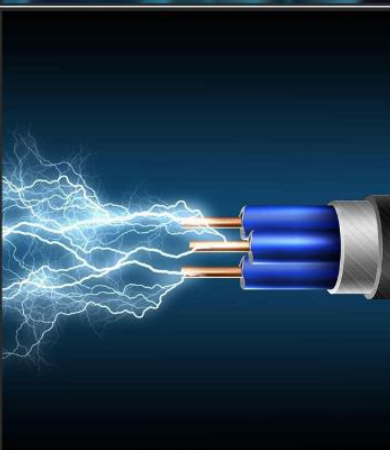


Catalogue of Ph.D. Theses



Prepared
by
LIBRARY
Indian Institute of Technology
Gandhinagar



Contents

Introduction to the Catalogue.....	1
Biological Science and Engineering	3
Chemical Engineering.....	63
Chemistry	122
Civil Engineering	207
Cognitive and Brain Sciences.....	266
Computer Science and Engineering.....	276
Earth Sciences.....	297
Electrical Engineering.....	344
Humanities and Social Sciences	430
Materials Engineering.....	488
Mathematics	526
Mechanical Engineering.....	560
Physics.....	583
Researcher/Author Index	768
Supervisor Index.....	774
Fact Sheet.....	777

Introduction to the Catalogue

Doctoral theses form an important part of the library collection. The library receives a softcopy and a hard bound of every PhD thesis, upon completion of the academic requirements after the submission. This collection in the library is growing steadily as a greater number of students are successfully graduating every year with their doctoral degree. As the PhD theses are unique and unpublished, the library puts in extra effort to collect, organize and provide access to this collection for the user community. Upon being awarded the degree at the convocation to the doctoral student, the library adds to its collection the copy of the thesis submitted to the Institute and then makes the basic information available. This basic information is maintained separately, with details accessible through the Library Catalogue (<https://catalog.iitgn.ac.in/>). Additionally, the Library maintains a Digital Repository (<repository.iitgn.ac.in>) that includes metadata and abstracts under each department name. This repository ensures that the research output of the doctoral students is preserved and made accessible to the broader academic community.

In addition, the Library Team has compiled a catalogue covering the basic details of each thesis where the degree was awarded during the period from 2013 to 2023 (347 Titles) to give a wider visibility to this important collection. This catalogue provides bibliographic information and abstract of the theses, to cater to a diverse scope and readership. The catalogue is divided into sections corresponding to 13 departments. For ease of browsing, a Researcher and Supervisor Index is included, guiding the readers to the specific page numbers where relevant theses can be found. Information included in this catalogue is sourced directly from the PhD theses submitted to IITGN, ensuring accuracy and comprehensiveness. By putting together this information about the research work undertaken at IITGN, current and future scholars can be inspired to explore these works and build upon the knowledge they represent. The PhD Theses Catalogue reflects the library team's effort in showcasing the doctoral students' high-quality research and scholarly achievements.

It is hoped that this catalogue serves as an invaluable source of doctoral research carried out at the Institute both for the internal community and the external scholars' community. Genuine feedback on this catalogue would be greatly appreciated.

Advisor (Library & Institute Archive)

June 2024



BIOLOGICAL SCIENCE AND ENGINEERING

Biological Science and Engineering

Title: Tau protein post-translational modification and small molecules interaction: molecular mechanisms of fibrillary assemblies, disassembly and aggregation inhibition

Researcher: Krishankumar, V. Guru

Supervisor: Gupta, Sharad

Year: 2018

Keyword's: Arginine-rich Eukaryotic Protein, Amyloid Fibrils, Vitro Aggregation

Call No.: 572.6 KRI

Acc No.: T00269

Abstract: Alzheimer's disease (AD) is a progressive neurodegenerative chronic disorder and is the most common form of dementia. Worldwide, there are more than 20 million cases of AD, expected to be doubled by 2030 and tripled by 2050. Owing to the increasing longevity of human population, AD is approaching epidemic proportions with no cures or preventative therapies. Amyloid beta (A β) peptide and tau protein, both are considered principal culprits but lately, the role of tau in AD pathogenesis has attracted significance as the severity of AD is well correlated with tau deposits in the human brain. Tau is an intrinsically disordered protein responsible for maintaining the structure and stability of microtubules in neurons. However, in AD and related tauopathies, tau undergoes abnormal Post-Translational Modifications (PTMs) such as hyperphosphorylation, resulting in amyloid deposits such as Neurofibrillary Tangles (NFTs). Therefore, understanding the mechanism of tau aggregation and correlation with PTMs is very critical in finding potential therapeutic agents that are capable of inhibiting or slowing the tau aggregation.

Simplified method for enhanced expression of tau protein

High Throughput Screening (HTS) of potential drug candidates which could modulate tau aggregation *in vitro* frequently requires milligram quantities of tau protein and is a major bottleneck for drug development efforts. As tau is a Proline and Arginine-rich eukaryotic protein, heterologous expression in *E. coli* often results in poor yield. We improved the expressed yield of tau by overcoming the codon bias and reported a simplified protocol for efficient tau extraction. The new method has two distinct features: (i) enhanced tau expression (up to eightfold) by supplementing deficient tRNAs (ii) direct-boiling of expressed *E. coli* cells to extract tau with no separate cell lysis step. We further demonstrated that tau extracted by direct-boiling is biophysically and biochemically similar to tau purified by size-exclusion chromatography and can be used for tau aggregation assays without any additional purification step.

Novel insights into the molecular mechanisms of tau protein and small molecules interaction

- a) *BODIPY derivatives as tau binding agents:* We screened styryl- BODIPY dyes derivatives to find a potential real-time molecular probe for *in vitro* tau protein fibrillization. Quinoxaline functionalized styryl-BODIPY derivative (Quin-BODIPY) exhibited significant fluorescence enhancement upon binding to tau fibrils. Tau-Quin-BODIPY interaction was further characterized by fluorescence emission kinetics, fluorescence microscopy, and Atomic Force Microscopy. The ability of Quin-

BODIPY to track real-time tau aggregation was at par with conventional Thioflavin T (ThT) dye. Post-fibrillization staining studies revealed that Quin-BODIPY preferentially binds to the growing end of tau fibrils, which hinted at a novel mechanism of tau-dye interaction previously not observed with ThT. Cell culture studies showed that Quin-BODIPY was cell permeable and non-toxic to live cells, and thus can be further developed for *in vitro* biological imaging application.

- b) *Remodeling tau-derived PHF6 fibrils by NQTrp hybrids*: NFTs are characterized by the conversion of natively unfolded monomeric tau protein into misfolded β -sheet rich aggregates. Therefore, inhibiting the aggregation cascade or disassembling the pre-formed aggregates becomes a pivotal event in disease treatment. We demonstrated that the Naphthoquinone-Tryptophan hybrids, i.e., NQTrp and Cl-NQTrp significantly disrupt the pre-formed fibrillar aggregates of tau-derived PHF6 (³⁰⁶VQIVYK³¹¹) peptide and full-length tau protein *in vitro*, in a dose-dependent manner as evident from ThS assay, CD spectroscopy, and TEM. Also, we found that the hybrid molecules disassemble the fibrils into non-toxic intermediates. Molecular dynamics simulation of PHF6 oligomers and fibrils with the Naphthoquinone-Tryptophan hybrids provided a possible structure-function based mechanism-of-action, highlighting the role of hydrophobic interaction and hydrogen bond formation during fibril disassembly. We inferred that π - π stacking of hybrid molecules with Tyr residue and hydrogen bond formation with Val of PHF6 caused the disassembly of amyloid fibrils.
- c) *High-Throughput Screening (HTS) of small molecule inhibitors for tau aggregation*: We carried out an *in vitro* HTS for the identification of potent inhibitors of tau aggregation using a proxy model; a highly aggregation-prone hexapeptide fragment ³⁰⁶VQIVYK³¹¹ (PHF6) derived from the tau protein. Using ThS fluorescence assay, we screened a library of 2,401 FDA approved, bio-active natural compounds, and found that palmatine chloride (PC) alkaloid was able to dramatically reduce the aggregation propensity of PHF6 at sub-molar concentrations. The results were further validated by the changes in β sheet content and reduced fibril density as observed by CD spectroscopy and TEM imaging, respectively. Also, PC disassembled pre-formed fibrillar aggregates of PHF6 and reduced the amyloid content in a dose-dependent manner. Insights obtained from molecular docking and molecular dynamics simulation showed that PC interacted by π - π stacking, π -cation stacking and formed hydrogen bonds with the key residues of PHF6 peptide responsible for β -sheet formation, which could likely be the mechanism behind inhibition and disassembly. Given that PC has been reported to cross the BBB, our findings suggest that it may serve as an attractive lead molecule for drug development towards AD and other related tauopathies.
- d) *Quercetin as a potent inhibitor of tau aggregation*: Polyphenols such as Resveratrol and Morin have been reported as potential small molecules to inhibit amyloid aggregation, including tau protein implicated in AD. To that end, we had tested quercetin; a polyphenol isolated from onion peel by magnetic nanobiocatalyst approach to target tau aggregation. ThT fluorescence assay showed that quercetin extract (MNP-quercetin) could effectively inhibit *in vitro* tau protein aggregation in a dose-dependent manner. The inhibitory effect of MNP- quercetin extract was further validated by fluorescence microscopy and Atomic Force Microscopy. We found that quercetin bound tau protein exhibited spherical morphology opposite to fibrillar. Also, MNP-quercetin extract efficiently disassembled pre-formed fibrillar aggregates of tau protein. MD

simulation with R2 domain of tau and quercetin revealed that the conformational changes in the monomeric protein upon interaction with quercetin could be plausibly due to specific hydrogen bonding interactions near the hexapeptide region, which is believed to be involved in the nucleation of tau aggregation. Additionally, we observed that quercetin increased the native random coil content by breaking secondary structures that favor fibrillization of R2 domain *in silico*, which could significantly reduce the overall aggregation propensity of tau. The ability of quercetin extract to inhibit tau aggregation expands the paradigm for application of bioactive polyphenols as therapeutic targets for AD.

Post Translational Modifications (PTMs) modulate *in vitro* aggregation of tau and tau derived peptides

- a) *Carbamylation: An age-related PTM promotes amyloidogenesis and induces structural changes in PHF6 fibrils:* Carbamylation is a non-enzymatic PTM, which involves the covalent modification of N-terminus of protein or ϵ -amino group of Lys. The role of carbamylation in several age-related disorders is well documented, however, the relationship between carbamylation and amyloid forming entities in neurodegenerative disorders including Alzheimer's disease remains unexplored. Using aggregation-prone tau-core hexapeptide fragments, i.e., ³⁰⁶VQIVYK³¹¹ (PHF6), ²⁷⁵VQIINK²⁸⁰ (PHF6*) and ¹⁶KLVFF²⁰ (A β 5) of amyloid β peptide models, we elucidated the effect of carbamylation on aggregation kinetics and overall changes in fibrillary morphology. We found that carbamylation promotes amyloidogenesis and converts the unstructured aggregates into fibrils, which were highly toxic to live cells. Electron microscopy images showed that carbamylation also altered the pitch length and twist of PHF6 fibrils. MD simulations of PHF6 variants and mutants (VQIVYA) revealed that the carbamyl moiety could form excess hydrogen bonds (3-fold higher than the acetylated peptide), which elevated the β -sheet content of fibrils. Our *in vitro* and *in silico* results corroborate each other and suggest that carbamylation could modulate the aggregation kinetics and cause structural changes in PHF6 fibrils.
- b) *Carbamylation promotes *in vitro* aggregation of full-length Tau:* We further extended our studies to the full-length tau protein and have shown that a similar change in aggregation pathway is observed upon carbamylation. The carbamylated tau protein self-aggregated rapidly in the absence of heparin opposite native tau, as observed by ThT fluorescence assay. The amyloidogenic aggregation of carbamylated tau was further validated by ANS fluorescence assay and Congo Red birefringence test. Not only the carbamylated tau protein aggregated faster than the unmodified tau, but also the resulting fibrils and oligomer preparations show significantly higher toxicity in neuronal cell culture model. MD simulation with R2 domain dimer of tau indicated that the carbamylated Lys residues (K²⁸⁰ and K³¹¹) located in the aggregation-prone regions (²⁷⁵VQIINK²⁸⁰) and (³⁰⁶VQIVYK³¹¹) primarily attributed for the onset of tau fibrillization, formed 7-fold excess hydrogen bonds than the native Lys residues. Carbamylation resulted in higher β -sheet content, which could plausibly be the reason behind the faster aggregation kinetics of modified tau protein. Perhaps, carbamylation, notoriously difficult to detect, is the missing link that could explain the sporadic nature and slow progression of neurodegenerative disorders such as AD.

Controlling PTMs to modulate PHF6 aggregation – a toolbox approach: To determine the combinatorial effects of PTMs on aggregation, we have designed a peptide toolbox containing N-terminus/Lys carbamylation (Cb), Tyr phosphorylation (pY) and N-terminus/Lys acetylation (Ac) of ³⁰⁶VQIVYK³¹¹. ThT Fluorescence assays indicates that only certain combinations of PTMs favor the aggregation, e.g., aggregation kinetics of peptide with Val (Ac) & Tyr (pY) was much rapid than Val (Ac), Tyr (pY), Lys (Ac) and Val (Cb), Tyr (pY), Lys (Ac). As observed in our previous studies, only aggregation kinetics cannot determine the amyloidogenicity of the matured fibrils. Molecular mechanisms such as hydrogen bonding, as well as charge-pairing could be the dominant determinants of amyloidogenic nature of aggregates. However, preliminary results indicated that PTMs indeed have a vital role in manifesting the aggregation kinetics of PHF6 peptide. In future, we intend to continue the in-depth analysis of these modified peptides to understand various factors responsible for modulating aggregation pathways and PTMs arbitrated polymorphism in amyloid fibrils.

Title: Interaction of dimeric carbocyanine dye with G-rich DNA
Researcher: Chilka, Pallavi
Supervisor: Datta, Bhaskar
Year: 2019
Keyword's: Quadruplex Research, Polymorphism, G-rich Oligonucleotides, G4-mediated Activity, Piperine
Call No.: 572.86 CHI
Acc. No.: T00523

Abstract: G-quadruplexes are four-stranded unorthodox nucleic acid structures formed by stacked G-quartets with Hoogsteen base paired guanine bases. The human genome consists of over 370,000 putative G-quadruplex-forming sequences. Most of these are found to localize at genomic regions with important cellular functions, such as the telomere, immunoglobulin switch regions, proto-oncogene promoters, and mRNA untranslated regions. G-quadruplex (G4) formation has been established at telomeres and a significant number of oncogene promoters. The bio-physical and structural characterization of G- quadruplexes has been subject of extensive research thereby providing valuable insights into structural nuances. However, their physiological functions remain open to investigation and interpretation. Small molecules that are capable of selectively binding G4 structures have emerged as important components of quadruplex research. Further, quadruplex-selective fluorescent probes have gained prominence for their ability to visualize quadruplex structures *in cellulo* in real time. The aim of this thesis was to investigate a small molecule fluorescence probe for specific targeting of G4 structures and to examine the scope of use of such a chemical agent. We have developed a novel class of dimeric cyanine dyes in our laboratory. In this thesis, we study the interaction of a dimeric cyanine dye with G4.

The thesis contains four experimental parts. In the first experimental part, interaction of 3,3'-(butane-1,3-diyl) bis (2-methylbenzo[d]thiazol-3-ium) bromide (hereafter dye 1) with various synthetic G-rich oligonucleotides has been studied. Notably, dye 1 displays nearly 1400-fold fluorescence enhancement upon interaction with specific type of G-rich sequences. This fluorescence enhancement is especially attractive alongside the nearly 30-fold fluorescence enhancement upon interaction with duplex and single stranded DNA molecules. The fluorescence enhancement of dye 1 is attributed to a de-aggregation induced mechanism wherein fluorescence quenched H-aggregated form of the dye is transformed to a highly fluorescent monomeric form upon binding specific G4 conformations. Interaction of dye is specific to G4 structures and not to the G-rich sequences. Changes in loop lengths and overall length of sequence influence topology of G4 also affecting interaction with 1. The de-aggregation induced mechanism is sensitive to conformational changes in G4 structures that can be effected by various experimental conditions. Dye 1 is able to convey differences in topology and stability of G4 through the extent of binding and concomitant fluorescence enhancement. Dye binding also stabilizes G4 structures based on increases in melting temperature.

In the second part, *in vitro* interaction of dye 1 is extended to physiologically relevant G- rich sequences that are known to exert G4-mediated activity. The behaviour of **1** against oncogene promoter sequences reinforces our findings from G-rich synthetic oligonucleotides, and also provide

support to the *in cellulo* use of 1. In particular, compared to K-Ras and c-Kit, substantial de-aggregation of dye is observed against c- Myc. The different behaviour of dye 1 in response to c-Myc as opposed to c-Kit or K- Ras is attributable to the G4 topologies formed in each case. Further, the dye is sensitive to the quadruplex-duplex equilibrium that can be effected by altering various conditions including the monovalent ion and choice of sequence. Dye 1 is potent for live cell imaging at low concentrations of usage and the application involves simple incubation. The purported de-aggregation induced fluorescence enhancement mechanism of 1 is used to visualize G4-containing regions of the cell. The staining profile of HeLa cells with the 1 is interesting as bright fluorescence is clearly observed at the nuclear periphery and certain regions of the nucleus. These regions are suggested as corresponding to mitochondrial guanine-rich DNA and nuclear r-DNA, respectively. Our studies support the ability of dye 1 as being a potent G4-visualizing dye that is comparable to a small number of known G4-selective fluorescent probes.

In the third part, we probe the *in cellulo* concomitant effect of G-quadruplex stabilizing property of dye 1 along with two known anti-cancer drugs on cancer cells. The quadruplex-selective drug piperine and the quadruplex-stabilizing dye 1 apparently compete for the G-rich DNA in cell nucleus. Piperine is found to prevail in this competition as evident from low fluorescence of dye inside the nucleus. Further, binding of the quadruplex-targeting drugs results in changes in cell morphology and/or changes in nucleus thereby permitting staining by the dimeric dye. The effects of piperine and olaparib are different in this regard. The latter produces more dramatic changes in staining profiles of the dimeric dye on drug treated cells. This work presents proof-of- concept for the use of quadruplex-selective staining as indicative of changes in the cellular environment. The sharp contrast between pre- and post-treatment by drugs (that are relatable to quadruplexes directly or indirectly), is not captured as well by a nucleus staining dye DAPI.

In the final part, we deploy dye 1-DNA complex as a reporter in two different contexts. The dye is used in conjunction with a G4 aptamer as a method of assaying the presence of toxin Bisphenol A. This approach relies on fluorescence quenching of the dye in presence of the aptamer-cognate target complex. Second, we use the dye 1-DNA complex as a reporter that can be applied for immunosensing applications. This thesis investigates and establishes scope of use of a G4-selective fluorescence probe thereby adding to a very small set of such known agents. It also poses questions in various contexts that form worthwhile future pursuits in our laboratory.

Title: Development of peptide-based inhibitors towards tau protein aggregation in Alzheimer's disease and sonic hedgehog protein in the hedgehog signaling pathway
Researcher: Ralhan, Krittika
Supervisor: Gupta, Sharad
Year: 2019
Keyword's: Solid Phase Peptide Synthesis, Neurofibrillary Tangles, Post-translational Modifications, Alzheimer's Disease
Call No.: 572.65 RAL
Acc. No.: T00528

Abstract: Peptides have emerged as an important class of biomolecules, which have found various therapeutics and diagnostic applications owing to their properties such as high target specificity, biocompatibility and the presence of pre-organised structure. In the past decade, peptide-based drugs have captivated an overall share of 10% in the pharmaceutical sector amounting to 40 billion dollars. There are currently 74 FDA approved peptide-based drugs in the market, and several others are in different phases of clinical trials. Despite the beneficial properties of peptides as prospective therapeutic agents, the major challenges remain such as their limited bioavailability, proteolytic stability and chemical stability. To counter these problems, several approaches are being used such as the introduction of molecular rigidity by forming disulphide cross-linkages, backbone modifications, non-canonical amino acids and D-amino acids are adopted. Present work details the efficient generation of peptide-based inhibitors targeting tau protein aggregation and Sonic Hedgehog/patched interaction. This dissertation explores the following approaches:

1. Novel deprotection strategy for difficult peptide synthesis

In Solid Phase Peptide Synthesis (SPPS), contamination with deletion sequences which often co-elute with the target peptide continues to be a major challenge as these impurities can significantly affect the target peptide's properties. Here, we report an efficient Fmoc- deprotection solution containing piperazine and DBU which can cause complete removal of Fmoc group in less than a minute. This combination rivals piperidine in speediness as revealed by kinetic studies. We demonstrate the efficiency of piperazine/DBU solution by synthesizing polyAla stretch with a significant reduction of deletion products occurring due to partial Fmoc- deprotection. We verify the utility of the deprotection solution by successfully synthesizing four aggregation-prone difficult peptide sequences. We further demonstrate that this combination can also be used to synthesize aspartimide and epimerization prone sequences when supplemented with 1% formic acid and is compatible with 2-chlorotrityl chloride resin. We conclude that piperazine/DBU can be used as a safer and effective alternative to piperidine in Fmoc-SPPS.

2. Effect of peptide length on the modulation of tau protein aggregation

The microtubule-associated protein tau is an intrinsically disordered protein which forms insoluble β -sheet rich assemblies in the human brain. Tau is implicated in several neurodegenerative disorders collectively known as tauopathies, where the most common tauopathy is Alzheimer's disease (AD) which is known to affect over 45 million people worldwide. Till date, there are no disease-modifying therapies available for AD. In an AD patient's brain, tau protein undergoes abnormal post-

translational modifications (PTMs) which allow it to self-assemble, resulting in the formation and deposition of Paired Helical Filaments (PHFs) and Neurofibrillary Tangles (NFTs). It is believed that tau protein can aggregate via the template-based conversion to form amyloids and may plausibly be a representative of prion-like protein. However, the precise mechanism of tau aggregation and molecular factors responsible for triggering the conformational conversion of unstructured tau monomers to form ordered assemblies remain elusive. Tau aggregation can be modulated by both intrinsic and extrinsic factors such as mutations in the *MAPT gene*, the concentration of protein, temperature, pH, salts, shear force, polyanions, PTMs and cross-seeding by other amyloidogenic proteins/ peptides. In the present study, we have evaluated the modulatory effect of the length and residue dependent short tau-derived peptides on the *in vitro* aggregation of full-length tau protein. Four short peptide variants were synthesized using SPPS: Tetra (IVYK), Hexa (VQIVYK), Octa (SVQIVYKP) Deca (GSVQIVYKPV). Complementary *in vitro* experiments demonstrated that tetrapeptide enhanced the tau protein aggregation, hexapeptide acted as complete inhibitor, whereas octa and deca peptides acted as a partial inhibitor of tau amyloid aggregation, respectively. Computational analysis of tetra and hexapeptides with R2 domain of tau protein (model dimer system) suggests that the addition of these peptide to tau system plausibly altered the structural conformation of the tau monomers in two different ways: (i) The tetrapeptide influenced the formation of intermolecular hydrogen bonds between the two tau monomers and increased the propensity of β -bridge formation, promoting aggregation (ii) hexapeptide promoted intramolecular hydrogen bonds within the tau monomers to form alpha-helix, thus facilitating aggregation inhibition.

3. Knottin based grafted peptides as Tau protein aggregation inhibitors

AD is the major form of dementia affecting over 45 million people worldwide. Till date, there are no disease-modifying therapies available for AD. Since the self-assembly of tau protein is closely related to AD and the initial stages of aggregation appear likely as the rate-limiting step, intervening in this process with aggregation-modulating agents might be an attractive strategy for AD therapeutics. Previously, few small molecules and peptide-based molecules have been reported to inhibit tau aggregation and disassemble pre-formed assemblies into non-toxic species. To this end, herein, we have rationally designed and synthesized potential knottin-based peptide inhibitors, which can perform targeted inhibition of tau aggregation. Knottins are cysteine rich miniproteins with characteristic disulphide bonding which helps in providing proteolytic, thermal and enzymatic stability to the synthesized knottin based peptides. Knottins have previously known to cross the blood-brain-barrier and hence we can use this property to our advantage for designing peptide based inhibitors for AD. Among the three synthesized peptide inhibitors, i.e., VQIVYK-knottin, VQIINK-knottin and Combo-knottin, VQIVYK-knottin was the most efficient peptide to inhibit tau-derived PHF6 hexapeptide aggregation as well as full-length tau protein aggregation in a concentration-dependent manner. The results were further validated using complementary biophysical characterization techniques. Cell culture studies revealed that VQIVYK-knottin peptide inhibitor was non-toxic to live cells and could permeabilize the cell membrane. Our findings signify the effectiveness of VQIVYK-knottin inhibitor towards tau aggregation and highlight the design to synthesize novel disease-modifying drugs for AD treatment.

4. Cysteine cross-linked macrocycle inhibitors for Hedgehog signaling pathway

Hedgehog signalling cascade is an important signalling pathway involved in embryonic development and organogenesis. In the case of aberrant expression, it can lead to the development of colon, lung and pancreatic cancers. The key player of the hedgehog signalling pathway is sonic hedgehog protein (Shh), which interacts with another protein named Patched to activate the downstream signalling cascade. In this work, we focus on the development of a macrocyclic peptide inhibitor against Sonic Hedgehog and patched interaction. The design is based on the specific binding site sequence of Hedgehog-interacting protein (HHIP) which competes with Patched protein for its binding site on Shh. We identified a 17 amino-acid long peptide sequence and subjected it to alkylation using several linkers reported previously. This reaction resulted in the formation of a bridge between the side-chains of two cysteine residues present in the sequence. The cysteine cross-linking provided molecular rigidity and resulted in several-fold improvement in the dissociation constant (Kd). Further, based on structural assessment of the native peptide, we replaced the canonical amino acid residues with non- canonical amino acids and subsequently generated a pool of peptides with unnatural amino acids and cross-linked cysteines. Using this approach, an optimized peptide named Biotin-M5St-DNle was obtained that binds to Shh with a Kd of 900 nM, corresponding to multi-fold improvement in affinity when compared to the parent peptide. This work introduces a new strategy to design potent peptide inhibitors against Shh/patched interaction.

Title: Theoretical investigation of carbohydrates and glycoproteins: elucidating structure, function and mechanism
Researcher: Pandey, Poonam
Supervisor: Mallajosyula, Sairam Swaroop
Year: 2019
Keyword's: Polarizable Simulations, Monosaccharide Systems, Drude Polarizable Force-field, N-acetyl-D-glucosamine, Antifreeze Glycoproteins
Call No.: 572.6 PAN
Acc. No.: T00529

Abstract: Carbohydrates; in the form of oligosaccharides, polysaccharides and glycoconjugates like glycopeptides, glycoproteins, glycolipids, and peptidoglycans; are amongst the abundant cell components. Glycans or oligosaccharides are an amazingly diverse class of macromolecules, varying in length, sequence order, linkages, substitution, and branching. Carbohydrates interact with a wide range of protein families, including antibodies, lectins, chemokines, and sugar transporters. Consequently, protein-carbohydrate interactions mediate a wide range of cellular processes. Owing to their structural and functional diversity, carbohydrates represent both therapeutic targets and tools. For example, glycans decorating the eukaryotic cell surface are often the hallmark of cancer and inflammation, while aberrant O-glycosylation may result in neurodegenerative disorders like Alzheimer's, Parkinson's and Huntington's disease.

Thus, a plethora of biological processes are directly or indirectly regulated by carbohydrates or their glycoconjugates, but the exact mechanism of their involvement in most of the biological events are still not clear. Therefore, understanding the physical and conformational properties of carbohydrates alone and in combination with their molecular scaffolds is crucial to elucidate the mechanistic role of these macromolecules in biological processes. It will also help to exploit these biomolecules for their utilization as therapeutic agents. Recent advances in experimental techniques allow the synthesis of naturally occurring oligosaccharides, polysaccharides and glycoproteins. However, the inherent structural complexity and variable-length complicate the experimental structural characterization of these molecules. For example, the flexible ring conformations and the flexible glycosidic linkage between carbohydrates generally lead to several possible low energy conformers, resulting in less well-ordered electron density for the entire carbohydrate unit in X-ray crystallography. Therefore the experimental studies are generally augmented with theoretical methods like Quantum mechanical (QM) calculations or molecular dynamics (MD) simulations. This thesis contributes to the understanding of carbohydrate interactions with water or proteins. The thesis is divided into seven chapters.

In chapter 1, we provide a brief introduction to carbohydrates and a comprehensive review of earlier experimental and theoretical studies on carbohydrates. The theoretical foundation of the computational techniques used in the subsequent chapters are discussed in detail in chapter 2.

In chapter 3, we use molecular dynamics simulations to gain atomistic insight into carbohydrate-water interactions and to specifically highlight the differences between additive (non-polarizable) and polarizable simulations. A total of six monosaccharide systems, α and β anomers of glucose,

galactose, and mannose, have been studied using additive and polarizable CHARMM carbohydrate force fields. The solvent was modeled using three additive water models TIP3P, TIP4P, and TIP5P in the additive simulations and the polarizable water model SWM4 in the polarizable simulations. The presence of carbohydrate has a significant effect on the microscopic water structure with the effects being pronounced for the proximal water molecules. Notably, a disruption of the tetrahedral arrangement of proximal water molecules was observed due to the formation of strong carbohydrate-water hydrogen bonds in both the additive and polarizable simulations. However, the inclusion of polarization resulted in significant bridge water occupancies, improved ordered water structure (tetrahedral order parameter) and longer carbohydrate-water H-bond correlations as compared to the additive simulations. Additionally, the polarizable simulations also allowed the calculation of the power spectra from the dipole-dipole autocorrelation function, which corresponds to the IR spectra. From the power spectra we could identify spectral signatures differentiating the proximal and bulk water structures which could not be captured from additive simulations.

In chapter 4, we report the development of Drude polarizable force-field parameters for the carboxylate and N-acetyl amine monosaccharide derivatives, extending the functionality of existing Drude polarizable carbohydrate force field. The force field parameters are developed in a hierarchical manner, reproducing the quantum mechanical (QM) gas-phase properties of small model compounds representing the key functional group in the carbohydrate derivatives. The optimized parameters were then used to generate the models for carboxylate and N-acetyl amine carbohydrate derivatives. The transferred parameters were further tested and optimized to reproduce crystal geometries and J-coupling data from NMR experiments. The parameter development resulted in the incorporation of D-glucuronate, L-iduronate, N-acetyl-D-glucosamine (GlcNAc) and N-acetyl-D-galactosamine (GalNAc) sugars into the Drude polarizable force field. The parameters developed in this study were then applied to study the conformational properties of glycosaminoglycan polymer hyaluronan, composed of D-glucuronate and N-acetyl-D-glucosamine, in aqueous solution. Upon comparing the results from the additive and polarizable simulations, it was found that the inclusion of polarization improved the description of the electrostatic interactions observed in hyaluronan resulting in enhanced conformational flexibility. The parameters developed in this study enabled us to investigate the influence of polarization on the structural properties of water around carboxylate (α/β -D-glucuronate and L-iduronate) and N-acetyl amine (α/β -N-acetyl-D-glucosamine and N-acetyl-D-galactosamine) monosaccharide derivatives. Unlike the unsubstituted monosaccharide-water system, a clear retardation in H-bond dynamics was observed for 1st hydration shell in polarizable systems, which is indistinguishable in additive simulations. We observed that the retardation dynamics also extended beyond the 1st hydration shell. This effect was due to the presence of the additional H-bond donating and acceptor groups present in carboxylate (COO^-) and N-acetyl-amine ($-\text{NHCOCH}_3$) side chains. The influence of these side chains is also captured by the fluctuations in tetrahedral order parameter.

In chapter 5, we carried out MD simulation studies to probe the microscopic properties of water brought about by structural variations of antifreeze glycoproteins (AFGPs). AFGPs are a distinctively riveting class of bio-macromolecules, which endows the survival of organisms inhabiting polar and subpolar regions. These proteins are supposed to hinder the microscopic freezing by interacting with the embryonic ice crystals and precluding their further growth. The underlying molecular

mechanism of AFGP binding to ice has remained elusive due to insufficient structural characterization, with conflicting hypothesis on the possible binding mode of AFGPs; either via the hydrophobic peptide backbone or via the hydrophilic carbohydrate side chains; when interacting with ice. Chemical synthesis has allowed researchers to access synthetic variants of natural AFGPs. These studies revealed that AFGPs exhibit huge variations in the thermal hysteresis and ice shaping behavior on slight structural variations, especially to the carbohydrate side chains. Four key structural motifs were identified as crucial to AFGP activity; the presence of threonine γ -methyl group, α -glycosidic carbohydrate-protein linkage, acetylamide group (-NHCOCH₃) at the C2 position of the carbohydrate linked to protein and the presence of carbohydrate hydroxyl groups. In this study, we use Molecular dynamics (MD) simulations to probe the microscopic properties of water along these structural variations of AFGPs. We find that these variations primarily influence the conformation space of AFGPs and also crucially control their hydration dynamics. Owing to the disordered nature of AFGPs, we use Markov-State modeling to identify conformational preferences for AFGPs. The simulations reveal the importance of steric bulk, intra-molecular carbohydrate-protein H-bonds, and conformational preferences (α - vs β - link-ages) in controlling the spatial segregation of hydrophilic and hydrophobic regions of AFGPs. We hypothesize that the hydrophobic component of AFGPs is crucial to its binding to ice, which determines the ice shaping ability of AFGPs. However, the hydrophilic carbohydrate hydroxyl groups and their ability to form bridge waters control the subsequent hydration dynamics, which is key to the antifreeze properties. Investigating the tetrahedral order parameter of water molecules around the carbohydrates revealed a competition between solute and bulk influenced the solvent structure, with maximum restructuring being observed in the interfacial region 2.5 Å – 4.5 Å away from the AFGPs.

In chapter 6, we report the development of CHARMM additive force-field parameters to enable the MD simulation studies of nucleotide-sugar. We used a hierarchical approach to develop the force field parameters. Initial parameters were adopted from the CHARMM nucleic acid and CHARMM carbohydrate force fields. Parameters were initially optimized using target data generated for small model compounds which were selected based on fragmentation approach. The optimized parameters were then used to generate the models for nucleotide sugars. The transferred parameters were tested and optimized to reproduce crystalline cell parameters and intra-molecular geometries. To ensure the compatibility of the developed parameters with the existing CHARMM additive force field, the parameters were also used to study the conformational properties of a family of nucleotide-sugar protein complexes. The developed force-field parameters in conjunction with the remainder of the CHARMM additive force-field parameters can be used for the future studies involving nucleotide-sugars in biological systems.

In chapter 7, we provide a overall summary of the work carried out in the thesis.

Title: Molecular Investigation of ATR and NFBD1 as therapeutic targets in cancer
Researcher: Bhakuni, Rashmi
Supervisor: Kirubakaran, Sivapriya
Year: 2019
Keyword's: Cancer, Chemo-therapy, mTOR Inhibitor, Immunoblotting, NFBD1
Call No.: 616.075 BHA
Acc. No.: T00539

Abstract: The 'graphene era', started in 2004 following the discovery of graphene by Geim and Novoselov, has laid interest in Graphene oxide (GO) research first as a starting material for the graphene synthesis and later as a unique material itself due to its structure and functionalities. GO is a two-dimensional (2D) material with plenty of oxygen-containing functional groups like carboxyl, epoxy, hydroxyl, carbonyl groups that play an exciting role in deciding properties of GO.

A single layer of GO, due to its homogeneity, large surface area ($2630 \text{ m}^2\text{g}^{-1}$) and occupancy of chemically active surface functional groups, are also manifested to have a high adsorption capability. Utilizing these properties, the scientific community has established its decontamination potential for a spectrum of organic substances related to various industries. However, the recovery of GO from water requires ultrahigh centrifugation for an extended time, which significantly increases the process costs and difficulty. Further, the long-term exposure to these graphene-family nanomaterials (GFN's) to water is reported to be toxic. To overcome these many biopolymers and chemicals are said to cross-link the individual GO sheet and make 3D networks. However, despite being too costly, all these cross-linked nanostructures show either weak mechanical strength or have very low efficiency towards the adsorption or removal of hazardous organic substances. Thus there is a constant requirement for the materials with higher mechanical strength, reasonable adsorption capacity, and minimum toxicity.

In this thesis work, we tried to investigate graphene-based two-dimensional (2D) and three-dimensional (3D) nanostructures with tunable mechanical strength and good adsorption capacity; further we report the rheological tuning mechanism for these gel-like aggregated nanostructures for the first time. We studied the microstructure, rheology and adsorption properties of aqueous dispersions of GO at an optimized volume fraction (ϕ_{GO}) = 0.018, which can be transformed into gels by cation induced charge shielding and cross-linking between the GO nanosheets. At similar ϕ_{GO} , cations of varying size and valence are systematically introduced with a range of electrolytes. Our results suggest that depending on the electrolyte concentration, size and the valence of the cation: low viscosity suspensions, fragile gels, and solid-like GO-electrolyte cross-linked gels are formed. These GO-electrolyte gels are shown to adsorb high quantities of oils and other organic contaminants. Along with higher oil and dye adsorption efficiency, GO-electrolyte gels are easy to recollect after the adsorption, thus avoiding the potential toxicity for bio-organisms in water caused by GO nanosheets.

Next to this, we explored the effect of size reduction and electrolyte addition on the rheology, microstructure, and adsorption capacity of the GO suspensions. We show that increasing the time of ultrasonication without any chemical treatment can promote aggregation of GO nanosheets

reflected by the increase in the storage modulus ($G'p$). The presence of electrolytes (NaCl, $MgCl_2$) increases the elastic moduli for GO aqueous dispersions by depending on the extent of aggregation and cross-linking. Stable gel-like suspensions with maximum $G'p$ are formed for GO nanosheets with the largest aspect ratio and maximum tested electrolyte concentration. The detailed XPS analysis is used to demonstrate the Mg^{2+} mediated bridging of GO is the primary factor of aggregation and the subsequent large $G'p$. Moreover, ultrasonication for prolonged time not only causes a reduction in the size of GO nanosheets but also leads to a reduction in the Mg^{2+} mediated crosslinking and hence a decrease in overall $G'p$.

We further synthesized composite photocatalysts using graphene-based nanomaterials GO and rGO as matrix components with TiO_2 using heat treatment and hydrothermal process. The unique feature is that these composites also show significant degradation efficiency for both the dyes in white light, making them suitable for practical applications requiring a wide range of the spectrum. In sum-up, lower bandgap, very efficient separation of e^-/h^+ pair, and the availability of $d-\pi$ electron cloud for the excellent e^- shuttling between the conduction band of TiO_2 and graphene matrix are some of the features that enhance the photocatalytic efficiency. One more unique feature of these photocatalysts is that they are equally efficient for the degradation of both MB and Eosin Y dyes with >95% efficiency in the extended wavelength region of the light spectrum.

Our next work reports the self-assembly of GO nanosheets at air-water interface using the LB method and obtained both monolayers and multi-layer films of graphene oxide at specific experimental conditions. We further explore the reproducibility of forming these GO films at similar experimental conditions by performing multiple compression-decompression cycles and observed the potential effect of various cycles on the hysteresis obtained. We also studied the impact of a significant factor, temperature, on the stability and properties of obtained GO LB films.

In conclusion, the first aspect of the thesis work has presented a new perspective on the science of graphene oxide suspension rheology. It is indeed the first study to explain the effects of systematic cation addition on the rheological properties of aqueous GO dispersions. It also establishes that the microstructural transformation of GO suspensions is actually governed by the hydrodynamic size of participating monovalent cation and the valence in case it's a multivalent cation. The second aspect of the thesis work emphasizes mostly on the nanosheets properties responsible for anchoring the cations from electrolyte dispersion to form cross-links between the adjacent GO sheets. The experimental results are evidencing that the carboxyl functionalities available on the rim of the nanosheets are indeed responsible for creating cross-links between the nanosheets. Thus, exposing the GO sheets to ultrasonication reduces their size and cross-linking efficiency that results in the GO suspension of low average storage modulus ($G'p$). This forms a fundamental discovery related to an aspect that has been associated with several research areas, yet remains unexplored. On the other hand, the third aspect of the thesis reveals the potential of graphene and its derivatives to be used as a suitable matrix material for the efficient anchoring of titania nanoparticles and form composites that are efficient to degrade both positively and negatively charged industrial dye wastes. In the end, the fourth aspect of the research reveals the ability to form monolayers on the air-water interface in optimized conditions. The monolayers of desired properties are of great scientific importance in designing the sensors and supercapacitors.

Overall, this thesis establishes a scope for using rheology as a modulation method for cation cross-linked GO-based macrostructures. It affirms that the mechanical strength and stability of these GO-based macrostructures depends on not only the external ionic conditions but also the size and functionalities of the GO sheets and can be optimized by controlling these critical factors. It not only provides certain fundamental additions to the current state of knowledge in 2D materials research but also raises so many questions in relevant contexts that open up new avenues of research in this domain.

Title: Two-dimensional films and three-dimensional macrostructures from the aqueous dispersion of graphene oxide: synthesis, rheology, and applications

Researcher: Ojha, Abhijeet

Supervisor: Thareja, Prachi

Year: 2020

Keyword's: Graphene-family Nanomaterials, Ultrasonication, Graphene-based Two-dimensional Structure

Call No.: 662.9 OJH

Acc. No.: T00540

Abstract: The 'graphene era', started in 2004 following the discovery of graphene by Geim and Novoselov, has laid interest in Graphene oxide (GO) research first as a starting material for the graphene synthesis and later as a unique material itself due to its structure and functionalities. GO is a two-dimensional (2D) material with plenty of oxygen-containing functional groups like carboxyl, epoxy, hydroxyl, carbonyl groups that play an exciting role in deciding properties of GO.

A single layer of GO, due to its homogeneity, large surface area ($2630 \text{ m}^2\text{g}^{-1}$) and occupancy of chemically active surface functional groups, are also manifested to have a high adsorption capability. Utilizing these properties, the scientific community has established its decontamination potential for a spectrum of organic substances related to various industries. However, the recovery of GO from water requires ultrahigh centrifugation for an extended time, which significantly increases the process costs and difficulty. Further, the long term exposure to these graphene-family nanomaterials (GFN's) to water is reported to be toxic. To overcome these many biopolymers and chemicals are said to cross-link the individual GO sheet and make 3D networks. However, despite being too costly, all these cross-linked nanostructures show either weak mechanical strength or have very low efficiency towards the adsorption or removal of hazardous organic substances. Thus there is a constant requirement for the materials with higher mechanical strength, reasonable adsorption capacity, and minimum toxicity.

In this thesis work, we tried to investigate graphene-based two-dimensional (2D) and three-dimensional (3D) nanostructures with tunable mechanical strength and good adsorption capacity; further we report the rheological tuning mechanism for these gel-like aggregated nanostructures for the first time. We studied the microstructure, rheology and adsorption properties of aqueous dispersions of GO at an optimized volume fraction ($\phi_{\text{GO}} = 0.018$, which can be transformed into gels by cation induced charge shielding and cross-linking between the GO nanosheets. At similar ϕ_{GO} , cations of varying size and valence are systematically introduced with a range of electrolytes. Our results suggest that depending on the electrolyte concentration, size and the valence of the cation: low viscosity suspensions, fragile gels, and solid-like GO-electrolyte cross-linked gels are formed. These GO-electrolyte gels are shown to adsorb high quantities of oils and other organic contaminants. Along with higher oil and dye adsorption efficiency, GO-electrolyte gels are easy to recollect after the adsorption, thus avoiding the potential toxicity for bio-organisms in water caused by GO nanosheets.

Next to this, we explored the effect of size reduction and electrolyte addition on the rheology, microstructure, and adsorption capacity of the GO suspensions. We show that increasing the time of ultrasonication without any chemical treatment can promote aggregation of GO nanosheets reflected by the increase in the storage modulus ($G'p$). The presence of electrolytes (NaCl, $MgCl_2$) increases the elastic moduli for GO aqueous dispersions by depending on the extent of aggregation and cross-linking. Stable gel-like suspensions with maximum $G'p$ are formed for GO nanosheets with the largest aspect ratio and maximum tested electrolyte concentration. The detailed XPS analysis is used to demonstrate the Mg^{2+} mediated bridging of GO is the primary factor of aggregation and the subsequent large $G'p$. Moreover, ultrasonication for prolonged time not only causes a reduction in the size of GO nanosheets but also leads to a reduction in the Mg^{2+} mediated crosslinking and hence a decrease in overall $G'p$.

We further synthesized composite photocatalysts using graphene-based nanomaterials GO and rGO as matrix components with TiO_2 using heat treatment and hydrothermal process. The unique feature is that these composites also show significant degradation efficiency for both the dyes in white light, making them suitable for practical applications requiring a wide range of the spectrum. In sum-up, lower bandgap, very efficient separation of e^-/h^+ pair, and the availability of $d-\pi$ electron cloud for the excellent e^- shuttling between the conduction band of TiO_2 and graphene matrix are some of the features that enhance the photocatalytic efficiency. One more unique feature of these photocatalysts is that they are equally efficient for the degradation of both MB and Eosin Y dyes with >95% efficiency in the extended wavelength region of the light spectrum.

Our next work reports the self-assembly of GO nanosheets at air-water interface using the LB method and obtained both monolayers and multi-layer films of graphene oxide at specific experimental conditions. We further explore the reproducibility of forming these GO films at similar experimental conditions by performing multiple compression-decompression cycles and observed the potential effect of various cycles on the hysteresis obtained. We also studied the impact of a significant factor, temperature, on the stability and properties of obtained GO LB films.

In conclusion, the first aspect of the thesis work has presented a new perspective on the science of graphene oxide suspension rheology. It is indeed the first study to explain the effects of systematic cation addition on the rheological properties of aqueous GO dispersions. It also establishes that the microstructural transformation of GO suspensions is actually governed by the hydrodynamic size of participating monovalent cation and the valence in case it's a multivalent cation. The second aspect of the thesis work emphasizes mostly on the nanosheets properties responsible for anchoring the cations from electrolyte dispersion to form cross-links between the adjacent GO sheets. The experimental results are evidencing that the carboxyl functionalities available on the rim of the nanosheets are indeed responsible for creating cross-links between the nanosheets. Thus, exposing the GO sheets to ultrasonication reduces their size and cross-linking efficiency that results in the GO suspension of low average storage modulus ($G'p$). This forms a fundamental discovery related to an aspect that has been associated with several research areas, yet remains unexplored. On the other hand, the third aspect of the thesis reveals the potential of graphene and its derivatives to be used as a suitable matrix material for the efficient anchoring of titania nanoparticles and form composites that are efficient to degrade both positively and negatively charged industrial dye wastes. In the end, the fourth aspect of the research reveals the ability to form monolayers on the air-water

interface in optimized conditions. The monolayers of desired properties are of great scientific importance in designing the sensors and supercapacitors.

Overall, this thesis establishes a scope for using rheology as a modulation method for cation cross-linked GO-based macrostructures. It affirms that the mechanical strength and stability of these GO-based macrostructures depends on not only the external ionic conditions but also the size and functionalities of the GO sheets and can be optimized by controlling these critical factors. It not only provides certain fundamental additions to the current state of knowledge in 2D materials research but also raises so many questions in relevant contexts that open up new avenues of research in this domain.

Title: Development of nanobioconjugates for the efficient extraction of bioactive compounds and for the detection of environmental and clinical analytes

Researcher: Kumar, Sanjay

Supervisor: Datta, Bhaskar

Year: 2019

Keyword's: Immobilizing Hydrolytic Enzymes, Conjugation Strategies, Atomic Force Microscopy (AFM), Transmission Electron Microscopy (TEM), RNA Detection

Call No.: 620.8 KUM

Acc. No.: T00547

Abstract: The field of nanobiotechnology combines the ability to prepare materials that typically measure between 1 and 100 nm with the ability to exert precise interventions in biological systems. Nanobioconstructs aspire to synergize the function and characteristics of nanomaterials with biomacromolecules. In this thesis I describe the development and investigation of various nanobioconstructs towards applications that can be broadly categorized under catalysis and sensing. The thesis is divided into two sections; in the first section I discuss reusable nanobiocatalysts for the efficient extraction of bio-active compounds. The first chapter provides a broad introduction of concepts and topics covered in the thesis.

In chapter 2, I examine the effect of immobilizing hydrolytic enzymes on nanoparticles. Hydrolytic enzymes cellulase and pectinase are immobilized on the magnetic iron oxide nano particles via established conjugation strategies. The size and morphology of the enzyme- nanoparticle constructs are characterized by Atomic Force Microscopy (AFM), the composition of the enzyme-nanoparticle constructs are characterized by X-Ray Diffraction (XRD) and Transmission Electron Microscopy (TEM) is used to assess the enzyme immobilization. The enzyme immobilized magnetic iron oxide nano particles are found to improve the yield of extraction of bioactive compounds by nearly 8-9 fold. In addition, the improved extraction of carotenoidic bioactive compounds bears a strong correlation with the extent of peel hydrolysis. There are relatively few approaches which address the issue of reusability of the biocatalyst in such extraction processes. In this work, the reusability of the enzyme-MNP constructs demonstrated towards the extraction of bioactive compounds from separate source batches of orange peel. The reusability of the nanoparticle-immobilized catalyst along with their improved stability compared to free enzymes bodes well for their active use. The elucidation of conditions for the extraction of bioactive compounds from a source like orange peel further enhances the value of the nano biocatalyst-mediated process.

In chapter 3, I scrutinize the construction and application of nanoparticle-immobilized hydrolytic enzymes. There are dearths of reports on the systematic examination of factors influencing nanoparticle-immobilized hydrolytic enzyme activity. First the effect of nanoparticle composition and chemical linkage has been investigated on the immobilized cellulase activity on onion skins. Our choice of onion skins as source material is aligned with our efforts in rendering value from waste. Onion skins are known to bear polyphenols such as quercetin. The products of hydrolysis of onion skin are assessed with respect to glycosidic and aglycosidic forms of polyphenols. Application of the cellulase-immobilized nanoparticles on onion skins results in release of a distinctive composition of polyphenols. The aglycosidic form of quercetin is the dominant product of onion skin hydrolysis

affected by cellulase nanobiocatalysts. The nanoparticles with different composition (such as IOMNPs, SNPs, S-IOMNPs and C-IOMNPs) and with different chemical linkers (C-5, C-6, C-14 and C-22) are synthesized and characterized. I assess these parameters towards achieving optimal hydrolytic activity of the immobilized enzyme. Chitosan-coated iron oxide nanoparticles with APTES-conjugated cellulase are found to be most effective for polyphenol release and for transformation of glycosidic to aglycosidic form of quercetin. Further, the quercetin-rich extracts exhibit a distinctive inhibitory activity on tau-fibril aggregation. In contrast, quercetin-diglucoside does not have an inhibitory effect.

The second section of the thesis is devoted to two different aspects of nanobiosensors.

In chapter 4, a novel immobilized-enzyme based strategy has been developed for the colorimetric detection of herbicide glyphosate. The latter is the most widely used herbicide in the world and has been at the center of an intense debate pertaining to its long-term effects on human health. Our method relies on concerted activity of laccase mediator system with syringaldazine as specific mediator. These oxidative systems catalyze the breakdown of glyphosate and simultaneously provide visual indication of the same. A combination of spectro-electrochemistry, NMR spectroscopy and glyphosate-derivatization based chromatography have been used to investigate and validate the assay. Presence of glyphosate enhances kinetics of the laccase-mediator by up to 30% and 10-200 ppm of glyphosate can be easily detected. These concentrations are well within the range of glyphosate concentrations that are likely to cause long-term harm to human populations. Reusability and superior sensitivity of our assay is enabled by use of silica-coated magnetic iron oxide nanoparticles with immobilized laccase.

In chapter 5, I deploy nucleic acid enabled biosensors for the detection of target DNA. Target DNA is detected by exploiting the response of pNIPAm-co-AAc microgel-based etalons to NaCl. NaCl in solution is capable of penetrating pores in the top Au layer of an etalon resulting in easily quantifiable color change. Probe DNA is immobilized on the top Au layer of an etalon that is capable of binding complementary target sequences. Upon binding of the complementary sequence to the surface (forming a double strand), the ability of the NaCl to penetrate the etalon's Au layer is hindered, while its response can be restored by removal of the DNA from the surface. Target DNA that has varying degrees of mismatches namely 3 base pair (BP), 10 BP and completely mismatched can all be distinguished by our approach. I validate the response of etalons through the removal of only hybridized nucleic acid sequences using specific enzymes (nuclease Bal-31). This system demonstrates a straight-forward detection method to sense target DNA without any modification or the use of labels.

My thesis highlights (1) the emergent behavior of nano-bioconjugates and (2) ability of nano-conjugates to expand the scope of application of distinctive biomolecular behavior.

Title: Mechanistic and characteristic investigation of recombinant eukaryotic hCD151 and prokaryotic HpIMPDPH protein

Researcher: Gayathri P.

Supervisor: Thiruvengatam, Vijay

Year: 2019

Keyword's: Tetraspanin CD151, Hydrogen Bonding, Helicobacter Pylori, Protein Production, HCD151

Call No.: 572 GAY

Acc. No.: T00548

Abstract: Compared to other expression systems, bacterial system (*E.coli*) remains the best candidate expression system due to their cost-effectiveness, well-studied genetics, high yield and short doubling time. The application of recombinant protein is widely present in the structural and functional characterization & biochemical studies of protein that requires a large amount of protein. In this work, we have studied the heterologous expression of eukaryotic (*Homo sapiens*) transmembrane protein, tetraspanin CD151, which is considered as one of the most challenging protein to express in the bacterial system and prokaryotic protein (*Helicobacter pylori*) Inosine- 5'-monophosphate dehydrogenase, which is an equally challenging protein to express in soluble and active form.

Tetraspanin CD151 is involved in the various crucial biological process. It plays a significant role in cancer by modulating different stages such as tumour growth, metastasis & drug sensitivity in various types of cancers (skin and lung) and viral infectious diseases. Targeting CD151 could be a promising therapy for cancer and viral infections, but this requires structural information to understand the mechanism of the protein. While considering the challenges in expressing & purifying transmembrane protein in *E.coli*, we have introduced a construct wise expression approach for the recombinant expression of hCD151 in the bacterial system. The full-length hCD151 protein has been constructed into four different constructs and cloned into pMALc- 5X-His. Construct-1 contains the full-length protein (28kDa), Construct-2 contains intracellular(IC) and large extracellular loops (LEL), and the 3rd and 4th transmembrane domain (TMDs) up to the C-terminal, the Construct-3 contains only the LEL, and the Construct-4 contains the LEL along with the 4th TMD helices up to the C-terminal end. Full-length hCD151 protein expression was not observed; however, in the other three constructs, the expression was observed. The reduction of TMD helices tailed by the presence of the extracellular region that fused with the MBP tag allowed the overexpression of the constructs. The recombinant expression of hCD151 constructs was confirmed by western blot and mass fingerprint analysis. The comparison of the CD curve of MBP and the hCD151 constructs clearly showed the presence of helical content in the recombinant hCD151 constructs.

Based on the recently reported full-length crystal structure of hCD81 [5TCX] complexed with cholesterol molecule, we have predicted and characterized the structure of hCD151. The docking study followed by the MD simulation showed an intramembrane pocket for the cholesterol moiety in hCD151 as seen in hCD81. The simulation results showed the apo-protein is stabilized by the hydrogen bond between Tyr²³ (TMD-1) and Gln²³⁴ (TMD-4) and the cholesterol bound structure is stabilized by salt bridge formation via Lys⁴⁵ (TMD-2) - Glu¹⁴⁰ (LEL) & Glu²¹⁸ (LEL) – Arg²²¹ (TMD-4).

These salt bridge formation and the hydrogen bonding between the apo and complex *hCD151* structure suggest that the *hCD151* protein also might undergo the open and closed conformations based on the cholesterol molecule presence as in *hCD81*. The crystallization trials were performed with the purified *hCD151* constructs fused with MBP protein. The initial crystal hit was observed in the screening condition, 0.2 Ammonium Sulfate and PEG-8000 at 16° (Crystal Screen HT C7). In this condition, microcrystals of 10-20µm were observed with poor diffraction quality. The conditions have to be optimized to get good quality crystal in a desirable size to proceed for the structural characterization of *hCD151*.

Helicobacter pylori (*H. pylori*) bacteria is the major cause of several gastric disorders and recognized as a type I carcinogen by WHO. Due to the resistance developed by *H. pylori* strains, currently used antibiotic based treatments demonstrate high failure rates. Recently, bacterial IMPDH enzyme involved in *denovo* guanine biosynthesis pathway has been studied as a potential target to treat bacterial infections. Differences in the structural and kinetic parameters of the eukaryotic and prokaryotic IMPDH makes it possible to target bacterial IMPDH selectively and hence, the IMPDH protein from the *H.pylori* can be a valid target for the infection.

To understand the functional and structural characterisation of *Hp*IMPDH, we have recombinantly expressed the *Hp*IMPDH protein and confirmed by western blot and peptide mass fingerprint. The presence of secondary structure elements in the *Hp*IMPDH is characterized by circular dichroism. The ability of the recombinant *Hp*IMPDH to convert the NAD⁺ to NADH shows the bioactivity of the recombinantly expressed *Hp*IMPDH. The kinetic profile of the recombinant protein showed the KM value of 18.36±1.53 µM and 76.37±1.09 µM respectively, for IMP and NAD⁺. To understand the structural characterization of the *Hp*IMPDH, crystallization trials were carried out. Crystal hits were observed in (a).0.2 M Sodium Fluoride, 20% w/v Polyethylene glycol 3,350 (PEG/ Ion screen™ HR2-126) at 16°C and (b). 0.2 M L-Proline, 0.1 M HEPES pH 7.5 10% w/v Polyethylene glycol 3,350 (INDEX) at 16°C). These crystals were tried for the X-ray diffraction experiment in RRCAT synchrotron facility, and no diffraction pattern was observed. Hence, these conditions have to be further optimised for the better quality crystal.

From our inhibitory studies, we identified, a new indole-based scaffold against *Hp*IMPDH and they showed non-competitive inhibition against IMP and NAD⁺, whereas the already reported benzimidazole compound C91 (IC50 0.18µM) was found to be an uncompetitive inhibitor. Further, we have identified indole-based diazo compounds to be the most potent inhibitors amongst the database with IC50 of 0.8 ±0.02µM and 1±0.03µM, and this can be a good lead for the further development of the selective and potent inhibitors of *Hp*IMPDH. Mutational studies were performed in the NAD⁺ binding domain (Asn²⁵²Ala and Tyr⁴³⁹Ala) and the flap region (Asp³⁹⁶Gly, Arg³⁹⁷Gly, Tyr³⁹⁸Gly, Arg³⁹⁷Lys & Tyr³⁹⁸Phe) of *Hp*IMPDH for a better understanding of the catalytic reaction. The enzymatic characterization of Asn²⁵²Ala, Asp³⁹⁶Gly and Tyr⁴³⁹Ala showed the binding pattern of the substrates and the cofactor had been affected in the mutant enzymes as compared to wildtype. The Asp³⁹⁶Gly showed Asp³⁹⁶ could be one of the critical factors in maintaining the open and closed equilibrium of the *Hp*IMPDH protein. The NADH product inhibition in the absence of RY dyad (Arg³⁹⁷Gly, Tyr³⁹⁸Gly, Arg³⁹⁷Lys & Tyr³⁹⁸Phe) revealed both the residues are equally crucial in the NADH release and their reported role of water activation as that of Euk-IMPDH. These studies would

aid for the better understanding of the catalytic reaction of *Hpl*MDH and designing of higher affinity inhibitory molecules with the host specificity.

Title: Validation of human tousled-like kinase 1B as a molecular target for anticancer therapy
Researcher: Bhoir, Siddhant Pandurang
Supervisor: Kirubakaran, Sivapriya
Year: 2020
Keyword's: Prostate Cancer, Clonogenic Assay, Carcinoma Drug Design, Radiotherapy, Genome and Epigenome
Call No.: 616.99 BHO
Acc. No.: T00574

Abstract: In the first chapter, we introduced and described the Tousled-Like Kinases (TLK1 and TLK2) which are highly conserved serine/threonine protein kinases responsible for DNA repair, chromatin assembly, transcription and chromosome segregation. We further explained their apparent role in the genome surveillance through different interacting partners, and in cancer development via efficient DNA repair mechanisms. Human TLKs are frequently overexpressed in breast cancer, prostate cancer and cholangiocarcinoma, and often correspond to reduced sensitivity towards chemo- and radiomimetic therapies. The mutations in the DNA repair genes and the checkpoint functions in most cancers makes them overly dependent on such alternative pathways for their survival. As high TLK1B expression is thought to be a critical transition during tumorigenesis, we hypothesized the pre-emptive inhibition of these kinases by the specific inhibitors which could choke a crucial step in the formation of tumours.

The development of new protein kinase inhibitors requires an in-depth knowledge of the kinase regulation, its activity and its ability to bind to the drugs. However, we understand that the detailed analysis of the protein structure and the mechanisms of protein-drug interaction through biochemical and biophysical techniques demands a method for the production of an active protein of exceptional stability and purity on a large scale. Hence, in the second chapter, we report a method for bacterial expression and purification of the full-length, wild-type hTLK1B by co-expressing it along with bacteriophage lambda protein phosphatase. With this approach, we could produce the homogeneously unphosphorylated hTLK1B protein in high yields (6 -12 mg/litre) for the structural and biochemical studies, and the protein was found to be stable and biologically active.

Similarly, in the third chapter, we contemplated if this simple, robust and efficient protocol (from the second chapter) can be extensively applied to the hTLK1B kinase domain construct as well, as the ability to engineer and express kinase domains of interest easily would foster the development of selective inhibitors, thereby, offering an advantage over currently available high throughput platforms. Impressively, we could obtain ample amounts (~20mg per litre of the bacterial culture) of the soluble and homogeneously unphosphorylated form of biologically active hTLK1B_KD with exceptional purity in a single purification step via 6x-polyhistidine tag, which can then be used for structural, functional and in-vitro drug screening studies. We further carried out the inhibitor sensitivity analysis and the first-stage in-vitro drug screening studies with the in house generated

TLK inhibitors, and the compounds 2a and 4b inhibited the protein slightly higher as compared to THD, a positive control for TLK inhibition.

In the fourth chapter, we evaluated the new phenothiazine inhibitor-J54 for its TLK1B inhibitory potential through in vitro, in silico, cell-based and the in vivo LNCaP xenograft studies in the prostate cancer (PCa) treatment. PCa is the second most commonly diagnosed cancer and the sixth leading cause of cancer deaths among men worldwide. A 65kDa TLK1B protein is an essential effector of chemoresistance that is overexpressed typically in the PCa cell lines and biopsies, and its expression is demonstrated as a critical driver of PCa. The androgen-deprivation therapy (ADT), which is the current standard of care for advanced PCa, results in translational upregulation of TLK1B via the mTOR-4EBP1 pathway, a crucial kinase upstream of NEK1 and ATR, thereby, mediating a DNA damage response (DDR)- ADT>TLK1B>NEK1>ATR>Chk1, that results in a temporary cell-cycle arrest of androgen-responsive PCa cells, while its abrogation leads to apoptosis, causing the suppression of PCa emergence. Hence, we targeted the TLK1B/NEK1 axis with novel TLK1B-specific inhibitor-J54 that is more effective and with fewer side effects, resulting in the complete response to

ADT. J54 was found to be potent and non-toxic to the healthy cells in-vitro and in LNCaP xenografts. It had a mild affinity for the dopamine receptor (DR2) in modeling studies, and weak detrimental behavioural effects in mice and *C. elegans* models.

I conclude my thesis by providing with the novel findings on the characterisation of a new phenothiazine-based TLK1B inhibitor, J54. Our experimental results collectively suggest that our drug combination (e.g., Bicalutamide and J54) will be successful and may result in a significant competitive advantage over similar DDR-based strategies that have not worked very well, thereby making phenothiazines (PTHs) as the promising anticancer agents and safety candidates for the future clinical trials in prostate cancer treatment. The high-throughput inhibitor screening assay platform developed in this thesis can be applied to other protein kinases as a useful contribution to the potential drug discovery applications.

Title: Crystal Engineering of poorly water-soluble drugs
Researcher: Indumathi, S.
Supervisor: Dalvi, Sameer V.
Year: 2020
Keyword's: Crystallography, Crystal growth, Cocrystallization, Salt-cocrystal, CUR-HXQ Crystals
Call No.: 548 IND
Acc. No.: T00692

Abstract: Several Active Pharmaceutical Ingredient (API) molecules in spite of having good medicinal properties and therapeutic ability are restricted for human administration because of their hydrophobic nature. Biopharmaceutics Classification System (BCS) of drugs have classified such hydrophobic drugs with poor aqueous solubility as BCS class II drugs (drugs with poor aqueous solubility but good membrane permeability) and class IV drugs (drugs with poor aqueous solubility as well as membrane permeability).

Cocrystallization is a crystal engineering approach which can be used to fine-tune the solubility nature of such poorly water-soluble drugs through introduction of non-covalent intermolecular interactions between drug and coformer molecules. The aim of this thesis is mainly focused on cocrystal formation of a BCS class IV drug, Curcumin (CUR) and BCS class II drugs, Nevirapine (NEV) and Carbamazepine (CBZ) for enhanced dissolution and bioavailability. CUR was observed to form cocrystal with hydroxyquinol (HXQ) and trimesic acid (TMA). CUR formed eutectics with salicylic acid (SAA), biotin (BIO), carbamazepine (CBZ), N-acetyl D,L-Tryptophan (N-ATP), paracetamol (PAR), tyrosine (TYR), glycine (GLY), succinic acid (SUC), ethyl paraben (ETP). With IBU, CUR remained as a physical mixture. CUR-HXQ (1:2) cocrystal showed highest dissolution, about 3 times and CUR-TMA (1:1) cocrystal exhibited 1.8 times higher than raw CUR in 40% ethanol-water (v/v ratio) at 37 °C. Further CUR-SUC (1:1) eutectic exhibited 4.84 times higher dissolution compared to raw CUR in 20% ethanol-water (v/v ratio) at 37 °C.

Multicomponent crystalline solid forms of NEV (a BCS class II anti-retroviral drug) have been prepared with paracetamol (PAR), trimesic acid (TMA) and trimellitic anhydride (TMEA) as coformers. NEV formed an eutectic with PAR at NEV-PAR stoichiometric ratio of 1:3. Evaporative crystallization and slurry conversion of NEV-TMA (1:1) yielded NEV-TMA (1:1) cocrystal methanol solvate. Interestingly, TMEA underwent conversion into trimellitic acetate (TMEA acetate) on its reaction with methanol during evaporative crystallization, resulting into NEV-TMEA acetate (1:1) cocrystal hydrate. NEV-PAR (1:3) eutectic and NEV-TMA (1:1) cocrystal methanol solvate exhibited 3 times and 2 times enhanced dissolution than raw NEV in deionized water (containing 0.1 wt % SDS) dissolution medium at 37 °C.

Apart from CUR and NEV, CBZ was chosen to investigate the role of cocrystallization in enhancing dissolution of drugs with poor aqueous solubility since it has been widely explored by researchers as a model drug in crystal engineering. In case of CBZ, efforts were made to enhance dissolution of CBZ by cocrystallizing CBZ with amide, acid and hydrazide coformer molecules possessing good aqueous solubility. CBZ was observed to form cocrystal with *para*-hydroxybenzamide (PHBAD) and acetamide (ACE) by solid-state grinding, evaporative crystallization, slurry conversion and slow

cooling crystallization. Interestingly, slow cooling crystallization of CBZ-ACE mixtures at stoichiometric ratios of 1:1 and 2:1 yielded CBZ dihydrate rather than cocrystals. The coformers salicylamide (SAL), pyrazinamide (PRZ), pimelic acid (PMA), suberic acid (SBA), azelaic acid (AZA), sebacic acid (SEA), isoniazid (ISN) and nicotinic acid hydrazide (NAH) formed eutectics because of the existence of weaker adhesive interaction between CBZ and the coformers. On the other hand, CBZ-maleic acid hydrazide (MAH) combination existed as a physical mixture symbolizing the absence of stronger non-covalent intermolecular interaction between CBZ and MAH. CBZ- PHBAD (1:1) cocrystals showed 8.73 times while CBZ-ACE (1:2) cocrystals displayed 7.47 times higher dissolution than raw CBZ. Among the various CBZ eutectics synthesized, CBZ-NAH (1:2) eutectic exhibited 4.93 times higher dissolution than raw CBZ in Phosphate Buffer Saline (PBS) at 37 °C.

The ultimate goal of cocrystallization was to enhance the bioavailability of NEV, CBZ and CUR. Therefore, to test the efficacy of the multicomponent solids prepared in this work, the anti-cancer and anti-invasion activity of some of the CUR multicomponent solids was evaluated against the 2D monolayers and 3D tumor models of MDA-MB-231 cells. The cytotoxicity and internalization assays conducted on 2D monolayers indicated that all CUR multicomponent solid forms except Curcumin-Folic Acid Dihydrate (CUR- FAD) (1:1) coamorphous solid exhibited enhanced bioavailability than raw CUR. Cell invasion assay conducted on 3D tumor spheroid models showed that CUR-HXQ (1:1) cocrystal completely inhibited cell invasion whereas CUR-FAD (1:1) coamorphous solid induced enhanced invasion of cells from spheroid models. Thus, we propose that CUR- HXQ (1:1) cocrystal possess an effective anti-cancer activity whereas CUR-FAD (1:1) coamorphous solid cannot serve as an ideal candidate for combinatorial drug therapy in the treatment of cancer.

Thus, this work illustrates that the simplicity and geometric compatibility of the coformer molecules to fit into a drug's crystal lattice, strength of the intermolecular interactions between a drug and a coformer, the solubility and therapeutic efficacy of the coformers were found to be the key parameters that determines the successful design of a new pharmaceutical entity with improved dissolution and bioavailability characteristics by cocrystallization.

Title: Investigation of protein-protein interactions in Tuberous Sclerosis Complex (TSC) and structural identification of Netrin-NTR

Researcher: Natarajan, Nalini

Supervisor: Thiruvengatam, Vijay

Year: 2020

Keyword's: Homology Modeling, Cloning, Dana-Farber Cancer Institute, Extracellular Protein, Tissues Inhibitors Metalloproteinases (TIMPS)

Call No.: 618.928 NAT

Acc. No.: T00693

Abstract: Protein-protein interactions (PPIs) are necessary for every cellular process. Understanding PPIs in a cell during a normal state and in diseased states give us an advantage of targeted therapy. Although wading through the interactome is a cumbersome process, the discoveries of novel PPIs often acts as a base for any successful drug discovery project. The recent advances in mass-spectrometry and yeast-2-hybrid screening have paved way for connecting the dots of the protein network resulting in an explosion of cellular signaling data. However, these data depict the physical contact of the proteins and rarely explains the functional significance of the interaction itself. The problem gets extremely complex in diseases like cancer, where a complete perturbation of cellular homeostasis occurs. In this thesis, I have worked on multifaceted cell signaling proteins like TSC1 (Hamartin), TSC2 (Tuberin), Hsp70 and Netrin-NTR. The **first chapter** of my thesis gives an overview of these proteins along with their physiological significance and cellular context.

TSC1 and TSC2 are heterodimeric tumor suppressor proteins that inhibit mTORC1. The mammalian target of rapamycin (mTOR) signaling pathway is a well-studied example of how the cell integrates both the extracellular and intracellular signals. mTORC1 positively regulates cell growth by responding to the proliferative external cues such as growth factors, energy status, oxygen and amino acids. On the contrary, TSC1/2 complex is a molecular switchboard, which responds to factors like stress, hypoxia and nutrient deprivation. Apart from its tumor suppressor function, TSC1 and TSC2 are involved in plethora of PPIs in the cell. Based on their interaction profile, TSC1 and TSC2 as a complex or individually can account to several important cellular functions like hypoxia, DNA damage stress and endoplasmic reticulum stress. TSC1/2 complex bridges several gaps in various cell signaling pathways. A significant part of the thesis was dedicated on identifying regions in TSC1 and TSC2 that have a rich propensity for PPIs and on investing in a maiden attempt to express, purify and characterize those domains. In a recent study, Hsp70 was found to be interacting with the TSC1, while the region of interaction or the mechanism of the interaction was not commented. Here, we have identified the regions of interaction in both TSC1 and Hsp70 and have shown that TSC1 inhibits human Hsp70.

The **second chapter** deals with the recombinant expression construct design and purification of TSC1 (302-420 aa) along with its interaction studies with the *E. coli* molecular chaperone DnaK. We have carefully designed the construct by incorporating the gene fragment corresponding to TSC1 (302-420 aa) in bacterial expression pGEX-6P1 vector with a GST fusion tag. The affinity purification using glutathione agarose was combined with an on-column HRV3C protease cleaving step. This

methodology upon optimization yielded pure TSC1 (302-420 aa). Interestingly, we observed that the eluted fractions of the purified TSC1 lead to the identification of a 70 kDa protein, which co-eluted along with TSC1 that was not understood till then. Based on the available literature and LC-MS/MS peptide mass fingerprinting analysis, the 70-kDa protein was found to be DnaK, a homologue of human Hsp70 in *E. coli*. Further, based on the net negative charge on both the proteins TSC1 and DnaK were separated via anion exchange chromatography. DnaK's ATPase intrinsic activity acts as readout of its interaction with the substrate and client proteins. The ATPase activity assay was performed using ADP-GLO assay kit (Promega). In the presence of Tsc1 (302-420 aa), Dnak was observed to have an increase in ATPase activity.

The **third chapter** deals with the initial experiments that showed a possible interaction of TSC1 (302-420 aa) with the human Hsp70 (HSPA1A) as well. This observation was further investigated in human Hsp70 (HSPA1A) using biochemical assays (GST Pull-down and ATPase assay) and resulted in identification of TSC1 (302-420 aa) as a novel binding region of Hsp70. Surprisingly, TSC1 (302-420 aa) showed a striking difference in the functionality on interacting with the evolutionarily conserved chaperone machinery (DnaK and HSPA1A). On adding TSC1 (302-420 aa), DnaK was activated and HSPA1A was inhibited. Though DnaK and HSPA1A are highly conserved, the C-terminal EEVD motif in HSPA1A's Substrate Binding Domain (SBD) has a unique role in signaling the co-chaperones in the eukaryotic chaperone complex. To assimilate the disparity in the chaperones' interaction pattern, the Nucleotide Binding Domain (NBD) and the Substrate binding domain (SBD) of HSPA1A were separately tested for interaction with TSC1 (302-420 aa). As expected, TSC1 (302-420) showed affinity towards HSPA1A SBD and not the NBD, which corroborates the earlier hypothesis of SBD and possible EEVD motif involvement. This also shows that TSC1 acts as a co-chaperone to Hsp70.

In the **fourth chapter** of the thesis, I have performed expression, purification and structural characterization of TSC2 (1-418 aa). TSC2 N-terminal is known to interact with TSC1 and knowing the structural information on that region would help in understanding the TSC1-TSC2 complex better. Zechet *al.* have reported the crystal structure of N-terminal TSC2 (TSC2-N) from thermophilic fungus (UniProtKB-G0SFF5) *Chaetomium thermophilium*. Unlike the human TSC2 (tuberin), *C. thermophilium* TSC2 is more stable and soluble. This could be due to the presence of several cysteines in tuberin N-terminal domain, which are predominantly free cysteines. Despite several reports of failed attempt in the literature to purify human TSC2 (1-418 aa), we have successfully obtained a pure GST-TSC2 fusion protein. The secondary structure of TSC2 (1-418 aa) was analyzed using circular dichroism and the protein was also screened extensively for crystallization. The crystal hits were optimized for cryo- protection and was subjected to data collection at the Advanced Photon Source (APS) synchrotron facility at Argonne National Laboratory, USA. Unfortunately, the required resolution could not be attained from the data collection to experimentally solve the crystal structure of TSC2. Further, to understand the structure and function of TSC2, we used *C. thermophilium* TSC2 N-terminal domain as a template, a homology model of human Tsc2 (1-418 aa) was generated using SWISS-MODEL. The model was further validated using a 100 ns molecular dynamic simulation using Desmond (Schrodinger suite). The results are discussed in detail in chapter IV.

The **final chapter** contains the structural study of Netrin's C-terminal domain (NTR). Netrin is an axon guidance cue molecule that is predominantly present in the neuronal growth cones. The term netrin is derived from the Sanskrit word 'Netr', which means to guide. Netrins are extracellular proteins that can diffuse and promote axonal outgrowth during embryogenesis. Netrin has three major domains. The N-terminal domain has homology to domain VI of laminin B. The second domain consists of EGF-like repeat sequence that is like the domain V of laminin B. The last domain in the c-terminal end is termed as NTR (Netrin like domain). This domain is known to be unique and highly basic in nature. The function of the NTR region of netrins is not completely understood. The NTR domain is also found to be present in other proteins like type I procollagen C-proteinase enhancer proteins (PCOLCE), complement proteins C3, C4 and C5, secreted/ soluble frizzled-related proteins (SFRPs) and putative *C. elegans* proteins. The function of NTR domain in other proteins like TIMPS (Tissues inhibitors Metalloproteinases) and PCOLCE indicate its potential function in inhibiting the metalloproteinases.

NTR was expressed along with sumo-tag and 6X His tag in the N-terminal. The affinity purification was performed using Ni-NTA chromatography and the subsequent cleavage of sumo tag using ULP1 (Ubiquitin like protease I). As NTR is highly basic and increased tendency to bind to nucleic acids, the purification of NTR required an extensive multi-step purification methodology. A detailed optimization for obtaining pure NTR is described in this chapter. The crystallization trials were performed using Phoenix liquid dispensing system and NT8 automated drop setter from formulatrix. The homology model of Netrin-NTR was build using PCOLCE-NTR and Complement proteins NTR as templates. The model built using SWISS-model, Schrodinger suite and I-TASSER were carefully analyzed for the characteristic structure of the NTR domain. The model from I-TASSER rendered the closest structure comprising of two terminal α - helices, six β -sheets, two disulfide bonds (C1-C4, C2-C5) and the correct positioning of the characteristic YLLLG and RGD motifs. I-TASSER uses multiple threading approach and identifies the templates from the PDB in a hierarchical method of protein structure and function prediction. The model was further validated using Ramachandran plot. The future direction of this work includes the crystal structure determination of NTR and functional characterization.

In conclusion, this thesis studies some of the less explored protein domains highlighting their structural and functional significance. The biochemical studies of TSC1 and TSC2 carried out in my thesis paved way for unraveling novel interplay of chaperones with the TSC complex. The chaperone biology is an active area of research and understanding the mechanistic pathways around it can be a very useful tool. Future studies involving TSC1-TSC2 and the chaperones Hsp70 and Hsp90 can provide molecular insights in the interaction event. Further, TSC1 and TSC2 are huge proteins with relatively less biochemical characterizations. Therefore, the studies done as a part of this work hold a great significance and provide a new perspective to TSC research. Another interesting and yet biochemically challenging signaling protein is Netrin-NTR. Both TSC and Netrin have a neurological significance, the former is known for the disease manifestation involving the nervous system and the latter regulates neuronal development. Finally, understanding the nature of these proteins and its signaling partners may help in targeting them for treating the disorders.

Title: Biochemical and Bioinformatic studies of THAP9 transposase and other THAP proteins
Researcher: Sanghavi, Hiral M.
Supervisor: Majumdar, Sharmistha
Year: 2020
Keyword's: DmTNP, Oligomerisation, Thanatos Associated Proteins, Transposase proteins
Call No.: 570.285 SAN
Acc. No.: T00694

Abstract: Transposable elements (TEs) are DNA segments that can move from one position in the genome to another, irrespective of any sequence homology between the excision and the integration sites. The movement of TEs is mediated by transposase proteins (maybe encoded by TE). TEs can provide raw material for generation of new protein coding genes in the host genome by the process of exaptation. The host often conserves the ancestral or slightly modified function of the TE-encoded protein while the ability to autonomously transpose is lost during evolution (molecular domestication). Studying active as well as domesticated transposases is of utmost importance for the basic understanding of how the conserved molecular protein architecture is adapted for diverse cellular functions over the course of evolution. For my doctoral dissertation, I have studied the conserved and divergent modular protein architectures of the well-studied *Drosophila* P element transposase (DmTNP; active transposase) and human THAP9 (hTHAP9; a DmTNP homolog of unknown function).

DmTNP is extensively characterized whereas hTHAP9 is only recently discovered. Based on sequence and structural homology, the domain organisation of hTHAP9 was found to be similar to DmTNP. An amino terminal zinc coordinating DNA binding domain (THAP domain) is conserved between both DmTNP and hTHAP9. Interestingly, the THAP domain is also conserved amongst eleven other human proteins, which are together grouped into the human THAP protein family. Interestingly, DmTNP as well as some human THAP proteins are known to form functional oligomers.

In the first chapter, I have adopted bioinformatic to explore the possibility of oligomerisation of human THAP proteins via a coiled coil region. This study identified a 40- residue long leucine rich region, which had an amphipathic pattern similar to leucine zipper regions (Fig. A), in all the twelve human THAP proteins including hTHAP9 (Fig. B).

The second chapter is an experimental continuation of the first chapter wherein I have established that hTHAP9 undergoes homo-oligomerisation using a combination of *in silico* prediction tools as well as biochemical techniques. Surprisingly, it was demonstrated that the amino-terminal regions of both hTHAP9 and DmTNP (after deletion of the predicted coiled coil region or mutating the leucines, either individually or together), retained the ability to form higher order oligomeric states (Fig. C). Moreover, this study also revealed that the oligomerisation of both hTHAP9 and DmTNP is partially mediated by DNA (Fig. D).

DmTNP binds GTP via an identified GTP binding region (G domain) as a prerequisite to forming the tetrameric synaptic paired end complex (PEC) bound to both ends of transposon DNA. However, there are no reports of GTP hydrolysis by DmTNP. Thus, it is speculated that GTP binding leads to DmTNP oligomerisation. It was interesting to speculate that hTHAP may also bind GTP as a prerequisite of oligomerisation. In the third chapter, I have predicted a GTP binding region (G-domain) in hTHAP9 by writing a customized Spacers and Mismatch Algorithm (SMA) (Fig. E) after failing to do the same using available *in silico* tools as well as an *in vivo* GFP solubility screen. The predicted G domains of hTHAP9 and DmTNP are now being used for experimental studies. The fourth chapter describes the extension of SMA such that it can be used to predict putative G boxes in any protein.

The DNA binding site of hTHAP9 is hitherto unknown. The DNA binding domain of hTHAP9 is the THAP domain. Despite having a similar structural fold, the THAP domains of different human THAP proteins have different DNA binding sites. Thus, in the fifth chapter, I have studied the synapomorphic (sequence and structural) variations in the THAP domains of human THAP family proteins (Fig. F) and their homologs using *in silico* motif prediction and secondary structure prediction tools. This study independently identified THAP domain size- and sequence-based sub-groups amongst the homologs of each human THAP protein.

Overall, the results of my thesis will direct future research towards better understanding of the evolution and cellular function of hTHAP9. The first chapter can be continued to study the possible protein interaction partners of human THAP proteins. This will also help advance the understanding of hTHAP9 hetero-oligomerisation which may be mediated either by one short motif or many motifs across the length of the protein as is suggested in the second chapter. The identification of a putative G domain in hTHAP9 in the third and fourth chapter is already being used to study possible GTP binding to hTHAP9 *in vitro*. The novel findings from the fifth chapter will not only help the ongoing studies to identify the DNA binding site of hTHAP9 but it can also be used to understand the evolution of the THAP domain in animals.

Title: Functional relevance of subtle patterns of cytosine methylation: a regulatory framework of human CGGBP1

Researcher: Patel, Manthan

Supervisor: Singh, Umashankar

Year: 2020

Keyword's: CGGBP1, Methylation, Stochasticity, CTCF, Asymmetry, Givinostat

Call No.: 574 PAT

Acc. No.: T00695

Abstract: The thesis is based on the work that describes the detailed characterisation of cytosine methylation regulation by the human protein CGGBP1 using WGBS and MeDIP-seq across three different cell types. It identifies sequence motifs where cytosine methylation is specifically affected by CGGBP1 depletion, of which CTCF motifs turn out to be prominent targets. By focusing on CTCF motifs, we report new CTCF-binding sites where cytosine methylation levels change dramatically. These CTCF-binding sites turn out to be different from another type of CTCF-binding sites where CGGBP1 regulates rapid transitions in H3K9me3 signals. A combination of WGBS, MeDIP-seq and CHIP-seq analysis allows us to identify these CGGBP1-regulated CTCF-binding sites as repeat-free motifs and motif-free repeats respectively. Such a distinction of the two types of CTCF-binding sites is a novel and important finding which this thesis deliberates upon.

An in-depth re-analysis of WGBS data describing cytosine methylation states in presence or absence of CGGBP1 allows us to draw a base-level resolution methylation landscape in all the three cytosine contexts: CpG, CHG and CHH. Furthermore, we also see a strand-specific increase in methylation changes in regions showing GC skew. We see methylation changes at candidate DNA-methylation regulatory genes such as DNMTs, MBDs, TET and APOBECs. Of multiple interesting findings in the report, my focus remained on finding out the significance of an equal abundance of gain and loss of cytosine methylation. By applying MeDIP-seq to understand the methylome regulation by CGGBP1, we see recapitulation of the near-identical presence of GoM and LoM at region-level. To determine the underlying contributor of such stochasticity, we study the allelic imbalance in methylation. The presence of AIM is observed under normal conditions, which is further enhanced upon knockdown of CGGBP1, suggesting the increment of stochasticity in methylation. To identify the determinant of the directed methylation regulation by CGGBP1, we analyse the methylation changes at the TFBS motifs (JASPAR-wide). Through this screen, we find about 72 TFs that show methylation disturbances in the absence of CGGBP1 in a cell-type-specific manner. Of all of these, CTCF was of the most affected TFBSs. When we studied a set of histone modification profiles at the CGGBP1-dependent CTCF-binding sites, we observed that CGGBP1 depletion causes gain- and loss- of H3K9me3 asymmetry in flanks of a subset of CGGBP1-regulated CTCF-binding sites. Next, we analysed the DNA methylation patterns in the flanks of these CTCF-binding sites. We see strong cytosine methylation asymmetries in the flanks of the motif-containing (RFM) peaks compared to repeat-positive (MFR) peaks, which exhibit only H3K9me3 asymmetry. CGGBP1 regulates cytosine methylation, and the majority of its cellular functions are dependent on its binding to the DNA. To identify the inhibitor of CGGBP1 by mimicking the methylation-sensitivity for its binding, we screen a small molecule library of 1685 compounds. We show that an anticancer drug candidate Givinostat, a known HDAC inhibitor, is also a direct inhibitor of CGGBP1.

This thesis proposes that cytosine methylation regulation by CGGBP1 hides subtle sequence preferences in an overall stochastic pattern. The studies on preferred site-specific cytosine methylation regulation by CGGBP1 reveals new types of chromatin regulatory CTCF-binding sites. Identification of Givinostat as an inhibitor also highlights the importance this epigenomic regulation by CGGBP1 has in cellular transformation.

Title: Modulatory crosstalk between chromatin components: the CGGBP1-CTCF axis
Researcher: Patel, Divyesh
Supervisor: Singh, Umashankar
Year: 2020
Keyword's: CGGBP1, CTCF, Insulator, Cytosine Methylation, Repeats
Call No.: 574 PAT
Acc. No.: T00696

Abstract: Genome organisation and gene expression are regulated by chromatin insulator elements. Chromatin insulator elements block the spread of silent chromatin as well as prevent interactions between transcription enhancers and gene promoters in *cis*. The CCCTC-binding factor (CTCF) binds to the insulator elements to partition the genome into chromatin domains that associate topologically. CTCF-binding sites at chromatin insulators are evolved from the retrotransposon Alu-SINEs and SVA elements. Cytosine methylation is one of the established regulators of CTCF binding to chromatin. Regulator of cytosine methylation at such a repeat would be the regulator of CTCF-binding. CGGBP1 is a ubiquitously expressed repeat binding protein. CGGBP1 binds to interspersed repeat Alu-SINEs and LINE-1s and negatively regulates constitutive methylation of repeats. Depletion of CGGBP1 affects cytosine methylation at CTCF-binding sites which may disrupt CTCF-binding. CGGBP1, as well as CTCF, binds to DNA in a methylation-sensitive manner. CGGBP1, a regulator of cytosine methylation, can be a regulator of CTCF-binding and its chromatin barrier function.

CGGBP1 depletion causes genome-wide disturbances in cytosine methylation in CpG and non-CpG context as well as gain and loss of cytosine methylation at GC skewed regions including LINE-1 repeats. CGGBP1 depletion increases cytosine methylation at known insulator elements, including many CTCF binding sites. Immunofluorescence study has shown colocalization of CGGBP1 and CTCF in the nucleus and at the mid-body. Endogenously expressed CGGBP1 and CTCF interact with each other. Further, DNaseI digestion of immunoprecipitated complex and antibody blocking assays have shown that CGGBP1-CTCF interaction is direct as well as mediated by a DNA-linker. CTCF ChIP-seq under normal or perturbed levels of CGGBP1 has shown that CTCF binds to canonical CTCF motifs and repeats. CTCF occupancy preference for canonical CTCF motifs is antagonised by CGGBP1. CGGBP1-regulated CTCF-binding sites at repeats exhibit a chromatin barrier-like function. ChIP-seq of histone modifications under the normal or depleted levels of CGGBP1 have shown that CGGBP1 regulates CTCF-binding sites exhibit loss as well as gain of chromatin barrier function with contrasting H3K9me3 levels. CGGBP1-dependent CTCF-binding sites exhibiting loss of chromatin barrier function are rich in LINE-1 repeats. Our results demonstrate that CGGBP1 levels regulate chromatin barrier activity of repeat-derived candidate insulators through regulation of CTCF occupancy. We have identified that the inhibition of CGGBP1, similar to CGGBP1 depletion that antagonizes CTCF occupancy at the repetitive elements, is achievable by a known anticancer agent Givinostat. The anticancer effects on CGGBP1 could be exerted through inhibition of CTCF binding at repeats.

Title: Molecular mechanism of intracellular cargo transport system
Researcher: Patel, Nishaben
Supervisor: Soppina, Virupakshi
Year: 2021
Keyword's: Antiviral Surface Coating, KIF1A, KIF16B Motors, Microtubules, Motor Proteins
Call No.: 574.22 PAT
Acc. No.: T00697

Abstract: Molecular motors are essential for multiple cellular functions, such as intracellular cargo transport, cell division, cell motility, cytoskeleton arrangement, etc. There are three classes of molecular motors: kinesin, dynein, and myosin. While kinesin and dynein are microtubule-based motors, myosin is actin-based. All molecular motors drive their movement by conversion of chemical energy into mechanical work. Malfunction of these molecular motors has been implicated in multiple disease conditions, such as neurodegeneration and cancer. Kinesin-3 is one of the largest families, consisting of KIF1, KIF13, KIF14, KIF16B, and KIF28 subfamilies. Kinesin-3 motors are inherently fast, superprocessive, and have increased microtubule landing rate. Kinesin-3 motors are crucial for various cellular processes and possess unique motility properties. Despite having significant physiological and clinical importance, the underlying chemomechanical properties and cellular functions of kinesin-3 motors remain poorly understood. In this dissertation, I aim to investigate molecular mechanisms underlying the unique properties of kinesin-3 motors using multiple *in vitro* and *in vivo* approaches.

Members of kinesin-3 family are inherently fast and superprocessive and exhibit increased microtubule landing rate, compared to other kinesin families. However, the mechanochemical properties of kinesin-3 family motors that enable their superprocessivity and higher microtubule landing remains poorly understood. Full-length and constitutively active kinesin-3 motors were purified from the Sf9-baculovirus expression system. Single-molecule motility analysis using Sf9-purified motors showed fast, superprocessive motility of kinesin-3 motors along the microtubules. Using colorimetric ATPase assays, we demonstrate that constitutively active kinesin-3 motors possess 10-fold higher ATPase activity compared to the well-studied constitutively active kinesin-1. In contrast, full-length kinesin-3 motors are inactive and exhibit minimal basal activity. Intriguingly, the velocities of kinesin-3 family motors inversely correlate with their microtubule-binding affinity. Furthermore, microtubule gliding assays of constitutively active kinesin-3 motors revealed smooth microtubule sliding and efficient crossing over. Moreover, microtubules propelled by kinesin-3 motors showed enhanced bending of microtubules without apparent change in the gliding velocities. These findings unveil the effect of enzyme catalysis and microtubule affinity on motor processivity. Thus, we propose that a fine balance between ATP hydrolysis rate and nature of motor interaction with the microtubule together can achieve family-specific mechanical outputs.

Membrane tubulation is a hallmark of recycling endosomes (RE), mediated by KIF13A, a kinesin-3 family motor. KIF13 motors are uniquely regulated by the presence of a proline residue located at the interface of neck-coil (NC) and CC1 domains. This proline induces a kink and favors intramolecular interaction between NC and CC1, which retains the motor in a monomeric and inactive state. Interestingly, deletion of proline (P390) releases this restraint and results in a stable

straight conformation, allowing motor dimerization and subsequent motility along the microtubule. Although wild type KIF13A is inactive *in vitro*, it plays an essential role in recycling endocytosis. Understanding the regulatory mechanism of KIF13A in RE tubulation and cargo recycling is of fundamental importance but is overlooked. Here, we report a unique mechanism of KIF13A dimerization modulated by Rab22A, a small GTPase, during RE tubulation. Remarkably, Rab22A plays an unusual role by binding to NC-CC1 domains of KIF13A, relieving proline-mediated inhibition, and facilitating motor dimerization. As a result, KIF13A motors produce balanced motility and force against multiple dyneins in a molecular tug-of-war to regulate RE biogenesis and homeostasis. Together, our findings demonstrate that KIF13A motors are tuned at a single-molecule level to function as weak dimers on the cellular cargo.

Next, we investigated whether KIF13B that belongs to same subfamily as KIF13A plays any role in recycling endocytosis. Interestingly, we report for the first time that KIF13B forms recycling endosome tubules, indicating that two different motors (KIF13A and KIF13B) are involved in the same process. We show that KIF13A is loaded onto recycling endosome before KIF13B and is able to overcome inactivity of KIF13B. In contrast, KIF13B was not able to overcome KIF13A inactivity. Interestingly, KIF13B forms more RE tubules compared to KIF13A. Results show that Rab10 relieves proline-mediated inhibition in KIF13B via binding to its NC-CC1 domains. We also demonstrate the role of CAP-Gly, an unusual domain, in KIF13B regulation. We conclude that although two motors are involved in the same cellular process, they both serve at different time and rate to ensure efficient cargo recycling. Overall these studies provide in-depth understanding of kinesin-3 motors regulation and functioning and pave way for future investigations regarding role of these motors in disease conditions.

Title: Mechanisms of DNA binding and transposition by THAP9
Researcher: Sharma, Vasudha
Supervisor: Majumdar, Sharmistha
Year: 2020
Keyword's: Transposons, SETMAR, Drosophila Cells, DNA, Zebrafish Embryos
Call No.: 572.869 SHA
Acc. No.: T00698

Abstract: Transposons or 'jumping genes' are dynamic DNA sequences that are ubiquitously expressed in all kingdoms of life. These DNA elements can move from one genomic location (using autonomous or non-autonomous enzymatic machinery) and integrate randomly or specifically into a different genomic location (using host cell DNA repair machinery). This movement often results in mutations, genome instability, changes in gene expression and DNA rearrangements. After being described as 'selfish' and 'junk' for decades, transposons are now recognized as important players in generating genomic diversity and evolution. Several transposons have been repurposed by host organisms to perform essential cellular functions. RAG1/2, CENPB, SETMAR, hTHAP9 are few examples of human genes that have domains recruited from DNA transposases but have evolved diverse functions.

Human THAP9 is a recently discovered, 'cut and paste' DNA transposase homologous to the well-studied *Drosophila* P-element transposase. The lack of transposon hallmarks, i.e., TIRs and TSDs in THAP9 indicate that it has undergone molecular domestication. THAP9 is a multi domain protein with a DNA binding THAP domain at its amino-terminal end, followed by a Leucine zipper motif, and a catalytic domain that appears to be disrupted by a GTP-binding insertion domain. The function of THAP9 in humans is yet to be discovered. The focus of this dissertation is to characterize and decipher the human THAP9 gene in both the genomic and molecular context.

Previous studies have reported that human THAP9 shows DNA excision and integration activity in cultured human and *Drosophila* cells. But nothing is known about its DNA binding or catalytic functions. ChIP-exo (Chromatin immunoprecipitation followed by exonuclease digestion) and ChIP-seq data was used to identify genome-wide binding sites of THAP9 in human cells and zebrafish embryos. The ChIP-exo method is a modification of conventional ChIP-seq that is used to reduce the background by digesting the unbound DNA. Several computational tools are available for analysing ChIP-seq data but most of these tools are unsuitable for processing ChIP-exo generated DNA reads. In Chapter 2, peak-callers designed for ChIP-exo were compared using publicly available datasets to select best performing tools. It was found that tools that select parameters based on the raw data perform better than the tools that require pairing of peaks on the opposite strands. In Chapter 3, the results from the software comparison study were used to establish a pipeline for analyzing THAP9 ChIP-exo and ChIP-seq data from HEK293, WIBR#3, HepG2 and NT2 cells. Our analysis revealed multiple binding sites of THAP9 in nuclear as well as mitochondrial DNA. In addition to a 'CCC' containing motif which is conserved in *Drosophila*, THAP9 has been found to bind a repeat-like motif 'ATTCCATTC' in mitochondrial DNA. The discovered motifs have been further validated by *in vitro* THAP9-DNA binding assays like size exclusion chromatography and gel-shift assays.

Many eukaryotic cut-and-paste transposase superfamilies are known to excise DNA via a DDE/D motif in an RNase-H like catalytic domain. THAP9 is known to cleave and integrate *Drosophila* P-element DNA flanked by intact inverted repeats. However, not much is known about THAP9's catalytic domain. In Chapter 4, the recently available cryo-EM structure of *Drosophila* P-element transposase was used as a template to predict the structure of THAP9. Secondary structure predictions and protein modeling were used to predict a putative RNaseH fold-containing catalytic domain in THAP9, along with acidic residues within the fold that might be involved in DNA excision. Site-directed mutagenesis of the predicted catalytic residues followed by plasmid-based screening for DNA excision and integration activity, has led to the identification of acidic residues (D304, D374, E613) in the RNaseH fold that could be a part of the catalytic triad in human THAP9. Besides, identification of the catalytic triad, D695 was also identified as an important residue which when mutated, increases the DNA excision activity of THAP9 in comparison to the wild type transposase.

Several transposable elements are known to be activated or repressed under stress. In Chapter 5, we investigated the effect of various stress conditions (DNA damage, oxidative, heat and osmotic stress) on THAP9 expression in synchronized cells in the S-phase of the cell cycle. The newly annotated THAP9-AS1 gene encodes for a lncRNA that is known to be upregulated in pancreatic carcinoma, neutrophil apoptosis and downregulated in septic shock. The promoters of THAP9 and THAP9-AS1 overlap with each other. Natural antisense transcripts and their corresponding sense transcripts often show inverse expression; thus, suggesting that one regulates the other. Thus, THAP9-AS1 expression was also quantified under the same stress conditions. It was observed that THAP9-AS1 is highly upregulated under different stress conditions whereas THAP9 exhibits varying patterns (both upregulated or unchanged) of expression.

Genomes are continuously evolving entities with transposons playing a crucial role in maintaining genomic diversity. They are reservoirs for providing gene-regulatory elements and may also give rise to new genes over the course of evolution. THAP9 is an example of a protein of unknown function, that evolved from an ancestral transposase (P-element in *Drosophila*). It is crucial to understand its role in humans in order to recognize the implications of 'molecular domestication' of transposases. This dissertation identifies potential DNA-binding motifs of THAP9 and sheds light on the important acidic residues required to cut and paste DNA. Furthermore, we suggest an important role of THAP9-AS1 in stress response. Although a significant amount of research still needs to be done to discover the function of THAP9, this dissertation paves way for designing further studies to investigate THAP9.

Title: Reservoir based co-delivery of CuO nanoparticles and Elesclomol to facilitate enhanced dissolution mediated intracellular oxidative stress

Researcher: Chakraborty, Swaroop

Supervisor: Misra, Superb K.

Year: 2020

Keyword's: Oxidative Therapy, PLGA, Gold, Polypads, Thermootherapy

Call No.: 574 CHA

Acc. No.: T00699

Abstract: Deregulation of cancer cell energetics is one of the emerging and prominent hallmarks of cancer. The alternation of Adenosine Triphosphate production pathways results in enhanced production of Reactive Oxygen Species (ROS) inside mitochondria. Cancer cells adapt to such high ROS production and get resistant to the majority of chemotherapeutic drugs. However, uncontrolled ROS production beyond the threshold in a cancer cell can be a potential target for oxidative therapy. In this study, an anticancer drug Elesclomol was used that requires divalent redox-active metal ions (Cu^{2+} , Ni^{2+} , Pt^{2+}), etc., to facilitate intracellular ROS production inside the cells. However, for the drug to function efficiently, it requires a constant supply of the divalent metal ions that can form complex with Elesclomol and selectively transport to mitochondria to induce ROS production via Fenton like reaction. In this study, Copper Oxide (CuO) nanoparticles were used as the reservoir of Cu^{2+} ions, wherein the divalent Cu ions were generated through the process of dissolution in the DMEM-cell culture medium.

The dissolution of nanoparticles is an important property that depends on various factors such as pH/temperature, exposure media, physicochemical properties of nanoparticles, exposure concentration of nanoparticles, etc. To examine the impact of CuO nanoparticles reservoir based oxidative therapy, a complete dissolution profile of CuO nanoparticles was established. Different filtration based separation methods (Dialysis, Centrifugal Ultrafiltration, Stirred Cell Ultrafiltration) were used with a molecular weight cut off of 3-3.5 kDa to investigate their advantages and limitations in assessing CuO nanoparticles solubility. Although all three separation methods were able to separate dissolved Cu efficiently in a range of biological (artificial lysosomal fluid) and environmental (artificial seawater, 1mM sodium nitrate) media, the dialysis membrane-based separation method was chosen for further evaluation of CuO nanoparticles dissolution. The main advantages of dialysis membrane-based separation methods were low experimental cost, less cumbersome sampling, time taken per experiment is less and less prone to membrane rupture as compared to the other two methods.

In the next study, the dissolution studies of CuO nanoparticles were performed in several biological media (artificial lysosomal fluid, simulated body fluid, DMEM-cell culture medium, and Muller Hinton Broth) to understand the extent to which CuO nanoparticles can generate dissolved Cu ions. Various parameters, such as rate constant (k), saturation concentration, size-based factors, and dissolution mediated antimicrobial activities, were investigated. To demonstrate the agglomeration behavior of CuO nanoparticles, Artificial Sea Water media was used wherein due to high ionic strength, the dissolution of CuO nanoparticles were <5%. However, the dissolution of CuO nanoparticles in biological media was very high, i.e., >80-85% in artificial Lysosomal Fluid and

artificial seawater. Although dissolution was happening in both biological media, significant differences were observed in the rate of dissolution in artificial lysosomal fluid ($k= 1.3 \text{ h}^{-1}$) and simulated body fluid ($k=0.325 \text{ h}^{-1}$). The rate of dissolution was much more rapid, and saturation concentration was achieved quickly in the case of artificial lysosomal fluid (5-6 hours) as compared to simulated body fluid (10-12 hours). A dissolution mediated antibacterial activity was also performed on *E.coli*, wherein it was inferred that 83-85% of the antibacterial activities are attributed to dissolved Cu ions.

After establishing an understanding of CuO nanoparticles dissolution behavior in biological media, the concept was exploited for Elesclomol based oxidative therapy. Dissolution mediated Elesclomol binding studies were carried out wherein dissolved Cu^{2+} were demonstrated to form a stable hydrophobic complex at a cell-free *in vitro* condition. Based on cytotoxicity assay performed on A549 (Lung Adenocarcinoma) cells, co-delivery of CuO nanoparticles at different concentrations with 50 ng/mL Elesclomol showed >80% reduction in cell viability after the end of 24 hours. The ROS quantification supports the cytotoxicity data wherein codelivery of 200 ng/mL CuO nanoparticles and 50 ng/mL of Elesclomol were showing more than 3 fold increase in ROS production when compared to control cells. Stable isotopically modified ^{65}CuO nanoparticles were also synthesized to understand the intracellular Cu accumulation in A549 cells when exposed with or without 50 ng/mL Elesclomol. More accumulation of ^{65}Cu was observed in the cells when exposed with Elesclomol signifies rapid and selective shuttling of Cu ions in the cells by Elesclomol. In conclusion, the results were supporting the hypothesis and demonstrated a promising approach towards dissolution mediated oxidative therapy.

Title: α -synuclein fibrillogenesis inhibitors and impact of charge neutralizing lysine post-translational modifications on α -synuclein and tau derived peptide aggregation

Researcher: Gadhavi, Joshna Dharmendrabhai

Supervisor: Gupta, Sharad

Year: 2022

Keyword's: Parkinson's Disease, α -syn Fibrillogenesis Inhibition, Carbamylation, Triazole-based Hybrids

Call No.: 612.8 GAD

Acc. No.: T00948

Abstract: Parkinson's disease (PD) is one of the most critical chronic neurodegenerative diseases. Worldwide, the burden of PD doubled between 1990 to 2016, from 2.5 million to 6.1 million patients. More than 10 million people are currently diagnosed with PD globally, and literature reports have predicted that this could go up to 17 million by the end of 2040. The Lewy bodies (LBs) and Lewy neurites (LNs) are pathological hallmarks of PD, and the aggregated α -syn protein is present in both LBs and LNs. α -Syn is a natively unfolded protein having 140 amino acid residues, and its aggregation plays a pivotal role in PD. Therefore, it is desirable to develop inhibitors that retain α -syn in a monomeric state or reverse prefibrillar α -syn into a non-aggregated state. As the α -syn sequence has 15 lysines and full-length tau consists of 44 lysines present, Post Translational Modifications (PTMs) that neutralize positive charge on the lysine side chain could significantly affect the structure and function of the affected protein. Therefore, we have further explored the relationship between carbamylation and acetylation, two major lysine charge neutralizing PTMs, and α -syn and tau aggregation by studying the aggregation propensities of protein derived modified small model peptides.

1. α -syn fibrillogenesis inhibition: Aggregation of α -syn is one of the central hypotheses for PD, and hence, its inhibition or disaggregation is a viable approach for PD treatment. We first expressed α -syn recombinantly and purified it by the DEAE sepharose anion exchange matrix. We screened two series of inhibitors (or modulators), Di-phenyl triazines and Triazole analogs, against α -syn fibrillization.

a. α -syn fibrillogenesis inhibition by diphenyl triazine hybrids: We studied the *in-vitro* efficacy of a series of synthesized diphenyl triazine hybrids (A1-A9) as potential inhibitors of α -syn fibrillogenesis. A1, A2, A4, A8, and A9 showed a significant lowering of the α -syn fibril formation as evidenced by Thioflavin-T (ThT) assay and fluorescence microscopy. In addition, these compounds A1, A2, A4, A8, and A9 also proved to be effective disaggregators for the pre- aggregated form of α -syn. All compounds exhibited no cytotoxicity in mouse embryonic fibroblast (MEF) and human adenocarcinoma alveolar basal epithelial cells (A549) except A2.

b. α -syn fibrillogenesis inhibition by triazole-based hybrids: A series of 12 triazole-based compounds were screened for the inhibition of α -syn fibrillogenesis and disaggregation of pre- formed fibrils. We observed that compounds Tr3, Tr7, Tr12, Tr15, and Tr16 exhibited a significant effect in inhibiting α -syn fibrillogenesis by ThT assay and fluorescence microscopy. α -syn fibril disaggregation was confirmed by fluorescence microscopy. The compounds that were suitable inhibitors or disaggregators had no toxic effects on the human neuroblastoma cells SH- SY5Y, as demonstrated by the MTT assay. Altogether, we concluded that these compounds have the potential to be

developed as therapeutic interventions against synucleinopathies, including PD and Lewy body dementia.

2. Amyloid materials synthesized from short carbamylated lysine repeats and their application

We demonstrated that short lysine repeats with varying hydrophobic N-terminal capping formed amyloid fibrillar structures upon carbamylation. These amyloid fibrillar assemblies were characterized by various biophysical methods, including ThT fluorescence enhancement, ANS binding assay, CD spectroscopy, congo red staining, fluorescence microscopy, SEM, and TEM to confirm their amyloidogenic nature. We determined that as low as three repeats of carbamylated lysine or homocitrulline were sufficient to observe the amyloid formation. DFT calculations further attributed this strong amyloidogenicity to cooperative hydrogen bonding resulting from favorable stacking of side-chain ureido functionalities. These formed amyloid materials could further be used as polymeric matrices for various applications.

3. Carbamylation reveals hidden aggregation hot spots in tau protein flanking regions

Tau protein is found abundantly in neurofibrillary tangles in Alzheimer's disease. The longest human tau isoform (2N4R) has 44 lysine residues. Several lysine-based PTMs such as glycation, acetylation, ubiquitination, and sumoylation have been implicated in Alzheimer's disease and other tauopathies. Carbamylation is one such lysine neutralizing age-related non-enzymatic PTM, which can modulate the aggregation propensity of tau. In the present work, we have studied the aggregation potential of lysine-rich regions of tau upon carbamylation, which do not aggregate in their native form. Using an array of biophysical and microscopic analyses such as ThT kinetic assay, fluorescence microscopy, Congo-red staining, and scanning electron microscopy, we demonstrate that peptides derived from 4 out of 5 such regions exhibit robust fibrillar amyloid formation. These regions are found in the N-terminal projection domain that encompasses the proline-rich domain (148-153, and 223-230), repeat domain R1 (253-260), as well as fibrillary core region (368-378) and, can be described as hidden aggregation hot spots which become activated upon carbamylation. We have compared the impact of carbamylation with acetylation on the aggregation propensity of lysine-rich peptide (²⁵⁴KKVAVV²⁵⁹) using biophysical experiments and MD simulations and deduced that carbamylation is a much stronger driver of aggregation than acetylation. Our findings may offer more insight into amyloid fibrils' interaction with hidden aggregation-prone nucleating sequences that act as hotspots for inducing tau fibrillation.

4. Carbamylation induces sequence-specific amyloidogenesis in the α -syn sequence-derived peptides and α -syn

KTKEGV repeat motif plays a crucial role in deciding the folded structure of α -syn and its function, including tetramer formation and interaction with membrane. PTMs that could neutralize the positive charge on lysine may also disturb the charge-charge interaction α -syn with the membrane, affecting the physiological function. Carbamylation is one such non-enzymatic age-dependent charge neutralizing PTM. While some reports have suggested that carbamylation is a pro-aggregation factor, others have assigned a protective role. In the present study, we have explored the aggregation propensities of KTKEGV repeat motif peptides and full-length α -syn protein. We observe distinct aggregation kinetics for various KTKEGV motifs of α -syn, including disease-specific mutated versions, which was confirmed by various biophysical techniques such as ThT assay,

turbidity measurements, Congo red staining, AFM, and SEM. We found that peptides derived from repeat motifs 3 (³²KTKEGVLYV⁴⁰), 5 (⁵⁸KTKEQVTNV⁶⁶), and 6 (⁷⁷VAQKTV⁸²) exhibit robust fibrillar amyloid formation when carbamylated. Also, repeat motif 4 (⁴³KTKEGVVH⁵⁰), when mutated (E46K, H50Q, and both), becomes an aggregation hot-spot even though the native sequence does not aggregate upon carbamylation. Carbamylation of full-length α -syn protein led to aggregates with a much higher β -sheet rich amyloid fibrillary content as indicated by several-fold enhancement of ThT plateau fluorescence. Such carbamylated α -syn aggregates could recruit unmodified α -syn and again led to the formation of well-organized amyloid fibrils. We further demonstrate that while some of these aggregated KTKEGV motif peptides can accelerate aggregation in full-length recombinant α -syn, others appear to be protective. This observation further reflects a site-specific role of charge-neutralizing PTMs such as carbamylation towards α -syn aggregation.

5. The interplay of acetylation on α -syn and tau sequence-derived peptides and their role in inducing fibrillation

The core-filament of tau protein fibril's structure as characterized by cryo-EM studies comprises eight in-registered β -sheets arranged in a C-shape unit. We wanted to understand the effect of lysine acetylation on the stability of the C-shape structure. We synthesized eight β -sheet regions of peptides that were in-situ acetylated by NHSA (sulfo-n-hydroxysulfosuccinimide acetate). The effect of acetylation on aggregation kinetics was confirmed by ThT assay and fluorescence microscopy. As β 1, β 2, and β 8 peptides, upon acetylation, formed amyloid structures readily, we hypothesize that acetylation might play a vital role in stabilizing the fibrillar core.

The mechanistic role of acetylation on α -syn sequence-derived peptides in various regions was investigated. The rigid amyloid core of α -syn was identified (L38 to V95) based on literature reports of cryo-EM studies of α -syn. Various peptides from different lysine-rich regions were selected, and the effect of in-situ acetylation on the aggregation kinetics was observed. Five out of seven selected peptides exhibited self-aggregation upon acetylation, which was further confirmed by ThT assay and fluorescence microscopy. Hence, we hypothesize that acetylation can modulate the aggregation propensity of α -syn locally, though the global effect on full-length α -syn remains to be explored.

Title: Studying endocytic uptake of nanostructures and pathogenic protein aggregates in model neurons
Researcher: Hivare, Pravin
Supervisor: Gupta, Sharad
Year: 2021
Keyword's: Endocytosis, Pathogenic Protein Aggregates, Hydrogels, Massive Endocytosis, Nanotoxicology
Call No.: 570 HIV
Acc. No.: T00956

Abstract: Endocytosis is the primary uptake process through which cells internalize extracellular materials and species. Endocytosis has a crucial role in the uptake of extracellular molecules essential for cellular function, clearance of unwanted extracellularly present species. It is also implicated in the intake of harmful aggregated protein species. Nanostructures have been widely used for delivering cargo inside cells or tissues, advanced molecular imaging, targeted delivery of drugs and small molecules across the blood-brain barrier. Nanostructures are programmable and can be created having specific dimensions, shapes, and geometries. Understanding the cellular and molecular endocytic pathways will help to devise targeting strategies and methods for therapeutic delivery in neurodegenerative diseases (NDs). Proteinaceous aggregates are characteristic features of several NDs such as Alzheimer's disease (AD) and Parkinson's disease (PD). Studying the endocytic pathways of such aggregates will give us an insight into the possible ways by which these characteristic aggregates spread in the nervous system. This will aid in the search for potential targets to decrease or stop the spread of the protein's pathological effects.

The thesis is broadly divided into two themes in which we have studied the endocytic uptake pathways of nanostructures and pathogenic protein aggregates. First, we have explored the differentiation of the SH-SY5Y cells using various hydrogels as a scaffold material which is followed by studies on molecular and cellular endocytic uptake pathways of Tetrahedral DNA nanocages and Carbon nanoparticles in model neurons. The second half of the thesis deals with studying the endocytic pathways of protein aggregates in SH-SY5Y neuroblastoma cells-derived differentiated neurons. To this end, we have used two different protein fibrils derived (i) synuclein and (ii) heparin and octadecyl induced-tau fibrils. A brief overview is provided below:

Exploring hydrogels for differentiation of SH-SY5Y cells into neurons

Hydrogels are an insoluble, physically or chemically cross-linked mesh-like network of hydrophilic polymers that can absorb water exceeding several times their original volume. They exhibit properties desirable for biomaterials such as large water content, flexibility in modification, multifunctionality, and biocompatibility. First, we have done optimization for SH-SY5Y cells differentiation on the 2D surface and confirmed the mature neurons formation. We further used three different hydrogels as support for three-dimensional cell culture and further explored utility for promoting neuronal differentiation. DNA hydrogel promoted the cellular growth of SH-SY5Y cells. The neuronal differentiation of SH-SY5Y cells on DNA hydrogel showed enhance neurite formation as compared to the non-treated surface. We also explored the modified chitosan-based hydrogels

(Carbamoylated or graphene oxide doped), which were found to be non-cytotoxic and promoted the attachment and cellular growth of SH-SY5Y cells. Further SH-SY5Y neuroblastoma cells were differentiated on these hydrogels, and mature neuron formation was confirmed with cellular staining and immunostaining. Hydrogels making an excellent scaffold for further neural tissue engineering applications.

Spatiotemporal Dynamics of Endocytic Pathways Adapted by Small DNA Nanocages in Model Neuroblastoma Cell-Derived Differentiated Neurons

Multiple endocytic pathways operate on the plasma membrane of cells at any moment with diverse but specific cellular functions. Knowledge of uptake of synthetic nanoparticles and ligands with respect to endocytic pathways is crucial to device the appropriate ligands for therapeutic delivery into differentiated neurons for targeting neuronal diseases. We herein explore the mechanisms of cellular uptake of 3D tetrahedral DNA nanocages at different stages of differentiating neurons. We monitored uptake, kinetics, and dynamics of DNA cages of different geometries, and interestingly we find a specific pattern and adaptability of the uptake of DNA devices with respect to the geometry of the ligand and specific endocytic pathways. We find that tetrahedral DNA nanocages get endocytosed mostly via clathrin-mediated endocytosis in fully mature neurons. These endocytic uptakes and intracellular choreography of DNA nanodevices will help us design the smartly targeted biotherapeutics for targeting neuronal disorders.

Red Emitting Fluorescent Carbon Nanoparticles to Track Spatio-Temporal Dynamics of Endocytic Pathways in Model Neuroblastoma Neurons

One of the biggest challenges limiting the biological applications of fluorescent carbon-based nanoparticles is their capacity to emit in the red region of the spectrum and simultaneously maintaining the smaller size. These two parameters always go in inverse proportion, thus lagging their applications in biological imaging. Here we have used red-emitting fluorescent carbon-nanoparticles smaller than 25 nm in size to study the dynamics of the endocytic pathway. Their small size and bright, red emission properties allow them to be internalized in live cells for extended periods of time, thus allowing to capture the Spatio-temporal dynamics of endocytic pathways in model SH-SY5Y derived neuroblastoma neurons. We find that these nanoparticles are preferably taken up via clathrin-mediated endocytosis and follow the classical recycling pathways at all the stages of neuronal differentiation. These nanoparticles hold immense potential for their size, composition, surface, and fluorescence tunability, thus maximizing their applications in tracking multiple cellular pathways in cells and tissues simultaneously at the resolution of single particles.

α -Synuclein Fibrils Explore Actin Mediated Macropinocytosis for Cellular Entry into Model Neuroblastoma Neurons

Alpha-Synuclein (α -Syn), an intrinsically disordered protein (IDP), is associated with neurodegenerative disorders, including Parkinson's disease (PD) or other α -synucleinopathies.

Recent investigations propose the transmission of α -Syn protein fibrils, in a prion-like manner, by entering in proximal cells to seed further fibrillization in PD. In spite of the recent advances, the mechanisms by which extracellular protein aggregates internalize into the cells remain elusive. Using a simple cell-based model of human neuroblastoma-derived differentiated neurons, we present the cellular internalization α -Syn preformed fibrils (PFF) to check cellular uptake and recycling kinetics

along with standard endocytic markers Tf marking clathrin-mediated endocytosis (CME) and Galectin3 marking clathrin-independent endocytosis (CIE). Specific inhibition of endocytic pathways using chemical inhibitors reveals no significant involvement of CME, CIE, and caveolae-mediated endocytosis (CvME). A substantial reduction in the cellular uptake was observed after perturbation of actin polymerization and treatment with macropinosomes inhibitor. Our results show the α -Syn PFF mainly internalizes into the SH-SY5Y cells and differentiated neurons via the macropinocytosis pathway. The elucidation of the molecular and cellular mechanism involved in the α -Syn PFF internalization will help in the understanding of α -synucleinopathies and PD and further design of specific inhibitors for the same.

Heparin and Octadecyl Sulphate Induced Tau Fibrils follow Clathrin-Mediated Endocytosis in SH-SY5Y Derived Differentiated Neurons

Tau is a microtubule-associated protein that is intrinsically disordered in nature and associated with more than 20 tauopathies in progressive neuropathological disorders (NDs). The intracellular proteinaceous aggregates of misfolded tau protein form the paired helical filaments (PHFs) and neurofibrillary tangles (NFTs). The aggregated tau species spread across neurons via transcellular propagation, and the mechanism of spreading remains unclear. The heparin-induced tau filaments differ structurally and may not reproduce the key structural features as found in Alzheimer's disease (AD) filaments raising questions to the use of *in vitro* tau assembly. Here in this study, we have prepared tau fibrils using heparin and octadecyl sulphate and characterized by using various biophysical techniques such as Thioflavin T assay, 8-anilino-1-naphthalenesulfonic acid (ANS) assay, fluorescence microscopy and congo red staining and studied the cellular internalization pathway in SH-SY5Y neuroblastoma cells and differentiated neurons. We studied the tau fibrils internalization using multiple cell-based approaches such as cellular uptake and recycling kinetics, standard endocytic probes, and protein colocalization. Transferrin is used to mark Clathrin-mediated endocytosis (CME), while Galectin-3 mark Clathrin-independent endocytosis (CIE). We further blocked the specific endocytosis pathway with inhibitors and found that tau fibrils follow the CME pathway. Identification of internalization pathway of tau fibrils formed by heparin and octadecyl sulphate will help understand the spread of tau aggregates in tauopathies and Alzheimer's disease.

Title: Design, synthesis and characterisation of organic fluorophores for visualization of cellular organelles
Researcher: Mukherjee, Tarushyam
Supervisor: Kanvah, Sriram
Year: 2021
Keyword's: Eukaryotic Cell Physiology, Cell Imaging, Mitochondrial Tracking, Plasmids, Lipid Vesicles
Call No.: 571.65 MUK
Acc. No.: T00957

Abstract: The dissertation focuses on the development of novel fluorophores to analyse the mysteries of microscopic cellular world through a combined approach of organic chemistry, spectroscopy and optical microscopy. Often, the organelles rapidly change and reorganize within the cellular compartments in response to the physiological requirements and internal environment. There are well-established fluorescent protein markers designed specifically to image such cellular changes and organelles. However, visualization with small organic molecules bring in great versatility. The incorporation of suitable substituents not only enables specific targeting of organelles but also enables detection of biological analytes and physiological processes, if any. In this study, we opted to tailor the traditional D- π -A scaffold to achieve visualization of sub-cellular organelles such as the mitochondria, lipid droplets, nucleolus and the plasma membrane.

Furthermore, the dissertation also discusses tracking of the live-cell mitochondrial dynamics, mapping mitochondrial viscosity, investigation of mechanistic details of the probe binding to cell organelles (structure-activity relationship), development of stress responsive probes for mitochondrial imaging and monitoring specific reactivity on plasma membrane utilising FRET (Fluorescence Resonance Energy Transfer) to distinguish between various stressed and cancer cells. Starting with a general introduction, we have derived the thesis into five chapters. Each chapter briefly introduces the objective of the work, relevant literature review, experimental methods and results and discussions. Summaries as well as references are compiled at the end of the thesis.

Title: Identification and screening of G-quadruplex structures in DNA and long non-coding RNAs
Researcher: Desai, Nakshi Nayan
Supervisor: Datta, Bhaskar
Year: 2022
Keyword's: RNA G-quadruplexes, Fluorescence Imaging, lncRNA, Circular Dichroism, MEG3, RNA
Call No.: 572.85 DES
Acc. No.: T00958

Abstract: Over the past two decades DNA and RNA G4 structures have emerged as a recurring motif in gene regulation and are suggested to play pivotal roles in disease onset and progression. G-quadruplexes are deeply intertwined with telomeric stability, genomic instability, transcription regulation and chromatin remodelling. DNA G4s have gained acceptance as a structural moiety and ligand binding receptor in supramolecular chemistry and materials science. RNA G4s are purported to influence RNA biogenesis, DNA processing and viral pathogenicity. In Part 1, we venture into identifying G4 formation in the non-coding transcriptome specifically long non-coding RNA (lncRNA). We probe and analyse lncRNAs that are capable of folding into stable G4s. We focus this investigation on lncRNAs that are functionally relevant to cancer. In Part 2, we investigate the visualization or screening of DNA and RNA G4s. Previous work from our group has established dimeric carbocyanine dyes as G4-selective ligands. In this thesis we expand the applicability of the dimeric carbocyanine dyes for *in cellulo* use and importantly for monitoring both DNA and RNA G4s.

In Part 1, we execute a systematic *in silico* and *in vitro* analysis of G4 possessing lncRNAs and predict their protein interacting partners and biological roles. Long non-coding RNAs are auxiliary regulators of gene expression and their presence in extracellular fluids manifests them as promising prognostic markers. We have focused on breast, cervical, lung and prostate cancers in this thesis. The systematic *in vitro* identification of G4 formation in lncRNAs can be a tedious and expensive proposition. Bioinformatics-based strategies offer comprehensive and economic alternatives when used in conjunction with suitable experimental validation. We began our workflow with lnc2cancer which is a manually curated database listing lncRNAs with association to specific cancers. The nucleotide sequences used in our study were obtained from lnc2cancer and subjected to QGRS mapper analysis. We subjected all lncRNA isoform sequences to QGRS mapper and selected sequences with G-scores > 60 for subsequent refinement and validation. This *in silico* workflow led to the identification of 14 lncRNA clusters, possessing 47 putative quadruplex forming sequences (PQS) nucleotide sequences. We define lncRNA consisting of all variants as one lncRNA cluster. To narrow our exploration, we chose lncRNA isoforms which are predominantly expressed and also harbour PQS. These considerations led us to the lncRNAs MEG3, CRNDE, LINP1 and SNHG20. We first conducted *in vitro* experiments on these lncRNAs with the objective of validating their quadruplex forming propensity. A combination of Circular Dichroism (CD) and fluorescence spectroscopic studies were performed on the PQS of MEG3, CRNDE, LINP1 and SNHG20. TERRA RNA G-4 quadruplex forming sequence was used as control molecule for the *in vitro* characterization experiments. All four lncRNAs adopted parallel G-quadruplex topologies. Use of an RNA G4-specific fluorophore, Thioflavin T, with the lncRNAs resulted in up to 275-fold enhancement of fluorescence. These results clearly demonstrated the quadruplex forming potential of the four lncRNAs, thereby

validating the *in silico* pipeline developed. We next used Kaplan-Meier curves from TCGA GDC data for cancer, to report the association of MEG3, CRNDE and SNHG20 expression on 5-year overall survival of cancer patients. We found that down-regulation of MEG3 and upregulation of CRNDE and SNHG20 are associated with poor survival of cancer patients. With the aim of identifying quadruplex interacting proteins in the G4 forming lncRNAs under study, we employed two strategies: (1) top-down approach, where we identified protein partners of lncRNAs under study for respective cancer from Inc2catlas database. A global score for interaction was obtained with a higher score indicating stronger interaction between the protein and lncRNA components. Owing to its large size, lncRNAs can have multiple protein binding pockets. Thus, even if the proteins obtained from our top-down approach do not directly bind G4 pockets of lncRNA, they may allosterically influence the functions of lncRNAs. (2) Our second strategy was a bottom-up approach. We used the RPISeq tool to predict interactions between MEG3, LINP1, CRNDE, SNHG20 with eight RNA G4 binding proteins. Brazda *et al.*, listed 8 RNA G4 binding proteins namely, FMR2, hnRNP A2, Nucleolin, DHX36, SRSF1, SRSF9, TLS and TRF2. We obtained RF and SVM scores for every lncRNA-protein pair and a score of >0.5 was inferred to denote significant probability of interaction. Interaction scores as well as subcellular localisation of lncRNA and protein led to the conclusion that FMR2 was a potential interacting partner for all four clusters. In addition to showing the lncRNAs MEG3, CRNDE, LINP1 and SNHG20 as influencing the progression of cervical cancer, our results provide insights into the RNA G4-interacting proteins. The work presented in this part is the first report of a pipeline for identification of G4s in lncRNAs and provides a viable handle for reducing experimental tedium and prioritizing expensive experiments.

The second part of this this thesis focuses on small molecules that are capable of selectively binding G4s. These molecules have enabled examination of structure-function correlations of quadruplexes. G4 interacting compounds can be classified into two classes: (1) G4 stabilizing ligands which have been suggested as chemotherapeutic agents, and (2) G4 targeting small molecules that enable *in vitro* and *in vivo* visualization. The transient nature of G4 structures challenges studying their formation in eukaryotic cells. In this context, the visualization of DNA and RNA G4 structures in cells has been an attractive tool to study their formation during various stages of cell cycle. BG4 and 1H6 antibodies are the most regarded visualizing agents providing an opportunity to elucidate the cellular role of G- quadruplexes. However, antibodies have unique constraints surrounding stability, immunogenicity and cell permeability leading to difficulties in live cell imaging. Small molecules are promising alternatives to these immune-based assays and probes. Further, G4 interacting molecules belonging to classes (1) and (2) can be converged to create promising theranostic agents. B6,5 had been developed previously in our laboratory and forms fluorescence-quenched aggregates which upon interaction with DNA G-quadruplexes disaggregates to generate substantial enhancement of fluorescence signal. In this thesis, we aimed to expand the scope of use of the dimeric carbocyanine dyes such as B6,5. For this purpose, we first tested the dye for use in a ligand displacement assay. In this regard, we wanted to compare the performance of B6,5 with the widely used fluorophore thiazole orange (TO). TO-assisted displacement assay is a widely cited strategy for primary screening of binding potential of small molecules towards DNA G4s. We deployed several DNA G4-interacting ligands such as TMPyP4, quarfloxin, piperine and olaparib in the B6,5 fluorescence displacement assay. Our results indicate that B6,5 is a superior alternative to TO for primary screening of G4 ligands, based on its ability to bind wider range of G4 topologies. Also, our results show that B6,5

exhibits comparable affinities for DNA and RNA G4s, thereby allowing it to be used across a broader range of G4 targets in comparison to TO. Notably, there is a dearth of RNA G4-interacting molecules in the reported literature. Interestingly, in conjunction to its use as a visualizing agent, B6,5 is capable of stabilizing G4s and displays remarkable duplex to quadruplex selectivity. Further, the molecule is cell permeable and enables visualization of quadruplex dominated cellular regions of nucleoli via confocal microscopy. We successfully extended the *in vitro* displacement assay to cellular displacement assay for primary screening of G4 specific ligands. The cell permeability and specificity of B6,5 for G4 structures was validated and displacement of B6,5 by quarfloxin was observed in real-time in live cells. The work presented in this part is the first report of an *in cellulo* G4-specific ligand displacement assay. Considering the dominant narrative about G4-specific therapeutics, this thesis is part of our on-going efforts towards developing quadruplex-specific diagnostic and theranostic strategies.

Title: Role of retrograde motor proteins in regulation of cellular endocytic processes, cell migration and invasion
Researcher: Mayya, Chaithra
Supervisor: Bhatia, Dhiraj
Year: 2022
Keyword's: Endocytosis, Clathrin Independent Endocytic (CIE), Dynein, Galectin
Call No.: 570 MAY
Acc. No.: T01028

Abstract: Endocytosis is an indispensable cellular process that assists in the uptake of various cargoes inside the cells such as nutrients, various signaling molecules and their receptors. The process involves cargo clustering at the plasma membrane which leads to the bending of the plasma membrane forming membrane invaginations and subsequent scission to generate endocytic vesicles. This process is hijacked by viruses and other pathogens to enter into the host cells. Multiple endocytic processes occur in tandem, which either require Clathrin proteins or act independent of it. Hence endocytosis is broadly classified as Clathrin mediated endocytic (CME) process or Clathrin independent endocytic (CIE) process. Caveolin mediated processes is still under debate. CME is by far mechanistically best understood endocytic process and this occurs in four stages, i) initiation of pit formation, ii) stabilization, iii) maturation, iv) fission. But the CIE is still a work in progress. Glycosylphosphatidylinositol (GPI)-anchored proteins are endocytosed without the requirement of clathrin or caveolin. This pathway is now named as Clathrin-independent carrier (CLIC)-GPI anchored-protein-enriched early endosomal compartment (GEEC). Galectins play a crucial role in building the endocytic pits during CIE processes by binding and clustering glycosylated proteins and lipids, thereby inducing membrane bending and biogenesis of clathrin independent vesicles. One of the members of galectin family, Galectin-3 is 30 kDa in size with carbohydrate recognition domain that help them in recognizing and binding to the carbohydrate rich regions on the plasma membrane receptors thereby assisting in internalization. Galectins also play pivotal roles in cell-cell adhesion, migration, cell-matrix interaction, angiogenesis, metastasis, apoptosis and various immunological functions. Glycolipid-lectin (GL-Lect) pathway is a mechanism where endocytosis take place with assistance of glycolipid and lectin (Hence, the name). It states that the sugar binding protein such as Gal3 bind to the carbohydrates of proteins like CD44, CD98, integrins and others. Gal3 oligomerizes on these proteins and activates its interaction with glycosphingolipids on the plasma membrane. The Gal3-membrane receptor-glycosphingolipids complex induce membrane bending, leading to the formation of endocytic pits. The whole process does not require clathrin for its pit formation. Various cytoskeletal components such as Rab GTPases, Rho GTPases and motor proteins act downstream of initial endocytic events. The actin and microtubule cytoskeletal system have significant roles in plasma membrane organization and remodeling, as well as in early endocytic events. Dynein and kinesins transport cargoes along microtubules whereas myosin superfamily of motor proteins perform cargo transport along actin networks. The ones mediating retrograde transport that is cargo transport from plasma membrane towards the interior of the cells are dynein and myosin VI. The role of retrograde motor proteins in CIE is minimally explored. Thus, in this thesis, I worked to explore the role of retrograde motor proteins, specifically with dynein and how it plays a role in GL-Lect pathway involving Gal3 for its internalization. *This background information forms the first chapter of my thesis and is already published as review in Journal of Cell Science, 2022.*

In the second chapter of my thesis, I have optimised the different concentrations of ciliobrevin D and Dynapyrazole A, which are small molecule inhibitors of dynein activity. I optimized the concentrations of the 2 drugs for inhibiting Gal3 uptake into the cells. The best concentration to be used for ciliobrevin D was 50 μ M and for dynapyrazole was 15 μ M in mouse embryonic cells (MEFs). These concentrations were enough to affect the uptake Gal3 but not transferrin, a well-known marker for CME. We found that the above mentioned concentrations were suitable for proceeding with other human cells lines as well such SUM159 and MDA-MB-231 and carry out mechanism studies involving Gal3 and transferrin.

In the third chapter of my thesis, the mechanism of Gal3 internalization was delineated. Previously it was shown that upon ATP depletion from cells, Gal3 was detected in the plasma membrane invaginations, demonstrating CLIC-like morphology and was microtubule dependent. In order to study the mechanism of membrane tubulation in CIE processes, cells were depleted with ATP to trap the Gal3 on the membrane invaginations. Interestingly we observed micron long tubules of Gal3 on the surface of the cells and the tubule lengths were significantly reduced on treatment with Ciliobrevin D. This indicated that Gal3 internalization provides pulling force from cytoskeleton thus leading to stabilizing the tubules on membrane and this process is thus dynein dependent.

It was previously shown that CD98 and CD147 follow CIE for their uptake. Hence we proceeded to check if these two cargoes depend on Gal3 for their internalization. The amount of CD98 internalization and its perinuclear localisation increased on increased concentration of Gal3. Next we used lactose, a competitive inhibitor of galectins to reduce Gal3 uptake into the cells. What we found is that on lactose treatment, along with Gal3, the uptake of CD98 was affected as expected but CD147 internalization was also affected. We wanted to move one step ahead that is to check if dynein motor protein was involved in these receptors uptake too just like Gal3. For this ATP depletion assays were performed to check the same and intriguingly these membrane receptors also formed tubules on the plasma membrane just like Gal3 tubules but relatively shorter tubules. Transferrin uptake was not affected in this inhibition experiment.

Another well-known cargo is B-subunit of cholera toxin is CTxB that follows CIE process for its endocytosis. We wanted to check if CTxB also followed Gal3 mediated internalization. We found that CTxB does not follow classical Gal3 mediated endocytosis neither it co-localised with transferrin vesicles (ruling out CME process) but it did form tubular structures on the plasma membrane which disappeared on ciliobrevin D treatment and reduction of tubular length on nocodazole treatment (microtubule depolymerizing agent) stating that CTxB required dynein motor protein and its associated track for its internalization.

Since dynein use microtubules as tracks to carry their cargo transport we also used nocodazole, a microtubule depolymerising agent and check if the endocytic uptake of Gal3 is getting affected or not. As expected nocodazole did affect Gal3 uptake. The gal3 vesicles were more dispersed in case of nocodazole. Even the transferrin uptake was partially affected. We also checked the role of actin in CIE process, hence cytochalasin D was used which does not allow actin to polymerise. Interestingly we found that cytochalasin D affected Gal3 and transferrin uptake. However, upon inhibiting myosin VI, another retrograde motor protein which use actin as tracks for its movement, it was seen that

Gal3 localisation was not affected but transferrin did get affected. These results shed new light on the role of cytoskeletal machinery on CIE as well as CME processes.

To validate the effects of Ciliobrevin D or Dynapyrazole, we performed siRNA treatment against dynein heavy chain (DYNC1H1) and checked if Gal3 uptake got affected. On 60 nM concentration upto 48 hours Gal3 internalization does get affected without affecting transferrin. We also checked if any of the dynein adaptors are involved in the early endocytic events. For this Hook1 antibody was used to check for its co-localisation on Gal3 tubules. Although Hook1 did not co-localise on gal3 tubules there were tubular structures of Hook1, which did get affected on CBD treatment.

In the fourth chapter of my thesis, Endocytosis is tightly coupled to multiple physiological processes like cell migration, division, differentiation. I checked the effects of dynein inhibition on cellular migration, invasion and wound healing processes. Cell migration and invasion potential studies was carried out in 3D spheroids as a model system. The method used to make the spheroids was hanging drop method. For wound healing scratch assay was performed in 2D cell culture system. The spheroids were treated with Ciliobrevin D or dynapyrazole to check the proliferation. Dynein inhibition affected invasion in spheroids and as well as wound healing. This gives a new insight on the role of dynein on cellular proliferation, migration and invasion.

The final results of my thesis are in the process of being written into a final manuscript which will soon be first published in Biorxiv and simultaneously will be submitted to a reputed journal. Taking the all results into account, we can conclude that Gal3 and its associated cargoes are dynein dependent and dynein would be playing crucial roles in CIE processes. Also from 2D and 3D cell culture systems, we could infer that dynein plays a role in cell migration, invasion and proliferation. There would be many other dynein associated adaptors/regulators assisting this process which is open for exploration. Gal3 has significant roles to play in cell migration, immunological processes, apoptosis, angiogenesis, inflammation and many more. Whether dynein and its regulators/adapters would be contributing to this process is still yet to be known.

Title: Geometry of DNA nanostructures influences cellular and *in vivo* uptake, stimulating differentiation and cell migration
Researcher: Rajwar, Anjali
Supervisor: Bhatia, Dhiraj
Year: 2022
Keyword's: DNA Nanotechnology, Geometry-DNA
Call No.: 572.86 RAJ
Acc. No.: T01040

Abstract: The fabrication of nanoscale DNA molecules to create 3D nano-objects with better control over shape, size, and ligand presentation has shown tremendous promise for therapeutic applications. The interactions between the cell membrane and different topologies of 3D DNA nanostructures are critical for developing practical tools for connecting DNA devices to biological systems. However, certain challenges limit their full potential by impeding their cellular targeting. Some of the major concerns in the field are *in vivo* clearance of these nanostructures by the liver, kidney, spleen, macrophages, etc. The low efficiency of cellular internalization, non-specific accumulation of DNA in non-targeted cells, and non-specific escape of cargo via the endolysosomal system. The practical applications of these DNA nanocages are still limited in cellular and biological systems due to the lack of detailed investigation of DNA nanostructures with the biological membranes, cellular, and *in vivo* systems. We can overcome these challenges by understanding the structural parameters that govern cellular internalization and delineating their interaction with the cell membrane and endocytic pathway. The correlation between the geometry of DNA nanostructures and their internalization efficiency remains elusive. Most published results have only used large-scale origami-based structures and are limited to 3D polyhedral nanostructures.

This dissertation focuses on investigating the influence of the shape and size of 3D DNA nanostructure on their internalization efficiency and studying their potential for cell differentiation. We found that one particular geometry, i.e., the tetrahedral shape, is more favored over other designed geometries for their cellular uptake in 2D and 3D cell models. This is also replicable to cellular processes such as cell invasion assays in the 3D cellular model and crossing epithelial barriers in zebrafish model systems. The geometry-specific bias can also be observed in stimulating *in vitro* angiogenesis. Taken together, this work can establish ground rules for future investigations involving DNA nanocages for biological and biomedical applications, explicitly applying their surface topologies in bioimaging, drug delivery, immune activation, differentiation, etc.

Title: Mechanochemical properties and function of kinesin-3 motors
Researcher: Shewale, Dipeshwari
Supervisor: Soppina, Virupakshi
Year: 2023
Keyword's: Kinesin-3, Molecular Motor Proteins, Cells Motility
Call No.: 572.6 SHE
Acc. No.: T01041

Abstract: A eukaryotic cell consists of different compartments that communicate in a well-orchestrated manner via a transport system comprising cytoskeletal tracks and molecular motor proteins. Cytoskeletal tracks, which include microfilament, intermediate filament, and microtubules, provide structural support and act as highways for motor proteins. Motor proteins like kinesin, dynein, and myosin utilize the energy from ATP-hydrolysis to transport various cargoes along these tracks. Among these motor proteins, kinesin is a plus-end- directed motor majorly involved in intracellular transport. There are over 45 kinesin genes divided into 14 families. These motors have a conserved N-terminal motor/ head domain that contains a microtubule (MT) binding region and ATP binding pocket for ATP hydrolysis, followed by neck linker and neck coil domain involved in motor dimerization and C-terminal tail domain for cargo binding and regulation. The kinesin-3 family consists of fast and superprocessive KIF1, KIF13, KIF14, KIF16B, and KIF28 subfamilies of motor involved in different cellular functions like long- range axonal transport, early and recycling endocytosis, and cell division. Any malfunction in these motors can lead to severe developmental defects, neurodegenerative diseases, and cancer. Despite its physiological and clinical implications, the mechanochemical properties and molecular mechanisms underlying the function of kinesin-3 motors remain unexplored.

This dissertation focuses on studying the motility properties of KIF1A, KIF13B, and KIF14 motors using in vitro assays and cellular studies. Cell-based assays employing an inducible targeting system were used to understand the effect of neurodegenerative disease mutations in the KIF1A motor domain on the motor's mechanochemical outputs and cargo transport. Furthermore, we investigated the significance of the C-terminal CAP- Gly domain of KIF13B in recycling endosome tubulation and cargo recycling using cellular and biochemical assays. Lastly, we also explored the motility properties of the KIF14 motor involved in cell division by using truncated KIF14 motors and generating chimeric KIF14 with KHC. This work gives us valuable insights into mechanochemical properties and regulation of kinesin-3 family members, KIF1A, KIF13B, and KIF14 in axonal transport, endocytosis, and cell division. The study performed with the KIF1A motor enhances our understanding of long-range transport by the motor and the effect of disease mutations in its motor domain on motility, force generation, and cargo transport by the motor. The present study with KIF13B, a homolog of KIF13A, shows colocalization on stable RE tubules and regulates cargo recycling. It demonstrates for the first time the physiological role of the CAP-Gly domain in the KIF13B motor in RE tubule formation. It also shows that KIF13B motors preferentially interact with tyrosinated microtubules through their C-terminal Cap-Gly domain during RE tubulation. Lastly, studies with chimeric KIF14 motors and truncated KIF14 demonstrated that its motor domain binds strongly to microtubules and is intrinsically designed to render KIF14 non-processive in cells.

Title: Investigating the conservation and disease association of THAP9 using sequence, structure, and expression data
Researcher: Rashmi, Richa
Supervisor: Majumdar, Sharmistha
Year: 2022
Keyword's: THAP9, DNA Transposons, Spacers And Mismatch Algorithm (SMA)
Call No.: 660.65 RAS
Acc. No.: T01046

Abstract: Transposable elements (TEs), which constitute 25- 50% of various genomes, are DNA segments that can move and duplicate within a genome. This can lead to an alteration in genome size and composition. Thus, TEs have a major role to play in evolution. There are many genes that are derived from TEs. Human THAP9 is one such gene that encodes the hTHAP9 protein which has more than 25% homology to *Drosophila* P-element transposase (DmTNP). The DmTNP protein mobilizes the P-element transposon which is the causative agent for Hybrid Dysgenesis in *Drosophila*. However, hTHAP9 is a domesticated human DNA transposase and probably does not transpose *in vivo* due to the absence of terminal inverted repeats and target site duplications. Despite being domesticated, it has retained its catalytic activity. Many THAP family proteins are known to be involved in human diseases. THAP1 has been associated with DYT6 dystonia and also plays a role in apoptosis with the help of the transcription repressor protein Par-4. Regulation of THAP5 by Omi/HtrA2 has been linked to cell cycle control and apoptosis in cardiomyocytes. LRRC49/THAP10 bidirectional gene pair is reported to have reduced expression in breast cancer. THAP11 is differentially expressed during human colon cancer progression and acts as a cell growth suppressor by negatively regulating the c-Myc pathway in gastric cancer. The exact functional role of THAP9 and its association with various diseases remains unknown, although the THAP9-AS1 (THAP9 antisense) gene is overexpressed in some cancers. Thus, in this study, we attempt to understand the role of THAP9 using sequence, structure, and expression data.

Chapter 2: Evolutionary analysis of THAP9 transposase: conserved regions, novel motifs

Phylogenetic analysis and evolutionary tests can help us understand the evolution and the type and extent of natural selection for the hTHAP9 gene and its associated protein. In this study, we performed *in silico* characterization of the hTHAP9 protein and its orthologs. We predicted already annotated Pfam and other functional domains (SMART) and novel motifs (ELM, MEME- suite, ScanProsite). We also predicted previously unreported functional features and post-translational modification sites that are highly conserved in mammalian orthologs. These include two myristoylation sites within the THAP domain and four adjacent motifs namely N-glycosylation site, Protein kinase C phosphorylation site, Leucine zipper domain, and Bipartite nuclear localization signal (NLS). The subcellular localization of proteins is sometimes regulated by zipper domains (HSF2) or phosphorylation at sites adjacent to the protein's NLS. Thus, it is tempting to speculate that these highly conserved features predicted in THAP9 may regulate its subcellular localization. Moreover, some THAP9 orthologs were observed to lack the THAP domain, suggesting that these orthologs may have disrupted DNA binding. To investigate the conservation of THAP9, we analyzed the evolutionary relations of its orthologs (both coding DNA and amino acid sequence using MEGAX, TimeTree, PAL2NAL, HyPhy). We created phylogeny aware multiple sequence alignments of amino

acid sequences (using CLUSTALW present in MEGAX,) and guide trees (using TimeTree). The coding DNA sequences of orthologs were codon aligned using PAL2NAL. The codon alignments and phylogenetic trees from above were used for a series of evolutionary selection tests using the HyPhy package. Analysis for selective pressure using HyPhy-FEL, HyPhy-FUBAR identified codon sites that evolved under the influence of pervasive (consistently across the entire phylogeny) positive/diversifying and negative/purifying selection. FEL predicted 8 diversifying sites and 514 purifying selected sites. Similarly, FUBAR predicted 1 diversifying selected site and 618 purifying sites. MEME identifies site(s) in a gene subjected to both pervasive or episodic (only on a single lineage or subset of lineages) diversifying selection. 197 codon sites distributed across hTHAP9 were observed to have evolved under episodic diversifying selection through this analysis. Based on the results from all 3 methods, we can say that THAP9 has evolved under a strong negative selection suggesting that THAP9 may have some stringent functional or structural requirements. The presence of many episodic positively selected sites suggests that certain essential mutations were favored across some lineages. However, there was only one common positively selected site at I829 detected by all three methods which support the role of THAP9 as an essential gene that is necessary to maintain its function through evolution.

Chapter 3: Analysis of AlphaFold-Predicted Structures of human THAP9 and other THAP proteins

Since experimentally derived protein structures of THAP9 are still unavailable, computational methods can be used to predict its structure from primary sequence and homologous structures. Three templates are available for THAP9 structure prediction namely THAP1, THAP2, and DmTNP with sequence identity between 31-44%. However, the query coverage for all three templates is very low, making homology modeling unreliable for structure prediction. The recently released AlphaFold and AlphaFold2 are advanced methods for predicting protein structures, which use evolutionary information to derive inter-residue distances. Thus, we used AlphaFold to predict the structure of THAP9 along with other THAP proteins. Protein domains with similar folds often share the same molecular function; wherein conservation is often restricted to a few residues in the functional sites. We compared individual domains in the predicted THAP protein structures with already characterized protein structures like DmTNP THAP domain (PDB ID:3KDE) and observed conservation in C2CH Zinc coordinating residues. In addition, we observed previously unreported hairpin structures in the DNA binding THAP domains of THAP5, THAP7, THAP8, THAP9 and THAP12. Comparison of catalytic domains of THAP9 and DmTNP suggested a D to K mutation in the DDE/D RNaseH catalytic triad of hTHAP9, which is responsible for the DNA excision in DmTNP. Lastly, we observed a novel C-Terminal domain structure in THAP9.

Chapter 4: Algorithm for G-domain prediction across the diversity of G protein families: A Gapped Motif Discovery Problem

DmTNP needs GTP as a cofactor for the DNA pairing, cleavage, and strand transfer stages of transposition. Thus, we speculated that hTHAP9 which is a homolog of DmTNP may also bind GTP via a conserved GTP binding domain. GTP binding proteins are characterized by a structurally and mechanistically conserved GTP-binding domain, indispensable for binding GTP. The G domain comprises five adjacent consensus motifs called G boxes, which are separated by amino acid spacers of different lengths. G-Domain identification can be treated as a gapped motif identification problem. So, we performed a detailed analysis of GTP binding protein sequences and created a

gapped motif identification algorithm called Spacers and Mismatch Algorithm (SMA) that can predict G-domains in a given G protein sequence, based on user-specified constraints for approximate G-box patterns and inter-box gaps in each G protein family. Using the SMA we predicted the G domains for hTHAP9, which are now being used for further analysis.

Chapter 5: Pan-cancer analysis of THAP9/THAP9-AS1 Sense-Antisense gene pair

The THAP9 and THAP9-AS1 genes are a putative bidirectional gene pair; their transcription start sites are located 166 bases apart, and they are arranged in a head-to-head or divergent manner on opposite DNA strands. THAP9-AS1 (THAP9 antisense) is a newly annotated lncRNA gene that has been implicated in pancreatic cancer, septic shock, and gastric cancer. It has also been reported recently that THAP9 and THAP9-AS1 exhibit differential gene expression patterns under stress such that THAP9-AS1 is consistently upregulated whereas THAP9 exhibits both up- and downregulation. Nevertheless, little is known about the functions of THAP9 and THAP9-AS1 or their role, if any, in tumorigenesis. Comprehensive studies of gene expression can help in predicting gene function. We thus conducted a pan-cancer analysis of THAP9 and THAP9-AS1 gene expression, patient prognosis, and genetic mutations in TCGA and GTEx datasets (RNA-seq) via TIMER2, GEPIA2, EdgeR, and cBio portal. Amplification appeared to be the most frequent DNA alteration. Genes that are activated or deactivated in tandem under a range of conditions may encode proteins that are part of the same multiprotein machine or participate in a complicated coordinated action. Characterizing the function of an unknown gene by associating it with known genes that share its transcriptional activity is frequently referred to as "guilt by association." Here, we also used Weighted gene co-expression network analysis (WGCNA) and Differential Gene correlation analysis (DGCA) to explore TCGA RNA-Seq datasets to study correlations between THAP9 and THAP9-AS1 gene expression and their correlation with the expression of other genes. Gene ontology (GO) and KEGG pathway enrichment analysis were performed to identify primary biological functions linked to the genes that share the THAP9 and THAP9-AS1 clusters in various tumor and normal samples. Our gene expression analysis using TIMER2, EdgeR, and GEPIA2 suggests that abnormal expression of THAP9 and THAP9-AS1 frequently occurred in various types of cancer. We observed that THAP9 was upregulated in CHOL, COAD, ESCA, LIHC, LUSC, LUAD, STAD, and THYM; and downregulated in KIRC, KIRP, PRAD, THCA, TGCT, and UCEC. THAP9-AS1 was upregulated in CHOL, THYM, DLBC, and PAAD, while it was downregulated in OV, SKCM, and THCA. Moreover, THAP9 and THAP9-AS1 were coordinately upregulated in CHOL and THYM and coordinately downregulated in THCA, compared with corresponding normal tissues. Independent and coordinated alteration in THAP9 and THAP9-AS1 expression in various cancers indicates that they may have different biological functions in different types of cancers. Also, since aberrant expression levels of the THAP9-THAP9-AS1 gene pair was associated with poor prognosis in many types of cancer, it is tempting to suggest that they may serve as potential prognostic biomarkers.

Conclusions: Transposable elements play a crucial role in genome evolution. Many TEs and TE-derived genes undergo domestication. THAP9 is one such gene that is a protein homolog of *Drosophila* P-element transposase. In this dissertation, I perform functional characterization of THAP9 using sequence, structure, and expression data. First, we used hTHAP9 and its orthologs to study its evolution and we observed high conservation of THAP9 within mammalian orthologs. Then, we used the THAP9 protein sequence to predict the structure of THAP9 using AlphaFold and

discovered a possibly disrupted catalytic domain. We further created an algorithm called SMA to discover the putative G-Domain in THAP9 and other GTP-binding proteins. Finally, we performed a pan-cancer analysis of THAP9 and THAP9-AS1, which are arranged head-to-head on opposite DNA strands forming a sense and antisense gene pair. My studies shed light on the possible functions of a relatively less understood TE in the human genome and set the stage for further studies to characterize its role.

* * * * *



CHEMICAL ENGINEERING

Chemical Engineering

Title: Hydrodynamics of solid-liquid fluidized beds: modelling and experimental studies
Researcher: Ghatage, Swapnil Vilasrao
Supervisor: Joshi, Jyeshtharaj
Year: 2014
Keyword's: Gas-solid-liquid, Computational Fluid Dynamic, Velocity, Regime Transition
Call No.: 660 GHA
Acc. No.: T00055

Abstract: Fluidized beds are widely used in chemical, petrochemical and process industries. They are preferred over other reactors for carrying out various gas-solid, solid-liquid and gas-solid-liquid processes due to enhanced contact between the fluid and solid particles. However, the efficient operation of a fluidized bed requires the accurate choice of design and operating conditions and the accuracy of prediction of fluidization behavior. With the developments in sophisticated measurement techniques and computational methods as well as increasing computational power, the detailed study of fluidized bed hydrodynamics is increasing extensively. In view of this, as a first exercise, the published literature on the hydrodynamics of these equipment has been systematically analyzed. The advances made in the experimental, modelling and simulations have been critically reviewed. The present status of application of computational fluid dynamic (CFD) simulations has been brought out. In three-phase sparged reactors such as fluidized beds and slurry bubble columns, gas is sparged in the form of bubbles. The gas phase flows in one of the two hydrodynamic regimes namely homogeneous or heterogeneous. The performance is known to depend strongly on the regime of operation. The estimation of critical gas holdup at which transition from homogeneous regime to the heterogeneous regime occurs is crucial for the design and scale-up of sparged reactors. A number of experimental and empirical studies are published in the literature; however, there exists a need of studies on mathematical modelling. In the present work, the theory of linear stability has been used to develop a mathematical model for the prediction of regime transition over a wide range of bubble size (0.7 to 20 mm) and terminal rise velocity (80 to 340 mm/s), particle settling velocity (1 to 1000 mm/s), particle concentration (0.0007 to 30 vol%) and slurry density (800 to 5000 kg/m³). It was observed that the developed model predicts the transition gas holdup within a standard deviation of 12 per cent for three-phase sparged reactors. It was also observed that the developed generalized stability criterion predicts the regime transition in gas-liquid two-phase systems satisfactorily within 10 per cent. In multiphase systems involving a dispersed phase, such as fluidized beds, the interphase exchange of mass, heat and momentum transfer can be very different from those from a single particle, droplet or bubble moving under terminal conditions. However, most existing methodologies still rely heavily on empirical relationships.

In this study the hindered settling/rising (slip) velocity of single steel particles ($d_{PD} = 5$ to 12 mm) and single air bubbles ($d_B = 1$ to 4 mm) has been measured in a solid-liquid fluidized bed of uniform size borosilicate glass beads ($d_P = 5$ and 8 mm) as a function of superficial liquid velocity. The homogeneity and intensity of the turbulence within the fluidized bed has been quantified using

article image velocimetry (PIV) and on the basis of the classification velocity of the foreign (steel or bubble) particle. It was found that the turbulence resulted in an increase in the computed drag coefficient under all the experimental conditions covered in this work. Eulerian-Eulerian simulations of a monodisperse solid-liquid fluidized bed (SLFB) have been carried out to study the effect of turbulence in SLFB on motion of the settling particle. The motion of foreign settling particle has been studied by the dynamic mesh technique provided in FLUENT 14.0. The results show that the model can satisfactorily predict the terminal settling velocity at lower fluidization. The possible reasons for deviations at high voidages have been explained. Also, computational fluid dynamics-discrete element method (CFD-DEM) has been applied for the simulation of the motion of foreign dense particle introduced in a monodispersed SLFB. The fluidization hydrodynamics of SLFB, settling behavior of the foreign particle and particle-particle collision effects have been investigated. Compared to those predicted by empirical correlations, the particle classification velocity predicted by CFDDEM provided better agreement with the experimental data (less than 10% deviation). The dimensionless collision frequency obtained by CFDDEM was found to agree with those predicted by the kinetic theory for granular flow (KTGF). The particle collision frequency was found to increase with an increase in the particle size ratio (d_{PD}/d_P) and become independent of the foreign particle size for high solid fractions. A correlation describing the collision force as a sole function of the average bed voidage was developed having a maximum error less than 20% in the prediction of particle collision force for $d_{PD}/d_P \leq 2$. In many industrial-scale fluidized-bed reactors, particle mixing and segregation play a vital role in determining the reactor performance. However, there exists a lack of studies wherein the fluidization of systems involving more than two types of particles is involved. Such systems are of high industrial importance in mineral and chemical process industries. Therefore, it was thought desirable to study the coupling between superficial liquid velocity and a multi-size (and/or multi-density) particle systems consisting of more than two types of particles. In the present work, Eulerian-Eulerian simulations have been carried out to investigate the effect of particle density and diameter on the minimum fluidization velocity, segregation and intermixing behavior in a fluidized bed comprising of three to five different types of solid phases. It was observed that the Eulerian-Eulerian model can satisfactorily predict the fluidization characteristics in multi-component fluidized bed including the minimum fluidization velocity. The stability analysis of multiphase reactors has been the focus of research for the past few decades. In the present work, the regime transition in SLFB has been analyzed using various experimental (PIV and measurement of settling velocity) and modelling (1D linear stability, 3D CFD and 3D DEM) methods. The characterization of turbulence in SLFB through these methods has been used to provide an insight into the mechanism of momentum transport and hence the transition. The transition conditions obtained using different approaches have been compared. The relative advantages and limitations of each method have been clearly brought out. Recommendations have been made for the estimation of some of the design parameters for SLFB. Suggestions have been made for the future work in the area of experimental and modelling studies.

Title: Hydrodynamic, mixing and mass transfer characteristics of multiphase reactors
Researcher: Kalaga, Dinesh Kumar
Supervisor: Joshi, Jyeshtharaj
Year: 2014
Keyword's: Solid-Liquid Fluidized Bed, Residence Time Distribution, Radioactive Particle Tracking, Computational Fluid Dynamic
Call No.: 660.2 KAL
Acc. No.: T00058

Abstract: The multiphase reactors such as solid-liquid fluidized beds and bubble columns are widely used chemical, petrochemical and allied industries. Their application ranges from manufacturing processes such as catalytic hydrogenation, oxidation, fermentation, waste water treatment, Fischer-Tropsch Synthesis and Chromatographic separations etc. The performance of these multiphase reactors depends on hydrodynamic, mixing and mass transfer characteristics. With this objective, in the present research work, an attempt has been made to understand the rational design procedures for multiphase reactors such as solid-liquid fluidized bed (SLFB), Solid-liquid multistage fluidized bed (SLMFB), Solid-liquid circulating multistage fluidized bed (SLCMFB) and Bubble column reactors. Liquid phase residence time distribution (RTD) studies have been performed in conventional SLFB and SLCMFB. RTD experiments for SLFB were carried out in the column having the same diameter as the down comer of SLCMFB. RTD has been estimated for both the riser column and the multistage down comer column of SLCMFB. Computational fluid dynamic (CFD) simulations of SLFB and riser section of SLCMFB have been performed to predict the RTD. In all the above cases, good agreement was found between the CFD predictions and the experimental measurements. Based on the experimental data, empirical correlations have been proposed for liquid phase axial dispersion coefficient. Solid-liquid mass transfer coefficient (k_{SL}) was measured in both conventional SLFB and SLMFB by using the system of dissolution of benzoic acid in water. The dependence of k_{SL} on important variables associated with the distributor design and the effect of inerts has also been studied. Based on the experimental data, generalized correlation has been proposed for the estimation k_{SL} for both SLFB and SLMFB. Radioactive Particle Tracking (RPT) technique was employed to quantify the hydrodynamic parameters in 120 mm diameter bubble column with and without internals using air/water system at different superficial gas velocities ranging from 15 mm/s to 265 mm/s. Experiments were performed for two internal configurations with percentage obstruction area in the range from 0 (no internals) to 11.7%. It is found that, the liquid phase hydrodynamics depends strongly on the superficial gas velocity and the internals. Suggestions have also been made for the future work.

Title: Quantification of acetone-butanol-ethanol (ABE) fermentation in *Clostridium acetobutylicum* using systems biology approach

Researcher: Kumar, Manish

Supervisor: Saini, Supreet & Gayen, Kalyan

Year: 2015

Keyword's: *Acetobutylicum*, Fermentation, Acidogenesis, ABE fermentation, Kinetic modeling, Materials

Call No.: 660 KUM

Acc. No.: T00095

Abstract: *Clostridium acetobutylicum* exhibits a two-step metabolic pathway where substrates are first converted to organic acids accompanied by a decrease in pH. The acids are then assimilated to organic solvents. The transition from the acid-producing (acidogenesis) to the solvent-producing phase (solventogenesis) is controlled by integration of a number of cellular and environmental cues, whose precise mode of action are not well understood. In this study, a series of batch experiments were performed to understand the impact of extracellular cues in regulating the dynamics of acidogenesis and solventogenesis. It is demonstrated that the two phases operate independently of each other and the growth phase of the cell, i.e. the cues controlling a phase are not linked to the status of the other phase or the growth phase of the cell. Kinetic experiments demonstrated that there exist two previously uncharacterized negative feedback loops controlling the amounts of acids produced in the acidogenesis phase. In the next investigation of this work, we have used Elementary Mode Analysis (EMA) to quantify fluxes of metabolic network of *C. acetobutylicum* under different physical and chemical conditions. Biochemical reactions and their stoichiometry based metabolic model helped to reveal that, in response to external stresses, the organism invokes Elementary Modes which couple acidogenesis and solventogenesis. This coupling leads to the organism exhibiting physiological characteristics of both, acidogenesis and solventogenesis at the same time. Significantly, this coupling was not invoked during any “unstressed” conditions tested in this study. Overall, this work highlights the flexibility in *C. acetobutylicum* to modulate its metabolism to enhance chances of survival under harsh conditions. During this thesis work, we have also developed a pH based phenomenological model of fermentative production of butanol from glucose using *C. acetobutylicum* in batch system. The model relates the dynamics of growth and metabolite production with the extracellular pH of the media and was validated using data from a number of fermentation experiments, and was found to be successful in predicting the fermentation dynamics in *C. acetobutylicum*. Further, the proposed model can be extended to represent the dynamics of butanol production in other fermentation system like fed-batch or continuous fermentation using single and multi-sugars.

Title: Liquid antisolvent precipitation of curcumin: polymorphism, particle formation pathways and long term stability

Researcher: Thorat, Alpana Ankush

Supervisor: Dalvi, Sameer V.

Year: 2016

Keyword's: Curcumin, Concomitant Polymorphism, Polymorphic Transformation, Aqueous Suspensions, Bovine Serum Albumin, Hydroxyl Propyl Methylcellulose, Curcumin Induce by Ultrasound, Water-soluble Drugs, Antisolvent Precipitation

Call No.: 660 THO

Acc. No.: T00103

Abstract: The main objective of this work was to understand particle formation pathways and polymorphism of curcumin. Curcumin is a poorly water soluble ingredient found in turmeric (*Curcumin longa*). In this work, curcumin was precipitated by liquid antisolvent (LAS) technique in presence of ultrasound and additives. The curcumin particles precipitated in presence of ultrasound and with (or without) additives were found to be in orthorhombic forms (Forms 2 or 3), whereas raw curcumin and curcumin particles precipitated without ultrasound and without additives were found to be in monoclinic form (Form 1). Solid-state characterization studies of these particles revealed that the orthorhombic forms (Forms 2 and 3) undergo polymorphic transformation to monoclinic form (Form 1) during differential scanning Calorimetry (DSC) heating studies. These polymorphic transformations were found to occur below the melting points of all three curcumin forms, hence polymorphs could be enantiotropically related to each other. However, further research is required to establish relationship between the curcumin polymorphs. Curcumin particles precipitated with ultrasound and bovine serum albumin (BSA), hydroxyl propyl methylcellulose (HPMC), and polyvinyl pyrrolidone (PVP) were found to follow non-classical particle formation pathways. These particles precipitated as micron sized superstructures formed by aggregation of several primary curcumin nanoparticles. The particles appeared to be the loose aggregates (of $\sim 1\text{--}5\ \mu\text{m}$ in size) composed of several curcumin nanoparticles ($\sim 50\text{--}200\ \text{nm}$ in size). Curcumin particles precipitated with ultrasound and other additives such as, SDS (at concentration below and above critical micelle concentration (CMC)), Tween 80 (at concentration below, and above CMC), Sodium Alginate (Na-Alg), Polymer JR 400, and Pluronic F68 (PF68) however, appeared to be completely fused particles. Hence, hypothesizing particle formation pathways in these cases was difficult. Curcumin particles precipitated in presence of ultrasound and additives such as, Tween 80 (at concentration below CMC), Sodium Alginate (Na-Alg), and Pluronic F68 (PF68) were found to be mixture of both Form 3 and Form 1. This concomitant behavior of polymorphs could be the result of the nucleation of Form 3 and Form 1, when precipitated in presence of these additives and ultrasound. The morphology of curcumin particles was found to be dependent on the polymorphic form of the precipitated curcumin particles. Rice seed like morphology was found to be indicative of orthorhombic form whereas rectangular plate-like morphology was the indication of monoclinic form. The long term stability of precipitated curcumin particles in terms of polymorphic as well as morphological transformations was also studied. Curcumin particles precipitated with higher ultrasound energy (105W) were stable in terms of particle size and size distribution for nearly 2 years. However, the particles precipitated with lower ultrasound energy (13W) or without ultrasound (0W) were found to grow to larger particles. Similarly, the precipitated curcumin particles

stored in aqueous suspensions at room temperature (25°C) were found to remain stable in the same polymorphic form as that of freshly precipitated particles with no significant change in particle morphology even after 3 years. The results presented in this work demonstrate that the particle formation pathways of curcumin could be manipulated to obtain desired polymorphic and morphological characteristics through a judicious choice of additives and mixing techniques (ultrasound vs. stirring). Moreover, the methodology developed could be applied to other poorly water-soluble drugs as well as other organic and inorganic materials.

Title: Mass transfer and kinetic characteristics of activated sludge digestion process

Researcher: Hariharan P.

Supervisor: Joshi, Jyeshtharaj

Year: 2016

Keyword's: Wastewater, Activated Sludge Process, Effluent Treatment Plants, Degradation and Detoxification

Call No.: 628.354 HAR

Acc. No.: T00177

Abstract:

The wastewater generated by industry, municipal and household contains a complex mixture of both organic and inorganic substances. The treatment of this wastewater is highly important before discharging into the ecosystem to avoid pollution of water-bodies. Industrial wastewater contains a diverse range of toxic compounds that cannot be released directly into the environment. Their degradation is mostly

carried out by the activated sludge process (ASP) either at Effluent Treatment Plants (ETPs) for wastewater generated by large-scale industries or Common Effluent Treatment Plants (CETPs) that treat wastewater generated by a cluster of small-scale industries. The wastewater treatment processes carried out in ETPs are relatively economical and widely accepted methods for the degradation and detoxification of domestic as well as industrial wastewaters. The wastewater can be treated by physical, chemical and/or biological methods. The cost of chemical treatment is too high for large wastewater quantities. The ASP involves the transformation of dissolved and suspended organic contaminants to biomass and gases such as CO_2 , CH_4 , N_2 and SO_2 . The effectiveness of ASP depends upon the development of an adequate microbial community and dissolved oxygen and usually operates in the mixed liquor suspended solids (MLSS) range of 4000 to 9000 mg/L. The high levels of MLSS may become attractive if the corresponding need of dissolved oxygen can be met. However, scant information is available in the published literature regarding the kinetics of ASP in the high range of MLSS (15000 to 40000 mg/L) and a systematic study was undertaken to enhance the understanding of associated processes.

In the present work, waste from an agrochemical plant was used. For wastewater treatment oxygen was supplied by either sparging air from bottom of the sparged reactor (BCR) or by surface aeration in stirred tank reactor (STR). The mass transfer coefficient ($k_L a$) for activated sludge in STR and BC were experimentally measured for agrochemical industry wastewater. The MLSS concentration was varied in the range of 6000 to 40000 mg/L. In STR, the superficial gas velocity and the impeller speed were varied in the range of 0.188 to 0.5 mms^{-1} and 5 to 11.67 rps, respectively. In BCR, the superficial gas velocity was varied from 0.6 to 2 mms^{-1} . For the measurement of $k_L a$, the physical method of transient oxygen uptake was

employed. In both the reactors, the value of $k_L a$ was found to decrease with an increase in the MLSS concentration covered in this work. However, the extent of reduction was found to be a factor of 2.5 to 4.5 in BCR as compared with a factor of only 1.6 to 1.8 in STR. In both reactors, the reduction was found to vary because of increase in viscosity with an increase in MLSS. However, the extent of such decrease was nominal in STR as compared with substantial decrease in BCR.

In addition to mass transfer characteristics, the kinetics of reduction of COD was investigated over a wide a range of MLSS (6000 to 40000 mg/L). Experiments were performed in surface aerators as well as in classical STRs with air sparging. The agitator speed was varied from 3 to 15 rps. Two modes of operations were investigated: (a) constant dissolved oxygen [1 and 2.5 mg/L] (DO) at different levels of impeller speed with respect to time and (b) variable DO [0.5 to 7 mg/L] at a constant speed with respect to time. The kinetics was investigated with and without nutrients. The kinetics was represented by the following equation:

$$\frac{dS}{dt} = -S_t k_0 \left(\frac{MLSS_0}{MLSS_0 + k_1} \right)^A \left(\frac{DO_t}{DO_t + k_2} \right)^B$$

Where A, B, k_0 , k_1 and k_2 are kinetic coefficients from the equation. The k_2 value was 0.25 taken from literature [1]. The values of other kinetic coefficients were obtained by fitting the experimental data. The overall values of k_1 and k_0 were obtained for experimental sets. The results on mass transfer characteristics and the reaction kinetics are expected to be useful for the design and optimization of aerobic biological reactor at high MLSS.

Aerobic digestion, an alternative method for treatment of waste activated sludge is carried out in the endogenous respiration phase of aerobic bacteria. As the supply of available food (substrate) is depleted, microorganisms begin to consume their own protoplasm to obtain energy for cell maintenance

reactions thus achieving endogenous oxidation of cell tissue. This in turn stabilizes the sludge with substantial reduction in its volume. Some of the cell material, utilized at a negligible rate, is non-biodegradable. The rate of destruction of activated sludge during its endogenous respiration phase can be expressed as a first order function of the concentration of the degradable biomass present, expressed as degradable volatile suspended solids (VSS). The endogenous decay rate was found to depend on the type of wastewater on which the sludge was grown, sludge concentration, sludge age (the time for which the sludge is aerated prior to digestion) and on the environmental factors such as pH and digestion temperature.

The excess activated sludge degradability was studied from an agrochemical industry wastewater treatment plant. The objective was to understand the kinetics of sludge digestion using air and oxygen. Experiments were performed in 2 L stirred tank reactor. The impeller speed was varied in the range of 1.67 to 11.67 r/s. The superficial air and oxygen velocities were maintained at 0.39 mm/s. The value of MLSS was also varied in the range of 6 to 90 g/L. The rate of digestion of MLSS/MLVSS was found to be of the first order. The kinetics of digestion is presented by the following equation:

$$\frac{d(M)}{dt} = -k_d * \left(\frac{M_0}{S_0} \right)^A M$$

The values of k_d and A have been reported in this work. This equation has been used for both MLSS and MLVSS to obtain the decay rate coefficient.

Title: Strategies for enhanced performance of single & multi-objective optimization using evolutionary algorithms: application to dynamics optimization

Researcher: Patel, Narendra M.

Supervisor: Padhiyar, Nitin

Year: 2016

Keyword's: Box Complex Member, Constraint Handling, Evolutionary Algorithms, Rosenbrock's Function

Call No.: 519.3 PAT

Acc. No.: T00189

Abstract: Evolutionary Algorithm (EAs) are often criticized for their large computational cost for solving practical optimization problems. Moreover they are naturally designed for unconstrained problems and hence require an additional mechanism for constraint handling. On the other hand, Voz complex method is a gradient free local search optimization technique having good convergence and constraint handling capabilities. Furthermore, the Box-Complex method being the multi-start numerical optimization technique, its hybridization with the EAs is quite straight forward. We explore this hybridization for enhancing the convergence and constraint handling capabilities of the EAs. We add one or more population members created by Box-Complex method using the current population and replace and replace the equal number of worst population members violating the constraints are projected through the centroid of a geometric complex made of a few feasible points using Box-Complex method for constraint handling. The success measure of the single objective EAs is its capability to converge to the global optimum. On the other hand, there are three measures for multi-objective optimization (MOO), namely convergence to the global pareto, the uniform spread of the solutions, and the coverage of the pareto front. Box-Complex is guided based in the objective (fitness) function value. This makes its hybridization with SOO EAs quite straightforward. However, such hybridization is not straightforward for the MOO problems since there are multiple conflicting fitness criteria in MOO. This motivated us to develop a novel sorting mechanism for MOO EAs by discretizing the objective space into an m-dimensional mesh, where m is the number of objectives. In this mesh sorting, the overall fitness is defined based on the location of the population member in the mesh. Furthermore, the additional MOO criteria can easily be incorporated with the novel mesh sort framework. The above, mentioned proposed strategies are quite generic and can be implemented with any population based EA. However, in the current work, we use Genetic Algorithm (GA), Cuckoo Search (CS), and Differential Evolution (DE) to demonstrate their performance. All the proposed strategies are first tested using the benchmark test problems. The strategies have been further validated using various engineering applications. Dynamic optimization (DO) is a class of optimization that optimizes the temporal profiles of the process inputs satisfying the process dynamics. Solving such DO problems is computationally expensive and quite challenging compared to the static optimization problems. Hence, we also validate the proposed strategies in the EAs using single and multi-objective DO problems. With increased computational advancements, there is a significant scope of utilizing the multi-objective optimization tool for enhancing the process efficiency. We in this work also propose novel multi-objective dynamic optimization problem formulations for a class of fed-batch bioreactors. We solve four bi-objective problems and a three-objective problem for an application of the secreted protein production in a fed-batch bioreactor. The four objectives considered in this study are maximization of productivity, maximization

of yield, minimization of fed-batch operation time, and minimization of the endpoint substrate concentration.

Title: Property improvement of fine pharmaceutical powders under varying humidity conditions through nano-coating
Researcher: Karde, Vikram Ashok
Supervisor: Ghoroi, Chinmay
Year: 2017
Keyword's: Colloidal Silicon-di-oxide, Relative Humidity, Hydrophilic Powders, Nanocoating
Call No.: 620.43 KAR
Acc. No.: T00219

Abstract: Majority of the pharmaceutical dosage forms are manufactured from powders as a starting material. The handling and processing problems in pharmaceutical manufacturing still revolves around unpredictable bulk behavior of powders in different manufacturing conditions. This work is an attempt to improve and study the particle properties and bulk behavior of some of the commonly known fine cohesive powders under varying humidity conditions through surface modification using nano-coating technique. The effect of surface modification on bulk behavior and surface characteristics of three pharmaceutical excipient powders viz. Avicel PH105, Lactochem fine powder and Corn starch was studied. Hydrophilic (Aerosil 200P) and hydrophobic (Aerosil R972) colloidal silicon-di-oxide were used as guest particles for dry coating (nano-coating). An overall improvement in the flow and packing (bulk density and compressibility) properties of all the three excipients were observed after nano-coating. The results also confirmed that the quality of nano-coating achieved is strongly influenced by surface morphology of powder particles. The effect of surface modification on wettability and surface energy characteristics of these pharmaceutical excipients were also studied. The results showed that wettability increases with increasing specific component of surface energy (γ_s^{sp}) of particles and successfully demonstrated that surface wettability and energetics of powders can be modulated by varying the type and level of surface coating. Influence of relative humidity (RH) on the surface energy characteristics of fine cohesive powders (Corn starch, Avicel PH105 and Ibuprofen) and its relationship with powder flow variations was explored. The γ_s^d component of surface energy barely changed with RH variation, whereas the γ_s^{sp} component of surface energy increased with increasing RH for hydrophilic powders. It was proposed that the γ_s^{sp} component of surface energy can be used as an effective indicator for tracking flow behavior of fine powders under varying humid conditions. The present study also brought out the existence of different regimes of probable interparticle forces which dictate the bulk flow behavior of fine hydrophilic powder under humid conditions. Subsequently, the effect of RH on the bulk behavior of raw and surface modified corn starch powder was studied. Powder bulk behavior like flow and packing properties of uncoated and coated corn starch powder, surface modified using hydrophobic (Aerosil R972) nano-silica, were studied at different relative humidity conditions (30%-90% RH). It was found that flow and packing properties of uncoated powder deteriorated at elevated RH conditions, with prominent changes observed above 60% RH. However, surface modification using nano-coating of particles countered the detrimental effects of humidity on its bulk behavior by preventing capillary bridge formation owing to increased nanoscale roughness and subsequent

modification of interparticle contacts. Also, the interparticle adhesion force developed in these powders, under varying humid conditions and applied consolidation stresses, was estimated using tensile strength determination approach. For uncoated powders, the results indicated that, at low consolidation and high RH, capillary force is the prevailing force contributing to the total interparticle adhesion in contrast to higher consolidation conditions where load induced contact force plays a dominant role. The study also identified a stable humidity zone (45-60% RH) for uncoated powder, where interparticle forces were minimal or stable. Further extension of this work involved identifying and investigating the RH dependent stick-slip regime of frictional behavior and its effect on flow properties of corn starch. The stick-slip friction of the particles under stress increased with the reduction in RH whereas it diminished with the increase in humidity. This frictional behavior was attributed to the alternate sticking of the contacts into the discretely or very thinly distributed moisture on the particle surface at lower RH. On the other hand, at higher RH levels, the presence of thick lubricating moisture film reduced the frictional forces between the particles and improved powder flow. Three different fluid film lubrication regimes viz. boundary, mixed and hydrodynamic regimes were identified for corn starch particles, within the studied RH range. Moreover, nano-coating led to alleviation of such frictional behavior at all RH levels.

Title: Viscoelastic properties of colloidal particles in liquid crystals and anchoring transitions at interfaces
Researcher: Kulkarni, Siddharth Vijay
Supervisor: Thareja, Prachi
Year: 2017
Keyword's: Viscoelastic Properties, Colloidal Particles, Cellular Networks, Amphiphilic Molecules
Call No.: 530.429 KUL
Acc. No.: T00220

Abstract: Liquid Crystals (LCs) are soft materials with molecules possessing an orientational order similar to solids but with mobility similar to liquids. Addition of colloidal particles to LCs disturbs the molecular order and leads to the formation of topological defects. It has been shown that the particle - defect interactions lead to several types of self - assembled particle structures of 1 - D linear chains, 2 - D sheets, 3 - D cellular networks, which have not been observed in isotropic liquids. Moreover, the external field required to align LC molecules is also reported to be significantly reduced by addition of particles. This work aims to understand the factors influencing the particle self - assembly and the resulting viscoelastic properties of particles-in-LC composites. Two types of ordered matrices are explored in this work: 1) hexagonal (H_1) LCs which are composed of cylinders of amphiphilic molecules arranged in a H_1 lattice and 2) Nematic LCs (NLCs) which have rod like molecules oriented in a direction, without a positional order.

We first present the self - assembly and rheology of colloidal particles in H_1 LC phase constituted by mixing a non - ionic surfactant, nonaethylene glycol monodecyl ether ($C_{12}E_9$) and DI water in 1:1 proportion by weight. The size of colloidal particles is in the range of 100 nm - 500 nm which is substantially greater than the characteristic spacing between the surfactant cylinders (5.7 nm). We show that the colloidal particles assemble at the grain boundaries (GBs) of the H_1 LC with particle structures dependent on the particle shape. The results reveal that while elongated and irregular particles form end to end interconnected particle networks, spherical particles form only aggregates at the H_1 GBs. The difference in particle shape - driven self - assembly also manifests in the rheological response as the formation of interconnected network at the GBs increases the elasticity of the H_1 LC phase more significantly than the presence of aggregates. In addition, the interplay of factors influencing the efficiency of the partitioning of the particle at the H_1 GBs and their resultant effect on rheology is also investigated. Our results demonstrate that with increase in particle loading, density and fast phase transition kinetics, efficiency of partitioning of particles at the GBs decreases. We show that while complete partitioning of particles at the H_1 GBs leads to a monotonic increase in the elastic moduli with particle loading, a decrease in partitioning efficiency leads to a non - monotonic trend in elastic moduli with particle loading. Changing the dispersing medium to NLCs presents a very different scenario. The rheological response resulting from the particle self - assembly of the hydrophilic Titania (TiO_2) nanoparticles in a NLC, N-(4-Methoxybenzilidene)-4-butylaniline (MBBA) is investigated. Our results show that while particle aggregates are formed at low particle loadings, a sample spanning network of particle flocs is formed above a threshold particle concentration and the NLC is confined in the network. We show that as the concentration of particles increases, the nematic order is progressively disturbed and a metastable, structurally disordered composite is formed. Further extension of this work involves studying the anchoring

transitions of NLC, 4-cyano-4'-pentylbiphenyl (5CB) at 5CB - aqueous and 5CB - solid interface. 5CB drop decorated glass surfaces are fabricated by flow coating, and the anchoring transition of 5CB is studied in response to varying surfactant concentrations and structures. The ordering transition of 5CB at 5CB - aqueous interface from tilted to perpendicular anchoring occurs at concentrations close to the critical micelle concentration (CMC) of surfactants, depending on the organization of the surfactant tails at the interface. The anchoring of 5CB molecules at 5CB - solid interface is also shown to correlate with the surface energy of solid surfaces (γ_{sa}), the sign of the anisotropic 5CB - surface interfacial energy ($\Delta\gamma_{si}$), spreading coefficient (S) and 5CB surface tension (γ_{5CB}). We also demonstrate with an empirical model that the dipolar interactions dominate during the perpendicular anchoring of 5CB, whereas dispersion forces dominate during the parallel anchoring of 5CB at 5CB - solid interface.

Overall, our work illustrates that controlling the partitioning efficiency of particles at the H_1 GBs provides a valuable strategy for engineering the particle self - assembly which subsequently governs the rheological manifestation. These results can be extended to engineering polycrystalline materials wherein impurities are added to improve mechanical strength. We further demonstrate that confining the NLCs in a network of particle flocs paves a way to systematically introduce structural disorder to tune the rheology of particles-in-NLC composites. This presents a different view point of studying structurally disordered glasses as systems in which order is disturbed by introducing external random quench disorder. Our study also shows that the surfactant driven orientational transition of NLC molecules at the NLC - aqueous and NLC - solid interfaces is dictated by the surfactant concentration and configuration of the surfactant tails at the interfaces.

Title: Engineering stable and biocompatible microbubble formulations for biomedical applications
Researcher: Upadhyay, Awaneesh K.
Supervisor: Dalvi, Sameer V.
Year: 2018
Keyword's: Biomedical Applications, Bovine Serum Albumin, Cell-viability Studies, Perfluorobutane
Call No.: 660.284 UPA
Acc. No.: T00265

Abstract: Microbubbles are gaseous colloidal particles with size ranging from 1 to 10 μm . Microbubbles consist of a protective shell made up of lipids, proteins, polymers, etc. which encapsulates a gaseous core. The core generally consists of gases with high molecular weight, low diffusivity, and low solubility in aqueous media. The shell of microbubbles can contract and expand when subjected to ultrasound. This phenomenon enables the use of microbubbles in applications like contrast imaging, sonoporation, microbubble cavitation, and as drug/gene or IV O_2 gas carriers etc. However, in order to use these microbubbles in biomedical applications, it is necessary to first estimate their shelf stability, in-vitro persistence, biocompatibility, response to ultrasonic radiation as well as their drug loading capacity. Understanding the effect of shell material, additives, storage medium and transport properties of core gas etc. on the stability and biocompatibility can help in engineering a microbubble formulation which is stable and can be used for medical diagnosis as well as for therapeutic applications.

The main objective of this work has been to engineer a stable and biocompatible microbubble formulation for biomedical applications. Microbubbles were synthesized using Bovine serum albumin (BSA) as a main ingredient and the effect of various additives on the shelf life and in-vitro persistence was studied. The microbubble formulations with highest shelf stability were tested for in-vitro immunogenicity using a complement preserved human serum. Further, in-vitro contrast enhancing capability, drug loading ability, in-vitro drug uptake and cell-viability studies were also carried out. Some of the major contributions of this work are briefly discussed below.

BSA microbubbles were made of Perfluorobutane (PFB) gas and were produced by probe sonication method using formulations containing BSA, Caprylic acid (CA) and N-acetyl-DL-tryptophan (Tryp) in different combinations. The freshly prepared polydisperse (0.5 – 20 μm) microbubble samples were then size isolated by centrifugal differentiation to produce microbubble suspensions with a narrow size range of 3 to 5 μm . The formulation containing BSA and Tryp yielded microbubbles with a shelf life (~8 months). This stability was observed when microbubbles were stored in an aqueous solution consisting of original solution [containing BSA and Tryp in phosphate buffer saline (PBS)] used to make microbubbles (80% v/v), 1, 2 propane-diol (10 % v/v) and glycerin (10 % v/v). Fluorescence and Circular Dichroism (CD) spectroscopic analyses were carried out to comprehend the enhanced stability of microbubble suspension by understanding the effect of additives such as CA and Tryp, and heating and sonication on the secondary and tertiary structure of BSA. It was found that the use of Tryp in the formulation favors greater unfolding of BSA as compared to a formulation where CA was used. This in addition to a lower diffusivity of PFB, and lower solubility of BSA in the solution

containing Tryp, leads to a relatively stable microbubble suspension. The microbubbles were mixed with PBS maintained at 37 °C, to check their in-vitro stability. It was observed that microbubbles produced from BSA formulation containing Tryp persisted longer than other microbubbles.

A comparative study was conducted to understand performance efficiency of protein and lipid microbubbles in terms of their shelf life and in vitro persistence. Lipid microbubbles were produced using a mixture of 1, 2 distearoyl-sn-glycerol-3-phosphocholine (DSPC) phospholipid as a main ingredient and polyethylene glycol 40stearate (PEG40S) as emulsifier (9:1 molar ratio). A narrow sized range (3 – 5 µm) microbubble suspension was produced using sonication method followed by size isolation using centrifugation. The shelf stability, in vitro stability, immunogenicity and contrast producing ability of lipid microbubbles was compared to that of BSA microbubbles (PEGylated and non-PEGylated). After 4 weeks of observation period, a least reduction in concentration of around 18% was observed for PEGylated BSA microbubbles whereas highest reduction of 38% was observed for DSPC-PEG40S microbubbles. *In-vitro* persistence performance for PEGylated BSA microbubbles was found to be better than non-PEGylated BSA microbubbles as well as DSPC-PEG40S microbubbles. Non-PEGylated BSA microbubbles were found to be immunogenic whereas PEGylated BSA and DSPC-PEG40S microbubbles were found to be non-immunogenic.

To test the ability of these microbubbles to produce contrast during ultrasonography imaging, microbubbles were mixed with PBS in a dialysis bag of 25 mm flat width and subjected to sonography. The ultrasonography contrast enhanced significantly in presence of microbubbles. It was found that the contrast in terms of grey scale value produced by DSPC-PEG40S microbubbles was maximum (212) followed by BSA microbubbles (194) and PEGylated BSA microbubbles (154) as compared to the control, consisting of PBS solution (17.5).

Further, BSA microbubbles were tested as drug carriers with curcumin loaded on the microbubble surface. Curcumin found in traditional Indian spice turmeric is an active ingredient with anticancer properties. In order to load curcumin on microbubble surface, curcumin was dissolved in ethanol and added to BSA solution in 5:95 (v/v) ratios. Curcumin-BSA conjugation was characterized by UV and fluorescence spectrophotometry. This solution was sonicated in presence of PFB gas to make microbubbles loaded with curcumin (CuB). The drug loading and kinetic release of curcumin from CuB microbubbles (in presence and absence of therapeutic ultrasound with frequency of 1 MHz, intensity 0.5W/cm², and exposure time of 5 sec) was carried out in PBS maintained at 37°C. It was observed that around ~50% of curcumin was released from CuB microbubbles in 1 hour in presence of ultrasound, while only ~14% curcumin was released when there was no sonication applied. Also, more than 90% of curcumin from CuB microbubbles was released within 4 hours when exposed to ultrasound, while only ~30% curcumin was released in the same time duration when sample was not exposed to ultrasound.

Further, drug (Curcumin) uptake studies conducted on HeLa cells confirmed that microbubbles along with ultrasound can effectively enhance the curcumin uptake by ~250 times when compared to a situation where HeLa cells are mixed with curcumin solution. *In-vitro* cell viability studies showed that curcumin loaded BSA (CuB) microbubbles were more effective in reducing viability of cells by ~62% when used along with ultrasound.

In this work we have shown an efficient way to prepare a drug loaded protein microbubble formulation which can be used to efficiently deliver a low bio- available drug to cancer cells. This work can be extended to formulate microbubble of different proteins or protein-lipid combinations using different additives. Also, to extend the therapeutic applications of microbubbles other poorly water soluble anticancer drugs delivery to different cancer cell lines. Further, in-vivo studies using animal models can be conducted to estimate the efficiency of these microbubbles constructs to inhibit growth of cancerous tumor cells.

Title: Solid state reactions and influence of additive for different applications in materials: experimental & thermo kinetic analysis

Researcher: Maiti, Sanat Chandra

Supervisor: Ghoroi, Chinmay

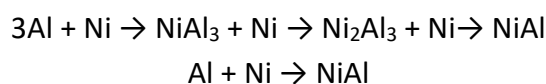
Year: 2018

Keyword's: Solid-state Reaction, Nano-additive, Thermo Kinetic Stabilization, CO2 Sorption, Doping

Call No.: 660.287 MAI

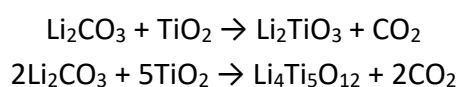
Acc. No.: T00395

Abstract: Understanding the kinetics of solid-state reactions and influence of different additives during reaction invite immense interest due to its application in material preparation. This dissertation presents research on four different solid-state reactive systems: Nickel aluminide (Ni-Al), Lithium titanate (Li_2TiO_3 / $\text{Li}_4\text{Ti}_5\text{O}_{12}$), Calcium silicate (Ca_2SiO_4) and Calcium oxide (CaO). In nickel aluminide system, the behavior of the complex reaction (series and parallel) has been carried out by thermo-kinetic analysis. The kinetic data were generated using dynamic temperature program at 5, 10, 15, 20 K min⁻¹ in a differential scanning calorimeter.



The phase formation was studied by the Rietveld refinement of X-ray data. The activation energy for the reaction was calculated from model-free isoconversional technique. The variation of activation energy with conversion shows the complex behavior of the reaction in between Ni and Al. In this work, Šesták Breggren (auto-catalytic model) has been applied by Málek's method to account for NiAl formation through complex reaction.

In case of anode materials of Li-ion battery, ionic mobility improves the quality of the anode materials. Generally, improvement in ionic mobility is measured using the electrochemical impedance spectroscopy (EIS). In this work (Li_2CO_3 - TiO_2 system), we demonstrate a unique approach to correlate influence of doping on ionic mobility through thermo-kinetic analysis. We discovered that Li_2TiO_3 / $\text{Li}_4\text{Ti}_5\text{O}_{12}$ synthesized in the presence of Mo+6 ion reduces the oxygen vacancy by charge compensation method.



The reaction mechanism was predicted by Master plot approach. We have shown that the rate controlling step shifted from three-dimensional diffusion (D_3) for undoped Li_2TiO_3 to a chemical reaction (F_n) for doped Li_2TiO_3 . For $\text{Li}_4\text{Ti}_5\text{O}_{12}$, the reaction mechanism (or rate controlling step) is found to be chemical reaction (F_n) for undoped and nucleation (A_n) for doped material. The results show that diffusion of ions becomes faster in the Mo+6 doped materials by reducing the charge transfer resistance.

For CaCO_3 -CaO system, nano- TiO_2 promoted CaO was synthesized from different wt.% of nano- TiO_2 coated micron CaCO_3 ($\text{CaCO}_3 \rightarrow \text{CaO} + \text{CO}_2$). This nano- TiO_2 promoted CaO were extensively studied to understand the effect nano- TiO_2 on crystal- lite size, surface area and morphology after decomposition. The nano- TiO_2 promoted CaO was then deployed for CO_2 sorption at different temperatures. We demonstrate that nano- TiO_2 (5 wt.%) promoted CaO (Ca-Ti-5) has 10 times more CO_2 sorption property than pure CaO obtained from micron- CaCO_3 . In-fact the sorption capacity is also higher than CaO obtained from nano- CaCO_3 . In addition, the experimental results (carbonation reaction) are fitted with theoretical kinetic models based on the shrinking core model. The kinetics parameters are evaluated and correlated with the crystal level properties.

For the CaO- SiO_2 system, several polymorphs of C_2S ($2\text{CaO} \cdot \text{SiO}_2$) are formed during the solid- state reaction between CaO and SiO_2 ($2\text{CaO} + \text{SiO}_2 \rightarrow \text{C}_2\text{S}$). In room temperature, undesired polymorph (γ - C_2S) is formed. In this work, selective and desired phase (β - C_2S) was stabilized by introducing nano- and micron-size additives. We demonstrate that efficiency of nano-additive is several times higher than micron- size additive. Also, hydration study of β - C_2S stabilized by nano-additive was also carried out in the presence of CaCl_2 , NaCl, NaOH and distilled water and demonstrate the role of different ions on hydration rate. The morphology of the hydrated product also depends on the ions present in the solution and play major role during hydration.

The scientific concepts obtained from this area of research will significantly ap- plied to other solid- state reactions for different applications in industry.

Title: Synthesizing a new class of two-dimensional boron based nanosheets and zero-dimensional carbon based quantum dots in a liquid medium

Researcher: Das, Saroj Kumar

Supervisor: Jasuja, Kabeer

Year: 2019

Keyword's: Quantum Dots, Liquid Phase Exfoliation, Ultrasonication, Analogous To Graphene, Chemical Composition

Call No.: 660 DAS

Acc. No.: T00511

Abstract: The ability to synthesize materials with nanoscale dimensions has transformed the science and technology of advanced functional materials. This is because nano-dimensional materials exhibit physical and chemical properties distinct from the properties characteristic to bulk forms. Furthermore, because these properties sensitively depend on the dimension of nanomaterials, a broad range of interesting properties can be realized. Based on dimensionality, the nanomaterials are classified as – zero-dimensional (quantum dots), one-dimensional (nanoribbons, nanotubes, and nanowires), two dimensional (nanosheets), and three-dimensional (nanoballs and nanocones). In this thesis work, we have reported the exfoliation of layered magnesium diboride (MgB_2) to enable the realization of quasi two-dimensional (2D) nanosheets comprising chemically modified boron honeycomb lattice. This thesis also reports a new insight about the process of liquid phase exfoliation, that we discovered inadvertently, and that led us to a method which can be used to synthesize 0D carbon quantum dots (CQDs); we have explained more about this in the following overview.

There are certain compounds in which the constituent atoms are arranged in the form of layers. In 2004, it was reported for the first time that from such a layered compound, it is possible to separate a single layer of atoms to realize a stable 2D material. This was demonstrated by isolating graphene, a single layer of carbon atoms, from its van der Waals bonded layered parent graphite. Inspired by graphene, the research focus is gradually shifting towards exploring layered materials in which the layers are more tightly bonded compared with van der Waals layered materials. Metal diborides (MB_2) represent one such family of strongly bonded layered materials in which metallic atoms are sandwiched in between boron honeycomb planes. Their chemical composition presents a rich opportunity to investigate the prospect of realizing quasi-2D forms of boron, analogous to graphene. One compound of particular interest belonging to this family of layered metal diborides is magnesium diboride (MgB_2), a material that has been primarily researched for its superconducting properties. In this thesis, we show that it is possible to exfoliate this non-van der Waals compound to synthesize a quasi 2D boron-rich material. We were able to achieve this through two main approaches explained as follows.

In the first approach, we show that MgB_2 can be exfoliated into few-layer-thick boron based nanosheets using forces generated by sonication-induced cavitation. In the second approach, we show that a step by step recipe involving chemical intercalation can be used to partly exfoliate MgB_2 and obtain multi-layer-thick (~300-400 nm) lamellae, which we referred as nanoaccordions as these resemble the shape of accordions. Subsequently, these nanoaccordions can be sonicated in water

to yield few-layer-thick boron-based nanosheets (~3-5 nm). We show that these nanosheets are photoluminescent and have an extremely small absorptivity. We also demonstrate that the nanoaccordions synthesized by us can be used to impart an extraordinarily high degree of flame retardancy to a polymer matrix that is otherwise flammable.

Although we were able to synthesize boron based nanosheets successfully using the above two approaches, we had found these to be densely functionalized by oxygen-based moieties. This functionalization had led to a transformation of their native chemistry and thereby limited the rich range of the properties inherent to bulk metal borides. Thus, we started exploring the possibility of nanoscaling without associated functionalization, such that we can obtain pristine nanosheets from MgB_2 . Because the functional groups were being acquired from the aqueous medium during ultrasonication, we hypothesized that if we select a solvent that does not contain oxygen as its constituent, the oxy-functionalization of these nanosheets could be minimized. In pursuit of this, we started exploring the exfoliation of layered metal diboride by ultrasonication in acetonitrile. We made an unexpected discovery when, as a control to the above experiment, we ultrasonicated only acetonitrile. We found that a simple ultrasonication of acetonitrile without any layered material results in the formation of photoluminescent carbon quantum dots. This finding contradicts an assumption routinely followed in the liquid phase exfoliation (LPE) strategies wherein it is presumed that ultrasonication of bare organic solvent would not have any effect on the molecules. There are no earlier reports that consider this important control experiment. Sonication within organic solvents is inherent to several research themes, and yet, the fact that this itself can lead to the formation of CQDs has remained unexplored. We observed that the CQDs which were forming had dimensions <10 nm and thickness in the range of ~3-4 nm. They were amphiphilic and exhibited blue, cyan, green, and yellow emissions depending upon the excitation wavelength.

In conclusion, the first aspect of the thesis work on exfoliation of metal diborides to yield boron based nanosheets and nanoaccordions have presented a new perspective to the science of metal diborides. The second aspect of the thesis work evidences that a mere sonication or shear mixing of organic solvents can enable the formation of CQDs. This addresses a major shortcoming in the liquid phase exfoliation strategies which involve ultrasonication of layered materials in organic solvents to synthesize 2D materials. Both these research aspects are expected to form seminal additions to the current state of knowledge on the synthesis of 2D materials.

Title: Boron based nanosheets from layered metal diborides: synthesis, physicochemical characterization and their nanoscale interfacing

Researcher: James, Asha Liza

Supervisor: Jasuja, Kabeer

Year: 2019

Keyword's: Chemical Engineering, Graphene Carbon's, Magnesium Diboride, Borohydride, Hydrogen Evolution Reaction

Call No.: 660 JAM

Acc. No.: T00541

Abstract: The isolation of graphene - carbon's famed two-dimensional allotrope - in 2004, inspired ground-breaking research in the field of two-dimensional materials. The unique properties of graphene and its versatile applications have inspired forays into other two-dimensional (2D) materials. While graphene remains the archetypal example of 2D materials, its incredible properties have inspired extensive research to develop analogous nanostructures. Boron, carbon's neighbor in the periodic table, has been seeking significant attention regarding the feasibility of its existence in planar forms analogous to graphene. The rising excitement associated with two-dimensionality has created new waves in the nanoscience of boron. Boron, being carbon's row neighbor in the periodic table, has also been envisioned to exhibit a similar 2D allotrope. Elemental boron possesses a host of unique properties – high melting point, low density and high hardness, moderate inertness to oxidation, and remarkable optoelectronic properties. 2D Boron has been in the limelight since 2015, when the first reports on the bottom-up synthesis of 'borophene' nanosheets were published. However, the synthesis of such boron based 2D structures has been restricted by experimental challenges and stability issues. Synthesis of boron nanosheets has been mainly limited to ultra-high vacuum, molecular beam epitaxy processes that are expensive and suffer from low yield. Although several theoretical studies predict the structures, stability, and feasibility of such quasi-planar forms of boron, their experimental realization remains challenging. The apparent absence of a suitable layered 3D precursor has precluded the top-down synthesis of boron sheets by exfoliation.

We present a fundamentally new perspective to this growing science of 2D Boron by proposing to use layered metal borides as starting materials towards the exfoliative synthesis of boron based nanosheets. Metal borides represent a family of layered compounds that are constituted of (graphene-like) honeycomb planes of boron sandwiched between hexagonal layers of metal atoms. Magnesium diboride (MgB_2) is a flagship compound belonging to this family of borides, a compound that rose to fame in 2001 owing to its superconducting properties. We hypothesized that suitable strategies to isolate these honeycomb boron planes from the bulk structure would enable access to boron in its quasi-planar forms. Hence, we proposed to utilize a "selective extraction" of magnesium ions from bulk MgB_2 using appropriate chelating agents to enable the delamination. To this end, we developed a novel chemical exfoliation strategy, which employs chelation by organic ligands to selectively extract the metal ions from layered MgB_2 in an aqueous medium, thereby causing delamination into few-layer-thick boron-based nanosheets.

These nanosheets are found to be metal-deficient in stoichiometry and are constituted of chemically functionalized boron honeycomb planes. The fundamental physicochemical properties of the boron-based nanosheets were established by extensive characterization. The morphological details were obtained from FESEM, TEM, and AFM studies. The chemical make-up was analyzed using FTIR, XPS, Raman, NMR spectroscopy. These uniquely functionalized nanosheets derived from metal borides offer interesting platforms to utilize the rich chemistry of nanoscaled boron. We were also successful in extending this approach to delaminate another layered metal diboride, namely AlB_2 .

Detailed chemical characterization indicated that the nanosheets possessed hydride, hydroxy, and oxy based functional groups. The presence of borohydride groups was a unique aspect because, in conventional chemistry, borohydride based reagents are well known for their chemically reducing property. We were curious to explore the possibility of whether the functional groups could confer a unique chemically active character to the nanosheets. We tested this by using an aqueous dispersion of nanosheets to reduce several organic and inorganic molecules. Carefully planned experiments to evaluate the action of the nanosheets on specific quinone to quinol conversions, revealed that the boron based nanosheets could reduce only a select range of compounds, namely those with a standard reduction potential >0.16 V (versus SHE) in a neutral aqueous medium. This ability was leveraged for synthesizing gold nanoparticles by an in-situ reduction of gold(III) chloride trihydrate in water by the nanosheets. Mixing these nanosheets with gold salt resulted in a spontaneous formation of ultra-small gold nanoparticles that subsequently anchor onto the nanosheets and form mixed-dimensional (0D-2D) heterostructures in solution. The nanosheets were shown to serve a dual role - as active chemical agents to reduce the Au^{3+} ions in the gold salt into Au^0 , and as swimming templates to stabilize the nanoparticles. We were also able to achieve a similar reduction of two more noble metal salts (silver nitrate and chloroplatinic acid hexahydrate) to obtain silver nanoparticle and platinum nanoparticle decorated nanosheet hybrids. This process neither required any reducing-stabilizing chemical nor an external inducing aide like sonication, electrochemical, or thermal treatment. Our initial experiments indicated that the noble metal nanoparticle-nanosheet hybrids are excellent electrocatalysts for hydrogen evolution reaction.

We went on to demonstrate that these nanosheets can also reduce graphene oxide to reduced graphene oxide, subsequently forming quasi-2D boron-carbon nanohybrids. This is the first report on interfacing boron planes with graphene, that too, in an aqueous solution. The concurrence of reducing nature and planarity makes these nanosheets an intriguing alternative over conventional reducing agents. A wide range of possibilities can be realized by employing these as nanoscale reagents, as well as building blocks towards assembling heterostructures with other low-dimensional systems. Such a method for the colloidal assembly of heterostructures in solution is of immense practical merit considering that while newer 2D materials are being discovered, there is also a surging interest in combining these with other nano-dimensional materials to create heterostructures which exhibit a synergistic blend of the constituent properties.

Despite these unique possibilities, the chelation assisted exfoliation had a major limitation, namely the relatively low yield ($\sim 7\%$). In terms of using the nanosheets in practical applications, it is imperative to be not limited by the yields, and hence there is a requirement for efficient, low- cost, and scalable methods for synthesis. In order to circumvent this challenge and make a substantial

amount of boron based nanosheets available for exploring practical applications, we developed an aqueous peroxy route towards synthesizing nanosheets from another metal boride titanium diboride (TiB_2). The one-pot synthesis employs hydrogen peroxide (H_2O_2) as the chemical oxidant and achieves processable aqueous dispersions of nanosheets derived from TiB_2 , in high yields of up to 3 mg/ml.

Interestingly, we encountered some unexpected observations while performing detailed electron microscopic characterization of the nanomaterials. We found that TiB_2 undergoes a reaction with H_2O_2 to form peroxy-titanium and peroxyborate complexes, which act as molecular precursors in synthesizing the nanostructures. Hence, contrary to our initial hypothesis of exfoliation, this route presented a bottom-up approach towards synthesizing the boron based nanomaterials, wherein condensation of the peroxy species into oligomeric units and their subsequent self-assembly into low dimensional structures (as revealed by TEM studies) is the possible growth mechanism. These nanostructures also exhibit a unique gelation behavior as well as the tenacity to be assembled into free-standing hierarchical macrostructures. These hydrogels and paper-like macrostructures are a timely development in the growing science of nanomaterials derived from metal borides. The possibility of using the nanosheets as building blocks towards assembling such hierarchical 3D structures enable smoother transition into the realm of applied studies.

We anticipate that the synthesis approaches demonstrated by us can provide an additional impetus to the recent advances in realizing boron based quasi two-dimensional materials and open up newer avenues to utilize their rich chemistry. We expect that a detailed elucidation of the unique characteristics of these nanosheets would enable rational incorporation of these nanomaterials in a broad spectrum of applications, especially in supercapacitors, plasmonics, hydrogen storage, catalysis, and sensing.

Title: Engineering pharmaceutical formulations for modulated release of NSAID and anticancer drugs
Researcher: Varghese, Sophia
Supervisor: Ghoroi, Chinmay
Year: 2020
Keyword's: Improving Dissolution, Dry Calcination, Bio-based Nano-carrier, Control Release, pH Responsive, Biopolymers
Call No.: 660 VAR
Acc. No.: T00542

Abstract: The major challenge for pharmaceutical industries is effective drug delivery. While the low solubility of Active Pharmaceutical Ingredient (API) results in poor bio-availability, and the burst release of highly soluble API causes toxicity to the body. Hence, improving the dissolution and modulating the release of these drugs with simple, green techniques especially using bio-based nano-carriers, is of great interest. The current work presents both the aspects of improving the dissolution of BCS class II drugs and control release of the anticancer drugs as well as Non-Steroidal Anti-Inflammatory Drugs (NSAID). The model drugs used in the study are ibuprofen (IBU) as NSAID drug and doxorubicin (DOX) as an anticancer drug. The improvement in wetting and dissolution of hydrophobic drug ibuprofen is carried out by a solventless co-milling approach (solid dispersion) using hydrophilic Micro Crystalline Cellulose (MCC) in a planetary ball mill. The dissolution studies are carried out using the USP Paddle type II apparatus. The results exhibited a reduction in contact angle from 60.6° to 18° indicating improved wetting and the increase in dissolution up to 96 % in 90 min as compared to 59 % of only ibuprofen. The improvement in wetting and dissolution is attributed to the changes in crystal level properties such as increased dislocations, defects, and a decrease in crystallite size and surface properties such as the increase in polar surface energies and the basicity on the surface of ibuprofen. The study shows that appropriate changes in crystal level property and surface-level property can play a crucial role in improving the wetting and dissolution of BCS class II drugs.

For control release studies, the conventional method includes solvent-based approaches with a multi-step process to host the nanoparticles in the carbon-based matrix. In the present work, the bio-based nano-carrier is developed for control release application using the one-step dry calcination process without the usage of any solvents. The newly developed material is explored in detail using different characterization techniques. The developed nano- biocomposite (nano Fe-CNB) is a carbon-based layered material of thickness 7-8 nm with Fe-based nanoparticles of 5-10 nm embedded in it. The nano Fe-CNB is porous in nature, with the surface area of 184.2 m²/g and a pore diameter of 3.19 nm. It exhibits pH and magnetic responsive behaviour and is thermally stable. The presence of Fe₃O₄, α-Fe₂O₃, and graphitic carbon in nano Fe-CNB is confirmed by P-XRD, Raman spectroscopy, and SAED pattern of HR-TEM. Due to the pH and magnetic responsive behaviour of the nano Fe-CNB, the developed material is incorporated in the biopolymeric matrix alginate (CA) for the controlled release of anticancer drug DOX. The nano Fe-CNB exhibits higher DOX loading ~ 94 % and control release, i.e., ~8 % of DOX release in physiological pH (7.4) and enhanced release of DOX ~38 % in the tumour cell pH (5.4) at the end of 2 days. The *in-vitro* HeLa cell line studies indicate the slow and controlled release of DOX from the DOX-loaded Fe-CNB alginate matrix into the nucleus

of the cells. The cell viability assays further confirm more viable cells (~ 63 %) as compared to free DOX (~ 43 %) at the end of 24 h. Thus, the results indicate the superiority of the developed bio-based nano-carriers.

An alternative formulation for the controlled release of DOX using mesoporous silica nanoparticle (MSN) is proposed using a simple electrostatic Layer by Layer (LbL) technique. To develop a bio-compatible core-shell matrix, the bi-layer coating of DOX loaded in MSN is performed using charge reversal biopolymers. The coating of positively charged amine groups of chitosan followed by negatively charged carboxyl groups of sodium carboxymethyl cellulose. The encapsulation efficiency of the DOX loaded the core-shell matrix is observed to be ~ 93 %. The controlled release of DOX is observed from the core-shell matrix, ~ 21 % release in 7.4 pH, and improved release of ~ 67 % in 5.4 pH, respectively, at 48 h. Further, the studies are extended to an *in-vitro* cell line using MDA MB 231 cells. The results confirmed the controlled release of DOX from the core-shell matrix. In addition, the cell viability assay confirmed more viable cells (~76 %) from the engineered core-shell matrix as compared to free DOX (~ 49 %) at the end of 24 h. Thus, the developed bio-compatible formulation of the core-shell matrix by the LbL technique is capable to guard the pores of MSN and prevents the premature release of DOX and thereby attains the controlled release of DOX.

The newly developed nano-biocomposite (nano Fe-CNB) is further used for the controlled release of ibuprofen (NSAID) required at certain chronic conditions such as post-operation, colon targeting, rheumatoid arthritis, etc. The nano Fe-CNB is incorporated into the biopolymeric alginate hydrogel matrix and β -CD alginate matrix to introduce hydrophobic sites and pH responsive behaviour. The incorporation of nano Fe-CNB into the alginate hydrogel matrix enhances the drug loading of IBU from ~ 23 % to ~ 45 %. The nano Fe-CNB impregnated hydrogel matrix exhibited pH responsive behaviour with less release of drug at initial 2 h, ~ 20 % in stomach pH (1.2) and improved release of ~ 49 % in physiological pH (7.4) at the end of 12 h. This formulation makes it more suitable for colon targeting drug delivery due to the ability of β -CD and alginate to protect the GI tract and mucosal lining. The incorporation of β -CD into alginate matrix (without nano Fe-CNB) enhances the IBU loading but does not exhibit pH responsive behaviour. The viscoelastic property of the hydrogels exhibits, the gels having higher viscosity have a higher swelling ratio. Moreover $G' > G''$ is observed for formulations independent of frequency sweep and time indicating the gel-like behaviour. The pH-dependent swelling ratio studies exhibit that all the formulations are intact in stomach pH 1.2 irrespective of the polymeric concentration. Thus, the prepared hydrogel formulations, which are pH responsive, are best suited for the controlled release of hydrophobic NSAID ibuprofen.

Thus, overall the thesis provides different engineered formulations for improved dissolution of hydrophobic drug IBU (NSAID) and control release of anticancer drug DOX as well as NSAID-IBU. The thesis proposes the solid dosage formulation for improving the dissolution of hydrophobic drug ibuprofen using the solventless co-milling technique. It shows that the co-milled mixture exhibits improved dissolution due to the changes in crystal level and surface properties. The newly developed bio-based nano-carrier prepared with one step dry calcination process exhibits pH and magnetic responsive behaviour and is thermally stable. The nano-carrier impregnated biopolymeric hydrogel matrix exhibits a controlled release of DOX at physiological pH. Thus, the formulation helps to minimize the side effects associated with burst release at physiological pH with anticancer drugs.

Further, an engineered formulation of a bio-compatible core-shell matrix using MSN is developed for the controlled release of DOX. The developed formulation helps to prevent the premature release of DOX from the pores of MSN and maintain minimal release at physiological pH (7.4). At the same time, it releases higher ~ 67 % of DOX at the cancer cell pH (5.4). The thesis also proposes a formulation to increase the loading of hydrophobic drugs in the hydrophilic matrix and achieve control release of NSAID drugs. The nano Fe-CNB incorporated biopolymeric alginate hydrogel matrix in combination with β -CD enhances the hydrophobic drug loading capacity at the same time the formulation also exhibits pH responsive behaviour. The drug releases in a minimum amount ~ 21 % in stomach pH (1.2) followed by control release at physiological pH (7.4). This indicates it is suitable for application in protecting the GI tract and mucosal lining and colon targeting drug delivery.

Title: Role of engineered nanoscale surface roughness for tuning the wetting behavior of micron-size particles
Researcher: Dixit, Deepa
Supervisor: Ghoroi, Chinmay
Year: 2020
Keyword's: Nanoscale Surface Roughness, Surface Chemistry, Surface Wettability, Water Disinfection, Anti-bacterial Surface
Call No.: 667 DIX
Acc. No.: T00549

Abstract: There is a growing interest in designing wetting and non-wetting surfaces using micro or nanoscale roughness (or combination of both) for various industrial applications like antibacterial surfaces, anti-corrosion surfaces, oil-water separations, etc. This dissertation studied the role of micro/nanoscale engineered surface roughness on the wettability of particles and flat surfaces for various applications in powder processing, water disinfection, and antibacterial surfaces. The surface is engineered via three approaches: (a) inert gas plasma surface modification, (b) chemical etching, and (c) photolithography tool.

The individual contribution of surface roughness and surface chemistry in transforming surface wettability is discussed in detail. The surface characterization is carried out using state of the art facilities, and the potential applications are demonstrated. While the surface morphology/topography is visualized and quantified using Scanning Electron Microscope (SEM) and Atomic Force Microscope (AFM), respectively, the surface chemical composition is studied using X-ray Photoelectron Spectroscopy (XPS) analysis. The changes in the wetting characteristic of the surfaces are measured using the contact angle (CA) analysis via a sessile drop method.

The first approach explores inert gas (Argon) plasma surface modification to improve the wettability of pharmaceutical powders (cornstarch and ibuprofen). The powder and pellets are exposed to the Argon (Ar) plasma for different time intervals (5 min to 20 min) at optimized pressure and voltage. AFM and XPS results show that during initial exposure, new active sites are build-up, and the surfaces become more hydrophilic. Further exposure to the plasma (> 5min) damages the active sites, and no significant improvement in wettability is observed. Based on the obtained results, wetting behavior for both powders is divided into two distinct regimes. The regime I (up to 10 min) corresponds to the change in surface groups where surface spreading and work of adhesion increases very rapidly. In regime II (beyond 10 min), spreading is mainly due to the combined effect of surface groups and nanoscale surface roughness.

In the second approach, the first of its kind highly hydrophobic surface engineered particles (SEP) is designed directly from hydrophilic soda-lime-silica particles (referred to as original particle) using alkali treatment (without coating with low surface energy material). The XPS study points out that alkali treatment of particles not only alters the surface topography of SEP but also induces Si-OH, which is expected to turn the SEP surface into a more hydrophilic surface. In contrast, the advancement in CA from 79° to 147° with strong solid-liquid adhesion shows the dominating role of engineered nanoscale roughness over the limited influence of surface functional groups. The

silanization of the OP and SEP confirms that an increase in CA from original particle (OP)~79° to silanized original particle (Si-OP)~113° portrays the role of surface chemistry (larger RMS roughness and higher peak-to-peak distance). The further gradual rise in CA from Si-OP~113° to SEP100~147° (SEP100 referred to surface engineered particle treated with alkali for 100 mins) is due to the governing role of smaller RMS roughness and minimum peak-to-peak distance.

Further, the developed hydrophobic SEP are explored for its usage as a low-cost, gravity- driven, and non-electric water filter for point-of-use (POU) water disinfection. We discovered that the SEP-based filter has the remarkable potential of arresting the 99.48% (~ 2 to 2.5 log₁₀ reduction) of gram-negative bacteria *Escherichia coli* (*E. coli* OP50) on its surface from the water containing 3×10⁸cells/ml. The performance of the SEP bed filter corresponds to the nanoscale surface roughness, its distribution along with the surface charge, and surface hydrophobicity that is favorable to attract and adhere to the bacteria in the water passing through the bed. Moreover, the SEP surface with 0.05 mM Ag⁺ loading (SEP+) completely inactivates (> 99.99999%) bacteria and protects any bacteria recontamination in the purified water. Besides, it eliminates any health hazard due to low silver leaching in the purified water.

In the last approach, the wettability and bacterial adhesion are correlated to the surfaces that are designed in a precise manner using photolithography where surface feature size is kept much larger than the bacterial size (unlike previous studies features size ≤ bacterial size). The study shows that smaller spacing (P~30 μm) and lower aspect ratio leads to the hydrophobic contact angle (132°≤CA≤138°) with strong solid-liquid adhesion (solid-liquid fraction: f~0.562, Wenzel wetting state) at the interface. The antibacterial test showed that the high solid-liquid contact area provides a highly accessible area to bacteria, which in turn leads to higher bacterial adhesion on the surface. Whereas, the higher aspect ratio (height to width~3.5-4.5) with large spacing (P~130 μm) mitigates the bacterial adhesion that corresponds to the superhydrophobic nature (Cassie-Baxter wetting state) of the surface. The results are implicated in the low solid-liquid fraction (f~0.035), which allows air to form cushion beneath the droplet and repels the bacterially contaminated droplet to pin the surface. Besides, the anti-adhesion potential of the superhydrophobic surface for the long-term is tested, and results indicate strong stability for the surfaces designed with large spacing and higher aspect ratio. Thus, the thesis demonstrated the surface design specifications for its usage in designing the biosensors, tools used in hospitals, surgical instruments, microfluidics, etc. to avoid chronic bacterial infections.

Title: Butylated urea formaldehyde resins: reaction mechanisms, kinetic model and multi-objective optimization based reactor design

Researcher: Amin, Shital A.

Supervisor: Padhiyar, Nitin

Year: 2020

Keyword's: Amino Resins, Urea Formaldehyde (UF) Resins, Butylated Urea Formaldehyde (BUF), Gas Chromatography

Call No.: 668 AMI

Acc. No.: T00721

Abstract: Amino resins are widely used as a cross-linking agent with primary film formers (such as alkyd, polyester, epoxy and acrylics resins) in paint and coating industries. They are made from substrates that have an amino (-NH₂) group, including urea, melamine, benzoguanamine, and glycoluril. In each case, amino resins for coatings are prepared by reacting the amino group with formaldehyde to form methylol intermediate and then reacting the resulting methylol groups at least partly with alcohol (R-OH) to form alkylated ether groups. When the coating is cured, the methylol or alkylated ether groups react with hydroxyl, carboxyl, urethane (carbamate), or amide groups of co-resins, to form a cross-linked network in surface coating application. It has been known that modified Urea Formaldehyde (UF) resins for cross-linking have a significant impact on the properties of the cured films.

UF is usually treated with butanol for its diverse applications in the paint and coating industry. The extent of butylation of UF plays a crucial role in the end applications of such butylated UF (BUF) resins. Moreover, BUF resins exhibit excellent water-resistant properties due to the presence of butyl/alkoxy groups in its molecular structure. Such BUF resins are typically synthesized in two steps via addition and condensation reactions. During the addition step, methylol and butylated methylol intermediates are formed, and these intermediates subsequently polymerize to form oligomers, in the second step, via condensation reactions through methylene (-CH₂-) linkages. Here a detailed reaction mechanism has been developed for the BUF synthesis and develop the kinetic model for the addition and condensation steps. The species in the reaction mechanism are represented in a generic fashion, and thus, the mechanism can be utilized not only for the BUF reactions but also for the synthesis of other amino resins. Additionally, the kinetic model is developed based on the experimental data obtained from a semi-batch reactor with transient conditions of pH, Bu addition and water removal during the synthesis. Finding in this work suggests approximately 2% Bu is consumed during the addition reactions, while 37.92% of Bu is consumed during the condensation reactions indicating that the low pH favors butylation reactions. Further, it has been demonstrated that the predictions from the kinetic model match with the experimental observations for reaction synthesis under different initial conditions. Therefore, the proposed model is further employed in predicting useful resins property, such as molecular weight distribution.

The proposed kinetic model is employed for designing the batch operation for the synthesis of resins with tailor-made properties. However, please note that owing to the complex kinetics involved in their synthesis, it has been a challenge to establish multiple design criteria for optimum reactor operations. For instance, for better water-resistant properties and for synthesizing specialty

nanocomposites, from BUF, maximum butylation and maximum X- condensates ($-\text{CH}_2\text{-O-CH}_2\text{-}$ linkages) are respectively required, along with minimum formaldehyde. Therefore, multi-objective optimization approach is employed to establish optimal trade-offs among various mutually conflicting objectives. In particular, process design criteria are established by performing 2 and 3 objective optimizations and demonstrate that the latter provides wider range of choices and better trade-offs for reactor operation compared to the former. For instance, 9.24% and 3.21% improvements in $F(t_f)$ and t_f are observed for 1% compromise in $\text{Bu}(t_f)$. Further, optimal temperature trajectories are also calculated and reaction times to achieve these objectives. Bi-objective optimization results are shown for the simultaneous maximization of X-condensate and butylation.

The finding suggests, maximum X-condensates in the resins result in minimum butylation and therefore, reduces the water- resistant properties of the BUF resins. Three representative trade-off solutions are also shown, which represented by points, A, B, and C corresponding to maximum butylation, maximum X- condensates, and equal compromise between the two respectively and also represented the corresponding optimum temporal temperature trajectories. The findings in this work can be utilized to determine operating conditions for optimizing the resin quality of particular specifications. For instance, it is possible to determine process conditions that can enable the BUF resins with higher X-condensates (species with $-\text{CH}_2\text{-O-CH}_2\text{-}$ linkages). Aforesaid X- condensates are important for the production of specialty resins that offer possibilities for grafting nanomaterials by utilizing the oxygen functionality present in these linkages. On the other hand, for synthesizing BUF resins with better impact resistance, water resistance, chemical resistance, solvent compatibility, and pot life, one can enhance the degree of butylation by operating reactor. On the other hand, methylol functionality can be increased for enhanced hardness, cross-cut resistance, and decreases the cure time.

Title: Design of self-oscillating chemical reactions catalyzed by nanoparticle-graphene composites and their utility in locomotion, sensing and detection

Researcher: Kumar, D Jaya Prasanna

Supervisor: Dayal, Pratyush

Year: 2020

Keyword's: Belousov-Zhabotinsky (BZ) Reaction, Chemical Oscillations, Nanoparticle-graphene, Composites, Thermodynamics

Call No.: 660 KUM

Acc. No.: T00722

Abstract: Designing synthetic systems to exhibit features similar to living systems has been one of the grand challenges in the field of science and engineering. Specifically, the biochemical oscillations and motions in living systems have been performing specific tasks with utmost efficiency. This efficient conversion of chemical energy to mechanical actions in living systems has aroused significant impetus to research aimed at developing synthetic systems. Recently researchers have succeeded in developing self-oscillating polymer gels using unique properties of the oscillatory Belousov-Zhabotinsky (BZ) reaction that undergo sustained mechanical oscillations. Precisely, the intrinsically powered chemical oscillations of the BZ reaction induces the mechanical oscillations and motion of the droplet.^{1,2} Till today, BZ gels are popularly known materials that transduce chemical energy to mechanical work. The objective of the present work is to tune and harness the phenomenon of the BZ catalyst that occurs at minuscule to realize its applications in diverse fields. Specifically, we utilize the unique properties offered by nanoparticles decorated graphene-based 0D-2D heterostructures as a multi-functional catalyst for the BZ reaction. Since, BZ reaction is comprised of redox states of the catalyst, incorporating electron-rich graphene, we believe that the frequency of chemical oscillations can be significantly increased.

In the present investigation, we manipulate the oscillatory dynamics of the BZ reaction by incorporating graphene-based nanosheets, namely graphene oxide (GO), reduced graphene oxide (rGO), and graphene as a promoter for the commonly used catalyst. Additionally, we also incorporated composites of ceria and ruthenium decorated nanoparticles on GO, rGO, and graphene as a catalyst. The BZ reaction catalyzed with composites demonstrated a significant increase in oscillating frequency in comparison with the bare nanosheets. The increase in the oscillating frequency of the BZ reaction is attributed to the rapid shuttling of electrons on the highly conductive graphene, which brings about a rapid transition in the redox states of the catalyst, i.e., oscillating frequency. We validated these results using a three variable Oregonator model and found that the nanoparticle decorated graphene specifically enhances the rate constant k_5 , i.e., the reduction rate step of the metal ion catalyst. The enhanced rate constant k_5 , in turn, influences the rates of all the other processes of the BZ reaction and ultimately increases its oscillating frequency. Further, we also estimated the activation energy of the ceria nanoparticle decorated graphene and the estimated values are lower than the activation energy of the commonly used solution-based cerium catalyst. Thus, the lower activation energy denotes higher reaction rates and thus the increase in oscillating frequency.

Having realized the enhance in the oscillating frequency, we further move on to incorporate these BZ nanocatalysts (nanocomposites) to augment the speed of the BZ reaction droplet in the oil-surfactant medium. Here, the droplet motion is due to the reaction between the bromine, an intermediate of the reaction, and the surfactant. The reaction generates an imbalance in surface tension over the droplet which in turn brings about the spontaneous droplet motion. Our results show an ~20-fold increase in velocity than it is reported in the literature. An increase in oscillating frequency with the previous experimental results suggests that an increase in bromine production is possible, which is a fuel for the BZ reaction. Finally, we have used the oscillatory Briggs-Rauscher (BR) reaction to quantify the antioxidants in the organically and commercially grown foods by measuring the magnitude of cessation of oscillations (inhibition time) using image processing methodology.^{3,4} Organically grown foods are known for their high antioxidants in comparison with the commercially grown counterparts, and our results demonstrate higher antioxidants with organically grown foods.⁵ In essence, we have demonstrated that the dynamics of the oscillatory BZ reaction are tailored with the nanoparticle decorated graphene-based nanosheets.

Title: Particle formation of poorly water soluble drugs & their incorporation into polymeric films for enhanced oral & transdermal drug delivery

Researcher: Pandey, Komal

Supervisor: Dalvi, Sameer V.

Year: 2020

Keyword's: Active Pharmaceutical Ingredients (API), Biopharmaceutical Classification System, Drug Administration, Thermogravimetric Analysis

Call No.: 660 PAN

Acc. No.: T00723

Abstract: Active Pharmaceutical Ingredients (APIs) are the main components of drug delivery systems. The physical characteristics of APIs such as particle size, size distribution, polymorphic form and crystallinity play a crucial role in the effectiveness of APIs. These properties not only affect the powder flow behavior but also significantly influence the dissolution rates and hence their bioavailability. Nearly 40% of the New Chemical Entities (NCEs) identified by the pharmaceutical industry fall in the category of being poorly water soluble, i.e. in Biopharmaceutical Classification System (BCS) class II and IV drugs. Poor aqueous solubility of drugs and limited drug absorption results in poor bioavailability which is the major problem encountered during pharmaceutical formulation development. This work was therefore focused on enhancing the efficacy of poorly water soluble drugs by formulating these (BCS class II and IV) drugs as ultrafine particles in aqueous suspensions and incorporating drug particles into polymeric films for effective transdermal drug delivery. Reduction in particle size increases the interfacial area for dissolution and hence enhances drug dissolution rates and increases the effectiveness of drug action. Further, the use of drug loaded films can improve the bioavailability since the polymeric films can either be used for transdermal drug delivery or for sublingual delivery. Such a route of drug administration can take advantage of highly vascularized nature of oral or buccal mucosa where drug can directly enter into a systemic circulation without having to pass through hepatic first-pass metabolism.

In this thesis, Fenofibrate and Curcumin were used as model drugs. Fenofibrate is a lipophilic drug used to lower cholesterol levels in blood whereas Curcumin is a naturally occurring ingredient found in turmeric (*Curcuma longa*). Curcumin is known to exhibit anti-inflammatory, antimicrobial and anticancer properties. Liquid Anti-Solvent (LAS) precipitation technique was used to produce aqueous suspensions of drug particles and different grades of hydroxyl propyl methylcellulose (HPMC) were used to produce polymeric films loaded with drug particles. These films were then evaluated for their effectiveness for *in-vitro* drug release.

Sonoprecipitation of fenofibrate was carried out in the presence of different additives. The particle size and morphology were found to be significantly affected by mixing conditions and the use of additives. In order to understand the mechanism by which additives control fenofibrate particle growth and affect particle morphology, intermolecular interactions between additive and fenofibrate were simulated using molecular dynamics simulations. HPMC was found to be the most suitable additive to produce submicron particles while ultrasound helped in stabilizing fenofibrate particles in all the cases. Powder X-ray Diffraction (PXRD) analysis indicated no polymorphic change in the precipitated fenofibrate particles where all the precipitated fenofibrate particles were found

to be Form I particles, a stable polymorphic form of fenofibrate. Particles precipitated with Tween 80 exhibited a needle-like morphology whereas fenofibrate particles precipitated with HPMC and Polyvinyl Pyrrolidone (PVP) showed a plate-like morphology. The particles precipitated with Bovine Serum Albumin (BSA) resulted in a mixture of rod and plate-like morphology. The dissolution rate of fenofibrate particles precipitated with additives and ultrasound was highest (about 99% in 6 hrs) as compared to the fenofibrate particles precipitated with additives and without ultrasound. Thus, HPMC was found to be the most effective additive for FNB while PVP was found to be the least effective additive.

Understanding the thermodynamic stability relationship among polymorphs of API is a necessary step for drug formulation development. Knowledge of such relationship enables identification of a stable polymorphic form at the prevalent conditions. Curcumin, a pharmaceutically active ingredient found in herbal spice turmeric, exists in three polymorphic forms; a monoclinic form (Form 1) and two orthorhombic forms (Form 2 and Form 3). However, thermodynamic stability relationships among curcumin polymorphs have not been ascertained yet. One part of the work was therefore focused on understanding thermodynamic stability relationships among curcumin polymorphs. During purification of curcumin, the pressure applied for vacuum evaporation of organic solvent was found to significantly affect the polymorphic outcome. Curcumin Form 2 was found to precipitate when the vacuum pressure in the range of 100-200 mbar was used whereas Form 1 was obtained when pressure in the range of 300-400 mbar was used. Thus, higher pressure was found to result in the nucleation of a stable form (Form 1) which also involves significant hydrogen bonding among curcumin molecules whereas lower pressures were found to facilitate nucleation of a metastable form (Form 2) in accordance to the Ostwald rule of stages. Application of the Burger and Ramberger rules such as heat of fusion, entropy of fusion and heat of transition rules indicates that the thermodynamic stability relationships among the curcumin polymorphs are of monotropic type with Form 1 being the most stable form. The irreversible transformations of Form 2 to Form 1 and that of Form 3 to Form 1 confirmed through DSC heating and cooling cycles and variable temperature XRD studies further prove that monotropic relationships exist between Form 1 and Form 2 and Form 1 and Form 3. Also, Solution Mediated Transformations (SMT) of polymorphic mixtures at 0, and 25 °C to Form 1 confirm that Form 1 is the most stable form among all three forms. The van't Hoff plot prepared based on the solubility of curcumin polymorphs in ethanol did not show any point of intersection between the solubility curves of these polymorphs which once again confirms that these polymorphs are monotropically related to each other. It can therefore, be summarized that the curcumin polymorphs are monotropically related to each other and the monoclinic form (Form 1) is the most stable form among three curcumin forms.

One aspect of the work was carried out to demonstrate that continuous LAS precipitation process can successfully produce aqueous suspensions of ultrafine particles of curcumin with narrow size distribution and desired polymorphic form. The use of ultrasound during precipitation process has a tremendous impact on particle size, size distribution, polymorphic form, and suspension stability. It prevents uncontrolled particle growth due to annealing of particle surface and also decreases the mixing time and increases the nucleation rates during LAS precipitation. Mixing time obtained during precipitation with ultrasound is 100 times lower than that without ultrasound. The polymorphic form of the precipitated particles can also be controlled by using ultrasound and additive.

Orthorhombic curcumin form was found to precipitate when ultrasound and additives were used and a monoclinic form was found to precipitate when precipitation was carried out without ultrasound and additives. The observations made in this work demonstrate that by the judicious choice of additives and different process conditions like sufficient use of ultrasound, a highly scalable continuous LAS precipitation process can be developed to produce ultrafine particles of curcumin with desired particle size and polymorphic form. Further, this process can also be used for continuous precipitation of other poorly water soluble drugs.

Next, we focused on precipitation of ultrafine particles of curcumin polymorphs at higher drug loading and their incorporation into polymeric films for transdermal drug delivery. Curcumin polymorphs i.e., Form 1 (monoclinic), Form 2 (orthorhombic) and Form 3 (orthorhombic), was precipitated using LAS precipitation incorporated into polymeric films in order to test their efficacy for transdermal drug delivery. Curcumin particles obtained at higher curcumin concentrations from acetone solutions in presence of ultrasound and additives were found to precipitate as stable Form 1. However, the particles obtained at high curcumin concentrations from DMSO solutions (with ultrasound and additives) were found to precipitate as metastable Form 3. The cytotoxicity of curcumin polymorphs was studied on SK-MEL 28 cell line. The free radical scavenging activity of Form 3 was found to be highest, followed by Form 2 and Form 1. Form 3-loaded films showed higher release profiles, both at the pH of 5.5 and 7.4. These studies imply that wound healing might accelerate for Form 3 loaded films as compared to Form 2 and Form 1 loaded films and that the films prepared in this work are suitable candidates for transdermal drug delivery.

To summarize, this work provides a basic understanding of particle formation process which can be used to control the particle morphology and polymorphism of poorly water- soluble drugs during LAS precipitation. It was found that particle size, polymorphism and morphology can be altered by mixing conditions and the use of additives both at batch and at a continuous mode of precipitation. Thus, judicious choice of precipitation conditions can significantly impact and modulate the dissolution profiles of the precipitated drug particles. This work also presents a systematic evaluation study to assign thermodynamic stability relationship between the polymorphs which is very important in understanding the occurrence domains of several polymorphs. Moreover, it is shown that the patches made of HPMC [with triethyl citrate (TEC) as a permeation enhancer] serve as an effective drug carrier for curcumin in the transdermal drug delivery. Curcumin Form 3 exhibits the highest release and permeation profiles among all the curcumin polymorphs studied in this work.

Title: Crystallization of active pharmaceutical ingredients: implications of intermolecular interactions on morphology and polymorphism
Researcher: Prasad, Rupanjali Gurprasad
Supervisor: Dalvi, Sameer V.
Year: 2020
Keyword's: Active Pharmaceutical Ingredients, Griseofulvin, Carbamazepine, Curcumin
Call No.: 660 PRA
Acc. No.: T00724

Abstract: The overall objective of this work was to understand how the intermolecular interactions between drug molecules, solvent and additives during crystallization affect the morphological and polymorphic behaviour of poorly-water soluble active pharmaceutical ingredients (APIs). In this work, three polymorphic APIs namely griseofulvin (anti- fungal), carbamazepine (anti-epileptic) and curcumin (anti-cancer) were used as model drugs. Liquid antisolvent (LAS) technique was used to precipitate drug particles under different mixing conditions (ultrasound vs stirring) and with different additives. Different hierarchical structures of griseofulvin (GF) were obtained under stirred conditions and in the presence of additives. An umbrella like morphology was obtained with hydroxypropyl methylcellulose (HPMC), hexagonal particles elongated along the c- axis were observed with Tween 80 and the use of polyvinylpyrrolidone (PVP) yielded long needle-like particles. Moreover, the use of bovine serum albumin (BSA) gave rise to interesting six-branched hierarchical structures, which are seldomly reported for API molecules. An aggregation-based pathway followed by ostwald ripening and directional secondary nucleation influenced the formation of GF structures.

LAS precipitation of carbamazepine (CBZ) was carried out from its solution in an ionic liquid, [BMIM][Cl], in the presence of HPMC, BSA and PVP with and without sonication. In-situ Raman spectroscopy revealed that the Dihydrate (DH) form of CBZ precipitates from the ionic liquid (IL) solution. Further analysis showed that DH CBZ underwent dehydration during freeze-drying and transformed selectively to anhydrous Form III (P- monoclinic) and Form I (triclinic) in the absence and presence of additives respectively. The presence of additives impeded the formation of CH...O CBZ dimers that are essential for stabilization of Form III, thereby “kinetically entrapping” the metastable Form I during dehydration. Hierarchical structures of CBZ were also observed which seemed to be a result of a non-classical pathway followed by secondary nucleation and growth.

The last part of the work was focused on elucidating polymorphic behaviour of curcumin (CUR). LAS Precipitation from acetonitrile yielded stable Form 1 while, ethanol led to the precipitation of Form 3. In-situ Raman spectroscopy revealed the presence of twisted curcumin clusters interacting through the phenolic ends (like Form 1) in acetonitrile while parallel stacks of curcumin molecules (like Form 3) dominated in ethanol. These clusters facilitated the formation of structurally similar curcumin polymorphs. The existence of these solvent induced curcumin clusters was further validated using computational tools such as density functional theory (DFT) and molecular dynamics (MD) simulations. The understanding developed experimentally and computationally was further validated using two additional solvent systems, acetone and methanol which led to the formation

of Form 1 and 3 respectively during LAS precipitation. Finally, a quantitative framework was presented to predict the polymorphic outcome across these solvents.

The results presented in this work demonstrate that the intermolecular interactions can be manipulated to obtain the desired morphological or the polymorphic outcome of APIs by a careful selection of additives or the solvents. The work also demonstrates that the extension of these methodologies to other APIs could enable better control over characteristics of drug particles.

Title: Rheology and microstructure of fumed, colloidal particles suspended in isotropic and anisotropic media: role of particle shape, surface chemistry and applied external fields

Researcher: Kumar, Saket

Supervisor: Thareja, Prachi

Year: 2020

Keyword's: Particulate Suspensions, Isotropic Dispersing Media, Anisotropic Dispersing Media, Silica Particles

Call No.: 660 KUM

Acc. No.: T00725

Abstract: The fundamental understanding of the behaviour of particulate suspensions in isotropic and anisotropic dispersing media is of critical importance for applications pertaining to hydraulics, robotic, microfluidic, sensory and display devices. While the isotropic silicone oil enables instantaneous polarization of electrically polarizable particles to form chain-like structures in the direction of an electric field (E), incorporation of particles in an ordered matrix of anisotropic liquid crystals (LCs) leads to the generation of different self-assembled structures. The present thesis systematically investigates the interplay of different factors controlling the rheology, structure and phase behaviour of suspensions. Two types of dispersing media are explored in this work: 1) the isotropic silicone oil and 2) Nematic LCs (NLCs) having rod-like molecules with only orientational order.

The first aim of the thesis is to understand the effect of addition of fumed alumina (Al_2O_3) nanoparticles (primary particle size ~ 21 nm) in silicone oil medium on the rheology, electrorheology and structure of Al_2O_3 /silicone oil suspensions. Our results demonstrate that in the absence of E, the suspensions form gels at and above the nanoparticle loading of 10 wt%, resulting in plateau of G' (storage modulus) at the low angular frequency (ω). We further show that these suspensions are extremely sensitive to the pre-shearing history and exhibit thixotropic behaviour, exemplified by the transient step-down in shear rate experiments. When the 0.5 wt% - 5 wt% Al_2O_3 /silicone oil suspensions are subjected to an external $E = 0.25 - 2$ kV/mm, a transition from liquid-like to solid-like behavior occurs, marked by diverging low shear viscosity, frequency independent G' and appearance of yield stress. Moreover, our results suggest that the above the threshold $E = 0.5$ kV/mm, the suspension electrorheological (ER) response is not dependent on the applied pre-shear and the relative viscosity does not follow the $\dot{\gamma}/E^2$ scaling ($\dot{\gamma}$: shear rate) based on the polarization force model.

We next investigate the implication of using elongated Goethite (α -FeOOH, length (l) = 488 ± 20 nm, aspect ratio = 5 ± 0.8) particles in the same silicone oil medium on the rheology and microstructure of α -FeOOH/silicone oil suspensions at different E. Even at a low E of 0.25 kV/mm, the liquid-like suspensions with ϕ of 0.025 and 0.039 transform into solid like gels, marked by ω independent G' and yield stress which varies with $E^{1.5}$, consistent with the conduction model framework. The optical microscopy demonstrates that the α -FeOOH particles dispersed in the silicone oil medium are capable of forming an electric field driven network under equilibrium conditions of no shear.

We now presents a completely different perspective by replacing the isotropic silicone oil with the anisotropic NLC medium, N-(4-methoxybenzylidene)-4-butylaniline (MBBA), for dispersing fumed Al_2O_3 nanoparticles. The suspensions with nanoparticle $\phi \geq 0.014$ form solid-like self-supporting gels with $G' > 10^3$ Pa and follow the soft glassy rheology (SGR) model, described by $G' \sim \omega^{(x-1)}$ scaling, where x is the effective noise temperature representing the structural disorder in suspensions. We also show that unlike fumed Al_2O_3 /silicone oil suspensions, fumed Al_2O_3 /MBBA suspensions can recover 60% of the original structure even after the application of large amplitude oscillatory strain (γ). The optical microscopy coupled with the differential scanning calorimetry (DSC) reveal that fumed Al_2O_3 nanoparticles cause a significant depression in the nematic-isotropic transition temperature (T_{NI}) relative to the particle-free MBBA, due to the quenched random disorder (QRD) resulting from the confinement of NLC in the network of nanoparticles. We further demonstrate that the reversible E-driven phase transition occurs only at and above a critical nanoparticle ϕ of 0.005.

The next aim of the thesis is to systematically study the role of particle surface chemistry on the rheology and structure of suspensions of fumed and colloidal silica particles in the NLC, 4-cyano-4-pentylbiphenyl (5CB). We show that the suspensions of hydrophilic fumed and colloidal particles in 5CB undergo sol to gel transformation at a lower particle ϕ than the hydrophobic fumed and colloidal silica particles. Moreover, the hydrophilic silica/5CB suspensions exhibit SGR characteristics while the hydrophobic particles-in-5CB suspensions show the features of flocculated gels. We show that below T_{NI} , the NLC domains get restricted in the existing network of fumed hydrophilic silica particles, leading to confinement and subsequently, SGR characteristics. In contrast, the well dispersed hydrophobic fumed silica in 5CB gets expelled at the isotropic-nematic interface during phase transition to form a network. We believe that the observed rheological response and underlying microstructure is due to different anchoring of 5CB molecules on the surface of silica particles.

In conclusion, our work has demonstrated the capability of fumed Al_2O_3 /silicone oil and FeOOH /silicone oil suspensions to serve a positive ER response system. On the other hand, dispersing fumed Al_2O_3 nanoparticles in the NLC paves a way to produce structurally disordered particles-in-NLC suspensions which can respond to an external E. We also show that depending on the particle surface chemistry and the NLC anchoring on the particle surface, the suspensions rheology can be tuned. To summarize, our work illustrates how the behaviour of suspensions can be engineered as a function of dispersing medium, particle loading, shape, surface chemistry and external E to provide a basis for various applications pertaining to sensing, display, E-driven phase changing and temperature measuring devices.

Title: Scalable synthesis of two dimensional nanosheets from magnesium diboride: a new class of nanomaterials for solid-propellants and hydrogen storage

Researcher: Gunda, Harini

Supervisor: Jasuja, Kabeer

Year: 2021

Keyword's: Magnesium Diboride, Solid Propellants, Hydrogen Storage, Ammonium Perchlorate, MgB₂

Call No.: 665 GUN

Acc. No.: T00932

Abstract: Boron has always intrigued the scientific community because of its rich inherent properties – low density, high melting point, high thermal resistance, ability to absorb neutrons, and high chemical resistance. Recent advances in the science of two- dimensional (2D) materials have motivated researchers to investigate whether planar nanostructures can also be constituted from boron. Such nanostructures are expected to serve as platforms for utilizing the inherent properties of boron to its full potential.

In this thesis, we present a new set of perspectives that we developed in our pursuit to obtain 2D boron from metal diborides, a family of layered materials that have been primarily investigated and utilized in their pristine forms. For example, magnesium diboride (MgB₂), a pioneering member of this family, is widely known for its superconductive nature; aluminum diboride (AlB₂) is used as a reinforcing material for polymer composites, and titanium diboride (TiB₂) is used in ballistic armors. However, the notion that these materials can be used in their native bulk forms is fast evolving. Researchers are revisiting these materials with a viewpoint to delaminate their layered structure into 2D nanosheets. The first such report appeared in 2015 when our research group showed that it is possible to exfoliate MgB₂ into boron-rich nanosheets simply by ultrasonically these crystals in water. In the ensuing years, we further demonstrated that this exfoliation could be achieved by other means, such as selective extraction of the interlayer metal atoms using chelation or expansion of the interlayer space using long-chain molecules.

While the method of ultrasonically MgB₂ crystals in water yielded boron-based nanosheets, we also observed a concurrent formation of ultra-small quantum dot-like nanostructures (< 10 nm in diameter). The formation of such nanostructures was unintended, and the mechanism underlying their formation of these nanostructures was not clear. This observation led us to a path forming this thesis's first research aspect. As we delved deeper to understand the mechanism governing the formation of boron-based nanosheets when MgB₂ crystals are exposed to ultrasonication in water, we discovered that, in addition to undergoing exfoliation to yield nanosheets, MgB₂ crystals also undergo a chemical reaction with water which results in their dissolution to form gaseous boron hydrides and quantum dot-like precursors. These precursors are found to be short-lived – they subsequently ripen to form boron-rich nanograins and nanoflakes. While the precursors are observed to be < 10 nm in lateral dimensions, the nanograins and nanoflakes have a lateral dimensional range of ~ 50- 400 nm. These nanostructures are few-layer thick (~ 6-8 nm) and are found to be decorated with hydrides and oxy-functional groups. We found that by simply tuning the recrystallization time, we can obtain various morphologies of boron-based nanostructures, including

quantum dots, nanograins, and nanosheets. This ability of MgB₂ crystals to yield in precursors, which can self-seed to form nanostructures comprising chemically modified boron honeycomb planes, presents a new facet to the physico-chemical interaction of MgB₂ with water. Further investigations suggested that the dissolution does not require ultrasonication and results in nanosheets with lesser defects. This discovery led us to a simple and scalable route to obtain boron-based nanosheets in high yield (apparent yield ~92%) by simply dissolving the MgB₂ crystals in water under the right conditions and allowing these to recrystallize.

What made this approach especially appealing was its inherent scalability; this is because scalability is a critical bottleneck in translating the nanomaterial research to a tangible application. Thus, the observations we had stumbled upon also presented an opportunity to advance an application that could benefit from enhanced access to boron. In this pursuit, we found that these 2D boron-based nanostructures can help address a critical challenge experienced in boron-based fuel additives. Boron is an excellent candidate as a fuel additive due to its high volumetric and gravimetric heat of combustion. Yet, scientists cannot effectively utilize boron's potential because, upon combustion, boron forms a viscous boron oxide layer on the surface that limits further oxidation. We postulated that an inherent presence of metal atoms in the nanosheets derived from MgB₂ should prevent the formation of such a passive layer, and the 2D nature of the material should optimize the accessibility to boron atoms. This forms the second research aspect in this thesis. We initiated our work on this front by studying the effect of boron-based nanosheets (obtained from the dissolution-recrystallization recipe) on the exothermicity of solid-propellant ammonium perchlorate (AP). We observed that these nanostructures catalyze AP's thermal decomposition and significantly enhance the release of energy. We then postulated that we could obtain even more efficient fuel additives if the degree of functionalization could be minimized during delamination. To achieve this, we endeavored to exfoliate MgB₂ in solid-state using planetary ball milling. Although we could not achieve complete exfoliation in this path, the resultant micro-derivatives, referred to as mechanically activated MgB₂ (MA- MgB₂), resulted in an unprecedented energy enhancement. Adding one wt.% of MA- MgB₂ to AP remarkably enhances the energy release by 78% and significantly lowers the fuel decomposition temperature by ~73 °C. By carrying detailed kinetic studies and using an integral model-free iso-conversional method, we could develop foundational insights on the mechanism that results in such extraordinary enhancements.

Because we could not achieve complete exfoliation using a planetary ball mill, we revisited the liquid-phase exfoliation approaches with a specific aim to obtain a minimally functionalized or pristine form of MgB₂ nanosheets. This forms the third research aspect of the thesis. For achieving this objective, we needed to rationally select a suitable solvent media that can exfoliate and form the stable dispersion of nanosheets. However, the presently available theories suggest solvents for potential exfoliation are available only for van der Waals layered materials. Thus, we adopted the approach where we would test exfoliation of MgB₂ in a range of organic solvents, and based on the stability of the dispersion; we would identify an optimal solvent. We tested the sonication-assisted exfoliation of MgB₂ in 1,4-Dioxane, Cyclohexane, Toluene, THF, DMF, ACN, Ethanol, Acetone, Ethylene glycol (EG), co-solvent mixtures of isopropyl alcohol (IPA) and Ethanol with H₂O. From the TEM, MAS-NMR, SEM, FTIR, XPS, EDX, and XRD characterizations, we found that exfoliation of MgB₂ in anhydrous IPA resulted in a high yield of nearly pristine MgB₂ nanosheets. For the first time, we

achieved delamination of MgB_2 in a pristine 2D form without any change in chemical composition. The ability to obtain nanosheets in pristine form led us to postulate that we may achieve a completed exfoliation in solid-state as well if we were to carry out the process in a high energy ball mill (HEBM). This was an important missing link for us to bridge, as the ball-milling methods are scalable alternatives to liquid phase exfoliation and are preferred modes for advancing an application. Tuning the parameters of HEBM resulted in successful delamination of MgB_2 , as evident from XRD, TEM, and AFM studies. The nanosheets were ultra-thin with thickness ranging from 3-4 nm. To our knowledge, no reports exist showing the successful delamination of MgB_2 in the 2D form via solid-state mechanical milling.

This ability to make pristine nanosheets from MgB_2 on a large scale was an important turning point, as we could now advance applications where the surface chemistry of native MgB_2 can be used to advantage. This seed thought led us to the frontier of hydrogen storage and formed the final research aspect of the thesis. Lightweight metal borohydrides like $\text{Mg}(\text{BH}_4)_2$ are found to be promising candidates and are gaining much attention because of their high hydrogen storage capacity of ~ 14.9 wt.% H_2 . The dehydrogenation pathway of $\text{Mg}(\text{BH}_4)_2$ is well-reported and reviewed, but the hydrogenation of MgB_2 to $\text{Mg}(\text{BH}_4)_2$ is not well understood, and complete reversibility has not been achieved so far. We were curious to test whether the MgB_2 derived 2D nanostructures can enhance hydrogenation compared to bulk MgB_2 . We conducted high-pressure hydrogenation experiments, and the dehydrogenation studies revealed a remarkable hydrogen release of ~ 5.1 wt.% H_2 from ultra-thin MgB_2 nanosheets compared with ~ 0.1 wt.% H_2 from bulk MgB_2 . These results suggest that the hydrogenation pathway of MgB_2 to form $\text{Mg}(\text{BH}_4)_2$ is more favorable when it is exfoliated. The observed value surpasses the 2020 target of 4.5 wt.% H_2 set by the US Department of Energy (DOE) for hydrogen storage materials, indicating the immense promise that this new class of 2D materials displays.

In summary, the work in this thesis presents a new paradigm to the science of metal diborides. It exemplifies how nanoscaling a layered material into its 2D counterparts can have implications that are not entirely intuitive. MgB_2 was considered a water-insoluble compound, but we discovered that it not only undergoes dissolution in water under the right conditions, but it also recrystallizes in a non-classical manner to form 2D boron-based nanostructures. MgB_2 was never viewed from the perspective of an additive in solid propellants. However, our results led us to establish that MgB_2 derived nanostructures are better than state-of-the-art catalytic and energetic nanoadditives for solid propellants. The ability of 2D MgB_2 nanosheets to store hydrogen at ~ 5.1 wt.% H_2 makes this new class of nanomaterials truly multifunctional in nature. In the near future, we sincerely hope to study how these nanosheets can be utilized to advance other applications including sensors, batteries, supercapacitors, and superconductors.

Title: Role of rheology on the hydraulic conveying of slurries of particulate solids through pipelines
Researcher: Prasad, Vighnesh
Supervisor: Thareja, Prachi
Year: 2022
Keyword's: Particulate Solid, Rheological Characteristics, Coal Ash Slurries, Frictional Head Loss, Shear Yield Stress
Call No.: 621.867 PRA
Acc. No.: T00933

Abstract: The hydraulic conveying of solids in the slurry form through pipelines is significantly more advantageous over other conventional modes of transportation such as rail, road, conveyor belt and barge. However, obtaining a favorable flow behaviour of slurries in pipelines remains a major challenge for its universal acceptance. Subsequently, a detailed rheological investigation is critical to identify the main influencing parameters which control the slurry flow characteristics. In the present thesis, we have studied the rheological response of various particulate slurries in the presence and absence of additives as a function of particle loading and particle size distribution. Our results show that 0.1 wt.% of Cetyltrimethyl Ammonium Bromide and 0.1 wt.% of Sodium salicylate salt prevent the sedimentation of coal ash particles up to 5 hours. We further demonstrate that the shear rate ($\dot{\gamma}$) range of 10 - 500 s^{-1} is free from the Taylor Vortices and wall slip effect, and is suitable for reliable rheological analysis. The 60 wt.% coal ash slurries exhibit the shear thinning flow behaviour irrespective of particle size. However, the slurries with fine coal ash have higher slurry viscosity (η) which can be reduced by adding coarse coal ash particles. η of fine coal ash slurries does not further decrease with addition of coarse coal ash particles beyond 30 wt.%. The effect of particle size and $\dot{\gamma}$ on η is demonstrated using a detailed rheo-microscopy analysis, which reveals that the incorporation of coarse particles in fine coal ash slurries disintegrates the densely packed floc structure, resulting in the lower η . However, the microstructure of slurry does not change appreciably after 30 wt.% of coarse coal ash, in agreement with the rheology data.

We also show that 60 wt.% coal ash, 60 wt.% gibbsitic bauxite and 35 wt.% lignite coal slurries have predominantly shear thinning flow behaviour in the absence of additives. The rheology data is suitably explained by the power-law model (Ostwald-de Waele model) to obtain the flow behaviour index (n) and consistency coefficient (k), which are used to estimate the head loss (hL), and consequently specific energy consumption (SEC) and energy cost. Our analysis indicates that the presence of coarse particle not only reduce η but it also lowers hL and SEC during pipeline transportation.

The wall slip, shear deformation and spillage condition in 70 wt.% coal ash (Volume fraction, $\phi = 0.54$) slurry is visually demonstrated. The experimental relative viscosity (η_r) data of coal ash slurries with varying concentration from 30 – 70 wt.% ($\phi = 0.17 - 0.54$) agrees well with Dabak and Yucel's viscosity model. On the other hand, 75 wt.% coal ash ($\phi = 0.6$) slurries have the thixotropic nature, also explained by the rheo-microscopy study. Furthermore, 70 wt.% coal ash ($\phi = 0.54$) slurry shows a significant increase in η with time (t) when slurry temperature (T) exceeds to 25°C. The shear yield stress (τ_y) for coal ash slurries is determined using stress sweep test, oscillatory sweep test and

rheological model, which exponentially increases with coal ash loading from 60 – 75 wt.% ($\phi = 0.43 - 0.6$).

h_L values estimated from the rheological data are compared with the actual h_L value measured in a closed pilot pipe loop experimental facility for 44 – 53 wt.% coal ash ($\phi = 0.272 - 0.349$) slurries. These experiments are carried out in pipelines having diameters (D) = 0.025 and 0.05 m. The detailed analysis suggests that the rheological h_L is in reasonably good agreement with the pipe loop h_L at higher slurry velocity (v_m) ($\sim 2 - 3$ m/s) during transport of coal ash slurries. The experimental results from the pipe loop indicate that h_L increases with an increase in v_m from 0.5 – 3 m/s and coal ash concentration from 44 – 53 wt.% ($\phi = 0.272 - 0.349$). The minor h_L and loss coefficients (K) across the gradual contraction and bend pipe are found to be functions of ϕ and v_m . Similar pipe loop experiments are performed for coarse river sand ($d_{50} = 690 \mu\text{m}$) and calcined bauxite ($d_{50} = 800 \mu\text{m}$) slurries in the concentration range of 38 – 49 wt.% ($\phi = 0.191 - 0.27$) and 40 – 50 wt.% ($\phi = 0.182 - 0.25$), respectively. The higher magnitude of h_L for these systems is attributed to the larger size and irregular shape of sand and bauxite particles. Our results also indicate that the coal ash, river sand and calcined bauxite slurries are in the laminar region during the pipe flow.

Overall, we suggest that the rheology can be serve as an accessory and supportive tool for better understanding of the pipeline transportation of slurry, which not only characterize the slurry under shear, t and T but it also predicts the transport parameters to design a low-cost and efficient slurry transportation system.

Title: Estimation and control strategies for smart water grids: a cyber-physical systems approach
Researcher: Kartik, Mankad Jaivik
Supervisor: Padhiyar, Nitin
Year: 2022
Keyword's: Smart Water Grids, Cyber-physical Systems, Water Distribution Networks, Fault Type Identification, Sensor Placement, Plant-model Mismatch, Graph Neural Network
Call No.: 621.319 KAR
Acc. No.: T00937

Abstract: The infrastructure of water distribution systems is of “vital importance” as they accommodate the water supply needs of the society. A water distribution network (WDN) is designed with the primary objective to supply the required quantity of water to a population at an adequate pressure. Critical Infrastructure Partnership Advisory Council Working Group (CIPAC Workgroup) has listed the potential impacts on water networks caused by manmade and/or natural disasters, including pipe breaks, loss of facility/supplies, pressure losses in the network, power outage, deterioration in quality, infrastructure damage/loss and other financial and environmental aspects. Disruptions in water networks degrade its performance in terms of pressure losses and/or reduced supply. This leads to the wastage of water and energy, driving the system to a non-optimal state. Besides these, climatic changes and the ever-increasing global population necessitate continuous monitoring of water networks for efficient management. Hence, modernization of WDNs is identified as necessary for sustainability and careful utilization and allocation of water. Intelligent water distribution systems must be developed to maintain serviceability during disruptive scenarios. This necessitates designing a network in a cyber-physical framework that can operate in real-time such that the objectives of a WDN are satisfied and it being sustainable. The term *Smart Water Grid* has become popular in the water domain, which takes a cyber-physical systems (CPS) approach. CPS, a newer concept, involves integrating the digital and physical systems for intelligent monitoring and decision making using data.

The first step to achieving the resilient cyber-physical design of WDNs is the detection of abnormal situations. Hence, metrics that provide an insight into the WDN's performance at a nodal-level have been developed. The present study focuses on physical failures caused due to disruptions such as pipe bursts and operational failures such as excess demand in WDN. During such events, parameters such as pressures, flow, or nodal heads are instrumental in determining the network's performance. The developed metrics also behave differently during some common faults occurring in the WDN and help identify the nature of the fault. However, it expects the availability of pressure and flow information from each node in the network, which is not practical. Hence, the problem of combined sensor placement (SP) and state estimation (SE) is addressed next using the notion of sparsity for solving an underdetermined SE problem. This approach exploits the underlying correlation structure in the data, along with the principles governing the flow through circular pipes. The problem of SE maps to a matrix completion (MC) problem, which is solved with certain physical and logical constraints. The completed matrix represents the state of WDN at any given time. Benchmark networks used in literature were used to evaluate the proposed approach. The MC problem assumes

smoothness in the states and the knowledge of model parameters. Further, it requires solving an optimization problem at every sampling interval, making real-time implementation difficult. Hence, a graph neural network (GNN) was used for real-time implementation of SE since they can learn the interactions between the variables and need to be trained only once. The GNNs allow representing structured data with complex interconnections in a graphical form.

With the knowledge of states, the next objective is pressure management in WDN. The goal of pressure management in a WDN is to avoid losses due to excessive pressure while meeting the minimum target pressure set for satisfying nodal demands. Since nodal demands can fluctuate, real-time control of nodal pressures is critical for normal network operation. Optimizing the operation and control of WDN based on a model with uncertain parameters and unaccounted nodal demands generate solutions that are not truly optimal and may even be infeasible. The aim for real-time control is to achieve optimal WDN operation in the presence of various uncertainties. A modifier-adaptation (MA)-based real-time optimization (RTO) strategy is used to drive the WDN to its optimal point. However, the MA-based RTO scheme assumes knowledge of all the variables of interest, which may not be available in practice. Therefore, a Bayesian MC approach for robust SE is used to impute unknown model parameters with limited measurements. The ability of the MC informed MA-based RTO approach for optimally operating the WDN is demonstrated via simulations on a practical WDN.

Title: Enhanced mechanical properties of chitosan hydrogels: rheology, 3d extrusion printing, and applications
Researcher: Marapureddy, Geetha
Supervisor: Thareja, Prachi
Year: 2022
Keyword's: Chitosan Hydrogels, Rheology, Graphene Oxide, Formation of Hydrogels
Call No.: 660 MAR
Acc. No.: T00955

Abstract: Hydrogels are 3D network-like structures comprising hydrophilic polymers holding copious amounts of water in the interstitial spaces of crosslinked networks and thus are promising materials in various biomedical applications. Biopolymers are preferred over synthetic polymers for the synthesis of hydrogels due to their biodegradability and biocompatibility. Chitosan (CH) is one of the biopolymers that are abundantly available in nature (extracted from crab and shrimp shells) and is made up of N-acetyl-D-glucosamine and D-glucosamine units. It resembles the extracellular matrix (ECM) component glucosaminoglycans; thus, it can mimic the in-vivo environment suitable for cell culture. The amino groups on CH protonate in an acidic environment, thus facilitating the dissolution of CH in water. Hence, CH shows a pH-responsive nature where it swells at acidic pH and shrinks at basic pH. The biodegradable, biocompatible, ECM mimicking nature, pH-responsive characteristics of CH has drawn the attention of researchers to use it in wound dressings, tissue engineering, and drug delivery applications.

Despite many advantages, the low mechanical strength of CH refrains its usage in many applications. The crosslinks are introduced on the hydrophilic groups of CH polymeric chains to synthesize hydrogels. Crosslinking techniques are categorized in two ways: chemical and physical. Chemical hydrogels are held together by irreversible covalent links, whereas physically crosslinked hydrogels are formed by molecular entanglements or secondary forces like ionic, hydrogen bonding, and hydrophobic interactions. The work in this thesis systematically investigates different routes for improving the strength of CH hydrogels and their effect on tissue engineering and drug delivery applications. Rheology is used extensively throughout the thesis to understand the structure-property relationships of CH hydrogels.

The first objective of the thesis focuses on the carbamoylation reaction of 1 w/v% of CH by adding potassium cyanate (KCNO). It was observed that the free amino groups converted into carbamyl functionalities by reacting to cyanate ions. The formation of carbamyl functionalities is confirmed by FTIR and XRD studies. Carbamoylation reaction led to sol to gel transition through hydrogen bonding between the newly formed carbamyl groups. The modified carbamoylated CH hydrogel (CCH) has better thermal stability than the pristine CH. The gelation kinetics of CH was studied by conducting the rheological experiments where cross-over of storage modulus (G') and loss modulus (G'') manifests the sol-gel transition. The gelation behavior is observed at a $[KCNO] \approx 0.1$ M. An increase in the $[KCNO]$ decreases the gelation time, and a G' of 10^4 Pa is obtained with 0.5 M KCNO. The cell attachment and proliferation of two different cell lines: A549 lung cancer cells and SH-SY5Y neuroblastoma cells was investigated on CH and CCH using an Alamar blue assay. The fluorescence intensity of A549 cells is higher on CCH than CH, indicating an increase in the cell proliferation rate

on CCH. The confocal microscope z-sectioning images show an increase in the cell density in the midsection of the CCH hydrogel, indicating the migration and attachment of cells. CCH promotes the differentiation of SH-SY5Y neuroblastoma cells to neuron cells, and the immunohistological studies confirm the mature neuron formation.

The next aim of the thesis focuses on the rheology and 3D printing of graphene oxide (GO) containing CH hydrogels to synthesize scaffolds. The mechanical strength of the printed CH filaments should be considerably high to self-support and avert the deformation of scaffolds induced by the gravity of the deposited filaments. To improve the mechanical strength, GO nanosheets have been added to the CH hydrogels to enhance the printability of printed structures. The oxy-functional groups interact electrostatically with the $-NH_2$ groups of CH, resulting in the multifold increment in the mechanical strength of GO-loaded CH gels. The structural recovery of the hydrogels is investigated by three intervals thixotropic test (3ITT) and 0.5 wt% GO loaded 3 wt% CH hydrogel shows a 94% recovery of G' after seven sequential stress cycles. The incorporation of GO decreases the Barus effect and improves the printability of GO-loaded 3 wt% CH hydrogels. 3 wt% CH hydrogel with no GO could not form multilayered structures with good fidelity as the CH filaments completely spread out, affecting the subsequent printing of layers. The improved printability of GO-CH nanocomposite hydrogels is attributed to the rheological properties of shear thinning, high viscosity, yield stress, and high structural recovery. Further investigation of SH-SY5Y neuroblastoma cell growth and differentiation on 3 wt% CH hydrogel and the 0.5 wt% GO loaded 3 wt% CH hydrogel reveals that GO promotes differentiation of SH-SY5Y cells. In contrast, no differentiation is observed in pristine CH hydrogel.

We further investigated the synergistic effect of chemical crosslinking by glutaraldehyde (GA) and physical crosslinking induced by GO nanosheet addition on CH to enhance the mechanical strength of CH hydrogels and their films. The rheological properties of 1 wt% CH are studied with varying [GA] from 17.6 mM to 53 mM and GO concentrations from 0.025 wt% to 0.5 wt%. G' value of 0.5 wt% GO incorporated 53 mM GA crosslinked CH hydrogel is 7.2 times greater than the pristine 53 mM GA crosslinked CH hydrogel. Oscillatory strain sweep studies indicated that the network of CH-GA yields earlier after incorporating the GO due to an increase in the crosslinking density. The morphology studies by FESEM show the microporous structure of CH hydrogels with an increase in the porosity with [GA]. These nanocomposite hydrogels are cast as films and characterized with a dynamic mechanical analyzer (DMA), which shows 20 times higher Young's modulus than the pristine CH. These results are in line with the observed rheological signatures. Drug delivery studies carried on these films show a pH-responsive behavior where the drug elution is higher at pH 4 than pH 7.4. Sustained drug delivery is observed in 0.1 wt% GO-loaded CH film crosslinked with [GA] = 35 mM. The GA crosslinking and GO nanosheets incorporation play a prominent role in reducing the burst release by 92 % from CH films.

To summarize, an understanding of the structure-property relationship is important in the fabrication of different hydrogels. This work elucidates the effect of modification of CH by carbamoylation, incorporation of GO nanosheets, and combined effect of chemical crosslinking by GA and incorporation of GO nanosheets on the mechanical strength of CH hydrogels and their applications in tissue engineering and drug delivery platforms. CCH and CH-GO hydrogels provide a

suitable environment for cells and open the possibility for use as scaffolds. The crosslinked CH films regulate the burst release of the drug. Thereafter it would be possible to use the CH-GO-GA films as local drug delivery agents.

Title: Cognitive workload analysis of control room operators using Electroencephalography (EEG) and eye-tracking
Researcher: Iqbal, Mohd Umair
Supervisor: Srinivasan, Babji
Year: 2023
Keyword's: Human Factors, Electroencephalography (EEG), Eye-tracking, Cognitive Workload
Call No.: 616.891425 IQB
Acc. No.: T01017

Abstract: Chemical and process industries are highly hazardous, and these hazards frequently result in disastrous accidents. Even though there have been tremendous increases in safety due to better process design and technical safety approaches, mishaps still happen. A significant majority of these accidents can be traced back to human errors. With the advancements in technology in the form of digitalization and concomitant automation (Khan et al., 2021), the role of human operators has changed more towards monitoring (during regular operation), diagnosis, and prognosis (during abnormal situations). To maintain adequate situational awareness, operators must prioritize, acquire, segregate, and integrate information from multiple sources in DCS. An abundance of information, coupled with the increased complexity of modern plants, makes these tasks cognitively challenging for an operator. As a result, operators' cognitive workload can drastically increase if they are not adequately trained and assessed. An increase in cognitive workload is known to result in the degradation of performance (Islam et al., 2017). This work addresses the critical need to understand and evaluate the cognitive performance of control room operators using electroencephalography (EEG) and eye-tracking.

Traditional methods of operator assessment often ignore cognitive aspects of operators' performance. Evaluation is carried out based on metrics such as the number of errors committed during a task, reaction time, number of successes and failures, and expert judgments (Lees, 2001). Such metrics fail to unravel the underlying reasons for shortcomings in operator performance; factors such as cognitive workload, the correctness of mental models, and the impact of HMI design on performance are overlooked. With advances in sensor technology, it is now possible to acquire various physiological data that can provide critical insights into an operator's cognitive performance.

The potential of EEG and eye-tracking in providing critical insights into cognitive aspects of human performance (such as thought process) has been demonstrated in several domains (Srinivasan et al., 2018). In this work, we demonstrate the potential of eye-tracking and EEG in assessing the cognitive workload of control room operators' performance. We use a simulated ethanol process testbed for conducting experiments. A typical experiment requires an operator to monitor the process and take corrective action(s) in case of any disturbance. During each experiment, the operator's gaze data

and EEG are recorded using a Tobii eye tracking set-up and single electrode EEG device, respectively. In addition, process data, alarm data, and operator actions are also recorded during each task.

In our eye-tracking-based work, we analyzed the relationship between operators' gaze data (recorded using a Tobii eye-tracking setup) and their learning to control a process abnormality. Our results reveal that as the operators learn to control a particular disturbance, the entropy of their gaze decreases, which could be used as a learning marker.

We also assessed the relationship between EEG data and operator performance. Our results reveal that the power spectral density (PSD) of theta waves (4-7 Hz) obtained from the recorded EEG signal is an indicator of the workload experienced by operators during process abnormalities. We found that if there is a mismatch between the operator's understanding of the process and the actual process behavior, then theta PSD shows an increasing trend otherwise a decreasing trend. The inability to bring the process variables within normal operating limits increases cognitive workload, which is captured by an increase in theta PSD.

Next, we explored the potential of EEG for quantifying cognitive aspects of performance during training where an operator performs several trials of the same experiment. Accordingly, we proposed an Electroencephalography (EEG) power spectral density-based metric that can quantify the cognitive workload and provide detailed insight into the evolution of the operator's mental models during training. We identified two clusters representing high and low cognitive workload levels by analyzing the participants' EEG data (PSDs in the 1-30 Hz) using k-means clustering. We then obtained the fraction of each of these clusters for each task. Our results reveal that the fraction of the low-power cluster captures training progress. If the fraction of low power cluster during a task is high, it reflects good cognitive performance (reflected by low workload), otherwise sub-optimal performance.

Finally, we assessed the benefits of the fusion of eye-tracking and EEG-based metrics in assessing the cognitive workload of operators and performance. Some aspects of performance may not be sensitive to the metrics obtained from one sensor, while the other sensor-based metrics can capture the same (Debie et al., 2021). We extracted EEG and eye-tracking-based metrics for each task to populate a feature matrix. These metrics include power spectral densities of pupil diameter in the range of 0-2 Hz, average pupil diameter, fixation duration-based (gaze) metrics, and power spectral densities of EEG in the range of 1-30 Hz. We trained a decision tree-based model, based on several feature set combinations, for estimating operators' cognitive workload. Our results indicate that the fusion of metrics results in a marked improvement in assessing the cognitive workload of control room operators compared to using features from EEG or eye tracking alone. We also developed an operator-independent generic model for classifying cognitive workload into three classes.

The work has the potential to assess cognitive aspects of performance and evaluate expertise during training, thus providing a comprehensive and robust performance assessment. This will help ensure the safety and quality of products in process industries. From a broader perspective, it can guide the application of human factors for improving safety in industries by providing objective information about the cognitive aspects of performance.

Title: Fouling monitoring and foulant identification in heat exchangers and heat exchanger networks
Researcher: Shankar, Patil Parag
Supervisor: Srinivasan, Rajagopalan
Year: 2022
Keyword's: Heat Exchanger, Heat Exchanger Networks, HEN-fouling, Network Thermal Performance
Call No.: 621.4025 SHA
Acc. No.: T01024

Abstract: Heat exchangers are widely used in process industries. As operational time progresses, unwanted material in incoming streams (foulants) starts depositing in heat exchangers (fouling). Since the conductivity of foulant is less than the heat exchanger's material, fouling reduces overall heat transfer rate. Also, it reduces the cross-sectional area for the fluids to pass through heat exchangers increasing the pressure drop. The reduced performance is compensated by spending additional utility and pumping power. As per an estimate, a temperature drop of 1°C in heat exchanger networks (HENs) in refineries costs about £ 2,50,000 per year (Macchietto et al., 2011), translating to \$2.26 billion in all US refineries annually (Coletti et al., 2015). Besides this, foulant deposition produces a substantial amount of greenhouse gases. An estimate suggests the production of ~88 million tons of CO₂ annually due to fouling in refineries (Müller-Steinhagen et al., 2011). Hence, mitigating fouling is necessary to minimize its economic and environmental impacts.

The fouling can be tackled when heat exchangers are under design or operation. The former includes proactive approach of overdesigning heat exchangers based on TEMA standards. On the other hand, approaches in operational heat exchangers can be divided into three sequential tasks: (a) Monitoring fouling state, (b) Characterizing deposited foulants, and (c) Cleaning using a suitable method based on the type of foulants. This thesis work is focused on operational heat exchangers and heat exchanger networks (HENs). The work contributes by providing novel fouling monitoring techniques and a foulant identification approach.

The monitoring is expected to convey an accurate degree of fouling based on reduced performances, either simultaneously or separately. We observed that existing methods based on the overall heat transfer rate fail to convey accurate thermal performance in common industrial scenarios, such as changing inlet conditions and in the presence of temperature control. To address this issue, we proposed a novel monitoring chart called *xTH monitoring charts* based on excess thermal and hydraulic loads on the heat exchangers. Once the fouling results in excessive-performance deterioration, heat exchangers must be cleaned to reinstate the original performance. An accurate information on foulants is necessary to decide on an appropriate cleaning method as different industries encounter foulants of distinct natures. Usually, the identification is conducted by laboratory analysis of deposit samples collected from an overhauled heat exchanger. However, it is not always reliable due to the challenges of maintaining the same industrial and laboratory conditions and the requirement of expensive equipment. The identification can also be based on heat exchanger models and plant measurements. However, the dependency on the overall heat transfer rate makes it unsuitable in case of change in inlet conditions and the presence of

temperature control. Alternatively, we proposed a model-based approach based on simple heat exchanger models. We showed that the proposed method can accurately estimate foulants in common industrial scenarios. In the case of HENs, it is observed that the inlet temperatures in the downstream heat exchangers tend to vary due to fouling in upstream heat exchangers, changing nominal overall heat transfer rates. As a result, the conventional approaches based on the heat transfer rate fail to indicate correct degree of fouling. We extended the usage of xTH monitoring charts *for the HENs*. Since the method considers changing inlet conditions, it can accurately estimate the degree of fouling. We proposed two charts: 'Network thermal performance monitoring chart' for thermal performance and 'Network hydraulic performance monitoring chart' for hydraulic performance. The proposed monitoring charts can be used for the HENs, with and without temperature controllers.

Overall, we conclude that combined use of the proposed fouling monitoring and foulant identification approaches can help identify heat exchangers with excessive fouling and identify deposited foulants to choose a cleaning method. Such an approach can help industries from regular mechanical to condition-based cleaning, saving cleaning time and associated costs. In the future, the current work can be extended in various directions. The effect of temperatures and flow rates on fouling rates and controllers can be considered. Also, detailed shell-side modelling can be also considered. As mentioned before, the fouling mitigation strategies require cleaning of heat exchangers as the final task. Towards this end, our future work considers identifying optimal cleaning schedules in HENs with various optimization strategies based on mixed-integer linear and mixed integer nonlinear programming.

Title: Engineered pharmaceutical formulations for improved dry powder inhaler (DPI) performance: particle engineering and mechanistic insights
Researcher: Varun, Neetu
Supervisor: Ghoroi, Chinmay
Year: 2022
Keyword's: Particle Engineering, Drug Excipient Interactions, Hollow Particles, Principal Component Analysis (PCA), Dry Powder Inhaler (DPI)
Call No.: 615.19 VAR
Acc. No.: T01025

Abstract: With the surge in respiratory diseases including COVID 2019, there are continuous efforts to achieve high-efficiency pulmonary drug administration. One of the major drug administration routes through inhalation includes Dry Powder Inhaler (DPI). Most commercial DPI formulation functioning involves drug-carrier mixing and drug aerosolization for delivery to lungs. However, clinically mostly carrier-based DPI has reported low drug delivery where fine particle fraction, FPF < 30%, (represents the mass of drug particles with aerodynamic diameter, $d_{aero} < 5 \mu m$ that reaches respirable region). The DPI efficiency is majorly influenced by formulation along with patient (inspiratory flow rate) and inhalation device (type of inhalers). Multiple issues associated with carrier-based DPI formulations are reported such as improper mixing, poor flow, inefficient drug dispersion, complex correlations between different drug-carrier properties and aerosolization performance. Literatures report incompatibility between drugs (containing polar protic groups) and carrier (lactose monohydrate) for solid dosage but remain unexplored for DPI mixtures. Beside, lactose cannot be given to lactose-intolerant people due to hypersensitivity reactions. Furthermore, current carrier-based formulation approach has limitations to deliver high drug dosage (10–250 mg/dose) to treat chronic diseases (like chronic obstructive pulmonary disease, cystic fibrosis, tuberculosis). Thus, carrier-free formulations are increasingly in demand for high drug doses. Recently, bio-polymeric aerogel particles are gaining much attention for sustained pulmonary drug administration. However, designing inhalable porous polymeric particles is challenging and costly.

This dissertation identifies the gaps associated with DPI formulation and explored various mitigation techniques to improve DPI efficiency using particle engineering approach. Here, model drugs (aceclofenac and salbutamol sulfate) and lactose monohydrate (commonly used excipient in commercial DPI formulation) are used to prepare binary mixtures separately. Further, formulations are characterized for their physicochemical properties and the complex correlations related to drug-excipient mixtures and DPI efficiency are comprehended using multivariable statistical approach (Principal component analysis, PCA). The engineered pharmaceutical formulations are explored for (a) carrier-based low dose application, (b) carrier-free formulation for high dose and (c) sustained pulmonary drug administration. The thesis work is summarized in four major sections as discussed below:

Firstly, we investigated the drug-excipient incompatibility in the physical mixtures and its influence on bulk homogeneity and flowability for DPI applications. Here, binary mixtures with model drugs (aceclofenac and salbutamol sulfate) and lactose monohydrate (commonly used excipient in commercial DPI formulation) are prepared separately at varied drug loading (1–33 w%). The DSC, P–

XRD and FT-IR studies show a significant shift in the signature peak of drug and excipient while ss-NMR, LC-MS show the absence of peaks. In contrast, new peaks are observed in LC-MS and GC studies. The findings indicated the formation of condensed or addition compound. This is attributed to an interaction between polar protic groups ($-\text{NH}-$, $-\text{COOH}$, $-\text{OH}$) and hemi-acetal carbon ($\text{HO}-\text{C}-\text{OR}$) of drug and excipient in the solid-state. It induces crystal strain and alters bulk properties related to mixing (relative standard deviation %RSD), cohesion and flow function coefficient (FFC). However, surface modification of excipient using magnesium stearate (MgSt) and Aerosil R972 (model nano-particle) guard or protect the highly active protic groups of LM to reduce the drug-LM interaction which improves the drug content uniformity and bulk flow properties of these mixtures pivotal for DPI performance.

While the above study determines the possibility of drug-excipient incompatibilities in DPI mixtures, the thesis also comprehend the **correlation of particle-bulk properties of lactose carrier with aerodynamic performance**. In this prospect, two different morphology lactose particles (LM_x , LM_f) are engineered for inhalation application using liquid anti-solvent crystallization method and compared with commercial lactose carriers (Inhalac 251; LM_c). The characterization of engineered lactose particles LM_x and LM_f confirm significant differences in properties such as higher surface area, roughness, surface energy and superior aerodynamic properties compared to commercial lactose carrier (Inhalac 251, LM_c). The inhalation performances of formulations with 1.48% w/w SS were examined. The in-vitro aerosolization results show the high emitted dose (92.62%) and high fine particle fraction (FPF 44.85%) for formulations with LM_f compared to that with LM_x (~33.23%) and LM_c (~23.40%). Further, the impact of physicochemical properties of the three carriers (LM_c , LM_x and LM_f) on aerosolization performances %FPF was assessed using principal component analysis (PCA) for 18 formulations (three carriers (LM_c , LM_x and LM_f) with two model drugs (SS and AC) at three drug loading (1, 1.48, 5% w/w). The PCA reveals that the improvement in %FPF of the formulations consisting of lactose particles (LM_f) is majorly attributed to higher surface roughness, surface area, surface energy and permeability. The study attributes can be better used to guide DPI performance.

In addition to carrier-based formulations for low drug dosage (as mentioned above), we also **designed the carrier-free formulation** as an alternative to drug-excipient formulation for high drug dose inhalation. Here, inhalable balloon-like hollow spherical salbutamol sulfate (model drug, $\text{SS}_{\mu\text{b}}$) particles is engineered from commercial salbutamol sulfate (SS, active pharmaceutical ingredient) through ultrasound-assisted crystallization coupled with stirring technique. The optimized processing variables such as drug concentration, sonication time, stirring time, solvent/antisolvent ratio significantly influence in tailoring particle shape and size. The insights into the mechanism of particle formation reveal that a hollow microsphere is formed by the density difference of SS within the droplet core to that of a droplet's surface. The analytical investigations of $\text{SS}_{\mu\text{b}}$ display 87.19% crystallinity with same chemical identity as SS and better flowability. The in-vitro aerosolization for $\text{SS}_{\mu\text{b}}$ shows 37.4% fine particle fraction and 95.1% emitted dose compared to 5.9% and 75.9% respectively for SS as carrier-free formulation. This is attributed to the hollow, porous, spherical particles with low surface charges and comparatively large particle size, surface roughness.

Further, there is growing interest for **designing inhalable aerogel microparticles for sustained pulmonary drug administration**. However, designing porous polymeric particles with aerodynamic diameter (d_{aero}) < 5 μ m remains major challenge. This study documents the low-cost design of inhalable calcium-alginate aerogel microparticles using hydrogel templated approach coupled with supercritical drying. Drug (salbutamol sulfate, SS) encapsulation is carried out using direct antisolvent crystallization. Optimized process conditions yielded porous spherical microparticles with d_{aero} 3.28 μ m and superior aeration properties. Optical, SEM images reveal nano/micron-size drug within hydrogel core and on the surface of microparticles. Analytical and simulation studies confirm crosslinking and drug-alginate non-bonded interactions while preserving crystal structure of drug. Sustained drug release upto 58.69% in phosphate buffer (pH 7.4) is achieved in 12h when compared with the burst dissolution of SS. Aerogel with ~10% drug loading resulted in higher fine particle fraction (51.40%) and emitted dose (95.96%). Overall, the method is simple, affordable and potent for DPI application.

In summary, this dissertation advances the fundamental understanding of the development of DPI formulations and provides effective formulations design for pulmonary drug administration. Detail insights of interactions between drug and excipient in physical mixtures are investigated. Further, designed surface engineered lactose carrier particles for improve FPF (maximum 44.85% from the current work). The thesis also came up with alternate carrier-free formulation (balloon-shaped inhalable drug particles) for high drug delivery (95.1% emitted dose and 37.4% FPF). Also, designed affordable bio-polymeric inhalable aerogel microparticles for sustained drug release through DPI. The state-of-art featuring different morphological aspects can be applied for various other pharmaceutical applications.

Title: Building stimuli-responsive nanoparticle assemblies by tuning charge correlations
Researcher: Pothukuchi, Rajesh Pavan
Supervisor: Radhakrishna, Mithun
Year: 2022
Keyword's: Nanoparticle, Coarse-grained Molecular Dynamics (CGMD), Self Assembly
Call No.: 620.5 POT
Acc. No.: T01039

Abstract: The dissertation, "Building stimuli-responsive nanoparticle assemblies by tuning charge correlations," focuses on understanding the role of electrostatics in the self-assembly of polyion grafted nanoparticles (NPs) in solutions and their response to external stimuli using the principles of statistical mechanics, molecular dynamics simulations, and experiments. Nanoparticle self-assembly in solution has gained immense interest due to the enhanced optical, chemical, magnetic, and electrical properties, which manifest at the macroscale. The self-assembly is driven by molecular forces, including van der Waals interactions, hydrophobic forces, and electrostatics. Solvent plays a significant role in understanding the self-assembly of NPs in solutions. Grafting NPs with polyions increases functionality and provides a wide range of tuning parameters like graft length, graft density, chain flexibility, NP size, molecular weight, and polydispersity of polyions. This thesis work presents a fundamental perspective on building nanoparticle assemblies by utilizing the electrostatic interactions of the polyion grafted NPs (PGNs).

We performed coarse-grained molecular dynamics (CGMD) simulations to understand the charge-driven self-assembly of spherical NPs grafted with polyelectrolyte (PE) chains. PGNs self-assemble to different structures driven by both excluded volume and electrostatic interactions. Our study shows that by tuning the graft density, the chain length, and the charge density of the grafts, we could build and control a variety of self-assembled structures ranging from rings, dimers, strings, coil-like aggregates, and disordered to ordered aggregates. The rings and aggregates obtained are quantified by calculating the probability of formation. The ordered nature of aggregates was measured by plotting the pair correlation functions by extending Voronoi analysis and calculating crystal cell data. These nanoassemblies built by these PGNs respond to external stimuli like pH, temperature, and electric or magnetic fields. CGMD simulations were performed to understand the stimuli-responsive behavior of these nanoassemblies in the presence of salt and polyelectrolytes. At low grafting density, a transformation from ring morphology to form dimers/strings/dispersed NPs was observed upon the addition of divalent/trivalent salts. Further, in the presence of polyelectrolytes, these transitions occurred at lower monomer valency due to the stronger electrostatic interactions between the grafted chains and oppositely charged free polyelectrolytes in solutions. Disordered and ordered aggregate assemblies formed at higher grafting density were broken into smaller NP assemblies in the presence of salt. Drug encapsulation studies in the presence of salt and polyelectrolytes were performed on model drug moieties to demonstrate the potential use of the modeled stimuli-responsive nanoparticle assemblies in drug delivery applications.

DNA-mediated directed self-assembly of gold nanoparticles (AuNPs) has garnered immense interest due to its ability to precisely control supramolecular assemblies. By engineering DNA-peptide interactions, the self-assembly and stimuli-responsive behavior of AuNPs grafted with single-stranded DNA (ssDNA), and poly-L-lysine (PLL) chains were studied. Our findings show that the electrostatic interactions between the negatively charged ssDNA grafts and positively charged PLL grafts drive the self-assembly of AuNPs of different sizes into 3D nanostructures. The transmission electron micrographs confirm that the smaller AuNPs grafted with PLL chains form a corona around the large AuNPs grafted with ssDNA like the petals around a flowery core to drive aggregation of large AuNPs. The presence of excess ssDNA / PLL chains in solutions affected both the morphology and the mechanism of aggregate formation. CGMD simulations qualitatively matched the experimental findings and provided a scientific rationale for the above findings highlighting the role of chain entropy, molecular connectivity, and charge correlations on the self-assembly of AuNPs.

At low grafting densities, despite the fast-evolving synthesis techniques, it is still experimentally difficult to precisely control the position of tethers/grfts on the surface of NPs. CGMD simulations were performed to study the effect of graft angle on the self-assembly of PGNs at low grafting densities. A wide range of morphologies like dimers, rings, strings, coils, tetramers, and aggregates are formed depending on the angle between the grafts. The effect of grafting angle is further amplified in the case of semi-flexible and rigid chains tethered on NPs. Studies on a system comprising an equimolar mixture of NPs grafted with polyions at varying grafting angles showed that the polyions grafted at low/high grafting angles preferentially interact with oppositely charged polyion grafts tethered at low/high graft angles. The results obtained from our graft asymmetry studies act as a template for understanding the molecular-level aspects of grafting, thereby aiding experimentalists in building assemblies for diversified applications. This thesis work also highlights how simple coarse-grained models can provide deep insights into the interactions occurring at the nanoscale.

* * * * *



CHEMISTRY



Chemistry

Title: Synthesis and photoinduced processes of donar-acceptor substituted diarylbutadienes

Researcher: Agnihotri, Harsha

Supervisor: Kanvah, Sriram

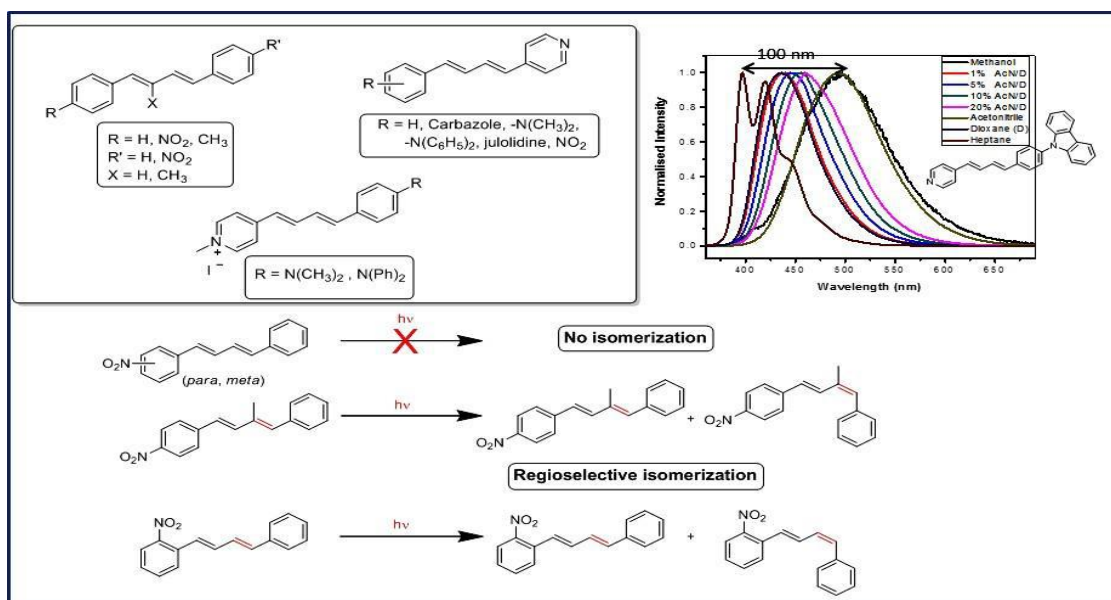
Year: 2015

Keyword's: Diarylpolyene Scaffold, Fluorescence and Photochemical Properties, Photoisomerization, Bathochromic Emission, Hydrochloric Acid

Call No.: 540 AGN

Acc. No.: T00097

Abstract: Several donor- π -acceptor systems based on diarylpolyene scaffold were synthesized and examined for their fluorescence and photochemical properties. The fluorescence investigations of these dienes reveal weak to strong solvatochromism attributed to intramolecular charge transfer (ICT). The systems containing nitro as acceptor, exhibit very weak quantum yields. Changing the position of nitro group from *para*, *meta* or to *ortho* results in further loss in emission. Interestingly, simple *para* (or *meta*) nitro diarylbutadienes show inefficient photoisomerization. However, introduction of a methyl group on the double bond in the same system yields regioselective isomer of methyl substituted double bond. Likewise presence of nitro group at *ortho* position also yields regioselective isomer of the double bond distal to the aromatic nitro group. Such behaviour is explained by (a) steric effect of methyl group that induces non-planarity and (b) the intramolecular C – H ... O hydrogen bonding that inhibits the isomerization of the proximal double bond. Similar photoisomerization observations were seen with a pyridyl group in place of phenyl ring. NMR and single crystal X-ray data substantiates these observations. Incorporation of suitable donating groups on phenyl ring of an arylpolyene scaffold bearing pyridine as an acceptor reveals remarkable fluorescence properties with strong bathochromic emission shifts. Methylation of pyridine results in a positively charged pyridinium ion which enhances the electron withdrawing ability and show strongly red-shifted emission near $\sim 700\text{nm}$. Such a strong emission, coupled with water-solubility can have useful applications as fluorescence probes for biological media



Title: Synthesis and studies of meso-functionalized porphyrins, N-confused porphyrins and metal dipyrriina to complexes
Researcher: Das, Sudipta
Supervisor: Gupta, Iti
Year: 2016
Keyword's: N-confused Porphyrins, Energy Donor-acceptor, Triphenylamine Dipyrriinato, Photophysical Studies
Call No.: 547.593 DAS
Acc. No.: T00178

Abstract: Porphyrins and its derivatives have been well studied for their potential application in biology, medicine and catalysis. Porphyrin derivatives have also been used as artificial light harvesting systems to capture and store energy. Porphyrins are important for its rich photophysical properties and coordination chemistry. Inspired by these interesting properties of porphyrin derivatives, venture has been made to synthesize and characterize novel difunctionalized porphyrins, Functionalized N-confused porphyrins (NCPs) and metal dipyrriinato complexes have drawn attention in recent times due to various applications. All the synthesized molecules have been thoroughly studied for understanding the photophysical and electrochemical, more specifically, redox properties. The present thesis consists of three main chapters viz. synthesis and studies of di- and mono- functionalized NCPs. Energy donor-acceptor type trans-A₂B₂ type porphyrins and triphenylamine dipyrriinato metal complexes. Along with these, an initial chapter consisting of the synthesis of common precursors which has been utilized in various projects has been drafted. The second chapter accounts for the synthesis, characterization photophysical and electrochemical studies of functionalized NCPs. Even though, there are several reports of the synthesis of tetra meso substituted NCPs, only few studies have been reported where synthesis of asymmetric of functionalized NCPs have been carried out. Moreover, unlike porphyrins, NCPs are less explored as light harvesting systems and in energy donor-acceptor based conjugates. Therefore an attempt has been made to synthesize di- and mono-functionalized NCPs which can be utilized in the synthesis of energy donor-acceptor type dyads or triads. Synthesis of these functionalized NCPs are challenging and therefore our first objective was to synthesize the molecules with modified synthetic strategy which is versatile to produce functional NCPs in better yield. Finally, a detailed study has been made to synthesize donor-NCP-donor (D- π -A) type triads employing the difunctionalized NCPs.

The third chapter consists of the synthesis, characterization and studies of energy donor- acceptor (D-A) type trans- A₂B₂ type porphyrins where sterically bulky and electron rich meso substituents have been chosen as donor. There are several reports of the synthesis and studies of trans- A₂B₂ type porphyrin, however, such bulky meso substituent based donor-acceptor system are novel of its kind. These molecules have been studied thoroughly by UV-Vis, steady state and time resolved fluorescence spectroscopy and cyclic voltammetry, Zn(II) and Pd(II) metal complexes have also been synthesized and studied especially for photophysical studies. The energy-transfer efficiencies of the different donors viz. N-butylcarbazole, N-butylphenothiazine and triphenylamine have also been studied qualitatively and quantitatively. The final aim of this work is to employ these molecules for bioimaging studies which require few more synthetic steps and is beyond the scope of the present work. The fourth chapter presents the synthesis, characterization, photophysical and

electrochemical studies of the triphenylamine dipyrinato metal complexes. Dipyrins structurally resemble to be the half part of porphyrins. However, their photophysical and electrochemical properties are very much different compared to the porphyrins. In the last decade metal dipyrinato complexes have been well studied and much of its potential applications in luminescent materials, sensing, sensitized solar cells and metal organic frameworks have been revealed. In the present context, our interest lied in the understanding of the role of different metals on the same dipyrinato ligand and studying the photophysical and electrochemical properties of the complexes. A set of homoleptic, heteroleptic and bimetallic type metal complexes have been synthesized and studied. The metals have been chosen on the ground of their coordination [Ni(II), Co(II)] and photophysical [Zn(II), Pd(II), In(III)] properties.

Finally, the experimental results have been summarized and conclusions have been drawn which is certainly a juxtaposition of objectives accomplished and future scopes.

Title: Design, synthesis and photoinduced behavior of π -conjugated substrates: aggregates and self-estimate

Researcher: Palakollu, Veerabhadraiah

Supervisor: Kanvah, Sriram

Year: 2016

Keyword's: Substituted Aryl Polyenes, Aggregation Induced Enhanced Emission, Dimethylamino Donor

Call No.: 541.35 PAL

Acc. No.: T00180

Abstract: π -Conjugated substrates containing donor and/or acceptor substituents gained tremendous attention because of their wide applicability in materials to biology. Several variants of such π -conjugated aryl and heteroaryl derivatives were designed, synthesized and investigated for their photoresponsive behavior. In this work, we have synthesized a series of donor (dimethylamine, triphenylamine, carbazole) or acceptor (nitro, cyano, isoxazole) substituted aryl polyenes and examined their fluorescence response in organic solvents and in heterogeneous media of micelles and sodium cholate. Upon substituting, a cyano group on the double bond, remarkably enhanced emission characteristics was observed in aqueous media. This emission is attributed to the formation of aggregates and this phenomenon is generally known as Aggregation Induced Enhanced Emission (AIEE). Such aqueous media emission response is used in determining critical micelle concentration (CMC) of the surfactants and to study pH sensitivity. Cholesterol tethered substrates containing dimethylamino donor and nitro acceptor result in large solvatochromic emission changes while presence of the cyano group on the double bond result in formation of nano structural assemblies. These cholesterol conjugates have been utilized to probe the changes in bile salts and surfactant assemblies. In presence of bile salts, cyano substituted stilbene and its cholesterol conjugates have exhibited nanostructures. The π -conjugated systems can find greater applications in their polymeric state compared to their monomeric form as many of the physical properties will improve. Therefore, to address this coumarin, thio coumarin and naphtho coumarin monomer derivatives have been synthesized and the optical properties have been examined. Polymers of the conjugated systems containing coumarin have been synthesized by step growth polymerization techniques and subsequent formation of photodimers is investigated.

Title: Lead identification and development against histone deacetylase, carbonic anhydrase cyclooxygenase-2 and thromboxane prostanoid receptor
Researcher: Shabbirali, Hadianawala Murtuza
Supervisor: Datta, Bhaskar
Year: 2017
Keyword's: Bioisosterism, Design Multi-target Ligand, Drug Design
Call No.: 616.24 SHA
Acc. No.: T00205

Abstract: Drug discovery is a highly time consuming and costly process. Lead identification and development are key steps in the drug discovery programme. Studies have suggested that a large number of commercially available drugs exhibit deep structural similarity to the lead compounds from which they were developed. Quality lead identification in terms of compounds with high potency and selectivity, favourable physicochemical parameters and invitro Absorption Distribution Metabolism and Excretion (ADME) parameters is the foremost requirement for the success of drug discovery process. In the present work we focus on lead identification for specific pharmaceutically important targets.

In our current investigations we exploited the principle of bioisosterism for lead identification across various targets. In particular, we have developed sulfonylurea derivatives as lead compounds for Histone Deacetylase (HDAC) activator and Carbonic Anhydrase (CA) inhibitor. Starting with HDAC, systematic Structure Activity Relationship (SAR) studies were performed using known HDAC inhibitors. SAR studies suggest that a modular architect of zinc binding group (ZBG), linker and cap require for effective HDAC inhibition. A set of a novel compounds with sulfonylurea as zinc binding group (ZBG), alkyl chain as linker and phenyl group as cap were designed. Length of linker chain was optimized using docking studies. All the designed compounds were synthesized by sodium cyanate mediated synthesis of sulfonylurea method. Synthesized compound were screened for its HDAC inhibitory activity using HDAC1 isoform. Interestingly, some of these compounds show HDAC1 activation rather than inhibition. Compound 1 shows approximately 2 fold activation at 100 μ M concentration. Numerous controls were performed in order to verify the results and to finally conclude that the designed compounds show HDAC activation rather than inhibition. Molecular docking studies of compound 1 revealed that sulfonylurea group of compound 1 binds with zinc metal present in the active site of HDAC2 (HDAC2 isoform were used because of unavailability of HDAC1 isoform crystal structure). Similarly a new set of compounds were designed with tosylureido group for another pharmaceutically important zinc metalloenzyme, namely carbonic anhydrase. All designed compounds were synthesized by using the same sodium cyanate mediated synthesis of sulfonylurea method. Screening of these compounds for their carbonic anhydrase inhibitory properties using human carbonic anhydrase II (hCAII) led to identification of compounds 12 and 13 with IC_{50} of approximately 600 nM. A FRET based assay implicates the lead compounds i.e. compound 12 and 13 as binding in proximity to the active site region of the enzyme. Molecular docking studies reveal that compound 12 and 13 bind to residues at the entrance of the active site thereby blocking access and resulting in enzyme inhibition. Based on our results, analogues of the lead compounds were designed and synthesized for Structure Activity Relationship (SAR) and isoform-selectivity studies. Preliminary studies of newly synthesized compound against hCAII

inhibitory activity show promising results and its detailed investigation for its isoform selectivity is under way in collaborator's laboratory.

In developing sulfonylurea-derivatives as zinc metalloenzyme modulators, we have expanded the scope of a hitherto unexplored method of synthesis of sulfonylureas from sulfonyl chlorides and amines using sodium cyanate. In our lead identification programme for HDAC, we were able to access aliphatic sulfonylurea using sodium cyanate mediated synthesis of sulfonylurea method. In case of aliphatic sulfonylurea for HDAC i.e. compound 1-5, the scope of reaction was explored using various sulfonylchlorides. Further scope of reaction in term of amine was examined by using various sulfonylchlorides and employing aniline as amine. Reaction of propylamine with ethanesulfonyl chloride yields novel sulfonylureas with aliphatic side chains on both sides. Similarly scope of reaction in term of aromatic sulfonylchloride and amine were studied in our programme for lead identification for CA using the compounds 11-23.

Results clearly indicate that nature of both the substrates influence the reaction. In case of electron donating groups on both the substrates, the reaction works well but in case of electron withdrawing group on them, the reaction does not yield desired product. In case of p-chlorophenyl sulphonyl chloride, the reaction shows interesting by-product profile. Isolation and characterization of by-product with the help of ¹HNMR, ¹³CNMR and LCMS led to discovery of novel sulonyltriuret compounds. Initial attempts to decrease formation of sulfonyltriuret by varying various reaction parameters such as equivalents of sodium cyanate, time of addition of amine, solvent and temperature were in vain. The formation of sulfonyltriuret in each case is predictable. We thus investigated sodium cyanate mediated method for synthesis of sulfonylurea, as a method for synthesis of sulfonyltriuret. We have successfully isolated and characterized the corresponding sulfonyltriuret in some of the above reaction and the scope of the single-step reaction has also thus been investigated as a method for preparation of sulfonyltriurets. The unique structural features of the sulfonyltriurets, namely the presence of pseudo-peptide bonds and resemblance to triurets indicate potential applications.

In the last part of our work we used a Design Multi-target Ligand (DML) approach for drug design. Inspired by bioisosterism of pharmacophores and by combining essential pharmacophores for their cognate targets, we attempted to identify a lead for dual inhibition of cyclooxygenase-2 (COX-2) and Thromboxane Prostanoid (TP) receptor. Such dual inhibitors are still in a nascent stage of development and have been suggested as the next generation of anti-inflammatory and pain-relieving medicines. We combined the essential pharmacophores from an established COX-2 inhibitor (Celecoxib) and a TP receptor antagonist (BM-573) into designing one class of molecules. Designed compounds were retrosynthesized and the synthesis of designed compound using the scheme intermediate C2 was achieved. Reaction of intermediate C2 (possessing primary amine group) with sodium cyanate and tosylchloride (sodium cyanate mediated synthesis of sulfonylurea) towards corresponding desired sulfonylurea derivatives was unsuccessful mainly because of presence of nitro group on one of the phenyl ring in intermediate C2. Since nitro is not an essential pharmacophore for both targets i.e. COX-2 and TP, proposed dual inhibitor was modified without nitro group. Based on the synthetic scheme of intermediate C2, intermediate C15 (without nitro group) were synthesized. Reaction of intermediate C15 (have primary amine group) with sodium

cyanate and tosylchloride yield the desired corresponding sulfonylurea derivative. However in the current context we fail to purify desired sulfonylurea from its sulfonyltriuret derivative. In order to provide proof of our hypothesis and to avoid synthetic challenge, we have repurposed desired dual inhibitor by using Terutroban as a known TP receptor antagonist instead of BM-573. Terutroban is a nonprostanoid TP receptor antagonist and sulfonamide is essential pharmacophore. Thus in repurposed dual inhibitor, sulfonylurea group was replaced by sulfonamide and synthesized by treatment of intermediate C15 (possessing primary amine group) with tosylchloride. All synthesized compounds were screened for their COX-2 inhibitory activity. However, compounds bearing this phenomenological design fail to display any activity against the COX-2 target. Since all of these compounds fail to show promising results against the principle target COX-2 we did not screen them for their TP receptor activity. We thereafter explored an entirely bottom-up design strategy using various techniques of computational structure based drug design (SBDD). Starting from the basic scaffold of flavonoid, activity of Design 4 was optimized for its COX-2 activity using docking studies. In the absence of structural information for TP receptor, model for TP receptor was generated based on fold recognition method. Loops were refined using prime and the quality of model was judged by using Ramachandran plot. MMGBSA based binding free energy of a known TP receptor antagonist was predicted and its correlation with experimental activity of the compound was calculated. Enrichment studies were performed to predict ability of docking protocol to distinguish active molecules from inactive ones using a set of 133 decoy compounds. The goodness of hit (GH) score was used to confirm that the docking protocol was capable of distinguishing active molecules from inactive ones. Docking and repeated iterations of structural modification finally led to design 6 which shows good docking score and binding pose in TP receptor. Docking of design 6 in the active site of COX-2 results into better stabilization due to flipping of B ring from hydrophilic to hydrophobic region. MD studies of Design 6 show that the compound is stable in TP receptor over entire simulation of 50 ns and does not diffuse away. The compound designed using the above methodology could be a potential lead as a dual COX-2 inhibitor and TP receptor antagonist and may overcome the side effects associated with COXIBs.

Title: Donor acceptor systems based on corroles, porphyrins and NIR Aza-BODIPYS
Researcher: Balsukuri, Naresh
Supervisor: Gupta, Iti
Year: 2018
Keyword's: Light-harvesting Antenna Systems, Fluorescence Spectroscopy, Tetrphenylethylene, Ethyne Linkage, Electrochemical Properties
Call No.: 547.593 BAL
Acc. No.: T00267

Abstract: Porphyrins and corroles are promising building blocks for panchromatic dyes due to their intense absorption in the visible range, high fluorescent quantum yields and high radiative rate constants. The porphyrins and corroles show interesting optical properties strong absorption and emission and they are part of the natural light harvesting systems such as chlorophyll, bacterio chlorophyll. Many covalently linked Donor-Acceptor (D-A) type systems based on porphyrins and its derivatives e.g core modified/expanded/contracted porphyrins have been synthesized to mimic natural light-harvesting systems. Also, photophysical and electrochemical studies have been carried out to understand intramolecular energy transfer and photoinduced electron transfer in such systems. In past two decades the chemistry of corroles has seen significant growth. Several mono and di functionalized corroles have been synthesized and utilized for the construction of D-A systems. The introduction of other donor chromophores at β and *meso*-positions altered the electronic properties of the corroles. Furthermore, porphyrin and corrole derivatives have found many applications in biology, materials and catalysis. Inspired by the bioimaging agents/photosensitizers interesting properties of these molecules, we prepared a series of Donor-Acceptor (D-A) type carbazole linked porphyrins, corroles systems for bio-imaging applications. All the synthesized molecules were characterized by standard spectroscopic techniques; optical studies were done using UV-vis and fluorescence techniques. The electrochemical studies were performed for target compounds by cyclic voltammetry in solution. Also, single crystal X-ray was done for selected compounds.

The thesis mainly highlights the synthesis, optical and electrochemical properties of D-A type systems based on porphyrin, corroles and aza-BODIPYs. Such D-A systems with NIR absorption and emission properties have potential applications in light-harvesting antenna systems, bio-imaging of live cells /deep tissue imaging and as photosensitizers in photo dynamic therapy (PDT).The present thesis consists of four chapters. In the first chapter, we described the synthesis of reported precursor molecules and they were characterized by standard spectroscopic techniques like IR, MS, NMR, UV-vis and fluorescence spectroscopy. The remaining three main chapters describe the synthesis and studies of D- π -A type carbazole-corrole/porphyrin systems, energy/electron donor groups bearing D-A type near-infrared (NIR) aza-BODIPYs and tetrphenylethylene (TPE) substituted aza-BODIPYs. The second chapter accounts for the synthesis and studies of D- π -A type carbazole corrole/porphyrins dyads and triads. All the molecules have been studied in detailed by absorption, fluorescence, time-resolved and electrochemical spectroscopy. The length of the spacer between the D and A was varied from "phenyl-ethyne" to "ethyne" linkage. The effect of the linker length on the spectral properties of these dyads and triads were studied. The introduction of carbazole unit at *meso* position of corrole/porphyrin with "phenyl-ethyne" or "ethyne linkage" showed significant

changes on the spectral properties of molecules. The absorption and emission properties of “ethyne” bridged dyads showed more red shifts as compared to “phenyl-ethyne” bridged dyads and triads. Efficient energy transfer (ETE) was observed in these dyads and triads between 48-84%. The maximum ETE up to 84% was observed for dyads with short “ethyne linkage” as compared to longer dyads/triads with longer “phenyl-ethyne” bridge.

In aza-BODIPYs the presence of electron donating groups, extending π -conjugation at *para* positions of 1,7 and 3,5-positions of phenyls and formation of B-O bond altered the electronic properties of aza-BODIPYs, which caused red shifts in the absorption and emission spectra of molecules. The third chapter of the thesis consist of D-A systems based on near infrared (NIR) aza-BODIPYs. A series of D-A type aza-BODIPYs and corresponding aza-dipyrrins containing bulky energy/electron donor groups at their 1,7- positions were designed and synthesized. The donor moieties at 1,7-positions of aza-BODIPY core have been changed from naphthyl, *N*-phenylcarbazole, *N*-butylcarbazole and ferrocene in the aza-BODIPYs. Also 3,5- positions were substituted with phenyl or thienyl groups. The presence of energy/electron donor groups affected the spectral properties of these compounds and comparative studies of optical and electrochemical properties were carried out by changing the donor groups. The absorption and emission spectra of aza-BODIPYs were significantly red shifted as compared to the parent 1,3,5,7- tetraphenylaza-BODIPY (TPAB), owing to the presence of donor moieties at 1,7 position of aza-BODIPYs. However in case of ferrocene blue shifted absorption and emissions were observed as compared to TPAB. Furthermore, the presence of thienyl groups resulted in better electronic interactions between the aza-BODIPY core and thiophene rings, which in turn caused redshifts in the electronic spectra of such compounds relative to their 3,5-phenyl counterparts. Fluorescence studies suggested effective energy transfer (up to 93% ET) from donor groups to the aza-BODIPY core in all the compounds. Density functional theory (DFT) studies revealed effective electronic communication between the donor groups and acceptor aza-dipyrrin moieties in all the aza-BODIPYs.

In fourth chapter of the thesis, the design and synthesis of tetraphenylethylene (TPE) appended aza-BODIPYs have been reported. In this chapter, we wanted to understand the effect of TPE units on the photophysical and electrochemical properties of aza- BODIPYs. The 1,7 positions of aza-BODIPYs varied from phenyl to thiophene and *N*- butylcarbazole; whereas, the *para*-positions of 3,5 phenyl group of aza-dipyrrin ligands were connected with TPE unit. The presence of phenyl, thiophene, *N*-butylcarbazole and TPE units significantly altered the electronic properties of aza-BODIPYs. The red shifted absorption and emission were observed for *N*-butylcarbazole-TPE aza-BODIPY due to presence of strong electron donating ability and extended conjugation of *N*- butylcarbazole and TPE units. Furthermore, the AIE behavior was observed for TPE appended phenyl and thiophene aza-BODIPYs whereas, ACQ property was shown by *N*- butylcarbazole-TPE aza-BODIPY.

Final aim of this thesis is to prepare water soluble derivatives of porphyrins/aza- BODIPYs which requires more synthetic steps and is beyond the scope of the present work. The synthetic challenges to create the library of D-A systems based on porphyrins/corroles/aza-BODIPYs are over come in this thesis. The photophysical and electrochemical studies of such D-A systems shed light as the energy/electron transfer processes within the molecule. These NIR dyes have tremendous potential in biology as photosensitizers/fluorescent labels for applications as diagnostic/therapeutic aggens.

Title: Synthesis and spectroscopic investigations of neutral and water soluble fluorophores: charge transfer, aggregates and self-assemblies

Researcher: Anuji, K. V.

Supervisor: Kanvah, Sriram

Year: 2017

Keyword's: Biological Environment, Supramolecular Hosts, Aggregation-Induced Emission, Protein Binding

Call No.: 543.5 ANU

Acc. No.: T00278

Abstract: Donor- π -acceptor conjugated systems have been extensively studied owing to their unique properties as photoresponsive materials for optical and biological applications. In particular, our focus is design and synthesis of neutral and water-soluble fluorophores and investigations of their photophysical properties. Absorption, steady-state fluorescence, and fluorescence lifetime measurements were used to investigate the effect of solvents (organic solvents and ionic liquids) on nitrodiphenylbutadienes. A red shift in absorption maxima is observed in ionic liquid media concerning polar organic solvents. We observed no effect in absorption maxima, and very little difference in emission maxima of the dienes by altering cationic components of the ionic liquids have different alkyl chain lengths, and the shifts in absorption in ILs are attributed to the viscosity effect and not due to solvent polarity effect. All the nitro-substituted diphenylbutadienes show dual emission in ILs and ethanol due to the presence of locally excited (LE) state and charge transfer (CT) band. Moreover, Interestingly, we observed excitation wavelength dependent emission in ethanol for p-methoxy p-nitro diphenylbutadiene. The multi- exponential decay of the dienes from time-resolved experiments and emission studies verify that fluorophores experience differential interaction with diverse microenvironments of ionic liquids.

Many donor-acceptor substituted organic molecules exhibit excellent charge transfer character, but for their biological use, it is important also to have water solubility. A way of introducing water solubility is to derivatize suitable groups through the introduction of an anion or cation or by the introduction of the suitable water-soluble moiety. Covalent conjugation with carbohydrate moieties can induce water solubility and can result in specific target detection through protein-carbohydrate interaction. This led us to a detailed investigation of the water-soluble cyanostilbene-glycoconjugate system and its interactions with solvents and biological media. We reported the synthesis of a novel water-soluble stilbene and its absorption and fluorescence behavior in organic solvents, binary-solvent mixtures, water and in the presence of proteins, concanavalin A (Con A), bovine serum albumin (BSA) and human serum albumin (HSA). We observed unique aggregation-induced emission (AIE) behavior of this stilbene molecule in 1, 4- dioxane/hydrocarbon solvents solvent pair with large Stokes shift. The aggregation behavior is characterized by FESEM and DLS studies. To check its potential application in protein binding we used serum albumins and Con A. The investigations reveal role play of both hydrophobic and hydrophilic interactions in binding with BSA and HSA while in Concanavalin A, carbohydrate-mediated hydrophilic interactions facilitates the binding. The results imply preferential binding interactions of the fluorophore with proteins.

Can a positively charged molecule target an anionic surfactant? With this objective, we studied the interaction of a water-soluble red emitting cationic in different surfactant media by using absorption, emission, and time-correlated single photon counting techniques. We observed a multi-

fold intensity enhancement in emission in the presence of anionic surfactants such as SDS, AOT and zwitterionic surfactants such as CHAPS and no significant effect with a positively charged surfactant, CTAB, and neutral surfactant TX-100. The fluorophore- surfactant interaction induces distinct color changes and optical properties indicating the selectivity and sensitivity towards negatively charged surfactants, and this is attributed to the electrostatic attraction between the negatively charged surfactant head group and the positively charged pyridinium ring of the fluorophore. Such distinguishable emission behavior and colorimetric sensing are major advantages in the industrial and biological field for targeted detection.

An important feature of water-soluble cationic dyes is its photophysical and self- assembly formation induced by host-guest interactions with macromolecule in aqueous media. We demonstrated the effect of encapsulation of cucurbituril 7 (CB-7) in varied pH solution using absorption, steady-state fluorescence, scanning electron microscopy (SEM), atomic force microscopy (AFM), optical microscopy and ¹H NMR measurements. We observed tunable photophysical characters and 1:2 guest-host binding interactions accompanied by the formation of different nanostructures. These findings highlight the importance of host-guest interactions for tunable emissive properties. We anticipated that the introduction of long alkyl chain could improve self-assembly formation of the donor-acceptor scaffold. To understand the response of alkylated chain over the non-alkylated ones, we synthesized two novel AIE active α -cyanostilbene fluorophores with nonpolar octyl and hexadecyl chains and investigated its self- assembling property in different solvents. To get insight into the self-assembly formation, we used different experimental techniques includes absorption, steady-state fluorescence, transmission electron microscopy (TEM), scanning electron microscopy (SEM) and dynamic light scattering (DLS) studies and monte-carlo simulations. Our results emphasize self-assembly formation in aqueous solution into well-defined nanospheres and aggregates because of the hydrophobic interactions. Self-organization of small organic molecules into nanostructures have promising material applications.

Title: Design and development of dimeric-cyanine dyes: self-assembly and interaction with biomolecules

Researcher: Patlolla, Prathap Reddy

Supervisor: Datta, Bhaskar

Year: 2019

Keyword's: Dimeric Carbocyanine Dye, Biomolecules, Fluorescence Intensity, Fluorescence Enhancement, Self-assembly

Call No.: 541.382 PAT

Acc. No.: T00503

Abstract: Cyanine dyes have been extensively researched for their ability to self-assemble into aggregates with distinctive photo physical properties. The unpredictable character of such self-aggregation has led to the development of strategies that can render greater control on aggregate formation. The template-directed aggregation of cyanine dyes has been comprehensively examined as a mechanism for formation of controlled dye aggregates. Templates such as polymeric DNA duplexes and polyanions have been found to play a crucial role in controlling the aggregation of symmetrical dicarbocyanine dyes. Also, DNA-templated dye aggregation has highlighted the importance of dye-dimers as the building blocks of supramolecular assembly.

In our work, we have designed and developed a series of dimeric cyanine dyes that are capable of template free self-assembly. A series of N-linked dimeric benzothiazole containing carbocyanine (trimethine) dyes and dicarbocyanine (pentamethine) dyes have been synthesised and characterised by 1D NMR, 2D NMR and ESI mass spectroscopy. Self-assembly of these dyes has been confirmed with a variety of spectroscopic techniques. We observe a strong correlation between the length of linker connecting two dye units with their ability to preferentially dimerise and form extended aggregates. Aggregation propensity of dimeric carbocyanine dyes are distinctly different from monomeric carbocyanine dyes. The dimeric dyes are found to form H-dimers and H-aggregates without the need for external templates and the resulting fluorescence is quenched. In addition The N-propyl linked dimeric dicarbocyanine dye exhibits pronounced H-aggregation at micromolar dye concentrations with the absorption maxima blue-shifted by nearly 200 nm. In contrast, an N-hexyl linked dye preferentially folds into H-dimers. Similar aggregates of the monomeric dicarbocyanine dyes are known to be observed at much higher dye concentrations or only in the presence of suitable templates. The aggregate species of the dimeric dicarbocyanine dyes are identified based on shifts in their absorbance maxima and quenched fluorescence. Further, introduction of DNA molecules with AT-tracts leads to transformation of the spontaneously formed dimeric dye H-aggregates and H-dimers into DNA-bound dye species. The calculated electronic structure of the all dimeric cyanine dyes supports their observed aggregation behaviour.

Pronounced aggregation of dimeric dyes raises the prospect of using fluorescence quenched H-dimers and H-aggregates as turn-on fluorescence probes in response to specific targets. The interaction of fluorescent dyes with serum proteins and nucleic acids has garnered significant interest owing to potential for non-covalent labeling and imaging applications. The interaction between aggregates of dimeric carbocyanine dyes and biomolecules such as BSA, [poly(dA- dT)]₂ and CT-DNA have been investigated in our work. Propyl linked dimeric carbocyanine dye aggregates

are disrupted by BSA protein resulting in more than 100-fold fluorescence enhancement in contrast to 59-fold enhancement for hexyl linked dimeric carbocyanine dye. The formation of dye-bound monomeric conformations and free H-dimers are responsible for this large amplitude of fluorescence enhancement. Notably, dimeric carbocyanine dyes interact with [poly(dA-dT)]₂ at lower concentrations resulting in fluorescence turn-off due to possible formation of dye aggregates on nucleic acid template. Propyl linked dimeric carbocyanine dye also interacts with CT-DNA showing more than 40-fold fluorescence enhancement as compared to ca. 30 fold enhancement for hexyl linked dimeric carbocyanine dye. The interaction of dimeric carbocyanine dye aggregates interaction with BSA, [poly(dA-dT)]₂, CT-DNA provide clues pertaining to the inter as well as intra-molecular character of the aggregates. Intra-molecular aggregates of hexyl linked dimeric carbocyanine dye display a more favourable interaction with BSA and CT-DNA resulting in larger amplitude of fluorescence enhancement. Monomeric cyanine dyes also show fluorescence enhancement in the presence of BSA and CT-DNA but at a lower fold as compared to dimeric dyes.

We have studied the interaction between aggregates of dimeric carbocyanine dyes and BSA in non-aggregated form. The dimeric dye self-assembly is disrupted by BSA resulting in substantial fluorescence enhancement when the dye is associated with protein over a period of time. Monomeric cyanine dye behaves in an opposite manner with dye aggregation on BSA resulting in a decrease in fluorescence intensity. The magnitude of dimeric dye fluorescence enhancement upon association with BSA is several folds greater than that experienced by a standard reporter such as Thioflavin T. The interaction of dimeric carbocyanine dye with BSA does not disrupt the secondary structure of the protein and an association constant of $\sim 1.49 \times 10^5 \text{ M}^{-1}$ is calculated for propyl linked carbocyanine dye. Aggregated forms of BSA are recognized by the propyl linked dimeric carbocyanine dye within 0.5 h via fluorescence microscopy. The ability of the dimeric cyanine dye to reveal fibrillar character of BSA aggregation in conjunction with the low background fluorescence of the dyes makes them attractive for use as non-covalent labels of protein aggregation events. Our work examines an hitherto less explored aspect of cyanine dyes and provides tools for controlling the dye self-assembly as well as their use in fluorescence sensing applications.

Title: Synthesis studies and application of porphyrins and boron dipyrromethenes appended with energy donor groups
Researcher: Praseetha, E. K.
Supervisor: Gupta, Itri
Year: 2019
Keyword's: BODIPY, Precursor Molecules, Fluorescence Spectroscopy, Phenylene
Call No.: 540 EKP
Acc. No.: T00509

Abstract: Porphyrins, a class of naturally abundant fluorescent dyes with multiple applications in the day-to-day biological process proved their applicability in multiple scientific streams. Similarly, BODIPYs, which resembles with the half portion of porphyrin, possess remarkable photophysical properties like intense absorption in the 480-600 nm region, high quantum yield, negligible triplet-state formation and excellent thermal and photochemical stability. Good solubility and easy functionalization of the BODIPY core has made them very popular among chemists. The utilisation of BODIPYs and porphyrins in several clinical and material applications have always created a scope for synthesising and studying their new derivatives. The main objective of this thesis is to synthesise novel BODIPY and porphyrin derivatives for various applications. This thesis consists of eight major chapters, comprising of synthesis, characterisation and energy transfer efficiency analysis of BODIPYs and porphyrins. Also, we reported DSSC and bioimaging studies of some of the synthesised novel BODIPYs. First chapter of the thesis described the synthesis of reported precursor molecules and their characterization by standard techniques like IR, MS, NMR, UV-vis and fluorescence spectroscopy.

Remaining seven chapters are divided into two parts; part A and part B. Chapters 2-6 in part A are mainly dealing with the synthesis, characterisation, energy transfer studies and photovoltaic and biological applications of some new BODIPYs. The second chapter gives a brief introduction on the recent developments in carbazole substituted BODIPYs. The third and fourth chapters describe the synthesis and dye-sensitized solar cell application of carbazole based D-A type BODIPYs. Substitution of electron rich carbazole donor moiety on C8-position of BODIPY affected its electronic properties. This was reflected in the higher extinction coefficient, red-shifted emission maxima, increased quantum yields and large Stokes shifts. Fluorescence studies indicated an efficient energy transfer from *meso*-carbazole moiety to boron-dipyrroin core. Modification of this BODIPY by substituting an anchoring group, cyanoacetic acid, we could convert this BODIPY as a potential photosensitizer for dye-sensitized solar cell (DSSC). Though photovoltaic performance revealed lower solar-to-electric power conversion efficiencies (PCE) for these sensitizers, improved design of BODIPYs having more electron donor groups and extended π -conjugated systems can be a strategy to have better sensitizers in the near future.

The fifth chapter explains the effect of linker size on the photophysical and electrochemical properties of bis-BODIPYs. Change in the linker size from bulky carbazole to phenylene to smaller thiophene and furan rings, affected the spectroscopic properties of bis-BODIPYs. The absorption and emission maxima were blue shifted for bis-BODIPYs having bulky aromatic spacers and red shifted for bis-BODIPYs having smaller thiophene/furan spacers. Also, the X-ray crystal structures of three

bis-BODIPYs were solved. The reduced dihedral angle between the bridging ring and dipyrroin core in all their X-ray single crystal structures indicated better interactions between the two constituting boron dipyrroin units.

Chapter six dealt with the synthesis and bio-imaging applications of thioglycosylated neutral water-soluble BODIPYs. Glucosylated and galactosylated BODIPYs showed IC₅₀ values of 23.83 to 48.61 μM in HaCaT and HeLa cells. These BODIPYs are more active in HaCaT cells with IC₅₀ values in between 23.83- 38.15 μM. Fluorescent microscopy colocalisation experiments demonstrated the ability of these thioglycosylated BODIPYs to target mitochondria in live cells. Selective mitochondrial localisation of these neutral water-soluble thioglycosylated BODIPYs make them promising candidates for cancer treatment as theranostic agents. As a future direction, the similar synthetic strategy and application can be extended for the synthesis of water soluble porphyrin.

Part B of the thesis comprises of two chapters; dealing with the synthesis and energy transfer studies of *beta* and *meso* substituted D-A type porphyrins. Chapter seven describes the synthesis, characterisation and energy transfer analysis of *beta*-substituted energy donor-acceptor type porphyrins; where, bulky electron-rich groups *viz.* *N*-butylcarbazole and triphenylamine have been employed as donor moieties. Along with two free base porphyrins, their Zn(II) and Pd(II) metal complexes have also been synthesized and characterised. Substitution of electron rich carbazole/triphenylamine donor affected directly to the electronic properties of the porphyrins and this was evident from the red-shifted absorption and emission spectra of these dyads. Introduction of Pd(II) to the core made the porphyrins phosphorescent with significant triplet emission. Energy transfer studies from the donor (e.g. *N*-butylcarbazole and triphenylamine) to the acceptor porphyrin core were carried out by using both steady state and time-resolved fluorescence techniques and these molecules showed 66-78% Förster energy transfer.

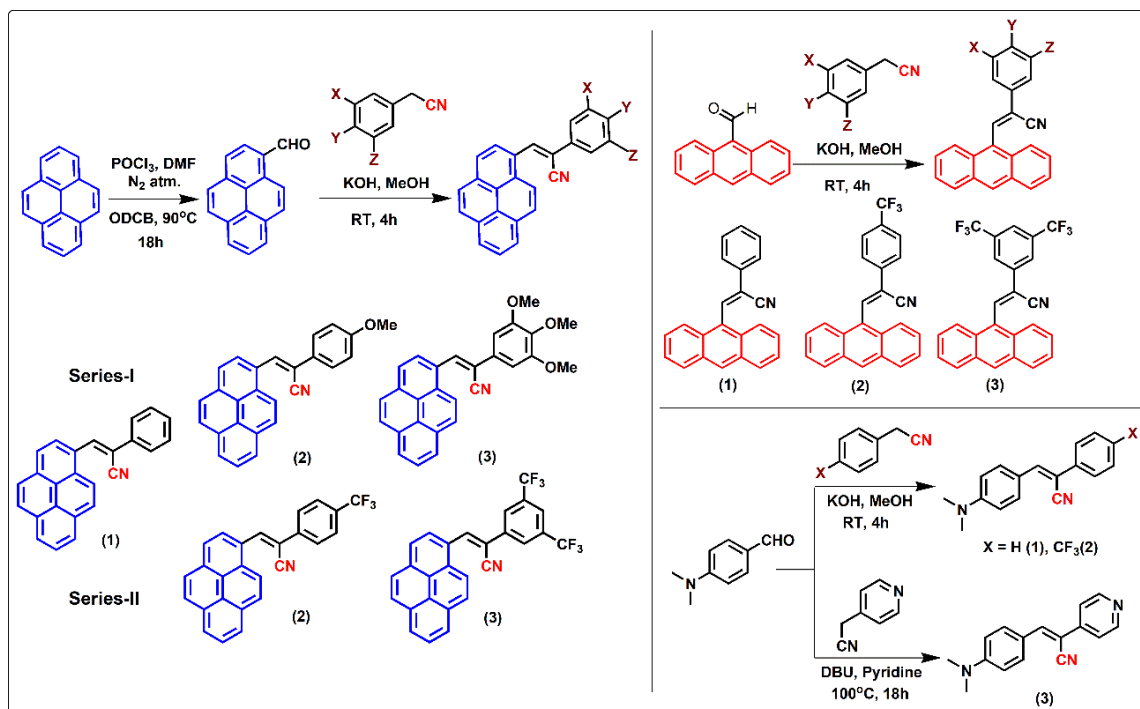
In the last chapter of the thesis, we described the synthesis and characterisation of a series of tetraphenylethylene (TPE) substituted A₂B₂ and A₃B type zinc porphyrins where, two or three TPE are present on the *meso* positions. The target compounds were obtained after multistep synthetic procedures. Acid catalysed mixed condensation of aldehydes and pyrrole ended up in the formation of desired free base porphyrin precursor. Zn metalation of these porphyrins followed by Suzuki coupling with TPE boronic acid produced the final compounds. All the target molecules were characterised by using NMR and MALDI-MS spectrometry techniques. Photophysical data showed red-shifted absorption and emission compared to ZnTPP (Reference porphyrin molecule). Thus, such TPE substituted porphyrin derivatives will have remarkable potential in biology and materials application. Energy transfer studies for all the five porphyrin derivatives were carried out in toluene and they showed an energy transfer efficiency of 54-60%. Solution based self-assembly analysis revealed that A₂B₂ Zn porphyrin with carbazole and TPE showed aggregation induced emission behaviour in THF/water solution. Further detailed analysis of aggregation behaviour of all the porphyrins is underway in our laboratory.

Title: Design and synthesis of small organic fluorophores:
Researcher: Kumar, Katla Jagdish
Supervisor: Kanvah, Sriram
Year: 2019
Keyword's: α -Cyanostilbenes, Light Emitting Diodes (LEDs), Spectroscopic Probes
Call No.: 547.1 KUM
Acc. No.: T00520

Abstract: This dissertation entitled "Design, Synthesis of Small Organic Fluorophores for Aggregation Induced Emission, Gelation, Sensing and Bio-conjugation" is focused on the synthesis and characterization of π -conjugated organic molecules with donor (D)- acceptor (A) moieties and their photophysical investigations. Starting with a general introduction, we have divided the thesis into three chapters. Each chapter contains (a) introduction, (b) literature review, (c) results and discussion and (d) experimental section. For ease of explaining the results and due to similarity of structural scaffolds, chapters 1 and 2 were divided to subsections. All the isolated new compounds are characterized by NMR, mass spectral analysis (HR-MS). The SEM, TEM analysis, and X-ray crystal structures are also determined, wherever needed. Summaries as well as references are compiled at the end of each section.

Chapter-1: Anthracene and Pyrene derivatives of cyanostilbene: Aggregation Induced Emission, and Gelation

This section deals with the synthesis and photophysical studies of anthracene and pyrene derivatives of cyanostilbene (Scheme-1.1) and their aggregation induced emission behaviour and organogel formation.



Scheme- 1.1. The cyanostilbene derivatives synthesized for this research.

α -cyanostyrenes bearing a pyrene and anthracene scaffold were synthesized using a condensation reaction of the corresponding aldehyde with the phenylacrylonitrile derivatives. The synthesized styrenes are weakly emissive in solution state but show enhanced emission in water attributed to the formation of aggregates. The restrictions of intramolecular rotations, increased intermolecular interactions contribute to the strong emission of the fluorophores in the aggregated state.

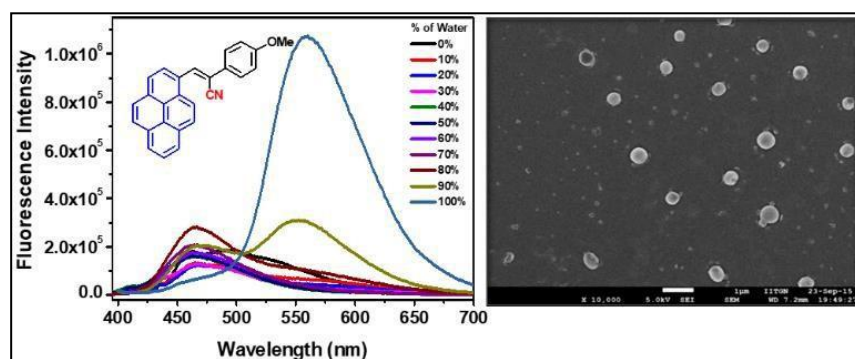


Figure 1.1. Fluorescence spectra in dioxane/water system (left) and SEM reveals the formation particles of (2) in water (right).

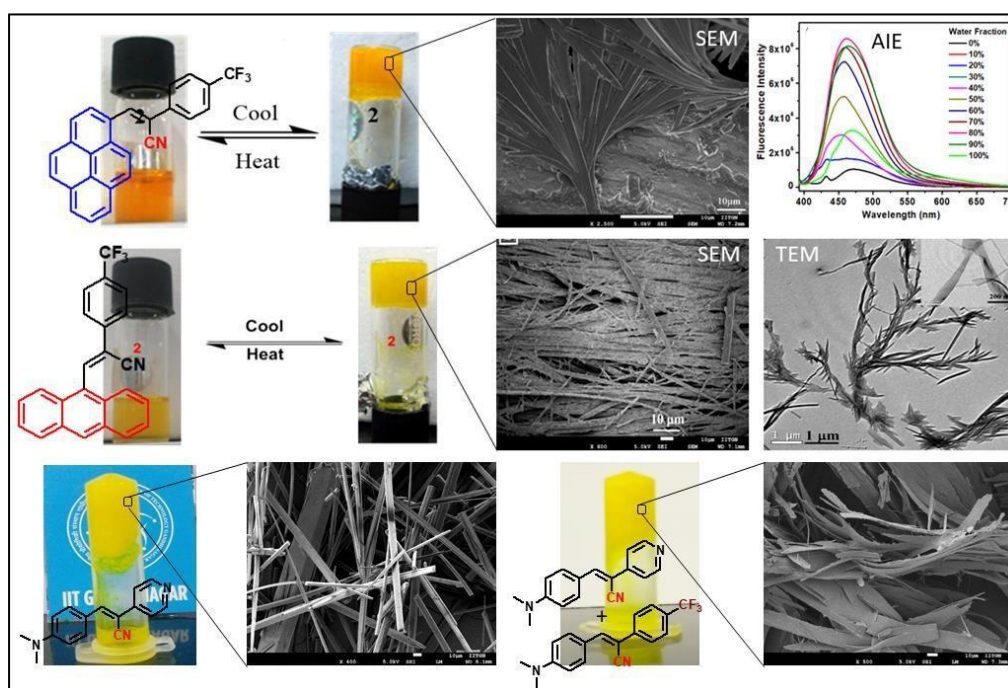


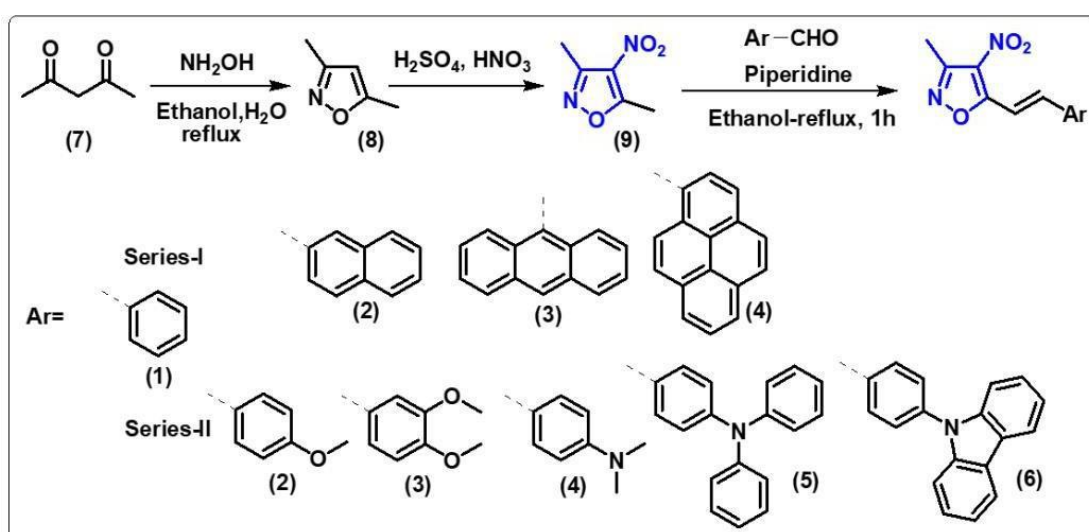
Figure 1.2. Organogels formed by cyanostilbene derivatives, SEM, TEM images of the xerogels and fluorescence spectra in dioxane/water system.

The molecules bearing CF_3 substituents show good gelation properties despite the absence of long alkyl chains, cholesterol moiety, sugars, or amide linkages. This gelation is aided by the favourable π - π interactions from the fused ring systems with CF_3 boosting the interactions through non-covalent interactions such as F...H and F...F. It was also observed that simple pyridyl substituted cyanostilbene also form organogels but their stability is enhanced upon addition of another but

dissimilar cyanostilbene. The stability of the gels was assessed using rheology investigations and rationalized by single crystal X-ray data. The formation of the aggregates, gelation and was investigated by using electron microscopy (SEM & TEM) and dynamic light scattering (DLS) studies.

Chapter-2: Styrylisoxazole Derivatives for Hydrogen Sulfide Detection and Non-Linear Optical Properties

In this section, we synthesised a set of diarylethylenes bearing a heterocyclic isoxazole containing a NO₂ group for the quantitative detection of H₂S and for investigation of non-linear optical response. The presence of the nitro group yields lower fluorescence quantum yields due to strong non-radiative transitions but upon treating with H₂S, yields distinct color and emission spectral changes upon reduction of NO₂ to NH₂. The molecular systems are greatly sensitive to H₂S compared to thiol containing molecules such as cysteine, homocysteine and glutathione. We also examined the solvatochromic behavior of other styrylisoxazole systems bearing methoxy and amino donors in various solvents and hyperpolarizability was measured [Scheme 1.2]. Such D-A derivatives showed strong intramolecular charge transfer and energetically contributed toward the second harmonic generation



Scheme-1.2. Synthesis of styrylisoxazole derivatives.

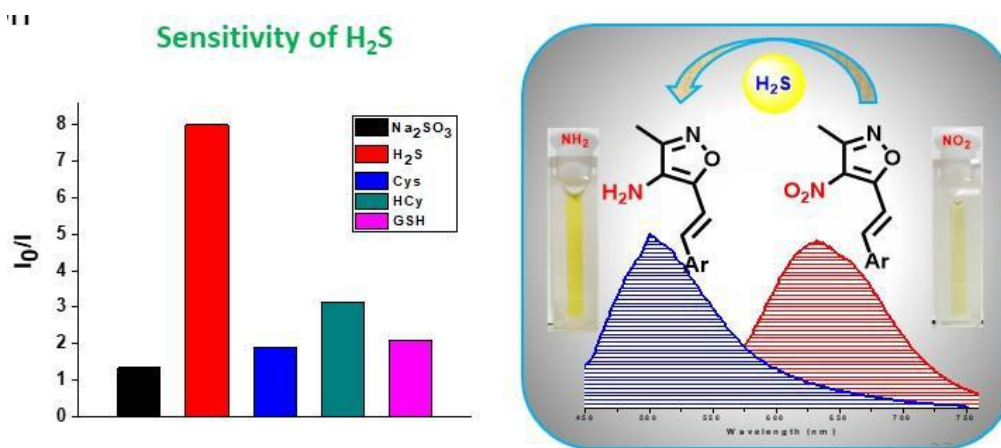


Figure 1.3. Comparative fluorescence intensity (I_0/I) ratios of [series-I (4)] in DMSO-Water (9:1) solution (10 μM) upon addition of other sulfur analytes measured at 200 μM of Cys, Hcy and GSH, Na_2S and SO_3^{2-} at $\lambda_{\text{ex}}/\lambda_{\text{em}}=450\text{ nm}/631\text{ nm}$. Each spectrum was recorded after 3 min (left). The graphical abstract shows the sensing mechanism and spectral changes on H_2S sensing.

Chapter-3: Surface Modifications of Feraheme Nanoparticles Using Click Chemistry For Multimodal Functionality

In this section, we successfully prepared biomedically applicable nanomaterials by combining Heat-Induced Radiolabeling (HIR) of the core and surface click chemistry. The core and surface coating of Feraheme nanoparticles (FHNPs) provide distinct modification sites for the generation of multifunctional nanomaterials. Besides inherent superparamagnetic properties enabling visualization by magnetic resonance imaging (MRI), HIR adds isotopes permitting radioactive detection by positron emission tomography (PET). Click surface modifications add moieties allowing fluorescent detection and provide targeting capabilities. In the context of nanoparticle modifications, we observed that the click reaction rates were kinetically affected by the particle's surface properties, reaction media, and ligands. The present study advances our understanding of the surface copper-free click chemistry between Azide-FH and Dibenzocyclooctyne (DBCO) derivatives, including the heat stability of azido groups, the ligands and buffers influences on reaction rates. Carboxymethyl dextran (CMD) coated feraheme nanoparticles (FHNPs) with $-\text{COOH}$ functional groups modified by copper free click chemistry, a covalent conjugation of fluorescent dye DBCO-Cy5.5 using EDC (1-ethyl-3-(3-dimethylaminopropyl) carbodiimide-HCl), HOBT (Hydroxybenzotriazole). Our results indicate that azido groups sustained the heating challenge of HIR (120 $^\circ\text{C}$, 2h). The click reactions of DBCO-Cy5.5 were carried out in 10 mM buffers for 2h, the click yields showed a sharp difference as >90% (DPBS), 50% (MES and Tris), and < 40% (HEPES and pure water).

Title: Design, synthesis, and identification of novel kinase inhibitors: biological and structural studies
Researcher: Shaik, Althaf
Supervisor: Kirubakaran, Sivapriya
Year: 2019
Keyword's: Enzymes, Cancer Therapy, ATR Kinase, Gefitinib
Call No.: 540 SHA
Acc. No.: T00530

Abstract: Protein kinases are enzymes that catalyze the transfer of phosphate group (PO₄³⁻) from ATP to hydroxyl-containing amino acid residues (Serine, Threonine, and Tyrosine) of the substrate. The human genome contains 518 protein kinases and 20 lipid kinases. They are involved in several essential cellular activation processes such as cell division, cell growth, development, DNA damage and repair, and signal transduction pathways. Deregulating and activating mutation in kinases has been considered crucial to the pathogenesis of human cancers. For this reason, kinases are considered an attractive clinical target for cancer therapy. The development of novel kinase inhibitors was spurred by the success of Gleevec (Imatinib), a 2-phenyl pyrimidine amine derivative that inhibits tyrosine kinase. Imatinib came to be commonly known as “magic bullet” when it transformed the treatment of chronic myeloid leukemia (CML). Nevertheless, the kinase inhibitors in the market bind to more than one kinase due to the highly conserved ATP binding site. This has led to the cross-reactivity or lack of selectivity, and toxicity, increased side effects and development of resistance against these anticancer agents. Therefore, kinase inhibitors with more selectivity, less toxicity, and high potency have been a major challenge in cancer drug discovery.

In order to overcome such challenges in kinase drug discovery, we have followed the combinatorial approach. In this approach, we have targeted the kinases involved in DNA damage and repair pathways since DNA repair mechanism greatly affect the response to cytotoxic agents. Ataxia-telangiectasia mutated Rad3 kinase (ATR) is one such kinase that induces cell cycle arrest in response to chemo or radiotherapy. Torin2 is a second-generation ATP competitive mTOR kinase inhibitor (EC₅₀ = 250 pmol/L) that exhibits potent biochemical and cellular activity against ATR (EC₅₀ = 35 nmol/L) kinases. Even though Torin2 inhibits ATR and mTOR in nanomolar range, it needs further optimization to reduce the cross-reactivity, improved water solubility, and metabolic stability. This work utilizes the classical approach of medicinal chemistry for optimizing the drug properties (lead to drug design) such as cross-reactivity, water solubility and metabolic stability of Torin2. In this study, Torin2 analogs were designed and synthesized through multistep synthesis and were characterized by NMR and mass analysis. The newly synthesized analogs were evaluated for their cytotoxicity. The compounds 13 and 14 showed significant inhibition for ATR and mTOR substrates against HCT-116 cell lines, i.e., p-Chk1 Ser 317 and p70 S6K Thr 389, respectively. Further, a comparative model of ATR kinase was generated using the SWISS- MODEL server and validated using PROCHECK and ProSA analysis. Synthesized compounds were docked into the ATP-binding site of mTOR and ATR to understand the binding modes and for the rational design of new inhibitors. 14 exhibited improved aqueous solubility of 11.02 µg/ml which was noticed to be almost 10 folds greater than Torin2 (1.29 µg/ml). It also displayed improved T_{1/2} = 157 min on incubation with

mouse liver microsomes. Which suggest that 14 may display enhanced metabolic stability compared to Torin2 ($T_{1/2} = 11.7$ min) for potential dual mTOR/ATR kinase inhibitor for cancer therapy.

The other scaffold that was explored during the process of development of ATR kinase inhibitors was pyrazolo[4,3-c] quinoline-3-ones. We have explored the simple and efficient, base free synthesis of pyrazolo[4,3-c] quinoline-3-ones from aryl hydrazines and 4-chloroquinoline esters. The scope of the reaction was studied with respect to various aryl hydrazine. We have successfully isolated and characterized the synthesized compounds and studied their cytotoxicity in HCT-116 and HeLa cell lines. Interestingly, these compounds showed selectivity towards HCT-116 cell lines (colon cancer cell) when compared to HeLa cell lines (cervical cancer cell). Our understanding has led to the identification of phosphodiesterase 5A (PDE5A) as a target for pyrazolo[4,3-c] quinoline-3-ones since PDE5A expressions levels are elevated in the HCT-116 cell line. Therefore, we have carried out the molecular docking studies of synthesized compounds with human PDE5A protein (PDB ID: 2H42) to understand their binding mode. All the compounds exhibited good docking score in comparison with the known PDE5A inhibitor Sildenafil and Tadalafil. Particularly, morpholine series of pyrazolo[4,3-c] quinoline-3-ones showed good affinity with PDE5A protein in the docking studies. Thus, these derivatives can be studied as potential inhibitors of PDE5A for the treatment of cancer.

As the other part of our work, we have explored YSK1 as a potential target for anticancer drug development. High throughput screening (HTS) of GSK-PKIS library compounds were carried out to discover new chemical scaffolds for targeting unexplored human YSK1. We have utilized Lab chip EZ reader mobility shift assay (MSA) assay with specific fluorescent-labeled peptide substrate for HTS against YSK1. Approximately 550 compounds have been screened (at 1 μ M) in which 12 compounds inhibited YSK1 activity more than 70%. These hits were structurally and chemically diverse. Further analysis of hits showed that 12 compounds had $IC_{50} < 110$ nM. Out of all the hits, GSK1660450B (tetrasubstituted pyridine derivative) compound showed potency in subnanomolar range $IC_{50} = 0.3$ nM. Four compounds were selected as leads based on potency and chemical structure. These leads can form the basis of for the development of YSK1 inhibitors that will have application in the development of anticancer drugs.

In the last part of our work, we have crystallized and solved the structure of Gefitinib and nine drug intermediates. Theoretical and experimental studies have been performed to quantify various weak inter and intramolecular interactions like O...H, N...H, X...X, O...N, C...C etc. This investigation has led to the identification of possible active conformation of drug and drug intermediates and understanding their supramolecular architecture. To summarize, this work advances the understanding of how subtle aspects of design, synthesis, biological study, HTS, and structural studies determine lead identification and pave the path towards drug optimization process that is required for the development of next-generation anticancer therapeutics.

Title: La₂O₃ and its doped analogs: physicochemical, optical and catalytic properties
Researcher: Gangwar, Bhanu Pratap Singh
Supervisor: Sharma, Sudhanshu
Year: 2020
Keyword's: Combustion Synthesized, X-ray Diffraction, X-ray Photoelectron Spectroscopy, Photoluminescence
Call No.: 540.3 GAN
Acc. No.: T00531

Abstract: The present thesis is an overview of the research results obtained during my doctoral research, and it is submitted in candidacy for the Ph.D. degree from the Indian Institute of Technology Gandhinagar. Physicochemical, optical and catalytic properties of undoped and doped lanthanum oxide have been investigated in detail during the studies. The catalytic activity of some selected compounds was studied for three selected heterogeneous reactions, namely Knoevenagel and Hantzsch reactions (organic reactions), dry reforming reaction (DRM) and CO oxidations. Each chapter gives an introduction, explain the aim of work, describe the experimental procedure, results, and the final conclusions. In this work, lanthanum oxide (La₂O₃) and various series of metal-doped lanthanum oxide (La_{2-2x}M_{2x}O₃, M = Pr, Nd, Sm, Ru, Bi) have been synthesized by solution combustion method and their corresponding pure hydroxides (h-La_{2-2x}M_{2x}O₃, M = Pr, Nd, Sm, Ru, Bi) are obtained upon exposure to an open atmosphere at different time intervals. Structure and morphology have been characterized by respective instrumentation techniques prior to their optical and catalytic behavior for various heterogeneous organic and inorganic gas-phase reactions.

In the first chapter, an overview of the physicochemical (hygroscopic behavior, basicity and reducibility/oxygen storage capacity), optical and catalytic properties of lanthanum based materials are explained in detail. A review of literature related to the influence of doping, dispersion, temperature effects on the optical and catalytic properties was discussed in detail.

In the second chapter, physicochemical and hygroscopic properties of combustion synthesized La₂O₃, La_{2-2x}Pr_{2x}O₃ (x = 0.025-0.30), La_{2-2x}Nd_{2x}O₃ (x = 0.025-0.50), La_{2-2x}Sm_{2x}O₃ (x = 0.025-0.30) nanocrystalline powders have been studied. All the compounds have a pure hexagonal phase, which was confirmed by X-ray diffraction (XRD). The hydroxylation reaction (reactivity with water) of oxides in an open atmosphere was monitored by X-ray diffraction (XRD). All of these oxides hydroxylate to form stable hydroxides at room temperature upon exposure to open atmosphere for certain interval of time. La₂O₃ shows a rapid hydroxylation reaction as compared to other oxides (La_{2-2x}M_{2x}O₃, M = Pr, Nd, Sm). It was observed that La_{2-2x}Pr_{2x}O₃ indicate slowest hydroxylation reaction compared to La_{2-2x}Nd_{2x}O₃ and La_{2-2x}Sm_{2x}O₃. The hydroxylation reaction becomes slower continuously as dopant concentration increases in La_{2-2x}Pr_{2x}O₃ (x = 0.05, 0.15 and 0.30), La_{2-2x}Nd_{2x}O₃ (x = 0.05, 0.15, 0.30 and 0.50) and La_{2-2x}Sm_{2x}O₃ (x = 0.05, 0.15 and 0.30). Overall, 30 atom% Pr doped La₂O₃ (La_{1.40}Pr_{0.60}O₃) shows the highest stability (slowest rate of hydroxylation) in open atmosphere at room temperature.

In the third chapter, physicochemical and optical properties (absorbance, reflectance, band gap and photoluminescence) have been further investigated for La_{2-2x}Pr_{2x}O₃ (x = 0- 0.30) and h-La_{2-2x}Pr_{2x}O₃ (x = 0-0.30) systems. X-ray photoelectron spectroscopy (XPS) confirms the presence of both Pr³⁺ and

Pr⁴⁺ in 15 atom% Pr doped La₂O₃. The band gap of La₂O₃ and La(OH)₃ decreases significantly after Pr doping. The photoluminescence (PL) studies of Pr doped La₂O₃/La(OH)₃ compounds show a sharp green emission due to ³P₀→³H₄ transition of Pr³⁺ ions, and the emission properties (intensity) depend upon the doping concentration. The emission intensity of Pr³⁺ is also optimized with concentration and 1 atom% Pr doped La₂O₃ (La_{1.98}Pr_{0.02}O₃) show the highest emission intensity in all the compounds (oxides/hydroxides). Hydroxides show slightly lower emission intensity compared to oxides because of the presence of quenching centres in the compounds (OH and CO₂ groups). One atom% Pr doped La₂O₃ (La_{1.98}Pr_{0.02}O₃) heated at higher temperatures shows slightly higher emission intensity compare to heated at low temperature due to the increase in crystallites size.

In the fourth chapter, the effect of Bi ions concentration on the physicochemical and optical properties of La₂O₃ and Bi doped La₂O₃ (La_{2-2x}Bi_{2x}O₃, x = 0-0.04) compounds (nanopowders) have been investigated. X-ray photoelectron spectroscopy (XPS) results of 4% Bi doped La₂O₃ reveals the presence of both Bi³⁺ and metallic Bi. Temperature programmed reduction (TPR) results of La₂O₃ and La_{2-2x}Bi_{2x}O₃ (x = 0.0025-0.04) indicate that the oxygen storage capacity (available surface oxygen) changes with the dopant (Bi) concentration. Hygroscopic studies show higher stability of La_{2-2x}Bi_{2x}O₃ (x = 0.04) in the open atmosphere at room temperature compared to pure La₂O₃. The band gap of La₂O₃ and La(OH)₃ decreases significantly after Bi doping. Further, photoluminescence (PL) studies of Bi doped compounds show a blue emission at 458 nm (³P₁-¹S₀ transition) of the Bi³⁺ ion substituted in La₂O₃ and maximum intensity is obtained with 0.5 atom percent Bi doping. Higher doping (>0.5 atom % Bi) decreases the emission intensity due to concentration quenching.

In the fifth chapter, catalytic properties of Pr and Bi doped La₂O₃ compounds (La_{2-2x}M_{2x}O₃, M = Pr, Bi) and Ru dispersed over Pr doped La₂O₃ compounds (Ru/La_{2-2x}Pr_{2x}O₃) for CO oxidation reactions is studied. Both Pr and Bi doped compounds are synthesized by solution combustion method, and Ru dispersed over Pr doped La₂O₃ catalysts are prepared by chemical reduction method using hydrazine hydrate as the reducing agent. The X-ray diffraction (XRD) analysis confirms the pure phase and hexagonal structure of compounds. Catalytic studies show that Pr doping decreases the CO oxidation activity of La₂O₃ and La(OH)₃ significantly. On the other hand, when Pr doped compounds are used as the catalytic support for Ru metal, activity is high compared to La₂O₃ alone. 2 wt% Ru/La_{1.40}Pr_{0.60}O₃ shows better catalytic activity (T₅₀ = 317 °C) than 2 wt% Ru/La₂O₃ (T₅₀ = 338 °C) for CO oxidation reaction. Bi doped La₂O₃ (4 atom%) shows higher catalytic activity compared to La₂O₃, other Bi dopants and Bi₂O₃ alone. Thus, contrast to Pr doping in La₂O₃, Bi doping increases the catalytic property of La₂O₃ significantly for the same reaction and under similar conditions. Overall, 2 wt% Ru/La_{1.40}Pr_{0.60}O₃ shows highest catalytic activity (T₅₀ = 317 °C) for CO oxidation among all the catalysts.

In the sixth chapter, dry reforming of methane was carried out over La₂O₃ and 0.5 and 0.1 atom% Ru doped La₂O₃ compounds (La_{2-2x}Ru_{2x}O₃, x = 0.005 and 0.01). Results indicate that just 0.5 atom% of Ru in La₂O₃ enhanced the activity by 20 times in terms of conversion when compared to the activity exhibited by La₂O₃. The oxygen storage capacity (calculated using H₂-Temperature programmed reduction) of the Ru doped sample was considerably higher than undoped La₂O₃, which resulted in the higher conversions of CH₄ and CO₂. The measured conversion of CH₄ and CO₂ was 72 and 80%, respectively, at 850°C while the conversion for undoped La₂O₃ under the same

experimental conditions was approximately 4%. Further, we also corroborated our experimental results by thorough DFT analysis of the surface structure of the proposed catalyst. DRIFTS studies demonstrated the role of specific types of carbonates in promoting the activity of the catalyst. DRIFTS studies demonstrated the role of a specific type of carbonates in promoting the activity of the catalyst. DFT calculations provided the rationale behind the selection of Ru-in-La₂O₃ methane dry reforming catalyst. The surface structures of pure and Ru-substituted compounds were determined, supporting the experimental observation of enhanced oxygen storage capacity on Ru substitution. Different active surface oxygen species were identified, and their roles in improving reducibilities and reactivities were established. Experimentally observed surface carbonates species were also identified in the calculations. The combined experiment and calculations approach proved ionic Ru in La_{2-2x}Ru_{2x}O₃ to be a novel and efficient dry reforming catalyst.

In the last chapter, the basicity of combustion synthesized La₂O₃ and subsequently produced La(OH)₃ have been utilized for liquid-solid phase heterogeneous catalysis (base catalysed Knoevenagel and Hantzsch reactions). XRD confirms the pure phase of compounds. The reaction of aldehydes with suitable substrates containing active methylene groups led to Knoevenagel and Hantzsch products in good to excellent yields in organic solvents, water and under dry or solvent-free conditions. Catalytic activity remains unchanged even after multiple (nine) cycles. Detailed mechanistic investigation using the simple adsorption reveals the prevalence of Eley-Rideal type adsorption where only one of the reactant is adsorbed for the reaction.

A brief summary of all the outcomes of the Thesis work has been presented in the conclusion part. We hope that the results presented in the thesis are a worthwhile contribution to optical materials and catalysis.

Title: Molecular insight into the mechanism of human GSAP and *P. aeruginosa* G6PI: biochemical and biophysical studies
Researcher: Angira, Deekshi
Supervisor: Thiruvencatam, Vijay
Year: 2019
Keyword's: *E. coli*, γ -Secretase Activating Protein, G6PI, Circular Dichroism
Call No.: 541.22 ANG
Acc. No.: T00532

Abstract: Structural biology plays an instrumental role in studying the functional aspects of the proteins in living system. The major prerequisite for the structural biology is the high yield of expressed and purified recombinant protein. *E. coli* expression systems have proven its dominance over other expression systems in terms of yield, cost and efficiency. Hence, in this work, we have used bacterial expression host *E. coli* to express and study the proteins, γ - Secretase Activating Protein (GSAP) and Glucose 6- Phosphate Isomerase (G6PI) that play an important part in diseases like Alzheimer's disease and cystic fibrosis respectively.

γ - secretase activating protein present in β -amyloid pathway orchestrates the formation of β - amyloid plaques by γ -secretase activation and is an emerging therapeutic target for the treatment of Alzheimer's disease. It forms a ternary complex with γ -secretase and the C-99 fragment of amyloid precursor protein. However, there are limited reports for the interaction of APP C-99 with GSAP. The work in this thesis discusses the characterization of purified maltose binding protein tagged human GSAP and its interaction with synthetic APP C-99 peptide fragments (⁷¹²IATVIVITLVMLKKQ⁷²⁷ (⁷¹²IQ⁷²⁷), ⁷¹⁹TLVMLKKKQYTSIHGGVVEVDAAVT⁷⁴³ (⁷¹⁹TT⁷⁴³) ⁷³⁴GVVEVDAAVTPEERHLSKMQQNGY⁷⁵⁷ (⁷³⁴GY⁷⁵⁷), and ⁷⁴⁶ERHLSKMQQNGYENPTYKFFEQMQN⁷⁷⁰ (⁷⁴⁶EN⁷⁷⁰)). The results emphasize the selective interaction of peptide (719TT743) with MBP-GSAP with a dissociation constant of 0.136 μ M. Further, computational modeling of the GSAP - 719TT743 complex finds an optimal bound pose of 719TT743 within an extended groove on the surface of GSAP. The preliminary results highlight the interaction between the two major proteins in the plausible ternary complex; APP C-99-GSAP- γ secretase. It paves a futuristic path to investigate the GSAP- APP C-99 binding in detail and accentuates the role of GSAP in the β -amyloid pathway. Along with canonical isoform 1 i.e. GSAP, for the first time GSAP isoform 4 (GSAP_I4) has been expressed in bacteria expression host *E. coli* and purified from inclusion bodies. The protein has been characterized using mass spectrometry, western blotting and circular dichroism. In order to explore the functionality of this new isoform, the binding studies have been performed with APP C-99 using ELISA and dot-blot far-western techniques.

Another protein under investigation, having moonlighting properties is *G6PI* from *Pseudomonas aeruginosa*. It is known to catalyse the second step in glycolysis in the reversible interconversion of an aldohexose glucose 6-phosphate, a six-membered ring moiety to a ketohexose, fructose 6-phosphate five membered ring moiety. This enzyme is of utmost importance due to its multifunctional role like neuroleukin, autocrine motility factor, etc. in various species. G6PI from *Pseudomonas aeruginosa* is less inspected for its multifunctional ability, which in turn can be predicted by studying the active site conservation of residues and their interaction with the reported

ligand. In this part of the work, we study G6PI in a self-inducible construct in bacterial expression system with its purification using IMAC Ni-NTA chromatography. The secondary structure of pure G6PI is estimated using circular dichroism to further predict the proper folding form of the protein. The bioactivity of the purified enzyme is quantified using phosphoglucose isomerase colorimetric kit from Sigma Aldrich with a value of 12.5 mU/mL. Differential scanning fluorimetry and isothermal titration calorimetry are employed to monitor the interaction of G6PI with its competitive inhibitor, erythrose 4-phosphate and calculated the T_m , K_d and IC_{50} values. Further, the homology model for the protein was prepared using human G6PI as the template to study the interaction with the erythrose 4-phosphate. Molecular dynamic simulation of the complex was performed at 100 ns to identify the binding interactions. We identified hydrogen bonds and water bridges dominating the interactions in the active site holding the protein and ligand with strong affinity.

Title: Electrocatalysis and gas solid catalysis by Pt ions in perovskites and CeO₂: a comparison between supported and the doped catalysts
Researcher: Bisht, Anuj
Supervisor: Sharma, Sudhanshu
Year: 2019
Keyword's: Catalytic Metals, Methanol Electro-oxidation, Electrochemical Studies, CO Oxidation
Call No.: 541.37 BIS
Acc. No.: T00543

Abstract: The present thesis is an overview of the research results obtained during my PhD studies and it is submitted in candidacy for the PhD degree from the Indian Institute of Technology, Gandhinagar. Three selected reactions have been investigated in detail during the studies, namely the oxygen evolution reaction (OER), formic acid electro-oxidation and CO oxidation. Each chapter will give an introduction to the subject, explain the aim of my work, describe the experiments, the results, and present the conclusions. In this work, ceria and La_{1-x}Sr_xCoO₃ perovskite have been synthesized and characterized and used as a host oxide for Pt doping and Pt supported system by solution combustion and chemical reduction method. The catalytic and electro-catalytic differences between the Pt doped and Pt-supported system has been studied. It was found that there are significant differences between the Pt-doped and Pt-supported for electro-catalytic and catalytic reactions. Activity of the catalyst depends on the particular reaction selected for comparison. We hope that the results presented in the thesis are a worthwhile contribution to catalysis.

Title: Regio and enantioselective vinylogous functionalization of α , β unsaturated aldehydes using dienamine catalysis

Researcher: Kutwal, Mahesh Shantaram

Supervisor: Appayee, Chandrakumar

Year: 2019

Keyword's: Dienamine Catalyzed Vinylogous, Unsaturated Aldehydes, Alkylation Reactions
Asymmetric Vinylogous

Call No.: 547 KUT

Acc. No.: T00554

Abstract: One of the greatest challenges in synthetic organic chemistry is to achieve highly selective organic transformations. There is much more emphasis on enantioselective reactions due to the increasing demand for the single enantiomer drugs. Organocatalytic chemo-, regio- and enantioselective reactions are found to be very much attractive because of avoiding tedious separation procedures to obtain pure products and is environmental-friendly. The enamine activation has been greatly studied for the selective α -functionalization of aldehydes and ketones utilizing distinctive electrophiles and subsequently applied in the synthesis of biologically active natural products. Comparatively, asymmetric vinylogous functionalization of α,β -unsaturated aldehyde using dienamine catalysis is one of the important yet less explored areas of amine catalyzed reactions. Mostly the dienamine intermediates that have been utilized in enantioselective pericyclic reactions and are relatively less explored in nucleophilic addition/substitution reactions.

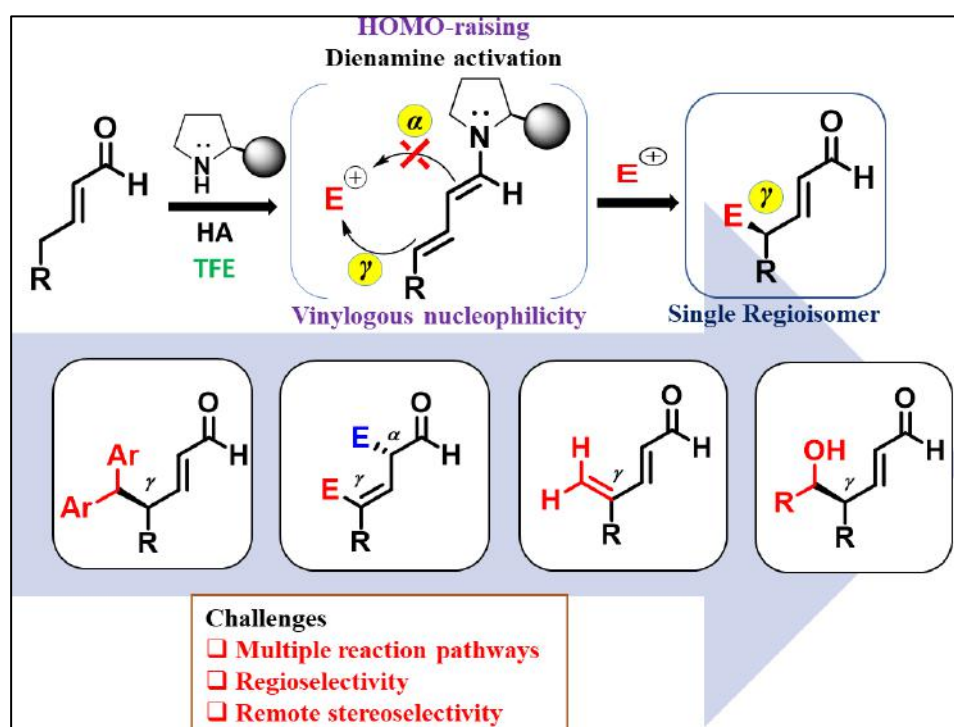


Figure 1. Dienamine activation for the vinylogous processes: challenges and scope

The dienamine intermediate was first demonstrated for the γ -amination of α,β unsaturated aldehydes and the high regio- and enantioselectivities were attributed to a proposed [4+2] cycloaddition mechanism. However, achieving high regio- and enantioselectivities were found to be difficult with other SN-type electrophiles. The main reason behind this is the multiple reaction pathways, the formation of a mixture of regioisomers, and complexity in controlling the stereoselectivity at the remote γ -position (Figure 1). The prime objective of this thesis is to overcome the challenges associated with the dienamine catalysis and the development of novel organocatalytic methodologies for regio- and enantioselective vinylogous functionalization of α,β -unsaturated aldehydes and the detailed experimental studies, mechanistic insight and application. The products of vinylogous remote functionalization of α,β -unsaturated aldehydes importantly, have free α and β reactive centres which could be further functionalized in a cascade fashion, and thus can be manipulated orthogonally for synthesis of challenging and potentially useful chiral building blocks. The entire thesis work has been divided into the following five chapters.

In chapter 2, a methodology for the highly regio- and enantioselective γ -alkylation of linear α,β -unsaturated aldehyde using dienamine activation is described. Further, we have demonstrated the use of TFE (trifluoroethanol) as a co-solvent to achieve excellent regioselectivity in the γ -alkylated products while an in-situ kinetic resolution has contributed to the product enantioselectivity. In chapter 3, we disclose the experimental evidence obtained to understand the role of TFE in regioselective γ -alkylation. During the detailed mechanistic investigation of the dienamine catalysed γ -functionalization of α,β -unsaturated aldehydes, we have understood the formation of a new dienamine intermediate from the γ -functionalized products. Therefore, we have envisaged a further reaction of this product dienamine intermediate with another electrophile to achieve a cascade α,γ -double functionalization.

In chapter 4, we have shown a new method for the regio- and enantioselective cascade double alkylation of α,β -unsaturated aldehydes. After successful regioselective γ -alkylation with SN- type electrophiles, another SN-type electrophile was added to functionalize the α -position. The substrate scope for the cascade α,γ -dialkylation α,β -unsaturated aldehydes with different electrophiles has resulted in the dialkylated products up to 70% yield and up to 99% *ee*. The formation of α,γ -dialkylated products not only confirms the γ -alkylated dienamine intermediate formation but also provides a new route for the selective double functionalization of α,β -unsaturated aldehydes.

In continuation of our interest to achieve a highly regioselective vinylogous γ -functionalization, we further envisaged a γ -hydroxymethylation of α,β -unsaturated aldehydes via the vinylogous aldol reaction using formaldehyde. In chapter 5, an organocatalytic methodology for the remote regioselective γ -methylenation of α,β -unsaturated aldehydes under mild reaction conditions is demonstrated. An excellent γ - selectivity has been obtained with a variety of α,β -unsaturated aldehydes in the presence of TFE as a co-solvent. This organocatalytic direct γ -methylenation is successfully applied for a short synthesis of α -triticene (an antifungal agent). γ -Methylenated products have been further transformed into synthetically important building blocks. The reaction of crotonaldehyde with formaldehyde has led to unusual double γ -

functionalized products. A vinylogous Mannich-type reaction mechanism is proposed for the γ -methylenation of α, β -unsaturated aldehydes based on the experimental evidence. We have also developed highly regio and enantioselective vinylogous γ -hydroxymethylation of α, β -unsaturated aldehydes using phenylglyoxal. We have optimized the reaction condition for the γ -hydroxymethylation of 2-decenal in 92% *ee* and *dr* > 20:1. Upon further exploration of the reaction of phenylglyoxal with β -substituted α, β -unsaturated aldehydes, we have observed a lactol intermediate which has been *in situ* transformed into a chiral dihydroxy cyclopentene carbaldehyde via vinylogous double cascade annulation reaction. The dynamic kinetic resolution was observed during the transformation of lactol to cyclopentene carbaldehyde obtained in 57% yield, 76% *ee* and >20:1 *dr*.

Title: Design and synthesis of π -conjugated organic fluorophores for biological and organic electronics applications

Researcher: Kumari, Beena

Supervisor: Kanvah, Sriram

Year: 2020

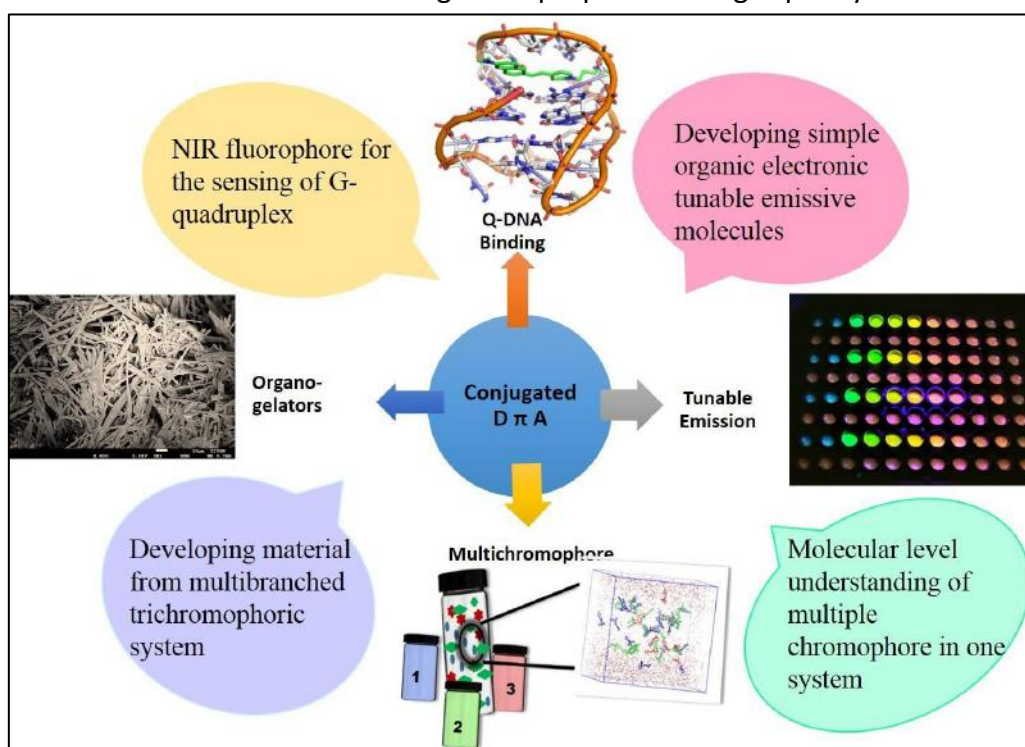
Keyword's: Pharmacological Applications, Solar Cells, H-bonding, Van der Waals, Forces Microorganisms

Call No.: 547.1 KUM

Acc. No.: T00572

Abstract: This dissertation entitled “Design and synthesis of small organic fluorophores for biological and organo-electronics applications” focuses on the synthesis and characterization of π -conjugated organic molecules with donor (D), acceptor (A) moieties and their photophysical investigations. The first chapter of the thesis discusses binding preference of fluorescent derivatives of naphthalene with G4DNA over duplex DNA. The thesis also discusses synthesis of various triphenylamine derivatives for obtaining tuneable emission leading to white light and organogel formation. The major objectives of the thesis are given below.

1. Design and synthesis of red-emitting fluorophores for the binding of G-quadruplex
2. DNA Developing simple organic electronic tuneable emissive molecules utilizing the triphenylamine scaffold.
3. Structural modifications to achieve gel-like properties using triphenylamine core.



A pictorial outlook of this thesis that represents the development of conjugated D- π -A based fluorophores for various applications.

Chapter 1. Cationic Red Emitting Fluorophore: A Light-up NIR Fluorescent Probe for G4-DNA

Guanine (G) quadruplexes (G4) are nucleic acid secondary structures formed by G-rich sequences, which are commonly found in human telomeric and oncogene-promoter regions, and they have emerged as targets for regulation of multiple biological processes. Considering their importance, targeting the G-quadruplex structure with small molecular binders is extremely pertinent. In this work, red emitting water soluble fluorophores bearing push-pull substituents were synthesised and examined for their interaction with human telomeric G4 and duplex (ds) DNAs. The presence of a strong electron donating (dimethylamino) and electron withdrawing (cationic pyridinium) groups linked through a conjugated double bond helps in water solubility and enabling the emission in the near IR region (>700-720 nm). Binding of this cationic dye to the G4-DNA yields multi-fold emission enhancement (~70 fold with G4-DNA vs ~7 fold with ds-DNA) along with hypsochromic wavelength shifts (35 nm with G4-DNA and 8 nm with ds-DNA). The remarkable emission changes, ~2-4 fold enhanced binding efficiency noted with the antiparallel conformation of G4-DNA indicates preferential selectivity over ds-DNA. The molecular docking and dynamics studies of the ligands with duplex and interactions of the ligands with duplex and G4 DNA were performed and they provided insights into the mode of binding of these dyes with G4-DNA and supplemented the experimental observations.

Chapter 2. Color Tuning & White Light Emission of Styryltriphenylamines through Admixtures of Donor-p-Acceptor Stilbene Siblings: Experiment and Simulation

White light emitting diodes are potential energy efficiency replacement of conventional lighting sources. Herein we report, the luminescent behaviour of three simple styryltriphenyl amines bearing different electron withdrawing groups. We have utilized two design strategies with D- π -A architecture to achieve red, green, and blue-emitting fluorophores i) with molecules emitting aggregation-induced emission and ii) with molecules that do not show aggregation-induced emission.

Part A: AIE active cyanostilbene siblings for tunable & white light emission.

Herein we report, the luminescent behaviour of three simple styryltriphenyl amines bearing different electron withdrawing groups phenyl, pyridyl, and p-nitrophenyl in a common Donor (D)- π -Acceptor (A) α -cyanostilbene construct along with their thermal and electrochemical properties. The DFT studies reveal that AIE characteristic feature of the D- π -A dyes is inversely proportional to the intramolecular charge transfer (ICT) effect i.e., phenyl and pyridyl substituted compounds show characteristic aggregation induced emission in water while ICT effect is dominant for the nitro derivative. The extent of intramolecular charge transfer and the solvatochromic emission shifts from blue to red, depends on the strength of the electron withdrawing group. White luminescence and tuneable emission colors are obtained by careful admixtures of these cyanostilbenes bearing triphenylamines. The results rationalized through DFT and TDDFT calculations follow a consistent trend with the energy levels measured from the electrochemical and optical studies. Thermogravimetric analysis and differential scanning calorimetry studies showed the excellent thermal stability of the compounds. The scanning electron microscopy (SEM) and dynamic light scattering (DLS) measurements were performed to reveal the formation of aggregates. This strategy

involving synthetically simple and structurally similar molecules with differential emission properties have potential applications in the fabrication of multicolor and white light emitting materials.

Part B: AIE inactive stilbene siblings for tuneable & white light emission

In the extension of this work, the donor-acceptor π -conjugated molecules with triphenylamine donor and different acceptor (H, cyano and pyridinium) units with a double bond spacer (without cyano) were synthesized. These compounds exhibit bathochromic shifts in absorption and emission with an increase in the acceptor strength. Solvatochromic measurements in water revealed emitting states characterized by a polar nature with three distinct emission spectral regions from blue to red. Interestingly, binary mixtures of the stilbenes in acetonitrile and water gave white light emission. MD simulations of the admixtures reveal that the emission data directly correlates to the structural arrangements of the molecules driven by intermolecular and solvent interactions with micelle-like structural arrangements for one set and uniform homogenous mixing for the other two sets. Such tuneable emitting strategy using simple structural siblings could offer great potential towards designing novel emitting systems. The modified set of TPA stilbenes without cyano group at double bond but consisting of H, CN and pyridinium acceptors gave white light emission in water and acetonitrile.

Chapter 3. Branching Effect on Triphenylamine-CF₃ cyanostilbenes: Enhanced Emission and Aggregation in Water

Six linear and branched α -cyanostilbene derivatives bearing triphenylamine donor and electron withdrawing trifluoromethyl on the phenyl ring and cyano on the double bond were synthesized and examined for their absorption, emission properties in solution and solid state. The molecules showed characteristic solvatochromic emission and aggregation induced emission in water. Interesting absorption and emission changes were observed upon branching, however extension of the third arm exerted negligible effect. Dropcast SEM images of these molecules in water revealed unique morphological features with the formation of uniform structures. The triply branched triphenylamine formed stable organogel aided by intermolecular interactions. The results were substantiated using DFT calculations.

In conclusion, we have designed and synthesized several solvatochromic fluorescent dyes and studied their absorption, and emission in organic solvents for potential use as DNA binding and tuneable emitting materials.

Title: New and emergent motifs in drug development: inhibition of enzymes sphingosine kinase 1, carbonic anhydrase VA and soluble epoxide hydrolase, and potent antibiotics

Researcher: Mahapatra, Amarjyoti Das

Supervisor: Datta, Bhaskar

Year: 2020

Keyword's: Drug Development, Sphingosine Kinase 1, Carbonic Anhydrase VA, P-aminobenzenesulfonamide

Call No.: 540 MAH

Acc. No.: T00709

Abstract: Sulfonamides or sulfa drugs were the pallbearers of antibiotic revolution in 20th century medicine. In the years preceding use of penicillin, sulfa drugs were used to treat variety of bacterial infections. A red dye Prontosil was first sold by the German chemical company IG Farben based on its pronounced antibacterial effects in mice. The activity of Prontosil was subsequently attributed to p-aminobenzenesulfonamide or sulfanilamide, that was produced upon metabolism of the dye. Sulfonamides were widely used in early World War II, especially by British and American soldiers, to treat wounds and infections. While interest in the antibacterial potential of sulfonamides waned by the mid-20th century, emergence of medicinal chemistry as a systematic area of study led to extensive explorations of sulfonamides as pharmaceutical and agricultural agents. A high degree of structural diversity of sulfonamide analogues provides a rationale for further drug discovery in search of potential therapeutic agents. The design and development of sulfonamide motif bearing pharmacologically important scaffolds has been an important paradigm of medicinal chemistry. This thesis expands on sulfonamides and further on to novel sulfonyl motifs in terms of identifying their therapeutic potential towards a variety of targets. This thesis fits within a broader theme of discovery of new and emergent small molecular motifs that are capable of blocking activity of established disease-relevant targets. Chapter 1 provides a comprehensive introduction to the conceptual framework of the work performed. The experimental section of the thesis comprises four chapters beginning with chapter 2.

Chapter 2 explores antibacterial activity of small organic molecules in conjunction with cell-penetrating peptide octaarginine. A series of N-(4-(4-(methylsulfonyl)phenyl)-5-phenylthiazol-2-yl)benzenesulfonamide derivatives were designed, synthesized and investigated for their antibacterial activity, in isolation and in complex with the cell-penetrating peptide. Several of the synthesized compounds displayed potent antibacterial activity against both gram-negative and gram-positive bacteria. Two compounds exhibited attractive antibacterial activity against multiple strains. The comparative antibacterial behaviour of peptide along, drug molecule along and drug-peptide complex were also investigated which revealed a fascinating syncretic mode of action of the drug-peptide complex. The syncretic framework of activity that our research group has elucidated thus far closely resembles the syncretic mode in which this specific project was pursued with another research group in our institution. Ongoing works in our laboratory are attempting to fully understand the scope of use of such antibacterial agents.

Chapter 3 examines and compares the nuances of supramolecular architecture of sulfonyl-molecules namely sulfonylurea, sulfonyldiurea and sulfonyltriurea using X-ray crystallographic analysis. Sulfonylureas are a prominent class of therapeutic agents and are notable for use as oral antidiabetic agents for management of Type 2 diabetes mellitus. The scope of use of aryl sulfonyl-oligomeric compounds has not been explored in drug discovery. In an attempt to examine such compounds from a fundamental structural perspective, we designed, synthesized and prepared crystals of three aryl sulfonylurea oligomeric molecules. The molecular packing analysis of these three derivatives reveals significance of N-H...O and C-H...O intra and intermolecular hydrogen bonding. A complete and detailed understanding of the intermolecular interactions was investigated employing the Hirshfeld surface analysis and 2D Fingerprint plots. Notably, the overall geometry of the molecules undergoes a dramatic change when comparing a sulfonylurea with a sulfonyltriurea. The ability to synthesize sulfonyldiureas or sulfonyltriureas has thus opened a new paradigm for influencing the activity of analogous sulfonylureas.

Previous efforts in our laboratory have shed light on the ability of sulfonylureas to exercise isoform-selective inhibition of enzyme carbonic anhydrase. These studies had sought to examine the bioisosteric modification of sulfonamides that hold sway as a dominant class of carbonic anhydrase inhibitors. Section A of chapter 4 is built on the theme of bioisosterism, albeit in a broader context that includes urea, sulfonamide and sulfonylurea motifs. A diverse set of molecules were investigated towards their ability to inhibit the enzyme sphingosine kinase 1 (SphK1). Within the sphingolipid metabolic pathway, SphK1 is a critical component of the sphingolipid metabolic pathway and has been established as an attractive chemo- therapeutic target. Synthesis of an array of compounds bearing urea, sulfonylurea, sulfonamide and sulfonyltriurea groups were followed by standard spectroscopic characterization (^1H and ^{13}C NMR and mass spectrometry). Four of the molecules displayed promising enzyme inhibitory activity with IC_{50} values between 0.14 to 2.94 μM . *In silico* assessment of the active compounds suggest promising scope of refinement of the corresponding molecular architectures towards selective inhibition of SphK1. Interestingly, a novel sulfonyltriurea motif shows significantly superior inhibition of SphK1 as opposed to sulfonylureas. The presence of two more -NH-CO- groups in the sulfonyltriurea motif raises prospects of additional weak interactions, in addition to influencing the molecular conformation. This chapter presents the first known application of a sulfonylurea-oligomer towards enzyme inhibition.

As further proof-of-concept of the applicability of sulfonylurea-oligomers, in section B of chapter 4, the potential scope of sulfonyldiureas molecules as novel inhibitors of the enzyme soluble epoxide hydrolase (sEH) is discussed. Synthesis of sulfonyldiureas as per our protocol, necessitates preparation of suitable N-monosubstituted ureas. A catalyst-free simple approach for the synthesis of mono substituted aryl and alkyl ureas from commercially available primary amines at room temperature is reported here. Further, a solvent-free single-step approach for the synthesis of sulfonyldiureas from N-monosubstituted urea are also developed. This single step methodology provides several advantages such as short reaction time, no expensive catalyst or reagents, simple work up and reasonable yields. The choice of targeting sEH was based on a survey of enzymes that were receptive to urea, sulfonylurea and amide-based inhibitors. sEH has emerged as a prominent

therapeutic target for addressing conditions ranging from pain, eye disease, hypertension, diabetes, immunological disorders, neurological diseases and cancers. In silico assessment of designed sulfonyldiurea molecules suggested suitable fit in the active site of the enzyme with effective hydrogen bonding interactions with key amino acid residues. Screening of enzyme inhibitory activity of a few sulfonyldiurea derivatives indicates modest success (high micromolar IC_{50}), while greater potency is expected with specific designed compounds. Detailed structure activity study (SAR), molecular dynamics studies, in-vitro enzyme inhibitory studies and cytotoxicity studies are underway.

In chapter 5, C2 and C4 substituted oxazole-5(4H)-one derivatives have been repurposed for the selective inhibition of human carbonic anhydrase VA (hCAVA). Inhibitors of carbonic anhydrase (CAIs) have been suggested for combating several cancers, diabetes, and metabolic syndromes. CAVA and CAVB are the only isoforms present in mitochondria and owing to their distinctive localization are correlated with a unique set of disease conditions. C2 and C4 substituted oxazole-5(4H)-one derivatives were designed, synthesized and evaluated for in vitro human hCAVA, hCAIX and hCAII inhibitory activity. Two compounds from among those tested, displayed pronounced selectivity for hCAVA as compared to hCAIX and the ubiquitous hCAII. In silico studies suggested that these compounds may be following a similar mechanism of CA inhibition as the standard compound acetazolamide. The active compounds have an attractive cytotoxicity profile, and the combination of in vitro and in silico results point to the potential for refining the oxazole-5(4H)-one derivatives for obtaining superior CAVA inhibitors. While the work in chapter 5 is not aligned with the stories about sulfonyl-motifs, it is a thematic extension of scrutinizing existing scaffolds towards less-explored targets.

Chapter 6 is devoted to a discussion connecting the questions, hypothesis and main results presented in the thesis. The chapter also engages in ideation for future works.

As mentioned at the outset, two broad themes are presented through this thesis:

- (1) discovery of entirely new chemical motifs that can be deployed in drug development, and
- (2) eliciting distinctive medicinal behaviour from established motifs.

Title: Design and synthesis of organic fluorescent molecules: sensing, cellular imaging and organogels

Researcher: Jana, Palash

Supervisor: Kanvah, Sriram

Year: 2020

Keyword's: Intramolecular charge transfer (ICT) processes, Biomolecules, Organic Fluorescent, Viscosity

Call No.: 540 JAN

Acc. No.: T00710

Abstract: Abstract not available

Title: Computational approach to systematically compare protein phosphorylation and O-GlcNAcylation
Researcher: Rani, Lata
Supervisor: Mallajosyula, Sairam Swaroop
Year: 2021
Keyword's: Protein Phosphorylation, O-GlcNAcylation, Genetics, Quantum Mechanical
Call No.: 540 RAN
Acc. No.: T00711

Abstract: The “central dogma” of molecular biology states that genetic information is stored in DNA, which is transcribed into mRNA and then is translated into proteins. Proteins undergo several biochemical modifications after being translated; these modifications are known as post-translational modifications (PTMs). These are known to be essential mechanisms by which eukaryotic cells diversify their protein functions beyond what is dictated by gene transcription. The resulting change in structure, as well as properties of proteins, allows them to dynamically regulate signal integration and physiological states. PTMs are crucial to form the mature protein products which carry out cell signaling, protein-degradation, regulation of gene expression, and protein-protein interactions. Over 450 different types of protein post-translational modifications have been known to date. In the present work, the two most common and concurrently occurring covalent modifications of proteins, i.e. phosphorylation and O-GlcNAcylation have been discussed in detail. The objective of this work is to compare and understand the conformational effects of phosphorylation versus O-GlcNAcylation on the same grounds.

Phosphorylation is the addition of the phosphate group at the side chain of serine, threonine, and tyrosine. Approximately 30% of human proteins are known to be phosphorylated which accounts for more than 2% of the human genome. Phosphorylation stimulates protein interaction with other proteins due to the high interactive capacity of the phosphate group. It acts as a regulatory mechanism for cellular processes such as protein synthesis, cell division, signal transduction, cell growth, cell development, and aging. O-GlcNAcylation is the addition of O-linked β -N-acetylglucosamine (O-GlcNAc) in nuclear, cytoplasmic, and mitochondrial proteins that are destined for secretion. The key substrate for protein glycosylation, uridine diphosphate GlcNAc (UDP-GlcNAc) is synthesized by the hexosamine biosynthetic pathway (HBP). O-GlcNAc is a key glucose sensor and regulates glucose uptake, insulin signaling, glycogen synthesis, gluconeogenesis, lipogenesis, and mitochondrial function. O-GlcNAcylation and phosphorylation can occur on the same Ser/Thr side chain. It is considered that every O-GlcNAcylated protein can be phosphorylated. As per the “Yin-Yang” relationship between phosphorylation and O-GlcNAcylation, there is direct competition between both modifications for the same site. However, it is not true for each event. Several studies have depicted reciprocal as well as synergistic effects of both modifications. It must be noted that even though O-GlcNAcylation is abundant and important it remained undetected until the early 1980s because glycosylation is largely undetected by commonly used analytical techniques like gel electrophoresis and HPLC. This difference is evident when one investigates the experimentally verified PTM site statistics available at the database of protein post-translational modifications

(dbPTM, <http://dbptm.mbc.nctu.edu.tw/1.0/>). Only 6340 experimentally verified O-linked Glycosylation sites have been reported, in which O-GlcNAc forms a subset. On the other hand 571032, experimentally verified phosphorylation sites have been reported. Issues with isolation of protein and inherent conformational flexibility associated with the glycosidic bond have also affected structural characterizations, with only a handful of O-GlcNAc containing structures being deposited to the Protein Data Bank. The lack of structural insight into O-GlcNAcylation and its comparative influence with phosphorylation at the same PTM site form the basis of this investigation. We carried out comprehensive theoretical studies to explore the atomistic interactions involved in post-translational dependent structural transitions of biological relevance. While both Phosphorylation and O-GlcNAcylation have been studied earlier using MD and QM calculations, we note that these studies primarily focused on only one of the PTM. In this thesis, we perform a series of studies using both quantum mechanical and molecular dynamics simulations on a range of biosystems to elucidate the impact of phosphorylation and O-GlcNAcylation. The work presented in this thesis has been divided into the following four chapters.

Chapter 1: A detailed structural and conformational analysis of phosphorylation and O-GlcNAcylation.

The chapter is divided into three sections:

[1.A] Conformational analysis of phosphorylated and O-GlcNAcylated Serine and Threonine residue reported in Protein Data Bank (PDB).

To acquire structural trends of serine and threonine upon phosphorylation and O-GlcNAcylation as observed in experiments crystal structure data was obtained from the Protein Data Bank database. Initially, two data sets were extracted from PDB; the first dataset consisted of protein structures containing phosphorylated Serine (SEP) and Threonine (TPO) while the second dataset consisted of O-GlcNAcylated Serine (O-GlcNAc (S)) and Threonine (O-GlcNAc (T)). To avoid redundancy in data similar proteins having a sequence similarity of > 90% were clubbed in a group from which the highest resolution structure was selected. Proteins with multiple subunits were analyzed to select only one subunit. For NMR resolved structures only the representative structure based on RMSD clustering was included in the dataset. Moreover, the dataset was also analyzed for missing residues immediately before or after the PTM site. Any PTM site with missing adjacent residues (coordinates) was removed. To analyze the influence of the absence of the PTM at a known PTM site a new dataset was then created which contained all the structures present in the PDB database except residue identifiers SEP and TPO, ie phosphorylated serine and threonine. From these obtained structures, the entries having > 90% sequence similarity with sequences present in the SEP and TPO datasets were selected. For each curated PTM site i , φ ($C_{i-1}-N_i-C_{\alpha i}-C_i$) and ψ ($N_i-C_{\alpha i}-C_i-N_{i+1}$) dihedrals were evaluated. As per the distributions analysis SEP was found to favor the compact conformation while TPO preferred extended conformation. We also observed presence of strong intra-residue phosphate-amide H-bond and distant inter-residue phosphate-lysine interactions possibly responsible for preferred conformations. On contrary, unmodified serine preferred both compact and extended conformations while threonine was mainly found in compact ψ -helical conformation. Moreover, we also extracted and analyzed each serine and threonine site present in the PDB which revealed a preference for the compact ψ -helical structures for unmodified serine and threonine. The

analysis revealed clear structural trends for the phosphorylated systems, but due to lack of sufficient O-GlcNAcylated serine and threonine sites in PDB, observing structural trends upon glycosylation was not possible. Therefore, we performed extensive QM calculations at the model dipeptide level.

[1.B] Quantum mechanical analysis on model serine and threonine dipeptides and modified forms. Model serine and threonine dipeptides and their phosphorylated and O-GlcNAcylated form were generated using CHARMM protein and carbohydrate topology. The minimal dipeptide design accounts for ϕ (C-N-C $_{\alpha}$ -C) and ψ (N-C $_{\alpha}$ -C-N) dihedrals by adding acetyl (-COCH $_3$) and methylamine (-NHCH $_3$) groups at amino and carboxyl terminal respectively. Dipeptide conformations were generated at 15° intervals for both ϕ and ψ dihedrals in the ϕ/ψ space amounting to 576 QM calculations per model dipeptide. As per PDB survey and NMR studies the N-C $_{\alpha}$ -C $_{\beta}$ -OG (χ) dihedral was fixed at 60° for the O-GlcNAc (S/T) model dipeptides, while all for SEP and TPO dipeptides the N-C $_{\alpha}$ -C $_{\beta}$ -OG (χ) and C $_{\alpha}$ -C $_{\beta}$ -O-P dihedrals were fixed at -60° and 110° respectively. Additionally in the SEP and TPO QM scans the N-H bond length was fixed to a value of 1.023 Å, obtained from averaging the N-H bond lengths from QM optimized geometries of the model compounds, to eliminate the possible shift of the acetyl or amine hydrogen's to the phosphate oxygen's. The QM calculation were performed at the B3LYP level employing the 6-31+G(d) functional. The 2D energy profiles obtained from the scans showed that unmodified serine and threonine preferred the extended β -sheet conformations as well as γ -turn region an intermediate space between the β -sheet and α -helix regions. In contrast to Ser and Thr dipeptides SEP and TPO dipeptides preferred the canonical α -helical region and second energy minima was located at γ -turn region. For O-GlcNAc (S) global energy minima was located at γ -turn region whereas for O-GlcNAc (T) global minima shifted towards compact conformations. We observed significant intra-residue H-bonding responsible for global minima conformations obtained from the scan.

[1.C] Molecular dynamics simulations performed on model serine and threonine dipeptides and modified forms as well as extended peptides: α -helical peptide and protein tau short motifs. Following DFT analysis on dipeptides extensive MD simulations were performed on model dipeptides to include the effect of solvation. The systems were generated using CHARMM protein, carbohydrate force fields and the TIP3P water model. For all the systems three simulations were initiated with the N-C $_{\alpha}$ -C $_{\beta}$ -OG (χ) dihedral initially fixed at 60°, -60° and 180°. These restrains were removed during the simulations allowing complete conformational flexibility. The equilibrated structures were subjected to production simulations with GROMACS simulation package. We analyzed relative free energy as a function of ϕ/ψ for each dipeptide system which revealed that both serine and threonine dipeptides favored compact α -helical as well as PPII conformation. SEP favored PPII while TPO favored α -helical geometry, whereas O-GlcNAcylated (S) and (T) both favored PPII conformation with significant decreased preference for α -helical conformation. The structural preferences observed were based on strong electrostatic interactions in SEP and TPO and weak H-bond in O-GlcNAcylated dipeptides. In addition to H-bonding significant water bridges were observed in the simulations highlighting the influence of solvation. To understand the influence of both PTMs on larger systems, MD simulations were performed on Baldwin (Ac-AKAAAAKAAA-AKAA-NH $_2$) peptide and short Tau fragments (KSPP and KTRP) as a

prototype for α -helical and PPII conformations based on the NMR and CD studies performed by Zondlo and co-workers. PTM's were introduced into the Baldwin structure at the interior (position 5) to study their influence on the structure. We analyzed secondary structure as a function of simulation time based on DSSP algorithm which showed that both modifications when introduced at middle of the helical peptide (at N5 position) destabilized the helix. Phosphorylation induced destabilization was due to intra residue H-bonding and phosphate salt-bridge with Lys while O-GlcNAcylation induced destabilizing effects were governed hydrophobic collapse and steric interactions as a result of bulky carbohydrate side chain.

Simulations performed on Tau peptides (KSPP and KPPP) showed the significance of electrostatic interaction of SEP and TPO with Lys residue on conformation preference. The interaction has been found to be strong enough to lock the geometry of SEP and TPO in PPII geometry. O-GlcNAcylated peptides on the other hand preferred extended geometries. The analysis highlights the importance of non-covalent interactions *i.e.*, intra-residue H-bonding and phosphate salt-bridge with lysine residues in controlling the overall conformation upon phosphorylation.

Chapter 2: Site specific stabilization and destabilization of α -helical peptide upon phosphorylation and O-GlcNAcylation

MD simulations were extended further to understand the site specific role of phosphorylation and O-GlcNAcylation on stability of α -helices. The model Baldwin peptide (Ac-AKAAAKAAAKAA-NH₂) was phosphorylated and O-GlcNAcylated at N-terminus (N1), interior N10 position and C-terminus (N14). We observed that phosphorylation and O-GlcNAcylation introduced at N-terminus stabilized the helical conformation. Helix stabilization was the direct result of favorable electrostatic interactions of phosphate and O-GlcNAc side chain with helix backbone. While phosphorylation and O-GlcNAcylation introduced at middle (N5) and near C-terminus (N10) of the helix were shown to be disrupting the helicity. The presence of intra-residue phosphate side chain-main chain H-bond was the key factor for disturbing the helicity in case of phosphorylation. This interaction blocked the main chain carbonyl oxygen and amide hydrogen atoms of phosphorylated serine and threonine residues to participate in helix characteristic $i, i-4$ interaction hence disturbed the helicity. In addition to electrostatic interactions, salt-bridges were also present in phosphorylated peptide between phosphate side chain and Lys residues. In case of O-GlcNAcylation steric hindrance was the main factor leading to disturbed helicity. It is evident here that both modifications imparted similar effects on α -helical peptide as observed in experimental studies.

We also explored the positioning effect of Lys residue relative to phosphorylation site as per the experimental study by Doig *et. al.* MD simulations were performed on Doig peptides and observed that phosphate-Lys salt-bridge can have both stabilizing and destabilizing effect on helicity of the peptide. Lys placed prior ($i, i+4$) to phosphoserine stabilizes the helix as phosphate-Lys side chain interaction locks the geometry of the serine in such a way that support characteristic helical main-chain hydrogen bonding. On the other hand, Lys placed after phosphoserine residue in the peptide, upon interaction with phosphoserine changes the pull out the serine residue in such a way that hindered the main chain helix hydrogen bonding pattern, which leads to helix opening.

Chapter 3: Influence of phosphorylation and O-GlcNAcylation on proline-rich domain of tau.

To explore the conformational influence of both PTMs on a disordered peptide we selected tau proline-rich region. As per the “jaws” microtubule-binding model proposed by Mandelkow et. al. and global hairpin structural model of tau, structural changes in the proline-rich regions of tau could have a major effect on microtubule binding affinity. We carried out enhanced sampling metadynamics simulation is carried out in order to investigate the phosphorylation and O-GlcNAcylation induced conformational effects on a Tau segment (Tau₂₂₅₋₂₄₆) from the proline-rich domain (P2). Enhanced sampling technique was employed for this study as biological molecules are known to have rough energy landscapes, with many local minima separated by high-energy barriers, due to which it is easy to fall into minima and get trapped and is hard to jump out of in conventional simulations. Parallel tempering-well tempered ensemble technique allow the simulation trajectory to explore all possible conformation space without getting trapped in local minima. For this study five systems were generated i.e. two unmodified peptide simulated with Amber ff99SBws and the CHARMM36m force fields respectively designed especially for simulating intrinsically disordered proteins, two phosphorylated systems having different phosphorylation patters: Tau₂₂₅₋₂₄₆ phosphorylated at residues T231 and S235, and Tau₂₂₅₋₂₄₆ phosphorylated at T231, S235, S237, and S238, and system O-GlcNAcylated at T231 and S235. The CHARMM protein and carbohydrate force fields were used to account for the phosphate and carbohydrate PTMs for the simulation of modified peptides. The starting geometry was set up by generating a random coil configuration of Tau₂₂₅₋₂₄₆ peptide. For each system Sixteen replicas are generated within a temperature range of 300 to 518.4 K. Each temperature replica was equilibrated for 200 ps to equilibrate the potential energy of the replicas. The potential energy was biased using 500 kJ/mol Gaussian widths, 1.2 kJ/mol initial Gaussian heights, with Gaussian potentials added every 2000 steps, with a bias factor of 36 to conduct simulations in the well-tempered ensemble (WTE). Each temperature replica was simulated for 200 ns NVT production simulations performed with the GROMACS for a total simulation time of 3.2 μ s, using a time step of 2 fs. We only analyzed 300 K temperature replica. As per secondary structure analysis the coil state was the dominant conformation for every peptide ensemble. We observed slight differences arising due to the underlying force field in unmodified systems simulated with Amber ff99SBws and the CHARMM36m force fields. We find a slight preference for helical structures, α -helix (6%) and 3_{10} -helix (4%), exhibited by the Amber ff99SBws force field, while the CHARMM36m force field favors the β -sheet structure (6%) for the native peptide. The secondary structure analysis revealed that PTMs (phosphorylation or O-GlcNAcylation) do not influence the conformation of the 225KVAVVR230 region, with no appreciable change in chemical shifts being observed in the simulations which agrees with the NMR derived chemical shifts data. Close contact analysis revealed that phosphorylation lead to the formation of strong salt-bridge contacts with adjacent lysine and arginine residues, which disrupted the native β -sheet structure observed in Tau₂₂₅₋₂₄₆. A transient α -helix (238SAKSRLQ244) was also observed when Tau₂₂₅₋₂₄₆ was phosphorylated at all four sites. In contrast, O-GlcNAcylation conformational effects resembled the native form of the peptide. The analysis showed non-bonding interactions based opposing structural effects of both PTMs.

Chapter 4: Influence of phosphorylation and O-GlcNAcylation on stability of tau paired helical fibril. Abnormal hyper-phosphorylation of the tau protein result in the self-assembly of tangles of paired helical filaments and straight filaments, which are involved in the pathogenesis of Alzheimer's disease, fronto-temporal dementia and other tauopathies. Tau contains a repeat domain consisting of four imperfect repeats (R1-R2-R3-R4) that forms the core of tau filaments and is capable of self-assembling into filaments in vitro. We carried out all-atom MD simulations to explored the effects of both PTMs on stability of paired helical filaments (PHF) formed by R3-R4 repeat domains of tau making it infinitely long in z-direction. Each simulation system consists of five-dimeric layers of Tau. The starting geometry for the five-dimeric layers of Tau was extracted from the Cryo-EM structure (PDB id: 503L) deposited in the Protein Data Bank, which has two peptides in each layer. The peptide consists of Tau residues 306-378 covering the R3 and R4 section of the repeat domain of Tau protein. Phosphorylation was attempted at Ser324 and Ser356, wherein both the residues have been experimentally proven to be crucial for maintaining PHF stability as well as binding of the tau repeat domain to MTs using CHARMM36m protein force field. O-GlcNAcylation was introduced only at the experimentally verified Ser356 site using CHARMM carbohydrate force field. To explore the conformational characteristics of the native and PTM systems we carried out microsecond long MD simulations. The main objective of the study was to understand key non-covalent interactions responsible for unique C-shaped structure of the PHF fibril. As per secondary structure DSSP analysis a slight reduction in β -sheets propensity upon phosphorylation was observed, which restored upon O-GlcNAcylation, confirming the opposing structural effects of both PTMs on tau. This was as a direct result of three different types of non-bonding interactions: salt-bridge, hydrophobic contacts and H-bonding, playing crucial role in stabilizing and maintaining the filament dimers as well as C-shape of the PHFs. We observed phosphorylation being the most disturbing modification to the characteristic C- shape architecture.

In conclusion, the present thesis significantly highlight the strong relationship between non-covalent interactions, salt-bridge and hydrophobic contacts in deciding the local conformation of the peptide upon phosphorylation and O-GlcNAcylation. These interactions have been known to influence protein folding and thermodynamically stabilizing the native protein conformation. More importantly, phosphate-Lys salt-bridge are crucial in the biological systems such as in kinases, wherein the activation loop changes conformation due to the $i, i-x$ arrangement of Thr and Lysine residues necessary for kinase activity. We hope that the work presented here provides reasonable contribution to the field of computational methods for protein secondary structure conformations.

Title: Synthesis and studies of new myo-inositol and phenothiazine derivatives as next-generation protein kinase inhibitors
Researcher: Javeena
Supervisor: Kirubakaran, Sivapriya
Year: 2020
Keyword's: Myo-inositol, Phenothiazine Derivatives, Protein Kinase Inhibitor, Immunotherapies
Call No.: 540 JAV
Acc. No.: T00712

Abstract: Protein kinases are the most studied targets in modern drug discovery majorly for cancer due to their key role in significant cell signaling pathways. In this thesis, we emphasize some of the chemical biology approaches across the two diverse chemical scaffolds, Myo-inositols, and phenothiazine. The first part of the thesis consists of the design and synthesis of the above scaffolds. These molecules are also studied for their novel structures using Single-crystal X-ray diffraction analysis. In the second part, the biological evaluation of these small molecules based on in vitro studies such as cell viability assay, cell death analysis, cell cycle arrest, and western blotting using specific antibodies of its downstream signaling protein.

In the second chapter, we have studied the Holy Grail of cancer called "RAS". RAS gene family is involved in multiple cellular functions consist of cell proliferation, survival, and gene expression is directly related to cancer pathogenesis, and often mutated in most of the human cancers. They have highly conserved G-domain (GTP/GDP binding regions) and share almost analogous activation/deactivation processes. In this prospect, in silico method has been used to recognize potential binding sites on RAS as a preliminary study to synthesize small molecules. In brief, the first objective of this chapter was to design and synthesize phosphate derivatives of Myo-inositol molecules as RAS inhibitors and designing of small molecules based on the recently reported inhibitors. We have also done biological studies on breast cancer cell lines of synthesized small molecule inhibitors for RAS inhibition. Our first-stage in-vitro screening of the in-house synthesized inhibitors showed that the compound 1b (C2-O-phosphate derivative of Myo-inositol 1,3,5-orthobenzoate) inhibited the RAS-RAF-MEK-ERK signaling pathway. Besides, we also found that this compound induced cell death and causes cell cycle arrest at S phase. This class of molecules may work as a potential inhibitor of breast cancer caused by a mutation in KRAS and its downstream proteins. Though the efficacy of the molecules is in the micromolar scale, they have not been explored previously for RAS inhibition. This result could be helpful further to explore its detailed biological studies to get better candidates as RAS inhibitors and advance the hunt of the small molecule in the mutant KRAS driven cancers.

In the third chapter, we have studied new kinase inhibitors for a novel kinase called TLK (Tousled-like Kinase, TLK1/1B). The prominent expression of TLK1B was observed in approximately ~30% of breast cancer antigens. Targeting TLK1/1B, which is S-phase active kinases and its connection to these functions, can cause effective and selective druggable targets for cancer therapy. Thioridazine (THD) is known as a lead compound for anticancer drug discovery in the field of TLK1/1B, and it has been researched extensively in preclinical studies. However, THD has not been successful further in

clinical studies. The primary objective of this chapter was the design and synthesis of the THD based scaffolds, which have phenothiazine as parent molecule by modifying the substituents at C2, N10 positions, and also changing the functional group at the C5 position. J3-54 showed promising results against prostate cancer in the combinatorial approach. Further, SAR studies based on the selectivity or potential of the J3- 54 would be proposed to improve the therapeutic properties.

In the last chapter, we have explored the packing features of the novel small molecules, which are presented in previous chapters with the help of single-crystal crystallography with supporting theoretical studies. Several small molecules were crystallized, and their structures have been solved by diffracted using single-crystal X-ray diffraction. The main motive is to identify the various molecular interactions generated among the molecules were studied using Hirshfeld surfaces (HS), and 2D fingerprint plots. The Hirshfeld surfaces of all the crystallized compounds have been mapped over a d_{norm} , shape index and curvedness to visualize the significant intermolecular interactions. These plots are mostly accountable for the distribution of strong and weak intermolecular interactions in the crystal packing of solid networks of the compound. From the experimental studies of the crystal structures, it is found that C–H···O, P–O···H, C–H···C, and π – π interactions play an important role in the stabilization of the crystal packing. The intermolecular charge transfer property of these compounds was studied by the density functional theory (DFT) calculations (B3LYP/6-31G* level). The theoretical values of bond length and bond angle were compared to the experimental ones obtained by single-crystal X-ray diffraction. This investigation may lead to the categorization of the promising active conformation of inhibitor and its intermediates additionally to the understanding of their structural packing.

In brief, the summary of the thesis is conceptualized around the designing, synthesis, structural and biological studies of new molecules to target kinases responsible for the growth of cancer cells. The studies reported here would lead to the pathway for advancing the drug-like properties of small molecules further.

Title: Asymmetric syntheses of substituted- γ -butyrolactones: application to the total syntheses of natural products

Researcher: Madhukar, Sarkale Abhijeet

Supervisor: Appayee, Chandrakumar

Year: 2020

Keyword's: Primary Metabolites, Bioactive Natural Products, Secondary metabolites, Therapeutic Agents, Enantiomeric

Call No.: 540 MAD

Acc. No.: T00713

γ -Butyrolactone is a five-membered heterocyclic compound, and this structural framework is ubiquitous in natural products. Considering the broad biological activity profiles and synthetic applications of the optically active γ -butyrolactones, the methodology development for synthesis of such challenging structural motifs has been an attractive goal for organic chemists. Several stereocontrolled synthesis of chiral γ -butyrolactones has been achieved using chiral pool, chiral auxiliary, and asymmetric catalytic methodologies.

This thesis describes the catalytic methodology developments for the asymmetric synthesis of substituted- γ -butyrolactones and their uses in the total syntheses of natural products.

In Chapter 2, the first organocatalytic approach for the short asymmetric synthesis of (*R*)-paraconyl alcohol is described in four steps with 35% yield and 95% *ee* after a single column purification. The asymmetric α -hydroxymethylation of aldehyde with aqueous formaldehyde in the presence of (*S*)-diaryl prolinol catalyst was conceived as a key step. The total syntheses of IM-2 and SCB2 are achieved through the direct aldol reaction in just three steps from (*R*)-paraconyl alcohol with a 38-42% overall yield. The application of (*R*)-paraconyl alcohol for the asymmetric synthesis of A-factor through acylation is also accomplished.

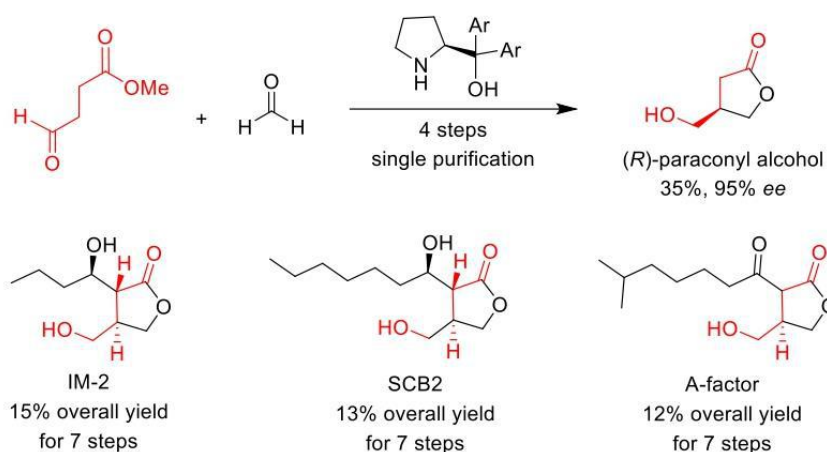


Figure 1. Asymmetric synthesis of (*R*)-paraconyl alcohol and total syntheses of IM-2, SCB2 and A-factor γ -butyrolactone autoregulators.

In chapter 3, a stereodivergent syntheses of the paraconic acids starting from commercially available maleimides and alkyl aldehydes is detailed. N-heterocyclic carbene catalysis is established for one-step syntheses of 3-acylsuccinimides with excellent yield. The first dynamic kinetic resolution of 3-acylsuccinimides is accomplished through asymmetric transfer hydrogenation to achieve the alcohols in good yields and high stereoselectivities. Syntheses of

trans-paraconic acids are fulfilled with DBU catalyzed epimerization of the alcohols followed by hydrolysis and cyclization under the basic conditions. Conversely, syntheses of *cis*-paraconic acids is achieved by mild hydrolysis followed by cyclization. Using this stereodivergent synthetic methodology, both the enantiomers of *trans*-paraconic acids are synthesized in three steps with 47–52% overall yield and 96% ee. On the other hand, both the enantiomers of *cis*-paraconic acids are obtained in four steps with 54–57% overall yield and 94–95% ee. We have also shown the application of paraconic acids for the total syntheses of (–)-methylenolactocin, (–)-phaseolinic acid, (+)-nephrosteranic acid, and (+)-nephrosterinic acid natural products.

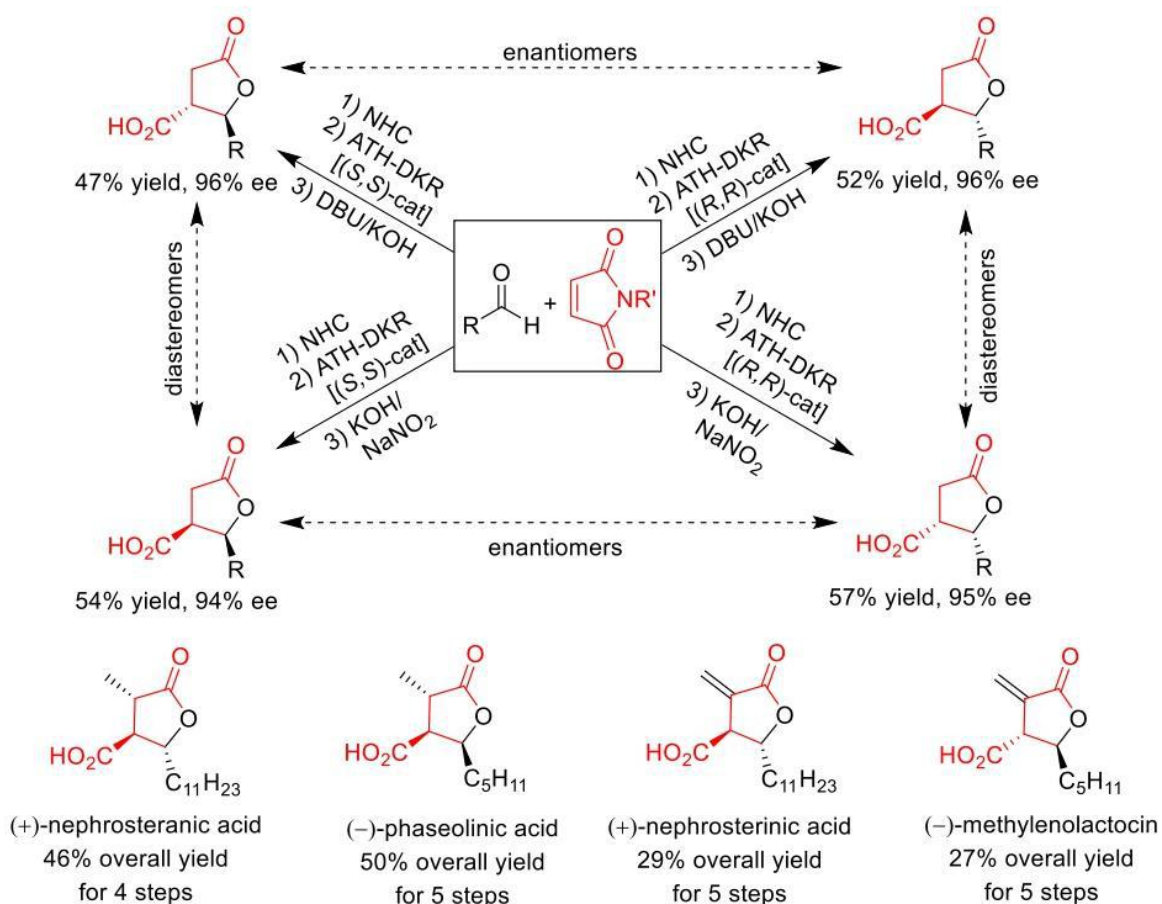


Figure 2. Stereodivergent syntheses of chiral paraconic acids and total syntheses of bioactive natural products.

In chapter 4, the first stereodivergent strategy for the asymmetric synthesis of all four stereoisomers of 1-hydroxymethylpyrrolizidine alkaloids, namely, (+)-isoretronecanol, (–)-isoretronecanol, (+)-laburnine, and (–)-trachelanthamidine using the common β -substituted- γ -butyrolactone intermediates. The self-Mannich reaction of methyl 4-oxobutanoate with PMP-amine catalyzed by chiral secondary amine to afford β -substituted- γ -butyrolactone

intermediate is considered as the key reaction. The optimization of the self-Mannich reactions of methyl 4-oxobutanoate with PMP-amine for stereodivergent syntheses of β -substituted- γ -butyrolactones is successfully achieved. The conversion of all stereoisomers of β -substituted- γ -butyrolactone to 1-hydroxymethylpyrrolizidine alkaloids is accomplished in 6 steps with 29–33% overall yield. The total syntheses of 1-hydroxymethylpyrrolizidine alkaloids are completed in 8 steps with 22–26% overall yield and 93–98% *ee* from commercial available starting materials.

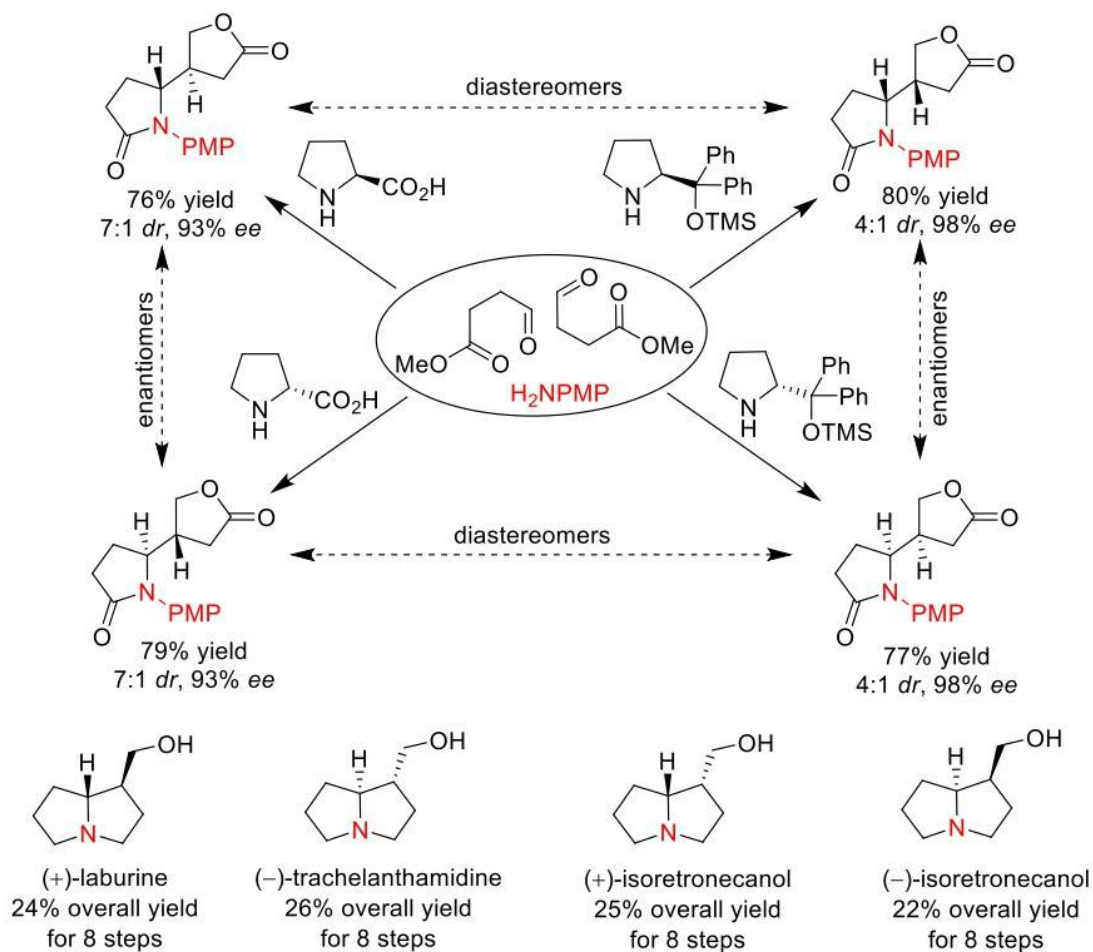


Figure 3. Stereodivergent syntheses of β -substituted- γ -butyrolactones and total syntheses of 1-hydroxymethylpyrrolizidine alkaloids.

Title: Synthesis and application of Trans A₂B₂ porphyrins for photocatalysis, energy transfer, and photodynamic therapy

Researcher: Pandey, Vijayalakshmi

Supervisor: Gupta, Itri

Year: 2020

Keyword's: Trans A₂B₂ - Porphyrins, Photocatalysis, Photodynamic Therapy, Catalytic Photooxidation

Call No.: 540 PAN

Acc. No.: T00714

Abstract: Porphyrins are tetrapyrrole containing aromatic compounds, found naturally in photosynthetic systems and oxygen-carrying biomolecule like hemoglobin. Porphyrins possess various remarkable applications in nature to make our life easier. The best examples are oxygen transport, photosynthesis, and electron transfer by cytochrome 450. Fischer and Gleim first approached the attempted synthetic methodology of making porphyrin synthesis in 1935. They focused on acid condensation of pyrrole and aldehyde in formic acid, which resulted in only 0.26% of porphyrin. Tetra-phenyl porphyrin or H₂TPP is the *meso* first substituted porphyrin designed and synthesized by Alder Longo in formic acid in the 1960s. The noteworthy photo-physical properties of porphyrins play a significant role in their applications. The typical photophysical properties; four Q bands followed by the strong absorption in UV-Visible region Soret band and red-shifted emission (600-900 nm) are the key features that make these porphyrins different from other non macrocyclic chromophores. The scope for design and alternation in the porphyrin is an immeasurable curiosity for the researchers working in this area. The remarkable photophysical properties, moderate quantum yield, excellent thermal & photochemical stability, good solubility makes these molecules promising for synthetic challenges. These molecules can be used for several applications like DSSC, organic photovoltaics, bioimaging, and photodynamic therapy. This thesis's main objective is to synthesize novel trans A₂B₂ porphyrins targeting three different applications: photo-oxidation, energy transfer, and photodynamic therapy. The thesis can be divided into four synthetic chapters, starting from synthesizing starting material to targeted designed *trans* A₂B₂ porphyrins. The molecules synthesized in this thesis have been carefully characterized by MALDI, ¹H-NMR, and ¹³C-NMR and explored for catalytic efficiency, energy transfer, and photodynamic efficiency. The *first* chapter is about the literature review on catalysis, energy transfer donor acceptor systems and glycosylated porphyrins used for photodynamic therapy. The *second* chapter of the thesis described the synthesis of reported precursor molecules and their characterization by standard techniques like IR, MS, NMR, UV-vis, and fluorescence spectroscopy.

The *third* chapter includes the synthesis and the characterization of carbazole and triphenylamine appended palladium metallated porphyrins. All the porphyrins synthesized were characterized by MALDI, ¹H-NMR, and ¹³C-NMR spectroscopy. Our lab's previous results made us curious to find out the catalytic efficiency of *trans*- A₂B₂ metalloporphyrins for photo-oxidation of aldehydes to a carboxylic acid. After screening the metalloporphyrins' singlet oxygen efficiency in different solvents, it was found that PdP3 is capable of generating 63% singlet oxygen in tetrahydrofuran.

However, the photo-oxidation reactions performed gave the exciting result in acetonitrile with a 98% yield. The sequential reactions were performed and the results implied that various factors decide the outcome of photo-oxidation reaction like a solvent, temperature, solubility, and time duration. Depending upon the kind of substituent attached to porphyrins core, the photocatalyst's catalytic efficiency is varied. The presence of electron-withdrawing donating groups decides the capacity of the photocatalyst. Electronegativity of fluorine plays an essential role in enhancing the speed of the reaction mechanism. On the other hand, the heavy atom effect of palladium enhanced the singlet oxygen generation.

The *fourth* chapter is about the donor-acceptor systems where the thiophene linker is used between the donor (thiophene functionalized carbazole or phenothiazine) and acceptor (porphyrin). To incorporate thiophene between the donor and acceptor, Suzuki coupling was employed between bromo/ iodo carbazole or phenothiazine and thiophene aldehyde to get functionalized aldehyde. Further Acid condensation between functionalized aldehyde and dipyrromethane of pentafluorophenyl was carried out using Lindsey's method. Zinc and palladium metals were also chosen to get the metalloporphyrins with fluorescence and phosphorescence properties. To gauge the electron density migration between the donor and acceptor, DFT calculations were carried out using the B3LYP/6-31G* level of approximation. We were able to get the crystal structures for free base and zinc metallated carbazole thiophene meso substituted trans A_2B_2 porphyrin in chloroform/hexane solvent mixture at room temperature. The ORTEP structure showed dihedral/torsion angle between donor and porphyrins ring, supported the expected orientation of thiophene to porphyrins core which is responsible for the improved electronic communication from donor to acceptor and energy transfer efficiency between 67-88%. Steady-state fluorescence and lifetime studies were carried to know the total energy transfer taking place in this kind of system.

The *fifth* chapter was designed to explore the trans A_2B_2 porphyrins for biological applications. A series of glycosylated porphyrins were synthesized using carbazole, phenothiazine, and triphenylamine at meso position. Carbohydrates have biological importance and it is well known that their selectivity for cancer cells is more as compared to normal cells, for the same reason glycosylated porphyrins were examined against A549 cell line. Out of the twenty glycosylated porphyrins, the glycosylated porphyrins synthesized have shown significant photodynamic efficiency in the presence of visible light with IC_{50} values between 23.3-44.2 μM in dark; whereas after visible light exposure, the photosensitizers exhibited IC_{50} values around 11.1-23.8 μM . The water-soluble thioglycosylated zinc(II) porphyrins having two *meso-N*-butylcarbazole groups exhibited an excellent degree of photocytotoxicity ($IC_{50} = 4.6-8.8 \mu M$). The flow cytometry analysis revealed that cellular uptake and ROS (reactive oxygen species) generation efficiency of water-soluble thioglycosylated zinc (II) porphyrins were considerably higher than non-metallated porphyrins. Confocal microscopy images displayed substantial distribution in the endoplasmic reticulum with partial co-localization in mitochondria and lysosomes of water-soluble thioglycosylated zinc (II) porphyrins in A549 cells.

The *sixth* chapter is based on the palladium complexes of glycosylated porphyrins. To get improved and check IC_{50} value heavy atom effect palladium metal was incorporated in glycosylated porphyrins. The synthetic method developed in the previous chapter did not synthesize palladium-appended glycosylated porphyrins; hence direct attachment of sugar to porphyrins was preferred, which gave a promising result of 90-92% product conversion. A different synthetic strategy was approached to synthesize palladium glycosylated porphyrins. The photophysical studies performed in toluene gave the effects similar to non-glycosylated porphyrins, which means attaching sugar does not alter the spectral properties in the non-polar solvent.

For the same reason, after deprotection, the studies were performed in methanol. The reduction in molar extinction coefficient was observed, which may be due to aggregate formation by free OH. Further, singlet oxygen generation studies were performed using DPBF as an oxygen quencher, which resulted in 60-65% singlet oxygen generation it was much higher than zinc-glycosylated porphyrins. The other biological studies to support the *in vitro* studies are underway.

At last, the summary of the work done from the thesis is given. In the *third* chapter, phosphorescent porphyrins synthesized have been used for photocatalysis. These porphyrins have become very promising, which can be used to explore different kinds of epoxidation sulphoxidation and C-H activation reactions. The porphyrins designed and synthesized in chapter *four* can give profitable energy transfer from donor to acceptor; hence, *it* can be used for DSCC applications. Apart from this, they can also be explored for photocatalysis reactions. The later part of the thesis, chapter *fifth* and *sixth*, focused on glycosylated porphyrins and provided promising results for targeting cancer cells. As these compounds possess high molar extinction coefficient and red-shifted emission, they can be used for *in-vivo* studies to target cancer cells.

Title: Synthesis and studies of luminescent metal dipyrinates: NIR emitters for application as triplet sensitizers in photo-dynamic therapy

Researcher: Manav, Neha

Supervisor: Gupta, Itri

Year: 2020

Keyword's: Luminescent Metal Dipyrinates, NIR Emitters, Metal Dipyrinates, Dichloromethane

Call No.: 540 MAN

Acc. No.: T00715

Abstract: Metal dipyrin chemistry has always been a center of attention for researchers from years. The small change in structure can vary the optical properties, and the change can either be of ligands or the metals. However, the absorption mostly observed as dipyrin centered but variations in photostability, singlet oxygen efficiency, and the lifetime can be expected. This makes the dipyrin chemistry more interesting for photodynamic therapy as well as OLEDs. Tricarbonyl Re(I) and cyclometalated Ir(III) complexes are the two important d^6 which have been extensively explored for OLEDs and solar light-harvesting systems. Their high spin-orbit coupling helps in populating the triplet state, or in other words, enhances ISC. Hence, the objectives of the thesis are to design metal dipyrinates (d^6 systems) based photosensitizers for biological studies, such as PDT. We explored this field starting from the strategy of changing meso-substituents around rhenium dipyrinates. We found interesting results in terms of high Stokes shifts, good singlet oxygen quantum yields, microsecond lifetimes, and photostabilities. This encouraged us to use these systems in biological applications. The metal dipyrinates were further modified and a series of sugar and oligoethylene conjugates were synthesized. These metal-sugar and OEG conjugates were prepared for their role in enhancing cellular uptake of the photosensitizers. In preliminary studies, such systems showed no dark toxicity and this makes them interesting candidate to explore in PDT, further studies are underway. Similarly, iridium dipyrinates were also explored with modification at meso-substituent, on pyrrole ring, and their conjugation with sugar moieties. Such systems provided good agreement with huge Stokes shifts and their predominant localization in the endoplasmic reticulum (ER). This makes them more interesting in co-cellular localization applications. More importantly, ER is very close to the nucleus where it's easy for photosensitizer to induce effective action of DNA damage by singlet oxygen generation. In the later part of the thesis, we have extended our approach from molecular systems to nano-assembly; where we prepared metal-lipid conjugates and explored the formulation of nano-assembly. The preliminary bio studies confirmed their good cellular uptake, and no dark toxicity up to 72 h with effective photo-toxicity. However detailed studies are under process in the lab but these systems have potential in exploring further as triplet sensitizer.

In the first chapter, rhenium(I) dipyrinate with 4-fluorophenyl and N-butylcarbazole substituents on the dipyrin ligand can also be explored in photo-catalysis reactions using sunlight like oxidation of aldehydes, epoxidation or sulfoxidation. They exhibited a good triplet excited-state lifetime of 29-17 μ s and high singlet oxygen generation ability (~98%) and efficient catalytic activity (~75-95%). These systems can seek applications in triplet-triplet annihilation, photocatalytic systems for CO₂ reduction, where certain rhenium complexes are proving their potential, Such complexes can also

be explored in the fields where lifetime in microseconds are anticipated such as solar light conversion and OLEDs. Furthermore, they can be modified for cellular uptake and their further potential in biology can be explored.

The glycosylated rhenium, palladium, and iridium complexes described in the second and third chapters can have potential applications in antimicrobial PDT; as they are neutral photosensitizers and could turn out to be more effective than already reported cationic and anionic PS in antimicrobial PDT. Such systems can be also be explored in photo-catalysis in water-soluble reactions using sunlight. The observed predominant localization of iridium dipyrinates opens up more avenues of exploring such systems as the compounds to target ER known to have better selectivity towards cancer cells over non-cancer cells. The predominant subcellular localization can induce anticancer activity in nanomolar concentrations. Other than this they have better potential than nucleus targeting agents, as sometimes for such systems DNA mutation can occur. However, being in close proximity to the nucleus, they can induce better toxicity after generating singlet oxygen and DNA damage.

Chapter four of the thesis opens up the platform for nano-conjugates importance and varied liposome surface-based modifications. In the future, there is a scope to develop metal dipyrinates and liposome hybrids for selective accumulation in cancerous cells and better renal clearance. This would be an effective approach to enhance photodynamic therapy.

The metal dipyrinates discussed in this thesis were anticipated in the fields where visible absorption and emission are useful. In this thesis, we synthesized neutral photosensitizers with NIR emission. The NIR emission can eventually be useful in eliminating the background fluorescence for bioimaging. As the cellular components mitochondria and lysosome emit mostly in the visible region. The high Stokes shifts of such systems can help to overcome the problem of autofluorescence in biological applications. We focused on neutral metal-based photosensitizers that are more useful than their charged analogs in the cellular system. The charged complexes were known to enhance the cellular uptake but eventually, they are also found to be toxic to the cells in dark conditions. This limits their application and hence neutral metal dipyrinates with high singlet oxygen in the presence of light (good photo-toxicity) could be the better option to overcome that limitation.

Synthetically the iridium(III) and rhenium(I) dipyrinates with different meso-substituents can be modified further to enhance the singlet oxygen quantum yields. It might help to shift their absorption and emission towards red to near infra-red (NIR) region, similar to the compounds reported with modified pyrrole in chapter 3. Such systems have a wide scope in modifying the pyrrole to shift its absorption. Overall, the field of metal dipyrinates can be refined further by conjugating other chromophores (BODIPYs, porphyrins, aza-BODIPYs) to the iridium /rhenium metal dipyrinates. Such panchromatic conjugated dyes could have promising photophysical properties with high molar extinction coefficient and NIR absorption and emission, for applications in anti-cancer treatment and as luminescent probes for deep-tissue imaging in biomedicine.

Title: Precise and in-situ control of surface plasmon resonance of gold nanorods via post-synthesis modifications
Researcher: Thambi, Varsha
Supervisor: Khatua, Saumyakanti
Year: 2020
Keyword's: In-situ Control, Surface Plasmon Resonance, Metal Nanoparticle, Plasmonic Nanoparticles
Call No.: 540 THA
Acc. No.: T00716

Abstract: The contribution of this thesis is towards developing three different methods for tuning the longitudinal surface plasmon resonance of gold nanorods. In pursuit of this, we have used the pre-existing study on post-synthesis modification and have brought various development and control over different methods. To summarize, Chapter 1 introduces the origin of surface plasmon resonance by the interaction of metal NP with the light and their decay through various pathways. These pathways open up various areas of application of AuNP. Here, we discuss the importance of tuning the plasmon resonance and the different methods available in the literature for such tuning. In Chapter 2, we were able to tune the LSPR of AuNR both at higher and lower wavelengths by changing the pH of the growth medium. Moreover, the developed method also helps in creating many different complex geometries like water chestnut, octahedron, dog bone, icosahedron, and nano bar by overgrowing gold nanorod. In Chapter 3, we have developed a new structure called peanut by simultaneous deposition of Ag and Au on AuNR and then dealloyed the structure to create a broken shell peanut structure. These broken shell peanut structures were found to be 12 times more efficient in catalyzing the reduction reaction of 4 nitrophenol. The creation of a hollow broken shell peanut structure allowed us to tune the plasmon resonance to higher wavelength and also use these structures as an efficient catalyst. At last, in Chapter 4, we have done *in-situ* tuning of LSPR by etching the nanorods in the presence of light and FeCl_3 . The method developed in this work is new, and one of its kind as both rate and directionality of the reaction could be tuned by changing the excitation power. Also, etching being light-driven, it could be selectively done on single NR and allow stopping the reaction at any time by switching off the laser.

5.2. Future Prospects

The work done in this thesis opens up many other areas to explore and develop. Some of the work that our group will try to take forward are given below:

In our work, we were able to synthesize many different geometries just by controlling the growth kinetics of the reaction. Here we have studied the effect of pH on the overgrowth of the nanorod. Several other parameters, like the effect of surfactant, reducing agent, and nanorod concentration, can also be studied by simultaneously varying the pH of the growth solution. This will help us in understanding the mechanistic details of overgrowth. The complex structures synthesized by the above methods can be further explored in various plasmonic metal driven catalytic reactions. This

will allow us to investigate the role of a highly faceted structure towards the rate and directionality of the reaction.

Furthermore, we have concluded from our study that the hollow core-shell structure is a better catalyst compared to its solid counterpart. In this, we used HCl as a dealloying agent. In the future, we can use many other etching agents (like HNO₃ and H₂SO₄) and their combination to achieve better control in the hole size and wall thickness of the shell structure. Further, we can use the same method to develop other multi-metallic alloy structure that includes a combination of metals like Au, Ag, Pd, Pt, Co, Cu, etc. These multi-metallic anisotropic systems would be beneficial to carry out catalytic reactions more efficiently. We can also investigate dealloying in these systems to create a library of anisotropic hollow structure and then compare their catalytic activity with each other.

Also, peanut and broken peanut structure (formed in Chapter 3) of various hole sizes can be used in the various electro-catalytic and photo-electro catalytic reactions. Recently, we have started some work in this area, where we have compared the electro-catalytic activity of nanostructures, i.e., nanorod (NR), peanut (BP0), and broken shell peanut (BP240) without any support towards methanol oxidation. These structures have a varied concentration of Ag and Au content, both of which are known to catalyze methanol oxidation. For this, nanostructures were deposited on the ITO surface, which was then used as a working electrode in a three-electrode system to study their catalytic behavior. We found peanut structure to be more catalytically active towards methanol oxidation compared to broken shell peanut and nanorod with the order: NR < BP240 < BP0. The enhanced activity of peanut structure was attributed to high concentration of Ag and Au present in the structure, which together gave the highest current density. Further, we evaluated the response of nanostructures in the presence of white light where broken shell peanut structure displayed the highest change in photocurrent as compared to the peanut structure with the order: NR < BP0 < BP240. The large change in photocurrent in the presence of white light is attributed to the porous structure, which allowed the strong coupling of light with the Au and Ag atoms present on the core as well as on the inside and outside the shell structure. The details of the experiment are given in Annexure A.

In the last chapter, we studied the effect of light in the etching of gold nanorod in the presence of ferric chloride. We found that the rate and directionality of the reaction can be controlled by excitation power. The reaction being light-induced and hot carrier driven, a systematic study of the wavelength dependence of excitation could be performed in the near future. Here, different light wavelength will excite the plasmon to create hot carriers of different energy and number, which in turn will affect the rate of the reaction. We have partly done this study, where we have performed *in-situ* etching of gold nanorod using FeCl₃ and 633 nm excitation source. We found that both rate and directionality can be controlled by the power of the laser. The details of these experiment is given in Annexure B. Furthermore, we can also study the effect of polarisation of light since circularly, and linearly polarised light interacts with the NP differently. We believe that circularly polarised light can interact with all atoms irrespective of their position on the NR. This will etch Au atoms from tips as well as on the lateral facet of the NR. But linearly polarised light will be able to

target either atoms from the tips or corners. In this, we can use different shaped nanostructure like gold nano triangle/nano prism and change the directionality of etching by changing the polarisation of light.

Apart from etching, we can also perform overgrowth of gold nanorod at the single-particle level. We believe that the growth at a single particle on the surface will give us many insights and development to understand the mechanism involved during the growth process. Our work in chapter 2 can be extended to the single-particle level. Here, we will deposit gold nanorod on the glass surface and use both chemical precursors and light to carry out the reduction of Au ions on the surface of NR. This will help in understanding the role of each precursor used during the growth of nanorods. Further, the role of light in terms of wavelength and power dependence can also be studied. We can also target the dealloying process discussed in chapter 3 to be performed at the single-particle level. Here, we can deposit the peanut structure and perform the dealloying process on the glass surface. This will allow us to study this process in detail.

Title: Developing bio-inspired molecular complexes for catalytic oxidation and reduction reactions

Researcher: Ali, Afsar

Supervisor: Dutta, Arnab

Year: 2021

Keyword's: Catalytic Oxidation, Molecular Complexes, Oxygen Reduction Reaction, Electrocatalysts

Call No.: 540 ALI

Acc. No.: T00717

Abstract: Abstract not available

Title: Development of asymmetric organocatalytic methodologies and their applications to the syntheses of bioactive natural products
Researcher: Maurya, Vidyasagar
Supervisor: Appayee, Chandrakumar
Year: 2021
Keyword's: Organocatalytic Methodologies, Bioactive Natural Products, Substrate Scope, Cyclobakuchiols
Call No.: 540 MAU
Acc. No.: T00718

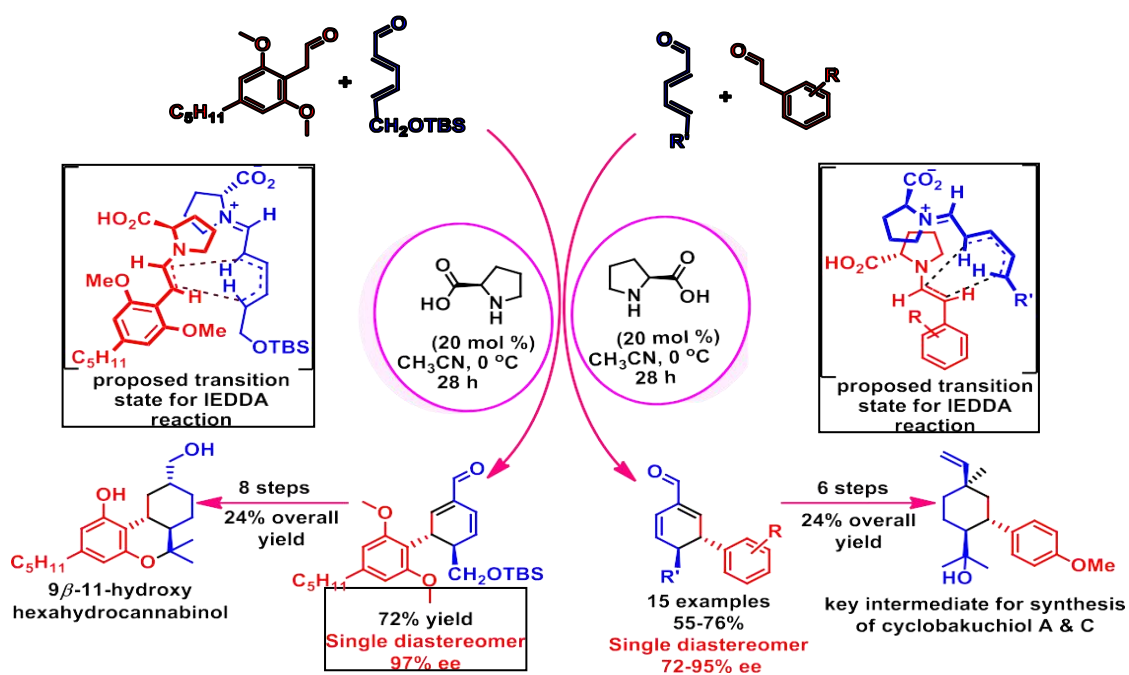
Abstract: My thesis work focuses on developing new organocatalytic methodologies for the asymmetric synthesis of multi-substituted six-/five-membered cyclic carbonyl compounds and further application to the asymmetric synthesis of bioactive natural products. During my Ph.D., I have developed new methodologies for proline catalyzed first asymmetric IEDDA reaction of $\alpha,\beta,\gamma,\delta$ -unsaturated aldehydes and arylacetaldehydes for the synthesis of highly stereoselective 3,4-disubstituted cyclohexadienecarbaldehydes. Further application of IEDDA reaction for the formal total synthesis of cyclobakuchiol A, an antipyretic and anti-inflammatory agent, cyclobakuchiol C, and the first total synthesis of 9 β -11-hydroxyhexahydrocannabinol, a potent cannabinoid. Another methodology for the first acetone functionalization for the asymmetric synthesis of disubstituted 4-oxocyclohexane carbaldehydes using organocatalysis. Apart from that, I have also worked on the concise total synthesis of chiral bioactive natural products, (+)-rocellaric acid, (+)-protolichesterinic acid, and (-)-nephromopsinic acid.

I have acquired a strong ability to independently plan, organize, and successfully perform the work within a team environment in a timely bound manner. First, two Ph.D. chapters involve very novel target synthesis for which there were no reports available in the literature. This opportunity gradually empowered me to develop new methodologies using organocatalysts. I have learned many scientific skills and management to perform multistep synthesis strategies, analysis, and various purification techniques. The whole thesis work aims to develop new approaches for accessing the highly substituted chiral motifs shortly and efficiently without harming the natural harmony and applying for the asymmetric synthesis of natural bioactive molecules. The entire thesis work has been divided into the following three chapters.

Chapter I. Asymmetric Synthesis of 3,4-Disubstituted Cyclohexadiene Carbaldehydes *via* Organocatalytic IEDDA Reaction

Inverse-electron-demand Diels–Alder reaction is one of the fascinating methods for the construction of six-member carbocyclic compounds and their application in the synthesis of natural products and biologically active molecules. Metal catalysis and organocatalysis are attractive areas for the synthesis of six-membered carbocycle rings. Because of the ecofriendly, cost-effective, and metal-free approach, asymmetric organocatalysis has been one of the most popular methods for the construction of chiral six-membered carbocyclic natural and biologically active molecules. In this chapter, we have developed the first asymmetric organocatalyzed [4+2] cycloaddition reaction of

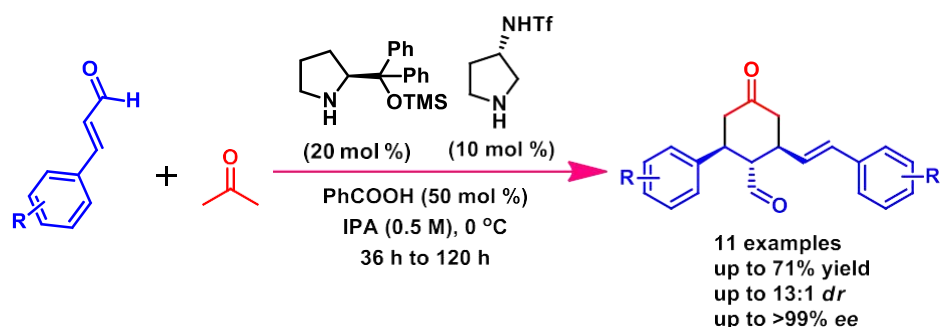
$\alpha,\beta,\gamma,\delta$ -unsaturated aldehydes and arylacetaldehydes via inverse-electron-demand Diels–Alder (IEDDA) reaction pathway. We have successfully synthesized 3,4-disubstituted cyclohexadienecarbaldehydes as the single diastereomers in up to 76% yields, 95% *ee*.



Further, we have successfully applied this methodology for the formal total synthesis of cyclobakuchiol A, an antipyretic and anti-inflammatory agent, and cyclobakuchiol C by obtaining the key intermediate from 3,4-disubstituted cyclohexadienecarbaldehyde in 6 steps and 24% overall yield. Using this asymmetric organocatalytic IEDDA reaction as a key step, we have achieved the first total synthesis of potent cannabinoid, 9β-11- hydroxyhexahydrocannabinol from 3,4-disubstituted cyclohexadienecarbaldehyde in 8 steps and 24% overall yield.

Chapter II. Direct Asymmetric Organocatalytic Reaction of Acetone with Cinnamaldehyde Derivatives to form Chiral Disubstituted 4-Oxocyclohexanecarbaldehydes

Chiral cyclohexanones are a common structural motif of many natural products, biologically active molecules and are used as a building block in organic synthesis. Several methodologies have been developed in the literature for the asymmetric synthesis of cyclohexanones frameworks because of their useful applications. However, there is no catalytic method reported so far in the literature for the asymmetric synthesis of disubstituted 4- oxocyclohexanecarbaldehydes. Acetone is one of the common organic solvents used in organic chemistry. The use of acetone as a substrate for chemical reactions is always a challenging and attractive task for organic chemists because of its inert nature, inexpensive, and easy availability. This chapter described the first organocatalytic stereoselective domino reaction from the readily available acetone and cinnamaldehyde derivatives to disubstituted 4- oxocyclohexanecarbaldehydes in up to 71% yield, up to 13:1 diastereoselectivity, and up to >99% enantioselectivity using two secondary amine catalysts.



Chapter III. Asymmetric Synthesis of Bioactive Paraconic Acid Natural Products

Paraconic acids are natural bioactive molecules that possess different biological properties like an antibiotic, antimicrobial and antitumor etc. This chapter has developed an efficient and short synthetic route for the synthesis of *cis*- & *trans*-paraconic acids starting from commercially available maleimides and alkyl aldehyde. NHC catalysis is established for the one-step synthesis of 3-acylsuccinimides. The first dynamic kinetic resolution (DKR) of 3-acylsuccinimides is accomplished through the asymmetric transfer of hydrogenation (ATH) to achieve the β -hydroxysuccinimides in good yields and high stereoselectivities. Synthesis of *trans*-paraconic acid is achieved by DBU catalyzed epimerization of the β -hydroxysuccinimide, followed by the hydrolysis and cyclization under the basic conditions. Similarly, the synthesis of *cis*-paraconic acid is achieved from the alcohols by mild hydrolysis followed by cyclization. Using this methodology, total synthesis of bioactive paraconic acid natural products, (+)-rocellaric acid is achieved in four steps with 38% overall yield, (+)-protolichesterinic acid and (-)-nephromopsinic acid are achieved in five steps with 23% and 56% overall yields.

Title: Modulating the photo and electro-catalytic small molecule activations by Cobaloximes with enzyme-inspired ligand design

Researcher: Mir, Ab Qayoom

Supervisor: Dutta, Arnab

Year: 2021

Keyword's: Cobaloximes, Elctro-catalytic Small Molecule, Photo-catalytic Small Moleule, Petrochemical

Call No.: 540 MIR

Acc. No.: T00719

Abstract: Non-renewable, carbon-based fossil fuels, which satisfy the major share of the existing demand for energy sources, are declining at an alarming rate. With a rapidly escalating population, there arises a need for more energy to meet the ever-increasing demand.^{1,2} The existing energy requirement comes mostly from non-renewable carbon-based sources such as coal, natural gas, and oil. Their continuous usage has a detrimental impact on the environment as they produce greenhouse gases like CO₂. Hence, the scientific community has turned their attention to non-traditional alternative energy resources that can still balance the global energy supply with minimal effect on our biosphere.³ The most abundant and exploitable energy source on planet earth is solar energy, but its intermittent nature has restricted its worldwide usage. In view of this limitation, efforts are being made to utilize this solar energy in an indirect albeit effective way. Natural photosynthesis is the primary inspiration behind this school of thought, where solar energy is converted into chemical energy (i.e., carbohydrate) for proper storage and timely exploitation. Researchers have effectively imitated the natural photosystem to convert solar energy into relatively simpler chemical energy via small molecule activation-based redox chemistry. Hydrogen is considered a leading green fuel. It has high energy density, and during redox cycling, for energy harnessing, it produces chemically benign H₂O as the sole by-product.⁴ Renewable energy can be efficiently stored into the H-H bond and later extracted in the form of electricity using the proton exchange membrane (PEM) fuel cell. Economical production of H₂ from a renewable source of energy is critical for large-scale H₂ generation.

Hydrogenase enzymes are known for the proton reduction with TOF of around TOF ~20000 s⁻¹ with minimal energy penalty (also known as the overpotential) of ~50-100 mV. However, the practical application of these hydrogenase enzymes is not feasible as they are functional only at a narrow chemical space matching the physiological conditions. The enzymes typically degrade under harsh, industrially relevant reaction conditions.⁵

However, the unique architecture of the enzyme always remains as the source of inspiration for the development of biomimetic synthetic catalysts. The surrounding protein scaffold (also known as the outer coordination sphere/OCS) of hydrogenase is a vital clog in its mechanistic reactivity, where it modulates the movement of protons, electrons, and H₂ gas in and out of the active site effectively via specific channels.⁶ The primary attempts to mimic the enzyme were limited to its Ni- and Fe-based active sites. Most of those structural model complexes failed to match the fast and energy-efficient H₂ production activity by hydrogenase. DuBois and coworkers introduced a pendant amine around the synthetic core of nickel *bis*-diphosphine complexes following the architectural clue from

the enzyme, and it significantly improved the H₂ evolution reaction (HER) catalytic activity.⁷ Later, Shaw and co-workers extended the peripheral functionalities with the incorporation of natural amino acids to generate one of the best reported artificial HER catalysts. Despite the remarkable catalytic performance, these nickel *bis*-diphosphine core-based DuBois catalysts are misfit for a large-scale usage due to their acute oxygen sensitivity.⁸⁻¹¹

On the other hand, Co-diimine-dioxime (cobaloxime) complexes are known to be oxygen tolerant but exhibited only a moderate H₂ production rate with appreciable overpotential values.¹² previously, our group has included amino acid-based functionalities around the cobaloxime core to induce water solubility while improving the H₂ production rate by ~10 times compared to the parent complexes. However, these amino acid decorated cobaloximes exhibited HER activity mostly at near-neutral conditions (pH ~7), and they lose its reactivity below pH 5.0.^{13,14} In this thesis, we have employed otherwise poorly active or inactive metal complexes as the central core and introduced non-amino acid and vitamin-based OCS imitating the enzymatic hallmark of proton relay. This inclusion not only imparts water solubility for the complexes but improves their reactivity under acidic conditions for catalytic HER activity. The reactivity of the complexes was probed under both electro and photocatalytic conditions. Each chapter in this thesis unravels the specific influence exerted by diverse modifications to the catalytic core by non-amino acid-based OCS.

We have introduced the otherwise inactive cobaloxime complex with non-amino acid-based vitamin B6 analogs as OCS as proton relay in the initial chapter. The synthesized complexes are having different basic functionalities such as alcohol, amine, and phosphate. All the catalysts having OCS were found highly active for H₂ production ranging from neutral to acidic conditions (pH 3-7). Of the three complexes with different basic functionalities, C1 (containing alcohol group) has maximum catalytic rate (turn over frequency/TOF) with 5400 s⁻¹, while C3 (containing alcohol, amine, and phosphate) exhibited the minimal rate. In terms of overpotential requirement, C3 demonstrated the best energy efficiency with a value of 430 mV (overpotential), which is one of the lower overpotential at neutral aqueous conditions reported for cobaloxime-based catalysts. Interestingly, all these complexes retained significant HER activity (~30%) even in acidic conditions compared to the amino acid-bound cobaloximes, which run at ~10% of their reactivity under similar conditions. The vitamin B6-analog- containing complexes were also probed for photocatalytic HER activity in 100% aqueous conditions in the presence of organic photosensitizer and triethanolamine as a sacrificial electron donor. Interestingly, all the complexes displayed substantial H₂ production under natural sunlight and aerial conditions (~21% O₂). Hence, the inclusion of vitamin molecules as outer coordination sphere opens up a new direction for incorporating OCS functionalities around synthetic cores with improved catalytic reactivity.

In the next chapter, we continued our journey by modifying the synthetic catalyst molecule (cobaloxime) with non-amino acid-based OCS features. For this purpose, we included a series of nuclear bases (hypoxanthine: an adenine analog), nucleoside (adenosine), and nucleotide (adenosine-mono-phosphate/AMP). The addition of these molecules not only conferred high aqueous solubility for the modified cobaloximes but also induced better performance for both photo

and electrocatalytic H₂ production. The inclusion of multifunctional groups directly influenced the catalytic turn over by the cobaloximes, which was evident from their relative order as cobaloxime-hypoxanthine (C4) < cobaloxime-adenosine (C5) < cobaloxime-adenosine-AMP. The highest catalytic rate for complex C6 was attributed to the interactive proton exchange between the peripheral functionalities improves with the presence of phosphate, carbohydrate, and nuclear base motif. The exchange of protons around the cobaloxime core by the basic functional groups was further probed by the two-dimensional nuclear Overhauser exchange spectroscopy (NOESY) experiment. In this experiment, the appearance of cross-peaks between various exchangeable groups such as oxime -NOH, heteronuclear base molecule, ribose -OH, and phosphate confirmed that the swapping of protons. The same trend continued even for photocatalytic H₂ evolution reaction in aqueous solution at neutral pH (7.0).

So far, we have monitored the photocatalytic reactivity of our complexes in the presence of untethered organic photosensitizers in the same solution. In the following chapter, we have directly integrated a stilbene-based organic dye moiety into a cobaloxime core-periphery via a distinct axial pyridine linkage. This strategy allowed us to develop a photosensitizer-catalyst hybrid structure with the same molecular framework. The structural and optical studies have exhibited an intense electronic interaction between the cobaloxime core and the organic photosensitizer. The cobaloxime was active for H₂ production even in the presence of water as the proton source. Here, we have developed a simple airtight system connected with an online H₂ detector to investigate the photocatalytic activity by this hybrid complex. This photosensitizer-catalyst dyad present in the experimental setup continuously produced H₂ once it was exposed to natural sunlight. This photocatalytic H₂ production by the hybrid complex was observed in aqueous/organic mixture media in the presence of a sacrificial electron donor under complete aerobic conditions.¹⁵ Thus, this photocatalysis measurement system, along with the photosensitizer-catalyst dyad, provides valuable insight for the development of next-generation photocatalytic H₂ production devices.

In the final chapter, we have constructed an artificial photocatalytic assembly by directly ligating a molecular cobaloxime motif to the plasmonic gold nanomaterial. Here, our goal was to explore the photosensitizing property of gold plasmons for photocatalytic water splitting, which is reckoned as the key step in the pursuit of a solar-driven renewable energy economy. Here, we have fabricated a covalently linked gold nanoprism-cobalt molecular catalyst construct that stimulated efficient photo-electrocatalytic water oxidation reaction. This assembly generated significant photocurrent ($\sim 50 \mu\text{A}/\text{cm}^2$) in neutral aqueous conditions with a minimal onset overpotential ($\sim 250 \text{ mV}$). This dyad imitates the light-harvesting properties of natural photosystem-II by producing 0.66 μmoles of O₂ and 1.32 μmoles of H₂ simultaneously per hour (0.8% photon to chemical fuel conversion efficiency) following complete water splitting under the light with $\sim 0.075\text{--}0.01\%$ incident photon to photocurrent conversion efficiency (IPCE). The presence of the plasmonic gold nanomaterial in this assembly instigates broad-band absorbance spanning from the visible to NIR region (400–1200 nm), covering the majority of the natural solar spectrum.¹⁶ This dyad construct also exhibited appreciable durability under photo electrocatalytic conditions to demonstrate its prospective applications in alternative energy fields.

In conclusion, we have been able to mimic the key features of hydrogenase enzyme successfully by strategically positioning different naturally occurring functionalities (vitamin and nuclear bases) around a cobaloxime core as OCS, which resulted in an improved H₂ production reactivity in an aqueous solution under both electro and photocatalytic conditions. Moreover, the appended core with non-amino acid-based basic functionalities not only increased the water solubility of the complexes it also expands the possibility of utilizing these catalysts under acidic conditions (pH < 5.0), which was lacking for the hydrogenase enzyme. The designed catalyst can be employed in the ideal system, as it can work under the natural sunlight at neutral aqueous conditions and is tolerant to the presence of O₂ in the environment. Later, we have developed artificial photocatalytic assemblies with direct ligation of the cobalt- based molecular catalysts to the organic or plasmonic photosensitizer motif. These photo- catalytic dyads were active from visible to NIR region for water splitting, which is a unique example of combining the molecular catalyst with the gold nano-prism chromophore. Additionally, the plasmonic-molecular catalyst assembly provides significant durability over a long period to highlight their potential for practical applications. This unique catalyst design can be extended for other small molecule activation involving proton and electron exchange processes.

Title: Bio-inspired catalyst design strategies for activating dormant transition metal cores for hydrogen evolution
Researcher: Khandelwal, Shikha
Supervisor: Dutta, Arnab
Year: 2021
Keyword's: Catalyst, Hydrogen Evolution, Dormant Transition, Spectroelectrochemistry
Call No.: 540 KHA
Acc. No.: T00720

Abstract: The global energy demand is skyrocketing with every passing day with urbanization and the progress of human civilization. A significant portion of current energy requirements is fulfilled by fossil fuels, primarily including coal, natural gas, and oil. The continuous usage of fossil fuels in the near future is under scrutiny for two reasons: (i) they are diminishing at an alarming rate, and (ii) during the energy extraction process, they produce an enormous amount of CO₂. CO₂ is a greenhouse gas and has a devastating effect on the surrounding environment. In the present circumstances, renewable energy resources have emerged as one of the best and abundant alternatives to fossil fuels. Taking inspiration from the natural photosynthesis process, scientists have attempted to imitate the photo to chemical energy transformation via Artificial Photosynthesis. In this biomimetic model, researchers have ventured to store energetically dilute sunlight into energy-rich chemical bonds. The hydrogen molecule is the simplest chemical vector one can imagine for this process as it requires only two electrons and two protons for the reversible conversion to H₂. Hence, renewable energy can be efficiently stored into the H-H bond and later extracted in the form of electricity using the proton exchange membrane (PEM) fuel cell. Cost-effective and energy-efficient H₂ production is one of the most critical steps for successful utilization of renewable energy resources. Proton to hydrogen conversion reaction is inefficient in the absence of a catalyst. Platinum-based materials are the best available catalyst for hydrogen production to date, but the low natural abundance and high cost of Pt have restricted its large-scale industrial implication. On the other hand, hydrogenase enzyme transduces energy in biology by interconverting proton and electron to hydrogen at an excellent rate and energy-efficiency under ambient condition using naturally abundant first-row transition metals. However, the enzymes' direct usage is not practical as they are evolved to be operational at physiological conditions, rather than the harsh fuel cell conditions. Enzyme simply degrades under highly acidic conditions. In addition, the purification of the enzyme is an expensive and tedious process, which also limits its practical implementations. Researchers have aimed to replicate the active site of the hydrogenase enzyme, containing Ni and Fe, but these structural mimics are not found to be catalytically active. Another class of catalysts has evolved over the past few years that are known as the functional mimics. Here, this set of model complexes showcases the essential features of the enzyme with appropriately patterned functional groups. The famous DuBois complex [Ni(N₂P₂)₂] and traditional Co-diimine–dioxime complexes are the prime examples of this category. [Ni(N₂P₂)₂] displayed an excellent catalytic rate for H₂ production in organic solvents. Their excellent catalytic activity was even translated into aqueous conditions with the improvised addition of natural amino acids in the periphery of the catalyst core. Such peripheral groups are called the outer coordination sphere (OCS)

that imitates the surrounding protein atmosphere observed in the enzymes. Despite having remarkable catalytic performance, these DuBois catalysts are misfit for a large-scale usage owing to their acute oxygen sensitivity. On the other hand, Co-diimine–dioxime complexes are known to be oxygen tolerant but exhibited only a moderate H₂ production rate with appreciable overpotential values. The introduction of artificial OCS features enhances the catalytic H₂ production rate by these cobalt complexes without any significant improvement in the overpotential requirement. Hence, there is a scope of developing a new genre of metal complex cores illustrating high catalytic rate and low overpotential for H₂ evolution reaction (HER). In this thesis, we have employed otherwise poorly active or inactive metal complexes as the central core and introduced several enzymatic hallmarks such as proton relay, redox partner, steric hindrance, and electronic effects to activate those dormant metal cores towards remarkable electrocatalytic HER. Each chapter in this thesis unravels the specific influence exerted by diverse catalyst design strategies.

In the first chapter, we have initiated our catalyst design around a Co-salen like core and decorated natural amino acids having protic functionalities like carboxylic acid and phenolic –OH groups on the periphery. The inclusion of such basic groups activates an otherwise inactive Co-salen like core for electrocatalytic hydrogen evolution in the aqueous medium. Co-salen complex with the non-carboxylate version of natural amino acids was also synthesized to investigate the role of each protic moiety (i. e., carboxylic acid, and phenolic –OH group) during the catalysis. The Co-salen complexes with peripheral carboxylic acid exhibited a unique pH switchable catalytic activity triggered around pH 4, which matched with the pKa (~ 4) of the carboxylic acid group. Below pH 4, –COOH act as a proton relay in its protonated form to showcase an active catalyst. On the contrary, the same functionality gets deprotonated to originate- COO⁻ above pH 4 and coordinates with the metal core at the prospective protonation site. Hence, no catalysis was observed at conditions pH > 4. The complementary 2D NMR studies suggested that the possible H-bonding network evolved from these basic functionalities in aqueous media controls the catalysis. Such a pH-regulated labile coordination geometry that switches between primary and secondary coordination sphere is the key for inducing catalytic HER activity into Co-salen like core. This approach can be extended further to other small molecule activation reaction where the proton transfer step is involved. Although these complexes displayed low catalytic rate (170-270 s⁻¹) and high overpotential (600-840 mV) for H₂ production activity, and an upgraded catalyst design was our next goal.

In the next stage, we have introduced a redox-active partner to the metal core via the primary coordination sphere. In metalloproteins, the redox partners play a vital role in facilitating the electron transfer and correlated catalytic process. We have synthesized Co-phenylenediamine (Co-PDA) complex where the *o*- phenylenediamine motif was blended in the metal core. Here, our primary goal was to exploit the π - interactive properties of the phenylene moiety. Electrochemical studies of Co-PDA displayed no catalytic activity in organic medium. Interestingly, the same complex sprang into life with moderate electrocatalytic H₂ production response in the aqueous medium. This complex was mostly active in the near-neutral pH range before losing its activity with increasing acidity. This complex became inactive below pH 3. The inclusion of an electron-donating axial ligand in the form of an unsubstituted pyridine improved the catalytic response of the Co-PDA core. The Co-PDA-pyridine [Co-PDA-Py] complex exhibited positive HER activity even in organic media in the

presence of organic acid (Trifluoroacetic acid/TFA). The catalytic activity in water improved by ~ 4 times for the Co-PDA cluster following the addition of pyridine as an axial ligand. These results indicated that Co-PDA and Co-PDA-Py represent an improved genre of HER electrocatalysts compared to the parent Co-*bis*-(dimethylglyoxime) [Co(dm_g)₂] complex in both organic and aqueous solutions. This study highlighted the importance of the role of hydrogen-bonded oxime moiety during catalysis. Curiously, the Co-PDA complexes established that the presence of only one such hydrogen-bonded oxime network is sufficient for the HER catalysis in contrast to the well-studied Co(dm_g)₂ core that contains two sets of such H-bonded oxime moieties. This unique coordination geometry design strategy accentuates the importance of both redox-partner and proton relay during the formation of HER active electrocatalysts. Despite the significant improvement in the catalytic rate for the Co-PDA-based complexes, the overpotential requirement altered only slightly. Thus, further modification of the ligand design can be implemented to originate a fast and efficient HER catalyst.

In chapter 3, we were focussed on incorporating another hallmark of the metalloenzyme architecture, the *entatic state*, into the catalyst design. The protein scaffold of metalloenzymes distorts the central metal ion to stabilize it in an otherwise uncommon coordination geometry (known as the entatic state) to fine-tune its redox properties. Here, we have thrust steric hindrance around a Co-*bis*-(dimethylglyoxime) [Co(dm_g)₂]-derived metal core by strategically positioning bulky phenyl groups in the place of hydrogen-bonded oxime network on one side of the complex. This new catalyst is designated as Co-(monoxime)-aniline motif. We have also altered the *para*-substituents on the phenyl groups to explore the electronic effect exerted by -OCH₃ and -CH₃ groups on the catalytic hydrogen production by the otherwise identical core. We have observed that the Co-(monoxime)-aniline and its derivatives demonstrated catalytic H₂ production in DMF in the presence of TFA. These complexes showed impressive acid-stability compared to the parent [Co(dm_g)₂] complexes, which were HER-inactive and unstable under analogous conditions. Our study has revealed that the introduction of bulky phenyl rings caused distortion around the cobalt center that triggers HER activity. However, the intramolecular π - π interaction between the phenyl rings locks the flexibility around the hydrogen-bonded oximes to aid the stability of the hydrogen-bonded nexus, even in strongly acidic conditions. The detailed electrochemical analysis suggested that the presence of a strongly electron-donating (-OCH₃) stationed in the *para*-position of the phenyl motif can enhance the rate of HER catalysis by ~ 5 times compared to the unsubstituted complex (50 s⁻¹) containing a similar core.

In the final chapter, we have probed the effect of the entatic state-inspired catalyst design on the energy efficiency of the H₂ production activity in aqueous conditions. For this purpose, we have studied Co-(monoxime)-anisidine [the -OCH₃ group containing Co-(monoxime)-aniline derivative] due to its impressive HER activity in organic media and enhanced aqueous solubility compared to the other derivatives. The Co-(monoxime)-anisidine produced H₂ in aqueous conditions at a broad pH range (pH 2- 7). Interestingly, the catalytic HER rate of this complex improves slightly as the solution changed from neutral (pH 7.0) to acidic (pH \sim 2.0). This observation is in contrast with the parent Co-*bis*-(dimethylglyoxime) [Co(dm_g)₂]-based complexes, which exhibit the maximum

catalytic rate in near- neutral pH before fading out in acidic conditions. This stark difference in the pH-effect on catalytic response is attributed to the presence of the intermolecular π - π interaction between the adjacent anisidine motifs. The stability of the H-bonded oxime motif even in the acidic condition was further corroborated with the complementary ^1H NMR experiment. The influence of the phenyl-phenyl interaction-induced entatic state on the catalysis was also evident from the trend of the overpotential requirement of Co- (monoxime)-anisidine at all pH conditions. This complex displayed an overpotential requirement of ~ 240 - 290 mV in pH 2.0-7.0, which was significantly lower compared to the $[\text{Co}(\text{dmg})_2]$ -based complexes (overpotential value varies ~ 500 mV). Hence, this study establishes that the inclusion of enzyme-inspired entatic state features can improve both the HER catalytic rate and energy efficiency of synthetic metal cores.

In conclusion, we have probed different routes to activate the dormant synthetic metal cores towards hydrogen evolution reaction. We have vividly followed the blueprint of enzyme structure and specifically included features like proton-relay, redox-partner, and entatic state to regulate the redox potential, catalytic rate, and overpotential requirement of the resultant complexes. Hence, these results indicate that the protein-based outer coordination sphere features of metalloenzymes should be imitated via rational ligand design. Such an enzyme-inspired catalyst design will ensure the inclusion of an essential but minimal feature in the form of an artificial OCS feature in bio-mimetic complexes for exhibiting H_2 production catalysis. This smart catalyst design strategy can be extended for developing complexes for other small molecule activating reactions, especially involving multiple proton and electron exchange steps.

Title: Membrane-targeting methacrylamide-based antibiotic polymers to combat drug-resistant bacteria: synthesis, characterization, and investigation of biological properties

Researcher: Tyagi, Anju

Supervisor: Mishra, Abhijit

Year: 2021

Keyword's: Antibiotic Resistant, Synthetic Polymers, Antibiotic Polymers, Hydrophobicity

Call No.: 615.329 TYA

Acc. No.: T00939

Abstract: Globally, multidrug-resistant pathogens are growing at an unprecedented pace jeopardizing the efficacy of most conventional antibiotics. In the quest for the development of new drugs, host-defense antimicrobial peptides (AMPs) have received tremendous attention due to their remarkable properties in the biomedical field. However, their chemical and pharmacokinetic instability, as well as the high manufacturing cost are stymieing the use of AMPs. Synthetic mimics of antimicrobial peptides (SMAMPs) as antimicrobial polymers engineered to replicate the prominent structural traits of host defense peptides are a new class of emerging materials in the fight against superbugs. It is well known that AMPs require an optimal balance of cationicity and hydrophobicity for targeting bacterial membranes.

The primary aim of this study is to develop compounds that meet the following design objectives.

- To investigate the role of hydrophobic aromatic benzyl units in methacrylamide-based polymers by optimizing an amphiphilic balance (an average number of cationic and hydrophobic residues linked in a polymer chain) to obtain biocompatible antibiotic materials.
- To develop an in-depth understanding of the mechanism by which these polymers perform their antimicrobial activity.
- Resistance study to ensure that the polymers remain useful for an extended time.

A series of water-soluble cationic antibiotic polymers with varying hydrophobicity (from 0.10 to 0.44) and degree of polymerization (from 10 to 66) were designed and synthesized to define an extent to which selective toxicity could be optimized for producing non-toxic bio-compatible polymers by finely tuning an amphiphilic balance using aminopropyl- methacrylamide (AMPA) and benzyl methacrylamide (BMA).

Various biological assays are performed to gain a thorough understanding of their mechanism, which is crucial in determining the structure-activity relationship (SAR). All synthesized polymers are characterized using proton NMR (Nuclear Magnetic Resonance) spectroscopy. Antibacterial efficacy is examined against gram-positive *S. aureus* and gram-negative *E. coli* by determining MIC (minimum inhibitory concentration) values which is the minimum polymer concentration that completely inhibits the growth of bacteria. Bactericidal kinetics was determined to investigate the effect of the bacterial growth phase on polymer activity by sub-culturing the bacteria from early and late exponential phases. Live/dead bacterial viability assay, liposome dye leakage assay, confocal and scanning electron microscopy (SEM) studies are carried out to find the antimicrobial mechanism of the polymers. Hemolysis and cytotoxicity assays using human juvenile fibroblast cells are performed

to examine their biocompatibility. A serial passage study is done by passaging *E. coli* and *S. aureus* at a sub-inhibitory concentration of polymers to find out any development of resistance. Hydrophobicity and average molecular weight play a significant role in regulating the activity, selectivity, and biocompatibility of polymers. All the synthesized polymers are active against both the examined bacteria with MIC values ranging from 2.5 to 25 μM against *E. coli* and 3.8 to 28 μM against *S. aureus*. These polymers have a remarkable bactericidal property and kill bacterial cells primarily by disrupting the cytoplasmic membrane which supports the generally accepted cationic AMPs mechanism of action. Moreover, the polymers activity is independent of the growth stages of bacteria, and the mechanism may not depend on bacterial metabolic activity specific to growth. No detectable resistance in bacteria is observed for these polymers. These results are significant in the current scenario, where multidrug-resistant pathogens endanger the efficacy of conventional antibiotics.

These results show that polymers with a ≈ 20 -mole percentage of a hydrophobic group and an average molecular weight of ≈ 5 kDa are suitable to act as a non-toxic polymeric material that shows exceptionally high activity and selectivity with MICs comparable to naturally found peptides. Feasible synthesis, along with high antibacterial efficacy, and selectivity make these polymers a potential pharmaceutical candidate for the future development of inexpensive biocompatible membrane-active antimicrobial polymeric materials.

Title: Preparation of bulk and thin-film conducting metal oxides electrodes and their electrochemical properties
Researcher: Vyas, Divya
Supervisor: Sharma, Sudhanshu
Year: 2021
Keyword's: Metal Oxide Electrodes, LSCO, Electrocatalysts, Electrochemical
Call No.: 530.4175 VYA
Acc. No.: T00940

Abstract: Electrocatalysis is a science that provides a connection between the rates of chemical reactions and the bulk and surface properties of the electrodes on which these reactions proceed. A range of metal oxides and perovskites have been explored as electrocatalysts by many researchers for sustainable energy source reactions like OER (oxygen evolution reaction), ORR (oxygen reduction reaction) and FOR (formate oxidation reaction) etc. Preparing a complex oxide by forming a solid solution between two compatible cations in an optimized ratio having an anion lattice is a popular approach to designing a desired electrocatalyst. Different synthesis methods like conventional solid-state method, coprecipitation, hydrothermal, sol-Gel, solution combustion etc offer different significance and advantages over others. Through the alteration of oxygen vacancies and the related crystal structure as well as surface properties, electrocatalytic activity can be adjusted.

In our work, we have observed that not only a single parameter but a combination of processing techniques, and the physical appearances of the material affect its catalytic activity. In the first chapter, we have studied a well-known system of antimony doped tin oxide (ATO). The low electronic conductivity of metal oxides limits their electrocatalytic activity. Through an appropriate amount of antimony doping, ATO achieves higher conductivity than tin oxide. ATO, having good stability and low cost, has been extensively studied. We reported, for the first time, its synthesis by solution combustion method. The prepared material has a very high surface area with a mesoporous surface. The synthesis method is rapid and gives particles of sizes 9 to 13 nm. The material has a specific surface area of 84 m²/g as estimated by the Brunauer-Emmett-Teller (BET) model. The comparative study of Sn_{1-x}Sb_xO₂ (0.01 ≤ x ≤ 0.05) indicates that the composition of Sn_{0.95}Sb_{0.05}O₂ has the lowest resistance with the highest carrier concentration. Electrochemical properties of the material are analyzed by cyclic voltammetry in both acidic and neutral media showing the Sn_{0.95}Sb_{0.05}O₂ with high electron transfer properties.

Perovskites are better catalysts for many reasons. Their ABO₃ arrangements offer simultaneous tuning of A-site and B-site cations to enhance the conductivity as well as the creation of oxygen vacancies. Other methods like quenching, post-annealing and thermal reduction have been explored too to tune its properties. Platinum-supported lanthanum strontium cobalt oxide (Pt/LSCO) has been explored by Anuj Bisht et al, for its OER activity. In our second chapter, we have extended the work with the same system by tuning its OER activity simply by heat treatment. By optimizing the temperature, we were able to increase its OER activity. The detailed surface analysis by XPS shows that synchronization between different oxidation states of platinum on the catalyst surface is contributing to its enhanced activity. Later, we extended our work to prepare the thin film of the

same perovskite system of LSCO. In our third chapter, by a combination of sol-gel and spin coating, we prepared a homogenous LSCO thin film on FTO (fluorine-doped tin oxide) substrate. Interestingly to explore the further effect of electrolytes, we studied the stability and activity of LSCO/FTO for OER in different mediums. Post catalysis analysis by XPS confirms degradation of surface in KNO_3 medium. However, the electrode remains stable for a long time in phosphate buffer solution (PBS). The enrichment of Co (II) on the surface confirms the involvement of cobalt as a reaction centre. As we confirmed the stability of LSCO/FTO in PBS, we used this electrode for FOR (Formate oxidation reaction) in our fourth chapter. Formic acid fuel cells are a propitious candidate for energy conversion. Formate salts are less toxic and less volatile than formic acid. We have used sodium formate as a precursor of formate ion in our work. LSCO/FTO, being a noble metal-free catalyst, offers an economic option. The electrochemical measurements confirm its activity and stability. It is a unique method to produce oxygen, hydrogen and carbon dioxide simultaneously.

Title: Quinoline-based small molecules as ATM kinase inhibitors: design, synthesis and applications
Researcher: Srimadhavi R.
Supervisor: Kirubakaran, Sivapriya
Year: 2021
Keyword's: Cancer, Protein Kinases, Quinoline, PIKK Family Proteins
Call No.: 572.6 SRI
Acc. No.: T00946

Abstract: Resistance towards DNA damaging agents like radiation and certain chemotherapeutics is of significant concern while treating cancer. This resistance is developed due to the active kinases of the DNA Damage and Response (DDR) pathway. These kinases have the ability to repair any damage imposed on the DNA due to which treatments which rely solely upon damaging the DNA face resistance. Therefore, we have designed, synthesized and characterized quinoline-based small molecules for studying their potential to be anticancer agents. The first part of the thesis focuses on the design, synthesis, characterization, and biological evaluation of the molecules against various cancer cell lines. Western blotting was performed to confirm the inhibition of the ATM kinase. The second part of the thesis focuses on *in silico* and Single Crystal X-ray crystallography studies for some of the synthesized compounds.

We aimed to study the key mediator of the DDR pathway, the ATM kinase, which is responsible for the regulation of the cell cycle, apoptosis, chromatin relaxation, and DNA double-strand break (DSB) repair. On inhibiting the kinase activity of ATM, the double-strand break repair process is hindered leading to the accumulation of DNA DSBs and finally bringing about cell death owing to genomic instability. Also, it is established that inhibition of ATM kinase radiosensitized cancer cells. Though the importance of ATM inhibition is well established, there are no FDA approved small molecule inhibitors for the same. Most of the existing inhibitors fail in the clinical trials either due to their high lipophilicity or their tendency to show off-target activity. Therefore, the primary objective was to design inhibitors that are selective towards the ATM kinase. Hence, we designed quinoline-based inhibitors for inhibiting ATM based on the crystallographic evidence that the quinoline nitrogen binds to the hinge region of PI3K- γ (a close homolog of ATM kinase).

The designed molecules were synthesized and characterized. Cell growth inhibition studies (performing CTG assay) for the synthesized molecules against various cancer cell lines were performed. Three of the molecules showed significant GI₅₀ (μ M) values against these cell lines. Cell viability studies were performed against HEK-293T cells and were found to be 3-fold less toxic. Also, it was observed that MDA-MB-468 (PTEN negative) cells were more sensitive towards our compounds in comparison with MDA-MB-231 (PTEN wt), unlike the existing ATM inhibitor KU60019. Furthermore, we were able to confirm the down-regulation of ATM by Western-Blotting. In conclusion, these experiments will lay the groundwork for the evolution of potent and selective ATM inhibitors for the radio- and chemo-sensitization of cancer cells.

The quinoline-3-carboxamides synthesized were further optimized and modified in positions 4 and 6 of the quinoline ring. These modifications were based on the article published in 2016 by Degorce et al. The Cl in position 4 and Br in position 6 were substituted with secondary, tertiary amines and pyridine, respectively. A molecule similar to 7 was synthesized by Degorce and the team, the only variation being the amide in position 3 was kept intact as a primary amide (-CONH₂). Surprisingly, when they converted the primary amide to a secondary amide (a simple methyl substitution) rendered the resulting molecule inefficient. Therefore, we aimed at synthesizing variants of molecule 7 and check the cytotoxicity. The cytotoxicity studies for the molecules are in progress.

Finally, we have performed *in silico* and structural characterization of selected molecules of scaffold 6. The molecules were docked against all the three DDR kinases, mTOR and PI3K γ . The synthesized molecules showed high selectivity towards ATM kinase even though the mentioned proteins shared a significant sequence similarity. Molecular dynamics simulations were performed for one of the inhibitors against all the enzymes to establish the stability of the interactions involved. ADME properties of the inhibitors were predicted using the QikProp manual in Maestro. Finally, three molecules were crystallized, and their structures were solved. Hirshfeld surface analysis and 2D fingerprint plots were generated to understand the various interactions involved in stabilizing the supramolecular arrangement of the molecules. DFT calculations were performed in order to analyze the intramolecular charge transfer property of the molecules.

To summarize, this thesis focuses on the design, synthesis, characterization, and biological evaluation of quinoline-3-carboxamides as effective inhibitors of ATM kinase. The results obtained in this study will pave the way for developing potential and selective ATM kinase inhibitors as cancer therapeutics.

Title: Synthesis and photoinduced chromic studies of a new class of alkylated unsaturated carbonyl compounds and their derivatives
Researcher: Duppalapudi, Venkata Mani Padmaja
Supervisor: Appayee, Chandrakumar
Year: 2021
Keyword's: Morita-Baylis-Hillman, Photoinduced chromic studies, Photoinduced Fluorescent Organic, UV-visible, Reactive Oxygen Species
Call No.: 547 DUP
Acc. No.: T00949

Abstract: The invention of a new synthetic methodology for the regioselective carbon-carbon bond formation has been one of the most attractive research in synthetic organic chemistry. The Morita–Baylis–Hillman (MBH) reaction plays a major role in creating a highly regioselective carbon-carbon bonds. Due to the tremendous applications in the synthesis of bioactive natural products, the MBH reaction has gained more attention in the past few decades. Although The MBH reaction of unsubstituted conjugated alkenes were well studied, substituted conjugated alkenes are relatively less explored. Moreover, the MBH reaction of $\alpha,\beta,\gamma,\delta$ -unsaturated compounds was found to be quite challenging due to the formation of a mixture of products with low yield under harsh reaction conditions. Particularly, the functionalization of $\alpha,\beta,\gamma,\delta$ -unsaturated aldehydes using the MBH reaction were not reported in the literature. On the other hand, several organic compounds were identified with photochromic property. Azobenzenes, spiropyrans, spirooxazines, and naphthopyrans, dithienylethenes, fulgides, and donor-acceptor Stenhouse adducts are some of the notable photochromic organic compounds so far reported in the literature. Due to the tremendous application of the photochromic organic compounds in molecular switches, memories, actuators, sunglass, rewritable papers, and optical materials, there is an increasing demand for the development of novel photochromic compounds. Although there are several photochromic compounds reported in the past few centuries, they can be classified into very few types based on the chemical reactions that occur during the photochromic process. Among them, *cis-trans* photoisomerization and cyclization reaction are the major types of chemical reactions that take place during the photochemical process. This thesis contributes to the development of novel methodologies for the α -functionalization of $\alpha,\beta,\gamma,\delta$ -unsaturated aldehydes *via* the MBH-type reaction pathway. This thesis also explores the photoinduced chromic properties of the novel alkylated unsaturated aldehydes and their derivatives.

In part-A section-2, a new methodology for the α -alkylation of $\alpha,\beta,\gamma,\delta$ -unsaturated aldehydes *via* MBH-type reaction pathway under a mild reaction conditions is described. Several $\alpha,\beta,\gamma,\delta$ -unsaturated aldehydes with aryl and alkyl substitutions have been successfully functionalized using simple pyrrolidine as the organic catalyst. The SN-type electrophiles such as Michler's hydrol, xanthidrol and thioxanthidrol, and acridinium ion have been utilized as the electrophilic reagents. Based on the reaction results, a reaction mechanism is proposed for the regioselective α -alkylation of $\alpha,\beta,\gamma,\delta$ -unsaturated aldehydes. In part-A section-3, a new methodology for the asymmetric MBH-type reaction of $\alpha,\beta,\gamma,\delta$ -unsaturated aldehydes with glyoxal derivatives is disclosed. Further we have

investigated the reaction optimization with several catalysts, acids, additives, and solvents to achieve the chiral MBH-type product in 39% yield and 61% *ee*. Using this asymmetric synthetic methodology, a bioactive natural product, (*R*)-avellaneol, an antibiotic metabolite of *Hypocrea avellanea* is achieved in one steps from the commercially available starting materials and catalyst. In part-B section-2, we described a serendipitous photoinduced chromism in the MBH-type products obtained from the reaction of $\alpha,\beta,\gamma,\delta$ -unsaturated aldehydes with Michler's hydrol. Upon UV irradiation, these new class of photoinduced chromic organic compounds exhibit intense visible color and show the new absorption band at around 650 nm in the UV-visible absorption spectra. The photoswitching property of one of these compounds is also demonstrated in solution (methanol) and in solid state (silica). This photoinduced chromism due to the hydride removal is proved by the extensive NMR studies and related chemical reactions. An application of these photochromic compounds for the detection of nitric oxide (NO) gas and cellular reactive oxygen species (ROS) is also showcased. In part-B section-3, we explored the photoinduced chromic fluorescent properties of the MBH-type products obtained from the reaction of $\alpha,\beta,\gamma,\delta$ -unsaturated aldehydes with xanthidol and thioxanthidol. After the UV irradiation one of these MBH-type products (derived from xanthidol), a benzo[*k*]xanthene derivative, which is responsible for the fluorescence emission, was isolated and characterized. In part-B section-4, we described the asymmetric synthesis of α,γ -dialkylated α,β -unsaturated aldehydes starting from α,β -unsaturated aldehydes and SN-type electrophiles. The photoinduced chromic properties of these chiral molecules is demonstrated through their UV-visible absorption spectra and their circular dichroism spectra.

Title: Developing methods for controlled spatial ordering of anisotropic gold nanoparticles for enhanced spectroscopy at the nanogaps
Researcher: Kar, Ashish
Supervisor: Khatua, Saumyakanti
Year: 2021
Keyword's: Plasmonic Nanoparticles, Gold Nanorods, Anisotropic Nanoparticles, Polyelectrolyte
Call No.: 540 KAR
Acc. No.: T00954

Abstract: Single-molecule imaging and spectroscopy has emerged as a powerful tool to gain molecular- level insights to various processes, such as subwavelength arrangement of cellular components, DNA conformational changes and dynamics of enzyme and proteins. Single-molecule techniques provides the advantage of studying molecules individually thereby eliminating the possibility of loss of information from ensemble averaging. Typically, fluorescence signal is used for single molecule spectroscopy as it provides high contrast, low background and fast detection. This technique, however, can only access species with high emission rates due to the weak light-matter interaction limited by diffraction of light. However, there are numerous strongly absorbing molecules including biologically relevant proteins and metal complexes such as hemes, which fluoresce only weakly. Thus, enhancement of the emission rates of weakly emitting species can extend the reach of single-molecule studies to gain various insightful information.

Gold nanorods have been shown to enhance the rate of fluorescence of weak emitters. This arises from the nanoparticles' capability to confine incident electromagnetic fields to a tiny area near their surface thus enabling light-matter interaction beyond the diffraction limit. These optical properties are drastically altered when two nanorods are placed in close proximity, due to coupling of their surface plasmon resonances. The field enhancement at the gap region of end-to-end coupled nanorods is enormously larger compared to isolated nanorods, commonly referred to as 'hot-spots', making them useful in enhanced spectroscopies.

The strength of the field at the hot spots in the coupled structures is also determined by the orientation and spacing between the individual nanostructures. The realization of these collective properties thus requires synthetic strategies to assemble such anisotropic nanoparticles with tailored configuration in terms of orientational preference, gap dimension and degree of assembly. This underpins the work carried out in this thesis to develop a versatile wet-chemical synthetic method to assemble anisotropic gold nanoparticles with high tip- specificity, control the degree of assembly formation, and utilize them as substrates for single- molecule fluorescence enhancement. And finally, a light driven technique is developed to tune the dimensions of individual nanoparticles immobilised on a substrate. This could provide avenues for in-situ control of the gap dimension in assembled nanostructures. Brief overview of the chapters that constitute the thesis are given below.

Chapter 1 provides an introduction to the optical properties of plasmonic gold nanoparticles and the various physical processes accompanying excitation and decay of surface plasmon resonance in such nanoparticles. Then the origin of optical properties in coupled nanostructures is described followed by discussion of the available methods for synthesizing tip-specific assemblies of gold nanorods.

In Chapter 2 we introduce a new method to synthesize end-to-end dimers of gold nanorods and stabilize them in acetonitrile medium. This is done by coating the nanorods with anionic polyelectrolyte (PE) and assembling the nanorods by a dithiol linker. The pH dependent configuration change of the polyelectrolyte chains was then used to quench the aggregation at the dimer stage by addition of a strong base, DABCO. This strategy was next utilised to create stable long-range end-to-end ordering of thousands of gold nanorods by tuning the surface charge by a comparatively weaker base, Et3N during the assembly formation.

In Chapter 3, the critical role of surface charge in triggering the assembly formation by dithiol ligands was then assessed. We studied the effect of varying surface charge of polyelectrolyte coated gold nanorods and establish it as the controlling parameter for linker driven assembly formation of anisotropic gold nanoparticles. By systematically modulating the nanorods' surface charge with different acids, we show that tip-specific assemblies are obtained reproducibly in a zeta-potential range of -10 mV to -17 mV. Uncontrolled aggregates form below this range and above this, no aggregation occurs. Further we show the formation of end-to-end assemblies of gold nanobipyramids, which are first of its kind showing the effectiveness and broad applicability of the polyelectrolyte coating strategy.

Next in Chapter 4, we move onto utilise the synthesized tip-specific assemblies of gold nanorods to enhance emission of a weak emitter. We describe the results and methodology of single molecule fluorescence enhancement experiment and the details of setting up a home-built confocal microscope. Here correlation between electron and optical microscopy was used to identify exact configuration of the assembly used. We show that the long-range assemblies of gold nanorods contain strong hot-spots that enhances the fluorescence of single crystal violet dye by 104 fold which is an order of magnitude larger than single nanorods and is comparable to the maximum enhancement factors obtained by lithographically made nano antennas.

Finally, in Chapter 5 we focus on light-driven tuning of dimensions of individual isotropic gold nanotriangles deposited on ITO substrate. We studied the oxidative dissolution of gold in presence of NaCl and applied anodic potential under linearly and circularly polarized laser excitation of 594 nm. The localization of the reactivity was tracked from the change in shape of the nanotriangle caused by the etching. Correlated SEM imaging was used to identify the same nanotriangle before and after the reaction. Anisotropic etching was observed in case of linear photoexcitation with etching occurring more predominantly in one of the vertex aligned with the polarization axis. Whereas, in case of circularly polarised excitation, uniform etching from all directions is observed with the formation of sphere like morphology after etching. Generation of local chemical reactive

sites on nanoparticles by polarization-controlled photoexcitation could open up possibilities to obtain in-situ control over the gap-dimensions in end-to-end assemblies of nanorods.

Title: Towards development of plasmonic antenna-reactor based catalytic construct for photo-electrochemical solar to fuel conversion

Researcher: Paital, Diptiranjana

Supervisor: Khatua, Saumyakanti

Year: 2022

Keyword's: Gold Nanoparticles-AuNP, Gold Nanorods-AuNR, Gold Nanoprism-AuTNP, Photo electrochemical Solar

Call No.: 660.2832 PAI

Acc. No.: T01042

Abstract: The rapid increase in the global energy demand and major reliance on fossil fuel burning put us in a difficult situation of energy crisis and global warming. Therefore, most of the countries are spending billions from their economy in searching for an alternate energy source. Among various alternate resources sun light is highly recognized as it is replenishable and available throughout the year. Thus, photocatalysis is considered as an appealing technique for harvesting solar energy for long-term solar fuel production. It has been noticed that, semiconductor based photocatalytic systems are mainly explored in last few years, however the efficiency of many of these materials are limited to the UV-Vis range of solar radiations and low absorption cross-sections. It is noteworthy to mention that solar light consist of large fraction of near infrared (NIR) radiation, whereas UV radiation consists of only 4% of overall solar radiation. In this context, plasmonic gold nanostructures (AuNS) have garnered significant attention due to its unique optical property called as Surface Plasmon Resonance (SPR); the collective oscillation of the conduction electron under incident light. This SPR is localized and can be tuned to cover entire Vis-NIR region depending upon their size, shape and refractive index of surroundings.

Under Light excitation, the excited plasmon decays non-radiatively into energetic charge carries known as "hot" electron and hole. These hot carriers have the tendency to induce and/or accelerate many uphill photocatalytic reactions. However, the short lifetime of these carriers restricts their efficient extraction and utilization, as a result low photocatalytic performance. In an alternate approach, placing a co-catalyst on the plasmonic nanostructure enhances the life time of these hot carriers by providing an elongated recombination route, and hence the better photocatalytic activity. Furthermore, few recent studies demonstrated that the photocatalytic efficiency of this system can be significantly enhanced by tuning appropriate size, shape and surface morphology. Understanding the nature of the hot carriers and their extraction efficiency by means of these geometrical parameters underpins the basic footprint for designing plasmonic antenna-reactor catalyst. In addition, the energy and relative location of the hot carriers also play a major role in activating various catalytic processes, and is dependent upon the excitation wavelength. For example, d-band hot holes and sp-band hot electrons are formed near the Fermi level at shorter wavelength excitation, whereas both hot hole and hot electrons are formed in the sp-band below and above the Fermi level at excitation of longer wavelengths. Thus, due to diverse location of hot

holes in the both the bands, they exhibit different catalytic properties. However the role of shape, size and surface morphology in enhancing the catalytic activity of the hot hole are often ignored and are limited only to few systems in the domain of

hot electrons. Thus, there is a need of understanding the role of certain unexplored parameters such as surface porosity and presence of active co-catalyst in the context of hot holes. This research gap motivates us to design projects to study the hot hole dynamics in metal-metal, metal-porous metal and metal-metal oxide core-shell catalytic systems.

In Chapter 1, we established a new method for preparing various complex nanoparticle geometry, such as nano dogbone, arrowhead and dumbbells shape of gold nanorods. This has been done by overgrowth of gold nanorod by tuning the solution temperature in presence of CTAB, AgNO₃ and HQ. Here, we found that at higher solution temperature, 35 and 40 oC arrow head shape gold nanostructures are formed while at 25 and 30 oC dog bone shape gold nanostructures were formed. This work demonstrates that, at higher temperature the rate of deposition of gold ad-atoms on the corner facets and migration to tips of the nanorods of gold become facile, because the reduction is so fast that they don't get enough time to get stabilize on the corner facets, as result arrow head geometry has formed. In Chapter 2, plasmonic metal- alloy consisting of AuNR core and alloy Au/Ag shell peanut and porous peanut shapes gold nanostructures were utilized to study the photo electrochemical methanol oxidation. Here we found that the presence of pores on the surface of Au/Ag alloy improves the catalytic activity and prolong stability by reducing the poisoning effect drastically. Furthermore, this porous structure exhibited higher photo activity towards hot hole driven oxidation of methanol in the Vis-NIR region. Next In Chapter 3, we established the synergistic effect of gold nanoparticle in providing basis for light harvesting and provide interfacial sites with MnO_x, which promotes the water oxidation reaction. Here, we found that the core-shell structures of Au@MnO_x having gold nanoparticles core and MnO_x shell, boosts the water oxidation reaction by lowering onset potential and increasing current density. Furthermore, the hot hole mediated water oxidation was monitored at different wavelength and a maximum photocurrent was achieved near the dyads absorption maxima. The presence of photo induced energetic holes on the gold nanoparticle core, boost the electron injection from water molecule by the catalytic MnO_x shell, and the mechanism of complete water oxidation cycle by changing the oxidations state of Mn is discussed. Lastly in Chapter 4, we modified the plasmonic core from sphere to gold nanoprisms (AuTNP) to extend the light harvesting window into Near Infrared region (NIR). This AuTNP@MnO_x dyad exhibits an improved performance in harvesting solar energy in the NIR region. Hence, to understand the underlying mechanism during such enhancement under NIR radiation, we analyse the shape of photocurrent time trace and its relative magnitude to deduce the effect of photocatalytic and photo thermal heating.

Interestingly, we found that the photo thermal heating dominates in all region of wavelength and is maximum at 808 nm i.e. at intraband transition and decrease gradually when excitation wavelength decreases towards interband region.

Title: Functional cyanostilbenes: sensing to imaging
Researcher: Dahiwadkar, Rahul
Supervisor: Kanvah, Sriram
Year: 2023
Keyword's: Cyanostilbenes, Aggregation-induced Emission (AIE), Low Molecular Weight Organogels
Call No.: 547.1 DAH
Acc. No.: T01045

Abstract: This dissertation focuses on the utilization of π -conjugated α -cyanostilbene systems for sensing and cellular imaging applications. These molecules are renowned for their distinctive Aggregation Induced Emission (AIE) phenomenon in aqueous media. AIE refers to the phenomenon wherein the fluorescence intensity of a molecule increases upon aggregation in a solution, contrary to the usual decrease in fluorescence intensity caused by the quenching of the excited state. This occurs because the electronic transitions in the aggregates experiences fewer hindrances compared to the isolated molecules. AIE is observed in various types of organic molecules, particularly those with π -conjugated systems, and finds application in diverse fields, including sensing, imaging, and organic light-emitting diodes.

Donor-acceptor compounds hold great importance in materials science and chemistry due to their distinct electronic and optical properties. The presence of a conjugated system in stilbenes enables efficient electronic and energy transfer between the donor and acceptor groups. This characteristic results in enhanced light absorption and emission, making them valuable for applications such as sensing, imaging, and optoelectronics. Moreover, the incorporation of both donor and acceptor groups within a single molecule allows for precise adjustment of their properties by modifying the chemical structure of these groups. Consequently, donor-acceptor compounds represent a versatile class of materials with a wide range of potential applications. This thesis work is divided into four chapters (2- 5), with each chapter addressing a specific research objective.

The general introduction (Chapter 1) provides an overview of the thesis and the research focus. The introduction includes an extensive review of numerous α -Cyanostilbene molecules for various applications, ranging from sensing to imaging. Each chapter begins by introducing the specific research objective, followed by a review of relevant literature. The experimental methods and results are then presented, along with a discussion of the findings. Finally, each chapter concludes with a summary of the main points and a comprehensive list of references

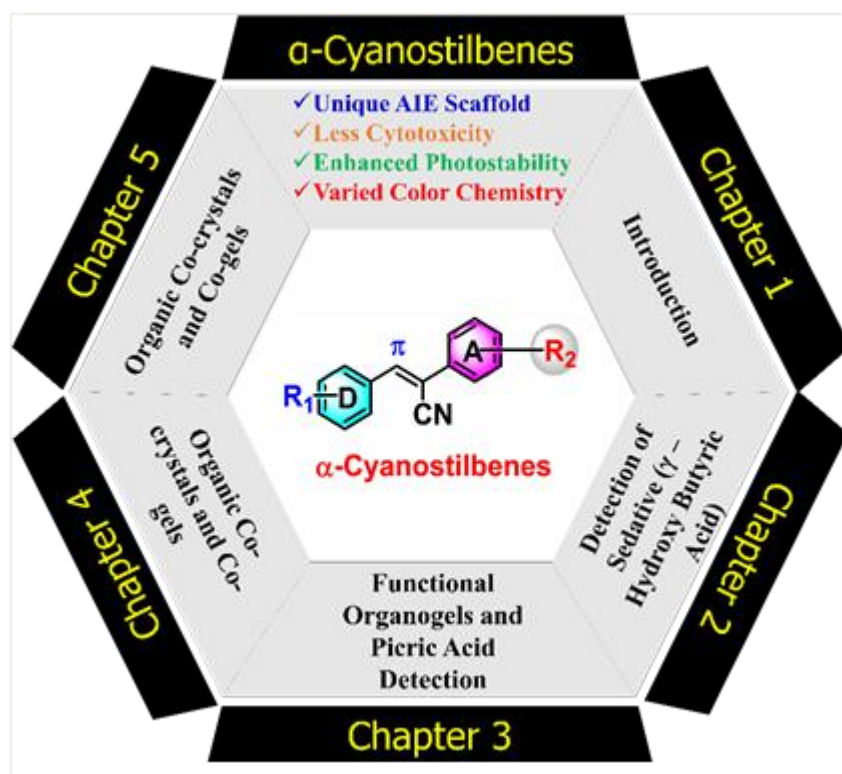
The Second chapter utilizes hydroxyl-substituted α -cyanostilbene systems to detect sedative γ -hydroxy butyric acid (GHB). Gamma-Hydroxybutyric acid (GHB) is a sedative and central nervous system depressant and is a treatment for conditions such as insomnia. While this is naturally occurring in small amounts in the human brain and tissues, the use of the compound for medicinal use has been discontinued because of its potential for abuse as a "club drug" or due to its ability to cause sedation, amnesia, and loss of inhibitions. The sensor uses the unique emission behavior of the cyanostilbene system, which results in a turn-ON fluorescence effect when the sensor comes into proximity with GHB. The sensor is selective for GHB as it only responds to the presence of the

drug and not other control molecules or fluorescence derivatives without hydroxyl groups. This sensing ability of the α -cyanostilbene system can be used for detecting GHB in alcoholic drinks and for on-site detection by law enforcement.

The third chapter discusses the design, synthesis, and evaluation of a series of alkyl-substituted trifluoromethyl cyanostilbene derivatives, study of their photophysical properties, and ability to form organogels. In water, the molecules exhibit excellent Aggregation-Induced Emission (AIE) properties and the molecules with bis (3,5- trifluoromethyl groups form stable organogels in ethanol under ambient conditions. The organogels could also detect nitro aromatic compounds such as picric acid both in gel and solution state.

We explored the propensity of pyridine containing α -cyanostilbene systems to form stable cooperative organic co-crystals in chapter-4. The cyanostilbenes systems were chosen in such a way that one unit contains pyridyl ring and the other contain iodophenyl unit so that favourable N...I interaction assists the formation of stable co-crystals in organic solvents. The formation of two component organogels with these molecular systems was also investigated.

In the fifth chapter, we utilized the trifluoromethyl (CF₃) cyanostilbenes and their AIE behavior for studying the imaging of sub-cellular organelles. Trifluoromethyl groups are important in various areas of chemistry and biology and are used as a bioisostere in medicinal chemistry to create potent substrates with improved bioavailability and specificity. The lipophilic properties of the CF₃ containing cyanostilbenes could be well-suited for imaging lipid rich organelles such as lipid droplets, endosomes and the like. We observed selective imaging of the lipid droplets and visualization of lipid droplets dynamics during oleic acid stimulation.



Title: Chemical Biology and nanotechnology-based tools for targeting Mitochondria in cancer
Researcher: Bajpai, Aman
Supervisor: Basu, Sudipta
Year: 2022
Keyword's: Chemical Biology-tools, Mitochondria-cancer, Chimeric Nanoparticle
Call No.: 572 BAJ
Acc. No.: T01086

Abstract: Mitochondrion, the powerhouse, is one of the most important organelles inside the cells due to its involvement in a plethora of biological functions including cellular energetics, biosynthesis, stress response, and cell death control signaling. Interestingly, mitochondria also contain genomic materials in the form of mitochondrial circular DNA (mt-DNA), mitochondrial RNA (mt-RNA), and ribosomes (mt-ribosomes) to produce proteins required for oxidative phosphorylation (OXPHOS). As a result, mitochondrial dysfunction is highly implicated in different diseases including cancer. Moreover, mitochondria are the ubiquitous powerhouses of healthy as well as cancer cells. Hence, selective subcellular targeting of mitochondria in cancer cells, keeping them unperturbed in healthy cells, could be of central importance for the development of novel cancer therapeutics.

To address this, in this thesis, in Chapter 2, we have engineered mitochondria-targeted antibiotic (tigecycline)-loaded cationic nanoparticles from cholesterol conjugates. Dynamic light scattering and electron microscopy confirmed the spherical morphology and a less than 200 nm hydrodynamic diameter for these nanoparticles. The triphenylphosphine-coated tigecycline-loaded nanoparticle (Mito-TPP-Tig-NP) was shown to be homed into the mitochondria of A549 lung cancer cells. These Mito-TPP-Tig-NPs indeed triggered mitochondrial morphology damage and generation of reactive oxygen species (ROS). Mito-TPP-Tig-NPs showed improved efficacy in A549 and HeLa cervical cancer cells compared to free tigecycline. Moreover, Mito-TPP-Tig-NPs showed much less toxicity toward noncancerous human embryonic kidney cells (HEK293) compared to free tigecycline. These antibiotic-loaded mitochondria-targeted nanoparticles can open up an avenue towards anticancer therapy.

Interestingly, it was found that mitochondria also have their own DNA repair mechanisms that help them to overcome mt-DNA damage. To overcome the mt-DNA repair mechanism, in Chapter 3, we have successfully designed Chimeric Nanoparticles (mt-CNPs) which consist of three different drugs simultaneously to damage the mitochondrial-DNA, mitochondrial-ribosome, and mitochondrial-topoisomerase I. These mt-CNPs were characterized to be positively charged, spherical in shape, and found to be less than 200 nm in diameter. Confocal microscopy confirmed that these mt-CNPs efficiently localized into the mitochondria of A549 lung cancer cells within 6h, followed by mitochondrial morphology damage and subsequent generation of reactive oxygen species (ROS). These mt-CNPs showed remarkable cancer cell killing ability compared to free drug combinations in A549 (lung), HeLa (cervical), and MCF7 (breast) cancer cells. These mitochondrial-targeted lipidic Chimeric Nanoparticles can be explored further to impair multiple targets in mitochondria to

understand mitochondrial translational and transcriptional machinery as well as a new strategy towards cancer therapy.

Furthermore, recent studies revealed that in some cancer cell lines (colon, lung, breast, gastric, etc.) the internalization of COX-2 enzyme along with heat shock protein HSP60 into the mitochondria, catalyzes the conversion of arachidonic acid (AA) into prostaglandin, thus acting as a sink for AA which is a major component in the mitochondria-mediated natural apoptosis. To overcome the anti-apoptotic mechanism regulated by the COX-2 enzyme in mitochondria of cancer cells, in Chapter 4, we have synthesized a small library of triarylphosphonium derivatives (8 molecules) of indomethacin V and ibuprofen, clinically approved non-steroidal anti-inflammatory drugs (NSAIDs). From this library, two small molecules were identified to induce mitochondrial morphology damage through outer membrane permeabilization (MOMP) followed by the generation of reactive oxygen species (ROS) leading to remarkable breast cancer cell death. These novel mitochondria-targeted NSAID derivatives can open a new direction to understand mitochondrial chemical biology as well as next-generation cancer therapy.

In summary, this thesis focuses on the development of novel small molecules and nano- platforms to impair mitochondria in cancer cells towards next generation organelle targeted anti- cancer therapy.

* * * * *



CIVIL ENGINEERING

Civil Engineering

Title: Drought monitoring and prediction in India
Researcher: Shah, Reepal
Supervisor: Mishra, Vimal
Year: 2017
Keyword's: Drought Monitoring System, Global Ensemble Forecast System, Bias Correction Methods, GEFSv2 for Drought Prediction
Call No.: 551.5773 SHA
Acc. No.: T00207

Abstract: Drought is one of the costliest natural disasters. Due to the erratic nature of the Indian summer monsoon, frequency and severity of droughts in India have increased during the recent decades and are likely to increase under the warming climate. Since 2000, India has faced five major droughts, 2002, 2004, 2009, 2014, and 2015. Drought in 2015 affected 33 million people and resulted in an estimated loss of 65000 crore (INR) in India. Despite the increased frequency of droughts in India and their impacts on water resources, agriculture, and socioeconomic conditions of people, a real-time drought monitoring and prediction system has been lacking. The present study aims to develop a near real-time high resolution drought monitoring and prediction system for India. First, the performance of model-based reanalysis products (in absence of real-time ground observations) was evaluated for drought monitoring in India. We found that the three latest generation reanalysis products [MERRA (change in Precipitation:-26%, Temperature:- 0.42°C), ERA-Interim (7%, 0.24°C), and CFSR (-8%, 0.54°C) largely failed to capture long-term trends in observed precipitation (-0.2%) and air temperature (0.13°C) obtained from the India Meteorology Department (IMD). Climate Forecast System Reanalysis (CFSR) product showed moderate skills in capturing interannual variability in observed precipitation and droughts. The ensemble mean of drought from the three reanalysis products showed more skill as compared to any individual product. Despite the potential of the reanalysis dataset for drought monitoring in India, the major challenge remains to provide information in real-time as most of the reanalysis products have latency of one to two months from the current period.

To develop a real-time drought monitoring system, the potential of remotely sensed precipitation was evaluated. We evaluated precipitation from the Tropical Rainfall Measurement Mission (TRMM) and found that it overestimated observed precipitation and underestimated number of rainy days in India. Moreover, monthly precipitation from the TRMM exhibited considerable bias against the observed precipitation from IMD. The daily maximum and minimum temperature data were obtained from the Global Ensemble Forecast System (GEFSv2) reforecast which was also evaluated against the observed data. Notwithstanding the availability of precipitation and maximum and minimum temperatures in real-time, the bias in these products hampered their skill in providing reasonable information on drought and its characteristics (frequency, areal extent, and severity) over India. Bias correction methods were used and evaluated to improve bias in the satellite driven precipitation and maximum and minimum temperatures from the TRMM and GEFSv2, respectively.

We found that bias correction resulted in improvement in bias in precipitation from 91.86 to 34.44 mm while -1.5°C to 0.5°C in air temperature during testing. Therefore, bias-corrected precipitation from TRMM and temperature from GEFSv2 can provide satisfactory information required for drought monitoring in real-time over India. Since the aim was to develop a real-time drought monitoring system that provides not only meteorological drought but also hydrological and agricultural droughts in India. Hydrologic variables (runoff and soil moisture) were simulated using the Variable Infiltration Capacity (VIC) model after successful calibration and evaluation. Standardized Precipitation Index (SPI), Standardized Runoff Index (SRI), and Standardized Soil moisture Index (SSI) were used to categorize meteorological, hydrological, and agriculture drought in India. The real-time monitoring system and drought information was evaluated against the satellite driven drought severity index and it was found that the developed system can successfully monitor drought in India.

Along with the real-time drought monitoring, short and sub-seasonal (7-45 days lead) drought prediction in India can assist farmers and water managers. Moreover, a skillful drought prediction can help in mitigating the adverse impact of drought and avoid associated economic losses. Initially, we evaluated 7 day lead forecast of precipitation and air temperatures (maximum and minimum) from the GEFSv2 for drought prediction in India. We found that precipitation and temperature forecast from GEFSv2 for 7 day lead showed reasonable skill during the non- monsoon (correlation: 0.6, 0.8) and the monsoon (June to September) seasons (correlation: 0.5, 0.6). Results showed that temperature predictions from the GEFSv2 showed higher forecast skill than precipitation in majority of India. Bias in the temperature and precipitation forecast was corrected using the observed data from IMD. The bias corrected forecast was used to run the VIC hydrologic model to simulate runoff and soil moisture. SRI, and SSI were used to categorize hydrological and agriculture drought forecasts India. The drought forecast was evaluated against the observed drought indices estimated using the satellite data and observed meteorological forcing. We found that the bias corrected GEFSv2 forecast can provide reasonable skills for medium range (~ 7 days) droughts over India; however, a majority of skills is driven from the observed initial hydrologic conditions. Skills of drought prediction in India were also evaluated at longer leads (15, 30, and 45 days) for forecast from the Climate Forecast System (CFSv2), GEFSv2, and Indian Institute of Tropical Meteorology (IITM). A careful evaluation of forecast skills in these products demonstrated that the ensemble forecast from the IITM showed a better skill at almost all the lead-times than the two other products in India. Moreover, the bias corrected ensemble mean of forecast from the IITM showed substantially higher skills for prediction of hydrological and agricultural droughts in India at 45 days lead-time. Overall, the real-time monitoring and predication system can be valuable for water resources and agriculture sectors in India.

Title: Dynamic behaviour and suction characteristics of CH combination soil
Researcher: Pandey, Saloni Prashant
Supervisor: Sachan, Ajanta
Year: 2018
Keyword's: Matric Suction, Cyclic Triaxial, Dynamic Triaxial, Unsaturated Cohesive Soil
Call No.: 624.17 PAN
Acc. No.: T00273

Abstract: Combination soils possessing mixture of coarse and fine grained with varied fractions are naturally encountered in several geotechnical engineering projects. Naturally available combination soils are subjected to various types of dynamic loading including high strain (earthquake & blast loading) & low strain loading (machine vibrations & traffic loading). This leads to particle structure breakdown inducing instability within the soil mass causing severe damages to various geotechnical structures under dynamic loading conditions. Assessment of strength & stiffness degradation characteristics of such soils under dynamic loading conditions is essential for stability analysis of structures. Evaluation of dynamic behavior of soil is imperative for solving various problems involving soil-structure interaction and other geotechnical issues. Unsaturated soils comprising of three phase system (air, water & soil mass) and possessing water content less than saturation (Degree of saturation; $S_r < 100\%$) are encountered in numerous geotechnical engineering issues especially in arid and semi-arid regions. Soil layer above hydraulic datum possess negative pore pressures frequently denoted as soil suction. Mechanical response of soil in unsaturated state remains non-consistent with conventional soil mechanics due to presence of negative pore water pressure. Current research involves the study on dynamic behavior of *CH* (Clay of high compressibility/plasticity) combination soil along with matric suction and collapsible characteristics under unsaturated state. Cyclic behavior, energy dissipation and stiffness degradation rate of *CH* combination soil is also studied under saturated state at varying amplitude and frequency under consolidated and unconsolidated testing conditions. In addition to this, the relationship of collapse potential and swelling pressure with suction measurements of expansive soils with different *DFSI* (Differential free swell index) has been evaluated.

A natural *CH* combination soil was chosen for the current research, which was collected from Ahmedabad (Gujarat, India) consisting of 1% gravel, 15% sand, 52% silt and 32% clay. Ahmedabad cohesive soil under unsaturated state was used to perform dynamic triaxial tests to evaluate the influence of matric suction and initial static loading on its hysteresis response, dynamic properties and stiffness degradation behavior. Application of initial static loading identified a unique dynamic response on compacted specimens of *CH* combination soil. Shear modulus of unsaturated combination soil increased with increase in matric suction. Soil specimens possessing higher matric suction experienced higher stiffness degradation with increasing number of loading cycles. Variation of collapse potential and cyclic degradation index with matric suction of unsaturated *CH* combination soil exhibited meta-stable behavior of specimens comprising of high matric suction indicating soil skeleton to be highly volatile and unsafe under dynamic loading conditions. Unsaturated shear strength of Ahmedabad cohesive soil was also determined by employing

conventional triaxial testing and matric suction measurements. Angle of shearing resistance w.r.t matric suction was obtained to be the maximum for lower degree of saturation and higher matric suction. Ahmedabad cohesive soil under saturated conditions was used to study the influence of initial void ratio, loading frequency and amplitude on hysteresis response, dynamic properties, energy dissipation, rate and magnitude of stiffness degradation by performing dynamic triaxial tests under consolidated and unconsolidated conditions. Specimens possessing lower initial void ratio exhibited greater loss in strength and stiffness of saturated *CH* combination soil. Loading frequency and amplitude significantly impacted the hysteresis response and dynamic properties of saturated Ahmedabad soil under consolidated and unconsolidated testing conditions. Pore pressure evolution under consolidated conditions improved when subjected to dynamic loading with higher amplitude and lower frequency. Rate and amount of stiffness degradation enhanced with increment in amplitude, however negligible influence of loading frequency was attributed from the present study. Consolidated state of soil attributed higher shear modulus as compared to unconsolidated state. Energy dissipation was found to be the maximum for higher amplitude, higher frequency and first cycle of dynamic loading. The suction and collapse potential study was extended to expansive soils (shrinkage-swelling), which would exhibit large amount of matric suction at their unsaturated state. Four such *CH* combination soils with different *DFS* ranging from 134% to 30% were explored to study the relationship of collapse and swelling with their suction parameters. Presence of large amount of Montmorillonite resulted in higher *DFS* and higher matric suction. Higher matric suction contributed to higher affinity of water causing larger amount of crystalline swelling resulting into the greater swelling pressure. Sudden reduction of high magnitude inter-particle resistive force in the soil skeleton possessing higher matric suction might have caused excessive volume change within the soil mass leading to higher collapse.

Title: On the causes of observed and projected changes in daily and sub daily precipitation extremes in major urban areas in India
Researcher: Ali, Haider
Supervisor: Mishra, Vimal
Year: 2018
Keyword's: Meteorology, Climatic Changes, Atmosphere, Global Mean Temperature
Call No.: 551.5 ALI
Acc. No.: T00279

Abstract: Urban areas are the centers of population, economic growth, and wealth. Daily and sub- daily extreme precipitation events in urban areas cause flooding, disrupt transportation, damage urban infrastructure, and often result in loss of human lives. Despite the implications of precipitation extremes for urban infrastructure and stormwater designs, our understanding of the major drivers of daily and sub-daily precipitation extremes in urban areas remains limited. In this dissertation the following major questions are addressed:

- 1) To what extent daily extreme precipitation events have changed during the past and if rapid urbanization in India has contributed to the observed changes in precipitation extremes?,
- 2) How do local surface air temperature (SAT) and dew point temperature (DPT) affect daily and sub-daily precipitation extremes in India?,
- 3) What is the contribution of dynamic and thermodynamic scaling in sub-daily precipitation extremes in India? And
- 4) How will daily and sub-daily precipitation extremes that are relevant to urban stormwater infrastructure change under the 1.5 and 2.0°C warming worlds?

To address the above questions, we used observations and model simulations from different sources including Indian Meteorological Department (IMD), Global Summary of the Day (GSOD), Climate Hazards Group Infra-Red Precipitation with Station data (CHIRPS), Tropical Rainfall Measuring Mission (TRMM), Climate Prediction Center morphing technique (CMORPH), Multi-Source Weighted-Ensemble Precipitation (MSWEP), Coordinated Regional Climate Downscaling Experiment (CORDEX) and phase five of Coupled Model Intercomparison Project (CMIP5). First, we studied the changes in extreme daily precipitation due to the climate change (pre and post-1955) and urbanization (pre and post-1983) in urban areas in India using observed IMD precipitation data (1901-2010). Our results do not indicate any significant change ($p > 0.05$) in mean and distribution of the daily extreme precipitation indices for the pre and post 1955 and 1983 periods revealing an insignificant role of climate change and urbanization respectively, on daily precipitation extremes in urban areas. We further used daily precipitation projections from Regional Climate Models (RCMs) to estimate precipitation maxima (1-3 day duration and 100-year return period). We find that the number of urban areas with significant increases in precipitation maxima under the projected future climate is far larger than the number of areas that experienced significant changes in the historic

climate (1901-2010), which warrants a careful attention for urban stormwater infrastructure planning and management.

Since understanding the relationship of precipitation extremes with temperature is helpful in predicting future precipitation extremes, next, we studied the sensitivity of precipitation extremes in response to warming (scaling: the relationship between precipitation extremes and temperature) at the selected urban locations where long-term (1979-2015) daily station data from GSOD are available. We used 3-hourly precipitation from TRMM and found a negative relationship between (sub-daily and daily) precipitation extremes and SAT in India at the majority of urban locations. The negative relationship between precipitation extremes and SAT in India can be attributed to cooling (SAT) due to the monsoon (June to September) season precipitation events suggesting SAT alone is not a good predictor of precipitation extremes. In contrast, a strong (higher than 7%/K) positive relationship between precipitation extremes and DPT and tropospheric temperature (T850) is shown at most of the locations, which was previously unexplored. Moreover, sub-daily precipitation extremes were found to be more sensitive to DPT and T850 than daily precipitation extremes. We, subsequently, used DPT and T850 as covariates for non-stationary daily design storms and found higher magnitude design storm under the assumption of a nonstationary climate.

As daily and sub-daily precipitation extremes are influenced by both local and large-scale processes, for a better understanding of the scaling relationship of precipitation extremes under the warming climate, consideration of both dynamic (controlled by the large-scale atmospheric processes) and thermodynamic (controlled by the saturation of atmospheric moisture) scaling is important. We, therefore, evaluated the role of dynamic and thermodynamic scaling in changes in sub-daily and daily precipitation extremes at urban locations in India. We find that the contribution of dynamic scaling in the rise in the frequency and intensity of sub-daily precipitation extremes is higher than the thermodynamic scaling indicating the controls of large-scale factors. Furthermore, half-hourly precipitation extremes show higher contributions from the both thermodynamic (~10%/K) and dynamic (~15%/K) scaling than daily (6%/K and 9%/K, respectively) extremes indicating the role of warming on the rise in the sub-daily precipitation extremes in India.

Next, we analyzed the scaling relationship of sub-daily precipitation extremes with global mean temperature (GMT). We find that the sub-daily precipitation extremes show the scaling coefficient 9-10%/K with GMT indicating that extreme precipitation events in India are sensitive to the rise in GMT. Since the Paris agreement aims to limit the rise in GMT below 2.0°C and with a more ambitious target of 1.5°C from the pre- industrial level, we evaluated the sensitivity of rise in GMT on sub-daily precipitation maxima relevant to urban stormwater designs. For this, we used observations and projections of the sub-daily precipitation from 15 General Circulation Models (GCMs) over urban areas in India. We find that a rise of 1.5 (2.0°C) in GMT from the pre- industrial level is projected to cause 20 (25%) increase in 3-hourly precipitation maxima at 100 year return period under the stationary condition, which can further rise by 10% under the nonstationary condition. Projected warming results in a much faster (almost twice) increase in 3-hourly precipitation maxima than 24-hourly 100 year precipitation maxima. Moreover, 3-hourly 100 year precipitation maxima is

projected to increase significantly at 78 locations (out of 89) if GMT rises from 1.5 to 2.0°C from the pre-industrial level. Our findings provide a better understanding of the observed and projected changes in daily and sub-daily extreme precipitation events in India. Moreover, we identify the major drivers that contribute to the changes in precipitation extremes at urban locations. Changes in daily and sub-daily precipitation extremes driven by the local and large-scale factors under stationary and nonstationary conditions provide robust estimates of precipitation extremes that are relevant to urban stormwater designs in India.

Title: Fully coupled multi physics nonlinear analysis of reinforced concrete and steel structural systems subjected to fire
Researcher: Prakash, Patnayakuni Ravi
Supervisor: Srivastava, Gaurav
Year: 2018
Keyword's: Reinforced, Steel Structural, Heat Transfer
Call No.: 624.38 PRA
Acc. No.: T00397

Abstract: This dissertation develops a fully coupled computationally efficient framework for multi- physics nonlinear analysis of structural systems subjected to fire with heat transfer analysis, pore pressure analysis and mechanical analysis as the multi-physics components. This is achieved through a two-level spatial discretization strategy. Such an approach is utilized to formulate a fiber type beam-column element using the direct stiffness method (DSM), a finite element (FE) layered shell element, and a zero-length spring element for modeling flexible connections. The beam-column element utilizes updated Lagrangian co-rotational formulation with local force deformation relationships deduced from the classical Euler- Bernoulli beam column theory. The superiority of the developed beam-column element lies in developing the DSM for structural fire analysis, which enables use of a much coarser spatial mesh when compared to existing fire analysis frameworks. Effects of large deformations, temperature-dependent material properties, spalling and transient states of strain are directly integrated into the stability and bowing functions in the construction of the member stiffness matrix. This alleviates the need to perform element-level numerical quadrature, typically required by all existing finite element based approaches. Permanent plastic deformations for steel are integrated into the beam-column element formulation by considering an isotropic hardening plasticity model in conjunction with the von Mises yield criterion.

The layered shell element, developed for modeling slabs, utilizes a total Lagrangian formulation and is developed from the Reissner-Mindlin thick plate theory. It accounts for large deformations, tensile membrane action, temperature-dependent material properties and transient states of strain. Material nonlinearity is considered in the shell element by considering a smeared rotating crack model. Such a layered shell element with smeared rotating crack model facilitates precise formulation especially in scenarios involving change in principal directions during the course of loading unlike the fixed crack model. Subsequently, equilibrium equations of all structural elements are assembled together to form a global system of nonlinear equations and are solved iteratively in a computationally efficient manner with the aid of sub-structuring. The efficacy of the developed framework has been demonstrated through several numerical examples. These numerical examples include verification studies, validation studies and applications pertaining to structural fire analysis of large scale structural systems.

Title: Effect of mica content and its crushability on compactability compressibility shear strength and dynamic behavior of micaceous sand
Researcher: Seethalakshmi.P
Supervisor: Sachan, Ajanta
Year: 2018
Keyword's: Mica Content, Crushability, Compactability, Compressibility, Geotechnical Sand
Call No.: 624.1821 PSE
Acc. No.: T00398

Abstract: Micaceous soils are considered to be detrimental due to low compactability, high compressibility and low shear strength behavior; which results in failures of pavements under traffic loading, earthen dams, embankments, cuts & excavations of retaining walls etc. Mica particles are platy, fragile and resilient in nature with inherent material anisotropy due to numerous intact mica flakes foliated over each other with low stiffness & hardness unlike spherical sand particles. Presence of mica particles substantially affects the geotechnical behavior of micaceous sand under different drainage (drained & undrained) and loading (impact, incremental, monotonic, dynamic) conditions. Hence, micaceous sand with more than 10% mica is considered unsuitable for construction to avoid damages in earthen structures. Micaceous sand comprises of complex geometric arrangements caused by bridging, ordering and pore filling phenomena leading to unique geotechnical behavior. Bridging represents the irregular arrangement of sand particles below mica and ordering represents the regular arrangement of sand particles above mica creating larger void spaces. Bridging and ordering occur when mica particles are larger than sand ($L_{mica} > D_{sand}$), and pore filling occurs when mica particles are smaller than sand ($L_{mica} < D_{sand}$). In previous studies, macroscopic behavior of micaceous sand was explored with respect to the size and quantity of mica; while the interpretations at micro level with respect to microstructural configuration were remained unexplored. The current study focuses on the effect of mica content and its crushability on compactability, compressibility, monotonic shear strength and dynamic behavior of micaceous sand incorporating the variations in geometrical arrangement of sand and mica particles.

Sabarmati sand was mixed with commercially available mica powder (muscovite) at varying percentages: 0%, 5%, 10%, 15%, 20%, 25% & 30% by weight to obtain different micaceous sand samples. Crushing of mica particles under impact loading simulates the particle breakage under traffic loading conditions. A study on successive cycles of impact loading was performed on micaceous sand with 15% & 30% mica (15MS & 30MS) to evaluate the degree of mica crushability on its compactability and compressibility behavior. Mica flakes were evaluated using Scanning Electron Microscopic (SEM) image to interpret the variation in microstructure at successive impact loading cycles. The modified compactability and compressibility behavior of micaceous sand due to crushing needs to be considered during construction of pavements and embankments to avoid failure. The effect of microstructure on shear behavior of micaceous sand (MS) in comparison to pure sand (PS) was also studied through three series of consolidated undrained (CU) triaxial tests with varying initial soil-structure before shearing due to looser & denser configuration, particle crushing and K_0 consolidation. PS microstructure was stable structure of sand particles which were closely & uniformly packed with larger interparticle contacts. MS microstructure was emerged as

metastable structure having less interparticle contacts with non-uniform void space among sand & mica particles due to bridging, ordering and pore filling phenomena. The ductile stress-strain response with higher peak stress along with contractive pore pressure response was observed in 30MS specimen as compared to PS at looser configuration; and the opposite response was observed for denser configuration. Consecutive *CIUC* triaxial testing cycles of 30MS specimens showed decreased peak stress and change of pore pressure from dilative to contractive indicating mica particle breakage. *CK_oUC* tests revealed an improved shear strength response of 30MS with higher peak stress and more dilative nature as compared to PS. Hence, the influence of boundary conditions (void ratio, isotropic/anisotropic, crushing, compression/extension) needs to be given importance to understand the microstructural changes in micaceous sand unlike pure sand and to decide the appropriate shear strength parameters for the design of earthen structures. The impact of varying mica content on shear strength behavior of micaceous sand was analyzed through a series of *CIUC* tests at different confining pressures. The peak stress was reduced and excess pore pressure evolution was observed to change from dilative to contractive response with mica upto 20% mica content. The response showed reverse pattern from 20% to 30% mica content. 20% mica was observed to be the critical mica content for Sabarmati sand, which showed the least shear strength and highest contractive pore pressure response (not 10% as suggested in previous studies). Hence, the critical percentage of mica may vary depending on the relative density, particle size & shape, sample preparation, mode of loading, etc., by affecting particle microstructure which also needs to be considered in deciding the vulnerability of micaceous sand in earthen structures. The critical micaceous sand with 20% mica was further experimented to examine the effect of drainage (drained & undrained) and loading (compression & extension) conditions under isotropic consolidation as well as the effect of stress induced anisotropic (stress- path) consolidation on shear strength behavior of micaceous sand. The dynamic behavior of micaceous sand under the influence of mica was also studied through a series of strain controlled cyclic triaxial tests. Pure sand & micaceous sand with 5% mica content exhibited liquefaction. However, the increment of mica content from 10% to 30% increased the cyclic stability of micaceous sand. The comparative study of micaceous sand (0% to 30% mica content) showed that the compactability, recompression index, peak deviatoric stress of monotonic compression and pore pressure evolution in extension mode of dynamic loading exhibited nonlinear parabolic response with respect to percentage of mica. Compression index, secant Young modulus in monotonic & cyclic triaxial tests, pore pressure evolution of cyclic loading in compression mode followed linear trend with respect to percentage of mica. The permissible mica content and possible design recommendations for design of various earthen structures on micaceous soil are also provided based on the obtained results from the current study.

Title: Characterisation and simulation of spatially varying ground motion
Researcher: Rodda, Gopal Krishna
Supervisor: Basu, Dhiman
Year: 2019
Keyword's: Cross-spectral Density, Auto-spectral Density, Amplitude Variability, Conditional Simulation, Apparent Translational Component
Call No.: 624.1 ROD
Acc. No.: T00505

Abstract: Spatially varying ground motion (SVGM) refers to the differences in the phase and amplitude of ground motions recorded over an extended area. Phase and amplitude variability may affect the SVGMs to various degrees depending on the separation distance. Amplitude variability is contributed from the change in magnitude (scaling) and spectral shape of auto-spectral density (ASD). The recorded ground motions represent the characteristics of seismic excitation at one single point. Past studies have demonstrated that the SVGMs could have significant effect on the structural response of certain civil engineering structures. Coherency, which is generally used as a descriptor of the spatial variability, is defined as the normalized (with ASD) cross-spectral density (CSD) and lagged coherency is given by its absolute value. Several procedures are available to simulate the spatially varying ground motion using lagged coherency conditioned to a seed ground motion. Most of the existing procedures assume the spatially uniform ASD and use either CSD or the evolutionary cross-spectral density (ECSD) to simulate the spatially varying ground motion around a chosen reference station. These CSD / ECSD based procedures account only for the phase variability and hence, lead to a good prediction at short separation distance (for example, 0~20 m). Since these procedures do not account for the amplitude variability, the resulting SVGMs do not exhibit close resemblance with the recorded data, at moderate to large separation distances.

One way of investigating the extent of spatial variability in ASD is through its parameterisation. For this purpose, a multi-modal lognormal functional form is proposed and a close resemblance with the ASD from the recorded components is observed. Possible correlation of the parameters of the proposed ASD model against site characteristics is investigated based on selected ground motions from PEER database. An attempt has been made in synthetically predicting the ASD at a given site. ASD of the recorded components at LSST and SMART1 arrays is parameterised through the lognormal form and similarity of spectral shapes of ASD is assessed through the "spectral contrast angle" based on "distance correlation". At short separation distances (for example, LSST array), spatial variability of ASD of horizontal motions is negligible while that for the vertical motion varies considerably. All three translational components exhibit considerable variability in ASD over the footprint of a large array (for example, SMART1 array) and hence, the assumption of spatially uniform ASD in simulating SVGMs is questionable.

Conditional simulation of SVGM requires a calibrated coherency model and a seed ground motion. For this purpose, a new coherency model is proposed accounting for the phase as well as amplitude variability of ASD and assessed that along with some of the other coherency models available in the literature against the data recorded over the footprint of LSST and SMART1 arrays. However, the scope of the coherency model was first restricted to the variation of lagged coherency against

frequency for a particular separation distance (and not to study its variation along the separation distance). Numerical studies on the spatial variability of ASD did not show a monotonic decay against the separation distance. Attributing this to the contribution from random component, the same coherency model is then extended so as to account for the contribution of random component to ASD.

A new framework for conditional simulation of SVGGM based on ASD is proposed. This ASD based framework simulates the SVGGM through the calibrated coherency model (proposed) and mapping of the ASD over the footprint of an array. The proposed ASD based framework accounts for both the phase as well as amplitude variability and hence, exhibited good resemblance with the horizontal components recorded over LSST and SMART1 arrays. Hence, for conditionally simulating SVGGM, use of the proposed ASD based framework is recommended over the CSD based framework. However, investigations specific to the recorded vertical components are limited in the literature and the proposed ASD based framework is further explored using the vertical components. Once again, a close resemblance between recorded vertical components and those from the proposed ASD based framework is noted.

Description of the ground motion input cannot be completed without specifying the rotational ground motion. Rotational motion is the spatial derivative of the associated translational motion and hence, rotational coherency model does not exist precluding the study of its spatial variability. However, if the rotational component can be expressed as a time derivative of an apparent translational component (ATC) with due scaling through apparent velocity, one may prove that the lagged coherency of rotational components computed by treating it as a mere time series is identical to that of its ATC. A semi-empirical procedure has been proposed to estimate ATC without the knowledge of rotational motion a priori. Time derivative of ATC has been assessed against the rotational components extracted using the single station procedure (SSP) reported by Basu et al. (2012). Both rocking and torsional components are found to be reasonably well described by the respective ATC. A novel window-based procedure has been proposed to estimate the required apparent velocities without the knowledge of rotational motion. Next, applicability of proposed ASD based framework for simulation of spatially varying rotational ground motion (SVRGM) is explored. SVRGM is simulated using the proposed framework through two approaches. In the first approach, spatially varying translational components simulated using the proposed framework are considered and SVRGM are extracted through the SSP by Basu et al. (2012). In the latter approach, SVRGM is directly simulated using the proposed framework on extracted rotational components. SVRGM from both the cases exhibit close resemblance with the extracted rotational components irrespective of separation distance unlike the CSD based framework. Therefore, proposed ASD based framework is recommended for conditional simulation of spatially varying rotational ground motion. As a closure, this thesis presents a novel framework for conditional simulation of six-component spatially varying ground motion (6C-SVGM) for seismic design of structures with spatially extended sub- and / or super- structures.

Title: Influence of irrigation and reservoirs on water budget and land surface temperature over Indian subcontinental river basin

Researcher: Shah, Harsh L.

Supervisor: Mishra, Vimal

Year: 2019

Keyword's: Water Budget Components, Variable Infiltration Capacity, Hydrologic Changes, Evapotranspiration, Air Temperature

Call No.: 624 SHA

Acc. No.: T00506

Abstract: Land use/land cover and climate change are the two major factors that affect the water cycle. Additionally, land surface water budget can be significantly influenced by anthropogenic activities such as irrigation and reservoir operations. Understanding the water budget is essential for planning and management of water resources. The Indian subcontinental river basins are largely influenced by the rapid land cover change, intensive agriculture, and use of surface and groundwater resources for irrigation. Notwithstanding the strong influence of irrigation and surface water storage on the water budget, most of the previous estimates of water budget over the subcontinental river basins ignore the role of irrigation and reservoir storage. Irrigation helps to meet the water demand during the weak monsoon and dry seasons. In result, the net irrigated area in India has expanded from 56.93 to 63.60 million hectares between 2001 and 2010. Moreover, about 4000 dams were constructed to supply irrigation water, flood control, and hydropower generation in India. Despite the massive irrigation and presence of reservoirs, our understanding of their influence on water, energy budgets and the land surface temperature remain poorly constrained.

We studied long-term (1901-2012) change in water budget components (Precipitation (P), Air Temperature (T_a), Evapotranspiration (ET) and Total Runoff (TR)) in the 18 river Indian subcontinental basins using observations and simulations from the Variable Infiltration Capacity (VIC) macroscale hydrologic model and a stand-alone routing model. We used daily precipitation, maximum temperature, and minimum temperatures from the India Meteorological Department (IMD) for 1901-2012, which were used to simulate the water budget components from the VIC model. Prior to the assessment of the water budget components, the VIC model was successfully calibrated and validated against in-situ (streamflow) and satellite (MODIS ET and ESACCI soil moisture) observations. Long-term (1901–2012) changes in hydroclimatic variables in the 18 Indian subcontinental basins were examined with hydrology simulated using the VIC. Change point analysis using the sequential Mann-Kendall test showed two distinct periods (1901–47 and 1948–2012) for the domain-averaged monsoon season (June–September) precipitation. Hydrologic changes for the entire water budget were estimated for both periods. In the pre-1948 period, a majority of the river basins experienced increased monsoon season precipitation, ET, and surface water availability (as defined by TR). Alternatively, in the post-1948 period, monsoon season precipitation declined in 11 of the 18 basins, with statistically significant trends in one (the Ganges basin), and most (15) basins experienced significant warming trends. Additionally, in the post-1948 period, the mean monsoon season ET and surface water availability declined in eight (with significant declines in four) basins.

The results indicate that changes in ET and surface water availability in the pre- and post-1948 periods were largely driven by the changes in the monsoon season precipitation rather than the air temperature, despite prominent warming after 1975. Coupled modes of variability of sea surface temperature (SST) and surface water availability indicated El Niño–Southern Oscillation (ENSO) as the leading mode. The second mode was identified as the trend mode for surface water availability in the subcontinental river basins, which was largely driven by SST anomalies in the Indian and Atlantic Ocean regions. This indicates that surface water availability in India’s subcontinental basins may be affected in the future in response to changes in large-scale climate variability.

Irrigation modulates the terrestrial water budget in intensively irrigated regions. However, the influence of irrigation on water budget and land surface temperature (LST) has not been quantified in Indian sub-continental river basins. Here, using the in-situ and satellite-based observations and the VIC model with irrigation scheme, we show that the presence of irrigation (no water constrained scenario) substantially alters water budget (especially ET) and LST in the sub-continental river basins. While irrigation results in increased ET in all the 18 sub-continental basins, mean annual ET of Indus and Ganges basins increases by 47% and 12%, respectively due to irrigation. TR has increased in the most basins due to irrigation. Irrigation has a remarkable influence on LST with the cooling of 0.2–0.65°C. Compare to other basins; irrigation water demand is high in Indus and Ganges basins during the post-monsoon season (October-January). Our results show that between 1951 and 2012, irrigation demand has decreased in 13 out of the 18 basins during the pre-monsoon season (February-May). However, irrigation water demand increased in 12 out of the 18 basins in the post-monsoon season. Changes in irrigation demands are largely driven by changes in soil moisture due to weakening/strengthening of the summer monsoon precipitation. Our findings have implications for water budget estimation over intensively irrigated basins, where ET might be substantially underestimated in the previous studies that do not consider the role of irrigation.

Constrained water management activities (e.g., irrigation practice and reservoir construction) alter the water and energy budgets over irrigated agricultural land. Moreover, these activities modify streamflow seasonality. The role of water management activities and their interaction with the terrestrial water and energy budgets have not been sufficiently studied over Indian subcontinental Basins. In this study, we coupled a well-evaluated water management model with the VIC model to examine the impacts of irrigation and reservoir operations on terrestrial water and energy budgets over the Indian subcontinental basins. We conducted two simulations: NATURAL (i.e., no irrigation and no reservoirs) and water management scenario (i.e., with irrigation and with reservoir regulations, referred to as MANAGED) over 18 basins from 1951 to 2012. Our results show that the water management activities have significant (p -value < 0.05) impacts on ET, latent heat flux (LHF), and LST in most of the river basins during the pre-monsoon season (February-May). Comparing to the NATURAL scenario, ET and LHF under the MANAGED scenario are significantly increased in most of the basins during the pre- and post-monsoon seasons, especially in semi-arid regions. LST and sensible heat flux (SHF) are reduced due to the presence of irrigation and reservoirs mainly in the pre-monsoon season when irrigation water demand is high.

Title: Instabilities granular media with flexible boundaries
Researcher: Bhattacharya, Debayan
Supervisor: Prashant, Amit
Year: 2019
Keyword's: Strain Accumulation, Proportional-Integral-Derivative, Post-bifurcation Regime, Elastoplastic Framework
Call No.: 624 BHA
Acc. No.: T00512

Abstract: Instability in granular media is associated with the emergence of non-uniform deformation modes suddenly from its state of uniform material behaviour. It is manifested in the form of localized strain accumulation (shear banding), surface buckling, bulging, liquefaction (“solid-fluid”) and volume instability. Such instabilities act as precursor to failure influencing material strength owing to which, investigation regarding its inception is of prime concern in geomechanics research. Onset of diverse instability modes can be attributed to several factors viz. inherent heterogeneity of the material medium, type of loading, boundary and drainage conditions. One needs to have an idea of handling the global material response in the post-bifurcation regime with its first stepping stone being assertion of instability onset strain since, the material behaviour does not remain uniform (“single element” behaviour) with instability outset. Initiation of non-uniform material response in Plane Strain (PS) conditions has been explored numerically within a continuum elastoplastic framework with the aid of a nonassociative generalized 3D material model that takes into account kinematic hardening. Emergence of instabilities have also been probed at the grain scale level within a discrete (discontinuum) framework that incorporates actual grain morphology while experimental findings augmented with digital image analysis techniques unravel local strain evolution in soil specimens subjected to different boundary conditions.

Since most of the geotechnical structures encountered in the field are idealized as plane strain problems (viz., slope stability, strip footing etc.) with their strength parameters still being estimated from axisymmetric triaxial tests, soil behaviour has been explored in PS conditions ($\epsilon_2 = 0$) in the present study. Existing PS testing of granular media (sands) have been restricted to rigid boundaries (frictional and lubricated to some extent) in the loading direction. Interestingly boundary conditions in laboratory experiments significantly influencing the mechanical response resulting in triggering of various non-uniform deformation modes suddenly from its homogeneous material behaviour, the present study employs flexible boundaries (FBs) in PS testing of sand specimens. FB-PS tests thus becomes imperative for development of material models and yield or failure criteria so that they can be employed to mimic field conditions which may result in more realistic predictions.

Onset of instability in sands has been explored in this study at different length scales from numerical as well as experimental perspectives. Coupled (diffusion) undrained instability analysis (globally undrained locally drained) in sands have been executed in ABAQUS v6.14 with the implementation of a user defined material model (UMAT). Instability onset within a numerical framework was found to be a mesh dependent phenomenon for a particular magnitude of inhomogeneity. Perturbation (required to trigger instability within any numerical framework) was introduced in terms of initial

void ratio (e_0) of the sand specimen locally in a few elements and its magnitude was found to significantly influence the instability onset strain. Influence of patch area of perturbation on instability onset was found to be relatively insignificant.

Furthermore, in order to resolve “pathological mesh dependence” with “phenomenological” material models, instability onset and its signatures have been captured within a discontinuum framework. Macroscopic response obtained from FB-PS test simulations are in good agreement with the experimental findings and the markedly comparable resemblance of the deformed sand specimens gives confidence on high reliability of the discrete element simulations. Localisation initiation was observed at smaller axial strain levels that manifested into distinct zone of shear strain accumulation at large strains with multiple shear bands (in conjugate arrays) at later stages. These zones were also associated with significant grain rotation asserting that sand grains undergo significant rotation inside shear band(s).

A multiaxial cubical device with provisions of FB-PS testing has been developed with three-axis electro-pneumatic Proportional-Integral-Derivative (PID) based real-time feedback control system. Transparent plexiglass in (imposed) PS directions allowed images to be taken at regular intervals during shearing stage of the specimen in order to characterise the local strain evolution in sand specimens. A customised software has also been developed in this regard which can automate various processes including consolidation and shearing stage along any predetermined stress or strain path in the generalised stress space. A series of FB-PS tests have been carried out by pre-compressing the sand specimen to a desired mean stress state and then by shearing it along a predetermined stress path following a particular stress ratio ($\Delta\sigma_3/\Delta\sigma_1$). A simplified yield function in 2D stress space has also been proposed that is in good agreement with the experimental findings along different stress paths with constant $\Delta\sigma_3/\Delta\sigma_1$. Local strain evolution in the material domain has also been examined by employing image analysis techniques during a set of carefully performed FB-PS tests and triaxial compression tests on cuboidal sand specimens so as to segregate the deformation modes encountered in these two conditions. An attempt thus has been made in the present study to characterise how instabilities and localisation emerge in pressure-dependent granular media and what are their various signatures across different length scales viz., continuum, discrete and laboratory “single element” scale.

Title: Deformation-based seismic design of cantilever retaining walls
Researcher: Jadhav, Prajakta Ramesh
Supervisor: Prashant, Amit
Year: 2019
Keyword's: FE Model, Shear Key, LRFD Framework, Soil
Call No.: 624 JAD
Acc. No.: T00516

Abstract: Case studies have reported failure of cantilever retaining walls under earthquake loading due to lack of sufficient understanding on the seismic design of these structures. As damage can be quantified better in terms of displacements, the primary aim of the current study is to propose displacement-based design methodology for cantilever retaining walls with due consideration to sliding and rotational failure modes. At present, practitioners analyze and design these walls like gravity retaining walls by considering vertical column of soil above the heel of wall to be part of wall. Experimental investigations have documented the formation of v-shaped rupture planes in the backfill evolving from the heel of wall. This v-shaped mechanism is primarily responsible for deformations in these walls which has been simulated in the current study by developing a simplified analytical model, i.e., double wedge model. This model computes seismic sliding displacements of these walls due to the applied earthquake motion and the tangential downward movement of soil wedge along the rupture planes. This rigid-plastic model considers wall with adjacent locked soil mass and soil wedge to traverse with distinct dynamic yield accelerations on non-deformable base. In practice, two different possible cases depending upon the intersection and non- intersection of rupture plane with the wall-stem has been simulated by model.

A two-dimensional plane strain FE model has been developed to understand the rotational behavior of cantilever walls. Analysis has been performed on six different classes of foundation soil defined by AASHTO. Many retaining walls are placed on class C type of foundation soil representing medium-dense sand, this soil type has been considered in the further simulations. In order to capture interface deformability at lower PGA, bilinear curve has been proposed to compute equivalent base-interface friction angle. To compute residual and peak rotational displacements at the top of wall in simplified manner, residual displacement factor and peak displacement factor have been proposed as 2 and 3, respectively, to be multiplied with sliding displacements computed from double wedge model. These factors have been determined based on the rotational displacements from 144 cases of FE model.

Past case-histories have also witnessed the failure of walls provided with shear key under earthquake loading. There exists ambiguity about position of shear key and slip plane to be considered in the analysis. From dynamic analysis, the shear key below the heel of wall has been deduced as the suitable location and the slip plane has been observed at some depth below the shear key of wall. The double wedge model has been extended by considering the passive resistance due to shear key and slip line at the depth of shear key. By analyzing 64 different cases, the residual displacement factor and peak displacement factors have been proposed as 2.5 and 3.5, respectively, to compute residual and peak in-plane rotational displacements of wall with shear key.

Further, a displacement-based seismic design methodology using LRFD framework is proposed for retaining walls with and without shear key. It accounts for the uncertainties associated with the variation in earthquake characteristics getting reflected in the deformation response of wall. Two different approaches of factoring load and factoring displacements have been explored and compared by considering 30 different earthquakes, each scaled to 4 different PHAs, 0.16g, 0.24g, 0.36g and 0.48g. The approach of factoring load is found to be a more suitable approach and accordingly, load factors for 0.16g-0.25g, 0.26g – 0.35g, 0.36g-0.45g and beyond 0.45g have been proposed as 1.5, 1.3, 1.1 and 1, respectively, corresponding to 15% probability of exceedance for wall without shear key. For walls with shear key, load factor of 1.25 for PGA less than 0.45g and that of 1 for PGAs greater than 0.45g have been proposed. The same factors have proved to be applicable for the rotational displacements as well. As a much simpler alternative, design charts based on double wedge model have been proposed by relating displacements to the ratio of length of heel L and height of wall H . Subsequently, equations have been proposed to estimate the minimum heel-length to be provided for the earthquake peak ground acceleration and peak ground velocity expected on site. Further, simple equations are proposed to estimate the subsidence extent and depth of backfill for the desired L/H ratio of wall, where H is the height of wall. A simplified LRFD-based methodology using design charts has been also proposed for the convenience of engineers.

Title: Static and cyclic liquefaction characteristics of Kutch soils
Researcher: Hussain, Majid
Supervisor: Sachan, Ajanta
Year: 2019
Keyword's: Geotechnical Investigation, Cyclic Liquefaction, Volumetric Compressibility, Clays With Fines Content, Silty-sands
Call No.: 624.1517 HUS
Acc. No.: T00569

Abstract: Liquefaction is a phenomenon in which the loose saturated granular soil mass loses its strength under undrained loading conditions. It is the consequence of solid-fluid instability resulting from shear-induced excess pore water pressure (Δu) leading to negligible effective stresses within the soil mass. The saturated granular soil can undergo either static or cyclic liquefaction depending on the type of loading; Monotonic or Cyclic. Static liquefaction is a pervasive failure mode in loose saturated granular soils. However, cyclic liquefaction manifests both in loose and dense saturated granular soils. Liquefaction during past earthquakes has led to huge damage to civic facilities (1906 San Francisco, 1964 Niigata, 1971 San Fernando, 1989 Loma Prieta, 1999 Chi-Chi, 2001 Bhuj, 2011 Christchurch). The 2001 Bhuj earthquake resulted in widespread liquefaction and related failures over an area exceeding 10,000 km². The liquefaction severely damaged a large number of dams, port facilities, embankments, underground pipelines, and foundation systems. However, no extensive geotechnical investigation of soil deposits of the Kutch region is available. Current research involves the extensive geotechnical investigation of soils of the Kutch region including 10 locations (five dams and five residential areas) at depths up to 2.5 meters. The liquefaction response of soils of the region under different loading and boundary conditions including monotonic compression, two-way cyclic triaxial (CTX) and cyclic simple shear (CSS) was evaluated at their respective in-situ densities. Basic geotechnical investigation identified most of the soils of the region as silty-sands (SM) with their grain size index (IGS) and mean grain diameter (d_{50}) falling in a narrow range of 0.1 mm to 0.3 mm, typical to those of liquefiable soils. However, a significant number of soils classified as clayey-sand (SC) and clays with fines content (FC) with plasticity index (PI) was found to be varying over a wide range. The volumetric response during shearing revealed highly contractive nature of the soils indicating large liquefaction susceptibility. The behavior of Kutch soils under isotropically consolidated undrained compression (CIUC) triaxial tests displayed a strong influence of FC and PI on the static liquefaction characteristics. Volumetric compressibility (m_v) of soils increased with an increase in the FC and PI. The microstructure of typical silty-sand and clayey-sand of the region revealed silt particles sitting on the sand grains and at sand-to-sand contacts creating a fragile metastable structure for silty-sands; however, for clayey-sands the sand fraction was clothed by the clay particles with voids either empty or filled by the fines resulting in open or compact microfabric respectively. State-dependent non-associative elastoplastic material model was used to explore the instability characteristics under undrained compression of one of the medium dense silty-sands (from Chang dam) of Kutch region. The change in the sign of second-order work (d^2W), the evolution of hardening modulus (H_p), and liquefaction

flow potential (ξ) captured the onset of instability and the subsequent liquefaction at pressures up to 300 kPa as observed in CIUC triaxial tests.

CTX results indicated that the Kutch soils were found to be prone to severe to moderate liquefaction with a strong influence of FC and PI on their cyclic behavior. Silty-sands exhibited liquefaction within 31 cycles whereas clayey-sands did not liquefy up to 50 cycles. This could be attributed to the collapsible nature of the metastable inter-particle structure of silty-sands; however, clayey-sands had compact collapse resistant microfabric due to the presence of plastic fines. Post-liquefaction reconsolidation deformations were governed by the magnitude of Δu developed during the cyclic loading. Post-liquefaction reconsolidation and undrained cyclic response of silty-sand of Chang dam were investigated under multi-level cyclic loading to simulate the behavior of soils under earthquake aftershocks and other cyclic loads. It exhibited increased liquefaction resistance under subsequent levels of reconsolidation and undrained cyclic loading. Improved material response with multi-level reconsolidation and undrained cyclic loading were identified with the increased slope of the envelope bounding the peak of effective stress path. The conditions triggering static liquefaction and cyclic liquefaction of medium dense silty-sand of Chang dam were observed to be the same. Liquefaction characteristics and dynamic properties of medium dense silty-sand of Fatehgarh dam under different loading conditions (frequency and strain amplitude) and stress-history ($OCR = 1-10$) were explored. Liquefaction resistance was observed to decrease at higher strain amplitudes. However, no substantial effect was observed at higher frequencies. At higher overconsolidated states, increased cyclic strength and reduced Δu led to increased liquefaction resistance. The increase in cyclic strength was found to follow a power function relationship with the degree of overconsolidation, which was explored under two scenarios: (a) constant pre-consolidation pressure, (b) constant pre-shear pressure. Very low inherent liquefaction resistance of silty-sand of Fatehgarh dam could be due to its collapsible inter-particle structure and material state. Presence of fines plays an important role in the constitutive behavior of the silty-sands. Under CIUC triaxial test, the influence of inter-granular void ratio (e_g) on the volume compressibility and undrained material behavior of base-sand and natural silty-sand of Fatehgarh dam was more vivid as compared to the global void ratio (e). Increased volume compressibility and decreased shear strength of silty-sand were captured better by e_g rather than e . Liquefaction and settlement behavior of saturated and in-situ moist soils of Kutch region under strain-controlled CSS conditions were examined. The liquefaction resistance was obtained to be very low (less than 40 cycles) for silty-sands at saturated conditions, whereas the loading at in-situ moist condition led to large vertical deformations. For silty-sands, liquefaction resistance was observed to be predominately governed by the FC. However, clayey-sands exhibited cyclic degradation with the rate and the magnitude of degradation controlled by the PI. Few clayey-sands with low PI and FC attained liquefaction within 6 cycles, whereas other clayey soils displayed cyclic degradation owing to the high PI. The magnitude and rate of generation of D_u were observed to be higher under cyclic simple shear conditions as compared to cyclic triaxial conditions by a factor of 1.5 and 1.3 after 1st and 5th cycle respectively. Cyclic behavior of the Kutch soils under either of the two loading conditions, CTX and CSS, revealed that the soils were prone to intense degradation which in extreme cases led to liquefaction in silty-sands. Further, the two states of saturated and in-situ moist conditions under CSS testing revealed Kutch soils to be prone to

liquefaction and large settlements with large susceptibility to damage in either of the two conditions.

Title: Studying planar and spatial dam breach hydraulics
Researcher: Kaurav, Rajkumari
Supervisor: Mohapatra, Pranab K.
Year: 2020
Keyword's: Dams, CFD Software, FLOW-3D, Turbulence Models, Sediment Scour Model
Call No.: 627.8 KAU
Acc. No.: T00700

Abstract: Dams are generally built for various purposes, including flood mitigation, water supply, and generation of electricity. Earthen dams are vulnerable to breaching due to overtopping, piping, or foundation/structural defects. The massive outburst due to dam breaching may cause immense losses to lives and properties. Predictions of breach profile flow through the breach, and its propagation in downstream locations are useful in early warning and damage mitigation systems. Dam breach studies are carried out using two different approaches. The first approach considers the breach to be planar, in which the dam overflow is identical along the length of the dam. The second approach is closer to real-life dam breach events, and it considers the breach to be spatial. In the present study, both planar dam breach and spatial dam breach are simulated using commercial CFD software, FLOW-3D.

For planar breach, the FLOW-3D model parameters are calibrated by comparing the results of the dam surface elevations at different time instants with those of an earlier experimental study. In addition, the results for maximum velocity and turbulence characteristics (the turbulent kinetic energy, the turbulence intensity, and, the excess shear stress) are presented for the calibrated model. Effects of the dam material, the dam height, the downstream slope, the width of the crest, and the inlet discharge, on the erosion rate and the peak discharge through the breach section are studied. Empirical equations for peak breach discharge and erosion rate are developed. The study reveals that the dam material, the inlet discharge, and the downstream slope of the dam are among the most influential factors affecting the planar breach.

Previous experiments on spatial dam breach studies have considered various shapes, sizes, and locations of pilot channels. In these studies, the choice of the shape, size, and location of pilot channels is arbitrary. For example, the ratio of the depth of the pilot channel to dam height varies from 0.0167 to 0.231. Therefore, the effect of different pilot channel parameters on the evolution of spatial dam breach is studied. The numerical model is validated by comparing the simulated results against experimental results available in the literature. Sixteen different cases of pilot channel to study the effect of size, shape, and location of the pilot channel on dam breach are considered. Three phases of spatial dam breach are identified. Results for breach profile, discharge through the breach, and erosion rate of breach volume indicates that the effect of the pilot channel

is limited to the first phase only. Based on the cases studied, important recommendations on size, shape, and location of the pilot channel to conduct dam breach studies are made.

The spatial breach experiment using a triangular pilot channel is conducted in the Hydraulics Laboratory of the Indian Institute of Technology Gandhinagar. The breach width profiles at the dam center are recorded using Kinect XBOX 360 and are considered as the reference values. The model parameters in FLOW-3D are calibrated using the breach profiles obtained from the experiment. The Renormalized Group (RNG) turbulence model, along with the Meyer-Peter and Muller (MPM) equation, simulates the breach satisfactorily. The effect of turbulence model (κ - ϵ , RNG and Large eddy simulation, LES model) and parameters used in the scour model (density, Critical Shield Number, CSN and, bedload transport equation) on the evolution of breach are studied. The effect of the turbulence model on breach parameters (breach profiles, erosion rate, and breach discharge) is more prominent for the Nielson equation (NE) and Van Rijn Equation (VR) as compared to the MPM equation. When the NE equation is used, breaching is lower for RNG and higher for κ - ϵ model. Using the VR equation, breaching is lower for LES and higher for κ - ϵ model. For different densities, the erosion is higher for the VR equation and, it is similar to the NE equation. For the MPM equation, the effect of density is negligible. However, for NE and VR equations, the breaching is higher when the density is decreased. The study for CSN shows that for all three bedload transport equations, the erosion increases when CSN decreases.

The last part of the thesis deals with dam breach studies concerning the rheological characteristics of the fluid. The effect of viscosity and density of the reservoir fluid on the spatial breach evolution is studied. The breaching is higher for higher densities when the viscosity is equal to or greater than water. However, the breach width increment dominates the breaching process if density is higher and the viscosity is less compared to the respective values for water.

Title: Drought risk in South Asia under observed and projected future climate
Researcher: Aadhar, Saran
Supervisor: Mishra, Vimal
Year: 2020
Keyword's: South Asia, Drought, Climate, Variable Infiltration Capacity (VIC)
Call No.: 624 AAD
Acc. No.: T00701

Abstract: Drought is one of the deleterious and complex natural disasters that affect water availability, crop production, and gross domestic product (GDP). Unlike other natural disasters, drought is difficult to identify, predict, and mitigate. Drought may have extensive spatial coverage extending up to continents, and large temporal coverage lasting to multiple years, which make drought one of the costliest natural disasters. For instance, the 2015 drought affected more than 330 million people in India. In the last few decades, the frequency of severe droughts has increased in South Asia, causing several challenges to agricultural production and water availability. Moreover, the intense and long-lasting droughts are likely to occur in the warming climate. South Asia is vulnerable to droughts due to its large population and agriculture driven economy. Therefore, understanding the drought risk in the observed and projected future warming climate is essential for adaptation and mitigation.

Observed and projected change in the drought characteristics (intensity, areal extent, duration, and severity) and water availability can be valuable for society, food security, and water management. First, we show the changes in the dryness (the ratio of PET and precipitation) over South Asia in the observed and future climate using data from the Climate Research Unit (CRU) and global climate models from the Coupled Model Intercomparison Project Phase-5 (CMIP5-GCMs), respectively. We find the significant increase in the dryness over the Gangetic Plain and parts of Pakistan during 1951-2016. An increase in the dryness is projected over the majority of South Asia under the 1.5°, 2.0°, and 2.5°C warming worlds. Moreover, increased dryness in the future is projected to affect more than 790(±336) million people living over half of South Asia under the 1.5° warming world. An additional 0.5° and 1.0°C rise from 1.5°C will increase the dryness risk and affect 890 (±485) and 1960 (±1033) million people living in South Asia, respectively. Our results based on the skillful GCMs (the high skill to simulate monsoon features) show contrasting results in comparison to the previous studies based on the multimodel (32 models) ensemble mean. It is noteworthy that the earlier studies based on multimodel ensemble mean show a decline in dryness over South Asia under the warming climate. This contrast in the dryness projection is associated with the low skill GCMs, which contribute to multimodel ensemble mean. Moreover, the low skill GCMs show higher sensitivity of convective precipitation, which results massive (~25%) increase in rainfall and decline in dryness in the multimodel ensemble mean.

Apart from the GCMs, considerable uncertainty in the estimation of potential evapotranspiration (PET) influences drought projections under the warming climate. Using the European Centre for Medium-Range Weather Forecasts Reanalysis version 5 (ERA5) and skillful CMIP5-GCMs, we show

the changes in PET and drought frequency in the observed and projected future climate in different climatic regions over South Asia. We find considerable uncertainty in the PET change during the observed period of 1979-2018, which is primarily due to different methods used for PET estimation. We used five methods to estimate PET (Thornthwaite: PET-TH, Hargreaves- Samani: PET-HS, Penman-Monteith: PET-PM, modified Penman-Monteith: PET-MPM, and Energy: PET-EN) for our analysis. Among the five methods, PET-TH method showed a significant increase in PET during the observed period. However, the other four methods (PET-HS, PET-EN, PET-PM, and PET-MPM) showed a decline in mean annual PET over the majority of South Asia during 1979-2018. The substantial increase in PET-TH is associated with the high-temperature sensitivity of PET-TH in comparison to the other methods (PET-HS, PET-EN, PET-PM, and PET-MPM). Moreover, the drought frequency estimated using these five PET methods showed a similar uncertainty (high drought frequency in SPEI-TH) during the observed period 1979-2018. Further, using the better skill CMIP5-GCMs, we find the increase in PET and drought frequency based on these five methods under the 1.5, 2.0, and 2.5°C warming world over the majority of South Asia. Moreover, the projections of drought frequency based on PET-EN and PET-MPM are consistent with the projection based on soil moisture drought index (SSI) under the warming climate over South Asia. However, the drought projections based on PET-TH are not reliable in the warming climate. Therefore, the projection of drought risk in the warming should be either based on the PET-EN/PET-MPM or based on soil moisture (SSI).

Similar to CMIP5-GCMs, recently, a new generation CMIP6-GCMs are available to assess the water availability and drought risk in the future climate. The studies based on the CMIP6-GCMs reported a decline in the drought frequency over South Asia in the future warming climate. We evaluated sixteen CMIP6-GCMs to examine the potential causes of declining droughts in future climate over South Asia. Consistent with the findings from the CMIP5-GCMs, the multimodel ensemble mean of CMIP6-GCMs is not reliable for drought projections over South Asia. The multimodel ensemble mean of CMIP6-GCMs is considerably influenced by the low skill GCMs. Moreover, the GCMs with lower skill in simulating the key monsoon features are highly sensitive to convective precipitation (20-30% increase) under the warming (1.5, 2.0, and 2.5°C worlds) climate. The high sensitivity of convective precipitation results in a large increase in precipitation under the projected future climate. We show that the skilful GCMs (with better seasonal cycle representation and less monsoon precipitation bias) project an increase in the drought frequency under the 1.5, 2.0, and 2.5°C warming, which consistent with our previous finding. Therefore, the drought risk based on the multimodel ensemble mean of CMIP6-GCMs is underestimated under the projected future warming in South Asia. Overall, the skill of GCMs to simulate the summer monsoon (June-September) in the observed climate need to be estimated before using them for the assessment of water availability and drought risk.

Finally, we examined the worst drought and its implications that occurred in South Asia in the observed climate (1951-2016). Besides, we estimated the risk of the worst observed drought under the projected future climate. We identified the worst drought during the 1951-2016 period using the Variable Infiltration Capacity (VIC) model-simulated soil moisture from the four global observational products [Climate Research Unit: CRU, WATCH-Forcing-Data-ERA-Interim: WFDEI, University of Delaware: UDEL, and Princeton]. Using the observed records, we show that the worst

drought occurred in 2002 with a substantial impact on agricultural production in South Asia. Moreover, our results showed a considerable uncertainty in the number of drought spells and their characteristics due to the four observational products. We conducted soil moisture simulations using the VIC model and meteorological forcing from Community Earth System Model-Large Ensemble (CESM-LENS) to estimate the risk of the worst observed drought in the projected future climate. Our results showed that the frequency of the worst droughts is projected to rise by 1.5 times in the future climate. Moreover, we find a considerable role of industrial aerosols in the occurrence of the worst droughts in South Asia. Overall, our findings have implications for understanding the drought risk in the observed and projected future climate in South Asia, which is essential for planning and management of water resources in one of the most populated regions of the world.

Title: Geotechnical and structural modulation for strength and adsorption enhancement of urban sewage sludge
Researcher: Taki, Kaling
Supervisor: Kumar, Manish
Year: 2020
Keyword's: Urban - Sewage, Underground Construction, Geotechnical And Structural Modulation, Scanning Electron Microscopy (SEM)
Call No.: 624.19 TAK
Acc. No.: T00702

Abstract: Sewage sludge (SS) is the semi-solid slurry obtained as a byproduct in wastewater treatment plant. It is rich in nutrients and harmful compounds such as metals, nano particles, antibiotics, pharmaceutical products, pathogenic bacteria and viruses. Presence of such life-threatening and environmental polluting substance demands efficient management of SS. In the past, different techniques have been explored for the management of SS, such as pyrolysis-gasification, combustion, landfill, incineration and wet oxidation. These techniques are efficient; however, it is not viable for a developing nation like India due to resource constraints. Also, the composition of SS produced in India is dynamic, which further result in additional problems. Unlike developed nations, we do not have a proper lined system, which makes the quality and quantity of SS highly unpredictable. The lack of lined drain arrangement leads to a significant amount of sediment content in wastewater, generating vast amounts of SS. Present thesis work put an effort on developing a green sustainable engineered way to address the management issue of harmful SS towards a cleaner environment. For the study, SS was gathered from the primary settling tank of Jaspur sewage treatment plant, Ahmedabad (India) on June 2018. SS was consisted of 68% silt and 27% clay. Liquid limit (LL) and plastic limit (PL) was 52% and 24%. Based on the obtained geotechnical parameters SS was classified as CH (Highly compressible) type. Upon testing for the critical geotechnical property such as differential free swell index (DFSI), it was observed that SS exhibited expansive behaviour. Change in volume and swell pressure was obtained as 47% and 57 kPa. Volume change behaviour was due to the presence of the expansive mineral montmorillonite. Swell shrink behaviour of SS added another engineering challenge, to use it effectively. To check the applicability of expansive SS for civil geotechnical purpose, SS was treated with lime (CaO). For the study five different SS samples were constituted using 0, 2, 4, 6, and 8% of lime by weight of the SS and cured for 7, 14, and 28 d. Stability of the lime-modified SS was evaluated through the determination of geotechnical, microstructural, and mineralogical properties. A significant improvement in unconfined compressive strength (UCS) from 207 to 1102 kPa was achieved after 28 d of curing SS with 6% lime. Improvement in UCS was due to formation of cementing compounds as a result of pozzolanic reaction.

Marked reductions in swell pressure of 47, 51, 54, and 58% was obtained with 2, 4, 6, and 8% lime treatment. Also, plasticity index decreased with surge in lime percentage for different curing periods, indicating SS has become much more workable and less expansive. Scanning electron microscopy (SEM), X-ray diffraction (XRD), Thermogravimetric analysis (TGA), and Fourier transform

infrared spectroscopy (FTIR) after lime treatment confirmed generation of new compounds, responsible for the improved engineering properties of SS. It was concluded that lime treatment can be an efficient alternative to stabilize SS for potential use as a construction material, for subbase of flexible pavement as per IRC (Indian Road Congress) 37-2012 guidelines. Applicability of SS for civil engineering purpose was further extended by utilizing it as a source material for bricks. One of the motives behind the study, apart from addressing the disposal and management of SS, was to conserve the natural arable soil. In India, the pure alluvial soil is generally utilized as a source material of brick, which affects the crop yield; and exploitation of natural alluvial soil and sands causes immense environmental degradation. In the present work, SS was amended with fly ash (FA) as an admixture, FA was obtained from Gandhinagar thermal power plant (India). Upon geotechnical testing, it was found that FA contains 17%, 82%, 1% of sand, silt and clay fraction type particles and classified as MI (silt of intermediate compressibility) type. LL and PL was reported as 44 and 0%. For the study, FA composition was varied from 0, 10, 20, 30, 40, 50, 60, 70, 80, 90, and 100% in the SS+FA mixture. The study was conducted to understand the dimensional and firing temperature effect on the mechanical properties of synthesized bricks. For exploring the dimensional effect, two extreme size of brick D1 (2x2x2 cm³) and D2 (7x7x7 cm³) was considered and compared with each other. The study found that for all FA combinations, the D1 sample demonstrated higher strength than D2. The increase in load-carrying capacity of smaller sample might be because of the formation of triangle wedges, which was not observed in the case of D2 sample. In order to understand the effect of firing temperature on the mechanical properties of bricks, three different firing temperature i.e., 900, 1000 and 1100°C was selected for the present study.

Study revealed that the maximum strength was demonstrated by the 1100°C fired brick sample, which was due to densification effect achieved by vitrification. It was concluded that the strength exhibited by 1000°C and 1100°C fulfills the requirement for civil engineering construction work as per IS standards (IS 13757:1997 Reaffirmed 2007). Whereas for 900°C, the strength obtained was below the codal provision. Towards the end, research work investigated the potential of utilizing SS as a source material for synthesizing magnetized geopolymer nano adsorbent for removing Arsenic (As) from the aqueous solution. As SS is rich in alumina and silica due to presence of 27% clay fractions, it was proposed to carry out the synthesis of magnetized geopolymer by utilizing SS. The batch experiment was conducted at different initial concentration of As(V) i.e. 10, 20, 30, 40, 50, 70 and 100 ppb for a contact time 15, 30, 45, 60, 75, 90, 120 and 180 min. It was observed that maximum sorption capacity of magnetized geopolymer towards As(V) ($51.6 \pm 3.97 \mu\text{g g}^{-1}$) was obtained at near neutral pH (~ 6.0). Increasing the initial As(V) concentrations from 10 to 100 $\mu\text{g L}^{-1}$, the sorption efficiency also surged from 4.37 to 27.0 $\mu\text{g g}^{-1}$. Adsorption of As(V) onto magnetized geopolymer followed pseudo-second-order ($R^2 \geq 0.95$) and Freundlich ($R^2 \geq 0.98$) kinetic and isotherm models, respectively. Competition studies supported field-scale applicability of the present waste material (SS) converted into a porous, low-cost magnetic geopolymer for removing metalloid As.

Overall, the major highlights of the present thesis work can be summarized as:

- I. 6% lime treatment improved strength, swelling and plasticity characteristics of SS. Also, the treated SS was suitable for subbase pavement construction.
- II. Dimensional effect and firing temperature had a significant influence on compressive strength of bricks. It was found that the 1100°C fired bricks confirms to Indian standards provision for construction purpose.
- III. SS can be utilized for synthesizing geopolymer. Maximum sorption by magnetized geopolymer occurred at near neutral pH (~6). Adsorption of As(V) followed Freundlich ($R^2 \geq 0.98$) isotherm and Pseudo-second-order ($R^2 \geq 0.95$) model.

The present study was carried on SS collected from one treatment plant; it is suggested to conduct studies on samples from different locations. As the composition of SS will vary depending upon the catchment area, season, and monitoring period. The research work demonstrates various framework for successfully utilizing SS to address its management issues. Also, the multidisciplinary utilization of SS demonstrated in the present study as a potential resource will enable researchers to dive deeper and perform comparisons with the present state of art.

Title: Small and large strain shear characteristics of compacted high plasticity clay subjected to static and dynamic loading

Researcher: Kantesaria, Naman Pranilal

Supervisor: Sachan, Ajanta

Year: 2021

Keyword's: Plasticity, Small and Large Strain, CH soil, Geological Formation, Volumetric Behaviour

Call No.: 624 KAN

Acc. No.: T00703

Abstract: High plasticity clays cover a large land area in India and around the world. The high plasticity clayey soils (CH soil) contain a substantial amount of fine-grained particles (<0.075mm) with clay minerals as a primary mineral constituent. CH soils are used in the construction of embankments in water barrier cores of earthen dams, levees, compacted clay liners, canals, etc. They are often used as the most economical material alternative for the construction in the absence of high-quality fill materials. Most of the geotechnical structures involve soil compaction to improve the engineering behaviour of soil. The compaction process significantly alters or destroys the natural microstructure of soil formed during the prolonged geological sedimentation process in several years. The dissimilarity within the microstructural formation has led to significantly different mechanical response of reconstituted and compacted clayey soils. Hence, it is essential to understand the shear behaviour of high plasticity clays under compacted state to develop the reliable constitutive formulations and ensure the safe design of man-made infrastructures. The majority of results, correlations, charts and models available in the literature are based on the experimental investigations of undisturbed or reconstituted clay specimens; while the static and dynamic shear characteristics of high plasticity compacted clays were remained unexplored. Current research involves extensive experimental investigation of the shear strength and yielding response of compacted high plasticity clay in conjunction with the pore pressure and strain energy characteristics under different stress paths and stress states. The influence of combined static and cyclic loading conditions on the dynamic response of compacted CH soil is also evaluated. To cover the entire spectrum of hydromechanical characteristics of compacted CH soil, the experimental study is extended from saturated to unsaturated state with the inclusion of matric and total suction. The experimental results and their analysis presented in the current research can contribute to the knowledge in the field of static and dynamic behaviour of high plasticity compacted clays.

The soil used in the present study was collected from the Left Bank Canal of Gosikhurd dam, Nagpur, India. Stress induced-anisotropy impact on compacted CH soil under saturated and undrained conditions was evaluated by conducting the series of K_0 , anisotropic and isotropic consolidation stress path triaxial testing. The compression and extension triaxial tests were performed on normally and over consolidated ($OCR = 1-10$) specimens of Nagpur soil under different degrees of stress-induced anisotropy ($K_c = \sigma_h'/\sigma_v' = 0.70-1.00$). The results showed that the undrained shear strength reduced with anisotropic consolidation, and its relationship with consolidation stress ratio (K_c) was found to be linear at each OCR levels. The reduction in strength was the highest for extension loading

conditions at normally consolidated state. Strain energy dissipation response displayed that the governing strain energy mechanism shifted from volumetric to shear strain energy, as consolidation state changed from anisotropic to isotropic. The volumetric strain (ϵ_v) during anisotropic consolidation was higher than that of isotropic consolidation at a given mean effective stress. The void ratio was a function of both, the mean effective stress (p') and the deviatoric stress (q) applied during the consolidation. The rate and magnitude of pore pressure generation with increment in deviatoric stress were higher for anisotropically consolidated soil in comparison to isotropically consolidated soil at NC state. Based on the obtained yield surfaces, pre-failure shear behaviour of compacted CH soil was found predominantly elastic for compression loading and elastoplastic for extension loading conditions.

The small strain stiffness and yielding characteristics of compacted CH soil in conjunction with the deformation response at relatively larger strains were studied under undrained boundary conditions. K_0 -consolidated undrained triaxial compression and extension stress path tests have been conducted on compacted Nagpur soil with bender element measurements at different stress path angles (ϑ) ranging from 0° to 304° . The undrained conditions were chosen during stress path shearing to decouple the effect of void ratio variation and stress state variation in the small strain shear modulus (G_{max}) measurement. The experimental results showed that the stress path direction significantly impacted the stress-strain-strength properties of soil as the peak deviatoric stress was found to increase with the increase in stress path angle. The strain at peak deviatoric stress (ϵ_f) was decreased in compression loading and increased in extension loading with the increment in θ . The measured small strain shear modulus (G_{max}) value was observed to be a function of the mean effective stress (p') with a slight dependency on deviatoric stress (q). G_{max} was found to reduce with the increase in strain level during shearing. An empirical correlation was formulated for compacted cohesive soil based on the elastic shear stiffness in pre-yield conditions. The equation to predict the G_{max} was developed as a function of void ratio, effective axial stress and effective radial stress. This correlation was further used to determine the yielding criteria of compacted cohesive soil along with the other two well-established criteria of stress-strain and strain energy. The yield points defined by these methods correspond to a constant strain energy lines, except for the extension stress paths at $\vartheta = 225^\circ$ and 252° . The obtained yield surface was asymmetric around the K_0 consolidation axis, which did not pass through the origin of q - p' stress space.

The cyclic degradation and cyclic pore water pressure response of compacted CH soil under the influence of undrained initial static stress and various dynamic loading conditions were also studied in the current research. A series of strain-controlled undrained (constant volume) cyclic simple shear (CSS) tests were conducted on the saturated specimens of compacted Nagpur soil. The effect of initial static shear stress ($\tau_s/S_u = 0-0.87$), cyclic strain amplitudes ($\gamma_c = 0.5\% - 3.75\%$), frequency ($f = 0.1\text{Hz}-2\text{Hz}$) and number of loading cycles ($N = 1-10000$) was investigated. The results reveal that the presence of initial static shear stress had a detrimental effect on cyclic strength of soil. Initial static shear stress significantly increased the magnitude (δ) and rate (t) of stiffness degradation and cyclic pore water pressure (r_u) generation. The strength under cyclic loading reduced below static shear strength within only five loading cycles. Evolution of cyclic pore water pressure increased with the

increase in cyclic strain amplitude and frequency. Under higher cyclic load, the pore pressure changed its phase and decreased after the certain number of load cycles due to undrained creep effect generated through long-term cyclic loading. The shear modulus (G) increased, and damping ratio (D) reduced with the increase in frequency and decrease in cyclic strain amplitude. The enhanced rate of stiffness degradation was observed to follow a power-law functional relationship with cyclic strain amplitude. The experimental results clearly demonstrated the coupling between cyclic degradation and pore water pressure generation. Strain-based empirical equations were also formulated for the risk assessment of compacted CH soil subjected to combined static and cyclic loading. The equations and design charts were proposed to estimate δ and r_u based on the input parameters of τ_s/S_u , γ_c and N . Comparisons were made between the results of compacted CH soil from present study and the results published in the literature for undisturbed and reconstituted clays. The comparison displayed distinctly different characteristics of compacted clay.

The influence of suction on compacted soil is important to evaluate for the analysis and design of geotechnical structures under unsaturated conditions. In the current study, the effect of a broad range of suction ($\psi_m = 52 \text{ kPa}-97930 \text{ kPa}$) and saturation ($S_r = 10\%-95\%$) on shear and volumetric deformation characteristics of compacted high plasticity clay have been evaluated. The matric and total suction values were obtained using filter paper and dew-point potentiometer tests. Small to large strain dynamic responses were analysed through a series of bender element and cyclic simple shear (CSS) tests. CSS tests were conducted under both stress-controlled and strain-controlled conditions. Additionally, the volumetric deformation response was evaluated using swell pressure and double oedometer tests. Results showed that micro/macro porosity evolutions with different suction and saturation strongly affected the hydromechanical behaviour of compacted high plastic clay. The shear strength (S_u) under static loading and stiffness (G) under large strain dynamic loading increased with the decrease in as- compacted saturation. These parameters attained maximum values at the critical degree of saturation (S_c) around 50%. Afterwards, their values decreased with further reduction in saturation. A similar response has been obtained for collapse potential (CP). The increase of interaggregate capillary water in the form of water-bridges in macro pores is responsible for the enhanced shear behaviour till S_c . In contrast to that, the small strain shear modulus (G_{max}), swell pressure (P_s) and swell potential (SP) increased continuously with the increase in matric suction and reduction in the degree of saturation. The obtained experimental results contradict the general perception regarding the behaviour of unsaturated clays. The results indicated that the strength, stiffness and collapse potential do not always increase with the increase in suction for compacted clays, unlike naturally drying clays. Hence, in addition to suction, the compaction state and generated microstructure should also be considered for the analysis of compacted clay response.

Title: Detection of blockages in a pipeline using fluid transients
Researcher: Kumar, Prabhat
Supervisor: Mohapatra, Pranab K.
Year: 2021
Keyword's: Blockages, Pipeline Fluid Transients, Underground Construction
Call No.: 624.19 KUM
Acc. No.: T00704

Abstract: The network of pipelines irrefutably out-rates other transportation means like truck/train owing to its cost effectiveness, convenience, high land use efficiency, higher reliability, higher degree of security and environmental friendliness over great distances. During their lifetime, pressurized conduits transporting liquids such as freshwater, seawater, sanitary and storm-water, oil, and blood may develop full or partial blockage at discrete locations or distributed over considerable portion of the affected pipeline. The blockages are due to reduction in pipe cross-sectional area caused by various physical and/or chemical processes. Blockages waste energy and financial resources by reducing pipe carrying capacity and can increase the potential for in-pipe water contamination. Since most of pipeline in Water Distribution System are concealed underground, therefore, unlike leaks, the detection of blockages is difficult.

A partial constriction is established due to an unplanned incomplete closure of an in-line valve, formation of ice during cold weather, other physical (sediment deposits) and chemical depositions. Blockages cause minor head loss, diminish the flowing capability, which indirectly amplifies the pumping and over-all business cost to unmanageable positions. Over-pumping also means that escalating air contamination by producing greenhouse gas, thereby raising the carbon footprint of the system. The constrictions deteriorate water quality as they act as a food source supplier for microbes and room for proliferation. Detection of localized deterioration, which is distributed along pipelines in its early stages, helps authorities to maintain, replace, and rehabilitate their pipeline assets cost- effectively and prevents potential pipe failure.

Traditional methods for detecting faults in any faults in a fluid system are either based on manual (or semi-autonomous) examination done either on entire or on a substantial portion of the pipe-network. These approaches are time-consuming and costly, such as semi-autonomous investigation procedures for sewer maintenance. Later, new techniques were developed based on scientific advancements, such as pulse-echo analysis, Vibration analysis, Acoustic Reflectometry, Radioisotope technology and Gamma-Ray Emission. These methods provide useful information about the state of the pipe, but they are highly time-consuming and costly techniques. Low-cost and quick techniques are of paramount importance in detecting partial blockages because, in addition to cost reduction, they also help to diminish service interruption times.

Hydraulic-based technique and tools are put forward to detect location and magnitude of faults such as pipe leaks, constrictions and for estimation of unknown model parameters. Transient pressure waves are considered as capable and smart tool for rapid, cost-effective, and noninvasive detection of localized and distributed deterioration in fluid carrying pipelines. These techniques require the creation of a transient disturbance and the measurement and analysis of the subsequent pressure

responses. Pressure waves accumulate a vast amount of information during their fast propagation through the pipeline system. Such a high-speed transmission of data can be utilized in many practical applications, such as pipe defect detection, condition monitoring, as well as system management. The technique significantly reduces both the interference with the regular functioning of the system and the personnel costs — and the possibility of using low-cost pressure probes. Concerning test duration, unlike acoustic techniques, which require a time-consuming survey of pipes, during transient tests, pressure waves travel fast along the pipe pointing out singularities.

The current research aims to fulfil multiple objectives and research gaps. Precisely:

- [1] The research on transient-based fault detection methods has taken small and steady leaps in the past two decades, and a need for reviewing and compiling them is experienced. Therefore, one of the study's objectives is to compile and publish all the prominent transient-based blockage detection methods.
- [2] Conventionally transient-based methods for detecting faults (e.g., leak or blockage) in the frequency response analysis require measurements that are performed with a large number of valve frequencies. The graphical method proposes a novel technique to overcome obscurity by reducing the number of required oscillating frequencies at the valve.
- [3] Recently few pieces of literature propose an RMOC method for estimation of pipe deteriorations and system parameters. In the current study, the method is modified, and a more generalized edition of the method is proposed. The novelties of the research on Reconstructive MOC (RMOC) methods are as follows: (a) the RMOC method is derived for discrete blockages; (b) the same technique is applied for discrete and extended blockages with due consideration of pipe friction; (c) The method is extended for viscoelastic conduits. The chapter examines the importance of the insertion of viscoelasticity in mathematical modeling. The technique is simple to apply when evaluated with other reconstruction methods.
- [4] Transient laboratory experiments were conducted in which the setup consists of a 26m long GI pipe with an inner diameter of 65 mm. A Machine learning approach coupled with transient is used to determine the size and location of a discrete blockage. Three classes of detection were built. These classes were (a) to distinguish between blocked-unblocked conditions, (b) classification for blockage location, and (c) classification for the magnitude of the blockages. The accuracies of the respective classification were 93.4%, 90.0%, and 80.7%, respectively. Finally, a fourth classifier is put up with the amalgamation of all three cases producing 86.6 % precision.

Title: Uncertainty quantification and design optimization of steel plate shear walls
Researcher: Khan, Nasar Ahmad
Supervisor: Srivastava, Gaurav
Year: 2021
Keyword's: Simulation-based Design, SBD, SPSW, Computational Complexity, Genetic Algorithm
Call No.: 624.1762 KHA
Acc. No.: T00936

Abstract: In recent decades, steel plate shear wall (SPSW) has received widespread attention as a robust and cost-effective lateral load resisting structural system for highrise buildings. Its unique combination of robust post-buckling strength, high initial stiffness, large ductility, stable hysteretic characteristics, and economic viability makes it an ideal lateral load resisting system in highly seismic zones. The SPSW consists of a boundary frame (usually a moment frame) and thin infill plates, either welded or bolted to the confining boundary frame. The system resists lateral load primarily through diagonal tension field (DTF) action in the infill plates, and the boundary members anchor the infill plate forces. Current seismic design provisions require the boundary members to be capacity designed assuming the infill plate has fully yielded in tension and forms a DTF to resist the lateral loads. In this type of SPSW, the columns (VBEs) and beams (HBEs) are designed to anchor the tension field forces. The tension field forces on the frame elements require heavy steel sections, making the construction expensive. Further, the current design provisions have limitations in considering openings in SPSWs.

The design of the SPSW is an iterative process, and one needs to rely on high-fidelity computer models in addition to physical experiments to reduce the overall time, cost, and risk. Such computer models have been a powerful tool that help in understanding and achieving true performance-based designs. Computational advancement and parallel processing have made this choice immensely popular over the last few decades. However, the complexity of these simulations still makes them computationally very intensive. The computational complexity involved in the SPSW is mainly due to its highly nonlinear behavior. Since a large number of simulations are required to be carried out to identify interesting regions in the design space, it can be computationally prohibitive to use such models. The present work focusses on three aspects related to SPSWs: (a) developing a detailed understanding of the behavior (load carrying capacity, stiffness, plate-frame interaction) of SPSWs with respect to their design parameters, (b) developing improved models for prediction of strength and stiffness of SPSWs with different types and configurations of openings, and (c) development of a novel surrogate approach to enable uncertainty quantification and design optimization of SPSW systems.

The behavior was explored through a large number of finite element simulation of different SPSW systems with and without openings. The relative importance of different design parameters was quantified through performance indices and simulation based models for reduction in strength and stiffness due to openings were postulated. The proposed models were found to be better than the earlier available models and are expected to enable a more rational design approach. It was

observed that sufficiently accurate finite element models can take significant amount of computational time (of the order of a few hours on a high-end workstation). Consequently, such full-fidelity computer models cannot be employed for design optimization or even a detailed sensitivity analysis or reliability analysis. To mitigate this, a novel framework was developed to construct surrogate models for SPSWs which could subsequently be used for the required uncertainty quantification procedures.

A number of surrogate modeling strategies were explored out of which, Kriging, polynomial response surface, and radial basis functions were finally selected. An ensemble average approach (weighted average surrogate) was also considered and was found to be the most effective. The overall optimization framework utilized Genetic Algorithm and was designed to primarily utilize the surrogate model with an adaptive mechanism to perform truth checks (executing the full finite element models) based on a cross-validation error metric. A similar approach was developed for reliability analysis (full Monte Carlo as well as first-order reliability method) and sensitivity analysis (using Sobol indices).

It was found that this surrogate-based approach enabled design optimization, sensitivity analysis and reliability analysis which could not have been possible otherwise. For instance, design optimization using the developed SBO framework yielded optimal design parameters using 3.4×10^6 number of surrogate model evaluations and 144 number of full model evaluations taking a total 6.5 days of computational time. However, if the same was to be carried out using the full model the projected computation time requirement would be about 21 years. It is expected that the present work will not only give insights into the behavior of SPSW systems with and without openings, but also pave way for uncertainty quantification of SPSWs (and other complicated engineering systems) for a better design approach.

Title: Development of hydrologic outlook at short to sub-seasonal time scales for India
Researcher: Tiwari, Amar Deep
Supervisor: Mishra, Vimal
Year: 2021
Keyword's: Hydrological Model, Hydrology Sub-season Time, Meteorological Forecast, Streamflow Prediction, Droughts
Call No.: 627.0954 TIW
Acc. No.: T00943

Abstract: At short to sub-seasonal time scales, hydrologic prediction is crucial for water management, agricultural activities, and reservoir operations. Prediction of inflow and storage of reservoirs can be valuable for decision making, which, apart from protecting downstream from flooding, provide water for irrigation and hydropower generation. Reservoirs also reduce the influence of interseasonal and interannual streamflow variability. Climate change has increased the frequency of extreme hydrological events such as droughts and floods, posing water management and food security challenges. Extreme hydrologic events influence reservoir storage and the smooth functioning of reservoir operations. Despite several meteorological forecast products, a comprehensive hydrological prediction system has been lacking in India. Moreover, previous studies on hydrologic prediction in India are mainly focused on drought. In addition, the role of bias correction of meteorological forecast and post-processing of hydrological forecast has not been examined over the Indian river basins. Notwithstanding the importance of a comprehensive hydrologic outlook at short to sub-seasonal lead in India, efforts have been limited. The present work fills this critical research gap in the direction of the development of a hydrologic outlook for the country.

Reservoirs provide water for irrigation and hydropower and protect downstream regions from flooding. Reservoir storage is affected by drought, which hampers the ability to provide water for irrigation and hydropower. Although reservoir storage prediction is needed for planning and decision-making, a reservoir storage forecast system at 1- to 3-month lead has been lacking for major reservoirs in India. Here we evaluate the potential of observed accumulated precipitation, standardized precipitation index (SPI), standardized precipitation evapotranspiration index (SPEI), standardized streamflow index (SSI), and observed reservoir storage to provide a reservoir storage anomaly forecast at 1- to 3-month lead for the dry season (February to May) using a statistical approach. We find that accumulated precipitation for 3–11 months is strongly associated with India's monthly reservoir storage anomalies. Moreover, accumulated precipitation and observed reservoir storage provide a reasonable ($R^2 = 0.7$) forecast skill for reservoir storage anomalies at 1- to 3-month lead. Similarly, SPI and SPEI can predict reservoir storage anomalies at 1- to 3- month lead in India. Since the prediction skill from SPI and SPEI is similar, reservoir storage at a monthly timescale is primarily affected by accumulated precipitation instead of variability in air temperature. We find that the forecast skill for the 1-month lead from SPI, SPEI, and SSI is similar for Indira Sagar (Narmada) and Minimata (Mahanadi) reservoirs. However, prediction skill for reservoir storage anomalies improves substantially using SSI for 2- to 3-month lead. Reservoir storage anomalies

forecast at 1-to 3-month lead can be valuable for water management-related decision-making and planning during the dry season in India.

Meteorological and hydrologic prediction at short to sub-seasonal scales is essential for reservoir operations to mitigate droughts. We examine the skills in the meteorological forecast from the SubX and Extended Range Forecast System (ERFS) for precipitation, maximum and minimum temperatures at 1, 7, 15, and 30 days lead. We bias-corrected meteorological forecasts using the Multivariate Bias Correction (MBC) method for hydrologic prediction. The Variable Infiltration Capacity (VIC) model simulated total runoff and root-zone soil moisture for India. We also developed a streamflow forecast for the five major river basins that have large reservoirs. Bias correction of meteorological forecast (precipitation, maximum and minimum temperatures) resulted in a considerable improvement in hydrologic and meteorological forecast skills. The Environmental Modeling Center (EMC) model from the SubX provides either better or equal forecast skills for the raw meteorological forecast compared to ERFS, an operational product in India. We examined the forecast skills of the meteorological and hydrological products for the two major droughts that occurred recently. We find that most forecast models effectively captured the onset, peak, and termination of the North Indian drought in 2015-16 and the South Indian drought in 2016-17 at a 30-day lead. Bias correction of the meteorological forecast improved the streamflow forecast for the selected drought event upstream of the major reservoirs. The EMC model showed better forecast skills for the two major droughts than other forecast products. Overall, the SubX products show potential for short-to-sub seasonal scale hydrologic prediction that can assist water management in India.

Existing efforts to develop a hydrologic model-based operational streamflow forecast in India are limited. We evaluate the role of bias correction of meteorological forecast and streamflow post-processing on hydrological prediction skills in India. We use the Variable Infiltration Capacity (VIC) model to simulate runoff and root zone soil moisture in the Narmada basin (drainage area: 97,410 km²), which was used as a testbed to examine the forecast skill along with the observed streamflow. We evaluated meteorological and hydrological forecasts during the monsoon (June- September) season for the 2000-2018 period. The raw meteorological forecast displayed relatively low skill against the observed precipitation at 1-3 day lead time during the monsoon season. Similarly, the forecast skill was low with a mean normalized root mean squared error (NRMSE) of more than 0.9 and a mean absolute bias larger than 60% for extreme precipitation at the 1-3- day lead time. We used Empirical Quantile Mapping (EQM) to bias correct the precipitation forecast. The bias correction of the precipitation forecast resulted in significant improvement in the precipitation forecast skill. Runoff and root zone soil moisture forecasts were also significantly improved due to bias correction of the precipitation forecast where the forecast evaluation is performed against the reference model run. However, bias correction of precipitation forecast did not cause considerable improvement in the streamflow prediction. Bias correction of streamflow forecast performs better than the streamflow forecast simulated using the bias-corrected meteorological forecast. The combination of the bias correction of precipitation forecast and post- processing of streamflow

resulted in a significant improvement in the streamflow prediction (reduction in bias from 40% to 5%).

Real-time monitoring and early warning systems are essential for decision making for managing water resources and agricultural activities. Notwithstanding the considerable progress in operational weather and climate forecast in India, efforts to develop hydrologic prediction systems utilizing the meteorological forecast have been lacking. We develop a hydrologic outlook for precipitation, temperature, runoff, soil moisture, and streamflow at a short-to-monthly lead time. We examined the role of bias correction of the meteorological, hydrological, and both meteorological and hydrological forecasts on the prediction skills of hydrologic outlook components. The raw forecast from the Extended Range Forecast System (ERFS) showed dry bias in precipitation and warm bias in minimum temperature, which was significantly improved after the bias correction. As the bias correction of meteorological and hydrological forecasts resulted in the best prediction skills, we developed the hydrologic outlook. Hydrologic outlook demonstrated reasonable forecast skills at 1-30 day lead time for extreme dry and wet conditions and streamflow upstream of major reservoirs. The developed framework of hydrologic outlook can assist the decision making in water resources and agriculture in India.

Title: 3D CFD modeling of the open channel junction flow on fixed and mobile beds
Researcher: Pandey, Abhishek Kumar
Supervisor: Mohapatra, Pranab K.
Year: 2022
Keyword's: Computational Fluid Dynamics (CFD), Flow Separation Zone (FSZ), Largeeddy Simulation (LES), Kelvin-Helmholtz Instability, Bed Morphology
Call No.: 624 PAN
Acc. No.: T00968

Abstract: Combining open channel junction flow occurs in natural and human-made hydraulic systems. Channel junction may pose risks related to flooding, pollutants dispersal, and morphological changes of bed and banks. A proper understanding of the junction flow dynamics is essential to analyze the associated processes like bed morphology, pollution transport, etc. The present doctoral dissertation identifies five major research objectives, which are relatively unstudied about combining open channel junction hydraulics. Three-dimensional (3D) computational fluid dynamics (CFD) simulations are conducted to achieve the research objectives. The junction hydraulics is strongly three-dimensional (3D), and the flow separation zone (FSZ) is one of the main flow characteristics. The FSZ is formed downstream of the junction corner as the tributary flow separates. The earlier studies concerning the flow separation were conducted for which the maximum junction angle was up to 90-degree. Other than the considered channel junction in the literature, there could be the case of opposing channel flow in which the junction angle is 180-degree. The 180-degree channel junction is common in drainage networks. As the flows from the opposing channels meet, two flow separation zones are formed at the junction corners, reducing the effective width significantly. Characterization of the flow separation zone at the opposing channel flow is required. Eighty-one different cases are simulated using the CFD model (Ansys Fluent) to study the effect of the flow conditions, downstream Froude number, width ratio, and aspect ratio of exit channel on opposing channel flow hydraulics. The model is validated against the published experimental data of the flow field. Empirical equations for contraction coefficient, flow depth ratio, and minimum water depth in the contracted flow region are developed as a function of the flow conditions, downstream Froude number, and width ratio using regression analysis.

The flow separation zone is associated with turbulent eddies, reduction of effective width, increased shear stress, momentum deficit, and energy loss. Hence, the reduction of the FSZ is desirable. The effect of continuous suction and blowing perturbations in reducing the FSZ at a right-angled open channel junction is quantified. The flow field is simulated using CFD software Ansys Fluent. The numerical model is validated by comparing the simulated velocity field, water surface elevation, and energy loss for the unperturbed junction flow with corresponding experimental results available in the literature. The continuous suction and blowing perturbation is generated by a sinusoidal function with zero net discharge and is applied through a rectangular slit. Three different slit locations are considered downstream of the junction. The simulated results (time-averaged) show that the sinusoidal perturbation is effective in reducing the dimensions of the FSZ and, consequently,

the energy loss and bed shear stress. The results demonstrate the enhanced effectiveness in reducing the energy loss when the slit is more proximate to the junction for the present flow configuration and choice of the characteristics of the sinusoidal perturbation.

Other than the flow separation zone (FSZ), the shear layer is one of the essential flow features at the junction. It is characterized by a high turbulence level and populated with coherent structures. The present understanding of the turbulence at the junction is limited to the shear layer of the mixing interface, which is predominantly two-dimensional and almost stable. Apart from the shear layer of the mixing interface, the shear layer is also developed between the flow separation zone and the tributary inflow. The turbulence within the shear layer associated with the FSZ may show incoherence, unlike those associated with the mixing interface. As the FSZ is a momentum deficit region, the shear layer developed between the FSZ and tributary inflows may undergo the Kelvin-Helmholtz instability (K-H) to a larger extent owing to the enormous momentum difference. Though the FSZ may not be fully evolved at the natural river confluence due to the rounding of the downstream confluence corner or the topographic steering owing to the deposition bar, the presence of the FSZ becomes indispensable in the many human-made systems of drainage and water distribution where the downstream junction corner is sharp. Hence, a comprehensive study is required for the shear layer of the flow separation zone. Moreover, the coherent structures govern pollutant transport; the present study attempts to understand the role of the turbulent structures in the pollutant transport at the junction. The knowledge about the pollution transport at the junction is helpful for the environmental management and evaluation of risk associated with the accidental release of the hazardous pollutants. The Large-eddy simulation (LES) model is chosen to resolve the turbulent structures. To study the pollutants mixing patterns at the junction, the mass fraction of the neutrally buoyant, conservative tracer is predicted by solving the convection-diffusion equation. The numerical model is validated against detailed measurements of the velocity field and turbulent kinetic energy. The distributions of the tracer mass fraction at different locations show the enhanced mixing for the deformed bed junction arising from the strong lateral currents. The present study highlights the major role of turbulent structures in the evolutions of pollutants transport at the junction.

Understanding the flood wave propagation and its accurate predictions at the channel junction is essential for water management, flood mitigation, and environmental protection. The flood routing at a channel junction by shallow water equations does not accurately represent the dynamic interaction between the main flow and tributary flow. Therefore, the study uses a 3D CFD model. The transient Reynolds-averaged Navier-Stokes (RANS) model is validated against the published experimental results of the unsteady channel junction flow induced by the dam-break flow. Three different cases (Cases 1, 2, and 3) are considered by applying a half-cycle sinusoidal flood wave at the inlet of the main channel, tributary channel, and both the channels, respectively. The steady-state junction flow with equal discharge in both the upstream channels is considered as the initial condition. The simulated results show that the rising flood flow in the main channel acts as an obstruction for the tributary channel flow in Case 1, while vice versa in Case 2. This leads to partial flow passage into the junction while part of the flow is reflected upstream, leading to stage rise. The

maximum stage rise occurs in Case 3 due to the pronounced combined effects of the rising flood wave and flow obstruction simultaneously. The evolution of the flow obstruction at the junction is visualized using the velocity vectors at different time instants.

The bed morphology in a channel junction shows characteristic features, including the scour zone and the deposition bar. Predicting the bed morphological changes at a junction is crucial from the environmental, ecological, design, and management perspectives. The transient RANS equations with the renormalized group (RNG) $k - \epsilon$ as turbulence closure are solved to simulate the flow field. The bed-load sediment transport rate is computed using the Meyer-Peter and Muller equation. The convection-diffusion equation is solved for the sediment concentration distribution, and the sediment continuity equation is used for the bed evolution. The numerical model is validated against the published laboratory data for junction bed morphology. The mutual relationship between the bed morphology and flow field evolution is investigated. The helical cell developed near the bed region generates an elongated tube-shaped turbulent structure. The helical cell and, thus, the tube-shaped turbulent structure grows wider due to the junction bed deformation, which ultimately results in enlargement of the zone of the high values of bed shear stress. The simulated results show that the length of the flow separation zone is reduced due to the topographic steering.

Title: Predictive modelling for the occurrence, prevalence, fate and transport of contaminants in the aquatic system

Researcher: Singh, Ashwin

Supervisor: Kumar, Manish

Year: 2022

Keyword's: Geogenic Contaminants, Inorganic and Biotic ligand Based Metal Speciation, Biotic ligand Model (BLM), Anthropogenic Nutrient Enrichment

Call No.: 624 SIN

Acc. No.: T00969

Abstract: The northern floodplains of India are believed to be the world's most anthropogenic stressed regions. Evaluating the aquatic system's vulnerability in terms of evolution and resilience is a challenging and stimulating task at the same time. The complexities in predicting the toxicity is characterized by extreme population density, high geomorphic differentiation and intricate contaminant enrichment process. Thereby making the study of the different aquatic systems an exhaustive science to explore. Through the current thesis work an attempt has been made to identify, quantify and propose a probabilistic model to reveal the interaction mechanism of various geogenic and anthropogenic contaminants across seasonal variability and geomorphic shifts. Based on available literary evidence, geological formations, hydro-chemical understanding, atmospheric sensitivity and fluvial dependency, different geographical proxies were identified in respective aquatic systems that acted as a closest link in establishing an interaction pathway. Therefore, for the study area two groundwater Alluvial setups were selected in the Mid-Gangetic floodplain (MGF) (Buxar and Darbhanga) and one in the Brahmaputra floodplain (BFP) (Guwahati), followed by one study setup each in the lake (Deepor Beel lake in Guwahati) and coastal water of Bay of Bengal. *In-situ* and secondary data analysis established that within the floodplains, arsenic enrichment via hydrolysis from the secondary sulphide minerals causes major population vulnerability. Natural recharge and groundwater fluctuation during monsoon season cause Fe-OOH production, facilitating mobilization of arsenic in the groundwater system. Further, high groundwater pumping brings these contaminants in close proximity with ecologically sensitive aquatic system like lakes and coastal water. In order to evaluate the sensitivity of the static surface water system, different modelling techniques including inverse methods, biotic ligand models, satellite and in-situ derived datasets were used. The model for water quality assessment has been developed using an autotrophic species (*ceriodaphnia dubia*) as a possible marker which signifies the lake health by acknowledging the contributions of labile metal loading and vacant biotic ligand sites. Finally, the role of nutrient in possibly changing the marine bio-geochemistry has been studied in details. The thesis when put together provides a comprehensive evaluation scheme for developing a robust methodology for assessing risk.

CHAPTER 1: Prediction of Geogenic Contaminants in the Urban and Alluvial Aquifer Systems

This chapter of the thesis deals with understanding the mechanism that is responsible for the release of contaminant, especially arsenic, in the groundwater system of MGP and BFP. Kriging based probabilistic mapping and ANN trained Markov-chain based

urbanization prediction schemes were applied in tandem to demarcate the specific contributions of physico-chemical parameters controlling the enrichment process. Using a bottom-top approach, firstly different small geomorphic settings at district level, designated as arsenic hotspots by the government agencies of India, were identified. The different settings were selected based on the criteria of its (i) population, (ii) reported arsenic exposure, (iii) proximity to fluvial disturbances and (iv) soil physical characteristics. While the degree of arsenic exposure remained relatively similar in both the floodplains but the factors controlling the dissolution and mobilization were altogether different. In case of MGP, the theory of natural recharge led arsenic dissolution was found to be most viable whereas in case of BFP, the dissolution of arsenic from iron-oxy-hydroxide surfaces remains the most appropriate answer that could explain the situation. After an initial assessment of the situation through the district level study, the activity of the processes in the floodplains were compared. It was found to be tracing the pattern and behaviour in terms of the arsenic mobilization process similar to their respective smaller geomorphic settings. The sensitivity of the fluvial loading on the enrichment process was evaluated by demarcating the contribution of river formations on the arsenic enrichment process for which another geomorphic setting (Buxar) was selected. Through this study, it is established that fluvial forcing does bring a sharp characteristic change in the physico-chemical behaviour of the soil which seems to be directly promoting the concentration of the arsenic in the groundwater.

The core objectives of the chapter in a nutshell are:

- Developing a probabilistic spatial model for tracing the hydrogeochemical processes aiding in arsenic enrichment over time.
- Modelling the future urbanization pattern through a stochastic land change model to identify the gaps and incoherence in the city planning in arsenic hotspot zones.
- Establishing a framework to quantify the contribution of meandering scars in promoting arsenic vulnerability in the floodplains.

CHAPTER 2: Inorganic and Biotic Ligand based Metal Speciation and Toxicity Prediction in the Lake Environment

While the groundwater had highest exposure of geogenic contaminants but an altogether different scenario was revealed in case of static surface water systems, especially lake. This led us to focus on demarcating the evolving hydro-dynamics at a lake level. This chapter of the thesis deals with developing a risk assessment model for the lakes located in the northern floodplains of India. In this regard an ecologically sensitive lake (Deepor Beel located in the Brahmaputra floodplain) was selected for understanding the existing risks in the lake system due to a combination of factors, including (i) anthropogenic leaching of toxic metals from the industries reaching as surface runoff, (ii) geogenic contaminant like arsenic intruding possibly through water table fluctuation, (iii) soil mediated responses and (iv) abnormality with regards to behaviour of lower autotrophic species in terms of growth and mortality. To tackle the problem from an ecological vulnerability perspective, ceriodaphnia dubia species was used as a marker to model the anthropogenic threat using Biotic Ligand Model (BLM) and other inverse modelling techniques. Time varying Hazard risk of different metal species and their corresponding competition with major

cations were evaluated to suggest the existing risk in the lake for the survival of the different aquatic species. This chapter brings forward a new approach towards assessment of lake health in the northern floodplains of India, currently facing direct human interferences and are on a verge of ecological destruction. The core objectives of the chapter are:

- Investigating the variability in the contaminant enrichment process in a static lake water source as compared to the groundwater.
- Developing an Inorganic/Biotic ligand model to simulate the vulnerability over major autotrophic species in the lake accounting the major operative hydro-chemical processes.
- Assessing the potential of soil and immediate landforms in providing feedback to the lake resilience.

CHAPTER 3: Drivers of Anthropogenic Nutrient Enrichment in the Coastal Setup.

A major question however, remained unanswered regarding the status of the nutrient led eutrophication in the coastal water of the Bay of Bengal, which certainly is contributed majorly by the surface run-off from these floodplains. Therefore, the last chapter is devoted towards understanding the final outcome of nutrient loaded river and lake discharge of the Gangetic and the Brahmaputra floodplains in the Bay of Bengal. In this case the data from NASA Ocean Biogeochemical Model (NOBM) regarding the various phytoplankton species including (i) coccolithophores, (ii) cyanobacteria, (iii) diatoms and (iv) chlorophytes was used to understand spatially and temporally the extent of the active nutrient enrichment process. Further, the concentration of iron and chlorophyll an in terms of mmoles/liter provides an active account of the biogeochemical mixing. It is established that these phytoplankton species, though sensitive to iron recycling capacity, reciprocate to changes in the discharge caused by the draining rivers. Our understanding of the chapter could be used directly for predicting the ocean health in event of a catastrophe observed in the river discharge of Ganga and Brahmaputra. The core objectives of the chapter in a nutshell are:

- Developing a satellite-based monitoring framework for quantifying the spatial and temporal extent of the nutrient enrichment process.
- Exploring the relationship between the major plankton species and their symbiotic role in controlling the ocean biogeochemical cycle.
- Developing a conceptual model of understanding to identify a near future eutrophication outbreak.

The present thesis provides a detailed investigation and a novel framework of risk assessment particularly to the water quality issues of the MGP and BFP which have often been ignored. The outcome of the thesis will be stepping stone towards developing a high precision model to predict the toxicity in different aquatic system at a high spatial and temporal scale

Title: Urban heat island in India: drivers, variations, and interactions
Researcher: Kumar, Rahul (15310055)
Supervisor: Mishra, Vimal
Year: 2021
Keyword's: Surface Urban Heat Island, Moderate Resolution Imaging Spectroradiometer (MODIS), Community land Model (CLM), Hysteresis Patterns
Call No.: 624.1 KUM
Acc. No.: T00970

Abstract: India has witnessed unprecedented urban growth that is likely to increase in the coming decades. Moreover, India experienced some of the most severe heat waves (e.g. 2015) that caused substantial mortality. Understanding the role of urban and surrounding non-urban areas on the UHI intensity can provide policy insights that can help urban planning and managing public health. We studied the Surface Urban Heat Island (UHI/SUHI) effect in 89 cities/urban areas that the Government of India considered developing smart cities, using Moderate Resolution Imaging Spectroradiometer (MODIS) satellite derived Land Surface Temperature (LST) data. We, for the first time, evaluated the role of agriculture, irrigation, and atmospheric aerosols using the combination of in-situ and remotely sensed data and land surface and climate models. Our observations and climate models show that agriculture and irrigation are the two dominant drivers of UHI in India. Moreover, our modelling results demonstrate that a significant presence of atmospheric aerosols over the urban areas can influence UHI. The findings have implications for future planning and decision making as rapid growth in urbanization and irrigation is expected in the coming decades. Rapidly growing urban areas in India show a robust UHI phenomenon at night with an intensity of 1-5°C in the pre and post- monsoon seasons. Nighttime UHI can have implications during the heat waves when the daytime temperature is substantially high. Moreover, nighttime UHI and heat stress may increase further in response to climate warming. Therefore, to avoid detrimental impacts of nighttime UHI in rapidly urbanizing India, additional mitigation strategies are required, which can help diminish the impacts of climate warming. Our results show that during the peak summer months (April to May) when heatwaves occur in India, the daytime surface temperature of urban-core regions is lower than their surrounding non-urban areas (Urban Cool Island (UCI) effect). The UCI phenomenon is largely driven by agriculture and irrigation in non-urban areas, while atmospheric aerosols can also partially contribute to daytime urban cooling. Our study highlights the complexity of attributing the UHI/UCI phenomenon across India and contributes to an improved understanding of the role of human effects (irrigation) and agricultural activities as well as aerosol loading that has remained largely unexplored in the past. These findings, as well as the scale of the study, are new in the field.

After ascertaining the mechanisms and factors affecting UHI/UCI, we studied the response of urban systems with heatwaves, a large scale event. Several studies suggested an amplification of temperatures during heatwaves to a larger extent than the surrounding rural regions. However, such responses were not observed in the Indian context; rather, we observed that the surrounding rural region experienced a higher degree of amplification during heatwaves. This was attributed to

summer term loss in crop and moisture because of prevalent agricultural practices around the urban setups. We evaluated the changes in extreme hot days/nights and heatwave intensification at the 89 major urban locations in India using in-situ, satellite and simulation datasets. We observed that the majority (44%) of the selected locations show a significant rise in extreme hot-day frequency in 1951-2016. In comparison, 35% of the urban locations experienced a decline in extreme hot-nights frequency in the same period. Our results show a significant decline in the change in frequency of hot nights concentrated in the Indo- Gangetic Plain (IGP). Using Community Land Model (CLM) simulations, we show that intensive irrigation is associated with significant cooling in IGP, which can be attributed to the decline in the frequency of extreme hot nights as compared to the rest of India. We further examined the amplification of differences in temperatures in urban and non-urban systems (SUHI) during heatwaves as an indicator of the impact of urbanization on heatwave intensification using MODIS LST datasets. We used changes in SUHI during heatwaves with respect to reference non-heatwave days since LST is closely related to land-use change and can better explain the urban and non-urban temperature contrast. We show that the majority of the urban locations (63% and 74%, respectively) show a decline in SUHI intensities during heatwaves both at day and night times. Our observations are in contrast with studies showing synergistic responses between heatwaves and UHI. The effect of urbanization can be explained by disentangling the urban and non-urban responses during heatwaves. We find that during heatwaves the daytime LST amplification in non-urban regions was significantly higher (1.94 °C) than the amplification in the urban areas (0.14 °C) for all selected locations [on top of higher non-urban base temperature than urban areas]. Our results show that heatwaves do not amplify SUHI intensity in India have implications for urban planning in India. Such observations were never reported worldwide as urban setups had predominantly faced UCI effect, which is contrary to the rest of the world.

Finally, we examined the seasonal variation of UHI for the urban areas. UHI can be affected by the radiation budget and land-use configuration of the local and urban-rural environment. But, the impact of background climate on seasonal variation is largely not well understood. Few studies based on remotely sensed data identified seasonal hysteresis like patterns in SUHI with the surrounding Reference Temperature (T_{ref}). The hysteresis pattern is usually seen with monthly average UHI and T_{refs} , which highlights the non-linear response of UHI with T_{ref} . The major hypothesis explaining the hysteresis is based on time-lags between the surface energy budget of cities, with a major contribution of solar radiation and energy/water fluxes of rural areas, regulated by regional climate and vegetation seasonality. The major focus was on the regional effect of hysteresis patterns and the association of shape parameters with seasonal temperature. We categorized the hysteresis patterns into five categories to explain the underlying regional effects. The urban areas in Indo-Gangetic Plain (IGP), which has relatively higher irrigation and agricultural activities, have the most concentration of type 1 hysteresis pattern. The type 1 pattern shows a relatively higher seasonal difference in UHI with respect to T_{ref} . We did not find much evidence of background climate on the hysteresis shapes or patterns. The daytime and nighttime hysteresis patterns were largely distinct, indicating different drivers at play. The type 4 hysteresis pattern is sparsely distributed in the mid and southern parts of India in the daytime. This type of pattern indicates nearly (or inversely) proportional T_{ref} with respect to UHI values. We then attempted to identify the sensitivity of

seasonal UHI with changes in Ref. T with shape factors of hysteresis ranges. The UHIs in IGP and Kerala region, for both summer and winter term, shows higher sensitivity towards T_{ref} in IGP. The nighttime UHIs in IGP during winters show the least sensitivity. However, the correlation between UHIs and T_{ref} anomaly shows different patterns. In contrast to the ratios indicating sensitivity in the IGP, the region has a low correlation. Most of the regions for both summer and winter term show a negative correlation with more prominent at day time than nighttime. In conclusion, the urban area with type 4 hysteresis does not show much seasonal differences in UHI with T_{ref} . Most of these areas follows negative relation between UHI and T_{ref} . Majority of the seasonal variation observed is in the types 1-3 at day time while a weak response is observed in the nighttime. The type 1 and type 2 hysteresis at nighttime show an upper threshold, and UHI inclines for a few months from Dec-Jan to Feb-March and declines as temperature rises. The UHI patterns are affected by the background climate and vegetation as observed in the IGP region. The region also has more irrigation and agricultural activities. The IGP region although has low correlation values at night and weak negative during daytime in summer; however, shape factor ratios show changes in response to low vegetation and irrigation cooling available in the non-urban belt.

Title: Characteristics and drivers of riverine floods in India
Researcher: Nanditha, J. S.
Supervisor: Mishra, Vimal
Year: 2023
Keyword's: Natural Calamity - Flood, Percipitation-riverine, Global Circulation Models
Call No.: 624 NAN
Acc. No.: T01018

Abstract: Floods are a recurrent natural disaster in India, directly impacting the lives of a large section of people and indirectly affecting the socio-economic facets of the country at large. Indian subcontinent has witnessed many of the world's largest floods, mainly during the summer monsoon season from June-September. According to the Central Water Commission, over a hundred thousand lives were lost to floods in the 65 years from 1952 to 2018. On the contrary, Global Flood Database indicate floods caused the death of over a hundred thousand people in India from 2000-2018 and displaced over 0.2 billion people. India houses a few of the world's most flood-affected river basins, like Ganga, Brahmaputra and Indus, making over 14% of Indian land area prone to flooding. Of which, 16% of the flood-prone area (over 75,000 km²) is affected annually, directly exposing over 100 million people to floods. Flood exposure in India increased by more than 20% in 2000-2015, which can be mainly attributed to increased urbanization and the vulnerability of people, forcing them to settle in flood-prone regions. Due to the increased population exposure of floods, the economic losses are growing every year. For instance, the economic losses in 2018 exceeded 2.6 times that of 2017, with an annual average flood damage of 18 billion INR. The total economic loss from 1952-2018 is over 4.69 trillion INR. Floods and the associated direct and indirect losses significantly impede the socio-economic growth of developing countries like India. Proper management and adaptation plan is necessary to reduce the fatalities and impacts of flooding.

Floods are a complex natural phenomenon driven by multiple factors, of which precipitation plays an important role. The antecedent catchment conditions, land use land cover, direct human interventions like reservoirs and river training, the characteristics of catchments, and the intensity, duration and orientation of precipitating storms generate flooding. However, there is a lack of understanding of the prominent flood drivers in the Indian river basins. There is high confidence that climate change has increased the frequency and intensity of extreme precipitation. Therefore, it is imperative to know the impact of extreme precipitation on floods as it is one of the primary drivers. Identifying the prominent causative drivers and mechanisms of flooding is inevitable to devise suitable adaptation and mitigation policies in a warming climate.

An in-depth understanding of the relative role of various flood drivers in the Indian subcontinental basins has been lacking. Multiple factors, including atmospheric and land surface conditions and moisture sources and pathways, are relevant in flood generation in rain-fed river basins. However, floods in Indian river basins are mainly studied considering the role of extreme precipitation. We conducted a pilot study in the Narmada River basin in central India. We investigated the combined role of extreme precipitation, soil moisture, atmospheric characteristics and moisture sources on

floods in the basin during 1951 – 2018 period. Most of the high flow events in the basin occur during August and September, and about 80% of them are caused by extreme precipitation on wet antecedent soil moisture. The atmospheric characteristics associated with flood producing storms reveal a high amount of vertically integrated water vapor flux, low mean sea level pressure, and strong westerly winds. The Arabian Sea is the primary moisture source for flood producing storms. However, the hitherto unrecognized north Indian plain is also a dominant source of flood producing storms in the upstream subbasins during the mid and late monsoon season. In the upstream subbasins, the moisture recycled from the land surface is the prominent moisture source. In contrast, moisture from the Arabian Sea is higher in the downstream subbasins. The linkage between land, ocean and atmosphere can assist in developing a skilful early flood warning system for the Indian river basins.

Understanding the prominent flood drivers in the observed climate will help monitor the changes to these drivers in a warming climate and their impact on flood projections. However, there is a lack of understanding of flood rivers in the Indian river basins in the observed and projected future climate. We used a novel framework to determine the immediate flood trigger based on the antecedent moisture conditions and precipitation characteristics before high flow events. We used four flood drivers, a combination of antecedent soil moisture and extreme precipitation. We estimated the probability of occurrence of these flood drivers and their association with peak flood magnitude in Indian river basins. We found multiday precipitation, a proxy for heavy precipitation on wet soil conditions, is the predominant flood driver in the observed and projected future climate. We show that multiday precipitation is a more prominent driver than extreme soil moisture conditions in larger river basins, while extreme precipitation drives floods in smaller river basins. The frequency of high flows and their drivers is projected to rise, which may pose a greater risk to agriculture and infrastructure under the warming climate.

Widespread floods that simultaneously affect multiple subbasins in a river basin are more disastrous than localized flooding. Therefore, understanding the mechanisms, drivers and probability of widespread flooding is pertinent for devising suitable policy measures. We investigated the occurrence and drivers of widespread flooding in seven Indian sub-continental river basins during the observed climate (1959-2020). We used a novel framework for identifying widespread floods. Further, we used non-stationary extreme value distribution to identify the mechanisms of widespread flooding. We found that the peninsular river basins have a high probability of widespread flooding (>15%), while the transboundary basins of Ganga and Brahmaputra have a low probability (<10%). We found considerable variability in widespread probability across the subcontinental river basins, which can be attributed to the antecedent catchment moisture conditions and the relative rareness of high flows across different subbasins. Favourable antecedent baseflow and soil moisture conditions, uniform precipitation distribution, and streamflow seasonality determine the seasonality and probability of widespread floods. Large atmospheric circulations are associated with widespread floods, which result in near-uniform precipitation within a river basin. However, we found no significant relation between widespread floods and oceanic

circulations. Our findings highlight the prominent drivers and mechanisms of widespread floods with implications for flood mitigation in India.

Due to the large spatial extent, widespread floods cause substantial challenges to disaster management and flood rehabilitation measures. We found a high probability of widespread floods in the observed climate in the Indian subcontinental river basins. However, there is a lack of understanding of the projected changes in widespread floods in a warming climate. We used 15 Global Circulation Models (GCMs) from the Climate Model Intercomparison Project Phase 6 (CMIP6) to evaluate the future changes in widespread floods. Catchment-scale uniform distribution of precipitation is an important driver of widespread floods. Therefore, we identify the linkage between the spatial extent of extreme precipitation and high flows in Indian river basins. In the observed climate, the fragmented increase in the trends in extreme precipitation precludes the translation of extreme precipitation to high flows. Nevertheless, the fraction of the catchment area that receives extreme precipitation is projected to increase in a warming climate along with the frequency of extreme precipitation leading to an increased frequency of widespread floods.

The CMIP6 GCMs exhibit substantial variability in future projections. Our results show that caution is needed in selecting suitable models representing the spatial variability of extreme precipitation to reduce the uncertainty in flood projections. We find significant differences in the frequency of flood projections between the BEST and POOR performing GCMs in a warming climate. POOR GCMs overestimate the frequency of extreme precipitation and widespread floods compared to BEST GCMs which can be attributed to the underestimation of monsoonal break spells in POOR GCMs. The break and active spells are part of the intraseasonal oscillations (MISO) of the Indian Summer Monsoon Rainfall (ISMR). The accurate predictions of MISO are crucial in improving precipitation and flood projections in a warming climate. Despite the high inter-model variability, a robust increase in widespread floods is projected across the GCMs, which has implications for flood management in Indian river basins.

The thesis broadens the understanding of the causative drivers of riverine floods in the Indian river basins. Our results identify the relative role of catchment factors, atmospheric characteristics and precipitation dynamics in driving high flows in the observed and future climates. Moreover, the results highlight the possible uncertainties in projecting riverine floods using GCMs.

Title: Development of design tools for serviceability design of rigid-faced GRS walls
Researcher: Krishna, Kolli Mohan
Supervisor: Prashant, Amit
Year: 2023
Keyword's: Geosynthetic Reinforced Soil (GRS), Rigid-Faced, Planar Polymeric Materials
Call No.: 624.17 KRI
Acc. No.: T01020

Abstract: The increase in the infrastructure needs over the past three decades around the globe resulted in the diverse applications of Geosynthetic Reinforced Soil (GRS) walls. The critical applications include embankments and load-bearing abutments for highways and railways other than typical retaining walls. The serviceability of such structures is an essential part of the design, which involves limiting displacements of the structure to a certain level based on the importance/requirement of the application. A comprehensive methodology for serviceability/deformation-based design of full-height panel rigid fascia (RF) GRS walls is missing in the literature and design practice. Further, innovative design configurations and component designs must handle the serviceability challenges raised due to differential settlements.

Initially, the mechanical behaviour of RF-GRS walls is studied by two-dimensional (2-D) Finite Element (FE) analysis in OpenSEES. Estimating realistic displacements is important for GRS walls' serviceability/deformation-based design. The mechanical response of the RF-GRS wall depends significantly on the considered modeling approach for soil-reinforcement interfaces. The bonded soil-reinforcement modeling approach is inadequate in many situations, like high walls, where large interface displacements are expected as per design. The selection of interface shear stiffness for frictional contacts is critical under working stress conditions to estimate displacements precisely. A simplified method is proposed to calibrate interface stiffness and strength from laboratory interface tests. The results at the end of construction show that the bonded soil-reinforcement interface underpredicts the total fascia displacements and external displacements of the RF-GRS wall compared to the frictional interface. The effect is 2-6 times in a 6 m high wall and 1.5-3 times in a 3 m high wall. It is also observed that the high shear stiffness of the interface generally leads to low displacements. The surface settlement of the wall with bonded soil-reinforcement interface is 2-3 times less than the frictional interface. The bonded interfaces produce local stress concentrations at the end of reinforcements creating a much different force distribution profile at local zones than the frictional interface.

Further, it is observed the toe is a load-carrying component in RF-GRS walls and significantly affects the mechanical response. The effect of toe conditions on the design of GRS walls has been generally ignored. Development of tools for serviceability designs and refinement of current design methods require a complete understanding of the role of toe conditions. 2-D FE analysis of RF-GRS walls is carried out by considering different toe conditions, such as fixed, rotating and frictional toe, representing different possible construction methods. The analysis of fixed toe conditions shows 3 to 5 times lower deformations and 10 to 20 times less load in bottom reinforcements compared to other toe conditions. Reduced reinforcement lengths at the bottom of the wall for a fixed toe

condition do not affect the deformations. The fascia experiences high bending moments at the bottom in such toe conditions, which the present designs do not consider. Frictional toe condition mobilized sliding and rotation mode of deformation of the wall. It also shows the toe force increasing by 5- 20% for embedment depth increase by 6 times. The results for rotating toe with restrained sliding show higher top displacements than other toe conditions. The use of stiffer reinforcements at the wall top reduces such rotations.

The conventional force-based limit equilibrium design suggested by present design guidelines is insufficient in applications requiring stringent deformation criteria. The observed load transfer mechanisms from the first two studies are used to develop three mechanistic models to estimate the horizontal displacements of a full-height panel RF-GRS wall. The models capture the possible deformation modes of the RF-GRS wall at the end of construction and during the operational stages. A beam with springs model subjected to earth pressure is proposed for estimating internal deformations of the reinforced zone considering the active and pull-out mechanisms. A multi-sliding model is proposed to capture external displacements caused by sliding at reinforcement levels. Also, a model for sliding at the foundation level is proposed. The superposition of these three mechanistic models predicts the total fascia displacement profile of the RF-GRS wall. The predictions of the proposed integrated model are compared with available deformation estimation equations in literature and FE results. It is found that the present ensemble is more reliable due to its mechanistic nature.

The relative settlement of fascia and reinforced fill induces reinforcement loads additional to service loads in Geosynthetic Reinforced Soil (GRS) Walls. The fascia- reinforcement connections are crucial to be taken care of in such conditions as they can affect the stability and serviceability of GRS walls. Sliding connection is an alternative to avoid the buildup of high reinforcement connection loads under the transverse relative settlement. 1-g model tests have been carried out in a relative settlement simulator tank on full-height panel RF-GRS walls with two types of positive connection systems. The corresponding sliding connection systems modifying the positive connections have also been tested. The reinforcement loads increase by 100-500 times for positive connections under 50 mm relative settlement compared to the end of construction. The increase in strains is 2-4 times from 50 mm settlement to 200 mm relative settlement. The top of the fascia is pulled towards the fill during the relative settlement of the fill. The developed sliding connection systems reduce the stress concentrations at the connection and allow free settlement of fill relative to the fascia. The increase in reinforcement loads in sliding connections is minimal compared to conventional non-sliding connections under the relative settlement.

Further, a numerical study is conducted to understand the behaviour of RF-GRS walls in different scenarios of transverse relative settlement. 2-D large deformation FE analysis of a 6 m high RF-GRS wall has been carried out for two relative settlement scenarios, i.e., fill w.r.t fascia and fascia w.r.t fill. The results show that a 400 mm relative settlement of fascia w.r.t fill leads to excessive outward displacements, about 6% of the wall height. The reinforcement loads increase by 44 times in bottom reinforcement and 10 times in top reinforcement compared to the end of construction. The

connections of bottom reinforcements show progressive failure with the increasing relative settlement of fascia w.r.t fill. Toe fixity slightly changes the deformation behaviour and reinforcement strain distribution in top reinforcement under the two relative settlement scenarios. Fascia stiffness in the practical range does not affect the response. Stiffer reinforcements reduce the mobilized strains under the relative settlement. The developed sliding connection in this study can allow free vertical movement of connection in all scenarios of transverse settlement.

Title: Analysis of seismically isolated fast reactors considering fluid-structure interaction
Researcher: Saboo, Anirudh
Supervisor: Kumar, Manish
Year: 2023
Keyword's: Generic Fast Reactor (GFR), Lumped Mass Stick Models -- (LMSMs) Earthquake Engineering, Nuclear Reactors
Call No.: 624.1762 SAB
Acc. No.: T01026

Abstract: Paris agreement signed in 2015 envisages net zero carbon neutrality by the year 2050. Nuclear energy is being considered as a frontrunner towards achieving the zero carbon goal. Government of India recently announced its plans to adopt nuclear energy over the coming decades (see the statement of the government of India at <https://pib.gov.in/PressReleasePage.aspx?PRID=1879298>, and plans of the National Thermal Power Corporation at <https://www.ntpc.co.in/en/about-ntpc-nuclear-venture>). Nuclear reactors are required to withstand extreme earthquakes. While it may be possible to design the structural systems for such loads, it may be prohibitive to attempt the same with the reactor and its components. A sustainable use of nuclear energy is possible when a reactor design is deployed across regions with varying seismic hazard. Seismic isolation of structures has been a proven technology to reduce earthquake loads in the structures, and is being seen across the world as a key towards the standardized reactor designs. Among the most advanced reactors under development in the world are sodium-cooled fast reactors. The prototype fast breeder reactor (PFBR) being developed by the Indira Center for Atomic Research (IGCAR), Kalpakkam, India is one such reactor. The overarching goal of the present work is to understand the influence of seismic isolation on the response of the generic fast reactor (GFR), which is similar to the PFBR.

This thesis is divided into three parts. The first part focuses on understanding the dynamics of a fluid-shell system representative of the GFR. The dynamics of a pressure vessel (i.e., inner vessel) present inside the reactor vessel (i.e., main vessel) is studied next. The third part deals with the influence of seismic isolation on the response of GFR internals subjected to seismic excitation. The three parts are described briefly in the subsequent paragraphs.

The first part presents a study on the dynamic behavior of three partially-filled interconnected cylindrical shells. This system can be considered to represent a portion of the GFR. Shells were considered elastic, while fluid was considered ideal. An energy-based formulation was used to derive the governing equations, which on minimization yielded the dynamic properties of the system. The formulation is flexible in a way that appropriate changes in the parameters of the solution can produce results for a large class of fluid-shell systems. The sloshing frequencies were of the order of 0.3 Hz, which can be comparable to that for an activated isolation system (e.g., 0.2 – 0.6 Hz).

The second part deals with the development of an analytical formulation to describe the vibration of a partially-filled joined cylindrical-conical-cylindrical vessel. Since the fluid-structure system is axisymmetric in nature and variants of this system are used in aircraft fuselages, storage tanks, submarine hulls, pressure vessels and components of nuclear power plants, the solution developed

herein will be of engineering importance to a large class of joined fluid-filled vessels. This vessel can be considered to represent the inner vessel of the GFR. Compatibility and interface conditions were utilized to derive the energy functional, which led to the natural frequencies and mode shapes of the fluid-shell system. Sloshing frequencies were found to not be affected significantly by the fluid height if most of the vessel was filled; coupling between bulging and sloshing frequencies may need to be considered for such cases. The bulging frequencies were found comparable to the shell-only frequencies for low fluid heights.

The third part of the thesis deals with the influence of seismic isolation on the response of GFR internals under earthquake excitation. While the preceding parts of the thesis presents some information potentially useful to develop lumped stick mass models (LMSMs) considering fluid-structure interaction (FSI), additional research is required to explicitly consider FSI in the LMSM for the GFR. Most of the past studies have ignored FSI effects in LMSM. Detailed finite element model of the components of GFR was developed first, which paved the way for the development of LMSM through suitable static analyses. An LMSM has nodes where relevant masses and mass moments of inertia are lumped, and sticks that represent the flexural, shear and axial stiffnesses of the respective segments. A representative fluid-shell system was analyzed with and without incorporating the FSI effects. The acceleration responses were found similar in both the cases. The LMSM was subjected to sets of ground motions representing hazard in low, moderate and high seismicity regions. Seismic isolation led to a substantial reduction (e.g., up to 10 times) in the median floor accelerations. If the PFBR at Kalpakkam is considered to be designed for a 0.25g peak ground acceleration hazard, the same reactor's response was found considerably smaller for 0.60g and 1.00g regions (compared to fixed-base configuration subjected to 0.25g hazard) if the reactor was isolated using a range of seismic isolation devices. These results show that seismic isolation can be used to deploy the PFBR at locations with varying seismic hazard across India.

Title: Hydrogeochemical unravelling of land-sea interaction along the Gujarat coast, India
Researcher: Bhagat, Chandrashekhar
Supervisor: Mohapatra, Pranab K.
Year: 2022
Keyword's: Seawater Intrusion, Submarine Groundwater Discharge, Ground Water-Gujarat
Call No.: 624 BHA
Acc. No.: T01081

Abstract: Interaction between two hydrologic masses, i.e., sea and land, manifests through two major processes, which are seawater intrusion (SWI) and submarine groundwater discharge (SGD). These processes can be intensified due to the tidal influences, unregulated industrialization, and urbanization in the coastal regions, which often lead to severe water stress on the coastal ground water (GW) resources. These unregulated developed regions are the hotspots for the discharge of contaminant enriched GW in the sea, which poses a threat to the marine ecosystem. SWI and SGD complement each other and have severe consequences on the coastal aquifer and sensitive marine ecosystem. SWI leads to salinization of the coastal aquifer and deteriorates the GW quality by elevating the dissolved solids. In contrast, SGD results in the loss of fresh GW from the aquifer (Fig.1), causing depletion of GW level (GWL) and acts as a pathway for contaminant discharge into the coastal ecosystem leading to an increased threat to the marine ecosystem. These processes are governed by several factors such as aquifer characteristics, GW potential, rainfall pattern, the topography of regions, recharge and discharge pattern, industrial and agricultural pattern, tidal influence, and density gradient. Therefore, identifying hotspots for these processes in the coastal areas and quantifying contaminant load becomes a complex problem. The coastal region of Gujarat is facing unregulated industrial and urban development and water contamination issues and is at high risk of turning into a hotspot for contaminant-enriched groundwater. These hotspots have been increasing contaminants in GW and SW, consequently deteriorating the GW quality and raising the health risk of coastal communities, and the increase in toxicity to aquatic life in the Arabian sea. Also, the beaches on the Gujarat coast modify the contaminants reaching the Arabian sea via SGD. Given the concerns posed above, the present study is oriented towards the following three objectives:

- To delineate the SGD hotspot along the Gujarat coast for quantification of SGD and associated contaminant flux reaching the Arabian sea;
- To unveil the GW salinization processes in the coastal aquifers of Gujarat and impact of salinity ingress on the trace metal toxicity; and
- To quantify the attenuation capacity of beaches to understand their role in modifying contaminant concentration in SGD flowing into the sea.

The thesis is presented through three major chapters to achieve these objectives, which are briefly described in the following sections.

CHAPTER 1: Quantification of submarine groundwater discharge and associate contaminants flux
This chapter focuses on identifying hotspots of SWI and SGD and quantifying the magnitude of SGD and contaminant load reaching the coastal ecosystem. For identifying SWI and SGD zones, site-

specific water characteristics and ground water levels were used as a proxy. For delineation, 540 water samples at a distance of 5–10 km (SW, PW, and GW) and several porewater (PW) measurements were taken from the entire coastline of Gujarat. Further, a three-tier validation system was adopted for delineating SWI and SGD zones, followed by physical verification of the locations through the integration of (i) Groundwater fluctuation dynamic, (ii) MODIS derived sea surface temperature (SST) anomaly, and (iii) Electrical conductivity (EC) based gradient mapping, respectively. The study has identified nine out of 14 districts as vulnerable to SWI, whereas the remaining five districts from south Gujarat and the Saurashtra coast are suspectable for SGD. Further to delineate the specific locations, a salinity gradient approach integrated with stable isotopes of oxygen ($\delta^{18}\text{O}$) and strontium ($^{86}/^{87}\text{Sr}$) was employed in order to confirm the presence of SGD before quantification. A total of seven sites were identified for SGD, among which three locations were found on the south coast, three on the Saurashtra coast, and one in Diu (Union Territory of India). Further, quantification of SGD flux reaching to sea was done using seepage meters and 1-D solute (salinity) and heat (temperature) transport models. Terrestrial and recirculated SGD significantly contributed to flow and contaminant load, ranging from 12.93 to 2251.79 $\text{m}^3\text{m}^{-2}\text{year}^{-1}$ and 0 mol Co Day⁻¹ to 40322 mmol Zn day⁻¹ in the Arabian sea.

The nutrient load reaching in marine ecosystem varies from 3.2 to 3358 mmol NO₃ day⁻¹ across the coast. The highest magnitude of SGD estimate was relatively less than the SGD reported for the eastern coast along the Bay of Bengal and comparable to the South Chennai coast. The order of estimated contaminants flux was Zn > Fe > Cr > Pb > Ni > Cu > Mn, and the highest flux of Zn (3234 mmol Zn day⁻¹) was found at Fansa beach, which was seven times Fe-flux and 45 times Cr-flux, respectively. The results revealed that the south Gujarat coast received a higher nutrients load compared to other coastal areas indicating the high vulnerability of eutrophication, algal blooms, and the formation of biotic ligands in aquatic species.

CHAPTER 2: Unveiling salinization processes and impact of salinity ingress on metals toxicity in coastal aquifers of Gujarat

While identifying the SGD locations, it was observed that GW quality along the coast deteriorated due to the salinization of the aquifer. The previous studies reported that increased GW salinity due to SWI was a significant threat across the coastal aquifers worldwide due to the anthropogenic activities and evaporative dissolutions. In India, especially across the western coast, high urbanization and industrial growth have caused over-exploitation of the GW resources, inhibiting the natural recharge tendencies and intensifying the SW movement in the aquifer. Thus, this chapter investigates the existing spatial vulnerability of GW quality and unveils the salinization processes through a comprehensive hydrochemical and isotopic analysis of the GW. Also, it focuses on the impacts of salinity ingress on the toxicity of trace metals. The specific observation from the study includes GW evolution rate and pattern, which changes the facies of GW from Ca-Mg-Cl type in southernmost Gujarat to Na-Cl type towards the Gulf of Khambhat. Results reveal that GW in the Gulf of Khambhat was heavily intruded by seawater and anthropogenic contamination due to various physical and chemical means and suggest remediation over the SWI problem. Statistical findings supplemented with isotopic signatures, ionic ratios, and cross plots identified four classes of GW, which vary with the degree of anthropogenic and seawater influences. Results suggest that

SWI heavily influences 42% of the total GW sample sites and 58% show vulnerability towards SGD. Salinity ingress reduces the toxicities of all trace metals except Cu, which may be due to the increase of Ca in GW, leading to the dissociation of CuCO_3 . Reactive species are dominant for Zn and Cd, whereas the M-CO_3 ligands are dominant for Cu and Pb. This dominance of metal carbonate ligands may be due to the undersaturation of dolomite and calcite in the aquifer system. The study also suggests feasible locations for the check dams as are medial measure for controlling the SWI in the coastal aquifers.

CHAPTER3: Interaction of contaminants and beach sediments in the mixing zone

The metal load and contribution of SWI in aquifer contamination found in the first and second chapters revealed the interaction of aquifer and sea, which eases the contaminant transport through concealed pathways. This transport of contaminants intensified SW contamination, posing a threat to sensitive marine ecosystems and deteriorating the SW quality. The measured hydrochemical parameter along with nutrients (N, P, and Si) and trace metal (Fe, Mn, Zn, Ni, Pb, and Cu) concentration in GW, PW and SW indicate that the aquatic system was heavily contaminated. However, the observed concentration in PW is relatively increased/decreased than the predicated concentration of PW for contaminants. Based on this observation, it has been hypothesized that the beaches alter the SGD composition before reaching the sea. Thus, this chapter focuses on investigating the proposed hypothesis and assessing the contamination level in GW, PW, and SW and the vulnerability of eutrophication. It was observed that SGD reaching the coast carried immense nutrient flux ($155.62 \text{ mmol NO}_3 \text{ day}^{-1}$; $35 \text{ mmol P day}^{-1}$ and $12.41 \text{ mmol DSi day}^{-1}$) and trace metal load ranging from 0.03 to $14.85 \text{ mmol day}^{-1}$. The nutrient fluxes were higher in the upper saline plume compared to the lower freshwater discharge plume. The muddy beach attenuated the nutrients in the varying percentages, such as 9.72 to 22% (NO_3), and 1.9 to 25.5% (P), probably due to denitrification and absorption of P, and 19.6% reduction of SO_4 . The average attenuation capacity of this muddy beach varied from $3.5(\pm 9.8)$ to $19.6(\pm 6.1)\%$, and the capacity of trace metal leaching varied from $2.0(\pm 13.5)$ to $7.1(\pm 20.1)\%$. The reduction in SO_4 leads to the formation of sulfide (HS^-), which may promote the precipitation of trace metals, resulting in the removal of Pb and Cu. The attenuation capacity of Dehri beach was less than the attenuation capacity of Varkala sandy beach Kerala. However, it showed good agreement with the attenuation capacity of Werribee beach, port Phillip Bay, Australia. This attenuation and leaching of contaminants lead to a change in the composition of SGD, resulting in a change in nutrient ratio in STEs and increasing the trace metal load. The attenuation of nutrients led to the change in the nutrient ratio ($\text{N/P}=7\text{-}11$) approaching the Redfield ratio, indicating the vulnerability of eutrophication at the Dehri beach. Overall, the muddy beach can play a dual role by acting as a natural biogeochemical reactor (as it attenuates the nutrients) and serves as a source for certain trace metals (Fe, Mn, Zn, and Ni). Hence, the muddy beaches play a significant role in altering the composition of SGD.

Finally, this thesis concludes that provides a holistic framework to investigate the land-sea interaction processes induced by nature/anthropogenic forcing in the coastal region of Gujarat and associate threats to the sensitive marine ecosystem and coastal GW aquifers.

* * * * *



COGNITIVE AND BRAIN SCIENCES

Cognitive and Brain Sciences

Title: John Henryism in the Indian context
Researcher: Gopal, Anvita
Supervisor: Subramanyam, Malavika A.
Year: 2021
Keyword's: Sciences Socioeconomic Positions, John Henryism Active Coping Scale, JH and Stress, Psychological Construct, Psychology and Public Health
Call No.: 305.0954 GOP
Acc. No.: T00944

Abstract: John Henryism (JH) is a term coined by Prof. Sherman James, who defined it as “a behavioral predisposition to engage in high effort coping with social and economic adversity” The John Henryism Hypothesis (JHH) states that the increase in the risk of physiological or disease outcomes among those from lower socioeconomic positions (SEP) compared to those from higher SEP will be greater among those who score higher on JH as compared to those scoring low on JH. It is the combination of high JH and low socioeconomic status (SES) that increases the risk of ill health, as per this hypothesis. JH is measured by a 12-item scale called the John Henryism Active Coping Scale (JHAC). JH has not been studied in India, there are several reasons to suspect that it may be a valid psychological construct in the Indian context and therefore merits a thorough investigation. Moreover, if support is found for the JHH in the Indian context, it has implications for both psychology and public health. Therefore, the primary focus of this thesis is on the relevance of JH in the Indian context and therefore, it further explores the JHH and its physiological implications in the Indian scenario.

Theoretical underpinnings and motivation:

JH, a form of active coping, may be relevant in India because a great proportion of Indians also undergo chronic socioeconomic adversity and cope with it. However, their coping may vary as per their background and position in society. In order to explore whether the concept of JH is relevant in the Indian context, we sought to learn about the socio-cultural context in which individuals live, experience, and cope with stress, specifically in Hindi-speaking areas of India. Essentially, the goal was to understand the stressors faced by individuals, their perceptions about them, and their ways of coping. The motivation for exploring the relevance of JH in India was the fact that if JH is indeed applicable in India, it suggests an aspect of a personality trait that has not been heretofore explored in India and deserves attention.

Moreover, if JH is relevant in India, it has potential implications for health. Previous research finding support for the JHH has focused on increased stress-related outcomes such as cardiovascular risk factors/diseases (CVD). Given the rising number of CVD cases in India, any evidence suggesting that the JH is relevant in India, and further exploration of any support for the JHH, is timely and necessary in India. This work which focuses on JH and JHH, therefore, has the potential to unveil a new cardiovascular risk factor.

Thus, a study exploring JH in the Indian context in a comprehensive manner has the potential to add to the knowledge in various disciplines such as psychology and public health about stress, its impact, and finally mitigation strategies.

Aims:

With rampant socio-cultural adversities, JH as a form of active coping might exist as an aspect of a personality that has yet not been explored in India and deserves attention. Therefore, the first aim of this study is to investigate if the construct of JH is relevant in the Indian milieu. If JH is indeed found to be relevant, the second aim is to design a way to measure JH in India using a modification and/or translation of the existing JHAC scale which is also valid and reliable. The third aim is to develop a psychological profile for high JH individuals. We hypothesize that constructs known to be similar to JH, such as self-efficacy, resilience, and conscientiousness, would be positively associated with JH. Finally, the study aims to test the JHH in the Indian context.

Methods:

Study design:

The study was carried out in multiple phases: Formative research, scale validation, psychological profiling, and a preliminary test of the JHH.

The formative research phase comprised three phases, the first was a phase of initial assessment, followed by an iterative testing phase. The third phase of scale development included steps such as numerous translations and back translations of the scale, seeking feedback from content and language experts, and from participants on the scale items. Finally, a Hindi and an English version of the JHAC scale suitable for the Indian population were developed. We launched a website in late 2019 to collect survey responses that were used in the validation study. Simultaneously, responses were also collected with the help of paper-pencil-based forms. This helped us to access a diverse sample, as well as to study whether the online and offline versions worked in a similar manner. The paper-pencil tests were administered at different sites, such as workplaces, educational institutes, occasionally on the streets with randomly approached strangers, and a few via personal contacts. After this phase of data collection, the onset of the COVID pandemic necessitated further data collection in the online mode only. Data were collected at 6-time points: T1: 29th March, the first week of the lockdown (n = 793); T2: 14th April 2020 (n = 478); T3: 2nd May 2020 (n = 511); T4: 24th May 2020 (n = 485); T5: 29th July 2020 (n = 457); and T6: 10th October 2020 (T6: 471), where JHAC was administered at T5 and T6.

For establishing validity, we assessed the face validity of the JHAC scale with the help of external evaluators as well as cognitive interviews. Content validity was evaluated by seeking feedback from experts and a sub-sample of the participants. Concurrent validity was assessed by measuring the association of JHAC with an active coping subscale of the Brief COPE while predictive validity was tested with the relationship of JH with perceived stress scale-PSS, self-rated health (SRH), and self-rated poor mental health (SRPMH). To assess construct validity, we examined the association of JH with other theoretically related constructs such as self-efficacy, resilience, locus of control, approach coping, conscientiousness, and stress, while also testing nomological network validity. The data

collected for the validation study was also used for creating a psychological profile and testing the JHH.

Sampling and recruitment:

We aimed to recruit Indian adults (>18 years of age) of any gender and geographical location across India. The goal was to include participants from varied educational and occupational backgrounds. During the entire process, participants were recruited by employing a mix of convenience and snowball sampling methods, with a few participants recruited with the help of personal contacts. At the formative research stage where we explored the construct, data were gathered through preliminary field visits (4-5 visits), informal conversations with a few residents of the village (n = 12), short informal interviews (n = 4), focused group discussions (FGDs) with women (groups of ~11 women and 5 women), and free-flowing (n = 5) and semi-structured interviews (n = 21). For construct validation, we also performed cognitive interviews (n=40) and respondent validations (n=8), plus survey data was collected at 7-time points: T0: (n=1421); T1: (n = 793); T2: (n = 478); T3: (n = 511); T4: (n = 485); T5: (n = 457); and T6: (T6: 471), where the JHAC was administered at T0, T5 and T6. Data for validating these newly developed modified scales were obtained by administering the scale in English (n = 893) and Hindi (n = 312); using either online (n = 962) or offline (n = 243) modes.

Ethical considerations:

Guidelines set by the IIT Gandhinagar Institutional Ethics Committee were followed.

Data analysis:

The formative research yielded audio records and written notes from interviews, which were transcribed by the selective verbatim transcription method, coded, and analyzed to identify themes. The quantitative analysis comprised scale validity assessments using convergent, concurrent, and predictive validity checks. We also performed reliability evaluations using Cronbach's alpha and temporal stability reliability assessments. Furthermore, correlation coefficients (both Pearson and Spearman) were calculated as required, while evaluating the validity and reliability of the scale. We used multivariable regression analysis, with the use of linear regression for continuous and logistic regression for binary outcomes while investigating the association of JH with other outcome variables as well as to test for the JHH. STATA version 12 was used for data analysis.

Results:

The formative research, including preliminary field visits, informal conversations, interviews, FGDs, cognitive interviews, and respondent validations, found that JH was relevant as a form of active coping. The analysis of the self-reported behaviors helped identify four main themes: Individual-level stressors, societal-level stressors, family responsibilities, and coping mechanisms. This suggested the relevance of JH in the Indian context. The findings further helped us make appropriate modifications to the JHAC scale.

The JHAC scale was adapted and modified for use in the Indian context in both English and Hindi language. Cronbach's α in different sub-groups ranged from 0.66 to 0.78, which established that the scale was reliable across both languages and modes of administration. The correlation of JHAC scores measured repeatedly over 3-time points among the same respondents was greater than 0.6, suggesting decent temporal stability. External evaluators found the JHAC to have decent face and content validity. Correlation of JHAC with active coping of the Brief COPE (0.32 ($p < 0.001$)) established concurrent validity; PSS (-0.20 to -0.37 ($p < 0.001$)), SRH (0.21 to 0.28 ($p < 0.001$)), and SRPMH (0.15 ($p = 0.080$) to -0.17 ($p = 0.009$)) helped with predictive validity. Nomological network validity as well as association between JH with other theoretically related constructs such as self-efficacy (0.45 to 0.56 ($p < 0.001$)), resilience (0.53 ($p < 0.001$)), approach coping (0.28 ($p < 0.001$)), conscientiousness (0.25 ($p < 0.001$)), established construct validity.

The psychological profile that emerged suggested that a high JH individual is someone who is resilient, has high levels of self-efficacy and conscientiousness; and deals with stressors with problem-focused coping strategies of planning and positive reframing in a non-emotion-focused manner. The distribution of JHAC scores showed a few interesting trends: individuals in the 40 to 65 age group showed the highest proportion (61%) of high JH (>median JH value). The underprivileged caste groups had a greater prevalence of high JH (61%) than the privileged group (51%). In the Hindi offline subsample, 83% of rural residents scored high on JH compared to 59.80% at urban locations. High JH was seen in 53.65% Hindus; 71.25 % of Muslims; and 29.58% of Christians. We found evidence supporting the JHH, though limited. For instance, among those with high JH, we found that those in the privileged caste group reported significantly lesser depressive symptoms than the participants in the underprivileged group, and this pattern was not seen in participants with low JH. Similarly, the higher household income group reported significantly lesser anxiety than the participants in the lower income group among those with high JH, and this pattern was not evident in participants with low JH. Nevertheless, the evidence supporting the JHH was modest.

Discussion:

The findings of the formative research helped conclude that individuals from all walks of life, diverse ages, gender, socio-economic background: privileged and underprivileged, had various levels of problems and stresses. Despite this, they coped actively. Their responses to, and understandings of, the scale items, though subjective, were similar. The learnings from the formative research helped us develop a modified JHAC scale suitable for use in India.

The modified JHAC was found to be a decently valid and reliable scale. However, we highlight a few key patterns. First, both the interviewer-administered as well as the self-administered scales were found to be effective. However, in the interviewer-administered version, the respondents raised some questions, and the presence of an interviewer proved to be beneficial because it allowed for further probing the responses, which might have been missed by some of the respondents in the self-administered mode. While both the online and offline administration of the scales worked efficiently, the offline version helped us increase the diversity of the sample, as it allowed us access to the less educated, and to those without easy access to the internet. An urban versus rural

residence mattered. Though we had fewer participants from rural areas, we found that the samples from both urban and rural areas gave consistent results. All our studies highlight that Indians engage in JH as a means of overcoming socio-economic stressors. The JHAC scale was effective across various modes of administration. We found our modified version of JHAC to be a validated scale for use on the Indian adult population in English and the Hindi language. A high-JH individual exhibited a psychological profile comprising self-efficacy, resilience, conscientiousness, and active coping. Though the evidence was limited, JHH was supported in the Indian context.

The thesis helped demonstrate that the previously under-researched psychological research construct John Henryism is applicable in the Indian context. This further opens another avenue of research in psychology, and arguably its applications. The work has helped develop a scale to measure JHAC in the Indian context in large community-based samples as well as in the clinical setting by psychologists and health researchers. The development of JHAC in one of the most spoken languages of India (Hindi) might help researchers reach a wider population and accelerate research in this process. The study of JHH might help unveil a potentially new cardiovascular risk factor in India. The JHAC scores were found to be distributed differently for minority participants. The experience of minorities deserves more attention. Our work helps to further generate hypotheses related to the study of active coping with stress in religious minorities represented by Muslims and Christians in a Hindu dominant nation. The work also helped towards profiling a high JH personality—a direct contribution to social and personality psychology. Our work also adds to the knowledge in fields such as personality and health psychology and has implications for public health and social epidemiology.

Title: Role of priors in audio-visual temporal binding and visuospatial attention
Researcher: Jagini, Kishore Kumar
Supervisor: Sunny, Meera M.
Year: 2023
Keyword's: Temporal Binding, Visual Perception, Cognitive Neuroscience
Call No.: 153.1 JAG
Acc. No.: T01019

Abstract: Our perception of the world is multisensory. For a unified and coherent multisensory perception of the world, our brain needs to bind multisensory signals belonging to a common causal event/object. One of the classic examples to demonstrate the binding of multisensory signals is temporal ventriloquism effect. Typically, in temporal ventriloquism, the observers perceive the slightly asynchronous audio-visual stimuli as a unified and synchronous percept. This temporal unification or binding of asynchronous audio-visual stimuli was demonstrated to occur by perceptual adjustment to the apparent onset time of vision toward audition – because our judgements of auditory time is typically more reliable than vision. From the Bayesian causal inference perspective, numerous causal priors or simply ‘priors’ help us in determining the multisensory signals belonging to a common causal event/object (Vilares & Kording, 2011). The ‘priors’ denote a priori information about the statistical regularities in the environment, which include, but are not limited to, spatial, temporal, and semantic congruency between multisensory stimuli. The Bayesian framework allowed the researchers to quantify and predict the strength of multisensory binding based on the combination of ‘prior’ and ‘sensory reliability’. Another line of research suggested that multisensory binding is bi-directionally linked to attentional mechanisms (Talsma et al., 2010). On the one hand, binding enhances the sensory saliency and attracts attentional resources. On the other hand, the availability of attentional resources determines the extent of multisensory binding. This thesis explores some of the unresolved questions on the role of ‘priors’ in audio-visual temporal binding and visuospatial attention.

Past research showed that when an unisensory event (e.g., a brief sound) is followed or preceded by observers’ motor action, the perceived onset time of that event is altered, and is shown to be inversely dependent on its reliability. In typical environments, however, multisensory events can be followed or preceded by our actions. Chapter 2 investigated the audio-visual (AV) temporal binding in the context of action. The first experiment investigated the modulations in AV binding window when the stimuli were presented as a consequence of observers’ action (keypress action) relative to the identical stimuli presented passively. In contrast, the second experiment investigated the modulations in AV binding window when these sensory stimuli were preceded by the observers’ action. To measure the temporal binding window widths for AV stimuli, a binary simultaneity judgment (SJ2) task was utilized for both experiments. The temporal delay between action and AV pair was manipulated. The temporal proximity between action and AV pair was considered as a causal prior which determine action influence on AV temporal binding. If the action alters the perceived onset times of auditory and visual stimuli differently, considering our judgments of onset times of audition are more reliable than vision, the action is expected to alter the AV temporal

binding. The results showed an altered AV binding, specifically for vision leading trials, when the stimuli were followed the action but not preceded and in close temporal proximity with the action. The results suggest that the action can influence the perceived onset times of auditory and visual stimuli differently, and that lead to the changes in AV temporal binding window widths. The cross-modal semantic congruency is known to guide observer's spatial attention toward the target of visual search. However, the degree to which the cross-modal semantic congruency influences the observers' spatial attention independent of goal-oriented behaviour is not clear. By systematically manipulating the task-relevancy of semantic congruency, the chapter 3 investigated the extent of audio-visual semantic information influence spatial attention independent of top-down goals. Toward this aim, multiple experiments were conducted by adopting the irrelevant singleton visual search paradigm. The search displays were presented simultaneously with speech sounds with verbalizations of colour of singleton in the search display. As control conditions, we used auditory white noise and/or no sound conditions. The results show evidence that the audio-visual colour semantic information modulates the search task efficiency in both goal-independent and goal-dependent manner. However, when the semantic information was task-irrelevant, the RT advantage for colour singleton targets suppressed. Whereas when the semantic information was task-relevant, RT advantage for colour singleton targets was facilitated. This pattern of results suggests that the audio-visual semantic interactions influence the visuo-spatial attention priority maps and influence attention differently depending on their relevancy to the task.

Past research has shown that participants can utilize statistical regularities of target and distractor stimuli independently within a modality either to enhance the target or to suppress the distractor processing. Utilizing statistical regularities of task-irrelevant stimuli across different modalities also enhances target processing. However, it is unknown whether distractor processing can also be suppressed by utilizing statistical regularities of the task-irrelevant stimulus of different modalities. Chapter 4 investigated whether the spatial (Experiment 1) and non-spatial (Experiment 2) statistical regularities of task-irrelevant auditory stimulus could suppress the salient visual distractor. We used an additional singleton visual search task with two high-probability color singleton distractor locations. Critically, the spatial location of the high-probability distractor was either congruent (valid trials) or incongruent (invalid trials) with the task-irrelevant auditory stimulus. The results replicated earlier findings of distractor suppression at high-probability locations compared to the locations where distractors appear with lower probability. However, the results did not show any RT advantage for valid distractor location trials compared to invalid distractor location trials in both experiments. When tested on whether participants can express awareness of the relationship between specific auditory stimulus and the distractor location, they showed explicit awareness only when auditory stimulus regularities were spatial. Overall, results indicate that irrespective of awareness of the relationship between auditory stimulus and distractor location regularities, there was no reliable influence of task-irrelevant auditory stimulus regularities on distractor suppression. Future research directions proposed conditions in which task-irrelevant sounds could modulate the distractor processing. The present thesis reports the behavioral effects of causal priors on audio-visual temporal perception and visual attention by utilizing typical behavioral/psychophysical measures such as simultaneity judgments and response times. The findings broaden our

understanding of how ‘priors’ influence human multisensory perception and attention in varied behavioral contexts.

Title: Characterizing active noise control headphones with psychoacoustics of amplitude modulation

Researcher: Bandyopadhyay, Sohhom

Supervisor: George, Nithin V.

Year: 2022

Keyword’s: Active Noise Control, Psychoacoustics, Shallow-envelope Chimera, ANC Headphones

Call No.: 153 BAN

Acc. No.: T01027

Abstract: Active noise control (ANC) headphones work by electronically generating an ‘anti-noise’ that interferes with external sounds, thereby creating a zone of quiet at the listener’s eardrum. Such headphones are supposed to deliver a superior audio experience because the desired i.e. the playback signal is less corrupted by external noise. However, despite being popular in the consumer electronics market and also as a research tool in a variety of disciplines, the effect of the ANC on the playback signal is not usually investigated. This thesis is an initial investigation into the possibility of the playback signal being physically improved (less degraded) due to the ANC, and any consequent psychoacoustic changes.

A signal can be distorted in many ways, and the corresponding space of psychological outcomes can be vast. Hence, this thesis is focused on only one aspect of the playback signal; its amplitude (a.k.a temporal) envelope. An acoustic signal can carry information for a brain in different ways, notably by amplitude and frequency modulations. Amplitude modulation is a mathematical process whereby a carrier signal’s amplitude is changed according to an envelope signal. The amplitude envelope’s role in human hearing has been studied in a large number of psychological and neuroscientific contexts; e.g. a speech signal can be understood by humans with only the information from its envelope.

This thesis carries out a perceptual evaluation of four commercially available ANC headphones as ‘black boxes’, i.e. without modifying the internal working of the ANC algorithm. The first two chapters elucidate the modulation transmission characteristics of headphones across the modulation frequency axis with modulated sinusoids, and the last two chapters do so by showing the variation of intelligibility and quality for speech with parametrically degraded envelopes. Overall, this work provides the first direct evidence that the playback signal produced by an ANC headphone has a relatively intact amplitude envelope when the ANC is enabled compared to when it is turned off. By quantifying this phenomenon with various acoustic and psychoacoustic models, and subsequently by studying the psychological effects on humans, we also provide evidence that ANC is helping the brain process the sounds more efficiently. Given the rising popularity of the ANC algorithm in ‘hearables’, headphones, hearing aids and potentially also cochlear implants, these

findings may have implications for the audio industry as a whole, as well as for clinicians working with hearing impaired individuals. In addition, by linking these findings with the remainder of the knowledge of the human auditory system, ANC headphones could also be utilized as a tool for designing new kinds of psychophysical experiments to better understand the cochlear functions and phenomena such as masking.

* * * * *



COMPUTER SCIENCE & ENGINEERING

```
text-align: center;
}
.App-logo {
  height: 40vmin;
  pointer-events: none;
}
@media (prefers-reduced-motion)
.App-logo {
  animation: App-logo-spin infinite
}
}
}
.App-header {
  background-color: #282c34;
  min-height: 100vh;
  display: flex;
  flex-direction: column;
  align-items: center;
  justify-content:
  font-size: calc(
  color: wh
}
}
@keyframes
from {
  tran
}
```

Computer Science and Engineering

Title: Graph isomorphism algorithms for graph with bounded structural parameters
Researcher: Enduri, Murali Krishna
Supervisor: Das, Bireswar
Year: 2018
Keyword's: Algorithm, Polynomial-time Algorithms, Tree-depth Graphs, Computation Planar Graphs
Call No.: 004.015115 END
Acc. No.: T00268

Abstract: Two graphs are said to be *isomorphic* if there exists a bijective mapping from the vertices of one graph to the vertices of other graph such that the adjacency is preserved. Given a pair of graphs as input the problem of deciding if the two graphs are isomorphic is known as the *graph isomorphism problem* (GI). Whether this problem has a polynomial-time algorithm is one of the outstanding open problem in the field of algorithms and complexity theory for the last forty years. The graph isomorphism problem is not known to be in P. It is in NP but very unlikely to be NP-complete. Recently Babai designed a quasi-polynomial time algorithm (STOC 2016) to solve GI problem improving the previously best known $e^{O(\sqrt{n} \log n)}$ time algorithm (FCT 1981, Theory of Computation I 1982, STOC 1983). Although no polynomial time algorithm for graph isomorphism problem for general graphs is known, efficient algorithms for GI have been discovered for various restricted classes of graphs, e.g., planar graphs, bounded degree graphs, graphs with bounded genus, etc.

A *graph parameter* is a function mapping from a graph to a non-negative integer. Many problems that are not known to be in P admits polynomial-time algorithms when restricted to graphs with a bounded parameter. These polynomial time algorithms are useful in practical and theoretical point of view. This thesis consists of four major chapters, all dedicated to the design of polynomial-time (P), fixed parameter tractable (FPT), logspace (L) and parameterized space (Para-L) algorithms for the graph isomorphism problem for restricted graph classes. In this work, we consider some well-known graph parameters such as tree-depth, clique-width, distance to H -free graphs, vertex cover number, twin-cover number, etc.

- The tree-depth is a parameter which measures how close a graph is to star graphs. We give logspace algorithms to recognize bounded tree-depth graphs and compute tree-depth decomposition using a recursive definition of tree-depth. We design a logspace algorithm for GI for bounded tree-depth graphs.
- We show that the graph isomorphism problem is fixed parameter tractable (FPT) for a parameterized graph class where the graph parameter is the length of the longest cycle.
- We give a clique-width preserving Turing reduction from GI to prime graph isomorphism by using modular decomposition. We design a polynomial time isomorphism algorithm for graphs with clique-width at most three. This can be done in two phases, in the first phase we give a dynamic programming algorithm to test if two given parse trees are structurally

isomorphic. In the second phase, we prove that the Corneil et al. 2012 algorithm can be slightly modified to produce structurally isomorphic parse trees for isomorphic graphs with clique-width at most three.

- Let $H = H_1, \{H_2, \dots, H_l\}$ be a finite set of graphs where vertices of H_i at most d for all i and for some constant d . Let G be an H -free graph class i.e., every graph G in G does not contain H as an induced subgraph for all H in H . We show that GI parameterized by vertex deletion distance to G is in Para-AC^1 , provided the colored graph isomorphism problem for graphs in G is in AC^1 . From this, we deduce that GI parameterized by the vertex deletion distance to cographs is in Para-AC^1 . We also show that the graph isomorphism problem parameterized by vertex cover number or size of twin-cover is in Para-TC^0 .

Title: On structural parameterizations of intractable graph problems
Researcher: Reddy, Vinod Kumar
Supervisor: Das, Bireswar
Year: 2018
Keyword's: Graph Motif, Polynomial Kernel, Vertex Deletion Distance
Call No.: 004.015115 RED
Acc. No.: T00270

Abstract: In this thesis, we study the parameterized and parallel complexity of hard graph problems for various structural parameters. Our main objective is to study a problem with respect to different structural parameters to obtain a better understanding of the problem's complexity. The problems we consider in this thesis are GRAPH MOTIF, FIREFIGHTING, GRAPH COLORING, HAPPY COLORING, CONFLICT-FREE COLORING and RECOGNITION OF BOUNDED RANK-WIDTH GRAPHS. We study the parameterized complexity of the above problems with respect to several distance-to-triviality parameters. Our notion of distance to a graph class is the vertex deletion distance. More precisely, for a class F of graphs, we say that the distance of G to the class F is k if there is a k -sized subset $X \subseteq V(G)$ such that $G \setminus X \in F$.

- We show that GRAPH MOTIF is fixed-parameter tractable (FPT) when parameterized by the distance to threshold graphs. We give a polynomial kernel for GRAPH COLORING parameterized by the distance to clique.
- We show that FIREFIGHTING is FPT when parameterized by the distance to threshold graphs and distance to disjoint unions of stars. We also show that FIREFIGHTING admits a polynomial kernel when parameterized by the distance to clique, while it is unlikely that it admits a polynomial kernel when parameterized by the distance to disjoint unions of stars.
- We show that MAX HAPPY VERTICES and MAX HAPPY EDGES problems are FPT when parameterized by the treewidth and the number of colors used in the precoloring. Further, we show that both the vertex and edge variants of the problem is FPT when parameterized by either vertex cover number or distance to clique. We also show that the problem of maximizing the number of happy edges is FPT when parameterized by the standard parameter, the number of happy edges in the solution. We show that the MAXIMUM HAPPY VERTEX (EDGE) problem is NP-hard on split graphs and bipartite graphs. We give a polynomial time algorithm to the MAX HAPPY VERTICES problem on cographs.
- We show that CONFLICT-FREE COLORING is FPT when parameterized by the cluster vertex deletion number of the input graph and admits an additive constant approximation algorithm when parameterized by the distance to threshold graphs. We also study the complexity of the problem on special graph classes, split graphs, cographs and intervals graphs. We also study the conflict-free coloring of points with respect to a set of double intervals. We show that this problem is NP-complete and obtain upper and lower bounds on the number of colors required for the special case when none of the intervals are contained in any other interval.
- We also study about the graph parameter rank-width. We show that for a fixed k , there is an NC algorithm that separates the graphs of rank-width at most k from those with rank-width

at least $3k + 1$. We also show that some problems which have polynomial time algorithms on bounded rank-width graphs admit NC algorithms on bounded rank-width graphs if a balanced rank-decomposition of bounded width is given as input.

Title: Models and algorithms for information diffusion
Researcher: Choudhari, Jayesh
Supervisor: Dasgupta, Anirban
Year: 2020
Keyword's: Diffusion of Information, Hidden Markov Hawkes Process (HMHP), Dual Network Hawkes Process (DNHP), Topical Interactions User Network
Call No.: 005.1 CHO
Acc. No.: T00558

Abstract: Social networks, whether real ones or online services, act as important platforms for the propagation of ideas, thoughts, innovation, rumors, infection, etc. The propagation of information from one user to others results in the formation of information cascades. These cascades can be thought of as conversations between the users that can be characterized by the topics being discussed, the time at which the conversation is going on, as well as the complex interactions (who responds to whom) between the users involved in the conversation. In this thesis, we first propose a series of generative models for this complex process of diffusion of information. The first model, Hidden Markov Hawkes Process (HMHP), incorporates the interaction between the users (influence of one user on another), users' topical preferences and, temporal patterns between posting and response times, as is the case with number of other models in existing literature; the novelty of HMHP is in incorporating topical interactions. We also propose a scalable algorithm based on Gibbs sampling that jointly infers the strength of interactions between the users, the path of diffusion of information, the topics of the posts, as well as the topical interactions. Experiments on synthetic data show that HMHP can recover user-user influence, parent identification, and topic identification more accurately as compared to the state-of-the-art baselines. More interestingly, HMHP finds insightful interactions between topics in real tweets which no existing model is able to do.

However, in HMHP, as well as in all the previous models in the literature, the time of the event is dependent only on the users (and their interaction), which is not the case in the real world. We propose the Dual Network Hawkes Process (DNHP) in which the event rates depend on the topic (topical-interaction) in addition to the user (user- interaction). In DNHP, in parallel to the user network, we model a network over the topics as well, so that the events propagate over a two dimensional space indexed by users and topics. This sets up an interaction between the two spaces, where the estimates of user- user weights depend on topic-topic weights, and vice versa. This resultant joint estimation of weights allows evidence to flow across weight variables. As compared to the HMHP, DNHP is not benefited from collapsed Gibbs sampling for the inference task. However,

experiments on synthetic data show that DNHP outperforms state of the art models in terms of parent identification, and user-user weight estimation.

In addition to the proposed generative models, we also look at the information diffusion problem from an algorithmic perspective, specifically, in the context of parameterized algorithms. Note that it is not always the case that we want the information to propagate. For e.g., consider a piece of information which is a rumor or fake news, or from the view of the epidemiology, consider an infection or a disease. In these cases, the goal would be to prevent or at least curb the spread of the contagion. Thus, in contrast to the previously mentioned works, which are centered towards understanding the propagation of information and the factors responsible for the same, the goal here is to propose algorithms for preventing the spread of information. In this work, we focus on the firefighting problem which formalizes the question of designing inoculation strategies (termed as firefighters) against a contagion (termed as fire) that is spreading in the network. There could be different objectives in the firefighter problem, but we concentrate on the objective of saving a specific set of nodes (termed as a critical set) and prove some results for the same. First, we show that saving a critical set on trees is fixed-parameter tractable (FPT) when parameterized by the number of firefighters and propose an algorithm with time complexity $O^*(4^k)$. We also show that the problem is FPT on general graphs when parameterized by the number of firefighters. Additionally, we claim that there is no polynomial sized kernel on trees for saving a critical set on trees. Finally, we consider the spreading model of the firefighting problem, where the firefighters spread as well, similar to the fire. For this model, we show that the problem of saving a critical set parameterized by the number of firefighters is $W[2]$ -hard (i.e. as hard as k -DOMINATING SET), which contrasts our FPT result for the previous non-spreading model.

Title: Challenges in deep visual recognition: algorithms and novel architectures
Researcher: Kumawat, Sudhakar
Supervisor: Raman, Shanmuganathan
Year: 2020
Keyword's: Deep Neural Networks, Convolutional Neural Networks, 2D Short Term Fourier Transform, Datasets
Call No.: 006.42 KUM
Acc. No.: T00726

Abstract: With the advent of digital technologies such as the internet and easy availability of visual sensors such as camera devices, there has been an explosion of visual data in the form of images and videos. In fact, the current growth rate of the visual data is so much that it has become infeasible for human manpower to process it in order to extract any valuable information. The field of computer vision attempts to solve this problem by training computer-based visual recognition systems to automatically interpret, understand, and extract valuable information from visual data. The past few years have witnessed a tremendous growth of visual recognition systems both in terms of precision as well as the complex tasks that they can perform. Recent visual recognition systems can not only answer simple questions such as “what object is in the image” or “where is particular object present in the image”. They can also address complex questions such as “whether a object is falling in the image” or “if it will break on falling”. A part of the above success of recent visual recognition systems can be attributed to the advances in computing systems such as Deep Neural Networks (DNNs) especially Convolutional Neural Networks (CNNs).

Recently, with the use of deep CNNs, the field of computer vision has achieved impressive results on a wide range of applications such as image classification, object detection, semantic segmentation, image super-resolution, action recognition, and pose detection. In general, the trend is to achieve higher performance by developing deep and complex models using large computational resources. However, this progress is not necessarily making the networks more efficient with respect to memory and computational cost. In many real world and resource constraint applications such as robotics, satellites, drones, and self-driving cars, the tasks are required to be carried out in a computationally efficient manner. Therefore, there is the need to develop space-time efficient models for such applications. In this thesis, we focus on developing resource efficient CNNs for various core computer vision tasks such as image classification, medical image segmentation, and human action recognition.

A key source of high space-time complexity in CNNs is the convolutional layer itself. The standard implementation of the 2D convolutional layer learns the spatial and channel correlations simultaneously. We propose space-time efficient alternative to this layer that partitions this process into two parts. First, we capture spatial information using non-trainable channelwise 2D Short Term Fourier Transform (STFT). Next, the 2D STFT feature maps are passed through trainable pointwise convolutions in order to learn the channel correlations. Such an architecture leads to significant saving in memory and computations since the only learnable part here is the pointwise convolutions and the 2D STFT is applied in a depthwise fashion. Our experiments on various benchmark datasets on different computer vision tasks e.g., image classification and segmentation show that the

proposed layer achieves better performance compared to the standard convolutional layer despite using less trainable parameters and computations.

The problem of high space-time complexity becomes more prevalent in deep 3D CNNs. Here, the 3D convolutional kernels need to learn the temporal correlations along with the spatial and the channel correlations. The standard implementation of the 3D convolutional layer learns all the three correlations simultaneously. We extend the 2D STFT based layer discussed above to the 3D domain and propose three alternatives to the standard 3D convolutional layer. The *first* alternative captures the spatial and temporal information using non-trainable channelwise 3D STFT. The *second* alternative captures the spatial information using the non-trainable channelwise 3D STFT and temporal information using the trainable depthwise convolutions. The *third* alternative captures the temporal information using the non-trainable channelwise 3D STFT and spatial information using the trainable depthwise convolutions. The outputs of these layers are then passed through the pointwise convolutions in order to capture the channel correlations. Our experiments on various benchmark human action recognition datasets show that capturing temporal information using 3D STFT significantly improves the performance achieving state-of-the-art results along with a significant saving of memory and computations. In another variant of the 3D convolutional layer, we also propose to replace the non-trainable 3D STFT with a local binary volume layer followed by pointwise convolutions in order to reduce the space-time complexity and improve performance for the task of face expression recognition. Thus, the proposed methods show that partitioning the process of learning various correlations and capturing them using non-trainable techniques such as STFT and local binary filters improves the space-time complexity of CNNs as well as their performance.

Finally, we propose a challenging human pose estimation dataset. Existing datasets for learning human poses are observed to be not challenging enough in terms of pose diversity, object occlusion, and view points. This makes the pose annotation process relatively simple and restricts the application of the models that have been trained on them. To handle more variety in human poses, we propose the concept of fine-grained hierarchical pose classification, in which we formulate the pose estimation as a classification task, and propose a dataset, Yoga-82. We also present modifications of the DenseNet architecture in order to utilize the hierarchy of our dataset for achieving better pose recognition.

Title: Fair multiparty computation using blockchain
Researcher: Shrivastava, Ananya
Supervisor: Paul, Souradyuti
Year: 2021
Keyword's: Multiparty Computation (MPC), Fairness, Fine-based Robustness, Cryptography, Blockchain, Bilinear Pairing, Data Trading.
Call No.: 005.82 SHR
Acc. No.: T00727

Abstract: The last decade has been marked by the unprecedented rise in the Internet-based applications (e.g., secure computation, e-commerce, blockchains, and FinTech). On the heels of the exponential growth of the Internet, have come a slew of novel technologies for storing and processing data intelligently (e.g., Artificial Intelligence (AI), Machine Learning (ML), Internet-of-Things (IoT), Cloud, Edge). This rapid increase in communications between various parties, nodes and other stakeholders on the Internet has, however, exposed the data to unauthorized use and illegitimate possessions, leading to various forms of cyber-crimes as well as the reduction in business activities. This thesis is mainly about developing powerful peer-to-peer (P2P) *computing* and *data storage* platforms by combining traditional *secure multiparty computation* (SMPC) and *Blockchain*. In an *SMPC*, a set of mutually distrusting parties can jointly execute an algorithm (or a program) without revealing their individual secrets. For real-life deployments, a P2P communication platform – in addition to having the traditional privacy and correctness properties – should have the *fairness* property as well; the *fairness* property guarantees that either all the parties learn the final output or nobody does. While *unconditional* fairness is impossible to achieve in any SMPC protocol, as shown by Cleve in 1986, the advent of Blockchain technology has shown great promise that a smart combination of an SMPC protocol and Blockchain may rescue this property in various useful applications, if designed with adequate caution and ingenuity.

Concretely, in this thesis, we have designed and analyzed four Blockchain-based MPC protocols solving as many distinct problems with varying degrees of security properties. We explain them briefly below.

In the first part, we designed two MPC protocols to compute an *arbitrary* function in the malicious model with the dishonest majority that guarantees *fairness*; this protocol is built on the Blockchain and critically uses *trusted hardware*. Our protocol achieves security even when the underlying MPC component is allowed to output an incorrect value. We also showed that under the same assumption, the *fairness* property of the existing protocols by Choudhuri *et al.* (ACM CCS'17) and Kaptchuk *et al.* (NDSS'19) collapses.

Next, we built from scratch a *fair* Blockchain-based data exchange protocol in which a seller can obviously trade files against a matching keyword. It turns out that our protocol is more efficient as well as better security than the existing protocols of Boneh *et al.* (Eurocrypt 2004), Popa *et al.* (USENIX-NSDI 2014), Jiang *et al.* (FGCS 2017), and He *et al.* (ICISC 2018).

Finally, we focus our attention on constructing an MPC protocol to compute an *arbitrary* function guaranteeing a stronger security notion than the fairness property called *fine-based robustness*. The *fine-based robustness* property guarantees that all the parties will either receive the output of the function or get compensated (that is, the protocol does not abort, unlike in *fairness*), once the protocol finishes the initial round of execution. Our protocol improves upon the verification time of the previous KZZ protocol (Eurocrypt 2016) from $O(n^6)$ to $O(n^3 \log n)$.

For all the above protocols, we have provided rigorous security proofs by exploiting the well-established mathematical hardness of some of the existing primitives such as bilinear maps, hash functions, signature scheme, and authenticated encryption. We have also mentioned several interesting open problems that arose out of our work.

Title: Deep feature learning: training with no prior examples and its applications
Researcher: Mastan, Indra Deep
Supervisor: Raman, Shanmuganathan
Year: 2020
Keyword's: Deep Image Prior, Deep Contextual Feature Learning Framework, GAN Framework, Deep Internal Learning for Image Enhancement
Call No.: 004.6 MAS
Acc. No.: T00728

Abstract: Many computer vision tasks could be formulated as image feature learning tasks where the objective is to perform image restoration or image synthesis. Image restoration is an ill-posed problem aiming to restore an image from a corrupted observation. The image synthesis task is related to synthesizing a new image while preserving various properties such as image context and object structure. The deep learning framework to perform image restoration and image synthesis without using paired samples for training was not explored until 2017. Recently, we have witnessed various research frameworks that are able to perform such tasks without using paired samples. By paired samples, we mean a training dataset consisting of pairs of source and target images, e.g., a clean and noisy image pair for image denoising.

Deep feature learning without using prior examples has practical applications for situations where one has limited computational resources, the training samples are difficult to collect, and one needs image output having no influence through bias from the training samples. Initial frameworks that do not use paired samples for training were proposed for image restoration tasks such as denoising and super-resolution. The key observation was the network structure itself works as an implicit image prior to perform image restoration as in Deep Image Prior (DIP). We propose a general framework (*MED*) to study how the structure of the network influences the quality of restoration. Our framework allows various network structures by modifying the network components such as skip links and the composition of the encoder-decoder subnetworks. These handcrafted network structures illustrate how the construction of untrained networks influence the following image restoration tasks: denoising, super-resolution, and inpainting.

Later, the deep internal learning-based single image GAN framework (InGAN and SinGAN) was proposed for the image synthesis task. Inspired by InGAN, we propose a single image GAN framework Deep Contextual Internal Learning (DCIL) for image restoration and image synthesis tasks. There are two interesting challenges here. (1) What aspects of the network would help in the GAN framework for image generation when there is a lack of feature learning from the training samples? (2) What should be the structure of the loss function when the source image and the target image are not aligned and do not have spatial correspondence? Our DCIL framework investigates the challenges above. It uses the internal learning of image context to perform various tasks. We perform image resizing application in the following setups: classical image resizing using super-resolution, a challenging image resizing where the low-resolution image contains noise, and content-aware image resizing using image retargeting.

The challenge in learning deep features without prior examples is to learn the semantics of the scene. We proposed a Deep Contextual Feature Learning framework (DeepCFL) to preserve and synthesize contextual features when performing image restoration and image synthesis. The contextual features are simply high dimensional vectors representing the semantics of the given image. DeepCFL is a single image GAN framework that learns the distribution of the context vectors from the input image. We show the performance of contextual learning in various challenging scenarios: outpainting, inpainting, restoration of randomly removed pixels, and object synthesis. We also propose a framework Deep Object-based Style Transfer (DeepObjStyle), where the task is to synthesize a new image that incorporates content features from the content image and style features from a style image while minimizing the content mismatch due to feature correlation in content and style images. Another interesting problem we address is the image enhancement of corrupted images to improve image quality. Our Deep Internal Learning for Image Enhancement framework (DILIE) shows the generalizability of deep learning methods for diverse applications such as hazy and noisy image enhancement.

Our novel strategies for image restoration, image synthesis tasks, and the related methods have shown that training deep IR models without using training samples (i.e., source and target image pairs) can be performed and applied to solve several low-level vision problems efficiently.

Title: Algorithms and space efficient representations for finite groups
Researcher: Sharma, Shivdutt
Supervisor: Das, Bireswar
Year: 2020
Keyword's: Algorithms, Data Structures, Computer Programming, Hamiltonian
Call No.: 005.73 SHA
Acc. No.: T00729

Abstract: In this thesis, we study algorithms and data structures for problems related to group theory. We design linear and nearly linear-time algorithms for the group isomorphism problem for some restricted group classes. We also design space efficient data structures for groups and compact data structures for Dedekind groups and finite rings.

Given two objects, the problem of checking whether they have the same structure or not is known as the isomorphism problem. Two groups are said to be isomorphic if and only if there exists a bijective homomorphism from one group to the other. Given two input groups by Cayley tables, deciding if the given groups are isomorphic is known as the group isomorphism problem. The group isomorphism problem is polynomial-time reducible to the graph isomorphism problem. The graph isomorphism problem is unresolved, a well-known problem in the field of theoretical computer science and it is interesting to many researchers due to its complexity status. Apart from its connection to the graph isomorphism problem, the group isomorphism problem is also of independent interest. Several attempts have been made in the past to solve the problem efficiently. Designing efficient algorithms for restricted group classes have been explored to a great extent in the past. Several restricted group classes admit polynomial-time algorithms for the group isomorphism problem. We study the group isomorphism problem for restricted group classes. Kavitha gave a linear-time isomorphism algorithm for abelian groups (JCSS 2007). Although there are isomorphism algorithms for certain nonabelian group classes, the complexities of those algorithms are usually super-linear. We design linear and nearly linear-time isomorphism algorithms for some nonabelian groups. In the process, we also design efficient algorithms for several other group theoretic problems.

More precisely,

- We design a linear-time algorithm to factor Hamiltonian groups. This allows us to obtain an $O(n)$ algorithm for the isomorphism problem of Hamiltonian groups, where n is the order of the groups.
- We design a nearly linear-time algorithm to find a maximal abelian direct factor of an input group. As a byproduct we obtain an $O(n)$ isomorphism for groups that can be decomposed as a direct product of a nonabelian group of bounded order and an abelian group, where n is the order of the groups.
- We observe that testing normality, computing the center of a group, finding a logarithmic sized generating set, computing quotient groups for groups given by their Cayley table could be done in linear or nearly linear-time.

Next, we study space efficient data structures for groups and rings. Our aim in this part is to develop space efficient data structures for groups and finite rings that can answer multiplication queries (and addition queries for rings) quickly. We focus on designing data structures in the standard random-access memory (RAM) model and its variants defined in the past. To represent the Cayley table of a group of order n in the RAM model it needs $O(n^2)$ words. A multiplication query in the Cayley table representation can be answered in time $O(1)$. Therefore, to ask if there is an $O(n^2)$ space representation of groups that still has $O(1)$ query time is an interesting question. We proved that for any δ with $1/\log n \leq \delta \leq 1$, there is an $O(n^{1+\delta}/\delta)$ space representation with $O(1/\delta)$ query-time for groups of order n . We also show that there are $O(n)$ space representations with logarithmic query-time for simple groups and several group classes specified as a semi-direct product, where n is the group size.

There is a computational model for a group representation described by Farzan and Munro (ISSAC'06). Farzan and Munro proved that abelian groups can be represented in this model with $O(1)$ space and $O(1)$ query time. They asked if their result can be extended to categorically larger group classes. For Hamiltonian groups and some other classes of groups, we construct data structures with constant query-time in their model. A data structure that achieves the optimum information theoretic lower bound asymptotically is known as a compact data structure. Farzan and Munro (ISSAC'06) gave an information theoretic lower bound of $n \log n$ bits to store a group of size n . This lower bound implies an $\Omega(n)$ lower bound on the number of words required to store a group in word-RAM model.

For functions $s, t : \mathbb{N} \rightarrow \mathbb{R}_{\geq 0}$, we say that a data structure is an $(O(s), O(t))$ -data structure if it uses $O(s)$ space and answers a query in $O(t)$ time. Except for cyclic groups it was not known if we can design $(O(n), O(1))$ -data structure for interesting classes of groups. We achieve information theoretic lower bound by designing $(O(n), O(1))$ -data structures for several classes of groups and for any ring. More precisely, we design $(O(n), O(1))$ -data structures for the following algebraic structures with n elements: Dedekind groups, groups whose indecomposable factors admit $(O(n), O(1))$ -data structures, groups whose indecomposable factors are strongly indecomposable, groups defined as a semidirect product of groups that admit $(O(n), O(1))$ -data structures and finite rings

Title: Streaming coresets for machine learning algorithms
Researcher: Shit, Supratim
Supervisor: Dasgupta, Anirban
Year: 2021
Keyword's: Streaming, Coreset, Sampling, Tensor Contraction, Subspace Embedding Bregman Divergence
Call No.: 006.31 SHI
Acc. No.: T00730

Abstract: Machine learning algorithms typically consist of optimizing some objective in a high dimensional space. The huge size of the data causes many learning algorithms to suffer from scalability issues. In this thesis, we address this problem by creating coresets. A coreset is a judiciously selected (and reweighted) set of points, often from the input points themselves, such that solving the optimization problem on the coreset gives a guaranteed approximation to the solution of the optimization problem on the full data. We present algorithms for streaming coresets, for various machine learning methods such as latent variable models, ℓ_p subspace embedding and clustering via Bregman divergence. We propose importance sampling based coresets, which rely on sensitivity framework. Our coresets can also be used in the restricted streaming (online) setting where, for every incoming point the algorithm maintains a small set of statistics of the data that has arrived so far and based on this it takes the sample/no-sample decision before looking at the next point. The coresets for latent variable models are based on robust tensor factorization. Here we worked on symmetric tensors for which we present coreset that preserve *tensors contraction*. We show a relation between p -order tensor contraction and ℓ_p subspace embedding for integer valued p . Our coresets ensure relative error approximation for even ordered tensor contraction and ℓ_p subspace embedding, whereas for odd order tensor, it ensures additive error approximation. For a dataset of n samples in d dimension, here we present two novel methods LineFilter and KernelFilter. The LineFilter can quickly take the sampling decision, but it ends up with $(n^{1-2/p}d\epsilon^{-2})$ expected samples. The KernelFilter first *kernelizes* each point to a higher dimensional space and then takes the sampling decision. It has an expensive update time but only have $(d^{p/2}\epsilon^{-2})$ expected samples for even p and $O(n^{1/p}d^{p/2}\epsilon^{-2})$ for odd p . Due to the online nature of the two modules, we propose various algorithms using them. The resultant coresets either match or improve upon the current state of the art results in terms of size, running time, and working space. As we can use tensor factorization for learning neural network parameters, so our algorithms can also be used in such cases to improve the running time for learning neural networks.

We also present coreset algorithms, which ensures a deterministic ℓ_p subspace embedding. We give two algorithms DeterministicSampler and DeterministicFilter. For DeterministicSampler we show that by sampling (deterministic) enough points in the coreset, we can ensure the deterministic guarantee. This algorithm is particularly useful when the *sensitivity scores* follow some power law decay. The DeterministicFilter does random sampling, yet its coreset ensures a deterministic ℓ_p subspace embedding. Our algorithm is similar to the elegant technique of barrier potential based sampling used for spectral sparsification (ℓ_2 subspace embedding). In combination with LineFilter and KernelFilter, we show that it can be extended to get random coresets, which ensures

deterministic guarantee for ℓ_p subspace embedding. Our coresets are useful for problems like regression and low rank approximations. We also present LiteFilter which gives lightweight coreset for l_p subspace embedding. The algorithm returns a small coreset in just input sparsity time at the cost of a small additive error approximation.

We propose an algorithm (ParametricFilter) to create online lightweight coresets that ensure a small additive error approximation for the clustering with Bregman divergence. Our algorithm works for Bregman divergence, which is μ -similar to some squared Mahalanobis distance. The algorithm is easily scalable as it only takes $O(d)$ update time and working space. Our coreset size only has logarithmic depends on the structure of the input data,

$$i.e., O \frac{\log n + \log(f_\phi(\mathbf{A}))}{\epsilon^2}$$

where n is the input size and $f_\phi(\mathbf{A})$ is the sum of distances of each points from the mean ϕ . We also present an algorithm (NonParametricFilter) which gives a non-parametric coreset, whose sample size is independent of both dimension of input points and the number of clusters. Such a non-parametric coreset is only possible as our coreset ensures an additive error guarantee. We achieve this using sensitivity based framework along with barrier potential functions. It is challenging to estimate the scores for clustering, unlike ℓ_p subspace embedding. For this we use *empirical sensitivity scores*, where we sample enough query points to estimate the true sensitivity scores. At a high level, our coresets are non-parametric because the expected upper bound of these scores (used to define sampling probability) is independent of both dimension of the input point and the number of centers. Here due to the use of barrier potentials, we do not need a union bound of a query set to show a strong coreset guarantee.

We have also presented empirical results on real datasets to compare our algorithms' performance with known baselines.

Title: On coresets for regularized and fair machine learning problems
Researcher: Chhaya, Rachit
Supervisor: Dasgupta, Anirban
Year: 2022
Keyword's: LASSO, Machine Learning, Socially Fair Clustering, Automated Data, Clustering
Call No.: 005 CHH
Acc. No.: T00950

Abstract: Most applications of machine learning require large amounts of data to train models and hence computational efficiency is a cause of concern. A common strategy is to train the model on a judiciously selected subsample of the data. A coreset is a subsample of appropriately reweighted points from the original data which can be used to train models with competitive accuracy and provable guarantees. The size of a coreset is usually much less than the size of the original dataset, making training on them more efficient. Coresets are known for many machine learning problems like regression, clustering etc. In our work we focus on coresets for problems which either have a regularization term or some fairness constraints. These constraints can impact the guarantees for the coreset as well as the size of the coresets. Construction and analysis of coresets for ML problems with additional regularization term or fairness guarantees is the main focus of the thesis. We focus on the scenario where the number of points n is much larger than the number of dimensions d .

In the chapter - "On Coresets for Regularized Regression", we study the effect of norm based regularization on the size of coresets for regression problems. Specifically, given a matrix $\mathbf{A} \in \mathbb{R}^{n \times d}$ with $n \gg d$ and a vector $\mathbf{b} \in \mathbb{R}^n$ and $\lambda > 0$, we analyze the size of coresets for regularized versions of regression of the form $\|\mathbf{Ax} - \mathbf{b}\|_r/p + \lambda \|\mathbf{x}\|_s/q$. Prior work has shown that for ridge regression (where $p, q, r, s = 2$) we can obtain a coreset that is smaller than the coreset for the unregularized counterpart i.e. least squares regression. We show that when $r \neq s$, no coreset for regularized regression can have size smaller than the optimal coreset of the unregularized version. The well known LASSO problem falls under this category and hence does not allow a coreset smaller than the one for least squares regression. We propose a modified version of the LASSO problem and obtain for it, a coreset of size smaller than the one for least square regression. We empirically show that the modified version of LASSO also induces sparsity in solution, similar to the original LASSO. We also obtain smaller coresets for ℓ_p regression with ℓ_p regularization. We extend our methods to multi-response regularized regression. Finally, we empirically demonstrate the coreset performance for the modified LASSO and the ℓ_1 regression with ℓ_1 regularization.

Automated data driven decisions play an increasingly important role in a number of settings, and correspondingly, the need for ensuring fairness of such automated procedures has become critical. This has naturally led the machine learning research community to propose various measures of fairness. Notions of fairness can apply to some protected group setting or to each data point individually. Fairness notions have been defined for both supervised and unsupervised learning setting. Incorporating fairness notions into the optimization can often increase the complexity of

the resulting optimization that needs to be solved (evident, for instance, in the fair regression with statistical parity setup, for which current algorithms are roughly $O(n^2)$ for n points). This is not always desirable from a practical standpoint, since it could lead to the unintended consequence of fairness definitions not being adopted widely. In the next part of the thesis we employ the use of coresets to mitigate this additional computational burden.

In the chapter - “On Coresets for Fair Regression”, we present algorithms to construct coresets for three different notions of fairness for regression. For a dataset of n points in d dimensions and having some discrete-valued protected attribute, fair regression with statistical parity requires predictions to be almost independent of the protected attributes. The algorithm to solve this problem on full data takes roughly $O(n^2)$ time. Since the constraints here are data dependent, the set of feasible solutions may change. Hence the definition of coreset for problems without constraints may not be enough. To remedy this, we first modify the notion of a coreset for fair regression and give a coreset that incurs only a small additive error in satisfying the constraints and a relative error in the objective function. The coreset size is linear in ℓ , the number of unique values the protected attribute can take, and the dependence on dimension is near linear ($d \log d$). For fair regression with mean residual difference and group residual difference penalties, we give a coreset of size $O(\frac{d \log d}{E^2})$, by casting these problems as instances of regularized least squares regression.

We also present algorithms to create coresets for two different notions of fair clustering problems in the chapter - “On Coresets for Fair Clustering”. The first fairness notion is an individual notion of fairness and the second is a group based fairness notion called *socially fair clustering*. Individual fair clustering intuitively requires each point to have a cluster center within its n/k nearest neighbours where k is the number of clusters. Existing algorithms take $O(n^4 k^4)$ time to give a bicriteria solution to the problem. Here again, we modify the notion of coreset and give a coreset of size logarithmic in n which approximates the cost function with relative error and the fairness criteria with a small additive error. In socially fair clustering the idea is to minimize the maximum average cost of clustering across all groups. For socially fair clustering, we give coresets of size $O(\ell B)$ where B is the size of a coreset returned by any coreset algorithm for the particular clustering problem and ℓ is the number of distinct groups. To the best of our knowledge these are the first coresets for the said notions of fairness for both regression and clustering.

Title: Decoding cognitive states from brain rhythms: insights from media perception and meditation studies
Researcher: Pandey, Pankaj
Supervisor: Miyapuram, Krishna Prasad
Year: 2023
Keyword's: Electroencephalography (EEG), Brain Rhythms, Emotion, Music, Meditation
Call No.: 616.891425 PAN
Acc. No.: T01087

Abstract: Studying how complex stimuli are dynamically processed by our brains is a very fascinating and challenging area. Historically, the field of Artificial Intelligence and Machine learning has been inspired heavily by understanding brain function, including recent developments in deep convolutional neural network architectures. Non-invasive measurement of brain function using electroencephalography (EEG) makes it possible to study brain oscillations (rhythms) at different frequency bands that are relevant to various cognitive processes. Human neuroscience research often uses laboratory-based experimentation that has limited ecological validity. While we are far away from studying cognition in the wild, studying naturalistic scenarios offers a good middle ground. Recently, wearable neurotechnology products such as wireless EEG have started penetrating the consumer market which has provided further impetus to research and application development for everyday scenarios such as listening to music, playing video games, or practicing meditation.

The non-invasive study of brain activity is primarily carried out through EEG due to its high temporal precision, broad accessibility, and portability (low-cost wearable devices). EEG rhythms have been identified that could be putative neuromarkers that map to specific cognitive states. The potential of developing EEG-based predictive models of media and self-induced experiences is still largely untapped. Researchers have already shown the potential neural markers of different experiences using standard analysis approaches such as event-related potentials in the time domain and spectral analysis i.e. power of different frequency bands. Past research efforts to identify neural correlates of experience pave the way for this thesis to develop machine learning models to predict different cognitive states with a specific focus on brain rhythms.

This thesis explores the efficacy of various features of brain rhythms to build machine learning prediction models for decoding cognitive states in media perception (listening music, watching movie clips) and meditation studies. While the former scenarios represent externally presented stimuli, the latter signifies self-induced cognitive states. Decoding the cognitive states from such scenarios would therefore be indispensable to develop neuro-feedback systems leveraging the potential of neurotechnological tools. This thesis addresses the significance of brain rhythms for developing machine learning models that demonstrate a rigorous attempt to identify personalized and shared features for a common task. We study three cognitive scenarios: movie-clip watching, music listening, and meditation.

We use 12 EEG naturalistic datasets in this thesis to develop machine learning models for classifying the various cognitive states elicited during movie watching, music listening, and meditation. Neural signatures for the western classification of emotions have been widely discussed in the literature. The ancient Indian treatise on performing arts known as *Natyashastra* categorizes emotions into nine classes, known as *Rasas*. *Rasas* opposed to a pure emotion - is defined as a superposition of certain transitory, dominant, and temperamental emotional states. Although *Rasas* have been widely discussed in the text, dedicated brain imaging studies have not been conducted in their research. Our study examines the neural oscillations, recorded through Electroencephalography (EEG) imaging, that are elicited while experiencing emotional states corresponding to *Rasas*. We identify differences among them using network based functional connectivity metrics in five different frequency bands. Further, Random Forest models are trained on the extracted network features, and we present our findings based on classifier predictions. We observe slow (delta) and fast brain waves (beta and gamma) exhibited the maximum discriminating features between *Rasas*, whereas alpha and theta bands showed fewer distinguishable pairs. Out of nine *Rasas*, Srīngaram (love), Bibhatsam (odious), and Bhayanakam (terror) were distinguishable from other *Rasas* the most across frequency bands. On the scale of most network metrics, Raudram (rage) and Srīngaram are on the extremes, which also resulted in their good classification accuracy of 95%. This is reminiscent of the circumplex model where anger and contentment/happiness are on extremes on the pleasant scale. Interestingly, our results are consistent with the previous studies which highlight the significant role of higher frequency oscillations in the classification of emotions, in contrast to the alpha band that has shows non-significant differences across emotions. This research contributes to one of the first attempts to investigate the neural correlates of *Rasas*. Therefore, the results of this study can potentially guide the explorations into the entrainment of brain oscillations between performers and viewers, which can further lead to better performances and viewer experience.

Naturalistic music typically contains repetitive musical patterns that are present throughout the song. These patterns form a signature, enabling effortless song recognition. We investigate whether neural responses corresponding to these repetitive patterns also serve as a signature, enabling recognition of later song segments on learning initial segments. We examine EEG encoding of naturalistic musical patterns employing the NMED-T and MUSIN-G datasets. Experiments reveal that (a) training machine learning classifiers on the initial 20s song segment enables accurate prediction of the song from the remaining segments; (b) β and γ band power spectra achieve optimal song classification, and (c) listener-specific EEG responses are observed for the same stimulus, characterizing individual differences in music perception. EEG oscillatory correlates of expert meditators have been studied in the time-frequency domain. Machine Learning techniques are required to expand the understanding of oscillatory signatures. In this work, we propose a methodological pipeline to develop machine learning models for the classification between expert and nonexpert meditative state. We carried out this study utilizing the online repository consisting of EEG dataset of 24 meditators that categorized as 12 experts and 12 nonexperts meditators. We have proposed two pipelines comprising wavelet analysis and synchronization. The first pipeline consists of four stages that include feature engineering, machine learning classifiers, feature

selection, and visualization. We decomposed signals using five wavelet families consisting of Haar, Biorthogonal(1.3-6.8), Daubechies(orders 2-10), Coiflet(orders 1-5), and Symlet(2-8), followed by feature extraction using relative entropy and power. We classified the meditative state between expert and non-expert meditators employing twelve classifiers to build machine learning models. Wavelet coefficients d8 shows the maximum classification accuracy in all the wavelet families. Wavelet orders Bior3.5 and Coif3 produce the maximum classification performance with the detail coefficient d8 using relative power. We have successfully classified the meditative state between expert and non-expert with 100% accuracy using d5, d6, d7, d8, a8 coefficients. The second pipeline, exploit four dimensions (Temporal, Spectral, Spatial and Pattern) of EEG data and present an analysis pipeline employing machine learning techniques. We discuss the significance of different frequency bands in relation with distinct primary 5 scalp brain regions. Functional connectivity networks (PLV) are utilized to generate features for classification between expert and non-expert meditators. We find higher accuracy using lower frequency θ and α oscillations over the frontal region. Overall, this works contributes a pipeline to analyze EEG data utilizing various properties and suggests potential neural markers for an expert meditative state.

Studying brain waves elicited during perceptual activity is a rapidly growing interdisciplinary research area encompassing experts from cognitive science, signal processing, and machine learning. In this research, we specifically focus on three naturalistic scenarios including music listening, movie watching and meditating. We use 10 EEG naturalistic datasets acquired at six different nations including USA, Greece, UK, Belgium, India, and China comprising 330 participants to demonstrate feature representation of EEG signals to identify the person. Our primary objective is to identify the personalized differences across datasets and bring a specific features and oscillatory signature. Our objective is to implement a interpretable pipeline incorporating understandable features on five primary brain waves. Previous studies didn't experiment utilizing naturalistic datasets and providing a holistic understanding for getting the information more relevant to personalized differences. We employ linear and non-linear features while training Random Forest classifiers and show the best feature which predicts maximum subjective discrimination. Our research demonstrates the significance of higher oscillations in generating the maximum subjective differences. Beta waves show the maximum contribution in predicting the differences and reaching to maximum 95% accuracy and an average across all datasets of 88.7%. Hjorth Mobility provides the maximum predictive ability. This result has a significant implication in the personalized and generalized models. Our findings exhibit that higher oscillatory β and γ rhythms are more predictive for perceptual activity, including music listening and movie watching. The slow oscillatory rhythms θ and α indicate features for meditation progress. We discuss the implications of our research for the advancement of personalized headset design that rely on feedback on the depth of meditation by learning from expert meditators. The implication of our result on person identification has massive space in the brain-computer interface (BCI) by removing person-specific EEG components that may minimize inter-subject variability to promote generalizability. We contribute two EEG datasets in the public repository, including emotional movie watching clips and music listening.

* * * * *



EARTH SCIENCE

Earth Sciences

Title: Investigating linkages between surface-subsurface processes and its control on geomorphic evolution of river systems in the tectonically active Nahan salient, NW Himalaya, India

Researcher: Kaushal, Rahul Kumar

Supervisor: Jain, Vikrant

Year: 2019

Keyword's: Structural Mapping, OSL Chronology, Kinematic Global Positioning System, Holocene

Call No.: 551 KAU

Acc. No.: T00513

Abstract: This thesis presents geomorphic analysis to understand subsurface neotectonic deformation in the Nahan salient, a tectonically active window of the Sub-Himalaya. The Sub-Himalaya and its south bounding Main Frontal thrust (MFT) is the most tectonically active region of the Himalaya, as total shortening across the Himalaya (~14-21 mm/yr) is mostly accommodated within the Sub-Himalayan thrusts. However, the process understanding of deformation pattern, stress partitioning and shortening rates along active thrusts in the Sub-Himalaya are still lacking or poorly constrained in some windows of the Himalayan arc. A detailed tectono-geomorphic investigation is needed for all such windows, and the Nahan salient is one such less studied area.

My study on the Earth's surface (geomorphology)-subsurface (tectonic) process interaction includes structural mapping, estimation of various geomorphic indices, landform mapping in lab and field, OSL chronology, bed-material grain size analysis, quantification of rock erodibility, semi-quantitative modelling and 1-D modelling of long profile though incorporation of hydrological and hydraulic parameters. Initial analysis using geomorphic indices, structural mapping and field investigations suggest that the Nahan salient is actively undergoing neotectonic deformation along a number of thrust faults in the Sub-Himalaya. The western part of the Nahan salient has been relatively more deformed and significantly uplifted during neotectonic activity. I have also proposed a new buried fault in the central part of the Nahan salient. The major deformation in the Nahan salient seems to be along thrusts at the north of the MFT.

Further, quantitative information of neotectonic deformation was achieved by analyzing chronologically-constrained fluvial landforms. The geometry of uplifted river terraces was mapped using high-precision, Real Time Kinematic Global Positioning System (RTK-GPS) and chronology were established through optically stimulated luminescence (OSL) dating of the fluvial sediments overlying the strath. Field data based structural cross-sections were superimposed with uplifted terraces to estimate uplift /shortening rates. The estimated Holocene average uplift rates are consistently higher in late Holocene as ~6-7 mm/yr (averaged over ~2-4 ka) in comparison to Early Holocene rate as ~1 mm/yr (averaged over ~11-12 ka) on the MFT (~30 km) within the Nahan salient. Late Holocene average uplift rates are also spatially variable along the MFT and it is higher in the

northwest and southeast part of the Nahan salient. Minimum late Holocene average shortening rate across the MFT ranges from $\sim 1\text{-}3$ mm/yr (averaged over $\sim 11\text{-}12$ ka) to $\sim 10\text{-}11$ mm/yr (averaged over $\sim 2\text{-}4$ ka) (considering MFT fault plane dip 30°). These rates are in agreement with the Holocene slip rate of ~ 9 mm/yr from nearby area (Dehradun recess). This study also suggests that most of the ongoing crustal shortening (~ 14 mm/yr) is accommodated along the MFT during late Holocene, and hence the MFT is the most active fault in the Sub-Himalaya of the Nahan salient.

I have extended regional understanding from the Nahan salient to further analyse linkages of surface-subsurface processes through a semi-quantitative approach by incorporating the hydrology and hydraulic parameters. River response to tectonic perturbation is reflected in slope and channel width variability. Though, sensitivity of these parameters will vary in rocks having different erodibility. Hydraulic parameters like shear stress and unit stream power are sensitive to uplift rates as well as to rock erodibility. Peaks in downstream variability of these parameters can be used as a proxy to identify active uplift along the faults, though regional variability in these parameters will reflect variation in rock erodibility. These hydraulic and hydrological indices were further used to identify and classify channel reaches into transport-limited and detachment-limited, because the cause-effect relationship between morphology and subsurface tectonics may vary from transport-limited to detachment-limited rivers. Long profile is the most important and sensitive landform to tectonic disturbances. Hence, I have simulated long profile evolution process for transport-limited reaches through a 1-D model using the stochastic distribution of discharge. I infer that channel steepness is not only sensitive to uplift rate but also to grain size. Hence, gradient of the transport-limited river can be set by changing grain size, even if uplift rate is constant. Further, new quantitative data on erodibility and abrasion rates highlight the role of lithology in river bed-material characteristics and hence on river sensitivity to tectonic perturbation. Semi-quantitative and 1-D model suggests that river morphology and incision patterns are also controlled by the lithological variability by modifying the shear stress/unit stream power.

My thesis finally presents a multi-disciplinary approach to (a) develop tectono- geomorphic understanding of a tectonic active area and (b) to address key research questions on the sensitivity of fluvial landforms to tectonic perturbation. It highlights that in-depth understanding of Earth's surface-subsurface processes could be achieved through multi-disciplinary study by including structural geology, geomorphology, GIS, hydrology and hydraulics through integration of lab, office (modelling) and field investigations.

Title: Causality of river long profile shapes and its implications on river morphological processes
Researcher: Sonam
Supervisor: Jain, Vikrant
Year: 2019
Keyword's: Energy Distribution, Tectono-climatic Settings, Total Stream Power, Geomorphic Processes
Call No.: 550.9 SON
Acc. No.: T00514

Abstract: River long profile (LP) is a plot of the downstream distribution of elevation along a river channel. Rivers are the most dominant agents responsible for shaping the morphology of the Earth's surface. Energy distribution pattern and channel processes along the LP of the trunk stream of a river drainage network set the base level for all erosion and deposition processes within its catchment. Hence, basin-scale analysis of river long profiles (LPs) is of importance to understand its evolutionary trajectory and the resultant controls on river process dynamics. This thesis presents an analysis of the river LPs of some of the major rivers river basins in Indian sub-continent. LPs from the diverse tectono-climatic settings of India have been chosen to capture the maximum diversity of controls on LP shapes. These include the LP of river channels from (1) the tectonically active and humid Himalayan tributaries of the Ganga River basin in bedrock setting, (2) the tectonically active and tropical climate of the Ganga River alluvial plains, (3) the tectonically passive Peninsular India with tropical climate, and (4) the tectonically active Kuchchh region in semi-arid western India. The purpose of this study is to evaluate the role of inherent geological controls on the shape of river LP. The river LP shape further governs geomorphic processes by shaping the stream power distribution pattern in a river channel. Hence, the main thesis objective is to analyse river LP data to assess the inherent geological controls on geomorphic processes.

Shuttle Radar Topographic Mission (SRTM)-Digital Elevation Model (DEM) data of 90 m resolution were used to derive the river LPs of major rivers, and the mapping of geological features (rock types and faults) was done using Geological Survey of India (GSI) Seismotectonic Atlas (scale-1:1,000,000). Hydrological data sets were obtained from Central Water Commission (CWC) and National Remote Sensing Centre (NRSC) archives. Rainfall variability was analysed using TRMM data sets.

Different shapes of river LPs exist in the four different tectono-climatic settings of India. Differences in shape is a reflector of one or a combination of factors such as heterogeneity in lithological (rock erodibility), climatic and tectonics, which result in differences in the rate of downstream change in channel slope along LP.

Sum of two exponential functions can be an appropriate representation of LP shape in regions with high uplift rate and where rock erodibility increases downstream e.g. the Himalayan tributaries of the Ganga River basin. However, the smaller river channel (length 20 to 35 km, in the tectonically active semi-arid Kuchchh region) which are flowing over uniform lithology do not have much concavity in their LP shape. Such LPs of smaller rivers can be represented by linear function. Further, in tectonically stable landscapes (of Peninsular India) where the LPs of river channel have a

downstream decrease in rock erodibility, do not have a well-defined shape and may not be represented by simple mathematical functions (linear or exponential).

The LP shape further governs the stream power distribution pattern along river channels. The downstream distribution of total stream power (TSP) can be mathematically modelled for rivers with a well-defined LP shape. The TSP distribution pattern obtained based on the sum of two exponential functions successfully explains the spatial variability in geomorphic processes. On the other hand, rivers which do not have a well-defined LP shape, have a randomly distributed TSP variability. For smaller river channels flowing over uniform lithology do not have much concavity in their river LPs and have nearly linear shape. However, owing to tectonic uplift along faults several small knick points are preserved in their LPs. The high Ks_n (normalised steepness index) zones correspond to knick points formed owing to tectonic activity along active faults. The Ks_n values also serve as a proxy of TSP.

My thesis presents a quantitative approach of LP analysis to unravel the role of geological (landscape) memory on geomorphic processes. Geological control on geomorphic processes is fundamental in nature, and its quantitative understanding establishes the significance of geological characteristics in basin-scale stream management studies. Analysis of the downstream distribution of TSP further establishes river LPs as fundamental units of landscape evolution.

Title: Quantitative geomorphic study of river networks and topography in the northwest Himalaya, India
Researcher: Sahoo, Ramendra
Supervisor: Jain, Vikrant
Year: 2019
Keyword's: Landscape Patterns, Drainage Network, Terrain Slope Variability, Clustering Technique, Hydrological Behavior
Call No.: 551.4 SAH
Acc. No.: T00533

Abstract: Fluvial landscape patterns are excellent markers of the inherent processes governing the evolution of rivers and its landscape. Hence, fluvial patterns are often used as proxies in geomorphic analysis to infer the geological history of a river basin. To this end, this thesis carries out a thorough examination of river or drainage network (DN) pattern and topography geometry in a tectonically active setting of the Northwest Himalaya, India. The main objective of this thesis was to quantify the relationship between river basin geology (including tectonics and lithology) and topography geometry, DN and subsequent modern-day hydrological behavior of a river basin. I used the freely available digital elevation model (DEM) data provided by Shuttle Radar Topography Mission (SRTM) for all my analysis.

In the first part of the thesis, I investigated the sensitivity of the synthetic hydrological response of a river basin to the spatial resolution of the DEM data. I found the river planform (DN)-based hydrological model, which is a function of DN morphometric parameters, to be consistent with DEM resolution. Next part of the thesis probed into the accuracy of different channel initiation functions for extraction of river network. My results showed that a slope-area initiation function is more efficient than a fixed-area initiation function in river basins with higher slope variability. Further, a slope-area initiation function was found to better capture the variability in drainage density resulting from terrain slope variability. The third part of the thesis addressed the effect of geology (lithology, tectonics, and long-term climate) on the geometry of fluvial topography. I characterized the topography as a fractal surface using its fractal dimension and topographic amplitude. Using basic clustering technique, I demonstrated that these two features together can accurately discriminate different physiographic settings. Further, my results revealed lithology to be a stronger control on topographic geometry even in a tectonically active fluvial setting. Last part of the thesis looked into the impression of tectonic uplift on the topology of DN topology. My results showed a significant effect of tectonic uplift on DN pattern, which also led to defining an indirect control of tectonic uplift on the hydrological response of a river basin. This also underlines the role of geological memory in modern-day process-response relation in a fluvial system. Moreover, discharge is an important governing variable in landscape evolution models and is regulated by climate parameters like precipitation characteristics. My results indicated that discharge is also likely to be very sensitive to change in tectonic uplift. Overall, my thesis highlighted the importance of an integrated multi-faceted study to fully understand the long-term effect of geological processes on fluvial system morphology, its landscape and its modern-day hydrological behavior.

Title: Climate and anthropogenic contribution to groundwater storage variability in India
Researcher: Akarsh A.
Supervisor: Mishra, Vimal
Year: 2020
Keyword's: Sustainable Agriculture, Climate Variability, Teleconnection, Terrestrial Water Storage
Call No.: 551 AKA
Acc. No.: T00559

Abstract: A significant fraction of the Indian population is directly or indirectly involved in agriculture. Over 70% of food grain production in India comes from the irrigated agriculture in which groundwater plays a considerable role. Groundwater has been one of the major driving forces in the irrigated agriculture growth over the last three decades in India, and now about 60% of total irrigated crop production is dependent on groundwater resources. Moreover, groundwater is considered as stored water to meet the requirements during extreme drought conditions and to supplement surface water resources. In the initial stages of the green revolution, surface water was the primary source of irrigation in Indian agriculture. Irrigation using the groundwater resources expanded exponentially from the 1970s due to the availability of mechanical pumps and subsidized electricity supply. This rapid expansion in irrigated areas and resources to pump groundwater caused a noticeable decline in groundwater in many parts of India. Therefore, sustainable management of groundwater resources is essential to meet the requirements of the growing population and for food production. However, our understanding of the relative contribution of groundwater pumping and climate variability on groundwater and terrestrial water storage in India remains limited.

Groundwater plays a major role in food and freshwater security in India that could be compromised in some regions by groundwater depletion primarily due to abstraction for irrigation. Another coincident and generally unacknowledged threat to groundwater resources is the increasingly erratic Indian summer monsoon that has decreased precipitation in many parts of north India and is influenced by sea surface temperature anomalies in the Indian Ocean. However, it remains unclear how the groundwater storage variability in India is driven by abstraction for irrigation or the monsoon season precipitation. To assess the relative influence of pumping and climate variability on groundwater storage in India, we use the groundwater observations from Gravity Recovery and Climate Experiment (GRACE) satellite and well level observations. Our results show that long-term change in the monsoon season rainfall is a major driver of groundwater resource variability in most parts of India either directly by changing recharge or indirectly by changing abstraction. We observed a decline in groundwater storage in northern India at the rate of 2 cm yr⁻¹ and an increase in south India at the rate of 1 to 2 cm yr⁻¹ between 2002 and 2013. The changes in precipitation can explain a large fraction of the total variability in groundwater storage in north-central and southern India. Groundwater storage variability in north-western India can be explained predominantly by variability in abstraction for irrigation, which is, in turn, influenced by changes in precipitation. Declining precipitation in northern India is linked to Indian Ocean warming, suggesting a previously unrecognized teleconnection between ocean temperatures and groundwater storage.

Precipitation intensity has changed in the observed climate and likely to change under the future climate in India. However, the crucial impact of precipitation intensity on groundwater recharge in India remains unknown. We evaluate the role of year to year variability of precipitation amount and characteristics (low and high intensity) on groundwater storage variability in India. Using groundwater well level observations, we show the strong linkage between precipitation intensity and groundwater recharge in India. In the northwest and north-central India, the low-intensity precipitation is strongly linked with groundwater recharge, whereas in South India, the major driver is high-intensity precipitation. We observed a decline in the low-intensity precipitation in the northwest and north-central India that are strongly driven by sea surface temperature over the Pacific Ocean. Increases in the high-intensity precipitation in South India are linked with the sea surface temperatures in the Atlantic Ocean. Our results highlight the importance of precipitation intensity for the monsoon season groundwater recharge in India, which can provide insights to manage rapidly declining groundwater resources in India sustainably.

The role of vegetation growth on groundwater storage variability is quantified at annual and seasonal scale using Gravity recovery climate experiment (GRACE) groundwater storage anomaly (GWSA) and Solar-induced chlorophyll fluorescence (SIF). At an annual time scale, precipitation is positively correlated with groundwater storage variability in north-central (NCI), and south India (SI). Whereas in northwest India, precipitation is negatively correlated with GRACE groundwater storage anomaly. The negative correlation between GRACE groundwater storage variability and precipitation in northwest India is attributed to groundwater depletion due to anthropogenic pumping from deep aquifers. We show that crop growth is negatively correlated with groundwater storage variability at annual time scales in north India. Analysis of the two main crop growing seasons (Rabi and Kharif) showed that crop growth is negatively related to groundwater storage in both Kharif (June-September) and Rabi seasons in north India (NWI and NCI). Groundwater contributes more than precipitation in NCI during the Kharif season and in NWI and SI during the Rabi season. We observed an increase in soil moisture and evapotranspiration in Rabi season during 2002-2016, attributed to irrigation for growing crops. Our findings based on three regions (NWI, NCI and SI) and two crop growing seasons (Kharif and Rabi) highlight the need for effective management of groundwater resources by introducing efficient water management practices in India.

To quantify the change in groundwater and terrestrial water storage due to climate variability and anthropogenic pumping, we use Variable Infiltration Capacity Simple Groundwater Model (VIC-SIMGM) and GRACE datasets for the major Indian river basins. The GRACE and well level observations have limitations in their spatial and temporal resolutions. The GRACE observations can be effectively utilized for the regional planning but limited in real-time monitoring of groundwater at high spatial resolution. Moreover, GRACE and well level observations are influenced by the anthropogenic factors, especially in the irrigated regions. We address these critical challenges by establishing a hydrologic modeling framework that integrates satellite observations and high-resolution meteorological forcing. The model was calibrated and evaluated against observed streamflow, well observations, and GRACE terrestrial water storage anomaly. We observed that under anthropogenic influence, groundwater storage anomaly explains the majority of the

variability in terrestrial water storage. However, under natural conditions, soil moisture is the major contributor to terrestrial water storage in the majority of India. Moreover, we observed a considerable difference in groundwater drought characteristics under anthropogenic influence compared to natural conditions. Hence, the groundwater droughts can be intensified under the anthropogenic influence, which emphasizes the need for sustainable groundwater management in India.

Title: Rate of chemical weathering in tropical region and its controlling factors: small catchment perspective from Western India
Researcher: Prasad, Ravi Kant
Supervisor: Jain, Vikrant
Year: 2020
Keyword's: Chemical Weathering Rates, Small Catchments, Bayesian Brain, Implicit Learning
Call No.: 621.3 PRA
Acc. No.: T00745

Abstract: Attentional processing of objects in the environment is critical for our experience of conscious perception. The control of attention is traditionally classified into either a goal-driven process or a stimulus-driven process. However, two streams of evidence have recently emerged that challenge this dichotomous notion. First, it has been shown that expectation about the impending sensation changes its sensory representation in a way that imitates the effects of attention (Wyart et al., 2012; Cheadle et al., 2015). Two, attention has been shown to be biased by the regularities in the sensory environment through the process of statistical learning Awh et al. (2012). Although the classical paradigms investigating attentional selection have employed probabilistic cueing, they have not isolated the effects of expectation and statistical learning from that of attention. The present thesis reports four empirical studies that report a total of 12 experiments that further our understanding of the effect of expectation and statistical learning on attentional selection. According to the Bayesian account of perception (Clark, 2013; K. Friston, 2005), statistical regularities about the sensory environment are formed through continuous interaction as an active agent. Previous studies have shown that these regularities (or predictions) modulate attentional selection (Wang & Theeuwes, 2018a, 2018b).

The first empirical chapter investigated whether the attentional selection is affected when there is a deviation or error to the predicted regularity. The extent to which attention is modulated by the task-based reliability of the error in prediction was also examined. The results showed that the reliability of the prediction error influences attentional guidance. The attentional guidance was found to change over time, reflecting an online re-calibration of the reliability of the prediction error.

The second empirical chapter investigated the learning-based effects on feature binding, which is traditionally considered to require attentional deployment. In light of recent evidence showing attention-independent learning effects on feature binding (Yashar et al., 2015), this study investigated whether the probabilistic association between the individual features that constitute an object influences learning. The results showed that training participants with a broad range of feature-combinations lead to a better transfer of learning. Follow-up experiment showed that this learning does not happen when the pre-exposed item is task-irrelevant.

The third and fourth empirical chapters investigated the extent to which expectation and attention contributes to effects that were earlier proposed to be exclusive to either expectation or attention. In previous studies, attention is shown to modulate the gain of psychometric function. However, the

manipulation of attention in these studies is conflated by concurrent information about the expectation associated with the stimulus. Thus, studies employing traditional attentional paradigms have conflated the effect of attention and expectation Summerfield & Egnér (2009). The third empirical chapter aimed to dissociate the effect of expectation and attention on psychometric function gain. The results showed that gain in psychometric function due to attention depends on the feature expectation. The study also finds marginal effects of feature expectation on the gain. The fourth empirical chapter extends the paradigm employed in the third chapter to investigate the mechanism underlying sensory attenuation, which is an effect typically ascribed to expectation. The study found that sensory attenuation depends on two factors, one, whether action precedes sensory signal, two, whether attention is deployed to the sensation.

The present thesis reports expectation-dependent and learning-dependent effects by demonstrating changes to traditional measures linked to attention, such as reaction time, search slope, sensitivity, and gain of the psychometric function. The findings broaden our understanding of attention and define it beyond traditional dichotomies. The present findings also challenge the modular notion of perception by re-defining attention as a process that dynamically alters the statistical properties of the sensory representation at every stage of processing.

Title: Topographic variability across a tectonically passive margin and its process dynamics at millennial timescale: a landscape to landform-scale study of the Western Ghat escarpment, India

Researcher: Guha, Shantamoy

Supervisor: Jain, Vikrant

Year: 2020

Keyword's: Western Ghat, Mountainous Terrain, Geomorphic Processes, Rifting History, Gridded Hypsometry

Call No.: 550 GUH

Acc. No.: T00746

Abstract: Evolution of the topography in mountainous terrain results from the interaction between the tectonic, lithology and climate. However, the passive margin escarpments situated at the present-day continental margins are relatively tectonically quiescent for 103-105-year time-scale. Therefore, these landscapes are ideal to evaluate the role of lithology and climate on the landscape evolution process. Additionally, hydraulic (channel width) variability plays a vital role to modulate the effectiveness of the water discharge in bedrock channels, though it is less studied in passive margins. Western Ghat (WG), a prominent high-elevated escarpment with diverse lithology and rainfall distribution is a natural laboratory to assess the role of external controls on the landscape evolution processes. I use the topography, hydrology, hydraulics and millennial-scale erosion to investigate a cross-over scale analysis of the external controls on the topographic characteristics.

The WG escarpment stretches ~1500 km along the west coast of India. First, I took the whole WG escarpment considering forty-five major west-flowing river basins with a cumulative area of $\sim 1 \times 10^5$ km². I carried out a landscape-scale topographic analysis utilizing the local relief, hypsometric integral, channel steepness in distinct lithology zones of the WG escarpment. I observed that the relief and channel steepness increase southward with a lithology transition from Deccan basalt to cratonic Precambrian and Archean igneous and metamorphic rocks (e.g. Granites, Gneiss, Charnockite and other granulites). The hard rock yields higher reach-steepness whereas the rainfall gradient does not play a major role. Additionally, the sediment rating relationship suggested that modern-day sediment erosion processes are inherently controlled by the underlying rock types. Relief is increased or sustained due to the balance between the interfluvial consumption and channel incision process.

Geomorphic processes were further analysed at landform or local scale. I measured the channel width along the main channel for four river basins underlain by different lithologies. The discharge was calibrated and validated through a physically based, semi-distributed and continuous-time hydrological model SWAT. Scaling relationships were estimated for network-scale channel width estimation. I estimated SP, SSP and shear stress along the main channel as well as in the network. The SP values were observed to be generally higher in the downstream part, whereas higher values of SSP and shear stress in the upstream part suggests a considerable role of channel width in SSP

distribution pattern. These data collectively suggest that the erosion is the highest in the vicinity of the escarpment and supports escarpment retreat in the WG escarpment.

To bridge the gap between the modern-day and millennial-scale processes, I have further estimated eight ^{10}Be and one ^3He basin-wide denudation rates. The new data suggests that the erosion rate in the Deccan basalt (~ 60 m/Myr) is significantly higher than the cratonic rivers (< 40 m/Myr). However, integration of my data with previously measured ^{10}Be erosion rates suggests a southward increase in the erosion rates in the cratonic part. Four topographic variables (i.e. basin-mean hillslope, normalized steepness index, local relief and elevation) were considered to evaluate the correlation between topography and erosion rates. Previously, the bivariate relationship between the topographic parameters and erosion rates suggested a moderate relationship and indicated that topography plays a major role in the modulation of the erosion rates. However, the erosion rate for the new dataset does not show any correlation with the normalized steepness index, mean relief and mean elevation which suggests strong local control. Multiple linear regression model and a dominance analysis suggest that the basin-mean hillslope is the most dominant factor. Mean basin SSP also portrays a positive correlation with the erosion rates, albeit when considered a narrow range of erosion rates (~ 40 - 70 m/Myr). This indicates that the hydrological processes are important even though the rainfall does not affect the millennial-scale erosion rates. Collectively the results suggest a lithological control on the millennial-scale erosion rate.

The extensive data from this thesis and synthesis of the landscape evolution processes across different passive margin indicate that the lithology plays the most important role in landscape evolution of passive margins. Although the role of the spatial variability of rainfall is less important, SSP has an important role in the millennial-scale erosion rates. This variation of the hydrological condition is further controlled by spatially varying channel width.

Title: High resolution paleoclimatic study using corals
Researcher: Raj, Harsh
Supervisor: Bhushan, Ravi
Year: 2020
Keyword's: Corals, Lakshadweep And Andaman, Bay of Bengal, Radiocarbon Records
Call No.: 551.6 RAJ
Acc. No.: T00747

Abstract: Corals are important natural archives of environmental records that can provide continuous, long term, high resolution proxy data. Coral records provide insight to the processes governing variability in the sea surface conditions, which can be helpful in understanding the climatic and oceanic changes. This work primarily focuses on the corals from the northern Indian Ocean to understand changes in sea surface conditions recorded in them by studying different geochemical and isotopic proxies. Samples of *Porites* corals were collected from the Lakshadweep and the Andaman islands. These samples were investigated for their stable oxygen and carbon isotopes, Sr/Ca ratios and radiocarbon composition.

The Lakshadweep and the Andaman corals show mean annual growth rate 14.7 ± 4.8 mm/yr and 9.4 ± 2.4 mm/yr respectively. Both corals show a decline in their annual growth rate towards present, which could be related to thermal stress on these coral due to the warming Indian Ocean.

The bimonthly stable oxygen and carbon isotope record from the Lakshadweep show seasonal variability. There exists inter-colony variability in the oxygen isotope values of Lakshadweep corals. This suggests that oxygen isotopic composition of fossil corals from the region should be carefully analysed to decipher past sea surface conditions. The Lakshadweep corals oxygen isotope were used to determine the seawater oxygen isotope of the region. It is observed that period of depleted seawater oxygen isotope corresponds to enhanced Indian rainfall period. It indicates that Lakshadweep coral records can potentially provide information about enhanced Indian monsoon rainfall period. The reconstructed seawater oxygen isotopic values along with available coral oxygen isotope records from literature were used to determine a $\delta^{18}\text{O}$ -SST relation, and the derived relation can be used to reconstruct past changes sea surface temperature variability. The Lakshadweep corals oxygen isotope values of monsoon period record sea surface temperature variations more robustly when compared to summer period. The carbon isotope values of Lakshadweep coral shows depletion during monsoon period. It is observed that $\delta^{13}\text{C}$ variability in Kadmat coral is not only modulated by photosynthesis, but some other processes that contribute to the observed $\delta^{13}\text{C}$ variability.

Paired Sr/Ca and $\delta^{18}\text{O}$ (oxygen isotope) measurement on the Andaman coral was carried out. It was found that coral Sr/Ca values show good correlation with sea surface temperature, but $\delta^{18}\text{O}$ showed weak correlation with sea surface temperature. This indicates significant contribution of seawater $\delta^{18}\text{O}$ variability to coral $\delta^{18}\text{O}$ variations. Using paired Sr/Ca and $\delta^{18}\text{O}$ measurements, seawater $\delta^{18}\text{O}$ changes were calculated. Both sea surface temperature and rainfall influence the seawater $\delta^{18}\text{O}$ of

the region. A linear correlation between monsoon rainfall and coral derived seawater $\delta^{18}\text{O}$ value of corresponding period is observed. Such a correlation can be used to understand past monsoon rainfall. Long term running average value of Andaman coral $\delta^{18}\text{O}$ values show depletion (enrichment) when NINO 3.4 region in east central tropical Pacific Ocean shows warmer (cooler) conditions, suggesting SST conditions in NINO 3.4 region influences the sea surface conditions in the Andaman region. The carbon isotope of Andaman coral shows a good correlation with outgoing longwave radiation values over the region, implying that it is mainly modulated by photosynthesis process in coral.

First radiocarbon records of corals from these islands are reported, which provides important insight on the oceanic conditions prevailing in these regions. These radiocarbon records suggest that the Lakshadweep region is influenced by upwelled waters, whereas surface waters in the northern Andaman region are less influence by upwelling as it is relatively stratified due to fresh water input from rivers. The coral radiocarbon records were used to determine air-sea CO_2 exchange rate over these regions. The air-sea CO_2 exchange rate over the Lakshadweep region is calculated to be $13.4 \pm 2.1 \text{ mol m}^{-2} \text{ yr}^{-1}$, whereas for the northern Andaman region it is $8.8 \pm 1.3 \text{ mol m}^{-2} \text{ yr}^{-1}$. It is observed that air-sea CO_2 exchange rates over the northern Indian Ocean show positive correlation with wind speed. The calculated net regional CO_2 flux from the Lakshadweep region is about 2.5 Tg C yr^{-1} and for northern Andaman region it is $-0.3 \text{ Tg C yr}^{-1}$. This shows that the Lakshadweep region acted as a source of atmospheric CO_2 but the Andaman region behaved like sink for atmospheric CO_2 . The pre-bomb radiocarbon record from the Andaman coral (1948-1951) yields reservoir age correction (ΔR) value of $-138 \pm 61 \text{ yr}$, which is the lowest reported for the northern Indian Ocean. The ΔR values reported from the Andaman basin shows significant variation, wherein southern Andaman ΔR value is higher than that of the northern Andaman and the Bay of Bengal. As the northern Andaman basin receives more freshwater flux as compared to the southern Andaman, such differences in reservoir age could be observed. The obtained ΔR value will be useful for radiocarbon dating of marine samples from the northern Indian Ocean.

Title: Understanding hydrometeorological processes concerning Indian precipitation: insights from oxygen and hydrogen stable isotopes in conjunction with meteorological parameters

Researcher: Oza, Harsh

Supervisor: Deshpande, R. D.

Year: 2020

Keyword's: Hydrometeorological Processes, Isotope Fingerprinting of Waters of India, Evaporation, Orographic Barrier, Socio-Economic Consequences

Call No.: 550 OZA

Acc. No.: T00748

Abstract: Hydrometeorological processes govern the availability and distribution of water in space and time. In the current scenario of global climate change, various trends in amount, intensity and spatial distribution of rainfall, are well recognized with reference to rising temperatures. However, the underlying subtle hydrometeorological processes governing rainfall pattern and distribution are still not quite clearly understood. Until climate driven major changes in hydrological cycle and its socio-economic consequences are identified, understanding contemporary hydrometeorological processes is very much important because it serves as an early warning system. In an agrarian country like India, with its unique geographical and climatic conditions, slightest vagaries in weather systems can disrupt the socio-economy of country. Indian weather systems are predominantly known to be governed by seasonal reversal of winds and the rainfall (monsoon) associated with it. Even though the broad patterns of monsoon and its linkages with other synoptic scale pressure-temperature systems are well known, there are still considerable knowledge gaps in understanding of various hydrometeorological processes operating at different spatial and temporal scales. Insights into these processes, derived from large scale circulation models, have limitations due to constraint on the spatial resolution, and yet pending ground validation through independent means. Therefore, an alternate approach to understand hydrometeorological processes is desirable. Stable isotopes of oxygen and hydrogen in rainwater can be used as tracers to understand the origin, movement and mixing of water molecules, in conjunction with meteorological parameters. Thus, it can be used to identify and understand various hydrometeorological processes governing distribution and availability of precipitation. With this backdrop, under the aegis of a National Programme on Isotope Fingerprinting of Waters of India (IWIN), precipitation samples were collected from 41 Indian stations spread across the country for their oxygen and hydrogen isotopic analysis, and interpretation of isotope data in light of various meteorological parameters.

Study was done to discern various hydrometeorological processes operating at three spatial scale viz., mega-scale (~1000 km), mesoscale (~100 km) and microscale (~1 to 5 km), which concern precipitation in India. Some of the important inferences drawn from the interpretation of isotope data in the present study are: (i) despite being surrounded by marine water bodies in three directions (east, west and south) and bounded by Himalayan mountains in the north, which restricts the moisture laden winds from travelling further north, evaporation from the falling raindrops is one of the dominant processes across the country; (ii) during pre-monsoon and post monsoon the

contribution of continentally derived moisture is significant; (iii) Orographic barrier posed by the Western Ghats to the southwest monsoonal winds causes nominal isotopic depletion in precipitation in leeward side compare to windward side, which indicate enormity of moisture drawn from Arabian Sea (AS) during southwest monsoon season; (iv) continentally recycled moisture predominantly contributes the northern Indian precipitation; (v) in northeast India maximum moisture for rainfall is derived from continental recycling from wetlands, and variation in the availability and isotopic makeup of local surface waters govern the isotopic composition of precipitation (vi) systematic pattern of depletion in precipitation isotope during late southwest monsoon (Aug-Sep), observed from long-term (2005 – 2016) isotopic study, is attributed to multitude of processes such as increased continentally recycled moisture in precipitation, increased rainout fraction due to decreased wind velocity, lowering of cloud base temperature and increased proportion of convective rain; (vii) during the post-monsoon season, contrary to expectation in southern Indian peninsula, isotopic signatures show significant continentally derived precipitation, instead of precipitation derived from the Bay of Bengal (BOB) vapour.(viii) The estimated evaporative loss from falling raindrops for the four representative stations is Jammu: Maximum 52% and Minimum 8%; Jorhat: Max 15% and Min 4%; Ahmedabad Min 8% and Hyderabad Max 29% and Min 15%. (ix) Based on the backward wind trajectory analysis done for four stations, maximum estimated contribution of continentally derived moisture in annual precipitation was found to be ~87% at Jammu and minimum contribution of continentally derived moisture in annual precipitation was found to be ~19% at Ahmedabad.

Title: Biogeochemistry of dissolved aluminium and manganese in the Indian ocean
Researcher: Singh, Naman Deep
Supervisor: Singh, Sunil Kumar
Year: 2021
Keyword's: Aluminium (dAl) And Manganese (dMn), Indian Subtropical Gyre, Arabian Sea, Thermocline Waters
Call No.: 577.14 SIN
Acc. No.: T00749

Abstract: This thesis presents extensive studies on the biogeochemical cycling of dissolved aluminium (dAl) and manganese (dMn) over the vertical water column in the tropical and subtropical Indian Ocean. Towards this, trace metal clean seawater sampling and analytical protocols were established for precise and accurate measurements of dAl and dMn concentrations in seawater. In the Bay of Bengal (BoB), fluvial discharge of lithogenic sediments and subsequent release of labile Al from the sediments play a dominant role in controlling the surface dAl distribution. Considering the steady-state balance between dAl input from lithogenic sediments and removal via passive scavenging, the fractional solubility of Al from the lithogenic sediments supplied to the BoB surface waters is constrained to lie in the range of 1.1-4.7%. During the late winter monsoon period (January-February), advective mixing between the low-salinity, dAl-rich BoB surface waters and the high-salinity, dAl-poor surface waters of the open southern Arabian Sea governs the surface dAl distribution in the eastern and central Equatorial Indian Ocean. Deep-water (>2000-3500m) dAl concentrations in the equatorial Indian Ocean region are generally low and uniform (~2.0-2.5 nM). A steady-state and vertical advection-diffusion-scavenging model is used to estimate the deep-water scavenging residence time of dAl in the equatorial Indian Ocean and found to vary in the range of 92-141 yr. The deposition of Australian dust and advection of Indonesian Throughflow Water translates to the dAl enrichment in the upper water column (<500m) at the northern end of the Indian Subtropical Gyre. Surface dAl distribution in the Arabian Sea demonstrates an east-west gradient, i.e., elevated dAl (12.7-20.9 nM) close to the Indian coastal region and low dAl (1.5-3.3 nM) along the western boundary of the Arabian Sea. Rapid surface dAl removal, due to relatively high biological productivity and a decrease in atmospheric dust deposition flux during the fall-intermonsoon, results in the low surface dAl levels observed in the western Arabian Sea region. Given that the Arabian Sea is marked by significant spatio-temporal changes in surface dAl levels, a simple one-dimensional, non-steady-state model was constructed to simulate, for the first time, the seasonal variability in surface dAl concentrations in the west-central Arabian Sea region (14-20°N, 57-65°E) and to understand the control of seasonal changes in dust deposition input and scavenging removal fluxes on the surface dAl distribution. Such a model could be utilized as a first-order tool to estimate the seasonal variations in dust deposition flux using the surface dAl variations, and vice-versa, in highly meteorologically dynamic basins such as the Arabian Sea. In the western equatorial Indian Ocean, a relative increase observed in the surface dAl concentrations, compared to the western Arabian Sea and the central equatorial region, suggests a local dAl input, presumably, due to the dust influx from the Somali coast.

The intrusions of the high salinity water masses (the Arabian Sea High Salinity Water and the Persian Gulf Water) in the thermocline depths (~75-300 m) are observed to carry the dAl-rich signal of their formation regions to the open Arabian Sea; however, mostly restricted to the northern and north-western Arabian Sea during the period of this study (fall intermonsoon). In the deeper waters (>1000m), elevated dAl levels were observed at the stations sampled near some of the major ridges, i.e., the Murray Ridge (~13.0 nM), the Laxmi Ridge (~10.0 nM) and the Carlsberg Ridge (~4.5 nM), in the Arabian Sea and the equatorial Indian Ocean. dAl input from the Al dissolution/desorption from the margin sediments and/or influx of dAl-rich sediment pore waters to the ambient ocean water column could explain the observed rise in dAl levels close to the ridges.

Dissolved Mn (dMn) distribution is determined in the southern and central Arabian Sea water column to understand the biogeochemistry of dMn in these regions. dMn distribution show surface maxima at all the sampled regions of the Arabian Sea. The estimated mean annual dMn input flux to the Arabian Sea surface waters from the atmospheric mineral dust deposition (dry) ranges between 28.6-239.4 nmol m⁻² d⁻¹, across the Arabian Sea. Compared to the atmospheric dMn input, dMn removal from the surface waters via bio-assimilation is insignificant (4.4-24.3 nmol m⁻² d⁻¹). Surface dMn removal through Mn-oxidation and passive scavenging (51.9-276.0 nmol m⁻² d⁻¹) is estimated to set a dominant control. The residence time of dMn in the Arabian Sea surface waters is calculated (1.0-9.3 yr) considering the steady-state condition and using the atmospheric dMn input and surface mixed layer dMn inventory.

Significant positive dMn anomalies were observed in the oxygen-deficit, lower thermocline waters (~200-600m) near the western continental margin of India (dMn anomaly ~0.2-0.5 nmol kg⁻¹) and in the perennial denitrification zone of the Arabian Sea (dMn anomaly ~2-4 nmol kg⁻¹). dMn diffusion from pore waters of the reducing sediments of the western Indian continental margin to the ambient seawater and subsequent lateral advection may lead to dMn-enrichment in the thermocline depths close to the margin. Mn release due to organic matter remineralization and/or *in situ* reductive dissolution of Mn-oxyhydroxides over the thermocline water column results in highly elevated dMn levels in the denitrification zone of the Arabian Sea.

Title: Impacts of Irrigation on hydroclimatic extremes in India
Researcher: Ambika, Anukesh Krishnankutty
Supervisor: Mishra, Vimal
Year: 2021
Keyword's: Land Surface Temperature (LST), NVSWI, WRF Simulations, Enhanced Vegetation Index, Solar-induced Chlorophyll Fluorescence
Call No.: 627.50954 AMB
Acc. No.: T00960

Abstract: In India, a massive irrigation expansion occurred after the green revolution in the 1970s due to a significant rise in groundwater wells and irrigation potential. India has the largest irrigated area globally, with more than 57 million ha irrigated through surface and groundwater sources. Irrigation expansion in India has played a tremendous role in improving the socio-economic condition of the population and ensuring food security. However, irrigation expansion significantly impacts land-atmospheric coupling by modulating moisture availability over land, modifying cloud formation and boundary layer, changing precipitation over the region, and dry-moist heat extremes. Moreover, the rapid expansion of irrigated areas and excessive groundwater pumping has caused groundwater depletion over northern India. The widespread increase of irrigation in the past and projected rise in the future can negatively impact moist heat stress and water management. However, the irrigation modulation on climate variability is less explored for the Indian region.

To assess the modulation of irrigation on meteorological and agricultural drought, we quantified the irrigation influence on vegetation health, land surface temperature (LST), and vegetation drought. Here, we develop a high-resolution (250m) remotely sensed data of enhanced vegetation index (EVI) and LST from Moderate Resolution Imaging Spectroradiometer (MODIS) for 2000-2017 at 8-day temporal resolution for India to quantify the role of irrigation in the modulation of EVI, LST, and vegetation stress. High-resolution (250m) EVI and LST derived from MODIS show that irrigation dominated regions have significantly (p -value < 0.05) higher EVI cooler (1-2 K) LST during the crop-growing season in the Indo-Gangetic Plain. Vegetation in highly irrigated regions is poorly correlated with meteorological drought primarily due to irrigation. Irrigation in Indo-Gangetic Plain resulted in vegetation growth and groundwater depletion during 2002-2016. Our results indicate that irrigation has a significant role in land-atmospheric coupling along the Indo-Gangetic plain. Further, modulation in land-atmospheric coupling aggravates soil moisture drought and high vapour pressure deficit (atmospheric aridity). Despite a significant expansion in an irrigated area in India, the role of irrigation on soil moisture and atmospheric aridity is not examined. We used observations, reanalysis datasets, and high-resolution simulations from the Weather Research and Forecasting (WRF) model to show that irrigation significantly modulates soil moisture and atmospheric aridity in India. The Indo-Gangetic Plain, which is one of the most intensively irrigated regions in the world, experienced significant (P -value =0.03) cooling ($\sim 0.8^\circ\text{C}$) and an increase in Solar-induced chlorophyll fluorescence (SIF) during the crop growing season (November-February). Atmospheric aridity has significantly (P -value=0.0002) declined (-1.38kPa) while soil moisture ($1.6\text{ m}^3/\text{m}^3$) and relative humidity (2.0%) have increased over the Indo-Gangetic Plain during 1979-2018.

We conducted high-resolution simulations using the WRF model to examine the role of irrigation on atmospheric aridity. Irrigation strongly modulates soil moisture drought, and atmospheric aridity by increasing latent heat and relative humidity and reducing sensible heat. Our findings indicate irrigation modulates compound extremes of soil moisture drought, and atmospheric aridity.

Compound extremes of low soil moisture and high vapor pressure deficit (VPD) impact terrestrial carbon sequestration, vegetation growth, and net primary productivity. Yet, the role of irrigation on the occurrence of compound extremes remains unexplored in India. We used satellite observations, reanalysis datasets, and high-resolution simulations from the Weather Research and Forecasting (WRF) model to show that irrigation significantly reduces the frequency of compound extremes of low soil moisture and high vapour pressure deficit in India. The Indo-Gangetic plain witnessed a significant ($p < 0.05$) increase in mean annual soil moisture while a substantial reduction in VPD during 1979-2018. Moreover, irrigation caused considerable cooling over the Indo-Gangetic Plain during 1982-2018. The increase in soil moisture and the decline in VPD resulted in a substantial rise in Normalized Difference Vegetation Index (NDVI) and Net Primary Productivity (NPP). We conducted high-resolution simulations using the WRF model to examine the role of irrigation in the modulation of the frequency of compound extremes during 1979-2018. The WRF simulations under irrigation-on show a considerably reduced frequency of the compound extremes compared to the irrigation-off simulations. Irrigation modulates the occurrence of compound extremes by changing the land surface energy budget and planetary boundary layer height. Therefore, there is a need to consider irrigation's role for reliable projections of compound extremes under the warming climate in the intensively irrigated regions. Our results highlighted the importance of sustainable irrigation practices in intensively irrigated areas.

Intensive agriculture and irrigation have played a crucial role in India's food security. However, irrigation has considerably impacted regional climate and groundwater sustainability. Notwithstanding the profound implications of irrigation on dry and moist heat and groundwater depletion, the role of efficient irrigation technology on moist heat stress reduction and water savings remains unexplored. Here, we use observations and simulations from the Weather Research Forecasting (WRF) model to examine the impact of efficient (drip) irrigation on moist heat and water savings over the Indo-Gangetic Plain. Irrigated area has increased more than 20% over the Indo-Gangetic Plain during the 1970-2005 period. As a result, irrigation water use has increased dramatically over the region. The irrigation expansion partly contributed to the rise of 0.46 °C (P -value < 0.05) in the summer (April- May) season wet-bulb temperature over the Indo-Gangetic Plain, which measures moist heat stress. The Indo-Gangetic plain exhibited a strong land-atmospheric coupling between soil moisture and dry and moist heat. Our WRF simulations conducted using ERA5 reanalysis as boundary conditions show that switching from the conventional (channel) to the efficient (drip) irrigation leads to a moderate warming ($\sim 0.2^\circ\text{C}$) and a significant decrease in specific humidity over the Indo-Gangetic Plain. The reduction in specific humidity due to efficient irrigation significantly lowers the moist heat stress (wet-bulb temperature) and increases water savings. Our findings show the double benefits of efficient irrigation to curb the rapidly declining groundwater and increase moist heat stress in the region.

Title: Non-redfieldian C:N:P ratios in the inorganic and organic pools of the northern Indian Ocean

Researcher: Sahoo, Deepika

Supervisor: Singh, Arvind

Year: 2021

Keyword's: Redfield Ratio, Bay of Bengal, Arabian Sea, Particulate Organic Matter, Dissolved Organic Matter, Nutrients, Biological Nitrogen Fixation, Denitrification, Mesoscale eddy, Picoplankton

Call No.: 551 SAH

Acc. No.: T00963

Abstract: Availability of nitrogen (N) and phosphorus (P) determine the strength of the ocean's carbon (C) uptake, and variation in the N:P ratio in inorganic nutrients is key to phytoplankton growth. A similarity between C:N:P ratios in the plankton and deep water inorganic nutrients was observed by Alfred C. Redfield around 85 years ago, who suggested that biological processes in the surface ocean are controlled by deep ocean chemistry. This notion of similarity in the ratios has been a tenet in ocean biogeochemistry until a phytoplankton physiology model and an empirical data set suggested that the Redfield Ratio is not a universally optimal value rather it merely reflects the average stoichiometry of phytoplankton. Recent studies revealed that the C:N:P ratios in organic matter and inorganic nutrients deviate from the Redfield Ratio. At present, however, understanding of the (environmental) factors governing the C:N:P stoichiometry remains poor. The northern Indian Ocean due to its geographic setting and monsoonal wind forcing offers a natural biogeochemical laboratory to explore the effect of environmental and physical factors on C:N:P stoichiometry. A handful of studies on the C:N:P ratios in phytoplankton, particulate organic matter (POM), dissolved organic matter (DOM), and nutrients have been reported from the Atlantic Ocean, and to a lesser extent from the Pacific Ocean with a few studies in the Indian Ocean. Despite the fact that the northern Indian Ocean is distinct from other oceans in terms of the biogeochemical and physical phenomena, particularly due to the reversal in monsoonal wind forcing, not much emphasis has been given to the region to understand the mechanisms regulating the elemental proportions.

This thesis reports the results on C:N:P ratios in nutrients, POM and DOM in three depth layers (top: surface to the depth of chlorophyll maximum, subsurface: depth of chlorophyll maximum to ~300 m, and deep layers: 300 m to a maximum of 3000 m) in the northern Indian Ocean, i.e., the Bay of Bengal and the Arabian Sea. The role of physical processes – eddies, convective mixing, riverine discharge, and biogeochemical processes – N₂ fixation and denitrification, in changing the elemental ratios is discussed in this thesis. We observed that the elemental ratios deviated greatly from the Redfield Ratio in both the northern Indian Ocean basins. Our observations of low N:P ratio (< 16:1) in the top layer nutrients indicate the N stressed productivity in these tropical basins. C:N:P ratios in particulate organic matter (POM) in the Bay of Bengal were 232:25:1 during summer and 249:39:1 during spring. Although the Bay of Bengal receives large riverine influx, but its influence in changing the C:N:P ratios was small during spring. In the Arabian Sea, the C:N:P ratios were 245:32:1 in the top layer POM during winter. The elemental ratios in nutrient and POM in the top layer were

affected by the winter convective mixing in the northern Arabian Sea. Comparatively high nutrient concentrations and low POM elemental ratios were observed in the northern Arabian Sea. Overall the high C:N:P ratios in POM in the northern Indian Ocean might be attributed to the prevalence of *picoplankton* which typically possess higher elemental ratios than the microplankton. The variation of ratios in the subsurface and deep layers was mostly driven by the preferential remineralisation of organic P over N and C.

The Bay of Bengal is often prevailed by mesoscale eddies. Anticyclonic eddies, mode water eddy and non-eddy regions were identified in this basin during summer. The eddy and non-eddy stations exhibited a mixed effect on C:N:P ratios of nutrients and POM in the top layer. However, comparatively low N and P nutrients were observed at the anticyclonic eddy regions during spring. A similar effect of anticyclonic eddy on the nutrient concentrations and their ratios was observed in the southeastern Arabian Sea during winter. In the Bay of Bengal, the elemental ratios (357:30:1) of DOM in the top layer were higher than the Redfield Ratio during summer but less than the global average of elemental ratios (640:44:1) for the surface bulk DOM. The ratios (2338:146:1) were higher than the global average during spring in the Bay of Bengal. However, the top layer DOM elemental ratios (635:47:1) in the Arabian Sea were similar to the global average values during winter.

Contrary to our hypothesis, N₂ fixation does not seem to have a role in changing the N:P ratios in the top layer POM pool and subsurface nutrients in the Bay of Bengal. But the role of N₂ fixation should be interpreted with caution as our N₂ fixation rates were low during the observational period. Denitrification in hypoxic waters of the Arabian Sea leads to lowering of the N:P ratio of nutrients in its subsurface and deep layers. The data generated for this thesis might be useful for ocean biogeochemistry modellers who have begun to represent a variable elemental stoichiometry of phytoplankton and nutrients.

Title: Quaternary ventilation of the Indian ocean deep basins, foraminiferal isotopic and abundance approach
Researcher: Bharti, Nisha
Supervisor: Bhushan, Ravi
Year: 2022
Keyword's: Accelerator Mass Spectrometry, Neodymium Isotope, Indian Ocean, Paleo-ventilation Age, Radiocarbon Ventilation, Accelerator Mass Spectrometry
Call No.: 551.461824 BHA
Acc. No.: T00964

Abstract: The ocean covers ~71% surface area of the earth with a maximum depth of ~11,034 m. Ocean stores huge amount of heat and balances Earth's heat budget, and contributes to ~96.5% water available on the earth, which has high heat-storing capacity. It stores almost 50 times more CO₂ than the atmosphere. Thus, the ocean plays a key role in regulating the earth's climate by regulating heat and atmospheric CO₂. Earth has witnessed several warm and cold phases since its formation, primarily due to the astronomical and orbital forcing of the sun, known as glacial and interglacial events. Numerous studies around the globe have suggested that the earth was ~5°C colder during the last glacial maxima (LGM: 18,000-25,000 cal yrs BP) compared to the pre-industrial time. Deglaciation commenced ~15000 yrs ago and sustained up to present. These global climatic excursions accompanied by changes in the global ice sheet extension led to the modification in the ice-melt freshwater flux. Changes in the atmospheric condition along with freshwater flux modified the convective process in the deep water formation regions, mainly the Northern Atlantic and the Southern Ocean. Various paleoclimatic data suggested that global deep ocean circulation or thermohaline circulation was either slowed down or was shut down during the LGM. The thermohaline circulation acts as a cardiovascular system of the ocean by distributing nutrients, dissolved gases, heat, and CO₂ in the global ocean. In response to the modification of the deep water or thermohaline circulation, the biological, physical as well chemical process of the global ocean got altered.

Foraminifera, a marine microorganism dwelling in the ocean since early Cambrian, precipitate calcium carbonate shell in equilibrium with the seawater having planktic as well as benthic mode of life, records the paleoclimatic as well as paleo deep water signature. Isotopic, elemental, and species abundance analysis in the well- preserved foraminifera have been used globally to reconstruct the past climate as well as deep-sea conditions. The disequilibria between surface and deep-sea radiocarbon concentration recorded in calcite shells of planktic and benthic foraminifera have been measured in various marine sediment cores from the Pacific, the Atlantic, as well as the Southern Ocean. Most records suggest that the deep ocean was poorly ventilated during the glacial time. However, few records suggest no change in the glacial ocean ventilation. Paleo-ventilation records along with other supporting proxies compared with the past atmospheric CO₂ and $\Delta^{14}\text{C}$ records from the Pacific, Atlantic, and the Southern Ocean suggest that the ocean probably played a key role in glacial depletion and deglacial increase of the atmospheric CO₂. The decrease and increase in the air- sea gas exchange during the glacial and deglacial period respectively were probably the reason

for this atmospheric CO₂ changes. However, it remains to be resolved in view of some studies which differ from this understanding. Additionally, the role of the various ocean in global average poor deep-sea ventilation remains to be explored, with some ocean basins sparsely studied for their role in glacial-interglacial climatic changes. The Indian Ocean, which contributes ~20% to the global oceanic volume, remains one of the most understudied ocean basins. There is no ventilation age record from the deep Indian Ocean so far, except one from the Southern Ocean sector.

In view of this, three major basins of the Indian Ocean i.e. Western, Central, and Eastern basin have been investigated in this study based on Accelerator Mass Spectrometry (AMS) radiocarbon dating of the coexisting planktic and benthic foraminifera in four marine sediment cores. Along with this, stable carbon isotope was measured in planktic and benthic foraminifera to decipher the past changes in the contribution of different water masses, and oxygen isotope for the past temperature variations. Additionally, benthic foraminifera species abundance was analysed to understand the changes in the past deep-sea environment in terms of food supply and dissolved oxygen. Replicated radiocarbon ventilation age record from two sediment cores of the Central Indian Ocean (CIO) and other supporting parameters along with published Neodymium isotope data suggest isolation of the CIO during the last glaciation. The peak of the ventilation age during Heinrich Stadial-1 and Heinrich Stadial-2 suggested the response of the CIO to the hydrographic changes in the Northern Atlantic. Much higher glacial radiocarbon ventilation age record from the CIO compared to the global paleo ventilation age record proposes the contribution of hydrographic changes originating in the Indian Ocean as well. Paleo ventilation age records from the CIO, the South West Indian Ocean (SWIO), and the Eastern Indian Ocean (EIO) show a remarkable difference in the evolution of paleo-deep circulation in the western, central, and eastern basin of the Indian Ocean. However, during a certain period, contribution of mantle-derived dead CO₂ was also evident in the SWIO as well as in the EIO.

Summarizing the whole thesis work, the present study was able to reconstruct the first paleo-ventilation age record for the deep water from major deep basins of the Indian Ocean. It highlights the under-estimated and under-appreciated role of the glacial Indian Ocean in the global average poor ventilation of the deep ocean during the last glaciation and the subsequent changes in the carbon cycle.

Title: Insights into the geological history of Mars through impact craters
Researcher: Harish
Supervisor: Vijayan S.
Year: 2021
Keyword's: Mars, Impact Craters, Martian Geological History, Surface Processes, Water Ice, Volcanic, Fluvial, Glacial, Tectonic, Graben, Pit
Call No.: 551.7 HAR
Acc. No.: T00965

Abstract: The geological history of Mars is complex as the planet has gone through various widespread processes such as volcanic, fluvial, glacial, tectonic, magmatic, and impact- cratering. These processes left shreds of evidence on the surface of Mars in the form of surface features, depositional and erosional landforms. The study of these processes is of paramount importance to understand the history of the planet. Impact-cratering is one of the fundamental processes in the Solar System, and impact craters are pervasive on the surface of the planet Mars. Thus, in this thesis work, impact craters are used to study various geological processes (glacial, fluvial, volcanic, tectonic, and magmatic), which prevailed on Mars from the Amazonian (younger) period to the Noachian (older) period. Impact craters located in different latitudes are used to study 1) Water-ice exposing scarps within the northern midlatitude craters on Mars 2) Fluvial and glacial processes within the southern low-latitude impact craters that excavated into a Noachian volcanic dome, and 3) Graben and collapse-pit formation processes associated with impact craters in the vicinity of Valles Marineris region of Mars.

Near-surface exposed water-ice was recently discovered on Mars, though the discovery is majorly limited to southern mid to high-latitudes. In this regard, this thesis work revealed near-surface water ice deposits exposed by erosional scarps within two impact craters located in the northern midlatitude of Mars. These two craters are ~5000 km spatially apart and provide ample evidence that the water-ice is widespread just a few meters below the Martian surface. This study also substantiated that snow/ice may have deposited and accumulated within the last 100 to 10 million years, and water-ice got exposed within the last 1 million years. In the northern lowlands, this thesis work mainly focused on the recent (Amazonian) depositional (snow) and erosional (scarp) history of Mars.

In the southern highlands, this thesis work focused on Degana crater, a ~50 km diameter impact crater, which formed on top of a ~4 billion-year-old volcanic dome. After the Degana formation, the climatic condition favored snow/ice precipitation and which formed multiple depositional fans within this crater. In a later stage, these fan deposits are superposed by glacial remains (moraine ridges). This study found that the volcanic dome contains Mg-rich olivine and low-calcium pyroxene, excavated by Degana and superposed crater Degana-A. This study provided evidence for volcanic material, fluvial-related depositional fan, and glacial moraines within the same crater on Mars. In the equatorial region, ~4000 km long canyon system is located, which is called Valles Marineris (VM). Such an extensive canyon system has been modified over time by tectonic and magmatic

processes. Thus, studying the spatial and temporal modification of this vast canyon system is essential to understand the tectonic and magmatic processes on Mars. The VM region is modified and developed through graben and collapse pits, which are surface expressions of tectonic and magmatic processes. To study these processes, this thesis work used those craters, which are: 1) located within the ~100 km distance from the boundary of Valles Marineris and 2) associated with graben and collapse pits. 1516 craters (diameter >1 km) are studied, and out of these, 48 craters have an association with graben and collapse pits. The detailed chronological analysis revealed that the modification of VM varies spatially as well as temporally (~3.7 to 1.2 Ga). The result from this study substantiates that the modification of VM occurred until the Middle Amazonian epoch, which is much younger than previously thought.

Overall, this thesis work provided new insights into the geological history of Mars by exploring the impact craters, which recorded and preserved the evidence for diverse geological processes that occurred at different epochs.

Title: Basin-scale hydrological mass budgeting using dynamics of glacial components and its incorporation in hydrological SWAT model: a regional study from NW Himalaya, India

Researcher: Chakravarti, Pritha

Supervisor: Jain, Vikrant

Year: 2022

Keyword's: Hydrology, Himalayan Glaciers, Hydrological Modeling, Soil & Water Assessment Tool (SWAT)

Call No.: 551.480151 CHA

Acc. No.: T01030

Abstract: Around 1.4 billion people in South Asia depend on the waters from the rivers originating from the Himalaya (Immerzeel et al., 2010). The snow and ice/glaciers upstream of these rivers help them sustain water throughout the year. Glaciers and permafrost (snow cover and rock glaciers) are the most important storehouse of freshwater in the region. They are also sensitive indicators of climate change (Thompson, 2000; Devkota and Gyawali, 2015). Any changes in their mass due to climate change may affect the discharge of these rivers significantly (Immerzeel et al., 2010). All presently available climate models predict a warming trend under the influence of rising levels of greenhouse gases in the atmosphere (Barnett et al., 2005). This warming trend may bring about significant changes in the hydrological cycle, particularly in regions where water supply (runoff) is currently dominated by melting snow or ice. Firstly, due to the enhanced melting of snow and ice, streamflow will increase, causing floods downstream. The recent IPCC report (2019) on high mountain areas suggests a decline in low elevation snow cover, glaciers, and permafrost and an increase in runoff. This will lead to the hazards of the thaw of glaciers and permafrost. It will destabilize the mountain slopes, causing frequent landslides and floods caused by outburst lakes. Later, as the melting continues, these changes will lead to water shortages in the future, which may likely worsen as the temperature soars. These glaciers and snow not only account for the water resource in the mountains but also influence lowland areas and help recharge river-fed aquifers (Bolch et al., 2012). Thus, it is essential to study the change and fate of the glaciers and snow cover to understand the changes in meltwater generation runoff in these areas, the most sensitive parameters that govern them, and the uncertainty that drives them (Rashid et al. 2020). Rock glaciers are landforms that is now understood to have a major role as water reservoirs in the mountains (Millar and Westfall, 2019, Azócar and Brenning, 2010). Rock glaciers are landforms that originate either through mountain creeping permafrost or glaciers or hillslope processes like mass wasting and talus creep (Barsch, 1996; Humlum, 1996; Humlum, 1998). They are indicators of permafrost in the mountainous region and are also very sensitive to climate change (Humlum, 1998; Konrad et al., 1999). Rock glaciers contain ice, which affects the hydrological cycle under the influence of freeze and thaw (Azócar and Brenning, 2010). Thus they have become very relevant in water-stressed regions in many parts of the world (Brenning, 2005).

For using any hydrological model for streamflow simulation and to study changes in meltwater generation runoff, we generally need glaciers and snow cover input. Studies discussed so far have not given the methodology which can address the issue of providing both snow and glacier boundaries at regional or basin scale (Kaushik et al., 2019). Such data at basin scale are essential to incorporate glacial parameters in the hydrological models. I adopted an integrated methodology that provided these components when mapped using an extensive dataset. Appropriateness of data is also checked along with the methodology for such an inventory study. Further, basin scale map of rock glaciers are not available for the entire northwest Himalaya. It is important to figure out the extent and quantity of these rock glaciers to estimate the potential locked up water that might help us in the water-stressed months. For the transboundary rivers of India, estimating discharge is a difficult task as there are no observed data sets released for common use. So, estimation and simulation of streamflow and snowmelt is very difficult for these rivers. In this thesis, I included a study where I compare streamflow from various hydrological models to understand the seasonal variability in discharge for these river basins. I further modelled the same for the future scenario to estimate the changes concerning the predicted climate change.

Thus, the following questions are addressed in the thesis:

- How to improve basin-scale mapping of clean and debris-covered glaciers in snow-dominated high relief terrain using optical data of different spatial resolutions?
- What is the present state of glaciers, ice pockets, and snow in the northwest Indian Himalaya, and how much did they change in the last 2.5 decades?
- What is the basin-wise distribution of rock glaciers in the northwest Himalaya, and how much water is locked in them?
- How to incorporate basin-scale glacial parameters into the hydrological model (SWAT), which will improve streamflow estimation of the river?
- Which parameters are more sensitive, and how are the future projections of streamflow and other water balance components considering two scenarios of climate dynamics?

The study area is the northwest Himalaya, where the rivers have a catchment area of 1,34,125 km² consisting of Beas, Ravi, Chenab, Sutlej, and Yamuna River basins. All river basins are characterised by glacier cover. This region receives precipitation two times a year- by the Indian summer monsoon in the summer (June-September) and the westerlies in the winter months of November to February. A basin-scale approach was adopted, which included the following steps, (a) basin-scale mapping of glacial components and preparation of the inventory and change detection in five major river basins, (b) mapping of rock glaciers and estimation of water content in them, and (c) incorporation of glacial components mapping data in the SWAT model to estimate the hydrological mass budget, glacial contribution to hydrology as well as changes in water balance components in different scenario of climate change effect.

In the first part of the thesis, I developed an integrated methodology to better map glaciers and their components at the basin-scale. The existing methods to carry out high-resolution mapping of glaciers are limited to smaller areas, which are insufficient to map glacial and its component at the basin scale. Hence, various existing approaches were integrated to carry out basin-scale mapping of the glacier and its component. I created a workflow that enables me a quick and effective procedure to bring out the areal extent of these individual features. I further examined the sensitivity of glacial mapping output to the scale and sensor's spatial resolution. Sensitivity analysis highlights that the spatial resolution of the sensors doesn't affect the mapping results when Landsat 8 and Sentinel 2A are compared. However, mapping scales do affect the areal output, especially for snow. The spectral resolution also plays a vital role in the mapping of the glaciers. Using thermal bands for mapping debris-covered glaciers is found to be more robust. So, Landsat 8 is better for mapping debris cover even though it is one-third in terms of spatial resolution when compared to Sentinel 2A. A most recent inventory of the glacier components in the five major river basins is developed with this workflow. Further, a change detection study is done on the state of glaciers in the region and their changes in the last couple of decades. I found the maximum loss is about 42% of glaciers and ice and about 70% of permanent snow and is in the Ravi River basin. In other basins, the loss has been less with an increase in permanent snow in the Yamuna basin. Controls on glacial dynamics were further analyzed. The significant loss in glacier area is due to rising temperature in this region, which we have found by examining the ERA5 surface temperature data. Receding snowlines and an increase in a glacial lake in the area correlate with temperature data showing a shift towards a warmer climate in this region.

The second part of the thesis was focused on the permafrost region, where rock glaciers are important glacier features containing water mass. 967 rock glaciers of 306 km² were identified and mapped in these five river basins. As many as 77% of the total are glacier derived, and 23% are talus derived as hill slope failures. I studied their geomorphic characteristics and the main controls for their distribution. I believe that the lithology or the hardness of the rocks does play an essential role in their formation, like the topography, such as the elevation and slope of the adjoining rocks from which they are weathered. They have been known to be hydrologically significant, especially in hydrologically stressed regions. I further calculated empirically the amount of water potentially stored in them. The hydrological impact of the rock glaciers is finally discussed in this study showing a total of 8.5 billion m³ volume of water stored in the rock glaciers. I observed that the rock glaciers would have an additional 9%, 4%, 14%, 39%, and 6% of the annual water volume in Beas, Chenab, Ravi, Sutlej, and Yamuna rivers, respectively.

In the third part of the thesis, the details of the areal extent of snow and glaciers are then used in the hydrological model, Soil Water and Assessment Tool (SWAT). I have used elevation bands and Equilibrium Line Altitude (ELA) to consider the effect of glaciers and snow that is already present in the catchment in generating the streamflow. The most sensitive parameters affecting the discharge from all the basins are the snow parameters. I have also analyzed other water balance components from the basin outlets. I compared the results with the streamflow obtained from other models like VIC and ERA5 and studied the variability produced using different weather forcing (IMD and ERA5).

I also studied the variability in streamflow that may be seen with and without considering glaciers in the basins. Further, I used 5 Global Climate Models (GCMs) from CMIP6 data and quantified the changes predicted in streamflow and other components in the next 80 years. I see future temperature and precipitation changes using the climate models; the corresponding change is the streamflow, especially in the winter and the spring months. For all the basins, the changes in streamflow in the winter months are almost 50% to 60%, and not much change is seen in the monsoon months. The result matches with the IPCC reports, which had predicted the same for the Nepal Himalaya.

Finally, rock glacier-based water mass estimation was integrated with the output of the hydrological model after the incorporation of glacial components. This study provides a holistic detail of the water budget of the present and the future for five different glaciated river basins of the NW Himalaya. The thesis also provides a new methodology to assess current and future hydrological variability by considering the glacial and climate dynamics in glacierised river basins. The approach can be further extended to other glacier basins of the Himalaya or elsewhere.

Title: Glacial landforms and gully formation on Mars
Researcher: Sinha, Rishitosh Kumar
Supervisor: Ray, Dwijesh
Year: 2023
Keyword's: Mars, Glacial, Gullies, Lobate Debris Aprons (LDA)
Call No.: 551.7 SIN
Acc. No.: T01048

Abstract: Two of the most common landforms in the mid-latitudes of Mars are glaciers and gullies. Their ubiquitous presence has substantiated evidence of multiple ice-related episodes that played a key role in landscape evolution during the last one to hundreds of millions of years. The primary objectives of this thesis were to analyze the nature of glacial activities at locations away from the dichotomy boundary and then examine the potential of debris-flows in forming gullies that are similar in morphology and morphometry to terrestrial gullies. I have conducted a survey of the northern mid- latitudes of Mars and found Erebus Montes region with glacial landforms, which were examined in detail to infer the history of glaciation in this region. To address the role of debris-flows in Martian gully formation, I first discovered 20 new locations (craters) where gullies have preserved morphological attributes of terrestrial debris-flow like deposits and then performed a comparative analysis of the morphometry of Martian and terrestrial gully systems to infer the potential involvement of debris-flow like processes.

The study of glacial landforms in the Erebus Montes region revealed that this region has mainly formed lobate debris aprons (LDA) which were extensively mantled by LDM during the recent past, and lacks the evidence for superposed lobate deposits on the main LDA. This suggests two things in particular: (1) LDA deposits in this region may have once been more extensive in the past and have undergone significant modification/degradation due to the emplacement and removal of LDM, and (2) there is a lack of alcove-fed multi-stage glaciation of a more limited magnitude and shorter duration in the Erebus Montes region. The observational evidence of linear-curvilinear ridges on LDA deposits help substantiates the proposal of LDA degradation in this region. We find that the LDA in this region is one of the youngest (~30 Ma) LDAs on Mars, although we attribute this as a manifestation of extensive mantling of the surface of the debris apron that resulted in burial and modification of the craters on LDA surface. The small size and the closely-packed spacing of the mound-LDA systems precluded the detection of buried extant ice in this region. We find that the LDA deposits examined here are more consistent with the cold-based glacial behavior - morphological observations support the existence of the sublimation process in the region. Taken together, the findings presented in this thesis support the results of previous studies carried out elsewhere along the dichotomy boundary that find evidence for the past presence of extensive debris-covered glacial land systems in the northern mid-latitudes of Mars. Detailed investigation of gullies formed inside newly found 20 gullied craters widespread in the northern and southern mid-latitudes led to the finding of morphological attributes of debris-flow like deposits on the gully fan surfaces. The debris-flow like deposits typically include leveed channels and overlapping lobate deposits with abundant embedded clasts. At first, the finding of levees and lobate deposits aided in

proposing that debris-flow like processes were not rare on Mars in the past. This inference is contrary to what was proposed in the previous studies. Furthermore, I proposed that the preservation of lobate deposits is the key to their paucity in the gully population. Subsequently, upon adding some more gullied craters to my study, I embarked on a detailed investigation of the influence of substrates within which gullies have formed on Mars and found that the morphology and morphometry of gullies formed in latitude dependent mantle (LDM) and glacial deposits differ from gullies formed in bedrock. My work has provided new insights into the role of LDM in the formation and evolution of glaciers and gullies found on Mars. Then, I calculated several morphometric variables to characterize the catchment and fan of the gully systems in order to infer the flow types that led to Martian gully formation. The analysis of combinations of the relationships between alcove length and fan gradient with Melton ratio of Martian gully systems were compared with the terrestrial gully systems, which aided in the interpretation that Martian gullies at some of the locations are from terrestrial debris-flow like processes in the past. Although it is important to note that formation of Martian gullies could not be related to just one process or a set of processes because the integral role of water and/or CO₂ frost might vary on Mars, both in spatial and temporal context. Therefore, the morphological attributes of debris-flow like deposits identified in this work were formed by aqueous or sublimation-driven processes remains to be a matter that likely only future detailed laboratory investigations can resolve. As far as the present-day activity in gullies is concerned, I have discovered several new locations where currently active gullies are evident. A comparison of changes in both dust/sand-filled gully channels and dune gullies led to the proposal that the currently active processes have similar effects on the loose, unconsolidated substrate in both gully types. Identification of CO₂ frost inside the dust/sand-filled gully channels in the image acquired during winter and prior to the image in which recent changes have been observed suggests a connection with the sublimating frost inside the channels and indicates a seasonal control that subsequently produces extensive changes during defrosting seasons in approximately a Mars year.

Title: Geological and geochemical study of martian volcanic provinces: implications for igneous evolution of Mars
Researcher: Rani, Alka
Supervisor: Sarbadhikari, Amit Basu
Year: 2022
Keyword's: Mars, Noachian Period, Igneous Provinces, Arabia Terra, Tectono-volcanism, Geochemical Trends
Call No.: 551.7 RAN
Acc. No.: T01051

Abstract: Over the last four decades, planetary missions to Mars have highlighted that the red planet has been volcanically active throughout its history, starting from Noachian (>3.6 Ga) to Late Amazonian (<150 Ma). The temporal evolution of volcanism on Mars implies that volcanic activity has played a significant role in the geologic evolution of the Martian crust and mantle. Martian volcanic provinces are of great geologic interest as the composition of igneous rock formed from the eruption of magma tends to preserve the record of its thermochemical properties.

Overall, this thesis aims to develop a perspective view of spatiotemporal changes in thermochemical conditions and evolution of the Martian mantle. We have used the link between magma chemistry and mantle thermal state to rationalize the compositional variations in Martian magmatism. In this context, detailed geological and geochemical investigations of Arabia Terra, the newly discovered Noachian aged (>3.6 Ga) volcanic province, helps to estimate the mantle source composition and magmatic processes. This study further evaluates the role of Arabia Terra in the geologic evolution of early Mars. Detailed morphological and structural analysis of the Arabia Terra region indicates that various volcanic landforms developed in response to putative regional tectono-volcanism, which further provides pieces of evidence for volcanism in Arabia Terra. Our finding of igneous landforms within the Ramanathan crater represents a broader extent of the thinned Arabia Terra crust. We also observe a preferred orientation of the igneous features, which show parallel alignment to regional linear tectonic features. We suggest that the igneous intrusions within the crater were controlled preferably along the pre-existing weak planes (i.e., faults) in response to the regional tectonism, while the magmatism was primarily triggered by the crater-forming impact event. This study discusses the possible extent of volcanism in Arabia Terra and shows that the proposed super-volcanic activity is not only confined to the NW part of Arabia Terra, but is plausibly spread over the entire Arabia Terra.

Furthermore, the compositional analysis of Arabia Terra is carried out to demarcate the geochemical extent and deduce the bulk composition for geochemical and petrological investigations. In this study, we present a set of consolidated chemical provinces of Mars, which delineate the geochemical extent of Arabia Terra. These consolidated geochemical provinces correlate with temporal changes in elemental abundances, suggesting evolving intrinsic primary processes and mantle sources. This relation of age versus compositional variability reveals significant information about Martian crustal and mantle evolution. Our geochemical investigation also shows that Arabia

Terra has a coherent compositional signature and uniformity in mapped geology. Lastly, temporal changes in element abundances of the Noachian-aged Arabia Terra are analyzed to understand the magmatic processes and formation pressure- temperature (P-T) conditions.

To improve our understanding of magma genesis in Noachian-aged (>3.6 Ga) volcanic regions, a detailed geochemical and petrological analysis based on model melting/crystallization simulation has been carried out. Our investigation demonstrates that the magma of the Noachian age was produced by 8-12% partial melting of the primitive Martian mantle at a pressure ranging from 1.3 to 1.8 GPa. Furthermore, our study demonstrates that the formation pressure (1.3 ± 0.2 GPa) of Noachian-aged Arabia Terra is relatively lower than the younger Hesperian and Amazonian-aged volcanic provinces. This lower pressure corresponds to a shallow melting regime for Noachian- aged Arabia Terra, supporting our geological observations. Furthermore, a decreasing trend of the calculated mantle potential temperature of the Martian volcanic provinces from Noachian to Amazonian is quite discernible.

In this thesis, through the geological and geochemical investigations, the age- specific Martian volcanic provinces are undertaken to obtain insights into the spatiotemporal changes in the Martian mantle, most notably of the early Noachian Mars.

Title: Oxygen and Hydrogen isotopic characterization of groundwaters of India: insights into hydrogeological processes
Researcher: Pandey, Amit
Supervisor: Deshpande, R. D.
Year: 2022
Keyword's: Groundwater, Seasonal Isoscapes, Isotopic Composition-Hydrogen-Oxygen
Call No.: 551.490954 PAN
Acc. No.: T01052

Abstract: Groundwater is the largest freshwater reservoir on Earth which sustains major water requirements for drinking, agriculture, and industrial usage. Groundwater also maintains the health of the riverine ecosystem by providing water through base flow. For India, Groundwater is even more important as it supports > 60% of irrigated agriculture and >85% of drinking water supplies. With ~250 km³ of annual extraction, India is the large extractor of groundwater in the world. Although groundwater is known to be a limited natural resource, India depends heavily on it due to erratic and unevenly distributed rainfall and heterogeneous surface water availability. High dependency on groundwater has led to indiscriminate exploitation of groundwater in India over the last several decades, which has gradually resulted in various groundwater-related issues such as depletion in groundwater levels and severe scarcity, quality deterioration by geogenic and anthropogenic contaminants, high cost of pumping deeper groundwater, and marine water intrusion along the coastline. Groundwater is also lost to the sea through submarine groundwater discharge (SGD) along some stretches of India's 7500 km long coastline. Superimposed on these problems are the climate-change-related adverse impacts on groundwater resources.

Since groundwater is a precious but threatened natural resource of India, it is very important to understand hydrogeological processes concerning groundwater recharge. Groundwater recharge is conventionally estimated in India using the Groundwater Level Fluctuation Method and the Rainfall Infiltration Factor Method. These methods do not provide scientific information about the hydrogeological processes and factors concerning surface water groundwater interactions that govern groundwater recharge. Having this knowledge is important to take more informed policy decisions about groundwater development and management.

In the above backdrop, the broad scientific objective of this doctoral research is to understand the surface water-groundwater interaction and to identify the underlying processes and factors such as the effects of hydrogeology, lithology, orography, drainage, evaporation, and proximity to surface water bodies, the southwest and the northeast monsoon systems, vapour sources. Oxygen and hydrogen isotopic composition ($\delta^{18}\text{O}$, δD and d-excess) are useful tracers to characterize different water sources (groundwater, river, surface reservoirs, rain) and to understand their interaction and mixing. In this doctoral research, seasonal variation in $\delta^{18}\text{O}$, δD , and d-excess of groundwater have been examined and interpreted in conjunction with the isotopic composition of its complimentary components (rainwater, river water, surface reservoirs) and other hydrogeological and meteorological aspects. While this thesis is largely based on the use of stable isotope composition

of groundwater, other methodological components also include isotope mass balance, a two-component mixing model, backward wind trajectory analyses, and uncertainty analyses to strengthen the isotope-based inferences.

As the major scientific outcome of this doctoral research, it has been possible to broadly identify different regions in India where groundwaters are recharged by different types of recharge source waters (e.g., monsoonal rains, canal waters, surface waters, deeper groundwaters) and due to different types of recharge mechanisms (e.g., preferential recharge pathways, preferential sources, irrigation return flow). Overall, this doctoral research provided important new hydrological insights into the surfacewater-groundwater interaction in different parts of India. This is the most extensive groundwater isotopic study ever carried out in India based on more than 5000 groundwater samples over one seasonal cycle of pre-monsoon and post-monsoon collected under the aegis of a multi-institutional collaborative national programme on isotope fingerprinting of waters of India (IWIN).

The general findings from this doctoral research are provided in one of the chapters on seasonal isoscapes ($\delta^{18}\text{O}$ and δD) of groundwater in India and underlying hydrogeological processes. The finer details emerging from certain states in India have been presented in subsequent chapters. In one of the chapters, the changes in the isotopic composition of groundwater within a decade have also been examined for a particular region. The last chapter of this thesis will discuss the limitations of this research and the future scopes of research emerging from this thesis.

Title: Biological fixation of nitrogen and carbon in the northern Indian ocean
Researcher: Saxena, Himanshu
Supervisor: Singh, Arvind
Year: 2022
Keyword's: Nitrogen Fixation, C Fixation, Photosynthesis, Chemosynthesis, Oxygen Minimum Zone
Call No.: 589 SAX
Acc. No.: T01058

Abstract: The elements carbon (C) and nitrogen (N) form the backbone of life, since all the major cellular components such as genetic materials, proteins and energy carrier molecules are stemmed from these elements. In the marine environment, the scarcity of N often limits the growth and productivity of phytoplankton in most of the surface oceans. Though the most abundant form of N, i.e., dinitrogen gas (N₂), comprises about 78% of the Earth's atmosphere, it is inaccessible to most of the phytoplankton. The majority of phytoplankton are unable to assimilate N₂ but require the bioaccessible or reactive forms of N, such as ammonium (NH₄⁺), nitrate (NO₃⁻) and nitrite (NO₂⁻). Notably, a specialized group of prokaryotes, termed diazotroph, is capable of N₂ fixation — a process of breaking the highly stable triple bond in the N₂ molecule and converting (or fixing) it to NH₄⁺.

N₂ fixation fuels the cellular N-needs of phytoplankton and thus, constrains the Earth's climate by influencing marine C fluxes through sequestration of atmospheric CO₂. Therefore, understanding the process of N₂ fixation by which newly fixed N is added to the ocean is essential for accurate quantification and ultimately to forecasting oceanic productivity. Additionally, in order to forecast accurate quantification of oceanic productivity, it is also essential to precisely estimate the present marine C budget. The prerequisite estimate of marine C budget is imprecise owing to inaccurate estimations of CO₂ sources and sinks. One such area for recognition in the C budget is the unaccounted sink of CO₂ via chemoautotrophic inorganic C assimilation (i.e., chemoautotrophic C fixation) within the aphotic zone. N₂ fixation rates based on direct field measurements are scarce with extremely high variability both spatially and temporally, lacking large regions of the global ocean especially the Indian Ocean. The northern Indian Ocean is a unique basin which contains different biogeochemical gradients with eutrophic, oligotrophic and O₂ deficient waters, and experiences a strong seasonal reversal of monsoon circulations. Yet, the studies on N₂ fixation so far conducted in the Indian Ocean before the commencement of this thesis work have mostly focused on regions with *Trichodesmium* (photoautotrophic diazotroph) blooms in the northwestern part of the Indian Ocean (i.e., the Arabian Sea). Hence, the thesis, primarily focuses on marine N₂ fixation and its contribution in the regulation of marine primary production, with an additional effort to assess the significance of C fixation within the aphotic zone of the water column. The thesis reports the results of N₂ fixation rates from the euphotic and aphotic zone of the Bay of Bengal (i.e., the north-eastern Indian Ocean) and the Arabian Sea for the summer and spring monsoon and the winter monsoon, respectively. The results of C fixation rates from the euphotic zone of the Bay of Bengal and the euphotic and aphotic zone of the Arabian Sea are also discussed in the thesis.

The euphotic zone N_2 fixation rates were mostly low ($< 1 \text{ nmol N L}^{-1} \text{ d}^{-1}$) in the oligotrophic Bay of Bengal contrary to the traditional assumption of oligotrophy favouring the diazotrophy. However, the upper bound of the observed N_2 fixation rates was higher than that reported in other oceanic regimes, such as the Eastern Tropical South Pacific, the Tropical Northwest Atlantic, and the Equatorial and Southern Indian Ocean. N_2 fixation contributed maximum up to 2% of primary production in the Bay of Bengal. The anticipated reason for low N_2 fixation rates in the Bay of Bengal could be cloud cover and turbidity due to copious riverine discharge during the summer monsoon and unexpected instability of the water column owing to the least fresh water induced stratification during the spring inter-monsoon. Volumetric N_2 fixation rates measured in the euphotic and aphotic zone of the Bay of Bengal were equally low, but interestingly, significantly higher N_2 fixation rates occurred below the oxygen minimum zone (OMZ) ($> 600 \text{ m depth}$) with $0.5 < O_2 \leq 1.6 \text{ mL L}^{-1}$, rather than within the OMZ with $O_2 \leq 0.5 \text{ mL L}^{-1}$. This suggests that low concentrations of O_2 and NO_3^- are not a firm niche requirement for diazotrophs.

N_2 fixation rates in the Arabian Sea were higher in the convection dominated regions than in the convection unaffected regions during the winter monsoon owing to lower N:P ratios and higher iron availability in the convection dominated regions. The aphotic zone N_2 fixation rates were low ($< 0.1 \text{ nmol N L}^{-1} \text{ d L}^{-1}$), but accounted for up to 95% of whole water column rates. N_2 fixation rates in the OMZ of the Arabian Sea were modest and comparable with another OMZs of the Eastern Tropical North and South Pacific.

The average C fixation rates in the suboxic waters of the OMZs of the Arabian Sea were significantly higher than in the hypoxic waters of the OMZ, which was likely related to nutrients availability and to the preferential dominance of nitrite oxidisers and anammox bacteria in the suboxic waters of the OMZ. The extrapolation of measured aphotic zone C fixation to the global ocean amounts to up to 15% of primary production of the global ocean. The results obtained during the course of this thesis work provide quantitative evidences that N and C budget are largely unbalanced owing to overlooked N_2 and C fixation potential in the aphotic zone of the global ocean.

Title: Geochemical and isotopic studies of Sarnu-Dandali-Kamthai Carbonatite-Alkaline complex, India
Researcher: Mahala, Milan Kumar
Supervisor: Ray, Jyotiranjana S.
Year: 2023
Keyword's: Alkaline Silicate Rocks, Carbonatites, Isotopic
Call No.: 551 MAH
Acc. No.: T01062

Abstract: Carbonatites, rich in carbonate minerals, are unique magmatic rocks because they are derived from a silicate-rich mantle. Being the largest extractor of mantle carbon, they play a vital role in Earth's deep carbon cycle. Although they represent less than 1% of all mantle-derived magmas, their presence throughout the geologic time, overwhelming presence in continental settings, close association with alkaline silicate rocks, special affinity towards deep mantle plumes, and extremely high contents of rare earth elements make them one of the most interesting rocks for studying the fluids in the Earth's mantle and many unusual magmatic processes.

The carbonatite research has come a long way since its first identification as magmatic rocks in 1950. We now understand many aspects of its origin and evolution; however, many other characteristic features and responsible processes remain undecipherable. To contribute to the global effort of unraveling the mysteries of carbonatite magmatism, I took up the study of one of several carbonatite complexes of the Deccan Traps magmatic province that came into existence during the late Cretaceous Period. This carbonatite complex is located in the Sarnu Dandali and Kamthai localities of Rajasthan. It exposes diverse alkaline silicate rocks along with minor carbonatite and is believed to represent one of the earliest magmatic manifestations of the Deccan-Reunion plume activity in the Indian subcontinent. In my Ph.D. work, I studied all different rock types of the complex for their field relations, mineralogy, geochemical, and C-O-Sr-Nd-Pb isotopic compositions and determined the timings of various magmatic phases using ^{40}Ar - ^{39}Ar dating method with the following major objectives: (1) Ages of emplacement of various magmatic bodies; (2) Nature of differentiation and evolution of carbonatites and their relationship with the associated alkaline silicate rocks; (3) Role of crustal assimilation (if any) in the origin and diversification of carbonatites; (4) Nature of the mantle source(s) for different magmatic activities in the complex and role of the Reunion-Deccan plume in their origin; (5) Nature (source) of carbon in carbonatites. Our age data reaffirm the recurrence of magmatic activities in the Sarnu-Dandali and Kamthai during two main phases; one during 89-79 Ma and the other during 69-66 Ma, with the older phase likely related to the continental breakup of India and Madagascar, and the latter clearly linked to the Deccan Traps activities. Based on field-age-geochemical-isotopic data and models, we clearly establish that liquid immiscibility is the main magmatic process responsible for the generation of carbonatite-alkaline silicate rock association in the complex and that crustal assimilation likely played a key role in the immiscibility process as well as subsequent differentiation leading to diversification of rocks. Isotopic data suggest plume origin for carbonatites; however, the metasomatized continental lithosphere appears to have played a significant role, particularly in enriching the parental magma

with rare earth elements. Primordial carbon appears to have remained a major source for carbonatites in the Deccan Province.

Title: Applications of cosmogenic nuclides in understanding quaternary events
Researcher: Jena, Partha Sarathi
Supervisor: Bhushan, Ravi
Year: 2022
Keyword's: Cosmogenic Nuclides, Quaternary Glaciation, Isotopes
Call No.: 523.12 JEN
Acc. No.: T01064

Abstract: The cosmogenic nuclides are produced from the interaction of highly energetic cosmic ray particles with terrestrial and extra-terrestrial material. In this study, both meteoric (formed in the earth's atmosphere) and in-situ (formed on the earth's surface) cosmogenic nuclides were employed to understand paleoclimatic and paleomagnetic processes during the Quaternary period.

In the northwestern (NW) Himalaya the spatial and temporal changes in the late Quaternary glaciation were modulated by a combination of two contrasting moisture sources viz., the Indian Summer Monsoon (ISM) and the mid-latitude westerlies. This study attempts to understand late Quaternary glacier fluctuations in the NW Himalaya and to infer the climatic factors responsible for driving glaciation cycles based on detailed geomorphological mapping and chronology obtained from the Terrestrial Cosmogenic Nuclide (TCN) exposure age dating method. The bedrock-derived ages show less spread (compared to boulders), suggesting a minimal effect of post and pre-depositional changes, and thus, are the most appropriate samples for TCN dating. The oldest Tirith II glaciation event in the Nubra Valley was dated to be Marine Isotopic Stage (MIS)-5/4, while the younger Tirith I (contemporaneous with the Puche Glacier Advance 1 in Ganglas valley) event was dated to be MIS-2. Reduction in temperature was found to be the primary factor driving the late quaternary glaciation in the northwestern Himalaya, while the glaciers were sustained by the moisture derived from the westerly precipitation.

A near-continuous proglacial relict lake sediment succession exposed at Spituk, Leh, was investigated to reconstruct the hydrological changes during the late Quaternary period. The sedimentology supported by geochemical proxies indicates that the lake sedimentation was modulated by the hydrological fluctuations controlled by the valley glaciers. The varve sedimentation between 27.5 ka and 22 ka indicates an overall cold phase. This hypothesises that the valley glaciers began to expand, although there was moderate humidity. The increase in precipitation during mid MIS-2 can be attributed to the enhanced contribution from the westerlies. Based on beryllium isotopic measurements on surface sediments from the central and northern Indian Ocean, an attempt has been made to understand the processes controlling beryllium isotopic distribution. Owing to higher terrestrial flux, the sediment samples from the Bay of Bengal show a high ^9Be concentration and a low $^{10}\text{Be}/^9\text{Be}$ ratio. The study suggests that scavenging by sediment particles plays a vital role in the distribution of Be isotopes in well-mixed open ocean. The higher

residence time of beryllium observed in the central Indian Ocean indicates low scavenging in the water column due to reduced particulate concentration.

$^{10}\text{Be}/^9\text{Be}$ records estimated from the marine sediment cores have the potential to serve as an important proxy to reconstruct past geomagnetic field strength. High-resolution beryllium isotopic measurement in a sediment core (SK-312/10) from the central Indian Ocean shows a higher $^{10}\text{Be}/^9\text{Be}$ ratio during 26 to 21 ka, which can be associated with lower geomagnetic field strength. A peak of $^{10}\text{Be}/^9\text{Be}$ ratio observed at ~ 41 ka in two sediment cores (SK-312/09 and 08), can be ascribed to the Laschamp event. During this event, a $\sim 40\text{-}60\%$ increase in the $^{10}\text{Be}/^9\text{Be}$ ratio was observed, which can be attributed to an increase in ^{10}Be production due to low geomagnetic field intensity.

One of the essential components of Quaternary studies is the use of appropriate dating techniques to build chronology of the marine sediment cores. With a relatively long half-life of 1.39 Ma, cosmogenic ^{10}Be has the potential to provide chronology of marine sediment cores as old as 10-12 Ma. We present the results of measurements made in a sediment core from the central Indian Ocean for both beryllium isotopes (^{10}Be and ^9Be). While ignoring the points showing a high anomalous $^{10}\text{Be}/^9\text{Be}$ ratio (associated with magnetic field intensity variation), a continuous decrease in the $^{10}\text{Be}/^9\text{Be}$ ratio with depth was observed. Based on the decay of ^{10}Be , the 5.7 m long sediment core was dated to be ~ 350 ka with an average sedimentation rate of 1.6 cm/ka.

To summarise, the present study has exploited the use of cosmogenic nuclides (^{10}Be , and ^{14}C) to investigate paleoclimatic and paleomagnetic studies. The study could delineate the major factors driving the Quaternary glaciation in the NW Himalaya using both glacial and paleolake deposits. Significantly diverse Be isotopic distribution and residence time of Be observed in the central and northern Indian Ocean Basins indicates strong control by terrestrial flux. Temporal records of Be isotope show a drastic increase in ^{10}Be production during the Laschamp event (~ 41 ka). Based on the ^{10}Be decay method, the applicability of meteoric ^{10}Be to date marine sediment cores older than the radiocarbon dating limit has been established.

Title: Aqueous evolution of CM Chondrites
Researcher: Baliyan, Shivani
Supervisor: Ray, Dwijesh
Year: 2022
Keyword's: Meteorites, CM Chondrites, Aqueous Alteration, Geochemistry, Mineralogy, Spectroscopy
Call No.: 523.51 BAL
Acc. No.: T01071

Abstract: The CM, Mighei-like carbonaceous chondrite, one of the primitive solar-system materials, experienced variable degrees of aqueous alteration early in its geological history. The primary objective of this thesis is to analyze the secondary minerals of the highly altered CM groups of chondrites belonging to petrologic type 2 (Murchison, Mighei, Murray, Nogoya, Cold Bokkeveld, and Mukundpura) to understand the degree, extent of alteration and aqueous evolution of parent asteroid. During the progressive alteration in the parent asteroid, the formation of secondary minerals, including phyllosilicates, tochilinite, and carbonates occurs with sulfate, phosphate, and magnetite as accessories. Phyllosilicates range a wider variability in their composition from Mg-rich serpentine (Chrysotile, Antigorite) to Fe-rich serpentine (Cronstedtite), common in the matrix of the meteorite or fine-grained rims around the chondrules, calcium-aluminum-rich inclusion and mineral clast. However, tochilinite generally occurs as intergrowths with cronstedtite, known as TCIs. Carbonates are usually common as tiny grains (generally, 20-80 μm across) as fluid precipitates within the matrix. Despite the existence of various models of alteration currently existing in the literature, the length-scale alterations and the role of the microenvironment in the CM parent body are poorly constrained. In the thesis work, a suite of CM type 2 fall samples (including one of the recent falls, Mukundpura), with different petrologic sub-types (2.0 to 2.5) are analyzed to gain further insights into the aqueous alteration processes. The role of a low-temperature hydrothermal process was evaluated based on minor element zonation in relict, refractory forsterite grains based on color CL and mineral chemical studies (for the first time in CM).

The qualitative and quantitative approaches adopted to constrain the aqueous alteration include different microtextural, mineralogical (including the modal proportion), and chemical compositions of matrix components and secondary minerals. This integrated approach is aimed at understanding the nature, condition, extent, and episodes of alteration. An attempt has been made to link the various microtextural characteristics and microchemical constraints to identify and evaluate the "microenvironment" that existed during the aqueous alteration process in the CM parent asteroid. The minor elemental distribution of carbonate grains is consistent with the microenvironment hypothesis and also suggested a changing carbonate fluids composition during the progressive alteration. This study suggests that even in thin section scale microenvironments exist and mineral chemistry further suggests more than one episode of aqueous alteration event.

The Fe oxidation record further helps to better evaluate the redox potential of iron species during aqueous alteration and this study suggested an oxidizing environment for the formation of TCI as suggested in a reducing environment in the earlier studies. Thus, the aqueous alteration formation environment is likely to become oxidizing, as alteration progresses.

The understanding of the role of impact and its linkage with aqueous alteration in the CM parent(s) is often difficult to ascertain due to the abundance of the fine-grained matrix (>70%) and the lack of suitable silicate minerals to record the shock metamorphism. Due to the paucity of mafic silicate and the rapid dispersion of shock waves via a fine-grained matrix, the imprint of shock is least understood in CM. This study demonstrates that the influence of shock metamorphism even in CM chondrites can be analyzed via the structural fingerprint using Raman. Impact-induced modifications probably induce a higher degree of alteration in highly altered CM. Additionally, based on this study, shock-induced heat may help to elevate the formation temperature locally at which TCI and carbonate form and moderate peak-metamorphic temperature based on the D and G band of matrix carbon in highly altered CM, playing a part in the parent body's thermal evolution.

Title: Drivers and implications of regional and global flash droughts
Researcher: Mahto, Shanti Shwarup
Supervisor: Mishra, Vimal
Year: 2022
Keyword's: Flash Drought, Soil Moisture-vapor Pressure Deficit, Land-atmospheric Coupling
Call No.: 551.5773 MAH
Acc. No.: T01083

Abstract: Drought is one of the deleterious and complex natural disasters that affect water availability, crop production, and gross domestic product (GDP). Unlike other natural disasters, drought is difficult to identify, predict, and mitigate. Conventional droughts evolve slowly with time and often last for months to years. Typically, drought does not show immediate consequences; however, people have recently noticed that crops and vegetation started dying suddenly in a few days to weeks under certain circumstances. Studies found that events of quick soil moisture desiccation were primarily common during the periods of vegetation mortality. The newly identified drought is termed a flash drought, uniquely characterized by a rapid rate of drought development.

India has one of the largest cropland areas globally (~140 million ha), of which 54% of the land depends on summer monsoon season (June-September) rainfall for agriculture. Agriculture plays a vital role in India's economy. Nearly 60% of India's workforce is engaged in agricultural and allied activities, accounting for 20% of the country's GDP. Flash drought in India can cause serious food crises and economic instability. An intense and widespread flash drought can be even more detrimental, making India's costliest natural disaster. The frequency of severe dry events has increased in India, which are expected to occur more frequently in the warming climate. Notwithstanding, India is vulnerable to flash droughts due to its large population and agriculture-driven economy; we do not know much about their occurrence, driving mechanism, and consequences. Therefore, understanding the flash droughts in the observed and projected future climate is essential for adaptation and mitigation under India's climate change scenario.

First, we check the reliability of state-of-the-art global reanalysis products that can be used for hydrologic applications in India. Observed climatic variables are difficult to acquire because of fewer monitoring stations and accessibility issues. In such a case, atmospheric reanalysis becomes the only data source that can be used to examine the drivers of flash drought in India. Moreover, coupled reanalysis datasets make it possible to analyze the land-atmospheric processes involved in flash drought development. We selected five global reanalysis products, mainly ECMWF 5th generation reanalysis (ERA5), Climate Forecast System Reanalysis (CFSR), ERA-Interim, Modern-Era Retrospective Analysis for Research and Applications version 2 (MERRA2), and Japanese 55-year Reanalysis Project (JRA55), to evaluate their performance against observations for hydrological applications in India. We used a well-calibrated and evaluated hydrological model [the Variable Infiltration Capacity (VIC) model] to simulate hydrologic variables using the forcing (daily precipitation and temperature) from India Meteorological Department and reanalysis products during the 1980-2018 period. Our results show that ERA5 outperforms the other reanalysis products

for the monsoon season precipitation, T_{max}, evapotranspiration, and soil moisture, which are essentially the key variables for flash drought study. However, CFSR performs better than ERA5 for monsoon season total runoff in India. Performance for streamflow and annual water budget for ERA5 is either better or comparable to the other reanalysis products in the two river basins. Overall, we find that ERA5 performs better than the other reanalysis products and can be used for flash drought assessments in India.

Next, we evaluate the occurrence of flash drought in India. Since flash drought characteristics can be evaluated using land hydrological variables, we used VIC simulated observed soil moisture (60cm depth) to identify flash droughts in India for the 1951-2018 period. We show that flash droughts predominantly occur during the summer monsoon season in India. More than 80% of the country-level flash droughts occurred during the monsoon season in India. The major country-level flash droughts occurred during the monsoon season of 1979, 2001, 1958, and 1986. About 10-15% of rice and maize grown area each year is affected by flash droughts during the monsoon season in India. We selected six regions based on homogeneous precipitation patterns to evaluate the regional characteristics of flash drought in India. Four out of six homogeneous precipitation regions experienced more flash droughts during the monsoon season than during the non-monsoon season. The Himalayan and Peninsular regions experience more flash droughts during the non-monsoon season primarily due to precipitation caused by western disturbance and northeast monsoon. Long dry spells with significant negative precipitation anomalies during the monsoon season and positive air temperature anomalies rapidly deplete soil moisture, causing flash droughts. Overall, we find that flash droughts directly affect crop production, which also poses indirect challenges for meeting increased irrigation water demands under soil moisture deficit conditions.

To mitigate the losses due to flash droughts, we should identify the regions and the rate at which flash droughts are changing in a warming climate. Moreover, the severity is another aspect of flash drought which may cause significant damage, even from a single flash drought event. We hypothesize that land-atmospheric feedback influences the occurrence and severity of flash droughts. Therefore, the observed and projected changes in flash droughts and associated land-atmospheric coupling were examined over India. We also examined the causes of the rapid depletion of soil moisture during the flash drought to prove our hypothesis true. Since VIC is not a coupled land-atmospheric model, we used ERA5 reanalysis and simulations from coupled model intercomparison project-6 (CMIP6) models to identify major flash droughts and associated soil moisture-vapor pressure deficit (SM-VPD) coupling in India. The summer monsoon season (June-September) witnesses more than 60% of total flash drought events and a relatively higher rate of flash drought development. Although flash drought frequency has mainly decreased during India's observed climate (1980-2019), the flash drought development rate has significantly increased. The flash drought frequency (development rate) is projected to decline (enhance) further in the future warming climate. The SM-VPD coupling during the flash drought onset-development phase is considerably higher (three to five-fold) than during the normal condition (in the absence of flash drought). The high (low) SM-VPD coupling explains the faster (slower) flash drought development rate in the observed and future warming climate. The strength of the SM-VPD coupling has increased

during the observed climate, which is projected to increase in the future. The increased SM-VPD coupling can intensify the future flash droughts in India, especially during the summer monsoon season, with considerable implications for agriculture, water resources, and ecosystems.

Flash droughts are decreasing in India, whereas they are expected to develop faster than usual (less than a week) if they occur. However, whether decreasing flash drought frequency in India significantly impacts worldwide crop production is unknown. Flash droughts have detrimental impacts on global agriculture, causing crop production to reduce, which may lead to an economic recession. Despite their serious consequences worldwide, flash droughts have not been examined in multiple aspects of the global cropland regions. We use ERA5 reanalysis and CMIP6 models to evaluate the flash drought occurrence in the observed (1981-2020) and the future (2020-2100) climate, respectively, for the sixteen selected cropland regions globally. More than 80% of the cropland regions have shown an increasing trend in flash drought frequency, except South Asia. The area affected by the flash drought has moderately increased during the 1981-2020 period, caused due to a significant rise in flash drought co-occurrence in multiple cropland regions. Due to decreasing flash drought frequency in India, global rice regions showed decreasing impacts of flash drought. Moreover, central Africa and southern South America will also experience fewer flash drought events in the future. Nevertheless, flash drought frequency will continue to rise in ten of sixteen cropland regions, especially in developed countries such as the United Nations, Europe, and China. The increase (decrease) in the flash drought frequency is strongly attributed to the decrease (increase) in soil moisture anomaly in the observed and the future warming climate. Moreover, VPD is projected to be the dominant driver of flash drought in a warming world. Monitoring and predicting VPD will be crucial for mitigating the agricultural and economic losses due to flash droughts in the global croplands, including India.



ELECTRICAL ENGINEERING

Electrical Engineering

Title: Grid converter synchronization techniques for distributed generation systems
Researcher: Chandrasekaran S.
Supervisor: Ragavan K.
Year: 2015
Keyword's: Discrete Fourier Transform, Shunt Active Power Filter, Grid Voltage, DG Units, Power System
Call No.: 621.3 CHA
Acc. No.: T00059

Abstract: The exponential growth of renewable energy resources based distributed generation (DG) systems is due to the ever increasing power demand and environmental concerns. The DGs are integrated to the grid through power electronic converters and they contribute to the enhancement of reliability and efficiency of power system. However, due to the increased penetration, DGs cause concern about stability due to their interaction with the grid. Hence, grid codes stipulate that DGs must have fault ride through capability and specify the range of values of voltage and frequency for which they should remain connected to the grid. Therefore, fast and accurate estimation of grid variables such as amplitude, phase and frequency is essential. Further, these information are vital in the reference current generation for converters. In this regard, this thesis focuses on developing grid variables monitoring scheme suitable for normal and abnormal grid conditions. This thesis presents sliding DFT prefiltered synchronous reference frame phase locked loop (PLL) for tracking the grid voltage attributes. With this prefilter, dc offset and harmonics present in the input are blocked from entering PLL. Further, the input voltage is amplitude normalized. The proposed scheme is suitable for single phase as well as three phase applications.

In the single-phase scheme, sliding DFT acts as prefilter and orthogonal signal generator. In case of three phase scheme, with the help of sliding DFT, the instantaneous symmetrical components (ISC) method succeeds in identifying the fundamental positive sequence (FPS) component. With this capability, even during severe disturbance and unbalance, rapid and precise tracking of utility variables is achieved. Synchronous sampling is essential for the deployment of sliding DFT. However, when the grid frequency deviates from the nominal value, sampling becomes asynchronous. To address this problem, two variants of this scheme are proposed. In the first scheme, adaptive sampling rate adjusted sliding DFT is deployed as pre-filter to the SRF PLL. When the grid frequency drifts from the nominal value, the required synchronous sampling condition is achieved with an adaptive sampling frequency adjustment scheme based on numerically controlled oscillator. With this technique, the attributes can be tracked without any steady-state error. However, the improvement in transient response is not substantial. Further, it is suitable for applications where variable sampling period is acceptable.

With the second scheme, pre-filtering is achieved with fixed sampling period sliding DFT. In this technique, under grid frequency drift, sampling frequency is not adjusted. As a result, sampling becomes asynchronous due to which there will be errors in the amplitude and phase of the SDFT output. However, the frequency information is error-free. By simulation study, these errors are found for a range of frequencies. Using these error data, the relation between these errors and frequency deviation is established. With these it is possible to account for the errors. However, when the grid frequency is off-nominal, the harmonics present in the input signal could not be completely blocked by the sliding DFT filter. This will cause oscillating error in the estimation of frequency and hence in the estimation of amplitude and phase. To address this issue, the moving average filter is deployed to attenuate the oscillations in the frequency estimation. This method is appropriate for applications demanding fixed sampling period. Major contributions of this thesis are enumerated below:

- sliding DFT used as pre-filter and orthogonal signal generator in single-phase SRF PLL
- sliding DFT together with ISC method used for FPS component extraction in three-phase SRF PLL
- with error compensation, fixed sampling period sliding DFT is deployed as pre-filter for single-phase and three-phase applications

The techniques proposed in this thesis have been implemented in Matlab-Simulink environment. These are experimentally validated using real-time controller board (dSPACE DS1104) and three-phase programmable power source. Various grid disturbances are emulated using the power source and the results are presented. With the fixed sampling period sliding DFT as pre-filter (second technique), irrespective of type and severity of disturbance, tracking of parameters is achieved within 30 ms. Such improved tracking of grid parameters will enhance the operation and control of DGs during normal and faulty grid conditions.

Title: Characterizing high-frequency behaviour of transformer by reduced-order circuit model and assessing the severity of mechanical deformations
Researcher: Shah, Krupa Rajendra
Supervisor: Ragavan K.
Year: 2015
Keyword's: Synthesizing Circuit, Radial Deformation, Single-winding, Axial Displacement
Call No.: 620 SHA
Acc. No.: T00096

Abstract: Stability and reliability of the power system is highly affected by the state of apparatus connected to it. High voltage power transformer is one of the crucial elements associated with transmission and distribution of electrical energy and hence its uninterrupted functioning is of utmost importance. Abnormal forces generated during short-circuit and transportation would cause permanent mechanical deformations in transformer. Such incipient fault grows and eventually would lead to catastrophic failure. Therefore, identifying mechanical deformation and assessing its severity is paramount for smooth functioning of transformer and power system. Mechanical deformation of windings gets reflected as changes in the high-frequency behaviour of transformer. Hence, characterizing its high-frequency behaviour is essential. For this purpose, physically realizable ladder circuit corresponding to the high-frequency behaviour of the transformer winding can be built. On this line, ladder circuit incorporating electrical and magnetic couplings has been widely accepted as suitable representation. In order to develop circuit model, certain terminal quantities are required. In this work, a generalized procedure is proposed to estimate various quantities such as effective shunt-capacitance, equivalent inductance and capacitance from the terminal data. It is found in literature that estimating effective series capacitance is not straightforward. To this end, an algorithm is presented. The algorithm is validated considering case studies on circuit model, single-winding and two-winding transformer. To assess the status of transformer winding with regard to mechanical deformation, an approach is proposed. Utilizing the above mentioned terminal quantities and by performing sequential iterations, high-frequency behaviour is represented by an equivalent circuit model. The circuit model is synthesized such that its natural frequencies, terminal inductance and capacitance are nearly same as that obtained through measurement.

This methodology involves comparing the circuit model corresponding to its present state with that of its counterpart when it was healthy. The location of deformation is identified by the changed parameter in the circuit. Further, the amount of change reveals the severity of introduced deformation. In practice, the transformer has many windings. In such scenario, extending the proposed approach for fault diagnostics becomes very challenging. As there is a need to model the high-frequency behaviour of winding by a ladder circuit, multiple winding unit corresponds to multiple ladder circuits. All these ladder circuits are electrically and magnetically coupled. Using such complex multi-ladder network for the purpose of diagnostics is really cumbersome. To this end, an approach is presented for simplifying this complex network. In this work, multi-winding transformer unit is realized by a reduced-order circuit model, that is, single ladder circuit. Once such ladder circuit

is available, the same principle of comparing two circuits is followed. The algorithm is demonstrated with a two-winding transformer unit. Further, a novel method is proposed to minimize resonance effects in transformer. This method involves designing transformer winding corresponding to power frequency excitation. Utilizing such geometrical information, estimation of its constants such as inductances and capacitances is achieved. Then, these parameters are utilized for constructing physically realizable ladder circuit model. From the circuit model, natural frequencies are estimated. If any of the natural frequencies coincides with the dominant frequency of the incoming surge then winding geometry is modified. The new set of natural frequencies can be obtained such that the resonance phenomenon is avoided.

Title: Controls for moderating generation-demand mismatch in wind-solar-hydro energy conversion system
Researcher: Ramprabhakar, J.
Supervisor: Ragavan K.
Year: 2016
Keyword's: Battery Energy Reserve, Reactive Power Support, Power Management Control, Energy Conversions Systems, Distribution Generation
Call No.: 621.04 RAM
Acc. No.: T00098

Abstract: Distributed generation (DG) is related with the use of small generating units installed at locations of load centres. DG can be used in an isolated way, supplying consumers' local demand, or integrated into grid supplying the energy to the remainder of the electric power system. DG technologies can run on renewable energy resources, and its capacity ranges in size from less than kilowatt to tens of megawatts. DG has attracted a lot of attention world wide, since it decreases the dependency on fossil fuel and also in reducing the emission of the greenhouse gases. The power derived from renewable sources such as wind flows and solar irradiance are unreliable owing to its seasonal and diurnal variations. To surmount the said defiance, power electronics and controls are used to coordinate the renewable power systems. This thesis is focused on modelling, control and power management of electronically interfaced distributed energy resources. To this end, mathematical model of each energy conversion system is developed and they are interfaced through power converters. For this integrated hybrid system, frequency control, voltage amplitude regulation and moderation of generation-demand (G-D) mismatch are the primary control requirements. In order to achieve this control schemes are proposed for the power electronic converters to regulate the power flow under balanced and unbalanced load conditions. For the hybrid scheme to operate effectively in integrated mode, effective control has to be done in order to meet the changing demand, despite variation in generation. An objective function is formulated to forecast the power harvested from the renewable sources. Moreover, the objective function also estimates the energy reserve available to meet the demand. In order to maintain the dc-link voltage constant, despite variations in G-D gap, an adaptive control technique is devised. In this technique, dc-link voltage is shown to be maintained by adaptive gain control that relates dc-link voltage to the power output of battery system. Further, the proposed objective function is such that, it can quantify the uncertainty with renewable generation forecast and battery power output. Further, this research work is extended to provide reactive power support by connecting static compensator (STATCOM) at point of common coupling. With this, it is possible to provide control measures to protect the system under emergency situations like sudden rise in demand. The STATCOM control is modified to maintain balance currents in the converter, despite unbalanced load conditions.

Title: Anomalous Narrow width effect in gate first high-k metal gate MOS transistor
Researcher: Satya, Sivanarsh. M
Supervisor: Mohapatra, Nihar Ranjan
Year: 2016
Keyword's: Threshold Voltage, HKMG MOS Transistors, Anomalous Behavior
Call No.: 621.381522 SAT
Acc. No.: T00179

Abstract: HIGH K dielectrics and metal gate stacks (HKMG stacks) are currently being used in place of conventional silicon dioxide and poly-silicon gate stacks (SiO_2 /Poly gate stack) for 45nm or below CMOS technology generations. The transistor dimensions (length and width) are small and also continuously shrinking in these technology generations. Therefore, the deeply scaled geometries coupled with HKMG stack give rise to many anomalous effects. These anomalous effects were never observed in earlier nodes. One of these effects is increase in both the threshold voltage (V_T) and the trans-conductance (g_m) with decrease in the transistor width (W) of nMOS transistors. The main focus of this thesis is to study and understand the details of the Narrow Width Effect (NWE) observed in HKMG MOS transistors and to access its impact on the analog/ digital circuit performance.

We have studied and explained in detail different geometry effects exhibited by the HKMG MOS transistors fabricated using a 28nm gate first CMOS technology. It is shown that the V_T of the nMOS transistors increases with the decrease in channel width (W) and this effect is amplified with the reduction in gate length (L_G). The pMOS transistors show decrease in $|V_T|$ with the reduction in width. It is also shown that this NWE is enhanced for nMOS and pMOS transistors with thicker HfO_2 film and thicker capping layer. Through detailed measurements on different test structures, the reason behind this anomalous behavior is attributed to the annihilation of positively charged oxygen vacancies (VO^{++}) and interface dipoles in the gate dielectric stack at the corners of the gate-active overlap region after post gate high temperature process steps. In addition, the said annihilation of positively charged oxygen vacancies will strongly depend on the layout and design rules. To confirm this, we investigated the effect of active to active spacing on the V_T of the HKMG MOS transistors. It is observed that V_T increases with increase in active to active spacing for nMOS transistors and decreases for pMOS transistors due to the higher annihilation of the oxygen vacancies at the corners of the active-gate overlap region. It is also found that the dependence of V_T on active to active spacing is higher for nMOS transistors with thicker La capping layer thickness, which again confirmed the annihilation of both VO^{++} and interface dipoles. It is also shown that the observed NWE could be reduced by optimizing the thickness of HfO_2 , SiO_2 interfacial layer, La capping layer and by using the dummy actives. An empirical model for the said NWE is also developed. The accuracy of the model is verified by comparing it with the measurement data. The model can accurately predict the V_T of different device geometries and for a wide range of HfO_2 and La capping layer thickness. We have discussed the effects of device dimensions on the analog performance of gate-first HKMG MOS transistors. It is observed through detailed measurements that the trans-conductance (g_m) of HKMG MOS transistors increases with reduction in the channel width. The 80nm nMOS and pMOS wide

transistors have shown ~28% and ~26% higher intrinsic gain compared to the 1 μ m wider ones respectively. And 80nm nMOS and pMOS wide transistors have shown ~26% and ~21% improvement in transconductance generation efficiency (g_m/I_d) compared to the 1 μ m wide transistors respectively. The similar behavior is observed for all gate lengths. This has been attributed to the reduction in the remote coulomb scattering (lower V_0^{++} in narrower transistors) for narrow width transistors. It is finally shown that longer and narrower HKMG MOS transistors will provide more benefit with respect to the analog performance metrics. We have also studied the analog performance of HKMG MOS transistors for low voltage applications such as mobile applications and medical electronics. It is found that at a lower bias current, the analog performance is marginally better for narrow width HKMG MOS transistors.

We have also investigated the effect of active to active spacing on the analog performance of the HKMG MOS transistors and it has been shown that the analog performance is better with increase in active to active spacing due to the higher annihilation of the positively charged oxygen vacancies at the corners of the active-gate overlap region. In addition, we have also shown that the analog performance can further be improved by dividing the single active into multiple actives or by eliminating the active dummies. In this way, the net reduction in V_0^{++} over the total width will be more and the corresponding analog performance will be better.

Title: Calibration- free 1f and 2f wavelength modulation spectroscopy with in-situ measurement of laser parameters
Researcher: Upadhyay, Abhishek
Supervisor: Chakraborty, Arup Lal
Year: 2016
Keyword's: Quadrature Modulation Frequency, Vertical Cavity Surface Emitting Laser (VCSEL), Calibration-free, RAM Nulling Method
Call No.: 621.361 UPA
Acc. No.: T00204

Abstract: Over the past few decades tunable diode laser spectroscopy (TDLS) has established itself as a highly reliable technique for the measurement of gas parameters, specially in systems that require high sensitivity, high specificity and rapid in-situ measurements. In TDLS a narrow linewidth tunable diode laser is tuned across the rotational-vibrational absorption line of the target gas. The relative transmission obtained is used to infer the gas parameters. A variant of TDLS known as wavelength modulation spectroscopy (WMS) where a high frequency sinusoid superimposed on a low frequency ramp is used to modulate the laser. The information bearing signal is shifted to its baseband with the help of a lock-in amplifier (LIA) resulting in an improvement in the signal-to-noise ratio (SNR) by about two orders. Initial WMS methods were not calibration-free and were not suitable for field measurements in harsh environments. Over the last decade several calibration-free WMS methods have been proposed which have enabled the deployment of TDLS based gas sensors in harsh environments. However, there were some limitations of these techniques. The calibration-free first harmonic (1f) WMS methods such as residual amplitude modulation (RAM) method and phasor decomposition (PD) methods were limited to low modulation index values (m-values) and suffered from the problem of large absorption independent background RAM which lead to the early saturation of the detection electronics. These methods were extended to high m-values by replacing the Taylor series analysis with the Fourier analysis of the transfer characteristics of the absorption signal. Also, the RAM nulling methods were able to remove the large absorption independent background accompanying the RAM signal. However, these methods were not immune to rapidly varying absorption independent losses such as those due to vibrations and beam steering. Second harmonic (2f) WMS methods such as 2f/1f method were able to overcome both these issues. The 2f/1f WMS signal had a negligible absorption independent background and was immune to the absorption independent systematic losses. However, this method relies on the pre-characterized laser parameters for the simulation of the 2f-WMS signal. These laser parameters may drift due to temperature variation and aging and would lead to an error in the measurement. The frequency modulation (FM) component of the 2f-WMS signal which is main measurement signal of the 2f-WMS methods, is always weaker than the FM component of the corresponding 1f-WMS signal. Despite this compromise in SNR, 2f-WMS methods were preferred over 1f-WMS methods because of low absorption independent background accompanying these signals. Hence different WMS techniques in their present form suffer from different types of limitations and there is a need to overcome these limitations either by making changes in the existing WMS methods or by proposing new methods that can overcome these limitations.

This work can be broadly divided into three parts, in the first part we have optimized the RAM method by operating at the phase quadrature modulation frequency (f_q) of 125.5 kHz. In the RAM method only a component of RAM signal is used for the measurement when operating at any other frequency instead of f_q . The PD method overcomes this problem and uses the full RAM signal. However, this method relies on the measurement of the phase between the intensity modulation (IM) and the FM of the laser which is susceptible to errors for lower concentrations and for smaller phase difference between the IM and FM. Hence operating at the f_q has the advantage that full RAM signal is used for the measurement of the gas parameters, without any limitations being imposed by the accuracy of measurement of phase between the IM and the FM of the laser. Although this advantage of operating at f_q was known for a long time but it had not been utilized because the f_q reported earlier were of the order of 1MHz. The cost of the supporting electronics when operating at such high frequencies increases. Along with operating at this low f_q , optical RAM nulling was used to remove the absorption independent background RAM. In optical RAM nulling the laser output is divided into two parts. The light output in the first part known as gas arm is transmitted through the absorbing gas sample and a polarization controller. The other part goes through a delay arm comprising of a single mode fiber of appropriate length, a variable optical attenuator and a polarization controller to generate an absorption independent RAM signal equal in magnitude but 180° out of phase with the absorption independent RAM signal in the gas arm. When operating at a $f_q = 125.5$ kHz the length of the fiber in the delay arm is 0.814 km which is much greater than the typical coherence lengths. In contrast when operating at a f_q of the order of 1 MHz this length would be close to 100 m and would lead to an optical interference when the signals from the gas arm and delay arm recombine in a 3dB coupler. Thus by operating at the f_q and implementing RAM nulling at this frequency to remove the absorption independent background RAM and using Fourier analysis of the transfer characteristics, RAM method was fully optimized. In the second part of this work a new calibration-free 2f-WMS method was proposed and its detailed description was provided. In this method all the relevant laser parameters are measured from the signals captured in traditional WMS, that is the transmitted output, the LIA output and the resonator output. Therefore, any change in experimental WMS signal due to variations in these parameters because of the non-absorbing losses are incorporated in the simulated signal as well. Hence this method is immune to the rapidly varying non-absorbing losses such as those due to vibrations, beam steering and fouling of the coupling optics. It is also immune to the slowly varying absorption-independent systematic losses such as those due to drift, aging and temperature variation. The applicability of this new method has been established by implementing it on three different types of lasers, namely 5250 nm continuous wave distributed feedback quantum cascade laser (cw-DFB-QCL), 2004 nm vertical cavity surface emitting laser (VCSEL) and 1650 nm edge emitting distributed feedback (DFB) laser for the measurement of nitric oxide, carbon dioxide and methane respectively. If there is significant nonlinearity in the intensity versus current characteristics of the laser such as for the cw-DFB-QCL laser used in this study, the 2f-WMS signal can be accompanied by a significant background RAM signal. The WMS signals for higher harmonics are weaker in signal strength but their signal to the absorption independent background ratio increases. Therefore, for such lasers it would be advantageous to use higher harmonics. By extending this technique to third harmonic for the three lasers used in this study, it has been established that this technique is not limited to 2f-WMS and is

applicable to higher harmonics as well. Using the same technique of in-situ real-time measurement of laser parameters a new calibration free 1f-WMS method which uses the magnitude of 1f-WMS signal as the measurement signal was proposed. The large absorption independent background of the 1f-WMS signal was removed through a new RAM nulling method proposed in this work.

In this method the transmitted signal detected by the photo-detector is divided into two parts. One part goes through a microcontroller that uses a software LIA of large dynamic range to generate a signal which is equal in magnitude but 180° out of phase with 1st order IM signal received at the photo-detector. The other part combines with the signal generated by the microcontroller through an analog summing amplifier. The output of the summing amplifier which is free from the absorption independent 1f background RAM is given as an input to a second LIA that has a much smaller dynamic range. Since the full dynamic range of the second LIA is used to measure the absorption dependent signal it leads to an increase in sensitivity of measurement. The quantization noise present in the output of the summing amplifier does not affect the final measurement because this noise is filtered by the second LIA as it is outside the bandwidth of the second LIA. This method obtains the RAM component, the FM component and the magnitude of the 1f-WMS signal. Since the FM component of the 1f-WMS is always stronger than the FM component of the 2f-WMS signal this method would provide a larger SNR as compared to 2f-WMS techniques. The RAM signal can be stronger or weaker than the FM signal, depending upon the operating modulation frequency and the tuning coefficient. However, it is demonstrated that the magnitude of 1f-WMS signal is the strongest WMS signal. Therefore, this method would always provide a higher SNR as compared to other WMS methods. The new WMS schemes have been validated by implementing them on different types of lasers for the measurement of different gases at various concentration and pressure values. A detailed explanation of each of these techniques has been provided. The advantages and limitations of each of these schemes have been discussed in detail.

Title: Physiology-sensitive virtual reality based system for children with autism
Researcher: Kuriakose, Selvia
Supervisor: Lahiri, Uttama
Year: 2017
Keyword's: Technology-assisted Tools, Intervention Paradigm, Physiology-sensitive, Social Communication
Call No.: 621.3 KUR
Acc. No.: T00206

Abstract: Autism Spectrum Disorder (ASD) with prevalence rate of approximately 1 in 150 in India is defined as a neurodevelopment disorder often characterized by impairments in communication, reciprocal social interaction and explicit expression of affective states. There is a growing consensus that intensive behavioral and educational intervention programs can significantly improve short and long term outcomes for individuals with ASD and their families. However, with limited availability of trained professional resources, lack of widely available efficacious intervention facilities and the enormous costs of treatment, a majority of these individuals fail to achieve adaptive independence as adults. Recent research shows that emerging technology can play an important role in providing more accessible, intensive and individualized intervention in the future. Many studies have investigated application of technology-assisted tools, such as, computer technology, Virtual Reality (VR), and robotic systems for individuals with autism. In our present work, we chose VR because of its malleability, controllability, modifiable sensory stimulation, individualized approach, safety, simplified but explorative training environment due to potential reduction of problematic aspects of human interaction particularly during initial skill training. Since VR mimics real environments in terms of imagery and contexts, it may offer efficient generalization of skills from VR environment to real world. The currently available VR environments as applied to intervention are designed to chain learning via aspects of performance alone (correct, or incorrect) thereby limiting individualization of application. In conventional techniques, a therapist adjusts the intervention paradigm by monitoring the affective state, such as, anxiety of these individuals for effective floor-time-therapy. In our study, we choose anxiety as the target affective state, since anxiety is a common concern in clinical samples with autism and this can have adverse effects on one's performance in a social task. To foster effective social communication skills, the technology-assisted system should intelligently adapt itself to a user's anxiety states with high degree of individualization. However, adolescents with autism often possess deficits in explicit expression of their anxiety state thereby posing limitations on traditional observation based techniques. Thus, researchers have been studying the potential of other modalities, such as, physiological signals that are continuously available and not directly impacted by one's communication deficits. Also, the physiological signals might offer an avenue for recognizing one's anxiety state that is less obvious for humans but easily decipherable by computers.

The primary goal of our research was to develop a VR-based technology with potential relevance to ASD intervention. To achieve the broader objective of offering an adaptive VR based social communication platform to participants, we designed usability studies that aimed to address the

following questions: (i) whether the VR-based social communication system has potential to have implication on one's performance and physiological indices, (ii) whether the system has the potential of mapping one's physiological indices to the anxiety level while interacting with the VR-based social communication tasks and (iii) finally whether the Physiology-sensitive VR-based social communication system has potential to contribute to improving one's performance in a social task. Results of our usability studies indicate the potential of VR-based social communication system to have effect on one's performance and physiological indices (used as biomarkers of one's anxiety level). Our novel VR-based Adaptive Response Technology (ART) was equipped with Anxiety-Sensitive feature. Specifically, this Anxiety-Sensitive (AS) system was capable of objectively identifying and quantifying one's anxiety level from physiological biomarkers to adaptively offer tasks of different challenge levels in an individualized manner thereby helping to foster improved social communication-related performance. Our research showed that our intelligent adaptive VR-based Anxiety-Sensitive system has a potential to contribute to improved performance among individuals with ASD in at least some of the core social communication aspects. Also, this can help to identify elements of social interaction that might be anxiety-provoking for this target group in a very individualized manner. Additionally, such an individualized VR-based Adaptive Response Technology can provide information on one's physiological profile and thereby can serve as a potent complementary tool in the hands of the interventionist. The inherent design flexibility of the VR-based system can be used to provide a portable home-based social communication skill learning platform that can be used by an individual with ASD beyond the clinical setting. Further, the ability of such a VR-based system to offer individualized feedback and reinforcement strategies can aid the therapist to monitor and work on improving the social communication skill learning of an individual with ASD. We hope that the realization of such a system may pave the way for intensive, intelligent, and individualized intervention paradigms in future. Thus, we believe that this novel technology can serve as a stepping stone in our endeavors to develop a comprehensive social skill learning platform that can improve the functioning and quality of life of individuals with ASD.

Title: Adaptive algorithms for active sound control
Researcher: Patel, Vinal
Supervisor: George, Nithin V.
Year: 2018
Keyword's: ASP Systems, Adaptive Algorithm, Health Issues, Active Sound Profiling
Call No.: 621.38224 PAT
Acc. No.: T00276

Abstract: The Air (Prevention and Control of Pollution) Act, 1981 considers noise present in the environment as a constituent of air pollution. Long term exposure to noise may lead to health issues including hearing loss. Passive noise control approaches like usage of barriers, mufflers etc. are not effective for mitigating low-frequency noise. Active sound profiling (ASP), which uses a secondary sound source to regulate the noise level, is a promising scheme for noise control. The secondary sound source, which is usually a loudspeaker, is controlled by an adaptive controller. The core of this controller is an adaptive filter, which is regulated using a suitable adaptive algorithm in such a way as to obtain the desired noise spectrum. ASP can achieve noise cancellation as well as sound enhancement of selected frequency components. This thesis aims at designing ASP systems, which can provide robust sound profiling under different usage scenarios. Low- cost implementations of such systems introduce non-linearity in the system, which can produce new frequencies when attempted to profile the sound using a linear controller. A set of non-linear controllers, which can handle such scenarios has also been designed. Promising results were obtained when sound profiling was implemented in real-time on a dSPACE^R platform.

Title: Technology assisted screening and balance training systems for stroke patients
Researcher: Kumar, Deepesh
Supervisor: Lahiri, Uttama
Year: 2018
Keyword's: Stroke Patients Training, Biomarker, VR-based CoP-assisted Balance Training, Kinect Sensor, Oculomotor Signature
Call No.: 621.3 KUM
Acc. No.: T00287

Abstract: Stroke is the second most common cause of death and fourth leading cause of disability worldwide. The morbidity and mortality rate due to stroke can be addressed at least to some extent if the treatments are given in short time window post the onset of stroke symptoms. This makes early screening of stroke critical. Some of the common symptoms of stroke are sudden trouble seeing in one or both eyes and visual neglect. These symptoms can be identified as related to stroke by expert clinicians. Unfortunately, lack of adequately trained neurologists and healthcare workers has limited its use only in major urban centers in countries like India. Faced with such challenge, a cost-effective, simple-to-use, a clinically valid device that can pick up potential biomarkers representative of neurological dysfunction can be critical and useful in both urban and rural healthcare settings. One such biomarker can be captured by picking up one's oculomotor signature for screening stroke cases. This is because one's oculomotor system connected with a vast network of brain areas become vulnerable to various neurological disorders such as stroke resulting in unique clinical patterns. Thus, the oculomotor examination can serve as a sensitive and also early indicator of neurological dysfunction. In this research, my first objective was to develop a cost-effective, simple-to-use and clinically-valid device (SmartEye) for screening one's probable neurological disorder from oculomotor signature. To achieve this objective, I designed a gaze-sensitive computer-based system called SmartEye. Results of the SmartEye-based study indicate that one's gaze-related indices such as gaze fixation, smooth pursuit, and blinking might serve as potential quantitative biomarkers for screening of stroke cases.

Once screened for the possible neurological disorder, it is also critical to address at least some of the accompanying deficits such as those related to balance and mobility. As a result of stroke, individuals often succumb to hemiplegia causing complete or partial paralysis on one side of the body. These patients show impaired balance due to asymmetric body posture which causes them to fall while performing activities of daily living. Such deficits are usually addressed by rehabilitation exercises done under the supervision of trained therapists spanning over repeated exposures. These conventional techniques, though powerful often suffer from subjectivity, restricted availability of trained therapists particularly in primary health centers, monotonicity with repetitive training/exercises stealing away patients' motivation. Thus, investigators have been exploring technology-assisted training. Among the technology-assisted balance rehabilitation systems use of robot-assisted, computer-based and Virtual Reality (VR) based techniques have started gaining popularity. Among these techniques, I chose VR augmented with peripheral device such as Balance Board and Kinect (to determine center of pressure (CoP) and center of mass (CoM)) for developing a balance training system that offers the flexibility of design, controllability, and individualized

approach to balance rehabilitation. My system offers individualization along with variations in tasks used for balance training that is not there in the currently existing VR-based systems that use off-the-shelf games (designed with an entertainment perspective) along with limited individualization thereby restricting the applicability for rehabilitation. Thus, the second objective of my research was to develop and study the implication of intelligent adaptive VR-based balance training platforms on one's task performance in a balance training task. To achieve this objective, I have explored the applicability of different VR-based training systems through three studies.

In the first study, I developed a VR-based CoP-assisted Balance Training (VBaT) platform, where VR-augmented user-interface using a single wireless balance board (WiiBB) was used. The VBaT offered tasks of varying challenges to the participants and was adaptive to one's performance quantified through weight-shifting capability during balance training. During the weight-shifting task, the position of a virtual object in the VR environment was controlled with CoP excursion measured by the WiiBB. Results of a usability study indicate the potential of the VBaT system to cause improvement in overall average task performance over the course of the training.

In my second study, I explored another modality such as use of CoM instead of CoP. For this, I developed a VR-based CoM-assisted Balance Training (Virtual CoMBaT) system interfaced with WiiBB and Kinect instead of marker-based motion capture systems as used by other researchers. In this system, I have used one's personalized CoM, estimated using Kinect sensor while offering individualized VR-based balance exercises. Here, the participant was allowed to interact with the VR-based tasks by shifting weight in different directions while standing on the ground. During the weight-shifting task, the position of a virtual object in the VR environment was controlled with CoM excursion. Results of a usability study indicate the potential of the Virtual CoMBaT system to (i) provide one's quantitative estimates of direction-specific residual balance capability and (ii) contribute to improvement in one's weight-shifting capability through an increase in performance in balance-related tasks of different challenge levels. Though both the VBaT and Virtual CoMBaT systems were able to contribute to the improvement in one's balance (weight-shifting ability) in the course of the training, yet these systems did not give the contribution of each of the two legs (Affected leg and comparatively healthy (Unaffected) leg of a hemiplegic patient) of an individual towards the improvement of his/her balance. This information on the relative contribution of each leg to one's weight-shifting ability is important to the clinician since it can assist a clinician in modifying the training paradigm so as to condition the rehabilitation effort in a way that the Affected leg gains greater usage by the participant. To achieve this, clinicians use targeted weight-shifting training for the patients in which the clinicians instruct the patients to increase the usage of Affected leg. However, these techniques operate as in open loop without any real-time visual feedback.

To achieve this, in my third study, I have designed a VR-based Balance Training platform interfaced with two WiiBB (V2BaT) augmented with a distributed weight paradigm (conditioning) coupled with a closed loop visual feedback. Here, during the weight-shifting task, the position of the virtual object in the VR environment was proportionally controlled with CoP excursions measured by two (one for each leg) WiiBB. Results of a usability study indicate the potential of the V2BaT system to contribute to (i) the improvement in one's balance (weight-shifting ability) in the course of the training and also (ii) increased usage of the Affected leg along with the Unaffected leg.

Having seen the use of VR-based systems augmented with peripheral devices in balance rehabilitation and the use of oculomotor signature as a screening biomarker of stroke, I wanted to understand the connectivity between one's eye movement and balance while performing a goal-directed balance task offered by the V2BaT system. Thus, the third objective of my research was to extend the previous study using V2BaT augmented with operant conditioning to examine the implication of such a paradigm on one's gaze fixation behavior during a goal-directed balance task. Similar to the previous study, here an individual was expected to maneuver a virtual object from a start location to a pre-defined static target location through CoP excursion while using distributed weight paradigm. At the same time, I monitored the individual's fixation pattern. The results of my study indicate that after the participant was exposed to the balance task augmented with operant conditioning, the participants demonstrated improved task performance coupled with increased fixation towards the static target location and decreased fixation towards the dynamic virtual object.

Title: Singnificance of tengential component of magnetic flux density in reaction torque and cogging torque
Researcher: Endla, Naveen Kumar
Supervisor: Ragavan K.
Year: 2019
Keyword's: Conformal Mapping, Magnetic Flux Density, Reaction Torque, Cogging Torque
Call No.: 621.2106 END
Acc. No.: T00391

Abstract: Magnetic field distribution in the airgap of rotating machines, consisting of tangential and normal components, determines the instantaneous value of torque. Lorentz Force (LF), Maxwell Stress Tensor (MST) and Virtual Work (VW) methods are commonly used to estimate torque. With regard to rotating machines, and in their general forms as used by design engineers, these methods show distinct significance of field components for numerical value of torque. LF method does not require the distribution of tangential component to compute torque whereas MST and VW require tangential component. A comprehensive understanding on field components and their significance in deciding the numerical value of torque is useful in developing effective design optimization methods.

A methodical way to appreciate the equivalence between LF, MST and VW is through analytical expressions. Equivalence of these methods for computation of global force (net force) is well addressed in classical literature. This equivalence can also be extended to torque, as torque is moment of force. A thorough literature review reveals that analytical equivalence with final torque expression is not previously presented. Such an equivalence is useful to understand the significance of field components and flux paths with regard to three methods.

In the first part of this thesis, torque expression based equivalence of LF, MST and VW methods is presented starting from a simple two coil conceptual system. Subsequently, similar torque expressions for smooth airgap systems with multiple coils is derived. Using these expressions and with certain assumptions, few indicative factors are derived. These factors reflect the method-specific significance of field components. In addition, these factors can also be regarded as reference values for relative sensitivity of the three methods to errors in field distributions. These factors are derived for both average torque and its ripple.

In the second part of the thesis, focus is mainly on cogging torque and separation of ripple components in reaction torque. In earlier publications, closed form expressions for pole embrace corresponding to minimum cogging are derived considering only radial fields. In this thesis, a compact equation for cogging torque is derived for SPM motors. This compact form explicitly reflects the contributions of both radial and tangential field components. Reduced order expressions are derived to easily identify the effects of key design parameters on the constituents of cogging. The analysis on cogging presented here, helps in determining search domains in which optimum embrace for minimum cogging can be found when tangential field component is not negligible.

A reduced order modeling of instantaneous torque is presented in Chapter 4 that helps in investigating the constituents of ripple content. The method used is a slightly modified version of Conformal Mapping based approach proposed in literature. The modification is done to obtain a torque expression that helps to explicitly identify the ripple induced by phase-belt and slot harmonics in SPM motors. The total effect of slot and belt harmonics on armature field can be obtained either using FEA, Conformal Mapping or Subdomain models. However, these methods are not suitable for explicit separation. The method given in Chapter 4 yields a suitable expression which can be used in a computational platform to perform a quick explicit investigation on slot and belt harmonic effects on armature field and torque ripple in SPM motors.

The discussion presented in this thesis on method-specific significance of tangential component and flux paths would be helpful in improving the lumped models of machines. The search zones to find optimum pole embrace for cogging given here, can be used by the designers to foresee the behavior of cogging sources before performing a rigorous analysis and hence reduce the time required in design optimization.

Title: Assessing the performance of estimation and control: from data to knowledge
Researcher: Das, Laya
Supervisor: Srinivasan, Babji
Year: 2018
Keyword's: Estimation Control, Data, Knowledge, Hurst Exponents
Call No.: 621.381531 DAS
Acc. No.: T00393

Abstract: Estimation and control constitute tasks of significant importance to industrial processes. This work addresses the task of assessing the performance of estimation and control algorithms in the presence of modeling uncertainties. The main theme of the work revolves around exploiting the relation between predictability of the errors made by a given algorithm and the performance of the algorithm. The predictability of individual estimation/control errors are used to quantify the performance of an individual variable with respect to its estimation/control. Hurst exponent is used to quantify the predictability of errors. With deteriorating performance, the predictability of individual errors are observed to increase as suggested by the Hurst exponents.

Modern systems predominantly being large scale multivariate systems, it is desirable to have single index that can quantify the performance of the overall system. The Hurst exponent however can only quantify the performance with respect to a single variable. The Mahalanobis distance, which is a single measure quantifying the degree of dissimilarity between a data point and a predefined mean and covariance structure is used to address the multivariate performance assessment challenge. This allows extending the Hurst exponent to multivariate systems, while providing a single index of performance. The use of Mahalanobis distance however requires that the mean and co- variance structure of the data (Hurst exponents) corresponding to ideal/optimal operating conditions be available beforehand. However, owing to the lack of knowledge of delay in a system, this cannot be obtained (for the purpose of control). We therefore turn to historical data to extract the data corresponding to the practically achieved best operating conditions. We employ a recursive binary segmentation technique referred to as interval halving to achieve this objective – for univariate as well as multivariate systems. The Hurst exponent is then used for assessing the performance of state estimation for a large scale unit. The anaerobic digester unit of a dairy plant is used for this purpose. The model of Amul dairy plant, consisting of 24 ordinary differential equations is used for simulating the plant. The Hurst exponent is used to quantify the performance of the four measurements available from the model. A comparison of the performance of three different nonlinear estimators is provided.

Finally, quantification of the performance of multivariate state estimators is done by first developing a benchmark and then assessing the performance. This is in contrast with the method adopted for performance assessment of control loops wherein specific properties (Hurst exponents of errors) of the benchmark controller are not available, preventing the benchmarking step. The theoretical optimum conditions of the Hurst exponent are derived which are used as a benchmark for assessing the performance of state estimators.

Title: Cognitive engineering approaches to understand the cognitive behavior of control room operators during plant abnormalities
Researcher: Bhavsar, Punitkumar
Supervisor: Srinivasan, Babji
Year: 2019
Keyword's: Cognitive Engineering, Prognostic Signatures, fNIR Imaging
Call No.: 621.3 BHA
Acc. No.: T00504

Abstract: Process industries continue to suffer from accidents despite significant regulatory intervention and major developments in process control, monitoring and supervision technologies over the last four decades. Human error is widely agreed to be the major contributor to most accidents today. The most common approach in practice today to tackle human error is to consider human failure during process hazard analysis. The role of humans in the process and the expected types of human failures are taken into account qualitatively in checklist analysis, HAZOP studies, etc. These consider human error as the initiating event of incidents, one that has a given likelihood of occurrence, similar to the way that a piece of hardware is expected to fail at some frequency. Just like equipment monitoring relies on detecting prognostic signatures of its impending failure, well in advance of the actual occurrence so as to trigger timely intervention, one can ask, is it possible to detect human error before it is committed? Cognitive engineering provides one such possibility and is concerned with the mental processes of the human actor, such as perception, memory, reasoning, and motor response especially in the context of his/her interactions with other elements of a system. Real-time evaluation of such actors provides information about the cognitive state of a human operator which can be used to infer about the likelihood of human failure.

Recent advancements such as eye tracking, EEG (Electroencephalography), fNIR imaging (functional Near Infrared) and GSR (Galvanic Skin Response) act as a valuable tool to understand the cognitive behavior of humans. Among these tools, eye tracking captures the eye movements in a non-invasive way and has a relatively simple instrumentation system. Typically in an eye tracker, the light source is used to illuminate the eyes and a camera is used to capture the image of eyes showing this reflection. The image captured is then used to locate the reflection of the light source on the cornea and in the pupil to estimate the gaze point. Eye tracking has been used to understand the cognitive behavior of operators in several safety critical domains such as aviation, healthcare, nuclear power plants and driving. In addition to monitoring the operator's attention allocation and distribution using metrics from gaze location, the cognitive states such as fatigue, stress and workload can also be inferred from the variations in pupil size. Eye tracking thus allows systems engineering techniques to be extended to the human component of fairly automated systems that are operated under human supervision. Moreover, the noninvasive nature opens the door for its applicability in the real-world environment without affecting normal operation. The goal of this thesis is to develop measures and methods from eye tracking which can be used in near real time fashion to analyze cognitive behavior of control room operators during abnormal plant condition.

In this work, the experiments were conducted using ethanol process simulator to study the cognitive behavior of control room operator. The HMI for the simulator is designed considering human factor principles. The process consists of an exothermic reaction between ethene and water to produce ethanol in a continuously stirred tank reactor (CSTR). The mixture of water and ethanol from CSTR is then sent to the distillation column for the separation. The process does not employ any automatic controllers; hence monitoring and control need to be performed by the operator. Alarms for the process variable are configured to provide an indication of the abnormal condition. Participants have carried out various disturbance rejection tasks while performing the role of control room operator. Eye tracking data along with process data, mouse click data and alarm data are collected to analyze the cognitive behavior of human participant.

In the first study (Chapter 4), the investigation is carried out for the operators' dwell duration distribution on various information sources (AOI) during the abnormal condition. Dwell duration distribution provides information about the distribution of participant's visual attention. Larger attention on the irrelevant information sources, during abnormal condition, is indicative of poor knowledge about the interrelationship between the variables which may lead to human error. The analysis reveals the dwell duration distribution is more focused on the primary- root cause variables for the performances in which the participant used only root-cause manipulated variable and succeeded (Group I) whereas the distribution contains major portion of the dwell duration on irrelevant information sources for the failed performances (Group III). The study also reveals a category of performance who used other manipulated variable along with primary root-cause manipulated variable and managed to succeed in the scenario (Group II). The dwell duration distribution for such category highlighted intermediate behavior by Group II as distinct from Group I and Group III.

In the second study (Chapter 5), the situation awareness is quantified based on the randomness in the gaze behavior. The randomness in gaze behavior is quantified using the derived measure of entropy. The low value of entropy during the action phase is observed for the participants who focused on a few related variables and exhibited proper situation awareness. Relatively larger value of entropy is observed for the participants who focused on relatively more number of variables and lacked to have adequate situation awareness about the abnormal condition.

The third study (Chapter 6) investigates the cognitive workload profile during the disturbance rejection tasks. Consistently high workload has been cited as a dominant factor responsible for the human error in the plant operation. Pupil size variations are considered to infer about the perceived level of the cognitive workload while handling an abnormal situation. The analysis from this study reveals increased workload level for all the participants just after the occurrence of the first alarm, as measured by the pupillary dilations. The participants who successfully handled the scenario using only root-cause manipulated variables, showed the decrease in the demand as observed by the dilations coming to the rest towards the end of the scenario. On the other hand, the failed performance remained in the higher workload demand even towards the end of the scenario. The fourth study (Chapter 7) investigates workload demand considering the time-frequency analysis of

pupil size variations. The analysis is able to quantify the demand at time localized events which happens during the interaction with HMI. An increase in the workload is observed for the time localized events when process behavior is not in coherence with the mental model. The similar trend is also observed with the tasks of flight control.

In summary, the experimental studies in this work uncover the potential of eye tracking technology to infer about the cognitive behavior of the control room operators. Almost real-time window into the operator's cognitive state, derived from the eye tracking metrics, provide the likelihood of the human failure dynamics during plant operation. Incorporating systems engineering techniques to the human component through eye tracking method can help identify the human error providing better safety and security of the process plants.

Title: Modeling and optimization techniques for efficient lithography simulation
Researcher: Kumar, Pardeep
Supervisor: Srinivasan, Babji
Year: 2019
Keyword's: Principal Component Analysis, Discrete Cosine Transform, Optical Proximity Correction, Lithography Simulation
Call No.: 621.3 KUM
Acc. No.: T00507

Abstract: This thesis presents new methods and models in optical lithography to improve the efficiency of full-chip level lithography simulation used for mask design in optical projection printing. For mask design, Optical Proximity Correction (OPC) has become an integral part, specifically for sub-wavelength optical lithography to improve pattern fidelity. The success of lithography simulation to perform the OPC on an entire chip relies heavily on the performance of lithography process models and the optimization algorithms. As feature sizes scale into the nanometer dimension, the reduction of computational time for full-chip lithography simulation along with the incorporation of new process effects into lithography models to improve the accuracy is still an open problem for lithography industry. Any small enhancement in the performance of process models and optimization algorithms can result in a valuable improvement in the OPC results and hence increase the yield. This research work is focused on the incorporation of new methods and models for optical simulation, sample plan selection, resist simulation, and OPC simulation.

In the optical simulation part, we proposed a nonlinear Principal Component Analysis (PCA) based light source optimization method for computation of the aerial image. The proposed approach is more general and considers both continuous as well as discontinuous intensity distribution from different types of lithography light sources with better performance in variance coverage among discrete data sets in comparison with the existing techniques. We have also investigated the use of a Discrete Cosine Transform (DCT) for aerial image generation in the optical simulation. DCT is a computationally efficient technique to transform the mask design from spatial domain to frequency

domain and it can further be used to trim the high-frequency components to reduce the dimension of the mask in the frequency domain which resulted in the faster optical simulation.

After optical simulation, the next important step is the resist simulation where we have contributed at different stages. In the initial phase of compact resist model building, we addressed the sample plan selection issue for measurement data selection. The reduction of measurement data and the time needed to select the sample plan is crucial for the development of a compact resist model. We studied the strengths and weaknesses of existing sample plan selection techniques and proposed Locally-Linear Embedding (LLE) based sample selection technique. The proposed approach significantly reduced the measurement data demand and modeling turn-around time, while maintaining the model accuracy and stability. For the existing compact resist models, we identified their shortcomings and proposed the clustering algorithms based model building approach for further improvement in the accuracy and computational efficiency of resist simulation. We also discussed the major issues of conventional clustering algorithms and proposed to use the density peaks based clustering algorithm for robustness in multiple compact resist model building. In addition to clustering algorithms, we have described in details the role of regularization in empirically driven resist models to avoid/compensate for over-fitting and proposed a two-stage compact resist model which successfully breaks through the asymptotic accuracy limit, which seemingly hinders single-stage models. The effectiveness of these proposed methods is verified by modeling the pattern transfer of essential layers in 14nm and 22nm Complementary Metal Oxide Semiconductor (CMOS) technology.

The final stage of lithography simulation involves the OPC methods. There are two existing schemes for the addition of OPC. These are (a) the Rule-Based OPC (RBOPC) and (b) Model-Based OPC (MBOPC). In general, the full-chip designs have a different variety of shapes and all the shapes do not need MBOPC treatments. For simple and sparse designs in a full-chip, RBOPC can be used to deliver the OPC solution with relatively less computational time. Considering all these facts, a hybrid OPC approach based on clustering algorithm is proposed, where the complexity of localized structures will drive the respective OPC methodology, either RBOPC or MBOPC. The proposed method also flags the lithography hotspots from the input design for custom OPC treatments. We also proposed rectangular blocks based new OPC style to add more degree of freedom to perform OPC and to utilize the strengths of positive and negative scattering bars to improve the pattern fidelity.

To summarize, in this thesis, we worked on the optical part to reduce the simulation time by source and mask optimization. We developed a robust technique for sample plan selection to reduce the time for the selection of samples for compact resist model building. Further, we worked on the accuracy enhancement of existing compact resist models and proposed the multi-stage resist modeling to break the asymptotic accuracy limit of conventional single-stage models. Finally, we proposed the hybrid approach to select the OPC algorithm and demonstrated the new OPC style as a futuristic approach for efficient OPC solution. All these techniques could be used together for efficient lithography simulation.

Title: Compact modeling solutions for advanced MOC devices
Researcher: Ojha, Apoorva
Supervisor: Mohapatra, Nihar Ranjan
Year: 2019
Keyword's: MOS Transistor, CMOS Technology, HKMG MOS Transistor, Quantum Mechanical
Call No.: 621.3 OJH
Acc. No.: T00510

Abstract: The phenomenal growth of semiconductor industry was aided by the relentless scaling down of the MOS transistor over the decades. In the last two decades though, the traditional scaling down of transistors was impacted by physical limitations leading to adoption of various facilitators to sustain scaling, namely, the strained CMOS technology, High-k Metal Gate technology and Multi-Gate FETs (MuGFETs). These technologies also introduced different/new set of physical behavior and their accountability needs to be done in the state-of-the-art compact models. Thus, in this thesis, the changes in the MOS device behavior due to these technological solutions are analyzed and modeled retaining the physics-based flavor for universality. The research problems undertaken in this thesis are as follows:

- Strained CMOS technology was introduced to sustain the scaling of MOS transistors by enhancing the mobility and hence the drive current of the transistors. But, apart from mobility, the threshold voltage (V_{th}) also changes due to shift in the energy band levels. This V_{th} shift is larger and more significant in a high-k metal gate (HKMG) transistor than the traditionally used poly-silicon/ SiO_2 MOS transistors and thus it needs to be modeled. This large V_{th} shift cannot be predicted using conventional modeling methodologies that take only longitudinal stress into account. In this work, the analysis of strain induced V_{th} shift is done using both longitudinal and transverse stress components. Also, the stress distribution in a MOS transistor channel is non-uniform, hence the effective stress and its effect on V_{th} shift is dependent on device dimensions. So, a detailed analysis and modeling of stress profile (longitudinal and transverse) in the channel of MOS transistor is done for the first time that takes into account device geometry dependence on the strain-induced V_{th} shift.
- The shift from Poly-Silicon/ SiO_2 to HKMG MOS transistor helped sustain scaling by having thicker dielectric and thus limiting gate leakage. But the replacement of SiO_2 by high-k dielectric HfO_2 led to change in behavior of gate leakage current owing to presence of large number of oxygen defects. Because of this, the trap-assisted conduction of carriers through gate dielectric dominates over the direct tunneling current. The conventional gate current models (primarily BSIM models) based on direct tunneling thus cannot model the gate leakage properly. Also, the presence of more than one kind of gate conduction mechanism makes the state-of-the-art compact models inaccurate for HKMG MOS transistors. Thus, gate leakage is analyzed across different biases and temperatures to identify conduction mechanisms (namely, Trap-Assisted Tunneling and Poole-Frenkel conduction) and then a consolidated model is developed which is valid across all gate biases and temperatures. Also, the applicability of the popular WKB approximation (used to evaluate tunneling probabilities)

for low bandgap HfO_2 (in comparison to SiO_2) is analyzed and appropriate corrections are developed.

- The shift from planar MOS transistor to MuGFETs helped overcome the short channel effects and semiconductor industry started adopting it in 22nm CMOS node and beyond. But, the additional gates and the ultra- scaled MOS devices introduced quantum mechanical (QM) effects in the devices. Thus, for accurate charge description, inclusion of QM effects is necessary. The traditional TCAD simulators use Poisson solver in conjunction with quantum corrections to incorporate quantum confinement effects. These correction though are geometry and bias dependent and have empirical formalism in them. The accuracy too needs to be improved. The most accurate option is using a Schrodinger solver but its utility is limited to region-specific computation owing to computational complexity. Hence, a quantum-corrected Poisson solver is developed in order to capture QM effects, namely geometrical confinement and electric field confinement accurately without any empirical formalism.

Title: Multidimensional reflection symmetry: theory, algorithms, and applications
Researcher: Nagar, Rajendra
Supervisor: Raman, Shanmuganathan
Year: 2019
Keyword's: Triangle Meshes, Point Clouds, Reflection Symmetry, RGB-D Image
Call No.: 621.3 NAG
Acc. No.: T00517

Abstract: An object is called symmetric if it can be partitioned into more than one identical segments. The objects are stored in the computer memory mostly as digital images, point clouds, and triangle meshes. Characterizing and finding the symmetry has been an active research topic in computer vision and graphics due to its importance in solving problems such as shape matching, shape recognition, compression, surface reconstruction, real-time attention for robotic vision, and cultural heritage object reconstruction and restoration.

There exist approaches for reflection symmetry detection in digital images, point clouds, and triangle meshes. However, the performance of the existing approaches on the real world datasets still has to be improved since many impurities are added in the data while capturing. For example, occlusion, non-rigid deformations, and sensor noise. Our goal is to develop algorithms for detecting reflection symmetries in digital images, point clouds, and triangle meshes in the presence of noise, occlusions, and non-rigid deformations.

We propose two methods for detecting reflection symmetry in 2D images. We then use the detected reflection symmetry to over-segment an image into symmetry aware super pixels and to find the reflection symmetry map of an image. The reflection symmetry map represents a confidence score at every pixel having its reflection pixel and identifies the reflection pixel of each pixel. We present two methods for detecting reflection symmetry in 3D point clouds without feature descriptors and using images used in a structure from motion framework for constructing the 3D point cloud of the underlying object. Intrinsic symmetry in triangle meshes is used as a prior in various important problems of shape analysis. Therefore, off-the-shelf fast and accurate detection of symmetry in challenging settings is required. We propose a functional map-based approach which achieves state-of-the-art performance in terms of time and accuracy. Many physical data points reside in the space of dimensions greater than three, e.g., an RGB-D image captured using a Kinect sensor. Therefore, we develop the theory and present a method for detecting the reflection symmetry in d -dimensional point cloud without using features.

Title: Design of fault-tolerant permanent magnet motors and post fault control
Researcher: Veeramaneni, Naveen Deepak
Supervisor: Ragavan K.
Year: 2020
Keyword's: Electrified Transportation, Permanent Magnet Synchronous Motor, Fractional Slot Concentrated Winding, Tooth-wound Configuration, Traction Applications
Call No.: 621.34 VEE
Acc. No.: T00524

Abstract: Use of electric motors and drives has increased in several applications. These include electrified transportation, military, industrial and healthcare robotic systems. For these applications, the preferred choice is Permanent magnet synchronous motor (PMSM) due to its high torque density and efficiency. In addition to performance, these applications also demand fault-tolerance. Winding short-circuit fault poses threat to the reliability of PMSM due to the presence of permanent excitation in the rotor. Hence, PMSM are to be designed to achieve fault-tolerance with regard to winding short-circuit. With sufficiently high inductance, currents during winding shortcircuit can be limited to safe value. Further, high inductance value increases the constant power speed range of motors. Thus, PMSM with high inductance becomes a natural choice for traction applications.

This thesis addresses the design of fault-tolerant PMSM and its post-fault operation. Initially, a fault-tolerant Surface-Mounted PMSM (12-slots in stator, 10- poles in rotor) is considered. Fractional slot concentrated winding (FSCW) offers short end-winding and manufacturing flexibility. Further, alternate tooth-wound configuration provides magnetic and physical isolation between phases besides high inductance value. As this feature makes the machine suitable for fault-tolerance, PMSM is designed with alternate tooth-wound FSCW.

The proposed control involves modeling the motor in stationary reference frame. It involves determining the desired values of currents in the remaining healthy phases during post-fault operation. With these currents in those healthy phases, torque ripple would get reduced. Further, speed control for post-fault operation is proposed. Initially, the proposed control is implemented in ANSYS- Maxwell, Finite Element Analysis (FEA) simulation platform. It involves co- simulation of FE model of PMSM and power electronic drive model. Later, the designed PMSM is fabricated and then the proposed control is implemented. Performance of the proposed control is satisfactory both in simulation work and experimental implementation on the prototype.

The designed Surface-Mounted PMSM is fault-tolerant with regard to winding faults. Windings of these machines are energized based on the rotor position information. If the rotor position sensors malfunction, the machines cease to be fault-tolerant. Hence, there is a need to estimate rotor position in the event of a position sensor failure. It is possible to estimate the rotor position if the machine has adequate saliency ratio (ratio of quadrature-axis to direct-axis incremental inductances). As the designed machine has its quadrature axis and direct-axis incremental

inductances nearly equal, its saliency ratio becomes unity. This makes it not suitable to achieve position sensor fault tolerance.

Utilizing the similarities with Switched Reluctance Motor (SRM), an optimized alternate tooth-wound FSCW PMSM is designed with the PM in inset configuration. This design achieves an inductance variation similar to SRM. Guidelines for odd and even phase designs are discussed, and FEA results corresponding to 3-phase, 4-phase and 5-phase motors are presented. The inductance profile of 3-phase machine is experimentally validated. Corresponding to maximum torque per ampere operation, the designed motor is found to exhibit 25% reluctance torque contribution. This is significantly higher than the values reported in literature for alternate tooth wound PM machines. For estimating the rotor position, an algorithm is proposed which makes use of incremental inductance of each phase. With the increase in stator excitation, incremental inductance profile is significantly distorted. However, at rated current excitation, incremental inductance profile is relatively un-distorted over the span of $1/6$ th electrical cycle out of one electrical cycle. From the unaffected portion of the inductance profiles in all the phases, the incremental inductance is determined and hence rotor position is estimated. It essentially involves inductance tracking through high-frequency injection technique and comparing with the known inductance profile lookup table. Effectiveness of the proposed algorithm is demonstrated through co-simulation of the FE model of the designed alternate tooth-wound FSCW PMSM with PM in inset configuration and the model of power electronic converter. By comparing with absolute position information, it is understood that the rotor position information is estimated accurately.

Title: Virtual reality-based treadmill-assisted adaptive response technology for post-stroke gait rehabilitation
Researcher: Solanki, Dhaval
Supervisor: Lahiri, Uttama
Year: 2020
Keyword's: Cerebrovascular Accident, Frominterruption In Blood Flow, Treadmill-assisted Exercise, VT-HART, Spatiotemporal Indices
Call No.: 621.3 SOL
Acc. No.: T00525

Abstract: Stroke, often categorized as Ischemic stroke and Hemorrhagic stroke, can be defined as a cerebrovascular accident resulting from interruption in blood flow causing a sudden death of brain cells. The Ischemic stroke results from a clot or blockage in the artery and the Hemorrhagic stroke results from the rupturing of blood vessels carrying blood to the brain cells thereby interrupting blood flow to the brain. Irrespective of its type, the stroke can cause impairment in sensory, motor, cognitive, perceptual, and language functions making it one of the leading causes of death and disability across the globe. The ill-effects of stroke are also alarming in developing countries like India. Reports from the World Health Organization (WHO) show that stroke stands in the top three causes of death in India and 10% of total deaths in India are due to stroke. Apart from this, about two-thirds of the post-stroke survivors suffer from severe long-term disability. The extent of disability after stroke depends on the size and location of the lesion in the brain. Due to the lesion, impaired motor cortices can cause paralysis on both sides of the body (termed as paraplegia) or one side of the body (often known as hemiplegia). The hemiplegia can decondition the patient thereby adversely affecting the functionality of the upper extremity and/or lower extremity on the affected side of the body. The impairment in lower extremity can adversely affect one's mobility. This results in walking dysfunction, often known as gait disability, where gait can be defined as one's manner of walking. Nearly 83% of the post-stroke survivors suffer from gait disabilities accompanied with an increased risk of fall and fall-related injuries. The gait disabilities in post-stroke patients limit their activities of daily living making a post-stroke survivor dependent on the caregiver. Additionally, after stroke, one's community ambulation capabilities are deteriorated thereby limiting their community participation and making them mostly home-bound. Also, this adversely affects their ability to earn their own livelihood that takes a toll on their socioeconomic status. They are often referred to gait rehabilitation centers. However, the healthcare situation is alarming in developing counties like India, where the rehabilitation resources are limited and expensive, with a low clinician-to-patient ratio of 1.4 clinicians per 1000 people against the recommended 2.8 clinicians per 1000 people by WHO. In such a situation, technology-assisted solution can complement clinicians' efforts, since it can empower one clinician to perform clinical assessment and offer individualized gait rehabilitation services (while reconditioning them) to multiple patients at the same time.

The reconditioning regime starts with clinical assessment of the residual gait ability of post- stroke survivors followed by prescription of appropriate gait rehabilitation exercises. With regard to the clinical assessment, one's residual gait capability can be quantified in terms of spatiotemporal gait

parameters while the subject is asked to walk overground. A simple and inexpensive technique to quantify one's gait is to record the subject's footprints using ink, chalk etc. during the overground ambulation along with a stop-watch. The record of the footprints and time to cover a predefined walking distance can offer spatio-temporal gait parameters. Though these techniques are still widely used by the clinicians, these techniques are labor-intensive, prone to errors, offer limited gait parameters and can suffer from subjectivity. In contrast, there are complex, expensive, but highly accurate techniques, such as use of force plates coupled with cameras (e.g., VICON cameras that are considered as a gold standard in gait estimation) that can offer objective metrics that can quantify one's gait. Additionally, these technologies can suffer from portability, line-of-sight issues, etc. Thus, it is essential to have a technology-assisted solution that can offer a portable, cost-effective and objective assessment of one's gait. Motivated by this, the first objective of my research was to (i) develop a portable and cost-effective gait quantification unit that can offer objective measurement of one's gait-related indices followed by (ii) validating these indices using gold standards. To achieve this objective, I have developed Instrumented Shoes having shoe insole instrumented with Force Sensitive Resistors (FSRs) that can offer a portable and cost-effective technique to quantify one's gait. There is evidence from literature that researchers have used sensed shoes with the number of FSRs ranging from 2 to 32. Too few sensors might cause gait events (such as, heel-strike, toe-off, etc.) to be missed while recording. Again, too large number of sensors can add to the system complexity. In my research, I used three sensors impregnated into the shoe insole of each foot. Specifically, two FSRs were placed below the heel (to monitor heel-strike) and one was placed below the toe (to monitor toe-off) events during one's walk. The idea behind the placement of two FSRs below the heel (one towards the lateral side and other towards the medial side of the heel) was to account for foot inversion/eversion condition, often demonstrated by post-stroke patients. Additionally, the Instrumented Shoes had a digital interface that was used to integrate the Shoes with any computer offering a Graphical User Interface (GUI), designed to monitor the health of the FSRs in real-time. The GUI was equipped to record and process the FSR data to estimate the gait-related indices. To validate these gait-related indices vis-à-vis gold standards and to check the feasibility of using the Instrumented Shoes for post-stroke patients, I conducted Study 1 in two Phases, namely Phase I and Phase II. The study was volunteered by a group of healthy participants (Phase I) and post-stroke survivors (Phase II). The Phase I comprised of estimating the spatiotemporal gait parameters of healthy participants measured using the Instrumented Shoes and validating these indices with standard stereophotogrammetric (VICON) setup and conventional paper-based setup. Results showed good agreement between the gait-related indices measured using Instrumented Shoes and the standard setups. For Phase II, investigation of the gait-related indices measured using the Instrumented Shoes demonstrated the potential of the Instrumented Shoes to quantify gait abnormalities of post-stroke hemiplegic patients. Also, the results of this Study 1 showed that the Instrumented Shoes can offer reliable measures of one's gait that can be used to quantify the residual gait ability of post-stroke patients. This can be useful to prescribe gait rehabilitation exercises.

Having quantified the residual gait ability of the post-stroke survivor, the next step of the reconditioning regime is to offer him / her gait rehabilitation exercises based on his / her ability to do the exercise. The gait exercises can be repetitive overground walking, walking on a treadmill, etc. One of the important components of an effective exercise is its ability to retain the patient's motivation during the repetitive exercises. It is commonly seen that the repetitive exercises often lack diversity and become monotonous to the patient that can adversely affect the patient's retention in the exercise and consequently the rehabilitation outcomes. Use of a technology-assisted solution for gait rehabilitation can offer an avenue to project exercise environments that will have diversity and in turn break the feeling of monotony of the patient undergoing the rehabilitation. One of the ways to achieve this is to use a Virtual Reality (VR)-based exercise that can offer feedback to the participant (similar to that done by a clinician accompanying the patient doing the exercise) and offer motivating exercise environments. Previous research studies have shown the power of using VR-based exercise environments in which investigators have projected VR environments depicting city environments, open grounds and closed corridors, etc. Since my research was related to designing gait exercise platforms for post-stroke patients, I wanted to offer a VR-based roadview to the users with limited distractions (unlike that in the city environment), pre-defined pathway (instead of an open ground) and with unrestricted view of the surrounding environment (unlike that of a closed corridor). Thus, while incorporating different exercise environments, the second objective of my research was to design a VR-based treadmill-assisted gait exercise platform that can offer motivational audio-visual feedback to the users and understand the implication of such an exercise on the gait-related indices of users vis-à-vis a platform offering only treadmill-assisted exercise (without the VR). The VR-based environment comprised of an Avatar (i.e., a humanoid character) walking on the virtual road (pathway). Before applying a VR-based environment to post-stroke gait rehabilitation regime, I wanted to understand the efficacy of using a VR-based treadmill-assisted platform for gait exercise among healthy users. While setting up such a platform, I synchronized the VR-based roadway environment with a treadmill using a universal synchronizer module and designed Study 2 to carryout comparative analysis of the gait-related indices (measured using the Instrumented Shoes) while healthy participants walked on a treadmill both in presence and absence of the VR-based exercise environment. Additionally, the universal synchronizer module helped in offering real-time feedback related to the exercise intensity. The Study 2 involved a group of healthy participants. Results of this study showed that the VR-based gait exercise platform had a greater potential to contribute to the making the exercise motivational and to have implications on one's gait-related indices as compared to an exercise platform without VR.

Having identified the potential of a VR-based treadmill-assisted gait exercise platform to contribute towards improvement in one's gait performance, the next step of my research was to offer individualized gait exercise to post-stroke patients based on their capabilities to do exercise. Though my VR-based treadmill-assisted exercise platform designed in Study 2 was promising, yet it lacked the individualization aspect of the rehabilitation. Specifically, one's individualized capability to do exercise depends to a considerable extent on one's energy expenditure during an exercise. This is particularly crucial for post-stroke patients, since there is evidence from literature that shows that post-stroke patients spend nearly 55-100% higher energy compared to that of their healthy

counterparts, during exercise. Thus, it is important that the gait rehabilitation platform employed for post-stroke patients has the capability of monitoring the energy spent by the post-stroke survivor during the exercise and in turn offers individualized exercise with varying intensity based on the patient's exercise capability. One of the ways to get an estimate of the energy expenditure is to monitor the variations in one's physiological indices, such as heart rate (measured using an electrocardiogram). Motivated by this, I wanted to design an individualized VR-based treadmill-assisted gait exercise platform that is (i) sensitive to variations in one's heart rate and can offer (ii) adaptive (to patient's capability) and progressive (gradually increasing exercise intensity with patient's ability) exercise intensities to a user based on his / her capability to perform the gait exercise. Additionally, I wanted to make the gait exercise platform capable of (i) offering varying exercise intensities through varying treadmill speed and (ii) quantifying gait-related indices using a portable device, such as the Instrumented Shoes. Thus, the third objective of my research was to develop a Physiology-sensitive gait exercise platform for post-stroke patients offering individualized, adaptive and progressive rehabilitation exercises along with feedback. Finally, the fourth objective of my research was to design a study involving healthy individuals and post-stroke patients to understand the implications of undergoing gait exercise using this platform on their (a) gait-related spatiotemporal indices and (b) lower limb muscle activity (to compute global outcomes in terms of sEMG-related indices) corresponding to one's gait as quantified using the Instrumented Shoes. To achieve the last two objectives, I have designed a VR-based Treadmill-assisted Heart rate-sensitive Adaptive and progressive Rehabilitation Task (VT- HART) platform for post-stroke gait rehabilitation. To achieve the fourth objective, I have designed the Study 3 having Phase I and Phase II. Phase I was used to test the operation of the VT-HART platform and involved a group of healthy individuals who were offered one exposure to this platform. The Phase II had a group of post-stroke patients who were offered multiple exposures to the VT-HART platform. In both the Phases I and II, the participants' gait-related spatiotemporal indices (quantified by using Instrumented Shoes) were recorded. Added to the gait-related indices, in Phase II, I have also investigated the implication of repeated exercise using the VT-HART platform on the lower limb muscle activation (acquired using surface Electromyogram (sEMG)) pattern to understand the efficacy of such an exercise to increase the lower limb muscle strength and reduce muscle fatigue of post-stroke patients thereby contributing to gait rehabilitation. For this study, I designed different VR-based templates along with audio-visual feedback to offer a motivational exercise environment. An intelligent and adaptive speed engine was designed to monitor one's heart rate during exercise and accordingly offered varying exercise intensities by changing treadmill speed (while maintaining safety limits) in an individualized manner. The Instrumented Shoes were used to monitor the gait performance of the participants during the exercise. The FSR and sEMG data were synchronously collected during the exercise using an in-house developed data acquisition module. Additionally, one's heart rate was computed by acquiring his / her Electrocardiogram (ECG) data in a time-synchronized manner along with the FSR and sEMG data. Results of Phase I indicated that the VT-HART platform was working as intended. Again, the results of Phase II indicated positive contribution of the VT-HART platform towards the spatiotemporal gait-related indices (providing insights to one's gait pattern) and muscle activity (offering insights to one's muscle activation pattern) of the post-stroke patients after exposure to the platform. The findings revealed that the VT-HART platform has the potential to

contribute to improvement in the spatiotemporal gait-related indices of post-stroke patients along with a reduction in the energy expenditure leading to energy-efficient gait patterns. Additionally, the findings related to the patients' muscle activation revealed that the VT-HART platform has the potential to contribute towards the improvement in muscle strength and reduction in muscle fatigue during ambulation. Further, our data analysis revealed that these findings were clinically significant. Finally, I conducted a post-study feedback session. The idea was to understand the patients' perception on the usage of the VT-HART platform and the applicability of this platform to contribute to gait reconditioning and rehabilitation. The post-study feedback session revealed that the VT-HART platform was well-accepted by the target group. These findings show that the VT-HART platform can serve as a complementary tool in the hands of the clinician offering individualized gait rehabilitation and empowering one clinician to assist more than one patient at the same time.

To summarize, in my research, I have (1) designed a portable and cost-effective gait quantification unit (i.e., Instrumented Shoes) that can be used for clinical assessment of residual gait ability of post-stroke patients and designed studies to validate these gait-related indices (measured using the Instrumented Shoes) with that measured using the gold standards, (2) developed Virtual Reality (VR) based environments integrated with treadmill-assisted gait exercise platform that provided motivational audio-visual feedback to the user followed by comparative analysis of the implications of such a system on the gait-related indices (measured using the Instrumented Shoes) with a treadmill-assisted platform without any VR component and (3) designed a VR-based Treadmill-assisted Heart rate-sensitive Adaptive and progressive Rehabilitation Task (VT-HART) platform for offering individualized gait exercise to post-stroke patients based on their capabilities to perform the exercise. Also, I investigated the potential of such a gait exercise platform to contribute towards post-stroke gait rehabilitation quantified in terms of gait-related indices and lower limb muscle activation. I believe that such a rehabilitation platform can hold promise to bring in a paradigm shift in post-stroke healthcare in low-resource settings like India where rehabilitation resources are expensive, far and few.

Title: Advanced CMOS technologies for SoC applications: challenges and solutions from Analog/RF perspective
Researcher: Bhoir, Mandar S.
Supervisor: Mohapatra, Nihar Ranjan
Year: 2020
Keyword's: Internet-of-things, Digital Signal Processing, Mixed-signal SoC, CMOS Technologies, FinFETs, Ultra-thin Body
Call No.: 621.3815 BHO
Acc. No.: T00526

Abstract: The digital revolution started in late 60s' with the invention of microprocessors, digital signal processors (DSPs) and digital memories. Undoubtedly, it enabled end-applications like communication, entertainment, transportation, health-care, domestic and industrial automation thereby impacting every aspect of human life. Therefore, the common feeling is that the world is becoming digital. However, the 'real world' around us is analog. The continuous nature of signals (with respect to time and amplitude) that we see, hear and feel confirms this fact. Therefore, even after the success of the digital revolution, analog systems coexist as an interface between the real world and digital core. The Internet-of- things (IoT), smart-phones and self-driven cars are few noteworthy applications of such mixed-signal systems. They typically contain modules for sensing, signal-conditioning, digital signal processing, storage and communication. These systems are often portable thus need to operate at low-power. Various options like System-on-chip (SoC) and System-in-Package (SiP) have been explored for cost-effective integration of the digital core (logic and memory), analog/radio-frequency (RF) core, sensors and high-voltage (HV) devices on a single substrate or package. The SoCs generally prefer CMOS technologies because of their higher performance at lower production cost.

Numerous mixed-signal SoC technologies with bulk MOS transistors are already available. However, beyond 28nm CMOS technology node, the bulk transistors were successfully replaced by two different architectures - FinFETs and Ultra-thin body and BOX Fully Depleted Silicon-on-Insulator (UTBB FD-SOI) MOS transistors. Currently, the FinFET drives high-performance computing whereas the UTBB FD-SOI serves the low-power/high-frequency market segment. The logic-oriented applications continue to drive the FinFET and UTBB FD-SOI technology scaling and will continue to do so in future. Note that a good analog transistor should have attributes like high intrinsic gain, low device-to-device variability, high linearity, good frequency response and lower noise at low power and integration cost. However, the logic-oriented technology seldom focuses on all these attributes. In such a scenario, the impact of scaling on analog/RF performance of the transistors needs to be studied in order to develop advanced SoC/SiP technologies. In this thesis, challenges arising due to the technology scaling from analog/RF perspective are investigated. Through detailed experimental measurements and extensive TCAD simulations, the physics behind the observed behaviours is explored and various solutions to overcome the challenges are proposed.

The thesis is organized in two major parts. In the first part, the impact of fin-width scaling (in sub-10nm regime) on FinFET's analog performance is investigated. Through experimental measurements on FinFETs with different W_{fin} s (7.5, 6 and 4.5nm), we show that W_{fin} cannot be leveraged to reduce the gate length of analog transistors for better analog performance. The physics behind this behavior- mobility and source/drain series resistance (R_{SD}) degradation is discussed in detail. Therefore, different process- optimization techniques to continue the performance improvement are discussed. For instance, we demonstrate ~21% and ~23% improvement in FinFET's intrinsic gain by R_{SD} and EOT optimization respectively. Further to study process-induced variability, a systematic strategy to separate different variability sources in on/off current, conductance and threshold-voltage is proposed and validated. The strategy is simple, non-destructive and can be easily adopted in upcoming CMOS technology nodes. Subsequently, it is shown that threshold-voltage variations are mainly because of work-function (Φ_M) and oxide charge variations. Moreover, we also demonstrate that the FER induced W_{fin} variations won't escalate even in FinFETs having stronger quantum-confinement ($W_{fin} < 5\text{nm}$). Finally, a new gate barrier metal TiTaN with significantly low Φ_M variability (~44% less total and ~27% less random V_t variability) is introduced and discussed.

In the second part, the impact of BOX thickness (T_{BOX}) scaling and ground-plane (GP) doping on the analog performance of UTBB FD-SOI MOS transistors is investigated. For the first time, it is shown that the carrier mobility significantly degrades (~14%) for transistors with ultra-thin BOX and high GP doping. The additional mobility limiting factors are discussed in detail. It is shown that this degradation reduces transistor's intrinsic gain but improves linearity. Finally, the optimal design-spaces in scaled FD-SOI technologies ($T_{BOX}=10\text{nm}$ and no/n-GP) from the analog performance perspective are highlighted. The impact of technology scaling on device-to-device variability and the frequency response of UTBB FD-SOI MOS transistors is studied. It is reported that small-signal conductances increase anomalously with frequency. A simple concept of "negative feedback" is coined to explain this anomalous behavior. Finally, few cost-effective solutions to minimize such anomalous behavior are proposed.

Title: Compact electrostatics and transport model for high mobility iii-v channel gate-all-around MOS transistors
Researcher: Ganeriwala, Mohit D.
Supervisor: Mohapatra, Nihar Ranjan
Year: 2020
Keyword's: Semiconductor Materials, MOS Transistors, Circuit Simulators, Cross-sectional Geometries
Call No.: 621.3 GAN
Acc. No.: T00527

Abstract: With the increased demands for quicker and power-efficient chips, due to the ever-growing consumer electronics market, there is a pressing question amongst the industry, when will it all stop? In the past, several research groups have predicted the death of Moore's law, the guiding force behind the exponential growth of the semiconductor industry. However, the engineering ingenuity and innovation beyond the standard requirements have kept the progress of the semiconductor industries on track. The current scenario hints that Moore's law is still alive but has slowed down. Semiconductor industries are currently looking at several alternatives to push forward the end even further. The III-V compound semiconductor materials with better carrier transport properties compared to the conventional silicon, have created considerable interest. Experimental and simulation results have shown their integration and performance feasibility. Combined with gate-all-around (GAA) architecture, they present one of the most well-poised solutions to boost the transistor performance. Unlike other new solutions such as 2D materials and NC-FETs, which are still being explored, the III-V transistors are not new to the semiconductor industry. Though not used in the logic application, industries are well versed with the handling of the III-V transistors providing significant volumes of electronic components for use in smartphones, fibre optics and satellite communications. However, for successful adaptation for the III-V GAA MOS transistors into the mainstream CMOS technology, their circuit performance needs to be tested and benchmarked against state of the art MOS transistors. Circuit simulation is crucial for testing the circuit performance during any integrated circuit (IC) design. Circuit simulation needs compact models, which are a mathematical description of the device physics with emphasis on accuracy and computational efficiency. The popular industry standard compact models BSIM, HiSIM and EKV, used in many commercial and open-source circuit simulators, are mainly optimised for the silicon MOS transistors and are semi-classical. However, the III-V materials due to their lower effective mass (m^*) show increased quantum mechanical effect, which these models are unable to capture.

Till date, there are very few models reported in the literature for the III-V GAA MOS transistors. The available models are not suitable for use in the circuit simulators. They either obliterate the essential physics or are complicated and computationally extensive (requires higher simulation time). The aim of this thesis is, therefore, to develop a compact electrostatic and transport model for the III-V GAA MOS transistors, which capture the essential physics in a mathematically simpler form, accurate and computationally efficient for use in circuit simulators. This issue is tackled in the thesis in two parts. First, the transistor channel charges and capacitances are modeled followed by the transistor current. A unified model for the GAA MOS transistors is developed which capture the arbitrary cross-

sectional geometries viz. circular and rectangular. The structural variation due to fabrication deformities is also included and the model could capture elliptical cross-sections as well. A compact modelling framework is also proposed to add the conduction band nonparabolicity and the satellite L-valley in addition to the dominant Γ -valley. The proposed model is physics-based, mathematically less complicated, computationally efficient and extremely suitable for circuit simulators. The model is also validated by comparing its results with the solution of a 2D Poisson-Schrodinger (PS) solver for different III-V channel materials, channel dimensions, cross-sections and found to be accurate for a wide range of bias voltages. In summary, the proposed model is the first compact model for the III-V GAA MOS transistors, which capture arbitrate cross-sectional geometries, includes band non-parabolicity and L-valley charges.

Title: Distributed demand response in smart grid:
Researcher: Rajasekhar, Batchu
Supervisor: Pindoriya, Naran M.
Year: 2020
Keyword's: Energy Storage, Microgrid Level Aggregator, Distributed Energy Resources Artificial Neural Network, Support Vector Regression
Call No.: 621.3 RAJ
Acc. No.: T00534

Abstract: With the proliferation of distributed energy resources like stochastic renewable generation, dispatchable generation and energy storage, and flexible loads like electric vehicles and air-conditioners will have an increased need for balancing supply and demand in electricity markets. This requires new form of algorithms for distributed aggregation and coordination of resources by having a hierarchical structure (i.e., residential level, field/microgrid level aggregator, and system operator level etc.,) for the envisioned smart grid. And new methods to understand and quantify the load demand and users behavior. Meanwhile, undesirable line congestion and voltage limit violations may arise in the distribution network, when flexible resources respond to external control or price signals on a large scale. It also poses computational, coordination and privacy challenges in coordinating a large number of agents. Given such a context, in this thesis we conduct research on following problem scenarios.

Firstly, enforcing coupling constraints among the customers i.e., lower and upper limit on aggregate load at a particular interval must be satisfied in order to comply with physical constraints of the network or to reduce the peak-to-average ratio is one of the major challenges to be studied. Therefore, first part of this thesis proposes optimization and interaction models between the community aggregator and its customers (including passive and active type) based on game-theory and evolutionary optimization techniques for participating in smart pricing based demand response programs. This model not only incorporates customer level multiple objectives with individual preferences and local appliance constraints but also considers community aggregator level resources and global constraints. Here, a penalty pricing scheme is employed to enforce the global constraints in a distributed manner.

Secondly, air-conditioning load is one of the most power intensive and fast responsive load. Also building thermal storage capacity allows the air-conditioning load demand to perturb high or low for short period without inconvenience to its users. So its demand forecasting and predicting the aggregate load dynamics with respect to variation in parameters like weather, set temperature, and price etc., is a key component for demand-side management activities like peak load reduction, load shifting, and as a regulation reserve to the grid. The second part of the thesis demonstrates and compares the effectiveness of three machine learning models namely Support Vector Regression (SVR), Ensemble Trees (ET) and Artificial Neural Network (ANN) for 15 minutes ahead load forecasting. To the end, it proposes an effective hybrid model which reduces biasing in output compared to individual models. Also, it analyzed and discussed the various phenomena like effect

of spatio temporal features selection on prediction output, effect of amount of training data used on convergence characteristics, and effect of change in one of the input features on the prediction output. The effectiveness of the proposed approach is evaluated using half year data set consisting of data from an ongoing research on energy management of inverter air-conditioners in a 20 household-residential test bed set up at the faculty housing units of Singapore University of Technology and Design (SUTD), and weather data from the local weather station.

Further, another major challenge in incorporating dispatchable and non-dispatchable distributed energy resources (DERs) and demand response (DR) into electricity markets by management algorithms is consideration of the underlying power distribution network with its power flow and operational constraints. Therefore, in the third part of this thesis a distributed transactive energy management approach based on dual-decomposition is proposed for decentralized trading algorithm for participation of demand response aggregator (DRA) and distributed generation owner (DGO) in electricity markets with network congestion, and demand and generation prediction uncertainties. Simulation results on a modified 33-bus active distribution system with considerable penetration of DR and DERs, shows that the suggested framework can efficiently reduce the iterations to converge and returns an optimal schedule.

Title: ASOCC: an evaluation framework for asynchronous and synchronous network-on-chip architectures
Researcher: Sneha
Supervisor: Mekie, Joycee
Year: 2020
Keyword's: Synchronous Systems, Network-on-chip, PANE Models, Routing Algorithms, Router Architectures
Call No.: 621.3815 SNE
Acc. No.: T00535

Abstract: As the advancement in technology is pushing for more cores on a chip, the physical constraints limit the number of cores that can operate synchronously on a chip. These limitations include higher EMI in the synchronous systems [28], higher contribution of wire delays over gate delays in the critical paths, timing closure problems, crosstalk [29] etc., especially in the low sub-micron technologies. Also, there is a need for low power circuits that are constrained by the challenges in low-power synchronous circuits. In addition to these physical constraints, there is also a computational need for heterogeneous computing [30]. These limitations call for a shift in the design paradigm from synchronous to heterogeneous or mixed synchronous-asynchronous. Multiple cores on a chip required communication infrastructure or network-on-chip (NoC) to support the inter-core communication. The research in network-on-chip or on-chip communication networks is facilitated by high-level as well as low-level simulators.

Several high-level simulators are available for synchronous or homogeneous network-on-chips. This has enabled extensive research and development in this area. However, there is no high-level simulator available for asynchronous and heterogeneous on-chip communication networks that is comparable to the contemporary synchronous high-level simulator in terms of simulation capabilities. This severely hampers the research and development for heterogeneous on-chip networks. A unified high-level simulator would enable evaluation of synchronous, asynchronous and mixed synchronous- asynchronous on-chip communication networks on a single platform and for the same set of real or synthetic benchmarks. This will empower researchers and NoC designers to not only evaluate their asynchronous or heterogeneous NoCs, but to also compare it with synchronous counterparts.

In this thesis, PANE [31], a high-level simulator for synchronous, asynchronous and mixed synchronous-asynchronous NoCs is presented. PANE models the asynchronous handshake mechanism for asynchronous NoCs through event-driven control units modeled in OMNeT++. Using inter-process communication, PANE supports implementation of the data and routing control path of the NoC on an existing synchronous NoC simulator. Arbitration dependent variability, which is characteristic to asynchronous arbiters, is also modeled for arbitration units in PANE. To present all the features of PANE, an extensive set of use cases using PANE are also presented in this thesis. The use case studies are presented for different NoC sizes, NoC topologies, routing algorithms, traffic patterns, buffering schemes, injection rates, packet sizes and router architectures. This includes

research on GALS systems and in identifying GALS partitioning of systems. As a part of this thesis, two synchronous routers were proposed and implemented on hardware, and then also modeled in PANE for evaluation. No-Lane-Change router [15] and Route-on-Fly router [16] are designed and implemented as a part of this thesis. Finally, some future extensions and applications for PANE are also proposed in this thesis.

In the future, PANE can be used to further the research in heterogeneous and asynchronous NoCs by providing a framework for high-level simulation on real and synthetic benchmarks.

Title: Field deployable tunable diode laser spectroscopy systems for greenhouse gas and air pollutant monitoring

Researcher: Roy, Anirban

Supervisor: Chakraborty, Arup Lal

Year: 2020

Keyword's: Global Atmosphere Watch, Spatio-temporal Resolution, Tunable Diode Laser Spectroscopy (TDLS), Vertical Cavity Surface Emitting Laser (VCSEL), Wavelength Modulation Spectroscopy (WMS)

Call No.: 621.3 ROY

Acc. No.: T00550

Abstract: Accurate *in situ* measurements of greenhouse gases (GHGs) is a key requirement in modern climate science research. Reliable measurements are required to build accurate models that help to understand the sink and source patterns of GHGs and also to assess the effectiveness of international agreements that aim to reduce GHG emissions. Several atmospheric monitoring networks around the world provide continuous measurement of GHGs that are crucial for improving our understanding about the GHG budget, both at regional and global scales. The Global Atmosphere Watch (GAW) programme of the World Meteorological Organization (WMO) comprises 31 global stations, more than 400 regional stations and around 100 contributing stations operated by contributing net-works. Although India is the fourth highest contributor to global GHG emissions after China, United States and European Union, the need for GHG monitoring was largely unaddressed till the early 1990s. Since then, there have been some measurements at certain parts of the country. Data is therefore not available over long time intervals and over large geographical regions. This makes it difficult to understand the variations of GHGs over the Indian subcontinent. High-quality, long-term monitoring of GHGs over India needs highly reliable sensor technologies. It is also important that the technology be amenable to scaling up to build large sensor networks for long-term monitoring with high spatio-temporal resolution. Tunable diode laser spectroscopy (TDLS) has matured into a robust gas sensing technology over the last few decades. TDLS-based sensors are compact, rugged, lightweight and highly selective. Crucially, TDLS offers calibration-free measurements. Owing to these attributes, TDLS has firmly established itself the world over as the preferred method for high-sensitivity gas detection using robust and portable field measurement systems.

The work presented in this thesis aims to address the need for GHG monitoring in India through the design and deployment of TDLS-based systems to carry out calibration-free measurements of atmospheric CO₂, CO and water vapour. The robustness of the developed systems is demonstrated through field campaigns. This work constitutes the first instance of TDLS-based sensors being deployed in India for environmental monitoring.

The work can be broadly divided into three parts. In the first part of the work, a portable TDLS sensor is designed and used to carry out open-path CO₂ and water vapour measurements in six busy areas of Ahmedabad and Gandhinagar. A 2004 nm vertical cavity surface emitting laser (VCSEL) was

used for CO₂ measurements (using second harmonic wavelength modulation spectroscopy (WMS)) and a 1392.54 nm distributed feedback (DFB) edge-emitting laser was used for water vapour sensing (using direct detection). The measurements clearly reveal the high CO₂ content in the urban atmosphere at specific locations within the two busy cities. The highest recorded value during our measurements was 877 ppm, which is clearly much higher than the current global average of 411 ppm. Although reliable measurements were obtained during the campaigns, the sensitivity of CO₂ measurements was limited by the weak line strength of transitions in the near-infrared region. Subsequent measurements were therefore made using a quantum cascade laser (QCL) to exploit the much higher line strength in the mid-infrared region.

In the second part of the work, a 4320 nm distributed-feedback QCL-based TDLS sensor was developed. The system was deployed at Mt Abu, a hill station in western India, to carry out week-long measurements of background atmospheric carbon dioxide. The maximum and minimum mole fraction values were 419 ppm and 365 ppm respectively and the average was 396 ppm. The system was then deployed in Gandhinagar, the capital of the state of Gujarat, to make measurements in the urban location. The maximum and minimum mole fraction values were 652 ppm and 420 ppm respectively with an average of 503 ppm. The large difference between the background levels in Mt Abu and enhanced levels in Gandhinagar is evident. The mole fraction and pressure of CO₂ were simultaneously extracted in real-time by least-squares fit of a simulated Voigt line shape to the acquired gas absorption line. The detection limit of the system was determined to be 260 ppb for 20 cm path length and for an integration time of 58 s. The water vapour measurement system mentioned earlier was made compact and light-weight and then deployed for water vapour measurement. It consisted of the 1392.54 nm distributed feedback laser driven by a custom laser driver circuit and a digital signal processor to carry out waveform generation, data acquisition and post-processing tasks.

Finally, a new calibration-free WMS methodology is proposed and implemented for in-field measurement of gas parameters. During WMS-based in-field measurements, the signal received by the photodetector varies due to factors such as mechanical vibrations, temperature variations, wind, accumulation of dust on optical surfaces and aging of the laser (for long-term measurements). Consequently, the received signal intensity and the linear and nonlinear intensity modulation (IM) amplitudes also vary. In the proposed method, the first harmonic (1f) and second harmonic (2f) WMS signals are normalized by the linear and non-linear IM components respectively to make the signals immune to laser intensity variations. The advantage of this method is that the normalized signals appear on a background that is totally independent of the laser parameters. This sets the method apart from the earlier reported methods in the literature. The proposed technique is demonstrated through field measurements of ambient CO and CO₂ in Gandhinagar, India. The algorithm is shown to work robustly for very low mole fractions of gas in outdoor conditions and over long periods without any intermediate adjustments. This demonstrates that the detection technique is robust enough for it to be used for long-term environmental monitoring applications. The technique is not restricted to the optically thin approximation and this gives the technique an edge over the 2f/1f method. The system has a single-pass detection limit of 3 ppb for CO (using 1f

WMS and 4.05 m path length) and 45 ppb for CO₂ (using 2f WMS and 20 cm path length) for an optimum integration time of 17 s and 69 s respectively. The calibration-free WMS technique is especially important for automated long-term deployment in the remote monitoring stations where reliability of data is the biggest challenge. Various models that are developed are highly susceptible to the problem of unreliable data and data with low spatio temporal resolution. It is therefore important to use reliable measurement techniques to feed data into the simulation models.

Title: Novel strategies for image retargeting: energy design, acceleration, and scene awareness
Researcher: Patel, Diptiben
Supervisor: Raman, Shanmuganathan
Year: 2019
Keyword's: Energy Computation, Energy Map, Occlusion Map, Graph-cut Formulation, Text Region Warping
Call No.: 621.3 PAT
Acc. No.: T00552

Abstract: In the era of internet, digital media (such as image or video) and its access through diverse display devices have drawn a lot of attention. Diverse aspect ratios of display devices require adaptation of the image content to be displayed on them. Image editing in terms of size and aspect ratio of the target display device is termed as *image retargeting*. Content-aware image retargeting techniques achieve the image of target display size while preserving the salient or important information and thereby reducing visible artifacts in the retargeted image. Moreover, the shape and application-specific display such as folded mobile screens and concatenated flat displays require region-specific resizing of an image to have a better visual experience. Image retargeting is gaining a lot of attention in the computer vision field since a decade. However, there is a scope of improvement in better visual experience across numerous displays. Also, there are still some issues specific to the content-aware image retargeting which have not been addressed. Our goal is to develop image retargeting algorithms defining the better quality of viewing experience, accelerate the image retargeting process, and preserve high-level visual attributes during image retargeting process.

Content-aware image retargeting techniques demand additional information other than the image describing the relative importance of an image region. We propose two energy measures defining the relative importance of an image region. Seam carving, one of the efficient discrete content-aware image retargeting technique, suffers from the high computational time due to its iterative nature. We present two techniques for the acceleration of the seam carving by removing multiple pixel paths rather than a single pixel path in an iteration. We also provide adaptation of the width of the multiple pixel wide path according to the content present in the image, making it a content-adaptive acceleration of image retargeting. Most frequently captured attributes present in the world provide additional and essential information present in the image. These attributes need to be preserved while accessing the image through various display devices. We present the preservation of two such frequently occurring attributes, namely reflection symmetry and scene text while performing image retargeting. While achieving stereo image retargeting, we observed the advantage of allowing object occlusion to prevent object shape deformation. We propose a method for stereo image retargeting which provides object occlusion behind the object near to the camera to prevent object shape deformation.

Title: Low power architectures for assistive listening devices
Researcher: Ray, Dwaipayan
Supervisor: George, Nithin V.
Year: 2019
Keyword's: Energy Consumption Reduction, CMOS Technology, High-Speed Implementation, Digital Signal Processor, Adaptive FIR Filters
Call No.: 621.38 RAY
Acc. No.: T00568

Abstract: Assistive listening devices (ALDs) are smart and portable devices that assist people in carrying out the routine tasks that need them to be aware of the sound in their surroundings. ALDs consist of a set of microphones, a loudspeaker, a digital signal processor, and a battery. The primary objective of an ALD is to enhance the signal-to-noise ratio for the listener, which is achieved by implementing a set of fixed and adaptive digital filters in the processor. However, the limited battery power, constraint on computation time and demand for smaller form factor, put forward a demand for low power, low area, and high-speed implementation of digital filters in application specific integrated circuit (ASIC) technology. Digital finite impulse response (FIR) filters are the basic building blocks of the processor used in ALDs, where the filtering operation is performed using a set of fixed coefficients. Since these coefficients are fixed and known a priori, the constant multiplications involved between the input and multiplying coefficients are utilized to develop novel shift-and-add based hybrid form FIR filters. It is shown that the proposed structures provide a 40% reduction in power consumption and a 52% reduction in energy consumption in 65-nm CMOS technology. The fundamental operation involved in FIR filters is inner-product computation.

To enhance the overall efficiency of inner-product structures, this thesis explores the use of approximate computing technique in distributed arithmetic (DA) based structures and develops new approximate DA-architectures. It is found that the proposed approximate structures consume 20% less power, 27% less energy, and 63% less truncation error than existing approximate DA-architectures in 45-nm CMOS technology. One of the primary objectives of adaptive FIR filters in an ALD is to identify the acoustic path existing between the microphone and loudspeaker. The identification of this acoustic path is a critical step in reducing the acoustic feedback problem/generation of the annoying whistling sound, which occurs due to the proximity of the loudspeaker and the microphone. However, such acoustic paths usually exhibit a sparse impulse response. To selectively cancel the feedback signal present in the microphone signal, a unified framework for efficient realization of zero-attraction based sparse adaptive FIR filters is developed in this thesis. In addition, this thesis also explores the low-complexity implementation of nonlinear adaptive filters in the context of ALDs.

Title: Technology-assisted exergaming platform for upper limb rehabilitation of post-stroke patients
Researcher: Dash, Adyasha
Supervisor: Lahiri, Uttama
Year: 2020
Keyword's: Neurological Disorder, Clinical Syndrome, Hemiplegic Stroke, Surface Electromyogram, Multiscale Sample Entropy
Call No.: 621.3 DAS
Acc. No.: T00570

Abstract: Stroke is a neurological disorder that is defined as “a clinical syndrome, of presumed vascular origin, typified by rapidly developing signs of focal or global disturbance of cerebral functions” according to the World Health Organization. The deferred cerebral function is often manifested in the form of visual, motor and speech deficits along with paralysis making the disorder a common cause of death and the fourth leading cause of disability worldwide. Hemiplegic stroke is one of the major contributors to the disability that often adversely affects the upper and lower limbs of the patients which are contralateral to the hemisphere of the brain where the lesion has occurred. Reduced muscle strength, spasticity in limbs, reduced coordination in arms and legs and lack of mobility in limbs are few of the common symptoms that are seen on the paralyzed side of the hemiplegic stroke survivors. The motor dysfunctions in one’s upper limbs can affect the grip ability and hand coordination skill of a stroke survivor that in turn often limits the ability to independently execute daily living tasks, such as brushing of teeth, drinking from a glass, etc. To address such deficits, these patients are often prescribed rehabilitation exercises administered by expert clinicians. The therapeutic regime follows a standard protocol that starts with the assessment of a patient’s residual ability in the limbs, such as in one’s upper limb. Following the assessment, the patient is asked to undergo rehabilitation exercise whose intensity is adjusted to suit the residual capability of the patient. To alter the intensity of the exercise during the process of rehabilitation, the therapist intermittently changes the challenge level of the exercise based on the rehabilitation outcomes. For this, the therapist evaluates the patient’s capability by using some standardized scales. For example, the standardized scales are Modified Ashworth Scale (MAS) for measuring the spasticity in the arm, wrist and fingers of the upper limb, Fugl-Meyer Assessment (FMA) for measuring the coordination ability in the upper limb, Manual Muscle Testing (MMT) for measuring the force-producing ability of the muscles, etc. Also, the residual grip strength is measured using portable devices, such as Dynamometers. The evaluation carried out using measures, such as MAS, FMA, MMT, etc. are often subjective in nature and depends to a great extent on the expertise of the therapist doing the evaluation. Again, the measurements using standalone devices e.g., hand grip Dynamometer provide a gross measure of the patient’s grip ability without giving any insight into the physiological profile of the patients. Stroke being a neurological disorder, affects one’s ability to do a task, such as performing a grip action that can have physiological manifestations. Specifically, the inability to do a grip task is often related to anomalous muscle activation in one’s upper limb that can be adversely affected due to changed muscle tone, spasticity, etc. after stroke. Before addressing such a deficit, one needs to quantify the residual ability of a patient. An alternative to

quantify the post-stroke disability can be to study the muscle activation pattern during one's grip action. With the advancement in sensing technology, the use of surface electromyogram (sEMG) based monitoring of muscle activation has created an avenue to carry out technology-assisted quantification of residual grip ability after stroke. Taking advantage of the technology-assisted quantification, I have developed an sEMG-based framework for quantification of residual grip ability of post-stroke patients which is presented as the first objective of my research. In order to achieve this objective, I have designed and conducted a study with a group of post-stroke patients and monitored the sEMG activation of their upper limb muscles (both antagonist and agonist muscles) during the execution of an isometric grip task. Multivariate Multiscale Sample Entropy (MMSE) based analysis of the sEMG signals was used to compute the interactions between the antagonist and agonist muscle pairs (of the upper limb) and evaluated its possible clinical relevance. The result of the study indicated that the MMSE-based quantification of sEMG activation can be used as an objective measure to quantify residual grip ability in post-stroke patients.

After one's residual ability has been assessed, the patient is often referred to a rehabilitation regime aiming to address various issues related to post-stroke condition, such as grip ability, coordination skill, etc. In this, the patients are exposed to rehabilitation training exercises. The conventional therapeutic rehabilitation exercises aimed to improve the grip ability and coordination skill in the upper limb needs one to undergo repeated exercises, such as using sponge ball and putty along with making flexion, extension, abduction and adduction movements of the arm and elbow joints. These repetitive exercises (spanning across multiple exposures) are generally performed under therapist's supervision and have been proven to be promising. However, the conventional settings with one-on-one therapeutic intervention are often resource- hungry, need the continuous presence of expert therapists, monotonous and lacks in providing one with motivating exercises spanning across multiple exposures. Given these limitations, researchers have been exploring complementary technology-assisted solutions for rehabilitation.

Among the technology-assisted rehabilitation platforms, the robot-based and computer- based (with Virtual Reality (VR) mediated exercises) rehabilitation platforms have gained popularity. In my research, I have chosen the computer-based VR technology for designing individualized and adaptive exergaming platforms aimed towards improving the Grip ability and Hand coordination skills of post-stroke patients. In this, I have designed three VR-based exergaming platforms and have investigated the potential of these platforms to contribute to upper limb rehabilitation of post-stroke patients while targeting their grip strength and coordination skill. Thus, my second objective was to design and investigate the implications of VR-based exergaming platforms augmented with sEMG-enabled biofeedback mechanism on one's grip ability and grip strength. The third objective of my research was to design and investigate the implications of a VR-based performance-sensitive exergaming platform on the coordination ability of post-stroke patients.

To achieve my second objective, I have designed two VR-based platforms that were capable of providing the sEMG-enabled biofeedback in (1) Uni-Manual and (2) Disintegrated Bi-Manual modes. The target participant pool being hemiplegic post-stroke patients, the first platform was designed

to offer audio-visual biofeedback to the patients while they performed a grip task with their affected hand (Uni-Manual mode). Here, the audio-visual representation of one's grip strength was provided to the patients. Specifically, one's muscle activation (in terms of sEMG signal) in the paretic (affected) hand was mapped to vary the position of a dynamic VR object on the VR-based Graphical User Interface (GUI). In this, the dynamic VR object was programmed to be displaced and reach different goal levels (challenges) in the VR-based GUI depending on the amount of muscle activation in the affected hand during a grip. In order to facilitate an individualized grip exercise, the difficulty of goal levels was calibrated based on the sEMG activation while a patient did maximum voluntary contraction in the paretic hand during each exposure. Additionally, I have conducted a longitudinal study to provide the post-stroke patients with multiple exposures to the VR-assisted Uni-Manual exercise platform. The results indicated that multiple exposures to the VR-based sEMG-enabled biofeedback platform contributed to the improvement in the grip ability and grip strength of the patients, manifested in terms of (1) VR-based task performance, (2) sEMG activation pattern and (3) clinical measures. Though the results were promising, yet this VR-based platform augmented with Uni-Manual biofeedback mechanism adjusted the task challenge levels depending on the patient's maximum grip strength in the paretic hand. Given the fact that the maximum grip strength in the paretic hand of a hemiplegic patient is less than that of the other hand (non-paretic (i.e., unaffected) hand), deciding the thresholds for the task challenge levels might lead to limiting the rehabilitation outcome. One of the ways to address this is to use their maximum grip strength in their non-paretic hand to decide the thresholds for the challenge levels (considering that the grip strength in the non-paretic hand is larger than that in the paretic hand). Given this alternative, I have designed my second exergaming platform that is targeted to offer VR-based sEMG-enabled biofeedback for grip strength exercise in Disintegrated Bi-Manual mode. Here, the audio-visual biofeedback was designed to offer a representation of the muscle activation in both the upper limbs of a patient (i.e., Bi-Manual mode). Though the task was Bi-Manual, the VR-based feedback was offered in a disintegrated manner by demonstrating the muscle activation in both the upper limbs of a user separately thereby eliminating any element of compensatory mechanism (commonly used by post-stroke hemiplegic patients). This featured two dynamic VR objects on the VR-based GUI with each being mapped to the sEMG signal captured from respective individual hand. The Bi-Manual platform was individualized similar to the Uni-Manual platform. For this, the thresholds for the varying goal levels (challenges) of the Bi-Manual platform was adjusted based on the maximum grip strength of the patient in an individualized manner. Specifically, the goal levels were calibrated based on the muscle activation in the non-paretic hand when the patient performed maximum voluntary contraction while making a grip. To evaluate the rehabilitative potential of the platform, I have conducted a study with a group of post-stroke patients who were offered multiple exposures to my platform. The results of the study indicated a potential of this system to improve one's grip ability and grip strength quantified in terms of (1) VR-based task performance, (2) sEMG activation and (3) clinical measures.

To achieve my third objective, I have designed and investigated the implications of a VR-based exergaming platform on the coordination ability of post-stroke patients. The platform was programmed to be performance-sensitive i.e., the platform was programmed to vary the task

difficulty based on one's performance in the VR-based coordination exercise. The task difficulty of the coordination tasks was defined in terms of the extent of arm flexion and the number of changes in hand orientation required to complete a VR-based task. In this task, the patient was expected to lift his / her arm and maneuver his / her hand in the physical space to sketch patterns in the GUI displayed on the Task computer monitor. Delivering of audio-visual feedback was also a part of the study design. In order to map the arm movement in the physical space to the VR-based GUI, a Kinect Xbox-360 was used. This study involved a usability evaluation in which a group of stroke patients was offered multiple exposures. The results showed that this platform has the potential to contribute to rehabilitation in terms of improving one's (1) VR-based task performance, (2) ability to use tasks of higher difficulty levels after a limited number of exposures. However, given a limited number of exposures, no clinical improvement was noticed. The study with each of the three exergaming platforms ended with a survey to understand the usability of the system by the target group. The results of the survey indicated that the participants were very positive about using the platforms.

To summarize, the outcomes of my research were the design of (1) sEMG-based framework for quantification of residual grip ability, (2) VR-based sEMG-enabled exergaming platform (Uni-Manual and Disintegrated Bi-Manual) and (3) Kinect-assisted Performance- sensitive exergaming platform. Additionally, I investigated the implications of (a) Uni-Manual and Disintegrated Bi-Manual exergaming platforms on the grip ability and grip strength and (b) Kinect- assisted exergaming platform on the coordination skill of post-stroke patients that have been presented in my thesis.

Title: Investigating motion in image sequences: detection, removal, and inference
Researcher: Kanojia, Gagan
Supervisor: Raman, Shanmuganathan
Year: 2020
Keyword's: Convolutional Neural Network (CNN), SSA Layer, Image Sequencing, Image Completion Network
Call No.: 621.367 KAN
Acc. No.: T00731

Abstract: Nowadays, capturing images and videos of a scene or an event is an inherent component in our lives. When one captures an outdoor scene, it is very common to have dynamic (moving) objects present in the scene. Sometimes they are undesirable and sometimes they are the key source of information about the scene. In this dissertation, our focus is on both the aspects of dynamic objects.

Detection and Removal. Whether desirable or undesirable, the detection of dynamic objects is crucial in both the cases. We, first, propose a patch-based method to identify dynamic regions present in a set of images of a dynamic scene captured from multiple viewpoints. Our approach exploits the coherency present in the natural images. It does not require a dynamic object to be present in all the input images. For the case where the dynamic objects are not desirable, we propose a convolutional neural network (CNN) based architecture for removing them. It takes the multiple views of a scene as the input and fills the undesirable regions in one image using the information present in the remaining images. The network is trained using an adversarial approach and is observed to generate sharp output images, qualitatively. Later, we combine the task of detection and removal of dynamic objects in a single algorithm. We propose an algorithm that takes this set of multi-view images as input, detects the dynamic objects present in the scene, and replaces them with the static regions which are being occluded by them. The proposed algorithm scans the reference image in the row-major order at the pixel level and classifies each pixel as static or dynamic. During the scan, when a pixel is classified as dynamic, the proposed algorithm replaces that pixel value with the corresponding pixel value of the static region which is being occluded by that dynamic region.

Action Recognition. Automatic interpretation of actions is a challenging task, especially when it involves rapid changes and long-term dynamics. In action recognition, the task of recognition requires not only the spatial information but also the temporal information. We propose a convolutional block that captures both the spatial information and the temporal information by utilizing a 2D convolution and temporal differences, i.e., the change in the spatial information at different time instances, using simple operations of shift, subtract and add. In the case of competitive diving, a more fine-grained action recognition task, capturing motion associated with the diver is an essential. It is a challenging task due to the rapid and complex movements of the diver. We propose an attention-guided LSTM-based neural network architecture for the task of diving classification that also localizes the diver in the input video frames during the dive without being explicitly trained with such a supervision.

Image Sequencing. If there are large deformations in the adjacent frames of the input image sequence, then the extraction of temporal information could be very challenging. Hence, the desired situation would be when the temporal order (or the order of capture) of the frames is known. For the case when the temporal order is unknown, we propose an LSTM-based deep neural network that takes a set of unordered images and outputs their order of capture in an end-to-end manner. We, further, improve the results for the task of image sequencing by proposing a novel convolutional block which captures the spatial information through a 2D convolution kernel and captures the temporal information by utilizing the differences present among the feature maps extracted from the input images. We show that the proposed approach generalizes well on the dataset apart from the one on which the network is trained.

Title: Magnetic equivalent circuit incorporating core saturation and rotor motion, and a method for mitigating subharmonics in surface-mounted PMSM

Researcher: Bhashini, Manju V.

Supervisor: Ragavan K.

Year: 2021

Keyword's: Magnetic Equivalent Circuit, MMF harmonics, Electrical Equivalent Circuits, Windings

Call No.: 621.3 BHA

Acc. No.: T00732

Abstract: Electric machine design involves determining the physical dimensions of the machine for certain desired terminal characteristics. It is an added advantage if the design tools are able to predict the machine performance during design phase. The terminal behavior of the machines is characterized by electrical equivalent circuits (EEC) and are widely used to understand the requirements on the source side and are also used for machine control. However, these EEC do not reveal the internal behaviour in the machines. Knowing the internal behaviour is very much needed for carrying out the design of machines. To this end, magnetic equivalent circuit (MEC) plays a vital role as the internal behavior is depicted in it. Further there exists one-to-one correspondence between the MEC and the machine.

There exist challenges in representing the actual machine into MEC. In rotating machines, the flux profile changes with rotor movement. Hence, identifying the flux path between the stator and rotor during its movement, and representing it by appropriate position dependent reluctance in the MEC is the main challenge. Another challenge is accounting for saturation behaviour of the iron core. As the value of permeability in a core region depends on the value of flux density, permeability cannot be assumed the same for different parts of the core. It is to be determined with the aid of magnetization characteristics. Hence, depicting the rotor movement and core saturation at circuit level requires an appropriate modeling.

In this thesis work, a simplified MEC topology is proposed for modeling the surface-mounted permanent magnet synchronous motor (PMSM) and is analyzed with the aid of mesh analysis. Number of air-gap elements associated with a stator tooth could either be one or two depending on the position of nearby rotor poles. With this, the number of meshes in the whole MEC does not change with rotor movement. It is worth to mention that the proposed MEC topology makes use of less number of air-gap reluctance elements linking the stator and rotor. Saturation effects are accounted in the MEC by means of flux-density dependent reluctance elements, and the developed model is solved through mesh analysis and Newton-Raphson method. The instantaneous variation of flux density, flux linkage and torque obtained from MEC agrees reasonably with the results obtained from finite element analysis (FEA) performed in Ansys-Maxwell platform. Subsequently it is demonstrated how MEC can be utilized for assessing machine performance with regard to its flux weakening capability, contribution of reaction and reluctance torque, cogging torque evaluation. As the evaluation of various quantities by MEC analysis agrees reasonably with FE analysis and

experimental measurements, the proposed MEC topology and its analysis could be useful during design phase.

In case of surface mounted PMSM with distributed winding, the value of direct-axis inductance is very low and flux weakening is ineffective. By opting fractional slot concentrated winding (FSCW), it is possible to increase its value. However, FSCW introduces more space harmonics in the stator MMF. Among those, sub-harmonics severely influence performance of the machine. In this work, an analytical method is proposed to minimize subharmonic in the MMF profile of surface-mounted PMSM with FSCW. Initially significance of winding layer and slot opening on the MMF harmonics is investigated. From the results, four-layer winding is found to have its subharmonic's magnitude as low. A method is proposed to minimize subharmonics by determining the optimum number of turns in the phase coils. For this purpose, voltage induced in a phase due to subharmonic is considered. For assessing the performance of optimum winding distribution, MMF harmonic spectrum and winding factors are used.

To demonstrate the proposed method of minimizing subharmonic, a PMSM that has only one subharmonic is considered with 12 slots and 10 poles (Machine- 1). Later the proposed method is extended to a machine that has more than one subharmonic, a PMSM with 18 slots and 14 poles (Machine-2) is considered. Optimum winding distribution is achieved such that subharmonics are minimized (1 in Machine-1; 1 and 5 in Machine-2). It is worth to mention that the synchronous torque producing frequency component remains unaffected (5 in Machine-1; 7 in Machine-2). The results are validated through FE simulation. In PMSM with FSCW, space harmonics in the MMF gets increased and these space harmonics eventually leads to eddy current loss in magnets. For extending the life of the magnets, it is necessary that the eddy current loss in it is to be minimized. This requires a suitable winding distribution and optimum current control so that the impact of space and time harmonics is reduced. In this work, investigations are carried out for understanding the severity of eddy current loss in magnets corresponding to different winding layers.

An analytical model available in the literature is used for predicting the eddy current loss in the magnets. The results obtained from the analytical model are validated through FE simulation. It is found that the winding distribution with higher magnitude of subharmonic results in higher loss in magnets. Further the loss is found to be the least with four-layer winding (compared to single and two-layer winding distribution). Later, segmented rotor configuration is chosen for minimizing the eddy current loss in the rotor. It can be concluded that four-layer winding distribution in stator with segmented rotor would correspond to energy efficient design. The proposals and investigations are related to modeling the internal behaviour of the rotating electrical machine, identifying optimum winding distribution for minimizing subharmonics, and suitable winding distribution for minimizing the loss in magnets and rotor. The findings are validated through appropriate FE simulation and few experimental measurements. It is believed that these findings could be useful in the design phase of electrical machines.

Title: Non-invasive detection of microbial growth using tunable diode laser spectroscopy and its application to assess bacterial traits

Researcher: Zarina A. S.

Supervisor: Chakraborty, Arup Lal

Year: 2020

Keyword's: Metabolic Activity, Microbial Growth, Diode Laser, Photobacterium Leioagnathi, Spectroscopy

Call No.: 621.366 ASN

Acc. No.: T00733

Abstract: Metabolic activity in all living organisms leads to concomitant emission of various gases. Accurate measurement of these gases in microbial growth can help to understand the underlying physiological processes and to control microbial behaviour. Such measurements have importance in fundamental bio-science studies, pharmaceutical drug development, bioreactor monitoring, planetary science studies and clinical microbiology. The major challenge in microbial growth measurement is that measurements need to be non-invasive, non-destructive and must be made in real-time to capture the time evolution of microbial growth and the expression of specific traits. It is also essential to avoid contamination of the growth culture and to allow the growth process to continue undisturbed. Conventional growth measurement techniques are not able meet all of these requirements. This work demonstrates that calibration-free tunable diode laser absorption spectroscopy can be used as a versatile and reliable technique to make accurate, real-time, non-invasive measurement of the of the mole fraction of the metabolic carbon dioxide that is emitted by bacterial cultures into the head space of the culture vessel over several hours of the bacteria's life cycle. Measurements are made with a vertical cavity surface emitting laser emitting at 2004 nm and a mid-infrared quantum cascade laser emitting at 4320 nm.

The thesis first establishes that cumulative CO₂ emitted by a bacteria follows the sigmoidal curve, which is the characteristic of bacterial growth in a nutrient limited medium. It is shown that it is possible to extract various growth parameters from this curve. This is first tested on *E. coli* and then on *S. aureus*. Then the cumulative CO₂ based growth measurement technique was applied to assess two of the many bacterial traits that bacteria are known to express at specific stages of growth depending on the growth conditions. It is shown that the bioluminescence and simultaneous carbon dioxide emission from *Photobacterium leioagnathi* are correlated, with the bioluminescence peaking at the point of maximum growth rate. Such time-resolved non-invasive growth measurements would be useful to validate and improve mathematical models of microbial growth. Such cross-verification would contribute to improving the overall understanding of the dynamics of the underlying processes. Next, it is demonstrated that tunable diode laser spectroscopy can be used to reliably determine the minimum inhibitory concentration of a drug for a given microbial strain. The mole fraction of carbon dioxide emitted during the bacteria growth was recorded for different standardized doses of antibiotic to show the drastic suppression of growth as the antibiotic dose is increased to the recommended value. It is shown that ultra-rapid antimicrobial susceptibility testing is possible with this laser-based technique with growth suppression detected as early as 2 h which compares favourably with measurements times of 10-12 h using conventional methods.

The thesis concludes by demonstrating simultaneous time-resolved measurements of the emission of nitrous oxide and carbon dioxide from *Citrobacter sp*, which opens up the prospect of measuring multiple gases simultaneously to study the relation between growth and emission of a specific gas. In summary, this thesis demonstrates that near-infrared and mid-infrared calibration-free wavelength modulation spectroscopy implemented on tunable diode lasers is a potent investigative technique that should find widespread use in laboratory and in-field studies of microbial growth.

Title: Grid-integration of large-scale wind power generation with battery energy storage system
Researcher: Abhinav, Rishabh
Supervisor: Pindoriya, Naran M.
Year: 2021
Keyword's: Battery Energy Storage System, Wavelet Neural Network (WNN), Wind-BESS Hybrid System, Convolutional Neural Network (CNN)
Call No.: 621.45 ABH
Acc. No.: T00734

Abstract: The variation in production and higher intermittency of wind power generation makes it difficult to fit into conventional procedures of power system operations, planning, and scheduling. The latest advancements in energy storage technology provide an opportunity for utilizing energy storage systems to address the intermittency of wind energy. Recent studies suggest that the Battery Energy Storage System (BESS) can play a significant role in handling risks associated with wind power generation uncertainties and maximizing wind power producers' revenue (WPP). This thesis mainly focuses on two aspects of the grid integration of wind energy: (i) the active power management of wind farms and (ii) the wind energy trading in short-term electricity markets, both incorporating BESS.

A grid operator must foresee the day-ahead generation and demand, such that a proper dispatch schedule is prepared, and hence, wind power forecasting is essential. It further assists the WPP to participate in futuristic energy markets with optimal decision-making. Several wind power forecasting modules based on machine learning and deep learning algorithms are developed as preliminary work in this thesis. First, a Wavelet Neural Network (WNN) based forecasting model is created, which utilizes a multi-level discrete wavelet decomposition technique to analyze the nonlinearity present in the historical wind power profiles. Based on a similar WNN model, an electricity price forecasting model is also developed, which is instrumental in wind energy trading in electricity markets. Further, an ensemble forecast model is proposed that takes the benefits of four machine learning algorithms, which include Convolutional Neural Network (CNN), Long Short-Term Memory (LSTM), Light Gradient Boosting Machine (LightGBM), and eXtreme Gradient Boosting (XGBoost). It is found that the performance of the ensemble model reasonably performs well throughout the year as compared to the other models.

The next part of the thesis addresses the dispatchability problem of wind power plants. A two-layer Coordinated Model Predictive Control (CMPC) algorithm is devised that coordinates the operation of a wind-BESS hybrid system (WBHS). The optimized reference signals are then sent to the BESS subsystem controller at the lower level. The lower-level controller drives its subsystem subjected to the system constraints to track the reference signal and provides optimal charging/discharging instructions to the BESS. Thus, the combined WBHS power output is brought to the desired dispatch level. It also helps in smoothening the wind farm power output. Simulation results verify the efficiency of the presented MPC controller.

The following segment of the thesis focuses on a risk-constrained stochastic bidding strategy for a WPP to play in the short-term electricity market. The strategy is formulated considering the uncertainties present in wind power generation and electricity market prices, aiming to minimize the power deviation during real-time delivery utilizing BESS. CVaR as a risk-measure is incorporated, and a two-stage stochastic optimization problem is formulated where the first stage decides the day-ahead (DA) offering while the second stage deals with the real-time (RT) operation. The stochastic problem is further reformulated using Extended Mathematical Programming (EMP), which reduces the problem's mathematical complexity. The wind power generation profile from an actual wind farm located in Gujarat, India, is taken as a test study. Various potential case studies are presented to illustrate the effectiveness of the proposed bidding strategy.

In conclusion, this thesis presents effective wind power forecasting and electricity price-forecasting models, which are much robust to predict throughout the year accurately. A coordinated model predictive controller is proposed to improve the dispatchability of the wind power plants by optimally scheduling the BESS. After that, an optimal bidding strategy is devised for WPP to participate in short-term electricity markets and maximize their revenue. This work can be further extended to incorporate the grid operator's perspective, where the algorithm can be developed considering the network constraints and grid disturbances. Wind energy and BESS roles can be explored in the ancillary services markets for frequency regulation and demand response. This energy trading in the electricity market could also incorporate multiple players with distributed generators and electric vehicles. The stochastic optimization problem developed in Chapter 5 may be solved for numerous participants by employing distributed algorithms like ADMM, Bender's decomposition, etc. This would further reduce the problem's computational complexity and protect data privacy among the market participants.

Title: Right invertibility and relative degree in tracking control: theory and tools
Researcher: Kadam, Sujay Dilip
Supervisor: Madapusi, Harish Palanthandalam
Year: 2021
Keyword's: Multi-Input Multi-Output (MIMO), Tracking Control, Coordinated Model Predictive Control (CMPC), Extended Mathematical Programming (EMP)
Call No.: 621.3 SUJ
Acc. No.: T00735

Abstract: Tracking control, in which outputs of a dynamical system are made to follow desired reference commands by applying appropriate control inputs, is one of the primary objectives in a large proportion of wide-ranging control problems. The literature is rich in controllers and control algorithms to achieve tracking behavior of systems using a variety of approaches and in the context of various applications. Determining whether control inputs exist to track arbitrary reference commands and analyzing the achievable tracking behaviour in general and for given reference commands are altogether different problems from synthesizing a controller. *Right invertibility* of a system is a fundamental system property that is helpful in examining the existence of control inputs for tracking arbitrary reference commands. This thesis discusses three closely related problems connected to right invertibility and tracking control, along with their applications.

Firstly, we discuss the theoretical aspects of right invertibility starting from the idea of trackable and untrackable sets of reference commands and subsequently developing theoretical facts and tools for analysis and control synthesis in tracking control problems in the process. We define the concept of trackability for multi-input multi-output (MIMO) discrete-time LTI systems as an inherent system property (here, by 'inherent' we mean unchanged by similarity transformation/change of basis). We also present tools to determine *a priori*, the achievable tracking behavior of the system. Furthermore, we show that trackability is different from controllability and output controllability.

Secondly, we discuss in case of MIMO systems, the input-output delays or relative degree governing the interaction between the system's inputs and outputs, and its effect on, and the means to accommodate those in feedforward control inversion-based tracking control. In fact, we generalize the notion of relative degree to non-square systems by defining two input and output relative degree vectors thereby generalizing the notion of relative degree for MIMO systems. This treatment leads to a simple yet powerful insight linking system invertibility and existence of well-defined relative degree being equivalent to each other.

Thirdly, we bring in the idea of prioritized tracking of a system's outputs by assigning priorities to the output components of interest, if some outputs require an emphasis over others in certain situations. We also discuss prioritizing the usage of input components, when the available inputs are more in number than the outputs. Further, to validate the idea of prioritized tracking of system outputs, we present a two-link 'swirling pendulum' manipulator mechanism having rich dynamical properties that exhibits several challenges in control design. Furthermore, we present a perspective

on controller design for tracking control of MIMO systems (also applicable to non-square systems) that allows us to easily use an existing input reconstruction method for tracking control by breaking down the tracking problem into state estimation and input reconstruction problems.

The work presented in the thesis is expected to serve as a foundation for a systematic discussion on tracking control and also to provide a framework for disseminating new insights on tracking control theory, methods and applications.

Title: Compression history estimation and source identification for image and audio forensics
Researcher: Verma, Vinay
Supervisor: Khanna, Nitin
Year: 2021
Keyword's: JPEG, Digital images, Compression-based Forensics, Deep Learning
Call No.: 621.3 VER
Acc. No.: T00736

Abstract: Nowadays, multimedia content such as digital images, audios, and videos are being generated and shared rapidly, thanks to the cost-effective hardware and internet data bandwidth. Simultaneously, tools that can modify the original meaning of the content without leaving any perceptual artifacts are easily available. As a consequence, the trustworthiness of the multimedia content has been eroded. Tampered multimedia content becomes a severe threat when used in the court of law or influences public opinion by spreading misinformation. Hence, such situations demand forensics systems to establish the history of the concerned multimedia content in its authenticity, source acquisition device, and digital processing history after its acquisition. These broad spectra of issues related to the forensic history of multimedia content are tackled in the multimedia forensics field. In this thesis, we attempted to address two currently relevant problems: image authenticity and source acquisition device identification for digital audio recordings. The primary motive in these forensic tasks is to suppress multimedia content and try to devise or learn low-level forensic signatures that can help in establishing the forensic history of the concerned multimedia. All the systems designed in this thesis fall into passive multimedia forensics; consequently, they do not require any additional information (such as a watermark or digital signature explicitly inserted during the multimedia creation) except the multimedia under concern.

Specifically, the first problem regarding the authenticity of digital images, we focus on JPEG encoded images. JPEG is the most widely used compression standard in image acquisition devices and commercially available image processing tools. Due to the broad usability of the JPEG images, the forensics community, through the years, has given significant attention to JPEG compression-based forensics. For JPEG images, we have developed systems that can provide information on the authenticity of the images. We investigated forgery localization in JPEG images, and the problem of detecting the number of JPEG compressions an image has undergone. Domain knowledge, coupled with the use of deep-learning methods, resulted in improving state-of-the-art performances. In this thesis, we present the first data-driven deep learning based approach to detect the number of JPEG compressions an image has undergone. Earlier deep learning based approaches were restricted to double compression, while the proposed system can detect up to five compressions. Results evaluated on standard publicly available datasets highlight the relevance and importance of the proposed systems for JPEG-based forensics.

In the second problem considered in this thesis, given a digital audio recording, we present systems to identify the source acquisition device, the source cell-phone in the present case. Acquisition device identification helps in the verification of ownership and establishes the authenticity of the

concerned digital audio. If different segments of the concerned audio signal are detected to be originating from different cell- phones, then it indicates the possibility of tampering. For cell-phone identification, we present two approaches: a feature engineering-based approach and a data- driven deep learning based approach. In the data-driven approach, the system learns device-specific low-level fingerprints suppressing the audio content from the recorded audio by changing the representation of the time-domain audio signal to the frequency domain without explicit physical modeling of the device characteristics. The performance of the proposed system is also evaluated with the re-compressed audio recordings, the scenario which needs more attention, as the audio recordings available for the cell-phone identification task might be re-compressed in their life cycle. Proposed methods are evaluated on a publicly available dataset. Additionally, we also created a new dataset to explicitly assess the effect of speaker and speech content on the proposed audio source identification system.

Title: Opportunistic context-aware energy-efficient embedded memory solutions
Researcher: Surana, Neelam
Supervisor: Mekie, Joycee
Year: 2020
Keyword's: Embedded Memory, System On Chip (SOC), Read-Decoupled DICE, Binary Neural Networks (BNN)
Call No.: 621.3 SUR
Acc. No.: T00737

Abstract: Embedded memory is crucial for better performance of any electronic system ranging from self-sustaining low power IoTs to power-hungry servers. In most of the current electronic systems, embedded memory takes a large chunk of the chip area and power. Embedded memory occupies ~70% of the total SoC chip area and it is further expected to increase to ~80 by 2021 [10]. Embedded memories consume significant power of a System On Chip (SOC), which necessitates the design of efficient embedded memory. Moreover, the paramount shift of electronic systems from the general-purpose systems to the application-specific systems has motivated researchers to design embedded memory that meets the needs of an application or is application-specific. It exploits domain knowledge to make it efficient. In this thesis, we have designed the embedded memory at the circuit level for diverse applications with low-power and high-performance requirements, including space applications, multimedia applications, and hardware for neural networks. For space applications, the designed electronic system should be radiation tolerant. Existing radiation-hardened cells like DICE, Quatro require high read and write energy. To circumvent these, we propose two novel SRAM cells, namely Read-Decoupled DICE (RDDICE) and Dual Port DICE (DPDICE) SRAM. RDDICE has decoupled read and write ports, which enables simultaneous read and write operations in an array, whereas DPDICE has two read ports that allow dual read operations simultaneously. In terms of the power benefits, RDDICE (DPDICE) has 47.4%(62.7%), and 22.6%(39%) lesser read energy, and write energy respectively compared to the conventional DICE SRAM in 32x32 array in UMC-28 nm technology, and are robust to errors.

Unlike space applications having zero tolerance for error, multimedia applications are error-resilient. This feature is exploited in earlier works to build energy-efficient approximate memories such as heterogeneous 6T SRAM and hybrid 8T+6T SRAM architecture. However, heterogeneous 6T SRAM suffers from large power requirements, and hybrid 8T+6T SRAM suffers from the design complexity. We have proposed multiple design solutions for the H.264 video decoder to circumvent these issues including heterogeneous 8T SRAM architecture, seven different Mixed-VT 8T SRAM architectures, single-ended 6T SRAM cell, and assist techniques like word-line boosting in 8T SRAM for H.264 video decoder. The proposed architectures give at least 51% dynamic energy reduction as compared to that in heterogeneous 6T SRAM without significant loss in video quality.

We also explore the design of content-addressable memories (CAMs) being used alongside SRAM to build the complete memory module. CAMs also have utility in other applications such as network routers, image processing, video decoders, etc. It is known that, in the CAMs, a large portion of the total power is consumed in the charging and discharging of the match lines, and precharge-free

CAMs have been proposed as energy- efficient substitutes. We show that the existing precharge-free CAMs suffer from either slow speed or are susceptible to process variations. We proposed novel 10T precharge-free CAM to circumvent these issues. For an array size of 32×32, the proposed CAM exhibits 6.2× of energy-delay-product reduction compared to conventional NOR-type CAM.

Neural networks (NNs) are another category of error-resilient applications. They are both compute and data-intensive and consume significant power in accessing memory accesses and computations. We have used three different techniques for reducing power consumed in embedded memory. We have proposed a novel DPDICE based on in-memory computing (IMC) architecture that is robust compared to all earlier proposals. Another technique is based on quantization to reduce the storage requirements, which also reduced power consumption in memory. Through rigorous mathematical analysis, we establish that the number of bits required for representing weights in a neural network depends upon the number of layers in the network and the least magnitude weight (LMW) of trained weights. The third technique is for binary neural networks(BNN), where we have proposed a split memory architecture. Here the weights are stored in area-efficient 6T SRAM, and batch normalization parameters (BNPs) are stored in robust 12T SRAM. The split architecture allows memory to be operated at as low a voltage as 0.52V, resulting in a 43% power reduction in UMC 28nm, without loss in BNNs accuracy.

To summarize, in this thesis, we leverage domain knowledge and propose application- specific embedded memory solutions for space applications, video applications, CAMs and neural networks to achieve low-energy and/or high-speed.

Title: Linearity enhancement techniques in high resolution pipelined ADCs
Researcher: Mohapatra, Satyajit
Supervisor: Mohapatra, Nihar Ranjan
Year: 2020
Keyword's: Signal to Noise And Distortion, CMOS, SDR (Software Defined Radios), Spur Free Dynamic Range (SFDR)
Call No.: 621.3 MOH
Acc. No.: T00738

Abstract: CMOS data converters for high resolution space imaging and cellular base station applications envisage wide dynamic range and high throughput. Particularly, with the advent of SDR (software defined radios), the system designers today perceive a shift in paradigms from the conventional super heterodyne architecture to Nyquist IF sub-sampling or direct RF sampling approach. While these modern approaches primarily benefit in terms of system size, cost and power, they impose stringent linearity constraints such as signal to noise and distortion (SINAD) and spur free dynamic range (SFDR) that is challenging to be met in scaled submicron CMOS processes. The variability in modern processes limits the accuracy of fabricated analog components thereby leading to component mismatch. This severely impacts the conversion linearity and energy efficiency of high speed data converter architectures such as the pipeline ADC and current steering DAC. In any standard CMOS process, the global mismatch typically limits the “intrinsic linearity” of these architectures to 10-12 bit. The global mismatch experienced on any placement are because of several reasons such as mismatch in layout, fabrication gradients, packaging stress, proximity to heated modules such as amplifiers, drop across metal lines and non-uniformity in metal coverage. More importantly their relative magnitudes, i.e. [linear: quadratic] and [parabolic: rotated-parabolic] also vary with layout intricacies, process technology, fabrication batches, die location over wafer, chip packaging technique adopted as well as operating environment conditions such as temperature. Since most of these factors are beyond the designer’s control, the experiments on a single test chip cannot be used to validate a placement technique across all chips. The present study develops a robust placement scheme which compensates all possible global error components and is independent of technology related parameters such as relative magnitudes of various gradient profiles, edge effect variability, linear shifting or angular misalignment of gradient angles during layout, processing, packaging as well as real time operations.

Based on elaborate mathematical analysis, the current research have developed a technique to generate statistically rare device placement patterns, which completely eliminates the process induced mismatch. This indigenous optimisation primarily helps to overcome the linearity bottleneck in fabrication of high resolution data converters with pipelined and current steering architectures. The linearity of the converter so implemented is independent of turn on sequence and technological ratios. The algorithm provided there in, further unravels certain crucial facts to the classical rearrangement inequality bounds in the field of mathematics. The technique sets a trend in mismatch resilient DAC design and is an useful aide to state of the art data converters aspiring for resolutions higher than 16-bit on silicon. Critical high speed high resolution applications

such as satellite imaging, SDR assisted military jet aircraft and mobile base station transceivers will significantly benefit from this.

Title: Development of energy management frameworks for der integration in distribution networks
Researcher: Kiran, Patnam.Bala Sai
Supervisor: Pindoriya, Naran M.
Year: 2021
Keyword's: Distributed Energy Resources (DER), Distribution Locational Marginal Pricing (DLMP), Mixed-Integer Programming (MIP), Aggregator
Call No.: 621.042 KIR
Acc. No.: T00739

Abstract: Over the decade, the power system architecture is rapidly transforming towards a smart grid with the large-scale integration of the distributed energy resources (DER), smart communication devices, and controllable loads. The DERs, such as renewable energy generation, electric vehicles, and battery energy storage system, leverage technical and economic benefits to consumers and system operator. On the other hand, the combination of flexible loads, intermittent renewable energy generation, and uncertain EV load changes the traditional load demand profiles. The improper coordination of loads and DERs leads to power imbalance and network congestion and poses significant challenges to the system operation and maintenance. Optimal demand response and DER coordination are required to operate the grid reliably and efficiently. This thesis develops advanced energy management algorithms to address the operational challenges related to DER integration, coordination and network con- gestion in the active distribution network.

In the first part of the work, a stochastic centralized energy management algorithm is developed to integrate demand response into the active distribution network. The proposed algorithm helps both the DSO and consumers to minimize energy cost and energy procurement risk. The scheduling involves both the day-ahead (DA) and real- time (RT) operation. In real-time, the aggregator solves the RT energy management problem with BESS to minimize the cost of power deviations. It is implemented us- ing rolling window optimization and modeled as a mixed-integer programming (MIP). The second part of the work focuses on the distribution locational marginal pricing (DLMP) based EV aggregator bidding strategy to minimize network congestion with EV aggregator load. It is formulated as bi-level programming with the EV aggregator as a leader and DSO as a follower. The upper-level/leader problem objective is the EV aggregator cost minimization by satisfying the EV load demand. In contrast, the lower-level/follower problem objective is the social welfare maximization. The nonlinear bi-level problem is reformulated into the single level mixed-integer programming (MIP) using Karush-Kuhn-Tucker conditions and duality theorem. Further, a DLMP based hierarchical multi-microgrid coordination algorithm is developed to address the challenges in coordinating multiple energy resources. The algorithm is implemented in two stages: the first stage, DSO, solves the optimal power flow problem and calculates the DLMP at all the nodes. In the second stage, microgrids schedule their generation and load demands based on the DLMP given by the DSO. Later, microgrids trade the power with other microgrids based on their surplus/deficit energy. In the

end, the trading price is calculated by using the Nash bargaining theory. In the last part of the work, a decentralized distributed energy management algorithm is developed for a balanced and unbalanced distribution network to improve the consumer's privacy and convergence speed. The decomposition is implemented in the following stages: First, a DSO and load aggregator (LA) solves the optimization problem using a predictor- corrector and proximal multiplier algorithm. Next stage, DSO and LA problems are decoupled further to avoid temporal coupled constraints, and closed-form updates of the DSO and LA optimization problems are calculated. The algorithm is tested on the IEEE 13, 37, and 123 nodes balanced and unbalanced systems.

Title: Source device identification systems for printed documents and digital images
Researcher: Joshi, Sharad
Supervisor: Khanna, Nitin
Year: 2020
Keyword's: Network-Connected Devices, Mobile Connectivity, Energy Management Algorithm, Bi-level Programming
Call No.: 621.3 JOS
Acc. No.: T00740

Abstract: Traditional notions of privacy and security are challenged by the ubiquitous presence of a humongous number of network-connected devices having never-imagined-before memory and computational powers. Particularly in India, mobile connectivity is rapidly increasing, with ever-increasing smart- phone users having access to one of the lowest mobile data rates across the globe. This implies that a smartphone user can effortlessly capture and share a printed document. This exposes many printed documents like books or other materials protected by copyright, secret military documents, quotations, examination question papers, product plans of a company, and undisclosed legal documents to a large number of unauthorized users. Such scenarios may give a harder time to the investigating agencies. Moreover, the rapid development in technology, lack of awareness among common users, and lack of acceptability of active authentication approaches by sensor-based product manufacturers has propelled the need for multimedia forensics. Although printed documents have been partially replaced by their digital counterparts for many daily applications. However, many applications require a co- existence of both printed and digital documents due to ubiquitousness, ease of use, cost-effectiveness, and security of documents. Paper is still widely used for financial and judicial processes such as lease agreements, purchase invoices/bills, and court judgments. This requires continuous monitoring of bulk documents in an accurate manner. An important aspect of examining printed documents for potential forgeries and copyright infringement is the identification of source printer as it can be helpful for detecting forged documents and ascertaining the leak. Although a considerable amount of work has been done in forensic identification of natural images and videos originating from digital cameras, more work needs to be done in the forensic characterization of printed text documents, particularly those shared over social media.

This thesis is aimed at developing systems for identifying the source device of given multimedia, including a printed document, a camera-captured document image, or a natural image. A combination of handcrafted and data-driven features-based frameworks have been developed, and promising results are obtained to address many challenges in this field.

Title: Fiber Bragg grating sensor-based glove to accurately measure finger flexure
Researcher: Jha, Chandan Kumar (15350004)
Supervisor: Chakraborty, Arup Lal
Year: 2021
Keyword's: Heart Disease, Fiber Bragg Grating, FBG- Glove, Stroke, Apodized Gratings
Call No.: 681.25 JHA
Acc. No.: T00741

Abstract: Virtual reality (VR)-based interventions have gained huge research interest in the rehabilitation of the hand of stroke patients in recent years. A feature that provides VR with an edge over the traditional rehabilitation exercises is that the interaction of the patients with the VR environment can be recorded continuously and in real-time using multiple sensors. This recorded data can be used to quantitatively assess the quality of movement and the recovery progress made by the patients. It is, therefore, essential to develop accurate and reliable motion tracking systems that can be used to monitor hand function recovery during virtual rehabilitation. Although several such input systems have been developed, instrumented gloves have become an attractive option because they are more convenient to use and can track fine finger movements very precisely. Several instrumented gloves have been developed using various sensors such as the resistive flex sensors, the inertial measurement units (IMU) sensors, magnetic and optical sensors. However, these systems have significant limitations such as low accuracy and reliability, and complex calibration protocols, which makes them less suitable for clinical applications. Therefore, this thesis work proposes a fiber Bragg grating (FBG) sensor-based instrumented glove (FBG- Glove) that offers much better angular resolution, accuracy and reliability compared to the other gloves.

The work presented in this thesis can be broadly divided into three parts. In the first part, a cost-effective FBG interrogation system based on a narrow linewidth tunable distributed feedback (DFB) laser and a fiber-optic Mach-Zehnder interferometer for biomedical applications have been proposed. The technique proposed in this thesis aims to make the interrogation system cost-effective, battery-powered and wear-able without compromising the wavelength resolution and accuracy. A merit of the proposed system is that an optical spectrum analyser (OSA) that is prohibitively expensive is not required at any stage of development or use. The interrogation system offers a sub-picometer resolution of 0.47 pm. This system was used to interrogate the FBG sensors in the next part of the work.

In the second part of the work, an FBG-based flexure sensing mechanism that can measure finger flexure with very high accuracy and reliability is proposed. The sensing unit consists of an FBG that is very sensitive to axial strain induced by the flexing of fingers. The spectral shift of the reflection spectrum of the FBG varies linearly with the joint rotation angle, which makes calibration a fast and straightforward routine. The sensor offers a very high angular resolution of 0.1° with a very high sensitivity of $18.45 \text{ pm}/^\circ$. The accuracy evaluated using a mechanical setup, and the human hand was 0.13° and 0.67° , respectively. The FBG sensor showed excellent repeatability with a maximum standard deviation of 0.30° and 0.79° on a mechanical setup and the human hand, respectively. The

FBG sensor also exhibited much better dynamic response compared to the IMU up to a rotation speed of $80^\circ/\text{s}$.

In the third part, the design and evaluation of a complete and functional instrumented glove (FBG-Glove) developed using the FBG sensors is presented. The glove can measure the range of motion of the ten finger joints (five metacarpophalangeal, four proximal interphalangeal and one interphalangeal joint) simultaneously with a rate of 250 Hz. A Raspberry Pi-based module was also developed that interfaces the glove with custom VR games that run on an Android tablet or a VR headset. The accuracy and repeatability of all the ten sensors of the glove were tested and compared to an IMU sensor. The glove outperformed many earlier reported sensing gloves with a mean error of 0.81° . The standard deviation (1.01°) and range (2.60°) obtained in the reliability test performed on five healthy subjects was also smaller compared to many other gloves. These results strongly indicate that FBG sensors are potential option to develop instrumented gloves for clinical applications.

Title: Approximate designs and frameworks for error resilient applications
Researcher: Jha, Chandan Kumar (15350009)
Supervisor: Mekie, Joycee
Year: 2020
Keyword's: Error Resilient Applications, CMOS Logic, SEDA, Inexact Array Dividers
Call No.: 621.3 JHA
Acc. No.: T00742

Abstract: Error resilient applications related to recognition, mining and synthesis have enabled re- searchers with an additional dimension for optimization to obtain benefit in terms of area, delay, and power. Error resilient applications can produce acceptable quality outputs even after the introduction of approximation in data and/or computations. While a variety of works related to approximate computing exists, there are several gaps in using them for real-world applications, which we have attempted to fill in this thesis. We analyze the impact of approximating different bits in non-configurable approximate arithmetic circuits and find that they have limited scope, due to the need for exact circuits alongside them. This happens because an application has both exact and approximate sections. To circumvent this problem, we design configurable approximate integer arithmetic circuits such that they have minimal energy and performance overheads. These designs can be configured at runtime to switch between exact and approximate mode. We then identified that introducing configuration in floating-point arithmetic circuits outweighs the benefits of approximation and thus propose static floating-point approximate circuits. To support design automation with approximate computing, we also propose a unified framework that allows energy-quality tradeoff analysis for any circuit for a given application. Finally, apart from approximate compute, we also investigate approximating data for the energy-quality tradeoff.

In the context of non-configurable approximate integer circuits, we propose three approximate adders based on hybrid CMOS logic for integer addition and build a trace based framework for the analysis of error and energy consumption to evaluate the proposed adders. We have evaluated these adders for Moby benchmarks, a benchmark suite for evaluating mobile systems. We show that having an approximation in the carry-bit leads to errors in the most significant bit thus making it unsuitable for its use in processors. We then propose three approximate 16 by 8 restoring array dividers (IRADs). We have evaluated the proposed IRADs on three image processing applications using a similar trace-based framework developed in our prior work. We observed that the design which had the least approximation in borrow bits had the highest peak signal to noise ratio and structural similarity index values. Thus, from these two works, we observe that introducing approximation in carry bits and borrow bits is not ideal for the design of ap- proximate arithmetic circuits. The reason for this is that introduction of approximation in carry bits and borrow bits, even in the least significant bits, of the arithmetic circuits can cause errors in most significant bits.

Configurable approximate integer circuits are those that can be configured to perform exact or approximate compute dynamically during runtime. We propose two different set of configurable approximate adder designs. In a single exact single approximate (SESA) adder, we propose three fine-grained configurable approximate adders that can perform either single exact addition or single

approximate addition with limited overheads. In single exact dual approximate (SEDA), we propose a coarse-grained configurable approximate adder design that can perform either one-bit exact computation or two-bit approximate computation using the same hardware. We also propose SEDAAF, a design that enables SEDA functionality for FPGAs. For the same output quality each of these designs gives energy and performance benefits over exact counterparts.

Unlike integer arithmetic circuits, for floating-point arithmetic circuits we implement designs that are not configurable at runtime, as configurable approximate floating-point units have large energy-overheads, thus defeating the purpose of approximation. We propose both a floating-point approximate multiplier and divider which outperforms the state of the art approximate floating-point units in both energy and performance without much degradation in output quality. The proposed floating-point units also have a design methodology that allows users to systematically implement approximate designs with varying output quality. We evaluate the performance benefits of both image processing and neural network applications and show that the proposed designs outperform the state of the art approximate multipliers and dividers. We then propose a framework for the design space exploration of approximate circuits. The framework allows for the automated design space exploration to obtain a pareto-optimal design point for integer arithmetic circuits by using all approximation strategies in unison. We showed that our framework gives the most optimal design points as compared to the prior state of the art approximation frameworks. This framework helps us to further dive deep into the design of approximate circuits and perform comparisons with the state of the art approximation methodologies.

Apart from approximate compute, we have also investigated the effect of approximating data on output quality. We approximate data using temporal approximation i.e. the knowledge of input data distribution is exploited to obtain power delay product benefits. In temporal approximation, computations are skipped and past computed results are reused to save compute power at the cost of approximation. We first identified the data distribution which captures the worst case, i.e. the distribution which leads to the maximum degradation in output quality, for temporal approximation. We also showed that the knowledge of input data distribution can be exploited to obtain power delay product benefits in temporal approximation. Another place where we have applied data approximation is in DRAM channels. We propose an energy-efficient data encoding scheme for transferring the data over the DRAM channels. The proposed encoding scheme builds on top of the state of the art data encoding schemes for energy reduction. It reduces the energy of the data transferred over the DRAM channels. We also provide various knobs to control the amount of approximation. We analyze the proposed encoding scheme on a variety of machine learning applications to evaluate the trade-off between energy and output quality. We show that the proposed approximate encoding scheme, when used both during training and inferencing, can significantly improve the output quality.

In the context of emerging AI/ML workloads and multimedia applications, we envisage that the designs and tools proposed on approximate computing in the thesis will become even more relevant.

Title: Fast and low complexity adaptive signal processing algorithms for digital hearing aids
Researcher: Bhattacharjee, Sankha Subhra
Supervisor: George, Nithin V.
Year: 2020
Keyword's: Hearing Aids, Signal Processing, Signal Processing Algorithms, Nonlinear Active Noise Control (NANC)
Call No.: 621.38223 BHA
Acc. No.: T00743

Abstract: Currently, about 5% of people around the world suffer from one or another form of hearing loss. Hearing aids have emerged as the most common intervention to compensate for hearing loss. A basic digital hearing aid consists of one or more microphones, a loudspeaker, digital signal processing unit and a battery. In addition to amplifying the sounds based on the hearing profile of the user, the signal processing unit implements several algorithms including ones for feedback cancellation, noise reduction and dynamic range compression. The close proximity of the loudspeaker and the microphone(s) in a hearing aid leads to acoustic feedback, which deteriorates the quality of the processed sound produced by the hearing aid. The acoustic feedback path in a hearing aid usually has a sparse impulse response. In order to take advantage of this property of the acoustic path, this thesis proposes a class of feedback cancellation schemes which are sparse aware. The signal processing algorithms must adapt quickly to the changing environment of the hearing aid user to provide enhanced usability and hearing comfort. With this objective in mind, this thesis also proposes a set of adaptive algorithms to improve convergence and tracking performance. To further enhance the quality of feedback cancellation, a two-microphone feedback cancellation scheme based on a delay less multiband-structured subband adaptive filter has also been developed. Further, to reduce the deterioration of signal to noise ratio caused by leakage of unprocessed noise into the ear canal in an open fitting hearing aid, a low complexity integrated noise reduction and active noise cancellation algorithm has been proposed. Also, a set of nonlinear adaptive filtering schemes have been developed to deal with nonlinearities that may arise in a hearing aid.

Title: Designing photonic nanostructures for compact, high performance refractometric sensing
Researcher: Vyas, Hardik Shyam
Supervisor: Hegde, Ravi Sadananda
Year: 2021
Keyword's: Photonic Integrated Circuits, Limit of Detection (LOD), Localized Surface Plasmon Resonant (LSPR), Nanophotonic Sensing Element, Refractive Index Sensing
Call No.: 621.365 VYA
Acc. No.: T00744

Abstract: Optical sensors have shown promising capabilities in applications such as medical diagnostics, environmental monitoring, food safety, homeland security etc. In addition to being label free, such sensors exhibit high target specificity and immunity to electromagnetic interference. Despite these advantages, there are restrictions in their widespread adoption due to requirements of bulky interrogation setups and skilled personnel. In recent years, there is an interest towards compact optical sensing platforms with direct sample-to-answer capabilities along with multiplexed analyte detection. Photonic integrated circuits (PICs) are one of such promising platforms where the light source, readout and sensing element can be monolithically integrated. Alternatively, image sensor readouts directly integrated with sensing elements having topside illumination source can also serve as compact and high throughput sensors. In the last decade, there have been significant scientific advances in the field of nanophotonics. The incorporation of nanophotonic resonators as sensing elements can result in unprecedented sensitivity and low limit of detection (LoD). In particular, nanophotonics has the potential to make field-deployable, compact, high performance sensing a reality. This work includes theoretical and numerical investigation of novel nanophotonic resonators with the aim of realizing compactly interrogated refractometric sensors.

Modern PICs use high Q (quality factor) microphotonic resonators or interferometers for sensing application. However, the modal volume (V) of these structures are large which prevents lowering of their LoD. Incorporating individual localized surface plasmon resonant (LSPR) nanostructures into integrated photonics platforms could result in reduced LOD. The two key problems addressed in this thesis include: 1. Low Q in LSPR nanostructures (due to ohmic and radiation losses); and 2. Weak light coupling efficiency between the PIC waveguide and plasmonic nanoresonator. To solve problem 1, I proposed incorporation of a compound plasmonic nanoresonator in the integrated platform. In comparison with nanoresonators of simple shape, sensing elements based on compound nanoresonators are predicted to exhibit twice the sensitivity and figure of merit in both intensity and spectral shift based sensing modality. To solve problem 2, the waveguide is nanostructured to modify the mode profile and improve the amount of light coupled to the LSPR nanoantenna. The proposed waveguide configurations include high Q Fabry Perot resonant phase shifted Bragg grating and subwavelength gratings. In comparison with a strip waveguide, a 3-4 times improvement in coupling, 6-7 times improvement in intensity-shift sensitivity are predicted for the structured waveguide configurations. The proposed configurations are found to be robust to fabrication errors such as waveguide-nanoantenna misalignment, size dispersion. Additionally, they have low footprint $<70 \mu\text{m}^2$ which is considerably smaller than ring resonator or interferometer.

Thus, with nanostructuring, a highly sensitive, low LoD device can be realized with the possibility of compact readout based high throughput detection.

Several technical challenges exist related to other components in PIC sensors such as efficient on-chip light sources at visible wavelengths, on-chip spectrometry and rapid detection of ultra low volume analytes. In this context, there is a growing interest in another class of compact sensing platform consisting of free space interrogated nanophotonic resonators integrated with photodiode arrays or an imaging camera. Metasurfaces (array of sub-wavelength spaced nanophotonic resonators) have been investigated for the mentioned platform in the recent past. Plasmonic metasurfaces employing LSPR arrays possess low Q, thus broader linewidth, affecting their sensing performance. High Q can be obtained by using all-dielectric meta-surfaces exhibiting Mie resonances and guided mode resonances (GMRs). Although silicon has a high refractive index, high absorption losses at visible wavelengths lead to weak Mie resonances. Low contrast gratings (LCGs) exhibiting GMR possess high Q provided they have a large footprint (undesirable for high throughput detection) and thin profile (difficult to fabricate). In this work, I propose asymmetry-engineered silicon nitride based 1D dimerized medium contrast gratings (DMCGs) in aqueous background by perturbing the width and gap between the grating elements of a 1D MCG. Numerical studies predict the excitation of quasi-bound states in continuum (QBIC) resonances with typical Q of the order of 10^4 in the proposed structure for large footprints. Bulk and surface sensing results for the proposed asymmetrical gratings predict higher sensitivity, figure of merit (FOM) in the spectral and intensity modalities, particularly for high refractive index analyte detection. Followed by this, in view of realizing low footprint devices, the effect of reducing the grating lines on Q was studied. For a lateral device footprint of around $8\ \mu\text{m}$, Q of 735 was predicted for QBIC resonant gratings as compared to Q of 80 found in symmetrical gratings. To conclude, the proposed asymmetric 1D DMCGs show higher sensitivity than symmetric gratings at visible wavelengths. Besides this, they possess high Q even for smaller footprints, showing the possibility of high throughput detection. In this platform, a miniaturized sensor using LED sources and integrated photodiodes can be realized for monitoring intensity shifts in place of bulky light sources and spectrometers required to track spectral shifts at the output.

Title: Design, modelling and control of novel hybrid flux motor
Researcher: Balaganesh B.
Supervisor: Ragavan K.
Year: 2021
Keyword's: Hybrid Flux Motor, Hybrid Flux Motor Design, Soft Magnetic Composite, Hybrid Flux Motor Modelling, MATLAB
Call No.: 621.46 BAL
Acc. No.: T00941

Abstract: Advancement in the power electronic devices and magnetic core materials modify the design constraints of an electric motor. Electric traction application needs high power density drive for efficient operation. The electric motor used in the drive is to be operated at high frequency to achieve better power density, and it is to be designed with a large number of poles for direct-drive operation. Because of the geometrical decoupling between the magnetic and electric circuits, the transverse flux motor (TFM) is suitable for a large number of poles design. However, it operates at a low power factor, and the permanent magnets are underutilized in this motor. This research work is aimed to improve the magnet utilization of TFM by modifying its structure. In the first part of this thesis, a novel hybrid flux motor (HFM) topology with the soft magnetic composite (SMC) core design is proposed. For this topology, the magnetic flux is transverse in the stator core and longitudinal in the rotor core. Hence, it is called as hybrid flux motor (HFM-a combination of longitudinal and transverse flux topologies). The structure, working principle and design criteria of HFM are detailed. Comparative study is performed using the Finite Element Analysis (FEA) simulation. The HFM has 53% higher torque per magnet mass than that of TFM due to better permanent magnet utilization.

A manufacturable prototype design of HFM is given in the second part. In this design, the SMC is replaced with laminated silicon steel core. Numerical analysis of HFM is performed using magnetic equivalent circuit (MEC). A simplified Jacobian matrix is proposed for solving non-linear MEC. The MEC model of HFM is represented as a directed graph in MATLAB and it is solved using graph theory. The proposed simplified Jacobian method converges 17% faster than the conventional Jacobian method. The rotor movement is incorporated based on the interval theory. The induced EMF, average torque, and instantaneous torque are calculated from the solution of MEC. The results obtained by the MEC model are in good agreement with the FEA results.

The fabrication process of HFM prototype is detailed in the third part. Fabricated HFM prototype is coupled with a separately excited DC machine, and its EMF waveforms are captured at base speed. Per phase equivalent circuit parameters are determined. The dq-axis model of HFM phase stack is derived. In the dq-axis model, varying phase winding inductance is represented with constant inductances L_d and L_q . Both simulation and implementation of field-oriented control (FOC) of HFM are carried out in this thesis's final part. The design of current and speed controllers is explained. The controllers' transient behavior and stability are studied with the help of step response, root locus, and Bode plot. Different levels in implementing the FOC are detailed. The dynamics of current

and speed controllers are experimentally verified. The performance of HFM under various loading conditions is studied.

The comparative analysis done using FEA confirms the improved magnet utilization of HFM over TFM. The proposed simplified Jacobian method can improve the convergence speed of any non-linear MEC analysis. The working of the hybrid flux motor presented in this thesis has been successfully demonstrated. Future research would be on the design optimization of HFM, fabrication of HFM using soft magnetic composite core, comparison study with longitudinal flux motors, and sensorless operation of HFM speed control. The proposed HFM topology is suitable for low-speed high torque application and electric traction applications.

Title: Deep learning based representation, processing and inverse rendering of curves and surfaces
Researcher: Gangopadhyay, Aalok
Supervisor: Raman, Shanmuganathan
Year: 2023
Keyword's: Digital Images, Deconvolution, Image Processing, Deep Learning Framework
Call No.: 006.37 GAN
Acc. No.: T01015

Abstract: Numerous popular methods for processing, representing, and rendering shapes in visual computing are classical and leave the wealth of information in real-world datasets unutilized. Moreover, these existing methods involve subroutines that are not differentiable and thus unsuitable for gradient-based optimization techniques. In this thesis, we develop deep learning techniques for addressing problems in visual computing concerning curves and surfaces. We develop self-supervised deep learning frameworks for processing shapes and inverse rendering of shapes. We also develop differentiable rendering and differentiable representation techniques for shapes.

The following are the major contributions of this thesis:

- We design a self-supervised geometric deep learning framework for surface denoising.
- We address the human shape blending problem with unknown correspondences in a self-supervised geometric deep learning setting.
- We develop a self-supervised deep learning framework for solving the problem of curve extraction from line plots.
- We propose a differentiable representation of knots based on invertible neural networks and a differentiable rendering algorithm for rendering silhouettes of knot-based tubes.

Through results and experiments we demonstrate that deep learning based methods are effective for processing, representing and inverse rendering of shapes.

Title: Design improvements in two-phase switched reluctance motors
Researcher: Upadhyay, Parth Tarun
Supervisor: Ragavan K.
Year: 2023
Keyword's: Reluctance Motors, Switched Reluctance Motor (SRM), Electric Two-wheeler-SRM
Call No.: 621.46 UPA
Acc. No.: T01029

Abstract: This work aims to design a two-phase switched reluctance motor (SRM) exhibiting better electromagnetic performance. Two-phase SRM is suitable for high volume and low-cost applications. However, there are several challenges in terms of its performance. One such limitation is its on-load starting.

In the first part of this work, design modification of stator poles of a conventional two-phase SRM is proposed to achieve on-load starting in both directions. Stator poles are slanted in a particular direction at the pole tips. This creates a range of rotor positions where torque polarity is the same for both phases, so starting torque is available. A unique excitation scheme is also proposed to run the motor in a particular direction from any initial position. The sequence in which the two phases are excited and the duration of their first excitation decides the direction of continuous rotation. These changes are proposed for two specific stator-rotor pole number combinations. Hence, it becomes possible to use two-phase SRM in applications in which on-load starting is needed. Washing machine is selected as a potential application of the proposed work. Design parameters such as input voltage, rated current, and torque-speed characteristics are investigated to suit top-load washing machines. A 500 W, 4/6 two-phase SRM is designed and finite element analysis (FEA) based simulations are carried out in ANSYS Maxwell package. Relation between the slant angle of the stator pole tip and minimum starting torque is analyzed through parametric simulations. To validate the simulation results, the designed two-phase SRM is fabricated and experiments are performed. An incremental encoder is used for sensing rotor position. The proposed excitation scheme achieves on-load starting and rotation in both directions even though the initial position is not known.

In the second part of the work, initially a comparison is made between two-phase and three-phase SRM with regard to torque density. It is found that a two-phase motor offers an advantage over a three-phase motor. This is essentially because of the provision to accommodate more winding-turns. By utilizing this unique feature of two-phase SRM, a high-torque density design suitable for high-torque and low-speed application is proposed. Since there is a space constraint in two-wheel electric vehicles (EV), permanent magnet motors are widely used (due to high energy density magnets). Typically, those are brushless DC motors (BLDC). An attempt is made to explore the possibility of using SRM for such two-wheel EVs. It is possible if an high-torque density design of SRM is made. In line with this, a two-phase, 1.5 kW SRM is designed. With the aid of parametric FEA simulations, the design parameters are obtained. Key ratings of a commercially available BLDC motor used in a two-wheel EV are taken as reference in designing the two-phase SRM. The torque-speed profile of the two-phase SRM reveals its suitability for the two-wheel EV application.

From the contributions made in this work, it is believed that two-phase SRM could be considered as a potential candidate for low power and high torque density applications. Nevertheless, exhaustive research efforts are needed for exploiting the full potential of SRM. For instance, in EV applications, there is a need to operate the machine as a generator during regenerative braking. This would require the implementation of a complex control technique and this effort would be taken up in future.

Title: Nature-inspired techniques for nanophotonics inverse design
Researcher: Panda, Soumyashree S.
Supervisor: Hegde, Ravi Sadananda
Year: 2021
Keyword's: Nanophotonics, Nanotechnology, Diffractive Optical Neural
Call No.: 621.36 PAN
Acc. No.: T01047

Abstract: Nanophotonics, the study of light at the nanoscale, has become a vibrant field of research. A plethora of research showcase the use of metal/dielectric nanostructures to process light in fascinating ways (e.g. scattering, refraction, filtration etc.); other- wise impossible to achieve with classical geometries and materials. Such exquisite control over light has placed nano-photonics in a wide range of applications including integrated optics, optical computing, solar and medical technologies and many more. Thus high expectation has been set for novel discoveries in nano-photonics in the coming years.

In recent times metamaterials, specifically metasurfaces, have provided immense contributions to nanophotonics. Their electromagnetic characteristics are primarily governed by subwavelength structures in conjunction with surrounding media, resulting in the desired electromagnetic response and device functionality through structural engineering. The concept of the metasurface is realized by designing a 1D or 2D array of optical antennas (that function as scatterers) and engineering the light-matter interaction. In its most general form, the optical metasurface is a "surface-like" heterogeneous array of nanoresonators. Despite their promise, metasurface designs reported in the literature are still predominantly limited to ordered arrangements of primitive geometries; e.g., circular, elliptical, rectangular and cross-shaped nanopillars. With the current state-of-the-art nanofabrication facility, single or multi-layered wide-area patterning of optical antennae with unprecedented lateral resolution and stitching accuracy has been achieved. Metasurface design repertoire is slowly expanding to include complex geometries like polygon meta-atoms, free-form geometries, extended meta-atoms and volumetric structures. A wide choice of materials like plasmonic metals, high-index dielectrics, phase change materials and exotic 2D materials enhance the design possibilities even further. Although exciting, the high degree of freedom pertaining to such a vast design space of structures and materials makes the exploration difficult. Such high-dimensional explorations are extremely inefficient with simple parameter sweeps. The problem with high dimensionality is only exacerbated when multiple goals are considered, or non-linear constraints are applied to the input parameters. This necessitates the use of novel computational techniques in design parameter exploration. Inverse design, a functionality-driven structure discovery approach, uses optimization algorithms to directly follow the functionality surface. In other words, the functionalities and properties are declared by the user first and the algorithm searches for geometries or configurations to achieve them. Search algorithms like evolutionary optimizations (follow a set of rules inspired by biological evolution), swarm optimizations (follow the movement of a swarm of biological entities) etc. have been proven to learn the structure-functionality landscape efficiently; there- fore they require fewer configuration explorations. The

use of Deep Neural Networks (DNN), which mimics the learning ability of the brain, has made inverse design faster and computationally efficient. As the workflows of these inverse design algorithms are galvanized by natural phenomena, they fall under the bracket of 'nature-inspired computing (NIC)'. The thesis aspires to use these nature-inspired computing techniques to inverse design metasurfaces for achieving target functionalities. The key problems in evolutionary algorithm-based inverse designing of complex metasurface geometries, as identified in the thesis, are as follows: (1) Lack of parametric encoding methodology in the design repertoire that can represent a huge number of shapes; (2) Absence of evolutionary framework that takes lithographic perturbation related imperfection into consideration and designs robust metasurfaces. The thesis deals with the first problem by proposing a polygonal encoding methodology, where each structure is represented as a polygon and is encoded by the polar coordinates of its vertices. Polygon metasurface geometries designed by following these approaches are reported showing an improvement over their primitive counterparts under the same material platform. The second problem is addressed by evaluating a geometry along with its perturbed variants and minimizing the variance due to perturbation. On the second front, the thesis emphasizes exploring a more informative partial-fraction set of perturbed cases (determined by Taguchi's orthogonal array method) which statistically represent the full-factorial corner cases of perturbed geometries. Devices designed with this robust framework are observed to show less sensitivity to lithographic inaccuracies. The DNN-assisted inverse design of metasurfaces has been explored extensively in the last decade. However, the literature lacks the inclusion of workflow prior to the DNN model creation; i.e. encoding of DNN inputs and outputs, sampling strategies and choice of network architectures. This thesis aspires to address those lacking by providing a systematic framework for the creation of DNN-based prediction models to predict the optical characteristics from metasurface geometries. Through extensive statistical comparisons, we show the efficacy of smart encoding and sampling strategies assisted by network architectures with better learning ability; especially in cases where training data is not abundant. Later, these DNN models are implemented as surrogates to accelerate the evolutionary algorithm-based inverse design. An extension of inverse design is the emulation of Diffractive Optical Neural-network (DON) emulated on software. The network is built by cascading diffractive layers with the weights being channelized in the amplitude and phases of the constituent diffractive elements. The network weights are optimized by training the emulated model (in-situ training) and are later downloaded to the hardware. However, the emulation does not provide an exact picture of the wave propagating through the hardware system as the faults and noises pertaining to the constituent diffractive elements are needed to be considered. The thesis aims to not only analyze the faults and noises in the device performance but also provide robust in-situ training regimens like (fault/noise injection and fault/noise regularization) to ameliorate their effect on device performance.

To conclude, the thesis provides a broader perspective on the inverse design of metasurfaces with an emphasis on complex geometries in a perturbation-tolerant design framework. It aspires to show an improved, efficient and robust workflow in nanophotonics inverse designing. All the source codes and datasets associated with the research carried out are open-sourced and are provided in Appendix-I. Owing to the universality of the high-dimensional solution space search requirement,

we feel that the work carried out in this thesis will be helpful to all scientific inverse design communities.

Title: Indigenous technology development of high-voltage MOS transistors for power management applications
Researcher: Kaushal, Kumari Neeraj
Supervisor: Mohapatra, Nihar Ranjan
Year: 2023
Keyword's: Transistors, Integrated Circuits, High Voltage MOS (HVMOS)
Call No.: 621.381528 KAU
Acc. No.: T01079

Abstract: India is one of the largest markets for electronic equipment such as portable devices, consumer and automotive electronics. To draw power, these devices rely on Power Management Integrated Circuits (PMICs). In modern PMICs, various devices digital, analog and high-voltage/high-power transistors are integrated monolithically on the same substrate in order to reduce the overall system cost. This requires a Bipolar-CMOS-DMOS (BCD) technology platform that can offer a wide range of voltages with higher performance. The market for PMICs in India is forecasted to increase in coming years on account of continuously increasing production and sales of electronics goods. However, the Indian industries are facing a particular challenge i.e. lack of indigenous semiconductor manufacturing base and lack of availability of an indigenous high-voltage CMOS technology. The only strategic CMOS fab, SemiConductor Laboratory (SCL), at Mohali, Chandigarh, India has 180nm CMOS technology. But, it only supports voltage up to 5V.

In this thesis, we have developed a cost-effective methodology to fabricate High- Voltage MOS (HVMOS) transistors with voltage handling capability up to 40V. We have designed a unique process flow by augmenting existing 180nm CMOS processes (at SCL) with minimum additional steps. Note that the Figures-of-Merit (FoM) of a HVMOS transistor are high breakdown voltage at low on-resistance, better switching characteristics and good device reliability. However, the inherent trade-offs associated with device design and contrasting requirements for different electrical specifications, often complicate the design process, which necessitates careful device design and innovative solutions. As part of this work, detailed TCAD simulations are performed to decide the device architecture and additional process steps for different high-voltage devices. Innovative solutions like Channel Doping Gradient (CDG) and Source Underlap (SU), are used to improve HVMOS transistor on-state performance without degrading their off-state characteristics.

The designed devices are then fabricated at SCL facility and characterized at IIT Gandhinagar. The fabricated devices are also tested for long-term reliability by performing detailed Hot Carrier Induced (HCI) degradation measurements. For design enablement, a PDK (Process Design Kit) with compact models is developed. The industry-standard HiSIM-HV2 model is used as a framework and the anomalous device effects (specific to HVMOS transistors) are also captured through physics-

based models. The robustness of the models and PDK is verified by designing few HVMOS transistor based circuits. Finally, the behavior of developed HVMOS devices in cryogenic temperature range ($T < 123\text{K}$) is experimentally investigated. We have shown that carrier freeze-out and field-assisted ionization in the drift region are critical to high-voltage MOS behavior at cryogenic temperatures. The HiSIM-HV2 model is then augmented with new model equations to extend the model accuracy in the 77-300 K temperature range.

The work done in this thesis is a pure technology development work and the first technology development (in INDIA) of HVMOS devices in INDIA. The deliverables from this work are highly relevant to industries and academia.

Title: Robust and sparse-aware adaptive learning strategies for audio signal processing
Researcher: Kumar, Krishna
Supervisor: George, Nithin V.
Year: 2022
Keyword's: Audio Signal Processing, Adaptive Filters-champernowne, Logistic Distance Metric Adaptive Filter (LDMAF)
Call No.: 621.3822 KUM
Acc. No.: T01080

Abstract: Conventional adaptive signal processing algorithms, based on a mean square error-based cost function, are not robust to strong disturbances picked up by the error sensor. This thesis proposes a class of robust adaptive signal processing algorithms to overcome this limitation. One of them is a class of adaptive algorithms based on a modified Champernowne function. The new Champernowne adaptive filter (CMAF) has been shown to provide robust behaviour in a system identification scenario. Further, an arctangent cost function framework has been proposed, which can create robust algorithms for adaptive filtering by embedding a standard cost function into the arctangent framework. In order to take advantage of the sparse nature of system impulse responses when used in a system identification application, robust, sparse-aware algorithms have been developed. A generalized modified Blake-Zisserman (GMBZ) robust cost function has been introduced, and the corresponding robust, as well as robust and sparse-aware adaptive filtering schemes have been developed. This is followed by the design of signal processing algorithms for audio applications such as active noise control and acoustic echo cancellation. This includes the filtered-x exponential hyperbolic cosine adaptive filter (FxEHCAF) and algorithms based on a logistic distance metric.

* * * * *



HUMANITIES AND SOCIAL SCIENCES

Humanities and Social Sciences

Title: Role of attentional scope on altruistic decisions
Researcher: Mukherjee, Sumitava
Supervisor: Manjaly, Jaison A.
Year: 2013
Keyword's: Attentional Broadening, Charitable Donations, Social Behavior Socio-economic Backgrounds
Call No.: 153 MUK
Acc. No.: T00048

Abstract: Understanding the cognitive mechanisms involved in altruistic decisions could enable us to better comprehend complex social interactions and also help us achieve a larger social gain. I sought to identify domain-generic mechanisms that could underlie charitable donation and investigated how content-free processing style linked with scope of attention influence altruistic decision. Attention is an important cognitive process that can influence a variety of behavior including prosociality. Most previous studies are based on effects of the presence (or lack) of attention using the framework of attention as a resource. Comparatively, there has been hardly any work on how differences in scope of attention could influence altruistic decisions. The overall hypothesis of the thesis was that since global processing is linked with eager approach orientations, love, compassions, an interdependent-self model and widening of one's thought-action repertoire; it should increase altruistic behavior. Five studies were performed to investigate how attentional scope influence altruistic decisions. Study 1 and 2 experimentally manipulated scope of attention and found that priming a broad scope of attention using a global processing style increases propensity to donate money for poor children. Study 3 found that global processing leads to increased allocation towards charities whose appeal is framed in an approach orientation compared to appeals framed in an avoidance orientation. In study 4, even when socio-economic backgrounds were matched, global processing lead to more donations in an anonymous economic game among students. Study 5, showed that real-world motivational states like love and hunger which is linked with global and local processing respectively, influence donations in predictable ways.

This thesis conclusively shows that attentional mechanisms play important role in decision making. Specifically, it adds to the literature on attentional scope and perceptual processing styles by showing for the first time, global-local processing styles can influence altruistic decisions. One of the important contributions of this thesis is that some seemingly unrelated previous studies on donations and pro-social behavior can possible by seen in light of the domain-generic global-local processing framework. After discussing some limitations of these studies, I conclude with a model of attentional broadening and highlight possible applications to other fields.

Title: Role of sensory prediction on perceptual and motor mechanisms
Researcher: Kumar, Neeraj
Supervisor: Manjaly, Jaison A.
Year: 2014
Keyword's: Limb State Estimation, Motor Adaptation, Cognitive Processes, Error Monitoring
Call No.: 153 KUM
Acc. No.: T00049

Abstract: The ability to interact with the environment through action is an essential aspect of human existence. Predication of sensory action outcome allows us to optimally influence and manipulate the environment for a meaningful interaction. Four studies were performed to investigate the role of predication on limb state estimation, sense of agency, attentional selection, and perceptual decision mechanisms. In study 1, prediction was updated by both relevant and irrelevant predication error in a visuomotor adaptation task. Results showed the altered perceptual estimate of limb position after adaptation. Results suggest that somatosensory mechanisms use the predictions about the sensory consequences of movement commands and do not rely solely on the information provided by the sensory systems. Study 2 manipulated the feedback about the action performed and found that error monitoring mechanisms evoked through feedback recalibrate the prediction in real time and optimize the sense of self- agency. Study 3 investigated the role of predication on attentional selection mechanisms by employing irrelevant feature singleton paradigm of visual search. Feature singleton was either presented as results of an action or it appeared automatically. Results suggest that singleton captures attention when preceded by action. It suggests that predication could be considered as a third factor apart from top-down goals and bottom-up features of the stimulus which determines how attention is allocated to the environment. Study 4 investigated how updating sensory predictions through motor adaptation influences perceptual processing and subsequent decisions based on the outcome of those perceptual processes in a visual search task. Results demonstrate the strong influence of adaptation and updating of predictive mechanism that adaptation entails on perception and decisions based on perceptual processing. Perceptual decisions can be clearly modified by manipulating the relationship between movement commands and their sensory consequences, and the degree of the modification may depend on how strongly the adapted state is reinforced. This thesis provides a holistic perspective about the contribution of prediction in various cognitive processes. It also provides conclusive and novel evidence to supports the hypothesis that cognition emerges out of our interaction with the world.

Title: Uses of heritage in Ahmedabad's global self-fashioning
Researcher: Thomas, Pooja Susan
Supervisor: Kothari, Rita
Year: 2015
Keyword's: Ahmedabad, Global City, Global Capital, Signifying Gandhi, What is ahmedabad?, Self-fashioning, Bhadra Fort, Walled City
Call No.: 954.75 THO
Acc. No.: T00092

Abstract: In the last decade and a half, increased consciousness around Ahmedabad, commercial capital of Gujarat and the region's largest city, has centered on its projection as an important node in the network of global capital. To bolster its claim as an aspiring global city, the discourse around the city's heritage has been deployed to increase Ahmedabad's cultural attractiveness and indicate its global capability. However heritage sites also of the accretion of history. Even has heritage sites are used to mediate the image of the city. They are points of intersection of symbolic and cultural reuse, narratives of belonging and identity, discursive sites, they enable an unravelling of Ahmedabad's aspirational self-fashioning and a deconstruction of its projected global city image. Within this framework, I look at Ahmedabad's self-fashioning as a global city from three sites of heritage. These three sites of heritage. These locations or sites of heritages are Gandhi Ashram at Sabaramati, Bhadra Fort precincts and Sarkhej Roza. They connote the centers and peripheries of Ahmedabad's global city projection and spell out its symbolic spatial bounds. The Ashram reminds of Mahatma Gandhi's choice of Ahmedabad as his political headquarters thereby naming Ahmedabad to world. Through the Gandhi Ashram, I examine the ways the imagination of Ahmedabad's urban future draws legitimacy from an interpretation of Gandhian mythopoesis. I show how through spatial gestures of proximity of Gandhi's ideals, the aesthetics of Ahmedabad's contemporary transformation is sought to be validated. The redevelopment of Bhadra Fort precincts represents such transformation. The Bhadra Fort precincts is the city's symbolic and historical core. However, over the years, the in and around the Bhadra Fort, known as the walled city, have come to be marked by congestion and residential decline. The transformation and development of the Bhadra precincts have been envisaged in a redevelopment project monitored by Ahmedabad's municipal corporation and the Archeological Survey of India. I explore how it produces norms of belonging through the figure of the desired pedestrian. These norms of belonging are intuitively recognized by those that the spatial histories of Ahmedabad have forced to its peripheries. Sarkhej Roza, the mausoleum complex of Ganj Baksh Khattu, signifies those peripheries of Ahmedabad that many Muslims fled to in the wake of communal violence. At the same time, it signifies the centrality of Sarkhej to the foundational history of Ahmedabad that is not forgotten. I examine narratives of revival and rediscovery of the Sarkhej Roza that argue for the monument's relevance to the city's cultural and syncretic memory. I show that in the intersection with recent interest in developing these sub-urban areas, such narratives of revival and rediscovery mediate norms of claiming rightful presence in Ahmedabad's global city-space. Thus, even as these sites of heritage are used to fashion Ahmedabad for a global audience, I use these sites to unravel and deconstruct the processes of the

city's self-fashioning, the implications of norms of belonging and the aesthetics of its global transformation.

Title: Gender politics and Indian children's literature: a comparative analysis of adventure fiction in English and Gujarati
Researcher: Vyas, Diti Pundrik
Supervisor: Lahiri, Sharmita & Mathur, Suchitra
Year: 2015
Keyword's: Literary Split, Children's Literature, Materialist Feminist Approach, Regional Language Literature
Call No.: 890.0954 VYA
Acc. No.: T00094

Abstract: Gender emerges as a recurrent theme in debates about contesting merits of Indian Writing in English (IWE) and regional language literature (RLL) becoming a pivot that splits them along "progressive" versus "traditional", "parochial" versus "cosmopolitan" binaries. This thesis investigates if this literary split is mirrored in Indian children's literature through a comparative study of Indian children's literature in English (ICLE) and children's literature in Gujarati (CLG). It uses materialist feminist approach to unmask the operations of power, focuses on literature post critically hailed watershed of 1990 and looks at the dominant genre of adventure. Several locations where such gender politics are seen to be operational such as representation of femininity and masculinity, and the narrative structure of adventure genre are examined as is the intersection of gender with hegemonic structures such as caste, class and community. The conclusions reveal that hegemonic conception of gender invoked through "parochial" and "traditional", and its non-hegemonic aspect referred to in "progressive" and "cosmopolitan" are present in both ICLE and CLG, while differences emerge in how hegemonic norms are upheld or interrogated. Texts adhering to the wide spectrum of hegemonic masculinity defined by R.W. Connell exist in both ICLE and CLG alongside those that challenge these definitions using strategies from inversion to reconfiguration. Similarly, texts that embed hegemonic notions of femininity in both ICLE and CLG stand side by side those that attempt feminist revision using strategies from gender role reversal to gender-mix. Hegemonically gendered ICLE and CLG texts endorsing patriarchal conventions and definitions of the quest plot and resorting to patriarchal structuring, spatial and temporal politics, co-exist with non-hegemonically gendered ones re-gendering, redefining, reframing or rupturing these conventions. While these similarities in gender politics undermine the IWE/RLL split, feminist intersectional analysis of gender with other parameters, partially reverses its association. Though ICLE and CLG construct gendered anti-minority community stereotypes and "savarnize" the women's question, CLG seems more progressive in questioning intersectional class and gender hierarchies and projecting alternative dalit masculinity. These complex conclusions undermine the literary split between IWE/RLL and underline the relevance of studying children's literature through a dialogue with mainstream criticism.

Title: And a world between them: cosmopolitanism in select narratives of south Asia
Researcher: Mukherjee, Payel Chattopadhyay
Supervisor: Rath, Arnapurna
Year: 2016
Keyword's: Social Sciences Socratic School of Thought, Immanuel Kant's Cosmopolitanism, Discourse To Dialogue, Global Nodes, Polity To Proletariat, Polis Cosmopolis
Call No.: 954 MUK
Acc. No.: T00104

Abstract: Cosmopolitanism as a philosophical concept vulnerably lies “lost in translation” between academic jargons and the difficulties of practicing it in the everydayness of life. This thesis presents an analytical study of the term “cosmopolitanism” and opens the complex dialogical relationships that it shares with the cultural philosophical and literary trajectories. The term opens rich critical and creative interpretations that overlap across academic disciplines. The first part of the thesis initiates an exhaustive study of the conceptualization of the term in the western philosophical traditions. The approach is to closely analyze cosmopolitanism connecting itself to the ideas of the individual, the polis, and the world. Our analysis starts from the Socratic school of thought with emphasis on the freedom of knowledge; continuing through Immanuel Kant's cosmopolitanism, to the contemporary debates surrounding the ideas of thinkers like Martha Nussbaum, Arjun Appaduraj, and Walter Dignolo. Further, we attempt to challenge the stereotypes associated with western scholarship by opening the possibilities of experiencing cosmopolitanism in lived human spaces through the thought threads of Rabindranath Tagore, Sri Aurobindo and Mikhail Bakhtin. The purpose is to underscore the idea that cosmopolitanism is a pervasive concept that has mattered to thinkers across time and space. We envision cosmopolitanism as a way to acknowledge the non-similar and the heterogeneous terrains of human thoughts. In the second part of thesis, we extend the theoretical idea of cosmopolitanism initiated in the first part to the praxis of the contemporary South Asia literary context. We explore cosmopolitanism in select literary representations of the South Asian cities of India, Pakistan, and Bangladesh. The analysis is through three different matrices of; (a) transactional cosmopolitanism (b) cosmopolitanism-national, and (c) dialogical cosmopolitanism. In Suketu Metha's *Maximum City* (2004), we focus on understanding cosmopolitanism through transactions in the marketplace of Bombay. Further, with a close reading of Amit Chaudhuri's *A Strange and Sublime Address* (1991) and *Calcutta: Two Years in City* (2013), we focus on the emergence of the cosmopolitanism-national as an individual who is at home with world. In chapter nine of the thesis with a focus on the cities of Karachi and Dhaka, we creatively understand “dialogical cosmopolitanism” with characters like Alice in Mohammed Hanif's *Our Lady of Alice Bhatti* (2011) and Masud in Adib Khan's *Spiral Road* (2007). These individuals negotiate between the “roots” and the “routes” of emerging global narrative and continuing local histories. To conclude, cosmopolitanism in the contemporary world survives with the “aesthetics of hope” and opens a possibility of imagining “a world between them” through dialogues.

Title: Context sensitive computational mechanisms of decision-making
Researcher: Chawla, Manisha
Supervisor: Miyapuram, Krishna Prasad
Year: 2018
Keyword's: Drift Diffusion Models, Reinforcement Learning, Stimulus Values, Decision-making
Call No.: 153 CHA
Acc. No.: T00271

Abstract: In everyday life, we encounter many situations in which we need to make decisions that are often repetitive in nature. The process of decision-making involves at least two steps - we need to first represent the various alternatives and then compute the value of these alternatives. Given that both our perception and valuation is influenced by the surrounding context, we are interested to know how context influences the process of decision-making. Contexts can be manifested in two different ways - Spatial context refers to the value of other simultaneously available options whereas temporal context is the relative valuation of outcomes experienced across time. A general mechanism for decision-making can be understood by the notion of 'common currency' where the comparisons of various competing alternatives can be made over the same relative scale. We investigate the integration of reward information with perceptual decisions in conjunction with computational modelling to understand the various subcomponents of a decision process. In a two-alternative forced choice experiment, spatial context attaches differential reward values with the two alternatives; hence we call them as choice values. The value information in spatial context is presented as symmetric or asymmetric rewards, which in turn influences decision process in different ways. The temporal context refers to differential outcomes across multiple trials that we refer as stimulus values. By manipulating the processing order temporally between reward values and perceptual stimuli, we dissociate the mechanisms underlying the stimulus encoding stage and the response execution stage. We used drift diffusion models to estimate parameters that encode the evidence accumulation process for perceptual judgments that could be influenced by integration with reward values. We extend the evidence accumulation approach to value-based decision making in a new task setting that studies choice exploration as a sequential sampling process. A novel particle filter based reinforcement learning model is used for studying the dynamic evolution of decision parameters in value-based decisions. Neural correlates of integration of value and perceptual information are studied using two complementary approaches. EEG (electrical recordings from the scalp) provides a good temporal resolution to study the dynamics of integration process, and using meta-analysis of brain imaging studies, we aim at consistent and specific brain regions participating in different types of decision making. By studying the contextual influences, we have proposed and established that the valuation process involves prior information based on temporal context, and the simultaneously available information in spatial context determines the choice. Overall, our findings have suggested the fundamental processes involved by which an individual integrates multiple sources of information to arrive at a decision.

Title: Automatic and controlled processes in temporal selection
Researcher: Singh, Divita
Supervisor: Sunny, Meera M.
Year: 2018
Keyword's: Rapid Serial Visual Presentation Paradigm (RSVP), Emotional Arousal, Emotional Valence
Call No.: 153.4 SIN
Acc. No.: T00272

Abstract: One major challenge for a human information processing system is limiting the amount of information it has to process at any given point in time. Selective attentional mechanism plays a key role in ensuring the efficiency of this system. The control of attentional selection is typically understood to be implemented by a dynamic combination of top-down as well as bottom-up processes. There has been a significant research effort to understand this dynamics for attentional processing at spatial and featural level. However, relatively less is known about how top-down and bottom-up factors contribute to the control of attentional selection over time. This thesis employs Rapid Serial Visual Presentation Paradigm (RSVP) and the theoretical models provided by Attentional Blink (AB) and Emotion Induced Blindness (EIB) studies to understand the relative contribution of top-down and bottom-up factors in temporal selection. The thesis reports sixteen experiments, organized into five empirical chapters, and investigates, how different aspects of top-down and bottom-up attentional control determine temporal selection.

Study 1 examined the role of emotional arousal and emotional valence in EIB and showed that EIB is more affected by the changes in the arousal level of the emotional image as compared to the changes in its emotional valence. Study 2 investigated the relative contribution of emotion and attention in EIB and showed that EIB is not an emotion-specific effect rather a consequence of attention capture by the irrelevant emotional distractor. Study 3 follows up on the findings of the study 2 and showed a similar level of impairment for neutral distractor that captured attention and discredits the view that EIB is an emotion specific effect.

Study 4 examined the underlying mechanism of Lag-1 sparing and showed that working memory requirement associated with the stimulus identification plays a crucial role in the presence of Lag-1 sparing. Study 5 examined the role of saliency in temporal attention and how the strength of the signal leads to the attenuation of the impairment in AB. Result did not show any blink for both emotional as well as perceptual salient information; this shows that featural properties of the information presented in the RSVP determine the temporal limits of attention. The present thesis contributes to the current theoretical understanding of the temporal attention by providing novel findings of how automatic and control processes modulate information processing.

Title: Three essays in aging and intergenerational relationship: social capital, family dynamics and transnational arrangements
Researcher: Gangopadhyay, Jagriti
Supervisor: Samanta, Tannishtha
Year: 2018
Keyword's: Intergenerational Relations, Family Relationship Aging, Social Capital, Intergenerational Relationships
Call No.: 305.26 GAN
Acc. No.: T00277

Abstract: Population aging is gradually becoming a concern for both the developed and the developing nations. Demographic forces such as increasing life expectancy and rapidly falling fertility rates are contributing to a growing bulge in the age group of 60 and above. This global aging has the potential to transform economies and trade, migration, disease burdens and social relations, all very significantly. In this India is no exception. In fact, projections suggest that India's older adult population (60 and above) will rise from 8% in 2010 (~ 60 million) to 19% in 2050 (approximately 300 million) (UNESA, 2009; Census of India, 2011). This demographic bulge of older adults is growing at a time when India is also experiencing significant shifts in family structures, security provisions and social policies. Demographic work on population aging in India has often focused on issues relating to family structure, health outcomes and living arrangements. Despite this focus on the Indian family, an in-depth study of the complex dialectic of intergenerational relationships is often missing from the gerontological literature. Against the background of this gap, this dissertation adopts a socio-gerontological lens and studies the complex interactions of family and intergenerational relationships in Ahmedabad, India. As a corollary to studying intergenerational dynamics and family ties, this dissertation examines questions of social capital, non-familial ties and older adult wellbeing in elder care institutions (more commonly known as old age homes). This is particularly useful as India is undergoing dramatic transformations in family structure marked by a gradual, but steady, movement away from multigenerational settings to the individual, the market and the state - these being the emerging sites of aging and elder care. Finally, this dissertation engages in a cross-cultural and comparative interrogation of filial expectations, network ties, (transnational) identity and cultural meanings of religion and death in two transitional cities of Ahmedabad (India) and Saskatoon (Canada).

This dissertation project lies at the intellectual interface of gerontology and family sociology. Ever since gerontology's evolution as a scientific field of study, it has been repeatedly criticized for being a-theoretical with a dominant focus on amassing large datasets and for remaining practice-oriented, or as Bengtson and colleagues (1997) aptly describe, "data rich but theory poor". Subsequently, despite a large and an impressive array of topics covered by scholars, Indian gerontology remains highly empirical with an (unintended) neglect of theory use and advancement. This neglect has

motivated the present research and thus, a conscious effort has been directed in infusing theory with empirical observations from the field.

The thesis is organized as follows. The first essay (Chapter II), examines change and continuity of intergenerational relationships in joint families of Ahmedabad city. In particular, the study borrows from the social constructionist framework of gerontology in order to interpret individual processes of aging. Within this framework, the dissertation adopts one of the earlier theories in sociology of aging, the Disengagement Theory (Cumming and Henry, 1961) which suggests a gradual withdrawal of the older person from social roles and an overall personal decline. Though the Disengagement Theory has often been criticized for its poor empirical fit and its deterministic approach in explaining human behavior, this dissertation revisits this theory for its semblance with the process of growing old in India. By doing so, this study shows that though old age in India is marked by a gradual disengagement as a way of preparing for death - this process of withdrawal reconfigures intra-familial relationships in complex ways. Moving on, this dissertation also examines intergenerational relationships against the backdrop of shifting social and economic realities as well as that of changing attitude towards the aged. Another dominant theoretical framework - the Conflict-Solidarity-Ambivalence Model (Bengtson and Schrader, 1982; Bengtson and Roberts, 1991; Bengtson and Achenbaum, 1993; Bengtson et al, 1997; Bengtson, 2001) has been utilized to examine how older adults in urban settings navigate their later lives in joint households. Findings from the first essay demonstrates the changing nature of intergenerational relationships in Indian joint families.

In Chapter III, this dissertation adopts a Social Exchange perspective (Dowd, 1975) so as to understand how older adults in institutional settings (more commonly known as old age homes) adapt to these non-traditional sources of care and support. The analysis of the interviews with the residents of elder care institutions suggest a tension between compulsive self-care and an idealized way of growing old that emphasizes on bodily and social detachment. The findings also show that these elder care institutions, under the garb of discipline and safety regulation, often restrict outings and overall mobility. This restriction is often disproportionately directed towards older women. The study further highlights the role of social norms and how that translates to social control, creating different social realities for older men and women. Overall, this part of the dissertation highlights the remarkable continuity of patriarchal ideology along the life course while investigating questions of roles, mobility and support.

In Chapter IV, questions that lie at the intersection of normative roles, intergenerational relationships and the social process of growing old are all examined in the transnational context. This essay draws from the Successful Aging model (Rowe and Kahn, 1997) to understand the process of growing old in Saskatoon. The Successful Aging model suggests that lack of physical disability and high cognitive functioning are the main components to age successfully (Rowe and Kahn, 1997). Building on this model, this chapter shows how perceptions of aging, caregiving expectations and intergenerational relationships are shaped in Saskatoon (Canada).

In Chapter V, this exercise on utilizing competing models to understand the process and experience of growing old is further advanced when a comparative framework is also adopted to reflect on the commonalities and parallels between the two contextually dissimilar settings (Ahmedabad and Saskatoon). Specifically, two contrary micro perspectives of gerontology -Disengagement Theory and Successful Aging model are utilized to understand the (differing) cultural notions of death, role continuity, filial expectations and identity formation through the everyday experience of growing old. Significantly, the role of context and the associated normative culture is shown to be deeply influencing this experience. In this final chapter (Chapter V) the dissertation also focuses on the intersection of age and gender- that is it examines how gender roles and expectations around household autonomy and mobility differ not only between men and women but also within women living in two different cultural contexts. In the process this chapter offers reflection on the paradoxical relationship between religion and everyday construction of old age in both the cities.

The methodology adopted for all the three substantive studies involves utilizing a pre-tested and pre-determined semi-structured questionnaire and in-depth narrative style interviews to capture the perceptions of older adults as well as the co-resident adult offspring, wherever possible. Sampling method has been non-statistical; primarily snowball sampling given the nature of the questions and the overall study design.

Overall, by closely examining the complex interplay of intergenerational relationships, family dynamics and social norms with age, the dissertation hopes to expand the gerontological knowledge to understand the future of aging as a lived experience as opposed to an empirical exercise of population numbers. As a related contribution, the dissertation opens up areas of intellectual investigations that lie at the intersection of family sociology and gerontology.

Title: Texts and traditions in seventeenth century Goa: reading cultural translation sacredness and transformation in the *Kristapurana* of Thomas Stephens S. J.
Researcher: Royson, Annie Rachel
Supervisor: Rath, Arnapurna
Year: 2018
Keyword's: Cultural Translation, Transformation, Roman Script, Biblical, Puranic
Call No.: 300.87 ROY
Acc. No.: T00399

Abstract: The thesis entitled “Texts and Traditions in Seventeenth Century Goa: Reading Cultural Translation, Sacredness, and Transformation in the *Kristapurāṇa* of Thomas Stephens S.J.” is a critical study of *Kristapurāṇa* (1616), a missionary composition from seventeenth century Goa. Thomas Stephens’s translation of the biblical narrative into Marathi is one of the earliest printed works in South Asia. In this thesis, Stephens’s magnum opus, *Kristapurāṇa*, is studied as a work of cultural translation. The concept of “cultural translation” is itself examined through this reading. A study of *Kristapurāṇa* highlights the interplay of diverse textual traditions in the text and the methods that early missionaries adopted to negotiate through the complexities of cultural encounters. The meeting between Christianity and ancient sacred traditions that existed in colonial centres such as Portuguese Goa gave rise to novel translation “strategies”. The purpose of these strategies was to convince the masses regarding the significance of Christianity and also to negotiate the stringent regulations laid down by the Church.

Stephens’s transformation from a traveller to a poet-priest-translator is treated as key to understanding the cultural translation undertaken in *Kristapurāṇa*. The language of the text and the Roman script in which it was first printed are significant in understanding the socio-political background against which Stephens’s text was composed. The thesis is also an attempt to understand how early Christian texts in South Asia travelled, with *Kristapurāṇa* as the epicentre for analysis.

In *Kristapurāṇa*, Stephens made use of the purānic genre to negotiate the spaces between Christianity and Hinduism. As a part of this thesis, an attempt has been made to close-read the purānic genre in the light of the text. Stephens chose to call his composition a “*Purāna*”, placing it firmly within the tradition of purānic texts and the conventions of sacredness attached to the tradition by the locals. He negotiated two sacred textual traditions—the biblical and the purānic—adding to the intricacies of his translatorial enterprise. A close reading of select passages from the text demonstrates how both the biblical narrative and the genre of Purānas are transformed in this process of translation. In this context, a strand of this thesis analyses the novelization of the purānic genre in the light of *Kristapurāṇa*. In addition to these aspects, Stephens’s text opens a site that reveals the centrality of landscapes in the colonial enterprise, the fascination with distant geographies, and the transformation of the physical and cultural landscapes of conquered regions. The vast deserts, tropical gardens, and desolate cities in this narrative reveal a constant process of travel across space and time. A reading of landscapes in this text brings to light the ways in which Stephens’s landscapes were a (re)invention of the topology in which the locals could position their

memories and traditions. Landscape is treated as an aspect of cultural translation in the context of *Kristapurāṇa*.

Travel, transformation, genre, and landscapes are the lenses through which the concept of cultural translation has been approached. The anxieties faced by both the translator and the “translated” in the process of grappling with the “sacred” are important concerns of this study. In this thesis, select verses from *Kristapurāṇa* have been translated into English as a part of critically engaging with the text. Of the ten thousand nine hundred and sixty-two verses of *Kristapurāṇa*, the passages selected for translation are meant to bring out the nuances of the text and to contribute to the conceptual arguments put forward by this thesis. The transformations and (re)creations that occur when sacred texts and traditions undergo cultural translation are highlighted in the present reading of *Kristapurāṇa*.

Title: Translation as reflective praxis: three narratives from twentieth century Gujarat
Researcher: Shah, Krupa
Supervisor: Kothari, Rita
Year: 2018
Keyword's: Culture Studies, Twentieth Century, Gujarat literature, Khemi
Call No.: 300.86 SHA
Acc. No.: T00400

Abstract: Although the practice of translation has always existed, the emergence of translation studies as a discipline in the last quarter of the twentieth century is a recent phenomenon. Its emergence has shown most prominently, the need to understand translation not as a corollary to literature, nor as a transparent means of access nor even as a cultural bridge but instead as a significant and influential factor in cultural and textual relationships, in processes of canonisation and in the politics of selection, representation and intervention. The conceptual shifts that characterise the brief history of translation studies have drawn extensively from interdisciplinary approaches and domains as varied as linguistics, anthropology, culture studies, post colonialism, and feminism. This dissertation is historically grounded in twentieth century Gujarat and brings under the lens of translation three canonical short stories from the decades 1920s-1950 in Gujarati literature. It advances a notion of translation as a form of reflective praxis that enables a critical reading of literature and the various polysystemic contexts it straddles. These contexts are shaped out of what I consider 'well- intentioned' discourses of change, compassion, valour, and sacrifice in the period. The critical act of translating makes this archive available and also facilitates its discursive readings.

The short story itself as a form is chosen because of its emergence as an important social genre in the decades of the early twentieth century that foregrounded many of the narratives taken up in this thesis. The first chapter provides a broad literature review of important theoretical leaps in the discipline of translation studies and its many turns and goes on to locate my own approach and use of translation as a mode of critical reading in the way that it makes available the stories that I translate from Gujarati into English. I argue that translation as a mode of reflective praxis enables making these texts available but also makes it possible to read around them.

The second chapter is centred on the translation and analysis of a well- known Gujarati short story about untouchability "Khemi", written by Ramnarayan Vishwanath Pathak (1887-1955) in the late 1920s. In this chapter, I contextualise the historical discourses that underpin Khemi such as processes of naming and framing untouchability that began in the early decades of the twentieth century, Gandhi's influential position on untouchability and also go on to perform a close reading of various instances of the text and its strategies of representing the 'untouchable' in language. These examinations also enable me to explore meaningful linkages between translation and untouchability and the way that translation provides insight into the language of caste. The third chapter examines another important narrative through a medieval folk story "Hothal" that circulated in various parts of Western India and was compiled and published in a twentieth century collection of folk tales called *Saurashtrani Rasdhar* (1923-27) by Kathiawadi writer Jhaverchand Meghani (1896-1947).

The story of Hothal evokes, as many other narratives of a similar kind, the pride in region, in continuities of heroism and valour, and the integral relation between social identities and folk tales in Saurashtra. The fourth chapter looks at another celebrated story “Dariyav Dil” (The Bounteous Heart) by writer Vinodini Neelkanth (1907-1987) and examines its narratives of extraordinary moral greatness and feminine generosity that imagined and posited women’s psyches in a particular way that became for several generations of readers and viewers, a hallmark of laudable womanly behaviour. The popularity and the acclaim that such a narrative garnered calls for a critical rethinking and a rereading of the text that is made possible through a translational lens. In providing the canonical archive, but also readings around the canon, translation in this thesis is both the body and the ways of seeing the body of this literature. By translating the canon, it also sometimes disrupts canonical readings.

Title: Nature of hand-centric visuo-spatial processing differences for objects in the peripersonal space
Researcher: Thomas, Tony
Supervisor: Sunny, Meera M.
Year: 2018
Keyword's: Hand-proximity Effect, Singleton, Peri-hand Space, Spatial Arrangement
Call No.: 153 THO
Acc. No.: T00508

Abstract: Hands provide critical inputs that are essential for the multisensory integration of stimuli that are in the graspable space. Previous studies have shown that objects that are present in this space are processed differently compared to objects in the space that are beyond the graspable space. Previous studies have also shown these differences irrespective of any intention to act upon them, implying that these effects are not subject to voluntary control. In the present thesis, I report ten experiments organized into four empirical chapters examining issues of stimulus specificity and automaticity associated with visual processing in the peri-hand space. Paradigms used to study questions of control and automaticity of visual selection offer methodologies that are useful in testing these questions. Moreover, past studies have tried to theorize attentional processing differences in the peri-hand space. The present thesis builds on these foundations and extends the questions about the understanding of visual perception and attentional mechanisms in the space near the hands. In Chapter 1, I pit the existing explanations of the hand-proximity effect on attentional processing, namely perceptual prioritization account and slower disengagement account against each other. That is, the speeds of pre-attentive and attentional mechanisms for the targets appearing near the hand were compared to those for targets appearing relatively farther away and also compared against a baseline no-hand condition. Results showed faster pre-attentive processing of targets appearing near the hand compared to the far and the no-hand conditions. In contrast, the attentional processes seemed to be slower for objects near the hand compared to objects farther away. The findings suggest dissociable effects of hand-proximity on perceptual and attentional mechanisms. In Chapter 2, we followed up on the Modulated Visual Pathway (MVP) hypothesis (Gozli, West & Pratt, 2012) of hand-proximity. MVP proposes processing biases mediated by the magnocellular and parvocellular pathways for stimuli presented in the near and far regions of space of the hand, respectively. In Chapter 2, the role of relevance of the motion and color features was looked-at in the manifestation of hand-proximity effect. In four experiments the type of feature singleton as well as the probability of the feature singleton being the target was manipulated. The results showed hand proximity biasing attentional allocation to the feature singleton only when the feature singleton was irrelevant to the search task. Also, the relative distance of the hand from the feature singleton seemed critical for the feature specificity of the effect to be observed clearly. Chapter 3 tested the automaticity involved in the manifestation of the hand-proximity effect, by changing top- down factors and bringing in more predictability to the task setting. Results of Chapter3 highlighted the sensitivity of hand- related effects to the spatial arrangement of search items. When the search display had items presented either only near the hand or only far away from the hand, hand-proximity effects were eliminated, suggesting that the processing difference for

objects in the far space is not independent of items in the near- space. Similarly, presenting the display in a predictable configuration also removed hand-proximity effects. The set of findings questions the automaticity associated with hand-related effect, highlighting its dependence on situational factors.

Chapter 4 aims to look at the visual processing effects associated with performing a goal-oriented reach movement. Performance in the action condition was compared with a static hand condition and a baseline no-hand condition. An action-specific reduction in both keypress RT and saccade latency was obtained for targets presented in the absence of distractors as compared to both static and baseline conditions. Presence of distractors resulted in an interference effect only in the dynamic hand condition, highlighting the effects of the organization of motor resources associated with performing an action on visual processing. Overall, the current thesis highlights how the hands play an important role in interactions with the environment, by looking at how hand position and making reach movements influence the visual processing of proximal compared to distal objects. More importantly, it illustrates the conditions under which the hand proximity effect is seen and also demonstrates the limits of hand proximity in modulating visual processing. The thesis proposes that visual and motor systems partner each other, forming a functional unit, to properly engage with the environment.

Title: Exploring the affective consequences of creative tasks
Researcher: Mehta, Krishnesh S.
Supervisor: Manjaly, Jaison A.
Year: 2019
Keyword's: Creativity, Self-control, Pro-sociality, Holistic Perspective
Call No.: 153.35 MEH
Acc. No.: T00519

Abstract: Creativity is one of the most intriguing of human capabilities and an enigmatic facet of human brain and cognition. Creativity is usually considered a positive trait that promotes benevolent activities and is generally positive for the creator. However, recently some studies have started showing the unintentional negative consequences of creativity (e.g. depression, dishonesty, reduced integrity, narcissism, addictive behaviours, etc.) that can be detrimental to the creator as well as the society. From the literature review, it was found that the negative consequences of creativity are similar to those observed after the impaired self-control, reduced empathy and pro-sociality, and a narrow attentional breadth or local processing. Seven studies were performed using a combination of the interrogative, observational, correlational, subjective experiential account, and experimentation to explore the role that the self-control and the related factors play in modulating the creative task-induced affect/affective states leading to the positive or the negative affective consequences. In Study 1, we investigated what kinds of affect the participants reported while performing a creative task and found that while all the participants approached the task in their unique ways, all faced affective vulnerability provocations during the various stages of the task. Study 2 carried out an ethnography/design ethnography inspired qualitative research using semi-structured interviews and correlational participative observation of the participants from a design background to understand their feelings and the mental states and the possible triggers that may lead them to the affective vulnerabilities. Study 2 found that during the creative task performance, there might be about seven moments of affective vulnerability arousals/triggers that may lead to affective consequences. At these times, the interplay of the personality and situational pressures may decide the subsequent behaviour. Study 3 explored the influence of the creative task on self-control and found a significant decrement of self-control after a creative task. Perhaps that is the most crucial factor in producing the affective consequences. Study 4 explored the impact of the creative task on the juror severity and found that the creative activity might preferentially significantly reduce the severity shown towards crimes that are desirable, even if illegal. Thus, reinforcing the findings of the previous study. Study 5 explored the influence of the creative task on empathy on two separate groups from a design background and one additional group from the non-design background and found that the empathy was significantly reduced in the design groups after the creative task. No such effect was seen in the non-design group, which agrees with the prior research. Study 6 explored the influence of the creative task on pro-sociality using the Dictator (giving only) format and found that after the creative task participants kept a more significant sum of money for themselves suggestive of reduced pro-sociality, which can result due to the reduced self-control. Study 7 explored the impact of the creative task on the global/local processing and found no significant bias towards any specific processing, thus showing that cognitive processing

may not be directly interacting with the affective consequences. However, the affective processes might likely be modulating the cognitive processes. Previous studies have shown that the self-control strength impacts empathy, juror severity, pro-sociality, and global/local processing, and here we found that the creative task might impact self-control. This thesis provides a holistic perspective through the correlational combination of the subjective experiential and the experimental studies on the probable reasons for the affective consequences induced during or after the creative task. The thesis provides novel evidence that self-control strength might be one of the significant factors modulating the affective consequences after the creative task and opens up future research on the role of Executive functions in the consequent behaviours after the creative tasks.

Title: Critique of the conceptualization of sense of agency in experimental paradigms
Researcher: Reddy, Nagireddy Neelakanteswar
Supervisor: Manjaly, Jaison A.
Year: 2020
Keyword's: Cognitive Penetration, Sensory Attenuation, Epistemic, Operationalized Implicit SoA, Explicit SoA
Call No.: 153.7 RED
Acc. No.: T00522

Abstract: The Sense of agency (SoA) as conceived in experimental paradigms adheres to “cognitive penetration” and “cognitive phenomenology.” Cognitive penetrability is the assumption that agency states penetrate sensory modalities like time perception – the Intentional binding (IB) hypothesis – and auditory, visual and tactile perceptions – the Sensory attenuation (SA) hypothesis. Cognitive phenomenology, on the other hand, assumes that agency states are perceptual or experiential that are akin to sensory states. I critically examine these operationalizations and argue that the SoA is a judgment effect rather than a perceptual/phenomenal state. My thesis criticizes the experimentally operationalized implicit SoA (in chapter 2), explicit SoA (in chapter 3) and cue-integrated SoA (in chapter 4) by arguing that: (a) There is uncertainty in the SoA experimental operationalization (making the participants prone to judgment effects); (b) There are inconsistencies and incoherence between different findings and reports in the SoA domain; (c) The SoA reports are influenced by prior as well as online-generated beliefs (under uncertainty); (d) The SoA operationalizations had inaccuracy or approximation standard for measuring perception/experience of agency; (e) Under certainty and accuracy standard (for perception), the SoA (biased or nonveridical) reports might not have occurred at all; and (f) Reported inconsistencies and, the effects of beliefs can be parsimoniously accounted by compositionality nature of judgment. Thus, my thesis concludes that SoA reports are not instances of feelings/perceptions but are judgments.

Title: Caste-coded city: mobility and marginalization in the space politics of Ahmedabad
Researcher: Banerjee, Dyotana
Supervisor: Mehta, Mona G.
Year: 2019
Keyword's: Post-liberalization, Spatial Politics, Ahmedabad, Dalit Politics, Caste Oppression
Call No.: 305.5 BAN
Acc. No.: T00544

Abstract: The dissertation examines how caste operates as one of the principal axes of urban political economy of post-liberalization Ahmedabad. It uses an ethnographic study to capture the major shifts and continuities in the cultural and political production of two distinct kinds of pre and post-liberalization Dalit neighbourhoods in Ahmedabad. Highlighting the politics of identity, aspiration, resistance and marginalization in Dalit engagement with the urban spaces of Ahmedabad, the dissertation situates these local forms of spatial politics against the backdrop of urban political economy in post-liberalization India. It argues that greater economic mobility associated with rapid urbanization produces increasingly homogenous and exclusionary spaces in terms of class within caste and vice versa. In Ahmedabad, middle class and working class Dalit identities are articulated, materially and discursively, through a range of socio-cultural dispositions that are embedded within the dominant Hindutva politics of the state. The emergent Dalit politics and spaces draw on and simultaneously reconstitute hegemonic norms of aesthetics, political aspirations and contestations that reveal the complexities of the urban-caste nexus. The dissertation largely draws from the theoretical understanding on spatial reorganization of social relations in the urban political economy by Henry Lefebvre, Manuel Castell and David Harvey.

One of the chapters of the dissertation focuses on how the role of caste is both masked and intensified in the formation of new neighbourhoods in the backdrop of city-remaking projects. What are the mechanisms by which inter-caste (between upper castes and Dalits) and intra-Dalit exclusion get produced in emergent middle-class neighbourhoods? It analyzes the processes that underpin the migration of Dalit communities from Ahmedabad's old industrial centres such as Gomtipur to the emergent neighbourhood of Chandkheda in the city's periphery. The movement of relatively affluent upwardly mobile Dalits from poor Gomtipur to the more 'desirable' Chandkheda, where crores of rupees are being invested in real-estate development of middle-class neighbourhoods is riddled with many contradictions. I argue that the migration to and emergence of an exclusively Dalit middle-class section within the greater region of Chandkheda cannot be understood entirely in terms of 'aspiration', 'assertion' and 'passing' of an underprivileged caste. Economic capital provides the entry ticket for Dalits into Chandkheda, but mobility within the locality remains firmly circumscribed by caste, resulting in residential pockets that are not only exclusively for Dalits but meticulously segregated around Dalit sub-castes.

Another chapter investigates the making and remaking of Dalit working class neighbourhoods in the city. Gomtipur and Dani Limda are two of the many workers' neighbourhoods developed in the industrial belt of Ahmedabad in response to the textile mill industrialization in the early twentieth

century. Today Gomtipur and Dani Limda are spaces that are simultaneously inter-communal and Dalit working class where Dalit working class identity is profoundly shaped by its interface with its Muslims residents. This is an increasingly rare occurrence within Ahmedabad's otherwise intensely segregated religion-cohered neighbourhoods. This study critiques the existing academic scholarship that echoes the popular middle class rhetoric of the mill area being a hotbed of communal politics. The existing scholarship on Ahmedabad largely insists on looking at this space through the lens of Hindu-Muslim conflict. This study explores, instead, other crucial aspects of post-mill working class Dalit identity such as - shared feeling of exclusion from the post-liberalization urban imageries of a 'megacity', the tag that Ahmedabad officially acquired in 2005, Dalit and Muslim economic competition and, a specific space and class based subjectivity rather than a predominantly communal identity.

The final part of the study examines how urban and peri-urban spaces are used to design, perpetrate and normalize caste-based violence by specifically referring to the incident of public flogging of tanners by cow vigilantes in the Una district of Saurashtra in Gujarat in July, 2016. The protest led by Rashtriya Dalit Adhikar Manch (RDAM) (translated as National Dalits rights forum) in response to this incidence of caste violence foregrounds the aspirations, anxieties and assertions of Dalit youth that are closely connected to the urban. This part of the study asks: why did an event of caste atrocity in rural Gujarat trigger protest mobilizations by Dalit-Bahujan youth in urban spaces like never before? How did Jignesh Mevani, an almost novice in politics, become the face of Dalit churning in urban Gujarat and what is his support base like? I argue that RDAM unleashes a sense of a collective or a 'team', as the RDAM members put it, that makes the processes of 'un-hiding' of a new brand of Dalit political self possible, for the aspirational urban Dalit youth. Through its engagement with the urban and digital, the youth seem to position themselves on a Dalit platform that seems, as my ethnographic inquiry reveals, 'cool' and 'attractive' to participate in. The process of 'unhiding' needs to be understood in the context of an often common defence mechanism among urban Dalits against caste discrimination where they change their surnames or hide caste identity under a caste neutral surname.

Title: Contextual factors in moral judgment and decision making
Researcher: Sahai, Abhishek
Supervisor: Manjaly, Jaison A.
Year: 2020
Keyword's: Moral Decisions, Economic Context, Utilitarian, Deontology, Moral/Material Value, Moral/Material Cost, Decision Speed
Call No.: 153.4 SAH
Acc. No.: T00553

Abstract: Morality refers to codes of conduct prescribed by society, state, or religion. Over the ages, morality has served an important functional role in the social lives of people, often guiding the distinction between right and wrong, permissible and impermissible, and justice and interpersonal expectations. Moral situations produce 'victims' and 'agents.' An agent is the perpetrator of 'action' while a victim is the recipient of the agent's action. The nature of the interaction between a victim and an agent determines the perceived morality of the action. If action is 'personal' through 'physical contact' the action is deemed to be immoral, whereas deemed morally permissible. If the agent helps the victim at 'personal material cost' the action is deemed moral, while if an agent harms the victim for 'personal material gain' the action is deemed immoral. If the decision to act was 'quick' indicating little evaluation or 'slow' indicating comparatively detailed evaluation process. However, most of this research has been studied in decision silos, and little research has been conducted to understand how contextual factors modulate moral decisions and their judgments. In this thesis, I hypothesized that contextual factors, specifically economic context will influence moral decisions and judgments. I investigated this hypothesis in 3 studies and found that, first, proceeding economic decisions increase the probability of utilitarian choices in tragic moral scenarios. Second, I found that economic inequality increases the probability of trading-off moral value against the economic value in deprived individuals. Third, I found that the economic status of the moral/immoral agent influences the judgment of character by observers.

Title: Decisions under risk: factors affecting descriptive choices
Researcher: Goyal, Shruti
Supervisor: Miyapuram, Krishna Prasad
Year: 2020
Keyword's: Discriminability, Probability weighting, Loss aversion, Prospect Theory, Gain loss asymmetry, Framing
Call No.: 153.4 GOY
Acc. No.: T00555

Abstract: The current thesis is an attempt to understand the decision making process under uncertainty. Uncertainty refers to scenarios where the outcome associated with an action is not known for sure. Uncertainty is generally studied in terms of risk for research purposes where probabilities associated with events can be calculated. However, the existing literature has mainly focused on descriptive scenarios ignoring the experiences associated with the decisions. The current thesis adds to the literature by investigating scenarios where both experience and description are available to the decision maker. This thesis further investigates the role of emotional experience on descriptive choices. We further looked into the factors that can diminish the effect of experience on descriptive choices. Framing as a possible moderating factor was manipulated to examine its effect on choices. Lastly, effects of initial information were investigated on loss aversion. Findings support the current debate on the loss aversion with arguments against general loss aversion. Choices under mixed uncertain scenarios that contain both gain and loss were studied to understand gain-loss asymmetry.

These investigations lead to the following findings, firstly, predictions of prospect theory hold true on Asian (Indian) population with more intense results in the gain domain. Secondly, feedback provided on descriptive choices influence probability estimation, specifically attractiveness, reversing the usual overweighting of small probabilities to underweighting. Thirdly, providing positive emotional feedback on the zero outcomes in gain domain moderates the effect of feedback on descriptive choices under risk. Emotional feedback does not work for loss domain. Fourthly, framing zero outcome as loss moderates the effect of feedback on descriptive choices under risk in gain domain but framing the zero outcome as gain does not influences choices in loss domain. Lastly, initial information acts as a reference point and directs gain-loss asymmetry either to the direction of loss aversion or symmetry, depending upon the starting point. Findings provide empirical support for the value construction account of loss aversion. The thesis concludes with suggesting a feedback module in the belief- based account of descriptive choices.

Title: Towards the design of multi-user virtual reality based interactive social communication platform for individuals with autism and its implications on eye-gaze
Researcher: Pradeep Raj K. B.
Supervisor: Lahiri, Uttama
Year: 2019
Keyword's: Autism Spectrum Disorder, Intervention Services, Behavioral Intervention Program, Technology-Assisted Platforms, Eye Tracking Technology
Call No.: 155.6 RAJ
Acc. No.: T00557

Abstract: Autism Spectrum Disorder (ASD) is a complex neurodevelopmental disorder characterized by impairments in social communication, reciprocity and understanding the preferences of social partners that can be critical during collaborative task execution. Given the deficits characterizing ASD along with high prevalence of ASD (about 1 in 69 children in India being diagnosed), easy access to appropriate intervention services is critical. However, in countries like India, specialized observation-based conventional intervention services are available only in selected urban pockets. This demands emphasis on carrying out deeper exploration into designing platforms that can make effective intervention services accessible to these individuals. There is consensus that an intensive and structured behavioral intervention program targeting the core deficits in communication skills while considering various social aspects can mitigate some of the difficulties faced by the individuals with ASD. This can possibly result in long term benefits for the target population by bringing positive outcomes in terms of improved social communication and interaction skills.

The conventional observation-based intervention techniques practiced by skilled therapists have been reported to be potent in bringing about such positive outcomes. Additionally, given the heterogeneous nature of the Autism Spectrum, offering an individualized service is essential for the intervention to be effective and this is practiced by trained therapists in conventional intervention settings. However, the limitations such as lack of availability of adequately trained therapists and the exorbitant costs in availing such services can make such intervention inaccessible for the common man. These challenges call for alternative solution in which the technology-assisted platforms can play a significant role in delivering more accessible, intensive, quantified and individualized services. Researchers have been investigating the use of technology-assisted platforms such as computer based Virtual Reality (VR) and robotic technologies in providing intervention services to the individuals with ASD. With the rapid progress in computer graphics, it is argued that the computer- based VR technology can be harnessed to provide effective intervention for individuals with ASD. In our current research, we have used computer-based VR technology, due to its flexibility in design, avenue to develop controlled and interactive 3D virtual environments that can project subtle nuances related with various real-life social situations in the form of audio-visual presentation which can be both entertaining and informative for the children with ASD. Also, using VR, we have manipulated some of the social aspects such as proximity and eye-gaze of a virtual character (avatar) serving as a communicator or facilitator.

Further, to facilitate the intervention process, the VR-based system needs to have an ability to obtain quantitative estimates on the affective states of each individual that might offer useful information to therapists. This is important, since the individuals with ASD often demonstrate difficulties in making explicit expression of their affective states in social situations. The VR-based system can be equipped with mechanisms that can tap into one's affective state using some of the implicit cues while being exposed to simulated social situations having varying challenges. One of the ways can be through monitoring one's gaze-related physiology and behavioral looking pattern while individuals interact using the VR-based platform which can be achieved by augmenting the platform with eye tracking technology. In our current research, we have augmented the VR-based social communication platform with eye tracking technology.

While such exploration into the social communication aspects of children with ASD using single-user (single participant with ASD interacting with avatar) VR-based platforms is important, investigation of VR-based social communication skill training using multi-user platforms (multiple participants with ASD interacting with each other using the training platform) is also critical. This is because, instead of interacting with an avatar (simulated character) individually, the multi-user platform will necessitate the multiple individuals with ASD to interact with each other (using the VR platform). Thus, each individual would be expected to put himself/herself into the shoes of the partner while understanding each other's preference on a topic of interest before reciprocating. This is one of the core difficulties faced by individuals with ASD. Thus, training these children to overcome such difficulties is necessary so as to foster fluid interpersonal social communication, essential for healthy community living.

In my present research, a multi-user VR-based environment was designed as an interactive platform where multiple participants interacted with each other while executing a collaborative task having shared goals. Additionally, one of the important components (that are missing in the currently available systems) during social interaction is to promote the participants to understand each other's preference on a topic of interest while collaboratively executing a task. The multi-user VR environment (developed in my work) can offer a facility to foster interaction among multiple users/players through appropriate reciprocation while understanding each other's preference on a topic of interest thereby helping in successful collaborative execution of a task. The task required them (multiple users or players) to jointly frame (while deploying interaction strategy based on understanding of each other's preference) a cohesive story by collating glimpses of social situations presented in front of them on a computer-based canvas. Once they completed a task, an avatar (facilitator) empowered by an intelligent engine was tuned to narrate the story framed by knitting the glimpses of the social situations as chosen by the players. Here we used the story narration, since evidences from literature show the potential of short social stories (in VR-based scenarios) in imparting social communication skills in individuals with ASD. The avatars followed social norms as far as proximity and eye gaze were concerned while narrating the stories. Usability studies were conducted by recruiting participants with ASD and TD to investigate the potential of both single-user and multi-user VR-based social communication platforms augmented with eye tracking technology.

Results indicated the acceptability of such platforms by the target population. Additionally, the results of the usability studies show (i) the implications of social aspects such as communicator's proximity and eye-gaze on one's task performance and gaze-related indices during the VR-based task, (ii) the potential of gaze-related behavioral and physiological indices in characterizing individuals with ASD and their TD counterparts, (iii) the potential of VR-based multi-user task platform to empower participants with ASD to perform better within the simulated world (and outside the VR-based environment) and (iv) the underlying linkage between the collaborative performance capability and their gaze-related behavioral indices.

We hope that using such a VR-based technology can help in fostering effective social communication and interaction skills in individuals with ASD. Also, this can serve as a complementary tool in the hands of the therapists involved in Autism intervention. We believe that the novel technology-assisted VR-based multi user social communication platform promoting mutual understanding of each other's preference (as developed in the present research) can pave a milestone towards offering comprehensive social skill training thereby contributing to the improvement in the community living of our target population.

Title: Law, crime and justice towards an understanding of criminal justice in colonial Assam, 1826-1905
Researcher: Bharadwaj, Jahnu
Supervisor: Sengupta, Madhumita
Year: 2020
Keyword's: Colonial Regime, Uniform And Universal, Political And Legal Ideology, Annexation, Administrative and Judicial Organizations
Call No.: 345 BHA
Acc. No.: T00560

Abstract: How law operates has always been a subject close to my heart, right from the time I had started taking an interest in history as a discipline. Two works, which I had read during my school days, influenced me greatly. The first one was Agatha Christie's *The Witness for the Prosecution* and the other was Benudhar Sharma's biographical work titled, *Maniram Dewan*. I have henceforth been a keen follower of how trials are conducted and verdicts delivered. I have been an avid reader of prominent verdicts as well as of case histories. It was this interest in court cases that perhaps germinated into an idea of working on the history of criminal law in colonial Assam. Contemplating a doctoral thesis on the history of law, without any formal training in law, was perhaps an ambitious plan and surely indicated my naivette. Yet, now that the project is almost completed, I must admit that it has been an immensely satisfactory journey for me. The archival research that I have undertaken during the course of my doctoral study, has been the most difficult, and yet, the most memorable episode in the last few years of my life. The sheer joy of finding a relevant source of information in a sea of archival documents, that sets you off on a trail towards something fruitful, can be the most exciting aspect of archival research, and this is known to only those who visit the archives. I have been very lucky as there have been occasions when I could use the archive meaningfully. However, there were also occasions when the archive restricted me by its erasures or increased my confusion by deliberately misleading me, and those were the occasions when I realized the limitations of a colonial archive. I was led towards alternate sources and I must admit that I found a wealth of information lying for me in vernacular literature. I may not have been able to do justice to all that I found, and I claim full responsibility for lapses if any. Overall, however, the project has been an immensely enriching and absorbing one that kept me engrossed for all of the five years that I took to complete the work.

Title: Social determinants of menstrual health: a mixed-methods study among Indian adolescent girls and boys
Researcher: Gundi, Mukta
Supervisor: Subramanyam, Malavika A.
Year: 2020
Keyword's: Socioeconomic Inclusivity, Social Construction Of Menstruation, Public Health Research, Gender, Public Health
Call No.: 362.1 GUN
Acc. No.: T00561

Abstract: Several studies on menstruation conducted among adolescent girls in India highlight that these girls face several menstrual taboos and restrictions in their daily lives, often impacting their health-related outcomes. Studies from different parts of India also specify that various socioeconomic (SE) factors, such as household wealth or quality of neighborhoods, can influence girls' menstrual health outcomes. Nevertheless, significant knowledge gaps remain concerning the menstrual health outcomes of Indian girls, particularly as there seems to be a dearth of mixed-methods studies on menstrual health that are gender and SE inclusive. Indeed, the intricate ways in which menstruation is understood by boys as well as girls, potential SE patterns in adolescents' social construction of menstruation, and various pathways through which menstruation-related knowledge, beliefs and other health-related outcomes are affected remain unaddressed. In this thesis, we address three such important pathways that address the latter knowledge gaps. The first pathway that we explore concerns knowledge gaps regarding menstruation-related interpersonal (IP) communication between adolescent girls and boys. The nuances and social patterns in IP communication on menstruation remain understudied as public health research frequently views health communication as an information dissemination strategy, thus neglecting the intricacies involved in interpersonal communication regarding a culturally taboo topic. As several studies show a close linkage between communication and health outcomes, it is imperative to understand if adolescents' menstruation-related communication experience (or a lack of it) is unequally patterned and whether and how it impacts the knowledge, beliefs and menstrual health outcomes among girls and boys similarly/differently.

The second pathway that is explored in this thesis explores how gender, through its micro-interactive and macro-structural levels, makes menstruation a gendered experience for boys as well as girls. Although previous scholarship has investigated how gender creates unequal sexual and reproductive health outcomes, to our knowledge, no studies in the Indian context have explored how the social experience of being a boy/a girl puts one at an advantage or a disadvantage to possess knowledge and favorable beliefs regarding menstruation. Additionally, we also explore how a gendered experience of menstruation among girls in different social institutions such as family, school and community is influenced by girls' SE background and, concomitantly, how the gendered experience of menstruation influences girls' menstrual health.

The third pathway that we explore in this study attempts to look at the SE patterning in boys' understanding and experiences regarding menstruation. We, thus, examine the complexity in the need of involving and engaging boys by looking at the sub-population of boys as a heterogeneous entity with existing social patterning in their menstruation-related understanding, beliefs and attitudes.

We draw from the theoretical lenses of social constructionist approach and the social determinants of health framework to address these three knowledge gaps using a social epidemiological perspective.

Title: Interlimb generalization of newly learned motor skills
Researcher: Yadav, Goldy
Supervisor: Mutha, Pratik
Year: 2021
Keyword's: Motor Skills, Neuronal Plasticity, Motor Adaptation, Interlimb Transfer, Ipsilateral Hemisphere
Call No.: 153.4 YAD
Acc. No.: T00705

Abstract: The ability to learn and execute a variety of movements, ranging from complex dance forms to martial arts, is a hallmark of human behaviour. This capacity has been studied using two approaches: motor adaptation and motor skill learning. Motor adaptation requires modification of motor output to account for externally applied perturbations, and is thought to be driven by updating an internal forward model of the relationship between motor commands and their sensory consequences (Krakauer and Mazzoni, 2011; Morehead et al., 2017). In contrast, skill learning evolves as a practice-mediated ability to overcome performance-limiting relationships such as the speed accuracy trade-off, and can be characterized by improved acuity, reduction in trial-to-trial variability, offline gains and adoption of new control policies (Dayan and Cohen, 2011; Shmuelof et al., 2012; Telgen et al., 2014). Understanding how learning generalizes or transfers to unpracticed conditions can provide a deeper understanding of the underlying learning mechanisms. In this context, generalization of motor adaptation within and across effectors has been widely investigated. Most of this work has confirmed substantial intra and interlimb generalization, although its direction and magnitude are strongly influenced by task constraints. However, generalization of newly acquired motor skills remains poorly understood. The empirical work presented in this dissertation is aimed at understanding mechanistic features of motor skill learning and its generalization across limbs, and also tries to probe the neural basis of certain effects seen with such generalization in healthy young adults.

Our first study (Chapter 2) investigates the directionality of generalization of newly acquired skilled movements across the right and left arms. Right-handed individuals (n=58) used their right or left arm to train on a task that required them to move fast and accurately at the same time, thus overcoming the typical speed- accuracy trade-off. Generalization, or transfer, was characterized by comparing naïve performance of an arm to its performance following training of the opposite arm. We observed robust and symmetric interlimb transfer across the arms in contrast to an asymmetry observed in a number of motor adaptation studies. Interestingly, neither the magnitude nor the directionality of transfer was affected by task level variability, although such variability differentially influenced the rate of learning of the two arms. Additionally, the mechanism used to reduce errors during learning, though heterogeneous across subjects, transferred to the untrained arm. These effects likely reflect the operation of cognitive strategies during the early stages of motor skill learning. In the second study (Chapter 3), we ask whether interlimb transfer of skill learning requires the memory to be in a labile form for transfer to occur, as has been proposed in studies of motor sequence learning (Robertson, 2009; 2012; Mosha and Robertson, 2016). A set of right-handed participants (n=48) learned the same task as in chapter 2, but were tested for transfer 24 hours after

initial learning. This window allows for motor memory consolidation, moving the memory from a labile to a stable state. We again found robust and symmetric interlimb transfer, even at 24 hours. We also found that the amount of interlimb transfer was similar to the magnitude of retention in subjects who were trained and tested on the same arm. This work suggests that the same stabilized memory mediates both transfer and retention of the learned skill.

To test this idea, we leveraged previous work from our lab which revealed that intralimb retention of a skill learned in a variable task environment could be disrupted if people engaged in a visuo-spatial working memory task following motor practice. In Chapter 4, we probed whether, like retention, interlimb transfer would also be disrupted using a visuo-spatial working memory task. Participants ($n=50$) trained on a novel motor skill under variable or constant practice conditions, followed by “Corsi Block” task known to engage dorsolateral prefrontal cortex based spatial working memory processes (Courtney, 2004; Klauer and Zhao 2004; Fregni et. al., 2005). They were then tested for interlimb transfer 24 hours later. We found that transfer was indeed impaired when learning occurred under variable (but not constant) practice conditions, which was strikingly similar to our previous work on intralimb retention. These results provide support to the view that once stabilized, both interlimb transfer and intralimb retention of skill learning arise from common underlying processes. Neurally, learning with one arm is thought to produce plastic changes in both brain hemispheres, which may facilitate interlimb transfer (Parlow and Kinsbourne, 1989; Cramer et al., 1999; Wiestler and Diedrichsen, 2013). However, recent work has shown that transfer is associated with ipsilateral changes that are not linked to changes in cortical excitability (Stöckel et al., 2016). We speculate that one reason for this could be that cortical excitability in the ipsilateral hemisphere is downregulated by the contralateral hemisphere through interhemispheric coherence. As a first step towards testing this, we studied how each hemisphere contributes to corticomotor output in the absence of any learning and memory storage (Chapter 5). We used a TMS-EEG setup in young individuals ($n=20$) and found that neither resting neural oscillatory activity (μ and β) over ipsilateral sensorimotor regions nor interhemispheric coherence significantly impacted corticomotor output; rather, this output was best predicted solely by contralateral activity. These results suggest that the lack of ipsilateral hemisphere contribution is potentially because of inhibition from the contralateral hemisphere. This can be causally probed further in future work that specifically employs skill learning paradigms and tests for interlimb transfer. Taken together, the current work broadens our understanding of learning and generalization of motor skills in humans. It provides support for the view that early stages of skill learning are mediated by cognitive or deliberative processes and highlights differences in transfer of new motor skills relative to actions adapted to counter perturbations. It challenges the notion that fragility/instability of the memory acquired as a consequence of learning is critical for generalization. It provides unique insight into the shared basis of interlimb transfer and retention of skills, and suggests that these can be used as behavioural tools to probe the fate of a motor memory post acquisition. Finally, by demonstrating the lack of contribution of the ipsilateral brain hemisphere to corticomotor output, the work also offers a preliminary hint as to why ipsilateral influences on interlimb transfer may not be excitability related. Going forward, these findings could be valuable inputs for the design of rehabilitation interventions for patients with motor deficits following neurological injury.

Title: How expectation and statistical learning shape attentional selection
Researcher: George, Nithin
Supervisor: Sunny, Meera M.
Year: 2021
Keyword's: Expectation, Statistical Learning, Attentional Selection, Feature Binding, Orbitofrontal Cortex
Call No.: 153.4 GEO
Acc. No.: T00706

Abstract: Attentional processing of objects in the environment is critical for our experience of conscious perception. The control of attention is traditionally classified into either a goal-driven process or a stimulus-driven process. However, two streams of evidence have recently emerged that challenge this dichotomous notion. First, it has been shown that expectation about the impending sensation changes its sensory representation in a way that imitates the effects of attention (Wyart et al., 2012; Cheadle et al., 2015). Two, attention has been shown to be biased by the regularities in the sensory environment through the process of statistical learning Awh et al. (2012). Although the classical paradigms investigating attentional selection have employed probabilistic cueing, they have not isolated the effects of expectation and statistical learning from that of attention. The present thesis reports four empirical studies that report a total of 12 experiments that further our understanding of the effect of expectation and statistical learning on attentional selection.

According to the Bayesian account of perception (Clark, 2013; K. Friston, 2005), statistical regularities about the sensory environment are formed through continuous interaction as an active agent. Previous studies have shown that these regularities (or predictions) modulate attentional selection (Wang & Theeuwes, 2018a, 2018b). The first empirical chapter investigated whether the attentional selection is affected when there is a deviation or error to the predicted regularity. The extent to which attention is modulated by the task-based reliability of the error in prediction was also examined. The results showed that the reliability of the prediction error influences attentional guidance. The attentional guidance was found to change over time, reflecting an online recalibration of the reliability of the prediction error.

The second empirical chapter investigated the learning-based effects on feature binding, which is traditionally considered to require attentional deployment. In light of recent evidence showing attention-independent learning effects on feature binding (Yashar et al., 2015), this study investigated whether the probabilistic association between the individual features that constitute an object influences learning. The results showed that training participants with a broad range of feature-combinations lead to a better transfer of learning. Follow-up experiment showed that this learning does not happen when the pre-exposed item is task-irrelevant.

The third and fourth empirical chapters investigated the extent to which expectation and attention contributes to effects that were earlier proposed to be exclusive to either expectation or attention. In previous studies, attention is shown to modulate the gain of psychometric function. However, the

manipulation of attention in these studies is conflated by concurrent information about the expectation associated with the stimulus. Thus, studies employing traditional attentional paradigms have conflated the effect of attention and expectation Summerfield & Eger (2009). The third empirical chapter aimed to dissociate the effect of expectation and attention on psychometric function gain. The results showed that gain in psychometric function due to attention depends on the feature expectation. The study also finds marginal effects of feature expectation on the gain. The fourth empirical chapter extends the paradigm employed in the third chapter to investigate the mechanism underlying sensory attenuation, which is an effect typically ascribed to expectation. The study found that sensory attenuation depends on two factors, one, whether action precedes sensory signal, two, whether attention is deployed to the sensation.

The present thesis reports expectation-dependent and learning-dependent effects by demonstrating changes to traditional measures linked to attention, such as reaction time, search slope, sensitivity, and gain of the psychometric function. The findings broaden our understanding of attention and define it beyond traditional dichotomies. The present findings also challenge the modular notion of perception by re-defining attention as a process that dynamically alters the statistical properties of the sensory representation at every stage of processing.

Title: Action planning in response to affective stimuli
Researcher: Mehta, Veli Milind
Supervisor: Manjaly, Jaison A.
Year: 2021
Keyword's: Theory of Event Coding (TEC), Valence-Compatible Stimuli, Cognitive and Emotional Processes, Residual Activation
Call No.: 153.4 MEH
Acc. No.: T00707

Abstract: Early theories regarding actions in response to affective stimuli considered these reactions to be automatic. However, even affective responses tend to be context-sensitive and goal-oriented. The affective extension of the Theory of Event Coding (TEC) equates action planning in response to affective stimuli to the process involved during action planning in response to non-affective stimuli. Accordingly, perception and action planning processes in response to affective stimuli lead to activation of features from a common representational framework. During the process of action planning in response to affective stimuli, this activation is followed by integrating all features relevant to the most appropriate response, followed by actual execution. The features remain activated in a residual fashion after execution for some time, followed by gradual disintegration. This thesis explores the processes of feature activation residual activation of these features following action execution in response to affective stimuli.

Three experiments in Chapter 2 demonstrate the facilitatory effects of affective feature activation during affect-based action planning on the perception of a concurrently presented valence compatible stimulus. These findings support the hypothesis that perception and action in response to affective stimuli make use of common features by demonstrating a significant influence of affect-based action planning on the concurrent perception of an affectively compatible stimulus. Two more experiments suggest that affective feature activation during affect-based action planning may last from 100 to 250 ms. Two experiments in Chapter 3 provide evidence in favor of residual activation of affective features following an affect-based response's execution. Further, two experiments in Chapter 4 suggest that affective and non-affective features may play a role in affect-related processes of perception and, especially, action planning. This thesis's findings have important implications for the current perspectives on response processes in the face of affective stimuli and the interactions between cognitive and emotional processes in general.

Title: Virtual reality based joint attention task platforms for individuals with autism
Researcher: Jyoti, Vishav
Supervisor: Lahiri, Uttama
Year: 2020
Keyword's: Autism Spectrum Disorder (ASD), Joint Attention (JA) Skills, Inverted Hierarchical Prompt Protocol, Applied Behavior Analysis
Call No.: 153.4 JYO
Acc. No.: T00708

Abstract: Autism Spectrum Disorder (ASD) is a neurodevelopmental disorder characterized by repetitive and stereotypical behaviors coupled with impairments in social communication and interaction. Such impairments can be attributed to these individuals having problems in understanding the verbal and non-verbal cues from partners during social communication. This is often manifested as deficits in Joint Attention (JA) skills. The JA refers to the process in which different individuals share attention towards a common target in the visual space. The JA skill is considered as one of the core deficits in individuals with ASD. The execution of tasks requiring JA has two facets, namely Response to Joint Attention (RJA) and Initiating Joint Attention (IJA). The RJA occurs when an individual follows a directional cue (towards a target stimulus) issued by a partner followed by attending to the stimulus, e.g., looking in the direction of a pointed finger. The IJA refers to the act of initiating an intentional pointing cue to draw the attention of a partner towards a stimulus. Both the RJA and IJA are equally important for effective social communication. Though children with ASD experience milestones both with respect to RJA and IJA skills, yet it might be critical to study the RJA (referred to as JA in this thesis) since the RJA needs one to understand the directional cue issued by a partner followed by appropriate reciprocation to successfully complete the JA bid initiated by the partner. Deficits in JA skill (a hallmark of ASD) can adversely affect one's social communication and interaction, community participation, ability to earn a livelihood, etc. This added to the high prevalence of ASD (about 1 in 65 children within the age group of 2-9 years being diagnosed in India as per a research published in 2017 in Indian Pediatrics), necessitates the availability of easily accessible and effective intervention services that can at least partially address such deficits. There is a common consensus that conventional behavioral interventions by trained therapists can have the potential to improve the core deficits in social communication, such as the JA skill of individuals with ASD. These conventional behavioral interventions have the potential to bring long-term benefits in terms of improvement in the skills of individuals with ASD. Though powerful, several limitations associated with behavioral interventions, such as resource limitations, high cost, the requirement of long hours of therapy from interventionists during one-on-one sessions, reduced flexibility in the hands of the therapists to bring in variations to the JA task environment in the clinic and scarcity of trained therapists have sparked interest in the research community to search for alternatives. Additionally, given the spectrum nature of ASD, every individual is unique; thus, the delivery of the intervention services needs to be individualized.

In an attempt to explore alternative intervention solutions that can be cost-effective, easily accessible, quantifiable, and individualized, investigators have proposed technology-assisted solutions, such as robots, computer-assisted platforms, etc. Robot-based solutions can offer a sense of embodied presence along with individualized intervention services. However, these benefits come at the expense of a few limitations. For example, some of the limitations of robot-assisted intervention can be high cost, safety issues, power constraints, non-naturalistic motor activity, the need for special training for operation, etc. The other approach, commonly used by researchers, is the computer-based platforms. Though computer-based platforms lack in offering a sense of embodiment (in terms of physical presence, such as in the case of robots), with the advancement in computing technology, virtual characters (such as 3-D humanoids) can be easily designed, offering a sense of virtual embodiment. In addition, the cost of offering computer-assisted intervention can be less. Additionally, once programmed, this will not necessitate specialized training to operate and can offer flexibility in the hands of the interventionists to bring in variations in the intervention paradigm. Despite several advantages, currently available computer-assisted platforms mostly operate in the standalone mode with restricted interaction capability coupled with a lack of individualization. With an increase in computational power, investigators have been augmenting computer-based platforms with Virtual Reality (VR) technology since VR offers flexibility to the designer to bring in variations in the presented stimulus with a realistic audio-visual appeal that can be motivational. Additionally, VR can offer a number of other advantages, such as cost-effectiveness, controllability, safety, individualization, etc. Given these positive attributes of VR, in our current research, we have used computer-based VR-enabled technology to design interactive virtual environments that can project real-life JA task scenarios coupled with an audio-visual stimulus presentation. In addition, the JA task scenarios offered by our system projected different virtual objects and 3-D humanoid characters (Avatars serving as JA task administrators), providing different verbal and non-verbal JA cues.

Furthermore, our designed VR-based JA task environments were equipped with an ability to predict one's affective state (that can affect one's social communication) while interacting with the JA tasks by augmenting the environment with techniques that are not susceptible to one's communication vulnerabilities. This is particularly essential for individuals with ASD who are commonly found to be socially withdrawn and have a hard time in explicitly communicating their affective states. For this, we have integrated peripheral physiological acquisition and eye-tracking technology with the VR-based JA task environments, thereby making the task environments capable of predicting one's affective state from one's peripheral physiological and eye-gaze-related indices in an individualized manner, since such implicit measures can be mapped to one's affective states while an individual interacts with JA task scenarios having different components. Some of the important components of a VR-based JA task environment are (i) Avatars, (ii) Objects, and (iii) JA cues. While the role of the Avatar as the task administrator is critical, it is also essential to understand the role of different objects used in the JA tasks. This is because the JA task requires a triadic relationship among an individual with his/her social partner and the object used as a JA target. It is a known fact that children with ASD exhibit a greater inclination towards non-social stimuli, such as objects in a communication environment. This necessitates further exploration into the role of objects in JA task execution by

individuals with ASD. Motivated by this, the first objective of our research was to investigate the implications of objects in a VR-based JA task environment on one's task performance and looking pattern. By looking pattern, we are referring to one's gaze pattern that can be picked up by using eye/gaze trackers. To achieve the first objective, we have designed a virtual environment with virtual objects to understand the role of objects when projected in the JA task environment for individuals with ASD. We have created a database of virtual objects (these objects were taken from various research studies focused on JA tasks) and projected these objects using a computer-based VR-enabled JA task environment. Based on a survey, we have selected objects that were preferred by these children, with the rest being comparatively less preferred. Our experimental study involved presenting the virtual objects as Target (i.e., object cued by the Avatar) and Non-Target (i.e., object not cued by the Avatar) in the JA task trials. The VR-based JA task environment was augmented with a remote eye-tracker. The results of our study indicate differentiated implications of preferred objects presented as Target and Non-Target on the task performance and looking pattern of these children.

Added to investigating the role of objects in a VR-based JA task environment, it is also important to understand the role of JA cues demonstrated by an administrator while conducting a JA task. This is because, added to the use of objects in JA task administration, an administrator often uses various types of JA cues in conventional settings while interacting with children with ASD. Thus, the second objective of our research was to investigate the implications of different types of JA cues when offered in a randomized manner in a VR-based JA task environment on one's task performance and peripheral physiology. To achieve the second objective, we have designed a VR-based JA task environment that delivered different types of Avatar-mediated and object-mediated JA cues of varying information content in a randomized manner. The designed task environment was augmented with a peripheral physiological data acquisition device. The results of the study with individuals with ASD and their typically developing (TD) counterparts indicated the differentiated implications of different types of JA cues when offered in a randomized manner in a VR-based JA task environment on the task performance and peripheral physiology of both groups.

Besides investigating the significance of different types of JA cues when delivered in a randomized manner, we were also interested in studying the implications of standard conventional protocols named (i) least-to-most (LTM) and (ii) most-to-least (MTL), also called fading procedures that therapists often use to deliver the JA cues in conventional intervention settings. In this, instead of delivering the JA cues in a randomized manner, the therapists begin with a JA cue that is least informative for LTM (the most difficult for the child) and most informative for MTL (easiest for the child). Given the importance of these standard protocols for the delivery of JA cues used in conventional settings, we were interested in exploring these protocols in VR-based settings. Motivated by this, the third objective of our research was to design interactive VR-based JA task platforms that offered JA cues following the protocols used in conventional settings and investigate its applicability for individuals with ASD in the VR-based JA task settings. The third objective is divided into two parts. To achieve the two parts of the third objective, we have developed two different VR-based JA task platforms that offered JA cues following LTM hierarchy (we have named

this prompting protocol as Hierarchical Prompt Protocol (HPP) in this thesis) and MTL hierarchy (or fading procedures) (we have named this prompting protocol as Inverted Hierarchical Prompt Protocol (IHPP) in this thesis). With regard to implementing the HPP in the VR-based settings, we have developed a Virtual Reality based JA Task (VIJAT) platform augmented with HPP that offered different JA cues in a hierarchical manner starting from the JA cue, which was the least informative. The delivery of the JA cues was made adaptive to the individualized performance, and the system autonomously increased the level of prompting on demand. Results of the study with individuals with ASD and their TD counterparts indicated the potential of the VIJAT platform to identify JA skill deficits along with differentiated implications on the task performance of both the participant groups. With regard to implementing the IHPP in the VR-based settings, we have developed the TABLET based JA Task (TABJAT) platform augmented with IHPP that offered JA cues in an inverted hierarchical manner starting with the JA cue, which is the most informative. In addition, the delivery of JA cue was made adaptive to one's individualized performance, and the system autonomously decreased the level of prompting on demand. Results of a study with individuals with ASD indicated the potential of the TABJAT platform to identify the JA skill deficits, and the TABJAT platform had implications on one's task performance.

To summarize, in our research, we have designed interactive VR-based JA task environments and platforms for individuals with ASD. The results of the experimental studies show (i) the implications of different components of JA task environment (such as objects and different types of JA cues) on one's task performance, peripheral physiology, and eye-gaze-related indices during the interaction with VR-based JA tasks, (ii) the potential of VR-based JA task platforms to actively encourage the participants with ASD to perform better within the simulated world, and (iii) the underlying linkage between the JA task performance, peripheral physiological and eye-gaze-related indices. The promising results of our studies show the potential of the VR-based JA task platforms to serve as complementary tools in the hands of the therapists and pave a way towards offering a comprehensive solution for imparting JA skill training to individuals with ASD, thereby contributing to the improvement in the social living of the target population.

Title: Representation and lived experience(s) of Dalits in visual and verbal mediums
Researcher: Ingole, Prashant
Supervisor: Mehta, Mona G.
Year: 2021
Keyword's: Scheduled Tribes, Dalit Panther, Achhut Kanya, Dalit Panther Movement, Scheduled Castes
Call No.: 305.5688 ING
Acc. No.: T00750

Abstract: This dissertation is an attempt to understand how representation and lived experience(s) of the Dalits go hand in hand, but while one becomes visible, the other remains invisible. In other words, they are conjunctural in their relations. This study analyses the rich array of carefully selected texts that include, Graphic Narratives– *Bhimayana: Experience of Untouchability* (2011), and *Gardener in the Wasteland Jotiba Phule's Fight for Liberty* (2011); Dalitbahujan media portals –*Round Table India: For an Informed Ambedkar Age, Dalit Camera, Velivada.Com*; Hindi Cinema – *Achhut Kanya* (1936), *Sujata* (1959), and *Aarakshan* (2011); and Dalit life writing – *Baluta* (1978), and *Angaliyat (The Stepchild)*, 1986). Through the Dalit “standpoint”, the study interrogates how meaning, language, events and “critical narratives” produce casteless understandings and anti-caste analytical perspectives.

The study revolves around the new forms of institutionalized hierarchies that have emerged in the post-Ambedkar context through oppositions between Dalithood and Dalitness, power and authenticity, casteless (ness) and anti-caste(ness). Further, it tries to develop the connections with past and present Dalit resistance movements through the analysis of aforementioned texts. The study critically analyzes two broad articulations, *narratives about the Dalits* and *writings by the Dalits*. For analytical and methodological purposes this dissertation separates *the narrative* (narratives about caste and casteless relations) as a mainstream representation of Dalit suffering and *the writings* (Dalit self- expressions about anti-casteness) as voices of the Dalits that draws on the lived realities through their own words and imagination. In order to understand the above mentioned processes and the context, this study is developed through Gopal Guru and Sundar Sarukkai's (2012 and 2019) theoretical debates on the everyday lived realities of the Dalits and caste as discussed in the discipline of social sciences and humanities. In addition, it also engages with Stuart Hall's (1997) and bell hooks's (1992/2015) approach on representation to uncover and re-articulate the cultural worldviews about the Dalits.

The study makes two main arguments. First, the study argues that the distinction between the lived experience(s) and representation is much more than the mere difference between the insiders' and outsider view. Dalithood and Dalitness can be understood through a prism of casteless(ness) and anticaste(ness) in which casteless(ness) is a position available for upper castes while anticaste(ness) is rooted in the Dalit resistance. The mainstream representational narration of Dalithood and social oppression is marked by a naturalization of victimhood that does not provide the Dalit view of lived

experience(s) in an emancipatory manner. But on the other hand, writings by the Dalit scholars develops through Dalitness, with a focus not only on subjugation and humiliation, but also on the assertion for self-respect and dignity. These aspects of self-respect and dignity become radical in their articulation, and anger in their language comes through the lived reality of the “epistemic violence”. Secondly, the study also argues for an intersection of Dalit studies and Cultural studies in order to challenge the brahmanical cultural knowledge production. This intersection can extend the program begun by Dalit studies to reclaim power and knowledge in relation with the ‘politics of difference’ in the cultural realm. This can be done through the ways in which the Dalit aesthetics decenter the cultural production and circulation of the hitherto grand narratives. Further, it can also attempt to debrahmanize and decasteize the established disciplinary space by bringing a discourse of Dalit experience of caste and humiliation into mainstream academia.

Taking a cue from Guru and Sarukkai this dissertation expands on their subtexts of anger and *maitri* and attempts to foreground the Dalit anguish to show that the Dalit anguish is grounded in the ‘lived’ experiences of Brahminical society and its graded inequalities. Dalit anguish is a revolt filled with resentment directed not against any particular being but the undemocratic structure of the society. The Dalit anguish is produced through literature, protest movements, artistic expressions and so on. The dissertation suggests that the Dalit anger/anguish has an ability to uplift the burden of caste. Further, it also leads to the formation of *maitri* (love and compassion towards any being) among the “everyday different social”. Thus, this anguish generates an “ethical rationality” that opens up the possibility of having democratic conversations among caste communities who occupy highly diverse social positions.

Considering the developments in the field of Dalit Studies in the past few decades, the study concludes by making a case for *Dalit Cultural Studies* which has the potential to transform the discipline into a dynamic field of research.

Title: Nutrition promotion among indian children and youth: insights from three theory-driven studies

Researcher: Shah, Ankita Rameshkumar

Supervisor: Subramanyam, Malavika A.

Year: 2021

Keyword's: Public Health, Health Promotion, KIRAN Program, Non-Communicable Diseases (NCD), Behavioral Diagnosis

Call No.: 613.2083 SHA

Acc. No.: T00934

Abstract: On the continuum of problems related to nutrition, Indian children and youth experience a double burden – namely unresolved problems of undernutrition including micronutrient deficiencies, and emerging problems of overnutrition resulting in overweight and obesity. India features among the countries having the highest proportion and absolute numbers of undernourished children in the world, with nearly 38% of under-five children stunted and 36% underweight. India also carries one of the highest burdens of anemia globally, including among adolescents. On the other hand, evidence is building up suggesting that nutrition-related risk factors implicated in non-communicable diseases (NCDs) are increasing across age-groups, including youth. A range of social and biological determinants of undernutrition and nutrition-related risk factors of NCDs are conceptualized that extend from individual to societal and national as well as global levels. A comprehensive approach addressing multiple biological and social determinants of these complex problems, integrating individual- as well as population-based approaches have been proposed by scholars. The role of population-based health promotion efforts aimed at enabling people to increase control over their health, and its determinants is emphasized in addressing the nutrition-related problems among populations. While several health promotion efforts of varying scale and intensity addressing nutrition-related problems are underway in India, we have identified several gaps in the existing programmatic efforts and have tried to address those using a theory-driven approach in the present thesis. Broadly, our research work is situated in the paradigm of health promotion within the domains of public health. We conceptualized population-based health education efforts as a way to enhance health literacy among a large proportion of the target population, potentially initiating a social change. We employed a social-epidemiological perspective in our research work. We have drawn extensively from Krieger's Ecosocial theory, in framing the research questions, designing the inquiry and intervention, as well as interpreting the findings. Additionally, we have drawn from several concepts and theories suitable to specific research questions that we attempted to answer in the three core studies that we carried out as a part of this dissertation work.

The present thesis is organized in the form of three core chapters describing three research studies situated in the broad area of nutrition-promotion. In the first core chapter, we describe findings from a mixed-methods impact evaluation of a community-based nutrition- literacy intervention aimed at behavior change, targeting mothers of young children in urban socio-economically disadvantaged areas of Ahmedabad and Vadodara, Gujarat. In the second core chapter we describe

development of a NCDs-related nutrition-literacy curriculum for college-youth. Further, we discuss delivery and evaluation of the effectiveness of the curriculum in enhancing nutrition-literacy, using randomized controlled trial, among college- going youth in Ahmedabad and Mehsana, Gujarat. In the third core chapter we explored the potential impact of social context on adolescent undernutrition in India by carrying out secondary data-analysis of NFHS-4 data. By quantifying the relationship of community-level women's education with undernutrition related indicators in adolescents, we present evidence of the influence of social context on adolescent nutrition and highlight the need for addressing social contextual factors, a potential missing link in the existing efforts, in health promotion interventions targeting adolescent health and nutrition.

Conclusion:

To conclude, our findings from the first core chapter highlight the importance of conceptualizing nuanced ways in which socio-culturally embedded families --as opposed to decontextualized mother-child-dyads-- influence child-care and child-feeding; and addressing those in the design and delivery of child nutrition promotion interventions. By presenting robust evidence of the effectiveness of an NCD nutrition literacy curriculum in our second core chapter, we argue for enhancing NCD-related nutrition-literacy among youth by incorporating it in their academic training and leveraging the ability of youths as social change agents in curbing the increasing burden of NCDs. In our third core chapter, we argue for moving beyond an individual-focused perspective to address the social-contextual determinants of adolescent undernutrition.

Our findings highlight that socio-cultural norms related to the value placed on women's well-being in a patriarchal Indian society have an influence that extends beyond childhood into adolescence. Circling back to theory, we do acknowledge that health-promotion interventions that we have designed, evaluated and proposed, are unequivocally a short-term approach. While we can predict on a sound empirical and theoretical basis that improvements in broader structural determinants of nutrition and health can lead to much larger and long-lasting changes, there is empirical evidence that health literacy in individuals is capable of bringing positive changes in certain indicators related to child health and NCDs. Therefore, probably we could use this as a complementary approach to our efforts in improving broader structural determinants such as poverty, education, gender equality and so on. Our central argument is that tasked with developing such an intervention/program/policy, the policy maker/program designer not only needs to be aware about epidemiological diagnosis of the problem but also behavioral diagnosis and the environmental diagnosis of the associated behaviors/practices that require the change. It is important to continue our efforts towards behavior changes, but in a way that it is relevant to its recipients, and can increase the participants' control over behavior change within their given socio-cultural and economic setting. This could be important not only in improving nutrition related outcomes, but potentially instrumental in achieving significant changes in structural level determinants, given the inter-linkages between nutrition and education and poverty.

Title: Metaphors in the visual: a semiotic approach to select intermedial adaptations of the Mahābhārata
Researcher: Sharma, Shivani
Supervisor: Rath, Arnapurna
Year: 2022
Keyword's: Mahabharata, Religions Of Indic Origin, Mediascapes, Mahabharata Metaphor
Virtual Reality
Call No.: 398.20934 SHA
Acc. No.: T01032

Abstract: The *Mahābhārata* is an integral part of the literary and socio-cultural fabric of Indian epic traditions. The epic has traversed interregional, multilingual and intergenerational routes in its varied manifestations, creating a fine grid of cultural narratives. The epic has a grand structure formed by interlacing narration and interwoven stories. This study is a semiotic analysis of the *Mahābhārata's* adaptations in distinctive media forms, and their role in disseminating the epic traditions in diverse literary contexts. It argues that the graphic and digital metaphors function as enabling tools in the adaptation and develops a nuanced understanding of epic traditions that are transmitted through the modalities of media. The research makes three interlinked arguments: firstly, the transmedial representations of the epic have democratised the narrative space, expanding its intermedial articulation across mediums; secondly, the distinctive modalities of each medium attend the semiotic process of (re)imagining the epic in its narrative structure, generating new modes of exchange between the form of the epic and its narration; finally, the dissemination of the narrative of the epic on the intermedial plane through metaphors facilitates a semiotic framework for understanding new modes of (re)imagining the epic traditions. The process of semiosis is intrinsically metaphorical, generating a network of meanings in the epic. This semiotic study extends the semantic scope of metaphors that preserve the narrative paradigm in the mediated form of the *Mahābhārata*. The primary focus of this research is analysing the cautiously selected adaptations of the epic in the mediums of comics, graphic narratives, and new media platforms such as Twitter and virtual reality. Furthermore, this study explores how transmedia representations remake the epic by adding new semantic layers, and elaborates on the semiotic dimension of narratives that contributes to preserving the narratological transmutations of the Mahābhārata.

Chapter One, 'Introduction to the Indian Epic Traditions,' situates the discussion within the context of Epic studies. The chapter examines the dialogic nature of the Mahābhārata, highlighting the multiple modes of presentation through which it has been articulated. Drawing on dialectical negotiations, it provides an overview of the epic and the cultural and literary manifestations that have played an instrumental role in creating its tradition. With an array of intertextual references, the epic has transcended its epicness and has become a framework for interpretation. Foregrounding the epic's multiplicity and its textual-visual proliferation, this chapter discusses the possibility of analysing the intermedial forms of the *Mahābhārata*.

Chapter Two, 'The Approach of Semiotics, Metaphors and Epic Intermediality,' uses semiotics as a critical vantage point to examine how the narrative threads of the epic are intertextually reflected in media representations that continuously resurface tales through adaptation. This chapter elaborates on the semiotic paradigm of combining the intermedial plane with V.S. Sukthankar's three planes- the mundane, the ethical and the metaphysical, and suggests a holistic framework for reading the epic. The intermedial approach is crucial to investigate the cross-media representations of the stories and their retellings, which invite alternative readings of the epic. The semiotic understanding of the Mahābhārata's adaptations and the intermedial diffusion of the epic traditions equip this research with critical praxis and the framework for engaging with the mediation of the tales.

Chapter Three, 'The Mahābhārata as Immortal Picture Stories,' focuses on the adaptation of the selected stories from the epic in the medium of comics to analyse the transition of the narrative from its classical mode of narration to the popular visual-verbal media. With its presentation, aesthetic design and spatial layout, the Amar Chitra Katha emerges as a pedagogic tool for disseminating Indian cultural traditions and ethos. The Amar Chitra Katha retells the complex stories of the epic in simplified versions in its sanitised format. This chapter argues that the structural properties of the Amar Chitra Katha, such as gutters, typographical matrices, and sartorial codes, are extended graphic metaphors that facilitate the adaptation and weaving of the narrative. The critical discussion of each component highlights the way the epic is adapted in the collaboration of visual-verbal modes of narration.

Chapter Four, '(Re)Imagining the *Mahābhārata* in Graphic Narratives,' continues the semiotic understanding of the graphic metaphors and extends the discussion in the medium of graphic narratives. This chapter unravels these graphic textures in Amruta Patil's duology, *Adi Parva* (2012) and *Sauptik* (2016), and Jason Quinn and Sachin Nagar's trilogy, *The Kaurava Empire* (2015). The semiotic explanation of the threadbearers, the language of colors, and the trope of marginal voices provide critical insights into Patil's graphic narratives as the subversive dimension of retellings. In contrast, Quinn and Nagar's retellings explore the futurist epic narratives through their reimagination of the war.

The new media retellings of the Mahābhārata have 'turned' the epic into an experimental mode, creating metaphoric threads of narrative. Chapter Five, 'New Mediascapes of the Mahābhārata,' analyses C. Sreedharan's two Twitter tales, *Epic Retold* (2014) and *Autobiography of a Villain* (2019) narrated from the perspectives of Bhima and Duryodhana, respectively. The chapter strives to illustrate how the emergence of new media has led to the creation of new digital forms of interaction and participatory modes of interpreting the epic. By examining digital metaphors specifically, this chapter intends to show how the epic undergoes a creative transformation when told through interlinked tweets in the digital space of Twitter. In the new mediascapes, the popular renditions of the epic have been emphasized through hashtags and tweets having a diegetic shift of their own. The chapter addresses the question of how fragmented and restricted access to tweets captures the depth of narration and empowers the storyteller without necessarily discontinuing epic traditions. It investigates the semiotic inflection of the Twitter narratives through the extension of its characters from 140 to 280. In addition to discussing the distinctiveness of digital metaphors and their

comparison with other mediatic adaptations, the chapter examines the possible impact of the temporal nature of the new media age on the pastness of the epic. The chapter attempts to decode the following semiotic layers: (a) the critical examination of the tweets as a semiotic unit in literary narration and the metaphors of hashtags, (b) the microblogging of the hero, Bhima and the antihero, Duryodhana as the storytellers of the Twitter Mahābhārata, and (c) tweeting the chronicles of the war. This chapter probes how the epic is retold in a fragmented, nonlinear, and linguistically restrictive digital space of 'twitterature.' This thesis contends that the minimalistic narrative space of Twitter, organized through hashtags and tweeting techniques dramatises the layers of meanings in the stories.

Chapter Six, 'Virtualizing the Mahābhārata,' showcases the possibility of visualizing tales from the epic in virtual reality. It highlights the pedagogical potential of creating narratives such as the episode of the labyrinth in virtual reality as an immersive medium for retelling the epic. The practical experience of weaving the narrative in virtual reality supplements the semiotic discussion of the adaptation process and its role in the reinvention of the epic. Creating the virtual reality episode opens the possibilities of constructing a digital narrative tradition. The critical landscape of the intermedial transmissions and modes of operation of the epic narrative have shaped the Mahābhārata into a living tradition. Through the intermedial approach of graphic and digital metaphors, this thesis provides a framework for engaging with the subtleties of narratives while forming alternative interpretations of the epic. The mediatic understanding of metaphors weaves layers of meanings through forging semiotic connections between the mediums. By establishing the continued relevance of the epic and its narratological reframing across cultural contexts, this thesis contributes to the critical discourse on the epic and its adaptations.

Title: mHealth in maternal health: the role of autonomy and digital literacy
Researcher: Susanna G.
Supervisor: Subramanyam, Malavika A.
Year: 2022
Keyword's: mHealth, Maternal And Child Health, Digital Health Literacy, Gender Digital Divide
Call No.: 362.1042 SUS
Acc. No.: T01033

Abstract: Maternal and Child Health (MCH) is considered an indicator of the human development of any country in terms of increasing equity and reducing poverty. It is a reflection of broader economic, social and developmental indicators. Although India has improved MCH indicators over the last few years, maternal and child health remains a significant public health concern. Neonatal disorders, undernutrition, and iron deficiency feature in the top ten causes of premature death or disability despite decades of rigorous MCH research, policymaking, and programme implementation. Challenges still exist in the health system due to the malfunctioning of the three-tier referral system and the accessibility and affordability of various health services. Hence, the current system needs to develop and incorporate innovative and cost-effective methods to strengthen the existing healthcare delivery system. Global agencies, including the World Health Organisation and the World Bank, highlight and recommend the possibilities of incorporating technological innovations to tackle the existing challenges in public health in developing countries. They recommend adopting 'Digital Health', which is an application of information communication technology (ICT) including telemedicine, health information system, electronic health (eHealth), mobile technology in health (mHealth) etc., as possible alternatives. In light of this, the government of India decided to incorporate various digital health interventions to extend health services and empower healthcare providers and beneficiaries (those who are seeking care).

According to the latest statistics provided by the telecom regulatory authority of India (TRAI), India has an exponential increase in mobile phones that have covered a substantially higher number of rural households than the last decade. The widespread use of mobile technologies and advancements could be helpful in the health system in addressing various health priorities. This has evolved into a new field known as mobile health (mHealth). Mobile health offers the potential for enhanced reach by providing individually tailored and customised services, even among traditionally underserved communities, at a relatively low cost.

The Government of India has launched different electronic and mobile-based health initiatives for frontline health workers for better healthcare delivery, including health education and health promotion activities. Digital health literacy can be considered a key determinant in the success of eHealth tools to support healthcare delivery, especially health education and health promotion. Digital health literacy is "the ability to seek, find, understand, and appraise health information from electronic sources and apply the knowledge gained to addressing or solving a health problem". The additional challenge of eHealth relates to the skills required to use electronic devices such as mobile phones and computers and have adequate health literacy to make effective decisions regarding health. However, with these innovative developments, eHealth literacy among beneficiaries and

different groups of health workers has become an important area of investigation as they belong to diverse socio-economic and cultural backgrounds.

Broadly, this work is situated in the paradigm of health systems strengthening within the domains of public health. We conceptualised autonomy as a key determinant of ownership and use of mobile phones and the internet, enhancing health literacy among the target population. We employed a social determinant of health perspective to frame the research questions, design the inquiry and intervention, and interpret the findings. Additionally, we have drawn from several concepts, such as intersectional feminism, which are suitable for specific research questions that we attempted to answer in the three core studies we carried out as a part of this dissertation.

This thesis is organised into three core chapters describing three research studies in the broad area of digital health. In the first Chapter, we assessed the extent to which ownership and use of mobile phones by Indian women are associated with the utilisation of maternal health indicators such as antenatal care and institutional delivery services by carrying out a secondary data analysis of IHDS 2 data. In the second Chapter, we describe findings from a mixed-methods study focused on the role of women's autonomy and determinants of social inequality on the uptake and use of mobile phones, the internet and mobile health interventions. The study also projects the factors associated with digital decision-making and discusses barriers and challenges related to using, accessing and digital health interventions among women in selected districts of Kerala.

In Chapter Three, we describe the perceptions and practices regarding the access, use, and dissemination of digital information among grass-root level (community-based) health workers (GHWs) in selected districts of Kerala. This Chapter also explains the factors (socio-cultural and other factors such as work experience, gender, caste, autonomy, educational status, geographic setting, training sessions and social support) that play a role in the uptake and adherence of mHealth interventions (mHIs).

Chapter 1

Even with years of maternal and child health programmes and interventions, maternal and child health issues persist in India. Given the expansion in the ownership and use of mobile phones, mobile health (mHealth) interventions have been designed and implemented to facilitate MCH services. This study aims to assess whether ownership and use of mobile phones by Indian women are associated with the utilisation of maternal health indicators such as antenatal care and institutional delivery services. This study used publically available data on mobile phone use from a nationally representative household survey (N=12047) to examine the association between mobile phone ownership and use, such as access to the Internet or not, texting facility available on the phone or not and with having at least four ANC visits or an institutional delivery. The data fitted survey-adjusted logistic regression models adjusted for women's autonomy, access to mass media, and other socioeconomic and demographic covariates. Household mobile phone ownership was positively associated with receiving ANC (OR=1.21; CI=1.08-1.36) in fully adjusted models. Women with access to the Internet and SMS facility also had higher odds (OR=2.87; CI=1.54-5.34) of reporting an institutional delivery and receiving an ideal ANC (OR=1.25; CI=1.01-1.64) in the fully

adjusted models. Patriarchal social norms likely impact women's use of mobile phones. mHealth MCH interventions in India, especially those targeting underprivileged women, are unlikely to be effective unless efforts are made to increase access to, and autonomy in, mobile phone use. Partnering with social scientists during intervention design and other policy-relevant implications are discussed.

Chapter 2

As maternal and child health is one of the key focus areas of the Indian health system, women as the target population need special attention while implementing MCH-related beneficiary-centric mHealth interventions. However, we could not find scientific literature focusing on beneficiary perspectives, especially women's ownership, access, and use of mobile phones and the internet and the social determinants contributing to such disparities. We also identified a need to study the role of women's autonomy in the ownership and use of mobile phones as it is the key determinant in the success of various digital health interventions, acquiring digital literacy and digital decision-making capacity. Previous efforts identified the existing gender digital divide in India; however, we could barely find studies that explored the nuances and pathways leading to the gender digital divide. Our extensive literature review found a need to study the role of socio-political, contextual and individual factors such as autonomy levels among women that determine the uptake and effective use of digital health interventions and digital health literacy among women across different geographic regions (five districts in Kerala) and social and religious groups. This study also tries to understand the pathways associated with the above connections. This study also aims to understand the benefits and challenges of the target population's use, access to digital health information, and digital decision-making process. We have adopted a cross-sectional mixed-method design, including a qualitative phase followed by a quantitative survey. The study participants were women in the reproductive age group with a child up to three years of age. The sample size for the survey was 785, and we interviewed 42 participants for the qualitative phase. For the survey, from the information of the eligible mothers shared by the GHWs, we randomly selected our study participants. We have adopted a systematic random sampling technique, and mothers with odd serial numbers were selected. Qualitative data were analysed using framework analysis as it enables a structured way of analysis, considered a suitable method for public health research. Quantitative data were analysed using descriptive statistics and multivariate regression models. Our qualitative findings revealed the great extent of the digital gender divide, relating to ownership, access and use. The study also found that women's autonomy and bargaining capacity were strong determinants of digital decision-making capacity. The study also discusses the complex interplay of multiple factors situated at different levels, which shape women's general autonomy, autonomy in the digital space and digital practices. Larger societal factors such as patriarchy and its effects such as societal gender norms, narrow family expectations and gender-based discrimination potentially play an important role in digital decision-making. The study also highlights the barriers to the beneficiaries' use and access to digital health information.

From the quantitative strand of the study, we found a direct positive association between higher digital health literacy levels among women with medium ($\beta=0.72$; CI= 0.050-1.38) and high

autonomy levels compared to women with low autonomy levels, independent of their age, education, household location, caste, religion, membership in self-help groups and family type. We also found a direct positive association between higher digital health literacy levels and women belonging to the high autonomy and low-income group ($\beta=1.4$; CI=0.63-2.25) compared to women belonging to the low-autonomy and low-income group after adjusting covariates. Hence the higher autonomy levels, irrespective of their household income, are associated with higher digital literacy levels. Finally, we found a positive association between digital health information seeking during pregnancy with digital health literacy($\beta=0.45$; CI=0.40- 0.49).

The study concludes that the gender digital divide exists in the study population, and high levels of autonomy and bargaining power can narrow down the divide. Social determinants, such as caste, income, religion, geographic setting and level of education, along with the gendered norms, play a role in shaping women's autonomy levels in general and in the digital space. The study's findings also suggest that digital health literacy is also associated with women's autonomy, further influencing digital health practices among women. We thus find a need for gender progressive policy-making, which can ensure the digital inclusion of women and other underprivileged sections of society for the effective implementation of digital health interventions. The digital literacy programmes also need to focus on the weaker and neglected sections as digital sources have become a key source of health information and health promotion.

Chapter 3

India is the second-largest country globally in terms of population, with two-thirds living in rural areas. The demographic and environmental transition of the country is supplementing the already existing high burden of communicable, non-communicable and various other infectious diseases. Significant disease burden of communicable and non-communicable diseases, limited human resources, poor health infrastructure, high absenteeism of healthcare providers at government facilities, and accessibility issues related to healthcare by rural inhabitants contribute to the dire state of healthcare services in many areas of the country. Challenges still exist in the health system due to the malfunctioning of the three-tier referral system and the accessibility and affordability of secondary/tertiary-level health services. Current challenges in healthcare delivery demand an urgent need to incorporate innovative strategies that can improve the efficiency and reach of health systems. From the available literature evidence, mobile phone technology in the health sector has the potential to radically improve the face of global health systems. Grassroot level health workers are considered an integral part of the health system of middle-income countries like India. GHWs act as a link between the health system and communities by delivering a wide range of health services, including promotive, preventive and curative services in various domains. The Government of India has launched different electronic and mobile-based health initiatives for frontline health workers for better healthcare delivery, including health education and health promotion activities. Literature evidence suggests that the effective use of such mHIs is associated with different skills required to use electronic devices such as mobile phones and computers and internet and internet-related services.

This study aims to bridge the gap in evidence by assessing the gap in access, use, and dissemination of digital information among grass-root level (community-based) health workers (GHWs) in selected districts of Kerala. The study would also explore the determinants which determine such gaps and the associated pathways. This study explores the benefits, barriers and challenges related to the use, access and digital health information.

We have adopted a cross-sectional mixed method design, including a qualitative phase followed by a quantitative survey. The study participants were GHWs, including Auxillary Nurse Midwives (ANMs), Anganwadi Workers (AWWs) and Accredited Social Health Activists (ASHAs) from selected districts of Kerala. The sample size for the survey was 801, and we interviewed 38 GHWs and four key informants for the qualitative phase. Qualitative data were analysed using framework analysis as it enables a structured analysis, considered a suitable method for public health research. Quantitative data were analysed using descriptive statistics and multivariate regression models. Our qualitative findings suggest that the divide in ownership, use of mobile phones and internet use of GHWs are shaped by multilevel factors varying from the individual level, household level, health system level, local context and larger socio-political factors. Even though gendered social norms play a role in shaping the digital divide, the higher autonomy levels enabled GHWs to actively participate in digital decision-making. Our findings also suggest that the use of mHIs can enable GHWs to improve their service delivery. However, maintaining multiple records along with digital data entry doubled the efforts and adversely impacted the service delivery. We also found that the training sessions received by the GHWs enabled them to use mHIs better but not always translated into digital health literacy. Lack of digital skills, family support, workspace support and work burden were barriers to effective use of mHIs.

Similarly, digital skills among GHWs were found to be a significant determinant of digital health literacy. Even though the GHWs had technical and skill barriers to digital health literacy, as GHWs have acquaintance with qualified healthcare providers, compared to the general population, they could cross-check the credibility and authenticity of the digital health information. From the quantitative part, we found that 80% of GHWs owned smartphones, and most smartphone users were ANMs, followed by AWWs and ASHAs. More than half ASHAs reported that they have access to the internet, whereas 86% ANMs and 77% of AWWs reported the same. Regarding digital health literacy, more than half of GHWs reported searching for health-related information on their mobile phone at least once.

However, only 18.2% used internet sources to answer beneficiary questions. More than half of ANMs and AWWs stated that they know how to identify reliable health resources on the internet, whereas only 36% ASHAs reported the same. 97% of the GHWs received training sessions before starting using mHIs and 92% of them were satisfied with the training. 94% of AWWs and 90% ANMs reported that they are confident in using mHIs whereas 87% reported that mHIs improved the efficiency of the work. We also found a direct positive association between higher digital health literacy levels among GHWs with medium ($\beta=0.16$; CI= -0.85-1.174) and high autonomy levels ($\beta=0.085$; CI= -0.631-0.79) compared to GHWs with low autonomy levels.

To conclude, our study findings shed light on the importance of digital inclusion and digital empowerment among GHWs to ensure better service delivery through digital interventions. We also emphasise the significance of technical skills and digital literacy in effective access, dissemination and use of health information from digital sources. We find a need for further in-depth enquiries on digital health literacy and digital decision-making with a particular emphasis on different groups of GHWs. The training sessions focusing GHWs need to include basic digital literacy training sessions along with the technical training for mHIs. The comparatively disadvantaged groups of GHWs like ASHAs require special attention, in general, and digital empowerment programmes.

Conclusion

mHealth interventions can be a powerful tool in low- and middle-income countries with large population sizes and limited health workforce. The post-COVID-19 world may demand interventions which minimise direct contact but ensure better health outcomes. Our study emphasises the importance of incorporating beneficiary-specific factors in designing mHealth interventions. mHealth-based maternal and child health (MCH) interventions in India, particularly those targeting underprivileged/ disadvantaged women, are unlikely to be effective unless measures are made to increase access to, and autonomy in, mobile phone use. Patriarchal social norms potentially affect women's access and use of mobile phones, thus leading to lower digital health access and practice. Hence women's autonomy in the digital space must be studied in detail before designing and implementing mHIs.

Similarly, proper policymaking and planning for educating GHWs on how to evaluate the quality of health information in digital media and improving their skills of identifying relevant information among the vast amount of available health information by choosing the right search strategy can help promote GHW's digital health literacy to an optimal level.

Title: Kūṭiyāṭṭam between preservation and transformation investigating the challenges posed by modernity to this traditional performing art of Kerala
Researcher: Nair, Ankita
Supervisor: Danino, Michel
Year: 2023
Keyword's: Kutiyattam, Abhinaya, Performing Arts-Kerala
Call No.: 792.095483 NAI
Acc. No.: T01034

Abstract: Kūṭiyāṭṭam is a Sanskrit-based classical theatre art of Kerala, traditionally performed by the Cākyār and Nampyār communities for possibly well over a millennium. Its performances, which also give some room to Prakrits and Malayalam, are noted for their elaborate stage techniques and productions. Until the 1950s, the art was only performed within temple premises, often in *kūttampalams* (temple playhouses), after which the art moved out to larger audiences and learners.

This study endeavours to comprehensively map and interpret the recent, and mostly 20th- and 21st-century, evolution in Kūṭiyāṭṭam's pedagogy, dramaturgical techniques, performance spaces, and audiences. The central argument of this thesis is pivoted on the tensions this art has witnessed over time between orthodoxy and innovation, or, more positively, on the interplay of preservation and transformation, *mārga* (classical) and *deśi* (regional), sacredness and profaneness. The core-periphery model will help investigate these tensions by defining the art's unchanging core and its changeable periphery, since most changes in Kūṭiyāṭṭam's pedagogy, dramaturgical techniques, performance spaces and audiences, though critical to the art's renewal, can be situated at its periphery. Drawing from primary texts, secondary studies, also from my pilot studies, in-depth interviews with the Kūṭiyāṭṭam fraternity, focused-group discussions, and brief training in Nañnyārkūttu, the thesis brings to light the ways in which the art has transformed itself, while at the same time remained the same, and attempts to glimpse its forthcoming trajectory in the 21st century.

Title: Samuel Beckett and carescapes
Researcher: Joshi, Swati Satish
Supervisor: Chattopadhyay, Arka
Year: 2023
Keyword's: Samuel Beckett, Self-care Models, Proto-Models Of Care
Call No.: 848.91409 JOS
Acc. No.: T01085

Abstract: Chapter 1: Introduction

Samuel Barclay Beckett, presumably born on April 13, 1906 (Good Friday), “had memories of life in his mother’s womb” (Cronin 1). These memories of prenatal confinement seem to have played a vital role in shaping his oeuvre (poems, short stories, novels, plays, and doodles). His creative journey, which possibly begins with his 1930 poem, ‘Whoroscope,’ commences with the question, “What’s that?” (Beckett 40), and he continues to explore the “what” aspect throughout his writing career, finally ending with yet another poem, ‘What is the word’ written in 1988 in the nursing home, Le Tiers Temps. Dirk Van Hulle’s preface to the 2009 Faber and Faber edition of *Company, Ill Seen Ill Said, Worstword Ho, Stirrings Still* corroborates this argument: “‘Quel est le mot?’ was still the pressing question when he was in the Hôpital Pasteur, and then in the nursing home Le Tiers Temps, in July 1988” (Van Hulle xv-xvi). I have tried to answer the question with the care models in the thesis. But it wouldn’t have been possible to answer this question simply using Beckett’s works. I have juxtaposed Beckett’s texts with the contemporary English and French novels that resurrect him in the clinical care settings. While Beckett’s works provide description of only one side of the clinical care- communication (for instance, the caregiver’s side in *Murphy* (1938), the care-recipient’s side in *Malone Dies* ([1956]1994)), the contemporary texts that resurrect Beckett provide the holistic view by showing how the caregivers and care-recipients perceive the process of care-communication. This chapter will carefully elaborate the reasons to collocate the contemporary texts with Beckett’s and explain how this juxtaposition helps to analyse the patterns of clinical/non-clinical care-communication in the prescribed confined care settings to develop the following three models of care: triangulated material auto-care (chapter 2), dyadic narrative self-care (chapter 3), and monadic proprioceptive self-care (chapter 4). In chapter 5, I study Beckett’s doodles sketched in the manuscript of *Murphy* as proto-models of confined care to coherently weave all the arguments made while examining the aforementioned models of care. These models unfold the violent nature of care, wherein the clinical/non-clinical caregivers abandon their care-recipients or at least the literary care-recipients claim so. In the wake of this abandonment, the care-recipients are compelled to care for themselves.

The introductory chapter defines all the predominant key terms like caregiver, care- recipient, resurrection, interchangeability of the terms of enlivening and resurrection, models and their functions, and so on. It explains how the personal experience of spending long duration in the confined spaces owing to the chronic Bronchitis along with a wide range of theories like, the philosophical approach to study the materials, ethnographic studies of care, theories of narrative

medicine, proprioception, and so on have inspired to investigate the nitty- gritty of each self-care model.

Chapter 2: Triangulated Material Self-Care in Samuel Beckett's *Murphy* and Sam Thompson's *Jott*

This chapter studies the triangulated material auto-care/self-care model (explained in detail in the chapter) that emerges by juxtaposing Samuel Beckett's *Murphy* (1938) and Sam Thompson's *Jott* (2018) that is inspired by *Murphy* among other texts of Beckett. The analysis shows 'Sam Répond Sam' ('Sam Replies to Sam') scenario wherein Sam Thompson, the grandson of Beckett's friend and psychiatrist- Geoffrey Thompson, writes a novel as a reply to Beckett's *Murphy*. The analysis of the authors' portrayals of the interaction of human caregivers and/or care-recipients with the materials in the prescribed confined clinical spaces of care shapes the development and interpretation of this self-care model. Paul Graves- Brown's explanation to "re-examine how the things around" us "shape practice, and are used to shape practice" (Graves-Brown 1) in *Matter, Materiality and Modern Culture* (2000), and Steven Jackson's explanation of material care in *Debates in Digital Humanities* have shaped the concept of material self-care. In tandem with this analysis, Beth Preston's philosophical approach of understanding the function of materials (delineated in *Matter, Materiality and Modern Culture*) and the research of Julie Brownlie ('Liveable Lives') and Helen Spandler ('Landscapes of Helping') conducted between 2013 and 2015 have also helped me understand the how the interaction of the caregivers with the material world around them shapes their practice of care/self-care. The outcomes of the afore-mentioned projects helped me develop two subtypes of the present model.

In the first subtype based on Beckett's *Murphy*, the interaction of the eponymous protagonist, Sasha Murphy, and his rocking chair is important. This rocking-chair is made of "of undressed teak, guaranteed not to crack, warp, shrink, corrode, or creak at night. It was his own, it never left him" (Beckett 3). So, it becomes a reliable caring agent for him in his room. In the wake of anxiety, he rocks his chair "faster and faster and then stopped. Soon his body would be quiet, soon he would be free" (Beckett 8). In his world of coercive care, his rocking- chair acts as his rock support. He takes this rocking chair with him to the room in "Brewery Road between Pentonville Prison and the Metropolitan Cattle Market" (Beckett 42) when he relocates and starts living with Celia. Moreover, he takes his rocking-chair to the asylum with him when he decides to work there. This is because he perceives his rocking-chair as a caregiver and reciprocates his care for it by taking it with him everywhere he goes. The care that he receives from his rocking-chair equips him to care for his patients at the asylum. Even in the end, when he feels his care is not acknowledged by Mr Endon, he goes back to the garret, ties himself to the rocking-chair and keeps increasing the pace of rocking till "his body was quiet" (Beckett 158). Murphy's care-relationship with his rocking-chair is intriguing because the novel begins with Murphy tied to his rocking chair and ends on the suicidal note, again with him tied to his rocking-chair. His relationship with the rocking-chair gives rise to the care triangle: Chair-Murphy-Endon.

Similarly in the second subtype, the materiality of the writing process cares for the protagonist, Louis Molyneux, in Thompson's *Jott* (2018). The materiality of the writing process involves Louis's silent observation of the materials, buildings, etc. around him. He roams the city or visits his psychiatrist friend, Arthur Bourne, at his hospital to make his interaction with the material world efficient. "...he

spent his days tramping around Battersea Park or hiding out in galleries, museums and pubs. When all else failed he'd go back to his digs and try to work, until the attempt brought him to such despair that he would trek out to the hospital..." (Thompson 4). It is this silent interaction of Louis with the material world around him that makes him wonder "how wards were organised and what therapies were practised, about the attitudes of the nurses to patients, and of doctors to nurses, about the difficulties of caring for those who could not be held responsible for their words or actions" (Thompson 8). The information he collects from Arthur and his own perception of the material world help him write his short stories and novels, that further care for him. When he is not able to translate his thoughts into his literary works, he suffers from terrible headaches. Hence, his care-relationship with the material world is convoluted as it cares for him indirectly giving rise to the care triangle: Louis-Walker-Jott.

Lastly, speaking of the aspects of the care-relationship, it is important to accentuate the transition that demonstrates how the dominant presence of the caregivers in this self-care model keeps dwindling in the ensuing chapters.

Chapter 3: Dyadic Narrative Self-Care Model in Samuel Beckett's *Malone Dies* and Annabel Abbs's *The Joyce Girl*

Chapter 3 collocates Samuel Beckett's *Malone Dies* ([1956] 1994) with *The Joyce Girl* (2016) by Annabel Abbs to study the dyadic narrative self-care model. This model proceeds from the care catered by materials or the materiality of the process of writing to the content of writing that cares for the care-recipients in the prescribed confined spaces of care. The triangulated clinical care model transitions into the dyadic owing to the receding presence of the clinical caregivers. It reaches a point where the care-recipients either feel totally abandoned (in case of *Malone*) or cast aside after a session of strict supervision (as Lucia perceives it in Abbs's novel). While the previous model is predominantly caregiver centric, the present one is care-recipient centric. It shows that when the care-recipient (*Malone*) does not see his clinical caregivers for longer duration or when the care-recipient (*Lucia*) sees her doctor, Carl Jung, only for a short duration, they seek refuge in the narratives/prescribed memoir they write. These narratives unfold the care-recipients' representation of their clinical/non-clinical caregivers. This chapter shows how the performance of patienthood leads to the caregivers' abandonment or the reduced contact with their care-recipients who employ their fear to write the narratives/memoir which care(s) for them. They write their narratives in the hope that their caregivers will read them and cater the in-person care they expect. Writing narratives helps them calm down and perform the script of a good patient which might help them get the in-person care they desire. This chapter delves deeper into the idea of the ward as a stage wherein the performance of patienthood takes place. Moreover, the clinical active audience (the clinical caregivers) decides the course of the care-treatment depending on their observation of the care-recipients' performance of the good patient script. Taking a segue from performance of a good patient script to get the expected in-person care, the succeeding chapter delineates how the care-recipients accept the total absence or surveillance of their caregivers during the clinical care session and move their body parts or imagine their mobility as a form of self-care.

Chapter 4: Monadic Proprioceptive Self-Care in *Becketttopia*

This chapter shows how the self-care model has moved from the triangulated and dyadic to the monadic level and from the caregiver centric and care-recipient centric to the holistic view of clinical care-communication. This chapter juxtaposes Beckett's *Nacht und Träume* (1984) and Maylis Besserie's *Le Tiers Temps* (2020) and its English translation, *Yell, Sam, If You Can* (2022), by Clíona Ní Ríordáin for analysing monadic haptic proprioceptive self-care. And, by collocating Beckett's *Molloy* ([1955] 1994) and Besserie's novel and its translation for examining the model of monadic peripatetic proprioceptive self-care. The reason to include the English translation and the French text in the thesis is that it is the translation and not the French version that uses the word "patient" (Besserie, trans. Ní Ríordáin 7) for the old Beckett staying in the nursing home.

In the case of haptic proprioceptive care, we see how the old, lonely protagonist in Beckett's *Nacht und Träume* imagines the movement of his body parts and he extends his hand to join the hand of the imagined caregiver or the imagine self. He does not write the story of his monadic proprioceptive self-care, but he performs one. On the contrary, Besserie's novel shows that the old Beckett residing in the nursing home attempts to write in his diary despite the difficulty in writing owing to his trembling hands. Moving further with the discussion of the peripatetic proprioceptive self-care, we see that Beckett's *Molloy* portrays more of the protagonist's attempts at gaining proprioceptive independence with his bizarre bicycle than performing self-care. Whereas, Besserie's novel and the English translation demonstrate how the doctors and physiotherapists assign different proprioceptive tests among others for the old Beckett and how he tries to achieve proprioceptive independence despite failing some of them. The significant aspect of this model is that whether the care-recipients are abandoned or under constant surveillance, they feel lonely in their suffering. Hence, they have to rely on the movement of their body parts for self-care.

Chapter 5: Samuel Beckett's Proto-Models of Care

This chapter, albeit shorter than the rest, is important because it analyses the final component of *Becketttopia*: his doodles made in the manuscripts of *Murphy* as proto-models of care. They are studied as proto-models or the preliminary models of care because the doodles are not published independently or as part of the afore-mentioned novels. They remain in the archives. But they bear remarkable significance for the thesis. I believe while trying to perfect his phrases to represent confined spaces and care, Beckett was also expressing his thoughts through his doodles. His telling graphic representation of the themes of confinement and proprioception helped me understand the fervour of the proprioceptive efforts made by the suffering individual in the sketches and the gravity of their experience of confinement. The examination of Beckett's doodles binds all the arguments presented while studying the three models of self-care in the prescribed confined care settings. His doodles have not received much scholarly attention, not to mention in the context of clinical care. So, this study is the first of its kind.

Chapter 6: Conclusion

This thesis is a unique and innovative enterprise as it develops models of self-care by juxtaposing Beckett's texts with the contemporary English and French novels that resurrect him as a character in the prescribed confined spaces of care. These models of self-care reveal the nature of the clinical

care-communication taking place in these prescribed confined spaces of care and the gaps therein. This is a concluding chapter presents the graphic and tabular representation of the flow of arguments in the thesis. It showcases that all the preceding chapters corroborate how the artistic legacies of Beckett that include Beckett's works and the contemporary novels that resurrect him as a character address various aspects of confine care- communication. While Beckett's novels, some of his plays, and his doodles address the "what aspect of the crisis in the care-communication, the novels that resurrect him represent how this crisis can be overcome. Beckett's 'Le médecin' shows the consequence of the crisis in the care- communication: "Le médecin nage le malade coule" (225). (The doctor swims the patient sinks). But it is the contemporary novels that show the fears of the doctor when sees "nothing about how his patient saw the world" (Thompson 79) and how the doctor and the patient collaborate to overcome the crises in the care-communication in their own ways. For designing the self-care models, considering both the aspects of confined care-communication was important.

* * * * *



MATERIALS ENGINEERING

Materials Engineering

Title: Tool wear during friction stir welding an experimental and numerical study during welding of CuCrZr alloy
Researcher: Sahlot, Pankaj
Supervisor: Arora, Amit
Year: 2018
Keyword's: Heat Transfer And Material Flow, Friction Stir Welding, Welding, Tool Wear
Call No.: 671.52 SAH
Acc. No.: T00280

Abstract: Friction Stir Welding (FSW) is a solid-state joining process and provides many advantages over conventional fusion welding processes. FSW of high melting point metallic (HMPM) materials has limited applications due to tool wear and shorter tool life. Tool wear changes profile of the tool pin and affects weld properties. Thus, understanding tool wear during FSW of HMPM materials is essential to obtain consistent weld properties, optimize process parameters, tool design and tool life. Experimental and numerical analysis is carried out in this research to understand tool wear during FSW process. Tool wear has been quantitatively analyzed by conducting suitable experiments to determine the effect of process parameters on tool wear, wear rate and change in the tool pin shape. Different wear mechanisms have been also investigated for the tool wear during FSW of CuCrZr alloy. A three-dimensional heat transfer and material flow (HTMF) based numerical model has been developed to predict tool wear and worn-out tool pin profile along with temperature and material velocities.

A quantitative analysis of H13 steel tool wear during FSW of CuCrZr alloy is performed by conducting suitable experiments. Effect of process parameters such as rotation speed, traverse speed, and traverse distance on tool wear and progressive wear rate are experimentally measured. Higher amount of tool wear is observed for faster tool rotational speeds and slower traverse speeds. Progressive wear rate shows a similar relationship with these process parameters only during initial traverse. With further tool traverse, the wear rate decreases significantly and is not much affected by change in process parameters. Tool pin is a crucial component of FSW tool for proper material flow to produce the defect-free joint. The tool pin profile is analyzed at multiple traverse distances for welding with various tool rotational and traverse speeds. The results indicate that measured wear depth is small near the pin root and increases significantly towards the tip. Near the pin tip, wear depth increases with increase in tool rotational speed. However, change in wear depth near the pin root is minimal. Wear depth also increases with a decrease in tool traverse speeds. Tool pin wear from the bottom results in pin length reduction, which is greater for higher tool rotational speeds, and longer traverse distances. The pin profile changes due to wear and results in root defect for long traverse distance.

Understanding wear mechanisms during FSW is important to prevent or reduce tool wear and ensure longer tool life for joining of HMPM materials. The macroscopic and microscopic investigations of worn-out tool are conducted by performing stereo-, optical- and scanning electron-microscopy (SEM) with energy dispersive spectroscopy (EDS). Tribological analysis of worn out surface is conducted by using tribometer and open source Gwyddion software. The scratch and groove formation on the tool surface is analyzed to ascertain presence of abrasive wear mechanism. Adhesive wear is confirmed by investigating the tool- workpiece interface layer, which features diffusion of copper, and formation of stress concentration edges and cracks. The presence of both abrasive and adhesive wear is an important aspect of the process.

In past, numerical modeling of welding processes has been of great use to develop physical understanding of the processes and reduce experimentation cost. A three-dimensional HTMF based model is developed for FSW of Cu-0.8Cr-0.1Zr alloy. Temperature dependent thermo- physical properties such as specific heat, thermal conductivity and yield strength of the alloy are experimentally determined. Temperature evolution and material flow are computed by solving conservation of mass, momentum, and energy equations. The results from developed numerical model are validated by comparing thermal cycles, peak temperatures and torque for various welds. The developed model shows capability to simulate FSW of CuCrZr alloy successfully. The HTMF based model is further expanded to predict tool wear and worn-out pin profile of H13 steel tool during FSW of CuCrZr alloy. The model thus developed is validated for tool pin profile for various process parameters. Tool wear is predicted based on forces and stresses acting on the tool. Regression analysis is used to modify Archard's wear equation for FSW of CuCrZr alloy. Modified Archard's wear equation is applied to compute tool wear and worn-out tool pin profile. Predictions of tool pin profiles from the modified Archard's equation are compared with experimentally observed tool pin profiles for various parameters. The wear model successfully predicts the worn-out tool pin profile. The self- optimized phenomena for various process parameters are also explained by the developed model. The effect of process parameters is analyzed in detail using the developed model. These insights from experimental and numerical studies of tool wear during FSW of CuCrZr alloy will be useful to optimize the process parameters, tool shape and tool dimensions to reduce tool wear. This study will also be useful for predicting tool pin profile and tool life for FSW of CuCrZr alloy or any other HMPM materials with few experiments.

Title: Design and characterization of novel antibiotics based on membrane active antimicrobial peptides
Researcher: Arora, Ankita
Supervisor: Mishra, Abhijit
Year: 2018
Keyword's: Multidrug-resistant Bacteria, Antibiotics, Membrane, Hydrophobicity, Antimicrobial Peptides
Call No.: 620.22 ARO
Acc. No.: T00396

Abstract: Antimicrobial peptides (AMPs), known as host defense peptides are considered as promising candidates to combat emergence of multidrug-resistant bacteria. AMPs are a class of peptides that are efficient in killing most microbes and can be found in wide variety of eukaryotes. The mode of action adapted by many AMPs involves the disruption of bacterial membranes. This ability is derived from the shared fundamental motifs of AMPs: cationicity and amphipathicity. It is believed that the electrostatic interactions between the cationic AMPs and anionic bacterial membranes and AMP, followed by hydrophobic insertion, drives formation of pores which eventually leads to leakage of cellular components.

Since AMPs attack the fundamental nature of cell membranes it is difficult for bacteria to evolve resistance against them. Complex secondary and tertiary structures and difficulties in isolating AMPs, however, have limited their use as antibiotics. Short and unstructured peptides are, therefore, more desirable. It has been demonstrated that small peptides derived from full length antimicrobial peptides also show antibacterial activity. Here, we do a detailed characterization of the antibacterial activity of one such derivative of human beta defensin-3 (hBD-3): CHR01 [KSSTRGRKSSRRKK]. CHR01 is a 14 amino acid long peptide that is unstructured in solution yet shows antimicrobial activity but at much higher concentration.

To make such short peptides more effective, it is essential to understand the role played by individual amino acids within the sequence. A 'design rule' for AMPs has been studied that represents the fundamental motifs of cationicity & hydrophobicity in terms of Arginine and Lysine content, and hydrophobicity. It states that the number of arginine and lysine residues is strongly correlated to the average hydrophobicity of a peptide. Specifically, AMPs with high arginine content require low hydrophobicity while those with low arginine content require high hydrophobicity. Using this design rule we designed two analogues of CHR01: KSR [KSSRSRKSSRR] and KLR [KLLRLRKLRR] and evaluated their antibacterial potency. We find that both these peptides are random coiled in solution and are active against bacteria. However, KLR is highly potent, displaying very low MIC values. Scanning electron microscopy and fluorescence spectroscopy results indicate that the mode of action for both peptides is by formation of membrane pores. In addition, both the customized peptides are non-cytotoxic. Being short and unstructured, KLR can potentially be mass produced relatively cheaply and its pore-forming mechanism renders it less susceptible to bacterial resistance. Therefore, KLR can be considered as a potential antibiotic for future commercial use.

For enhanced pharmacokinetic properties and chemical stability, it is desirable to develop synthetic polymer-based antibiotics that mimic AMPs. According to the design rule the arginine/lysine content and hydrophobicity of such AMPs are correlated, with lower arginine content necessitating increased lysine content and increased hydrophobicity. Therefore, we developed a series of polymers using lysine-mimicking amino ethyl methacrylamide with butyl methacrylamide to add hydrophobicity, and studied their antimicrobial activities. These polymers are found to be effective against both the bacteria at low concentrations with no toxicity to human blood cells, thereby showing significant potential to be used as antibiotics.

Title: Microstructure influenced bulk optoelectronic and surface electrical properties of low cost materials for photovoltaic application: the case of Al doped ZnO and SnS

Researcher: Singh, Chetan C.

Supervisor: Panda, Emila

Year: 2018

Keyword's: Materials, ZnO SnS, Lower Electrical Resistivity, Higher Optical Transmittance
Optoelectronic, Microstructure

Call No.: 620.11 SIN

Acc. No.: T00401

Abstract: In the perspective of fabricating low-cost, environment-friendly photovoltaic (PV) devices using facile manufacturing techniques, earth abundant and less toxic semiconductor materials have received considerable interest. The commercialized wafer-based Silicon solar cells and thin film solar cells based on CuIn(Ga)Se₂ and/or CdTe either require expensive multi-step fabrication techniques or elements that are expensive due to their scarcity in the earth's crust and/or toxic. To this end, Al-doped ZnO (AZO) as a transparent conductor and SnS as an absorber are explored. AZO finds tremendous applications in technological domains because of its higher optical transmittance and lower electrical resistivity. Unlike optical properties, electrical properties are strongly dependent on the fabrication conditions with their underlying mechanisms being always not known. Similarly, SnS is a promising low cost, less toxic, earth-abundant semiconductor material with a direct band gap of 1.3-1.5 eV and has high absorption coefficient ($> 10^4 \text{ cm}^{-1}$). Intrinsically, it is a *p*-type semiconductor with theoretical efficiency of SnS single-junction cell being 32%. Yet its device performance is still very low, with the highest reported efficiency being 4.63%. The lower performance of these SnS-based solar cells is mainly attributed to the uncertainty in the electrical properties of these materials, attributed to the presence of large number of intrinsic point defect states and also to the trapped states developed because of the diffusion of the individual layer elements at the interfaces. This necessitates fundamental understanding of the microstructure, bulk optoelectronic and surface electrical properties of these materials with respect to the various process parameters, in order to arrive at the optimized optoelectronic properties.

In this PhD project, AZO and SnS thin films are fabricated on ultrasonically cleaned (1 cm × 1 cm) soda lime glass (SLG) substrates by varying a range of process parameters (i.e., substrate temperature (T_s), deposition time (t) and power (P) supplied to the target varying from 303 to 673K, 15 to 120 mins and 10 to 50 W respectively) using radio frequency (RF) magnetron sputtering. Additionally, SnS particles are prepared by varying the initial tin precursor concentration from 0.5 M to 1.0 M in solution chemical route. Then a detailed microstructural, bulk optoelectronic and surface electrical characterizations of these materials are carried out by using a combinatorial experimental tools, like, x-ray diffractometry (XRD), field emission scanning electron microscopy (FESEM), energy dispersive spectroscopy (EDS), atomic force microscopy (AFM), transmission electron microscopy (TEM), UV-Vis-NIR spectrophotometer, photoluminescence measurement system (PL), Hall effect measurement system (HEMS), scanning tunnelling microscopy/ spectroscopy (STM/STS), and x-ray photoelectron spectroscopy (XPS).

The work on the AZO films first addresses the variation in electrical properties with respect to its thickness and then correlates this with its defect chemistry. The carrier concentration (n_e) in these films are found to be strongly prejudiced by the presence of the shallow donor level defects instigated by zinc interstitials (Zn_i), extended zinc interstitials ($ex-Zn_i$), whereas, deep donor level defects (i.e., double charged oxygen vacancies (V_o^{++}) and excess surface oxygen) are not found to contribute to this carrier generation. Further, in order to know the threshold quantity of the electronic defect states because of the presence of Zn_i and $ex-Zn_i$ and their effect on the overall microstructure and optoelectronic properties of these films, in the subsequent work, Zn-rich AZO thin films are fabricated by adding excess zinc (from a metallic zinc target) during their deposition in RF magnetron sputtering. To understand fundamentally the role of zinc atoms in creating the electronic defect states and thereby tuning the overall microstructure and optoelectronic properties of these films, similar sets of experiments are also conducted with the ZnO films (i.e., co-depositing from the ZnO ceramic and Zn metallic targets). This intentionally added zinc in these AZO and/or ZnO films is found to enhance not only the Zn_i and $ex-Zn_i$ but also created single charged oxygen vacancy (Vo^+) which are also found to contribute to an increase in n_e in these films. Additionally, the surface electrical properties of the AZO films are found to be influenced by an overall microstructure and thereby associated defect chemistry. A link between the bulk and the surface electrical properties of these AZO films are then established; a higher bulk electrical conductivity resulting in higher average tunneling current along with increased heterogeneity in the local surface electrical properties. Finally, the AZO film deposited at 623K T_s for 60 minutes and by using only the single AZO ceramic target (of composition 98 wt. % ZnO and 2 wt. % Al₂O₃) is found to demonstrate the most oriented crystallite growth and best optoelectronic properties (i.e., the average transmittance in the visible range (T) = 91%, electrical resistivity (ρ) = $9.13 \times 10^{-4} \Omega\text{-cm}$, $n_e = 4.09 \times 10^{20} \text{ cm}^{-3}$, carrier mobility (μ_e) = $16.32 \text{ cm}^2 \text{ V}^{-1}\text{s}^{-1}$). 15 rpm substrate rotation, 7.0 cm substrate to target distance and 50 W power (supplied to the target) are used here.

Next, solution chemical route is used to synthesize the SnS particles by varying the tin precursor concentration from 0.5 to 1.0 M. All these SnS particles are found to be Sn-rich and p -type. However, distinctly different morphologies (i.e., flower-like and aggregated ones) are observed, which are then correlated with the electronic defect states, induced because of the presence of the Sn vacancies, Sn antisites and/or Sn interstitials. A combination of XRD, EDS, XPS and STM/STS data confirmed the presence of higher concentration of Sn vacancies along with lower quantities of Sn antisites in the SnS particles with flower-like morphologies, hence giving rise to higher hole concentration, which then lead to reduced transport, optical band gaps and barrier heights. Then SnS films are fabricated by varying T_s in the range of 303-623 K for 60 mins on the SLG substrate using RF magnetron sputtering are also found to be of Sn-rich and p -type. However, the concentration of point defects (i.e., Sn vacancies, Sn antisites and/or Sn interstitials) is found to vary in these films, thereby affecting their overall bulk and surface electrical behavior. Additionally, SnS films are deposited by varying t from 15 to 90 mins at T_s of 573 K (T_s at which SnS film on the SLG substrate yielded lowest electrical resistivity) on a stack consisting of a buffer (ZnO) and transparent conductor (AZO); i.e., ZnO/AZO/SLG stack configuration. Whereas, the local surface electrical properties measured using STS from the SnS films deposited only on the SLG substrates

demonstrates semi-metallic behavior, those deposited on the ZnO/AZO/SLG stack configuration shows ohmic behavior, because of an increase in the overall conducting domains from the substrate and/or films.

Title: Interrelation between electronic structure, microstructure and optoelectronic properties of Al-doped ZnO and Cu_{2-x}S
Researcher: Patel, Tvarit A.
Supervisor: Panda, Emila
Year: 2020
Keyword's: Transparent Conductor, Optoelectronic, Scanning Tunneling Microscopy, Stoichiometry
Call No.: 620.1 PAT
Acc. No.: T00521

Abstract: Selection of a semiconductor material with appropriate band gap is essential for specific (opto)electronic applications. Moreover, it is necessary to use earth-abundant and environment friendly materials that are easy to manufacture using cost-effective synthesis techniques onto a range of substrates. However, electronic structure and optoelectronic properties of these semiconductors are found to be highly sensitive to their overall microstructure, which in turn depend on the synthesis route as well as process parameters used for their fabrication. Moreover, choice of deposition technique plays an important role in designing efficient and cost-effective devices. It is also equally important to understand the surface and interface physics in terms of their variation in the surface microstructure and electronic structure along with bulk optoelectronic properties as these films are always present in a stack structure (consisting of multiple layers), thereby influencing the electrical properties of the next layers and thus the entire device. To this end, Al-doped ZnO (AZO) as a transparent conductor (TC) and Cu_{2-x}S as an absorber are investigated in this thesis. AZO is one of the most studied *n*-type TC because of its low cost, less toxicity, stability in hydrogen plasma, higher optical transmittance in visible range and lower electrical resistivity, hence, finding broader applications in technological domains, such as, thin film solar cells, touch-sensitive panels, light-emitting diodes, liquid crystal displays, organic electroluminescent and electrochromic devices. Similarly, Cu_2S is a promising low-cost, non-toxic *p*-type semiconductor with an optical band gap of 1.21 eV, which is in the optimum range for various applications, such as, photovoltaic, thermoelectric, gas sensor and optical filter. The optoelectronic properties of Cu_{2-x}S are highly sensitive to its stoichiometry, where a change in *x* (in the range of $0 \leq x \leq 1$) corresponds to distinct crystalline phases enabling significant variation in the optoelectronic properties (i.e., electrical resistivity of 0.8 $\Omega\text{-cm}$ for Cu_2S , 1×10^{-3} $\Omega\text{-cm}$ for $\text{Cu}_{1.8}\text{S}$ and 1×10^{-4} $\Omega\text{-cm}$ for CuS and optical band gap of 1.1-1.3 eV for Cu_2S , 1.5 eV for $\text{Cu}_{1.8}\text{S}$ and ~ 2.0 eV for CuS). Thus, a systematic interrelation between electronic structure, microstructure and optoelectronic properties of these materials with respect to the various synthesis methods and process parameters is very important to get optimized quality for specific application.

In this PhD project, AZO and Cu_{2-x}S thin films are deposited on ultrasonically cleaned ($1\text{ cm} \times 1\text{ cm}$) soda lime glass (SLG) substrates by varying the process parameters (i.e., substrate temperature (T_s) and deposition time (t)) in radio frequency (RF) magnetron sputtering. Additionally, Cu_{2-x}S (with x being 0, 0.25 and 1.0) microtubes are synthesized by thermally dissociating the self-sacrificed $\text{Cu}(\text{tu})\text{Cl} \cdot 0.5\text{H}_2\text{O}$ template and by varying the concentration of the reducing agent (Na_2SO_3) from 0 to 1.7 mmol in solution chemical route. In addition to above, Cu_{2-x}S films of varying stoichiometry are prepared by dissolving appropriate concentration of Cu and CuS particles in binary thiol-amine alkaline solvent mixture through molecular solution approach. Then a range of experimental techniques, such as, X-ray diffractometer (XRD), field emission scanning electron microscope (FESEM), energy dispersive spectroscopy (EDS), atomic force microscope (AFM), transmission electron microscope (TEM), UV-Vis-NIR spectrophotometer, Hall effect measurement system (HEMS), X-ray photoelectron spectroscopy (XPS), conductive atomic force microscopy/spectroscopy (C-AFM/C-AFS), scanning tunnelling microscopy/spectroscopy (STM/STS) are used to understand the overall electronic structure, microstructure and optoelectronic properties of these materials.

The work on the AZO films addresses the relation between microstructure and optoelectronic properties of these films by varying process conditions (i.e., varying T_s from 303 to 673 K and t from 15 to 120 mins) in RF magnetron sputtering. Here, 242 nm thick AZO film deposited at 623 K T_s for 60 mins and at 50 W RF power is found to show the most oriented crystallite growth and best optoelectronic properties (i.e., the average transmittance in the visible range (T) = 91%, electrical resistivity (ρ) = $9.38 \times 10^{-4}\ \Omega\text{-cm}$, carrier concentration (n_e) = $4.09 \times 10^{20}\ \text{cm}^{-3}$, carrier mobility (μ_e) = $16.28\ \text{cm}^2\text{V}^{-1}\text{s}^{-1}$). Furthermore, C-AFM is used to study the nanoscale surface conductivity of AZO thin films deposited onto SLG substrates by varying T_s from 303 K to 673 K for 60 mins. The obtained local surface electrical conductivity values are found to be influenced by their bulk electrical resistivity, surface topography and tip geometry. Further, the average (local) surface conductivity from the film surface is found to increase with increasing T_s from 303 K to 623 K, beyond which they decrease until 673 K. Additionally, the variation in the local surface electrical heterogeneity within and also for a thickening AZO film is studied using the C-AFM/C-AFS technique. To this end, these films were deposited by varying the t from 15 to 120 mins by RF magnetron sputtering. The local surface electrical heterogeneity was found to be strongly dependent on the overall microstructure of the film grown at a particular deposition time. XPS and TEM-EDS are used to discern the distribution of the chemical constituents over these film surfaces. This study correlates the presence of a large amount of chemisorbed oxygen and/or segregated Al_xO_y at the grain boundaries associated with relatively non-uniform and/or rough films to the overall lower surface current values. Subsequently, a uniformly thick AZO film with a homogenous microstructure grown at an optimum deposition time is found to have the least amount of chemisorbed oxygen along with an effective distribution of Al doping on the film surface, leading to an increase in the overall surface current. This higher surface current is then found to increase the surface electrical heterogeneity of the film due to increased difference between a defect and defect-free region, contrary for a non-uniform and/or rough film.

Next, a simple, cost-effective thermolysis route to produce single phase, stoichiometric, hollow Cu_{2-x}S microtubes of varied composition by using $\text{Cu}(\text{tu})\text{Cl}\cdot 0.5\text{H}_2\text{O}$ as a self-sacrificed template is devised. Here, the concentration of the reducing agent (i.e., Na_2SO_3) is precisely controlled to obtain these Cu_{2-x}S microtubes, which are confirmed by using XRD, EDX and FESEM. The optical absorption as well as the optical band gap of these compounds are found to be strongly influenced by its composition. Finally, the mechanism of formation of these precisely controlled compounds and direct impact of the shape of the self-sacrificed template on the ultimate tubular morphology of Cu_{2-x}S is discussed. Moreover, to study copper deficiency induced varying electronic structure and optoelectronic properties of Cu_{2-x}S thin films, here varying composition of Cu_{2-x}S (i.e., Cu_2S , $\text{Cu}_{1.96}\text{S}$, $\text{Cu}_{1.8}\text{S}$, $\text{Cu}_{1.8}\text{S} + \text{Cu}_{1.6}\text{S}$ and CuS) films are grown here by using a low temperature molecular solution based deposition method, following which a wide range of characterization tools were used to understand their microstructure, electronic structure and optoelectronic properties. The hole concentration of these films are found to vary from $3.32 \times 10^{19} \text{ cm}^{-3}$ to $2.54 \times 10^{22} \text{ cm}^{-3}$ as Cu_{2-x}S composition changes from Cu_2S to CuS . This is because of the induced Cu deficiency in Cu_{2-x}S films with decreasing Cu/S-molar ratio, which reduced the Cu *d*-band width in the valence band, thus pushing the Fermi level deep into the valence band. This leads the optical and transport gap to increase from 1.36 eV to 2.23 eV and 1.31 eV to 2.02 eV respectively with increasing copper deficiencies from Cu_2S to CuS . Moreover, in this work, both the valence and conduction band edge positions are found to shift negatively with increasing Cu deficiency in these films. Finally, this thesis addresses the influence of film thickness on the microstructure, electronic structure and optoelectronic properties of Cu_2S films. To this end, thickening Cu_2S films are deposited on the SLG substrate by varying *t* from 60 to 420 mins at room temperature (303 K) using RF magnetron sputtering. Following which a range of experimental techniques are used to characterize these films. Though films deposited at *t* of 60 to 360 mins are found to have pure Cu_2S phase, additional $\text{Cu}_{1.8}\text{S}$ phase is detected for the film deposited at 420 mins. The valence state of Cu is found to be +1 in all these films, though the binding energy positions of the core level 2p electrons are found to shift systematically and is correlated to the thickness induced compositional changes in these films. Sulfur is found to exist in two valence states in all these films; S^{-2} bound with Cu_2S and elemental or non-stoichiometric S^{-n} , the overall $\text{S}^{-n}/\text{S}^{-2}$ ratio being found to reduce with increasing film-thickness. This microstructural adjustment in the thickening film is found to alter the electronic structure and optoelectronic properties of these films, measured using XPS, STM/STS, UV-Vis-NIR spectrophotometer and HEMS. In the end, principle behind the microstructure alteration of this thickening film is proposed.

Title: Aluminium matrix friction stir surface composites study on mechanical and electrochemical performance
Researcher: Mahesh V. P.
Supervisor: Arora, Amit
Year: 2020
Keyword's: Base Alloy, Friction Stir Processing, Electrochemical Properties, Scanning Electron Microscope, Energy Dispersive X-ray Spectroscopy
Call No.: 620.11 MAH
Acc. No.: T00537

Abstract: Aluminium (Al) alloys are used in transportation, defense and aerospace applications owing to their light weight and high specific strength. However, low surface hardness, wear and corrosion resistance limit the use of these alloys in various strategic applications. Microstructural modification by surface composite formation can overcome these limitations. Metal matrix surface composites possess the combined properties of the base alloy and the reinforcement. Surface composites can be fabricated through liquid and solid-state processing routes. Liquid state processing may result in the formation of different intermetallics which lead to deteriorated mechanical properties. Solid state processing can avoid the drawbacks of liquid state processing such as reduced wettability and interfacial reaction between the matrix and the reinforcements. Friction stir processing (FSP) is an effective solid state processing route to develop surface composites. Formation of intermetallics can be avoided as FSP is done at temperatures lower than the base material T_m . The processing generates fine grained microstructure due to severe plastic deformation. Presence of reinforcement particles in the fine grain matrix enhance the surface hardness and reduce the thermal effects. Molybdenum (Mo) is a suitable metallic reinforcement for the surface composite owing to its high melting point, better wear and corrosion resistance compared to aluminium. Understanding the various parameters and their impact on the Al surface composites is important, yet not known. Here we present the effect of the friction stir processing parameters such as tool shoulder diameter, tool rotation speed, number of grooves, and number of processing passes as well as the reinforcement particle distribution on the resultant surface properties of Al surface composites.

The groove method is used to fabricate the materials using friction stir processing. The experiments are carried out at different process parameters such as reinforcement content, number of processing passes, tool rotational speed, tool shoulder diameter and type of reinforcement particles. The microstructural, mechanical and electrochemical properties of the base alloy are compared with the friction stir processed materials without reinforcement particles and surface composites fabricated after incorporating the reinforcement particles. The microstructural characterization is performed using optical microscope with image analyzer and Scanning Electron Microscope (SEM). The compositional analysis is carried out using Energy Dispersive X-ray Spectroscopy (EDS) and X-ray powder diffraction (XRD) techniques. Surface hardness of all the processed samples and the unprocessed base alloy in the top surface and the cross-section surface of the processed region is measured using a Vickers microhardness testing machine. The post-processing particle size and

distribution is analyzed using ImageJ analysis software. The electrochemical behavior of the base alloy, friction stir processed materials and the surface composites are studied using Potentiodynamic polarization and Electrochemical Impedance Spectroscopy. The preliminary analysis of tensile behavior of the materials is carried out using an Instron Universal tensile testing machine and the wear analysis is done using reciprocating wear testing equipment.

Single and double groove FSP experiments are carried out to study the effect of number of grooves on the hardness of surface composites fabricated using 22, 20 and 18mm tool shoulder diameter. The introduction of a second groove increases the Mo content in the surface composite. The incorporated Mo particles enhance the surface hardness of Al 1050 base alloy. The surface hardness of unprocessed material is 26 HV 0.1 and the hardness increases to 42 HV 0.1 on the top surface and 44 HV 0.1 on the cross-section surface of SGC (Single Groove Composite). The top and cross-section hardness for DGC (Double Groove Composite) are 46 HV 0.1 and 49 HV 0.1, respectively. Microhardness value of 51 HV 0.1 on the top surface and 52 HV 0.1 on the cross-section surface is observed in DGC sample processed with 18mm shoulder diameter tool. The amount of Mo particles incorporated in the composite material is increased with decrease in tool shoulder diameter. The amount of reinforcement is about ~8%wt Mo in SGC and ~12%wt in DGC samples processed with 22mm shoulder diameter tool, respectively according to the microstructural analysis. The amount of Mo particles in SGC and DGC is ~17%wt and ~22%wt, respectively for samples processed with 20mm shoulder diameter tool whereas SGC and DGC fabricated using a 18mm shoulder diameter tool possessed ~27%wt and ~31%wt Mo particles. Mechanical shearing through severe plastic deformation during the friction stir processing reduces the average Mo particle size in the surface composites. Molybdenum is distributed in its elemental form in the Al-Mo surface composites. The grain size in the processed samples reduces with decrease in tool shoulder diameter. Surface hardness improves due to the combined effect of Mo reinforcement and grain refinement induced by the friction stir processing.

The combined effect of number of passes and grooves on the corrosion resistance is also analyzed. Aluminium surface composites are prepared using single pass (SP) and double pass (DP) FSP groove method. Potentiodynamic corrosion testing of Al-Mo surface composites is carried out to study the change in the corrosion resistance. Surface composites exhibit better corrosion resistance with higher corrosion potential (E_{corr}) and lower corrosion rate (i_{corr}) compared to the unprocessed base alloy and friction stir processed materials without Mo addition. Amount of Mo particles is increased by the addition of a second groove. A second processing pass homogeneously distributes this higher amount of Mo particles. Double groove double pass sample exhibits best corrosion resistance. Electrochemical Impedance Spectroscopy (EIS) analysis confirms the higher corrosion resistance of the surface composites. Surface composites with Mo particles show a charge transfer controlled corrosion behavior whereas the Al 1050 base alloy exhibits a mixed corrosion behavior. The initiation stage of pitting corrosion is restricted by the presence of evenly distributed fine Mo particles on the surface composites. The second processing pass on the double groove composite also increases the hardness of Al-Mo surface composite due to the uniform distribution of reinforcements in the grain refined Al matrix.

Different tool rotation speeds and tool shoulder diameters are used to fabricate defect-free Al- Mo surface composites. Molybdenum particles are uniformly distributed in the aluminum matrix without formation of any intermetallics with various tool shoulder diameters (18, 20 and 22mm) and tool rotation speeds (780, 900 and 1200rpm). Higher amount of Mo is observed in the surface composite processed at higher tool rotation speed and lower tool shoulder diameter. Dynamic recrystallization during FSP and pinning effect due to the Mo particles results in the grain refinement. The hardness of surface composites increases with increase in tool rotation speed and decreases with increase in tool shoulder diameter. The surface composite hardness enhances due to the coupled effect of grain refinement and Mo reinforcement. A two fold increase is observed in the average hardness of surface composites compared to the unprocessed Al 1050 base alloy.

The corrosion behavior of aluminium surface composites with metallic, ceramic and hybrid reinforcement particles are also analyzed in this study. Molybdenum, possessing higher corrosion resistance compared to aluminium, is used as the metallic reinforcement and the third hardest known material boron carbide (B_4C) is used as the ceramic reinforcement. The effect of hybrid reinforcement addition on the corrosion behavior of Al surface composites is studied by the combined addition of boron carbide and molybdenum particles. The electrochemical behavior of the developed composites is analyzed through potentiodynamic polarization and EIS. The reinforcement particles distributed in the Al matrix affect the pitting corrosion behavior of the surface composites. The base alloy and the hybrid surface composites show diffusion controlled corrosion mechanism whereas the Mo and B_4C reinforced composites exhibit charge transfer controlled behavior. Single reinforcement addition enhances corrosion resistance of the base alloy whereas the hybrid reinforcement addition induces more corrosion. Post-corrosion microscopy analysis reveals the severity of pitting in hybrid composites. The surface composites developed with metallic, ceramic and hybrid reinforcements are free from general intermetallic phases possible based on the equilibrium phase diagram.

Al-Mo surface composites exhibit improved tensile strength and wear resistance compared to the unprocessed base Al 1050 alloy. The improvement in the wear resistance and tensile strength in the surface composites are attributed to the combined effect of reinforcement particles and grain refinement. The improved ductility in the surface composites compared to the unprocessed base alloy corresponds to the better interfacial bonding between the matrix and the reinforcement particles. The knowledge, regarding the effect of processing parameters and type of reinforcements on the aluminium surface composite properties by FSP, will be very useful in developing optimized surface composites for strategic applications.

Title: Microstructure modulated optoelectronic properties of Al-doped ZnO and CuInGaSe₂ films using cost-effective, scalable deposition techniques

Researcher: Bandaru, Narendra

Supervisor: Panda, Emila

Year: 2019

Keyword's: Scalable Deposition Techniques, Spin Coating Process, Single Charged Oxygen Vacancies, Microstructure And Optoelectronic

Call No.: 620.1 BAN

Acc. No.: T00538

Abstract: The need for developing cost-effective and scalable thin film techniques for fabricating semiconductor materials with promising optoelectronic properties have led researchers to explore a range of synthesis routes along with their process parameters. However a change in the process parameters and/or route would often alter the microstructure of the film, thereby also changing its optoelectronic properties. To this end, Al-doped ZnO (AZO) and CuInGaSe₂ (CIGS) thin films are synthesized here by varying a range of process parameters and using relatively cost-effective fabrication routes. Whereas, both the sol-gel followed by spin coating and RF magnetron sputtering techniques are used to fabricate the AZO films, single step deposition route combined with lower substrate temperature are used to deposit the CIGS films. Whereas, AZO is a wide band gap semiconductor, with a direct band gap of above 3.3 eV and lower electrical resistivity of the order of 10^{-3} - 10^{-4} Ω -cm, and so suitable to be used as a transparent conductor, CIGS because of its direct band gap in the range of 1.04 – 1.67 eV and higher absorption coefficient ($> 10^5$ cm⁻¹) is suitable as a solar absorber material. Though extremely important, literature detailing on the understanding of the process parameter induced variation in the microstructure and associated optoelectronic properties of these semiconductor materials using cost-effective, scalable deposition techniques is still limited, necessitating the present thesis work.

This PhD thesis discusses the process parameter induced variation in the microstructure and optoelectronic properties of the AZO and CIGS films deposited on ultrasonically cleaned (2 cm × 2 cm) soda lime glass (SLG) substrates. After fabrication, a range of experimental techniques, like, Grazing Incident X-ray Diffractometer (GIXRD), Field Emission Scanning Electron Microscopy (FESEM), Energy Dispersive Spectroscopy (EDS), UV-Vis-NIR spectrophotometer, Photoluminescence measurement system (PL), Hall effect measurement system (HEMS), X-ray Photoelectron Spectroscopy (XPS) and Scanning Tunnelling Microscopy / Spectroscopy (STM/STS) are used to characterize these films.

The work on the AZO films using the sol-gel followed by spin coating process first addresses the annealing induced transformation and/or enhancement of their electronic defect states. Here, the as-prepared samples are subjected to two annealing steps; first either in air or in low vacuum (LV; 1×10^{-2} mbar) and the second at higher vacuum (HV; 1×10^{-6} mbar); each at 500 °C for 1 h. Whereas, the overall microstructure and optical properties of all these films are found to change only marginally, the electronic defect states are found to significantly alter because of these repetitive

annealing, leading change in the electrical properties. The AZO films annealed under atmospheric pressure are found to contain deep donor level defects in the form of only excess oxygen. Further annealing of these samples at reduced pressure and at higher temperature leads to effective Al doping in Zinc lattice sites, which subsequently enhances the formation of the shallow donor level defects, like, Zn interstitial (Zn_i), extended Zn interstitials ($ex-Zn_i$, denoted as Zn_i^+ and Zn^{++i}) and single charged oxygen vacancies (V_o^+). However, in case of annealing in low vacuum, only shallow donor level defects (consisting of Zn_i , $ex-Zn_i$ and V_o^+) are found to form, the concentration of which is found to enhance when these films are annealed for a second time under high vacuum, which is associated to enhanced (i.e., effective) Al doping. This increase in the Al dopant concentration by a second step annealing for both these two cases and also for a wider range of initial dopant concentration (0.0 to 3.0 at. %) could also be evident from the observed increase in the optical band gap of these films. Subsequently, an increase in carrier concentration (n_e) in all these films after the second stage annealing is observed. Moreover, irrespective of the annealing condition, we found lowest electrical resistivity (ρ) for the AZO film doped only with 0.5 at. % Al, with the lowest of all being for the film annealed in LV + HV (i.e., $\rho = 1.439 \times 10^{-2} \Omega \cdot \text{cm}$).

Next, the role of excess Al and deposition rate in reducing the doping efficiency of Al⁺³ cations in AZO film is discussed. To this end, two series of samples are deposited using co-deposition either from an AZO (98 wt. % ZnO, 2 wt. % Al₂O₃) or a ZnO (100 wt. % ZnO) ceramic target and a metallic Al target. Whereas, the power provided to the ceramic target is kept constant of 50 W, the power provided to the metallic Al target is varied from 0 to 40 W to see the effect of varying Al concentration (along with deposition rate) on its doping efficiency. For both the series of these deposited AZO films, a higher deposition rate is found to increase both the Al and oxygen quantities in these films, while it reduced the overall zinc concentration. An increased Al concentration in these films leads to Al⁺³ substitution in Zn⁺² lattice sites initially, thereby increasing n_e in these films. However, excess Al concentration because of higher deposition rate along with increased oxygen concentration in these films then lead to the formation of higher quantities of Al_xO_y , thus reducing their doping efficiency and lowering their n_e . Moreover, the crystallite size of these films is also found to decrease with increasing deposition rate, which increases the concentration of trapped aluminum in these increased amorphous regions, thereby also contributing to the lowering of the doping efficiency of Al in AZO films, hence significantly affecting their optoelectronic properties. Finally, a lowest ρ of $0.91 \times 10^{-3} \Omega \cdot \text{cm}$ is obtained for the AZO film, which is deposited using only a single AZO target with 98 wt. % ZnO and 2 wt. % Al₂O₃ composition.

Then to understand the effect of heating and the thus induced changes in the microstructure and optoelectronic properties of the bottom layer and its effect on the top layer(s), here, AZO/ZnO bilayers are used as a model system. To this end, first ~ 242 nm thick AZO film is deposited on cleaned SLG substrate at 623 K substrate temperature (T_s) by using a set of optimized parameters. Next, thickening ZnO layers are deposited on this AZO coated SLG substrate by varying the deposition time of up to 15 mins at the same T_s of 623 K, but using the following two processes: in process I, ZnO layer is deposited on the AZO-coated SLG substrate for appropriate duration immediately after the deposition of the AZO film and in process II, the bottom AZO-coated SLG is cooled to room

temperature after its deposition and then reheated again to 623 K for depositing the ZnO layer. To compare and interpret the microstructure and optoelectronic properties of these bilayers with respect to the deposition time and/or process type, the bottom AZO layer is also reheated for the same duration (as that of process II). Reheating induced transition of the Al^{3+} cations from the substituted Zn^{2+} lattice sites is seen, which is then reacted with the excess oxygen present in these films to form Al_xO_y . The migration of these Al^{3+} cations is then associated with the repositioning of the Zn^{2+} cations from their interstitial to the lattice sites.

Finally, these atomic transitions in these films are found to alter the optoelectronic properties of these single and bilayers.

In the end, the changing microstructure, bulk optoelectronic and surface electrical properties of sputter deposited CIGS films on the SLG substrates as a function of altered film thickness is studied. To this end, these films are deposited by varying the deposition time from 180 to 540 mins in RF magnetron sputtering. Here a single step deposition and by use of a single quaternary CIGS target are employed. Moreover, T_s is kept lower (i.e., of 523 K) to deposit these thickening films. All these films are found to grow in single phase, chalcopyrite crystal structure, and with dominant (112) orientation. Moreover, CIGS film is found to make from a semimetallic to semiconductor transition with increasing film thickness that is correlated with the variation in the type, quantities and position of the intrinsic electronic defect states and also to the hole concentrations (p_h) in these films. Optical band gap (E_g) is found to decrease from 1.32 eV to 1.16 eV with increasing film thickness because of a change in film composition. Moreover, CIGS film deposited for 540 mins is found to yield a film thickness of about 2.85 μm , with p_h of $2.17 \times 10^{17} \text{ cm}^{-3}$ and optical E_g of 1.16 eV; optoelectronic properties that are appropriate for an absorber layer in photovoltaic application. Thus, in this work, a facile, cost-effective deposition technique for the growth of CIGS film is developed, where a relatively lower substrate temperature is used.

Title: Development of antibacterial surface coatings
Researcher: Majhi, Sasmita
Supervisor: Mishra, Abhijit
Year: 2019
Keyword's: Quaternary Ammonium Compounds (QACs), Antimicrobial Peptide (AMP), Water Contact Angle, Bromophenol Blue (BPB)
Call No.: 667 MAJ
Acc. No.: T00546

Abstract: Bacterial contamination aided by antibiotic resistant biofilm formation on abiotic surfaces is a major concern in healthcare and industrial environment. Antibacterial coatings on such surfaces are considered an effective way towards addressing these issues. A number of suitable antibacterial agents, including antibiotics, metal nanoparticles, quaternary ammonium compounds (QACs), antimicrobial polymers, have been investigated for such antibacterial surface coatings. However, emergence of multidrug resistant bacteria has emphasized the need for an effective alternative. A potential substitute is antimicrobial peptides (AMPs), class of short polypeptides usually associated with the host organisms innate immune system. AMPs exhibit broad spectrum antimicrobial activity, low propensity towards pathogen resistance, and low immune response. These properties make AMPs an ideal candidate to be used in antibacterial coatings in preventing bacterial adhesion and/or survival on commonly used surfaces. However, maintenance of peptide activity and stability after immobilization is a crucial prerequisite for the development of AMP-based surface coatings. A short (12 residues), random-coiled, pore-forming antimicrobial peptide (AMP) named KLR (KLLLRKLLRR), is designed based on a proposed 'design rule' that optimizes the cationicity and hydrophobicity of peptide. KLR is immobilized on multiple surfaces, namely polystyrene (PS), stainless steel (SS), and glass, to investigate the effect of surface immobilization chemistry on antibacterial efficacy of the designed AMP. Since PS, SS, and glass have wide applications in medical sector, therefore, bestowing them with antibacterial properties would be of great advantage. The effect of peptide orientation on its antibacterial activity is further studied by adding a cysteine residue at N-terminal of peptide, named CKLR (CKLLLRKLLRR), followed by its immobilization. The surfaces were analyzed by atomic force microscopy (AFM), water contact angle (WCA) measurements, and X-ray photoelectron spectroscopy (XPS), to confirm chemical modifications at each step. The findings show that KLR immobilized on to PS and SS surfaces results in almost complete inhibition of both *E. coli* and *S. aureus* irrespective of the orientation. The peptide-coated glass surfaces, however, inhibited *E. coli* but were ineffective against *S. aureus*. All peptide-modified surfaces were non-cytotoxic towards fibroblasts. Surface segregation of peptides determined from bromophenol blue (BPB) binding method indicated 20-25% of the total available peptide binds to PS surface. Microstructural examination, micro-hardness, and tensile test on peptide modified stainless steel surfaces (SS-KLR) suggest mechanical properties of SS-KLR substrates are unaffected by the chemical treatment employed for surface modification. Immobilized KLR on glass surfaces show pore-forming mechanism of action, thereby, suggesting less likeliness of development of antibiotic resistance. Thus, versatility of KLR makes it a potential

antibacterial candidate for development of broad-spectrum antibacterial coating on multiple biomaterial surfaces.

Title: Microstructure influenced variation in the electronic properties of the functional materials: the case of Nb doped anatase and TbFe_2
Researcher: Manwani, Krishna
Supervisor: Panda, Emila
Year: 2020
Keyword's: Functional Materials, Nb-doped anatase TiO_2 (NTO), Radio Frequency, Polycrystalline
Call No.: 621.37 MAN
Acc. No.: T00756

Abstract: 'Functional materials' represent the type of materials that perform specific functions under defined external stimuli. A broad classification of functional materials would include materials having a wide range of electronic properties (i.e., electrical, optical, and magnetic properties), which find applications in various technological domains. However, these properties are found to be highly influenced by their chemical composition and overall microstructure, thereby making it crucial to understand the correlation between these electronic properties with their overall microstructure, hence tuning these for the desired applications. To this end, Nb-doped anatase TiO_2 (NTO) as an optoelectronic material and TbFe_2 as a magnetostrictive material are examined in this thesis. NTO is a promising wide band gap transparent semiconductor because of its low cost, high chemical stability and long wavelength transparency, hence, can be used as an electrode layer in the optoelectronic devices. Similarly, TbFe_2 is a promising magnetostrictive material due to its large magnetostriction of 2500×10^{-6} at room temperature, hence, finds significant application in actuation and sensing. However, magnetic properties of TbFe_2 are strongly dependent on its chemical composition and overall microstructure and a change in its composition by means of oxidation, can substantially affect its magnetic properties. Hence a systematic understanding between the microstructure, chemical composition and electronic properties of these functional materials with respect to various process parameters is needed to achieve the optimized electronic properties.

In this PhD project, first the process parameter induced variation in the microstructure and associated optoelectronic properties of the NTO films are demonstrated. To this end, NTO films are deposited on 2 cm x 2 cm quartz and soda lime glass (SLG) substrates by varying the process parameters in radio frequency (RF) magnetron sputtering. A range of experimental techniques are then used to investigate the electronic structure, microstructure and optoelectronic properties of these films. Additionally, the oxidation induced variation in the overall microstructure, chemical composition and magnetic properties of TbFe_2 magnetostrictive material is discussed. To this end, a detailed thermodynamic study is first performed to understand the growth of the various oxides due to dry, thermal oxidation of TbFe_2 over a wide range of process conditions. Then TbFe_2 intermetallic

compound in the form of ingots is prepared by melting appropriate weight fractions of high purity Tb (> 99.99 wt.%) and Fe (> 99.95 wt.%) in an arc melting furnace followed by melt spinning in vacuum to obtain TbFe₂ ribbons. These TbFe₂ samples are then annealed and oxidized under various process conditions, followed by their overall microstructure and magnetic property investigation by using a range of experimental techniques.

The work on the NTO films first addresses the thickness dependent variation in the electronic structure, microstructure and optoelectronic properties of undoped and Nb-doped anatase TiO₂ thin films. To this end, these films are deposited at room temperature on the quartz substrates by varying the deposition time (t_d) from 1 to 5 hr, followed by annealing at 823 K for 1 hr and at 2.2×10^{-4} Pa. To compare these results with those of the undoped anatase TiO₂ system, similar series of anatase TiO₂ (TO) films are also fabricated by using the same deposition and post-annealing conditions. The observed shift in the valence and conduction band edge positions for both the TO and NTO films are found to be associated with their total O and Ti content in these films, respectively. Whereas, TO films are found to be highly insulating, NTO films show highly conducting characteristics. The lowest electrical resistivity (ρ) of $4.80 \times 10^{-3} \Omega \text{ cm}$ (with carrier concentration (n_e) of $0.6 \times 10^{21} \text{ cm}^{-3}$ and carrier mobility (μ_e) of $2.14 \text{ cm}^2 \text{ V}^{-1} \text{ s}^{-1}$) is obtained for ~ 74 nm thick film deposited at 3 hr. Additionally, the relative positions and intensities of the shallow donor level defect (SDD) states of anatase TiO₂ system are analyzed and then compared with ZnO system to gain fundamental insight into the differences in their electrical behavior. Along with the visible region, these films also exhibit high transmittance in the NIR region, thereby making these promising transparent conductors for the entire spectral range. Additionally, the role of the post-deposition annealing parameters (i.e., annealing time (t_a) and temperature (T_a)) in tuning the overall microstructure and thereby developed optoelectronic properties of NTO films are discussed. To this end, these films are first deposited on the unheated quartz substrates and then post-annealed at T_a ranging from 623 to 1023 K for various t_a of 0.5, 1 and 3 hr at $\sim 2.2 \times 10^{-4}$ Pa. Though all these post-annealed films are found to crystallize in a polycrystalline anatase TiO₂ crystal structure, their overall crystallinity, dopant atom activation and optoelectronic properties are found to be significantly influenced by the annealing process parameters. Only at an optimized annealing condition (i.e., 823 K for 1 hr) highest crystallinity in the film along with the most effective Nb doping in Ti lattice sites is seen, which eventually gives rise to highest n_e of $0.84 \times 10^{21} \text{ cm}^{-3}$, μ_e of $1.86 \text{ cm}^2/\text{V-s}$ and E_g of 3.51 eV in these films. Consequently this film is found to show the lowest ρ of $4.01 \times 10^{-3} \Omega \text{ cm}$ among all the post-annealed NTO films. Finally, the successful fabrication of high quality transparent conducting NTO films on cost-effective SLG substrate by altering the annealing conditions is demonstrated. The overall crystallinity of these films is found to significantly vary with T_a , which is found to have a strong influence on the dopant activation in these films, eventually leading to larger variation in their electrical properties. Consequently, NTO film with the lowest ρ of $9.84 \times 10^{-3} \Omega \text{ cm}$ (with n_e of $0.74 \times 10^{21} \text{ cm}^{-3}$ and μ_e of $0.85 \text{ cm}^2 \text{ V}^{-1} \text{ s}^{-1}$) and with an average visible transmittance of $\sim 76\%$ are fabricated at T_a of 823 K for 1 hr.

Next, the growth of various oxides due to dry, thermal oxidation of TbFe_2 over a wide range of process conditions is investigated. To this end, a thermodynamic formalism is developed to predict the type of crystalline oxide overgrowth on $\langle \text{TbFe}_2 \rangle$ substrate with respect to various parameters, such as, segregated iron (Fe) content at the substrate/oxide interface ($0 \leq x_{\text{Fe}}^i \leq 1$) growth temperature ($T_g = 298.15\text{-}900$ K), oxide film thickness ($h_{\langle \text{oxide} \rangle}$ up to 5 nm) and various low-index crystallographic surfaces of the substrate and oxide. To validate the outcome of this thermodynamic formalism, arc melted polycrystalline TbFe_2 samples are subjected to annealing and/or oxidation by varying the temperature (T_a), pressure and time. Overall, the formalism predict the overgrowth of $\langle \text{Tb}_2\text{O}_3 \rangle$ at $x_{\text{Fe}}^i = 0$ for all combinations of T_a and $h_{\langle \text{oxide} \rangle}$ because of its more negative total Gibbs energy. However at $x_{\text{Fe}}^i = 1$, where the original surface of the $\langle \text{TbFe}_2 \rangle$ substrate is fully covered with the Fe atoms, $\langle \alpha\text{-Fe}_2\text{O}_3 \rangle$ formation is found to be thermodynamically preferred over all other considered Fe oxides. Experimentally, this is also found to co-exist with $\langle \alpha\text{-Fe}_2\text{O}_3 \rangle$ at higher T_a .

Moreover, both the model and the experimental data suggest Fe to be segregated on to the TbFe_2 substrate surface. Finally, for the growth of a multi-phase oxide-film consisting of $\langle \alpha\text{-Fe}_2\text{O}_3 \rangle$ and $\langle \text{Tb}_2\text{O}_3 \rangle$ the interface and the surface energies are found to stabilize $\langle \alpha\text{-Fe}_2\text{O}_3 \rangle$ at the $\langle \text{TbFe}_2 \rangle$ - $\langle \text{oxide} \rangle$ interface and $\langle \text{Tb}_2\text{O}_3 \rangle$ on the oxide-film surface. Further, the thermal oxidation (by varying T_a and t_a) induced deterioration in the magnetic properties of TbFe_2 is systematically investigated. The characteristic parameters of magnetic properties (such as, coercivity (H_c) and remanent magnetization (M_r)) of TbFe_2 are found to decrease with increasing T_a (i.e., H_c and M_r are found to decrease from 798 to 4 Oe and 29 to 1 emu/gm with increasing T_a from 300 to 900 K, respectively) and/or t_{ag} (i.e., H_c and M_r are found to decrease to 10 Oe and 3 emu/gm with increasing t_{ag} to 4320 h, respectively), thereby indicating significant deterioration in the magnetic properties of TbFe_2 . Moreover, a strong correlation between the oxidation-induced microstructure, magnetic properties and magnetic domain structures are observed here.

Title: Antibacterial properties of Octaarginine-complexed hydrophobic drugs
Researcher: Ratrey, Poonam
Supervisor: Mishra, Abhijit
Year: 2020
Keyword's: Antibacterial Agents, Hybridizing Hydrophobic Drugs, Cell-Penetrating Peptide (CPP) – Octaarginine, Brominated Thiazolyl Benzenesulfonamide (BTB), Hydrophobic Drug
Call No.: 615.1 RAT
Acc. No.: T00757

Abstract: Bacterial infectious diseases represent an emerging public health threat. The crisis is further aggravated by antimicrobial drug-resistance, which leads to the ineffectiveness of a range of antibiotics. The need for new and potent antibacterial agents has led to forays into molecules with inhibitory effects; however, the majority of such compounds or molecules are hydrophobic in nature, restricting their clinical employment. Here, we present an approach of hybridizing hydrophobic drugs with a cell-penetrating peptide (CPP), octaarginine, to render them aqueous solubility and enhance the antibacterial properties. The drugs used are curcumin, and novel isopropyl and bromine substituted thiazolyl benzenesulfonamide derivatives.

Curcumin, a versatile drug with broad pharmacological properties, is challenged by its extremely low aqueous solubility and bioavailability. We modify curcumin non-covalently with the hydrophilic cell-penetrating octaarginine and find that linking peptide improves curcumin's solubility in water and enhances its biological activities. X-ray diffraction and differential scanning calorimetry establish the amorphization of curcumin through peptide while Fourier Transform Infrared (FTIR) and Raman spectroscopies detect hydrogen bonding between the two partners. UV-visible spectroscopy points towards the presence of electrostatic force between the cationic peptide and monoanionic curcumin. The peptide- curcumin complex shows synergistically enhanced antibacterial activity against the Gram-positive and Gram-negative bacterial cells in an aqueous medium. Electron microscopy images show membrane damage and punctures by the complexed drug but not by curcumin alone. Rapid killing kinetics of the complex is obtained, which, along with synergism in the growth inhibition, strongly suggests a distinctive and novel mode of antibacterial action of the complex. The propidium iodide uptake assay also indicates that the peptide-curcumin complex causes bacterial cell membrane damage, suggesting it to be the complex's primary target. Interestingly, the water-soluble complex of curcumin and polyvinylpyrrolidone (PVP) does not significantly inhibit bacterial cells, indicating the active role of octaarginine peptide for the antibacterial effects. The peptide-curcumin complex also shows anticancer activity against HeLa cells in an aqueous medium and internalizes into mammalian cells.

We observe a selective character of the octaarginine-drug complex with benzenesulfonamides, explored in detail with isopropyl substituted thiazolyl benzenesulfonamide (ITB). This hydrophobic drug shows potent antibacterial activity against a set of bacteria irrespective of the Gram character and morphology except against *E. coli* strains. We find that the peptide- ITB complex dissolves in water and shows antibacterial activity against *S. aureus*. Interestingly, the complex does not offer any inhibition of the *E. coli* cells, a behavior in line with its bare and unmodified drug. These

observations point towards the complex's selective character and that the overall activity of the complex is not a simple summation of individual constituents. Brominated thiazolyl benzenesulfonamide (BTB) in complexation with octaarginine presents results similar to the octaarginine- curcumin complex regarding physicochemical characterizations and antibacterial activity, with the addition of cell-selectivity like the peptide-ITB complex. Dye leakage study with giant unilamellar vesicles confirms the bactericidal feature of the peptide- BTB complex. The complex of BTB and octalysine does not cause membrane damage like the octaarginine complex, highlighting the pivotal role of CPP octaarginine.

In summary, the thesis investigates and establishes the potential of cell- penetrating peptide for antibacterial applications and highlights the distinctive underlying strategy that can be exploited to develop superior antibacterial agents. While revolving around a very applied arena, the study also adds up to the basic understanding of cell-penetrating peptides, the conventional non-antimicrobial peptide, which holds a lot of academic interest per se.

Title: Reactivity mediated energetics transformation of oxide based nanoparticles: critical determinant towards nanosafety

Researcher: Paruthi, Archini

Supervisor: Misra, Superb K.

Year: 2020

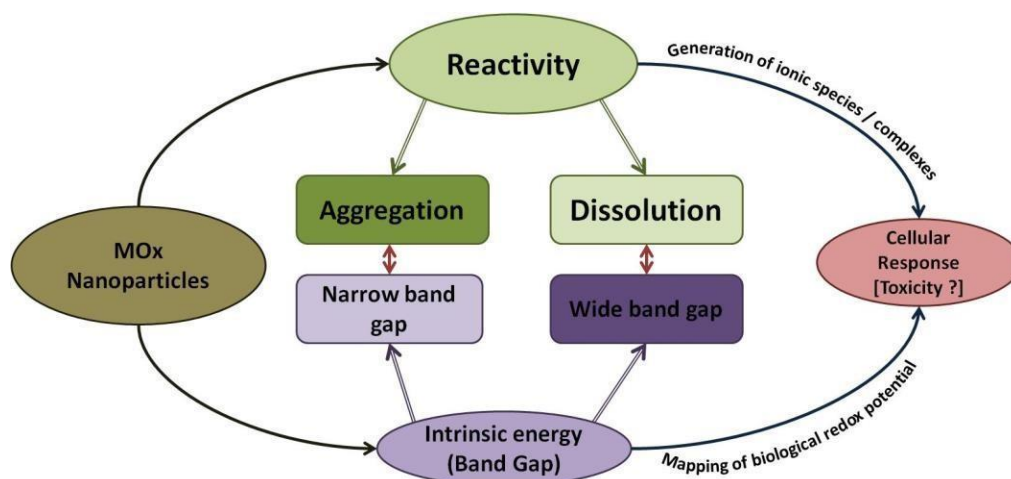
Keyword's: Nanomaterials, Nanotechnology, Bandgap Energy, Mitochondrial Membrane, CuO, ZnO

Call No.: 620.115 PAR

Acc. No.: T00758

Abstract: Incorporation of nanomaterials to enhance the properties of the products deployed in a multitude of fields in the current market (75 billion USD by December 2020) calls for ensuring its safety. From a regulatory standpoint, this specific class of materials (nanomaterials) must be thoroughly scrutinized, categorized, and defined appropriately. Despite the advantages and unique attributes of nanomaterials imparted to the product as a result of dimensionality, it concerns the health safety of the workers, consumers, and the ecosystem. The state of the art delivers that modes of toxicity encompass a wide range of physicochemical factors. Size, shape, surface area, composition, surface chemistry, crystallinity, and reactivity (rate of aggregation/dissolution) are the major physicochemical factors. These factors have the potential to impact both bandgap energy and non-oxidant paradigms (protein corona) in isolation in its native state. The established schools of thought dominantly regarded that highly dissolving nanoparticles (like CuO, ZnO) have their primary mode of toxicity as ion-mediated. However, for low dissolving metal oxide nanoparticles, bandgap could be a predictive paradigm leading to oxidative stress *in vitro* and *in vivo* through biological redox potential overlapping.

There is a strong gap that exists in terms of disassociating the degree of oxidative stress caused due to dissolved species and the effective bandgap of the remnant nanoparticles in the system. Rather, the intrinsic property of the material and its dynamic interaction with the surrounding media in terms of its energetics (bandgap/hydration/interfacial energetics) would be a reliable determinant of oxidative stress (as it deals with the transfer of electrons across the system boundary). This thesis aims to investigate the intertwined mechanisms of metal oxide-based nanoparticles underlying cellular toxicity. Energetics being the main emphasis of this work, the thesis navigates through the reactivity (dissolution/aggregation) mediated variation in the bandgap of selected semiconducting nano-oxides (CuO, ZnO, NiO, and Mn₂O₃). The variation in the bandgap energy (up to 122%), valence and conduction flat band potentials impact the ROS generation (up to 6 fold) which leads to oxidative stress. This study provides insight into the major stakeholders (particles vs ions/complexes) at different levels of oxidative stress-mediated toxicity. It also provides insight into the mode of cell death ranging from necrosis (up to 36%) to apoptosis triggered due to energetic parameter variation as a function of reactivity of nanoparticles. However, the overall cell response is dependent on the biological fingerprint that nanoparticles acquire. Energetics dependent variation in the biophysical features of the protein corona and its knock-on impact on cellular response/toxicity is yet to be investigated in detail and is beyond the scope of this thesis.



For investigating the intertwined mechanisms, metal oxide nanoparticles of high dissolving (CuO, ZnO) and low dissolving (NiO, Mn₂O₃, SiO₂) capacity were synthesized by wet chemical routes. Various morphological modifications with 0.5%- 6% Ni and Mn doped CuO nanoparticles were synthesized for the concept validation of bandgap energetics. XRD analysis was performed to confirm the phase purity and computation of percentage strain and crystallite size post Rietveld refinement. The morphology and size were confirmed through TEM measurements. The specific surface area, pore-volume, and pore diameter for all the synthesized nanoparticles were computed through BET measurements. The surface chemistry and oxygen defects were validated by employing XPS. The intrinsic energy (bandgap energy) of the synthesized metal oxide nanoparticles can be tuned by variation in the composition, size, shape, and introduction of defects in the nanoparticles. The intrinsic bandgap energy of all the metal oxides was computed via diffuse reflectance spectroscopy (DRS measurements). With a decrease in the size of the nanoparticles, the bandgap declined by 3% and with decreasing aspect ratio the increase was by 1.5%. For various compositions, the bandgap of CuO, NiO, Mn₂O₃, and ZnO nanoparticles ranged from 1.18eV - 2.92eV.

Suspension of oxide-based nanoparticles in biological (simulated body fluid, artificial lysosomal fluid, and cell culture media) and ecological media (algal growth media, 1mM NaNO₃ and artificial seawater) was observed for 24 hours to 7 days. The reactivity was assessed in terms of variation in hydrodynamic diameter, quantification of dissolved ionic species, and computation of the wetted surface area of nanoparticles based on ¹H NMR. The in situ tracking in the reactivity variation was conducted by spin-spin nuclear relaxation time under various factors (temperature, pH, presence of serum/organic matter, ionic strength of the media). The variation in reactivity (agglomeration/aggregation/dissolution) translated into changes in the surface composition of CuO nanoparticles quantified by change in the metal/oxygen ratio (range of 0.4 - 1.1) by XPS. Temporal treatment of CuO nanoparticles with 1mM NaNO₃ and simulated body fluid led to an increase in the fermi energy levels (up to 4.52eV) and shifts in the valence band maxima (up to 1.26eV). The temporal changes in the valence band maxima were attributed to an increase/decrease in the size of the nanoparticles. The experimentally found bandgap energy was used for the computation of valence flat band and conduction flat band potentials followed by the development of heat maps. The electrochemical redox potential of the commonly found aqueous redox species in the

environmental and biological milieu was computed by the Nernst equation. All the above potentials are strong indicators of the electronic transfers at the bio-nanointerface. The transfer/acceptance of electrons from the nanoparticles translates into depolarization of biological membranes and redox reactions across the biomolecules.

Correlation of the computed energy levels was done with the biological response of the RAW 264.7 cell line and validated by using the A549 cell line. The mitochondrial activity of the cells and the state of early/late apoptosis, viability, and necrosis of the cells on the treatment with nanoparticles was tracked by employing MTT and Annexin-V/PI assays. The intracellular ROS generation within the cells on the treatment with nanoparticles was assessed by DCFH-DA assay. Post various *in vitro* optimizations, the mitochondrial membrane potential depolarization of RAW 264.7 was tracked for 18 hours of particle separation duration. Mn_2O_3 and NiO nanoparticles demonstrated hyperpolarization of the mitochondrial membrane for the initial duration of 2 hours. However, ZnO and CuO nanoparticles demonstrated mitochondrial depolarization within 30 minutes of particle treatment signifying its potential toxicity. The immune response via the cytokine production tracking of pro-inflammatory (IL-6, IL-1 β , and TNF- α) and anti-inflammatory (IL-10) cytokines was tracked by time-dependent RT-PCR experiments.

In a nutshell, the complex interaction of nanoparticles with the biological milieu results in temporal variation in the reactivity which further causes a variation in the energetics of the remnant nanoparticles. The transformation in the surface availability, size, surface chemistry, and energetics of the nanoparticles impacts the interactions of nanoparticles with the cells. The energetics of the NPs predicted to facilitate the generation of redox couples leads to higher intracellular ROS generation and depolarization of mitochondrial membrane potentially translating into stronger inflammatory responses. It also leads flagging of cytotoxic biomarkers for cell apoptosis. This study is instrumental in unleashing the contribution of particles in isolation towards depolarization of mitochondria and reconsideration towards the construction of predictive paradigms. There is a strong need for the development of paradigms that takes into account the temporal variation of band energetics of the remnant particles in addition to dissolved species for assessment of nanosafety.

Title: Development and analysis of friction stir channeling process using experimental tools
Researcher: Pandya, Sheetal Rameshchandra
Supervisor: Arora, Amit
Year: 2021
Keyword's: Optical micrography, Material Flow Study, Material Flow, Thermo-hydraulic Performance, Heat Transfer Performance
Call No.: 671.52 PAN
Acc. No.: T00935

Abstract: Micro/mini-channel compact heat exchangers have widespread applications in biomedical appliances, electronic cooling systems, aerospace, automobiles, chemical, and nuclear reactors, medical diagnostics, cryogenics, and other reduced size and high thermal performance systems. The conventional manufacturing processes of micro/mini-channels in metal substrates (micro- milling, micro-drilling, micro electron beam machining, micro powder injection molding, microwire cut electro-discharge machining) have limitations if the channels fabricated to be integral, long linear, or non-linear. Besides, these fabrication techniques are very time-consuming and expensive. The Friction Stir Channeling (*FSC*) process is an alternative low-cost fabrication process for manufacturing continuous, linear, and non-linear internal channels in a metal body, overcoming these limitations. The channel geometry and uniformity along the path determine its heat transfer and fluid flow performance. Being an emerging manufacturing technology, *FSC* is required to exhibit the capabilities of manufacturing geometrically controlled and uniform channels along linear and non-linear paths.

The channel geometry is governed by the material flow and *FSC* parameters (tool geometry and process parameters). The fundamental understanding of the material flow, its implication on forming various channel parts, and the impact of *FSC* parameters on channel geometry is significant to produce channels with controlled geometry. In non-linear channels, the important factors other than *FSC* parameters (affecting channel geometry and uniformity along the path) are the change in path and the positions of advancing side (*AS*). The fundamental understating about how the change in path and position of advancing side drives the change in channel geometry is essential to produce controlled and uniform channels along non-linear paths. The fabricated channels by *FSC* are different from conventional channels due to irregular shapes and large surface roughness. Besides, the axial wall conduction and surface roughness effects significantly affects heat transfer in rough channels fabricated on a highly conductive and bigger metal substrate. Hence, it is significant to know the friction stir channels' heat transfer and fluid flow characteristics to illustrate their feasibility and capability as cooling channels. The main focus of this research work is to study the previously discussed three significant aspects of the Friction stir channeling process. In the present study, Friction stir channels are fabricated using Vertical *CNC* Machine Center (*VMC*) in 6061 T6 Aluminium Alloy plates using high- speed steel (*HSS*) tools. The concept of classic clearance-based *FSC* is utilised to fabricate entire channels.

The analysis of material flow and its association with different channel parts is carried out. We have used X-ray Micro Computed Tomography (*XR-MCT*) combined with optical microscopy to investigate material flow and its implication on channel formation. The fundamental understanding of the effect of tool geometry (Pin Diameter (*PD*), Shoulder Diameter (*SD*), and Pin Length (*PL*)) and process parameters (Tool rotation speed (*N*), Tool travel speed (*V*), Shoulder clearance (*G*)) on material flow and channel geometry is developed with the help of optical macrographs. The fundamental knowledge about the variation in channel geometry with the change channel path and position of advancing side in curved channels is developed. The synchronisation developed between the channel areas and real-time spindle torques is used to obtain an elementary explanation as to what drives the change in channel geometry. The torque variations due to the parametric variations (*N*, *V*, *G*), are investigated to establish the correlation with channel geometry. The thermo-hydraulic performance of a mini channel (Hydraulic diameter (D_h) = 1.939 mm) is explored using de-ionized water as a working fluid. The overall heat transfer performance and surface roughness effect on heat transfer are evaluated with the average Nusselt number. In fluid flow analysis, the variations in Friction factor are studied to determine the effect of surface roughness. The local wall temperature distributions are analysed to identify the impact of axial wall conduction. The impact of process parameters (*N*, *V*, *G*) on hydraulic diameters and channel performances of different channels is determined.

The results show that pin-influenced material region, (advancing side channel wall, retreating side channel wall, channel roof, and channel bottom) and shoulder influenced material region (top portion of channel roof) are responsible for forming four sides of the channel. An increase in pin diameter significantly affects the material flow and channel geometry behaviour. The reduction in pin length and rise in shoulder diameter resulted in the decline in cross-section area with no change in the channel shape. The decrease in the cross-section area of the channel is observed with the rise in tool rotation speed, tool travel speed, and reduction in shoulder clearance. The channel shape is significantly affected by shoulder clearance, in contrast to tool rotation speed and tool travel speed. It is found that the torques and areas of the curve_1 (C_1) are higher than curve_2 (C_2). The difference between the torque and area values of the linear segments is attributed to the difference in heat input, while to the change in path and position of the advancing side during curve segments. The torque and area are observed to reduce with increase in tool rotation speed, and increased with increase in tool travel speed. The torque is reduced, and the area is augmented with the increase in shoulder clearance. The local wall temperature distributions indicated that the axial wall conduction effect significantly affects heat transfer through the mini channel. The higher average heat transfer (Nusselt numbers) and flow characteristics (Poiseuille numbers) are obtained due to the presence of surface roughness. The higher heat transfer coefficient and pressure drop are obtained at the moderated tool rotation speed & shoulder clearance. The heat transfer coefficient and pressured drop are increased with a reduction in tool travel speed.

These findings are based on the study carried out on Aluminium Alloy as work- piece material. However, the fundamental understanding developed about the material flow, the impact of *FSC* parameters on material flow and channel geometry, geometry variations along curved channel paths, thermo-hydraulic and scaling effects behaviour of channels, will be stepping stone. It will provide the foundation for future work on other materials. Many of the *FSC* characteristics demonstrated for Aluminium can also be seen in the channeling of different materials, such as copper, magnesium, titanium, and steel. Further, these findings will help to design and develop the cooling channels produced through the *FSC* process for applications in thermal management systems.

Title: Quasi-coupled solidification and heat transfer-material flow modelling for directed energy deposition process of Al-0.5Sc-0.5Si alloy

Researcher: Singh, Amit Kumar

Supervisor: Arora, Amit

Year: 2021

Keyword's: Additive Manufacturing, Power Bed AM Process, Rapid Solidification, Energy Deposition Process, Thermal Gradient

Call No.: 621.4022 SIN

Acc. No.: T00938

Abstract: The Additive Manufacturing (AM) process has significantly increased over the conventional manufacturing process, primarily due to its broad application in automobiles, aerospace, electronics, medical, and sports industries. In aerospace, AM is used to manufacture complex objects such as turbine blades and fuel injector nozzles. Similarly, this process is applied in the biomedical field to produce implants and fabricate patient-specific prostheses at a reduced cost. Likewise, it is used in electronic industries to design new product features like six-sided gaming die and PCB circuits. The AM process also aids in manufacturing lightweight structures by optimizing the design, which ultimately reduces material wastage. It has been widely explored for fabricating stainless steel, nickel alloy, and titanium alloy components in industry and academia to reduce manufacturing costs. In this process, the post-processing techniques like joining and machining are eliminated during deposition, and intricate shapes of an object are created in a single step using metallic powder. However, the high-quality spherical metallic powders are costly and cannot be reused due to heavy oxidation, increasing production costs. Also, numerous defects such as porosity, delamination, warping, and residual stress adversely affect the mechanical properties. Thus, the hit and trial experiments are needed to minimize the defects. The defects formation is affected by the temperature distribution and fluid flow inside the melt pool. Therefore, to fabricate defect-free specimens, anyone must understand the underlying physics of heating, melting, solidification, and cooling phenomena in the AM process.

The powder feed method called Directed Energy Deposition (DED) process is a type of AM process. The heat transfer and material flow numerical model is developed for the Laser-assisted Directed Energy Deposition (DED-L) process using the Finite Volume Method (FVM). The multi-layer deposition of incoming materials is simulated for DED-L, including numerous assumptions. Various physics such as moving heat source, conduction, convection mode of heat transfer, solid and liquid phase change, the effect of turbulent mixing inside melt pool, Marangoni effect, and remelting of deposited layers are considered in the numerical model. The moving heat source with variable grid size is used to reduce the computation time in a model.

The temperature field and melt pool size are obtained by solving the mass, momentum, and energy conservation equations. The computed thermal cycles for multi-layered deposition in the DED-L process are tested and validated with the actual experimental results for Al-0.5Sc-0.5Si alloy. The computed thermal cycles and melt pool size for multi-layer deposits show better agreement with

the experimental results. The effects of process parameters such as laser power (P , Watt), deposition speed (V , mm/s), laser beam radius (r_b , mm), and build temperature (T , K) in the thermal cycle are studied in detail.

The solidification of a melt pool in AM process is relatively different than the conventional casting process. The rapid solidification in AM leads to the quick removal of thermal energy from the liquid melt pool to solidify the materials at room temperature. The Columnar-to- Equiaxed Transition (CET) diagram using the Kurz-Giovanola-Trivedi (KGT) model is developed for multi-component Al-0.5Sc-0.5Si alloy. Process-microstructure solidification map is generated for varying process parameters in the DED-L process. The thermal gradient (G , K/m) is mapped over the solidification map to predict the solidification morphology. The morphology of microstructure continuously varies equiaxed to columnar from top to 99.9% of melt pool depth. The process parameters such as deposition speed, laser power, laser beam size, and build temperature are varied to compute microstructure morphologies. The morphologies of solidification microstructure are studied using the Electron Backscatter Diffraction (EBSD), optical microscope, and Scanning Electron Microscope (SEM) technique. The predicted solidification morphologies show better agreement with the observed micrograph.

The room temperature and build temperature deposition micrograph show mixed columnar and equiaxed grains inside the melt pool. However, the fraction of grains varies with different process parameters, and the highest fraction of equiaxed grains is observed for maximum build temperature. The fraction of equiaxed grains and nano precipitates (Al₃Sc) correlate with the computed cooling rate and heat input from top to bottom and different process parameters. The maximum build temperature shows a lower cooling rate and larger remelting region than room temperature deposition. The multiple remelting of the deposited layer leads to very fine precipitates and equiaxed grains, resulting in higher mechanical strength. The microhardness value of the build temperature sample is compared with the sample deposited at room temperature. The build temperature sample shows higher microhardness than room temperature and is nearly equivalent to a heat-treated sample.

Title: A bicrystal-template based approach to study grain boundaries
Researcher: Dish, Nilabh
Supervisor: Gautam, Abhay
Year: 2022
Keyword's: HAGB, Transmission Electron Microscope, NaCl Crystal, Single-crystal Salt, Materials Genome Initiative
Call No.: 620.11299 DIS
Acc. No.: T00947

Abstract: One of the key goals of materials research is to develop models and tools to predict and simulate material behavior and, therefore, expedite materials development. The last few decades have seen a large-scale systematic effort to accelerate such research under various initiatives, including through-process modeling, integrated computational materials engineering (ICMR), materials Genome Initiative (MGI), etc. State-of-the-art calculations allow us to study the equilibrium structure of materials and simulate their behavior in various environments. However, our ability to deal with non-equilibrium aspects, especially materials defects such as grain boundaries (GB), and its contribution towards the material's overall performance is still quite limited. The current approach typically considers the statistically averaged influence of the GB and does not have a routine to account for the peculiarity of an individual GB. This capability is highly desirable for multiple reasons; for instance, abnormal grain growth can be triggered by a GB with specific crystallographic characteristics, which may not be possible to capture using a mean-field approach. These limitations become more evident as the push for material development explores designing at smaller length scales and therefore introducing larger interface content, making their contribution significant.

One of the most successful approaches to study GB phenomenon involves the use of bicrystal samples. They offer selectivity while minimizing the influence of other microstructural parameters. The sample for such studies is typically prepared through epitaxial or directional growth of a metal on a substrate or seed crystal, respectively. However, these techniques are either effective in the fabrication of a narrow range of GBs or lack specificity in terms of the choice of the GB. This work aims to develop a simple, cost-effective, reproducible, and relatively general method of preparing a bicrystal sample with single and specific GB. In this study, we propose a rock-salt (NaCl) bicrystal template-based approach to prepare a free-standing, bicrystal metal film to study the structure and property of a GB. The approach involves: Polishing the single-crystal salt to obtain desired crystallographic plane. This is achieved through a combination of mechanical polishing and etching of the surface to obtain a smooth surface. Diffusion bonding of the two salt crystals along the polished surface to obtain desired GB. This is achieved by heating the crystals under low pressure in a furnace while placing the polished surfaces of the two crystals parallel to each other with a desired in-plane rotation. The bonded crystal is then used as a substrate to epitaxially grow the metal films using a physical vapor deposition process.

The salt substrate is dissolved in distilled water to obtain a free-standing metal film that can be easily transferred to study the GB's structure and/or property. Extensive polishing and characterization of single-crystal NaCl were done to obtain optimum NaCl surface for joining and epitaxial growth of the metal film. Various oriented single-crystal films of copper, gold, and silver were prepared. These include [110], [111] and [112] metal films. The growth of high-index oriented metal film such as [112] was a significant finding of this work. Further, a systematic study of the various surface preparations, including a) ethanol- treatment, b) deionized-water treatment, and c) furnace-annealing, were also investigated. Observations from film grown on the treated surface reveal enhancement in the cube-on-cube oriented growth of face-centered cubic (fcc) metal films on the (110) and (111) surface of NaCl. While these results do support hydroxide substitution surface assisting the epitaxy, similar enhancement on the furnace annealed surface suggests an alternate mechanism that might be responsible for better epitaxial growth of fcc film on the air-cleaved or substituted surface of the NaCl crystal.

Bicrystal templates of salt crystals with (210) and (310) symmetric tilt grain boundary (STGB) were successfully prepared using the proposed technique. The work involved optimizing various mechanical polishing routines and surface preparations followed by diffusion bonding. The template prepared was then used to epitaxially grow the [001] oriented Cu film of thickness $\sim 50\text{nm}$. These Cu films were transferred onto a transmission electron microscope (TEM) grid for observation.

Both high-resolution TEM (HRTEM) and selected area electron diffraction (SAED) revealed that fabricated high angle grain boundary (HAGB) generally followed the intended misorientation between the two crystals. These boundaries did include some pinholes and minor deflection and modulation of the GB. However, regions of clean and well-defined GB segments were available and easy to find. In addition, the process was also used to prepare low- angle GB which was used to benchmark the electrical property measurements of a single crystal and across GB.

The GBs are well recognized for increasing the electrical resistance of metals due to increased electron scattering. A two-point probe technique was used to measure the electrical resistance across the fabricated GB, including the low-angle and the two HAGB. These measurements were compared with the experimental result from a single crystal. The measured values followed the expected trend where the electrical resistance of the single crystal region was found to be the lowest and comparable to the low-angle boundary. The two S5 HAGB had higher resistance values. Overall, the methodology presents a novel and straightforward approach for the fabrication of GBs that are both unique and cost-effective, would enable systematic investigations of the correlations between GB property and their structure in metals.

Title: Functionalization of Cu-centered MOF to enhance its hydrolytic stability and application in Pb(II) trapping with high adsorption capacity
Researcher: Goyal, Prateek
Supervisor: Misra, Superb K.
Year: 2022
Keyword's: Metal Organic Frameworks (MOFs), MOFs-Synthesis, Hydrolytic Stability
Call No.: 620.18 MIS
Acc. No.: T01021

Abstract: Metal-organic frameworks (MOFs) have established themselves as versatile material with applications in gas adsorption/storage, environmental applications, as well as membrane technologies (water harvesting, desalination membranes). High porosity, structural uniformity, multifunctionality, and site accessibility are some of the reasons making MOF an ideal candidate for adsorption/storage-related applications. This thesis aims to understand the lead (Pb(II)) adsorption mechanism for Cu-centered MOFs and to explore the strategies to improve the hydrolytic stability of Cu-centered MOFs. We established HKUST-1 to have an ion-exchange-dominated mechanism for Pb(II) removal. HKUST-1 MOF as an adsorbent showed exceptional selectivity and very high adsorption capacity (610 mg g^{-1}) for Pb(II) adsorption. Although HKUST-1 demonstrated high adsorption capacity, HKUST-1 MOF suffers from poor chemical stability and disintegrates in water. Partial Fe substitution ($\sim 5 \text{ mol\%}$) yielded a significant enhancement in the hydrolytic stability of HKUST-1, wherein the structure was intact for up to 10 hrs of water treatment. For the pristine HKUST-1, only 33.4% crystallinity was retained and 93.3% loss in specific surface area was observed after exposure to water for 2 hrs. In contrast, 86% crystallinity and 89% specific surface area (11% loss) was retained in the case of $\text{Fe}_{0.05}$ HKUST-1. Fe doped HKUST-1 showed exceptionally high Pb(II) selectivity, Pb(II) removal efficiency of $> 90\%$, and a high Pb(II) adsorption capacity of 565 mg g^{-1} . Along with doping as a successful strategy, we also replaced 1,3,5 benzene tricarboxylic ligand (used in HKUST-1) with imidazolate-based ligand (Cu-Imidazolate MOF) and niacin-based ligand (Cu-Niacin MOF) to improve the hydrolytic stability of Cu-centered MOF from under 2 hrs to more than 48 hrs. The Cu-Imidazolate MOF showed exceptional hydrolytic stability across acidic and basic pH, as well as at high temperatures. Cu-Imidazolate MOF also showed a high Pb(II) adsorption capacity of 492 mg g^{-1} . The Cu-Imidazolate MOF additionally showed Pb(II) adsorption for 4 cycles, with a removal efficiency after the 4th cycle of 99.5% and a desorption efficiency after the 3rd cycle of 92.68%. The environmental application of MOFs poses a risk of environmental toxicity, therefore understanding the toxicity of MOFs and their ecotoxicological impact is very important. Nano-sized MOFs (ZIF-8 MOF) were prepared due to their enhanced mobility and possible environmental transformations. RBITC functionalized ZIF-8 MOF were naturally exposed to *C. elegans* ($0.16\text{--}16.4 \text{ }\mu\text{g mg}^{-1}$) and fluorescence was detected in the pharyngeal and gut lumen regions of the worms after 4 h of treatment, for exposure concentrations $>0.163 \text{ }\mu\text{g mg}^{-1}$. The uptake of RBITC@ZIF-8 MOF for an exposure concentration of 0.163, 1.63, and $8.2 \text{ }\mu\text{g mg}^{-1}$ was found to be 52.1, 11.4 and 28.6%, respectively. Overall, the stable Cu-centered MOFs developed in this project showing very high adsorption capacity and high selectivity for Pb(II) could be promising adsorbent material for Pb(II) trapping from a highly Pb(II) rich system. Through this study, we successfully enhanced the

hydrolytic stability of Cu- centred MOFs either by doping or ligand engineering which will pave a way for commercial applications.

Title: Fabrication of Porous structure through vapor phase dealloying of Mg-Zn alloys
Researcher: Behera, Rakesh
Supervisor: Gautam, Abhay
Year: 2023
Keyword's: Porous Metals, Dealloying Vapor Phase Dealloying (VPD), FactSage Software
Call No.: 620.381531 BEH
Acc. No.: T01022

Abstract: Porous materials are increasingly used in applications where the requirements range from enhanced transport kinetics to higher specific surface area. Depending upon the pore size, distribution and connectivity, these porous structures are often referred to as foams, nano- porous materials etc. The conventional approach to fabricating porous structures includes the melt infiltration method (MI), spacer-based powder metallurgy (PM) route; Titanium wire space holder (TWSH); Hydrogen injection (HI), Additive manufacturing (AM) & mechanical perforation (MP). However, conventional approaches have limitations in controlling the pore size and 3D interconnectivity of porous materials. In the PM route, the fabrication of sub- micro pores is more challenging due to the difficulty of dispersing ultrafine spacer particles with metal powder. The TWSH technique imposes a challenge in thinning down Titanium wire diameter below 250 μm and forming an entangled 3D shape. However, in the MI technique, the process parameters (infiltration pressure, melt casting temperature, atmosphere and the preform template strength) make the entire process complicated. The absence of an interconnected porous network is the primary concern in the HI technique. Lastly, in AM technique, handling laser or electron beams is extremely challenging, especially flammable materials or high vapor pressure materials (Magnesium, Zinc, Cadmium & Calcium).

Efforts to achieve better control over the pore size and distribution, especially towards lower length scale, has led to significant interest in developing the dealloying route of pore formation. The pore formation involves a new lump forming-disintegrating mechanism which is assisted by spinodal decomposition. Chemical and liquid metal dealloying are two commonly used dealloying techniques to prepare bulk porous structures. The chemical route, however, is limited to noble metals, stable compounds, and easily passivated transition metals. In contrast, liquid metal dealloying is limited to elements that can satisfy the requirements of miscibility. One of the most recent developments in this area has been the vapor phase dealloying (VPD) for the fabrication of nanometer-scale pores is by dealloying. This method results in forming a well-defined 3D interconnected porous network structure. A wide range of elements, irrespective of their miscibility parameter and chemical activity especially high reactive metals such as Magnesium (Mg), can be used for fabricating the 3D interconnected porous structure. Mg is fascinating because it is one of the most abundant materials and has an outstanding strength-to-weight ratio. Its biodegradability, non-toxicity, and excellent mechanical and physical properties are similar to bone properties. Hence porous Mg has attracted

considerable attention due to its great potential as a biodegradable implant material. Therefore, this work aims to fabricate a porous Mg structure by using the VPD technique.

In the VPD technique, the difference in vapor pressure among the constituent elements present in the alloy system plays a critical role in fabricating the porous metal structure. To form a 3D interconnected porous structure, the element with the highest vapor pressure sublimates first, and the remaining components reorganize themselves due to surface diffusion to create a 3D interconnected porous structure. According to the pure elements' vapor pressure vs. temperature graph, Cadmium and Zinc exhibit higher vapor pressures than Mg. However, Zn was preferred over Cd (toxic element) as the sacrificial element to fabricate the Mg porous structure. The choice of alloy and its composition was limited to binary systems to avoid experimental complexity as well as to make data interpretation relatively straightforward. According to the equilibrium phase diagram of Mg-Zn alloy systems, various intermetallic compounds are formed in the Mg-Zn alloy system depending on the percentage of Zn & the alloy system is complex. Therefore, to begin the experiments, the Mg-Zn alloy's initial parting limit is calculated using the FactSage software. Based on the Zn activity coefficient, the initial composition of the alloys is identified. After identifying the alloy compositions, the entire experiment is conducted in three steps:

The approach involves:

1. Preparation of Mg-Zn alloy by varying the Zn percentages as 15 at%; 57 at%, 75 at% & 90 at%
2. Optimization of the dealloying parameters, i.e., the temperature and the time in a constant vacuum condition to fabricate the porous structure
3. Investigate the effects of temperature and time on the dealloying kinetics process

The Mg-Zn alloys needed for this study are prepared through an electric arc melting route. All the Mg-Zn as-cast alloys ($\text{Mg}_{85}\text{Zn}_{15}$, $\text{Mg}_{57}\text{Zn}_{43}$, $\text{Mg}_{25}\text{Zn}_{75}$, and $\text{Mg}_{10}\text{Zn}_{90}$) are prepared through a non-equilibrium cooling process. Therefore, the homogenization process is carried out at 280°C for 48 hours to improve phase stability, compositional homogeneity, and uniform distribution of phases in the alloy systems. The overall chemical composition of the alloy system remains constant during the homogenization process. The VPD process is performed on the Mg-Zn alloys by cutting them into 3 mm thick samples and polishing them with 1 μm alumina suspension. The dealloying process uses a home-built vacuum annealing chamber to fabricate the 3D interconnected porous structure. In the dealloying process, the vacuum condition of the chamber is kept constant. Dealloying experiments are done at a series of times and temperatures. According to the experimental results, the only successful Mg-Zn alloy composition is $\text{Mg}_{10}\text{Zn}_{90}$, which forms a 3D porous network structure. The structure of a full 3D interconnected porous network has been successfully fabricated at 265°C after the alloy has been held there for 6 hours. The pore size that is present within the 3D interconnected porous structure varies in the range of 2-75 μm . Furthermore, a systematic study is conducted by using various dealloying temperatures and dealloying holding times in order to investigate the VPD kinetic process & coarsening phenomena of the 3D interconnected porous structure of $\text{Mg}_{10}\text{Zn}_{90}$ alloy. According to the results, it is evident that in the VPD technique, the dealloying process

becomes faster as the temperature increases. Therefore, dealloying temperature plays a critical role in order to control the dealloying holding time and the coarsening phenomena of 3D interconnected porous structure. According to SEM cross-section micrographs, at constant dealloying temperature and vacuum conditions, the thickness of the porous structure increases with dealloying time. According to the kinetic study, the thickness variation of porous structures is controlled by reaction-controlled mechanisms. The phase analysis of the final 3D porous structure suggests that the porous structure is composed of $MgZn_2$ phase. Finally, the present study will pave a new way for fulfilling the aforementioned objective & developing new type Mg-Zn based porous materials for various advance applications. Overall, this dealloying technique has proven to be a straightforward approach & environment friendly for fabricating 3D interconnected porous structures.

Title: High temperature oxidation behavior of high entropy alloys
Researcher: Dehury, Ranjit Kumar
Supervisor: Gautam, Abhay
Year: 2023
Keyword's: High Entropy Alloys (HEA), Cantor Alloy, Oxidation-HEA, FeCoNi-CoCrFeMnNi
Call No.: 620.16 DEH
Acc. No.: T01031

Abstract: To improve the mechanical, physical, and chemical properties of an element, the conventional approach relied on the addition of a small amount of one or more elements to achieve the desired outcome. Recently, researchers have started systematically exploring multi-principal component material systems. Among these, high-entropy alloys (HEA) have received exceptional attention due to a combination of factors that make them a quite promising candidates for a range of applications. The four core effects-high entropy, lattice distortion, sluggish diffusion, and cocktail effect-are commonly used to explain the observed properties and microstructure of a HEA. High entropy alloys are defined as near-equimolar compositions of five or more elements. Almost two decades of active research have produced numerous HEA families, each with distinct intended applications. The potential of these alloys in industrial applications is being actively explored. This area, which is important for both academic and commercial applications, still has a lot of untapped potentials and offers a huge amount of space for both academic and industrial research.

One of the strategic areas of application of HEAs is at high-temperatures and/or aggressive environments such as nuclear, aerospace, marine etc. due to its promising mechanical properties, thermal stability, superior oxidation resistance and thermal fatigue. Superalloys such as those based on nickel are typically used for such high temperatures applications however, they are expensive. The temperature limit of Ni-based superalloys is typically up to 1000 °C. Moreover, properties like low creep strength, poor thermal conductivity, difficulty in machining and low fatigue resistance demand the innovation of new advanced materials. The development of new high-temperature oxidation-resistant materials has thus been one of the primary priorities of the high-temperature materials research field. Some HEAs, perform well under high-temperature oxidation but are less expensive compared to Ni-based superalloys. Therefore, they have certain cost advantages and have emerged as alternatives. Refractory HEAs may eventually take the place of nickel-based superalloys in high- temperature applications. They are expected to significantly improve gas turbines' thermal efficiency by sharply raising the application temperature to over 1300 °C.

CoCrFeMnNi also known as cantor alloy is one of the most researched alloys because of its unique structure and characteristics. This work aims to investigate the surface segregation thermodynamics of CoCrFeMnNi at high temperatures both in a vacuum and with a dry oxygen environment. While no such segregation was seen in a vacuum, exposure to O caused substantial segregation of Cr and Mn with minimal outer diffusion of Fe, Ni, and Co. In the CoCrFeMnNi alloy, the short-term vs. long-term evolution of different oxides as well as their evolution in real time were carefully examined. Additionally, by selecting CoCrFeNi and CoFeMnNi, the competition between the key alloying elements responsible for higher and lower oxidation rates was further investigated. A test was also

conducted to get some understanding of the oxidation behaviour brought on by the accelerated oxidation in the liquid state. CoCrFeNi alloy oxidation rate was low compared to those of CoCrFeMnNi alloy. The oxidation rate of CoFeMnNi alloy was highest among the three alloys. The high-temperature prolonged exposure of CoCrFeMnNi resulted in the formation of multiphase oxides with discontinuous scale and experienced severe oxide scale spallation.

Based on results from the comprehensive characterization of the base cantor alloy, an effort was made to improve the high-temperature oxidation behaviour of the alloy through the addition of Ta and Al. Both alloys display a parabolic kinetic behaviour, with CoCrFeMnNi and CoCrFeMnNiTa exhibiting comparable oxidation rates and CoCrFeMnNiAl showed a substantially lower oxidation rate than CoCrFeMnNi at 1000 °C. Both alloys exhibit considerable resistance to oxide scale spallation as well as developed multi-layered complex oxide scales. While CoCrFeMnNiTa primarily forms rutile-type CrTaO₄ oxide, which drastically reduces oxygen and nitrogen inward diffusion and suppresses the escape of other alloying elements, the superior oxidation resistance for CoCrFeMnNiAl could be related to the emergence of distinctive Cr₂O₃ and Al₂O₃ scale.

Furthermore, the microstructure of CoCrFeMnNi HEA Films was explored by growing the film on a (100) surface of a sacrificial NaCl substrate at a substrate temperature ranging from -143 °C to 600° C. The films grown at cryogenic temperatures were found to be amorphous while partially crystalline regions were observed for growth at room temperature. Polycrystalline films were commonly obtained when grown on heated substrates. However, in the narrow temperate range of 400 - 450° C the alloy film growth displayed partial epitaxy suggesting the possibility of growing crystallographically oriented films of the high entropy alloys under more refined growth conditions. Due to their unique properties, HEAs have the potential to be used as coating materials for high-temperature applications.

* * * * *



MATHEMATICS

Mathematics

Title: Investigations on biharmonic boundary value problems with qualitative questions
Researcher: Dwivedi, Gaurav
Supervisor: Tyagi, Jagmohan
Year: 2017
Keyword's: Biharmonic Boundary, Equation, Boundary Data Models
Call No.: 515.353 DWI
Acc. No.: T00217

The present work in the thesis deals with the existence and qualitative questions to biharmonic boundary value problems. More specifically, we establish the existence of solution to several type of biharmonic equations and systems. We also generalise several celebrated identities and inequalities to the biharmonic operator setting, such as Picone's identity, Caccioppoli's, Adams' inequalities and also consider some applications. This work is motivated by the interest of many researchers in the study of biharmonic equations. The Biharmonic equation $\Delta^2 u = f$ with suitable boundary data models various physical problems related to plates, e.g., Dirichlet boundary conditions ($u = 0 = \frac{\partial u}{\partial \nu}$ on boundary) model clamped plates, Navier boundary conditions ($u = 0 = \Delta u$ on boundary) model hinged plates etc. First, we consider the problem of the existence of a positive solution to the following biharmonic system:

$$\begin{cases} \Delta^2 u = \lambda a(x)f(v) & \text{in } B, \\ \Delta^2 v = \lambda b(x)g(u) & \text{in } B, \\ u = 0 = v & \text{on } \partial B, \\ \frac{\partial u}{\partial \nu} = 0 = \frac{\partial v}{\partial \nu} & \text{on } \partial B, \end{cases} \quad (0.1)$$

where B denotes the unit ball in \mathbb{R}^n with boundary ∂B , λ is a positive parameter, $a, b : \Omega \rightarrow \mathbb{R}$ are sign changing potentials, $f, g : [0, \infty) \rightarrow \mathbb{R}$ are continuous with $f(0) > 0, g(0) > 0$. We prove the existence of a positive solution to (0.1) with the aid of the Leray-Schauder fixed point theorem, by utilising the representation of the solution to (0.1) in a ball. We also establish the existence of a unique weak solution to the following system of biharmonic equations:

$$\begin{cases} \Delta^2 u = a(x)g(x, v) & \text{in } \Omega, \\ \Delta^2 v = b(x)h(x, u) & \text{in } \Omega, \\ u = 0 = v & \text{on } \partial\Omega, \\ \frac{\partial u}{\partial \nu} = 0 = \frac{\partial v}{\partial \nu} & \text{on } \partial\Omega, \end{cases}$$

without monotonicity assumptions on the nonlinearities, in a smooth and bounded domain Ω . We assume that $a, b \in L^\infty(\Omega)$ are sign changing potentials. We use theory of monotone operators to prove our existence results. Further, we establish the existence of a unique weak solution to the following singular biharmonic system:

$$\begin{cases} \Delta^2 u = a(x) \frac{g(x, v)}{|x|^4} & \text{in } \Omega, \\ \Delta^2 v = b(x) \frac{h(x, u)}{|x|^4} & \text{in } \Omega, \\ u = 0 = v & \text{on } \partial\Omega, \\ \frac{\partial u}{\partial \nu} = 0 = \frac{\partial v}{\partial \nu} & \text{on } \partial\Omega, \end{cases}$$

where $0 \in \Omega \subseteq \mathbb{R}^n, n \geq 5$ and $a, b \in L^\infty(\Omega)$ are sign changing potentials. We prove our result by utilising the theory of monotone operators and the Rellich inequality.

Next, we consider the problem of the existence of a solution to the following biharmonic equation:

$$\begin{cases} \Delta^2 u - \alpha |\nabla u|^r = \det(D^2 u) + \lambda f + \mu a(x)u^2 + vb(x)u^q & \text{in } \Omega, \\ u = 0 = \frac{\partial u}{\partial \nu} & \text{on } \partial\Omega, \end{cases}$$

where $\Omega \subseteq \mathbb{R}^2$ is a smooth and bounded domain, $\alpha \geq 0, \lambda > 0, \mu > 0, v > 0, a, b, f \in L^1(\Omega), r \geq 1$ and $0 < q < 1$. The special feature of this problem is that it involves the determinant of the Hessian with sign changing concave, quadratic and gradient nonlinearities. We remark that nonlinearities of the type $\mu a(x)u^p + vb(x)u^q$, where $0 < q < 1 < p < \infty$ are called concave-convex nonlinearities. The main difficulties arising in these problems are due to the determinant of the Hessian of the function and the involvement of sign changing concave, quadratic and gradient nonlinearities. Because of the presence of the gradient term, the problem is not variational, in general. To overcome this difficulty, we make use of an iteration technique introduced by Figueiredo et.al. We employ certain inequalities allowing to place the determinant of the Hessian in Hardy space and prove the existence and multiplicity of solutions by using critical point theory.

We also deal with Picone's identity for the biharmonic operator on the Heisenberg group. Picone's identity plays an important role in the qualitative theory of elliptic PDEs. The classical Picone's identity says that if u and v are differentiable functions such that $v > 0$ and $u \geq 0$, then

$$|\nabla u|^2 + \frac{u^2}{v^2} |\nabla v|^2 - 2 \frac{u}{v} \nabla u \nabla v = |\nabla u|^2 - \nabla \left(\frac{u^2}{v} \right) \nabla v \geq 0. \quad (0.2)$$

(0.2) has numerous applications to second-order elliptic equations and systems. We extend the identity (0.2) to biharmonic operators and also establish its nonlinear analogue. As an application of it, we establish a Hardy type inequality, a Picone inequality, a Caccioppoli inequality and the monotonicity of the first eigenvalue of the associated problem. We also obtain Picone's identity for operators of form $-div(a(x, u, \nabla u))$, whose coefficients $a : \Omega \times \mathbb{R} \times \mathbb{R}^n \rightarrow \mathbb{R}^n$ satisfy certain hypotheses. This operator generalises the Laplace and p -Laplace operators. As an application of Picone's identity, we establish a Hardy type inequality, a Sturmian comparison theorem, the monotonicity property of the first eigenvalue, nonexistence of positive supersolutions and a Caccioppoli inequality.

Further, we establish an Adams type inequality for the biharmonic operator on the Heisenberg group. Let $\Omega \subseteq \mathbb{R}^n$, $n \geq 4$ be a bounded domain. The Sobolev embedding theorem says that for $p < n$, $W_0^{2,p}(\Omega) \hookrightarrow L^q(\Omega)$, $1 \leq q \leq \frac{np}{n-p}$. For the limiting case $p = n$, we have $W_0^{2,n} \hookrightarrow L^q(\Omega)$, $1 \leq q < \infty$ but it is well known that $W_0^{2,n}(\Omega) \not\hookrightarrow L^\infty(\Omega)$. Then there is a natural question that what is the smallest possible space in which, we have embedding of $W_0^{2,n}(\Omega)$? This question was answered by D.R. Adams in the case of bounded domains in \mathbb{R}^n . We extend the Adams' inequality to the case of bounded domains in Heisenberg group \mathbb{H} . We make use of convolution results involving Reisz potential established by W.S. Cohn and G. Lu. We also establish an Adams type inequality with singular potential. As an application of Adams' inequality, we prove the existence of solution to the following biharmonic equation with Dirichlet's boundary condition on the Heisenberg group:

$$\begin{cases} \Delta_{\mathbb{H}}^2 u = \frac{f(\xi, u)}{\rho(\xi)^a} \text{ in } \Omega, \\ u|_{\partial\Omega} = 0 = \frac{\partial u}{\partial \nu} \Big|_{\partial\Omega}, \end{cases} \quad (0.3)$$

where $0 \in \Omega \subseteq \mathbb{H}$ is a bounded domain, $0 \leq a \leq Q$, $Q = 4$ is the homogeneous dimension of \mathbb{H} and the nonlinearity f satisfies certain hypotheses. The problem (0.3) has the following special features, which make it challenging to study. First, it contains the nonlinearity f , which is of exponential growth and the potential $\frac{1}{\rho(\xi)^a}$, $0 \leq a \leq Q$, which has singularity at $\rho(\xi) = 0$. This problem is handled with the use of Adams' inequality with singular potential. Second, the case $a = Q$, is critical for the potential. Since we do not have a singular Adams type inequality in the case $a = Q$, we use an approximation method. More precisely, we approximate (0.3) with a sequence of problems which are subcritical in the potential, i.e., $a < Q$ and then, we pass to the limit to conclude that (0.3) has a nontrivial solution in the case $a = Q$.

Finally, we establish the semi-stability of positive solutions to the following problem:

$$\begin{cases} \Delta^2 u = a(x)u - f(x, u) \text{ in } \Omega, \\ u|_{\partial\Omega} = 0 = \Delta u|_{\partial\Omega}, \end{cases} \quad (0.4)$$

where $\Omega \subseteq \mathbb{R}^n$ is a smooth and bounded subset. The nonlinearities of the type $a(x)u - f(x, u)$ are known as logistic nonlinearities. There have been several research works to study problems related to the existence and stability of solutions to the Laplace equation with logistic nonlinearities. To show the semi-stability of u , we show that the eigenvalues of the linearised operator associated with (0.4) at the point u are non-negative.

Title: Studies on the existence of positive viscosity solutions to fully nonlinear elliptic PDEs
Researcher: Verma, Ram Baran
Supervisor: Tyagi, Jagmohan
Year: 2018
Keyword's: Fluid Mechanics, Elliptic Equations, Laplace Equation, Viscous Flow
Call No.: 515.64 VER
Acc. No.: T00281
Abstract:

The present work in this thesis deals with existence and qualitative properties of solution of fully nonlinear elliptic equations. This type of fully nonlinear elliptic equations arise in the study of stochastic control problem, stochastic differential game theory, etc. More precisely, the value function in stochastic control problem and stochastic differential game theory satisfies fully nonlinear elliptic equations. In particular, if in a stochastic control problem, the diffusion coefficient is a control variable, then we get a very important class of second order fully nonlinear equations so-called extremal Pucci's equations. Extremal Pucci's equations involve extremal Pucci's operators. For given positive constants $0 < \lambda \leq \Lambda < \infty$, extremal Pucci's operators are defined as follows:

$$\mathcal{M}_{\lambda, \Lambda}^{\pm}(X) = \Lambda \sum_{\pm e_i > 0} e_i + \lambda \sum_{\pm e_i < 0} e_i, \quad (0.1)$$

where e_i 's are the eigenvalues of X and $X \in S(n)$, where $S(n)$ is the set of all $n \times n$ real symmetric matrices. From (0.1) it is clear that if $\lambda = \Lambda = 1$, then $\mathcal{M}_{\lambda, \Lambda}^{\pm}(D^2u) = \Delta u$. So naturally extremal Pucci's operators are generalization of Laplace operator. We point out that extremal Pucci's equations have only non-divergence structure and positive homogeneity, consequently, weak formulation emanating from integration by parts is not an appropriate approach for study of extremal Pucci's equations. The interesting property which extremal Pucci's operators share with Laplace operator is maximum principle. The maximum principle allows us to define a new notion of solution so-called viscosity solution. This notion of solution first of all appears in the study of first order Hamilton-Jacobi equation and later it has been generalized in the context of second order elliptic equations satisfying certain maximum principle, see [M. G. Crandall et al., User's guide to viscosity solutions of second order partial differential equations, Bull. Amer. Math. Soc., 27, 1 (1992), 1–67].

Singularly perturbed problems arise in many branches of science and engineering, like, in fluid dynamics, reaction-diffusion process, plate theory, aerodynamics, etc. First of all, these problems appear in [L. Prandtl, Über Flüssigkeitsbewegung bei sehr kleiner Reibung (Motion of fluids with very little viscosity), in Verhandlungen des III Internationalen Mathematiker-Kongresses, Heidelberg, 1904 (B G Teubner, Leipzig), 484–491]. Since then the investigations on the singularly perturbed problems for semilinear/quasilinear equations have been the interest of many researchers. The main progress in the study of singularly perturbed problem for Laplace equation was made by Ni and Takagi, see [W. M. Ni, I. Takagi, On the shape of least energy solution to a semilinear Neumann problem, Comm. Pure Appl. Math. 41 (1991), 819–851]. Later, these results have been generalized to different kind of problems including p -Laplace operator. While in the case of extremal Pucci's operators, such problems first of all have been considered by S. Alarcón et al., see [Existence and multiplicity results for Pucci's operators involving nonlinearities with zeros, Calc. Var. Partial Differential Equations, 45(3-4) (2012), 443–454]. Since last three decades, there has also been a good amount of interests on semilinear elliptic equations with singular nonlinearities due to appearance of these equations in study of non-Newtonian fluids, steady state of thin films, modelling of MEMS devices. The study of existence of positive solutions to such problems was started by M. G. Crandall et al., see [M. G. Crandall, P. H. Rabinowitz, L. Tartar, On a Dirichlet problem with a singular nonlinearity, Commun. Part. Differ. Equ. 2(2), (1977) 193–222] and later has been generalised by many authors in several directions. To establish the existence of positive solutions to these kind of problems, the method of monotone iteration, variational method and topological degree theory are used. In context of fully nonlinear elliptic equation such problems have recently been studied in [P. Felmer et al., Existence and regularity results for fully nonlinear equations with singularities, Math. Ann., 354(1) (2012), 377–400], where the authors show the existence of positive solution and also study its regularity properties.

In view of above mentioned research, we remark that very little research is known for fully nonlinear elliptic equations with gradient nonlinearity and fully nonlinear elliptic equations with singular nonlinearity. Motivation to study such kind of equations with nonlinear growth in the gradient comes from the appearance of these equations in risk-sensitive stochastic control problem, large deviation problems etc., see [W. H. Fleming,, H. M. Soner, Controlled Markov processes and viscosity solutions, Vol. 25, Second Edition, Springer, 2005]. In this thesis, we establish the existence of positive viscosity solutions to singularly perturbed problems for fully nonlinear elliptic equations. We also establish the existence of positive solution to extremal Pucci's equations with singular and sublinear nonlinearity as well as gradient nonlinearity. Lastly, we establish Lyapunov type inequality for extremal Pucci's equations. This thesis consists of seven chapters which are organized as follows:

Chapter 1 has a brief introduction to fully nonlinear elliptic equations and more specifically to extremal Pucci's equations.

In Chapter 2, we give the preliminaries required for the study of the existence of solutions to fully nonlinear elliptic equations and related results. Finally, we state a few important results which have been used in this thesis.

Chapter 3 deals with the existence of multiple positive solutions to the following class of singularly perturbed problems:

$$\begin{cases} -\varepsilon^2 F(x, D^2u) = f(x, u) + \psi(Du) \text{ in } \Omega, \\ u = 0 \text{ on } \partial\Omega, \end{cases} \quad (0.2)$$

where Ω is a smooth bounded domain in \mathbb{R}^n with $n > 2$, $f : \Omega \times [0, \infty) \rightarrow [0, \infty)$ and $\psi : \mathbb{R}^n \rightarrow [0, \infty)$. Here, we assume that $f(x, t)$ is locally Lipschitz in t variable as well as it has a positive zero and ψ is Lipschitz continuous. We show the existence of two positive solutions to (0.2) and the convergence of the solutions to the positive zero of f as $\varepsilon \rightarrow 0$. We remark that the multiplicity of the solutions are obtained by employing degree theory, see [J. Tyagi, R. B. Verma, Existence of solutions to fully nonlinear elliptic equations with gradient nonlinearity, to appear in Taiwanese J. Math, 21(5) (2017), 1037–1056] for the details.

In the continuation of the above problem, with the help of inf regularization, we also show that the Lipschitz continuity of f in the second variable can be relaxed, but in this case, the convergence of the solutions to the positive zero of f is not known, see [J. Tyagi, R. B. Verma, Existence of the solutions to fully nonlinear elliptic equations with non-Lipschitz nonlinearity (under review)].

In Chapter 4, we consider the fully nonlinear elliptic equations with singular and sublinear nonlinearity. More precisely, we consider the following problem:

$$\begin{cases} -\mathcal{M}_{\lambda, \Lambda}^+(D^2u) = \frac{\mu k(x)f(u)}{u^\alpha} - \eta h(x)u^q \text{ in } \Omega, \\ u > 0 \text{ in } \Omega, \\ u = 0 \text{ on } \partial\Omega, \end{cases} \quad (0.3)$$

where h, k are nonnegative bounded and continuous functions on Ω with $\inf_{\Omega} k > 0$ and f is non-increasing. Here, we establish the existence of a positive solution of (0.3) in three different cases: $f(0) > 0$; $f(0) = 0$; $f(0) < 0$. Note that, because of $f(0) < 0$, the problem (0.3) is semipositone and also contains sublinear term. We also show some nonexistence of the solution and monotonic properties of the solution of (0.3) with respect to the parameter η , see [J. Tyagi, R. B. Verma, Positive solution of extremal Pucci's equations with singular and sublinear nonlinearity, Mediterr. J. Math., DOI 10.1007/s00009-017-0950-6].

In Chapter 5, we consider the following problem:

$$\begin{cases} -\mathcal{M}_{\lambda,\Lambda}^+(D^2u) + H(x, Du) = \frac{k(x)f(u)}{u^\alpha} & \text{in } \Omega, \\ u > 0 & \text{in } \Omega, \\ u = 0 & \text{on } \partial\Omega, \end{cases} \quad (0.4)$$

and establish the existence of a positive solution to (0.4). The main feature of the above problem is that it has superlinear growth in the gradient. We remark that superlinear growth in the gradient has attracted a considerable attention in the case of Laplace equation as well as in the case of fully nonlinear elliptic equations, but no existence results are available for fully nonlinear elliptic equations which involve superlinear growth in the gradient as well as singular nonlinearity. In order to handle the general gradient superlinearity, we use the following inequality:

$$|Du|^q \leq (2-q)|Du| + (q-1)|Du|^2, \quad 1 < q \leq 2,$$

and then an appropriate transformation which absorbs the quadratic power of the gradient. In this case also, we show the existence of positive solutions in three separate cases: $f(0) > 0$; $f(0) = 0$; $f(0) < 0$. For the details, see [J. Tyagi, R. B. Verma, Positive solution to Pucci's extremal equations with singular and gradient nonlinearity (under review)].

In Chapter 6, we establish Lyapunov type inequality for extremal Pucci's equations. A. M. Liapunov [A. M. Liapunov, Problème général de la stabilité du mouvement, Ann. Math Stud., 17 (1947), 203–474], established a very famous inequality which gives a necessary condition for the existence of solutions to the boundary value problem for linear second order ordinary differential equations. Later, this inequality has been generalized for the partial differential equations involving Laplace, p -Laplace and fractional Laplace operators. In view of the above, it is a natural question to ask whether one can establish Lyapunov type inequality for extremal Pucci's equation. In this chapter, we answer this question. More precisely, we establish Lyapunov type inequality for the following problem:

$$\begin{cases} \mathcal{M}_{\lambda,\Lambda}^+(D^2u) + b(x)|Du| + a(x)u = 0 & \text{in } \Omega, \\ u = 0 & \text{on } \partial\Omega, \end{cases}$$

see[J. Tyagi, R. B. Verma, Lyapunov type inequality for extremal Pucci's equations(under review)]. Conclusion and future plans are a part of Chapter7.

Thesis ends with a bibliography.

Title: Predictive model development and validation for raised floor plenum data centers
Researcher: Fulpagare, Yogesh Shantaram
Supervisor: Bhargav, Atul
Year: 2018
Keyword's: Energy Efficiency, CFD Model, Effective Tile Properties, Energy
Call No.: 697.9316 FUL
Acc. No.: T00282

Abstract: Electronic data centers that handle enterprise and world wide web transactions typically consist of many servers, along with cooling units & power backup systems. With the explosion in digital traffic, the number of data centers as well as demands on each data center continue to increase. Concomitantly, the cost (and environmental impact of) energy expended in the thermal management of these data centers is of concern to operators in particular, and society in general. The most common data center is the air-cooled type, in which heat generated by computing and memory resources in servers is removed by computer room air conditioning (CRAC) units to maintain safe working temperatures inside the data center. In the absence of physics based control algorithms, CRAC units are typically operated at conservatively pre-determined set points, resulting in sub-optimal energy consumption. This problem is exacerbated in smaller, non-standard data centers that may be operated by relatively small enterprises who cannot own large, optimized data centers. For a more optimal control algorithm, predictive capabilities are needed. In this thesis, we develop a data-informed, experimentally validated and computationally inexpensive system level predictive tool that can forecast data center behavior for a broad range of operating conditions.

Initially, we developed a steady state CFD model of a typical raised floor plenum (RFP) data center system and performed parametric analyses. An important conclusion from this study was that to accurately simulate fluid flow through plenum tiles (and into the data center), effective tile properties must be carefully selected to satisfy mass and momentum balance. Using this tool, we also quantified the impact of plenum chamber obstructions on steady-state data center performance. Once reasonable agreement with literature and experimental data was achieved, we developed a transient CFD model.

Experimentation on live data centers is a challenge, since an increased risk of service disruption is unacceptable. In such cases, a scaled down testing facility enables safe testing and validation of CFD models, and further, to evaluate candidate control strategies. We developed a bench-top test facility (20 times scaled down). Using this scaled-down facility, we established that the CFD models agree well with experiments. This bench scale prototype allows experimentation with various arrangements of server racks (such as conventional RFP or the so-called "s- pod" layouts).

We then performed dynamic thermal response experiments on a full-scale experimental raised floor plenum data center laboratory. At the server, rack and facility levels, the effect of server heat load, CRAC air supply temperature, and CRAC air flow rate were experimentally quantified. The transient CFD models for rack & system level were developed and validated against experiments. CFD solutions incorporating Navier-Stokes equations are computationally expensive for a real-time

control of a data center. To reduce computational expense, we adopted a data driven model and expanded it for the system level non-linear multivariate problem.

The predictive modeling approach utilizes system input and output data to train a coefficient matrix. This coefficient matrix captures system information and is the key to mimic system dynamics in a predictive simulation. This coefficient matrix is unique to each data center; once the coefficient matrix is determined, the thermal behavior of the system can be predicted. We have tested this model against experiments as well as on (experimentally) validated transient CFD simulations. The validated model can accurately forecast temperatures and air flows in a data center (including the rack air temperatures) for ten to fifteen minutes into the future. Once integrated with control aspects, we expect that this model will form an important building block in a future intelligent, increasingly automated data center.

Title: Unboundedness of betti numbers of curves
Researcher: Mehta, Ranjana
Supervisor: Sengupta, Indranath
Year: 2018
Keyword's: Grobner, Betti Numbers, Curves, Arithmetics
Call No.: 515.112 MEH
Acc. No.: T00394

Abstract: This thesis is an attempt to answer the question that given e (embedding dimension), is it true that for all symmetric numerical semigroups with embedding dimension e the cardinality of a minimal presentation is a bounded function of e . For $e = 3$, Herzog in [9] and for $e = 4$, Bresinsky in [3] proved that the symmetry condition on the numerical semigroup imposes an upper bound on the cardinality of a minimal presentation of a numerical semigroup with embedding dimension e . This question remains an open question for $e \geq 5$: In this continuation we have constructed a class of symmetric numerical semigroup of embedding dimension $e \geq 4$; which is formed by concatenation of arithmetic sequences. This example generalize Rosales' result. We calculate the Apéry set and prove that the cardinality of a minimal presentation of the semigroup is a bounded function of the embedding dimension e .

This thesis also deals with the question that given e , how does one naturally generalize the examples of Bresinsky and Moh to construct examples of curves in general embedding dimension e , whereas both examples have unbounded Betti numbers. Bresinsky in [2] gave a family of semigroups in embedding dimension 4 to show that the number of minimal presentation of the family is unbounded above. We explicitly calculated a minimal generating set which is also a Gröbner basis of defining ideal with suitable monomial order. We also calculated all the syzygies of the defining ideal. Bresinsky proved that the minimal number of generators or the first Betti number of the defining ideal is unbounded above. We prove that the same behaviour of unboundedness is true for all the Betti numbers.

The integers n_1, n_2, n_3, n_4 defining Bresinsky's semigroups have the property that $n_1 + n_2 = n_3 + n_4$, up to a renaming if necessary. In an attempt to generalize the Bresinsky example for $e \geq 5$; we constructed a class of numerical semigroup of embedding dimension $e \geq 4$: Suppose $a = e+1$, $b > a+(e-3)d$, $\gcd(a, d) = 1$ and $d \mid (b-a)$. Let $M = \{a, a+d, a+2d, \dots, a+(e-3)d, b, b+d\}$, which forms a minimal generating set for the numerical semigroup $\Gamma_e(M)$, generated by the set M . We calculate the Apéry set and the Frobenius number of $\Gamma_e(M)$.

We also show that the minimal number of generators for the defining ideal p of the affine monomial curve parametrized by $x_0 = t^a, x_1 = t^{a+d}, \dots, x_{e-3} = t^{a+(e-3)d}, x_{e-2} = t^b, x_{e-1} = t^{b+d}$ is a bounded function of e . In an attempt to generalize the Moh's examples in higher dimensions we study Moh's example, which is in dimension 3. Let p_n be the defining ideal of Moh's curves and $P_n = p_n \cap k[x, y, z]$. Our objective was to find a Grobner basis for P_n . At first we study the case $n = 1$: The ideal p_1 is the defining ideal of the algebroid space curve under the parametrization

$$p_1(x) = t + t^{1+\lambda}; p_1(y) = t^2; p_1(z) = t^3;$$

which is complete intersection because $\mu(p_1) = 2$ by [14]. Our aim is to write an explicit minimal generating set for p_1 and show that it is a regular sequence of length 2. We will see that the complete intersection property of p_1 does not necessarily ensure that the contracted ideal P_1 always has the same property. We also find a Gröbner basis of P_1 .

Title: Studies on existence questions of solution to singular elliptic PDEs
Researcher: Kumar, Dharmendra
Supervisor: Tyagi, Jagmohan
Year: 2020
Keyword's: Elliptic, Amann-Sattinger Method, Hardy Potential, Bootstrapping Technique, Sobolev Spaces
Call No.: 510 KUM
Acc. No.: T00556

Abstract:

The present work in this thesis deals with the existence questions of singular elliptic partial differential equations (PDEs). The basic model problem on singular elliptic PDEs is described by

$$\begin{cases} -\Delta w = f(x, w) & \text{in } \Omega, \\ w > 0 & \text{in } \Omega, \\ w = 0 & \text{on } \partial\Omega, \end{cases} \quad (\text{a.1})$$

where $f(x, w) = \frac{1}{w^\delta}$, $\delta > 0$ is a positive real number and Ω denotes an open bounded subsets of \mathbb{R}^N . Problems of type (a.1) arise in different context of engineering and sciences. The investigations on the positive solutions are appropriate in most circumstances because of the meaning of the unknowns (populations, concentrations, etc.).

Let us mention that the first study in this direction is carried out by Fulks and Maybee in [Osaka J. Math., 1960], where they established existence of solution to (a.1) by fixed point method. The problem was then studied by Stuart in [Math. Z., 1976], which deals for the case of $f(x, s)$ exploding at $s = 0$ if $x \rightarrow y$, where $y \in \partial\Omega$. Later Crandall, Rabinowitz and Tartar in [Comm. Partial Differ. Equ., 1977] showed the existence and continuity properties of the solution of (a.1) for the case $f(x, s)$ that does not depend on x .

After the work of Stuart, and Crandall, Rabinowitz and Tartar, problems of type (a.1) with $f(x, s)$ singular at $s = 0$ have been intensively investigated by many authors in past, see, for instance by A. C. Lazer and P. J. McKenna in [Proc. Am. Math. Soc, 1991] and M. M. Coclite, G. Palmieri in [Comm. Partial Differential Equations, 1989] and many others. In the quasilinear case, see the works of J. Giacomoni et al. in [Ann. Sc. Norm. Super. Pisa Cl. Sci. 2007], [C.R. Math. Acad. Sci. Paris, 2012] and [Dyn. Syst. Differ. Equ. Appl. Proc. AIMS 2015].

We recall that the effect of the Hardy potential in elliptic problems has been studied in several papers, see for instance, by H. Brezis and X. Cabré in [Boll. Unione Mat. Ital. Sez. B Artic. Ric. Mat., 1998] and H. Brezis et al. in [Selecta Math., 2005] and many others.

Motivated by the above research, first, we establish the existence of a solution to the following singular elliptic problem:

$$\begin{cases} -\operatorname{div}(|x|^{-2\beta}\nabla w) - \mu \frac{w}{|x|^{2(\beta+1)}} = \frac{g(x)}{w^{\theta_1}} + \frac{f(x)}{w^{\theta_2}} & \text{in } \Omega, \\ w > 0 & \text{in } \Omega, \\ w = 0 & \text{on } \partial\Omega, \end{cases} \quad (\text{a.2})$$

under assumptions $\theta_1 \geq \theta_2 > 0$, $0 < \mu < \left(\frac{N-2(\beta+1)}{2}\right)^2$ and $0 \leq g \in L^k(\Omega)$, $0 \leq f \in L^k(\Omega)$, $1 < k < \frac{N}{2}$, $0 < \beta < \left(\frac{N-2}{2}\right)$. The interesting mention on this problem is that it has singularity at origin as well as on the boundary of Ω . Using Schauder fixed point theorem and an a priori estimate, we obtain existence and regularity results of (a.2), depending on θ_1 , f and g .

Going further in the study to singular elliptic problem, Coclite and Palmieri in [Comm. Partial Differential Equations, 1989] studied another type of following singular elliptic problem with supercritical

More precisely, he established that

$$\frac{4}{T} \leq \int_0^T |v(t)| dt \quad (\text{a.14})$$

is a necessary condition for a nontrivial solution of (a.13). Let us mention that the inequality (a.14) has many applications, for instance, in stability questions, eigenvalue bounds for ODE, a priori estimates and many others involve inequality of type (a.14).

In the nonlinear setting, Elbert in [Colloq. Math. Soc. János Bolyai, 1979] derived the following inequality

$$\frac{2^p}{T^{p-1}} \leq \int_0^T v(t) dt \quad (\text{a.15})$$

to p -Laplace problems

$$\begin{cases} (|w'|^{p-2} w')' + v(t)|w|^{p-2} w = 0, \\ w(0) = 0 = w(T), \end{cases} \quad (\text{a.16})$$

where $v \in L^1$, $1 < p < \infty$. He recovered the results to linear problem (a.13) for $p = 2$. It is natural to see that inequality (a.15) is the generalization to Lyapunov inequality (a.14) to p -Laplace problems.

There are also some results devoted to similar inequalities for PDEs. Let us recall the some of these here. Cañada, Montero and Villegas in [J. Funct. Anal., 2006] have studied the following problem

$$\begin{cases} \Delta w + v(x)w = 0, & x \in \Omega, \\ \frac{\partial w}{\partial \eta} = 0, & x \in \Omega, \end{cases} \quad (\text{a.17})$$

and they established a nonexistence of solution to (a.17) for general domains. They also prove some bounds associated with the second Neumann eigenvalue λ_2 . Recently, de Nápoli and Pinasco in [J. Funct. Anal., 2016] established the Lyapunov type inequalities to the following p -Laplace equation

$$\begin{cases} -\Delta_p w = v(x)|w|^{p-2} w & \text{in } \Omega, \\ w = 0 & \text{in } \partial\Omega, \end{cases} \quad (\text{a.18})$$

where Ω is an open bounded subset of \mathbb{R}^N and they considered two separate cases: $p < N, p > N$ and raised an interesting question whether one can establish a related Lyapunov inequality in case $p = N$, see pp. 1998 in [J. Funct. Anal., 2016].

Motivated by the above question and interesting studies on existence of a solution to N -Laplace equations, we establish a related Lyapunov inequality in case of $p = N$. In fact, we establish a Lyapunov type inequalities for the following singular partial differential equations (a.19) - (a.22) in an open bounded subset $\Omega \subset \mathbb{R}^N$ with C^1 boundary:

$$\begin{cases} -\Delta w - \mu \frac{w}{|x|^2} - \frac{|\nabla w|^2}{w} = v(x) w & \text{in } \Omega, \\ w = 0 & \text{on } \partial\Omega, \end{cases} \quad (\text{a.19})$$

where $N \geq 3$, $0 \in \Omega$, and $0 < \beta < \frac{N-2}{2}$, $v \in L^m(\Omega, |x|^{-2\beta m'})$, where $\frac{1}{m'} + \frac{1}{m} = 1$, $m > 1$, $0 < \mu < \left(\frac{N-2(\beta+1)}{2}\right)^2$;

$$\begin{cases} -\operatorname{div}(b(x, w, \nabla w)) - \mu \frac{g(x)}{|x|^p} |w|^{p-2} w = v(x)|w|^{p-2} w & \text{in } \Omega, \\ w = 0 & \text{on } \partial\Omega, \end{cases} \quad (\text{a.20})$$

has been widely investigated for different choices of λ and h . For instance, the existence of a solution to (a.7) with $\lambda = 0$ is obtained by V. Ferone, F. Murat in [Nonlinear Anal. T.M.A, 2000] provided that h is small enough, while for $\lambda < 0$, the existence is obtained by L. Boccardo et al. in [SIAM J. Math. Anal., 1992] for all h and in many others. The interest to investigate this type equation comes from the problems in the calculus of variations. Apart from the above mentioned works, this type of problems has also been investigated by several other researchers. There is a vast literature on the following type of problems:

$$\begin{cases} -\operatorname{div}(A(x)\nabla w) + f(w)|\nabla w|^2 = h(x) & \text{in } \Omega, \\ w = 0 & \text{on } \partial\Omega, \end{cases}$$

where f is singular at the origin and A is a uniformly elliptic matrix, which is also bounded, i.e., $\exists \alpha, \beta > 0$ such that $0 < \alpha \leq \beta$ with

$$\alpha|\xi|^2 \leq A(x)\xi \times \xi, \quad |A(x)| \leq \beta,$$

for each $\xi \in \mathbb{R}^N$, for almost each $x \in \Omega$. See for instance, the works of D. Arcoya et al. in [J. Differential Equation, 2009] and L. Boccardo et al. in [SIAM J. Math. Anal., 1992] and the reference cited therein. Problem (a.1) can also be thought of as the generalization to the following quasilinear singular problem:

$$\begin{cases} -\Delta w + \alpha \frac{|\nabla w|^2}{w} = g(x) & \text{in } \Omega, \\ w > 0 & \text{in } \Omega, \\ w = 0 & \text{on } \partial\Omega, \end{cases} \quad (\text{a.8})$$

with $0 < \alpha < 1$, and g is a nonnegative function. By transformation, $v = w^{1-\alpha}$, (a.8) reduces to the following form

$$-\operatorname{div}(A(x)\nabla v) = f(x, v), \quad (\text{a.9})$$

where $A(x)$ is an identity matrix and $f(x, s)$ is singular for $s = 0$ and $x = 0$, which has been intensively studied by many authors in the past.

Motivated by the above research work, one may ask whether we can obtain the existence of the solution to the following problem:

$$\begin{cases} -\Delta w - \mu \frac{w}{|x|^2} = \frac{|\nabla w|^2}{w} + f(x, w) & \text{in } \Omega, \\ w > 0 & \text{in } \Omega, \\ w = 0 & \text{on } \partial\Omega, \end{cases} \quad (\text{a.10})$$

where $\mu > 0$, $0 \in \Omega$, $N \geq 3$.

We prove the existence of a solution to (a.10) in $H_0^1(\Omega)$ under certain conditions on f . This problem is challenging due to the following reasons; (i) the problem is non-variational due to the quadratic gradient term (ii) the problem under consideration has strong singularity (i.e., singularity at origin $x = 0$ and at boundary $\partial\Omega$). These two reasons make this study quite challenging. We overcome these two difficulties by introducing a suitable transformation, which converts (a.10) into of the following type:

$$-\operatorname{div}(A(x)\nabla v) = f(x, v),$$

where A is a singular term. Thereafter, it turns out to be natural to investigate the transformed equation in the weighted Sobolev space and so, we define a suitable weighted Sobolev space and look at the

solution in the same space. The surprising thing about this transformation is that it takes care of the singularity $\frac{w}{|x|^2}$ and the quadratic term with singularity $\frac{|\nabla w|^2}{w}$ simultaneously.

We also make an attempt to investigate singular elliptic equations on Heisenberg group. For this, we consider the existence questions of singular elliptic problem on Sobolev space associated with Heisenberg group. Our motivation to study elliptic problems on Sobolev space associated with the Heisenberg group is due to the fact that there are some similarities between $\Delta_{\mathbb{H}^n} w$ and classical Laplacian. Also, following type of problem:

$$\begin{cases} -\Delta_{\mathbb{H}^n} w = f(x, w) & \text{in } \Omega, \\ w > 0 & \text{in } \Omega, \\ w = 0 & \text{on } \partial\Omega, \end{cases}$$

where Ω is an open (bounded or unbounded) subset of Heisenberg group \mathbb{H}^n and $\Delta_{\mathbb{H}^n} w$ is the subelliptic Laplacian on \mathbb{H}^n arise as Euler equations in some variational problems related to some geometry of CR manifolds.

Let us consider the following problem, which is closely related to problem (a.3):

$$\begin{cases} -\Delta_{\mathbb{H}^n} w = \mu V(\xi)w + f(\lambda, \xi, w) & \text{in } \Omega \subset \mathbb{H}^n, \\ w = 0 & \text{on } \partial\Omega. \end{cases} \quad (\text{a.11})$$

For $\mu = 0$ and $f(\lambda, \xi, w) = f_1(w)$ in (a.11), Garofalo and Lanconelli in [Indiana Univ. Math. J., 1992] established existence of a nonnegative solution by using mountain pass theorem and compact embedding. By using mountain pass theorem and linking theorem of Rabinowitz, Mokrani in [Commun. Pure Appl. Anal., 2009] studied the existence of a nontrivial solution to (a.11) under certain conditions on f and V .

Motivated by the above research and many others, we obtain the existence of the solution to the following problem:

$$\begin{cases} -\Delta_{\mathbb{H}^n} w - \mu \frac{g(\xi)w}{(|z|^4 + t^2)^{1/2}} = \frac{\lambda f(\xi)}{w^\gamma} + h(\xi)w^p & \text{in } \Omega, \\ w > 0 & \text{in } \Omega, \\ w = 0 & \text{on } \partial\Omega, \end{cases} \quad (\text{a.12})$$

under assumptions $\gamma > 0, p > 0, \lambda > 0$ small and $0 \leq f, g, h \in L^\infty(\Omega)$. We show that there exists a solution to this problem in $H_0^1(\Omega, \mathbb{H}^n) \cap L^\infty(\Omega)$, for small $\lambda > 0$.

We also investigate Lyapunov-type inequalities for a class of singular elliptic PDEs. In his classical work, Lyapunov established that the solution w of the following ODE

$$w'' + v(t)w = 0, \quad \text{in } (-\infty, \infty),$$

is stable if

$$T \int_0^T v(t)dt < 4,$$

where v is continuous, positive and periodic function with period T . Then, Borg in [Amer. J. Math., 1949] obtained the Lyapunov inequality for sign changing weights v . He obtained the necessary condition for a nontrivial solution of the following problem

$$\begin{cases} w'' + v(t)w = 0, \\ w(0) = 0 = w(T). \end{cases} \quad (\text{a.13})$$

where $N \geq 2$, $0 \in \Omega$, $1 < p \leq N$, $v \in L^m(\Omega)$, $m > 1$ and $|g(x)| \leq M$, $M < \infty$, $0 \leq \mu < \frac{\alpha}{MK_H}$, where K_H is constant appearing in Hardy inequality;

$$\begin{cases} -\Delta_N w - \mu \frac{g(x)}{(|x| \log \frac{R}{|x|})^N} |w|^{N-2} w = v(x) |w|^{N-2} w \text{ in } \Omega, \\ w = 0 \text{ on } \partial\Omega, \end{cases} \quad (\text{a.21})$$

where $0 \in \Omega$, $\Delta_N w = \operatorname{div}(|\nabla w|^{N-2} \nabla w)$, $|g(x)| \leq M$, $\forall x \in \Omega$, $0 < M < \infty$, $0 \leq \mu < \frac{(\frac{N-1}{N})^N}{M}$ and $R \geq \sup_{\Omega} \{|x| e^{\frac{2}{N}}\}$, $v \in L^m(\Omega)$, $m > 1$;

and

$$\begin{cases} -\operatorname{div}(|x|^{-2\beta} \nabla w) - \mu \frac{g(x)}{|x|^{2(\beta+1)}} w = v(x) w \text{ in } \Omega, \\ w = 0 \text{ on } \partial\Omega, \end{cases} \quad (\text{a.22})$$

where $N \geq 3$, $0 \in \Omega$, and $0 < \beta < \frac{N-2}{2}$, $0 \leq g \in L^\infty(\Omega)$, $v \in L^m(\Omega)$, $m > 1$, $0 < \mu < \left(\frac{N-2(\beta+1)}{2}\right)^2$.

The thesis contains eight chapters and the organization of the thesis is as follows.

Chapter 1 has a brief introduction to singular elliptic PDEs and earlier developments on this subject. Chapter 2 deals with useful preliminaries and important results, which are used in ensuing chapters. In Chapter 3, we study the existence and regularity of a non-trivial weak solution to (a.2). We establish positive solution to (a.6) in Chapter 4. Chapter 5 deals with the existence of a non-trivial weak solution to (a.10). In Chapter 6, we establish the existence of positive weak solution to (a.12). We establish a Lyapunov type inequality to singular elliptic PDEs in Chapter 7. Finally, the conclusions and future plans are a part of Chapter 8. Thesis ends with a bibliography.

The following are the research articles out of this thesis, which are published /communicated:

- D. Kumar, Semilinear elliptic problems with singular terms on the Heisenberg group, *Complex Var. Elliptic Equ.* 64 (2019), no. 11, 1844–1853.
- D. Kumar, Positive solution to singular elliptic problems with subcritical nonlinearities, *Nonautonomous Dynamical Systems*, 6(1):99-107 DOI: 10.1515/msds-2019-0007.
- D. Kumar, J. Tyagi, Singular elliptic equations with quadratic gradient term (under-review).
- D. Kumar, J. Tyagi, Existence and regularity of positive solution to singular elliptic problems (under-review).
- D. Kumar, J. Tyagi, Lyapunov-type inequalities for singular elliptic PDEs (under-review).

Title: Generalized Hurwitz zeta and modified Bessel functions and associated modular relations
Researcher: Kumar, Rahul 15310066
Supervisor: Dixit, Atul
Year: 2020
Keyword's: Hurwitz zeta Function, Ramanujan-Guinand Formula, Koshliakov Kernel, Lommel Function
Call No.: 515.53 KUM
Acc. No.: T00751

Abstract: The Hurwitz zeta function $\zeta(s, a)$ has been of great interest to mathematicians since it was introduced by Hurwitz in 1881. Its theory has been extensively developed since then, and yet new properties of this function continue to surface to this day. It has applications in fractals, dynamical systems and applied statistics. A fundamental formula in the theory of $\zeta(s, a)$ is Hurwitz's formula. In Chapter 2 of this thesis, we obtain a new proof of Hurwitz's formula beginning with Hermite's formula, which is another crucial result in the theory. The aim is to reveal a beautiful connection between $\zeta(s, a)$ and a particular case of the Lommel function $S_{\mu, \nu}(z)$.

This thesis focuses mainly on developing the theories of two new special functions which we naturally encountered in our work on modular relations, and on obtaining a generalized modular relation. This is explained next.

Modular forms are certain functions defined on the upper half-plane which transform nicely under $z \rightarrow -1/z$ and $z \rightarrow z + 1$. By a modular relation (or a modular-type transformation) for a certain function F , we mean that which is governed by $z \rightarrow -1/z$ but not necessarily by $z \rightarrow z + 1$.

Equivalently, the relation can be written in the form $F(\alpha) = F(\beta)$, where $\alpha\beta = 1$. There are many generalized modular relations in the literature such as the general theta transformation of the form $F(w, \alpha) = F(iw, \beta)$ or other relations of the form $F(z, \alpha) = F(z, \beta)$, etc. The famous Ramanujan-Guinand formula, equivalent to the functional equation of the non-holomorphic Eisenstein series on $SL_2(\mathbb{Z})$, admits a beautiful generalization of the form $F(z, w, \alpha) = F(z, iw, \beta)$ recently obtained by Dixit, Kesarwani, and Moll. This implies that one can superimpose the theta structure on the Ramanujan-Guinand formula.

A substantial part of the thesis arose from answering a similar question - can we superimpose the theta structure on a recent modular relation involving infinite series of Hurwitz zeta function $\zeta(s, a)$ which generalizes an important result of Ramanujan? In the course of answering this question in the affirmative, we were led to a surprising new generalization of $\zeta(s, a)$. This new zeta function, which we call the generalized Hurwitz zeta function and denote by $\zeta_w(s, a)$, is initially defined for $\text{Re}(s) > 1$ and represents an analytic function in this half-plane. It satisfies interesting properties, albeit they are much more challenging to derive than the corresponding ones for $\zeta(s, a)$. Chapters 3 and 4 are devoted to developing the theory of $\zeta_w(s, a)$. In Chapter 3, we obtain three important integral representations for $\zeta_w(s, a)$. One of these integral representations contain a generalization of Hermite's formula for $\zeta(s, a)$ in the setting of $\zeta_w(s, a)$. Later in Chapter 4, we employ this new generalization of Hermite's formula to analytically continue $\zeta_w(s, a)$ in $\text{Re}(s) > 1, s \neq 1$. We show that

$\zeta_w(s, a)$ has a simple pole at $s = 1$ with the residue essentially being the square of a confluent hypergeometric function ${}_1F_1(b; c; z)$. While obtaining Laurent series expansion of $\zeta_w(s, a)$ near $s = 1$ we find a new generalization of the digamma function $\psi(a)$. Some properties of this generalized digamma function are obtained in Chapter 4. In order to obtain the generalized modular relation (with the theta structure) involving $\zeta_w(s, a)$, one not only needs the theory of $\zeta_w(s, a)$ but also that of functions reciprocal in a certain kernel involving Bessel functions, namely, the second Koshliakov kernel. While developing the theory of reciprocal functions, we stumbled upon a new generalization of modified Bessel function $K_z(x)$. We call it the generalized modified Bessel function ${}_1K_{z,w}(x)$. This special function ${}_1K_{z,w}(x)$ is initially defined as the inverse Mellin transform of the product of gamma functions at two different arguments and confluent hypergeometric functions at two different arguments. Chapter 5 of the thesis is devoted to showing that ${}_1K_{z,w}(x)$ satisfies a rich theory comparable to that of $K_z(x)$. We provide several new series and integral representations for ${}_1K_{z,w}(x)$, and also derive asymptotic estimates for it for small as well as large values of x . A relation between the two new special functions, namely $\zeta_w(s, a)$ and ${}_1K_{z,w}(x)$, is also obtained at the end of Chapter 5.

Chapter 6 is devoted to providing a new pair of functions reciprocal in the second Koshliakov kernel. This new pair is crucial in obtaining the generalized modular relation with the theta structure which is of the form $F(z, w, \alpha) = F(z, iw, \beta)$, $\alpha\beta = 1$. A general theorem evaluating an integral involving the Riemann Ξ -function is also obtained here. Later in Chapter 7, this general theorem and the new pair of reciprocal functions are employed to evaluate an integral involving product of Riemann Ξ -function at two different arguments.

As mentioned earlier, Dixit, Kesarwani and Moll obtained a generalization of Ramanujan-Guinand formula, and in the course of doing that, they naturally found a new generalization of the modified Bessel function $K_z(x)$ (different from ${}_1K_{z,w}(x)$ that we encountered in our work). They call it generalized modified Bessel function $K_{z,w}(x)$. They developed the theory of $K_{z,w}(x)$. In the last chapter of this thesis, namely Chapter 8, we add a further little piece to this theory. We show that while $K_{1/2}(x)$ is an elementary function, $K_{1/2,w}(x)$ can be written in the form of an infinite series involving the well-known Humbert functions. As an application of this result, we generalize the transformation formula for the logarithm of the Dedekind eta function $\eta(z)$. We also establish a connection between $K_{1/2,w}(x)$ and the cumulative distribution function corresponding to the Voigt line profile.

Title: Koshliakov zeta functions, squares of odd zeta values, sum-of-tails identities, and mock theta functions

Researcher: Gupta, Rajat

Supervisor: Dixit, Atul

Year: 2021

Keyword's: Ramanujan's Lost Notebook, Theorem of Andrews and Freitas, FFW Function, Mock Theta Function

Call No.: 515.56 GUP

Acc. No.: T00959

Abstract: In 1949, Nikolai Sergeevich Koshliakov (Koshlyakov), an outstanding Russian mathematician, wrote two long memoirs during his correctional hard labour in prison (which he was put to on fabricated charges), one of them titled "Issledovanie odnogo klassa transtsendentnykh funktsii, opredelyaemykh obobshchennym yravneniem Rimana (A study of a class of transcendental functions defined by the generalized Riemann equation)". It was published in 1949, a year before Koshliakov was released. The second memoir was lost in transition from jail to the mathematical community. In his 1949 memoir, he gave a non-trivial example of a functional equation studied by H. Hamburger. The example involves two functions $\zeta_p(s)$ and $\eta_p(s)$, which we call the Koshliakov zeta functions. His memoir consists of nine chapters.

This thesis is divided into two parts. In the quest to examine the nature of certain Dirichlet series, the first part of the thesis is devoted to obtaining a formula for special values of certain Dirichlet series, namely, the Koshliakov zeta function $\zeta_p(s)$ and the square of the Riemann zeta function at odd integer arguments. The study also involves modular type transformations involving some special functions arising from the theory of Koshliakov zeta functions.

Chapter 2 of this thesis examines the aforementioned unstudied manuscript of Nikolai Sergeevich Koshliakov which was published in 1949. In this chapter we derive a generalization of Ramanujan's famous identity for $\zeta(2m+1)$ in the setting of the Koshliakov zeta function $\zeta_p(2m+1)$. When $p \rightarrow \infty$, it reduces to Ramanujan's formula. However, if we let $p \rightarrow 0$, we get a surprising new formula for odd zeta values. In particular, it enables us to find closed form evaluations of some infinite series. Later in this chapter we examine Chapter 9 of Koshliakov's manuscript and obtain an elegant extension of Ramanujan's modular relation found in the middle of page 220 of Ramanujan's Lost notebook. This identity is of the type $F(\alpha) = F(\beta)$ where $\alpha\beta = 1$. We also find a generalization of the integral involving Riemann function $\Xi(T)$ associated to this formula. Again, letting $p \rightarrow \infty$, we get Ramanujan's result whereas the case $p \rightarrow 0$ gives a new formula.

In Chapter 3, we study an infinite series whose summand involves the generalized divisor function $\sigma_z(n) = \sum_{d|n} d^z$ and a combination of the modified Bessel functions of the second kind. Koshliakov uses a special case of this function to obtain a very clever proof of the Voronöi summation formula. We use this function to obtain an identity for the square of odd zeta values, which is an analogue of Ramanujan's formula for $\zeta(2m+1)$. In course of obtaining the identity, we had to obtain the correct

analogue of Eisenstein series. This explicit construction of the series is crucial without which the full-fledged Ramanujan-type formula for $\zeta^2(2m + 1)$ is not possible to obtain. As a special cases of the main result, we obtain an identity involving the non-trivial zeros of the Riemann zeta function as well as a result which establishes that at least one of two quantities – an infinite series and $\zeta(5)$ – is irrational. The second part of the thesis is devoted to studying some topic in the theory of partitions.

This part of the thesis constitutes two chapters.

In Chapter 4, we study certain sum-of-tails identities. Identities of such type were first studied by Ramanujan. Later, sum-of-tails identities were studied by many mathematicians. We start this chapter by obtaining a finite analogue of a sum-of-tail identity of Andrews and Freitas. We then derive a new extension of Abel's lemma with the help of which we obtain a one-parameter generalization of a sum-of-tails identity of Andrews, Garvan and Liang, which, as a special case, gives identities involving half-Lerch sums. Later we introduce a new generalization of a function of Fokkink, Fokkink and Wang, namely $FFW_c(n)$, and derive an identity for its generating function. This gives, as a special case, a recent representation for the generating function of $spt(n)$ given by Andrews, Garvan and Liang. We also obtain some weighted partition identities along with new representations for two of Ramanujan's third order mock theta functions through combinatorial techniques.

Finally in Chapter 5, we discuss some problems related to mock theta function and their connections with certain partition counting function. Recently, George Andrews and Ae Ja Yee established beautiful results involving bivariate generalizations of the third order mock theta functions $\omega(q)$ and $\nu(q)$, which is an extension of their earlier result of them joint with Atul Dixit. Generalizing the Andrews-Yee identities for trivariate generalizations of these mock theta functions remained a mystery as pointed out by Li and Yang in their recent work. We partially solve this problem and generalize these identities. Several new as well as well-known results are derived. For example, one of our two main theorems gives, as a corollary, a special case of Soon-Yi Kang's three-variable reciprocity theorem. A relation between a new restricted overpartition function $p^*(n)$ and a weighted partition function $p_*(n)$ is obtained from one of the special cases of our second theorem.

Title: Asymptotic analysis of controlled dynamical systems with small random noise and fast sampling
Researcher: Dhama, Shivam Singh
Supervisor: Pahlajani, Chetan D.
Year: 2023
Keyword's: Perturbation-Mathematics, Differential Equations -- Asymptotic Theory, Non Differential Equations -- Asymptotic Theory
Call No.: 515.35 DHA
Acc. No.: T01016

Abstract:

In many control applications, one encounters situations where the dynamics of a system governed by an ordinary differential equation (ODE) evolves continuously in time, whereas the control actions are computed and updated at certain discrete time instants rather than being updated continuously. An example of this phenomenon is the sample-and-hold implementation of a feedback control law where using the state measurement at certain time instants, control action is computed, and held fixed until the next sample is obtained. This interplay between discrete and continuous dynamics makes this a hybrid dynamical system. This hybrid nature of systems arises quite naturally in the context of computer-controlled systems and networked control systems.

It is often noticed that systems of interest in various applications are subject to some uncertainties, and hence stochastic differential equations (SDE) are used to describe the dynamics in such cases. The asymptotic analysis of dynamical systems perturbed by small random noise has been extensively studied. Motivated by this study, we explore similar questions for a dynamical system under the combined influence of sampling and noise.

In this dissertation, we study the asymptotic analysis of a controlled dynamical system under the combined effect of fast periodic sampling with period δ and small noise (for the cases of both continuous and jump random perturbations) of size $\epsilon, 0 < \epsilon, \delta \ll 1$. Due to sampling effects, the measurements (samples) of the state are taken at periodically spaced discrete time instants, and the instantaneous rate of change of the state depends on both its current value and the most recent measurement. We show that the resulting stochastic process indexed by two small parameters ϵ, δ , converges—as $\epsilon, \delta \searrow 0$ —to the dynamics of an ODE on time interval $[0, T]$ for any fixed $T > 0$. The vector field of this ODE is obtained by replacing the state measurements at discrete time instants with their continuous-time counterparts. This result is interpreted as a law of large numbers (LLN) type result, and the dynamics of the resulting ODE capture the mean behavior of the stochastic process. Next, we explore the fluctuation analysis of the stochastic process of interest around its mean. Here, we find that the asymptotic behavior of the appropriately scaled fluctuation process depends on the relative rates at which the small parameters ϵ, δ approach zero. The key contribution here is the identification of an *extra drift* term in the SDE for the limiting fluctuation process which captures the combined influence of small noise and fast sampling. This result is in the spirit of the central limit theorem (CLT). As a consequence, we obtain a first-order perturbation expansion of the stochastic process of interest, together with error estimates on the remainder. Here, the zeroth- and first-order terms are characterized by the ODE describing the mean behavior, and the SDE which captures the fluctuations about the mean.

In addition, we report some preliminary results on the asymptotic analysis of a linear system with fast *random sampling* rather than periodic. Using the linearity of the system, we obtain an explicit solution representation in terms of a product of random matrices. We establish the limiting mean behavior and fluctuation analysis, as the temporal sampling rate tends to infinity, of an embedded discrete-time stochastic process using well-studied limit theorems for products of random matrices.

In more detail, Chapters 3 and 4 deal with SDE (0.1) and (0.2), respectively, mentioned below.

$$dX_t^{\epsilon, \delta} = \left[AX_t^{\epsilon, \delta} - BKX_{\pi_\delta(t)}^{\epsilon, \delta} - \epsilon BKV_{\pi_\delta(t)} \right] dt + \epsilon dW_t, \quad X_0^{\epsilon, \delta} = x_0, \quad (0.1)$$

and

$$dX_t^{\epsilon, \delta} = \left[f(X_t^{\epsilon, \delta}) + g(X_t^{\epsilon, \delta})\kappa(X_{\pi_\delta(t)}^{\epsilon, \delta}) \right] dt + \epsilon \sigma(X_t^{\epsilon, \delta}) dW_t, \quad X_0^{\epsilon, \delta} = x_0, \quad (0.2)$$

where $A \in \mathbb{R}^{n \times n}$, $B \in \mathbb{R}^{n \times m}$ and $K \in \mathbb{R}^{m \times n}$ are given matrices and the mappings $f: \mathbb{R}^n \rightarrow \mathbb{R}^n$, $g: \mathbb{R}^n \rightarrow \mathbb{R}^{n \times m}$, $\kappa: \mathbb{R}^n \rightarrow \mathbb{R}^m$ and $\sigma: \mathbb{R}^n \rightarrow \mathbb{R}^{n \times n}$ satisfy certain regularity conditions. $\pi_\delta(\cdot)$ is a time-discretization operator which rounds down the continuous time $t \in [0, \infty)$ to the nearest multiple of

δ , and W, V are two independent Brownian motions with V representing measurement noise and W representing state noise. Note that when $V = 0$, equation (0.1) is a special case of (0.2) with the particular choices of $f(x) = Ax, g(x) = B, \kappa(x) = -Kx, \sigma(x) = I$ (identity matrix). The equation (0.2) thus corresponds to a randomly perturbed sample-and-hold implementation of the nonlinear control system $\dot{x} = f(x) + g(x)u$ with control law $u = \kappa(x)$; the state x of the system is sampled at discrete time instants $k\delta, k \in \mathbb{Z}^+$, and used to compute the control action u , which is then held fixed until the next sample is taken. We show that the continuous-time non-Markovian process $X_t^{\varepsilon, \delta}$ solving (0.2) converges, as $\varepsilon, \delta \searrow 0$, to the deterministic model $\dot{x} = f(x) + g(x)\kappa(x), x(0) = x_0$ over time interval $[0, T]$ for any fixed $T > 0$. Next, we explore the fluctuation analysis of $X_t^{\varepsilon, \delta}$ about the mean $x(t)$ in the limit as $\varepsilon, \delta \searrow 0$. The results here depend essentially on the *relative rates* at which the small parameters ε, δ approach zero. Assuming that $\delta = \delta_\varepsilon$ and that the limit $c \triangleq \lim_{\varepsilon \searrow 0} \delta_\varepsilon / \varepsilon$ exists in $[0, \infty]$, we consider three different regimes

$$c \triangleq \lim_{\varepsilon \searrow 0} \delta_\varepsilon / \varepsilon \begin{cases} = 0 & \text{Regime 1,} \\ \in (0, \infty) & \text{Regime 2,} \\ = \infty & \text{Regime 3.} \end{cases} \quad (0.3)$$

In Regimes 1 and 2, we establish that over any finite time interval $[0, T], T < \infty$, the (rescaled) fluctuation process $Z_t^{\varepsilon, \delta} \triangleq \varepsilon^{-1}(X_t^{\varepsilon, \delta} - x(t))$ can be approximated by the limiting time-inhomogeneous Markov process Z_t satisfying

$$Z_t = \int_0^t [Df(x(s)) + J(x(s))]Z_s ds - \frac{c}{2} \int_0^t J(x(s))[f(x(s)) + g(x(s))\kappa(x(s))] ds \\ + \int_0^t \sum_{i=1}^m Dg_i(x(s))Z_s \kappa_i(x(s)) ds + \int_0^t \sigma(x(s))dW_s, \quad (0.4)$$

where for $f: \mathbb{R}^n \rightarrow \mathbb{R}^n$ and $x \in \mathbb{R}^n$, $Df(x)$ represents the Jacobian matrix of f at x , $J(x) \triangleq g(x)DK(x)$, $g_i \in \mathbb{R}^n$, and $\kappa_i \in \mathbb{R}, i = 1, \dots, m$ denote the columns of g and components of κ , respectively. As a particular case, in the linear setting (Chapter 3), equation (0.4) takes the form

$$Z_t = \int_0^t (A - BK)Z_s ds - BK \int_0^t V_s ds + \frac{c}{2} BK \int_0^t (A - BK)x(s) ds + W_t.$$

In Regime 3, viz., $\varepsilon \searrow 0$ faster than δ does, the limiting fluctuation process is purely deterministic.

Next, in Chapter 5, we extend the results of Chapter 3 for the case when the system of interest is perturbed by a jump noise. More precisely, we consider the stochastic process $Y_t^{\varepsilon, \delta}$ satisfying the SDE

$$dY_t^{\varepsilon, \delta} = \left[AY_{t-}^{\varepsilon, \delta} - BK Y_{\pi_\delta(t)-}^{\varepsilon, \delta} \right] dt + \varepsilon \sigma(Y_{t-}^{\varepsilon, \delta}) dW_t + \varepsilon \int_E F(Y_{t-}^{\varepsilon, \delta}, x) \tilde{N}(dt, dx), \quad Y_0^{\varepsilon, \delta} = y_0, \quad (0.5)$$

where A, B and K are matrices as mentioned above and $\pi_\delta(\cdot)$ is defined as earlier. Here, the mappings $\sigma: \mathbb{R}^n \rightarrow \mathbb{R}^{n \times n}$ and $F: \mathbb{R}^n \times \mathbb{R}^n \rightarrow \mathbb{R}^n$ satisfy certain regularity conditions, \tilde{N} is a compensated Poisson random measure and $E \triangleq \{x \in \mathbb{R}^n: 0 < |x| < 1\}$. We first demonstrate that the càdlàg process $Y_t^{\varepsilon, \delta}$ solving (0.5) converges, as $\varepsilon, \delta \searrow 0$, to the dynamics of $\dot{y}(t) = (A - BK)y(t), y(0) = y_0$ on time interval $[0, T], T < \infty$. In our second result of this chapter, we study the limit as $\varepsilon, \delta \searrow 0$, of the rescaled fluctuations of $Y_t^{\varepsilon, \delta}$ about $y(t)$. This result is again found to vary depending on the interaction of small parameters ε, δ . In Regimes 1 and 2 (see equation (0.3)), the rescaled process $Z_t^{\varepsilon, \delta} \triangleq \varepsilon^{-1}(Y_t^{\varepsilon, \delta} - y(t))$

converges, as $\varepsilon, \delta \searrow 0$ and $t \in [0, T]$, to the càdlàg process Z_t which solves the SDE

$$Z_t = (A - BK) \int_0^t Z_s ds + BK \frac{c}{2} \int_0^t (A - BK)y(s) ds + \int_0^t \sigma(y(s)) dW_s + \int_0^t \int_E F(y(s), x) \tilde{N}(ds, dx). \quad (0.6)$$

The novelty of this work (presented in Chapters 3, 4 and 5) stems from the identification of the extra drift terms $\frac{c}{2} \int_0^t J(x(s))[f(x(s)) + g(x(s))\kappa(x(s))] ds$ and $\frac{c}{2} BK \int_0^t (A - BK)y(s) ds$ —capturing the sampling effect—in the limiting SDE (0.4) and (0.6), respectively. The main results of Chapter 3 are proved through the explicit solution representations (possible due to linearity) of the stochastic process of interest, whereas proofs of results in Chapters 4 and 5 use the integral representations of the SDE (0.2) and (0.5). The stochastic quantities in the proofs are handled by the tools of stochastic analysis, viz., Burkholder-Davis-Gundy inequalities and Ito isometry for stochastic integrals.

Finally, in Chapter 6, we consider the random integral equation

$$x_n(t) = x_0 + \int_0^t \{Ax_n(s) - BKx_n(\tau_{N_t^n}^n)\} ds \quad \text{for } t \geq 0, \quad (0.7)$$

where $x_n(t)$ represents the state of the system, the renewal process $N_t^n, t \geq 0$, indexed by the parameter $n \in \mathbb{N}$, represents the total number of samples collected by time t , and the quantity $\tau_{N_t^n}^n, t \geq 0$, denotes the time of collection of the *most recent* (with respect to the “present” time t) sample. Here, for $k \geq 1$, $\tau_k \triangleq \sum_{i=1}^k \xi_i$ denotes the time of the k^{th} sample, $\tau_k^n \triangleq \tau_k/n$, and the i.i.d. holding times ξ_i 's satisfy certain integrability assumptions. In this case, $1/n$ gives the order of magnitude of the time between successive samples. The explicit solution representation for equation (0.7) is given as the product of random matrices, viz., $x_n(t) = \Phi_n(t)x_0$, where, $\Phi_n(t) \triangleq \varphi(t - \tau_{N_t^n}^n) \prod_{i=1}^{N_t^n} \varphi(\tau_i^n - \tau_{i-1}^n)$, and $\varphi(t) \triangleq e^{tA} - \int_0^t e^{(t-r)A} BK dr$, for $t \geq 0$. Now, recording the values of $x_n(t)$ at sampling times τ_k^n , we obtain the embedded discrete-time process $y_k^n \triangleq \prod_{i=1}^k \varphi(\xi_i/n)x_0$ for $k \geq 1$. In our first result of this chapter, we establish that the process y_n^n can be approximated, as $n \rightarrow \infty$, by $e^{m(A-BK)}x_0$, $m = \mathbb{E}[\xi_1]$, in a suitable sense. Our second result describes the fluctuations of the process $y_{n_2}^n$ in the limit $n \rightarrow \infty$ and shows that the rescaled process $e^{-nm(A-BK)}y_{n_2}^n$ converges, in a suitable sense, to $\Psi(1)$. Here, for $t \geq 0$, $\Psi(t) \triangleq \exp\{\zeta CW_t + (m^2 + \zeta^2)(AC - C^2)t/2\}$, $C = A - BK$, ζ^2 is the variance of ξ_1 and W_t is a standard, one-dimensional Brownian motion.

We illustrate our theoretical results in the context of a numerical example.

Title: On d-holomorphic connections and gauge theoretic aspects of parabolic bundles on Klein surfaces
Researcher: Jaiswal, Ayush
Supervisor: Amrutiya, Sanjay kumar
Year: 2023
Keyword's: Klein Surfaces, Riemann Surfaces, Parabolic Bundles, D-holomorphic
Call No.: 516.373 JAI
Acc. No.: T01036

Abstract: The notion of connections and curvatures is vital in many fields like Differential Geometry, Algebraic Geometry, Geometric Analysis, Mathematical Physics, etc. In this thesis, we have studied certain particular types of connections on vector bundles over Klein surfaces. Felix Klein (1882) first observed that non-orientable surfaces carry a dianalytic structure. Following his observation, a two-dimensional real manifold with a dianalytic structure is called a Klein surface. Later, Michael Schiffer and Donald C. Spencer established the theory of analytic functions and differentials on orientable and non-orientable Riemann surfaces with or without boundaries. They have used that a non-orientable Riemann surface with or without boundary admits an orientable double cover. Alling and Greenleaf (1969) have systematically established the equivalence between the following three categories:

1. the function fields in one variable over \mathbb{R}
2. compact Klein surfaces
3. compact Riemann surfaces with anti-holomorphic involutions

The classification of isomorphism classes of fixed rank and degree vector bundles is a fascinating problem in the theory of vector bundles, also known as the moduli problem of vector bundles. David Mumford (1963) introduced stable (semi-stable) vector bundles on a smooth complex projective curve. He developed the theory (known as GIT) of taking quotients in the category of schemes. He used it to prove that the moduli space is a non-singular, quasi-projective algebraic variety. On the other hand, Seshadri and Narasimhan (1965) demonstrated that the vector bundles arising from irreducible unitary representations of the fundamental group of compact Riemann surfaces are precisely stable.

In the commentary on volume 5 of his collected works (Geometry of Yang–Mills fields *Lezioni Fermiane Acad. Nazionale dei Lincei and Scuola Normale Sup. Pisa* (1979)), Atiyah wrote:

From 1977 onwards, my interests moved in the direction of gauge theories and the interaction between geometry and physics...the stimulus came from two sources: On the one hand, Singer told me about the Yang–Mills equations, which, through the influence of Yang, were just starting to percolate into mathematical circles...The second stimulus came from the presence of Roger Penrose and his group in Oxford.

After this, Atiyah and Bott (1982) developed the Yang–Mills theory for Riemann surfaces, which inspired Simon K. Donaldson (1983) to prove the Narasimhan–Seshadri theorem using differential geometric techniques (gauge theoretic methods) involving Uhlenbeck global compactness theorem. Florent Schaffhauser (2012) studied real points of coarse moduli space for vector bundles over Klein surfaces using the results of Donaldson. C. S. Seshadri first introduced the notion of the parabolic bundle. It naturally arises while studying the representations of the fundamental group of a punctured Riemann surface. V. B. Mehta and C. S. Seshadri (1980) constructed moduli of parabolic bundles on compact Riemann surfaces. Olivier Biquard (1991) used weighted Sobolev spaces to prove the generalized Narasimhan–Seshadri–Donaldson correspondence for parabolic vector bundles. One part of the thesis aims to study the gauge theoretic aspects of real (resp. quaternionic) parabolic bundles over a compact Riemann surface with an anti–holomorphic involution.

A connection on a smooth vector bundle always exists but may not be integrable, i.e., a vector bundle may not arise from a representation of the fundamental group of base space, which is a compact Riemann surface. In general, a holomorphic connection may not exist on a holomorphic vector bundle. André Weil (1938) first studied this problem and gave the following criterion:

Let $E = E_1 \oplus E_2 \oplus \dots \oplus E_k$ be a Remak decomposition of a holomorphic vector bundle over a compact Riemann surface X . Then E arises from a representation of the fundamental group of X if and only if $\deg(E_i) = 0$ for each $i = 1, 2, \dots, k$. In 1957, Atiyah developed the theory of connections on principal bundles over complex manifolds. He proved Weil’s theorem with a different viewpoint which involves a short exact sequence associated with the given holomorphic bundle, known as the Atiyah sequence. The following criteria is known as the Atiyah–Weil criterion for holomorphic connections. Let $E = E_1 \oplus E_2 \oplus \dots \oplus E_k$ be a Remak decomposition of a holomorphic vector bundle over a compact Riemann surface X . Then E admits a holomorphic connection if and only if $\deg(E_i) = 0$ for each $i = 1, 2, \dots, k$. The second part of the thesis aims to develop the theory of d –holomorphic connections on d –holomorphic bundles over Klein surfaces in the spirit of Atiyah’s work and provide a suitable criterion for the existence of d –holomorphic connections.

Title: Delta geometry and p-adic Hodge theory
Researcher: Pandit, Sudip
Supervisor: Saha, Arnab
Year: 2022
Keyword's: Geometry, Hodge Theory, Hodge-pink Structure
Call No.: 516.35 PAN
Acc. No.: T01038

Abstract: The notion of differentiation is a fundamental tool in the theory of functions over real or complex numbers. Based on a prior work of Joyal, Buium introduced the notion of p-derivation denoted as δ in order to derive arithmetic applications analogous to the theory of functions in differential algebra. This leads to the theory of delta geometry. At first, we develop the theory of δ -characters of Anderson modules. Given any Anderson module E , using the theory of δ -geometry, we construct a canonical z-isocrystal $H\delta(E)$ with a Hodge-Pink structure. As an application, we show that when E is a Drinfeld module, our constructed z-isocrystal $H\delta(E)$ is weakly admissible given that a δ -parameter γ is non-zero. Therefore the equal characteristic analogue of the Fontaine functor associates a local shtuka and hence a crystalline z-adic Galois representation to the δ -geometric object $H\delta(E)$. Moreover, we prove that γ is non-zero for a Drinfeld module of rank 2 which implies that $H\delta(E)$ is weakly admissible. Therefore, the equal characteristic analogue of the Fontaine functor associates a local shtuka and hence a crystalline z-adic Galois representation to our δ -geometric object $H\delta(E)$ unconditionally in this case.

As another consequence, if E is a Drinfeld module of rank 2 and does not admit a lift of Frobenius and K is the fraction field of the ring of definition, we show that $H(E) \otimes K$ is isomorphic to $H^*dR(E) \otimes K$ and the isomorphism preserves the canonical Hodge filtration. On the other hand, if E admits a lift of Frobenius, then $H(E) \otimes K$ is isomorphic to the subobject $Lie(E)^* \otimes K$ of $H^*dR(E) \otimes K$. The above result can be viewed as a character theoretic interpretation of de Rham cohomology. In the case of Carlitz modules, we show that the Galois representation associated to $H\delta(E)$ is indeed the usual one coming from the Tate module. Hence this dissertation further raises the question of how the above two apparently different Galois representations compare with each other for a Drinfeld module of arbitrary rank.

Secondly, we develop the theory of m-shifted π -typical Witt vectors which can be viewed as subobjects of the usual π -typical Witt vectors. We show that the shifted Witt vectors admit a delta structure that satisfy a canonical identity with the delta structure of the usual π -typical Witt vectors. Using this theory, we prove that the generalized kernels of arithmetic jet spaces are jet spaces of the kernel at the first level. This also allows us to interpret the arithmetic Picard-Fuchs operator geometrically. For a π -formal group scheme G , by a previous construction, one attaches a canonical filtered isocrystal $H_\delta(G)$ associated to the arithmetic jet spaces of G . In the final part of the dissertation, we show that $H_\delta(\text{ffi})$ is of finite rank if ffi is an abelian scheme. We also prove a strengthened version of a result of Buium on delta characters on abelian schemes. As an application, for an elliptic curve ffi defined over Z_p , we show that our canonical filtered isocrystal $H_\delta(\text{ffi}) \otimes Q_p$ is weakly admissible. In particular, if ffi does not admit a lift of Frobenius, we show that that $H_\delta(\text{ffi}) \otimes Q_p$

\mathbb{Q}_p is canonically isomorphic to the first crystalline cohomology $H^1(\text{ffi}) \otimes \mathbb{Q}_p$ in the category of filtered isocrystals. On the other hand, if ffi admits a lift of Frobenius, then $H^\delta(\text{ffi}) \otimes \mathbb{Q}_p$ is isomorphic to the sub-isocrystal $H^0(\text{ffi}, \Omega_{\text{ffi}}) \otimes \mathbb{Q}_p$ of $H^1(\text{ffi}) \otimes \mathbb{Q}_p$.

The above result can be viewed as a character theoretic interpretation of the crystalline cohomology. The difference between the integral structures of $H^\delta(\text{ffi})$ and $H^1(\text{ffi})$ is measured by a delta modular form f_1 constructed by Buium.

Title: Cohen-Macaulay graph ideals and the v-number of monomial ideals
Researcher: Saha, Kamlesh
Supervisor: Sengupta, Indranath
Year: 2022
Keyword's: Commutative Algebra, Cohen-Macaulay Rings, Monomial Ideals, Binomial Ideals
Call No.: 512.44 SAH
Acc. No.: T01043

Abstract: Ideals of polynomial rings associated with simple graphs, commonly known as edge ideals, binomial edge ideals, weighted oriented edge ideals etc. appear in studies of various fields of research like commutative algebra, algebraic statistics, coding theory, combinatorics, etc. In 1990, Villarreal initiated the study of ideals in terms of graph theory, known as edge ideals of simple graphs ([97]). Later, in 2010, the study of binomial edge ideals, which is a generalization of determinantal ideals, was started due to its connection with the theory of conditional independence by Ohtani ([79]) and Herzog et al. ([44]), independently. The study of edge ideals of weighted oriented graphs has been started very recently due to its appearance in the research of Reed-Muller-type codes ([82]). Also, in the same context, a new invariant, called the v-number of graded ideals, has been defined in [19].

The work done in this thesis is to study the Cohen-Macaulayness of graphs ideals and the v-number of monomial ideals. We divide this thesis into two parts: Part A and part B. In Part A, we have studied the Cohen-Macaulay property of binomial edge ideals and weighted oriented edge ideals. Part B is devoted to the study of v-number of monomial ideals. In Chapter 1, we briefly describe this thesis. The necessary prerequisites to describe our work are given in Chapter 2.

In Chapter 3, we introduce the notion of binomial edge ideals for clutters and generalize the concepts of gluing and cone for clutters. We derive results regarding the Cohen-Macaulay property of these ideals similar to those obtained for graphs by Rauf & Rinaldo in [84]. We also answer a question posed in their paper.

In Chapter 5, we study the combinatorial aspects of Cohen-Macaulay binomial edge ideals. For a graph G , Bolognini et al. in [10] have shown the following: J_G is strongly unmixed $\implies J_G$ is Cohen-Macaulay $\implies G$ is accessible and conjectured about the converse, where J_G denotes the binomial edge ideal of G . Accessible and strongly unmixed properties are purely combinatorial. We give some motivation to focus only on blocks with whiskers for the characterization of all G with Cohen-Macaulay J_G . We show that accessible and strongly unmixed properties of G depend only on the corresponding properties of its blocks with whiskers and vice versa. We give an infinite class of graphs whose binomial edge ideals are Cohen-Macaulay. From that class, we classify all r -regular r -connected graphs with the property that after attaching some special whiskers to it, the binomial edge ideals become Cohen-Macaulay. Finally, we define a new class of graphs, called *strongly r -cut-connected* and prove that the binomial edge ideal of any strongly r -cut-connected accessible graph, having at most three cut vertices, is Cohen-Macaulay.

Chapter 6 is devoted to the study of Cohen-Macaulay weighted oriented edge ideals. The study of the edge ideal $I(D_G)$ of a weighted oriented graph D_G , with underlying graph G , was started in the context of Reed-Muller-type codes in 2019 ([82]). We generalize some Cohen-Macaulay constructions for $I(D_G)$, which Villarreal gave for edge ideals of simple graphs in [97]. Our constructions can be used to produce large classes of Cohen-Macaulay weighted oriented edge ideals. We use these constructions to classify all the Cohen-Macaulay weighted oriented edge ideals, whose underlying graphs are cycles. We also show that $I(D_{C_n})$ is Cohen-Macaulay if and only if $I(D_{C_n})$ is unmixed and $I(C_n)$ is Cohen-Macaulay, where C_n denotes the cycle of length n . Miller generalized the concept of Alexander dual ideals (of square-free monomial ideals) to arbitrary monomial ideals (see [75]), and in that direction, we study the Alexander dual of $I(D_G)$ and its conditions to be Cohen-Macaulay.

Again, in 2020, during the study of Reed-Muller-type codes, Cooper et al. ([19]) have introduced a new invariant for graded ideals, known as the v -number, which is our topic of discussion in Chapter 7 (Part B). We show that the v -number of an arbitrary monomial ideal is bounded below by the v -number of its polarization and also find a criterion for the equality. By showing the additivity of associated primes of monomial ideals we obtain the additivity of the v -numbers for arbitrary monomial ideals. We prove that the v -number $v(I(G))$ of the edge ideal $I(G)$, the induced matching number $\text{im}(G)$ and the regularity $\text{reg}(R/I(G))$ of a graph G , satisfy $v(I(G)) \leq \text{im}(G) \leq \text{reg}(R/I(G))$, where G is either a bipartite graph, or a (C_4, C_5) -free vertex decomposable graph, or a whisker graph. There is an open problem in [50], whether $v(I) \leq \text{reg}(R/I) + 1$ for any square-free monomial ideal I . We show that $v(I(G)) > \text{reg}(R/I(G)) + 1$, for a disconnected graph G . We derive some inequalities of v -numbers, which may be helpful to answer the above problem for the case of connected graphs. We connect $v(I(G))$ with an invariant of the line graph $L(G)$ of G . For a simple connected graph G , we show that $\text{reg}(R/I(G))$ can be arbitrarily larger than $v(I(G))$. Also, we try to see how the v -number is related to the Cohen-Macaulay property of square-free monomial ideals.

Chapter 8 is the last chapter of the thesis, where we pose some open problems which appear naturally from our research work.

Title: Projective closure of affine monomial curves
Researcher: Srivastava, Pranjali
Supervisor: Sengupta, Indranath
Year: 2022
Keyword's: Numerical Semigroups, Affine Monomial Curves, Affine Semigroup Rings, Cohen-Macaulay Rings
Call No.: 512.44 SRI
Acc. No.: T01044

Abstract: Numerical semigroups in \mathbb{N} define Numerical semigroup rings, which are important objects in the study of singularities of algebraic curves. Numerical semigroups define an important class of curves in the affine space, known as the affine monomial curves, and these are curves having only one singularity at the origin. The higher dimensional analogue of numerical semigroups are called the affine semigroups in \mathbb{N}^d , which are equally important in the study of singularities in Commutative Algebra and Algebraic Geometry. The main aim of our research is to understand a particular class of affine semigroups in \mathbb{N}^2 , namely those which define the projective closure of affine monomial curves. A natural quest is to know which properties of affine curves are preserved under projective closure, which forms the central theme for this thesis. To be specific, this thesis is an attempt to understand the behaviour of the Betti numbers of projective closure and constructing projective closure which have Cohen-Macaulay property. Apart from these, we have also studied the structure of the derivation module and the Poincaré series of the projective closure, two important objects in the study of singularities. Lastly, we have expanded our study to the general context of affine semigroup rings and have studied their Associated Graded rings. The thesis is divided into seven chapters. The first chapter is an Introduction to the thesis and we discuss some preliminaries in the second chapter. The main body of the thesis appear in chapters 3 - 6. We discuss some open questions in chapter 7.

Chapter 3. Projective closure of certain family of curves. Backelin, Bresinsky, and Arslan constructed numerical semigroups of embedding dimension 4. Many authors studied these curves to understand the Cohen-Macaulayness of their tangent cone and the behaviour of the Betti numbers of corresponding affine monomial curves. In Chapter 3, we investigate the Cohen-Macaulayness of the projective closure of Backelin curves and the minimal free resolution of the projective closure of all three classes.

Chapter 4. Projective closure of the gluing of numerical semigroups and the Betti numbers of Projective closure. It is well known that the affine monomial curves are always Cohen-Macaulay, but their projective closure need not be Cohen-Macaulay. We give a method to construct infinitely many examples of the Cohen-Macaulay projective closures of numerical semigroups. To do so, we use the gluing technique of numerical semigroups. We introduce the notion of star gluing of numerical semigroups and show that this preserves the arithmetically Cohen-Macaulay (respectively Gorenstein) properties of the projective closure. In Chapter 4, we give a sufficient condition using the Gröbner basis of the defining ideal of an affine monomial curve so that the Betti sequences of

the affine curve and its projective closure are the same. We also study the effect of simple gluing on Betti sequences of the projective closure.

Chapter 5. Derivation module of the projective closure. The Poincaré series of the finitely generated R -module M is the series defined as $P_M^R(z) = \sum_{i \geq 0} \beta_i^R(M)z^i$, where $\beta_i^R(M)$ denotes the i^{th} Betti number of M over R . The well-known question is to answer when this series represents a rational function. In order to study this problem, Fröberg et al. computed the Poincaré series of the derivation module of a numerical semigroup ring and exhibited an relation of $P_{\text{Der}_K(R)}^R(z)$ with $P_{R_K}(z)$, where R is a numerical semigroup ring. In Chapter 5, we compute the Poincaré series of derivation modules of the Arslan curve and the Backelin curve. Note that both have the property that their projective closures are arithmetically Cohen-Macaulay. We use Tamone's description of the derivation module of projective closure of numerical semigroup rings for our computation. We compute the Poincaré series of the derivation modules of these families and show that the Poincaré series of the derivation module of the projective closure is related to the Poincaré series of a field K over the projective closure.

Chapter 6. Affine semigroup rings. Simplicial affine semigroups are the natural generalisation of a numerical semigroup and the semigroups corresponding to the projective closure. We want to generalise some results of affine monomial curves and their projective closures to the semigroup rings associated with simplicial affine semigroups. We give the necessary and sufficient conditions for the Cohen-Macaulayness of the associated graded ring of simplicial affine semigroup via Gröbner basis. We generalise the concept of homogeneous numerical semigroup for the simplicial affine semigroup and show that the Betti number of the corresponding semigroup ring matches the Betti numbers of the associated graded ring. We study some extension of affine semigroups.

Title: A study of certain affine semigroups and semigroup rings
Researcher: Prakash, Om
Supervisor: Sengupta, Indranath
Year: 2023
Keyword's: Affine Semigroups, Semigroup Rings, Maximal Projective Dimension
Call No.: 512.44 PRA
Acc. No.: T01082

Abstract: Affine semigroups and their associated semigroup rings are widely studied objects in the literature. They became important due to their applications in commutative algebra and algebraic geometry. The main link of affine semigroups to the algebraic geometry and commutative algebra is through toric varieties. Due to the increase in computational power in algebraic geometry and commutative algebra, last few decades have witnessed the extensive study of affine semigroups and semigroup rings. This thesis deals with certain type of affine semigroups and their corresponding semigroup rings. In Chapter 1, we summarize the results obtained in the thesis. In Chapter 2, we review the prerequisites to the thesis.

For a numerical semigroup S , there exists at least one element f in $N \setminus S$ such that $f + (S \setminus \{0\}) \subseteq S$. These elements are called pseudo-Frobenius elements. But for affine semigroups in N^r , the existence of such elements is not always guaranteed. In [31], authors prove that an affine semigroup S has pseudo-Frobenius elements if and only if the length of the graded minimal free resolution of the corresponding semigroup ring is maximal. Affine semigroups having pseudo-Frobenius elements are called maximal projective dimension (MPD) semigroups. A. Moscariello [49], introduced a tool associated with the pseudo-Frobenius elements of numerical semigroups, namely, row-factorization (RF) matrices, to explore the properties of semigroup rings. RF-matrices are important in studying the Cohen-Macaulay type, set theoretic complete intersection property, minimal free resolution, generic property, generating set, etc for the defining ideal of monomial curves.

In Chapter 3, we consider the numerical semigroup generated by an almost arithmetic sequence. In particular, we consider that S is generated by an almost arithmetic sequence $\{m_0, m_1, \dots, m_p, n\}$ such that $m_i = m_0 + id$ for $i = 0, \dots, p$, $d > 0$ and $\gcd(m_0, n, d) = 1$. In this chapter, we give a description of a possible row-factorization matrix for each pseudo-Frobenius element of S . Further, when S is symmetric and has embedding dimension 4 or 5, we prove that the defining ideal is minimally generated by RF-relations.

In Chapters 4, and 5, we generalize the notion of symmetric semigroups, pseudo-symmetric semigroups, and row-factorization matrices for pseudo-Frobenius elements of numerical semigroups to the case of MPD-semigroups in N^r . Under suitable conditions, we prove that these semigroups satisfy the extended Wilf's conjecture. We prove that the defining ideal of the associated semigroup ring of an MPD-semigroup is generic implies the uniqueness of the row-factorization matrix for each pseudo-Frobenius element. Further, we give a description of pseudo-Frobenius elements and row-factorization matrices of gluing of MPD-semigroups and consequently deduce

that the defining ideal of gluing of MPD-semigroups is never generic. We also explore the connection between the Hilbert series of the semigroup ring $K[S]$ and the set of pseudo-Frobenius elements of the MPD-semigroup S .

In Chapter 6, we consider simplicial affine semigroups. A simplicial affine semigroup in \mathbb{N}^r is the semigroup whose rational polyhedral cone has r extremal rays. It is well known that the defining ideal is one of the most important objects to study algebraic properties of the semigroup ring. For a Cohen-Macaulay simplicial affine semigroup ring, we give a sufficient criterion for an ideal to be the defining ideal. Further in this chapter, we study a special class of two dimensional affine semigroups in \mathbb{N}^2 , with the property that all the generators belong to the same line such that any two consecutive elements have the same distance.

Let a and d be two linearly independent vectors in \mathbb{N}^2 , over the field of rational numbers. For a positive integer $k \geq 2$, consider the sequence $a, a+d, \dots, a+kd$ such that the affine semigroup $S_{a,d,k}$ is minimally generated by $\{a, a+d, \dots, a+kd\}$. We study the properties of affine semigroup ring $K[S_{a,d,k}]$ associated to this semigroup. We prove that $K[S_{a,d,k}]$ is always Cohen-Macaulay and it is Gorenstein if and only if $k = 2$. For $k = 2, 3, 4$, we explicitly compute the syzygies, the minimal graded free resolution and the Hilbert series of $K[S_{a,d,k}]$. We also give a minimal generating set for the defining ideal of $K[S_{a,d,k}]$ which is also a Gröbner basis. Consequently, we prove that $K[S_{a,d,k}]$ is Koszul. Finally, we prove that the Castelnuovo-Mumford regularity of $K[S_{a,d,k}]$ is 1 for any a, d, k .

In Chapter 7, we study the derivation module and the Hilbert Kunz multiplicity of certain affine semigroup rings of dimension two, which are the co-ordinate rings of projective monomial curves in the projective space \mathbb{P}^n_k . Let n_0, n_1, \dots, n_p be a sequence of positive integers such that $n_0 < n_1 < \dots < n_p$ and $\gcd(n_0, n_1, \dots, n_p) = 1$. Let S be an affine semigroup in \mathbb{N}^2 generated by $\{(0, n_p), (n_0, n_p - n_0), \dots, (n_{p-1}, n_p - n_{p-1}), (n_p, 0)\}$. The semigroup ring $K[S]$ is the co-ordinate ring of the projective monomial curve in the projective space \mathbb{P}^{p+1}_k , which is defined parametrically by

$$x_0 = v^{n_p}, x_1 = u^{n_0} v^{n_p - n_0}, \dots, x_p = u^{n_{p-1}} v^{n_p - n_{p-1}}, x_{p+1} = u^{n_p}.$$

In this chapter, we consider that n_0, n_1, \dots, n_p forms an arithmetic sequence, and give an explicit set of minimal generators for the derivation module $\text{Der}K(K[S])$. Further, we give an explicit formula for the Hilbert-Kunz multiplicity of the co-ordinate ring of a projective monomial curve.

Title: Transformations of generalized Lambert series and analogues of a formula of Ramanujan, Hardy and Littlewood.

Researcher: Shivajee

Supervisor: Vatwani, Akshaa

Year: 2023

Keyword's: Number Theory, Ramanujan-Hardy-Littlewood (RHL), Riesz-type Criteria, Lambert Series

Call No.: 512.7 SHI

Acc. No.: T01084

A family of L -functions known as the Selberg class, which satisfies the fundamental requirements of the Riemann zeta function, was first studied by Selberg in 1991. Well-known functions like the Riemann zeta function $\zeta(s)$, the Dedekind zeta function $\zeta_{\mathbb{K}}(s)$ of a number field \mathbb{K} , Dirichlet L -functions, L -functions etc, are the elements of the Selberg class \mathcal{S} . The discussion for the non-trivial zeros of functions belonging to the Selberg class is similar to that on the Riemann zeta function. In this manner, there is a Grand Riemann Hypothesis (GRH), which asserts that all non-trivial zeros of any function belonging to the Selberg class lie on the critical line $\text{Re}(s) = \frac{1}{2}$.

The development of theories related to modular type transformations, Riesz-type criteria, and Lambert series is the main objective of this thesis. Another development is a new mean value theorem in the theory of moments. These developments are explained next.

Certain functions defined on the upper half-plane that transform nicely under the transformations $z \rightarrow -1/z$ and $z \rightarrow z+1$ are known as modular forms. For a specific function F , we refer to a modular relation (or a modular type transformation) as a relation that is controlled by $z \rightarrow -1/z$ but not necessarily by $z \rightarrow z+1$. The relationship can be expressed equivalently as $F(a) = F(b)$, where $ab = 1$.

In the first part of this thesis, we study a Ramanujan-Hardy-Littlewood-type identity which is a modular relation involving non-trivial zeros of the associated function. We give the Ramanujan-Hardy-Littlewood-type identity in the setting of a function belonging to the Selberg class and the Dedekind zeta function $\zeta_{\mathbb{K}}(s)$. While doing this, we also derive new transformation formulas involving special values of the Meijer G -function of the type $G_{0,n}^{n,0}$. New elegant transformations are obtained when \mathbb{K} is a quadratic extension, one of which involves the modified Bessel function of the second kind of order zero.

Hardy and Littlewood gave a Riesz-type criteria which is equivalent to the Riemann Hypothesis. In the context of L -functions belonging to the Selberg class, we derive a generalization of the Riesz-type criteria which is equivalent to the Grand Riemann Hypothesis. For L -functions obeying the axioms of the Selberg class, we find a criterion that is sufficient for the Grand Riemann Hypothesis (GRH) to hold without an application of the Ramanujan hypothesis to their coefficients. Additionally, we create a subclass of the Selberg class and prove a necessary criterion for GRH for L -functions in this subclass. A Riesz-type criterion for the Generalized Riemann Hypothesis for $\zeta_{\mathbb{K}}(s)$, using a slightly different kernel is also provided.

In the second part of this thesis, we explore Lambert series and discover a mean value theorem for $\zeta\left(\frac{1}{2} - it\right)\zeta'\left(\frac{1}{2} + it\right)$. A series whose general form is $\sum_{n=1}^{\infty} \frac{a(n)q^n}{1-q^n} = \sum_{n=1}^{\infty} \frac{a(n)}{e^{ny}-1} = \sum_{n=1}^{\infty} (1 * a)(n)e^{-ny}$, is known as the *Lambert series* of $a(n)$, where $q = e^{-y}$ with $\text{Re}(y) > 0$, and $a(n)$ is an arithmetic function with $(1 * a)(n) = \sum_{d|n} a(d)$ being the Dirichlet convolution. An

explicit formula for $\sum_{n=1}^{\infty} \frac{\log(n)}{e^{ny} - 1}$ for $\operatorname{Re}(y) > 0$, which takes y to $1/y$, is obtained in this thesis, for the first time in the literature. This transformation involves the digamma function and the logarithmic derivative of the Ramanujan-Deninger gamma function, that is, $\psi_1(z)$. We not only give an explicit formula for the series but also an asymptotic formula. In the explicit formula, the Lambert series transforms into a series containing the derivative of $R(z)$, a function studied by Christopher Deninger while obtaining an analogue of the famous Chowla-Selberg formula for real quadratic fields. It may seem fairly unexpected at first, but in order to obtain the transformation, new crucial properties of $\psi_1(z)$ (the derivative of $R(z)$) and a novel representation for the second derivative of the two-variable Mittag-Leffler function $E_{2,b}(z)$ evaluated at $b = 1$ are required.

A part of this thesis is devoted to the study of the moments $M_k(T)$, given by $\int_0^T |\zeta(\frac{1}{2} + it)|^{2k} dt$, which are of fundamental importance in the theory of the Riemann zeta function. It is conjectured that $M_k(T) \sim C_k T \log^{k^2}(T)$ as $T \rightarrow \infty$ for a positive constant C_k , although this has been proved only for $k = 1$ and 2 by Hardy and Littlewood and by Ingham respectively. Such results are known as mean-value theorems for the zeta function. The importance of the study of moments lies, for example, in the fact that the estimate $M_k(T) = O_{k,\varepsilon}(T^{1+\varepsilon})$ for every natural number k is equivalent to the Lindelöf hypothesis. These are significant because they can be used to determine the estimated maximal order of the zeta function, to obtain zero-density estimations as well as in the study of the distribution of prime numbers. Mean value theorems involving the derivatives of the Riemann zeta function have been well-studied. In the last part of this thesis we establish a mean value theorem for the smoothly weighted function $\zeta(\frac{1}{2} - it) \zeta'(\frac{1}{2} + it) e^{-\delta t}$, as $\delta \rightarrow 0$, $|\arg \delta| < \frac{\pi}{2}$ as an application of our asymptotic formula of the Lambert series of logarithm.

* * * * *



MECHANICAL ENGINEERING

Mechanical Engineering

Title: Global stability analysis of spatially developing boundary layers
Researcher: Bhoraniya, Ramesh
Supervisor: Narayanan, Vinod
Year: 2018
Keyword's: Fluid Mechanics, Boundary Layer, Axisymmetric Boundary, Global Stability Analysis
Call No.: 629.132 BHO
Acc. No.: T00266

Abstract: The laminar-turbulent transition of the boundary layers has been a subject of interest to many researchers in past few decades. The amplification of the disturbance waves is the first step in the transition process, and it is studied by linear stability theory. The linear stability analysis of the shear flows with parallel flow assumption is well understood by the solution of the Orr-Sommerfeld equation. The stability characteristics of a boundary layer are strongly influenced by the various factors such as pressure gradient, surface curvature, free-stream turbulence, etc.

The boundary layer formed over an axisymmetric body is qualitatively different from a flat-plate boundary layer. The boundary layer on a circular cylinder and cone develops continuously in spatial directions; hence the parallel flow assumption is not valid. Due to the wall normal velocity component, the boundary layer is non-parallel. The instability analysis of such two-dimensional nonparallel base flow is called global stability analysis.

The main motivation of present work is to study the stability characteristics of the spatially developing boundary layers using global approach. The flow transition takes place through instability of the base flow, and thus, the flow instability has the great role in the flow transition and its control. The knowledge of flow instability can help in deciding the control strategy also. Most of the earlier work in the area of flow stability uses the local stability approach, in which stability characteristics are studied based on the local velocity profile. The velocity profile is a function of wall normal coordinate only. The streamwise wavenumber is constant at each streamwise location. The numerical solution of Orr-Sommerfeld equation gives the local stability characteristics. In most of the cases, critical Reynolds number is obtained above which the flow becomes unstable. This approach is valid only when the base flow velocity profile is not varying in stream-wise direction. The fully developed channel flow is an example of parallel flow. In real-life situations, the flows are always non-parallel. The non-parallel effects are strong in the case of boundary layer flows at low and moderate Reynolds number. The base flow velocity profile varies drastically in stream-wise direction. The stability analysis of the base flow with streamwise variation can be studied using global approach. The main objectives of the present work are to investigate the stability characteristics of the spatially developing boundary layers and the effect of transverse curvature and pressure gradient on it. Some investigators have studied stability characteristics of the flat plate boundary layer with zero pressure gradients. We considered three different cases of spatially developing boundary layers.

In the first case, instabilities of the incompressible axisymmetric boundary layer over a circular cylinder is studied. The base flow is fully non-parallel and non-similar, the pressure gradient is zero and transverse curvature increases in the stream-wise direction. The range of Reynolds number from 261 to 693 is considered based on the displacement thickness at the inflow with azimuthal wavenumbers from 0 to 5. The Governing stability equations are discretized using Chebyshev spectral collocation method. The general eigenvalue problem is solved using Arnoldi's iterative algorithm. The computed global temporal modes show that the largest imaginary part of eigenvalues is negative for the range of Reynolds number and azimuthal wave-numbers. Hence the global modes are temporally stable. The two-dimensional spatial structures of the global modes show that the disturbances grow in size and magnitude while moving towards the downstream. The global modes with azimuthal wavenumber $N=0$ are least stable at lower Reynolds number; however, for $Re > 557$ the azimuthal wave $N=2$ are observed least stable one. Global modes with $N=3, 4$ and 5 are more stable. The global stability characteristics of axisymmetric boundary layer are also compared with the flat-plate boundary layer (zero transverse curvature). The comparisons show that the axisymmetric boundary layer is more stable than that of the flat plate boundary layer at small and moderate Reynolds number due to the transverse curvature effect. As Reynolds number increases, the transverse curvature reduces and the stability characteristics of axisymmetric boundary layer approach to that of the flat-plate boundary layer. Thus, the transverse curvature has the significant damping effect on the disturbances.

In the second case, we considered axisymmetric boundary layer over a sharp circular cone. The base flow is fully non-parallel & non-similar, the transverse curvature reduces and favorable pressure gradient develops in the streamwise direction. The increase in semi-cone angle α increases the effect of pressure gradient and reduces the transverse curvature effect. The Reynolds number is varying from 174 to 1047 based on the displacement thickness at the inflow and azimuthal wave numbers from 0 to 5 for different semi-cone angles (α). The global temporal modes are computed for a range of Reynolds number, and azimuthal wave numbers for various semi-cone angles shows that the largest imaginary part of eigenvalues is negative. Hence the global modes are temporally stable. The spatial structure of the of the eigenmode shows growth in the streamwise direction. The wave-like behavior of the disturbances is observed in the streamwise direction. As the semi-cone angle (α) increases for a given Reynolds number, the damping rate of the eigenmode increases, while the spatial growth rate of the disturbances increases in the stream-wise direction. Thus, the increase in α makes the flow temporally more stable. The azimuthal wavenumber $N = 1$ is found to be least stable among all.

In the third case, we considered flat-plate boundary layer. The base flow is fully nonparallel, and the transverse curvature effect is zero. The pressure gradient effect is favorable for positive wedge angle and adverse for the negative wedge angle. The Reynolds number computed based on the displacement thickness. The global temporal modes are computed for favorable and adverse pressure gradient conditions. The global modes are more stable with the favorable pressure gradient, while it becomes less stable for the adverse pressure gradient.

Title: Biomechanical view of parkinsonian rest tremor mechanism and its implication to therapy and early diagnosis
Researcher: Shah, Vrutangkumar V.
Supervisor: Madapusi, Harish Palanthandalam
Year: 2018
Keyword's: Biomechanics, Neurodegenerative Disorder, Tremulous Motion
Call No.: 612.76 SHA
Acc. No.: T00274

Abstract: Parkinson's Disease (PD) is the second most common neurodegenerative disorder of the central nervous system, and it is typically characterized by four cardinal motor symptoms: Rest Tremors, Bradykinesia, Rigidity and Postural Instability. The fundamental mechanism of these motor symptoms is still not well-understood, and further, differential diagnosis of PD remains a challenge. Fortunately, Deep Brain Stimulation (DBS) effectively alleviates motor symptoms of PD. Despite its success, the underlying mechanism of action of DBS also remains elusive. Hence, there is a tremendous opportunity to explore the fundamental mechanism of motor symptoms of PD and mechanism of action of DBS. In this thesis, we focus our attention on Rest Tremors in PD as it is one of the most common symptoms. While the various assumptions in our analysis are inspired by clinical observations and physiology literature, we primarily adopt a macro view and use a combination of systems theory, control theory, signal processing and other such engineering tools to analyse the symptoms and its underlying mechanism. Using such an approach, we draw insights and suggest future directions as discussed below.

1. Rest Tremors: Rest tremors are tremulous motion in body parts that are not voluntarily activated and are one of the most common symptoms in PD. To understand the mechanism behind rest tremors, along the lines of [1], [2], we view an increased sensorimotor loop delay as a key distinguishing feature in PD over healthy individuals, and theorize that this increased delay causes Parkinsonian rest tremors [3], [4], [5], [6]. With this as the starting point, several clinical observations related to Parkinsonian rest tremors are explained [6]. Thus, the present work provides a framework towards developing a deeper conceptual understanding of the mechanism of action of rest tremors, and it lays a foundation for developing tools for diagnosis and progress tracking of the disease by identifying some key trends. Further, we contrast this theory against the predominant central oscillator theory for rest tremor mechanism on the basis of established clinical observations with the help of simulation examples. Finally, based on our simulation analysis, we propose a few test-worthy experiments that could be explored further [7].
2. Deep Brain Stimulation (DBS): Next, we explore the underlying mechanism of DBS, a neurosurgical procedure involving the implantation of a medical device that generates high-frequency electrical signals and suppresses the tremors. Based on our simulation study, we conclude that the conceptual reason behind the working of DBS is that the high-frequency stimulation in combination with nonlinear elements in sensorimotor loop act to deaden the control actions and hence suppresses tremors [8] and [9]. We also show how a simple representation of sensorimotor loop is able to capture the key trend observed in real patients with PD [9]. Further, we propose that there

may be a potential link between the conceptual working of DBS and FES (Functional Electrical Stimulation) or other non-invasive techniques [9]. We further use the insights from this analysis to analyse the effectiveness of the different waveforms.

3. Early Diagnosis: It is known that the motor symptoms appear only when approximately 40%-60% of the dopaminergic neurons in the substantia nigra are lost. Further, when PD is clinically diagnosed, the disease may already have started some 4 to 6 years earlier. So there is a need for developing a test for detecting PD before the appearance of the motor symptoms (called Presymptomatic PD (PPD)). Hence, based on insights gained from rest tremors hypothesis, we propose a methodology for detecting PPD. The proposed methodology tracks the tendency of the sensorimotor delay to destabilize the sensorimotor loop. The proposed method is evaluated on simulated data of representative cases of healthy individuals and PPD [10], [11]. Our study suggests a need for a further in-depth clinical study to validate the proof-of-concept for the proposed methodology.

Title: Control of optimal growth of instabilities in fluid flows
Researcher: Kant, Ravi
Supervisor: Narayanan, Vinod
Year: 2020
Keyword's: Wall Transpiration, Linear Quadratic Regulator, Non-symmetric Base Flow Solutions, Symmetric Base Flow Solutions
Call No.: 620.106 KAN
Acc. No.: T00536

Abstract: The present thesis consolidates the comprehensive study on optimal control of instabilities in several flow scenarios such as plane channel, Jeffery-Hamel and channel flow with porous walls. The thesis also includes the study of adaptive control for flow profiling (the process of controlled attenuation and enhancement of amplitude) over flat plate boundary layers. The motivation behind aforementioned works are to delay the transition process, in turn achieving the desired flow conditions.

We have presented the effect of wall transpiration (a stability modifier) on optimal growth of perturbation energy in plane Poiseuille flow as the starting step of the work. There are substantial works done controlling of plane Poiseuille flow instabilities in the past. The starting step of controlling plane Poiseuille flow instabilities are useful to construct and deal with more complex flow scenarios such as control of Jeffery-Hamel flow, porous channel flow instabilities, which are not explored previously. We have adopted both modal and non-modal stability framework to analyze the flow problems. The state space model is constructed by integrating wall transpiration (a process in which small amount of fluid is periodically withdrawn/pumped through walls). The variational method is adopted to derive the optimal disturbance and associated optimal growth of the system. An optimal feedback control gain is acquired through Linear Quadratic Regulator. It utilizes the full knowledge of the states, and is feed- backed to the system to reduce the largest amplification of optimal growth of the disturbances. Upon controlled actuation, it has been found that the largest amplification of optimal growth is considerably suppressed. The G_{max} (for a supercritical case $Re = 8000$, $k_x = 1$, $k_z = 0$) is inhabited considerably (approximately 60 and 75 percent for single lower boundary control case and combined both boundary control case respectively). We have also synthesized an estimator by considering the wall shear as measurement equation. The estimator showed poor performance as compared with that of full state feedback. We have further analyzed the delay in transition in quantitative sense. It has been found that the maximum amplification of the growth function with no control case at $Re = 4000$ is identical with that of controlled plant's maximum amplification at $Re = 12000$, which shows that, with control application, the flow can further permit large Reynolds numbers without undergoing transition. We have also not confined ourselves with the same Fourier mode actuation. Actuation with double the wavenumbers/Fourier modes shows larger suppression of the optimal growths as compared with that of same and half the wavenumbers.

In the later section, we exhibit control of optimal growth of perturbations in Jeffery-Hamel flow through the standard stability modifier i.e. wall transpiration. The control of optimally amplified perturbations in converging/diverging Jeffery-Hamel flow with small angle, has not been studied previously to the best of our knowledge. The motive behind this study is to delay the transition phenomena in converging/diverging Jeffery-Hamel flows with small angles, where the parallel flow approximations are valid. The governing equations and the associated control model for the JH flow are developed with the parallel flow approximations, which gives the flexibility to work in the local stability framework. We have explored both modal and non-modal stabilities in this context. A similar variational method is utilized to calculate the optimal growth of the system. An optimal feedback control gain is developed through Linear Quadratic Regulator utilizing the knowledge of entire state, and is feed-backed to the system to reduce the largest amplification of optimal growth of the disturbances. It has been found that the optimally amplified growth in both converging as well as diverging JH flow is substantially reduced after applying controlled wall transpiration. The present study gives the possibility of a starting step towards the control of non-parallel global instabilities.

In the next section, we briefly study the control the optimally amplified growth of instabilities in porous channel flow through the standard stability modifier (wall transpiration), under the conditions of constant suction or injection through the porous walls. The methodologies and control modeling is similar to what has been applied for plane Poiseuille and JH flows. There are several base flow solutions in a channel flow with porous walls. We explore the stability and control of all possible base flow solutions. We apply controls for both symmetric and non-symmetric base flow solutions (type-I, type-II and type-III). We utilize the knowledge of full state, based on which, a linear quadratic regulator (LQR) is synthesized and an appropriate gain is feed-backed to restrain the largest amplification of optimal growth of the instabilities in the flow.

The last section of the thesis includes the wave cancellation method for flow control in contrast with all the previously used stability modifier (wall transpiration) method. we have introduced an adaptive control approach for flow profiling (the process of controlled attenuation and enhancement of amplitude) of a linear convectively unstable Tollmien-Schlichting (TS) alike waves. In many flow situations, we need to suppress the flow instabilities as it causes unnecessary drag and noise due to enhancement of perturbation amplitude, whereas in few other flow situations, we deliberately need the flow perturbations in some desired permissible set level to obtain a desired mixing or controlled enhancement of heat transfer in the fluid system. We introduce a flow profiling model (modified FxLMS) through which we can achieve controlled attenuation as well as enhancement in the amplitude of perturbation with single additional gain in the system. When the flow undergoes transition to turbulence, it is not easy to control the flow since it is chaotic and difficult to model. It is easy to apply the control while the flow is in unstable laminar state by keeping the amplitude of the wave in permissible set range. One dimensional linearized Kuramoto - Sivashinsky equation model (KS equation) is utilized to imitate the flow problem. The active flow problem is achieved by adaptive feedforward control which is extensively and effectively used in noise control. We make use of model- free adaptive method to further apply it for active flow

profiling in fluids. A structurally modified adaptive algorithm incorporating Filtered-x LMS (FxLMS) is designed and tested to get the desired set level of fluctuations in the fluid system. In this control model, with a set value of additional gain, we achieve cancellation, attenuation, enhancement, and neutralization of perturbation amplitude downstream of the flow. This profiling model also ensures that the set of troubling frequencies/modes are also attenuated/enhanced accordingly.

Title: Experimental insights on wettability induced enhancement in confined and unconfined pool boiling heat transfer

Researcher: Sarode, Ajinkya Ashok

Supervisor: Bhargav, Atul

Year: 2020

Keyword's: Heat Transfer Coefficient (HTC), Superhydrophobic, Heater Surface Rewetting, Fabrication Method

Call No.: 621.4022 SAR

Acc. No.: T00551

Abstract: Boiling utilizes latent heat of vaporization of the fluid to dissipate high heat fluxes at small temperature budgets. Consequently, nucleate boiling is widely pursued in a wide variety of applications such as thermal power plants, cooling of electronic devices, compact heat exchangers, engine cooling and, so forth. However, continuously rising heat flux requirements and efficient thermal management of miniaturized electronic devices demand an improvement in the boiling heat transfer performance. Surfaces with micro-/nano-scale wettability patterns have been shown to improve the heat transfer coefficient during pool boiling. In this dissertation, a simple and cost-effective technique to fabricate heterogeneous surfaces with macroscale wettability patterns comparable to the capillary length of the boiling fluid has been proposed. An enhancement up to 66% in the boiling heat transfer coefficient can be achieved in comparison to the bare surface. The proposed fabrication method facilitates a separate vapor/liquid pathway to achieve comparable heat transfer coefficients enhancements otherwise achieved through sophisticated and costly surface patterning techniques discussed in literature.

Applications such as cooling of 3D electronic stacks and portable electronic devices demand nucleate boiling in narrow gaps and often with inclined surfaces. In this regard, the individual effects of confinement and orientation (horizontal and vertical) on the heat transfer coefficient (HTC) obtained during boiling on macroscale patterned wettability surfaces has been experimentally investigated. For confined pool boiling condition, modified surface always demonstrated better heat transfer coefficient than the bare surface. The boiling heat transfer performance of modified surface was independent of surface orientation. While studies in the literature report the effect of various parameters such as gap dimensions, heater surface to confinement plate area ratio, surface modification and inclination on confined pool boiling heat transfer, the effect of wettability of the confinement plate has been completely missed. Here controlled experiments were performed to show that the heat dissipation capacity can be drastically improved by up to 82% if the conventionally used hydrophilic (HPI) confinement plates are replaced with a superhydrophobic (SHPo) ones. Side-view boiling visualization photography revealed that SHPo confinement attracts/pulls the nucleating bubbles away from the heater surface to provide a continuous pathway for liquid re-supply to facilitate efficient heater surface rewetting.

The ability to improve confined and unconfined boiling heat transfer performance has the potential to find wide applications in two-phase heat transfer.

Title: Ethanol autothermal reforming on Rh/CeO₂ catalyst: experimental and numerical studies
Researcher: Baruah, Renika
Supervisor: Bhargav, Atul
Year: 2021
Keyword's: Autothermal Reforming, Microkinetic Mechanism, Computational Fluid Dynamics, Global Rate Expressions, Artificial Neural Network
Call No.: 621.3 BAR
Acc. No.: T00752

Abstract: Hydrogen-powered Fuel Cell System has gained traction as a potential alternative source of power generation in remote area standalone applications like diesel generators. However, due to the high cost of storage and transportation of hydrogen to remote locations, it is generally desired to produce the hydrogen on-site via reforming reactions of hydrocarbons. Ethanol is a hydrocarbon and biofuel that is easily available in many parts, especially in agricultural areas. Ethanol can be reformed to hydrogen on-site using steam and oxygen (called autothermal reforming).

In this study, ethanol autothermal reforming on Rh/CeO₂ catalyst is studied experimentally and numerically. It is observed from literature that most studies in this area focus on novel catalyst development, optimization of reactor operating conditions, and reactor configuration. There is only a handful of literature available which studies the process numerically. Computational fluid dynamic (CFD) models at the reformer level incorporating detailed microkinetic mechanisms or global rate expressions are important for understanding the complex reactions process that accounts for the overall autothermal reforming process. It is a tool that can further play an important role in the design of the reactor and the reaction process as a whole. However, there are very few studies that incorporate detailed heterogeneous microkinetic mechanisms into their flow model. Moreover, a detailed microkinetic mechanism for ethanol autothermal reforming (ATR) on Rh catalyst is missing from the literature. Also, there are very few studies available which investigate the dynamic behavior of a reformer. Such studies are crucial to the understanding of fuel processing systems (FPS) and can contribute to improving the overall control strategies of small, autonomous fuel cell systems subjected to variable-load conditions. This thesis aims to address these gaps in literature. A test rig is developed to conduct experiments for the process. The reformer comprises of ceramic monolith reactors coated with Rh/CeO₂ catalyst. Experiments are carried out for a wide range of S/C and O/C ratios. The flow rate of ethanol is kept fixed at 0.5 g/min. The product composition at the outlet is analyzed through a Gas Chromatograph. A novel microkinetic mechanism for ethanol ATR on Rh catalyst is derived from a mechanism based on partial oxidation of ethanol on Rh catalyst already reported in literature using the top-down hierarchical method in a 1-D PFR reactor. The mechanism is then incorporated into a 3D CFD model to simulate Ethanol ATR on Rh/CeO₂ coated monolith reactor. The ceramic monolith reactor with washcoated channels is assumed to be a homogenous porous media with equivalent catalytic surface area and thermal properties to reduce computational effort. Using this model, we were able to predict the product composition and the

temperature profiles at various locations for different operating conditions with good agreement with experiment results.

3D CFD models using detailed kinetic mechanisms are computationally intensive. These models are useful in predicting the product concentration and reactor temperature for steady-state conditions. However, in case of dynamic conditions, such models are not feasible. Thus, a 3D transient CFD model using global rate expression has been developed. The model is simulated for varying oxygen flow rate at the reactor inlet, and the product composition response at the reactor outlet is monitored. An artificial neural network is trained on the transient CFD simulations to reduce computational time. This ANN model is then validated with CFD model results. We expect that the work in this thesis is an important step towards model-based real time control of autothermal reformers and could impact efficiency and robustness of reformer integrated fuel cell systems.

Title: Experimental investigations and prediction modelling of texture and thermo-physical changes during thermal processing of hygroscopic food materials

Researcher: Sinha, Ankita

Supervisor: Bhargav, Atul

Year: 2021

Keyword's: Food Processing Industry, Artificial Neural Network (ANN), Viscoelastic Nature - Food Materials, Hygroscopic Materials

Call No.: 621 SIN

Acc. No.: T00753

Abstract: The food processing industry has witnessed very high growth in India and in other countries due largely to the ever-increasing demand for processed food products. Process efficiency, health concerns, and product quality are some of the critical challenges faced by the industry. Researchers have worked on various aspects of these challenges in the past and have been successful in contributing to significant improvement in state of the art. However, a major limitation is the lack of comprehensive studies that could simultaneously focus on different aspects of a food processing technique and their interdependency on one another. Besides, the lack of well-defined protocols and methodologies have resulted in challenges during the generalisation and replicability of many experimental and computational procedures.

This dissertation focusses on addressing three broad segments of the food processing industry, namely (a) consumer satisfaction, (b) process efficiency and (c) development of new food products. While each of these segments is vast in itself; the current work focusses only on the three key aspects of these segments: texture, modelling of transport, deformation and chemical kinetics, and properties estimation. These segments are interrelated, and efforts have been made in this dissertation, to capture these aspects and then couple them with each other. Tuberos, hygroscopic food materials such as potatoes and sweet potatoes were chosen as the primary subject of study. However, the applicability and validity of work to other porous hygroscopic materials is also discussed.

In this dissertation, firstly, Young's modulus (a mechanical parameter) is chosen as the measure of texture and effect of various operating parameters (geometry, aspect ratio and strain rate) and thermal processes (air drying and deep frying) on Young's modulus is experimentally investigated. Importance of strain rate consideration (due to the observed viscoelastic nature of food materials) while conducting texture experiments is emphasised. Subsequently, the role of state transition and drying kinetics on texture development during air drying is investigated. Models have been proposed to relate local and effective Young's modulus with moisture content. For deep frying process, three models have been developed to capture the effect of starch gelatinisation along with moisture content on Young's modulus. This is followed by the development of physics-based models for analyses and prediction of transport (heat, mass, momentum), deformation and chemical kinetics behaviour during air drying and deep frying process. As a novel approach, a simplified physics-based porous media model is developed to predict shrinkage along with heat and mass transfer during low

temperature air drying processes. Using volume additivity and neglecting variation in gas porosity, the need for complex constitutive models and fitting parameters to predict deformation is mitigated. The model is then validated with experiments conducted here and with those reported in the literature; results show good agreement.

Similarly, for deep frying processes, a fully coupled porous media model that predicts heat, mass and momentum-based transport, chemical kinetics and texture behaviour during deep frying process is proposed. Health aspect associated with deep frying is taken into account by coupling acrylamide formation chemistry with the heat, mass and momentum-based transport. Developed texture model has been coupled with the physics-based model for predicting quality behaviour. The trade-offs between desired texture, moisture content and permissible acrylamide content is also discussed. This model is also validated with experiments from the literature and results show good agreement. Finally, a novel, artificial neural network (ANN) based inverse problem approach is developed for estimation of food properties which are critical for the physics-based model. A deep learning ANN model is trained to predict sensitive properties using temperature and moisture data from a set of simple standard control experiments. The framework to implement the estimated properties in physics-based modelling of drying process is discussed and the modelling results show good agreement with experiments.

The present dissertation serves as an initial step to capture and couple various mechanisms associated with a food process and aims to emphasise on the development of comprehensive methodologies, which could simultaneously utilise experimental procedures, physics-based models as well as neural network based techniques for better understanding of thermal food processes, their modification and optimisation.

Title: Determination of the thermophysical properties of Al₂O₃-CO₂ nanofluid: a molecular dynamics approach
Researcher: Ahmed, Zeeshan
Supervisor: Bhargav, Atul
Year: 2020
Keyword's: Carbon dioxide (CO₂), Thermal conductivity (*k*) - CO₂, Viscosity (μ) - CO₂, Molecular Dynamics, Thermo-Physical Properties
Call No.: 621.4 AHM
Acc. No.: T00754

Abstract: Carbon dioxide (CO₂) has an impact on global climate and is thus extensively studied. Worldwide, great attempts have been made to decrease CO₂ emissions in the atmosphere, for instance, by capture and sequestration procedures. Also, CO₂ is a widely used industrial fluid as a natural refrigerant in data center cooling, in the oil and gas industry to enhance the oil recovery, well-fracturing applications, and in CO₂ capture and storage. Transport properties such as thermal conductivity (*k*) and viscosity (μ) of CO₂ play an essential role in these rapidly evolving applications. A need arises to improve the *k* and μ of CO₂ to increase the process efficiency and reduce cost in such applications. One of the ways to enhance the *k* and μ is through nanoparticle addition in the base fluid, known as nanofluid. Nanofluids are known to have significantly different transport properties relative to the corresponding conventional base fluids. The enhanced heat transfer in nanofluids has made them the topic of many theoretical research efforts during the last decade. Molecular dynamics (MD) simulations are being increasingly adopted as a numerical method to obtain preliminary estimates of nanoparticle-fluid interactions and to understand the elementary properties of the system.

The nanofluid in this study consists of alumina (Al₂O₃) nanoparticle and CO₂ as a base fluid. The experimental data on *k* and μ of CO₂ based nanofluid are currently not available in the open literature. Even the parametric studies on *k* and μ estimation of CO₂ nanofluids are not found in the open literature. We screened the intermolecular interaction potential models available for CO₂-CO₂ interactions and found that the TraPPE-flexible model (with Morse potential) to be most suitable for conditions used in this work. Using quantum mechanical simulations, we estimated the CO₂-Al₂O₃ interaction potential. Using this combination for CO₂-CO₂ and CO₂-Al₂O₃ interactions, we explored the various influential effects including the volume fraction of nanoparticles, the diameter of nanoparticles, nanofluid temperature, Brownian motion of particles, Brownian motion induced micro-convection, interfacial layering, nanoparticle aggregation, surface wettability as well as the interfacial thermal resistance on the thermal conductivity and viscosity of Al₂O₃-CO₂.

In addition to this, diffusion coefficients are calculated for base fluid and nanofluid to investigate the Brownian motion effect. The thickness of the dense semi-solid layer formed at the Al₂O₃-CO₂ interface is studied through radial distribution function (RDF) and density distribution around the nanoparticle. Results indicate that the self-diffusion coefficient for CO₂ decreases, and the nanolayer thickness is found to increase with an increase in nanoparticle diameter. The Brownian motion does not appear to be the cause of the enhanced *k* and μ of the nanofluid. This enhancement can instead

be attributed to nanolayer formation. The thermal conductivity and viscosity enhancement of the nanofluid was 20%, 46% and 62%, and 25%, 54% and 65% for 1 nm, 2 nm and 3 nm diameter, respectively at a constant volume fraction of 1.413% and 1.54%. Various configurations of the aggregated nanoparticle cluster and its stability are examined using potential energy analysis, and results showed that the potential energy is inversely proportional to the enhancement in the thermo-physical properties, owing to the increased system stability and hence, yielded a different increase in thermal conductivity and viscosity. Results showed that the existence of the nanoparticle aggregation causes a maximum enhancement of 70% in thermal conductivity and 84% in viscosity of nanofluid at the volume fraction of 0.9%. Lastly, the thermal interfacial resistance was calculated, and its effect due to np diameter, temperature and surface wettability are studied. A study of the monolayer is done to see the interfacial resistance effect over k , and results show that the influence of thermal interfacial resistance (TIR) on k is negligible compared to the nanolayer. Also, it is observed that the TIR decreases with the increase in temperature and the effect of temperature at high surface wettability is almost negligible. The output of the current work demonstrates the enhancement in thermal conductivity and viscosity due to nanoparticles addition which has a potential to improve data center cooling efficiency, oil recovery, Brayton cycle efficiency, refrigeration and other thermal applications.

Title: Mechanisms and neural substrates underlying the acquisition of effector-independent motor memories
Researcher: Kumar, Adarsh
Supervisor: Mutha, Pratik
Year: 2021
Keyword's: Motor Adaptation, Neural Systems, Neuroanatomically - Adaptation, Myriad Mechanisms
Call No.: 621.3 KUM
Acc. No.: T00755

Abstract: Over the past 25 years or so, there has been considerable interest in understanding how humans learn to adapt to altered visual and dynamic environments. This work has explored two main questions: what are the mechanisms that drive this motor adaptation, and what neural systems are critical for it. While early work indicated that such learning occurs by implicitly updating our internal neural representations or models of the body and the environment (Shadmehr and Mussa-Ivaldi, 1994; Imamizu et al., 1995; Gandolfo et al., 1996; Sainburg et al., 1999; Wang and Sainburg, 2005; Tseng et al., 2007), newer studies have suggested that multiple mechanisms contribute to such learning. These include the use of fast-acting explicit re-aiming strategies (Fernandez-Ruiz et al., 2011; Taylor et al., 2014; Morehead et al., 2015), use dependent plasticity and operant mechanisms (Diedrichsen et al., 2010) that lead to reinforcement of successful movements (Huang et al., 2011). Neuroanatomically, adaptation has been shown to be critically dependent on intact processing within the cerebellum and the posterior parietal cortex.

Adaptation is deemed useful when it generalizes, or transfers, beyond the conditions in which learning has occurred. Accordingly, transfer of learning to conditions that a limb has not experienced during training has been shown in a number of studies (Imamizu et al., 1995; Krakauer et al., 2000, 2006; Malfait et al., 2002; Yan et al., 2012; Taylor and Ivry, 2013). These studies on within-limb generalization have yielded fairly consistent results, which has enabled a relatively clear understanding of its mechanistic basis (Tanaka et al., 2009). Interestingly, transfer from a trained limb to another which has not been exposed to the learning conditions at all has also been demonstrated (Criscimagna-Hemminger, 2002; Wang and Sainburg, 2003; Malfait and Ostry, 2004; Taylor et al., 2011; Wang et al., 2011a; Bock, 2013; Joiner et al., 2013; Lei and Wang, 2014; Sarwary et al., 2015; Poh et al., 2016; Bao et al., 2017a; Kumar et al., 2018). One way in which these results could be explained is by positing that learning to adapt movements with one limb gives rise to representations that are effector-independent, or common across limbs. While there is some support for this idea (Wang and Lei, 2015; Wang et al., 2015), the heterogeneity in the results of interlimb transfer makes this difficult to ascertain. For instance, transfer has been shown to occur completely (Poh et al., 2016), partially (Wang and Sainburg, 2004b; Taylor et al., 2011; Joiner et al., 2013) or not at all (Martin et al., 1996a; Kitazawa et al., 1997). In the absence of transfer, it is unclear whether an effector-independent representation even gets developed or whether it remains inaccessible to the untrained limb.

In our first study (Chapter 2), we used an interference paradigm to test the idea that an effector-independent representation is acquired when learning using a single limb. We used upper extremity targeted reaching movements under a visuomotor rotation as model for motor learning, and had healthy human subjects learn a CW 30-degree rotation with either left or right arm followed immediately (5 min) by adaptation to a CCW 30-degree rotation with the other, untrained arm. After 24 hrs, subjects relearned the CW 30-degree rotation with the same arm that they had used to learn the task the first time. We observed robust interference when the two arms adapted to opposite perturbations. We also observed a learning-order-dependent asymmetry in performance upon re-exposure, which could be attributed to asymmetric transfer of aftereffects from the left to the right arm but not vice versa. The clear interference between the memories indicated that learning with one arm leads to the development of memory representations that are effector-independent. Which of the myriad mechanisms that contribute to learning drive the formation of this effector-independent representation? We explored this question in the next study (Chapter 3) by specifically probing the contribution of the faster, likely explicit, processes and slower implicit mechanisms to interlimb transfer, the signature of the effector-independent component. Subjects first adapted to a counterclockwise visuomotor rotation with either left or right arm for different numbers of trials (40, 80, 160, 320) and then were tested for transfer to the other arm on the same task (40 trials). Performance on the first transfer trial of an arm was compared with first naïve learning trial performance of the same arm. We first confirmed that transfer was asymmetric and only occurred from left to right arm. We then noted that the amount of transfer scaled with the number of left arm training trials; thus, transfer magnitude was greatest in the 320 trials group and least in the 40 trials group. A dual-rate state-space model fit that included fast and slow learning processes revealed a strong association between the amount of transfer and the level of slow (but not the fast) process reached at the end of different learning trials.

Although in this study we were able to establish an association between the slow process and transfer magnitude, this association was essentially correlational in nature. In our next experiment (Chapter 4), we sought to more directly test whether transfer is associated with the slower, implicit mechanisms that operate during learning. We leveraged the idea that when subjects adapt to a perturbation A followed by an opposite perturbation B, they demonstrate “spontaneous recovery” of the behavior in A when they are exposed to “error-clamp” trials following brief exposure to B. This spontaneous recovery is thought to be the consequence of residual implicit processes that do not immediately get reset to zero in the error-clamp. We wondered whether spontaneous recovery would occur if subjects were adapted to perturbations A and B with one arm, and were then asked to perform the error-clamp trials with the other arm. Subjects first used either left or right arm to adapt to a 30-degree CCW visuomotor rotation over 200 trials, and followed by 20 trials of a 30-degree CW rotation. They then used the other, untrained arm to move in an error-clamp block of 80 trials. We found spontaneous recovery only in subjects who used the left arm to learn and were then tested in the error-clamp with the right arm, confirming the asymmetry in transfer. More importantly, since the spontaneous recovery is a signature of the slow process, this result also confirmed that the observed transfer was the consequence of the operation of the slower, implicit mechanisms. Thus, our studies in chapters 3 and 4 established through studies of interlimb transfer

that the effector-independent representation of the motor memory is acquired via gradually evolving implicit learning mechanisms.

In our final study, we aimed to determine the neural substrate essential for representing this effector-independent component. Specifically, we asked whether disrupting the posterior parietal cortex (PPC) of the left brain hemisphere using high-definition cathodal transcranial direct current stimulation (hd-tDCS) post adaptation would disrupt interlimb transfer. Subjects first learned a 30-degree CCW visuomotor rotation with their left arm for 200 trials and were then divided to receive either real or sham 2 mA cathodal hd-tDCS for 15 minutes. Subjects were then tested for transfer with their right arm on the same task. Unsurprisingly, subjects who received sham stimulation showed substantial transfer of learning from the left to the right arm. However, subjects who received real stimulation over the left PPC showed no transfer. Control experiments revealed that this was not due to non-specific effects of hd-tDCS since another group of subjects who received stimulation over the left primary motor cortex (M1) showed substantial transfer. This study enabled us to conclude that the left PPC is a critical substrate that participates in the formation of an effector-independent motor representation that leads to interlimb transfer. Collectively, our results provide fresh insight into the mechanistic determinants of interlimb transfer, and are also significant from the point of view of understanding the neural basis of effector-independent motor memories. In the future, these findings can be leveraged to design improved rehabilitation protocols that exploit such effector-independent representations to alleviate motor deficits post Stroke.

Title: Intermittent feedback control theory & its applications to human postural control
Researcher: Dash, Ranjita
Supervisor: Madapusi, Harish Palanthandalam
Year: 2022
Keyword's: Closed-loop and Open-loop Dynamics, Human Quiet Standing Posture, Posturographic Techniques, Energy Efficiency, Ground Vehicle Steering
Call No.: 629. 8312 DAS
Acc. No.: T00945

Abstract: Intermittent feedback control is a form of feedback control in which the variables of interest are observed continuously but corrective control action is only initiated intermittently. Further, if this intermittent action is triggered when certain threshold criteria are met (such as if the deviations in the variables of interest exceed certain thresholds), it is referred to as event-driven intermittent control. While intermittent control has received limited attention in the controls community, evidence of presence of intermittent control has been reported widely in many natural systems including various control strategies adopted by humans. Several studies related to tasks such as postural control, control of saccadic eye movement for tracking of objects with eyes, locomotion (whether it being on foot or controlling a vehicle) have shown that there is evidence that humans employ intermittent control. It has been reported by multiple groups in the literature that the Central Nervous System (CNS) likely uses an event driven intermittent control strategy to stabilize the human upright posture. In addition, intermittent control also finds applications in the field of physiological modelling, networked control systems, transportation, economic modeling, communication systems, manufacturing among many more.

While the focus in the literature has been to uncover evidence of the presence of an event-driven intermittent strategy, studies aimed at developing an in-depth understanding of intermittent control have been largely lacking. Further, with regard to human postural control, there have been almost no studies on the nature of the threshold criteria in an event-driven intermittent strategy and how it may change under different conditions.

This thesis investigates three key directions related to intermittent control. First, it examines through analysis, simulations and experiments the advantages of an intermittent control strategy over a conventional continuous control strategy. Second, the role of intermittent control and specifically the nature of and changes in the threshold criteria in the control of human quiet stance by the CNS is investigated through simulations and human subject trials. Finally, the applicability of intermittent control to an intuitive and common application such as vehicle lane keeping is examined to help illustrate some of the advantages of intermittent control.

The first line of research aimed at developing an understanding of intermittent control brings out several insights on stability, energy efficiency, and transient performance in comparison to corresponding continuous control. We show with the help of analysis and simulations that it is indeed possible to use an intermittent control strategy to improve stability of the feedback control

system as compared to an equivalent continuous control strategy. We also show that for some classes of systems, an intermittent control strategy also provides superior transient performance and lower energy consumption. In such systems, it is observed that the intermittent strategy allows one to use ‘a more aggressive’ control action intermittently and therefore obtain lower energy consumption and better stability properties. These findings are also demonstrated on a table-top experimental setup of an inverted pendulum.

In the second line of research, using human subject trials and simulations of Anterior-Posterior dynamics of human quiet standing, we analyze the role and nature of an intermittent control strategy in the control of human quiet stance. First, it is demonstrated through simulations that an intermittent control strategy indeed provides better stability and lower energy consumption in postural control tasks. Further, it is shown that intermittent control explains several clinical observations related to the Centre-of-Pressure (COP) trajectories observed in human quiet stance such as the presence of a bi-modal COP distribution and presence of limit-cycle oscillations. Moreover, several clinical observations including some contradictory observations related to COP trajectories of Parkinsonian patients reported in the literature are shown to be consistent with an intermittent control strategy. Next, in an experimental study recording COP trajectories from 51 young healthy individuals along with with Stabilogram-Diffusion, temporal and spectral analysis, we show that there is compelling evidence of changes in the threshold criteria governing the intermittent control strategy with a change in the task conditions. Specifically, we show that inducing a natural arm swing during quiet stance appears to lead to higher sensory dead zone in neuronal control reflecting higher intermittency in active feedback control and a corresponding lower sensory dependence. These results provide insights that may be useful to understand how postural control is affected under certain diseased conditions or with age and in assessment of future fall risk.

Finally, with the help of simulations, we analyze the impact of intermittent control on the lateral vehicle dynamics in an autonomous vehicle lane keeping problem. Consistent with our earlier findings, these results show improved transient performance at lower energy consumption over a continuous control strategy. In conclusion, the three directions investigated in this thesis demonstrate the advantages of intermittent control and generate insights about both intermittent control in general and its role in human quiet stance. These results not only have a direct role in understanding human quiet stance and deterioration in postural control under various circumstances, but also have direct applications in areas such as autonomous vehicle systems and autonomous robots.

Title: Studying the role of cable-driven leg exoskeleton in altering human-robot interaction for Gait training
Researcher: Sanjeevi, N. S. S.
Supervisor: Vashista, Vineet
Year: 2023
Keyword's: Human-robot Interaction, Artificial Limbs, Gait Rehabilitation, Central Nervous System (CNS)
Call No.: 629.892 SAN
Acc. No.: T01023

Abstract: Walking is the most convenient mode of locomotion among humans. It is accomplished through the integrated action of different components of the human musculoskeletal system. The musculoskeletal system is inherently redundant thus facilitating individuals to achieve the same movement goal in several different ways. Neuromusculoskeletal impairments, such as stroke, cerebral palsy (CP), and spinal cord injury (SCI), damage the central nervous system (CNS) pathways in an individual. These damages limit one's ability to contract muscles to normal amplitudes voluntarily. Additionally, muscle spasticity and inappropriately timed muscle activities are reported in individuals with these impairments. These abnormalities result in unstable and asymmetrical walking patterns and affect one's ability to walk correctly. Subsequently, different training and rehabilitation paradigms have been proposed in the literature to improve the functional walking of individuals by providing repetitive practice sessions. To this extent, exoskeletons have become popular for their advantages in providing controlled repetitive motion, better quantification of kinematic changes, and reduced labour need.

Despite the variety of robotic gait rehabilitation devices that have been developed and the studies performed with these devices, no consensus has emerged about the superiority of robot-aided gait rehabilitation over the traditional methods. The understanding of how to optimally plan an intervention by an exoskeleton and how the exoskeleton works in concert with a complex musculoskeletal system during walking is non-trivial. One possible way to elaborate on the complex interaction between humans and the robot can be by studying the imposed external dynamics, i.e., Human-robot interaction (HRI). Among the works on leg exoskeletons, cable-driven robotic architectures have also been used for movement rehabilitation. Due to the use of cables, these systems provide inherent advantages of being lightweight, flexible, and easily altering cable routing architecture. However, unlike a rigid link, a cable can only apply a pulling force on a body and can only be used for unidirectional force applications. Thus, redundantly actuated cables are required to control a cable-driven system fully. Such actuation redundancy adds to control complexities and makes the system's operation analogous to a human musculoskeletal system. In the context of a Cable-Driven Leg Exoskeleton (CDLE), actuation redundancy and flexibility in altering system architecture imply modulation of the robot's dynamics, i.e., a possible way to adapt the CDLE and human interaction.

The central focus of this dissertation is to formulate the external dynamics imposed on a human by a CDLE during a gait cycle and to systematically investigate the effect of altering the system parameters in modulating the imposed dynamics and study how the imposed dynamics of a CDLE can be tuned to promote a desired joint strategy or motion adaptation during a gait rehabilitation paradigm. The imposed dynamics are essentially the impedance that a robot imposes on the human musculoskeletal system and are typically modelled as a combination of the robot's inertia, damping, and stiffness elements. In the context of a CDLE being used for gait rehabilitation applications, the current work predominantly models the CDLE's impedance through its stiffness characteristics. As human anatomical architecture comprises thigh, shank, and foot segments connected in series, a typical leg exoskeleton is given a serial-chain manipulator architecture, where externally actuated elements are attached to the segments. Thus, as the first step, we began our analysis by analytical modelling for a cable-driven serial manipulator (CDSM) and computed its tensionable workspace. Later, we developed a formulation for stiffness analysis of a CDSM. We analyzed the effect of system parameters, namely, cable stiffness, cable tension, cable routing, and cable anchor positions, on the CDSM's stiffness characteristics. Further, the stiffness behaviour of a CDSM was evaluated across its tensionable workspace. We have also developed a lab-based experimental setup to validate the stiffness changes from altering CDSM parameters. Specifically, we devised three CDSM design conditions that enabled more significant variation in stiffness characteristics without affecting the tensionable workspace. Using the understanding developed from CDSM modelling, we extended the formulation to comprehend the multi-joint stiffness characteristics of a CDLE. In the context of CDLE-human interaction, this stiffness essentially represents the external impedance imposed on human anatomical joints. Subsequently, we analyzed the effect of system parameters on the stiffness behavior of a CDLE over a gait cycle. Out of different parameters, we observed that cable routing alteration facilitates diverse stiffness modulation for a CDLE. From the perspective of movement training during a rehabilitation paradigm, the analysis and results demonstrated the efficacy of performing architecture modulation for a CDLE in favourably tuning the HRI.

As the next step, a cable-driven lower limb musculoskeletal system model was developed, considering the bones as rigid links and muscles as cables. This modelling was intended to study the lower limb musculoskeletal joint stiffness variations during the sagittal plane limb motion of walking. We used an open-source biomechanical modelling software (OpenSim) to solve muscle forces required for a healthy gait. The muscle force values were input to the developed cable-driven model to compute the musculoskeletal joint stiffness. Accordingly, a musculoskeletal simulation paradigm was established to analyze the effect of external dynamics on human walking. Specifically, we simulated two modalities, differed only by the imposed impedance, for a similar passive swing phase intervention. The results showed significant changes in musculoskeletal stiffness variations and their interdependence with the imposed impedance characteristics. From the gait intervention perspective, the presented observations illustrated the importance of HRI and its effect on musculoskeletal adaptations.

Finally, healthy human walking experiments were conducted to elaborate on the role of altered HRI on human gait adaptation. A customizable CDLE was developed to apply an external force intervention during treadmill walking. The setup allowed alteration in the cable routings and cable attachment locations to modulate the imposed multi-joint stiffness on the human anatomical joints. A swing phase force intervention to increase the step height during walking was implemented with three different configurations of the CDLE. Eight healthy participants were recruited for each CDLE configuration. The results showed varied gait adaptation among the three groups such that the subjects used either predominantly their hip joint, knee joint, or a combination of both joints. Furthermore, the force intervention using only one CDLE configuration reported consistently increased step height. These human experiments demonstrated a CDLE's ability to alter HRI to promote a particular joint strategy during a gait training intervention.

Overall, the presented work in the dissertation illustrates the importance of HRI in governing the adaptation outcome of a gait intervention paradigm. The presented conclusions, though derived from the healthy subject experiments, bear significance in choosing gait rehabilitation paradigms, as the exoskeletons are used for individuals with disabled walking, and any undesired HRI can lead to undesired compensatory strategies by the individuals.

* * * * *



PHYSICS

Physics

Title: Inflationary scenario with non- standard spinors
Researcher: Basak, Abhishek
Supervisor: Bhatt, Jitesh R.
Year: 2013
Keyword's: Inflation, Elko, NSS, Cosmological Perturbation Theory, Dark Energy, Cosmic Coincidence Problem
Call No.: 539 BAS
Acc. No.: T00050

Abstract:

Inflationary scenario has been very successful in solving various problems associated with the standard Big Bang cosmology. But the nature of the field that drives accelerated expansion (inflaton) is still unknown to us. The inflationary models with scalar fields, under the slow-roll approximations, are well studied. In contrast, inflationary scenario with spinor fields have not attracted much attention. In earlier works the 'classical' Dirac spinor field was studied as a candidate of inflaton. However, there were some issues with inflationary scenario driven by the Dirac spinor. One of the most important problem with Dirac spinor is that it produces highly scale dependent power-spectrum (with spectral index $n_s \sim 4$), which is inconsistent with the CMB observations.

Recently, one special type of spinor was proposed by Ahluwalia (2005, 2013) which is an eigenspinor of charge conjugation operator, also known as Elko. This spinor is called the Non-Standard Spinor (NSS) as it has an unusual property: $(CPT)^2 = -\mathbb{I}$. NSS field is a spin- $\frac{1}{2}$ field with mass dimension *one*, whereas the 'classical' Dirac spinor is a spin- $\frac{1}{2}$ fermion with mass dimension $\frac{3}{2}$. This new spinor field obeys the Klein-Gordon equation instead of Dirac equation. NSS can interact only through Higgs and with gravity, therefore it is dark by nature. Thus it is worth investigating the role of NSS in the unknown dark sector of the universe like: Dark matter, dark energy and inflation etc. In this thesis our focus is on the NSS driven accelerated expansion of the universe.

In the earlier NSS theories there was one major inconsistency — the equation of motion of NSS obtained from the energy-momentum tensor did not match with the equation of motion calculated using the Euler-Lagrange equation. Recently a consistent theory of NSS was developed which removed this inconsistency. In this thesis we use a consistent NSS theory to study the first order cosmological perturbation theory for NSS. The NSS Lagrangian and the energy-momentum tensor can be expressed as follows:

$$\mathcal{L} = \frac{1}{2} \bar{\lambda} \overleftarrow{\nabla}_{\mu} \nabla^{\mu} \lambda - V(\bar{\lambda} \lambda), \quad T^{\mu\nu} = \bar{\lambda} \overleftarrow{\nabla}^{(\mu} \nabla^{\nu)} \lambda - g^{\mu\nu} \mathcal{L} + F^{\mu\nu}$$

where λ and $\bar{\lambda}$ is the NSS and its dual. The covariant derivatives are defined as: $\bar{\lambda}\overleftarrow{\nabla}_\mu \equiv \partial_\mu\bar{\lambda} + \bar{\lambda}\Gamma_\mu$ and $\nabla_\mu\lambda \equiv \partial_\mu\lambda - \Gamma_\mu\lambda$ where, Γ_μ is the spin connection. In the expression of energy-momentum tensor the $F^{\mu\nu}$ term, which was absent in the earlier works, appears because of the variation of Γ_μ with respect to the metric (Böhmer et al., 2010). Using a simple ansatz of the perturbed NSS and its dual, $\delta\lambda = \delta\varphi\xi$, $\delta\bar{\lambda} = \delta\varphi\bar{\xi}$ where φ is a scalar and ξ is a constant spinor with the property $\bar{\xi}\xi = 1$, we have calculated components of the perturbed energy-momentum tensor. The perturbation theory for NSS becomes like a scalar field theory. However, calculation of the energy-momentum tensor shows the presence of additional terms in comparison with the standard canonical scalar field. We construct the modified Mukhanov-Sasaki equation for the NSS. Unlike scalar field case, the sound speed square is shown to be $c_s^2 \neq 1$ in general. The spectral index for the scalar perturbation is shown to give a nearly scale invariant power-spectrum which is consistent with the observation provided that $\tilde{F} \equiv \frac{\varphi^2}{8M_{pl}^2} < 10^{-4}$. With this upper bound $c_s^2 \sim 1$. Thus in case of first order perturbation theory, NSS becomes indistinguishable with the canonical scalar field theories.

In this thesis we have also studied the attractor behaviour of NSS cosmology. In inflationary and dark energy theories it is difficult to find exact initial conditions. Therefore it is important that these theories show the attractor behaviour, which will allow a wide class of solutions with different initial conditions to have similar asymptotic behaviour. The search for an attractor in case of NSS was attempted before also (see Wei, 2011). But no stable fixed points were found in the earlier attempts. In this thesis it is shown that the NSS equations can give inflationary-attractor which corresponds to 60 e-foldings. We have also demonstrated, with a new definitions of variables, that in the presence of barotropic perfect fluid the dynamical equations of the NSS can have stable fixed points. The stable fixed points can give us late-time attractor for NSS which can be useful in alleviating the cosmic coincidence problem. The stable fixed points are achieved by redefining the kinetic and potential part of NSS.

Title: Effects of lower atmospheric and solar forcings on daytime upper atmospheric dynamics
Researcher: Laskar, Fazlul Islam
Supervisor: Pallamraju, Duggirala
Year: 2014
Keyword's: Atmospheric Coupling, Dayglow, Ionosphere, Upper Atmosphere, Sudden Stratospheric Warming, Sun-Earth Interaction, Gravity Waves, Planetary Waves
Call No.: 539 LAS
Acc. No.: T00054

Abstract: The upper atmosphere of the Earth is influenced by incoming solar radiation (UV, EUV, and X-rays) and by secondary effects like waves from the lower atmosphere. The EUV radiation is absorbed above about 100 km altitude of the Earth's surface by atomic and molecular constituents resulting in their excitation to higher energy states. These excited species while returning to their respective ground states give rise to radiations, which are called dayglow (or daytime airglow). Chemically excited atmospheric species can also contribute to dayglow emissions. The intensity of these dayglow emissions depends on the number densities of the reactants and on the temperature. The distribution in densities of the reactants can be affected by the waves, thereby leading to the variations in the intensities of the dayglow emissions. Thus, the dayglow measurements provide an effective means to investigate the upper atmospheric dynamics, which are influenced by both solar flux variations and lower atmospheric processes. Solar activity changes due to its internal dynamics giving rise to variations of different periods ranging from hours to years. The lower atmospheric waves are excited by topography, convection, etc., and in the presence of stable atmosphere they can propagate to the upper atmospheric altitudes. In this study we characterize various types of coupling processes in the atmosphere and their variations with waves and solar activity.

The main data set that has been used in this work has been retrieved using Multiwavelength Imaging Spectrograph using Echelle-grating (MISE). MISE is a unique instrument capable of obtaining daytime sky spectra at high-spectral resolutions over a large field-of-view. From such spectra of MISE oxygen dayglow emission intensities at 557.7 nm, 630.0 nm, and 777.4 nm wavelengths have been obtained. In addition to oxygen dayglow emission intensities, data sets of ionospheric total electron content (TEC), zonal mean winds and temperatures from the stratosphere to the lower thermosphere, and the equatorial electrojet (EEJ) strengths have been used. In this thesis, it has been shown that the lower atmospheric influence on the upper atmosphere through waves is affected by solar activity. This is because the latter is responsible for the alteration of the atmospheric background conditions on which wave propagation and dissipation depend. From an investigation of the oscillations of planetary wave regime in dayglow and other atmospheric parameters at three different levels of solar activity, it has been shown that the vertical coupling of atmospheres through these waves is solar activity dependent. It is proposed that: (i) the effect on upper atmospheric dynamics due to lower atmosphere exists at least until the average sunspot number (SSN) is ≤ 35 , (ii) there is a transition from the lower atmospheric forcing to mixed behavior between average SSNs of 35 to 52, and (iii) another transition from mixed effects to those of purely solar origin occurs between SSN

values of 52 to 123. Further, in this thesis it has also been shown that even during high solar activity period if a sudden stratospheric warming (SSW) event occurs then the vertical coupling is enhanced, as the SSW related processes provide additional energy to enable this coupling. A statistical study of gravity waves present in the thermospheric altitudes is made using the three dayglow emissions and the EEJ strength data obtained during the years 2011 to 2013. The gravity waves are found to be present in higher numbers in the thermosphere during higher solar activity of 2013 compared to 2011, which is attributed to a reduction in dissipation in the lower thermosphere during higher solar activity epoch. Investigations using long-term data sets of EEJ and TEC revealed that the vertical coupling during SSW events depends on the strength of the SSW. Also, the interaction between quasi-16-day planetary waves and semi-diurnal tides has been found to be very strong for the strong major SSW events. In another result, using both ground- and satellite-based optical remote sensing measurements, a new circulation cell in the mesosphere-thermosphere system has been shown to exist during SSW events, which has been alluded to in previous modeling studies.

Title: Vortices of light and their interaction with matter
Researcher: Prabhakar, Shashi
Supervisor: Singh, R. P.
Year: 2014
Keyword's: Singular Optics, Optical Vortex, Spontaneous Parametric Down-conversion, Entanglement, Wigner Distribution Function, Bell's Inequality, Vortex Dipole Annihilation
Call No.: 535 PRA
Acc. No.: T00057

Abstract: Optical vortices are singularities in the phase distribution of a light field. At the phase singularity, real and imaginary parts of the field vanish simultaneously and associated wavefront becomes helical. For an optical vortex of topological charge ℓ , there are ℓ number of helical windings in a given wavelength λ of light and it carries an orbital angular momentum of ℓh per photon. This dissertation concerns with the study of interaction of optical vortices with matter namely nonlinear optical crystal β -Barium Borate (BBO) and Bose-Einstein condensate. A new method to determine the order of optical vortex from just the intensity distribution of a vortex has been discussed. We show that the number of dark rings in the Fourier transform (FT) of the intensity can provide us the order. To magnify the effect of FT, we have used the orthogonality of Laguerre polynomials. We have studied the interaction of optical vortices with BBO crystal. The spatial-distribution of degenerate spontaneous parametric down-converted (SPDC) photon pairs produced by pumping type-I BBO crystal with optical vortices has been discussed. For a Gaussian pump beam, we observe a linear increase in thickness of the SPDC ring with pump size. On the other hand, the SPDC ring due to optical vortex forms two concentric bright rings with an intensity minimum in the middle. We also observe that if the beam size is lower than a particular value for a given topological charge ℓ of the vortex, then there will be no change in full-width at half maximum of the rings formed by down-converted photons. We have experimentally varied the quantum inspired optical entanglement for classical optical vortex beams. The extent of violation of Bell's inequality or continuous variables written in terms of the WDF increases with the increase in their topological charge. To obtain this, we have used the FT of two-point correlation function that provides us the WDF of such beams. Quantum elliptic vortex (QEV) is generated by coupling two squeezed vacuum modes with a beam splitter (BS). The Wigner distribution function (WDF) has been used to study the properties of this quantum state. We also study how this coupling could be used to generate controlled entanglement for the application towards quantum computation and quantum information. We observe a critical point above which the increase in vortices decreases the entanglement. We have also studied the annihilation of vortex dipoles in Bose-Einstein condensates. To analyze this, we consider a model system where the vortex antivortex pair and gray soliton generated by annihilation of vortex dipoles are static and the system could be studied within Thomas-Fermi (TF) approximation. It is observed that the vortex dipole annihilation is critically dependent on the initial conditions for their nucleation. Noise, thermal actuations and dissipation destroy the superflow reflection symmetry around the vortex and antivortex pair. It is note worthy that some of our theoretical results have already been verified experimentally.

Title: Stable water isotopologues in the Indian summer monsoon rainfall
Researcher: Midhun M.
Supervisor: Ramesh R.
Year: 2015
Keyword's: Indian Summer Monsoon, Stable Water Isotopologues, Amount Effect, Isotope Enabled General, Circulation Models, Paleomonsoon
Call No.: 551.90954 MID
Acc. No.: T00089

Abstract: Stable oxygen isotope ratios ($\delta^{18}O$) of tree cellulose and speleothem carbonate are useful proxies for past monsoon rain in many tropical regions, as in such region a decrease in rain $\delta^{18}O$ accompanies an increase in rainfall on a monthly time scale. This amount effect varies spatially; therefore a local calibration, with actual measurements of rain amount and its $\delta^{18}O$ is required. Such observations, however, are quite limited in space and time. This thesis is aimed to improve the understanding of factors that control the $\delta^{18}O$ of Indian monsoon rainfall. For the present study water vapor samples were collected from the marine atmosphere over the Bay of Bengal (BoB) and rainfall sampled from Central and Northern India. The multiple simulations from isotope enabled General Circulation Models (GCM) are also used to understand the variability of the $\delta^{18}O$ of the Indian Summer Monsoon (ISM) rainfall on daily to inter-annual time scales. Measurements of stable isotopic compositions ($\delta^{18}O$ and δD) of water vapor collected from the BoB helps characterize both ISM vapor and North East Monsoon (NEM) vapor. This study shows that vapor $\delta^{18}O$ is higher during ISM compared to NEM with higher d-excess during NEM. This seasonal deference is possibly due to the seasonality in sea surface conditions, change in circulation pattern and changes in the type of rain forming systems (monsoon depression during ISM vs. tropical cyclones during NEM). The stable isotopic composition of water vapor estimated using Craig and Gordon model with the closure assumption (i.e., evaporation from the BoB is the only source of vapor) matches well with the measured values during non rainy days of ISM, whereas, it shows a large deviation from the model estimate during NEM season. The deviation from model estimate is negatively correlated with the rainfall along parcel trajectory (upstream rainfall) during both the seasons. The convective downdraft associated with tropical cyclones during NEM also plays major role in the lowering of vapor $\delta^{18}O$.

During ISM 2013, rain water samples were collected on a daily basis from six different cities (Ahmedabad, Bhopal, New Delhi, Kanpur, Varanasi and Dhanbad) spread over central and northern India and stable isotopic analyses were carried out. A weak amount effect (negative correlation between local rain and its $\delta^{18}O$) is observed at five out of the six stations, which explains ~7-22 % of intrapersonal variation of $\delta^{18}O$ of rain. The nudged simulations from an isotopeenabled General Circulation Model (IsoGSM) is compared with the observations. Though the model has some limitation in simulating the accurate spatio-temporal pattern of rainfall, the model simulated rain $\delta^{18}O$ is in good agreement with the observations. This study suggests strong control of moisture transport pathways on daily rain $\delta^{18}O$ at Ahmedabad, Bhopal and New Delhi. At New Delhi this effect is observed on intraseasonal to interannual timescales. Many isotope enabled General Circulation

Models (GCM) are used to aid the interpretation of rainfall- ^{18}O based proxies; nevertheless, all such simulations taken together remained to be evaluated against observations over the Indian Summer Monsoon (ISM) region. This study also examine ten such GCM simulations archived by the Stable Water Isotope INtercomparison Group, phase 2 (SWING2). The spatial patterns of simulated ISM rainfall and its $\delta^{18}\text{O}$ are in good agreement with the limited observations available. Simulations nudged with observed wind ends show better skill in reproducing the observed spatio-temporal pattern of rainfall and its $\delta^{18}\text{O}$. A large discrepancy is observed in the magnitude of the simulated amount effect over the Indian subcontinent between the models and observations, probably because models simulate the spatial distribution of monsoon precipitation differently. Nudged simulations show that interannual variability of rainfall $\delta^{18}\text{O}$ at proxy sites are controlled by either regional (rather than local) rainfall or upstream rain out. Interannual variability of rainfall $\delta^{18}\text{O}$ over the East Asian region is well correlated with El Nino Southern Oscillation (ENSO) while it is only weakly correlated over the Indian sub-continent.

Title: Finite temperature effect in the condensates of dilute atomic gases
Researcher: Roy, Arko
Supervisor: Singh, Angom Dilip Kumar
Year: 2015
Keyword's: Bose Einstein Condensation, Hartree-Fock-Bogoliubov Theory, Bose-Einstein Condensates, Goldstone Modes, Thermal Fluctuations, Condensate Atoms
Call No.: 530.43 ROY
Acc. No.: T00091

Abstract: The stationary state solutions and dynamics of Bose-Einstein condensates (BECs) at $T = 0$ are well described by the Gross-Pitaevskii (GP) equation. BECs of dilute atomic gases have been experimentally achieved at ultracold temperatures of the orders of 10^{-9} K. To include the effects of finite temperature on these condensates one needs to generalize the GP equation. We report here the development of the Hartree-Fock-Bogoliubov theory with the Popov (HFB-Popov) approximation for trapped two component BECs (TBECs). It is a gapless theory and satisfies the Hugenholtz-Pines theorem. The method is particularly well suited to examine the evolution of the low lying energy excitation spectra at $T = 0$ and $T \neq 0$. Apart from the two Goldstone modes corresponding to each of the species in quasi-1D TBEC, we show that the third Goldstone mode, which emerges at phase-separation due to softening of the Kohn mode, persists to higher interspecies interaction for density profiles where one component is surrounded on both sides by the other component. These are termed as sandwich type density profiles. This is not the case with symmetry-broken density profiles where one species is entirely to the left and the other is entirely to the right which we refer to as side-by-side density profiles. However, the third Goldstone mode which appears at phase-separation gets hardened when the confining potentials have separated trap centers. This hardening increases with the increase in the separation of the trap centers in which the TBECs have been confined. Furthermore, we demonstrate the existence of mode bifurcation near the critical temperature. We also examine the role of thermal fluctuations in quasi-1D TBECs of dilute atomic gases. In particular, we use this theory to probe the impact of non-condensate atoms to the phenomenon of phase-separation in TBECs. We demonstrate that, in comparison to $T = 0$, there is a suppression in the phase-separation of the binary condensates at $T \neq 0$. This arises from the interaction of the condensate atoms with the thermal cloud.

We also show that, when $T \neq 0$ it is possible to distinguish the phase-separated case from miscible from the trends in the correlation function. However, this is not the case at $T = 0$. In a BEC, a soliton enhances the quantum depletion which is sufficient enough to induce dynamical instability of the system. For phase-separated TBECs with a dark soliton in one of the components, two additional Goldstone modes emerge in the excitation spectrum. We demonstrate that when the anomalous mode collides with a higher energy mode it renders the solitonic state oscillatory unstable. We also report soliton induced change in the topology of the density profiles of the TBEC at phase-separation. For quasi-2D BECs, at $T = 0$, we show that with the transformation of a harmonically to toroidally trapped BECs, the energy of the Kohn modes gets damped. This is examined for the case when the radial angular frequencies of the trap are equal. The other instance, when the condensate

is asymmetric, the degeneracy of the modes gets lifted. The variation in the anisotropy parameter is accompanied by the damping of the modes, the quasiparticle modes form distinct family of curves; each member being different from the other by the principal quantum number n . When $T \neq 0$, with the production of a toroidally trapped BEC, the maxima of the thermal density tends to coincide with the maxima of the condensate density profiles. This is different from the case of a harmonically trapped BEC in which due to the presence of repulsive interaction between the atoms, the thermal density gets depleted where the condensate atoms are the highest.

Title: Spectral and timing studies of accretion disk in black hole binaries
Researcher: Jassal, Anjali Rao
Supervisor: Vadawale, Santosh V.
Year: 2015
Keyword's: Accretion, Accretion Disks, Black Hole Physics, X-rays- Binaries, X-rays- Individual
Call No.: 530 JAS
Acc. No.: T00099

Abstract: Accretion around compact objects is the most efficient way of extracting energy from material in an accretion disk. Luminous accretion disks around black holes in mass transferring black hole binaries offer an opportunity to study accretion processes taking place in the extreme conditions of temperature and gravitational field. However, these astrophysical sources cannot be observed with ground based conventional telescopes because they emit mainly in X-rays. Therefore, data are collected with space borne X-ray observatories. Spectra, light curves and images extracted from data are used as probes to understand the radiative processes in accretion disks. Although a significant understanding of the sources has been developed with the help of several empirical and theoretical studies, there are several phenomena, which are not understood.

This thesis presents the efforts that have been made to understand some of these phenomena. A majority of black hole binaries are transient in nature and they keep on switching between quiescent and outburst states. It is generally believed that an accretion disk is truncated far away from the central black hole during quiescent states. However, the observational evidence for this general picture is indirect at best. We studied a transient black hole candidate MAXI J1659–152 during its 2010 outburst, which was detected during very early stages of the outburst. We investigated the variation of the inner disk radius with progress of the outburst and found that the disk is truncated at larger radii in the beginning. A systematic decrease in the inner disk radius was found as the source transitions towards the soft states. We estimated mass of the black hole to be $8.1 \pm 2.9 M_{\odot}$ with the help of normalization of the disk blackbody component. A transient black hole candidate IGR J17091–3624 is studied, which behaved like ‘normal’ black hole binaries except during its latest outburst in 2011. The source showed properties similar to a unique black hole binary GRS 1915+105, known for exhibiting extreme variability. High mass accretion rate is believed to give rise to extreme variability, therefore IGR J17091–3624 is expected to be a bright source. However, IGR J17091–3624 is about 20 times fainter as compared to GRS 1915+105. We performed a comparative study of the two sources by investigating ‘heartbeat’-type variability observed in their light curves. The light curves were folded and spectra were generated for the 5 phases of ‘heartbeat’ oscillations. The spectra were fitted simultaneously by tying the system parameters and leaving the accretion-process-dependent parameters independently free across the 5 phases. We found important constraints on mass, distance, inclination and spin of IGR J17091–3624. It was noticed that the estimated value of spin is low ($a_* < 0.2$) as opposed to the high value of spin for GRS 1915+105. We suggest that the low spin of the black hole in IGR J17091–3624 can be a reason behind its faintness as compared to GRS 1915+105 instead of showing variability patterns arising from high mass accretion rate. Black hole binaries are known for showing quasi periodic oscillations (QPOs) during hard states, which appear as narrow peaks superimposed on the broad band continuum in power

density spectrum. Several studies have shown the correlation between QPO properties and spectral parameters, indicating a close link between the two. However, the mechanism behind generation of QPOs is not well understood.

The thesis presents our attempts to understand the QPO mechanism by simulating light curves. We studied a NuSTAR observation of GRS 1915+105, which has a power law dominated spectrum and shows the presence of reflection component. Since there is only one primary component, we make a hypothesis that the QPO is generated as a result of oscillation of some of the spectral parameters (instead of spectral components) at frequencies close to that of the QPO. We test the hypothesis by finding whether the simulated results explain the observed energy dependence of QPO or not. It was found that the observed trend of increasing QPO power with energy can be reproduced qualitatively if the spectral index is varied with the phases of QPO. Variation of other spectral parameters does not reproduce the observed energy dependence. The variation of spectral index is verified by performing phase-resolved spectroscopy for the phases of QPO. The results clearly show the variation of spectral index with the phases of QPO. The finding of variation of spectral index is an important result and it puts significant constraints on the models explaining modulation mechanism for QPOs.

Title: Multi - wave length investigations of solar eruptive phenomena
Researcher: Kushwaha, Upendra Kumar Singh
Supervisor: Joshi, Bhuwan
Year: 2016
Keyword's: Solar Atmosphere, Solar Flare, Prominence Eruption, Confined Eruption, Sigmoid-to-arcade evolution, RHESSI ; NOAA; HXR coronal, Ultraviolet
Call No.: 530 KUS
Acc. No.: T00100

Abstract: Solar eruptive phenomena correspond to various kind of transient activities occurring in the solar atmosphere in the form of flares, prominence eruptions and coronal mass ejections. They mostly originate from solar active regions which consist of complex magnetic structures extending from the deeper sub-photospheric layers, crossing through the photosphere to the coronal heights. An eruptive flare typically spreads across all the atmospheric layers of the Sun and involves substantial mass motions and particle acceleration. Multi-wavelength observations are thus crucial to probe the underlying physical processes occurring at different layers and regions at and above the photosphere. In this thesis, I have studied some key aspects of solar eruptive phenomena such as solar flare, prominence eruption, coronal implosion, failed eruption, and sigmoid-to-arcade evolution. These investigations have employed contemporary multi-wavelength solar observations with superior resolution. The imaging and spectroscopic capabilities of Reuven Ramaty High Energy Solar Spectroscopic Imager (RHESSI) have been extensively utilized to investigate the thermal and nonthermal energy release processes associated with different stages of the eruptive phenomena. Complementary to RHESSI X-ray measurements, we have combined solar observations at Extreme Ultraviolet (EUV), Ultraviolet (UV), Microwave (MW), optical, and radio wavelengths to investigate the complex physical processes occurring at different atmospheric layers of the Sun during the eruptive events. We study two spectacular prominence eruptions and associated flare activities which occurred in active regions NOAA 10656 on 2004 August 18 (event I) and NOAA 11548 on 2012 August 18 (event II) with the motivation to identify the prominence destabilization through the observations of pre-eruption phase and pre-flare activity. The violent eruption of the prominences is accompanied by major flares. We also explore the signatures of magnetic reconnection in the corona and discuss the thermal and non-thermal effects driven by prominence eruption during their eruptive phase. During event I, three localized episodes of energy release were observed in the vicinity of the filament before the eruption that produced intense heating along with non-thermal emission. The prominence eruption was accompanied with an X1.8 flare during which multiple HXR bursts were observed up to 100-300 keV energies. We have noted striking HXR coronal source at 50-100 keV energy band that was formed at the time of detachment of the prominence from the source region. From the location, timing, strength, and spectrum of HXR emission, we conclude that the prominence eruption was driven by distinct events of magnetic reconnection occurring in the current sheet below the erupting prominence. During event II, we observed multitude of coronal activities in the form of a blowout jet, rapid evolution of a flux rope above the prominence, and events of episodic energy release. Out of these activities, the flux rope exhibited the most dramatic evolution, characterized by splitting and rotation along with localized brightenings during its

outward expansion. The prominence underwent catastrophic loss of equilibrium with the onset of an M1.8 flare, suggesting large-scale energy release by magnetic reconnection. During the impulsive phase of the flare, a plasmoid eruption was observed below the apex of erupting prominence at multiple EUV channels. The temporal, spatial and kinematic correlations between erupting prominence and plasmoid imply that the magnetic reconnection supported the fast ejection of prominence in the lower corona. Flare research has been dominated by the study of eruptive flares because of their large-scale structure and long duration. On the other hand, it is rather challenging to investigate energy release processes in confined flares due to their rapid evolution in a compact region that impose severe observational constraints. Now with the availability of observations at unprecedented temporal, spatial, and spectral resolutions from RHESSI and SDO, we have made an effort to investigate the triggering mechanism and magnetic reconnection scenario in a confined M4.0 flare in AR NOAA 11302 on 2011 September 26. From this case study, we infer some important conclusions about the evolution of flare loops and thermal/nonthermal emissions within the confined environment of active region corona. This event was associated with a magnetic transient which was observed ~ 1 minute prior to the flare onset at the early flare location within the inner core region. The spectral, temporal, and spatial properties of magnetic transients suggest that the sudden changes in the small-scale magnetic field have likely triggered the flare by destabilizing the highly sheared pre-flare magnetic configuration.

We have studied a confined eruption (or failed eruption) of a flux rope which occurred in AR NOAA 10646 on 2004 July 14. After striking pre-flare phase, we observed a major M6.2 flare during which a large flux rope and associated prominence material underwent confined eruption. A major highlight of the preflare phase lies in the observation of large-scale contraction in overlying coronal loops for a span of ~ 30 minutes during which the overlying loops underwent an altitude decrease of ~ 20 Mm (40% of the initial height) during pre-flare phase. The impulsive phase of the flare is characterized by multiple non-thermal peaks during which very high plasma temperature ($T \sim 30$ MK) and substantial nonthermal characteristics were observed. The time-evolution of thermal energy exhibits a good correspondence with the variations in cumulative non-thermal energy which suggest that the energy of accelerated particles efficiently converted to hot flare plasma implying validation of the Neupert effect in terms of flare energetics. Finally, we have presented a multi-wavelength investigation of a sigmoid-to-arcade development in AR 11719 on 2013 April 11. The study aims to explore several crucial aspects involved during the process of solar eruption right from the formation stage of coronal EUV sigmoid to the post-eruption phase of the source region. The evolution of sigmoid was observed at 94°A images which implies that the structure comprised of very high temperature plasma. The sigmoid eruption was accompanied with a large M6.5 two-ribbon flare which is characterized by a prolonged rise phase of ~ 21 minutes. We have especially emphasized morphological and spatial evolution of flare sources during the prolonged rise phase and discussed their observational disparities with the standard flare model.

Title: Generation and characterization of coherent beams of tunable spectral and spatial properties using optical parametric oscillators

Researcher: Aadhi A.

Supervisor: Singh, R. P.

Year: 2015

Keyword's: Nonlinear Optics, Optical Parametric Oscillator, Parametric Amplification, Phase Matching, Second Harmonic Generation, Ultraviolet Radiation, Laser Beam Shaping, Airy Beam

Call No.: 530 AAD

Acc. No.: T00101

Abstract: Optical parametric oscillators (OPOs) have become standard source of coherent radiation inaccessible to ordinary lasers. Based on nonlinear optical effect, the OPOs convert a fixed pump laser wavelength to a wide band of coherent radiations ranging from visible to far-IR. Additionally, development of new nonlinear crystals with improved crystal parameters including high nonlinearity, high damage threshold and wide wavelength transparency demands advancement in OPOs with extended wavelength coverage in all the time scales. While OPO based sources produce high output power in Gaussian spatial beam profile, optical beam in different spatial profiles such as optical vortex and Airy beams are of paramount interest for different scientific and technological applications. Therefore, the focus of this thesis is the development and characterization of OPO based sources of coherent optical radiation in continuous-wave (cw) and picosecond time scales with spectral and spatial tunability. The development of OPOs in singly-resonant configuration (SRO), the focus of the current thesis, is challenging due to high threshold. Additionally, photorefractive effect in visible pumping, thermal damage, and thermal effects are some of the important issues to overcome. Therefore, it is important to have proper cavity design while maintaining the overall cavity losses to a minimum. A proper selection of the nonlinear crystals and appropriate design of the diffractive optical element is required for spatial modification of the intra-cavity OPO beam into structured beams. A high power, single-frequency, tunable radiation source in the ultraviolet (UV) region have been developed using intra-cavity frequency-doubling of the resonant signal of a MgO:sPPLT crystal based SRO pumped in the green. Two different nonlinear crystals, BIBO and PPKTP have been used for frequency doubling. The BIBO based source produces UV radiation with output power as much as 770 mW at 398.24 nm, while pumping at 8W of green power. The UV source can be tuned across 355.2-418 nm with a continuous wavelength tunability of 62.8 nm in single frequency radiation with an instantaneous line-width of 14.5 MHz. On the other hand, the PPKTP based UV source generates maximum UV power of 336 mW at 398.28 nm and wavelength tunability of 18.1 nm in a TEM₀₀ spatial mode for 5W of green pump power. The BIBO and PPKTP based UV sources have Gaussian spatial profile with ellipticity of 0.66 and 0.93, respectively. The line-width of the UV radiation is measured to be 18.5 MHz. We have also demonstrated tunable UV radiation in ultrafast pulses at high repetition rate using a SRO based on MgO:sPPLT crystal synchronously pumped at green. The source produces high-repetition-rate picosecond UV pulses at 240 MHz with internal frequency doubling of the visible signal pulses of the SRO into the UV in BIBO. The device is tunable across 317-340.5 nm with a single set of mirrors, with

the tuning range currently limited by the available grating periods in the MgO:sPPLT crystal and cut angle of the BIBO crystal. In addition to UV generation, the OPO provides tunable signal pulses across 634-681 nm in the visible with a maximum average power of 800 mW at 642 nm, and corresponding mid-IR idler radiation over 2429-3298 nm with up to 147 mW of output power. In OPOs, the signal and idler radiations are constrained by energy conservation. Therefore, it is not possible to tune the wavelength of the signal and idler beams independently.

We have developed a novel approach based on two nonlinear crystals inside a single SRO cavity for the generation of two signal-idler wavelength pairs with truly independent and arbitrary tuning, which are unbound by energy conservation and phase-matching, using a simple design based on two nonlinear crystals in a compact four-mirror ring-cavity OPO. We have studied such novel SRO architecture theoretically and experimentally to understand various parameters in tuning the performance of a such scheme. The intra-cavity parametric amplification of the resonant signal of one crystal in the other crystal shows the possibility of using different combinations of crystals and pump radiation. We verified the coherent energy coupling between the intra-cavity resonant signal field resulting in Raman spectral emission. While we have demonstrated optical radiation in the wavelength range from UV to near-IR in cw and picosecond time scales, in all cases, the output beams have Gaussian spatial structure. To verify the possibility of generating output beam with a different spatial distribution other than Gaussian from a SRO, we have demonstrated a compact source of widely tunable, high-power, single frequency output beam in Airy intensity profile.

Based on cubic phase modulation of the intra-cavity beam of a MgO:PPLN crystal based SRO pumped at 1.064 μm , the source provides Airy beam tunable across 1.5 to 2 μm wavelength range with output power of 8.1 W at 42 W of pump power in the wavelength of 1.571 μm . In addition, it generates Gaussian beam across 2.3-3.6 μm wavelength range in the mid-IR with a maximum power of 10.1 W at 2.35 μm . We also examined all the peculiar properties of Airy beam such as self-acceleration, self-healing, nondiffracting fraction for different wavelengths. This generic approach can be used for the generation of different structured beams on demand through proper modulation of the intra-cavity beam of the SRO.

Title: Tropospheric greenhouse gases: emission characteristics and dynamical effects
Researcher: Chandra, Naveen
Supervisor: Lal, Shyam
Year: 2015
Keyword's: Atmospheric Temperature, Greenhouse Effect, Earth Climate, Urban Location, Energy Flow
Call No.: 530 CHA
Acc. No.: T00105

Abstract: The urban areas consist of more than half of the world's population and contribute about 70% of the fossil fuel CO₂ emissions (in 2010) as well as significant amount of anthropogenic emissions of CH₄ into the atmosphere. India is a fast developing country, where fossil fuel emissions have increased dramatically in last three decade and further predicted to continue to grow at least 6% per year through to 2025. In order to provide independent verification of future mitigation activities and predicting future climate, there is an urgent need of the measurements of greenhouse gases over representative urban regions.

Realising the importance of the study of greenhouse gases over urban locations, measurements of CO₂ and CH₄ along with an anthropogenic emission tracer CO have been initiated at a major urban site Ahmedabad in India, using a state of the art laser based cavity ring down spectrometer. The observed year-long data are analysed using suitable global chemistry transport models (JAMSTECs ACTM for CO₂ and CH₄, LMDz-OR-INCA for CH₄), and correlations among them. The effects of land ecosystem on CO₂ variation as well as anthropogenic emissions and atmospheric transport on CO₂ and CH₄ variations have been identified. The inventory (EDGAR) emissions of CH₄ and CO are tested using the observed data for the study location and found that the inventory emissions are underestimated. The CO₂ observations and model comparison brings out the need for improvement in the terrestrial flux simulated by the Carnegie-Anes-Stanford Approach (CASA) ecosystem model.

Furthermore, comparison of the seasonal cycle of CH₄ with both models reveal that the afternoon mixing ratios have the potential to represent the footprint of its emission of larger area and hence this data can be used in regional and global CH₄ inversion study with some caution. Analyses of vertical profiles of CO₂ and CO in the troposphere using aircraft measurements of CO₂ over Delhi and satellite data of CO over five selected regions in India are also conducted. The amplitude of seasonal variability in CO₂ shows direct, but a delayed link with the strength of the Indian summer monsoon rainfall in Delhi. The model simulations are more close to the observations in the upper troposphere (3-8 km) as compared to lower troposphere (below 3 km). Average seasonal distributions of CO in the troposphere over all the study regions show very large spatial and vertical variability. Significant contribution at 300 - 200 hPa, due to strong convection during the monsoon season as well as long range transport from the biomass burning regions of Central Africa and East Asia during other seasons particularly over south of Ahmedabad, have been observed. The annual variations in the CO concentrations at 900 and 300 hPa are found to be in opposite phase with lower values during monsoon at 900 hPa and higher values at 300 hPa. Simulations from two

photochemical-transport models (MOZART and EMAC) are able to capture these variations broadly. Measurements of CO₂ and CH₄ coupled with the atmospheric transport models could be used to assess the sources and sinks of CO₂ and CH₄ at regional level by inverse modeling studies. This is, however, an objective for the future, since it can only be achieved using data records covering multiple years and at a network of stations. In summary, this thesis contributes in providing precise atmospheric measurements of important GHGs - CO₂ and CH₄ along with the anthropogenic tracer CO over an urban location in India which is not done so far to the best of our knowledge. This dataset is very helpful for understanding processes and phenomena related to the land-atmosphere exchange of CO₂, constraining the CH₄ and CO emission inventories as well as understanding the contributions of anthropogenic sources in a mega-city to observed variations.

Title: Observational aspects of hard X-ray polarimetry
Researcher: Chattopadhyay, Tanmoy
Supervisor: Vadawale, Santosh V.
Year: 2015
Keyword's: X-ray Polarimetry, Compton Scattering, Hard X-ray Telescopes Geant-4 Simulation, Instrumentation, Astrosat, Cadmium Zinc Telluride Imager (CZTI)
Call No.: 522.65 CHA
Acc. No.: T00106

Abstract: Sensitive polarization measurements in X-ray may address a wealth of astrophysical phenomena, which so far remain beyond our understanding through available X-ray spectroscopic, imaging, and timing studies. Though scientific potential of X-ray polarimetry was realized long ago, there has not been any significant advancement in this field for the last four decades since the birth of X-ray astronomy. The only successful polarization measurement in X-rays dates back to 1976, when a Bragg polarimeter onboard OSO-8 measured polarization of Crab nebula. Primary reason behind the lack in progress is its extreme photon hungry nature, which results in poor sensitivity of the polarimeters. Recently, in the last decade or so, with the advancement in detection technology, X-ray polarimetry may see a significant progress in near future, especially in soft X-rays with the invention of photoelectron tracking polarimeters. Though photoelectric polarimeters are expected to provide sensitive polarization measurements of celestial X-ray sources, they are sensitive only in soft X-rays, where the radiation from the sources is dominated by thermal radiation and therefore expected to be less polarized. On the other hand, in hard X-rays, sources are expected to be highly polarized due to the dominance of nonthermal emission over its thermal counterpart. Moreover, polarization measurements in hard X-rays promises to address few interesting scientific issues regarding geometry of corona for black hole sources, emission mechanism responsible for the higher energy peak in the blazars, accretion geometry close to the magnetic poles in accreting neutron star systems and acceleration mechanism in solar flares. Compton polarimeters provide better sensitivity than photoelectric polarimeters in hard X-rays with a broad energy band of operation. Recently, with the development of hard X-ray focusing optics e.g. NuSTAR, Astro-H, it is now possible to conceive Compton polarimeters at the focal plane of such hard X-ray telescopes, which may provide sensitive polarization measurements due to flux concentration in hard X-rays with a very low background. On the other hand, such a configuration ensures implementation of an optimized geometry close to an ideal one for the Compton polarimeters. In this context, we initiated the development of a focal plane Compton polarimeter, consisting of a plastic scatterer surrounded by a cylindrical array of CsI(Tl) scintillators. Geant-4 simulations of the planned configuration estimates 1% MDP for a 100 mCrab source in 1 million seconds of exposure. Sensitivity of the instrument is found to be critically dependent on the lower energy detection limit of the plastic scatterer; lower the threshold, better is the sensitivity. In the actual experiment, the plastic is readout by a photomultiplier tube procured from Saint-Gobain. We carried out extensive experiments to characterize the plastic especially for lower energy depositions. The CsI(Tl) scintillators are readout by Si photomultipliers (SiPM). SiPMs are small in size and robust and therefore provide the compactness necessary for the designing of

focal plane detectors. Each of the CsI(Tl)-SiPM systems was characterized precisely to estimate their energy threshold and detection probability along the length of the scintillators away from SiPM.

Finally, we integrated the Compton polarimeter and tested its response to polarized and unpolarized radiation and compared the experimental results with Geant-4 simulation. Despite the growing realization of the scientific values of X-ray polarimetry and the efforts in developing sensitive X-ray polarimeters, there has not been a single dedicated X-ray polarimetry mission planned in near future. In this scenario, it is equally important to attempt polarization measurements from the existing or planned instruments which are not meant for X-ray polarization measurements but could be sensitive to it. There have been several attempts in past in retrieving polarization information from few of such spectroscopic instruments like RHESSI, INTEGRAL-IBIS, INTEGRAL-SPI. Cadmium Zinc Telluride Imager (CZTI) onboard Astrosat, India's first astronomical mission, is one of such instruments which is expected to provide sensitive polarization measurements for bright X-ray sources. CZTI consists of 64 CZT detector modules, each of which is 5 mm thick and 4 cm × 4 cm in size. Each CZT module is subdivided into 256 pixels with pixel pitch of 2.5 mm. Due to its pixelation nature and significant Compton scattering efficiency at energies beyond 100 keV, CZTI can work as a sensitive Compton polarimeter in hard X-rays. Detailed Geant-4 simulations and polarization experiments with the flight configuration of CZTI show that CZTI will have significant polarization measurement capability for bright sources in hard X-rays. CZTI is primarily a spectroscopic instrument with coded mask imaging. To properly utilize the spectroscopic capabilities of CZT detectors, it is important to generate accurate response matrix for CZTI, which in turn requires precise modelling of the CZT lines shapes for monoenergetic X-ray interaction. CZT detectors show an extended lower energy tail of an otherwise Gaussian line shape due to low mobility and lifetime of the charge carriers. On the other hand, interpixel charge sharing may also contribute to the lower energy tail making the line shape more complicated. We have developed a model to predict the line shapes from CZTI modules taking into account the mobility and lifetime of the charge carriers and charge sharing fractions. The model predicts the line shape quite well and can be used to generate pixel-wise response matrix for CZTI.

Title: Studies towards the possible temporal variation of the fine structure constant
Researcher: Nandy, Dilip Kumar
Supervisor: Sahoo, Bijaya Kumar
Year: 2015
Keyword's: Fine Structure Constant, Sensitivity Coefficient, Alkali-Doublet Method, Many-Multiplet Method, Atomic Clock
Call No.: 530 NAN
Acc. No.: T00107
Abstract:

In the standard model (SM) of particle physics it is a well-known fact that coupling constants of different fundamental interactions run with energy. The variations of these coupling constants under different local energy regimes have already been verified experimentally. But in the current scenario there is no law or symmetry principle, other than a presumption for the sake of simplicity, that restrains the physical constants of nature from varying in space and time. Hence, it is necessary to verify this assumption experimentally.

Investigations of temporal variation of fundamental constants have been gaining the ground steadily in both the theoretical and experimental physics for the last two decades [J. P. Uzan, *Rev. Mod. Phys.* **75**, 403 (2003), J. A. King, et al. *MNRAS* **422**, 3370 (2012), H. Chand, et al., *Precision Spectroscopy in Astrophysics*]. Important consequences of searching for such variations are to establish theories suggesting violation of Einstein's equivalence principle, to support unification of gravity with the other three fundamental interactions of nature [T. Damour, et al., *Phys. Rev. D* **89**, 081601 (2002), T. Damour, et al., *Phys. Rev. D* **66**, 046007 (2002), T. Kaluza, *Sitzungber. Press. Akad. Wiss. Phys. Math. Kl. L IV*, 966 (1921), O. Klein, *Z. Phys.* **37**, 895 (1926), A. Chodos and S. Detweiler, *Phys. Rev. D* **21**, 2167 (1980), W. J. Marciano, *Phys. Rev. Lett.* **52**], et cetera. This will also probe the multidimensionality to space as predicted by super-string theories [T. Damour and A. M. Polyakov, *Nucl. Phys. B* **423**, 532 (1994)]. These theories predict temporal variations of dimensionless fundamental constants including the electromagnetic fine structure constant ($\alpha_e = \frac{e^2}{\hbar c}$) in the low energy limit at the cosmological time-scale.

The primary objective of this thesis is to provide accurate results for the relativistic sensitivity coefficients which can be further used to investigate temporal variation of α_e . We have employed relativistic coupled-cluster (RCC) methods developed by us to determine these sensitivity coefficients in many astrophysically relevant atomic systems and also for some of the atomic clock transitions to study the possible temporal variation of α_e . It can be perceived that the anticipated relativistic effects are quite large in the highly charged ions, and seem to

be the promising candidates for such investigation. So we have considered many possible highly charged ions and investigated enhancement of relativistic effects in these systems. To give more accurate results for the sensitivity coefficients, we also estimate the contributions from the Breit interaction and the dominating quantum electrodynamic (QED) corrections in addition to the contribution from Dirac-Coulomb (DC) Hamiltonian.

For the above purpose, we have developed one-electron detachment and one-electron attachment RCC methods from a closed-shell atomic configurations. Using the above methods, we determine the sensitivity coefficients (or q -values) for three low-lying $3s^23p^5\ ^2P_{3/2} \rightarrow 3s3p^6\ ^2S_{1/2}$, $3s^23p^5\ ^2P_{3/2} \rightarrow 3s3p^6\ ^2S_{1/2}$ and $3s^23p^5\ ^2P_{3/2} \rightarrow 3s^23p^5\ ^2P_{1/2}$ transitions in the Cl-like Mn IX, Fe X, Co XI and Ni XII ions. We also calculate the sensitivity coefficients for the three low-lying transitions $2s^22p^5\ ^2P_{3/2} \rightarrow 2s2p^6\ ^2S_{1/2}$, $2s^22p^5\ ^2P_{3/2} \rightarrow 2s2p^6\ ^2S_{1/2}$ and $2s^22p^5\ ^2P_{3/2} \rightarrow 2s^22p^5\ ^2P_{1/2}$ in the F-like Ti XIV, V XV, Cr XVI, Mn XVII, Fe XVIII, Co XIX, Ni XX, Cu XXI, Zn XXII and Mo XXXIV ions very accurately. In addition to these ions, we have also calculated the sensitivity coefficients for a number of astrophysically relevant transitions in the Si IV, Ti IV and Zn II ions using our RCC methods. Since Si IV, Ti IV and Zn II ions are highly abundant in many quasars, we have provided q -values for a number of important transitions in these ions to achieve better statistical analysis in the estimation of α_e variation using the Many-Multiplet (MM) method.

We also carry out very accurate calculations of some of the physical quantities which are vital in the precise estimate of absolute frequencies in the atomic clock experiments. One of them is the quadrupole shift in the Yb⁺ ion clock which arises due to the interaction of electric field gradient with the quadrupole moment of the atomic systems. We have investigated quadrupole shifts for three prominent clock transitions, $[4f^{14}6s]^2S_{1/2} \rightarrow [4f^{14}5d]^2D_{3/2}$, $[4f^{14}6s]^2S_{1/2} \rightarrow [4f^{14}5d]^2D_{5/2}$ and $[4f^{14}6s]^2S_{1/2} \rightarrow [4f^{13}6s^2]^2F_{7/2}$, in the Yb⁺ ion by calculating quadrupole moments (Θ s) of the $[4f^{14}5d]^2D_{3/2,5/2}$ and $[4f^{13}6s^2]^2F_{7/2}$ states using our methods. We find an order of magnitude difference in the Θ value of the $[4f^{13}6s^2]^2F_{7/2}$ state between our calculation and the experimental result, but our result concur

with the other two calculations that are carried out using different many-body methods than ours. However, our Θ value of the $[4f^{14}5d]^2D_{3/2}$ state is in good agreement with the available available experimental results, and is the most precise estimate of the quadrupole shift

The other calculated systematic is the black-body radiation (BBR) shifts due to the magnetic dipole (M1) and electric quadrupole (E2) components of the radiation fields in the Ca^+ and Sr^+ single ion clocks. We have estimated contribution from the M1 and E2 multipoles of the radiation field for the $4s\ ^2S_{1/2} \rightarrow 3d\ ^2D_{5/2}$ and $5s\ ^2S_{1/2} \rightarrow 4d\ ^2D_{5/2}$ transitions in the singly ionized calcium and strontium, respectively. These shifts are obtained by calculating the corresponding multipolar scalar polarizabilities of the involved atomic states. Precise estimate of these systematics are quite important for determining uncertainties to the measured clock frequencies in these ions, which are further used for giving stringent bound on the temporal variation in α_e .

Title: Study of particle physics models implication for dark for dark matter and cosmic ray phenomenology
Researcher: Tomar, Gaurav kumar
Supervisor: Mohanty, Subhendra
Year: 2016
Keyword's: Dark Matter, Beyond Standard Model, Relic Abundance, Gauge Extension, Muon Magnetic Moment
Call No.: 539.72 TOM
Acc. No.: T00181

Abstract:

There are many observations in particle physics and cosmology, which seek physics beyond standard model for their explanation. Some of them are : The excess of positron over cosmic ray background observed by AMS-02 experiment, the 3.6σ discrepancy between muon $(g - 2)$ measurement by BNL and its standard model prediction, and the absence of Glashow-resonance in the PeV neutrino events at IceCube. As the thesis title indicates this work is about the study of particle physics models which not only explain the mentioned observations but also give a suitable candidate of dark matter with correct relic density.

In the work presented here we have proposed a gauged horizontal symmetry model for which we introduce a 4th generation of fermions into SM. We then introduce a $SU(2)_{HV}$ vector gauge symmetry between the 4th generation leptons and muon families. The 4th generation right-handed neutrino is identified as dark matter which annihilates into leptons final state $(\mu^+ \mu^-, \nu_\mu^c \nu_\mu)$ giving rise to correct relic density. In this model, dark matter is leptophilic in nature, so it can explain AMS-02 positron excess remaining consistent with stringent bounds from antiproton. It is also possible to alleviate the discrepancy in muon $(g - 2)$ from 4th generation charge lepton, $SU(2)_{HV}$ gauge boson, and from neutral and charged scalars. In this way, both the signals, muon $(g - 2)$ and the excess of positron can be explained simultaneously. We have also studied an alternative left-right model called dark left-right model, where it is possible to accommodate a suitable dark matter candidate. The second generation right-handed neutrino is identified as dark matter which dominantly annihilates into leptons final state. So it is possible to explain AMS-02 positron excess and lift the stringent bounds from antiproton. The singly and doubly charged scalars in dark left-right model also contribute to muon $(g - 2)$ and so both the signatures can also be related in this model.

Another part of this thesis deals with the absence of Glashow resonance at IceCube PeV neutrino events. The IceCube collaboration has observed neutrino of very high energy which goes upto ~ 3 PeV, but did not see any events at Glashow resonance. The Glashow resonance gives rise to an enhanced cross-section for $\bar{\nu}_e$

at resonance energy 6.3 PeV which increases the detection rate of $\bar{\nu}_e$ by a factor of ~ 10 . This implies that at least some of the events should have been observed at Glashow resonance, but none were. We proposed a new mechanism which can explain why neutrinos arising from astrophysical process may be suppressed. We assume a Lorentz violating higher dimensional operator, which modified dispersion relation of neutrinos (antineutrinos). As a result, pion and kaon decay widths get suppressed and we observe a cutoff in the neutrino spectrum which is consistent with IceCube data.

Title: Nonlinear interaction of structured optical beams
Researcher: Chaitanya, Apurv
Supervisor: Samanta, Goutam Kumar
Year: 2016
Keyword's: Second Harmonic Generation (SHG), Um Frequency Generation (SFG), Gaussian Intensity Profile, Ultrafast Femtosecond Laser
Call No.: 535.5 CHA
Acc. No.: T00182

Abstract: The general principles of Maxwell's electromagnetic theory and quantum mechanics were well established much before the invention of lasers. However, after the first report of laser in 1960 and subsequent advancement in the field of laser technology, these theories have been revisited to understand the effects of higher order interactions between intense laser light beams and matter in terms of nonlinear susceptibilities. As such, the study of behavior of light in nonlinear media, in which the dielectric polarization responds nonlinearly to the electric field of the light, has given birth to a new branch of optics called nonlinear optics. Typically nonlinear optical effects are studied using laser beams with Gaussian intensity distribution. However, in recent times, structured coherent optical beams including optical vortices, hollow Gaussian beam, and Airy beam have found wide range of applications in variety of fields in science and technology. All existing techniques used to date to generate such beams suffer from different limitations including lower output power and restricted wavelength range. On the other hand, interactions of such beams with nonlinear media are mostly unexplored.

During my PhD we have studied the nonlinear interaction of optical beams with different spatial structures. We have used second order nonlinear interactions such as second harmonic generation (SHG), where two photons from same laser get annihilated to produce a new photon of double energy, and sum frequency generation (SFG), where two photons of two different lasers get annihilated to produce a new photon of energy equal to the sum of the energies of the annihilated photons. The study also includes the nonlinear generation of structured beams such as Laguerre Gauss beams (optical vortices), a new class of vortex beam known as "perfect" vortex beams, hollow Gaussian beam, and Airy beam in different spectral and temporal domains.

Most of the lasers (but not all) produce electromagnetic radiation in Gaussian intensity profile. However, due to unavailability of suitable laser gain medium, the nonlinear optical effects play pivotal role in generating coherent optical radiation with wavelength inaccessible to lasers. Using an ultrafast femtosecond laser at 1064 nm we have studied the second order nonlinear interactions such as SHG and SFG in different nonlinear crystals to produce ultrafast coherent radiation at 532 nm and 355 nm in Gaussian intensity profiles. Such beams have variety of applications, including spectroscopy, material processing, pumping of optical parametric oscillators and generation of structured optical beams. The efficiency of nonlinear optical processes varies proportional to the square of the length of the nonlinear crystal and the intensity of the laser beam. However, use of longer crystal length and increase of laser intensity through tight focusing do not necessarily increase the overall efficiency of the nonlinear process. There is always an optimum focusing

condition for efficient nonlinear interactions, [1] have predicted such optimum condition for SHG of continuous wave (cw) or long-pulse lasers. However, the optimum focusing condition in the presence of temporal walk-off arising from the use of ultrafast lasers can be different from that of the cw and long-pulse lasers [2, 3]. We have also investigated the optimum focusing condition for single-pass SHG and SFG of ultra-short femtosecond pulses for generating the optical beams at 532 and 355 nm in Gaussian intensity distribution respectively. We have also done a comparative SHG performance study of the crystals having different temporal and spatial walk-off parameters. We have further investigated the effect of the ratio of confocal parameters (beam focusing condition) and power ratio of the interacting pump beams in SFG process.

Knowing the effect of Gaussian beam in nonlinear frequency conversion processes, we have studied the interaction of orbital angular momentum (OAM) of the laser beams with nonlinear medium. Unlike Gaussian beams, optical vortex beams, spatially structured beams with helical wave-front [4], carry photons with OAM. These beams have doughnut shaped intensity profile with zero intensity at the point of phase singularity. Optical vortices are characterized by its topological charge (order), or winding number, l and are found to carry OAM of $l\hbar$ per photon. Using second order nonlinear crystals we have studied the frequency doubling characteristics of high-power, ultrafast, optical vortex beams by generating optical vortices of order up to 12 at 532 nm and 266 nm wavelengths. We have experimentally verified the OAM conservation law, the OAM of the generated photon is equal to the sum of the OAMs of the annihilated photons, in SHG process. We have also demonstrated a new scheme to generate optical vortices of orders $l = 1$ to 6 by using only two spiral phase plates (linear optical elements to generate optical vortices of a fixed order) of phase winding 1 and 2. We further observed that the efficiency of vortex SHG process decreases with the order of the vortex. We attributed such effect to the increase of the area of vortex beam with its order. However, it was not possible to overrule the contribution (if any) of OAM in the SHG process as the area and order of the vortex are not mutually independent parameters.

The decrease of SHG efficiency of optical vortices with order restricts the study of nonlinear interaction of vortices to a certain order. Additionally, the dependence of beam area with its order does not provide clear information about the contribution of vortex order (OAM) in nonlinear frequency conversion process. However, a recent advancement in the field of structured beam has produced a new class of vortex beam, known as "perfect" vortex. These beams have area independent of the vortex order. Using such vortices we have experimentally verified that the vortex SHG efficiency does not depend upon the order (OAM) of the optical vortices. We have also studied the nonlinear frequency conversion of such beams to produce "perfect" vortex beam of order up to 12 with power as high as 1 W for all orders. We verified OAM conservation of "perfect" vortices in SHG process.

Due to the OAM conservation in SHG process, the OAM of the frequency doubled vortex beam is twice that the pump beam. But what will happen to the output beam if the interacting photons in the nonlinear process have opposite OAMs? To study such effect we have studied the SFG (SHG is the special case of SFG process) process of two pump beams having equal vortex orders but opposite in sign (direction of the helical phase variation). As expected, due to OAM conservation law the

output beam was found to have no OAM ($l=0$). However, the output beams have no light (dark) region at the center of the beam similar to the vortex beam. This is a new class of structured beam known as hollow Gaussian beam (HGB) [5] and our method gives a new way of generating HGB through nonlinear processes. The increase of annular ring radius of these beams with the order of the input vortex beams signifies that HGBs also have certain orders. However, there is no experimental or theoretical means to determine the order of such beams. We have devised a new way to determine the order of hollow Gaussian beams.

To broaden our study and to address other structured beams we have generated Airy beam and characterized its properties. Unlike other structured beams, Airy beam has peculiar properties such as beam shape invariance with propagation (non-divergence), propagation along curved trajectory in free space (self-acceleration), and self-restoration (self healing) of beam shape even after obstruction by small objects. Using intracavity cubic phase modulation of an ultrafast singly resonant optical parametric oscillator (SRO), we have generated ultrafast beam in 2-D Airy intensity distribution with wavelength tunability across the near-IR wavelength range. In addition to the Airy beam, the SRO produces Gaussian output beam in the near- to mid-IR wavelength range across 1.4 - 1.7 μm with power as much as 1.54 W.

Title: Constraining Physics beyond the standard model in post-higgs era
Researcher: Mondal, Tanmoy
Supervisor: Konar, Partha
Year: 2016
Keyword's: Vacuum Stability, Copositivity, Extended Scalar Sector, Beyond The Standard Model, Z 'Model
Call No.: 530 MON
Acc. No.: T00197

Abstract: In the history of elementary particle physics, the discovery of the Higgs boson at the Large Hadron Collider (LHC) in July 4, 2012 is an important breakthrough which completes the Standard Model (SM) of particle physics. Nevertheless, there exist experimental observations which cannot be explained by the SM, like the neutrino oscillations, dark matter, baryon asymmetry etc. With these experimental shortcomings it is evident that there exist some beyond the Standard Model (BSM) physics. There are several ways to extend the SM to explain some of the experimental phenomena which is still to be observed in the state-of-the-art experiment phenomena which is still to be observed in the state-of-the-art experiment like LHC. But the recent Higgs discovery can shed some light in the uncharted territory of theoretical physics. We are living at a minima of the Higgs potential where the Higgs field acquires a vacuum expectation value (vev) which is intertwined with the Higgs boson mass (m_H) measured at the LHC. The stability of the minimum is ensured by the condition that the Higgs quartic coupling should be positive.

But recent observation of m_H at the LHC indicates that the SM minima does not remain stable up to the Planck scale. This also indicates that there must be some new physics phenomena which will stabilize the minimum. Hence the stability analysis of the BSM scenarios is necessary to constrain parameters of the model. There are other constraints like perturbativity and unitarity of scattering amplitudes of longitudinal gauge boson modes which will also restrict the parameter space. The BSM models that include many scalar fields possess scalar potential with many quartic couplings. Due to the complicated structures of such scalar potentials it is indeed difficult to adjudge the stability of the vacuum. Thus one needs to formulate a proper prescription for computing the vacuum stability criteria. We have used the idea of copositive matrices to deduce the conditions that guarantee the boundedness of the scalar potential. We have discussed the basic idea behind the copositivity and then used that to determine the vacuum stability criteria for the Left-Right symmetric models with doublet, and triplet scalars and Type-II seesaw. As this idea is based on the strong mathematical arguments it helps to compute simple and stability criteria embracing the maximum allowed parameter space.

We study the B-L gauge extension of the Standard Model which contains a singlet scalar and three right-handed neutrinos. The vacuum expectation value of the singlet scalar breaks the $U(1)_{B-L}$ symmetry. The B-L symmetry breaks when the complex singlet scalar acquires a vev. We studied two different cases of B-L breaking scale. TeV scale and $\sim 10^{10}$ GeV. The TeV scale breaking scenario can have signatures at the LHC and we have constrained parameter space of this model. The high scale breaking scenario provides a constrained parameter space where both the issues of vacuum stability and high-scale inflation can be successfully accommodated. The Left-Right symmetric model

(LRSM) is theoretically well motivated and also contains rich phenomenology. We used idea of copositivity to calculate vacuum stability conditions for two variants of the LRSM. We incorporate the unitarity conditions in (LRSM) which can translate into giving a stronger constraint on the model parameters together with the criteria derived from vacuum stability and perturbativity. In this light, we demonstrate the bounds on the masses of the physical scalars present in the model and find the scenario where multiple scalar models are in the reach of Large Hadron Collider.

We have also studied a variant TeV scale seesaw model in which three additional heavy right handed neutrinos are added to the standard model to generate the quasi-degenerate light neutrinos. This model is theoretically interesting since it can be fully rebuilt from the experimental data of neutrino oscillations except for an unknown factor in the Dirac Yukawa coupling. We study the constraints on this coupling coming from meta-stability of electro-weak vacuum. Even stronger bound comes from the lepton flavor violating decays on this model, especially in a heavy neutrino mass scenario which is within the collider reach. Bestowed with these constrained parameters, we explore the production and discovery potential coming from these heavy neutrinos at the 14 TeV run of Large Hadron Collider. Signatures with tri-lepton final state together with backgrounds are considered in a realistic simulation.

Title: Decays of hadrons as probes of standard model and beyond
Researcher: Kumar, Girish
Supervisor: Mahajan, Namit
Year: 2017
Keyword's: Flavor Physics, Rare Decays, Semileptonic B Decays, Kaon decays, Baryonic B Decay
Call No.: 539.72 KUM
Acc. No.: T00208

Abstract: Flavor physics is the study of quark “flavors” and their interactions involving change of one type of flavor to another type of flavor. It is known that, historically, the study of flavor physics has played a key role in the development of the Standard Model (SM) of particle physics. The recent discovery of the last missing piece, the Higgs boson, in the first run of the Large Hadron Collider (LHC) marks the completion of the SM. The SM has been exceptionally successful in explaining the experimental data collected so far. However, there are many experimental measurements which point towards the existence of physics beyond the SM. Therefore, it is natural to consider SM as the low-energy limit of a more general theory above the electroweak scale. The next important task is then to look for hints of the physics beyond the SM. In this endeavour, the study of flavor physics continues to be an integral part of the searches at the intensity frontier. The study of flavor physics offers unique possibilities to study the weak inter- actions operating at the fundamental level governing the decays in conjunction with the strong forces responsible for keeping the constituents bound in various colorless hadronic states. In recent years, due to dedicated efforts by the Belle, BaBar, CDF, and LHCb experiments, a great theoretical understanding of the flavor dynamics of the SM has been achieved, and severe constraints on the new physics parameters have been imposed. The rare and flavor changing neutral current processes of b quark have been quite instrumental and valuable probes of new physics, thanks to their suppressed nature in the SM and high sensitivity to the new physics effects.

In this context, the exclusive semileptonic decay $B \rightarrow K^* \ell^+ \ell^-$ governed by the quark-level transition $b \rightarrow s \ell^+ \ell^-$ is one of the most interesting candidates, which has received great attention, experimentally as well as theoretically. The analysis of the angular distribution of its four-body final state gives access to a large number of experimentally accessible observables as a function of invariant mass squared of the dilepton system (q^2). Interestingly, the LHCb collaboration has found deviations from the SM predictions in the measurement of angular observables of $B \rightarrow K^* \mu^+ \mu^-$. These measurements are reported in bins of q^2 .

Particularly, the discrepancy in one of the angular observables, P'_5 , in two of low q^2 bins is quite intriguing. However, in order to be certain that the reported deviations are hints of new physics or artifacts of underestimated theoretical uncertainties, it is necessary to measure the observables which are as insensitive to hadronic effects as possible with more precision. In this thesis, we study some of these “theoretically cleaner” observables which are independent of hadronic form factors within the heavy quark effective framework. We show that zero crossing points of observables P'_5 , P'_4 , and of a new observable $O_{T^{\prime R}}$ in the standard model coincides with the zero crossing of the forward-backward asymmetry (A_{FB}) of the lepton pair. But in the presence of new physics

contributions they show different behaviors. Moreover, we show that there exist relations between the zeros of $P_5^i, P_4^i, O_{\tau}^{\text{LR}}$ and the zero of A_{FB} , which are also independent of hadronic uncertainties. We point out that precise measurements of these zeros in the near future would provide a crucial test of the standard model and would be useful in distinguishing between different possible new physics contributions to the Wilson coefficients. If the experimental observations are in fact due to NP in $b \rightarrow s\ell\ell$, then similar effects must also be seen in other $b \rightarrow s\ell\ell$ transitions involving different hadronic states. This fact sets the tone for our next work in which we study the semileptonic baryonic $b \rightarrow s$ decay, $\Lambda_b \rightarrow \Lambda\ell^+\ell^-$. We construct new angular observables and asymmetries; all of which have zero crossing points in the large q^2 region. The zeros of proposed observables in the heavy quark and large q^2 limit are again functions of Wilson coefficients only, and therefore have less sensitivity to hadronic effects. We discuss the potential of the decay $\Lambda_b \rightarrow \Lambda\ell^+\ell^-$ in probing the new physics effects in $b \rightarrow s\ell^+\ell^-$ along with the decays $B \rightarrow K^{(*)}\ell^+\ell^-$.

In the second part of the thesis, we present the explanation of some of the experimentally observed anomalies in the flavor sector within the framework of left-right symmetric gauge theories motivated by one of the low-energy subgroups of E_6 naturally accommodating leptoquarks. First, we explain the enhanced decay rates of $B \rightarrow D^{(*)}\tau\nu$ in E_6 motivated Alternative Left-Right Symmetric Model. We discuss the constraints from the flavor sector on the couplings involved in explaining the experimental data. We further consider the framework of E_6 motivated Neutral Left-Right Symmetric Model, and give simultaneous explanation for B decay anomalies in $B \rightarrow D^{(*)}\tau\nu$ and $B^- \rightarrow K^-\ell^+\ell^-$ together with the anomalous magnetic moment of the muon, consistent with the constraints from other flavor data.

In the last part of the thesis, we carry out a detailed study of the effects of new physics originating from a scalar leptoquark model on the kaon sector. It is known that kaon decays provide some of the most stringent constraints on various extensions of the SM. We consider a simple extension of the SM by a scalar leptoquark of charge $-1/3$ with $(SU(3)_C, SU(2)_L)$ quantum numbers $(3, 1)$, which is able to account for the deviations observed in B decays. The leptoquark we consider is a TeV-scale particle and within the reach of the LHC. We use the existing experimental data on the several kaon processes including $K^0 - \bar{K}^0$ mixing, rare decays $K^+ \rightarrow \pi^+\nu\bar{\nu}$, $K_L \rightarrow \pi\nu\bar{\nu}$, the short-distance part of $K_L \rightarrow \mu^+\mu^-$, and lepton-flavor-violating decay $K_L \rightarrow \mu^\pm e^\mp$ to obtain useful constraints on the model.

Title: Binary mixtures of ultracold quantum gases in optical lattices
Researcher: Suthar, Kuldeep
Supervisor: Singh, Angom Dilip Kumar
Year: 2016
Keyword's: Bose-Einstein Condensation, Multicomponent Condensates, Optical Lattice, Bose-Hubbard Model, Phase Separation
Call No.: 539 SUT
Acc. No.: T00209

Abstract: The stationary state, and dynamics of the ultracold bosons in optical lattices at zero temperature are well described by the discrete nonlinear Schrodinger equation (DNLSE). This equation is valid in the tight-binding limit, and used for the superfluid (SF) phase of bosons or Bose-Einstein condensate (BEC) in optical lattices. The recent experimental realizations of the binary mixtures of ultracold bosons in optical lattices provide the motivation to study the effects of finite temperatures in the lattice system. We report the development of the coupled DNLSEs, and the Hartree-Fock-Bogoliubov formalism with the Popov (HFB-Popov) approximation for the two-component BECs (TBECs) or binary condensate mixtures of dilute atomic gases in optical lattices. This method is ideal to study the ground state density profiles, and the evolution of the low-lying quasiparticle modes at zero as well as finite temperatures. The thesis can be broadly divided into three parts. The first two parts are results of the zero temperature calculations, which examine the quasiparticle excitation spectra of the TBECs in quasi-1D and quasi-2D optical lattices. The third part deals with the finite temperature results, and pertains to the investigation of the finite temperature effects on the quasi-particle mode evolution of the TBECs. The spontaneous symmetry breaking of $U(1)$ global gauge symmetry results into two Nambu-Goldstone (NG) modes corresponding to each of the species in quasi-1D TBECs. However, at phase separation an extra NG mode emerges with *sandwich* type density profile in the immiscible phase.

We investigate the role of quantum fluctuations on the quasiparticle mode evolution for quasi-1D TBECs. In the presence of the fluctuations, an extra NG mode which appears at phase separation gets hardened, and a symmetry broken *side-by-side* density profile appears in the immiscible phase. Furthermore, we examine the ground state geometry, and the quasiparticle spectra of quasi-2D TBECs. We observe that the TBECs acquire the side-by-side geometry when it is tuned from miscible to the immiscible phase. The energies of the quasiparticle modes are softened as the system is tuned towards the phase separation, and harden after phase separation. In the miscible domain the quasiparticle modes are degenerate, and this degeneracy is lifted after the phase separation. Furthermore, in the miscible domain, the quasiparticles have well-defined azimuthal quantum numbers, and hence shows a clear structure in the dispersion curve. On the other hand, the dispersion curve of the immiscible phase does not have a discernible trend due to the presence of the mode mixing. We also report the enhancement in the miscibility of the condensates of quasi-2D TBEC in the presence of the thermal fluctuations.

Title: Electronic transport properties of materials: the memory function approach
Researcher: Bhalla, Pankaj
Supervisor: Singh, Navinder
Year: 2017
Keyword's: Bloch-Boltzmann Approach, Electrical Conductivity, Relaxation Time Approximation, Generalized Drude Scattering
Call No.: 537.5 BHA
Acc. No.: T00216

Abstract: The study of the transport properties is very important for understanding various interactions in electronic systems. These properties such as electrical conductivity, thermal conductivity and thermoelectric coefficients have been widely studied within the Bloch-Boltzmann approach. In this approach, the transport equations are generally solved analytically under the relaxation time approximation (RTA) and in the zero frequency limit. Success of this approach is mostly limited to the zero frequency behavior. It becomes very complicated while investigating the finite frequency behavior of these transport coefficients especially beyond RTA. Thus, one needs an alternative approach which goes beyond RTA and captures the finite frequency features of these coefficients with much ease. This approach is known as the memory function approach. By construction, this formalism is beyond RTA and using this formalism one can calculate the time dependent correlation functions upto any order. It has been used by Götze and Wölfle (GW) to calculate the dynamical electrical conductivity for metallic electrons. It is successfully applied to study the transport behavior in presence of weak electron-phonon, electron-impurity interactions in metals under the assumption of constant electronic density of states (EDOS). An attempt to extend the GW approach beyond its original assumption of constant EDOS is made here and also we have applied GW approach to a wide variety of transport coefficients (dynamical thermal conductivity, dynamical Seebeck coefficient, etc). Sharapov and Carbotte have also calculated the generalized Drude scattering (GDS) rate for systems with gapped density of states based on Kubo formalism. We reconsider that problem here using the memory function formalism. We show the suppression in GDS due to the presence of gap. We also compare the resulting GDS with that calculated by Sharapov and Carbotte (SC). We find discrepancy in the scattering rate using both approaches in the low frequency limit. This is due to the crucial assumption made by SC approach which is not assumed in the memory function approach. We then study the dynamical thermal conductivity of metals within the memory function formalism. Here we introduce the thermal memory functions for the first time and calculate them for the cases of the electron-impurity and electron-phonon interactions. Several new results have been obtained and discussed in various temperature and frequency regimes. In the zero frequency limit, we find that the results are consistent with the results predicted by using the Bloch-Boltzmann approach and are also in accord with the experiments.

Furthermore, we also investigate the dynamical behavior of the thermo-electric coefficient, namely Seebeck coefficient. This analysis is done to explore the possibility of obtaining large figure of merit in various materials so that the efficiency of thermoelectric devices can be enhanced. We first confirm that at the zero frequency and in the high temperature case, the results of the Seebeck coefficient are in qualitative agreement with the experimental findings. We further find that the Seebeck coefficient increases with increasing frequency. This enhancement hints towards a possibility of greater figure of merit if the device is operated at a certain non-zero frequency. We have also applied the memory function approach to other systems such as graphene, a two dimensional system and we investigate the electronic thermal conductivity. In that, we explore the roles of different acoustic phonons, characterized by different dispersion relations. It is found that at the high temperature, the thermal conductivity saturates for all type of phonons. But the longitudinal phonons gives larger contribution to the total thermal conductivity. While at the low temperature, it follows different temperature power law behavior for different type of phonons. We have also found the results at finite frequency regimes which are identical to the case of conventional metals. In the above studies, we performed analytical studies of various transport coefficients that have been done for the weak perturbative interactions by using the memory function approach. However, with the increase in the interaction strength, one needs to go beyond GW approach. In this context, we propose a high frequency expansion of the memory function in term of its various moments. Taking simple example of the electron-impurity interaction for the case of the metal, we calculate the memory function upto the second order moment. It is found that the higher moments contribute more in the low frequency regimes and in the case of large interaction strength. In a nutshell, we extend the GW memory function formalism to various physical situations of interest with encouraging new results in the dynamical regime. While in the dc limit, our results agree with the traditional approaches.

Title: Physics beyond the standard model, LHC, and cosmology
Researcher: Hati, Chandan
Supervisor: Sarkar, Utpal
Year: 2016
Keyword's: Neutrino Masses, Matter-antimatter Asymmetry, Cogenesis Mechanism, Viable Models
Call No.: 539.72 HAT
Acc. No.: T00218

Abstract: The Standard Model (SM) of particle physics has been highly successful in explaining most of the experimental measurements in elementary particle physics. It has survived decades of precision tests at highest available energies and with the discovery of the Higgs boson in 2012 at the Large Hadron Collider (LHC) the last missing piece of the SM was confirmed. However, the SM suffers from a number of shortcomings, which strongly suggest that the SM is only an effective limit of a more fundamental theory of interactions. The aim of this thesis is to study various aspects of the physics beyond the SM ranging from the phenomenological implications of viable models to cosmological implications such as the matter-antimatter asymmetry of the universe, dark matter, and dark energy. In this thesis we study several models beyond the SM in the contexts of LHC phenomenology, neutrino masses, flavor anomalies associated with B-decays and gauge coupling unification. We also study the possibilities of explaining the matter-antimatter asymmetry via baryogenesis (leptogenesis) mechanisms in these models. We also touch upon the issues of potential candidates for dark matter and the realization of dark energy in models beyond the SM.

We study the implications of a right handed charged gauge boson W_R^\pm with mass of around a few TeV for leptogenesis. We point out how the discovery of a TeV scale W_R^\pm will rule out all possibilities of leptogenesis in all classes of the left-right symmetric extensions of the SM due to the unavoidable fast gauge mediated B-L violating interactions. We also study the framework of LRSM with additional scalar singlets and vector-like fermions in the context of the recent LHC excess signals and the phenomenological implications for the fermion masses and mixing. We also discuss how the introduction of a real bi-triplet scalar, which contains a potential DM candidate, can allow gauge coupling unification. Furthermore, we point out that the existence of new vector-like fermions can also have interesting implications for baryogenesis and the dark matter sector.

The effective low energy left-right symmetric subgroups of the superstring inspired E_6 model provide a rich phenomenology, thanks to many additional exotic fields including leptoquarks. We systematically study these low energy subgroups in the context of the LHC excess signals reported by the CMS collaboration, and high scale leptogenesis. We also study the left-right symmetric low energy subgroups of E_6 in the context of recent experimental results from the LHCb, BaBar and Belle collaborations on the decays of the B mesons: $\bar{B} \rightarrow D^{(*)}\tau\bar{\nu}$ and $\bar{B} \rightarrow K \ell\ell$, showing significant deviations from the SM, which hint towards a new physics scenario beyond the SM.

We use the leptonic decays $D_s^+ \rightarrow \tau^+ \bar{\nu} + \dots$, $B^+ \rightarrow \tau^+ \bar{\nu}$, $D^+ \rightarrow \tau^+ \bar{\nu}$ and D^0 - \bar{D}^0 mixing to constrain the couplings involved in explaining the enhanced B decay rates. We also study the E_6 motivated $U(1)_N$ extension of the supersymmetric SM in the context of the LHC excess signals and the baryon asymmetry of the universe. In light of the hint, from short-baseline neutrino experiments, of the existence of one or more light sterile neutrinos, we also study the neutrino mass matrices, which are dictated by the discrete symmetries in the variants of this model. We study aogenesis mechanism in which the observed baryon asymmetry of the universe and the dark matter abundance can be produced simultaneously at a low reheating temperature without violating baryon number in the fundamental interactions. This mechanism can also provide a natural solution for the cosmic coincidence problem. We also present a realization of mass varying neutrino dark energy in two simple extensions of the SM, where the SM is extended to include new TeV scale triplet scalars and fermions, respectively. We also discuss the possible leptogenesis mechanisms for simultaneously generating the observed baryon asymmetry of the universe in both the scenarios and the collider signatures for the new TeV scale fields.

Title: Investigations of daytime thermospheric wave dynamics over low latitudes using ground based optical technique
Researcher: Karan, Deepak Kumar
Supervisor: Pallamraju, Duggirala
Year: 2017
Keyword's: Dayglow, Thermosphere, Ionosphere, Upper Atmosphere, Equatorial Electrodynamics, Ionospheric-Thermospheric Coupling, Gravity Waves
Call No.: 551.5153 KAR
Acc. No.: T00275

Abstract: The equatorial- low-latitude ionosphere-thermosphere system (ITS) hosts several inter-coupled process during the daytime. Various dynamical effects due to winds and waves affect the ITS. Further, solar forcing and geomagnetic storm effects also modulate the low-latitude ITS coupling. The varying nature of these dynamics in response to different geophysical conditions bring in complexities in these coupled processes, which result small and large scale variations in the behavior of the ITS, both in temporal and spatial domain. Even though, investigations of the wave characteristics in spatial domain of the ITS have been carried out over several decades for nighttime conditions, such investigations during the daytime are in a state of infancy. Therefore, systematic investigations of the wave characteristics for daytime conditions are essential in order to gain a comprehensive understanding of the ionospheric and thermospheric system.

The optical dayglow emission intensity variations can be used as tracers of the neutral dynamical variations that exist at the altitudes of their origin. In the present thesis work, by using a high spectral resolution large field-of-view spectrograph, MISE, we have obtained the neutral oxygen dayglow emission intensities at three wavelengths (OI 557.7, 630.0, and 777.4 nm) from Hyderabad, a low-latitude location in India. These emissions are considered to originate from altitudes around 130, 230 and 300 km. The dayglow emissions are used as the primary data set for the investigations carried out in this thesis work.

The dayglow emission intensity patterns showed both symmetric and asymmetric diurnal behavior with respect to local noon. Considering purely photo-chemical nature of the production mechanisms of the dayglow, the asymmetric diurnal behavior is not expected and hence, it is clear that transport processes play a role. The extent of asymmetric behavior in the dayglow emission intensity is characterized in terms of Asymmetry in Time (AT), which is the product of difference in time of occurrence of peak intensity and local noon and the ratio of intensities at the peak and local noon. The days with $AT \leq 0.4$ h and $AT > 0.4$ h are considered to be the days with symmetric and asymmetric diurnal behavior in the emission intensities, respectively. Comparing the roles of neutral winds and the EEJ strengths on the days with $AT > 0.4$ h, it is conclusively shown that the dayglow emission intensities over the off-equatorial thermosphere are predominantly affected by the equatorial electrodynamics. It is also noted that this asymmetric diurnal behavior in the neutral emission intensities has a solar cycle dependence with more number of days during high solar activity period showing larger AT values as compared to those during the low solar activity epoch.

Periodogram analyses of the dayglow emission intensity have been carried out at all the three emission wavelengths in three distinctly different directions (west, zenith and east) which are separated by 3° - 8° depending on the altitude of day- glow emissions. Presence/absence of the time periods with similar values in these three directions indicates the non-existence/existence of longitudinal differences in the gravity wave (GW) features suggesting to a common/different source driving the waves at these locations. The non-existence of the similar time periods on the days with asymmetric diurnal behavior was attributed to the stronger equatorial electrodynamics. Moreover, GW features in terms of the zonal scale sizes and propagation directions also show different behavior on the days with and without the existence of longitudinal differences in the equatorial processes. Thus, our results show, for the first time, that there exist longitudinal variations in the equatorial electrodynamics in as small separations as 3° - 8° .

Variations in the dayglow emission intensities have been investigated for three geomagnetic disturbances that occurred in different seasons. It is found that the dayglow variations showed similarity with the variation of O/N_2 during geomagnetic disturbances that occurred in solstices. However, during the equinox, the dayglow showed similar variations with that of the EEJ strengths. Taken together, this shows the dominance of the equatorial electric field over the storm influenced neutral wave dynamics on low-latitude ITS during equinox times, and the effect of neutral wave dynamics from high-latitude during solstices. Moreover, contrasting distributions of the GW zonal scale sizes are observed on geomagnetically quiet and disturbed days in different seasons. This shows that changes are brought-in in the zonal GW scale sizes during geomagnetic disturbances irrespective of the season of the storm occurrence.

Near-simultaneous measurements of the spatial varying dayglow along both the zonal and meridional directions are obtained. From the wave number spectral analysis of these data, the zonal and meridional component of the horizontal waves are obtained. These values are used to calculate the horizontal scale sizes and their propagation angles. Such measurements on the horizontal scale sizes (in two dimensions) are first results of their kind. Moreover, these measured values have been used in conjunction with the GW dispersion relation to calculate the plausible wave features in the vertical direction. Thus, the first three dimensional GW characteristics in the daytime upper atmosphere has been derived. This technique opens up new possibilities in the investigations of the daytime wave dynamics.

Title: Origin and dynamics of the primordial magnetic field in a parity violating plasma
Researcher: Pandey, Arun Kumar
Supervisor: Bhatt, Jitesh R.
Year: 2017
Keyword's: Primordial Magnetic Field, Cosmology, EW Phase Transition, Left Right Symmetric Model, Turbulence Theory, Kinetic Theory
Call No.: 538.3 PAN
Acc. No.: T00283

Abstract: The Universe is magnetized on all scales that we have observed so far: stars, galaxies, cluster of galaxies etc. Recent observations indicates that typical magnetic field strength in a galaxy or a galaxy-cluster can have is about a few μG and its coherent length is around ten kpc. Recent observations suggest that the intergalactic medium (IGM) have magnetic field in the range of $(10^{-16} - 10^{-9})$ G with the coherent length scales around Mpc. Though it might be possible to explain the observed magnetic field of the galaxies and stars by some kind of astrophysical process, it is hard to explain the observed magnetic field of an IGM void. There exists an intriguing possibility of relating the origin of these large scale magnetic fields with some high-energy process in the early Universe. Thus it is of great interests to study the origin, dynamics and constraints on the magnetic field generated by such mechanism. This forms the prime focus of this thesis which considers the above problem in the context of a high-energy parity violating plasma.

In recent times there has been considerable interest in studying the magnetic field evolution in high-energy parity violating plasma. It is argued that there can be more right-handed particles over left-handed particles due to some process in the early Universe at temperatures T very much higher than the electroweak phase transition (EWPT) scale ($T \sim 100\text{GeV}$). Their number is effectively conserved at the energy scales much above the electroweak phase transitions and this allows one to introduce the chiral chemical potentials $\mu_R(\mu_L)$. However, at temperature lower than $T \sim 80$ TeV processes related with the electron chirality flipping may dominate over the Hubble expansion rate and the chiral chemical potentials cannot be defined. Further the right handed current is not conserved due to the Abelian anomaly in the standard model (SM) and it is the number density of the right handed particles are related with the helicity of the fields as $\partial_\tau (\Delta\mu + \frac{\alpha_2}{\pi} H_B) = 0$. (Here $\Delta\mu$, α_2 and H_B represents the chiral chemical imbalance, fine structure constant and magnetic helicity respectively). Therefore even if initially when there is no magnetic field, a magnetic field can be generated at the cost of the asymmetry in the number density of the left and right handed particles in the plasma. Recently, it has been interesting development in incorporating the parity -violating effects into a kinetic theory formalism by including the effect of the Berry curvature. Berry curvature term takes into account chirality of the particles. By using this modified kinetic equation, we show that chiral-imbalance leads to generation of hypercharge magnetic field in the plasma in both the collision dominated and collisionless regimes. We show that in the collision dominated regime, chiral vortical effects can generate a chiral vorticity and magnetic field. Typical strength of the magnetic field in the collision and collisionless regime are 10^{27} G at $10^5/T$ length scale and a magnetic field of

strength 10^{31} G at $10/T$ length scale at a temperature $T \sim 80$ TeV. We also show that the estimated values are consistent with the present observations.

We also show that in the presence of chiral imbalance and gravitational anomaly, a magnetic field of the strength 10^{30} G can be generated at a scale of 10^{-18} cm (much smaller than the Hubble length scale i.e. 10^{-8} cm). The idea is that in the presence of the gravitational anomaly, the current expression for the chiral plasma consists of a vortical current, proportional to square of temperature i.e. T^2 . The silent feature of this seed magnetic field is that it can be generated even in absence of chiral charge. In this work we have considered the scaling symmetry of the chiral plasma to obtain the velocity spectrum. Under this scaling symmetry in presence of gravitational anomaly, amount of energy at any given length scale is much larger than the case where only chiral asymmetry is considered. We also show that under such scenario energy is transferred from large to small length scale, which is commonly known as inverse cascade.

In the context of chiral plasma at high energies, there exist new kind of collective modes [*e.g.*, the chiral Alfvén waves] in the MHD limit and these modes exist in addition to the usual modes in the standard parity even plasma. Moreover, it has been shown that chiral plasmas exhibit a new type of density waves in presence of either of an external magnetic field or vorticity and they are respectively known as Chiral Magnetic Wave (CMW) and the Chiral Vortical Wave (CVW). In this regard we have investigated the collective modes in a magnetized chiral plasma and the damping mechanisms of these modes using first order and second hydrodynamics. Using first order conformal hydro, we obtained previously derived modes in the chiral plasma. However we show in addition that these modes get split into two modes in presence of the first order viscous term. By using second order conformal magnetohydrodynamics, we show that there are a series of terms in the dispersion relation and these terms are in accordance with the results obtained using AdS/CFT correspondence. We also calculated one of the transport coefficients related with the second order magnetohydrodynamics.

Title: Parity violating plasma-neutrino interaction: quantum kinetic and quantum magneto-hydrodynamic approach
Researcher: George, Manu
Supervisor: Bhatt, Jitesh R.
Year: 2017
Keyword's: Kinetic, Electromagnetic Plasma, Magneto Hydrodynamic, Depine-Lakhtakia
Call No.: 530.44 GEO
Acc. No.: T00284

Abstract: There has been a considerable interests in studying the properties of parity violating plasmas. Such plasmas are well studied as indicated by recent activities. New kinds of kinetic and hydrodynamic theories are developed which take into account of the quantum anomaly. And also their application to variety of astrophysical and laboratory situations has been considered. It is quite possible that the generation and dynamics of the primordial magnetic field, which is one of the open problem of cosmology, is intimately related with the study of parity violating plasmas. In these work the plasma is considered to have an excess of right-handed electron (quark) over the left-handed electrons (quarks). However neutrino sector also can play role in the magneto-genesis which has not been systematically explored in the literature. There exist many situations where the plasma neutrino interaction can play an important role in the dynamics of the system. In the case of neutrinos these type formalisms are not fully developed. In this thesis we study the effect of parity-violating neutrino interaction on an electromagnetic plasma.

We consider a plasma in presence background neutrino gas. We assume that the number densities of left-handed neutrino and right-handed neutrino are not equal. We develop the kinetic equation starting from the Lagrangian which contains the neutrino-charged lepton interaction. We calculate the polarization tensor for photon propagating in the plasma. Owing to the parity violating neutrino-plasma interaction, the polarization tensor receive an additional axial contribution. Using this polarization tensor, we show that the system support unstable modes in the quasi-static limit ($\omega \ll k$) which in turn can lead to the generation of a magnetic field. We show that the length scale associated with the unstable modes ($k^{-1}_{\max} \sim 10^4 \text{cm}$) at the time of the neutrino decoupling in the early Universe. It has also been shown that the strength of the magnetic field falls well within the bounds obtained for the present day universe. We construct the quantum hydrodynamic equations for a plasma composed of charged leptons and ions. We assume that there is an asymmetric neutrino gas present in the background. Linear analysis of these hydrodynamic equations are done to show that the asymmetry in the neutrino background drive a new kind of Alfvén wave. We also show that, in presence of asymmetric neutrino background, the Alfvén wave velocity is modified depending on the propagation direction with respect to the magnetic field. This modification in the velocity can contribute towards explaining the observed pulsar kick. Finally we study the refractive properties of a party violating plasma. We consider both chiral plasma as well as a plasma interacting with asymmetric neutrino background. It is shown that modifications in the photon polarization tensor due to the violation of parity can also modify the refractive properties of the medium. We show that the plasma exhibits the phenomena negative refraction for some value of ω as indicated by the Depine-Lakhtakia index.

Title: Measurement of solar magnetic fields: development of a polarimeter for multi-application solar telescope
Researcher: Tiwary, Alok Ranjan
Supervisor: Mathew, Shibu K
Year: 2017
Keyword's: Multi-Application Solar Telescope, Liquid Crystal Variable Retarders, Voltage, Helioseismic Magnetic Imager, Line-of-sight Observations
Call No.: 538.7 TIW
Acc. No.: T00285

Abstract: The solar magnetic field governs all the solar activities occurring at the outer atmosphere of Sun. The magnetic field lines in the solar atmosphere are stressed or deformed by the convective motion at the photosphere. These stressed magnetic field configuration is believed to be responsible for activity phenomena like flares, filament eruptions, coronal mass ejections (CMEs) etc. Majority of the eruptive events occur in the regions of strong and complex magnetic fields called as active regions. These eruptive phenomena directly affect near-Earth space weather by the accompanying high-energy radiation and charged particles. In order to predict these events a detailed investigation of solar magnetic structures is required. Thus, measurement of solar magnetic fields is of utmost importance in solar physics. However, measurement of solar magnetic field is done remotely by measuring the polarization of solar spectral lines induced by Zeeman effect. Polarization measurement is quite a challenging task because the polarization state of incoming light can be modified due to several factors/components (Earth atmosphere, Telescope, other optical components) coming in the path of light beam.

Multi-Application Solar Telescope (MAST), a 50 cm off-axis Gregorian telescope, was installed at Udaipur Solar Observatory (USO), India, which has been made operational recently. For understanding the evolution and dynamics of solar magnetic and velocity fields, an imaging spectropolarimeter has been developed at USO as one of the back-end instruments of MAST. This system consists of a narrow-band imager and a polarimeter. This instrument is intended for the simultaneous observations in the spectral lines at 6173 Å and 8542 Å, which are formed in the photosphere and chromosphere, respectively. The focus of this thesis is on the development of a polarimeter for measuring the polarization signal induced in the photosphere and chromosphere. The polarimeter includes a linear polarizer and two sets of Liquid Crystal Variable Retarders (LCVRs). It is known that the retardance of LCVR depends on the voltage and temperature. Voltage at a constant temperature is used for fast modulation.

However, fluctuations in the temperature and voltage reduces the accuracy in the polarimetric measurements. Thus we have characterized LCVRs of the polarimeter for various combinations of voltages and temperatures. Further, to achieve a sufficient polarimetric accuracy of 10^{-3} , it is necessary to calibrate the polarimeter and remove the cross-talk arising from the polarimeter itself. The calibration of the polarimeter is performed by introducing a calibration unit (CU) consisting of a linear polarizer and a zero order quarter wave plate (QWP). Both elements are placed in computer controlled rotating mounts. The calibration unit is placed just after the folding mirror (M6) of MAST.

Thus, during operations with MAST, calibration unit is used to generate known polarization by rotating QWP. The polarimeter response function or X-matrix is determined from a comparison between created input and measured output. The application of the inverse matrix X^{-1} on the measured Stokes vector removes the cross-talk arised due to properties of the polarimeter components.

In the thesis, spectropolarimetric observations of various active regions obtained with the imaging spectropolarimeter for MAST are also presented. For verification, we have made comparison of line-of-sight observations of a selected active region obtained from the Helioseismic Magnetic Imager (HMI) onboard the Solar Dynamics Observatory (SDO) with that obtained from observations in the spectral line 6173 Å from MAST telescope. We found good agreement between both the line-of-sight observations, considering the fact that MAST observations are limited by atmospheric seeing. It is important to note that MAST is a nine mirror system with two off-axis parabolic and seven plane oblique mirrors, the oblique reflections of these mirrors complicate the measurement as the instrumental polarization corrupts the incoming radiation. The polarization induced due to mirrors of telescope is linear. In order to get the vector magnetic field Stokes Q, and U profiles need to corrected using telescope matrix. We have planned to obtain the telescope matrix both theoretically and experimentally. The thesis is concluded with a discussion on the ongoing experiment for the determination of telescope matrix using sheet polarizer.

Title: Phenomenological aspects of neutrino masses, mixings and oscillations
Researcher: Nath, Newton
Supervisor: Goswami, Srubabati
Year: 2017
Keyword's: Neutrino Physics, Neutrino Oscillation, PMNS Matrix, Long-Baseline Neutrino Experiments, Atmospheric Neutrino Experiments, Texture Zero, Neutrino Mass Matrix, Flavor Antisymmetry
Call No.: 539.7215 NAT
Acc. No.: T00286

Abstract: Neutrino, meaning “*the little neutral one*” (in Italian) is a sub-atomic fundamental particle. It is the most abundant particle in the universe after the photon. In 1930, Wolfgang Pauli first postulated the existence of the neutrino to explain the conservation of energy and the angular momentum in nuclear beta-decay. In the Standard Model (SM) of particle physics, there are three types of neutrinos (namely electron, muon and tau neutrino) which are electrically neutral, spin-half and massless fermions. Neutrinos cover a wide range of energies from 10^{-6} eV to 10^{18} eV which have been detected by different experiments – starting from detection of MeV neutrinos e.g, in nuclear beta- decay, solar and reactor experiments to very high energy PeV neutrinos in the IceCube experiment. In this doctoral work, we study some of the very interesting aspects of neutrino physics from both phenomenological as well as theoretical point of view.

Last few decades have witnessed remarkable developments in the field of neutrino physics coming from the observation of neutrino oscillation in terrestrial experiments. Neutrino oscillation requires that at least two of the neutrinos possesses small but non- zero mass and there is mixing between different flavors of neutrinos. Since in the SM neutrinos are massless, the phenomenon of neutrino oscillation implies physics beyond the SM. The three-flavor neutrino oscillation framework containing six oscillation parameters (ϑ_{12} , ϑ_{13} , ϑ_{23} , Δm^2 , $|\Delta m^2|$ and δ_{CP}) is now well established. Global analysis of neutrino oscillation data have determined some of these parameters with considerable precision. At the current juncture, the three unknown neutrino oscillation parameters are the neutrino mass hierarchy ($\Delta m_{31}^2 > 0$, known as the normal hierarchy or $\Delta m_{31}^2 < 0$, known as the inverted hierarchy), octant of the mixing angle ϑ_{23} ($\vartheta_{23} < 45^\circ$, known as the lower octant or $\vartheta_{23} > 45^\circ$, known as the higher octant) and the CP phase δ_{CP} . A major part of this doctoral work is devoted to the determination of these unresolved parameters using different oscillation experiments.

The main obstacle for an unambiguous determination of these unknowns are the presence of parameter degeneracies which means different sets of oscillation parameters giving the same probability. In our study, we advocate a comprehensive way to study the remaining parameter degeneracies in the form of a generalized “*hierarchy- ϑ_{23} - δ_{CP}* ” degeneracy. To analyze this, we consider long baseline neutrino oscillation experiments NOvA and T2K and atmospheric neutrino oscillation experiment ICAL@INO. We discuss their physics reach and illustrate their synergistic effects to resolve the different degenerate solutions. We also explore the potential of the next generation super- beam experiment, DUNE to determine the different unknowns in neutrino oscillation parameters. Our study mainly focuses on the determination of the octant of ϑ_{23} and the

CP phase δ_{CP} . In particular, we emphasize on the role played by the antineutrinos, the broadband nature of the beam and the matter effect.

Theoretically, the challenge is to construct models of neutrino masses and mixing which can explain the observed values of the mass squared differences and the mixing angles. We discuss consequences of the assumption that the (Majorana) neutrino mass matrix M_ν and the charged lepton mass matrix M_ℓ satisfy, $S_\nu^T M_\nu S_\nu = -M_\nu$, $T_\ell^T M_\ell M_\ell^\dagger T_\ell = M_\ell M_\ell^\dagger$ with respect to some discrete groups S_ν , T_ℓ contained in A_5 group. These assumptions lead to a neutrino mass spectrum with a massless neutrino and a degenerate pair of neutrinos and also constrain the mixing among them. We derive possible mixing patterns considering the various subgroups of A_5 .

Another interesting question in neutrino physics is the existence of light sterile neutrinos. There are many experimental evidences which seem to support such a hypothesis. In this direction, we consider the “minimal extended type-I seesaw” (MES) model which naturally gives rise to a light sterile neutrino. We focus on the texture zero study of the various fermion mass matrices involving the charged leptons and neutrinos in this model. In this study, we obtain only two allowed one-zero textures in the neutrino mass matrix, m_ν , namely $m_{e\tau} = 0$ and $m_{\tau\tau} = 0$, having inverted hierarchical mass ordering. In the context of the MES model, we obtain extra correlations among neutrino oscillation parameters which can be tested in future oscillation experiments.

Title: Understanding the structure and emission processes in AGN using blazar variability
Researcher: Kaur, Navpreet
Supervisor: Baliyan, Kiran S.
Year: 2017
Keyword's: Electromagnetic Waves, Non-thermal Radiation, Mt Abu InfraRed Observatory, Duty Cycle Of Variation, Shock-in-jet Model
Call No.: 523.112 KAU
Acc. No.: T00288

Abstract: Active galactic nuclei (AGN) are centers of galaxies majority of which are 10^2 to 10^5 times more luminous than a normal galaxy and show signs of non-thermal activity. Since AGN are very compact and at relatively large redshift, they are non-resolvable by any existing facility. Therefore, understanding their structure and processes responsible for such high energy output is a big challenge. These are now broadly known to be powered by a supermassive black hole (SMBH) accreting matter through a disk surrounding it. An important diagnostic to investigate AGN phenomenon is temporal variability in blazars- a subclass of AGN. The emission in blazars is dominated by non-thermal radiation which is extremely variable at time scales ranging from a few tens of minutes to several tens of years across the whole electromagnetic spectrum (EMS). Rapid flux variability is capable of resolving features close to the central engine. In the present work, we have used variability of blazars to improve our understanding of the AGN in general and blazars in particular. The thesis is organized as follows.

We introduce the AGN phenomena, blazar properties and observational facilities which are used to obtain data at several energy regimes. The data reduction and analysis methods along with statistical techniques used to facilitate extraction of science from the data are also described. To address the microvariability (intra- night variations; INV) and long term variations in optical domain, we have carried out optical observations from the Mt Abu InfraRed Observatory (MIRO), complementing these with data from Steward Observatory, where available. Instances of INV and their time scales are determined for IBL 3C66A and S5 0716+71, duly verified using statistical techniques. The duty cycle of variation (DCV), sizes of the emission regions and possible mechanisms of emissions are discussed. The long-term behaviour of the source brightness, major outbursts and spectral properties of the two sources have been addressed using the entire dataset. The shock-in-jet model appears to be explaining the long term behaviour. We also studied the extent of variability as a function of source brightness and found opposite trends in the two IBLs. Though blazars are valuable sources of information, they become wonderful probes when in outburst. During these outbursts, source is normally detected across the EMS, providing opportunity to study the correlated variations among different energy bands. Two sources which exhibited unprecedented outbursts during last three years or so, 1ES 1959+650 (HBL) and CTA 102 (FSRQ), were studied using the multiwavelength data from optical observatories, Swift-XRT/UVOT (X-ray/UV/optical), Fermi-LAT(γ -rays) and 15GHz radio data from OVRO. The data were analyzed using standard techniques and multiwavelength light curves were generated. Both sources were at their historically brightest levels with several major outbursts and a number of rapid flares with significant amplitudes. It was possible to put constraints on the sizes of emission regions, distance of the high energy emitting

region from the black hole and infer processes responsible for flares. For CTA 102, we used 3-hour binned data to estimate the flux doubling time scale. The spectral energy distributions were constructed to study their spectral behaviour during pre-, post- and flaring periods. We infer that the jet has multiple emission regions in almost all the energy regimes, DCV depends on the duration of monitoring, variations at shorter time scales are stochastic in nature and long term outbursts are probably caused by shock moving down the jet, interacting with plasma over-densities (shocks/knots) or the changes in the viewing angle. The variability amplitudes appear to increase with frequency. The INV and LTV are possibly connected but such inference needs to be strengthened by an extensive study with densely sampled data.

Title: Investigations on ionospheric electrodynamics over low latitudes in Indian sector
Researcher: Rambabu, Pandey Kuldeep
Supervisor: Sekar, R.
Year: 2018
Keyword's: Low Latitude Ionosphere, Sq Electric Field, Plasma Drifts, Equatorial Counter Electrojet, Disturbance Dynamo
Call No.: 530.31 RAM
Acc. No.: T00392

Abstract: The central theme of the present doctoral thesis work is to understand the occurrence of equatorial counter electrojet (CEJ) or reductions in equatorial electrojet (EEJ) strength under geomagnetically quiet and disturbed conditions. Since variation in the ionospheric zonal electric field is central to any meaningful study on EEJ or CEJ, it is important to know the zonal electric field variations to understand these events. Since systematic measurements of electric fields covering all local times and seasons over the Indian sector are not available, the vertical drifts from the presently available global empirical models [Scherliess and Fejer, 1999; Fejer et al., 2008a] are used. Detailed investigations on the applicability of these empirical models over the Indian sector are carried out based on the comparisons with the measured and derived drifts. This investigation revealed that Fejer et al. [2008a] model drifts represent the quiet time vertical drifts over the Indian sector fairly well barring early morning hours. Therefore, the drifts obtained from Fejer et al. [2008a] model are used in the subsequent investigations, whenever applicable.

Observational studies over the Indian longitudes revealed that the occurrence of quiet time CEJ events is most frequent in afternoon hours during June solstice in solar minimum. An investigation carried out to understand the generation mechanism of these CEJ events showed that these CEJ events are caused by westward Sq electric fields and hence are part of the Sq current system extending from pole to equator. Further, the reversal of EEJ due to disturbance dynamo is investigated and it is found that reductions in the daytime electric field can be significantly large (0.7 ± 0.2 to $1.2 \pm 0.3 \text{ mVm}^{-1}$) during disturbance dynamo events. In order to explain such large westward electric field perturbations, additional role of semi-diurnal tides is indicated. Further, the strength of nighttime equatorial E-region current, used as the base level to determine the EEJ strength, are estimated to be about $0.3 - 0.7 \mu\text{Am}^{-2}$ based on three methods. The corresponding strength of the horizontal component of magnetic field induced at ground is found to be within 6 nT .

Title: Optical spectroscopic studies of minor bodies of the solar system
Researcher: Venkataramani, Kumar
Supervisor: Ganesh, Shashikiran
Year: 2018
Keyword's: Giant Planets, Comets, Orbits, Infra-red Observatory, Optical Spectrum
Call No.: 530 VEN
Acc. No.: T00515

Abstract: The minor bodies in the solar system comprise of asteroids, comets, trans-Neptunian objects, dwarf planets, planetary satellites, the Trojans of the giant planets, Centaurs and Kuiper belt objects. The widely accepted solar-nebula hypothesis for the formation of the solar system suggests that these minor bodies along with all the other planets formed within a disk of gas and dust called the proto-planetary disk. Formation of planets and their subsequent migration within the disk led to redistribution of the smaller bodies and formation of their various reservoirs at different distances from the Sun. Although a large number of ground based observations coupled with various space based missions have led to an advancement in our understanding of the formation of the solar system, a lot of questions about the composition of the small bodies, their dynamic behaviour, source location and formation scenarios are yet to be completely understood.

Due to their volatile nature, comets tend to become active as they move closer to the Sun. The various kinds of ices present in the cometary nucleus start to sublime at various temperatures at different heliocentric distances. The gases formed due to sublimation along with the dust particles forms the coma of the comet. This mixture of gas and dust arises from the icy volatile material which was trapped in the cometary nucleus ever since its formation in the proto-planetary disk. This makes them the signature bodies to understand the formation of the solar system. Comets carry a significant amount of pristine material from the early solar system and are relatively bright objects which can be observed and studied using even one meter class telescopes. Therefore the current work has focused on studying comets and near-Earth asteroids on comet like orbits. Optical spectroscopic studies of these objects have been carried out using the 0.5 m and 1.2 m telescopes at the Mount Abu Infrared Observatory with an aim of contributing towards answering some of the questions in cometary and solar-system science. A plethora of emission lines are seen in the optical spectrum of a comet. These arise due to the fluorescence excitation of the various molecular and ionic species of the gases present in comet's coma. In this work, we have monitored the activity in different comets by spectroscopically observing them at various heliocentric distances.

The thesis starts with a basic introduction to the minor bodies of the solar system, the effects of migration of giant planets on the distribution of these small bodies, the physical properties and classification of comets and asteroids and the optical spectrum of these objects. The facilities used for observations and the data reduction techniques have been described briefly. The low resolution spectrograph LISA has been used to obtain the optical spectrum of different comets and asteroids. The optical spectrum of comet C/2014 Q2 (Lovejoy) was obtained at four epochs in 2015. The comet showed a lot of molecular emissions in its spectrum. The production rates, production rate ratios, dust production and dust to gas ratio was estimated for this comet and its trend with the heliocentric

distance was studied. On the similar lines, optical spectra were obtained for three more long period comets: C/2013 US10 (Panstarrs), C/2013 X1 (Panstarrs), C/2015 V2 (Johnson) and two short period comets: 41P/Tuttle–Giacobini–Kresák and 45P/Honda–Mrkos–Pajdušáková. The fall in production rates of these comets with heliocentric distances have been examined. The comets 41P and C/2015 V2 have also been imaged using the Hale-Bopp Narrow band filters. Comet C/2016 R2 showed an unusual spectrum, quite different from the general cometary spectra. An in depth analysis of the optical spectrum of this comet has been carried out. First comet observations with the Hanle Echelle Spectrograph at the 2m Himalayan Chandra Telescope were done during the course of this work. The near Earth asteroid 2014 JO25 was spectroscopically followed during its close flyby of Earth in April 2017. A significant range of phase angle was covered during the observations of this asteroid. Results from these observations have also been discussed.

Most of the observations have been carried out using smaller class of telescopes and a small spectrograph. This demonstrates and exemplifies the importance of small telescopes and ground based observations of minor bodies of the solar system.

Title: Collective excitations of the hot QCD medium and quark-gluon plasma in relativistic heavy-ion collisions
Researcher: Jamal, Mohammad Yousuf
Supervisor: Chandra, Vinod
Year: 2019
Keyword's: Quark-Gluon-Plasma, Color Screening, Quasi-parton, Effective Fugacity, Gluon Selfenergy, Momentum Anisotropy, Heavy Quarkonia
Call No.: 530 JAM
Acc. No.: T00518

Abstract: The underlying theory of strong interaction force, namely, the Quantum Chromodynamics (QCD), predicts a transition from the normal nuclear (hadronic) matter to a deconfined phase where the quarks, anti-quarks and gluons are effectively free to move beyond the nucleonic volume. This deconfined phase of the matter, could be obtained at extremely high temperature and density and is commonly termed as Quark Gluon Plasma (QGP). The QGP is believed to exist in the very early universe, a few microseconds after the Big-Bang. One could create these conditions (Mini Bang) in the heavy-ion collision (HIC) experiments with the global collider facilities at Brookhaven National Laboratory (BNL) and European Organization for Nuclear Research (CERN). The nature of interaction in the QGP medium and their role in understanding its properties could be studied by investigating the collective excitations of the medium. In particular, it is essential to understand the plasma aspects such as color screening and energy loss in the QGP medium. This further helps in understanding the existence of the QGP in HIC and controls the physics of quarkonia dissociation and jet quenching in the medium. In this thesis, an attempt has been made to understand the collective excitations of the anisotropic hot QCD/QGP medium in the presence of collisions (with Bhatnagar-Gross-Krook (BGK) collisional kernel) in terms of gluon polarization tensor by invoking classical Yang-Mills equations. The hot QCD medium effects have been included via effective quasi-particle model, and the semi-classical transport theory approach has been adopted for the analysis. As an implication, we have been able to study the dielectric property and the possibility of negative refraction in the medium. The heavy quarks energy loss have also been obtained in terms of induce electric field which is determined by the gluon selfenergy. Finally, the analysis of heavy quarkonia dissociation has been presented considering the anisotropy in the medium. The medium effects, collision and anisotropy (momentum) have been found to have a significant impact on the above-mentioned aspects of the QGP in HIC.

Title: Synthetic magnetic fields and multi-component BECs in optical lattices
Researcher: Bai, Rukmani
Supervisor: Singh, Angom Dilip Kumar
Year: 2020
Keyword's: Optical Lattice, Bose-Hubbard Model, Quantum Hall States, Single-site, Cluster Gutzwiller Mean-field Theory, Exact Diagonalization
Call No.: 530 BAI
Acc. No.: T00545

Abstract: Quantum Hall states are robust and good choice for numerous potential applications and to study the physics of topological effects. These states have been observed experimentally in condensed matter systems. However, the observation of fractional quantum Hall states with high flux is difficult in these systems as they require high magnetic fields (≈ 100 T or more). In this respect, ultracold atoms trapped in the optical lattices are clean and appropriate systems as synthetic magnetic fields equivalent to 1000 T or more can be generated using laser fields. In this thesis, I study the occurrence of quantum Hall states and competing superfluid states in optical lattices for both homogeneous and inhomogeneous systems. And, I also study the physics of multi-component ultracold atomic gases in optical lattices. For the former, I solve the Bose-Hubbard model with synthetic magnetic field referred to as the bosonic Harper-Hofstadter model, using cluster Gutzwiller mean-field and Exact diagonalization methods. The synthetic magnetic field in the optical lattices can be implemented through the Peierls phase and experimentally using laser fields. For the homogeneous case, with the inclusion of the synthetic magnetic field, we obtain the quantum Hall states as the ground state of the bosonic Harper-Hofstadter model. As a first step, the parameters of the QH states are identified based on the compressibility. We obtain the quantum Hall states for different values of synthetic magnetic field with different cluster sizes for the hard core bosons and in the neighbourhood of zero Mott lobe. For the hard core bosons, the onsite interaction energy of the atoms is much larger than the nearest neighbour tunneling energy. As a possible experimental signature, I study in detail the two-point correlation function to distinguish between the quantum Hall states and superfluid states. The states so obtained as further studied in more detail with the exact diagonalization method. I identify the quantum Hall states and superfluid states based on the Penrose-Onsager criterion and Von Neumann entropy. Then, the identification of the quantum Hall states is confirmed by computing the many-body Chern number and ground state degeneracy. For the inhomogeneous case, I do recover all the quantum Hall states for hard wall boundary and for a shallow Gaussian potential, but not with the harmonic oscillator potential. For the multi-component ultracold atomic gases, I obtain the phase diagram for the Bose-Hubbard model for two species. I get the half-filled Mott lobes in presence of inter-species interaction strength. And, show that the width of half-filled Mott lobe varies linearly with increasing the inter-species interaction strength. I, then, consider the nearest neighbour interaction together with onsite interaction in the Bose-Hubbard model and study the phase separation for the strongly correlated phases of two-component ultracold atomic gases in optical lattices. I also study the phase diagram of the extended Bose-Hubbard model and observe the shifting of density wave lobe with the increase of the inter-species interaction strength with zero inter-species nearest neighbour interaction. While with finite

inter-species nearest neighbour interaction I observe the phase separation in density wave, super-solid and superfluid phase.

Title: Matter under extreme conditions and transport coefficients of hot and dense matter
Researcher: Abhishek, Aman
Supervisor: Mishra, Hiranmaya
Year: 2019
Keyword's: Quantum Chromodynamics, Chiral Symmetry, Confinement, Asymptotic Freedom, Heavy Ion Collisions, Transport Coefficients, Spin Polarization
Call No.: 536.41 ABH
Acc. No.: T00562

Abstract: In this thesis we have investigated the properties of strongly interacting matter at extremely high temperatures and densities. The interactions of strongly interacting matter are governed by the laws of Quantum Chromodynamics (QCD) which is a gauge theory based on $SU(3)_c$ symmetry group. The Standard model of particle physics contains six strongly interacting quarks and eight gluons which bind together to form baryons such as protons, neutrons, etc and mesons such as pions, kaons, etc. Collectively the baryons and the mesons are known as hadrons and make up the bulk of the observable universe. Strongly interacting matter exhibits peculiar features owing to the strong nature of its coupling, namely asymptotic freedom, confinement and spontaneous breaking of chiral symmetry. Chiral symmetry refers to the symmetry of the Lagrangian under a chiral transformation, that is upon replacing left-handed fields with right handed fields and vice versa. Spontaneous breaking of chiral symmetry in QCD results in mass generation and is responsible for about 98% of the visible mass of the universe.

Asymptotic freedom refers to the fact that the strong coupling decreases with increasing energy and thus at very high energies the theory becomes weakly coupled. Weak coupling allows one to use usual methods of perturbation theory to make predictions about experiments and study the hot and dense matter created in heavy ion collisions. There has been considerable success in the use of perturbation theory to explain the experimental data obtained in heavy ion collisions. Despite the successes there are many unresolved problems which remain. Predictions of the transport properties based on perturbative QCD(pQCD) are in disagreement with experimental data and Lattice QCD simulations which suggests non-perturbative effect remain strong in the matter produced in heavy ion collisions for temperatures atleast few times the transition temperature. Other than high temperatures, the picture is also unclear at high densities. Lattice QCD, which is a first principle implementation of QCD has the sign problem and perturbative calculations are inapplicable due to large coupling for realistic densities, e.g. in the core of neutron stars or the dense matter produced in heavy ion collisions. Moreover, it is also known that neutron stars have a very strong magnetic field. Origin of such high magnetic fields and its effect on hadronic matter is also a topic of active research. In view of these problems one turns to effective models which are based on phenomenological parameters and captures some of the basic properties of QCD. Two such

popular models are Nambu Jona Lasinio model (NJL) and Polyakov Loop extended Quark Meson Model(PQM).

Nambu Jona Lasinio model was proposed by Yochiro Nambu and Jona Lasinio as a low energy phenomenological model of strong interactions. The model is written on the basis of chiral symmetry with a four fermion interaction and exhibits spontaneous chiral symmetry breaking. Gluons are absent in the NJL model and hence lacks confinement. The parameters of the model are fit to reproduce low energy hadronic spectrum. The model has been successfully applied to the study of strongly interacting matter both at high temperatures and high densities. Quark Meson model(QM) is similar to NJL written on the basis of chiral symmetry. Whereas in NJL model the degrees of freedom are quarks, QM model includes mesonic degrees of freedom such as pions. The model has interactions between meson and quarks and mesons and mesons. Further Polyakov loop is added to QM model. Polyakov loop takes into account effects of confinement which both NJL and QM model lack and leads to statistical confinement of quarks below chiral transition.

Using these two models we have studied the properties of matter under extreme conditions of temperature and densities. Polyakov Quark Meson model(PQM) has been used to calculate the transport coefficients of hot matter created in heavy ion collision, namely the shear viscosity, bulk viscosity and thermal conductivity. Results have been obtained using kinetic theory and thermal averaging of scattering rates. Values obtained for the transport coefficients are consistent with experimental results and other phenomenological studies.

For quark matter at high densities and large background magnetic field, which is relevant for the interior of neutron stars, three flavor NJL model with determinant interaction has been used with background magnetic field to study color superconductivity at high densities. Constraints of charge neutrality have been imposed and resulting gapless modes have been studied. Impact of background magnetic field on the superconducting gap and neutrality conditions is also discussed. Spontaneous spin polarization has been suggested as a possible mechanism for the origin of large magnetic fields in neutron stars. In order to study spontaneous spin polarization in quark matter, a three flavor NJL model with tensor interaction has been used with non-zero current quark masses. Two independent spin polarization condensates arising from tensor interaction in three flavor NJL model, have been studied as a function of quark chemical potential. Magnetic field resulting from such condensates is estimated and found to be of expected order of magnitude.

Title: Test of new physics at neutrino telescopes
Researcher: Chauhan, Bhavesh
Supervisor: Mohanty, Subhendra
Year: 2019
Keyword's: Sterile Neutrino, Leptoquark, IceCube, MiniBooNE, Flavor Anomalies, Dark Matter
Call No.: 530 CHA
Acc. No.: T00563

Abstract: The Standard Model of particle physics is the most successful theory of interactions between elementary particles. But there are enough reasons to believe in particles and symmetries beyond standard model. In this thesis, I have studied two well motivated extensions, leptoquarks and sterile neutrino, in the context of IceCube and ANITA experiments. A TeV scale leptoquark can resolve the observed discrepancy in semi-leptonic decays of B meson (flavor anomalies). The leptoquark can also be resonantly produced in neutrino-nucleon interaction and explain the excess of PeV events at IceCube. We find that a simultaneous explanation using the scalar leptoquark $R_2 \sim (3, 2, 7/6)$ is ruled out from LHC searches such as dijet + E_T and monojet + E_T . The constraints obtained also limit other resonance based explanation of PeV excess. Moreover, the puzzle of EeV scale τ emerging from inside Earth as observed by ANITA can also be explained with leptoquarks. In our framework, the vector leptoquark $U_1 \sim (3, 1, 2/3)$, which can simultaneously address the charged and neutral current mediated flavor anomalies, also couples to a sterile neutrino. The leptoquark mediated interaction between astrophysical neutrino and nucleons in Earth produces a sterile neutrino that propagates without significant attenuation. If the mass of the sterile neutrino is a few GeV, it decays near the surface to τ lepton. On the other hand, if the sterile neutrino is very light, the astrophysical flux of sterile neutrinos can pass through Earth and produce a τ lepton near the surface by resonant production of leptoquark. These two scenarios significantly enhance the survival probability and provide a combined explanation of flavor and ANITA anomalies. In addition, the new particles proposed are within the reach of future LHC searches and B factories. A major challenge is to explain the flux of sterile neutrinos and one possibility is to consider oscillation from active neutrinos. This is plausible only if the sterile neutrino is very light and has large mixing angles. The existence of eV scale sterile neutrino is also hinted by short baseline experiments such as MiniBooNE and LSND. However, it is in conflict with big bang nucleosynthesis unless one postulates either non standard cosmology or new interactions. One possibility is to consider self-interaction in the sterile sector. Such interactions would result in absorption features in the astrophysical neutrino spectrum which can be tested by IceCube. We have claimed that the lack of 400-800 TeV neutrinos is due to absorption by cosmic sterile neutrino background. The lack of Glashow events is attributed to absorption due to heaviest active neutrino in the cosmic background. Furthermore, the self interacting sterile neutrino can also act as a portal to hidden and light self-interacting dark matter. A model is proposed where the relic density of dark matter is obtained from freeze-out of coannihilations and self-interaction is loop suppressed. The interesting parameter space that can be tested with supernova neutrinos is in conflict with observation of PeV events at Ice- Cube.

Title: (Semi) leptonic rare decays of B mesons as probes of the standard model and beyond
Researcher: Kindra, Bharti
Supervisor: Mahajan, Namit
Year: 2019
Keyword's: Flavor Physics, Semileptonic B Decays, Effective Field Theory, Wilson Coefficients, Form Factors
Call No.: 539.7 KIN
Acc. No.: T00564

Abstract: In particle physics, flavor refers to a generation of an elementary particle. Within standard model, there are six flavors of quarks and three flavors of leptons. Study of these elementary particles and their interactions is referred to as flavor physics. Historically, it has played a crucial role in development of Standard Model (SM) of particle physics. At present, there are compelling indications that the framework of Standard Model is not complete. However, there are no direct hints of any new particle from collider experiments. Flavor physics plays an important role here as it provides indirect probe to study new physics. Specially, the loop induced decay modes are sensitive to both SM and heavy new physics particles. Thus, dedicated efforts have been made to study flavor interactions both experimentally and theoretically. On experimental side, a paramount data on flavor physics has been accumulated which has improved the understanding of flavor interactions. However, some recent measurement of flavor changing decays of B mesons show some deviations from SM predictions. In particular, the angular observables of decay modes based on $b \rightarrow s\ell^+ \ell^-$ and $b \rightarrow c\ell\nu_\ell$ transitions have shown consistent anomalies. Global fits of all these observables suggest the presence of new physics but the solution is not unique. Due to lack of enough data and large uncertainties in SM calculations, the source of the deviations is not clear. In this thesis, we have studied more decays in Standard model and new physics scenarios suggested by the present data. The aim of the thesis is to have SM expectations values for the leptonic and semileptonic decay modes with contributions of QCD corrections included.

In Chapter 3, predictions of angular observables for semileptonic decays, $B \rightarrow \rho\mu^+\mu^-$ and $B_s \rightarrow K^{*\mu^+\mu^-}$ and their CP conjugate modes are given. It is found that the SM expectation for $B_s \rightarrow K^{*\mu^+\mu^-}$ is in agreement with the recent LHCb results. For $B \rightarrow \rho\mu^+\mu^-$ analysis is more involved as ρ is a CP conjugate state and the flavor of the decaying B meson can not be tagged. We consider the impact of $B - B^-$ mixing on the angular observables systematically and give predictions separately for LHCb and B factories.

In Chapter 4, we give predictions for angular observables corresponding to $B \rightarrow K_2^*\mu^+\mu^-$ with SM and other new physics scenarios. It has been shown that this mode is important as it is induced by $b \rightarrow s\ell\ell$ transition at the quark level. However, because K_2^* is a tensor particle, hadronic inputs are much different in comparison to other $b \rightarrow s\ell\ell$ processes. Thus, the study of this mode can be important to isolate the source of the deviations observed. Moreover, it has been shown that this channel can be used to lift the degeneracy in the solutions of global fits.

In Chapter 5, we have studied four-lepton decay of charged B meson. This channel is important as it can provide constraints on one of the most important hadronic parameters. The calculation for this channel is same as that of radiative decay with one difference. The photon in this case is not on-shell and hence the momentum squared of photon (q^2) is not zero. We have systematically retained q^2 terms in the calculation of form factors and given predictions for the four-lepton decays where final state can have electrons and muons.

In Chapter 6 we summarize the work done and discuss some future directions that can be pursued following the work done in this thesis.

Title: Some aspects of low scale seesaw models
Researcher: Vishnudath K. N.
Supervisor: Goswami, Srubabati
Year: 2019
Keyword's: Neutrino Mass, Seesaw Mechanism, Majorana Neutrinos, Neutrino-less Double Beta Decay, Vacuum Stability, Metastability, Low Scale Seesaw, Dark Matter, Naturalness
Call No.: 539.7 VIS
Acc. No.: T00565

Abstract: The Standard Model (SM) of particle physics has been very successful in explaining a wide range of experimental observations and the discovery of the Higgs boson at the Large Hadron Collider has confirmed the mode of generation of the masses of the fundamental particles via the mechanism of electroweak symmetry breaking. This has put the SM on a solid foundation. However, despite its success in explaining most of the experimental data, the SM cannot address certain issues, of which two of the most important are non-zero neutrino mass and the existence of dark matter. The most plausible way to generate small neutrino masses is the seesaw mechanism which implies neutrinos to be lepton number violating Majorana particles. This Majorana nature of the neutrinos can give rise to the neutrino-less double beta decay process in which the total lepton number is violated by two units. It is well known that the canonical high scale seesaw models are not testable in the colliders and there are various low scale seesaw models proposed in the literature motivated by their testability. Such models can have various phenomenological as well as theoretical consequences. For example, the heavy seesaw particles can lead to enhanced rates of various charged lepton flavor violating decays and the new couplings associated with the seesaw can alter the stability/metastability of the electroweak vacuum. In addition, these heavy particles can have interesting signatures in the collider experiments. In this thesis, we study various phenomenological and theoretical implications of massive neutrinos in the context of various low scale seesaw models. We also explore the possibilities of having viable candidates for dark matter in the context of seesaw models.

First, we explore the implications of the Dark-LMA (DLMA) solution to the solar neutrino problem for neutrino-less double beta decay ($0\nu\beta\beta$). The standard Large Mixing Angle (LMA) solution corresponds to standard neutrino oscillations with $\Delta m_{21}^2 \sim 7.5 \times 10^{-5} \text{ eV}^2$ and $\sin^2 \theta_{12} \sim 0.3$, and satisfies the solar neutrino data at high significance. The DLMA solution appears as a nearly-degenerate solution to the solar neutrino problem for $\Delta m_{21}^2 \sim 7.5 \times 10^{-5} \text{ eV}^2$ and $\sin^2 \theta_{12} \sim 0.7$, once we allow for the existence of large non-standard neutrino interactions in addition to standard oscillations. We show that while the predictions for the effective mass governing $0\nu\beta\beta$ remains unchanged for the inverted hierarchy, that for normal hierarchy becomes higher for the Dark-LMA parameter space and moves into the “desert region” between the two. This sets a new goal for sensitivity reach for the next generation experiments if no signal is found for the inverted hierarchy by the future search programmes. We also obtain the sensitivity for the DLMA region in the future ^{136}Xe experiments.

In the next part of the thesis, we study the minimal type-III seesaw model in which we extend the SM by adding two $SU(2)_L$ triplet fermions with zero hypercharge to explain the origin of the non-zero neutrino masses. The lightest active neutrino will be massless in this case. We use the Casas-Ibarra parametrization for the neutrino Yukawa coupling matrix and by choosing the two triplets to be degenerate, we have only three independent real parameters, namely the mass of the triplet fermions and a complex angle. The parametrization used allows us to have low masses of the triplet fermions and large Yukawa couplings at the same time. We show that the naturalness conditions and the limits from lepton flavor violating decays provide very stringent bounds on the model parameters along with the constraints from the stability/metastability of the electroweak vacuum. We perform a detailed analysis of the model parameter space including all the constraints for both normal as well as inverted hierarchies of the light neutrino masses. We find that most of the region that is allowed by lepton flavor violating decays and naturalness falls is stable/metastable depending on the values of the SM parameters.

In addition to neutrino masses, the existence of the dark matter is another issue that points towards the need for an extension of the SM. Hence, it is important to study the implications of the models that can simultaneously address these two issues. From this point of view, we consider singlet extensions of the SM, both in the fermion and the scalar sector, to account for the generation of neutrino mass at the TeV scale and the existence of dark matter, respectively. For the neutrino sector we consider models with extra singlet fermions which can generate neutrino masses via the so called inverse or linear seesaw mechanism whereas a singlet scalar is introduced as the candidate for dark matter. The scalar particle is odd under a discrete Z_2 symmetry which ensures its stability. We show that although these two sectors are disconnected at low energy, the coupling constants of both the sectors get correlated at a high energy scale by the constraints coming from the perturbativity and stability/metastability of the electroweak vacuum. The singlet fermions try to destabilize the electroweak vacuum while the singlet scalar aids the stability. As a consequence, the electroweak vacuum may attain absolute stability even up to the Planck scale for suitable values of the parameters. We delineate the parameter space for the singlet fermion and the scalar couplings for which the electroweak vacuum remains stable/metastable and at the same time giving the correct relic density and neutrino masses and mixing angles as observed.

In addition to the simple extensions of the particle content, we also consider a class of gauged $U(1)$ extensions of the SM, where active light neutrino masses are generated by an inverse seesaw mechanism. Along with the three right handed neutrinos needed for the cancellation of gauge anomalies, we add three singlet fermions. This allows us to consider large neutrino Yukawa couplings keeping the $U(1)'$ symmetry breaking scale to be of the order of $\sim O(1)$ TeV. Demanding an extra Z_2 symmetry under which, the third generations of both the electrically neutral fermions are odd gives us a stable dark matter candidate. We express the $U(1)$ charges of all the fermions in terms of the $U(1)$ charges of the SM Higgs and the new complex scalar. We perform a comprehensive study to find out the parameter space consistent with the low energy neutrino data, vacuum stability and perturbativity, dark matter bounds and constraints from the collider searches.

Title: Twisted single photons and their applications in quantum information processing
Researcher: Lal C.K., Nijil
Supervisor: Singh, R. P.
Year: 2019
Keyword's: Single Photon, Twisted Photons, Photon Statistics, Orbital Angular Momentum, Spontaneous Parametric Down-Conversion, Entanglement
Call No.: 539.7 LAL
Acc. No.: T00566

Abstract: Information theory based on quantum systems has shown to be amazingly advantageous over that based on classical systems in devising efficient and secure communication protocols. This is a manifestation of two unique properties of quantum systems such as the existence of an indivisible quanta of energy and entanglement. The advances in quantum information processing have led to the quest for suitable candidates to carry quantum bits of information. Single photons are proven to be a suitable qubit candidate as they are fast and do not interact with each other. However, generating stable sources of ideal single photons in an efficient and cost-effective manner is a challenging task. A unique non-linear phenomena called spontaneous parametric down-conversion (SPDC) has been widely explored as an alternate source of single photons over the past few decades. SPDC is a second order, non-linear optical effect where the dipole polarization depends on the electric field in a quadratic manner and photons incident on the non-linear crystal gets converted into two photons with lower frequencies. Heralding the detection of one of the photons by the detection of the other gives rise to single photon behaviour. Such heralded single photons generated in spontaneous parametric down-conversion provide cost-efficient, stable sources of single photons which can be manipulated easily using linear optics for applications in quantum information processing. Orbital angular momentum (OAM) of light is widely being studied to be used in communication as unlike other degrees of freedom of light, OAM provides an infinite dimensional basis. Orbital angular momentum of single photons is also being explored extensively aiming towards increased information transfer as well as robust entanglement protocols. The twin photons generated in paraxial SPDC are correlated in orbital angular momentum following OAM conservation. Thus OAM entanglement can be easily realized in SPDC. The projective measurements corresponding to OAM are generally carried out through phase-flattening technique using a spatial light modulator (SLM). However, the measurements based on phase-flattening have shortcomings in terms of efficiency and dependence on pump beam characteristics. Alternate interferometric methods for projective measurement and sorting of OAM modes form an active area of research. In this thesis, we study and characterize twisted single photon sources generated from parametric down conversion based on their statistical correlations. We build the probability distribution of numbers using photon detectors and an oscilloscope which is a ubiquitous instrument present in any undergraduate laboratory. We verify the Poissonian and super Poissonian statistics of different sources. For the heralded single photon sources generated in parametric down-conversion, we verify the sub-Poissonian behaviour.

Further, we study the second order correlation of these single photons in a heralded Hanbury Brown-Twiss experiment. We observe near-zero values for second order correlation coefficient at zero delay, $g^{(2)}(0)$. The correlation parameter is calculated using direct measurement of three-fold coincidences as well by only accounting for the probability of accidental triple coincidences. We show that the latter method gives the same value for the correlation parameter with reduced uncertainty. We investigate the variation of the statistical correlation with the OAM order of the twisted single photons. We observe that the non-classical behaviour of the heralded twisted single photons reduces for higher orders of OAM. We study the OAM distribution of the twin photons generated in the down-conversion process as well. The study reveals that using perfect optical vortices as pump we can obtain narrower OAM spectrum. We also study the effect of pump mode on OAM entanglement. Finally, we demonstrate that the OAM sorting process of indistinguishable photons generated from collinear parametric down-conversion can be utilized to reveal the polarization entanglement. We use even-odd basis of OAM to label and distinguish the photons from a pair. This increases the efficiency of available entangled photon pairs as we do not eliminate any pairs while selecting the photons in the two-dimensional Hilbert space of even and odd OAMs.

Title: Quantum phase transitions of Bose gases confined in 2D harmonic traps and optical lattices
Researcher: Bandyopadhyay, Soumik
Supervisor: Singh, Angom Dilip Kumar
Year: 2019
Keyword's: Quantum Fluctuations, Bose-Einstein Condensation (BEC), Polarized Dipolar Atoms, Vortices With Quantized Circulation, Miscible-Immiscible QPT
Call No.: 530.12 BAN
Acc. No.: T00567

Abstract: Quantum phase transitions (QPTs) can be probed at temperature $T \approx 0\text{K}$, when the quantum fluctuations are larger than the thermal fluctuations in a physical system. In experiments at several laboratories around the world temperatures $\sim 100\text{nK}$ have been achieved, and at these low temperatures Bose-Einstein condensation in trapped quantum degenerate gas of interacting bosonic atoms have been observed. So, Bose-Einstein condensates (BECs), which are macroscopic quantum states with long-range phase coherence, have become important candidates to explore properties of different quantum phases of matter and phenomena associated with QPTs. On the otherhand, BECs can host vortices with quantized circulation, which serve as probes for superfluidity and quantum turbulence. In this thesis, we explore the dynamics across miscible-immiscible QPT of harmonically trapped two-component BECs (TBECs) and novel quantum phases of BECs of dipolar atoms loaded in optical lattice potentials. Further more, we investigate on the stability properties and splitting dynamics of quantized composite vortices in the harmonically trapped miscible TBECs.

We induce the miscible-immiscible QPT, also referred to as phase-separation, in harmonically trapped quasi-two-dimensional (quasi-2D) TBECs by adiabatic quenching of the intercomponent interaction strength. We theoretically study the dynamics of the phase-separation by solving coupled time-dependent *Gross-Pitaevskii (GP) equations*, which are apt to describe the temporal evolution of the BECs at $T = 0\text{K}$. We examine the effects of quantized vortices on the phase separation, and demonstrate that the vortex induced superfluid flow can either enhance or suppress the phase-separation depending on the presence of vortices in the components of the TBECs. Afterwards, we analyze the stability properties of axisymmetric composite vortex states of the TBECs in the miscible phase. For this, we perform linear stability analysis of the stationary solutions and solve coupled *Bogoliubov-de-Gennes equations* for quasi-particle amplitudes. We infer about the dynamical and energetic instabilities from the quasi-particle excitation frequencies, and present stability diagrams of the composite vortex states. We, then, illustrate important splitting dynamics of dynamically unstable composite vortex states by evolving the stationary vortex state solutions using time-dependent coupled GP equations. We observe that the composite vortices can exhibit splitting dynamics which are strikingly different from the dynamics exhibited by quantized vortices in single-component BECs.

To explore quantum phases of BECs of polarized dipolar atoms in strongly interacting domain, we consider the atoms to be confined in optical lattice potentials. At $T = 0\text{K}$, the physics of such systems

is well described by the lowest band Bose- Hubbard model (BHM) with dipolar interactions. Minimal form of this model is to restrict the range of dipole-dipole interactions to nearest neighbour lattice sites. We solve this minimal model for 2D square optical lattice, and discuss the quantum phases of the system arising due to the variation in the tilt angle ϑ of the polarization axis. To solve the model, we employ site-decoupled mean-field theory with Gutzwiller ansatz.

Our study reveals that at low tilt angles $0^\circ \leq \theta \lesssim 25^\circ$, the ground state of the system are phases with checkerboard order. These are either checkerboard supersolid or checkerboard density wave phases. On the other hand, these phases have stripe order at high tilt angles $35^\circ \lesssim \theta \lesssim 55^\circ$. In the intermediate domain $25^\circ \lesssim \theta \lesssim 35^\circ$ metastable emulsion states or superfluid phase intervenes the QPTs between the phases with checkerboard and stripe order. The attractive dipolar interaction dominates for $\vartheta > \sim 55^\circ$, which renders the system unstable and density collapse occurs in the system. We report detailed phase diagrams illustrating possible QPTs of the system. We also analytically calculate the phase boundaries between an incompressible and a compressible phase by performing second order perturbation analysis of site-decoupled mean-field theory. The analytical results are in excellent agreement with our numerical results. Furthermore, we study the phases of hardcore dipolar atoms in the bilayers of the 2D square optical lattice. The ground state of this system can exhibit valence bond checkerboard solid phase with average occupancy per lattice site as $1/4$ and $3/4$, when the inter-plane hopping is strong. We obtain the phase diagrams of this system by varying the interplane hopping strength.

Title: Aspects of black hole thermodynamics in general relativity & beyond
Researcher: Fairuos C.
Supervisor: Sarkar, Sudipta
Year: 2019
Keyword's: General Relativity, Black Hole Thermodynamics, Higher Curvature Gravity Theories, Lanczos-Lovelock Theory
Call No.: 530.14 FAI
Acc. No.: T00571

Abstract: The goal of this thesis is to study certain aspects of black hole thermodynamics in general relativity (GR) as well as higher curvature gravity theories. In GR, it has been shown that the evolution of black hole entropy is similar to that of an ordinary fluid. In this thesis, we study the entropy evolution of black holes in Lanczos-Lovelock gravity by formulating a thermodynamic generalization of the null Raychaudhuri equation. We show that the similarity between the expressions of entropy change of the black hole horizon due to perturbation and that of a fluid, which is out of equilibrium, transcends beyond general relativity to the Lanczos-Lovelock class of theories.

An important aspect of the black hole thermodynamics is the issue of the validity of the cosmic censorship hypothesis (CCH). The formulation of the laws of black hole mechanics assumes the stability of black holes under perturbations in accordance with CCH. This conjecture, due to Penrose, asserts that the formation of naked singularities by a physical process from a regular black hole solution is not possible. However, earlier studies show that naked singularities can indeed be formed leading to the violation of CCH. We investigate the validity of CCH by considering the infall of charged massless particles as well as a charged null shell. We also discuss the issue of the third law of black hole mechanics in the presence of null charged particles by considering various possibilities. Further, we examine the problem of overcharging extremal and near-extremal black hole solutions of Einstein-Gauss-Bonnet gravity in any dimension.

This thesis also addresses the information loss paradox and the problem of correlation in the Hawking radiation. A re-analysis of Hawking's derivation including the effects of self-interactions in GR shows that the emitted radiation deviates from pure thermality. However, no correlations exist between two successively emitted Hawking quanta hence leaving the paradox unsolved. We extend these calculations to Einstein-Gauss-Bonnet gravity and investigate if higher curvature corrections to the action lead to some new correlations in the Hawking spectra. The physical process version of the first law can be obtained for bifurcate Killing horizons with certain assumptions. Especially, one has to restrict situations where the horizon evolution is quasi-stationary. Here, we revisit the analysis of this assumption considering the perturbation of a Rindler horizon by a spherically symmetric object. We demonstrate that even if the quasi-stationary assumption holds, the change in entropy, in four space-time dimensions, diverges when considered between asymptotic cross-sections. However, these divergences do not appear in higher dimensions. We also analyze these features in the presence of a positive cosmological constant. In the process, we prescribe a recipe to establish the physical process first law in such ill-behaved scenarios.

Finally, we discuss some fundamental aspects of the membrane paradigm description of black hole physics. We show that the dynamics of the boundary matter arises from the invariance of the bulk action under local symmetries in the presence of the inner boundary. If general covariance is broken in a semi-classical treatment of a quantum field near a black hole horizon, we argue that it can be restored by the inclusion of a quantum flux into the membrane conservation equation which should be exactly equal to the Hawking flux.

Title: Structured beam optical parametric oscillators
Researcher: Sharma, Varun
Supervisor: Samanta, Goutam Kumar
Year: 2020
Keyword's: Spatial Beam Shaping, Optical Vortex, High Power, Optical Radiation, Spatial Light Modulators
Call No.: 530 SHA
Acc. No.: T00573

Abstract: The applications of lasers cover almost all fields of science and technology including medical diagnosis, lithography, communication and material processing. Typically, lasers, the main source of coherent optical radiation, are characterised with the performance parameters such as output power, energy, temporal, and spectral features. However, they typically provide output radiation in the Gaussian spatial intensity distribution. While the majority of the scientific and technological applications require laser beams in Gaussian spatial distribution, however, in recent times laser beams with different spatial structures have also attracted a great deal of interest. For example, optical vortices are important for material processing, lithography, quantum information, particle manipulation and high-resolution microscopy. Similarly, Airy beam, a non-diffraction waveform, finds many applications in curved plasma wave-guiding, micro-particle manipulation for optically mediated particle clearing and light- sheet microscopy. The applications of all these different spatial structures extend across the entire electromagnetic spectrum. For example, optical vortices in the short wavelength region have their application in quantum and long-wavelength region such as mid-IR and THz vortices are essential for the spectroscopy. Similar, to optical vortices, Airy beam, and vector beams are prepared across the different spectral region from ultraviolet to mid-IR for various applications. For demonstrations of these applications, lasers in the Gaussian intensity distribution are used along with different phase elements. There are few conventional elements used for spatial beam shaping such as liquid crystal-based spatial light modulators (SLM) or dielectric phase elements. However, with new emerging and ever increasing applications of structured beams over different wavelengths, there is a humongous demand for their generation with high power and broad wavelength coverage.

Unfortunately, most of the commercially available lasers used for the generation of structured beams have certain drawbacks in terms of limited or no tunability, high cost, and complicated design. Some of the shortcomings can be overcome by choosing a proper system design. However, the generation of wide tunable radiation from a laser itself is limited by the availability of suitable gain medium. Such unavailability of gain medium restricts access to many wavelength regions ranging from the ultraviolet (UV) to mid-IR spectrum. Additionally, due to the normal dispersion, the phase elements used to generate structured beams are wavelength-selective. For example, a spiral phase plate used to generate optical vortices at 532 nm cannot be used for other wavelengths. While liquid crystal-based spatial light modulators can have limited wavelength coverage but such systems have lower damage threshold and do not provide high output powers. Moreover, all commercially available phase elements have limitations for the generation of structured beams in UV and the mid-

IR region due to the limitations of lithography techniques and high absorption in those wavelength regions. All these limitations restrict the generation of structured beams at a wide range of wavelengths using lasers

On the other hand, optical parametric oscillators (OPOs) have become a well-established technology to generate coherent radiations inaccessible to lasers. Based on the nonlinear frequency conversion process of a single pump laser, the OPOs produce optical radiation tunable over a wide wavelength range from UV to deep mid-IR region. Like lasers, the optical parametric oscillators have three basic requirements, pumping, gain medium and the optical cavity. However, in contrary to the lasers, the OPOs have instantaneous parametric gain along the direction of the pump. The OPO's are designed in various cavity configurations, like singly resonant, where one of the generated beams resonate, doubly resonant, where both the generated beams resonate, or triply resonant, where all the interacting beams resonate in the cavity to overcome the losses inside the cavity. While the parametric gain increases with the number of resonating beams in the OPO, however, the increase of the number resonating beams degrade the performance of the systems in terms of output power and the system stability. On the other hand, as the nonlinear parametric gain can be controlled using the pump intensity, the conventional OPOs utilize pump beam in Gaussian intensity distribution. Further, for efficient energy transfer among the interacting beams, the resonating beams oscillate in fundamental cavity mode of the oscillator producing output radiation in Gaussian intensity distribution. As such, to utilize the OPOs for structured beam generation, one need either manipulate the pump beam spatial structure or produce higher order cavity mode of the OPO through higher pump intensity. However, the spatial structuring of the pump lead to the lower parametric gain and subsequent increase in the OPO threshold as compared to conventional OPOs reported so far. On contrary, the increase of pump energy to increase the parametric gain to excite higher order cavity modes inside the OPO is restricted to the damage of the nonlinear gain medium. To overcome such challenges to generate structured beams directly from an OPO, one needs better OPO cavity designs for maximum gain extraction, and the selection of suitable cavity mirrors, nonlinear crystals and pump sources. In this thesis, we addressed the generation of various structured coherent beams including the Gaussian beam, optical vortex beam, vector vortex beams, Airy beam, and vortex Airy beam across the ultraviolet to the mid-IR region in all time scales (from ultrafast as well as continuous-wave) based on OPOs.

While the optical vortices are generated through the spatial mode conversion of the Gaussian beam using a transverse phase element, we tried to avoid the use of any phase element to generate optical vortices from a continuous-wave (cw), Gaussian beam pumped doubly resonating optical parametric oscillator (DRO). The basic principle of such vortex generation is the superposition of two Gaussian beams with lateral phase shift inside the OPO cavity. Using a 30-mm long MgO doped periodically poled lithium tantalate (MgO:sPPLT) crystal based DRO, pumped in the green by a frequency-doubled Yb-fiber laser in Gaussian spatial profile we have generated signal and idler beams in vortex mode of order, $\ell=1$, tunable across 970-1178 nm. Controlling the spatial overlap between the Gaussian pump beam with the fundamental cavity mode of the resonant signal and idler beams of the DRO through the tilt of the pump beam and/or the cavity mirror in the transverse plane, we

generated both signal and idler beams in vortex and vortex dipole spatial profiles. However, due to the high reflectivity of the cavity mirrors, the generated vortex and vortex dipole beams have substantially low output power. To increase the output power of the vortex beam we have explored the Gaussian beam superposition using an anti-resonant ring based picosecond OPO configuration. With the help of two mirrors of the anti-resonant ring, we introduced a linear phase in the superposed beams and successfully generated optical vortices in the near-IR region from 1457 to 1657 nm with output power in excess of 860 mW.

While we have successfully generated tunable vortex beam of substantial output power using an OPO without use of any transverse phase modulator, however, the order of the vortex by this technique is limited to $\ell=1$. Therefore, to generate higher order optical vortices using OPO, we have used vortex beam pumped OPOs. Conventionally, in singly resonant OPOs (SROs), the vortex pumping enables the generation of optical vortices in the non-resonant beam while resonating beam oscillate in Gaussian mode due to lower threshold and high gain. Therefore, we have demonstrated the control of orbital angular momentum (OAM) exchange among the interacting beams using a synchronously pumped by a picosecond SRO. Using vortex pump beam from a frequency-doubled Yb-fiber laser at 532 nm in the green we have demonstrated the successful transfer of the pump OAM mode to the non-resonant idler beam tunable across 1109-1209 nm, with OAM as high as $\ell_p=3$. Controlling the cavity loss and spatial overlap between the resonant signal and the pump beam in the nonlinear crystal, we have generated signal and idler OAM mode combinations, (ℓ_s, ℓ_i) of (0,2), (1,1) and (0,3), (1,2) for pump OAM mode $\ell_p=2$ and 3, respectively. Using a pump power of 1 W, we have generated idler OAM mode of orders, $\ell_i=1, 2,$ and 3, with maximum output powers of 202, 113, and 57 mW, respectively.

Further, we have demonstrated the generation of tunable, ultrafast optical vortices in mid-IR from a picosecond SRO. Using a SRO based on multigrating MgO doped PPLN crystal and synchronously pumped by a picosecond Yb-fiber laser centered at 1064 nm we have demonstrated for the first time an ultrafast OPO in the mid-IR spectral region pumped with pump vortex order as high as $\ell_p=5$. We have successfully demonstrated the transfer of pump optical vortices directly to the non-resonant idler beam, while the signal resonates in Gaussian cavity mode and generated optical vortices from 2538 nm to 4035 nm with a maximum output power of 1.6 W at vortex order of $\ell_i=1$.

To increase the span of wavelength coverage of the vortex beam OPO, we have generated optical vortices in the ultraviolet wavelength range using a continuous-wave (cw) OPO. Based on a MgO:sPPLT as the nonlinear crystal, the SRO is pumped by a cw vortex beam in the green, and deploying intracavity sum-frequency-generation (SFG) between the undepleted pump and the resonant Gaussian signal in the crystal second nonlinear crystal (BiB_3O_6), we have generated optical vortices of order, $\ell_{uv}=1$ and 2, tunable across 332-344 nm in the UV with a maximum power of 12 mW. Due to the conservation of orbital angular momentum in the parametric process, the OPO also produces non-resonant idler output beam in the vortex spatial profile of order, $\ell_i=1$ and 2, identical to the pump vortex, with the signal beam in Gaussian distribution. The idler vortex is tunable across 1172-1338 nm with a maximum output power of 1.3 W.

Given the nonlinear frequency conversion processes depend on the polarization state of the interacting beams, conventionally the OPOs so far produces vortex beams with uniform polarization in the transverse plane of the beam commonly known as scalar vortex beams. However, there exist another set of vortex beams known as vector vortex beams, where, the beams have space-variant polarization in the transverse beam plane. We have explored the possibility of generating tunable vector-vortex beams directly from the OPO source. Exploiting the orbital angular momentum conservation, we have systematically control the polarization of the resonant beam using a pair of intracavity quarter-wave plates to generate coherent vector- vortex beam tunable across 964-990 nm, with output states represented on the higher-order Poincaré sphere. The generic experimental scheme paves the way for new sources of structured beams in any wavelength range across the optical spectrum and in all time-scales from cw to the ultrafast regime.

While we have addressed the generation of vortex beams and vector vortex beams from OPO, however, each of those beams require a dedicated experimental setup. As a result, one need to design a dedicated experiment setup to generate the desire spatial structured beam. To avoid such difficulty, in the current thesis we have tried to address the possibility of generating tunable multiple structured optical beams from a single OPO source. Using vortex pumping and controlling the spatial mode and subsequent intracavity cubic phase modulation of the resonant beam of an OPO, we have successfully demonstrated the simultaneous generation of multiple spatial structures in the near-IR to mid-IR wavelength region. Using a synchronously pumped SRO with pump vortex order of $\ell_p = 2$ and controlling the pump OAM transfer between signal and idler, for OAM mode combination of $(\ell_s, \ell_i)=(0,2)$, we generated Gaussian and Airy beam in signal and vortex beam in idler wavelength range. On the other hand, for OAM mode combination of the signal and idler, $(\ell_s, \ell_i)=(1,1)$ we have further generated, vortex and vortex- Airy beam in signal and vortex beam in idler wavelength range. All these generated structures are tunable from 1457 nm to 1680 nm in signal and 2901 to 3944 nm in idler with excess power of 980 mW.

Title: Aspects of gravitational wave astronomy with coalescing compact binary sources
Researcher: Roy, Soumen
Supervisor: Sengupta, Anand S.
Year: 2020
Keyword's: Ground-based Interferometer, Gravitational waves - General relativity, Astrophysics, Data Stacking, Signal-to-noise Ratio
Call No.: 539.754 ROY
Acc. No.: T00759

Abstract: The detection of gravitational waves (GWs) from merging compact binaries by a global network of the highly sensitive ground-based interferometer has ushered in a new era in observational astronomy and fundamental physics. On the one hand, these sources provide a unique opportunity to carry out high-precision tests of general relativity, measure cosmological parameters, and understand the extreme astrophysics. On the other hand, they also pose several challenges, such as devising efficient ways of detecting such faint transient GW signals buried in non-stationary and non-Gaussian instrument noise, dealing with high-dimensional model space. In this thesis, we focus on two major aspects of these challenges and some of the challenges that remain. We begin with fundamental theories of gravitational waves in the theory of general relativity, review our present understanding of GW sources, and their possibility of detection with current and future detectors. We describe the techniques that have been developed to measure a tiny displacement in spacetime produced the GWs. We also briefly discuss the basic analysis strategies for searching the faint GW signals and reconstructing their source properties.

The detection of GW signals from compact binary coalescences relies on the matched-filtering of data against a set of theoretical waveforms. An efficient grid construction over the parameter space (template bank) has a direct impact on improving these searches' efficiency. For parameter spaces with flat metric, the construction of optimal template banks is an example of the *sphere covering problem*, which is achieved by the A_n^* lattice that is the best lattice-covering in dimensions $n \leq 5$. Unfortunately, the search parameter space of compact binaries is not flat. We present a new hybrid geometric-random template-placement algorithm that incorporates the efficiency of the A_n^* lattice and the robustness of the stochastic placement. We use this placement algorithm to construct an optimal template bank for non-precessing binary systems and compare with state of the art in template placement.

The higher-multipoles of GW signals from coalescing compact binaries play a vital role in the accurate reconstruction of source properties, bringing about a deeper and nuanced understanding of fundamental physics and astrophysics. The detection of higher multipoles of GW signals is exceptionally challenging due to its subdominant contribution to the full radiation. We present a new method for their detection by combining multiple events observed in interferometric GW detectors. Sub-dominant modes present in (the inspiral part of) the signal from separate events are stacked using time-frequency representation of the data. We demonstrate that this procedure enhances the signal-to-noise ratio of the higher-multipole components and thereby leads to increased chances of their detection.

Title: Improving low-latency gravitational wave search pipeline using numerical linear algebra

Researcher: Reza, Amit

Supervisor: Sengupta, Anand S.

Year: 2021

Keyword's: Gravitational Wave, Compact Binaries, Metric, Matched Filtering, Singular Value Decomposition, Random Projection, Matching Pursuit, Likelihood Ratio, Radial Basis Function

Call No.: 539.754 REZ

Acc. No.: T00760

Abstract: Improvements of sensitivity and bandwidth in advanced-Laser Interferometer Gravitational-Wave Observatory (LIGO) detectors pose a tremendous computational challenge for gravitational wave (GW) searches from astrophysical compact binary systems. Computationally improved algorithms for large scale data-analysis problems need to be incorporated to improve the search scheme. This thesis aims to develop advanced numerical methods to enhance the efficiency and scalability of the low-latency GW search pipeline, specifically focusing on the GstLAL-based inspiral pipeline.

Real-time search for a GW transient signal is an open and well-known problem in LIGO Scientific collaborations (LSC). Presently, there are four individual search pipelines- PyCBClive, GstLAL, MBTA, SPIIR that are being used for the detection of the GW signal from compact binary sources. However, none of them work in real-time due to the involvement of computationally expensive statistical measures such as Matched filtering. Hence, there is a need for alternative and efficient methods, which can reduce the latency of the search scheme, and enable the follow up of the electromagnetic counterpart of a GW signal. Addressing this research problem is crucial and challenging for the GW research community. The GstLAL pipeline has the lowest latency among all other current pipelines available for the search of the GW signal. The GstLAL search pipeline has several stages of analyzing the data collected by the detector. The first stage generated a set of the analytical waveforms and obtained a general representation of these waveforms based on a set of basis. The computation of the basis is done using singular value decomposition (SVD). However, the computational cost of obtaining a set of basis using SVD is not scaled well with the number of analytical waveforms. In the advanced LIGO era, it is expected that the number of waveforms will be increased. Therefore, the GstLAL pipeline is not optimal for the computation of the matched filtering with large and long waveforms. In this thesis, we proposed an advanced matrix factorization based on the randomized algorithms by which the computation of the basis for a set of a large number of waveforms is possible. Further, we have demonstrated the efficacy of the proposed algorithms for the fast decomposition of the large template bank.

In the second stage of the GstLAL search pipeline, vast numbers of triggers are generated as each detector collects and analyzes the data separately. Therefore, it is crucial to classify the noisy triggers, and the potential GW candidate triggers very quickly. However, it is a difficult task, as each detector has provided a massive number of triggers. In this thesis, we have proposed a fast multi-

detector coincidence test by which the classification of the triggers can be done in near real-time. Further, we have developed a fast interpolation scheme that can be used for the source reconstruction using the GstLAL framework. Currently, GstLAL does not have any source reconstruction module. We have shown that our proposed interpolation scheme can be useful for the development of the source reconstruction module. We have also developed an efficient algorithm for the computation of the components of the parameter space metric that can be useful for the optimal way of placing the template points in parameter space. The methods described in this thesis are directly applicable to the GstLAL pipeline, and incorporation of these methods will increase the computational efficiency of the GstLAL search pipeline. Hence, it will enhance the opportunity of discovering new transient astronomical phenomena in coincidence with GW triggers. In summary, this thesis mainly addresses the practical issues of the GstLAL search pipeline and tries to resolve them to improve its efficiency.

Title: Structure and dynamics of scientific collaboration networks of Indian researchers in APS publications
Researcher: Singh, Chakresh Kumar
Supervisor: Dey, Krishna Kanti
Year: 2021
Keyword's: Power-grid Network, American Physical Society - APS – Journals, Scientific Collaboration, Affiliation networks, Temporal Network Analysis
Call No.: 530 SIN
Acc. No.: T00761

Abstract: Many real-world systems such as power-grid network, a system of protein-protein interactions, traffic networks, internet, and scientific collaboration between researchers show complex dynamical patterns which cannot be explained just by its constituent elements. These systems are characterized by continuous interactions between their member elements. The study of complex networks has emerged as one of the most suitable fields to address both theoretical and application-based problems in diverse fields including Physics, Computer Science, Mathematics, Biology and, Social Sciences related to many real-world systems mentioned above. One such system is that of scientific collaboration. The nature and dynamics of scientific collaboration can be correlated with that of an organic entity that fits well with the definition of complex systems. Studies on both (i) aggregate large networks of scientific collaboration and (ii) more selective small-scale network studies have been abundant. This thesis is on the latter form of networks.

In my thesis, I have focused primarily on a community of Indian physicists who published in the American Physical Society journals between 1919 to 2013. I have presented an extensive analysis of the different forms of collaborations in various domains of Physics identified by different APS journals and explained their nature and dynamics as they evolve. This thesis constitutes three main contributions that have been published.

In the first study, we analyzed the evolution of the co-authorship network of Indian physicists publishing in the APS journals. This temporal study pointed out variations in trends in collaboration. The trends were quantified using network measures and were compared across different fields of Physics identified from the categories of APS journals. We found that while collaborations in PRA, PRB, and PRE are within smaller groups PRC, PRD, and PRL had larger group collaborations with more influence from foreign collaborators. On average the collaboration between Indian researchers was represented by short-living dynamic communities in the co-authorship networks in all sub-fields within the APS journals. In the second chapter, we used the metadata to construct affiliation networks between Indian research institutes. This work highlighted the collaboration between different academic institutes in India, categorized by the norms set by University Grant Commission (UGC) in India, and how it changed over time. We found that National Research Institutions (NRI), Central Universities (CU), and Institutes of National Importance (INI) dominated the research output in Physics based on APS data set Major cities in India like Delhi, Mumbai, Kolkata, Bangalore, Chennai were largest knowledge hubs for India followed by Kanpur, Allahabad, Ahmedabad, and Bhubaneswar. These cities are also known to host premier educational and research institutions in

the country. State Universities and State Colleges appeared to collaborate closely with institutions closer to them. Using citation exchanged within institutes we highlighted top knowledge sources and sinks in the institute-affiliation network.

Finally, the analysis was extended to correlated networks. We studied the simultaneous evolution of citation and co-authorship networks. In this work, we used probabilistic analysis to quantify the interdependence between evolving citation and co-authorship networks. We made inferences on the collaboration patterns by tracing the history of interactions between all possible author pairs in our data-set from 1970-2013. With a macroscopic approach, we found that majority of the citations exchanged were accounted for by co-author pairs. A very small fraction of pairs were connected with the shortest path greater than 1 in the co-authorship network but still had a significant contribution to the overall number of citations. Disconnected pairs, on the other hand, contributed to citations at the beginning of the network, but their contribution became negligible as the network grew and was more connected. Besides interactions between pairs, we also investigated the average probability of reciprocity in citations. The trends indicated that while, over time, the ratio of outgoing to incoming citations per author had increased. However, the ratio of pairwise outgoing citations that reciprocate citing authors decreased over time. We also observed the aging of collaboration strength, represented by mutual citations, between author pairs. Whereas, in microscopic calculations, we first calculated the average citations shared between all author pairs at all possible network distances to find that the number of average citations showed a steep decay up to shortest network distance ≤ 3 and then was almost stable for longer distances. That is, pairs that were more than distance three apart in the co-authorship network had a similar (and minimal) effect on citation patterns. To confirm the interdependence between citation networks and the associated co-authorship network we formulated a null model for the probability of an author and then using Bayes' formalism, we explicitly showed that the null model is indeed insufficient to explain the citing patterns. There is a significant effect caused by the distance between pairs of authors in the co-authorship network over their citing patterns.

Through the systematic analysis of the temporal networks constructed using our data-set, I have deduced how the structure of collaboration changes over time and what are the major factors that influence its dynamics. To the best of my knowledge, the work presented in this thesis is among the first studies that do such an intensive study on Indian physics researchers.

Title: Dynamical processes in brain networks: mass modelling approaches
Researcher: Tripathi, Richa
Supervisor: Miyapuram, Krishna Prasad
Year: 2021
Keyword's: Complex Networks, Nonlinear Dynamics, Synchronization, EEG, Neural mass models, Phase oscillators, Epilepsy, Spreading Depression, Modular brain network
Call No.: 612.82 TRI
Acc. No.: T00762

Abstract: The brain is arguably the most complex system that enables cognition owing to the presence of multiple spatial and temporal scales. The cumulative advances in neuroimaging technologies and experimental and theoretical neuroscience have exerted impetus on brain research. However, only when the research from the neuroscientific community is complemented by the principled approaches by physicists, larger aspects of the brain, and cognition can be understood. The theory of complex networks that leans on the framework of statistical physics and mathematics, and on graph-theoretical concepts from computer science, has seen growing attention from the physics community to understand non-trivial connection structure and its implications on the function of a complex system. Additionally, the framework is generalizable to incorporate characteristics of individual nodes on the top of simple connectivity matrices that describe network structure. The structural descriptors of brain network organization, (for example, the hierarchical structure, modularity, and small worldness) have been directly related to function through correlations with variables describing cognition and behaviour. The theory has also been successful in underpinning structural attributes to altered functional states; for example, the disease states like Alzheimer's, Schizophrenia, and Epilepsy. Moreover, the complex network modelling of the brain can be extended to various neuroimaging modalities such as EEG and fMRI. Another very important pillar that supports research in the brain is that of mathematical modelling and simulations of mechanisms and phenomena in the brain at various levels of the organization. Ranging from the simple model of action potential firing in neurons to sophisticated modelling of thalamocortical columns to understand sleep-wake transitions in animals, the computational neuroscience community has been successful in modelling brain functions at various levels of structural granularity. The neural mass models that capture a mean-field picture of a population of neurons and the synapses connecting them have successfully presented phenomenological descriptions of brain activity such as brain rhythms, synchronization- desynchronization transitions in the brain and sleep stages. The emergence of phenomenons in the brain from the interactions of complex patterns of its sub-systems obviates inherent nonlinearity. Hence, the dynamical systems theory and nonlinear dynamics are inevitable for the modelling and characterization of dynamics in the brain.

This thesis attempts to explore and understand the dynamics of brain activity at the mesoscopic level of brain organization i.e. at the level of brain areas/neuronal ensembles using tools from complex networks and nonlinear dynamics. Specifically, we aim to identify and characterize the complex non-linear dynamical patterns in brain activity and its implications on normal and pathological functioning. We use a plethora of neuro-computational models and use simulations on

networks to mirror the dynamics observed in the brain. In light of this goal, we did investigate the collective dynamics of coupled biological oscillators. Each of these oscillators (modelled using the Wilson-Cowan units) representing the mean activity of an ensemble of neurons, were connected to each other in a network framework. In an idealistic network topology, where each of the oscillators was identical in terms of external stimulation and its connectedness to the rest of the network, we find the existence of many complex non-linear patterns each characterized by a different basin of attraction as the coupling strength of these oscillators. Some of these patterns were: Exact synchronization, quasi-periodicity, gradient synchronization and chaos. Apart from the theoretical appeal of these collective oscillator states, these states, and their inter transitions hold significance in the biological aspects of brain functioning. For example, the transition to global synchronization mimics the transitions between interictal and ictal activity in the context of epilepsy. Similarly, transition to de-synchronization with increased coupling can explain the anesthesia-induced loss of consciousness in the brain. We also did a comparative study of variation in synchronization order parameter for the coupled thalamo-cortical oscillators and Kuramoto order parameter (when modelling the nodes as phase oscillators), due to the variation in the network topology. In other words, based on the collective dynamics observed for the two cases, we investigate which one of two scenarios is more apt for studying dynamics in the brain. Besides, we also investigated, which network structures (or connection topologies) support or make the network more prone to the seizure-like phenomenon (corresponding to large scale unwanted synchronization of neurons in the brain) than others. We explored aspects of synchronization in real brain topologies like the Macaque connectome and its surrogate counterparts. Further, we explored the effects of periodic stimulation on the collective dynamics of coupled oscillators. We find that periodic stimulation of coupled masses can lead them to coherence for a particular range of stimulation frequency, mimicking experimentally observed flickering- stimuli induced epileptic seizures in the human brain. In another neural mass modelling project aimed at modelling spatiotemporal patterns of Spreading Depression, we simulated the mechanism for initiation of Depolarization Block in compartmental neural masses of Hodgkin-Huxley neuron, excitatory neurons, inhibitory neurons. We aim to explore and identify the dynamical changes responsible for the seizure generation and propagation of depolarization block in a network of neural masses.

In our pursuit of exploring and modelling the mesoscopic brain activity, we carried out the analysis of EEG time series data to infer the modular structure of the functional brain networks in different frequency bands. In this work, the EEG time series from the human brain were recorded corresponding to different emotions to infer the specific functional connectivity of brain areas. This functional connectivity between brain areas was, in turn, dictated by the coherence or the amount of synchronization between the time series recorded from the overlying scalp region. Stronger functional connectivity indicates stronger synchronization or coactivity of the brain areas and vice versa. We then characterized the obtained brain networks using complex network measures to compare and contrast the brain functioning for the perception of different emotions. Further, we obtained the segregation of networks into modules and compared similarities and differences in the modular organization of the emotion networks. We identified the most important nodes or hubs for emotion perception using centrality measures.

In this thesis, we also propose an eigen-spectra based approach to identifying the important structure of complex networks. Such a formalism can be used to obtain a size-reduced representation of large complex networks that have redundant local structures. The subset network, as we show for a plethora of real and simulated networks, can be used to approximate the spectra of the full network; it also has enhanced information flow metrics than the original networks (measured in terms of path length and clustering coefficient). We also show that the subset can successfully be used to identify the modules of the network. Hence, in summary, this approach can be used to enormously reduce the computational burden for operations on large adjacency matrices i.e large complex networks. We provide the implementations of subset selection algorithms on the brain network of Macaque and extract its modular structure.

Title: Multiwavelength polarimetry of astrophysical sources
Researcher: Aarthy E.
Supervisor: Vadawale, Santosh V.
Year: 2021
Keyword's: X-ray Polarimetry, Cadmium Zinc Telluride Imager – CZTI, Gamma-ray Bursts – GRB, Infrared Polarimetry, Geant4
Call No.: 523.01 AAR
Acc. No.: T00763

Abstract: Polarization measurements of astrophysical sources could help in understanding phenomena that cannot be distinguished only through imaging, timing and, spectroscopy. Measuring polarization of the source over various regimes of the electromagnetic spectrum could address the nature of source geometry, emission mechanism behind the origin of photons, and magnetic field. Since polarization is not a directly measurable quantity, special components/techniques are needed to the measure polarization of any astrophysical source. In general, polarization measurement requires a large number of source photons. This makes measurement of polarization highly challenging, particularly in X-ray regime since X-ray instruments are space-borne. Polarization measurements in X-rays are achieved by measuring the modulation amplitude, which is the histogram of detected counts at various azimuthal scattering angles. The importance of polarimetry was realized in the early stages of X-ray astronomy and there were several attempts to perform polarimetry through rocket-based experiments. The first dedicated space-based polarimeter is a Bragg polarimeter onboard OSO-8 which reported the first reliable polarization measurement of Crab in soft X-ray band. Since then, over the past five decades, there has been no dedicated space-based X-ray polarimeter. Though there have been attempts to measure polarization through balloon-borne instruments, they have a disadvantage in limited exposure time. In the absence of dedicated polarimeters, there have been constant attempts to use the polarization capability of spectroscopic instruments. The modulation amplitude which gives the polarization fraction is a positive definite quantity. Hence, in case of low signal to noise, there are chances to measure definite polarization fraction even if the incident radiation is unpolarized. Hence it is important to experimentally verify the performance of a polarimeter with unpolarized X-rays. Major problems with utilizing imaging/spectroscopic instruments to do polarimetry is that they were not optimized experimentally for polarization measurements. Due to this reason, there are apprehensions in the scientific community to accept the results obtained from those instruments.

Cadmium Zinc Telluride Imager (CZTI), which is one of the payloads onboard India's first multiwavelength astronomical satellite AstroSat is one such imaging & spectroscopic instrument that could be optimized to perform polarimetry. Primary objective of CZTI is to perform imaging and spectroscopy over an energy range of 20 – 150 keV. The instrument employs pixelated CZT detectors that could be used to measure polarization. A major advantage of CZTI is that its polarimetric capability was experimentally demonstrated before launch using both unpolarized and polarized X-rays.

AstroSat was launched in September 2015, and post-launch CZTI was used to measure hard X-ray polarization of Crab pulsar and nebula, which is a standard candle in X-ray astronomy. While the hard X-ray (/soft gamma-ray) polarization of Crab was reported earlier (by INTEGRAL), the major advancement provided by CZTI is that it could measure polarization as a function of the pulse phase. Using Crab data obtained by CZTI over one year its operation, Vadawale et al 2018 (V18) showed a clear swing in polarization in the off-pulse region and the polarization properties are found to be different at two peaks of Crab. In addition to the data used in V18, CZTI has acquired Crab data over multiple observations. Here, we use this data to confirm the phase dependent signatures and also carry energy resolved phase dependent polarization analysis. Over the past 4 years of operation, Crab has been observed for ~ 1800 ks over multiple observations by CZTI out of which the results of ~ 800 ks data was reported in V18. Following up the work of V18, we perform phase resolved polarization analysis over 100 – 380 keV using ~ 1800 ks of CZTI Crab data observed over 4 years. The phase integrated and phase resolved polarization results over 100-380 keV are consistent with those reported by V18 with a better statistical significance. We obtain PF, PA of $33.4 \pm 4.1\%$, $143.6 \pm 1.7^\circ$ at 8.1σ for Crab and $35.2 \pm 7.4\%$, $144.2 \pm 3.0^\circ$ at 4.7σ for the off-pulse region. It is to be noted that, so far these are the results with the best statistical significance. Further, we extended the work by analyzing polarization over multiple energy ranges. A method of dynamic binning in energy, dividing the total energy range 100 – 380 keV into bins of 70 keV with a sliding window of 10 keV is performed for the first time. We obtained interesting results which show energy dependence in the polarization at both the peaks, bridge, and off-pulse region.

The polarization measurement of Crab in hard X-rays using CZTI prompted two branches of possibilities. First is to use CZTI to the measure polarization of other hard X-ray bright sources. The second is to probe the possibility of performing multiwavelength polarimetry of Crab.

Besides observing persistent sources like Crab, CZTI is also a prolific Gamma- Ray Burst (GRB) detector. This provides an opportunity to utilize CZTI to perform polarization of GRBs in hard X-ray regime. One advantage of GRB polarization using CZTI compared to Crab is the high signal to noise ratio, resulting in better sensitivity. However, a drawback is that GRBs are randomly distributed in space and time and they last for a very short time (fractions of seconds to few seconds). Hence in general Monte Carlo simulations are essential in GRB polarization analysis. We developed the AstroSat Mass model using Geant4 to perform required simulations for CZTI GRB polarimetry. CZTI detected 47 GRBs between October 2015 to October 2016 out of which we report polarization of 11 bright GRBs.

A statistical study on GRB polarization could help in understanding the emission mechanism behind GRB prompt emission and the nature of the magnetic field along the jet. This demands precise polarization measurement of a large number of GRBs. Hence, CZTI, which measured polarization of 11 GRBs detected over a year is of great importance to the GRB polarimetry community. However, one caveat is that the polarimetric capability of CZTI for off-axis sources is not experimentally demonstrated. Experimental confirmation of CZTI to be used to perform polarimetry in case of pointed observations is the factor that makes CZTI unique from other non-optimized polarimeters.

However, experimental confirmation for such capability is not available for non-dedicated GRB polarimeters including CZTI. In this context, we performed controlled experiments using CZT detector and complemented the experimental results with extensive Geant4 simulations. Our results show that CZTI can be used to measure the polarization of bright GRBs up to the off-axis angle of $\sim 60^\circ$.

With firm polarization measurements of Crab in X-rays, we explored the possibility of measuring Crab polarization in other wavebands. Although polarization reports of Crab are available in radio, optical, X-rays/Gamma-rays, interestingly no such report of polarization exists in the infrared regime. The Mount Abu Infrared Observatory (MIRO), is one of the facilities of Physical Research Laboratory (PRL) that has a 1.2 m Cassegrain f/13 telescope and various optical and infrared back end instruments. The Near Infrared Camera and Spectrograph (NICS) is a workhorse instrument which is capable of doing imaging and spectroscopy in the near IR regime. The accessibility of MIRO and NICS provided the motivation to explore the possibility of measuring the near IR polarization of Crab. We added imaging polarimetric capability to NICS (NICSPol) by mounting a rotating wire grid polarizer between the telescope optics and NICS. NICSPol covers a wavelength range of 0.8 to 2.5 μm over H, J and Ks bands. We verified the performance of NICSPol by observing a set of polarized and unpolarized standards. The results show that NICSPol can constrain polarization within $\sim 1\%$ for sources brighter than ~ 16 magnitude in JHKs bands. NICSPol is the only imaging IR polarimeter in India and would provide a fantastic opportunity to do simultaneous polarimetry of various astrophysical objects over a wide range of EM spectrum.

In a nutshell, we performed energy dependent polarization of Crab using AstroSat CZTI data with respect to the pulse phase. We obtained Crab polarization results with the best statistical significance so far in the hard X-ray regime. Apart from persistent sources like Crab, CZTI also serves as a good GRB detector. Hence we performed polarimetry of GRBs detected by CZTI over a year and obtained polarization of 11 bright GRBs with good statistical significance. The GRB polarization results using CZTI are promising, but to enhance the credibility of these measurements we carried out controlled experiments and simulations with polarized and unpolarized incident X-rays to validate the off-axis polarimetric capability of CZT detectors. This ensures that pixelated CZT detectors could be used to perform GRB polarimetry. These works which comprise the thesis have resulted in significant advancement in the field of astrophysical polarimetry. By achieving the hard X-ray polarization of Crab we explored the possibility to measure polarization of Crab in the infrared regime by developing NICSPol, as an add-on to NICS at MIRO, PRL. Currently, NICSPol is the only imaging infrared polarimeter in India.

Title: Infrared astronomical instrumentation and polarisation studies
Researcher: Rai, Archita
Supervisor: Ganesh, Shashikiran
Year: 2021
Keyword's: Optical Design, Multi-function Infrared Instrumentation, Dual Beam Polarimetry, Interstellar Polarisation, Optical Design, Dual Beam Polarimetry, Multi-function Infrared Instrumentation, Lynds Clouds
Call No.: 522.2 RAI
Acc. No.: T00764

Abstract: The spectacular night sky with its vibrant stars is our own Milky Way Galaxy. The observations for the Galaxy dates back to the time when Galileo first used a telescope (1608-10) to observe the night sky. His conclusion was that the Milky Way is a vast collection of stars. Subsequently, many astronomers have worked extensively to bring up our current understanding of the Milky Way as a spiral galaxy. Polarisation has been seen in the light from the stars in the Galaxy - particularly those close to the plane. Stars, being spherically symmetric, one does not expect the light to be polarised and certainly not in a coordinated (aligned) manner, hence it was realized that this was due to the medium through which the light had travelled. This was the discovery of interstellar polarisation. The current understanding is that the asymmetric dust grains in the interstellar medium get aligned in the Galactic magnetic field giving rise to interstellar polarisation. Hence, measurement of polarisation is a way to measure the Galactic magnetic field - both strength and direction, in some conditions.

The inner regions of the galaxy have always been obscured from our view at optical wavelengths, because of the intervening clouds of dust. Therefore, our knowledge of the Milky Way structure and how the different components have been formed and put together can only be enhanced by surveying the galaxy at near and mid-infrared wavelengths. But most of these large scale surveys, until recently, were confined to imaging and spectroscopic studies, leaving behind the polarimetric observations which demands a thorough study in the regions of heavy dust presence. By studying the polarization distribution, one can get additional information about the magnetic field (its geometry & strength) and study the dust present in the region. One expects that there should be a correspondence of the distribution of molecular clouds in different directions with the distribution of dust (which causes extinction and polarization). A polarimetric instrument in the near infrared is therefore a very valuable means to study the polarization distribution along the line of sight (in combination with distance determined using different techniques - e.g. red clump method, parallax etc).

The science part of the thesis has addressed the interstellar polarisation phenomena using the PRL 1.2 m telescope with the NICSPol instrument. The observations of a dark Lynds cloud L1340 have been undertaken and polarisation measurements for stars part of the cloud have been reported in the J, H & K_s bands. The plane of the sky magnetic field strength has also been estimated for the RNO 8 cluster and cloud core, which is a part of the L1340 cloud. The observations were taken using

a wire-grid module (WGP) as analyzer on the near-IR camera & spectrograph (NICS) instrument. This work underlines a very promising scientific approach and impresses on the need for a more versatile instrument with improved accuracy in polarisation measurements, and negligible thermal contribution from the optics. This is one of the major scientific goals which led us to develop NISP (Near-IR Imager, Spectrometer & Polarimeter) as a new multi-function near-infrared instrument for PRL's upcoming 2.5 m telescope at Mount Abu.

The major part of the thesis covers the instrumentation part and includes the optical design of NISP which has been completed with optimization of the design at each step. The instrument offers multimode capabilities of imaging, spectroscopy and polarimetry in a single package. The different modes in the instrument have been realised using components whose designs were custom made to achieve the specifications required in the instrument. Several options were explored with the manufacturers since the components would be fabricated at room temperature but used at cryo temperatures at NIR wavelength ($0.9 \mu\text{m} - 2.5 \mu\text{m}$). This posed various challenges and constraints. With several constraints of meeting instrument specifications, instrument size limit, performance at cryo temperature etc., the optical design had been completed. The collimator optics design is a F/8 system with a collimated beam width of 38 mm, and the camera design necessary for our instrument specifications is F/5. The design has achieved a full unvignetted imaging field of view of $10j \times 10j$, and a spectral resolving power ~ 2150 across all filters in the near-infrared. It implements single shot imaging polarimetry using wedged double Wollaston as an analyser. The dual beam polarimetry technique, will benefit many scientific projects with an improved precision in the observational data. The dual beam method helps in using the full light, by not wasting half of the orthogonal component of polarization. This also cancels the Earth atmosphere effects by the ratio of intensities taken amongst orthogonal components. Hence, this allows the observers to work on targets with low polarisation or sources with intrinsically variable polarisation behaviour on short time scales. Some example science programs are: polarisation study of the interstellar regions of the Milky Way, mainly involving polarisation study of larger molecular clouds, clusters, globules etc. & variability of AGN polarisation on short timescales, wherein polarisation variability has been noticed on short timescales (order of a few minutes) which need a simultaneous measurement mode, to obtain better polarisation accuracy. These will be addressed once the instrument is commissioned.

The thesis work illustrates the intricate details of the optical design of a near infrared multimode instrument and its fulfilment with robust attributes, in terms of the implementation of the various modules, in the NISP instrument for PRL's upcoming 2.5 m telescope.

Title: Understanding the properties of accretion powered Be/X-ray binary pulsars
Researcher: Gupta, Shivangi
Supervisor: Naik, Sachindranatha
Year: 2021
Keyword's: X-ray Binaries, Accretion Powered Pulsars, Magnetic Fields, Accretion, Pulse Profiles, Spectroscopy, Pulse Phase Resolved Spectroscopy, Critical Luminosity
Call No.: 522.6863 GUP
Acc. No.: T00765

Abstract: This thesis is dedicated to understand the timing and spectral properties of accretion powered Be/X-ray binary pulsars. Accretion powered binary X-ray pulsars are system of highly magnetized neutron stars which accrete matter from non-degenerate companion and subsequently get powered in X-ray regime. Neutron stars are among the most compact objects in the universe, which contain more than a solar mass confined within spheres of ~ 10 km radii. This results in an average density of a neutron star to be $\sim 10^{14} \text{g cm}^{-3}$, i.e. as high as that of the nuclear matter. Apart from the extreme density, the magnetic field of neutron star in these binary systems is of the order of 10^{8-12} G. These aspects make them one of the most exotic objects in the universe. Therefore, study of the accretion mechanism in these systems provide us with the opportunity to probe the properties of matter under extreme conditions, which otherwise is impossible to achieve through laboratory experiments.

During the process of accretion, the matter accreted from the non-degenerate optical companion follows the magnetic field lines and gets dumped onto the magnetic poles of the neutron star. This forms an accretion mound on the magnetic poles of the neutron stars. However, when the mass accretion rate is high, a column like structure, known as the 'accretion column', is formed at the magnetic poles of the neutron star. A radiation dominated shock is expected to form in the accretion column which decelerates the infalling plasma before settling on to the surface of neutron star. Consequently, the surface temperature at the magnetic poles reaches as high as 10^7 K, resulting in X-ray emission. The interaction of this radiation with the infalling plasma, through complex physical processes, shapes the resulting spectral continuum of the neutron star. As the spin and magnetic axes are usually misaligned, the beam of X-ray radiation from the magnetic poles of the neutron star can be detected once it sweeps through the line of sight of the observer. This result in apparent X-ray pulsations, hence the neutron star in these systems is known as pulsar.

The emission characteristics of this radiation depend upon the mass accretion rate and hence on the luminosity. Therefore, it is interesting to investigate the characteristic properties of these X-ray sources at different luminosities. One such class of X-ray binaries, showing extreme variability in terms of luminosity is, Be/X-ray binary pulsars. The neutron star in these systems revolve in a wide eccentric orbit around its Be optical companion and remain in quiescence most of the time. However, once it approaches the periastron, mass accretion from the circumstellar disk of the Be star becomes possible and the neutron star consequently show strong X-ray outburst activities, known as Type I outburst. The X-ray luminosity during these outburst events can reach as high as

10-100 times the quiescent luminosity ($L_{\text{quiescent}} \approx 10^{34} \text{ erg s}^{-1}$). Another kind of X-ray enhancement, i.e. Type II outbursts are also detected from these systems. The Type II outbursts are rare and independent of the orbital motion of the binary system. The X-ray luminosity during these (giant outburst) events may even reach as high as $\geq 10^{38} \text{ erg s}^{-1}$. Due to extreme variability and strong mass accretion rate during these X-ray outburst events, Be/X-ray binaries are ideal sources to study the luminosity dependence of the emission characteristics of the X-ray pulsars, which is the main focus of the present thesis.

In this work, I have carried out a detailed and systematic investigation of the spectral and timing properties of Be/X-ray binary pulsar 2S 1417-624. Using large number of *RXTE* pointed observations, taken during the 2009 giant X-ray outburst of 2S 1417-624, a systematic change in the shape of the pulse profile of the pulsar was observed. The pulse profiles were found to exhibit a transition from two-peak structure to three-peak during the rise of 2009 Type II outburst, while a reverse trend was observed during the outburst decline. At the same time, the pulsed fraction of the pulsar was found to be anti-correlated with the source luminosity. This kind of variation was never seen previously, for any kind of X-ray activity observed from this source. In order to probe the cause of such variation, a detailed phase averaged and pulse phase resolved spectroscopy was performed for each epoch of the observation. The spectral continuum was found to be described well with an absorbed cut-off power law model with an additional Gaussian component for the iron emission due to Fe K_{α} . The dependence of the spectral parameters on the source luminosity was studied for the first time in great detail. It was found that the observed changes in spectral and timing properties of the pulsar pointed towards the change in the accretion geometry close to *critical luminosity* regimes. This subsequently allowed to constrain one of the most fundamental physical parameter of the pulsar, i.e. magnetic field strength, by using the relation between critical luminosity and the magnetic field strength (Becker et al., 2012).

Recently in 2018, 2S 1417-624 showed another giant outburst activity and was observed simultaneously with *NuSTAR* and *Swift* X-ray observatories at the outburst peak. This was the most luminous outburst detected from the pulsar till date and provided a unique opportunity to carry out a systematic analysis of the emission characteristic of the pulsar at even higher luminosity. The pulse profiles of the pulsar during this event was found to evolve further to four-peak structure. This was a direct observational evidence of the strong dependence of the emission geometry of pulsar on the mass accretion rate. The phase averaged spectrum of the pulsar was different as compared to its previous outburst events and found to be described only with a composite model consisting of an absorbed cut-off power law model, a Gaussian component for iron fluorescence emission and an additional blackbody emission component with a temperature of $\approx 1 \text{ keV}$ (soft X-ray excess). The detection of soft-excess emission in the pulsar spectrum is quite rare. Therefore, a detailed pulse phase resolved spectroscopy was performed in order to probe the origin of this component. Moreover, a detailed physical modeling was carried out for the first time in this work to describe the X-ray spectrum of 2S 1417-624 self consistently, using physically motivated spectral continuum model COMPMAG (Farinelli et al., 2012). The results obtained from these studies are discussed in great detail in the thesis.

Title: Emission and atmospheric variability of volatile organic compounds over the Indian subcontinent and surrounding oceanic regions

Researcher: Tripathi, Nidhi

Supervisor: Sahu, Lokesh Kumar

Year: 2020

Keyword's: Volatile Organic Compound, BVOCs, Ozone formation potential, PTR-TOF-MS, Urban/suburban Arabian Sea, IGP, Isoprene, Alkenes

Call No.: 570 TRI

Acc. No.: T00766

Abstract: Volatile organic compounds (VOCs) are ubiquitous organic gases present in the Earth's atmosphere at trace levels. VOCs are categorized mainly into the major groups of non-methane hydrocarbons (NMHCs) and oxygenated-VOCs (OVOCs). NMHCs are primary VOCs emitted from biogenic and anthropogenic sources, while both primary and secondary sources contribute to OVOCs. However, based on their major global emission sources, VOCs are also classified as anthropogenic VOCs (AVOCs) and bio-genic VOCs (BVOCs). In the troposphere, VOCs are precursors for the formation of secondary organic aerosols (SOA), and ozone (O_3) in the presence of oxides of nitrogen ($NO_x = NO + NO_2$) and sunlight. The reactions of VOCs with hydroxyl (OH) radicals control the oxidation capacity of the atmosphere. Therefore, the levels of VOCs can change the atmospheric lifetimes of important trace gases such as methane (CH_4) and carbon monoxide (CO). Atmospheric chemistry is complex over the Indian subcontinent due to the vast geography with different climatic zones and the existence of a variety of both natural and anthropogenic sources. India is one of the fastest-growing countries in Asia experiencing severe air pollution due to the rapid urbanization and increased use of automotive vehicles. Thus far, the measurement-based studies of VOCs in India are limited and focused mainly on AVOCs in urban regions. Lack of representative parameterization of BVOCs emission, particularly from the tropical biosphere, is one of the largest sources of uncertainty in the chemistry-climate model.

This thesis presents important results based on the measurements of the mixing ratios of VOCs in different terrestrial and oceanic regions of the Indian subcontinent. The ambient concentrations of VOCs were measured using the proton transfer reaction-time of flight-mass spectrometry (PTR-TOF-MS) and thermal desorption-gas chromatograph-flame ionization detection (TD-GC-FID) in the urban, suburban, forest and oceanic regions of India. The results and discussion presented in this thesis are based on a large dataset of the ambient concentrations of various VOCs and other trace gases. The meteorological and biological parameters are also used to support the interpretations. Ocean microbes and dissolved organic compounds are important natural sources of many NMHCs in the remote marine atmosphere. The Arabian Sea is one of the most biologically productive ocean regimes and hence possesses a perennially intensive oxygen minimum zone. High productive oceans have the potential to modify the production and sea-to-air exchange of trace gases including VOCs. This study combines the NMHCs data measured in the marine air with the physical and biological parameters of seawater. In this interdisciplinary study, seawater parameters are used to explain the distribution of NMHCs in the marine atmosphere over the Arabian Sea. A brief comparison with

measurements reported over the Bay of Bengal and other oceanic regions of the world has also been presented. The emissions of NO_x from international ship traffic in the Indian Ocean (especially the Arabian Sea and the Bay of Bengal) have increased significantly. In summary, this study suggests strong interactions between marine-derived VOCs with anthropogenic emissions (shipping and transport from the land) over the Arabian Sea.

The contributions of natural and anthropogenic sources of VOCs can vary on the local and regional scales. In urban regions of the developing countries, fossil fuel use is one of main anthropogenic sources of VOCs in the ambient air. The other sources such as biomass/biofuel burning and biogenic emissions, also make significant contributions depending on the season. However, the separation of anthropogenic and biogenic contributions of VOCs in urban air is not straightforward because of their emissions from various common or co-located sources. The study highlights the complex emission and atmospheric processes of VOCs impacting atmospheric chemistry in the urban/suburban regions of India. In the urban region, emissions of BVOCs can have significant implications on regional atmospheric chemistry related to the production of ozone and secondary organic aerosols. The measurements of BVOCs, especially monoterpenes, were performed using PTR-TOF-MS at a semi-arid site in western India during the winter-to-summer transition period. This study presents the best data of monoterpenes for the Indian region owing to high time- and mass-resolutions of PTR-TOF-MS. Dependence of monoterpenes on meteorological parameters such as temperature, sunlight, humidity, etc. has been analyzed in detail. A significant increase of biogenic monoterpenes during the winter to summer transition was associated mainly with the change in the meteorological parameters.

Many urban regions, mostly over the Indo-Gangetic Plain (IGP) of India, face severe air pollution episodes. Simultaneous measurements of VOCs using two PTR- TOF-MS instruments at the urban and suburban sites of New Delhi were conducted during the winter season. This study presents the contributions of anthropogenic and biogenic/secondary sources of OVOCs and isoprene in ambient air. We estimated significantly higher biogenic contributions of isoprene at the suburban site than those at the urban site. The study also reveals the roles of the photochemical transformation of primary VOCs to OVOCs both in the urban and suburban regions. The data and results provide an improved understanding of the regional tropospheric chemistry leading to ozone and SOA formation in the urban and suburban regions. The thesis also briefly presents the results of the measurements of biogenic C₂-C₅ NMHCs emitted from the tropical evergreen forest of central Western Ghats (WG) of India. There is significant biodiversity in the WG due to the variation in altitude, soil, slope, etc. This is the first study reporting the measurements of light alkenes in the forested WG. We found the significant impact of biogenic emissions of VOCs in the forms of alkenes and isoprene from the tropical evergreen forest. This work indicates the significant implications of biogenic emissions on alkenes in atmospheric chemistry over remote terrestrial regions of India.

Overall, we have highlighted the critical needs to address the current lack of knowl- edge of BVOC and OVOCs emissions focused on atmospheric chemistry leading to the environmental and climate change over South Asia. The results presented in this thesis reveal significant roles of BVOCs in tropical atmospheric chemistry.

Title: Investigation of martian dust devil characteristics
Researcher: Uttam, Shefali
Supervisor: Sheel, Varun
Year: 2020
Keyword's: Mars, Martian Atmosphere, Dust Devil, Boundary Layer, Convective Vortex, Dust Lifting, Electric Field
Call No.: 551.51 UTT
Acc. No.: T00767

Abstract: The Martian Planetary Boundary Layer (PBL) is the lowest 10 km of the atmosphere that is directly influenced by the surface forcing, leading to a strong vertical mixing in the atmosphere. The dust, entrained into the PBL and consequently transported to large distances, affects the thermal and dynamical state of the Martian atmosphere. Thus, it is important to study the processes by which dust can enter in to the atmosphere, for which convective vortices have been proposed as an efficient mechanism. Convective vortices form due to heating of the surface by solar flux, leading to the formation of unstably stratified atmosphere, and hence a strong convection. The winds within the vortices have vorticity in it which makes the structure rotate. They are also accompanied by a pressure drop inside the vortex. The vortices in which winds and pressure drop are strong enough to pull dust from the surface into the atmosphere are called “dust devils”. The objective of my thesis is to study various characteristics of Martian dust devils, and their quantitative investigation. The research work comprising my thesis is based on the steady state vortex systems. Mean physical conditions, such as that for vortex wind speeds, size of vortex, atmospheric pressure and density, have been used to study vortex properties and characteristics using analytical and numerical approaches. Characteristics of convective vortices and dust devils have also been studied based on observations from a rover on Mars.

Using an analytic approach to solve the Navier Stokes equation, we have derived a simple equation for the mean tangential velocity for a vortex. Unlike other analytical solutions for vortices, our solution is dependent on the few atmospheric parameters that vary with altitude. Later, we use in-situ meteorological data recorded by NASA’s Curiosity rover, to detect convective vortex events on Mars. Some of these vortex events show obscuration in solar flux data which are identified as a possible dust devils. A seasonal variation of these events suggest that they are frequent during the local summer season, during which the pressure drop associated with the vortex events are also high compared to other seasons. Lifting and distribution of dust are yet not well estimated within dust devils, for which we have provided a quantitative estimate, based on our studies. Our simulations indicate a maximum concentration of particles near the surface and at the boundary of the vortex. The larger sized particles are lifted to lower heights, as compared to its smaller counterparts. This supports the fact that within a dust devil the dust particles are distributed as per their mass along the height. The larger (heavier) particles are mostly present in lower part of the dust devils whereas, the smaller (lighter) particles move to higher heights. Finally, we have modeled electric fields within the dust devils. Due to tribocharging the dust particles get charged depending on their size. A charge separation within the dust devil gives rise to an electric field, which has

important potential in lightning generation. We find that the electric field reaches the breakdown value faster in dust storm scenario as compared to non-dust storm scenario. A vertical exponential distribution of charged particles will lead to development of lower electric field than the dipolar configuration of charged particles.

Title: Probing New Physics with hadronic final states at the Large Hadron Collider
Researcher: Bhardwaj, Akanksha
Supervisor: Konar, Partha
Year: 2020
Keyword's: Beyond The Standard Model, Jet Substructure, TeV Scale Seesaw, Extended Scalar Sector, Compressed SUSY, Higgs CP Violation
Call No.: 530.1298 BHA
Acc. No.: T00768

Abstract: The Large Hadron Collider (LHC) fixes the last missing bit of the Standard Model by the remarkable discovery of the Higgs boson in 2012. The LHC now opens a new paradigm with the underlying motivation for determining properties of the Higgs boson and searching for new physics. Many Beyond Standard Model (BSM) theories predict heavy resonances which predominantly decay to particles like W , Z , the Higgs boson or the top quark. Study of these model in hadronic final states become very important due to high branching fraction of these particles into jets. However, large quantum chromodynamics (QCD) background makes the study of hadronic final states remarkably difficult. Recent techniques like jet substructure can be very useful in studying the boosted jets produced through the decay of highly energetic heavy particle. Many jet substructure variables are proposed which are inspired by the idea of different energy distribution between the decay of heavy boosted particle and fragmentation of highly energetic partons. These techniques are utilized to explore the TeV scale BSM models. In this thesis, we explore BSM models such as inverse seesaw, inert doublet model, compressed supersymmetric (SUSY) scenario and CP violation in the Higgs sector. These models can address some of the outstanding issues of the SM like neutrino mass generation, dark matter etc. We propose new search strategies using the boosted topology in hadronic final state to probe the BSM physics at the LHC.

First, we discuss the inverse seesaw model which is an elegant and simple mechanism to generate the small neutrino masses at TeV scale together with a large coupling to probe at the LHC. We study collider signatures of heavy pseudo-Dirac neutrinos with a sizable mixing with the SM neutrinos under two different flavour structures, viz., Flavour Diagonal and Flavour Non-Diagonal scenarios. We probe the heavy pseudo-Dirac neutrinos with the opposite-sign di-lepton associated with a fat jet signature at the LHC. The heavy mass sterile neutrinos decay leads to boosted fat jets arising from W boson hadronic decays and helps to overcome the enormous background of opposite sign di-lepton. This signature is very important as it is the characteristic for a class of models with Dirac or pseudo-Dirac type neutrinos. We perform a comprehensive collider analysis to demonstrate the effectiveness of this channel in both scenarios. The bounds on the right-handed neutrino mass and mixing angles are significantly enhanced and are at least an order of magnitude better than existing limits at the 13 TeV LHC.

Next, we explore the Inert Doublet Model (IDM) which is a minimal extension of the SM that can provide a viable dark matter (DM) candidate which satisfies the observed relic density in different parameter region of the model. We study the challenging hierarchical mass spectrum of the IDM where relatively light dark matter along with much heavier scalar states can fully satisfy the constraints on the relic abundance along with all other theoretical, collider and the astrophysical bounds. The significant mass differences between DM candidate and other scalars present in the model give rise to interesting signal topology characterized by two boosted jets along with large missing transverse energy (MET) from the DM production. With this topology, we capture a hybrid process where the di-fat jet signal is significantly enhanced by the mono-fat jet contribution. We adopt the method of multivariate analysis using jet-substructure observable as inputs. This study brings the entire parameter space well within reach of the 14 TeV LHC runs with the first phase of high luminosity (HL-LHC).

We also study the compressed SUSY scenarios with a higgsino-like X_1^0 as the next-to-lightest sparticle (NLSP) and a light keV-scale gravitino (G) as the LSP and potential dark matter candidate. A multi-TeV scale higgsino like NLSP decays highly boosted Higgs or Z bosons along with large MET. At this high energy, capturing the Higgs based on double b-tagger will not be useful as b-tagging deteriorates its efficiency at this high momenta. Rather we utilize 2-prong finder to capture Higgs as well as Z boson in the final state. This method can cover up to 3.2 TeV scale of such compressed SUSY spectrum at HL-LHC. We also design observables which can distinguish between the compressed and uncompressed spectrum.

The new physics signature may be hidden inside the Higgs sector itself. Hence the measurements of Higgs properties are crucial. Therefore, we study the CP properties of the Higgs by determining the CP-violating phase in the $H_{\tau\tau}$ Yukawa coupling. In this study, we present the several CP odd observables which are sensitive to the CP-violating phase of the $H_{\tau^-\tau^+}$ coupling. We also propose a novel method to reconstruct the τ momenta.

In this thesis, we demonstrate the efficacy of jet-substructure variable in various model and probe the most challenging parameter space of these models. The analysis presented in this thesis can be applicable to a wide range of BSM models due to its generic nature.

Title: Warm inflationary universe at the large and the small scales
Researcher: Arya, Richa
Supervisor: Rangarajan, Raghavan
Year: 2020
Keyword's: Cosmic Inflation, Warm Inflation, Dissipation Coefficient, Primordial Power Spectrum, Primordial Black Holes, Initial Mass Fraction of Black Holes
Call No.: 530 ARY
Acc. No.: T00769

Abstract: The Standard Big-Bang Model (SM) of Cosmology has been a widely accepted and successful framework in describing the post Big-Bang Nucleosynthesis (BBN) evolution of our Universe. But certain difficulties arise when one tries to explain the observations of the early Universe, like the extreme homogeneity and isotropy of the cosmic microwave background radiation, within this description. Thus, to overcome these shortcomings and probe an insight to the early Universe, a phenomenon known as '*Inflation*', is introduced. Inflation is a phase of a rapid accelerated expansion of the early Universe during which the physical distance between any two spatial points in the Universe grows tremendously (nearly exponentially) within a brief time. It is proposed to have taken place when the Universe was in its initial stages (within 1 second of its formation). The inflationary paradigm of the early Universe efficiently resolves the problems faced by the SM, as well as explains the current observations very precisely. As an additional feature, it also provides a mechanism to generate the density inhomogeneities that become the seeds of the Large Scale Structure (LSS) at late times, which supplements its importance and success.

There are two approaches to explain the dynamics of inflation. The first one is the standard cold inflation. In this description, as the Universe inflates, the number densities of all the species present at that time dilute away, and the Universe attains an almost supercooled state during the inflationary phase. On the other hand, there is a second description, known as *Warm Inflation*, in which the dissipation processes during the inflationary phase are taken in account. During expansion, a thermal bath of particles (radiation) is created from the inflaton dissipation and thus, the Universe has a non-zero temperature during warm inflation.

The two descriptions of inflation have different microphysics that governs them. In warm inflation, one accounts for the inflation couplings to the other fields during inflation, unlike in cold inflation where they are neglected. Because of these couplings, the inflation dissipates its energy, which is quantified in terms of a dissipation coefficient. Thus, warm inflation is a broader and more general description, with cold inflation as its limiting case. The dynamics of the Universe are different in the two scenarios and lead to significant distinctions in the theoretical predictions of the cosmological observables. In this thesis, I consider a few models of warm inflation and discuss their signatures in the large and small scale observations.

The observational test of any inflationary model is carried out by examining the imprints of inflation on the Cosmic Microwave Background (CMB) radiation. CMB radiation - the earliest signals of the Universe, refers to the primordial photons present in all directions of the sky. The CMB temperature is observed to be uniform over the entire sky to high precision, with some tiny anisotropies of the order of 1 part in 10^5 . The anisotropies in the CMB temperature is evidence for the existence of fluctuations in the energy density of the primordial Universe and is studied using the linear theory of cosmological perturbations. The origin of these anisotropies is attributed to the inflationary phase, therefore features in the CMB act as a probe to the physics of inflation. The correlations in the CMB anisotropies are described in terms of a primordial power spectrum, and are quantified by the amplitude of the primordial power spectrum, A_s , the scalar spectral index, n_s , and the tensor-to-scalar ratio, r . With the precision measurements of the CMB, stringent bounds have been put on the parameters n_s and r . Hence, in order that any inflationary model is a viable one, its theoretical estimates of the cosmological parameters must be consistent with the observational measurements.

Constructing a model of inflation from fundamental particle physics has always been elusive. The ultimate goal of model builders is to make a connection between the inflationary theory and the elementary particle physics theory of the early Universe. This requires a knowledge of the parameters of the inflation model such as the masses, couplings, and multiplicities of the fields involved. Therefore, an estimation of the model parameters consistent with the observations is essential for the inflation model building. In the first part of the thesis, I consider some models of warm inflation with monomial potentials and explore their microphysics in terms of the inflaton self-coupling, and its dissipation to other fields characterized by a dissipation parameter. Using the CosmoMC numerical code, I estimate the values of these model parameters for which these models are consistent with the CMB observations. In our analysis, it is seen that for some parameter values, these models are viable models of inflation. Further, I also calculate the n_s and r values for the mean values of the parameters and show that for the weak dissipative regime, r is within the sensitivity of the next generation CMB polarization experiments, which is an important observational test for these models.

In the second part of the thesis, I discuss the growth of small scale fluctuations generated during warm inflation in the context of Primordial Black Holes (PBHs), i.e., black holes with a primordial origin. PBHs are one of the exotic and remarkable probes to the physics of the early Universe. They are a very unique and efficient means to investigate various inflation models. PBHs can form in the early Universe when primordial small scale overdense fluctuations, generated during inflation, reenter the horizon and collapse by gravitational instability. In my thesis, I study a model of warm inflation and find that for certain parameter space, it has the features that it is consistent with the CMB as well as has a large amplitude of the primordial power spectrum at the small scales to form a significant abundance of PBHs. Further, I calculate the mass and the initial mass fraction of the generated PBHs and discuss the observational bounds on the abundance and other implications of the PBHs formed in our warm inflation model.

Title: Daytime thermospheric neutral wave dynamics over low- and equatorial-latitudes
Researcher: Mandal, Subir
Supervisor: Pallamraju, Duggirala
Year: 2020
Keyword's: Solar Flux, Astrophysics, Nano Technology, Thermo Dyanimics, Thermospheric Wave Dyanimics
Call No.: 530.189 MAN
Acc. No.: T00770

Abstract: Earth's ionosphere-thermosphere system is driven by forcing from the top (radiation & high energy particles of solar origin) and the bottom (atmospheric waves). In addition, over low- and equatorial-latitudes, these upper atmospheric regions are affected by several phenomena driven by the equatorial electrodynamics. Further, during geomagnetic storms, high-latitude processes influence the dynamics of these regions. As a result of all these processes, the upper atmospheric dynamics over the low- and equatorial-latitudes is highly inter-coupled in nature. Systematic information on the gravity wave propagation characteristics in different geophysical conditions at thermospheric altitudes is crucial to gain a comprehensive understanding of the atmospheric coupling and dynamics.

This doctoral thesis presents new results on the daytime thermospheric wave dynamics obtained from low- and equatorial-latitude locations over different seasons and geomagnetic conditions. These results have been made possible by using an innovative approach to derive propagation characteristics of gravity waves in the daytime thermo- sphere, which has been arrived at as a part of the thesis work. This method has opened up new possibilities for investigations of daytime thermospheric wave dynamics on a continuous basis. Furthermore, the gravity wave characteristics, such as the time periods, vertical phase speeds, and scale sizes, obtained using this approach correspond to the highest possible altitude region reported so far in the literature.

The prediction of the occurrence of one of the equatorial phenomena, the equatorial spread F (ESF), which refers to the generation of plasma irregularities in the nighttime, has been one of the missing elements in the understanding of the equatorial upper atmosphere. Some of the earlier works had suggested that the daytime thermospheric dynamics makes the conditions, conducive or otherwise, for the occurrence of plasma irregularities in the nighttime equatorial ionosphere. In the recent past, the possibility of gravity waves offering the seed perturbation has been proposed, and investigations are underway around the globe. In this context, as now an effective method is available to estimate the vertical propagation activity of gravity waves in the daytime, this aspect has been investigated further. It has been found that the vertical propagation activity is present on 85% of ESF days as compared to around 50% of non-ESF days. Also, the vertical propagation speeds of gravity waves on ESF days are higher compared to non-ESF days. ESF has been found to occur on 100% of occasions whenever the vertical phase speeds of daytime gravity waves were greater than 80 ms^{-1} . This threshold value of vertical propagation speeds of gravity waves can be used to predict the occurrence of ESF as early as 16 LT. The analysis shows that the time periods associated with these

upward propagating gravity waves that are present in the afternoon persists until late in the evening of ESF occurrence, thereby offering a plausible connection of gravity wave seeding of ESF bubbles in the daytime.

The gravity wave propagation characteristics were studied to investigate the seasonal behavior. It has been found that the magnitudes of vertical propagation speeds and wavelengths of gravity waves in the daytime thermosphere over low-latitudes are maximum during equinoxes and minimum in the summers. The comparison between the gravity wave characteristics and model-derived winds indicates that these gravity waves propagate mostly in the westward direction. During geomagnetic storms, the values of wave speeds and vertical scale sizes are significantly different than those seen on geomagnetically quiet days. These differences are very similar to the variation in energy inputs at the high-latitudes, as characterized by the strength of the auroral electrojet index. This result presented direct evidence of high-to-low latitude coupling in the neutral wave dynamics during geomagnetically disturbed times. Numerical relations have been arrived at to represent variations in the vertical propagation speeds of gravity waves during both geomagnetic quiet and disturbed conditions.

Even though the gravity waves in the thermosphere are considered to be omnipresent, their vertical propagation in the daytime upper atmosphere is observed on only around 40% of the days. Nevertheless, the days in which vertical propagation exists, it is seen that the vertical propagation activity increases with increasing solar flux. This is inferred to be due to an increase in the scale height and decrease in the Brunt-Väisälä period of the upper atmosphere with increasing solar flux. Further, the number of gravity waves in the daytime thermosphere increases due to the weakening in wave dissipations during the period of higher solar flux. These influences of solar flux on the gravity wave characteristics have been quantified, and empirical relations have been obtained.

Results obtained in this thesis work have provided new insights, which have significantly enhanced our understanding of the daytime neutral wave dynamics. The empirical relations established in this thesis work can form inputs to global-scale models of thermospheric dynamics. Furthermore, the innovative approach of using radio wave technique to derive neutral gravity waves, as demonstrated in this thesis, has opened up a new dimension in the investigations of Earth's upper atmospheric dynamics.

Title: Dynamics of heavy quark in a medium
Researcher: Singh, Balbeer
Supervisor: Mishra, Hiranmaya
Year: 2020
Keyword's: Quark Gluon Plasma, Thermal Field Theory, Magnetic Field, HQ Transport Coefficient, Quarkonia Suppression In QGP
Call No.: 530.697 SIN
Acc. No.: T00771

Abstract:

Heavy quarks (HQs) like charm (c), bottom (b), and their bound states such as J/ψ , Υ , etc. provide a unique framework and tool to systematically investigate the in-medium properties of strong interaction in high energy nuclear-nuclear collisions. This uniqueness is firstly because of the large masses (M) of the HQs compared to the inherent QCD scale (Λ_{QCD}) as well as the emergent scales such as temperature (T) in the thermalized medium that is believed to be created in these nuclear collisions. Indeed, due to a large mass threshold, HQs are not produced in the thermal medium for the temperature range achieved in nuclear collision experiments. Thus, both the production mechanism and number of HQs are controlled by the hard scatterings, mainly gluon-gluon fusion during the initial stages of the collision. Secondly, the vacuum properties of HQs and their bound states are quite well understood in pp collision. Therefore, any modification on HQ observables such as jets and quarkonia properties signals the presence of a thermalized bulk medium consisting of light quarks and gluons.

In nuclear collision experiments, the accelerated beam of charged ions is also responsible for the magnetic field generation. Indeed the strongest field in nature, i.e., $\sim 15m_\pi^2$ at LHC with Pb-Pb nuclei at $\sqrt{s} = 2.75$ TeV/A and $\sim m_\pi^2$ at RHIC Au-Au nuclei at $\sqrt{s} = 200$ GeV/A. Even though this magnetic field decreases rapidly in a vacuum, it may be possible that it stays reasonably strong for a longer time and directly affects the dynamics of light partons and HQ through its interaction with the light partons in a magnetized thermal medium as well as in pre-equilibrium phase. This situation may arise in the case when the system develops a finite electrical conductivity during the thermalization process. There have been many efforts to estimate electrical conductivity both in QGP as well as hadronic medium and its effects on the strength of the magnetic field and its phenomenological implications both theoretically as well as experimentally.

In order to characterize the in-medium properties of strong interaction at RHIC and LHC energy scales, perturbative QCD (pQCD) based analysis are not enough.

Since the non-perturbative nature of QCD arising from confinement and chiral symmetry is dominant near $\Lambda_{QCD} \sim 200$ MeV, one needs to go beyond perturbative analysis. Indeed, at finite temperature, this situation arises near a transition temperature of $T_c \approx 155$ MeV.

In this thesis, we study the magnetic field and non-perturbative effects on the in-medium binding potential of HQ and its anti-quark, collisional energy loss, and transport coefficients, namely the drag and diffusion coefficient. In order to see the magnetic field effect on quarkonia decay width, we first estimate modifications of the real and the imaginary part of quarkonia potential. An increase in the imaginary part of the potential with an increase in the magnetic field suggests that quarkonia dissociate earlier in a magnetic medium compared to its counterpart purely thermal medium.

For single HQ, the collisional energy loss in a magnetized medium suggests that the magnetic field may significantly contribute to the jet quenching. This is because the magnetic field contribution to the energy loss is of similar order as to the case of vanishing magnetic field, at least in the strong field limit where HQ is not directly affected by the magnetic field, i.e., $M \gg \sqrt{eB} \gg T \gg g\sqrt{eB}$. Further, in the low momentum regime, the magnetic field gives rise to anisotropy in the diffusion coefficient. In fact, depending on the relative direction of HQ velocity and magnetic field, one can define five diffusion coefficients. For HQ moving parallel to the magnetic field, diffusion in the transverse direction is larger than that of the longitudinal direction, i.e., $\kappa_{TT}^{\parallel} \gg \kappa_{LL}^{\parallel}$. However, for HQ moving perpendicular to the magnetic field, diffusion along the direction of HQ velocity and perpendicular to the magnetic field is gets, and dominant contribution and diffusion perpendicular to both magnetic field and HQ velocity get the least one, i.e., $\kappa_{TL}^{\perp} \gg \kappa_{LT}^{\perp} \gg \kappa_{TT}^{\perp}$. Out of these five diffusion coefficients, κ_{TT}^{\parallel} is the dominant one. Similarly, the transverse drag coefficient $\eta_{D;TT}^{\parallel}$ is the largest one out of five drag coefficients. These estimations suggest that the magnetic field can significantly contribute to the elliptic and directed flow of heavy flavor mesons.

In addition to the magnetic field effects, we investigate the non-perturbative contributions that are significantly large near transition temperature on HQ transport coefficients. This is done withing the matrix model of semi-QGP with input parameters as the expectation value of the Polyakov loop and constituent quark mass. It is observed that with the inclusion of constituent quark mass and Polyakov loop, the drag coefficient is significantly large compared to the one estimated within the pQCD framework. On the other hand, the diffusion coefficient decreases with the momentum. Furthermore, with the inclusion of shear and bulk

viscosities, it is observed that the momentum diffusion coefficient increases. This, in turn, gives a small value of the spatial diffusion coefficient. The consistency in the results of various models suggests that the non-perturbative effects on HQ transport are indeed very important for heavy ion collision phenomenology.

Title: Aspects of astroparticle physics in the precision measurement era
Researcher: Ashish
Supervisor: Mohanty, Subhendra
Year: 2020
Keyword's: Dynamical Dark Energy, Nano Science, Astronomy, Precision Givandage, Kerr-Sen Black Hole, KSBH, Gravitational Waves, Cosmic Rays
Call No.: 630.897 ASH
Acc. No.: T00772

Abstract: Astroparticle physics is a synthesis of particle physics, cosmology and astrophysics which enables us to study high energy particle physics phenomena in natural laboratories like early universe and black holes using natural probes such as cosmic microwave background radiation (CMBR), cosmic rays (CR) and gravitational waves (GW). Till the end of the 20th century, the standard model (SM) of particle physics, the standard model of cosmology (Λ CDM model) and Einstein general relativity (GR) were immensely successful at explaining the observed particle interactions, the observed evolution of the expanding universe and gravitational observations, respectively. The advent of the precise measurements at all these fronts have brought into light several shortcomings of these models and hence a need to go beyond the so called standard picture is indispensable. The observation of neutrino oscillation confirms that neutrinos have non-zero mass, which is in direct conflict with both SM and Λ CDM model. Moreover there is no particle candidate for dark matter (DM) in the SM. Additionally, in the Λ CDM model, there are discrepancies in determination of two derived parameters, namely the H_0 (Hubble parameter) and the σ_8 (density fluctuations at 8 Mpc length scale) between two different observations (CMBR and large scale structure) and also there is no theoretical explanation of the so called co- incidence problem. The recent observation of the M87* black hole shadow by the event horizon telescope (EHT) has a possible deviation (< 10 %) from the shadow predicted by Einstein's general relativity which opens a window to consider other theories of gravity.

In this thesis, the focus has been on extending the standard models to address the above mentioned issues. The ν 2HDM (Neutrino-philic 2-Higgs doublet model), which is an extension of the SM by one Higgs and three right handed neutrinos explains the non-zero neutrino mass and provides a viable dark matter candidate in the form of the neutral component of the second Higgs. This model also provides an explanation to the long-standing problem of non-observation of Glashow resonance at the IceCube neutrino detector. At the cosmological front, to address the cosmological parameter discrepancies, the coincidence problem and the incorporation of massive neutrinos in the cosmological model a comparative study of two dark energy models, namely Hu-Sawicki (HS) model and dynamical dark energy (DDE) model suggests that the resolution of parameter discrepancies prefers DDE model over HS model. At the gravity front, a study of Kerr-Sen black hole (KSBH), which emerges as a solution to 4-dimensional heterotic string theory and has axionic hair, in the light of EHT observation reveals that even more precise measurements of the shadow along with the polarimetric observation of the black hole are required to concretely conclude M87* to be a KSBH.

Title: Solar origin of space weather
Researcher: Sarkar, Ranadeep
Supervisor: Srivastava, Nandita
Year: 2020
Keyword's: Solar Active Regions, Solar Magnetic Fields, Solar Flares, Solar-Terrestrial Relations, Space Weather, Solar Coronal Mass Ejections
Call No.: 530.1278 SAR
Acc. No.: T00773

Abstract: Coronal mass ejections (CMEs), the most violent eruptive phenomena occurring in the heliosphere, are recognized as one of the major solar origins of space weather disturbances. CMEs erupt in the form of gigantic clouds of magnetized plasma from the Sun and can reach Earth within several hours to days. If the magnetic field inside an Earth-directed CME or its associated sheath region has southward directed component (B_z), then it interacts with the Earth's magnetosphere, leading to severe geomagnetic storms. Therefore, it is crucial to predict the strength of B_z inside an Earth impacting interplanetary CME (ICME) in order to forecast the intensity of the resulting geomagnetic storms. Forecasting the strength and orientation of CME magnetic field at 1 AU requires advance knowledge of near-Sun CME properties and its nature of evolution in the heliosphere. The source region characteristics of CMEs may help to acquire knowledge about the CME properties close to the Sun as well as the conditions leading to CME initiation. However, the understanding of CME initiation and its nature of evolution close to Sun are limited due to lack of continuous observations which can capture the CME evolution starting from its initiation to post-eruptive phase. Moreover, in absence of any direct measurement of vector magnetic field in solar corona, it becomes quite challenging to estimate the magnetic field strength of CMEs close to the Sun. Apart from the above mentioned challenges, further complexities arise in modeling the CME parameters from Sun to Earth in order to predict its strength and orientation of magnetic field at 1 AU. In spite of several numerical and analytical modeling efforts, to date there is no such model yet which is capable of giving reliable prediction of B_z at 1 AU.

In backdrop of the above scenario, in the thesis, we first explore the conditions leading to CME eruptions from its source active regions (ARs) by studying the source region characteristics of the largest AR (NOAA 12192) of the solar cycle 24. This active region is a unique representative case, as it gave rise to several non-eruptive X-class flares as well as an eruptive M-class flare, giving an excellent opportunity to compare the photospheric magnetic environments of confined and eruptive events originated from a same AR. Comparing the magnetic characteristics associated with both the confined and eruptive flares, we found that, although the flare-related permanent and abrupt changes in photospheric magnetic field and Lorentz forces are a common feature in large flares, the magnitude of those changes is smaller in the case of confined flares compared to the eruptive ones. In order to shed light on the physical scenario behind the confined nature of the high energetic flares originated from AR 12192, we have examined the magnetic environment over the source locations of both the confined and eruptive flares occurred in the AR. From the study of the extrapolated magnetic field, we have found that the critical decay index (1.5) for the onset of torus

instability was achieved at a higher height (52 Mm) over the non-eruptive core region of AR 12192, whereas this critical height was comparatively lower (35 Mm) over the eruptive part of the AR. This is an important finding which suggests that the decay rate of the overlying magnetic-field strength can be used as a key parameter to determine whether a flare productive active region will result in a CME eruption or not.

Further, we extend the studies of source region characteristics to the active regions leading to recurrent large eruptive flares in order to unveil the conditions leading to successive eruptive events. A longstanding unsolved problem in flare physics is that, whether these events occur due to the continuous supply of free magnetic energy to the solar corona or because not all of the available free magnetic energy is released during a single major flaring event. In order to address this question, we study the evolution of photospheric magnetic field and the associated Lorentz force changes in NOAA ARs 11261 and 11283, each of which gave rise to recurrent eruptive M- and X-class flares. The distinct rebuild-up of net Lorentz force in between the successive flares and its abrupt downward changes during each flare in ARs 11261 and 11283 as obtained in our study, are the first observational evidences found in the evolution of any non-potential parameter of solar ARs, that confirms the build-up and release scenario for magnetic energy storage in the solar corona. We conclude that the recurrent large flares reported in our study occurred due to the newly supplied energy to the AR, instead of consuming the available residual energy. In the context of space weather predictions, the evolutionary pattern of the net Lorentz force changes reported in our study has significant implications, in particular, for the forecasting of recurrent large eruptive flares from the same AR and hence the chances of interaction between the associated CMEs. Addressing the source region characteristics of CMEs, next, we have studied the CME initiation and its nature of evolution close to Sun. Since the morpho- logical and magnetic properties of coronal cavities hold critical clues to triggering mechanism behind the CME initiation, we have tracked the evolution of a solar coronal cavity from a quasi-static equilibrium in the lower corona to its eruption into the interplanetary space using the multiple vantage point observations from SDO, STEREO (A & B), PROBA2 and LASCO. Importantly, by comparing the cavity centroid height during different stages of its evolution from quiescent to pre-eruptive phases, we have found that the eruption of the CME is triggered when the cavity centroid height reached a critical height for the onset of torus instability. Therefore, we have concluded that monitoring the cavity centroid height can be a useful forecasting tool to predict the cavity eruption in the form of CMEs.

Utilizing the large field-of-view of SWAP EUV imager and combining the EUV observations with the white-light images obtained from LASCO coronagraph, we have captured the complete evolution of the erupting cavity by filling the observational gap between 1 to 2 R_{\odot} . By applying successive geometrical fits to the cavity morphology, we have found that the nature of expansion of the coronal cavity was not self similar in the lower corona, below a critical height ($2.2 \pm 0.2 R_{\odot}$). However, above that critical height the nature of expansion remained self similar throughout the rest of the observed propagation path. Our observations also revealed that the cavity exhibited a strong deflection at 1.3 R_{\odot} and after that, the direction of propagation remains approximately constant. The above mentioned results provide important observational constraints on both the nature of expansion and

direction of propagation of CMEs, which are useful to model the CME properties from Sun to Earth in order to forecast its space weather impact at near-Earth space.

Combining the knowledge of CME source region characteristics and the nature of evolution of its near-Sun properties as developed in the thesis, finally, we have attempted to model the CME magnetic field from Sun to Earth in order to forecast the strength of B_z at 1 AU. Using the near-Sun CME properties as initial inputs, we developed an observationally constrained analytical model, the INterplanetary Flux ROpe Simulator (INFROS), to predict the magnetic field vectors of the associated ICMEs at any heliocentric distance. As a proof of concept, we validate the model for a test case of an Earth-impacting CME which occurred on 2013 April 11. The predicted magnetic field-vectors of the ICME obtained from INFROS show good agreement with those observed by the WIND spacecraft at 1 AU. This shows promising results in forecasting of B_z in near real time. It may be highlighted that INFROS is advantageous in many aspects compared to the existing B_z forecasting models, as it uses the realistic inputs and is capable of predicting the time-varying axial field strength and the expanding nature of the ICME without involving any free parameters. Therefore, the model (INFROS) developed and described in this thesis could prove to be a promising space-weather forecasting tool for advance prediction of magnetic field vectors of ICMEs.

In short, exploiting both the observational and modeling efforts, this thesis provides novel techniques to predict the magnetic field vectors of ICMEs which build the stepping stones towards the forecasting of intensity of the associated geomagnetic storms at near-Earth space.

Title: Phenomenology of neutrino oscillations and masses
Researcher: Chakraborty, Kaustav
Supervisor: Goswami, Srubabati
Year: 2021
Keyword's: Neutrino Oscillation, Non-Unitarity, Double-beta Decay, $\mu - \tau$ Symmetry, Neutrino Physics, Sterile Neutrino, Flavour Symmetry
Call No.: 530.127 CHA
Acc. No.: T00774

Abstract: Neutrinos are one of the most abundant subatomic particles in the universe second only to the photons. Yet, they are one of the most mysterious particles in the universe. This particle is emitted along with the electron in a nuclear β -decay thus making it a three body decay and explaining the continuous spectrum of the electron. In fact neutrino was postulated by Pauli in 1930 to explain this continuous spectrum. Neutrinos are spin half, neutral particles which interact only via weak interactions and are mass- less in the Standard Model. But, the discovery of neutrino oscillations has established that neutrinos have mass.

Neutrino oscillation physics is an established field of research that has been posing many challenges over the past few decades. Neutrinos are produced in certain flavor states, but, when the same neutrino is detected after a certain time the flavor state might be different, this phenomena is called neutrino oscillations. Three flavour neutrino oscillations is governed by three mixing angles, two mass squared differences and one complex CP phase. With the help of many phenomenal experiments much progress has been made in precisely determining the oscillation parameters ϑ_{12} , ϑ_{13} , $|\Delta m^2_{31}|$ and Δm^2_{21} . This leaves determination of neutrino mass hierarchy i.e. the sign of $|\Delta m^2_{31}|$, CP phase δ_{CP} and the octant of ϑ_{23} as the primary objectives of the on-going and the upcoming neutrino oscillation experiments. Oscillation experiments are sensitive to the mass-squared differences but the absolute mass scale of the light neutrinos are still unknown and there exists only an upper bound on the sum of absolute neutrino masses from cosmology. Although neutrino oscillations among the three neutrino flavors have been well established there are various studies to explore if there can be other beyond the standard model scenarios at a sub leading level and their detectability in current and future oscillation experiments. This includes the existence of a fourth sterile neutrino, non-standard interactions, neutrino decay, non-unitarity of neutrino mixing matrix, neutrino decoherence, CPT violations, Lorentz violations etc.

The primary objective of the thesis is to study the physics potential of current and future accelerator neutrino experiments to determine the unknown parameters. Neutrino oscillations experiments are sensitive to the probability of oscillations. However, the determination of the parameters are challenging due to the presence of various parameter degeneracies. This can be resolved by exploring the synergies between various experiments. In particular we concentrate on the future experiments DUNE, T2HK/T2HKK, ESvSB and, perform a comprehensive and comparative analysis of the sensitivities of the current unknowns at these experiments.

The symmetry based approaches have been quite successful in predicting the inter- relations among these quantities and the structure of the leptonic mixing matrix. One such symmetry, called $\mu - \tau$ reflection symmetry leads to very successful predictions of mixing angles which are close to the present experimental values. The consideration of partial $\mu - \tau$ reflection symmetry leads to various correlations between the mixing angles and the CP phase. We study the possibility of studying these correlations in the future long baseline experiments like DUNE, T2HK/T2HKK.

We also investigate the predictions of the $\mu - \tau$ reflection symmetry in presence of a light sterile neutrino and find bounds on the unconstrained parameters. These predictions can be tested in neutrino oscillation experiments like DUNE as well as in neutrinoless double-beta decay experiments. Additionally we also consider a future proposal nuSTORM proposed primarily for accurate determination of neutrino cross-sections. We study the possibility of exploring sterile neutrinos and non-unitarity of neutrino mixing matrix in the context of this proposal emphasizing on the inclusion on neutral current events in the analysis.

Title: Laser induced breakdown spectroscopy utilising synthetic spectrum method for optically thick plasmas
Researcher: Kumar, Prashant
Supervisor: Singh, R. P.
Year: 2020
Keyword's: LTE Spectrum, Spectroscopy, CF-LIBS, Stark Parameter, Stark Broadening Measurements
Call No.: 530.179 KUM
Acc. No.: T00775

Abstract: Laser induced breakdown spectroscopy (LIBS) has emerged as one of the promising analytical technique for quantitative analysis. This method offers several advantages in terms of versatility and ease of setting up the experiment when compared with other analytical methods. Although there has been a substantial understanding of most of the basic processes involved in LIBS such as laser-matter interactions, plasma formation, its propagation and temporal evolution, etc, still a significant amount of research into utilising the emission spectrum from an evolving plasma to obtain accurate quantitative information is required. This has been a driving force for nearly two decades of active research in the field.

The present thesis is also aimed towards achieving the goal of obtaining more reliable and accurate results using LIBS for materials with varying degree of complexity in terms of analysis. Considering the advantage that no additional information or data of the analyte, apart from the emission spectra, is needed, the present thesis is based on an approach known as calibration-free LIBS. The work presented in the thesis is mainly focused on synthetic spectrum method for quantitative analysis. This method is based on comparing the experimental spectrum with a simulated LTE spectrum of the material under study where all plasma parameters including number densities of species and hence, concentration is obtained as a result of simultaneous fitting of multiple emission lines in a spectrum. Improvements to the technique have been realized by using a large number of emission lines in the analysis and an automated search procedure for line identification. The effectiveness and suitability of the developed method has been demonstrated on different samples, even for cases having dense spectrum with merged lines. The method has also been used for estimating detection limits for various trace elements in the sample as a function of experimental signal-to-background levels. This can help in deciding the experimental conditions tuned to analyze selected trace elements. A correct accounting of the emission line broadening, mainly due to self-absorption and Stark effect in the plasma is of utmost importance in matching the experimental spectrum with simulated one. Although the developed scheme of analysis automatically incorporates the effect of self-absorption in the plasma, much accurate estimate of Stark broadening still poses a challenge given the paucity of available data in literature. A correct estimate of this parameter becomes even more important as self-absorption in turn depends on Stark broadening of the emission line. Hence, a method utilising time resolved measurements have been proposed for Stark broadening measurements. This utilises the relation between various emission line parameters and the plasma opacity. The method has been successfully demonstrated on a few

resonant lines of neutral aluminum species. With these improvements, major objectives of the present thesis have been realized. The suggested procedure also paves a way to further research in some of the topics, such as obtaining temporal evolution of the detection limits for different elements, estimating error expected in quantitative analysis in CF-LIBS using synthetic spectrum method, Stark parameter database for LIBS, etc.

Title: Hot QCD matter in the influence of electromagnetic fields
Researcher: Kurian, Manu
Supervisor: Chandra, Vinod
Year: 2020
Keyword's: Quark-Gluon-Plasma, Magnetized QCD Medium, Effective Kinetic Theory, Shear and Bulk Viscosities, Electrical Transport, Thermal Transport, Heavy Quark, Drag And Diffusion Coefficients
Call No.: 530.128 KUR
Acc. No.: T00776

Abstract: The high-energetic/ultra-relativistic heavy-ion collision experiments at Relativistic Heavy Ion Collider (RHIC) and at Large Hadron Collider (LHC) have produced the deconfined phase of the matter, at extremely high temperature, in which quarks/antiquarks and gluons are effectively free. This phase (hot QCD matter) is commonly termed as Quark-Gluon-Plasma (QGP). The deconfined phase is characterized by quark, antiquark, and gluonic effective degrees of freedom, and the created medium seen to behave more like a near-ideal fluid (perhaps except near the QCD transition point) and most vortical one too. The quantitative analysis of the experimental observables of the final stage particles from the dissipative hydrodynamical simulation involves the dependence upon the thermodynamic and transport parameters of the hot nuclear matter. On the other hand, intense magnetic fields are produced in the initial stages of non- central asymmetric collisions and can affect the thermodynamic and transport properties of the nuclear matter. In this thesis, an attempt has been made to understand the impact of the magnetic field on the QCD equation of state and transport properties of the deconfined nuclear matter by employing an effective modelling of the magnetized medium. The charged fermions (quarks/antiquarks) are directly coupled to the strong magnetic field through the Landau level dispersion relation and have constrained $1 + 1$ dimensional motion along the direction of the strong magnetic field. Thus, the strong magnetic field violates the rotational symmetry and induces anisotropy in the medium. The electromagnetic responses of the collisional QGP medium have been analyzed with relaxation time approximation and Bhatnagar-Gross-Krook collisional kernels within the scope of covariant kinetic theory. The effect of the magnetic field on the momentum transport and thermal transport has been studied by estimating the longitudinal viscous coefficients and thermal conductivity in a strongly magnetized medium. Further, the analysis of thermal transport has been extended to the weak magnetic field limit. The interplay of thermal transport and electric charge transport in a weakly magnetized QGP has been studied in terms of Wiedemann-Franz law. Heavy quarks/antiquarks are created in the initial stages of the collisions and are considered as one of the effective probes to characterize the properties of the QGP. Owing to their large mass, a heavy quark/antiquark will not get affected directly by the magnetic field. The measurements of charge-dependent directed flow at the LHC and RHIC might provide insights about the electromagnetic fields in the medium. To that end, the heavy quark drag and diffusion coefficients have been estimated in the magnetized medium. Finally, the analysis of heavy quark transport has been extended to a magnetized bulk viscous medium. The effects of the magnetic field, collision, and equation of state have been seen to have a visible impact on the above-mentioned aspects of the QGP/hot QCD matter.

Title: Some novel studies of black holes in general relativity and modified theories
Researcher: Mishra, Akash K.
Supervisor: Sarkar, Sudipta
Year: 2021
Keyword's: General Relativity Theory, Black Holes Topology, Lovelock Gravity, Physical Process First Law
Call No.: 530.11 MIS
Acc. No.: T00942

Abstract: The primary motivation of this thesis is to study certain theoretical and observational aspects of theories beyond general relativity. This includes the horizon topology, thermodynamics of black holes, cosmic censorship conjectures, gravitational lensing, gravitational waves etc. The topology theorem by Hawking is considered as one of the most important results in classical black hole physics. The theorem asserts that the admissible topology of the event horizon cross-section of black holes in general relativity is either spherical (S^2) or toroidal ($S^1 \times S^1$). However, this result is specific to four-dimensional black hole solutions in general relativity. In this thesis, we have studied the topology theorem in the context of $f(R)$ theory of gravity. We have obtained a sufficient differential condition on the function $f(R)$ for which the allowed topological structures in $f(R)$ theory is identical to that of general relativity. We also extend this result to higher dimensions.

Further, we study the Physical Process First Law (PPFL) of black hole thermodynamics in an arbitrary diffeomorphism invariant theory of gravity. We have obtained the most general form of the variation of horizon entropy and use the result to understand the effects of the ambiguities present in the Wald entropy on the formulation of PPFL. We show that, for linear order perturbation, when the variation of entropy is computed between a past bifurcation surface and a future stationary slice, the PPFL is independent of the ambiguity terms. Finally, we calculate the change in entropy between two arbitrary non-equilibrium cross-sections of the event horizon. In this setting, we could express the variation of entropy as the first law by identifying the additional boundary term to be horizon membrane energy. We have explicitly illustrated this result in the context of Einstein-Gauss-Bonnet gravity and arbitrary order Lovelock theory.

This thesis also addresses the validity of cosmic censorship conjectures (weak and strong) in various non-trivial settings. The weak cosmic censorship negates the formation of naked singularity as the final state of a gravitational collapse. This is essential to ensure the stability of black holes under small perturbations. We examine the Gedanken experiment of overcharging a system of two extremal black holes via the process of charged particle absorption to test the validity of weak cosmic censorship. We show that, even for such a non-trivial system, the conjecture remains valid. Also, our work represents the first-ever study of weak cosmic censorship in a multi black hole setting. Furthermore, we study the strong cosmic censorship conjecture in higher curvature theories, which is a statement regarding the deterministic nature of the underlying theory of gravity. The primary motivation of this work is to understand the effects of higher curvature couplings on the violation of strong cosmic censorship conjecture. Our results indicate that the violation seems to be stronger

in the presence of higher curvature terms. We demonstrate this result for charged de Sitter black holes in Einstein-Gauss-Bonnet gravity and pure Lovelock gravity.

Because of the strong gravitational lensing effect, light can follow a circular path in the vicinity of black holes known as photon orbits. This gives rise to the formation of shadow structure around a black hole. Surprisingly, most of the previous studies of black hole shadow consider the spacetime to be stationary. This is only an idealization since an astrophysical black hole strongly interacts with the surrounding matter distribution and, as a result, cannot be represented by a stationary spacetime ansatz. In this thesis, for the first time, we study the evolution of the photon sphere and shadow radius around several black hole solutions in general relativity and Einstein-Gauss-Bonnet gravity. We obtained a general second-order differential equation that governs the dynamics of the photon sphere and illustrates some interesting results by applying it to various dynamical models.

Setting constraints on theories of gravity beyond general relativity has been of growing interest in recent years. With the recent advancement of gravitational wave detectors, we can access the previously unexplored strong and dynamical regime of gravity. The gravitational-wave observation provides an unprecedented opportunity to test the predictions of general relativity and constrain modified theories. The second part of this thesis attempts to connect theory and observations in gravitational physics. In particular, we have developed two general methodologies to obtain constraints on the parameters of modified gravity theories from gravitational-wave observations. Firstly, using the observed time delay between the gravitational-wave and electromagnetic signal in the GW 170817 event, we constrain the coupling of the quadratic gravity in four dimensions. Finally, using the observed quasi-normal mode spectrum of the GW 150914 event, we were able to constrain the tidal charge parameter of a rotating braneworld black hole. These formalism are entirely general and can be employed in several other class of modified gravity models.

Title: Viscous dark matter and its astrophysical and cosmological signatures
Researcher: Mishra, Arvind Kumar
Supervisor: Bhatt, Jitesh R.
Year: 2020
Keyword's: Dark Matter, Dark Energy, Self-interacting Dark Matter, Dark Matter Viscosity, CMB, EDGES
Call No.: 523.1126 MIS
Acc. No.: T00951

Abstract: The Standard Model (SM) of cosmology (Lambda Cold Dark Matter (Λ CDM)) successfully explains the large-scale structure and the cosmic microwave background radiation observations. However, it encounters some theoretical and observational challenges, which demand a modification from the standard behavior. The drawbacks of SM include an interpretation of the cosmological constant, small-scale structures observations, and anomaly in the 21-cm signal observed by the Experiment to Detect the Global Epoch of reionization Signature (EDGES) collaboration. The Λ CDM model assumes that the Dark Matter (DM) is a cold, collisionless, and dissipationless fluid. However, as the real Universe contains non-ideal species, one needs to explore beyond the ideal behavior and study the effects of imperfections in the cosmic fluid. In this thesis, we study the Viscous Dark Matter (VDM) and explore some of its possible signatures in the Universe. The Self-Interacting Dark Matter (SIDM) is a possible candidate to address the small-scale problems faced by the Λ CDM model. We calculate the mean free path of dark matter particles and argue that for SIDM particles, the hydrodynamic description is valid from galactic to large scale. We propose that the self-interaction between the DM particles may lead to viscosity in the DM fluid. We estimate the shear and bulk viscosity of the Viscous Self Interacting Dark Matter (VSIDM) fluid using the kinetic theory in relaxation time approximation. The astrophysical constraint on the ratio of DM self-interaction cross-section to its mass (σ/m) indicates that the viscosity is large at present and increases by two orders of magnitude from the galactic to cluster scale. Therefore, one may expect interesting cosmological consequences from such a large DM viscosity. Our calculation found that the SIDM viscosity is sufficiently large to account for the present accelerated expansion and hence mimic the Dark Energy (DE). Thus, the viscous SIDM model provides a unified description of the DM and DE. Further, we explore the effects of the VSIDM dissipation at a low redshift interval, $0 \leq z \leq 2.5$. For this, we assume the viscosities as a constant with the redshift and parameterize the fluid velocity gradients as a power-law form. Using the χ^2 minimization techniques, we obtain the averaging length scale is ≈ 20 Mpc, which is larger than a typical cluster scale. The best value of the model parameters indicates that the cosmic dissipation is large at present, $z = 0$, and decreases on the redshifts $0 \leq z \leq 2.5$. We report that the decreasing dissipation (as redshift increases) explains the late-time observations, whereas the constant dissipation fails to do so.

Furthermore, String theory provides a lower bound, called KSS bound, on the shear viscosity to the entropy density ratio as $\eta/s = 1/4\pi$. Using the cluster scale constraint on σ/m , we find that the SIDM fluid violates the KSS bound if the SIDM mass is above a GeV scale. Assuming that VSIDM respects the KSS bound, we constrain the DM mass and report that the DM mass should be sub-GeV. Our

result provides a new DM mass range, which can be explored in the DM detection experiment. Further, we also explore the evolution of the bulk and shear viscosity in the SIDM fluid, parameterizing them as redshift dependent. We find that the SIDM viscosities are large at present and decrease on large redshift, supported by the late-time observations.

We also study the evolution of the DM temperature in the presence of viscosity. The DM viscosity causes energy dissipation and hence increases its temperature. For a large DM viscosity, its temperature will be high, and so the DM may no longer be a cold fluid. Therefore it will affect the large scale and the CMB observation. We derive a condition on the DM viscosity parameters which is consistent with the CMB observation.

Further, we propose a possibility of photon production from viscous dark matter energy dissipation. The photon generation has been considered in two ways: first, when the DM directly dissipates into the photons, and second when the DM firstly dissipates into dark radiation and then generates the visible photons via kinetic mixing between the dark radiation and photons. We find that the photons obtained from the kinetic mixing increase the number density in the Rayleigh-Jeans limit of the cosmic microwave background radiation. As a consequence, it can explain the EDGES anomaly observed in the 21-cm signal. Further, using the EDGES observation, we explore the DM model parameters such as its mass, kinetic mixing parameter, and dark radiation mass, whose information is crucial for the DM viscosity estimation and dark radiation searches.

After that, we investigate the DM microphysics using the interacting viscous dark matter-gas formalism in light of the reported EDGES anomaly. The DM viscosity heats the DM and also the gas via its interaction with the gas. The gas heating increases as the mass and viscosity of the DM increases. Therefore, to explain the EDGES 21-cm signal, the DM mass should be small, but the DM-gas interaction cross-section ($\hat{\sigma}$) should be large in comparison with the ideal DM case. Further, using the CMB constraint on the DM-gas interaction cross-section, we report that the EDGES 21-cm signal allows a large viscosity compared to the bounds from structure formation. We find that the DM coldness condition provides a stringent limit on the dark matter viscosity.

Title: Dynamics of self-assembly in silicon-based nanostructures at surfaces and interfaces
Researcher: Utsav
Supervisor: Banerjee, Rupak
Year: 2021
Keyword's: Silicon-based Nanostructures, Silicon Nanowires, Silica Nanospheres, Tetraethyl Orthosilicate, Silsesquioxane Nanocages
Call No.: 537.622 UTS
Acc. No.: T00952

Abstract: Silicon-based nanomaterials, ranging from monomolecular to nano-sized frameworks, have been extensively deployed in a broad range of structural assemblies to be utilized (directly or indirectly) in various applications. Such versatility in applications stems from the large variety in size, symmetry, and tunable physicochemical properties of silicon-based nanostructures. The physicochemical properties of these nanostructures depend on the basic structural built of the core and the substitutions over the active surface sites of the framework. Silicon-based nanomaterials can be synthesized and assembled in many ways depending upon the targeted utility. In this thesis, we have focused mainly on Silica (SiO_2) and Silsesquioxane ($\text{RSiO}_3/2$, where R is an organic group) based nanomaterials. Depending on the synthesis or fabrication process, both Silica and Silsesquioxane based-frameworks exhibit precise tunability in their size, ranging from 10 - 2000 nm for Silica-based nanoparticles to 0.5 - 10 nm for Silsesquioxane nanoparticles. The nature, number, relative position of the substituents, and the geometrical shape and symmetry of the structural unit of the core dictate their interaction with each other and the surroundings.

This thesis aspires to investigate the dynamics of self-assembly in various types of silicon-based nanomaterials (viz. Silica and Silsesquioxane) at different surfaces and interfaces. The first part of the thesis explores the self-assembly and controlled restructuring of Silica nanospheres (SNs) into long-ranged periodic structures, which are further employed for energy storage and surface-enhanced Raman spectroscopy (SERS) applications. The latter part of the thesis focuses on the weak interaction mediated structural phase transitions in modified Silsesquioxane nanostructures when laterally compressed at the air-water interface.

Silica nanoparticles have been used extensively in device fabrication due to their excellent thermal and chemical stability, size selectivity, and ability to support and facilitate the growth of various nanostructures. Additionally, silica nanoparticles are known to self-assemble with a long-range structural periodicity that enhances the performance of devices. Long-ranged close-packed monolayers (CPM) of Silica nanospheres (SNs) were fabricated using a unique three-step spin-coating method and later used as nanocomposites and templates for energy storage, photoelectrochemical applications, size-selective nanowire fabrications, and SERS active surfaces. The CPM of SNs was restructured under controlled sintering and etching conditions via neck-growth and neck-dissolution to create templates for nanowires and SERS-active surfaces. The sintering ensures effective fixation of the restructured monolayer to the substrate while facilitating neck growth between neighboring SNs. Additionally, the thermal treatment induces segregation and

compactification of the growth domains. The structural transformations were emulated using a two-particle geometrical model parametrized by universal neck parameters. The model provides a handle over the thermal budget to effectively dock the monolayer, preserving the geometrical features of the nanoparticles. In addition to that, the model estimates quantitative values of the curvature radius and interpenetration depth of the SNs, thus providing insight into the dynamics of the sintering process for non-porous SNs. The sintered monolayers were restructured by using chemical etching to form non-close-packed monolayers (NCPM). The etching process could also be modeled by parameterizing the structural changes with the same universal neck parameters that influence the resultant morphology. Observed variations in the neck parameters, at different stages of restructuring, were corroborated with the model calculations. The effect of etching time and etchant concentration on different particle sizes was also investigated. This allowed template fabrication of predetermined geometry that could be used for Silicon Nanowire (SiNW) growth via metal-assisted chemical etching. Variation in the monolayer assembly, along with different etching sequences, led to the fabrication of SiNWs with desired dimensions.

Metal-assisted chemical etching of NCPM template (formed with pre-sintered SNs monolayer) was exploited to fabricate SiNWs of desired sizes using either monodisperse SNs or carefully chosen volume ratio of bi-disperse SNs. An appreciable increase in the photoelectrochemical performance of the tipped SiNWs was demonstrated with a photocurrent density of approximately $4\text{mA}/\text{cm}^2$ at a potential of -1 V vs. RHE. The sintering mechanism between SNs, which are chemically and geometrically identical but of different radii, scales in accordance with Herring's law and provides valuable insights into the dominant mass transport mechanism contributing to neck formation. An archetypal plasmonic-photonic nanocomposite of a 2D periodic array of SNs with gold (Au) crowning was realized, extending over a large surface area. Pre- and post-annealing morphological features reveal gold crowning on top of SNs, at different annealing temperatures for various thicknesses of the sputter-deposited gold. *In-situ* grazing incidence X-ray diffraction measurements were employed to structurally characterize the reconstruction in the Au-layer as a function of the annealing temperature. Finite element methods were used to simulate the interaction between the paired nanocomposites and the incident electromagnetic radiations to elucidate the crowning and nanodrop formation mechanism. Such paired nanocomposites allow prospective applications in optoelectronics, sensing, catalysis, and SERS. Another nanocomposite consisting of an inorganic SNs shell and an organic core constituting a phase change material (PCM) was employed for thermal energy storage applications. The encapsulation within the Silica shell makes it impervious for the PCM material to seep out during solid-liquid phase change. The nanocomposites exhibit enhanced pressure durability and thermal stability when compared to the pristine PCM material.

Silsesquioxanes are also silicon-based nanostructures that are amphiphilic and demonstrate exciting properties at the liquid-air interface. The Silsesquioxane materials are composed of an inorganic core with organic substituents and find widespread industrial usage in coatings, cosmetics, fire-repellants, nano-fillers, and composites for strength enhancement. We investigate the structural phase transitions, ordering, and crystallinity of a particular class of Silsesquioxanes, namely, Polyhedral Oligomeric Silsesquioxane (POSS) molecules, to explore the influence of variation in the

substitutional groups of the POSS core on the nature of crystalline states formed at the air-water interface on a Langmuir trough. X-ray scattering studies in the grazing incidence geometry with an intense and collimated synchrotron X-ray beam (with a wavelength of 1.24 Å), impinging over floating POSS layers exhibit unique diffraction profiles characteristic to the structural phase and ordering within the layers. The POSS variants exhibit transition from a weakly correlated monolayer to polycrystalline structures with a propensity of preferential orientations to single crystal-like ordering under the influence of regulated compression at the interface. The structural transformations of the differently substituted POSS molecules and their variations therein are attributed to the changing balance of the hydrophobic vs. hydrophilic interaction in the layers. This balance of interaction is determined by the anisotropic shape and distribution of the substitutional groups over the nano-sized core-cage of the monomer, steric interaction between nearest dimeric neighbors as well as the in-plane and out-of-plane assembly of the overlayers. Quantitative structural evaluation provides critical insights into the dynamic nature of the crystallization of amphiphilic molecules at the air-water interface by correlating the differences in the molecules' substitution to the final crystal structure attained under lateral compression.

Finally, within the scope of this thesis, we can subsume that the dynamics of self (and sometimes forced) assembly of Silicon-based nanostructures, by quantitative experimental characterization and modeling, reveal a multivariate dependence on the size, symmetry, basic structural framework, deforming forces, and physicochemical properties of the assembling units. Such knowledge is crucial not only for the fundamental understanding of the various aspects of self-assembly in different nanostructures at surfaces and interfaces but also for optimizing bottom-up approaches leading to the fabrication of various devices using such nanostructures.

Title: Aspects of beyond the standard model higgs phenomenology
Researcher: Sarkar, Agnivo
Supervisor: Coleppa, Baradhwaj
Year: 2021
Keyword's: Standard Model Higgs, LHC, Compact Linear Collider (CLIC), Higgs Boson, Collider Phenomenology
Call No.: 539.721 SAR
Acc. No.: T00953

Abstract: The discovery of the Higgs boson by the ATLAS [1] and CMS [2] collaborations at the LHC, found the last missing piece of the Standard Model's (SM) particle spectrum. In spite of the numerous experimental success of the SM, the theory fails to provide a complete picture of the dynamics of the fundamental particles at high energies. It does not give a natural explanation for the scale of electroweak symmetry breaking. Additionally, several theoretical and experimental issues like Higgs mass hierarchy, a candidate for dark matter or the non-zero neutrino masses motivate particle physicists to improve upon the existing SM. These advancements in model building avenues come under the collective banner of Beyond the Standard Model (BSM) scenarios.

The commonalities among these models is the presence of additional (usually heavy) bosonic and fermionic degrees of freedoms. The ultimate success of these models would be decided by detecting these particles at LHC. In the last decades various collider experiments probed mass ranges upto a few TeV in search for these additional particles. The non-observation of new physics signal at this energy scale strongly suggests that the production cross-section of the BSM signals are severely suppressed. However, the possibility remains that these new state produced by and subsequently decay via exotic channels not currently explored at the LHC. The central theme of this dissertation is to explore such phenomenological aspects of new physics signals in the context of BSM scenarios with enlarged gauge and scalar sectors.

We begin our discussion by presenting the study of a fermiophobic Z' boson in the context of the LHC and future Compact Linear Collider (CLIC). Since the Z' does not couple to SM fermions at tree level it can evade the present day collider limits from direct searches. Such a Z' is dominantly produced via vector boson fusion process and subsequently decays via the WW and Zh channels. Our analysis indicates that the final state offers favourable prospects to detect the Z' as opposed to traditional search strategies (that involve Z' decaying to a dilepton final state). We develop a cut-based analysis which systematically reduces the relevant SM back-ground events and helps us to extract a model-independent values of $\sigma \times BR$ that are required for a 5σ discovery at the LHC and CLIC. We further translate these numbers into the parameter space of an extended gauge model for illustration purposes. Our findings show that a heavy fermiophobic Z' boson can be discovered in the final state for a wide range of parameter choices.

Any class of models where several Higgs multiplets are involved in electroweak symmetry breaking can contain charged scalars (H^\pm) in the particle spectrum. We explore the discovery prospects of a charged Higgs in the context of the 14 TeV LHC in a generic model-independent fashion. Taking into account the recent experimental developments of the H^\pm search program, we look for novel production and decay channels for the H^\pm that involves other BSM neutral scalars (e.g. H , A). Depending on the tree-level couplings of the charged Higgs with the SM, we categorise these BSM scenarios into three classes: Chromophobic, Gaugophobic and Leptophobic. We analyse these classes separately and devise cuts for a 5σ discovery of the charged Higgs. We then translate these results into the parameter space of the Type II 2HDM to understand the scope of our analysis. Our findings suggest that the chromophobic case, (in which the H^\pm does not couple to the colored sector) offers maximum discovery potential. This is in contrast to traditional searches that rely heavily on the tb^- final state. Our study thus offers a complementary search paradigm at the LHC.

The thesis further considers a BSM model by enlarging the gauge symmetry of the SM with an additional $SU(2)$ gauge group. Two Higgs in doublet representations and one non-linear Sigma field acquire vacuum expectation values to engineer electroweak symmetry breaking (EWSB). After EWSB, the scalar spectrum of this model consists of two neutral CP-even Higgs, one pseudo-scalar, and a pair of charged Higgs - all together five scalar particles. We present the details of the gauge, scalar and fermion sectors of this model. Interestingly, the scalar sector of this model is analogous to the generic 2HDM model (specifically the Type-I 2HDM). Our primary objective of this study is to lay out the markedly different collider phenomenology offered by this alternative scheme of EWSB. We impose various theoretical (e.g. mass positivity, unitarity, vacuum stability and perturbativity) and experimental (h -125 discovery data, $Z \rightarrow b_L b_L^-$, Δp and $b \rightarrow s\gamma$) constraints to extract regions of the parameter space that are not disallowed. Furthermore, we discuss different decay channels corresponding to the neutral and the charged Higgs bosons.

Finally, we revisit the collider phenomenology of the charged Higgs boson in the context of a BSM scenario with a generic extended gauge and scalar sector. It is certainly possible in these scenarios for the charged Higgs to decay via heavy gauge boson mediated channels ($W' Z/WZ'$) along with the traditional decay modes. We set up the search strategy of the H^\pm in the channel $H^\pm \rightarrow W' Z$. Since the W_0 is assumed to not couple to SM fermions at tree level, it opens up interesting cascade decay chains like $H^\pm \rightarrow W' Z \rightarrow W^\pm ZZ$. As a result the charged Higgs can be discovered in final states with multiple hard leptons and/or b-quarks which can be probed by the future LHC experiments with sufficiently high luminosity. We demonstrate the reach at the LHC for luminosities of 500 fb^{-1} and higher.

Title: Various manifestations of accretion onto stellar-mass black holes
Researcher: Rout, Sandeep Kumar
Supervisor: Vadawale, Santosh V.
Year: 2021
Keyword's: Astronomy & Astrophysics, X-ray binaries, Accretion disks, Black holes, Quasi-periodic oscillations, General theory of relativity
Call No.: 520 ROU
Acc. No.: T00961

Abstract: The very definition of black holes makes their study extremely challenging by using electromagnetic waves as conventionally done for other astronomical objects. It is only through their impact on matter within their gravitational influence that any reasonable understanding about them can be obtained. Accretion of matter onto black holes results in X-ray emission and such X-ray observations provide the best opportunity to study their properties. The only other possibility being a study of black hole mergers using gravitational waves, which is still a nascent field. As a corollary, black hole accretion systems also provide fertile conditions for understanding the complicated process of accretion.

X-ray binaries with black hole as a component exhibit rich phenomenology in radiation due to accretion of mass from the companion star. The X-ray spectrum of a black-hole binary consists of three main components, i.e., thermal emission from the disk, power law due to inverse Comptonization of the disk photons from geometrically thick and optically thin cloud of electrons (called as corona), and reflected emission of the Comptonized hard photons that hit the disk. Likewise, a power spectrum, which is the Fourier transform of a time series, consists of many peaked and broad noise components. Following five decades of extensive study, these aspects of black-hole binary outbursts stand on a fairly strong observational footing. In general, the process of state transition during an outburst and the associated spectral and timing variability are reasonably well understood, although, every now and then some exceptions crop up. Despite considerable advancement in understanding the phenomenology, some fundamental questions regarding the inner geometry of the accretion flow and the origin of certain observed phenomena remains debatable.

The accretion disk in the vicinity of a black hole is strongly influenced by two of its fundamental properties - mass and angular momentum (or spin), which makes their accurate measurement extremely important. Mass and spin estimates of a large sample of black holes are also necessary for constraining the stellar evolution theories. The best measurement of mass is done using the dynamical methods i.e., by measuring the radial velocity of the secondary star from Doppler shifted lines and feeding it to the binary mass function. However, in many cases the secondary is too faint to be detectable. An estimate of mass can also be obtained by correctly modeling the thermal X-ray emission from the accretion disk during a disk-dominant state. The measurement of spin is more tricky. It can either be done by modeling the fluorescent Fe $K\alpha$ line reflected from the inner accretion disk or by modeling the soft X-ray continuum. This is based on the rationale that the inner boundary of the accretion disk is determined by spin of the black hole. The measurement of the spin is also

important as it can constrain the models positing that the jets are powered by the spin of the black hole.

In order to gain deeper insights into the accretion process we have studied black-hole binaries using X-ray spectroscopy and timing analysis as primary tools. We analyzed three low-mass X-ray binaries, namely GRS 1716–249, MAXI J1631–479, and MAXI J1659–152 and one high-mass X-ray binary, namely Cygnus X–1, using data from six X-ray observatories and one ground based infrared telescope. With our work, we were able to comprehend the geometry of the inner accretion flow by studying the properties of the QPOs in MAXI J1631–479. We have delineated the radiation emitting from inner accretion region in GRS 1716–249. We have also constrained the two fundamental parameters of a black hole, i.e., spin and mass, for two systems - MAXI J1659–152 and MAXI J1631–479, which has far reaching consequences on the binary evolution and jet propagation theories.

Title: Experimental investigation of biomolecules under impact induced shock
Researcher: Singh, Surendra Vikram
Supervisor: Sivaraman, Bhalamurugan
Year: 2021
Keyword's: Complex Macroscale Structures, Biomolecules, Flower Morphology, Organic Compounds, Nucleobases
Call No.: 550 SIN
Acc. No.: T00962

Abstract: Amino acids, nucleobases, and sugar-related compounds are among the organic compounds found in primitive meteorites, which may be the potential building blocks of life. These organic compounds would have developed and evolved in a variety of environments. Many of these may have arrived on the early Earth in meteorites, comets, and interplanetary dust particles. The origins and evolutions of organic compounds are not well established despite numerous meteorite analyses and experimental studies. Sample return missions like Hayabusa2 and OSIRIS-REx are expected to provide more information about the origin, evolution, distribution, and delivery of prebiotic molecules. Under simulated prebiotic conditions, laboratory studies have shown the synthesis of almost all life's building blocks and polymers. On the primitive Earth, however, it is mysterious how these compounds spontaneously assembled to produce proto-biological functions (e.g., metabolism, replication). One of the most important and exciting challenges of our time is discovering pathways that led to the transition. While tremendous progress has been made in prebiotic chemistry since the famous Miller's experiments in the 1950s that revolutionized the field of prebiotic chemistry, there are still major challenges that remain in our understanding of the origin of life. Many of these studies have focused on the role of endogenous sources such as hydrothermal vents, synthesis in the primitive atmosphere, the importance of minerals surrounding, etc. However, given the intensity of impact bombardment on the early Earth, these environments are equally crucial in the prebiotic scenario for the studies on the origin of life. Impact induced shock provides a sharp increase in pressure and temperature due to shock compression and subsequent cooling due to expansion within a very short time scale. Such thermodynamic conditions can offer various pathways for molecules to react, thus can lead to the synthesis of a variety of molecules. Consequently, the studies herein investigate the fate of amino acids and nucleobases under high temperature heating effect of impact induced shock using laboratory techniques.

To simulate impact induced shock environment in the laboratory, an experimental set up of shock tube (HISTA) is designed and developed in Astrochemistry Lab PRL India. The shock tube setup is capable of providing a high temperature of approximately 8000 K maintained over a 2 ms time scale. Variety of amino acids were shock processed at various temperature ranges leading to the formation of a variety of complex structures, including globules, threads, filaments, twisted and folded assemblies, tubular structures of various sizes ranging from micrometer to millimeter scale, as revealed from microscopic observation. Membrane-like structures were seen at the nanometer scale in TEM observations. Spectroscopic observations have shown the formation of the peptides in shock processed residue. Impact experiments were also performed using a light gas gun facility with

high-speed bullet firing on the amino acid-water ice target, and ejecta coming out of target were collected and analyzed. Complex structures were observed in the ejecta similar to dendritic pattern and flower morphology. TEM observations of these ejecta have also shown membrane-like structures as we observed in shock processed residues. Further, mass spectrometry has shown that long polypeptide chains were synthesized in the ejecta. The formation of such peptides containing complex structures has important implications for the origins of life. Nucleobases, the basic component of informational polymers RNA and DNA, were also shock processed and formed long threads spanning up to mm scale.

Overall, in the present thesis, a novel method is designed for simulating the high temperature and pressure condition as achieved in natural impact events using high intensity shock tubes. The effect of high intensity shocks on amino acids and nucleobases is studied. This is the first report on the formation of complex macroscale structures due to impact induced shock conditions which provide pathways for the origin of life. Given the widespread record of impact events across the solar system bodies, hypervelocity impacts experiments are performed on icy mixtures of amino acids to simulate the impact on icy bodies of the solar system using a light gas gun, showing the formation of the long polypeptide chain in the impact ejecta. These results demonstrate that extraterrestrial impact provided necessary life ingredients and assisted in the formation of complex architecture that can form the basis for cellular life. Future research endeavors will focus on the various combination of biomolecules, including amino acids, nucleobases, sugars and fatty acids under impact shock conditions to resolve the complex pathways that lead to the origin of life.

Title: Magnetic field and electric current in the solar atmosphere
Researcher: Nayak, Sushree Sangeeta
Supervisor: Bhattacharyya, Ramitendranath
Year: 2021
Keyword's: Magnetic Reconnection, Magnetohydrodynamics, Magnetic Fields, Corona, Flares, Activities
Call No.: 523.72 NAY
Acc. No.: T00966

Abstract: Transients like solar flares, coronal mass ejections (CMEs), coronal jets, etc. are ubiquitous in the solar atmosphere. For several decades, investigations including theoretical studies, numerical modeling and observations have been carried out to reveal the intriguing physics behind them. The events vary in energy, spatial and temporal scales; providing outstanding opportunities for a comprehensive study of the solar atmosphere. A better understanding of these events is not only of fundamental importance but is of practical significance to realize potential space-weather influences. A near-consensus exists in contemporary research that magnetic reconnection—a fundamental process in the solar atmosphere involving rearrangement of magnetic field line connectivity, conversion of stored magnetic energy to kinetic energy, heat and acceleration of charged particles—is responsible for the onset and the evolution of these events. Also, important is the site of magnetic reconnection where these transients are believed to be triggered. Magnetic null points (where the magnetic field vanishes), separators (connecting layers between null points), and quasi-separatrix surfaces (regions with a sharp change in field line connectivity) are the preferential locations where the vanishing of the magnetic field or local enhancement of the current density can initiate reconnection. Identifying these locations and realizing their influences on local magnetic field lines are interesting and important to investigate the dynamics near the transients. Therefore, the thesis aims to study the role of magnetic field and electric current in the transients and, specifically focuses on the topology near the locations of reconnection—highlighting their generation and evolution along with the impact on the neighboring magnetic flux systems.

The coronal magnetic field, where most of the transients are traced, is also important. The coronal magnetic field is obtained by extrapolating the photospheric magnetic field. Subsequently, the extrapolated field is used as an input to a magnetohydrodynamics (MHD) model to capture the evolution. The works in the thesis have utilized both extrapolated and analytically derived magnetic fields as the initial inputs. For the extrapolations, the non-force-free-field (NFFF) model is employed in conjunction with the photospheric vector magnetograms from Helioseismic and Magnetic Imager (HMI) onboard Solar Dynamics Observatory (SDO). For the numerical simulation, we have used the well-established magnetohydrodynamics model EULAG-MHD. We have studied a blowout jet and a near co-temporal C-class flare hosted by the active region NOAA 12615 on 2016 December 5 via extrapolation and simulation. Near the jet, we find a pair of three-dimensional (3D) null points and a flux-rope (or mini-filament) lying below the nulls. In the simulation, the reconnection near the nulls initiates the jet and the cool materials escape from the mini-filament through the channel made by the ambient field lines of the corresponding spine axis. The simulation results validate the

standard scenario where a mini-filament interacts with the ambient open field lines causing the jet material to eject (Sterling et al., 2015). In case of the C-class flare, we find the presence of a single 3D null and quasi-separatrix layer (QSL) in the extrapolated field. In the simulation, the dynamics near these topologies explain the flare onset and match well with the observational signatures.

We have then simulated an X-class flare on 2014 March 29, to understand the initiation process. In the extrapolated field we find one 3D null, a pair of flux ropes, a set of sheared arcades, and a set of magnetic loops connected to a distant region which, is affected by the flare. The MHD evolution also matches well with the observations. We have estimated the stored energy released during the process and found it to be $\approx 6.8 \times 10^{31}$ ergs, again which is in agreement with the corresponding observational value. Another promising result is the value of Pearson correlation coefficient of ≈ 0.7 between the observed and simulated transverse magnetic fields toward the end of the simulation. In the next work, we have explored a circular flare ribbon and found a 3D null co-located with the flare location. The footpoint motions of the field lines lying on the fan surfaces and spines are following the circular brightening and a distant region away from the ribbon location. These data-constrained simulations of different solar transients showcase the role of complex topologies and corroborate remarkably with observations, and hence, prove the efficacy of both the extrapolation and MHD model.

Albeit their impact on triggering the transients, the generation of such null points in the solar atmosphere is counterintuitive. We sought out this issue by employing a two-pronged approach: (1) with the relaxation of a deformed potential null, and (2) relaxation of a modified Arnold-Beltrami-Childress (ABC) field—chaotic in nature and devoid of any null. The simulations show a spontaneous generation of 3D nulls, indicating their omnipresence in the solar atmosphere. Further, we also explore magnetic reconnections in the vicinity of the QSLs. We have investigated the effect of multiple sites of reconnection in a computational domain. The simulation results examine the role of plasma flow in presence of various topologies favoring magnetic reconnection. Overall, the thesis explores the importance of magnetic reconnection in the different solar transients via numerical and observational studies. Future studies will accommodate high-resolution magnetic field data from upcoming space and ground-based observations. Toward simulating more accurate dynamics of the transients, a data-driven model is also envisaged as a future assignment.

Title: Probing new physics with cosmological observations
Researcher: Parashari, Priyank
Supervisor: Mohanty, Subhendra
Year: 2021
Keyword's: CMB, LSS, Viscous Dark Matter, Neutrinos, Sterile Neutrinos, Mini-BooNE, PBH, GW, NANOGrav
Call No.: 530 PAR
Acc. No.: T00967

Abstract: Our knowledge of the Universe is based on several observations, such as observations of cosmic microwave background (CMB) anisotropy, large scale structure (LSS), and gravitational waves (GWs). These observations give us insight into cosmological theories of structure formation, dark matter, inflation, GWs, and primordial black holes (PBHs). These observations can also provide an excellent probe to particle physics, e.g., properties of neutrinos. Neutrinos leave their signature in the CMB and LSS observations, making cosmological surveys a promising probe of neutrino properties. In this thesis, we study the underlying connection among these observations and use them to constrain the theories of dark matter, neutrinos, and inflation. However, there is no direct observational evidence of the physics of the Universe before the big bang nucleosynthesis (BBN) epoch. Interestingly, observation of GWs at current pulsar timing arrays (PTAs) and interferometers and proposed GW observatories like LISA can be used to probe these epochs. Specifically, we use the recent observation by the North American Nanohertz Observatory for Gravitational Waves (NANOGrav) to constrain the stochastic GW background and PBH abundance utilizing the coupling between the scalar and tensor perturbations in higher order perturbations theories.

The CMB anisotropy and LSS observations are very well explained within the standard cosmological model, the Λ cold dark matter (Λ CDM) model. However, some discrepancies between the values of r.m.s. fluctuation of density perturbations at $8 h^{-1}\text{Mpc}$ scale (σ_8) and Hubble parameter at the present epoch (H_0) obtained from these observations within Λ CDM model have been reported, which hint towards the new physics. We explore two such possibilities, namely effective viscosity in dark matter and massive neutrinos, to resolve these tensions and find that effective viscosity simultaneously reconciles both tensions. In contrast, massive neutrinos resolve only the H_0 tension. Interestingly, the amount of viscosity required to reconcile these tensions is of the same order as the viscosity predicted by the effective field theory of dark matter fluid on large scales. We also report that the constraint on neutrino mass is more stringent if dark matter has an effective viscosity. Next, we go beyond the standard neutrino physics and discuss the implications of sterile neutrinos with $m \sim \text{O}(\text{eV})$, as indicated by some short baseline experiments, in cosmology. Such sterile neutrinos conflict with the cosmological observations. Self-interaction between these sterile neutrinos can make them compatible with cosmology. We find that the cosmological model with self-interacting sterile neutrinos (SIV) fits the Planck CMB data as well as the fit in the Λ CDM model. Moreover, we find a lower value of the spectral index in the SIV model than in the Λ CDM model, which significantly impacts the validity of inflation models. For example, inflation models like the Starobinsky and quartic hill- top models allowed within the Λ CDM model are disfavored in the SIV

model, whereas inflation models, such as natural and Coleman-Weinberg inflation, are now favored in S_{lv} model.

There is also a possibility that PBHs may constitute a significant fraction of dark matter. We study the PBH formation and GW evolution in the nonstandard cosmological histories to probe the early Universe between the end of inflation and BBN. The dynamics of PBH formation and evolution of GWs in a nonstandard post-inflationary epoch are significantly different from that in the standard cosmology. In the standard cosmology, the abundant PBH formation requires a nonstandard power spectrum feature with large power on the small scales. In this thesis, we explore the PBH formation in the nonstandard cosmological evolution with the nonstandard primordial power spectrum. Specifically, in a pre-BBN kination dominated (KD) epoch, we find that abundant PBH formation requires a lower amplitude of the primordial scalar power spectrum than required in the standard RD epoch to reach the same abundance. We also find that both the first- and second-order GW spectra show an enhancement in the KD epoch, which may be probed by the current and future GW surveys. Next, we investigate the possibility of the recent NANOGrav signal being a first- or second-order stochastic GWs evolving through the nonstandard post-inflationary epochs. We find that the first order GWs evolving through a nonstandard cosmological history with a pre-BBN matter dominated epoch can fit the stochastic GW hypothesis of NANOGrav observation, whereas constraints from the BBN and CMB observations rule out the possibilities of the NANOGrav signal arising from the first order GWs in the standard RD or nonstandard KD epoch. On the other hand, for the second-order GWs, we find that the fit of the stochastic GW hypothesis of NANOGrav signal as a second-order GW background and abundant PBH formation in the standard RD epoch can be obtained simultaneously for different forms of power spectra under consideration. Furthermore, we show that fit of the stochastic GW hypothesis of NANOGrav signal as the second-order GWs and abundant PBH production in a nonstandard dustlike epoch can be obtained simultaneously only for a few of all the power spectra considered here, if these power spectra peak at scales (k_p) larger than the NANOGrav observed scales. However, in the case of a KD epoch, the abundant PBH formation is not consistent with the NANOGrav observation.

Upcoming experiments of CMB and LSS surveys like CMB-S4, Euclid, and LSST will refine our understanding of the cosmological models. Neutrino experiments like DUNE will give precise information about neutrino masses, mixing angles, and mass hierarchy. Current and future GW experiments, such as advanced LIGO/VIRGO, LISA, and PTA surveys, will expand the regions of frequency and amplitude of cosmological and astrophysical GWs. Therefore, the models of dark matter, neutrino interactions, PBHs and GWs we study in this thesis will be further validated or ruled out by the upcoming experiments.

Title: Chemically active systems as sensors and transducers
Researcher: Shukla, Ashish Kumar
Supervisor: Dey, Krishna Kanti
Year: 2023
Keyword's: Catalytic Motors, Microbial Active Matter, Sensors-Transducers
Call No.: 681.2 SHU
Acc. No.: T01035

Abstract: This dissertation discusses a few simple and inexpensive sensing and energy harvesting strategies that utilize self-propulsion and collective behaviors of both synthetic and biological active systems. Autonomous propulsion of particles was realized using polymer beads coated with catalytic nanoparticles that actuated in dilute hydrogen peroxide (H₂O₂) solutions. The behaviors of these self-propelled particles were found to be dependent on the properties and compositions of their surrounding media, which offered opportunities to use them for on-the-fly sensing and harvesting of useful energy in simple electrochemical chambers. Generation of energy based on bacterial enzyme-mediated redox reactions has also been demonstrated, which opens avenues for the development of microbial activity controlled small-scale power generators. The results and observations presented in this thesis provide key insights into the foundations necessary to fabricate multifunctional sensors and energy harvesting devices based on self-powered chemically active systems.

Chapter 1 aims at presenting a simple and pedagogical review of the literature to help the reader get an overview of the field of active matter. Various challenges and opportunities in this field are highlighted. Also, this chapter includes a comprehensive discussion on the importance and state-of-the-art of active matter-based sensing and energy harvesting in fluidic media. Noteworthy attempts made by various research groups towards developing such synthetic and biological systems are reviewed in brief; highlighting the significance and contributions of each of these approaches. The chapter is concluded with a justification for the need of scalable and cost-effective devices, as demonstrated in the current thesis work, that offer better flexibility in terms of ease of fabrication, mechanical stability and possible integration with biological systems.

In Chapter 2, the self-propulsion of catalytic motors fabricated using polymer particles coated with palladium nanoparticles (Pd NPs) and luminescent Zn-quinolate inorganic complex (Zn-QC) has been studied. This bi-functional motor shows oxygen (O₂) bubble powered vertical motion in dilute H₂O₂ owing to the catalytic decomposition of the peroxide by Pd NPs. The average vertical speed of the motor was found to be a measure of the viscosity of the medium, while its fluorescence was found to be correlated with the crowding conditions within the solution. This was demonstrated experimentally by observing the motion of the motor in different concentrations of reagents that are used in mimicking crowded cellular environments, such as Ficoll 400 and glycerol. Experiments performed with bacterial suspensions further suggested that these bi-functional motors can be used as a probe in measuring the spatio-temporal concentration fluctuations within active biological fluids.

The research results discussed in the previous chapter have been extended further in Chapter 3, in order to develop a simple, table-top technique for efficient detection of enzyme inhibitors and other harmful chemicals in various solutions and industrial effluents. The propulsion speed of the polymer nanoparticle composite motors has been shown to be enhanced in the presence of secondary catalysts like catalase and horseradish peroxidase, which generate auxiliary convections in the experimental chamber. The convections and motor propulsions are sensitive towards the presence of molecules that inhibit the enzyme activity, thereby offering a simple route for using these motors as dynamic sensing probes. It has been shown that the dynamics of these motors is sensitive enough to detect trace amounts of heavy metal ions, inorganic pollutants, aromatic dipeptides and toxins present in industrial effluents. This offers an inexpensive, easy-to-use, rapid method for toxin detection, health hazard monitoring and environmental remediation. A simple model connecting the enzyme inhibition and motor propulsion speeds has also been developed to support the experimental observations and results.

Chapter 4 discusses how self-propulsions of the polymer based catalytic motor can be harnessed in designing a non-Faradaic electrochemical energy generator or storage device. The experiments are performed within an electrochemical chamber containing the motors, 1% aqueous H₂O₂ as the fuel, a fluorine doped tin oxide (FTO) working electrode and a salt gradient. The polymer- supported motors, while moving through the fuel solution, periodically interacted with the electrode surface that was positioned at the top of the electrochemical chamber. While doing so, the motors facilitated the advective transfer of ions from the bottom of the fuel solution to the negatively charged FTO electrode, which resulted in the formation of an electrical double layer capacitor (EDLC). The magnitude of this EDLC charging has been estimated using open circuit potential (OCP) measurements against a reference Ag/AgCl electrode. The charge transport and electrode charging profile match well with that of a series resistor-capacitor (RC) circuit. The strength of the potential generated has also been found to increase with the number of motors. Interestingly, instantaneous voltage spikes were also observed over the OCP signal profiles when the motors struck the electrode surface; possibly due to the instantaneous and enhanced ion transfers. The frequency of such voltage peaks generated has been found to get enhanced with the increasing speed of the motors through the solution. These results are expected to find applications in diverse fields ranging from the sensing of analytes to power generation at the small scales, under complex environments.

Other than using synthetic active systems for energy harvesting applications, useful energy has also been generated using activity and motility of bacterial suspensions. These observations and results are presented in Chapter 5. Here, a simple and efficient energy harvesting strategy has been shown based on the activity of cupric reductase NDH-2 enzyme present in *E. coli* bacterial cells. The generation of energy has been recorded in an electrochemical setup with various strains of *E. coli*, indicating that this strategy may, in principle, be applicable to other microbial catalytic systems. We offer a simple mechanism of the energy transduction process based on the hypothesis of bacterial enzyme-mediated redox reactions occurring over the working electrode surface. The amount of energy generated has been found to be dependent on the motility of bacteria within the experimental chamber, indicating possible opportunities for developing microbial activity-

controlled power generators. We also show that the Faradaic electrochemical energy harvested is large enough to power a commercial light-emitting diode connected to an amplifier circuit. We expect the present study to generate sufficient interest within the soft matter and biophysics communities, and offer novel platforms for controllable energy generation at small length scales.

Chapter 6 provides the summary of the research work done, highlighting the key contributions of various projects. It also discusses the possible future research directions based on the work presented in the thesis.

Title: Free space quantum key distribution: experiments for improving security and key rate
Researcher: Biswas, Ayan
Supervisor: Singh, R. P.
Year: 2021
Keyword's: Quantum Cryptography, Quantum Key Distribution, BB84 Protocol, BBM92 Protocol, Orbital Angular Momentum
Call No.: 530.12 BIS
Acc. No.: T01037

Abstract: Security of Classical Key Distribution can be open to threats after the development of quantum computers. Shor's quantum algorithms can easily break the prime factorization and discrete log problem, which are crucial for providing security to classical cryptography. To provide unconditional security to the keys, Quantum Key Distribution (QKD) comes to the rescue. QKD is one of the most important applications of quantum mechanics in modern times. Photons are the most viable quantum system for QKD since they can be transported through free-space as well as through optical fiber. However, due to inherent loss in the fiber, it cannot be used for long distance QKD. Therefore, free-space quantum communication assumes importance as it is a precursor for satellite-based quantum communication needed for secure key distribution over longer distances. Though QKD provides unconditional security, practical implementation deviates from the ideal one, affecting the secure key rate. We have developed techniques to improve the key rates for BB84 and BBM92 QKD protocols and methods to characterize implementation loopholes. These loopholes create vulnerabilities in proving the absolute security to the QKD protocol. Although QKD provides information theoretic security but, due to unavailability of ideal sources and detectors, adversary can take the advantage and guess the key that is being shared between communicating parties. This can be a major setback in implementing QKD systems in real scenarios. Even though there are true single photon sources but their efficiency is very less that reduces the key rate. Therefore, one uses weak coherent laser pulses as a source for prepare and measure protocols which can increase the key rate, however, can compromise the security. Therefore, it is necessary to characterize the source to quantify the amount of information leakage due to the side channel. We have discussed how one can characterize the QKD source for side-channel leakage as a function of different source parameters. Also, we have quantified this information leakage in terms of cross-correlation between two signals. It is also seen that for some parameters this leakage is considerable, while it is negligible for others. Possible ways out to reduce the side channel have also been proposed. This can come in handy while making it ready for field deployment. For increasing the key rate using weak coherent laser pulses, the decoy state method is used, which adds complexity to the BB84 protocol. We introduce a novel quantum key distribution protocol, coincidence detection quantum key distribution protocol (Coincidence Detection (CD) QKD). We show that in this protocol, the Poissonian nature of weak coherent pulses instead of posing a security risk can be used to achieve a secure key rate over a longer distance compared to standard GLLP (Gottesman, Hoi-Kwong Lo, Lutkenhaus and Preskill) method for quantum key distribution. This protocol will also be able to track the presence of Eve (Eavesdropper) from the multi-photon (mainly consisting of two and three

photons) weak coherent laser pulses. Looking at the current trend for satellite-based optical communication, using satellite as a trusted device as in prepare and measure QKD protocols is fraught with danger. Therefore, entanglement-based protocols are preferred since, along with overcoming the distance limitation, one can take the satellite as an untrusted device. The most widely used EB QKD is the E91 protocol, but the key rate is less as a large fraction of the bits are sacrificed for Bell parameter (S) checking. This key rate can be increased by using the BBM92 protocol with a pre-characterized relation between S and QBER. This method efficiently increases the key rate without affecting the security of EB QKD.

Title: Hard X-ray spectro-polarimetric study of black hole binary Cygnus X-1
Researcher: Kumar, Abhay
Supervisor: Vadawale, Santosh V.
Year: 2022
Keyword's: Cygnus X-1, Black Hole, X-ray Polarisation, Compton Spectro Polarimeter
Call No.: 523.8875 KUM
Acc. No.: T01049

Abstract: The study of astrophysical sources is done with the help of electromagnetic radiation emitted by them, starting from γ rays to radio. In the X-ray sky, black hole binaries are one of the most peculiar astrophysical sources to understand the physics in the extreme conditions such as strong gravity, high temperature, and magnetic field. Black hole X-ray binaries are the binary systems in which the primary is a black hole and the secondary is a normal star. The black holes are the region of space time from where even light cannot escape. It is very challenging to study black hole because we do not get any radiation directly from it. It is mostly studied through the radiation emitted from the surrounding environment which is under its gravitational influence. Accretion of matter onto black hole gives rise to X-rays along with other wavelengths to study their properties. The typical geometry of accreting environment around the black hole is based on spectroscopic and timing studies.

The X-ray spectrum of a black hole binary consists of three main spectral components: thermal emission from the disk, power law continuum emitted as a result of inverse Comptonization of the thermal disk (or seed) photons from an optically thin medium of electrons (known as corona or Compton cloud), and the emission resulting from the reflection of the continuum photons hitting the disk. It is generally accepted that corona is responsible for the power law emission. However, the composition and geometry of the corona are still unclear. Different competing models have been developed based on timing and spectroscopic observations which successfully produce the powerlaw and other variability properties. Some of the geometries that have been incorporated are spherical, sandwich or slab, lamp post etc., but there is no general consensus on any of them. To break this degeneracy, X-ray polarisation studies can play a vital role. The degree of polarisation and the polarisation angle are the two additional observables that can help in the discrimination between different models. Astrophysical sources exhibit polarisation primarily as a result of scattering and synchrotron emission, which are determined by the geometry, magnetic field strength, and structure of the source.

In order to understand the geometry of the corona and the emission mechanism, we have studied black-hole binary Cygnus X-1 using X-ray spectroscopy timing and polarisation analysis as primary tools. Cygnus X-1 is a galactic black hole binary comprising a black hole of mass $\sim 21 M_{\odot}$ that accretes from the companion supergiant star (O9.7 type) with a mass of 40.6 solar mass. Its brightness and proximity (distance ~ 2.22 kpc) have made it an obvious choice of study by different instruments. It has been extensively studied using spectroscopy and timing analysis techniques in a wide energy range, but X-ray polarisation analysis remains mostly unexplored due to the requirement of relatively longer exposure times and instrumental limitations. In this thesis, we have

used AstroSat -CZTI data to study Cygnus X-1. The CZT detectors are of 5 mm thickness and hence have good efficiency for Compton interactions (double pixel events) beyond 100 keV, which are utilized for the polarisation study using CZTI in 100 to 380 keV. We explore the utility of polarisation double pixel events to do spectroscopy above 100 keV. We have used Crab observations, which is the standard calibration source in the X-ray sky, to refine the background selection and subtraction techniques. We get consistent hard X-ray flux and spectral index for Crab, which validates our techniques. We have also used AstroSat -LAXPC and SXT observations for the broadband spectroscopy. We have tried to comprehend the emission mechanism and geometry of the corona in Cygnus X-1 with the spectro-polarimetric study in the broad energy range of 1 - 380 keV. We further investigate the different hard X-ray spectral states in Cygnus X-1 and its polarisation dependence. For this, we measure the flux and spectral index in the 22 – 100 keV energy band and the short-term spectral and flux correlation index. We have identified distinct accretion modes in the source based on the hard X-ray data, consistent with the recent INTEGRAL results and its polarisation dependence.

We have discussed the implications of these results to understand the coronal geometry of the source and corona/jet contribution in the polarisation. Further, we show the necessity of the Compton spectro-polarimeter below 100 keV to get a complete picture of the source geometry and the emission mechanism. We provide a conceptual design of a Compton spectro-polarimeter and characterized the absorber's position sensitivity, which detects the scattered photons coming from the scatterer.

Title: Population of obscured active galactic nuclei
Researcher: Kayal, Abhijit
Supervisor: Singh, Veeresh
Year: 2023
Keyword's: Active Galactic Nuclei (AGN), Dust-obscured Galaxies (DOG)
Call No.: 523.112 KRO
Acc. No.: T01050

Abstract: Active Galactic Nuclei (AGN) are the manifestation of accretion onto the supermassive black holes (SMBHs) located at the centres of galaxies. AGN emit copiously across a wide range of wavelengths via various processes occurring in the material present around the accreting SMBHs. Moreover, the enormous radiative power in most AGN is often obscured by the gas and dust present in the circumnuclear environment and in the large-scale interstellar medium of the host galaxy. Thus, obscuration poses a challenge for uncovering the complete AGN population and understanding their cosmic evolution, in particular at high redshifts. The dust-obscured galaxies (DOGs), which are bright in the infrared wavelengths but relatively much faint in the optical wavelengths can be the potential hosts for obscured AGN. Due to the large content of dust and gas, the optical and UV emission from AGN gets heavily absorbed. Hence, optical and UV surveys can miss the AGN population residing in dusty environments. However, radio, infrared and X-ray surveys being less susceptible to absorption, can detect obscured AGN.

This thesis work delves into unveiling and understanding of a new population of AGN in DOGs using different observational techniques based on the deep radio, mid-IR and X-ray observations. Using deep radio observations from the upgraded Giant Metrewave Radio Telescope at 400 MHz, our study demonstrates that sensitive radio observations are one of the most efficient methods for detecting radio-emitting AGN residing in dusty environments. Our deep uGMRT observations have resulted in 29 per cent radio detection rate of DOGs, which is the highest among all the literature studies performed till date. With multi-frequency radio observations, we find that radio sources in DOGs are mainly compact steep spectra sources and peaked spectrum sources, which further infers that the radio sources are likely to be in the early phase of their evolution. Unlike our radio observations, we find that deep XMM-Newton X-ray observations detect a much smaller fraction (8 per cent) of AGN and the detections are limited only to the X-ray luminous AGN.

We performed X-ray spectral modelling of 34 DOGs ($0.59 \leq z \leq 4.65$) using all the existing *XMM-Newton* data, and *Chandra/ACIS* data, whenever available in the XMM-SERVS extragalactic field. The X-ray spectra of our DOGs can be well described with an absorbed power law and reflection component. The column densities derived from the spectral modellings show that all but four of our DOGs are moderately obscured ($N_{\text{H}} < 10^{23} \text{ cm}^{-2}$) and the fraction of heavily obscured DOGs is limited only to 11.7%. The high absorption corrected 2.0–10 keV X-ray luminosities ($10^{43} - 10^{45} \text{ erg s}^{-1}$) suggest for the presence of luminous AGN. The N_{H} versus Eddington ratio diagnostic plot infers that our DOGs represent a heterogeneous population containing Hot DOGs as well as reddened quasars. Only a few of our DOGs are likely to belong to an early phase (Hot DOGs) during which accretion and

obscuration peak, while the remaining DOGs possibly belong to a late phase during which radiative feedback from the dominant AGN blows away obscuring material.

In order to constraint the geometry of the circumnuclear obscuring material, we performed a detailed study of the multi-epoch broadband spectra of the heavily obscured AGN hosted in the nearby Circinus galaxy. We utilised all the available hard X-ray (> 10 keV) observations taken at ten different epochs in the span of 22 years from 1998 to 2020 from *BeppoSAX*, *Suzaku*, *NuSTAR* and *AstroSAT*. The 3.0-79 keV broadband X-ray spectral modelling using physically motivated models infers the presence of a torus viewed edge-on (inclination angle of 77° - 81°) with a low covering factor of 0.28, and Compton-thick line-of-sight column densities ($N_{H,LOS} = 4.13$ – 9.26×10^{24} cm $^{-2}$) in all the epochs. The joint multi- epoch spectral modelling suggests that the overall structure of the torus is likely to remain unchanged. However, we find tentative evidence for the variable line- of-sight column density on time scales ranging from 1 day to 1 week to a few years, suggesting a clumpy circumnuclear material located at subparsec to tens of parsec scales.

Title: Investigations on low latitude Ionosphere under varying space weather conditions
Researcher: Kumar, Ankit
Supervisor: Chakrabarty, Dibyendu
Year: 2022
Keyword's: Equatorial Ionosphere, Equatorial Ionization Anomaly, Equatorial Plasma Fountain, Zonal Electric Field, Pre-reversal Enhancement, Overshielding (OS) Electric Field, Total Electron Content
Call No.: 538.767 KUM
Acc. No.: T01053

Abstract: The central theme of the present thesis work is to understand the role of ionospheric electrodynamics over the equatorial ionosphere in the plasma distribution over the low latitude sector, in general, and the EIA crest region, in particular, during different seasons, solar fluxes, and solar activity conditions. The dip equatorial electric field perturbations related to space weather events are also investigated during post-sunset as well as post-midnight hours and their effects over low latitude plasma distribution are investigated.

Based on 10 years' of observations (2010-2019) of the vertical total electron content (VTEC) over Ahmedabad (23.0°N, 72.6°E, dip angle 35.2°) and campaign based observations of OI 630.0 nm airglow intensity over Mt. Abu (24.6°N, 72.7°E, dip angle 38.0°), enhancements in VTEC/airglow intensity are brought out during post-sunset hours. Morphologically, these enhancements are found to start any time after 1900 LT and peak around 2000 LT. It is found that these enhancements are primarily caused by the pre-reversal enhancement (PRE) of the zonal electric field over the dip equator through re-invigorated plasma fountain process assisted by the latitudinal plasma density gradients. Interestingly, the post-sunset enhancements in VTEC over the EIA crest region are conspicuous during the December solstice and Equinox in the high solar activity period only. This is consistent with the seasonal and solar activity dependence of the amplitudes of PRE-associated vertical drifts over the dip equator. This suggests that the post-sunset enhancements are related to PRE. The thesis propounds that as the daytime equatorial plasma fountain (EPF) process decides the plasma distribution over the low latitudes, the PRE-driven re-invigorated EPF determines the degree of post-sunset enhancements over the low latitudes. Interestingly, the response time of the EIA crest region corresponding to the PRE-driven plasma fountain is found to be ~ 1.7 hr in contrast to the 3-4 hrs of response time corresponding to the daytime plasma fountain. The TEC measurements by the Indian Satellite-based Augmentation System (SBAS) GAGAN (GPS Aided Geo Augmented Navigation) suggest that PRE drives plasma from 5°-10° magnetic latitude to the EIA crest region, leading to a shorter response time during post-sunset hours. Further analysis of Ahmedabad VTEC reveals that the post-sunset enhancements depend on the solar flux levels and are conspicuous if the solar flux level exceeds ~110 sfu during December solstice and Equinox. As PRE is also solar flux dependent, this provides further credence to the direct role of PRE in driving the post-sunset enhancements over the EIA crest region. However, it is suggested that PRE is a necessary condition but not a sufficient condition for the post-sunset VTEC enhancements over the EIA crest region. This is because plasma densities and vertical drifts obtained from the Thermosphere Ionosphere

Electrodynamics- General Circulation Model (TIE-GCM) suggest that latitudinal plasma gradients work in tandem with the PRE to determine the degree of post-sunset enhancements in plasma density over the EIA crest region.

In addition to the quiet conditions, the present thesis also brings out a few cases of space weather-induced electric field perturbations during post-sunset and post-midnight hours. These investigations are carried out to understand the changes in the post-sunset ionosphere over low latitudes during disturbed space weather conditions. Several kinds of space weather-induced electric field perturbations are investigated that often worked in tandem or in opposition. These investigations suggest that many anomalous electric field perturbation events cannot be explained based on the conventional penetration electric field paradigm that solely depends on the solar wind electric field related to IMF Bz and solar wind velocity. In fact, these investigations show that unconventional drivers like IMF By, substorm induced electric field etc., can play important roles in modulating the amplitude and polarity of penetration electric field perturbations during both post-sunset and post-midnight hours. These have ramifications for evaluating the state of the low latitude ionosphere at night during disturbed space weather conditions.

Title: Phenomenological applications of light cone sum rules
Researcher: Bansal, Anshika
Supervisor: Mahajan, Namit
Year: 2022
Keyword's: Light Cone Sum Rules (LCSR), Hadronic Matrix Elements, Baryon Number Violation Proton Decay, Quantum Chromodynamics
Call No.: 539.7548 BAN
Acc. No.: T01054

Abstract: Within the Standard Model (SM) of particle physics, the strong interactions are dictated by the gauge theory called quantum chromodynamics (QCD). QCD is a theory of quarks and gluons, which carry a gauge charge called color. Gluons are the mediators of strong interactions between colored particles, very much like the photon for electromagnetic interactions between electrically charged particles. However, unlike photons, the gluons themselves carry color charge due to the non-abelian nature of QCD. This leads to self-interactions of gluons, and hence to many exciting phenomena in QCD like *asymptotic freedom*, *color confinement*, etc. The quarks and gluons form colorless bound states like *mesons* (the bound state of a quark and anti-quark) and *baryons* (the bound state of three quarks), collectively called *hadrons*, at small energies because of the phenomenon of color confinement. As a result, we only detect colorless hadrons at the detectors. According to the scattering theory, experimental observables like decay width, scattering cross-sections, etc., can be calculated theoretically by calculating the matrix elements of quark-gluon operators between the initial and final hadron states called the *Hadronic Matrix Elements (HMEs)*. However, the difficulty arises as these hadrons are bound states i.e. are non-perturbative in nature, and hence, the perturbative QCD can not provide a complete solution to these HMEs. Consequently, these HMEs contain the non-perturbative effects in the form of hadronic quantities like form factors, decay constants, etc.

These hadronic quantities are very essential inputs for any prediction within or beyond the SM. Therefore, calculating these quantities is very crucial. There exist several methods like chiral perturbation theory (PT), lattice QCD (LQCD), QCD sum rules (QCDSRs), etc., to handle these objects. However, none can give precise results with the current techniques and computational skills, and different methods are found to typically work well in different regimes.

Therefore, estimations of these quantities, involved in the processes of interest, using different methods is very important to get reliable theoretical estimates for the experimental observables. In this thesis, we have discussed the applications of the method of Light Cone Sum Rules (LCSR), the QCDSRs on the light cone, to various processes within and beyond the SM, focusing on the calculation of the Form Factors (FFs) involved. LCSR is a QCD based method. It uses the analytic properties of the correlation functions, the matrix elements of the quark and gluon operators taken between the vacuum and the hadronic state, and the framework of Operator Product Expansion (OPE) to compute these FFs. Along with these properties, it uses Quark-Hadron duality which allows one to calculate the correlation functions at large Euclidean momentum transfers which can then

be analytically continued to the desired kinematical regime. As stated above, every available non-perturbative method has limitations and domain of applicability, and so does the method of LCSR. To explore the applications of LCSR and gain better understanding of its limitations, we considered several processes within and beyond the SM involving light as well as heavy quark hadrons. The considered processes are the radiative tau decay (involving a light meson called pion), the proton decay to a positron and a photon (involving a light baryon called proton), the baryon number violating decay of D-meson to an anti-proton and a positron, and the radiative decay of D_{K^*} -meson (both involving heavy quark D-meson). In all these cases, the method of LCSR is found to provide reasonable estimates for the form factors involved. All of these are the first applications of LCSR to such processes. Moreover, for the considered cases involving proton and D-mesons, we discussed the first theoretical estimates of the FFs involved which are of great phenomenological importance as they can be very helpful in constraining the Beyond SM (BSM) models, and probing the structure of the hadrons. The results can be further improved with the inclusion of higher-order effects which may also bring some new elements. This method also has the potential to be applied to several other situations like non-leptonic decay modes where systematic calculations still show some discrepancies.

Title: Observational analysis of cometary bodies in the solar system
Researcher: Aravind K.
Supervisor: Ganesh, Shashikiran
Year: 2022
Keyword's: Comets, 156P/Russell-LINEAR, Comet Spectroscopy, Interstellar Comets
Call No.: 523.6 ARA
Acc. No.: T01055

Abstract: As a supplementary to the eight major planets, there are countless minor bodies, belonging to various reservoirs, that go around the Sun in various orbits. They have their own characteristic behaviour and composition. Most of the minor bodies such as the comets, which are remnants of the proto-planetary disk that formed the Solar system, are faint and inactive at a large heliocentric distance. These bodies being the remnants contain pristine material from the early protosolar nebula. Owing to the small mass and long orbital periods of comets, they would have probably undergone less internal and external evolution. Hence, they embrace information regarding the composition and thermophysical conditions that existed in the protoplanetary disk. One of the key motivations to carry out research and study different comets and their characteristics is that they can advance our understanding of the Solar system and its evolution from the protosolar nebula.

Comets have been observed to be distributed into different reservoirs. Various theories suggests that these reservoirs would have formed as a result of multiple chaotic planetary migration that occurred at different stages of the Solar system formation. A major mixing up of the material distributed in the proto-planetary disk would have occurred during these chaotic movements. Hence, the average composition of a comet family or the overall composition of an individual comet cannot be linked to a particular place or time in the proto-planetary disk. As a result, observing and analysing pre- dominantly all the comets originating from different reservoirs is essential for having a general idea regarding the distribution of cometary material. At far off heliocentric distances, comets behave similar to asteroids as the ambient temperature would not be high enough to sublimate the volatile materials present in the comets. Short period and Long period comets keep orbiting in their respective orbital periods while new comets are injected into the Solar system from distant reservoirs like the Kuiper belt or the Oort cloud due to some external perturbations. As these objects start moving into the inner Solar system, based on the volatile nature of the materials present, sublimation occurs, producing an envelope made up of gas and dust, which is called the coma of the comet. It is at the onset of this phenomenon, comets are said to be active and hence become detectable. The observed coma is made up of material rising from the cometary nucleus, which formed at the initial stages of the Solar system. This makes comets a potential ticket to understand the history of the Solar system. Likewise, Interstellar comets, which were once part of another stellar system is a prospective messenger to understand and compare the composition of those systems with that of ours. Such comparisons can further help in confirming whether the formation of our Solar system was unique or general.

There are different aspects of a comet that needs to be studied. This includes the gaseous/dust activity and composition. The coma morphology can also speak for itself regarding the jet activity occurring within the coma. Therefore, the current work is intended in having a wide scale analysis of comets by examining the comets characteristics in different aspects. The gas activity/composition is studied by analysing the cometary emission spectra via low or high resolution spectroscopy. Dust activity/characteristics can be probed via imaging/spectroscopy and polarimetry, while the coma morphology and jet structures is studied by imaging the comet in various filters. The optical spectroscopic, polarimetric and imaging studies are carried out using the 1.2 m and 2 m telescopes at Mount Abu Infrared Observatory and Indian Astronomical Observatory respectively. In this work, a total of 22 comets, 10 Short Period Comets, 11 Long Period Comets and 1 Interstellar comet have been observed and studied. Out of these, all 22 of them have been studied via low resolution spectroscopy, 4 comets in high resolution spectroscopy and 5 comets by means of polarimetric observations. Low resolution spectroscopy has been used to analyse the relative abundance of various molecular emissions and Afp profiles corresponding to different filter bands, while high resolution spectroscopy was employed to probe and separate the different blended emissions. High resolution was also effective in identifying the emission lines within each molecular bands and in investigating the forbidden Oxygen lines as well different bands of NH₂. Optical imaging and polarimetry were carried out to analyse the coma morphology and to evaluate the variation in degree of polarisation with phase angles for different comets, respectively.

The thesis commences with a basic introduction to the structure of the Solar system. The various major cometary reservoirs, their interconnection, classification of comets based on different criteria and the theories explaining the role of planetary migrations on the formation of these reservoirs have been briefly explained. A brief introduction to comets, including details regarding their activity, volatile composition, optical spectrum and detected species, dust properties, etc is provided. The roadmap of speculations related to the existence of the Interstellar comets alongside the presence of exocomets have been briefed. Comet 156P/Russell-LINEAR was analysed with spectroscopic, polarimetric and imaging techniques to have a wider understanding of the comet's characteristics. Comets 46P/Wirtanen and C/2017 T2 (PANSTARRS) were observed extensively in low resolution spectroscopy to examine the fluctuations in the comet's activity along its orbit. The great comets of 2020 and 2021, C/2020 F3 (NEOWISE) and C/2021 A1 (Leonard), respectively, a peculiar Short Period Comet 29P/Schwassmann–Wachmann, interesting activity in comet 88P/Howell and many other interesting comets have been studied in optical spectroscopy and their activities have been examined and discussed. A few comets, including 46P, were observed in high resolution spectroscopy and different aspects of emission lines have been analysed. Once in a lifetime appearance of an Interstellar comet, 2I/Borisov, was observed in low resolution spectroscopy to report its pre and post perihelion activity to point at a possible heterogeneous nucleus of the comet. Imaging techniques were also employed to obtain the rough estimate of the comet's nucleus size. Results obtained from each individual analysis have been discussed in their respective chapters and all the obtained results have been put together to achieve a collective understanding. This work demonstrates the importance of observing all possible cometary bodies and the advantage of simultaneously employing different observational techniques to analyse the characteristics of a

comet. This work also exemplifies the significance of a common cometary database systematically updated with latest observational results, which can be later used for modelling and for cometary classification purpose.

Title: Investigating the coronal X-ray characteristics - from Sun as a Star to imaging spectroscopy
Researcher: Mondal, Biswajit
Supervisor: Vadawale, Santosh V.
Year: 2022
Keyword's: X-ray Spectroscopy, X-ray Imaging, X-ray Telescope, Solar Corona, Coronal Heating
Call No.: 523.7 MON
Acc. No.: T01056

Abstract: The specific physical mechanism underpinning the coronal heating mechanism, which causes the solar corona to be significantly hotter than the solar photosphere, remains a mystery. According to our current understanding of the problem, it is believed that the corona is heated by the continual deposition of small-scale energy, so called nanoflares. In addition to the coronal heating problem, the spectroscopic observation revealed that the abundance of low FIP elements (whose First Ionization Potential is less than 10 eV) in the closed-loop active corona is 3–4 times higher than their photospheric abundances. The difference in coronal and photospheric abundances is characterized by their ratio, termed as “FIP bias”. This phenomenon is known as the “FIP Effect”, and its true origin is yet to be known. However, with the recent understanding, the FIP effect is believed to be a bi-product of the coronal heating mechanism.

To comprehend the FIP effect in various coronal structures, we have used the disk-integrated spectroscopic observations acquired by the Solar X-ray Monitor (XSM) onboard India's Chandrayaan-2 satellite. The XSM is a broadband spectrometer with a good energy resolution of better than 180 eV at 5.9 keV. It operates in the soft X-ray energy range of 1 to 15 keV with a cadence of 1 s. We have determined the evolution of temperature (T), emission measure (EM), and elemental abundances for X-ray Bright Points (XBP) and Active Regions (AR) by analyzing the XSM spectra taken during the minimum of Solar Cycle 24. The estimated T and EM are found to be correlated to the measured X-ray flux, whereas the abundances are consistently higher than their photospheric values without much variation. The FIP bias of Mg and Si was found to be ~ 3 for AR, which develops within ~ 10 hours of the AR's emergence during its emerging phase and is almost constant irrespective of the AR's activity or age. The FIP biases of Mg and Si for quiet Sun XBPs, on the other hand, are found to be ~ 2 , which is smaller than the obtained FIP bias of AR. This is the first time we have provided a prolonged study of the abundances of XBPs, and it shows an intermediate FIP bias compared with the ARs and photospheric values. With our present theoretical understanding of the FIP effect, having the lower magnetic activity of the XBPs, it is expected to have a low FIP bias compared with the ARs. We also find that the lowest FIP element, Al, has a stronger FIP bias than Mg and Si, indicating a probable link between the degree of FIP bias and the FIP values of the low-FIP elements.

Performing the time-resolved spectroscopic analysis of the XSM spectra, we examined the evolution of FIP bias during multiple small flares. We have found a statistically persistent variation in FIP bias across all of these flares. During the impulsive phase of the flares, FIP bias became unity from their 3-4 times higher pre-flare coronal values. Beyond the flare peak, the FIP biases are seen to get enriched again and they recover back to the coronal values at the end of the flare. Our observation of quick recovery to the coronal values show that any process giving rise to such fraction must be occurring on a time scale of few tens of minutes. We have proposed two scenarios to explain these results. The first scenario is based on the evaporation velocity of the flaring plasma from the lower to the upper atmosphere, and the second relies on the flare-driven Alfvén waves.

Using the unique combination of disk integrated soft X-ray observations with XSM and imaging EUV observations with AIA/SDO, we have estimated the plasma emissions of the disk-integrated quiet Sun and XBPs at different temperatures, characterized by Differential Emission Measure (DEM). In the absence of any AR, XBPs are found to be the dominant contributor to disk-integrated X-rays with a radiative flux of $\sim 2 \times 10^5 \text{ erg cm}^{-2} \text{ s}^{-1}$. XBPs consist of small-scale loops associated with bipolar magnetic fields. We have simulated such XBP loops using the hydrodynamic model and have estimated their composite DEM, which is then compared with the observed DEM. A good agreement between the simulated and observed DEMs suggests that XBP heating can be attributed to the frequent heat deposition by nanoflares caused by the release of magnetic free energy within stressed loops.

During the minimum of solar cycle 24, when solar activity was at its lowest, it was possible to study the spatially integrated plasma parameters from XBPs, ARs, and tiny solar flares using XSM's sun-as-star observations. However, to examine the spatiotemporal evolution of the individual features on the solar disc (e.g., XBPs, ARs, etc.), an imaging spectroscopic observation in the X-ray energy range is required. We are stressing the need for a future X-ray imaging spectroscopic instrument for the Sun. An imaging spectroscopic instrument needs X-ray optics that rely on X-ray mirrors. A single or several thin (10–100 Å) layer of materials make up an X-ray mirror. We have initiated the development of X-ray mirrors by setting up a thin-layer coating facility. Additionally, we have developed a piece of software called "DarpanX" to design and characterize the X-ray mirrors. We also have proposed a conceptual design for the Solar Imaging X-ray Spectrometer (SIXS), which operates in the 0.5–10.0 keV energy range. The instrument offers an energy resolution of more than 150 eV at 5.9 keV and a spatial resolution of around 4". If such an instrument can be launched in near future, it can further advance our understanding of the FIP effect and coronal heating, two crucial problems that are studied in this thesis. We have stated the primary scientific aims of the proposed SIXS instrument and evaluated its ability to accomplish those objectives.

Title: Properties of strongly interacting matter under extreme conditions
Researcher: Kumar, Deepak
Supervisor: Mishra, Hiranmaya
Year: 2023
Keyword's: Strong Matter, Nuclear Matter, Quark Matter, Non-radial Oscillation
Call No.: 539.7 KUM
Acc. No.: T01057

Abstract: Normal matter (protons, neutrons, mesons) are expected to undergo a phase transition at extremely high temperature ($\sim 10^{12}$ degree Kelvin) and/or extremely high density ($\sim 10^{14}$ gm/cc) to a state where the relevant degrees of freedom are their constituents described in terms of quarks, antiquarks and gluons called quark gluon plasma. Such kind of matter is believed to be there upto few tens of microseconds after the big bang. The cold quark matter is also expected to be present in the core of ultra compact astrophysical objects for example neutron stars, hybrid stars. In laboratory, quark gluon plasma can be produced at the collision center by colliding heavy ions at relativistic energies and it cools through the QCD phase diagram. In the off-central heavy ions collisions, extremely strong magnetic fields ($\sim 10^{18}$ Gauss) is produced by the current of the relativistically moving ions in opposite directions. It is very interesting to study the properties of matter under such extreme conditions of temperature, density and magnetic field.

We have worked on the two regions of the QCD phase diagram (in $T\mu$ plane)

- (i) zero temperature and non-zero chemical potential, and (ii) non-zero temperature and zero baryon chemical potential regions.

In the first part, we estimate the chiral susceptibility at finite temperature within the framework of the Nambu–Jona-Lasinio (NJL) model using the Wigner function. We also estimate it in the presence of chiral chemical potential (μ_5) as well as a non-vanishing magnetic field (B). We use a medium separation regularization scheme (MSS) in the presence of magnetic field and the chiral chemical potential to regularise the infinities present in the chiral condensate and corresponding susceptibility. It is observed that for a fixed value of chiral chemical potential (μ_5), transition temperature increases with the magnetic field. While for the fixed value of the magnetic field, transition temperature decreases with chiral chemical potential. For a strong magnetic field, we observe non degeneracy in susceptibility for up and down type quarks.

We also estimate some of the transport properties of the strongly interacting medium produced in the heavy ion collisions. A thermal gradient and/or a chemical potential gradient in a conducting medium can lead to an electric field, an effect known as thermoelectric effect or Seebeck effect. In the context of heavy-ion collisions, we estimate the thermoelectric transport coefficients for quark matter within the ambit of the NJL model. We estimate the thermal conductivity, electrical conductivity and the Seebeck coefficient of the same. These coefficients are calculated using the relativistic Boltzmann transport equation within the relaxation time approximation. The relaxation times for the quarks are estimated from the quark-quark and quark-antiquark scattering through meson exchange within the NJL model. As a comparison to the NJL model estimation of the Seebeck coefficient, we also estimate the Seebeck coefficient within a quasi-particle approach.

In the second part, in the context of the cold quark matter, we study the possibility of existence of quark matter in the core of compact stars (hybrid stars) and non-radial oscillation modes in neutron and hybrid stars. The Walecka type relativistic mean field models - (i) NL3 parametrised and (ii) with density dependent coupling parametrised (DDB) are considered to describe the nuclear matter at low densities and zero temperature and the NJL model is considered to describe quark matter at high densities in the zero temperature limit. A Gibbs construct is used to describe the hadron-quark phase transition at large densities. Within the models, as the density increases, a mixed phase appears at density about $2.36\rho_0$ ($3.93\rho_0$) where ρ_0 is the nuclear matter saturation density and ends at density about $5.22\rho_0$ ($6.9\rho_0$) for NL3 (DDB) models and beyond which pure quark matter phase appears.

It turns out that a stable hybrid star of maximum mass, $M = 2.27 M_\odot$ with radius $R = 14$ km, can exist with the quark matter in the core in a mixed phase only. The hadron-quark phase transition in the core of maximum mass hybrid star occurs at radial distance, $r_c = 0.27R$ where the equilibrium speed of sound shows a discontinuity. Existence of quark matter in the core enhances the non-radial oscillation frequencies in hybrid stars compared to neutron stars of the same mass. This enhancement is more for the g modes. The non-radial oscillation frequencies depend on the vector coupling in NJL model. The values of g and f mode frequencies decrease with increase the vector coupling in quark matter.

The non-radial oscillations of neutron stars have been suggested as an useful tool to probe the composition of neutron star matter. With this scope in mind, we consider a large number of equation of states (EOS) that are consistent with nuclear matter properties and pure neutron matter EOS based on a chiral effective field theory calculation for the low densities and perturbative QCD (pQCD) EOS at very high densities. This ensemble of EOSs is also consistent with astronomical observations, gravitational waves in GW170817, mass and radius measurements from Neutron star Interior Composition Explorer (NICER). Apart from verifying the robustness of universal relations (URs) among the quadrupolar f modes frequencies, masses and radii with such a large number of EOSs, we find a strong correlation between the f mode frequencies and the radii of neutron stars. Such a correlation is very useful in accurately determining the radius from a measurement of mode frequencies in near future. We also show that the quadrupolar f mode frequencies of neutron stars of masses $2.0 M_\odot$ and above lie in the range 1.68 - 2.16 kHz in this ensemble of physically realistic EOSs. A two solar mass neutron stars with a low f mode frequency may indicate the existence of non-nucleonic degrees of freedom.

Title: Study of the evolution of velocity and magnetic fields in the solar atmosphere
Researcher: Kumar, Hirdesh
Supervisor: Kumar, Brajesh
Year: 2023
Keyword's: Sunspots, Magnetic elds, Quiet-Sun, Chromosphere
Call No.: 523.72 KUM
Acc. No.: T01059

Abstract: In 1962, Leighton, Noyes and Simon discovered velocity oscillations on the photosphere of the Sun at Mt. Wilson Observatory in the USA using a spectro heliograph. These oscillations were interpreted as the superposition of millions of individual acoustic modes generated beneath the photosphere via turbulent convection and trapped inside the Sun. The oscillatory motions showed a dominant period of 5-minutes with a maximum velocity amplitude of 500 m s^{-1} . In 1972, Wolf suggested that solar flares could stimulate free modes of oscillations of the entire Sun. Solar flares are highly energetic events in the solar atmosphere that take place within a few minutes to hours and release an enormous amount of energy in the electromagnetic spectrum and consist of accelerated charged particles. During the bombardment of highly energetic charged particles on the chromosphere, some of these particles and downward propagating shock strike the solar photosphere thereby generating acoustic events like sunquakes or seismic emissions. Kosovichev and Zharkova (1998), for the first time, discovered the seismic emissions from an X2.2 class flare on July 9, 1996, in the active region NOAA 7978. This phenomenon was identified as a “sunquake”. Moreover, apart from the back reaction of charged particles and shock, Hudson et al. (2008a) suggested that abrupt changes in Lorentz force (namely the “magnetic jerk”) can also induce seismic emission in the sunspots accompanying major solar flares. However, Qiu and Gary (2003) had suggested and later on, it was found that line profiles are prone to getting distorted in the flaring locations during solar flares, which could affect the measurements of the Doppler velocity and magnetic fields. Therefore, we have investigated seismic emissions in the sunspots away from flaring locations accompanying major solar flares. These locations are considered to be free from any flare-related contaminations in the observational data. We construct acoustic power maps in 2.5–4 mHz band from photospheric Doppler velocity observations obtained during pre-, spanning and post-flare epochs and overplot contours of H_{α} flare ribbons and hard X-ray footpoints in 12–25 keV band. We have identified seismic emission locations within sunspots and away from the flaring sites. Our detailed analysis shows an abrupt and persistent change in photospheric magnetic fields in the seismic emission locations in the range of 50–100 Gauss within a period of 10–20 minutes. Also, we find that the estimated change in Lorentz force of the order of 10^{21} dyne is sufficient to induce seismic emission in the sunspots during the major solar flares. Our investigation provides evidence that abrupt changes in the magnetic fields and associated impulsive changes in the Lorentz force could be the driving source for these seismic emissions in the sunspots during solar flares. It is crucial to study the seismic emission in the sunspots during solar flares because these excess wave energies propagate up in the solar atmosphere in the magnetized regions and thereby may contribute to the heating of the solar active region atmospheres.

Additionally, the trapped low-frequency acoustic waves beneath the solar photosphere in acoustic cavities are considered to leak along the inclined magnetic fields due to the reduction in acoustic cut-off frequency. The propagation of these low-frequency acoustic waves in the small-scale magnetic fields is important in terms of their contribution to the heating of the lower solar atmosphere. Moreover, acoustic waves interact with highly structured magnetic fields of the solar atmosphere in complex ways. Observational studies of such interactions and the magnetohydrodynamic waves that result from them are essential for the energetics of the solar atmosphere and recovering the background thermal and magnetic structures. The plasma $\beta \approx 1$ surfaces and the magnetic canopy in the solar atmosphere play decisive roles in propagation of these waves. The high-frequency fast mode waves are refracted at $\beta \approx 1$ in the higher atmosphere and are known to cause high-frequency acoustic halos around the sunspots. Thus, we analyze the propagation of low-frequency acoustic waves into the solar chromosphere within small-scale inclined magnetic fields over a quiet-magnetic network region utilizing photospheric and chromospheric Dopplergrams obtained from the Helioseismic and Magnetic Imager (HMI) onboard Solar Dynamics Observatory (SDO) and the Multi-Application Solar Telescope (MAST) operational at the Udaipur Solar Observatory, respectively. In view of the stochastic excitation of acoustic waves and their intermittent interaction with the background magnetic fields, we use the wavelet technique to detect these episodic signals. We report a one-to-one correspondence between the presence of oscillatory signals (2.5-4 mHz band) in the photospheric and the chromospheric wavelet power spectra, which are associated with the leakage of photospheric oscillations into the chromosphere. In addition to this, chromospheric power maps also show the presence of high-frequency acoustic halos around relatively high magnetic concentrations, which indicate the refraction of high-frequency fast mode waves around $v_A \approx v_s$ layer in the solar atmosphere.

The internal or atmospheric gravity waves (IGWs) are generated by turbulent subsurface convection overshooting or penetrating locally into a stably stratified medium. This is a normal response generated by a gravitationally stratified medium to any perturbations from its equilibrium position and buoyancy acting as a restoring force. Gravity waves in the solar atmosphere are now increasingly recognized as an important contributor to the dynamics and energetics of the lower solar atmosphere. While propagating energy upwards, their characteristic negative phase shift over height is a well-recognized observational signature. Since their first detailed observational detection and estimates of energy content, several studies have explored their propagation characteristics and interaction with magnetic fields and other wave modes in the solar atmosphere. Recently, numerical simulations have shown that gravity waves are suppressed or scattered and reflected back into the lower solar atmosphere in the presence of magnetic fields.

Here, we present a study of the atmospheric gravity wave dispersion diagrams utilizing intensity observations that cover photospheric to chromospheric heights over different magnetic configurations of quiet-Sun (magnetic network regions), a plage, and a sunspot, as well as velocity observations within the photospheric layer over a quiet and a sunspot region. In order to investigate the propagation characteristics, we construct two-height intensity - intensity and velocity - velocity cross-spectra and study phase and coherence signals in the wavenumber - frequency dispersion

diagrams and their association with background magnetic fields. We derive signatures of association between magnetic fields and much-reduced phase shifts over height from intensity-intensity and velocity-velocity phase and coherence diagrams, both indicating suppression/scattering of gravity waves by the magnetic fields and thereby provide a qualitative observational verification of numerical simulations of such phenomena.

Thus, in this thesis we have investigated the evolution of velocity and magnetic fields in the solar atmosphere with an emphasis to understand the propagation of waves in the lower solar atmosphere.

Title: Equilibrium quantum phases and quench dynamics of dipolar bosons in 2D optical lattices
Researcher: Sable, Hrushikesh
Supervisor: Singh, Angom Dilip Kumar
Year: 2022
Keyword's: Quantum Phase Transitions, Gutzwiller Mean-field, Bose-Hubbard Model-Equilibrium
Call No.: 530.414 SAB
Acc. No.: T01060

Abstract: Emergence of the novel phases of matter at low temperatures has been a motivation to cool systems to lowest temperatures possible. At low temperatures, quantum statistics become important and the quantum fluctuations dominate over the thermal fluctuations. These fluctuations drive the quantum phase transitions (QPTs) which are associated with a change in the ground state of the system Hamiltonian. The bosonic quantum gases cooled to quantum degeneracy temperatures exhibit the Bose-Einstein condensation phenomenon, which corresponds to the macroscopic occupation of the single particle level. These Bose Einstein condensate (BEC) atoms when loaded in optical lattice potentials can exhibit the quantum phases in the strongly interacting domain; and are novel quantum systems to study the quantum many-body physics and QPTs. In this thesis, we investigate the quantum phases of the neutral and dipolar ultracold bosonic gases trapped in square lattice, and the quench dynamics across the QPTs exhibited by these systems. Furthermore, we also study the quantum phases and phase transitions of these atoms loaded in disordered lattice potentials.

We study the quantum phases of the dipolar quantum gases, in particular, the parameter domain of the novel supersolid (SS) phase. The SS phase exhibits the properties of being a solid and a superfluid simultaneously. We model the system with the extended Bose-Hubbard model, and obtain the ground state phase diagrams. We utilize the single-site Gutzwiller mean-field (SGMF) and cluster Gutzwiller mean-field (CGMF) to obtain the ground states of the model. As a result of the quantum fluctuations incorporated in the CGMF method, the parameter domain of the SS phase is shrunked in comparison to the one obtained with the SGMF method. We also perform a cluster finite size scaling to find out the critical points of the QPTs in the exact calculation limit, demonstrating the role of quantum fluctuations. Furthermore, we show that the presence of the artificial gauge field enlarges the domain of the SS phase. This enlargement is due to the localizing effect of the Landau quantization due to the artificial gauge fields. We numerically demonstrate the gauge invariance of the phase boundaries obtained using the SGMF and CGMF methods.

Apart from studying the atoms in “clean” lattice potentials, we also investigate the equilibrium quantum phases in disordered lattice potentials. In particular, the Bose glass (BG) phase, characterized by superfluid (SF) islands in an MI background emerges, when the disorder is present. We apply the methods of percolation theory and numerically identify the SF domains in the BG phase and study their average size (or the correlation length). As the SF phase is approached, there

is a divergence of the correlation length, and the critical exponent is in good agreement with the value predicted by the 2D site percolation universality class. This suggests that the BG-SF phase transition belongs to 2D site percolation class of transitions.

Next, we study the dynamics associated with quenching a parameter of the system Hamiltonian across the critical point, over a finite time duration. We study the spontaneous symmetry breaking and the order parameter development in the dynamics following the Kibble-Zurek mechanism (KZM). The KZM categorizes the entire dynamics into three temporal regimes based on the competition between the relaxation time and the quenching rate. And it predicts the universal power-law scaling of certain quantities like the correlation length and the amount of defects generated as a function of quench rate. In this thesis, we consider quenching across certain second-order QPTs like the Mott-Insulator to superfluid QPT of the Bose-Hubbard model (BHM) and the stripe density wave to stripe supersolid QPT of the dipolar BHM and investigate the KZ scaling laws. The scaling exponents obtained satisfy the expected scaling relations. Next, we consider quenching the polarizing angle of the dipoles which results in the structural QPT from the stripe ordering to the checkerboard ordering in the system. We demonstrate the power-law scaling of the number of checkerboard ordered domains formed in the dynamics, which is reminiscent of the KZM.

Title: On the role of hall magnetohydrodynamics in magnetic reconnection: astrophysical plasmas
Researcher: Bora, Kamlesh
Supervisor: Bhattacharyya, Ramitendranath
Year: 2022
Keyword's: Magnetohydrodynamics, Hall magnetohydrodynamics, Solar active regions, Solar magnetic fields, Solar coronal mass ejections
Call No.: 523.72 BOR
Acc. No.: T01061

Abstract: Magnetic reconnection is a distinctive fundamental process that often causes explosive energy release phenomena in various astrophysical plasmas. Generally, the astrophysical plasmas are characterized by large magnetic Reynolds number ($R_M = Lv/\lambda$, in usual notations) owing to their inherent large length scale and high temperature. Large R_M causes the Alfvén flux freezing theorem—magnetic flux being frozen to the plasma flow—to be satisfied. Reconnection occurs due to the violation of Alfvén’s flux-freezing theorem at small length scales which generate as a consequence of large-scale dynamics. Such small-scales are characterized by large gradients in the magnetic field and may occur as current sheets (regions of high current density) and magnetic nulls (locations where the magnetic field vanishes; $B = 0$). The multiscale behavior of reconnection makes it challenging to study the physics at small-scales and capture its effect on large-scale dynamics simultaneously. Identification of the reconnection scale depends on the specific physical system under consideration. The outermost atmosphere of our nearest star Sun—the solar corona, serves as a prototype astrophysical plasma. Large-scale solar eruptions observed on the Sun, such as flares and coronal mass ejections (CMEs) are the manifestation of magnetic reconnection. In particular, solar flares are fast and impulsive phenomena since a huge amount of energy ($\approx 10^{32}$ erg) is released suddenly and rapidly within a very short time period (\approx a few minutes to hours). Therefore, the underlying reconnections must be fast and impulsive too. The reconnection length scale in the solar corona (based on the observed impulsive rise time of hard X-ray emission during the solar flares) turns out to be a few tens of meters. At this scale, the order analysis of the induction equation indicates that the order of the Hall effect is much higher than the resistive diffusion. This leads to the Hall MHD description which can account for impulsive behavior as compared to the traditional theoretical models of reconnection.

Against the above backdrop, this thesis focuses on the investigation of the Hall effect in 3D magnetic reconnection through numerical simulations. For this purpose, a Hall MHD solver is developed and benchmarked toward the known properties of Hall-assisted reconnection. For benchmarking, a comparative study using Hall MHD and MHD simulations is carried out. The simulations are initiated with an unidirectional sinusoidal magnetic field (contained in the xz plane of employed Cartesian geometry), having a non-zero Lorentz force which initiates the dynamics. In MHD simulation, the evolution of magnetic field lines is symmetric and confined within the xz planes. Magnetic reconnections within each plane generate magnetic islands which, when stacked together along the y direction, appear as magnetic flux tube made by disjoint magnetic field lines. Contrarily, the

Hall MHD simulation exhibits an asymmetric and three-dimensional (3D) evolution, owing to the development of an out-of-reconnection plane (xz plane) magnetic field component (B_y) which is quadrupolar. This is in agreement with the earlier Hall MHD simulations in the literature. Subsequently, the B_y component causes the formation of a magnetic flux rope (MFR) in the computational domain. In their 2D projections, the rope and the flux tube appear as magnetic islands. Subsequent evolution exhibits the breakage of primary islands into secondary islands followed by their coalescence in both the simulations. However, the dynamics are faster during the Hall MHD. An important finding is the formation of twisted 3D magnetic structures which cannot be apprehended from 2D calculations, although their projections agree with the latter. The volume-averaged current density rate shows abrupt changes during the Hall MHD—signifying impulsiveness. Alongside, we have also explored the Whistler wave mode numerically vis-a-vis its analytical model and found the two to be matching reasonably well in Hall MHD simulations. Overall, the results agree with the existing scenario of Hall-assisted reconnection, thus validating the model.

Since the evolution of an MFR is instructive to understand the CMEs and eruptive flares on the Sun, the numerical model is employed to perform Hall MHD and MHD simulations toward the generation and evolution of an MFR. The simulations are initiated with 2.5D and 3D bipolar sheared magnetic fields. In the 2.5D case, MFR is levitating and unanchored while in the 3D case, it is anchored to the bottom boundary. The generation of MFR due to primary reconnections is identical for both cases in the two simulations. However, the subsequent evolution of MFRs is influenced by the Hall effect. In the 2.5D case, Hall MHD evolution depicts the local breakage of MFR, owing to the internal reconnections. When viewed favorably, the structure appears reminiscent of the “number eight(8)”. The temporal evolution of average magnetic energies, in the presence and absence of the Hall effect, is near-identical for both cases and consistent with the theoretical expectation that the Hall term does not affect the magnetic energy evolution. In the 3D case, the primary MFR gets generated in both simulations due to repetitive reconnections at 3D null points. Subsequently, Hall MHD evolution features the swirling motion of small-scale twisted structures in the vicinity of 3D null points. The intermittent reconnections within these structures lead to the formation of large-scale MFR which indicates the association of small-scale dynamics with large-scale structure formation—a key finding emphasizing the role of the Hall effect in 3D reconnection.

Based on the accomplished knowledge about the Hall effect in 3D magnetic reconnection, finally, in this thesis, the role of the Hall effect is explored for a solar flare. To achieve the aim, a C1.3 class flare on March 8, 2019 in the solar active region (AR) 12734 is selected as a test bed and the numerical model is employed to perform the data-based Hall MHD and MHD simulations. Analysis of multiwave-length observations from the AIA instrument on board SDO reveals an elongated extreme ultraviolet (EUV) counterpart of the eruption in the western part of the AR, a W-shaped flare ribbon, and the circular motion of chromospheric material in the eastern part. Subsequently, the magnetic field line morphologies over the AR are explored by employing the non-force-free field (non-FFF) extrapolation which uses the photospheric vector magnetogram from the HMI instrument on board SDO. The analysis of the extrapolated field reveals the presence of 3D nulls and quasi-separatrix layers (QSLs) which are favorable sites for 3D magnetic reconnection. A null point with

fan-spine configuration is found in the middle of the active region whose Hall MHD evolution is in better agreement with the tip of the W-shaped flare ribbon. Further, the lower spine and fan remain anchored to the bottom boundary throughout the evolution, thus providing a pathway for post-reconnection plasma flow while in the MHD case, the lower spine gets disconnected. Notably, an MFR with QSLs as overlying field lines is found at the location of flare saturation in the SDO/AIA images. The Hall MHD simulation shows faster slipping reconnection of the flux-rope footpoints and overlying QSLs magnetic field lines. Consequently, the overlying magnetic field lines rise and reconnect in the corona, thereby providing path for plasma ejection. This finding agrees with the observed eruption in the western part of AR. Contrarily, such a significant rise of the flux rope and overlying field lines is absent in the MHD simulation, thus signifying the reconnection to be slower in MHD. Interestingly, such field line dynamics suggest a distinct mechanism of flux rope eruption in 3D, which is not widely documented in the literature. The result further emphasizes that null points and true separatrices in 3D may not be required for eruptive flares. Additionally, a “fish-bone-like structure” surrounding a null line is found in the eastern part of the AR. A salient feature captured only in the Hall MHD is that rotating magnetic field lines agree remarkably with the observed circular plasma motion, both spatially and temporally.

Overall, investigations of the Hall effect on 3D magnetic reconnection employing the numerical simulations initiated with both the analytical and observed magnetic fields display significant changes in the magnetic structures around and on the reconnection site which subsequently alter the large-scale dynamics making the evolution faster. Therefore, this thesis provides the Hall MHD as a potential description to understand the faster reconnections in 3D with particular emphasis on the effects of structural dynamics at small-scale on large-scale structures.

Title: Multi-wavelength studies of active galactic nuclei (AGNs)
Researcher: Kumari, Neeraj
Supervisor: Naik, Sachindranatha
Year: 2022
Keyword's: Active Galactic Nulcei, NGC 4051-NLS1 Galaxy, Seyfert Galaxies
Call No.: 523.112 KUM
Acc. No.: T01063

Abstract: Active Galactic Nuclei (AGNs) are the most luminous (luminosity $\sim 10^{42} - 10^{48}$ erg/s) persistent astronomical objects in the Universe, emitting in almost entire wavelength range of the electromagnetic spectrum, starting from radio to Gamma rays. This enormous radiation is attributed as due to the accretion of the surrounding material onto a supermassive black hole (SMBH) located at the centre of a galaxy. Usually, the AGNs are X-ray loud and emit profoundly in the 0.1 – 100 keV energy band. The spectral energy distribution of type 1 AGNs (e.g. Seyfert galaxies) shows the presence of primary spectral components such as a big blue bump in the UV range, soft X-ray excess below ~ 2 keV, Fe emission lines in 6 – 7 keV, reflection hump in 10 – 50 keV range and a power-law continuum emission with high energy cut-off. These components are thought to be originating from distinct regions of the AGN and are expected to vary differently. One of the most important properties of these objects is that they are highly variable on different time scales. The observed X-rays show rapid variability on the time scale of as short as an hour which is comparable to the size of the immediate region around the black hole. This makes X-ray emission, along with emission in other wavelengths, an important proxy to probe the extreme environment of the black hole. Our understanding of the variability properties of these objects is still not complete. Therefore, the spectral and timing studies of the AGNs can provide a better understanding of the central engine and its surrounding medium. The present thesis work is dedicated to the substantial understanding of three Seyfert galaxies: Mrk 509, NGC 1566 and NGC 4051. To fulfil the thesis objectives, the data from various space-based observatories, such as Swift, XMM-Newton and NuSTAR are utilized. To disentangle the origin of short-term variabilities in Seyfert 1 galaxy Mrk 509, long-term Swift data from 2006 to 2019 in multi- wavebands (X-ray, UV and optical) have been used. We analyzed a total of 275 pointed observations to study the variability properties of the source in the optical/UV to X-ray emission. The average spectrum over the entire duration of observations exhibits a strong soft X-ray excess above the power-law continuum. The soft X-ray excess is well described by two thermal components with temperatures of $kT_{\text{BB1}} \sim 120$ eV and $kT_{\text{BB2}} \sim 460$ eV. The warm thermal component is likely due to the presence of an optically thick and warm Comptonizing plasma in the inner accretion disc. We calculated the fractional variability amplitude in each band and found it to be decreasing with increasing wavelength i.e., from the soft X-ray (0.3 – 2 keV) to UV/optical emission. However, the hard X-ray (2–8 keV) emission shows very low variability. The strength of the correlation within the UV and the optical bands is found to be stronger (0.95–0.99) than the correlation between the UV/optical and X-ray bands (0.40–0.53). These results clearly suggest that the emitting regions of the X-ray and UV/optical emission are likely distinct or partly interacting. After removing the slow variations in the light curves, we find that the lag spectrum (time lag vs wavelength) is well described by the 4/3 rule of the standard Shakura–Sunyaev accretion disc when

we omit X-ray lags. Nearly zero time lag and marginal variability difference between UV bands suggest that the UV emitting region in the disc is not smooth but is instead a stratified region. All these results suggest that the real disc is complex and the UV emission is likely reprocessed in the accretion disc to give X-ray and optical emission.

Another detailed spectral and timing study has been performed for the 2018 outburst of the Changing-look AGN (CL-AGN) NGC 1566, where its intensity increased up to $\sim 25 - 30$ times its quiescent state intensity. This main outburst was accompanied by small recurrent outbursts. The CLAGNs are a newly emerging class of AGNs where an AGN switches its type over the years. The study was performed during pre-outburst, outburst and post-outburst epochs using semi-simultaneous observations with the XMM-Newton, NuSTAR and Swift Observatories. The broadband 0.5–70 keV spectra were fitted with phenomenological models as well as physical models. A strong soft X-ray excess is detected in the spectra during the outburst, while it was weak before and after the outburst. The soft excess can produce most of the ionizing flux necessary to create broad optical lines. The broad lines appeared during the outburst, therefore, could be due to the strong soft excess, leading to the changing-look event. The soft excess emission is found to be complex and could originate in the warm Comptonizing region in the inner accretion disc. Using the obtained results, we find that the increase in the accretion rate, which could be due to the disc instability, is responsible for the sudden rise in luminosity and rule out the possibility of a tidal-disruption event (TDE). This is supported by the ‘q’-shape of the hardness-intensity diagram that is generally found in outbursting black hole X-ray binaries. From our analysis, we find that NGC 1566 most likely harbours a low-spinning black hole with the spin parameter $a \sim 0.2$. We also propose a possible scenario where the central core of NGC 1566 could be a merging pair of supermassive black holes. This scenario could explain the recurrent outburst.

To investigate the cause of ubiquitous small X-ray flares in AGNs, a small flaring event of ~ 120 ks in narrow-line Seyfert 1 (NLS1) galaxy NGC 4051 has been studied in detail using simultaneous XMM-Newton and NuSTAR observations. The ~ 300 ks long NuSTAR observation and the overlapping XMM-Newton exposure were segregated into pre-flare, flare and post-flare segments. We found that during the flare, the NuSTAR count rate peaked at 2.5 times the mean count rate before the flare. We explored the variation of X-ray emission in three phases using various phenomenological and physical models. The 0.3 – 50 keV X-ray spectrum of the source is described by a composite model consisting of a primary continuum, reprocessed emission, warm absorber and ultra-fast outflows. From the spectral analysis, we find that the reflection fraction drops significantly during the flare, accompanied by the increase in the coronal height to $\sim 12.2 R_g$ from $\sim 9.6 R_g$ (during the pre-flare phase) above the disc. The spectrum became softer during the flare showing the “softer when brighter” nature of the source. After the alleviation of the flare, the coronal height drops to $\sim 7.4 R_g$, and the corona heats up to the temperature of ~ 228 keV. This indicates that there could be inflation of the corona during the flare. We did not find any significant change in the inner accretion disc or the seed photon temperature during the observation. These results suggest that the flaring event occurred due to the change in the coronal properties rather than any notable change in the accretion disc.

Title: 21 cm line astronomy and constraining new physics
Researcher: Natwariya, Pravin Kumar
Supervisor: Bhatt, Jitesh R.
Year: 2022
Keyword's: Astronomy, Dark Matter, Baryon-dark Matter, Black Hole
Call No.: 520 NAT
Acc. No.: T01065

Abstract:

The 21 cm signal appears to be a treasure trove to provide an insight into the period when the first generation of luminous objects sprung up in the Universe—hereafter, we will refer to these objects as first stars. The 21 cm line has been actively used to trace the neutral hydrogen in Milky Way for more than seven decades since its first observation in 1951 [1]. The 21 cm line corresponds to the wavelength for hyperfine transition between 1S singlet and triplet states of a neutral hydrogen atom, and the corresponding frequency is 1420.4 MHz. Hydrogen is the predominating fraction of the total baryonic matter during cosmic dawn (CD). Therefore, it is convenient and advantageous to study physics during CD using the 21 cm signal. The transition probability for the hyperfine states is once in $\sim 10^7$ years in the absence of any external sources. The presence of any

exotic source of energy can significantly affect the hyperfine transition, thus spin temperature of the hydrogen gas. The spin temperature (T_S) is characterized by the number density ratio in the 1S singlet and triplet states of the neutral hydrogen atom. In the cosmological scenarios, there are three processes that can affect the spin temperature: background radio radiation, Ly α radiation from the first stars and collisions of a hydrogen atom with another hydrogen atoms, residual electrons or protons. During CD era, the 21 cm signal is observed in the form of differential brightness temperature. If a light with initial brightness temperature (T_R) passes through a medium having optical depth (τ_ν) & excitation temperature (T_{exc}), there can be an absorption or emission by the medium resulting in a different final/emergent brightness temperature (T'_R). The divergence of T'_R from the T_R is known as the differential brightness temperature— observed temperature by antennas. In our case, the medium is neutral hydrogen gas and the T_{exc} for the 21 cm line is T_S . Therefore, we refer the observed antenna temperature by 21 cm differential brightness temperature [2, 3],

$$T_{21} = \frac{T_S - T_R}{1 + z} \times (1 - e^{-\tau_\nu}),$$

here, z is the redshift. Depending on spin and background radio radiation temperature, there can be three scenarios: $T_S > T_R$ ($T_{21} > 0$, emission signal), $T_S = T_R$ ($T_{21} = 0$, no signal), $T_S < T_R$ ($T_{21} < 0$, absorption signal).

Usually, in the Λ CDM model of cosmology, the contribution in the background radiation is assumed to be solely by the cosmic microwave background radiation (CMBR). Therefore, here, we will discuss the evolution of the global 21 cm signal when only CMBR is present as background radiation (T_{CMB}). At the redshift of interest ($z \sim 17$), gas temperature (T_{gas}) strongly couples to T_S due to Ly α radiation emitted from first stars by Wouthuysen-Field (WF) effect [2, 4]. During CD era, T_{gas} and T_{CMB} fall adiabatically as $\propto (1 + z)^2$ & $(1 + z)$, respectively. Therefore, $T_S \sim T_{\text{gas}} < T_{\text{CMB}}$, and it implies a 21 cm absorptional signal during

CD era. The presence of any exotic source of energy can inject energy into the intergalactic medium (IGM) and heat the gas. Subsequently, it can modify the absorption amplitude in the global 21 cm signal. Therefore, the absorption feature in the 21 cm signal can provide a robust bound on such sources of energy injection into IGM. In the thesis, the following four works has been considered done by me: sterile neutrinos and primordial black holes as dark matter candidates and constrain their properties in the light of the global 21 cm signal. Another two works discussed in the thesis are related to the constraining strength of primordial magnetic fields that might have been generated in the very early Universe.

In 2018, the Experiment to Detect the Global Epoch of Reionization Signature (EDGES) collaboration reported an absorption profile for the 21 cm signal in the redshift range $15 - 20$ [5]. Recently, many articles have questioned the EDGES measurement; for example, see the Refs. [6–8]. In the light of these controversies, in the recent two articles (A1 & A2), we do not consider the absorption amplitude reported by the EDGES collaboration. While in the older two articles (B1 & B2), we have considered the absorption amplitude reported by the EDGES collaboration.

Title: Application of relativistic coupled-cluster method to study P, T -odd properties in heavy and superheavy molecules
Researcher: Mitra, Ramanuj
Supervisor: Sahoo, Bijaya Kumar
Year: 2022
Keyword's: Electric Dipole Moment, Permanent Electric Dipole Moment, Diatomic Heavy Polar Molecules
Call No.: 530 MIT
Acc. No.: T01066

Abstract: Atoms and molecules are called the natural laboratories to probe electron-electron, electron-proton, electron-neutron, proton-proton, proton-neutron, and neutron-neutron interactions. Except for the electron-electron interactions, other interactions originate at the quarks levels. There have been immense interest to probe the nature of all possible phenomena involving these interactions. Direct probes of interactions involving electrons and quarks demand very large energy facilities like the Large Hadron Collider (LHC) at CERN owing to Heisenberg's uncertainty principle. However, using atoms or molecules, one can indirectly probe these interactions. These probes sometimes include evaluation of certain properties of fundamental particles, which can have further implications in fields like cosmology. One of the biggest cosmological mysteries in the present universe is the riddle of matter-antimatter asymmetry. According to Sakharov's conditions, it requires sufficient amount of CP (C : charge conjugation, P : parity) violation to properly explain the matter-antimatter asymmetry. Although there are a few known signatures of CP violation in the electro-weak interaction sector, those are insufficient to explain the matter-antimatter asymmetry. Therefore, it is imperative to search for new sources of CP violation. The electric dipole moment of electron (electron's EDM or eEDM, d_e) being a P, T -odd (T : time-reversal) property, is one such CP violating phenomenon which is yet to be observed. Therefore, the eEDM, if detected, would be regarded as a direct signature of CP violation and it can throw light into explaining matter-antimatter asymmetry.

Probing eEDM through accelerator method with a single isolated electron is impractical, as it demands huge amount of energy that is currently beyond the capacity of existing as well as projected laboratory set ups. However, in non-accelerator probes, many-electron systems like paramagnetic atoms or molecules are used as proxies in EDM experiments. Due to their better experimental sensitivities, heavy polar molecules have historically become superior choices over atoms for EDM experiments. Within an atom or a molecule, an electron with EDM experiences an internal electric field due to other electrons and nuclei. For molecules, this electric field can be viewed as an effective electric field (E_{eff}), a large value of which would imply a better sensitivity in EDM experiments. E_{eff} of a molecule is completely a relativistic phenomenon and cannot be measured in experiments, thus requiring a fully relativistic framework to perform theoretical calculations. Combination of relativistic many-body calculation of E_{eff} and experimentally measured molecular energy shift can together put a stringent bound to d_e . The best experimental upper limit on d_e comes from a heavy diatomic molecule, ThO, which is about ten orders larger than the upper

bound predicted by the Standard Model (SM) of particle physics. Experimentally set upper limit to d_e may constrain theories beyond the SM (BSM) which predict larger values of eEDM. An improvement in the upper bound to d_e through molecular EDM experiments and relativistic many-body calculations could guide us to reach near to the actual value of eEDM. In this thesis work, we mainly focus on exploring new molecular candidates for EDM experiments to obtain better sensitivity by means of our theoretical analyses. For this purpose, we employ the relativistic coupled-cluster (relativistic CC or RCC) method to carry out theoretical calculations relevant to EDM searches. Before employing RCC theory to calculate molecular properties pertaining to high-precision EDM experiments, it is essential to test the potential of the RCC method to produce accurate results. As we do not have the option to compare our RCC results of properties related to EDM studies of new molecular candidates with existing literature, we employ the RCC method to calculate a few molecular properties for a couple of systems for which previous theoretical studies and/or experimental results are available. To serve this purpose, we calculate static dipole polarizabilities and permanent electric dipole moments (PDMs) of closed shell heteronuclear alkali-dimers for which experimental values are available. We discuss in detail the relativistic and correlation effects in both the properties. We compare our results from relativistic calculations with existing non-relativistic results as well as experimental data.

We observe that our results obtained from RCC calculations agree well with experimental results and improves upon existing non-relativistic results. As open-shell paramagnetic molecules are considered for EDM experiments, similar exercise of testing the RCC theory needed to be performed with open-shell molecules also. For that matter, we considered open-shell alkali-alkaline earth (Alk-AlkE) molecules to calculate their PDMs and static dipole polarizabilities using the RCC method. Experimental results of PDMs and polarizabilities of these systems are not available. Therefore, we had to settle by comparing our RCC results with non-relativistic results from our calculations as well as from other works available in literature. We observe that our RCC calculations of PDMs of Alk-AlkE systems significantly improve over the non-relativistic estimates, while the relativistic effects in dipole polarizabilities become prominent for heavier systems. After checking the capability of the RCC method, we employ it to assess the suitability of new molecular candidates for EDM searches.

Diatomic heavy polar molecules have been very popular for both theoretical and experimental studies of eEDM. However, it is recently shown by Kozyrev *et al.* [Phys. Rev. Lett. 119, 133002] that due to the presence of internal comagnetometer states in triatomic molecules, they could offer extra advantages over diatomic molecules in EDM experiments. We know that HgF possesses the largest E_{eff} among the theoretically proposed molecules. Keeping this in mind, we chose HgF's triatomic isoelectronic counterpart HgOH for conducting theoretical analyses to assess its suitability in EDM experiment. Based on our RCC calculations and several experimental considerations, we provide the projected sensitivity of HgOH, which is better than the current best experimental limit set by the ThO experiment. We also explored feasibility of HgOH for different types EDM experiments.

As E_{eff} is a purely relativistic property, we expect its value to get enhanced for molecules which exhibit relativistic effects more prominently. Superheavy molecules are generally anticipated to exhibit larger relativistic effects than the non-superheavy ones. Therefore, in our next endeavour, we selected three superheavy molecules, namely LrO , LrF^+ , and LrH^+ to assess their prospects in EDM experiments. Using RCC calculations, we obtained the equilibrium bond-lengths of the molecules at their ground states from the minima of the corresponding potential energy curves (PEC). Once we found that stable bound state formation is quite possible for the considered Lr molecules, we employed the RCC theory to calculate E_{eff} and PDM of the chosen molecules. We observe that the values of E_{eff} for all the three molecules are almost 3 to 4 times larger than that of the current best theoretically proposed candidate HgF and experimentally considered molecule ThO . RCC values of PDM are also found to be quite large for the aforementioned systems. In superheavy molecules, along with the eEDM, another P , T -odd phenomenon that may significantly contribute to the molecular energy shift during an EDM experiment is the nucleus-electron scalar-pseudoscalar (S-PS) interaction. In the S-PS interaction, the properties analogous to d_e and E_{eff} are S-PS coupling coefficient k_s and S-PS enhancement factor W_s , respectively. Calculated values of W_s using RCC method for the chosen superheavy molecules are observed to be almost four to five times larger than that of HgF and ThO . We also provide a pathway to produce Lr atoms in larger numbers, which is crucial in the formation of Lr molecules during EDM experiments. Enhanced values of E_{eff} and PDMs of the chosen Lr molecules make them interesting for future EDM experiments. Our precise calculations of the molecular PECs and PDMs could also guide other future experiments with these molecules.

Title: Interaction of intense femtosecond pulses with polyatomic molecules: probing the ultrafast dynamics
Researcher: Das, Rituparna
Supervisor: Kushawaha, Rajesh Kumar
Year: 2023
Keyword's: Polyatomic Molecules, Molecular Dynamics, Pulse
Call No.: 532.05 DAS
Acc. No.: T01067

Abstract: Strong-field physics aims to understand the ultrafast nuclear and electron dynamics in atoms and molecules on their intrinsic timescale and eventually, control them. The development in laser technology made it possible to produce ultrashort (durations of few tens of fs or even shorter) bursts of light of intensities ranging from TW/cm² to PW/cm². Such intense fields are comparable to and sometimes stronger than the Coulomb potential in the atoms/molecules. To understand the ultrafast nuclear dynamics in polyatomic molecules using femtosecond laser pulses, the molecules are first ionized, thereby creating a molecular wavepacket in a ground or excited ionic state. Next, as the wavepacket evolves on the electronic state, the ion undergoes changes in its geometry leading to bond breakup, intramolecular migration of moieties and bond formation before it dissociates into fragments. Obtaining the complete kinematic information of the fragments in coincidence using a Recoil Ion Momentum Spectrometer (RIMS) reveals information about the excited-state dynamics of the molecular ion. For instance, the kinetic energy, momentum distribution and the angular distribution of the fragments provide information about the orbital from which ionization took place, the nature of the electronic state from which dissociation took place, the timescale of dissociation, and so on. Further, by shaping the laser pulses or tweaking the laser parameters, it is possible to manipulate these ultrafast nuclear dynamics and hence, control the yield of the dissociative pathways.

Although the control of light-induced reactions and molecular fragmentation has been studied extensively in the past decades, a complete understanding of H⁺ and H⁺ formation by the bond breakup, intramolecular H migration, and bond formation has not been achieved yet. Furthermore, the control of the H₂⁺, H₃⁺ yield by controlling the excited-state dynamics of the parent ion is of particular interest, as this will enable us to control bond breakup and bond formation in reactions. In this thesis, we have investigated the strong-field ionization and fragmentation of polyatomic molecules (CH₃OH, CD₃OH, and CH₃Cl) induced by intense femtosecond laser pulses in our in-house developed RIMS and Velocity Map Imaging (VMI) spectrometers. We focused on the formation of H⁺ and H⁺, which involve the bond breakup, intramolecular H migration, and bond formation processes, as mentioned above. We first demonstrated the influence of laser parameters like intensity, pulse duration, wavelength, and polarization on their yield. Next, a few two-body fragmentation pathways (that produce H⁺ and HCl⁺) of a molecular dication (CH₃Cl₂²⁺) using photoion-photoion coincidence were identified. The complete kinematic information of the fragments revealed the timescale of dissociation and the nature of the excited electronic states from which dissociation occurred. Using laser intensity and chirp, it was possible to control the excited-state dynamics of the parent dication and hence, its dissociation along the four pathways. Finally,

the complex fragmentation dynamics of CH_3Cl_2^+ along three-body breakup pathways were investigated using Dalitz plots, Newton diagrams, and the native frame method. The momentum sharing between the fragments and the fragmentation mechanism for the pathways were investigated. The most dominant fragmentation pathways were found to be concerted, along with some sequential processes. Chirped pulses were found to influence the excited-state dynamics of the dication and hence, the fragmentation mechanism. I have, therefore, investigated and demonstrated the control of the ultrafast nuclear dynamics in polyatomic molecules and their dissociation along two- and three-body breakup pathways by using different intensities and pulse durations, which is a significant step in the control of reactions.

Title: Study of cometary coma: from simple molecules to complex organics
Researcher: Ahmed, Sana
Supervisor: Acharyya, Kinsuk
Year: 2022
Keyword's: Comets, Comae, Comet Volatiles, Complex Organic Molecules
Call No.: 523.6 AHM
Acc. No.: T01068

Abstract: Comets are numerous objects surviving from the early formation stages of the Solar System, and they are made up of frozen volatiles and dust grains. The frozen volatile material of the cometary interior can be regarded as the oldest and largely unprocessed material of the Solar System. This makes comets the ideal candidates to study the early formation history of the Solar System. Cometary volatiles have been detected both in situ and by remote observations of the cometary atmosphere or coma. One of the major sources of knowledge about the structure and composition of comets comes from studies of the coma. Numerical modeling studies of the coma give a quantitative understanding of the physics and chemistry in the coma gas.

In this thesis work, a numerically robust chemical-hydrodynamical coma model has been built, which can be used to study the coma of comets having a wide range of volatile compositions. This model is based on applying fluid conservation equations to a spherically symmetric coma in a steady state. The model involves collision-dominated flow, a multifluid treatment of the coma-gas, active gas-phase chemistry, and heating and cooling mechanisms. An extensive chemical network is used, which includes chemical reactions involving complex organic molecules and ions. Cooling mechanisms due to vibrational and electronic excitation of CO molecules have also been added.

The model is used to simulate the coma of the interstellar comet 2I/Borisov. This comet shows a high CO/H₂O ratio (~ 1), which makes it a notable exception when compared with Solar System comets, which are dominated by the outgassing of water molecules from the nucleus. The model results show that the high CO/H₂O ratio will affect the chemistry and dynamics of the coma. It is found that the high CO abundance alters the temperature profile and results in high abundances of CO⁺ and HCO⁺ ions in the coma. These two ions affect the formation/destruction rates of other ions such as H₂O⁺, H₃O⁺, and N-bearing ions. In addition, higher abundances are seen for assorted organic neutrals and ions in the interstellar comet, compared to a typical Solar System comet of the Halley-type composition.

Improvements in observational capabilities have resulted in the detection of many new organic species in a large number of comets. While organic species can originate from the nucleus, comets showing moderate to high activity can reach sufficient coma densities for organic molecules to form by active gas-phase coma chemistry. The coma model has been used to study the comets C/1996 B2 (Hyakutake), C/2012 F6 (Lemmon), C/2013 R1 (Lovejoy) and C/2014 Q2 (Lovejoy) with respect to their organic abundances. The gas-phase organic formation pathways in the comae of these comets and the resulting coma abundances of organic neutrals and ions due to these gas-phase formation

mechanisms are examined. The efficiency of coma chemistry towards forming neutral organic molecules in the coma, as opposed to these molecules outgassing from the nucleus, is discussed. The volatile composition of 21/Borisov will provide insights into the prevailing conditions of its host system. A comparative study of the interstellar comet with Solar System comets will aid in making a chemical inventory of 21/Borisov's natal disk, including possible organics that could be present. Answering the questions of how organic chemistry works in cometary environments will improve our understanding of the formation and distribution of organics in the Solar System and the terrestrial delivery of organic molecules.

Title: Entangled photons and their applications in quantum information processing
Researcher: Mishra, Sarika
Supervisor: Singh, R. P.
Year: 2022
Keyword's: Quantum Entanglement, Quantum Cryptography, Quantum Communication, Quantum Key Distribution, BBM92 Protocol, Orbital Angular Momentum.
Call No.: 530.12 MIS
Acc. No.: T01069

Abstract: Entangled photons have been used to perform many quantum information protocols such as quantum teleportation, quantum superdense coding, quantum cryptography etc. Spontaneous parametric down-conversion (SPDC) process emerged as one of the best methods to generate entangled photons. The photon pairs generated through SPDC are indistinguishable and maintain a quantum correlation among themselves in different degrees of freedom (DoFs) which leads to the quantum entanglement in those DoF. Among all such DoFs, polarization and orbital angular momentum (OAM) are the two important bases which are widely used to study the fundamental properties of entanglement. We use polarization entangled state to study the BBM92 protocol, an entanglement-based quantum key distribution (QKD) protocol, over 35 meters and 200 meters free-space atmospheric channel, and simultaneously study the effect of aerosols on the secure key rate. This is the first study of its kind where the extinction coefficient of atmospheric aerosols is used to study the variation of entanglement, quantum bit error rate (QBER) and key rate. A quantum bit with more than two dimensions is known as a qudit. It enables access to a larger Hilbert space, which can provide significant improvement over qubit such as increasing the information capacity per photon in quantum communication, increasing the dimensionality of the Bell state in dense coding etc. Since entangled qudit states have more advantage over entangled qubit states in secure communication, we explore the dimensionality of the OAM entangled state. Higher dimensional entangled states (HD-ES) in OAM have been gaining more attention due to their easy scalability in dimension. Photon pair generated through SPDC theoretically show multi-dimensional entanglement in OAM. The OAM spectrum of the two entangled photons is known as spiral bandwidth (SB). Dimensionality of the entanglement depends on the size of the spiral bandwidth. We show how the beam waist of the pump mode can affect the bandwidth of the OAM spectrum and how it helps in engineering the higher dimensional entanglement.

We also investigate the entanglement between different DoFs (polarization and OAM) which is known as hybrid entanglement. It allows the generation of qubit-qudit entanglement. We propose a new method to generate arbitrary classical non-separable state which can be easily transformed into quantum hybrid entangled state through the SPDC process. The effect of random scattering such as through a ground glass plate (GGP) on hybrid entanglement is also investigated.

Title: Orbital angular momentum of light and quantum correlations
Researcher: Patil, Satyajeeet
Supervisor: Singh, R. P.
Year: 2022
Keyword's: Quantum Communication, Quantum Key Distribution, Orbital Angular Momentum, Spontaneous Parametric Down Conversion
Call No.: 530.12 PAT
Acc. No.: T01070

Abstract: Orbital angular momentum (OAM) modes of light or Laguerre-Gaussian beams are the solutions of the paraxial wave equation. These beams form a set of infinite-dimensional orthogonal solutions. Due to the azimuthally varying phase, they have a twist in their wavefront, which acts as a screw dislocation and produces a vortex. This OAM can be transferred to micron-sized particles placed along the propagation axis that finds practical interest in the field of optical trapping, optical tweezing, and spanning. Since LG modes expand the infinite-dimensional basis, they find applications in classical and quantum communication. Therefore, experimental techniques for their characterization are essential. Our work proposes and demonstrates a simple and novel technique to identify the order and sign of the optical vortex. The spontaneous parametric down-conversion (SPDC) that uses a second-order non-linear process is the most widely used method to generate entangled states of photons. Using the SPDC process, polarization, OAM, and position-momentum entanglement states can be generated. Information can be encoded in the entangled states of photons, known as qubits. Measurement on qubit gives the value of the classical bit. Efforts have been made in the direction to enhance the capacity of the qubit to encode and extract more information, and it is known as dense coding. Polarization-entangled states have been used to show the dense coding, but it has practical limitations. Therefore, we use the non-separability of polarization and OAM of light to overcome the limitations, showing the dense coding. Due to the strong position-momentum correlation between SPDC photon pairs, this correlation finds applications in quantum imaging and quantum sensing. Usually, the Gaussian pump beam is used to generate position-momentum entangled states, which give equal entanglement in transverse directions. We use an elliptical-Gaussian pump beam to show that entanglement in transverse directions becomes unequal, which we call anisotropic entanglement. Also, we show the death of entanglement in one direction while keeping it alive in another direction. Such anisotropic entangled states may seek application in secure communication. We also study the effect of OAM modes of light on the momentum correlation of SPDC photon pairs and near-field SPDC distribution. Finally, we demonstrate the amplitude transfer of partially coherent pump beams with OAM to the SPDC photons and discuss the future outlook of our work.

Title: Investigations of low- and equatorial-latitude upper atmospheric processes using optical and radio techniques
Researcher: Saha, Sovan
Supervisor: Pallamraju, Duggirala
Year: 2022
Keyword's: Equatorial Plasma Bubbles, Radio Techniques, Upper Atmospheric Variabilities, Optical Techniques
Call No.: 539 SAH
Acc. No.: T01072

Abstract: The ionosphere-thermosphere regions of the upper atmosphere consist of plasma and neutrals, which are intercoupled with each other, often referred to as the ionosphere-thermosphere system (ITS). Different electrodynamic processes, such as equatorial electrojet (EEJ), equatorial ionization anomaly (EIA), pre-reversal enhancement (PRE) in zonal electric field, and neutral dynamics play important roles in the distribution of plasma and neutrals over the equatorial and low-latitude regions. As a consequence, the magnitudes of the plasma and neutral densities, electric fields, and neutral winds get altered. Further, on occasions, plasma irregularities get generated over the magnetic equator due to the onset of Rayleigh-Taylor (R-T) instability which can span scale sizes of around seven orders of magnitudes and extend to the low-latitudes and beyond. These plasma irregularities adversely affect the radio wave communications at different frequencies. A comprehensive understanding is required on all these variations in plasma-neutral dynamics, in order to gain not only fundamental understanding of ITS science, but also aspects related to applications.

Therefore, systematic observations and accurate measurements of different parameters are needed for a critical understanding of the upper atmospheric processes. Optical, radio, and magnetic techniques have been used in this work to infer the intricate behaviour of the ITS. In this thesis, the OI 630.0 nm nightglow emissions (red line), which serve as tracers to the behaviour in the ITS, are used as the primary data. High Throughput Imaging Echelle Spectrograph (HiTIES) is used to measure the red line emissions at Mt. Abu, a low-latitude location over Indian longitude, typically situated under the crest of the EIA during high-solar activity periods. Data from digisonde and the magnetometer are also used to carry out a comprehensive study of the various dynamical processes which occur in the upper atmosphere.

The peak emissions of OI 630.0 nm nightglow emanate from around 250 km and provide information of the upper atmospheric dynamics prevalent, essentially in the bottomside of F-region. Dissociative recombination of molecular oxygen with the thermal electrons is responsible for the nighttime red line emissions. A photo-chemical model has been generated to estimate the OI 630.0 nm nightglow emissions wherein the digisonde measured electron densities are used as an input. The red line emissions primarily depend on the densities of electron, O^+ , and O^+ present at these altitudinal regions. Therefore, the variabilities in the OI 630.0 nm emissions provide information on the subtle changes occurring at those altitudes. Different kinds of variabilities have been observed in the OI 630.0 nm nightglow emissions from this location which fall in four broad types. The causes of such

variabilities have been addressed rigorously and the new understanding of the systemic behaviour that has emerged is reported in this thesis.

Investigation into the effect of equatorial electrodynamics on the latitudinal movement of the EIA crest has shown that, on several occasions, airglow emissions are larger along the northern direction after sunset compared to the southern direction. This is due to the movement of the EIA crest in response to the PRE. As the night progresses, the plasma motion changes towards the magnetic equator, which is known as reversal of the EIA. The speeds of this reversal range from 10 to 55 ms⁻¹ and are caused by the nocturnal equatorial westward electric fields. In the absence of information on the nighttime electric fields over the Indian longitudes, we use the simultaneous variations in the daytime EEJ data from an opposite longitude sector and compared them with the measured nighttime reversal speeds. We show that these two are consistent, as the global equatorial electric fields follow the curl-free condition ($\nabla \times E = 0$). An experimental evidence has been shown of the variation in the nighttime reversal speeds of the EIA in relation with the nighttime equatorial electric field. As a result of this information, it is proposed that the observed reversal speeds (equatorward movement) of the EIA crest can serve as a viable proxy to determine the behaviour of the nightly westward electric fields which are otherwise extremely difficult to obtain.

The OI 630.0 nm nightglow emission decreases monotonically with a decrease in the ionization after sunset. But, on several occasions, a bell-shaped enhancement in the OI 630.0 nm nightglow emissions were observed over Mt. Abu during post-sunset hours. The role of equatorial electrodynamics and meridional winds have been investigated to understand the plausible cause for such enhancements and found that the presence of poleward meridional winds or the cessation of equatorward winds over the low-latitudes can effectively account for the observed post-sunset emission enhancements. This effect of meridional winds on the thermospheric airglow emissions during the post-sunset time is a new finding, as it shows a consistent decrease in magnitude during Jan-Mar as predicted by climatological model winds in HWM-14. The OI 630.0 nm emission data considered was for the years 2013, 2014, and 2016 with varying solar activity, which asserts that the results arrived at are independent of the solar flux variation.

Multiple excursions in OI 630.0 nm nightglow emissions are seen over Mt. Abu. The presence of equatorial plasma bubbles simultaneously, as seen in the ionosonde data over Ahmedabad and the depletion in OI 630.0 nm emissions over Kolhapur, is further evidence of their influence. The strength of the PRE was found to be larger on the nights when the depletions in emissions were observed in the OI 630.0 nm emission over Mt. Abu. The zonal speeds of the plasma bubbles were found to vary from around 190 to 90 ms⁻¹ over the night. The wave number spectral analyses for the emissions in the zonal direction using data from around 1300 images show that the scale sizes in the range of 250-300 km are omnipresent, whereas shorter scale sizes (50-250 km) are observed only during the presence of EPBs. It is inferred that these shorter scale size gravity waves played a significant role as the seed perturbations to trigger the R-T instability which is an interesting and important result in terms of understanding the generation of EPBs.

Title: Phenomenological implication of particle dark matter models
Researcher: Show, Sudipta
Supervisor: Konar, Partha
Year: 2022
Keyword's: Particle Physics, Large Hadron Collider, Dark Matter, Radiative Neutrino Mass
Call No.: 523.1126 SHO
Acc. No.: T01073

Abstract: The standard model of particle physics provides an elegant description of matters and forces of nature as the building block in its most fundamental form. Decades-long theoretical and experimental journey, most of them through immense collaborative efforts from Humanity, finally established a self-consistent theory of particles and their gauge interaction, depicting the strong, weak, and electromagnetic force. An enormous amount of data so far from different collider and celestial experiments measured different parameters of this model very precisely, shaping this model.

Alas, we still firmly believe this only as an effective low energy theory - just revealed the tip of the iceberg. A considerable chunk remains imperceivable to us, probably describing a richer dark sector, which constitutes eighty percent of the matter of the Universe. The evidence of dark matter has spread over a wide range of scales, e.g., from the galaxy scale to the cosmological scale, in various experiments. Our standard model cannot provide any clue if it has anything to do with the particles and forces of fundamental nature. There are several other convincing results, such as matter anti-matter asymmetry and the tiny but non-zero neutrino mass, which only strengthens this impression. A fierce hunt for new physics is underway at the present high luminosity run of the Large Hadron Collider. Many exotic theories have been developed to make it work or address some of these puzzles. The present thesis studies some of these well-motivated new physics models winding around different dark matter scenarios.

The first set of analyses explores different extended realizations of the singlet doublet scenario. We start with examining a simple extension of the standard model with a pair of fermions, one singlet, and a doublet in a common thread linking the dark matter problem with the smallness of neutrino masses associated with several exciting features. In the presence of a small bare Majorana mass term, the singlet fermion brings in a pseudo-Dirac dark matter capable of evading the strong spin-independent direct detection bound by suppressing the dark matter annihilation processes mediated by the neutral current. Consequently, the allowed range of a mixing angle between the doublet and the singlet fermions is enhanced substantially. Interestingly, the presence of the same mass term in an association with singlet scalars also elevates tiny but non-zero masses radiatively for light Majorana neutrino satisfying observed oscillation data. We further extend to study an appealing alternative scenario of leptogenesis assisted by the dark sector, which leads to the measured baryon asymmetry of the Universe. The dark sector carries a non-minimal set-up of singlet doublet fermionic dark matter extended with copies of a real singlet scalar field. A small Majorana mass term for the singlet dark fermion, in addition to the typical Dirac term, provides the more favorable dark matter of pseudo-Dirac type, capable of escaping the direct search. Such a

construction also offers a formidable scope for radiative generation of active neutrino masses. In the presence of a (non)standard thermal history of the Universe, we perform the detailed dark matter phenomenology adopting the suitable benchmark scenarios, consistent with direct detection and neutrino oscillations data. Besides, we have demonstrated that the singlet scalars can go through CP-violating out of equilibrium decay, producing ample lepton asymmetry. Such an asymmetry then gets converted into the observed baryon asymmetry of the Universe through the non-perturbative sphaleron processes owing to the presence of the alternative cosmological background considered here. Unconventional thermal history of the Universe can thus aspire to lend a critical role both in the context of dark matter and in realizing baryogenesis.

In another work, we further discuss the non-thermal production of dark matter in a scalar extended singlet doublet fermion model where the lightest admixture of the fermions constitutes a suitable dark matter candidate. The dark sector is non-minimal with the MeV scale singlet scalar, which is stable in the Universe lifetime and can mediate the self-interaction for the multi-GeV fermion dark matter, mitigating the small-scale structure anomalies of the Universe. If the dark sector is strongly coupled, it undergoes internal dark thermal equilibrium after freeze-in production. We end up with suppressed relic abundance for the fermionic dark matter in a commonly conceived radiation-dominated Universe. In contrast, the presence of a modified cosmological phase in the early era drives the fermionic dark matter to satisfy nearly the whole amount of observed relics. It also turns out that the assumption of an unconventional cosmological history can allow the GeV scale dark matter to be probed at LHC from displaced vertex signature with improved sensitivity.

In our next set of investigations, we probed the importance of thermal effects in dark matter production. To realize the same, we examine a scenario for freeze-in production of dark matter, which occurs due to the large thermal correction to the mass of a decaying mediator particle present in the thermal bath of the early Universe. We show that the decays, which are kinematically forbidden otherwise, can open up at very high temperatures and dominate the dark matter production. We explore such forbidden production of dark matter in the minimal $U(1)_{B-L}$ model, comparing dark matter phenomenology in the context of forbidden frozen-in with the standard picture. We further investigate a freeze-in production of the dark matter considering the thermal effects in a minimally extended $U(1)_{\mu-L\tau}$ framework that remains consistent with the recent muon ($g-2$) data. Here, the scalar plays the role of the dark matter with a non-trivial charge under the additional symmetry $U(1)_{\mu-L\tau}$. This scalar dark matter obtains a thermally corrected mass at high temperatures for a not-so-small self-coupling. We show that the thermal correction to the dark matter mass plays a significant role in the dark matter phenomenology.

In this thesis, we explored diverse mainstream paradigms consisting of ‘weakly interacting massive particle’ (WIMP) and ‘feebly interacting massive particle’ (FIMP) as dark matter in the context of different models. We also discuss the scope of generating observed neutrino masses and the production of baryon asymmetry via the leptogenesis mechanism. Two important aspects, such as the thermal effects in masses and cosmological evolution in the early Universe, can affect the dark matter evolution. The significance of the same is probed by looking at the subtle footprint it may have left on dark matter phenomenology.

Title: Eruption of solar magnetic flux ropes and associated flaring activity: observational perspectives
Researcher: Sahu, Suraj
Supervisor: Joshi, Bhuwan
Year: 2023
Keyword's: Magnetic Flux Rope (MFR), Large Angle And Spectrometric Coronagraph (LASCO), Solar Observations, Magnetic Fields
Call No.: 522.1 SAH
Acc. No.: T01074

Abstract: The solar eruptive phenomena consist of various forms energetic and explosive activities occurring throughout the solar atmosphere. It is now well-understood that the solar eruptive events usually take the forms of filament eruptions, flares, coronal mass ejections (CMEs), solar jets, etc. The source of origin of these explosive events lies in the complexity of the magnetic configurations permeating the solar atmospheres from the photosphere to corona. The continuous photospheric motions shuffle the coronal magnetic field lines creating entanglement and this results in the storage of free magnetic energy, which ultimately releases drastically to give rise to the numerous explosive activities on the Sun. Usually, an eruptive flare expands and evolves through all the atmospheric layers and the associated radiative signatures span over the entire electromagnetic spectrum. The various ground- and space-based observational resources cover a wide range of spatial, temporal, and spectral domains, which help in understanding the different atmospheric layers through measurements of their physical parameters, viz., temperature, density, pressure, etc. In view of this, it is important to investigate the origin and evolution of the solar eruptive events through multi-wavelength and multi-instrument observational facilities.

It is now well-established that the magnetic flux rope (MFR) is the basic constituent of the solar eruptive phenomena. An MFR is defined as the bundle of field lines that wind around each other and wrap around a common axis. In this thesis, we focus on the exploration of the build-up, activation, eruption, and subsequent evolution of MFRs in the framework of the eruptive flares. Our analyses reveal a number of important observational results related to the physics of MFR with the aid of multi-wavelength data, complemented by the coronal magnetic field modeling techniques. The E(UV) imaging observations are obtained from the Atmospheric Imaging Assembly (AIA) instrument on board the Solar Dynamics Observatory (SDO) spacecraft. The photospheric magnetic field evolution is studied from the data gathered from the Helioseismic and Magnetic Imager (HMI) instrument on board SDO. The imaging and spectroscopic capabilities of Reuven Ramaty High Energy Solar Spectroscopic Imager (RHESSI) are extensively utilized to investigate the thermal and non-thermal energy release processes associated with different stages of the eruptive phenomena through analysis of the X-ray sources. The Large Angle and Spectrometric Coronagraph (LASCO) on board the Solar and Heliospheric Observatory (SOHO) spacecraft provides the white light observations of CMEs. The temporal information about the evolutionary stages of solar flares are obtained from the disk-integrated soft X-ray light curves in the 1–8 and 0.5–4 Å channels of the Geostationary Operational Environmental Satellite (GOES) system. In order to investigate the

precise coronal magnetic field structures, we use two different magnetic field extrapolation techniques. For the analysis of small-scale magnetic fields at lower coronal heights, we use the Non-Linear Force-Free Field (NLFFF) extrapolation technique, whereas, the large-scale coronal magnetic structures are investigated through the Potential Field Source Surface (PFSS) method. Both these extrapolation methods are based on the numerical techniques.

We analyze the processes responsible for the build-up and activation of a hot channel in high temperature EUV passbands, located over the polarity inversion line (PIL) of the flaring region within the NOAA active region (AR) 12371 during 2015 June 22. The activated hot channel erupts following the standard flare reconnection scenario giving rise to a major M6.6 flare and associated CME. Prior to the onset of the eruptive flare, the hot channel undergoes a prominent activation phase during which it displays co-spatial hard X-ray (HXR) emission up to energies of 25 keV. We obtain an MFR co-spatial to the hot channel through NLFFF modeling. To our knowledge, this is the first time a developing MFR/hot channel is being detected in direct HXR observations. These distinct, localized HXR sources from the central part of the MFR suggest its build-up and activation through magnetic reconnection among the sheared/twisted field lines representing the MFR magnetic structure. We observe significant changes in the AR's photospheric magnetic field prior to the flare onset, during an extended period of ≈ 42 hr in the form of rotation of sunspots, moving magnetic features, and flux cancellation along the PIL. During the activation phase of the MFR, it undergoes a slow rise phase ($\approx 14 \text{ km s}^{-1}$) for ≈ 12 minutes, which is thought to be the result of the ongoing magnetic reconnection occurring at multiple locations within the MFR core field. Suddenly, a fast transition ($\approx 109 \text{ km s}^{-1}$ with acceleration $\approx 110 \text{ m s}^{-2}$) in the kinematic evolution of the MFR is observed, which temporally marks the onset of the impulsive phase of the ensuing M6.6 flare. This sudden transition in the speed of the erupting MFR precisely divides the pre-flare and impulsive phase of the flare. This observation points toward the standard flare reconnection scenario, which entails the inherent feedback process between the early dynamics of the eruption and the strength of the flare magnetic reconnection. The erupting MFR finally blows out the constraining overlying field lines completely to be observed in the coronagraphic images as a CME.

An MFR may form at the base of the convective layer of the Sun due to dynamo mechanism. Buoyancy instability causes the MFR to emerge from the solar interior and overshoot the photosphere to break into the atmosphere. The footpoints of a bundle of emerged MFRs usually become visible in the white light intensity images as sunspot groups, forming the ARs. The various photospheric motions strongly affect the subsequent dynamics of an MFR after its emergence. In view of this idea, we try to explore the efficient coupling between the photospheric and coronal magnetic fields and associated processes through the investigation of a series of homologous eruptive flares. The flares originate from NOAA AR 12017 during 2014 March 28–29 and are of successively increasing intensities (M2.0, M2.6, X1.0). The EUV observations coupled with coronal magnetic field modeling reveal that the eruptive flares are triggered by the eruption of MFRs embedded by a densely packed system of bipolar loops within a small part of the AR. The evolution of photospheric magnetic field over an interval of ≈ 44 hr encompassing the three events undergoes important phases of emergence and cancellation processes together with significant changes near

the PILs where the flux ropes lie. In view of this, our observational results point toward the tether-cutting mechanism as the viable triggering mechanism responsible for the eruptions. Between the second and third event, we observe a prominent phase of magnetic flux emergence which temporally correlates with the build-up phase of free magnetic energy in the AR corona. This observation is suggestive of an efficient coupling between the rapidly evolving photospheric and coronal magnetic fields in the form of persistent flux emergence that leads to a continued phase of the build-up of free magnetic energy, which gets released episodically resulting into the three homologous flares of successively increasing intensities.

The homologous eruptive flares in AR 12017 are triggered by the eruption of compact MFRs within the flaring region. The spatial extent of the source region of eruptions is much compact compared to the CMEs produced as a result of the eruptions. Each of the three CMEs developed in the wake of the eruptions gradually attains a large angular width, after expanding from the compact eruption-source site. We analyze this remarkable observation of generation of broad CMEs resulting from compact eruptions. We find these eruptions and CMEs to be consistent with the “Magnetic-Arch-Blowout” (MAB) scenario: each compact-flare blowout-eruption is seated in one foot of a far-reaching magnetic arch, explodes up the encasing leg of the arch, and blows out the arch to make a broad CME.

In summary, our observational results obtained from the multi-wavelength and multi-instrument data, complemented by the coronal magnetic field modeling techniques, are useful to understand the build-up, activation, triggering, and subsequent evolution of MFRs in the framework of the eruptive flares. Our results can be used as important inputs toward the prediction of near-Earth space weather phenomena.

Title: Evolution of remnant radio galaxies
Researcher: Dutta, Sushant
Supervisor: Singh, Veeresh
Year: 2022
Keyword's: Black Holes, Active Galactic Nuclei (AGN), Radio Galaxies
Call No.: 523.112 DUT
Acc. No.: T01075

Abstract: Active Galactic Nuclei (AGN) are manifestations of accretion around the Super-Massive Black Holes (SMBHs) residing in the centres of galaxies. Radio galaxies, a subclass of AGN, emit copiously at radio wavelengths and exhibit a typical radio morphology comprising a core, a pair of highly collimated relativistic jets that eventually form radio lobes at their extremities. Understanding the evolution of radio galaxies is one of the important aspects of galaxy evolution, as AGN jet activity influences host galaxy and surrounding inter-galactic-medium (IGM) via feedback processes. In last few decades, multi-frequency radio observations probing radio emission at different spatial-scales have revealed that the AGN jet activity in galaxies is only a phase (active phase) lasting for several tens of Myr during which the radio size can grow up to a few hundred kpc and rarely, up to a few Mpc. After an active phase, AGN activity ceases or drops below a certain threshold level so that the outflowing jets are no longer supported and the radio lobes begin to fade away. During the fading period termed as the 'remnant phase' or 'dying phase', the radio core and jets disappear but the radio lobes can still be detected for a period of a few tens of million years before they disappear due to radiative and dynamical losses. The duration of remnant phase is arguably a small fraction of the duration of active phase, hence remnant sources are believed to represent a short-lived final phase of the radio galaxy's evolution. Remnant radio galaxies (hereafter 'remnants') are deemed to be less abundant owing to the relatively short duration of the remnant phase. Due to their relative paucity remnants are poorly understood. Specifically, AGN duty cycle and its dependence on various factors such as the jet kinetic power, host galaxy, and large-scale cluster environment are still a matter of investigation.

This thesis presents the search and characterization of remnants in the XMM-LSS deep field by using sensitive radio observations at 325 MHz from the Giant Metrewave Radio Telescope (), at 150 MHz from the LOw Frequency ARray (LOFAR), at 1.4 GMRT GHz from the Jansky Very Large Array (JVLA), and at 3 GHz from the VLA Sky Survey (VLASS). By using both morphological criteria viz., undetected radio core as well as spectral criteria viz., high spectral curvature, and ultra-steep spectrum, we identify a sample of 21 remnant candidates that are found to reside mostly in noncluster environments, and exhibit diverse properties in terms of morphology, spectral index ($\alpha_{\frac{1.4 \text{ GHz}}{150 \text{ MHz}}}$ in the range of -1.71 to -0.75 with a median of -1.10) and linear radio size (ranging from 242 kpc to 1.3 Mpc with a median of 469 kpc). Our study attempts to identify remnant candidates down to the flux density limit of 6.0 mJy at 325 MHz, and yields a stringent upper limit on the remnant fraction (f_{rem}) to be 5%, a lower value than those reported previously. The observed f_{rem} seems consistent with the predictions of an evolutionary model assuming power law distributions of the duration of active phase and jet kinetic power with index -0.8 to -1.2.

This thesis also highlights the fact that most of the previous studies searched remnants using morphological criteria and they have preferentially identified large angular size sources resulting into a bias towards the remnants of powerful FR-II radio galaxies. This thesis presents the first attempt to perform a systematic search for remnants of small angular sizes ($<30''$) by exploiting spectral curvature criterion in the 150 MHz— 1.4 GHz spectral window. We identify a sample of 48 small-size remnant candidates that exhibit strong spectral curvature *i.e.*, $\alpha_{325 \text{ MHz}} - \alpha_{1.4 \text{ GHz}} \geq 0.5$. Our study unveils a new population of small-size ($<200 \text{ kpc}$) remnant candidates, and contradicts previous findings suggesting that the small-size remnants mostly reside in cluster environments wherein dense surrounding medium confines the growth of radio source. We find that most of our small-size remnants reside in less dense environments. We speculate that a relatively shorter active phase and/or the low jet kinetic power can be plausible reasons for the small size of remnant candidates.

We model the radio spectral energy distributions (SEDs) of a subsample of remnants using band-3 uGMRT and ancillary radio observations. The continuous injection off model (CI_{OFF}), that assumes an active phase with continuous injection followed by a remnant phase, provides reasonably good fits to the SEDs. Our study finds the total source ages (t_s) in the range of 20 Myr to 42 Myr with t_{OFF}/t_s ratio distributed in the range of 0.1 to 0.6, which in turn suggests them to belong to different evolutionary phases. We note that, in comparison to the remnants reported in the literature, our sample sources tend to show lower spectral ages that can be explained by the combined effects of more dominant inverse Compton losses for our sources present at the relatively higher redshifts, and possible rapid expansion of lobes in their less dense environments.

Title: Enlightening the dark universe through light particles
Researcher: Poddar, Tanmay Kumar
Supervisor: Goswami, Srubabati
Year: 2022
Keyword's: Light Particles, Gravitational Waves, Dark Matter, Modified Gravity, Sterile Neutrino
Call No.: 535.4 POD
Acc. No.: T01076

Abstract: The Standard Model (SM) of particle physics and Einstein's theory of General Relativity (GR) are the two most important theories that can explain the four fundamental forces governing the interactions between the particles in nature. Since, gravitational interaction is not quantized, it cannot be accommodated in the SM of particle physics that deals with strong, electromagnetic, and weak interactions. The classical GR theory explains the gravitational interaction between massive objects very well. In fact, these two theories can explain a wide range of observational and experimental results with a high level of accuracy. However, there are theoretical, and experimental motivations for studying physics Beyond Standard Model (BSM) of particle physics and physics beyond Einstein's GR theory. The most prominent BSM signatures are the existence of dark matter, neutrino mass, matter-antimatter asymmetry etc. There are motivations to go beyond Einstein's GR theory as well to explain phenomena such as the massive gravity theory, fifth force, singularity problem, dark energy etc.

In this thesis, we have studied light particles such as axions (spin-0), light gauge bosons (spin-1), massive gravitons (spin-2), and sterile neutrinos (spin-1/2) to explore the unknown dark sector of the universe such as dark matter, neutrino mass, massive gravity, and fifth force. We obtain bounds on the properties of these particles through orbital period loss of compact binary systems (Neutron Star-Neutron Star (NS-NS), Neutron Star-White Dwarf (NS-WD)), gravitational light bending, Shapiro time delay, perihelion precession test, and neutrino experiments. If a compact star such as NS or WD is immersed in a low mass axionic potential then it can develop a long range axion hair outside of the compact star. Here, we have considered several compact binary systems like NS-NS and NS-WD and calculated the inverse of their orbital time period which is $\sim 10^{-19}$ eV or less. This mass range is in the ballpark of Fuzzy Dark Matter (FDM) which includes Axion Like Particles (ALPs). The orbital period loss of the compact binary systems is mainly due to the gravitational wave radiation. The orbital period can also decay due to the radiation of ultralight ALPs if its mass is smaller than the orbital frequency of the binary system. We consider four compact binary systems such as PSR J0348+0432, PSR J1738+0333, PSR J0737- 3039, and PSR B1913+16. Comparing with the experimental data, we obtain bounds on the axion decay constant $f_a \lesssim O(10^{11} \text{ GeV})$ with axion mass $m_a \lesssim O(10^{-19} \text{ eV})$. The result suggests that if ALPs are FDM, then they do not couple with quarks. If the NS is a pulsar, it can also emit electromagnetic radiation. The long range axion hair from a pulsar can change the polarization of the electromagnetic radiation which is called the birefringent effect. We calculate the birefringent angle due to the interaction of long range axions with the electromagnetic radiation as 0.42° . This value is within the accuracy of measuring the linear polarization angle of pulsar light. This value holds for the axions of mass $m_a < 10^{-11} \text{ eV}$ which is

constrained by the radius of the pulsar and axion decay constant $f_a \sim O(10^{17} \text{ GeV})$ which is constrained by the requirement that the axions are sourced by pulsars. Like NS, WD, pulsars, the celestial objects like earth and Sun can also mediate long range axion hair outside of these massive bodies. The range of the axion mediated Yukawa type fifth force is constrained by the distance between earth and Sun which sets the upper bound on the axion mass $m_a \lesssim 10^{-18} \text{ eV}$. The contribution of axionic Yukawa potential is within the experimental uncertainties in the measurement of light bending and Shapiro time delay. We have calculated the amount of light bending and Shapiro time delay due to the axion emission and by comparing with the experimental data, we obtain bounds on axion decay constant. The Shapiro delay puts the stronger bound on axion decay constant as $f_a \lesssim 9.85 \times 10^6 \text{ GeV}$. The result also implies if ALPs are FDM, then they do not couple with quarks.

We have also attempted to probe gauged $U(1)_{Li-Lj}$ scenario from orbital period loss of compact binary systems and perihelion precession of planets. Due to large chemical potential of degenerate electrons, the NS contains lots of muons and hence the compact binary systems can mediate gauged $U(1)_{L\mu-L\tau}$ force. The vector gauge bosons of $U(1)_{L\mu-L\tau}$ type can radiate from the binary systems and its contribution is within the experimental uncertainty in the measurement of orbital period loss of the compact binary systems. The mass of the gauge boson is constrained by the orbital frequency of the binary system and for the radiation of gauge bosons, the mass is restricted by $M_{Z'} < 10^{-19} \text{ eV}$. Comparing with the experimental data, we obtain a bound on $U(1)_{L\mu-L\tau}$ gauge coupling as $g < O(10^{-20})$. Presence of electron in the Sun and Planets is also responsible for the mediation of long range Yukawa $U(1)_{Le-L\mu,\tau}$ type of gauge force between the planets and the Sun. The mass of the $U(1)_{Le-L\mu,\tau}$ gauge boson is constrained by the distance between the Sun and the planets that puts the stronger bound on the gauge boson mass as $M_{Z'} < 10^{-19} \text{ eV}$. The contribution of $U(1)_{Le-L\mu,\tau}$ gauge bosons is within the experimental uncertainty in the measurement of the perihelion precession of planets. We calculate the perihelion precession of planets due to the mediation of $U(1)_{Le-L\mu,\tau}$ gauge bosons and by comparing with the experimental data, we obtained a bound on $U(1)_{Le-L\mu,\tau}$ gauge coupling as $g \lesssim O(10^{-25})$. We find that the planet Mars puts the stronger bound on coupling. Next, we have calculated the energy loss due to massless graviton radiation in Einstein's GR theory for a single graviton vertex process using Feynman diagram techniques. This gives the same result as one obtains from the quadrupole formula. Following the same technique, we have calculated the energy loss due to massive graviton radiation for several massive gravity theories such as Fierz-Pauli (FP) theory, Dvali-Gabadadze-Porrati (DGP) theory, and modified Fierz-Pauli theory. Theories of massive graviton has a peculiarity that at zero graviton mass limit, the massive graviton propagator does not go to the massless graviton propagator. This is called vanDAM-Veltman-Zakharov (vDVZ) discontinuity. We study the vDVZ discontinuity in these massive gravity theories. We also obtain bounds on the graviton mass in these massive theories from the binary pulsar timing.

Lastly, we analyze the effect of sterile neutrino on the effective Majorana mass ($m_{\beta\beta}$) governing neutrino-less double beta decay ($0\nu\beta\beta$) for Dark Large Mixing Angle (DLMA) solution. The later arises in presence of neutrino non standard interaction and admits a solution for the solar mixing angle $\vartheta_{12} > 45^\circ$. We have checked that the MSW resonance in the sun can take place in the DLMA parameter

space in the 3+1 scenario. Next, we investigate how the values of the solar mixing angle ϑ_{12} corresponding to the DLMA region alter the predictions of $m_{\theta\theta}$ by including a sterile neutrino in the analysis. We also compare our results with three generation cases for both standard large mixing angle (LMA) and DLMA. Additionally, we evaluate the discovery sensitivity of the future ^{136}Xe experiments in this context.

Title: Aspects of spectroscopic and polarimetric instrumentation for ground based optical telescopes with related observations
Researcher: Kumar, Vipin
Supervisor: Srivastava, Mudit K.
Year: 2022
Keyword's: Polarimetric Instrumentation, Faint Object Spectrograph And Camera (FOSC), Optical Telescopes, MFOSC-P
Call No.: 522.29 KUM
Acc. No.: T01077

Abstract:

Physical Research Laboratory (PRL) has been operating a 1.2m aperture diameter telescope and is recently in the process of setting up another 2.5m aperture diameter telescope at Gurushikhar, Mt. Abu, India. The 1.2m telescope is equipped with various back-end instruments capable of studying the visible and NIR regime of the spectrum. A variety of observational astrophysical research programs have been successfully explored with the existing telescope over the last couple of decades, such as star formation, novae & supernovae, active galactic nuclei, cometary sciences, exo-planets, etc. The upcoming 2.5m telescope would further enhance the prospects of these research domains as well as in new avenues like observations of transients (novae, supernovae, etc.), exoplanets, and their host stars, M dwarfs, etc.

The Faint Object Spectrograph and Camera (FOSC) type of instrument has been one of the most sought-after general-purpose, versatile instruments on any small or medium aperture telescope due to its ability to provide imaging and spectroscopy in a single focal reducer-based optical chain. As the requirements of a full-fledged FOSC instrument for the upcoming 2.5m telescope were being considered around late 2014, it was decided to develop a pathfinder instrument, named Mt. Abu Faint Object Spectrograph and Camera-Pathfinder (MFOSC-P) for the existing 1.2m telescope. MFOSC-P had been designed to provide low-resolution spectroscopy in three resolution modes ($R \sim 500, 1000, 2000$) and seeing limited imaging in astronomy standard Bessell's B, V, R, I, and a narrow band $H\alpha$ filters. At the time of starting this thesis work in mid-2018, the design of MFOSC-P was completed, and various components were being procured. Thus the overall structure of this thesis was planned around the MFOSC-P instrument and can be summarized in four broad projects,

1. Assembly-Integration-Test (AIT) of MFOSC-P instrument in the laboratory.
2. On-sky characterization and performance verification program of MFOSC-P using a sample of M dwarfs.

3. Science verification of MFOSC-P with the observational studies of Nova V2891 Cyg and a suspected symbiotic system SU Lyn.
4. Optical design of an extended version of FOSC instrument for the upcoming 2.5m telescope, named - Mt. Abu Faint Object Spectrograph and Camera-Echelle Polarimeter (M-FOSC-EP) and its prototype- named ProtoPol.

The Assembly-Integration-Test (AIT) of MFOSC-P in the laboratory formed **the early part of the thesis**. AIT is an important and essential phase of the instrument development process. It includes quality tests for various components, sub-assemblies, instrument integration, etc. It also includes various performance tests to cross-verify the photometric and spectroscopic performance of the instrument with their designed values. During the AIT procedure of MFOSC-P, various sub-systems were assembled and characterized on the optical test bench set-up. These sub-systems were then assembled within the instrument's enclosure, and the performance verification of the instrument was done in the laboratory. The imaging & spectroscopic performance had been verified & were determined as per the designed values. The AIT and laboratory characterization of MFOSC-P was conducted from October 2018 to January 2019. Optical performance verification of the optics components (e.g., lenses and lens sub-assemblies), motion sub-systems testing, imaging and spectroscopy performance verification, etc., were done during this period (see Fig. 1).

The next project of the thesis work was to commission the instrument on PRL 1.2m telescope (see Fig. 2). This was done through a long-term performance verification (PV) program, wherein a sample of M dwarfs were observed during February-June 2019. The primary goal of the PV observations is to ensure the functionalities of the instrument in varying observing conditions. Observations of various astrophysical objects conducted during this program were also utilized to evaluate the performance of MFOSC-P, such as its efficiency, signal-to-noise-ratio (SNR), etc.

During the MFOSC-P performance verification program, 80 M dwarfs were observed during February-June 2019 for their spectral type classification &



Figure 1: Panels (a.), (b.) & (c.) show the development of MFOSC-P lens barrels. Panels (d.), (e.) and (f.) show the completed lens barrels and their cage-rod assemblies. Panels (g.) and (h.) show the assembled MFOSC-P instrument in the laboratory.

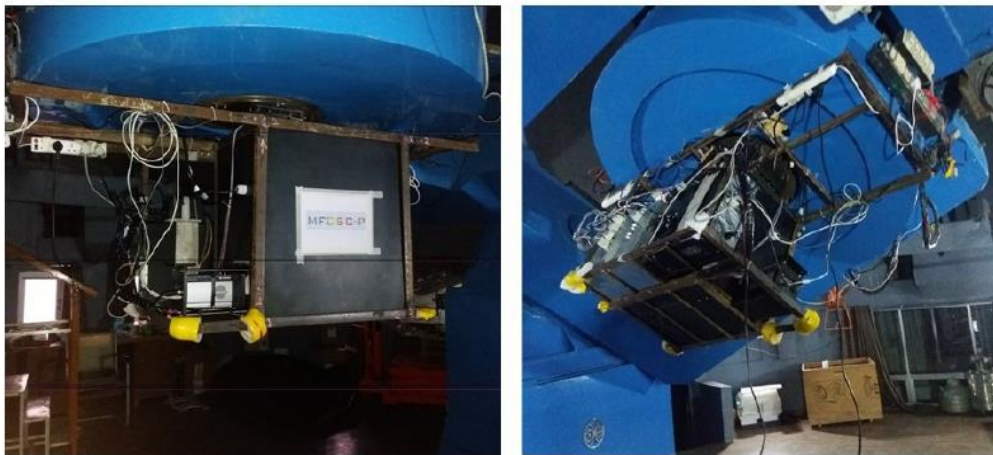


Figure 2: MFOSC-P on the PRL 1.2m telescope.

atmospheric properties using spectroscopy. $H\alpha$ emission was noticed in ten of these sources, indicating the activity in M dwarfs. As very few studies had been carried out to explore the short-term $H\alpha$ variability in M dwarfs. Therefore, it was decided to perform a follow-up spectroscopic study of the variability of the $H\alpha$ and $H\beta$ emissions at shorter time scales in a different sample of M dwarfs. Therefore, in another program, 83 active M dwarfs were observed from March

2020 to March 2021. In this program, we have performed the spectroscopic monitoring of 83 early M dwarfs to study the short-term (~ 5 minutes) variability of $H\alpha$ and $H\beta$ emissions over a few hours of time scales. This study was further complemented with the use of archival photometric light curves from TESS and Kepler/K2 missions. The derived variability parameters are then explored for any plausible systematics for their rotation periods and star-spot filling factors.

An automated data reduction pipeline was developed during the PV phase to reduce these raw observational data to science-ready data. The pipeline has been developed in PYTHON using open-source image processing libraries (e.g. ASTROPY, etc.). The pipeline consists of a series of tasks (codes) to be applied to the raw data in pre-determined sequences. It includes various spectroscopy data reduction steps like bias subtraction, cosmic ray removal, tracing and extracting the spectra, sky background subtraction, wavelength calibration, instrument response correction, etc.

Subsequently, a **science verification (SV) program** was undertaken with MFOSC-P to demonstrate the instrument's scientific potential, capabilities, and performance. Nova V2891 Cyg was selected as a science target for this purpose, and it was monitored for 13 months (November 2019 - December 2020) since its discovery using various imaging and spectroscopy modes of MFOSC-P. Supporting data from several other observatories were also used in this study. Novae are the outburst transients and show significant variations in their magnitudes and optical spectrum. Various phases of the nova outburst were, thus, traced and studied with MFOSC-P. The analysis showed that the coronal emission lines, most likely, are due to shock heating rather than photo-ionization, and the episode of dust formation is shock-induced. These phenomena are rare in the evolution of the novae.

An additional short-term program with MFOSC-P was the study of a suspected symbiotic system- SU Lyn. In this study, we have also utilized the UV spectroscopic data from the UVIT (Ultra-Violet Imaging Telescope) payload of

the AstroSat mission. Using this multi-wavelength data, we have successfully confirmed the symbiotic nature of SU Lyn and established that it belongs to a rare non-shell burning symbiotic system. These results are significant as they firmly establish the existence of non-shell-burning symbiotics without any prominent emission lines in optical.

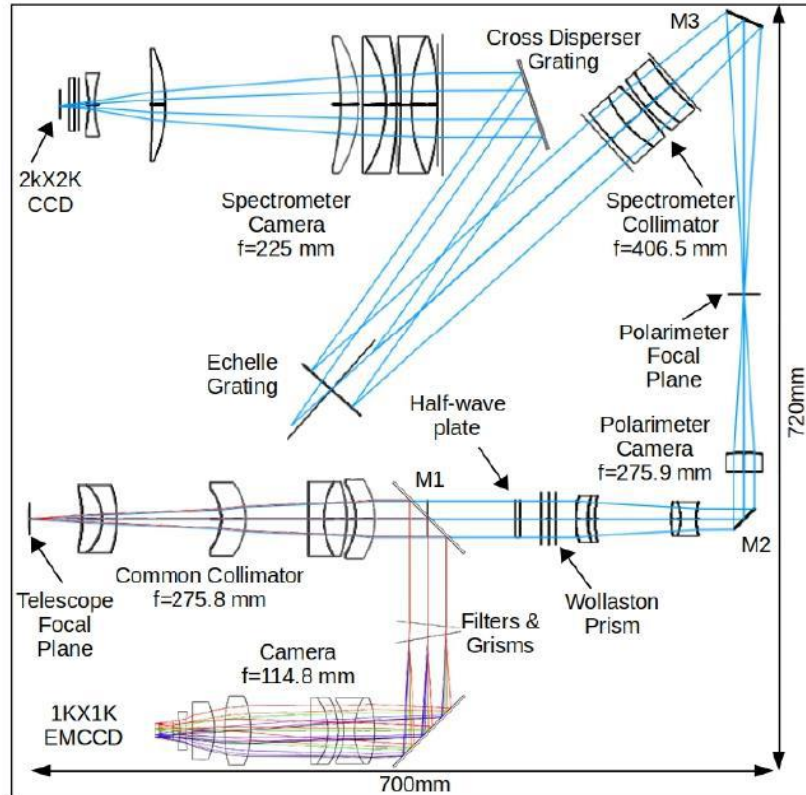


Figure 3: The figure shows ZEMAX optical design model of the M-FOSC-EP instrument. Fold mirrors are used to fold the design within the constraints of the mechanical dimensions. The movable fold mirror M1 would be used to choose the required mode between LRA & Spectro-polarimetry.

As the last part of the thesis, following the success of the MFOSC-P instrument on a 1.2m telescope, we have subsequently developed the optical design of a two-channel multi-mode instrument named Mt. Abu Faint Object Spectrograph and Camera - Echelle Polarimeter (M-FOSC-EP). M-FOSC-EP would have the capabilities of a typical FOSC instrument and the functionalities of an intermediate-resolution spectro-polarimeter. It would be having two detector systems for two of the optical arms. The first arm, the low-resolution

arm (LRA), would provide low-resolution spectroscopy ($\sim 500\text{-}800$) and seeing limited imaging in various filters. The second arm is designed for intermediate resolution (~ 15000) spectro-polarimetry.

The instrument's optical design has been completed and analyzed to ensure the required performance. The optical ZEMAX design is shown in Fig. 3. The instrument is being developed as a common facility instrument with wide-ranging science cases such as symbiotics, M dwarfs, AGNs, novae, supernovae, etc.

As a precursor of the M-FOSC-EP instrument, a prototype instrument-ProtoPol has also been designed with completely off-the-shelf optical components. ProtoPol can be used on the upcoming PRL 2.5m telescope and the existing PRL 1.2m telescope. We have completed the optical design of ProtoPol using ZEMAX software (see left panel of Fig. 4). An initial version of the 3-D mechanical CAD model was also developed using the "Autodesk Inventor" software (see right panel of Fig. 4). The ProtoPol would perform the spectro-polarimetry in the visible domain with a resolution of $\sim 6000\text{-}7000$. ProtoPol is currently being developed, and its various parts are being fabricated.

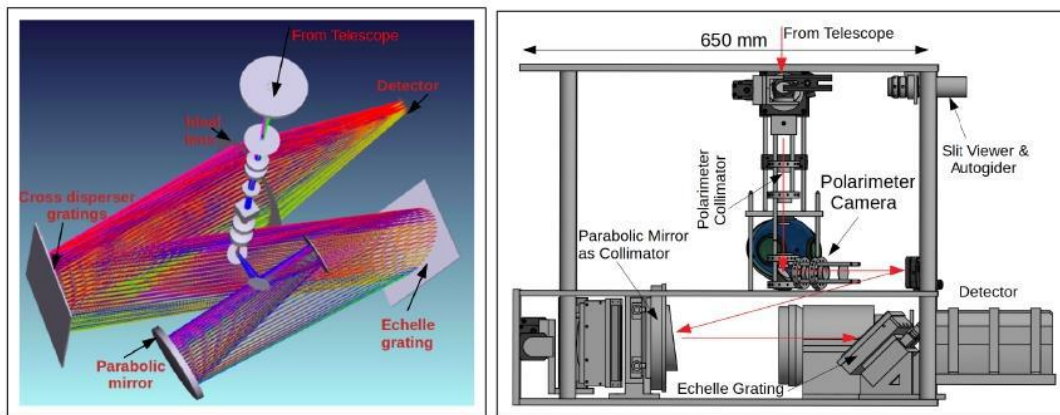


Figure 4: Left panel shows the ZEMAX 3-D model of the Echelle-polarimeter prototype instrument - ProtoPol for upcoming PRL 2.5m telescope. Right panel shows the opto-mechanical design of ProtoPol. The telescope beam enters from the top into the vertical polarimeter arm and then travels through the horizontal spectrograph section.

The thesis is organized into six chapters, as briefly described below:

Chapter 1 - Introduction: This chapter will describe the baseline optical and opto-mechanical designs of the MFOSC-P instrument. We will also discuss the requirements of intermediate resolution spectro-polarimeters on small to moderate aperture telescopes. Various science programs that can be executed with the M-FOSC-EP on the upcoming PRL 2.5m telescope are briefly described here, along with the primary design considerations of the intermediate resolution spectro-polarimeter.

Chapter 2 - Assembly-Integration-Test & laboratory characterization of MFOSC-P: We shall discuss the details of the AIT procedure of MFOSC-P in this chapter. This includes the development of optics/lens sub-assemblies, their quality checks, the laboratory characterization of MFOSC-P on the optical bench as well as within the instrument envelope, etc. The on-sky commissioning and characterization tests of MFOSC-P on the 1.2m telescope will also be discussed, along with the development of the MFOSC-P spectroscopy data reduction pipeline.

Chapter 3 - Performance verification of MFOSC-P with the statistical samples of M dwarfs: In this chapter, we will describe the performance verification studies of MFOSC-P with the sample of M dwarfs. Two observing programs will be discussed: (A.) the low-resolution spectroscopy program of a sample of M dwarfs to characterize them with the determination of their fundamental parameters, viz. effective temperature and surface gravity, and (B.) a follow-up spectroscopic study of short-term $H\alpha$ / $H\beta$ variability in another sample of M dwarfs.

Chapter 4 - Science verification of MFOSC-P: multi-wavelength studies of Nova V2891 Cyg & Suspected Symbiotic - SU Lyn: The two science programs will be discussed in this chapter that were chosen for science verification of MFOSC-P. First, the observing program for Nova V2891 Cyg will

be discussed. The observations of this nova include observations with various spectroscopy and photometry modes of MFOOSC-P, along with various data from other national and international observational facilities. In the second section, the multi-wavelength science observations of SU Lyn will be discussed, which include (in addition to MFOOSC-P observations) the UV spectroscopy data from the UVIT payload on-board the AstroSat mission.

Chapter 5 - Design of spectro-polarimeters for PRL telescopes: The optical design and analyses of M-FOSC-EP and its prototype instrument will be presented in this chapter. In the first section, the optical designs of various sub-modules of M-FOSC-EP -namely, the Low-Resolution Arm (LRA), Polarimeter module, and the Echelle spectrograph module, will be discussed, along with their optical performance and various design analyses. Several other aspects of the optical design like efficiency, resolutions, cross-talk of orders in Echelle spectroscopy, etc., will also be discussed for this instrument. In the second part of the chapter, the optical design of ProtoPol will be described along with its expected performance. A preliminary opto-mechanical design of ProtoPol will also be discussed.

Chapter 6 - Summary & Future Work: This chapter will summarize the content of this thesis and will also discuss some of the promising future research prospects that arise with the successful completion of this work.

Title: Searching for new Physics signatures in hadronic final states at the large hadron collider with deep learnings
Researcher: Ngairangbam, Vishal Singh
Supervisor: Konar, Partha
Year: 2022
Keyword's: Particle Physics, Large Hadron Collider, Vector Boson Fusion Higgs, Quantum Chromodynamics (QCD)
Call No.: 539.72 NGA
Acc. No.: T01078

Abstract: The Large Hadron Collider continues to search for signatures of new physics and scrutinise the properties of the Higgs boson. It has accumulated enormous amounts of highly complex high energy collision event data (and will collect even more data in the upcoming high luminosity phase) to pinpoint different parameters with extraordinary precision and constrain classes of new physics models.

The simultaneous development of very powerful deep-learning algorithms presents a genuine opportunity for their application, leveraging their unprecedented power to enhance experimental sensitivities in pursuit of new physics. Unlike many industrial applications, which can be almost entirely data-driven, the application of such deep-learning algorithms to fundamental physics provides unique challenges. The aim is not solely to utilise their superior performance, for instance, in segregating different signals from the background, but also to understand the features they extract, resulting in such an increase. Moreover, rigorous first principle motivation from the underlying physics provides useful priors whose knowledge can be built into architectural design. This thesis investigates some of the applications of deep-learning algorithms to phenomenological searches at the Large Hadron Collider, concentrating mainly on the challenging but abundant hadronic final states.

The Higgs invisible branching ratio, which is pivotal in ruling out many dark-matter-motivated BSM models, is still poorly constrained. The best available limit comes from the vector boson fusion (VBF) channel, which is experimentally challenging. We address the problem of finding the signal as a classification of images as inputs to Convolutional Neural Networks (CNNs) by using the analogy of the detectors to a camera. The energy's spatial distribution essentially forms a picture with the energy deposits as the pixels' values. Using these so-called 'Tower Images,' we trained CNNs to identify signal type events from background ones. We improved the upper bounds on the invisible-branching ratio of the Higgs by a factor of three compared to existing methods using the same amount of data. The differing nature of the QCD radiation pattern is exploited in traditional VBF searches and deep machine learning. Therefore, it is natural to ask: How accurate are the parton-shower models which simulate the predominant radiation patterns? This issue is, in fact, more pronounced in deep learning methods, which look into minute differences in the radiation pattern. The global parton-shower recoil scheme inherently assumes an Initial-Initial colour dipole structure. It fails to correctly produce the wide-angle radiation patterns in a VBF topology with an Initial-Final/Final-Initial dipole structure. Moreover, the next-to-leading order corrections to the tree level

VBF process are important in determining the kinematics of the third hardest jet, which would be the dominant information beyond the two-jet system. Therefore, we extend the analysis to explore the robustness of the CNN in identifying VBF Higgs signals to these essential factors in the signal simulation process. We find that the CNN's performance is more dependent on the recoil scheme when comparing models trained and tested with the same signal simulation. However, the higher perturbative accuracy of a next- to-leading-order matrix element simulation has better stability when tested on models trained on different signal simulations.

The findings of the previous investigation demonstrate that the training of CNNs is dependent on the nature of the data simulation. Infrared and collinear (IRC) safety guarantees the predictability of observables based on hadrons from quantum chromodynamics. It ensures that long-distance non-perturbative hadronic dynamics do not significantly modify observables. In the subsequent study, we devise an IRC safe framework for Graph Neural Networks, a different class of deep-learning algorithms that generalise the favourable properties of CNNs and generalise it to possibly non-Euclidean domains while forgoing the strictly ordered and sparse representation of the tower image. We also found that it performs as well as state-of-the-art IRC unsafe algorithms in identifying boosted hadronic decays of the top quark against QCD jets while being robust to soft and collinear emissions.

With the null results of various well-motivated new physics models, it is important to look at the background-only hypothesis in a model-independent approach. The subsequent studies explore such model-independent anomaly detection techniques. Although various convolutional autoencoders have been proposed for model-independent anomaly detection methods, it is challenging to design graph autoencoders for inductive graph-based purposes. To utilise the more favourable properties of graph neural networks for unsupervised anomaly detection, we devise a graph autoencoder with the ability to learn inductive graph representations with the help of edge-reconstruction networks. We train the model to efficiently reconstruct the constituent four vectors of large-radius QCD jets in such anomaly detection methods. When trained to reconstruct QCD jets, such models have a high reconstruction error on jets with higher n-prong multiplicities.

In the final study, we explore the power of quantum autoencoders based on variational quantum circuits to detect anomalous signals in a model-independent set-up. Available noisy-intermediate-scale-quantum devices have potential applications in quantum machine learning, where a variational quantum circuit is trained by classical means but utilises the quantum aspects within the circuit implementations. We find that compared to similar bit-based autoencoders with the same inputs, quantum autoencoders have a very efficient training, saturating the test loss reconstruction with as low as ten training samples. Moreover, they perform better than their classical counterparts in a few benchmark signal scenarios.

* * * * *

Researcher/Author Index

A

Aadhar, Saran 229
Aadhi A. 596
Aarth E. 660
Abhinav, Rishabh 400
Abhishek, Aman 635
Agnihotri, Harsha 122
Ahmed, Sana 742
Ahmed, Zeeshan 572
Akarsh A. 302
Ali, Afsar 178
Ali, Haider 211
Ambika, Anukesh Krishnankutty 315
Amin, Shital A. 92
Angira, Deekshi 146
Anuji, K. V. 131
Aravind K. 718
Arora, Ankita 490
Arya, Richa 673
Ashish 679

B

Bai, Rukmani 634
Bajpai, Aman 204
Balaganesh B. 419
Baliyan, Shivani 338
Balsukuri, Naresh 129
Bandaru, Narendra 500
Bandyopadhyay, Sohom 273
Bandyopadhyay, Soumik 644
Banerjee, Dyotana 449
Bansal, Anshika 716

Baruah, Renika 568
Basak, Abhishek 583
Behera, Rakesh 520
Bhagat, Chandrashekhar 262
Bhakuni, Rashmi 15
Bhalla, Pankaj 615
Bharadwaj, Jahnu 456
Bhardwaj, Akanksha 671
Bharti, Nisha 319
Bhashini, Manju V. 396
Bhattacharjee, Sankha Subhra 416
Bhattacharya, Debayan 221
Bhavsar, Punitkumar 363
Bhoir, Mandar S. 377
Bhoir, Siddhant Pandurang 25
Bhoraniya, Ramesh 560
Bisht, Anuj 148
Biswas, Ayan 708
Bora, Kamlesh 729

C

Chaitanya, Apurv 607
Chakraborty, Kaustav 683
Chakraborty, Swaroop 41
Chakravarti, Pritha 323
Chandra, Naveen 598
Chandrasekaran S. 344
Chattopadhyay, Tanmoy 600
Chauhan, Bhavesh 637
Chawla, Manisha 435
Chhaya, Rachit 291
Chilka, Pallavi 7
Choudhari, Jayesh 279

D

Dahiwadkar, Rahul 202
Das, Laya 362
Das, Rituparna 740
Das, Saroj Kumar 82
Das, Sudipta 123
Dash, Adyasha 390
Dash, Ranjita 577
Dehury, Ranjit Kumar 523
Desai, Nakshi Nayan 50
Dhama, Shivam Singh 544
Dish, Nilabh 517
Dixit, Deepa 90
Duppalapudi, Venkata Mani Padmaja
196
Dutta, Sushant 753
Dwivedi, Gaurav 526

E

Endla, Naveen Kumar 360
Enduri, Murali Krishna 276

F

Fairoos C. 646
Fulpagare, Yogesh Shantaram 531

G

Gadhavi, Joshna Dharmendrabhai 43
Ganeriwala, Mohit D. 379
Gangopadhyay, Aalok 421
Gangopadhyay, Jagriti 437
Gangwar, Bhanu Pratap Singh 143
Gayathri P. 23
George, Manu 623

George, Nithin 461
Ghatage, Swapnil Vilasrao 63
Gopal, Anvita 266
Goyal, Prateek 519
Goyal, Shruti 452
Guha, Shantamoy 307
Gunda, Harini 103
Gundi, Mukta 457
Gupta, Rajat 542
Gupta, Shivangi 665

H

Hariharan P. 68
Harish 321
Hati, Chandan 617
Hivare, Pravin 46
Hussain, Majid 225

I

Indumathi, S. 27
Ingole, Prashant 468
Iqbal, Mohd Umair 112

J

Jadhav, Prajakta Ramesh 223
Jagini, Kishore Kumar 271
Jaiswal, Ayush 547
Jamal, Mohammad Yousuf 633
James, Asha Liza 84
Jana, Palash 158
Jassal, Anjali Rao 592
Javeena 165
Jena, Partha Sarathi 336
Jha, Chandan Kumar (15350004) 412

Jha, Chandan Kumar (15350009) 414
Joshi, Sharad 411
Joshi, Swati Satish 482
Jyoti, Vishav 464

K

Kadam, Sujay Dilip 402
Kalaga, Dinesh Kumar 65
Kanojia, Gagan 394
Kant, Ravi 564
Kantesaria, Naman Pranilal 235
Kar, Ashish 198
Karan, Deepak Kumar 619
Karde, Vikram Ashok 73
Kartik, Mankad Jaivik 108
Kaur, Navpreet 628
Kaurav, Rajkumari 227
Kaushal, Kumari Neeraj 426
Kaushal, Rahul Kumar 297
Kayal, Abhijit 712
Khan, Nasar Ahmad 240
Khandelwal, Shikha 186
Kindra, Bharti 638
Kiran, Patnam Bala Sai 409
Krishankumar, V. Guru 3
Krishna, Kolli Mohan 257
Kulkarni, Siddharth Vijay 75
Kumar, Abhay 710
Kumar, Adarsh 574
Kumar, Ankit 714
Kumar, D Jaya Prasanna 94
Kumar, Deepak 722
Kumar, Deepesh 357
Kumar, Dharmendra 535
Kumar, Girish 612
Kumar, Hirdesh 724

Kumar, Katla Jagdish 137
Kumar, Krishna 428
Kumar, Manish 66
Kumar, Neeraj 431
Kumar, Pardeep 365
Kumar, Prabhat 238
Kumar, Prashant 685
Kumar, Rahul (15310055) 251
Kumar, Rahul (15310066) 540
Kumar, Saket 101
Kumar, Sanjay 21
Kumar, Vipin 758
Kumari, Beena 152
Kumari, Neeraj 732
Kumawat, Sudhakar 281
Kuriakose, Selvia 354
Kurian, Manu 687
Kushwaha, Upendra Kumar Singh 594
Kutwal, Mahesh Shantaram 149

L

Lal C.K., Nijil 642
Laskar, Fazlul Islam 585

M

Madhukar, Sarkale Abhijeet 167
Mahala, Milan Kumar 335
Mahapatra, Amarjyoti Das 155
Mahesh V. P 497
Mahto, Shanti Shwarup 340
Maiti, Sanat Chandra 80
Majhi, Sasmita 503
Majumdar, Sharmistha \f 32
Manav, Neha 173
Mandal, Subir 675

Manwani, Krishna 504
Marapureddy, Geetha 110
Mastan, Indra Deep 285
Maurya, Vidyasagar 179
Mayya, Chaithra 53
Mehta, Krishnesh S. 446
Mehta, Ranjana 533
Mehta, Veli Milind 463
Midhun M. 588
Mir, Ab Qayoom 182
Mishra, Akash K. 688
Mishra, Arvind Kumar 690
Mishra, Sarika 744
Mitra, Ramanuj 737
Mohapatra, Satyajit 408
Mondal, Biswajit 720
Mondal, Tanmoy 610
Mukherjee, Payel Chattopadhyay 434
Mukherjee, Sumitava 430
Mukherjee, Tarushyam 49

N

Nagar, Rajendra 369
Nair, Ankita 481
Nanditha, J. S. 254
Nandy, Dilip Kumar 602
Natarajan, Nalini 29
Nath, Newton 626
Natwariya, Pravin Kumar 734
Nayak, Sushree Sangeeta 701
Ngairangbam, Vishal Singh 766

O

Ojha, Abhijeet 18
Ojha, Apoorva 367

Oza, Harsh 311

P

Paital, Diptiranjana 200
Palakollu, Veerabhadraiah 125
Panda, Soumyashree S. 424
Pandey, Abhishek Kumar 245
Pandey, Amit 331
Pandey, Arun Kumar 621
Pandey, Komal 96
Pandey, Pankaj 293
Pandey, Poonam 12
Pandey, Saloni Prashant 209
Pandey, Vijayalakshmi 170
Pandit, Sudip 549
Pandya, Sheetal Rameshchandra 512
Parashari, Priyank 703
Paruthi, Archini 509
Patel, Diptiben 388
Patel, Divyesh 36
Patel, Manthan 34
Patel, Narendra M. 72
Patel, Nishaben 37
Patel, Tvarit A. 494
Patel, Vinal 356
Patil, Satyajee 745
Patlolla, Prathap Reddy 133
Poddar, Tanmay Kumar 755
Pothukuchi, Rajesh Pavan 119
Prabhakar, Shashi 587
Pradeep Raj K. B. 453
Prakash, Om 555
Prakash, Patnayakuni Ravi 214
Prasad, Ravi Kant 305
Prasad, Rupanjali Gurprasad 99
Prasad, Vighnesh 106

Praseetha, E. K. 135

R

Raj, Archita 663

Raj, Harsh 309

Rajasekhar, Batchu 381

Rajwar, Anjali 56

Ralhan, Krittika 9

Rambabu, Pandey Kuldeep 630

Ramprabhakar, J. 348

Rani, Alka 329

Rani, Lata 159

Rashmi, Richa 58

Ratrey, Poonam 507

Ray, Dwaipayan 389

Reddy, Nagireddy Neelakanteswar 448

Reddy, Vinod Kumar 278

Reza, Amit 653

Rodda, Gopal Krishna 217

Rout, Sandeep Kumar 697

Roy, Anirban 385

Roy, Arko 590

Roy, Soumen 652

Royson, Annie Rachel 440

S

Sable, Hrushikesh 727

Saboo, Anirudh 260

Saha, Kamlesh 551

Saha, Sovan 746

Sahai, Abhishek 451

Sahlot, Pankaj 488

Sahoo, Deepika 317

Sahoo, Ramendra 301

Sahu, Suraj 750

Sanghavi, Hiral M. 32

Sanjeevi, N. S. S. 579

Sarkar, Agnivo 695

Sarkar, Ranadeep 680

Sarode, Ajinkya Ashok 567

Satya, Sivanaresh. M 349

Saxena, Himanshu 333

Seethalakshmi.P 215

Shabbirali, Hadianawala Murtuza 126

Shah, Ankita Rameshkumar 470

Shah, Harsh L. 219

Shah, Krupa 442

Shah, Krupa Rajendra 346

Shah, Reepal 207

Shah, Vrutangkumar V 562

Shaik, Althaf 141

Shankar, Patil Parag 114

Sharma, Shivani 472

Sharma, Shivdutt 287

Sharma, Varun 648

Sharma, Vasudha 39

Shewale, Dipeshwari 57

Shit, Supratim 289

Shivajee 557

Show, Sudipta 748

Shrivastava, Ananya 283

Shukla, Ashish Kumar 705

Singh, Amit Kumar 515

Singh, Ashwin 248

Singh, Balbeer 677

Singh, Chakresh Kumar 655

Singh, Chetan C. 492

Singh, Divita 436

Singh, Naman Deep 313

Singh, Surendra Vikram 699

Sinha, Ankita 570

Sinha, Rishitosh Kumar 327
Sneha 383
Solanki, Dhaval 372
Sonam 299
Srimadhavi R. 194
Srivastava, Pranjal 553
Surana, Neelam 406
Susanna G. 475
Suthar, Kuldeep 614

T

Taki, Kaling 232
Thambi, Varsha 175
Thomas, Pooja Susan 432
Thomas, Tony 444
Thorat, Alpana Ankush 67
Tiwari, Amar Deep 242
Tiwary, Alok Ranjan 624
Tomar, Gaurav kumar 605
Tripathi, Nidhi 667
Tripathi, Richa 657
Tyagi, Anju 190

U

Upadhyay, Abhishek 351

Upadhyay, Awaneesh K. 77
Upadhyay, Parth Tarun 422
Utsav 692
Uttam, Shefali 669

V

Varghese, Sophia 87
Varun, Neetu 116
Veeramaneni, Naveen Deepak 370
Venkataramani, Kumar 631
Verma, Ram Baran 528
Verma, Vinay 404
Vishnudath K. N. 640
Vyas, Diti Pundrik 433
Vyas, Divya 192
Vyas, Hardik Shyam 417

Y

Yadav, Goldy 459

Z

Zarina A. S. 398

Supervisor Index

A

Acharyya, Kinsuk 742
Amrutiya, Sanjay kumar 547
Appayee, Chandrakumar 149, 167,
179, 196
Arora, Amit 488, 497, 512, 515

B

Baliyan, Kiran S. 628
Banerjee, Rupak 692
Basu, Dhiman 217
Basu, Sudipta 204
Bhargav, Atul 531, 567, 568, 570, 572
Bhatia, Dhiraj 53, 56
Bhatt, Jitesh R. 583, 621, 623, 690, 734
Bhattacharyya, Ramitendranath 701,
729
Bhushan, Ravi 309, 319, 336

C

Chakrabarty, Dibyendu 714
Chakraborty, Arup Lal 351, 385, 398,
412
Chandra, Vinod 633, 687
Chattopadhyay, Arka 482
Coleppa, Baradhwaj 695

D

Dalvi, Sameer V. 27, 67, 77, 96, 99
Danino, Michel 481
Das, Bireswar 276, 278, 287

Dasgupta, Anirban 279, 289, 291
Datta, Bhaskar 7, 21, 50, 126, 133, 155
Dayal, Pratyush 94
Deshpande, R. D. 311, 331
Dey, Krishna Kanti 655, 705
Dixit, Atul 540, 542
Dutta, Arnab 178, 182, 186

G

Ganesh, Shashikiran 631, 663, 718
Gautam, Abhay 517, 520, 523
Gayen, Kalyan 66
George, Nithin V. 273, 356, 389, 416,
428
Ghoroi, Chinmay 73, 80, 87, 90, 116
Goswami, Srubabati 626, 640, 683, 755
Gupta, Iti 123, 129, 135, 170, 173
Gupta, Sharad 3, 9, 43, 46

H

Hegde, Ravi Sadananda 417, 424

J

Jain, Vikrant 297, 299, 301, 305, 307,
323
Jasuja, Kabeer 82, 84, 103
Joshi, Bhuwan 594, 750
Joshi, Jyeshtharaj 63, 65, 68

K

Kanvah, Sriram 49, 122, 125, 131, 137, 152, 158, 202
Khanna, Nitin 404, 411
Khatua, Saumyakanti 175, 198, 200
Kirubakaran, Sivapriya 15, 25, 141, 165, 194
Konar, Partha 610, 671, 748, 766
Kothari, Rita 432, 442
Kumar, Brajesh 724
Kumar, Manish 232, 248, 260
Kushawaha, Rajesh Kumar 740

L

Lahiri, Sharmita 433
Lahiri, Uttama 354, 357, 372, 390, 453, 464
Lal, Shyam 598

M

Madapusi, Harish Palanthandalam 402, 562, 577
Mahajan, Namit 612, 638, 716
Majumdar, Sharmistha 39, 58
Mallajosyula, Sairam Swaroop 12, 159
Manjaly, Jaison A. 430, 431, 446, 448, 451, 463
Mathew, Shibu K 624
Mathur, Suchitra 433
Mehta, Mona G. 449, 468
Mekie, Joyce 383, 406, 414
Mishra, Abhijit 190, 490, 503, 507
Mishra, Hiranmaya 635, 677, 722

Mishra, Vimal 207, 211, 219, 229, 242, 251, 254, 302, 315, 340
Misra, Superb K. 41, 509, 519
Miyapuram, Krishna Prasad 293, 435, 452, 657
Mohanty, Subhendra 605, 637, 679, 703
Mohapatra, Nihar Ranjan 349, 367, 377, 379, 408, 426
Mohapatra, Pranab K. 227, 238, 245, 262
Mutha, Pratik 459, 574

N

Naik, Sachindranatha 665, 732
Narayanan, Vinod 560, 564

P

Padhiyar, Nitin 72, 92, 108
Pahlajani, Chetan D. 544
Pallamraju, Duggirala 585, 619, 675, 746
Panda, Emila 492, 494, 500, 504
Paul, Souradyuti 283
Pindoriya, Naran M. 381, 400, 409
Prashant, Amit 221, 223, 257

R

Radhakrishna, Mithun 119
Ragavan K. 344, 346, 348, 360, 370, 396, 419, 422
Raman, Shanmuganathan 281, 285, 369, 388, 394, 421
Ramesh R. 588

Rangarajan, Raghavan 673
Rath, Arnapura 434, 440, 472
Ray, Dwijesh 327, 338
Ray, Jyotiranjana S. 335

S

Sachan, Ajanta 209, 215, 225, 235
Saha, Arnab 549
Sahoo, Bijaya Kumar 602, 737
Sahu, Lokesh Kumar 667
Saini, Supreet 66
Samanta, Goutam Kumar 607, 648
Samanta, Tannishtha 437
Sarbadhikari, Amit Basu 329
Sarkar, Sudipta 646, 688
Sarkar, Utpal 617
Sekar, R. 630
Sengupta, Anand S. 652, 653
Sengupta, Indranath 533, 551, 553,
555
Sengupta, Madhumita 456
Sharma, Sudhanshu 143, 148, 192
Sheel, Varun 669
Singh, Angom Dilip Kumar 590, 614,
634, 644, 727
Singh, Arvind 317, 333
Singh, Navinder 615

Singh, R. P. 587, 596, 642, 685, 708,
744, 745
Singh, Sunil Kumar 313
Singh, Umashankar 34, 36
Singh, Veeresh 712, 753
Sivaraman, Bhalamurugan 699
Soppina, Virupakshi 37, 57
Srinivasan, Babji 112, 362, 363, 365
Srinivasan, Rajagopalan 114
Srivastava, Gaurav 214, 240
Srivastava, Mudit K. 758
Srivastava, Nandita 680
Subramanyam, Malavika A. 266, 457,
470, 475
Sunny, Meera M. 271, 436, 444, 461

T

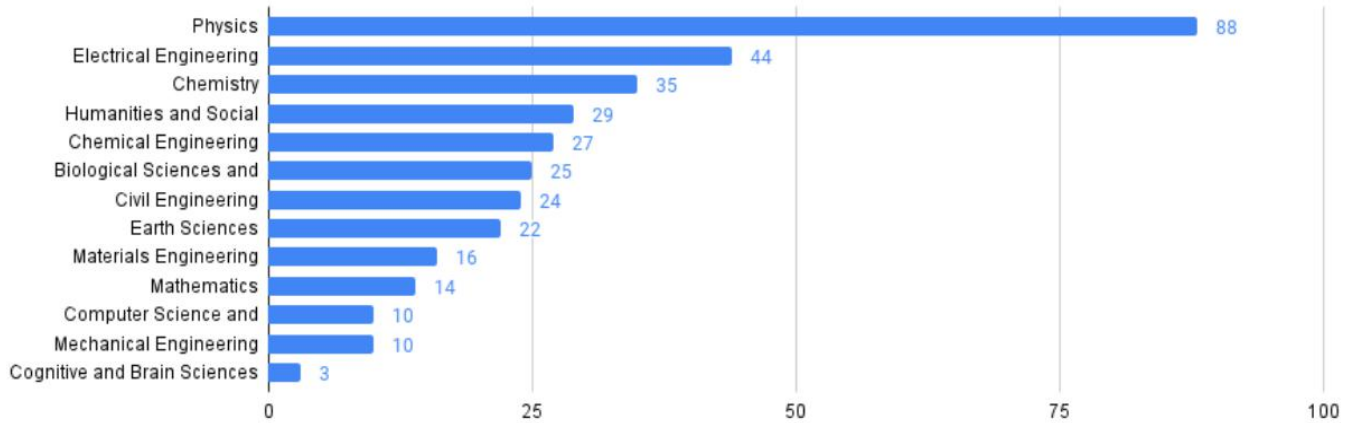
Thareja, Prachi 18, 75, 101, 106, 110
Thiruvengatam, Vijay 23, 29, 146
Tyagi, Jagmohan 526, 528, 535

V

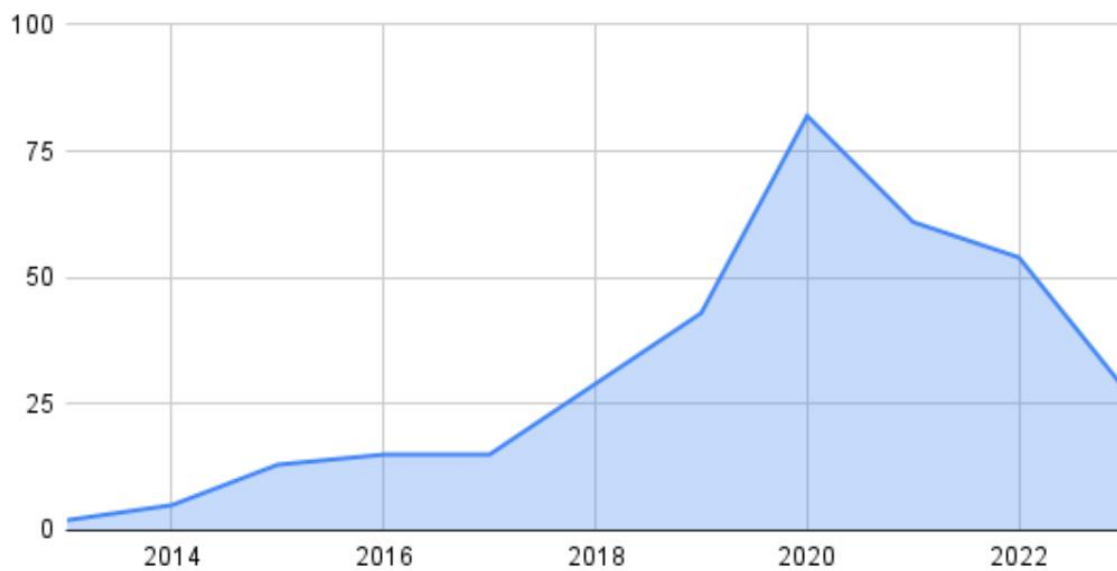
Vadawale, Santosh V. 592, 600, 660,
697, 710, 720
Vashista, Vineet 579
Vatwani, Akshaa 557
Vijayan S. 321

FACT SHEET

Department-Wise



Year-Wise Distribution



M.Sc Theses

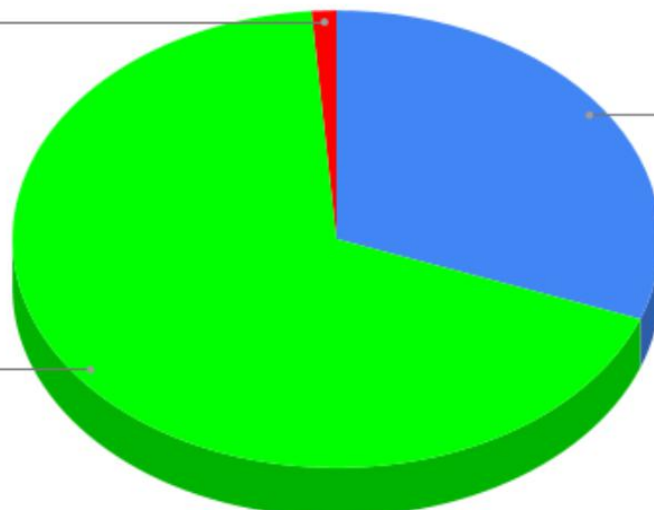
1.2%

PhD Theses

30.7%

M.Tech Theses

68.1%



Address:

Main Library

Academic Block 13A


Indian Institute of Technology Gandhinagar

Palaj, Gandhinagar 382055, Gujarat



Contact Us

 librarian@iitgn.ac.in

 079-2395-1129, 1127, 1128, 1126, 2431

Follow Us

